BULLETIN OF THE EARTHQUAKE RESEARCH INSTITUTE,
TOKYO UNIVERSITY. Vol. XXXIII, Part 1. March, 1955.

東京大學
地震研究所彙報

第 33 號　第 1 册

昭和 30 年 3 月

創立 30 周年記念号

目　次

論文及報告

			頁
1.	地球核内の電磁流体振動 (英文)	力武常次	1
2.	大地震前後に於ける平均海水面の変化について (英文)	山口生知	27
3.	分散した地震波の解析 I (英文)	佐藤泰夫	33
4.	チベット高原と日本海を通過する表面波について，及びある限られた地域を通過する表面波の速度を計算で見出す場合の二，三の注意 (英文)	三東哲夫 (旧姓秋間)	49
5.	大理石の弾性，特にその異方性に就いて (英文)	下鶴大輔 村井勇	65
6.	大理石の弾性に関するノート (英文)	下鶴大輔	73
7.	伊豆大島三原山昭和 25 年及 26 年の噴火 その 2 昭和 26 年の噴火 (B) 第 3 期の活動 (英文)	津屋弘逵 森本良平 小坂丈予	79
8.	建物の振動的性質と地盤の性質との関係 (実在建物における地震動観測) 第 2 報 (英文)	金井清 鈴木富三郎	109
9.	福井平野周辺地域の地質構造解析 (邦文)	村井勇	121
10.	1953 年 7 月 26 日の早雲山山津波の調査 (邦文)	岸上冬彦 小坂丈予	153
11.	青森県天間林地域における磁気探鉱 (邦文)	横山泉	163

(The titles in occidental languages are given on the back cover.)

本彙報ハ年4回 (但シ第1號ヨリ第6號マデハ不定期ニ，第7號ハ3冊トシテ發行セリ)，彙報別冊ハ不定期ニ發行ス.

本彙報掲載ノ論文及ビ報告ノ內容ニ關シテハ著者ノミニ其責任アルモノトス.

本彙報ニ關スル照會通信ハ東京大學地震研究所長ヘ宛テラレタシ.

The Bulletin is published quarterly. (Vols. I–VI were published at irregular intervals and Vol. VII consisted of three parts.)

Supplementary Volume is published at irregular interval.

The authors of the papers alone are responsible for the statements and opinions contained in their respective papers.

All communications relating to this Bulletin should be addressed to the Director of the Earthquake Research Institute, Tokyo University.

1. *Magneto-hydrodynamic Oscillations in the Earth's Core.*

By Tsuneji RIKITAKE,

Earthquake Research Institute.

(Read Dec. 21, 1954.—Received Dec. 24, 1954.)

Summary

Possibilities of magneto-hydrodynamic oscillations in the earth's core are discussed in relation to the stability of Elsasser-Bullard-Takeuchi's dynamo. If there are stable magnetic fields which are caused by the dynamo-action in the earth's core, there will be oscillations of magnetic field and fluid motion around the steady state. This sort of oscillation is here studied under some simplifications. Although the study is rather crude, it is tentatively concluded that the toroidal magnetic field is not so large, otherwise the small oscillations of dynamo would not be stable. Since the fundamental equations for magnetic changes in the earth's core are obtained, we may forecast the magnitude of magnetic field of certain type, say S_1^0-type, starting from suitable initial conditions. This is done in this paper on the basis of the spherical harmonic analyses for various epochs. Although no definite result is obtained because the observation period of the earth's magnetism seems too short for close comparison between the observation and theory, the conclusion concerning the internal magnetic field is compatible with that obtained in the stability problem.

The effect of the earth's rotation as well as that of the mutual dependence of various spherical harmonics are ignored throughout this study. That sort of study will be carried out later on.

1. Introduction

W. M. Elsasser[1]. E. C. Bullard[2], H. Takeuchi[3] and Y. Shimazu[3] have shown that the origin of the earth's main magnetic field seems

1) W. M. ELSASSER, *Phys. Rev.*, **69** (1946), 106, **70** (1946), 202.

2) E. C. BULLARD, *Proc. Roy. Soc. London A*, **197** (1949), 433, **199** (1949), 413.

3) H. TAKEUCHI and Y. SHIMAZU, *Journ. Phys. Earth.*, **1** (1952), 1. *Journ. Geophys. Res.* **58** (1953), 497.

to be explained by the self-exciting dynamo in the earth's core though further laborious works would be necessary in order to complete the theory. As far as the convection currents, magnetic fields and electric currents which are expressed by low degree spherical harmonics are concerned, however, it is likely that there will be a solution for the eigen-value problem which proves the existence of a self-exciting process. If this is to be taken for granted, we have steady motions which excite steady electric currents and consequently steady magnetic fields.

Since the earth's main magnetic field seems to be maintained over long periods, the dynamo must be fairly stable. Palaeomagnetic studies[4] suggest that the earth's magnetic field might have been reversed quite a long time ago, say 10^5—10^6 *years*. But there is no evidence that the reversal of the earth's magnetic field occurred after this epoch. So the dynamo must have been maintained during this order of years. It is believed that the study on the stability is also quite important to establish the dynamo-theory in the core. Bullard[5] studied the oscillation of a homopolar disc dynamo as the first step to this problem. Although the disc dynamo is quite different from the dynamo in the earth's core, his study is important and interesting for the stability problem. The writer would here like to make another approach to the stability problem which is approximately applicable to the real earth.

Now let us consider an equilibrium of convection currents, magnetic fields and electric currents. We shall introduce small deviations of these quantities from their steady values. The behaviour of these small quantities will be studied here. If they remain small enough for a long time, the small oscillation of the dynamo may be regarded as stable. If they increase indefinitely, it will not be stable.

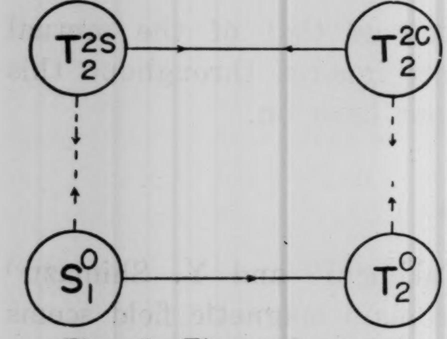

Fig. 1. The "A-approximation" of the self-exciting dynamo.

The writer takes the so-called "A-approximation" as the simplest model of the steady state. As shown in Fig. 1, it contains magnetic fields of S_1^0, T_2^0, T_2^{2c} and T_2^{2s} type and velocities of T_1^0 and S_2^{2c} type. The fundamental equations for small deviations are constructed in Section 2. In order to solve these equations, only small deviation of the magnetic field of S_1^0 type is taken into account ignoring all magnetic

4) T. NAGATA, *Spec. Rep. A.T.M.E.I.U.G.G. Rome Meeting* (1954).
5) E. C. BULLARD, Personal Communication.

fields of other types which will come out during the course of magneto-hydrodynamic interactions. Thus as shown in Section 3, we can solve the pressure equation which is deduced from the fundamental equations. Then the velocity is calculated in Section 4, getting T_1^0, T_3^0, S_2^0, S_2^{2c}, S_2^{2s}, T_3^{2c}, and T_3^{2s} motions. The couplings between these motions and the steady magnetic fields will give many types of magnetic field. But we pick up the couplings which give only the S_1^0-type magnetic field. So we can have an integro-differential equation for small deviation of S_1^0-type magnetic field as given in Section 5. In Section 6, this equation is solved assuming suitable distributions of the steady fields. Thus the periods of free magneto-hydrodynamic oscillations are approximately obtained. The above-stated procedure is similar to the studies of magnetic oscillations of highly conducting stars[6),7),8)] though there are some differences between both studies.

It is found out that the amplitude of the above-considered small deviations will increase tremendously unless the intensities of the steady magnetic fields satisfy certain conditions. In other words, this is a sort of stability condition from which we presume that the T_2^{2c} and T_2^{2s} magnetic fields would not be larger than the steady part of the S_1^0 field as will be discussed in Section 7. In that case the period of free oscillation of S_1^0 field will be of the order of scores or hundreds of *years*. However, as was suggested by Bullard[9)], the effect of Corioli's force due to the earth's rotation would be fairly large. If we take into account this effect, it is quite probable that the stability condition would become fairly modified. Strictly speaking, the error due to the present procedure in which we pick up only the S_1^0-type magnetic field is not clear though the effect of neglecting higher degree terms is thought to be not so serious from physical considerations. However, these points remain to be made clearer.

The integro-differential equation (45) which is obtained in Section 5 can be regarded as the fundamental equation which governs the small oscillations of the S_1^0 field superposed on the steady one. If we start from suitable initial conditions, we may forecast the behaviour of geomagnetic change which is thought to correspond to the secular variation. With the aid of the various spherical harmonic analyses we choose the initial condition at 1900. Then a forecasting is made in

6) M. SCHWARZSCHILD, *Ann. D'Astrophys.*, **12** (1949), 148.
7) V. C. A. FERRARO and D. J. MEMORY, *M.N.R.A.S.*, **112** (1952), 361.
8) C. PLUMPTON and V. C. A. FERRARO, *M.N.R.A.S.*, **113** (1953), 647.
9) E. C. BULLARD, Personal communication.

Section 8 and is also compared with the observed course of the secular change in the S_1^0-field. Since the observation does not cover a period sufficient for getting a definite result from the comparison between the forecasting and the observation, we failed to obtain any conclusive result. But the assumption that the toroidal field is not so large in the core as is discussed in Section 7 seems to hold good here also, otherwise the forecast curves would have become quite different from the observed one.

2. Fundamental equations

Assuming that the magnetic permeability is unity, the fundamental equations are given as

$$\vec{I}=\sigma(\vec{E}+\vec{V}\wedge\vec{H}) , \tag{1}$$

$$\mathrm{curl}\,\vec{E}=-\partial\vec{H}/\partial t , \tag{2}$$

$$\mathrm{curl}\,\vec{H}=4\pi\vec{I} , \tag{3}$$

$$\rho d\vec{V}/dt=\vec{I}\wedge\vec{H}-\mathrm{grad}\,P+\vec{G} , \tag{4}$$

where $\vec{I}$, $\vec{E}$, $\vec{H}$, σ, ρ, $\vec{V}$, P and $\vec{G}$ denote respectively the electric current density, electric field, magnetic field, electrical conductivity, density, velocity, pressure and non-electromagnetic force. We will write as

$$\left.\begin{aligned} &\vec{I}=\vec{I}_0+\vec{i}, \quad \vec{E}=\vec{E}_0+\vec{e}, \quad \vec{H}=\vec{H}_0+\vec{h}, \\ &\vec{V}=\vec{V}_0+\vec{v}, \quad P=P_0+p, \end{aligned}\right\} \tag{5}$$

in which the quantities with suffix o are not dependent on time, while those denoted with small letters are regarded as first order small quantities. Introducing (5) into the fundamental equations and ignoring the second order quantities, we have

$$\text{(I)}\begin{cases} \vec{I}_0=\sigma(\vec{E}_0+\vec{V}_0\wedge\vec{H}_0) , \\ \mathrm{curl}\,\vec{E}_0=0 , \\ \mathrm{curl}\,\vec{H}_0=4\pi\vec{I}_0 , \\ \vec{I}_0\wedge\vec{H}_0-\mathrm{grad}\,P_0+\vec{G}=0 , \end{cases} \qquad \text{(II)}\begin{cases} \vec{i}=\sigma(\vec{e}+\vec{v}\wedge\vec{H}_0+\vec{V}_0\wedge\vec{h}) , & (6) \\ \mathrm{curl}\,\vec{e}=-\partial\vec{h}/\partial t , & (7) \\ \mathrm{curl}\,\vec{h}=4\pi\vec{i} , & (8) \\ \rho\partial\vec{v}/\partial t=\vec{i}\wedge\vec{H}_0+\vec{I}_0\wedge\vec{h}-\mathrm{grad}\,p . & (9) \end{cases}$$

It is assumed here that the liquid is incompressible. So the relation

$$\mathrm{div}\,\vec{v}=0 \tag{10}$$

is taken into account in obtaining the equation (6).

The first system of equations (I) is precisely the one from which the self-exciting dynamo in the earth's core might be deduced. It has been shown by Bullard, Takeuchi and others that the solution of (I) would be so complicated that one can hardly solve it completely. But it is likely that the main feature of a self-exciting dynamo will be given with certain magnetic fields and velocity fields which may be expressed by spherical harmonics of low degree. Therefore the writer assumes that the solution of (I) is given by the "A-approximation" as was called by Takeuchi and Shimazu. The solution contains the T_1^0 and S_2^{2c} types of velocity and magnetic fields of the S_1^0, T_2^0, T_2^{2c}, and T_2^{2s} types.

Now we are in a position to solve (II) in which $\vec{V}_0$, $\vec{H}_0$ and $\vec{I}_0$ are given as the solution of (I). By taking curl of (6) and eliminating $\vec{e}$ with the aid of (7), we have

$$\mathrm{curl}\,\vec{i}=\sigma\{-D\vec{h}+\mathrm{curl}(\vec{v}\wedge\vec{H}_0)+\mathrm{curl}(\vec{V}_0\wedge\vec{h})\} \tag{11}$$

where we write D in place of $\partial/\partial t$. On the other hand we have from (8)

$$4\pi\,\mathrm{curl}\,\vec{i}=\mathrm{curl}\,\mathrm{curl}\,\vec{h}=-\nabla^2\vec{h}\ . \tag{12}$$

From (11) and (12), we have

$$\{D-(4\pi\sigma)^{-1}\nabla^2\}\vec{h}=\mathrm{curl}\,(\vec{V}_0\wedge\vec{h})+\mathrm{curl}\,(\vec{v}\wedge\vec{H}_0)\ .. \tag{13}$$

We also have from (9)

$$\rho D\vec{v}=(4\pi)^{-1}\{(\mathrm{curl}\,\vec{h}\wedge\vec{H}_0)+(\mathrm{curl}\,\vec{H}_0\wedge\vec{h})\}-\mathrm{grad}\,p\ . \tag{14}$$

If we make div. of (14), we obtain

$$\nabla^2 p=-(4\pi)^{-1}\{\vec{H}_0\cdot\nabla^2\vec{h}+\vec{h}\cdot\nabla^2\vec{H}_0+2\,\mathrm{curl}\,\vec{h}\cdot\mathrm{curl}\,\vec{H}_0\}\ . \tag{15}$$

3. The solution for pressure

Generally, $\vec{h}$ can be expressed as

$$\vec{h}=\sum_{n,m}\vec{h}_{s,n}^m+\sum_{n,m}\vec{h}_{t,n}^m \tag{16}$$

where $\vec{h}_{s,n}^m$ is of the poloidal type, the r, θ and ϕ components being written as

$$\vec{h}^m_{s,n}=\begin{cases} -n(n+1)s^m_n(r)r^{n-1}Y^m_n \\ -\left[r\dfrac{ds^m_n}{dr}+(n+1)s^m_n\right]r^{n-1}\dfrac{\partial Y^m_n}{\partial\theta}\,, \\ -\left[r\dfrac{ds^m_n}{dr}+(n+1)s^m_n\right]r^{n-1}\dfrac{\partial Y^m_n}{\sin\theta\partial\phi}\,, \end{cases} \tag{17}$$

and $\vec{h}^m_{t,n}$ is of the toroidal type which is written as

$$\vec{h}^m_{t,n}=\begin{cases} 0 \\ -t^m_n(r)r^n\dfrac{\partial Y^m_n}{\sin\theta\partial\phi}\,, \\ t^m_n(r)r^n\dfrac{\partial Y^m_n}{\partial\theta}\,, \end{cases} \tag{18}$$

in which

$$Y^m_n=P^m_n(\cos\theta)\frac{\cos}{\sin}m\phi\,. \tag{19}$$

Introducing (16) into (15), we obtain a partial differential equation from which we can determine p as a suitable solution with some constants. Since p becomes known, $\vec{v}$ will be obtained from (14). The constants should be determined by the condition that the radial component of $\vec{v}$ vanishes at the surface of the core whose radius is denoted by a in later statement. Putting both $\vec{h}$ and $\vec{v}$ in (13), we shall have an equation by which we may determine s^m_n and t^m_n under the condition that the magnetic field is continuous at the surface of the core. Theoretically speaking, we can thus obtain the magnetic field and velocity. However, as has been shown by Elsasser, Bullard, and others, an interaction between certain electric currents and magnetic fields produces many types of motions and that between motions and magnetic fields produces many types of electric currents. Thus it is almost impossible to treat the problem quite generally. As has been done in the study of self-exciting dynamo, we shall take an approximation.

As the simplest, we shall assume that the magnetic field is of the S^0_1-type which is the most predominant one in the earth's magnetic field. The magnetic field of other types which will appear in the righthand-side of (13) will be ignored.

The magnetic field $\vec{h}$, curl $\vec{h}$ and $\nabla^2\vec{h}$ are given as

$$\vec{h}=\begin{cases} -2s(r)P_1\ , \\ -\left(r\dfrac{ds}{dr}+2s\right)\dfrac{dP_1}{d\theta}\ , \\ 0\ , \end{cases} \qquad \text{curl}\,\vec{h}=\begin{cases} 0\ , \\ 0\ , \\ -\left(r\dfrac{d^2s}{dr^2}+4\dfrac{ds}{dr}\right)\dfrac{dP_1}{d\theta}\ , \end{cases}$$

$$\nabla^2\vec{h}=\begin{cases} -2\left(\dfrac{d^2s}{dr^2}+\dfrac{4}{r}\dfrac{ds}{dr}\right)P_1\ , \\ -\left(r\dfrac{d^3s}{dr^3}+6\dfrac{d^2s}{dr^2}+\dfrac{4}{r}\dfrac{ds}{dr}\right)\dfrac{dP_1}{d\theta}\ , \\ 0\ , \end{cases} \tag{20}$$

while the stationary magnetic field and velocity are given as

$$\left.\begin{aligned} \vec{H}_0&=\vec{H}_1+\vec{H}_2+\vec{H}_3+\vec{H}_4\ , \\ \vec{V}_0&=\vec{V}_1+\vec{V}_2\ , \end{aligned}\right\} \tag{21}$$

where

S_1^0 magnetic field :

$$\vec{H}_1=\begin{cases} -2S_1(r)P_1\ , \\ -\left(r\dfrac{dS_1}{dr}+2S_1\right)\dfrac{dP_1}{d\theta}\ , \\ 0\ , \end{cases} \qquad \text{curl}\,\vec{H}_1=\begin{cases} 0\ , \\ 0\ , \\ -\left(r\dfrac{d^2S_1}{dr^2}+4\dfrac{dS_1}{dr}\right)\dfrac{dP_1}{d\theta}\ , \end{cases}$$

$$\nabla^2\vec{H}_1=\begin{cases} -2\left(\dfrac{d^2S_1}{dr^2}+\dfrac{4}{r}\dfrac{dS_1}{dr}\right)P_1\ , \\ -\left(r\dfrac{d^3S_1}{dr^3}+6\dfrac{d^2S_1}{dr^2}+\dfrac{4}{r}\dfrac{dS_1}{dr}\right)\dfrac{dP_1}{d\theta}\ , \\ 0\ , \end{cases} \tag{22}$$

T_2^0 magnetic field :

$$\vec{H}_2=\begin{cases} 0\ , \\ 0\ , \\ a^{-2}r^2T_2(r)\dfrac{dP_2}{d\theta}\ , \end{cases} \qquad \text{curl}\,\vec{H}_2=\begin{cases} -6a^{-2}rT_2P_2\ , \\ -a^{-2}\left(r\dfrac{dT_2}{dr}+3T_2\right)r\dfrac{dP_2}{d\theta}\ , \\ 0\ , \end{cases}$$

$$\nabla^2 \vec{H}_2 = \begin{cases} 0\,, \\ 0\,, \\ a^{-2}\left(\dfrac{d^2T_2}{dr^2}+\dfrac{6}{r}\dfrac{dT_2}{dr}\right)r^2\dfrac{dP_2}{d\theta}\,. \end{cases} \tag{23}$$

T_2^{2c} magnetic field :

$$\vec{H}_3 = \begin{cases} 0\,, \\ -a^{-2}r^2T_3(r)\dfrac{\partial(P_2^2\cos 2\phi)}{\sin\theta\partial\phi}\,, \\ a^{-2}r^2T_3(r)\dfrac{\partial(P_2^2\cos 2\phi)}{\partial\theta}\,, \end{cases}$$

$$\text{curl}\,\vec{H}_3 = \begin{cases} -6a^{-2}rT_3P_2^2\cos 2\phi\,, \\ -a^{-2}\left(r\dfrac{dT_3}{dr}+3T_3\right)r\dfrac{\partial(P_2^2\cos 2\phi)}{\partial\theta}\,, \\ -a^{-2}\left(r\dfrac{dT_3}{dr}+3T_3\right)r\dfrac{\partial(P_2^2\cos 2\phi)}{\sin\theta\partial\phi}\,, \end{cases}$$

$$\nabla^2 \vec{H}_3 = \begin{cases} 0\,, \\ -a^{-2}\left(\dfrac{d^2T_3}{dr^2}+\dfrac{6}{r}\dfrac{dT_3}{dr}\right)r^2\dfrac{\partial(P_2^2\cos 2\phi)}{\sin\theta\partial\phi}\,, \\ a^{-2}\left(\dfrac{d^2T_3}{dr^2}+\dfrac{6}{r}\dfrac{dT_3}{dr}\right)r^2\dfrac{\partial(P_2^2\cos 2\phi)}{\partial\theta}\,, \end{cases} \tag{24}$$

T_2^{2s} magnetic field :

$$\vec{H}_4 = \begin{cases} 0\,, \\ -a^{-2}r^2T_4(r)\dfrac{\partial(P_2^2\sin 2\phi)}{\sin\theta\partial\phi}\,, \\ a^{-2}r^2T_4(r)\dfrac{\partial(P_2^2\sin 2\phi)}{\partial\theta}\,, \end{cases}$$

$$\text{curl}\,\vec{H}_4 = \begin{cases} -6a^{-2}rT_4P_2^2\sin 2\phi\,, \\ -a^{-2}\left(r\dfrac{dT_4}{dr}+3T_4\right)r\dfrac{\partial(P_2^2\sin 2\phi)}{\partial\theta}\,, \\ -a^{-2}\left(r\dfrac{dT_4}{dr}+3T_4\right)r\dfrac{\partial(P_2^2\sin 2\phi)}{\sin\theta\partial\phi}\,, \end{cases}$$

$$\nabla^2\vec{H}_4=\begin{cases} 0\,, \\ -a^{-2}\left(\dfrac{d^2T_4}{dr^2}+\dfrac{6}{r}\dfrac{dT_4}{dr}\right)r^2\dfrac{\partial(P_2^2\sin 2\phi)}{\sin\theta\partial\phi}\,, \\ a^{-2}\left(\dfrac{d^2T_4}{dr^2}+\dfrac{6}{r}\dfrac{dT_4}{dr}\right)r^2\dfrac{\partial(P_2^2\sin 2\phi)}{\partial\theta}\,. \end{cases} \tag{25}$$

T_1^0 velocity :

$$\vec{V}_1=\begin{cases} 0\,, \\ 0\,, \\ a^{-1}r\,V_1(r)\dfrac{dP_1}{d\theta}\,. \end{cases} \tag{26a}$$

S_2^{2c} velocity :

$$\vec{V}_2=\begin{cases} -6a^{-1}r\,V_2P_2^2\cos 2\phi\,, \\ -a^{-1}\left(r\dfrac{dV_2}{dr}+3V_2\right)r\dfrac{\partial(P_2^2\cos 2\phi)}{\partial\theta}\,, \\ -a^{-1}\left(r\dfrac{dV_2}{dr}+3V_2\right)r\dfrac{\partial(P_2^2\cos 2\phi)}{\sin\theta\partial\phi}\,. \end{cases} \tag{26b}$$

From (20), (21), (22), (23), (24) and (25), we can calculate the righthand members of (15) as follows ;

$$\begin{aligned}\vec{H}_0\cdot\nabla^2\vec{h}=&\frac{2}{3}\left\{2S_1\left(\frac{d^2s}{dr^2}+\frac{4}{r}\frac{ds}{dr}\right)+\left(r\frac{dS_1}{dr}+2S_1\right)\left(r\frac{d^3s}{dr^3}+6\frac{d^2s}{dr^2}+\frac{4}{r}\frac{ds}{dr}\right)\right\}\\ &+\frac{2}{3}\left\{4S_1\left(\frac{d^2s}{dr^2}+\frac{4}{r}\frac{ds}{dr}\right)-\left(r\frac{dS_1}{dr}+2S_1\right)\left(r\frac{d^3s}{dr^3}+6\frac{d^2s}{dr^2}+\frac{4}{r}\frac{ds}{dr}\right)\right\}P_2\\ &+2a^{-2}T_3r^2\left(r\frac{d^3s}{dr^3}+6\frac{d^2s}{dr^2}+\frac{4}{r}\frac{ds}{dr}\right)P_2^2\sin 2\phi\\ &-2a^{-2}T_4r^2\left(r\frac{d^3s}{dr^3}+6\frac{d^2s}{dr^2}+\frac{4}{r}\frac{ds}{dr}\right)P_2^2\cos 2\phi\,,\end{aligned}$$

$$\begin{aligned}\vec{h}\cdot\nabla^2\vec{H}_0=&\frac{2}{3}\left\{2\left(\frac{d^2S_1}{dr^2}+\frac{4}{r}\frac{dS_1}{dr}\right)s+\left(r\frac{d^3S_1}{dr^3}+6\frac{d^2S_1}{dr^2}+\frac{4}{r}\frac{dS_1}{dr}\right)\left(r\frac{ds}{dr}+2s\right)\right\}\\ &+\frac{2}{3}\left\{4\left(\frac{d^2S_1}{dr^2}+\frac{4}{r}\frac{dS_1}{dr}\right)s-\left(r\frac{d^3S_1}{dr^3}+6\frac{d^2S_1}{dr^2}+\frac{4}{r}\frac{dS_1}{dr}\right)\left(r\frac{ds}{dr}+2s\right)\right\}P_2\\ &+2a^{-2}\left(r^2\frac{d^2T_3}{dr^2}+6r\frac{dT_3}{dr}\right)\left(r\frac{ds}{dr}+2s\right)P_2^2\sin 2\phi\\ &-2a^{-2}\left(r^2\frac{d^2T_4}{dr^2}+6r\frac{dT_4}{dr}\right)\left(r\frac{ds}{dr}+2s\right)P_2^2\cos 2\phi\end{aligned}$$

$$\operatorname{curl}\vec{h}\cdot\operatorname{curl}\vec{H}_0=\frac{2}{3}\left(r\frac{d^2S_1}{dr^2}+4\frac{dS_1}{dr}\right)\left(r\frac{d^2s}{dr^2}+4\frac{ds}{dr}\right)$$
$$-\frac{2}{3}\left(r\frac{d^2S_1}{dr^2}+4\frac{dS_1}{dr}\right)\left(r\frac{d^2s}{dr^2}+4\frac{ds}{dr}\right)P_2$$
$$+2a^{-2}\left(r^2\frac{dT_3}{dr}+3rT_3\right)\left(r\frac{d^2s}{dr^2}+4\frac{ds}{dr}\right)P_2^2\sin 2\phi$$
$$-2a^{-2}\left(r^2\frac{dT_4}{dr}+3rT_4\right)\left(r\frac{d^2s}{dr^2}+4\frac{ds}{dr}\right)P_2^2\cos 2\phi$$

For the sake of simplicity, we may assume that S_1, T_2, T_3 and T_4 are independent of r. We shall be able to obtain a rough idea of the magneto-hydrodynamic behaviour in the earth's core by this simplification. In that case (15) becomes

$$\nabla^2 p=f_0+f_2P_2+f_2^{2c}P_2^2\cos 2\phi+f_2^{2s}P_2^2\sin 2\phi \tag{27}$$

where

$$-4\pi f_0=\frac{4}{3}S_1\left(r\frac{d^3s}{dr^3}+7\frac{d^2s}{dr^2}+\frac{8}{r}\frac{ds}{dr}\right),$$
$$-4\pi f_2=-\frac{4}{3}S_1\left(r\frac{d^3s}{dr^3}+4\frac{d^2s}{dr^2}-\frac{4}{r}\frac{ds}{dr}\right),$$
$$-4\pi\begin{pmatrix}f_2^{2c}\\ f_2^{2s}\end{pmatrix}=\mp 2a^{-2}\begin{pmatrix}T_4\\ T_3\end{pmatrix}r^2\left(r\frac{d^3s}{dr^3}+12\frac{d^2s}{dr^2}+\frac{28}{r}\frac{ds}{dr}\right). \tag{28}$$

The solution of (27) may be expressed as

$$p=\sum_{n,m} q_n^m(r)Y_n^m\,. \tag{29}$$

Putting (29) in $\nabla^2 p$, we obtain

$$\nabla^2 p=\sum_{n,m}\left\{\frac{1}{r^2}\frac{\partial}{\partial r}\left(r^2\frac{\partial}{\partial r}\right)-\frac{n(n+1)}{r^2}\right\}q_n^m(r)Y_n^m\,. \tag{30}$$

Comparing (27) with (30), we obtain a series of ordinary differential equations such as

$$\left.\begin{aligned}&\frac{1}{r}\frac{d}{dr}\left(r^2\frac{d}{dr}\right)q_0^0=f_0\,,\\ &\left\{\frac{1}{r^2}\frac{d}{dr}\left(r^2\frac{d}{dr}\right)-\frac{6}{r^2}\right\}\begin{pmatrix}q_2^0\\ q_2^{2c}\\ q_2^{2s}\end{pmatrix}=\begin{pmatrix}f_2\\ f_2^{2c}\\ f_2^{2s}\end{pmatrix}.\end{aligned}\right\} \tag{31}$$

q_n^m for the other combinations of n, m are disregarded without loss of generality.

The solutions of (31) which remain finite at $r=0$ are given as

$$\left.\begin{aligned} q_0^0 &= K_0^0 + \int_0^r r f_0 dr - r^{-1}\int_0^r r^2 f_0 dr\,, \\ \begin{pmatrix} q_2^0 \\ q_2^{2c} \\ q_2^{2s} \end{pmatrix} &= a^{-2}r^2\begin{pmatrix} K_2^0 \\ K_2^{2c} \\ K_2^{2s} \end{pmatrix} + \frac{1}{5}\left\{r^2\int_0^r r^{-1}\begin{pmatrix} f_2 \\ f_2^{2c} \\ f_2^{2s} \end{pmatrix} dr - r^{-3}\int_0^r r^4\begin{pmatrix} f_2 \\ f_2^{2c} \\ f_2^{2s} \end{pmatrix} dr\right\}, \end{aligned}\right\} \quad (32)$$

where K_0^0, K_2^0, K_2^{2c} and K_2^{2s} are constants which shall be determined later. Putting (28) in (32), we have, after some calculations, the following expressions :

$$\left.\begin{aligned} 4\pi q_0^0 &= L_0^0 - \frac{4}{3}S_1\left(r\frac{ds}{dr} + 3s\right), \\ 4\pi q_2^0 &= a^{-2}r^2 L_2^0 + \frac{4}{3}S_1 r\frac{ds}{dr}\,, \\ 4\pi q_2^{2c} &= a^{-2}r^2 L_2^{2c} + 2a^{-2}T_4\left(r^3\frac{ds}{dr} + 4r^2 s - 2r^{-3}\int_0^r r^4 s dr\right), \\ 4\pi q_2^{2s} &= a^{-2}r^2 L_2^{2s} - 2a^{-2}T_3\left(r^3\frac{ds}{dr} + 4r^2 s - 2r^{-3}\int_0^r r^4 s dr\right), \end{aligned}\right\} \quad (33)$$

where

$$L_0^0 = 4\pi K_0^0\,,\quad L_2^0 = 4\pi K_2^0\,,\quad L_2^{2c} = 4\pi K_2^{2c}\,,\quad L_2^{2s} = 4\pi K_2^{2s}\,.$$

Thus the solution for the pressure is given by (29) together with (33).

4. The solution for velocity

The velocity can be calculated from (14). We have

$$\left.\begin{aligned} \operatorname{curl}\vec{h}\wedge\vec{H}_1 &= \begin{cases} -\frac{4}{3}S_1\left(r\frac{d^2s}{dr^2} + 4\frac{ds}{dr}\right) \\ 0 \\ 0 \end{cases} + \begin{cases} \frac{4}{3}S_1\left(r\frac{d^2s}{dr^2} + 4\frac{ds}{dr}\right)P_2 \\ \frac{2}{3}S_1\left(r\frac{d^2s}{dr^2} + 4\frac{ds}{dr}\right)\frac{dP_2}{d\theta} \\ 0 \end{cases}, \\ \operatorname{curl}\vec{h}\wedge\vec{H}_2 &= \begin{cases} 0 \\ 0 \\ 0 \end{cases}, \\ \operatorname{curl}\vec{h}\wedge\vec{H}_3 &= \begin{cases} -2a^{-2}T_3 r^2\left(r\frac{d^2s}{dr^2} + 4\frac{ds}{dr}\right)P_2^2\sin 2\phi \\ 0 \\ 0 \end{cases}, \end{aligned}\right|$$

$$
\left.\begin{aligned}
\operatorname{curl}\vec{h}\wedge\vec{H}_4 &= \begin{cases} 2a^{-2}T_4r^2\left(r\dfrac{d^2s}{dr^2}+4\dfrac{ds}{dr}\right)P_2^2\cos 2\phi \\ 0 \\ 0 \end{cases}, \\
\operatorname{curl}\vec{H}_1\wedge\vec{h} &= \begin{cases} 0 \\ 0 \\ 0 \end{cases}, \\
\operatorname{curl}\vec{H}_2\wedge\vec{h} &= \begin{cases} 0 \\ 0 \\ -\dfrac{6}{5}a^{-2}T_2r\left(r\dfrac{ds}{dr}+5s\right)\dfrac{dP_1}{d\theta} \end{cases} + \begin{cases} 0 \\ 0 \\ \dfrac{6}{5}a^{-2}T_2r^2\dfrac{ds}{dr}\dfrac{dP_3}{d\theta} \end{cases}, \\
\operatorname{curl}\vec{H}_3\wedge\vec{h} &= \begin{cases} -6a^{-2}T_3r\left(r\dfrac{ds}{dr}+2s\right)P_2^2\sin 2\phi \\ -6a^{-2}T_3rs\dfrac{\partial(P_2^2\sin 2\phi)}{\partial\theta} \\ -2a^{-2}T_3r\left(r\dfrac{ds}{dr}+3s\right)\dfrac{\partial(P_2^2\sin 2\phi)}{\sin\theta\partial\phi} \end{cases} \\
&\quad + \begin{cases} 0 \\ 0 \\ \dfrac{2}{5}a^{-2}T_3r^2\dfrac{ds}{dr}\dfrac{\partial(P_3^2\cos 2\phi)}{\partial\theta} \end{cases}, \\
\operatorname{curl}\vec{H}_4\wedge\vec{h} &= \begin{cases} 6a^{-2}T_4r\left(r\dfrac{ds}{dr}+2s\right)P_2^2\cos 2\phi \\ 6a^{-2}T_4rs\dfrac{\partial(P_2^2\cos 2\phi)}{\partial\theta} \\ 2a^{-2}T_4r\left(r\dfrac{ds}{dr}+3s\right)\dfrac{\partial(P_2^2\cos 2\phi)}{\sin\theta\partial\phi} \end{cases} \\
&\quad + \begin{cases} 0 \\ 0 \\ \dfrac{2}{5}a^{-2}T_4r^2\dfrac{ds}{dr}\dfrac{\partial(P_3^2\sin 2\phi)}{\partial\theta} \end{cases}.
\end{aligned}\right\}
\tag{34}
$$

With these expressions we can calculate $\vec{v}$ from (14) in which p is given by (19) and (33). Hence we have

$$4\pi\rho Dv_r = -2\left(a^{-2}rL_2^0 - 2S_1\frac{ds}{dr}\right)P_2$$
$$-2a^{-2}\left(rL_2^{2c} + 6T_4r^{-4}\int_0^r r^4 s dr\right)P_2^2\cos 2\phi$$
$$-2a^{-2}\left(rL_2^{2s} - 6T_3r^{-4}\int_0^r r^4 s dr\right)P_2^2\sin 2\phi\ ,$$

$$4\pi\rho Dv_\theta = \left\{-a^{-2}rL_2^0 + \frac{2}{3}S_1\left(r\frac{d^2s}{dr^2} + 2\frac{ds}{dr}\right)\right\}\frac{dP_2}{d\theta}$$
$$-a^{-2}\left\{rL_2^{2c} + 2T_4\left(rs - 2r^{-4}\int_0^r r^4 s dr\right)\right\}\frac{\partial(P_2^2\cos 2\phi)}{\partial\theta}$$
$$-a^{-2}\left\{rL_2^{2s} - 2T_3\left(rs - 2r^{-4}\int_0^r r^4 s dr\right)\right\}\frac{\partial(P_2^2\sin 2\phi)}{\partial\theta}$$
$$-\frac{2}{5}a^{-2}T_3r^2\frac{ds}{dr}\frac{\partial(P_3^2\cos 2\phi)}{\sin\theta\partial\phi}$$
$$-\frac{2}{5}a^{-2}T_4r^2\frac{ds}{dr}\frac{\partial(P_3^2\sin 2\phi)}{\sin\theta\partial\phi}\ ,$$

$$4\pi\rho Dv_\phi = -\frac{6}{5}a^{-2}T_2r\left(r\frac{ds}{dr} + 5s\right)\frac{dP_1}{d\theta}$$
$$+\frac{6}{5}a^{-2}T_2r^2\frac{ds}{dr}\frac{dP_3}{d\theta}$$
$$-a^{-2}\left\{rL_2^{2c} + 2T_4\left(rs - 2r^{-4}\int_0^r r^4 s dr\right)\right\}\frac{\partial(P_2^2\cos 2\phi)}{\sin\theta\partial\phi}$$
$$-a^{-2}\left\{rL_2^{2s} - 2T_3\left(rs - 2r^{-4}\int_0^r r^4 s dr\right)\right\}\frac{\partial(P_2^2\sin 2\phi)}{\sin\theta\partial\phi}$$
$$+\frac{2}{5}a^{-2}T_3r^2\frac{ds}{dr}\frac{\partial(P_3^2\cos 2\phi)}{\partial\theta}$$
$$+\frac{2}{5}a^{-2}T_4r^2\frac{ds}{dr}\frac{\partial(P_3^2\sin 2\phi)}{\partial\theta}\ .$$

But it is more convenient to express velocity with a sum of poloidal and toroidal velocity fields. We can write as follows;

$$\vec{v} = \vec{v}_1 + \vec{v}_2 + \vec{v}_3 + \vec{v}_4 + \vec{v}_5 + \vec{v}_6 + \vec{v}_7\ , \tag{35}$$

where

T_1^0-motion :

$$4\pi\rho D\vec{v}_1=\begin{cases}0\\0\\t_1 r\dfrac{dP_1}{d\theta}\ ,\end{cases}\qquad t_1=-\frac{6}{5}a^{-2}T_2\left(r\frac{ds}{dr}+5s\right),\tag{36}$$

T_3^0-motion :

$$4\pi\rho D\vec{v}_2=\begin{cases}0\\0\\t_3 r^3\dfrac{dP_3}{d\theta}\ ,\end{cases}\qquad t_3=\frac{6}{5}a^{-2}T_2 r^{-1}\frac{ds}{dr}\ ,\tag{37}$$

S_2^0-motion :

$$4\pi\rho D\vec{v}_3=\begin{cases}-6s_2 rP_2\\-\left(r\dfrac{ds_2}{dr}+3s_2\right)r\dfrac{dP_2}{d\theta}\ ,\\0\end{cases}\qquad s_2=\frac{1}{3}\left(a^{-2}L_2^0-2S_1r^{-1}\frac{ds}{dr}\right),\tag{38}$$

S_2^{2c}-motion :

$$4\pi\rho D\vec{v}_4=\begin{cases}-6s_2^{2c}rP_2^2\cos 2\phi\\-\left(r\dfrac{ds_2^{2c}}{dr}+3s_2^{2c}\right)r\dfrac{\partial(P_2^2\cos 2\phi)}{\partial\theta}\\-\left(r\dfrac{ds_2^{2c}}{dr}+3s_2^{2c}\right)r\dfrac{\partial(P_2^2\cos 2\phi)}{\sin\theta\partial\phi}\ ,\end{cases}\qquad s_2^{2c}=\frac{1}{3}a^{-2}L_2^{2c}+2T_4a^{-2}r^{-5}\int_0^r r^4 s dr\ ,\tag{39}$$

S_2^{2s}-motion :

$$4\pi\rho D\vec{v}_5=\begin{cases}-6s_2^{2s}rP_2^2\sin 2\phi\\-\left(r\dfrac{ds_2^{2s}}{dr}+3s_2^{2s}\right)r\dfrac{\partial(P_2^2\sin 2\phi)}{\partial\theta}\\-\left(r\dfrac{ds_2^{2s}}{dr}+3s_2^{2s}\right)r\dfrac{\partial(P_2^2\sin 2\phi)}{\sin\theta\partial\phi}\ ,\end{cases}\qquad s_2^{2s}=\frac{1}{3}a^{-2}L_2^{2s}-2T_3a^{-2}r^{-5}\int_0^r r^4 s dr\ ,\tag{40}$$

T_3^{2c}-motion :

$$4\pi\rho D\vec{v}_6=\begin{cases}0\\-t_3^{2c}r^3\dfrac{\partial(P_3^2\cos 2\phi)}{\sin\theta\partial\phi}\\t_3^{2c}r^3\dfrac{\partial(P_3^2\cos 2\phi)}{\partial\theta}\ ,\end{cases}\qquad t_3^{2c}=\frac{2}{5}a^{-2}T_3r^{-1}\frac{ds}{dr}\ ,\tag{41}$$

T_3^{2s}-motion :

$$4\pi\rho D\vec{v}_7 = \begin{cases} 0 \\ -t_3^{2s} r^3 \dfrac{\partial(P_3^2 \sin 2\phi)}{\sin\theta\partial\phi} \\ t_3^{2s} r^3 \dfrac{\partial(P_3^2 \sin 2\phi)}{\partial\theta} . \end{cases} \qquad t_3^{2s} = \frac{2}{5} a^{-2} T_4 r^{-1} \frac{ds}{dr} , \tag{42}$$

The constants are determined by the condition $v_r=0$ at $r=a$. They are given as

$$L_2^0 = 2aS_1\left(\frac{ds}{dr}\right)_{r=a} , \quad L_2^{2c} = -6T_4 a^{-5}\int_0^a r^4 s dr , \quad L_2^{2s} = 6T_3 a^{-5}\int_0^a r^4 s dr . \tag{43}$$

5. The integro-differential equation for magnetic field

We introduce, then, $\vec{v}$ thus obtained into (13) together with $\vec{V}_0$ of (26). Although we obtain many types of magnetic field from curl $(\vec{V}_0\wedge\vec{h})$ and curl $(\vec{v}\wedge\vec{H}_0)$, we only pick up the components of the S_1^0 type. This can be done with the aid of the selection rules for electromagnetic couplings. The components which contribute to the S_1^0 type magnetic field are found to be as

$$\left.\begin{aligned}
&4\pi\rho D(\vec{v}_3\wedge\vec{H}_1) \rightarrow \begin{cases} 0 \\ 0 \\ -\dfrac{6}{5}S_1 r\left(r\dfrac{ds_2}{dr}+5s_2\right)\dfrac{dP_1}{d\theta} , \end{cases} \\
&4\pi\rho D\,\mathrm{curl}\,(\vec{v}_3\wedge\vec{H}_1) \rightarrow \begin{cases} \dfrac{12}{5}S_1\left(r\dfrac{ds_2}{dr}+5s_2\right)P_1 \\ \dfrac{6}{5}S_1\left(r\dfrac{d}{dr}+2\right)\left(r\dfrac{ds_2}{dr}+5s_2\right)\dfrac{dP_1}{d\theta} \\ 0 \end{cases} \\
&4\pi\rho D(\vec{v}_4\wedge\vec{H}_4) \rightarrow \begin{cases} 0 \\ 0 \\ -\dfrac{216}{5}T_4 a^{-2} s_2^{2c} r^3 \dfrac{dP_1}{d\theta} , \end{cases} \\
&4\pi\rho D\,\mathrm{curl}\,(\vec{v}_4\wedge\vec{H}_4) \rightarrow \begin{cases} \dfrac{432}{5}T_4 a^{-2} r^2 s_2^{2c} P_1 \\ \dfrac{216}{5}T_4 a^{-2}\left(r\dfrac{d}{dr}+2\right)(r^2 s_2^{2c})\dfrac{dP_1}{d\theta} \\ 0 \end{cases} ,
\end{aligned}\right\} \tag{44}$$

$$4\pi\rho D(\vec{v}_5 \wedge \vec{H}_3) \rightarrow \begin{cases} 0 \\ 0 \\ \dfrac{216}{5} T_3 a^{-2} s_2^{2s} r^3 \dfrac{dP_1}{d\theta} , \end{cases}$$

$$4\pi\rho D \operatorname{curl} (\vec{v}_5 \wedge \vec{H}_3) \rightarrow \begin{cases} -\dfrac{432}{5} T_3 a^{-2} r^2 s_2^{2s} P_1 \\ -\dfrac{216}{5} T_3 a^{-2} \left(r \dfrac{d}{dr} + 2 \right) (r^2 s_2^{2s}) \dfrac{dP_1}{d\theta} \\ 0 \end{cases} .$$

Hence (13) is satisfied if we have the following relation:

$$4\pi\rho D \left\{ Ds - (4\pi\sigma)^{-1} \left(\frac{d^2 s}{dr^2} + \frac{4}{r} \frac{ds}{dr} \right) \right\}$$
$$= -\frac{6}{5} S_1 \left(r \frac{ds_2}{dr} + 5 s_2 \right) + \frac{216}{5} a^{-2} r^2 (T_3 s_2^{2s} - T_4 s_2^{2c}) . \tag{45}$$

6. An approximate solution for the magnetic field

(45) is an integro-differential equation for s. It will be of great difficulty to obtain rigorous solutions for it. However, we may be able to find a solution for a simple radial distribution in the following way.

Let us assume that

$$s = \sum_{n=0}^{\infty} a_n (r/a)^n \tag{46}$$

in which we do not take into account the negative powers of r because the magnetic field should remain finite at the centre of the earth. Introducing (46) into (45), we have the following relation

$$4\pi\rho D^2 \sum_n a_n (r/a)^n - \rho D \sigma^{-1} a^{-2} \sum_n a_n n(n+3)(r/a)^{n-2}$$
$$= -\frac{4}{5} S_1^2 a^{-2} \sum_n a_n \{5 - (n+3)(r/a)^{n-2}\}$$
$$+ \frac{432}{5} \{(T_3)^2 + (T_4)^2\} a^{-2} \sum_n \frac{a_n}{n+5} (r/a)^2 \{1 - (r/a)^n\} . \tag{47}$$

Equating the corresponding terms of both the sides of (47), we can obtain the relations between the coefficients a_0, a_1, $a_2 \cdots$. If we ignore the terms for $n > 4$, the relations become

$$4\left(\rho D\sigma^{-1}+\frac{4}{5}S_1^2\right)a_1=0\ , \tag{48}$$

$$4\pi\rho D^2 a_0-10\rho D\sigma^{-1}a^{-2}a_2+16S_1^2a^{-2}a_4=0\ , \tag{49}$$

$$4\pi\rho D^2 a_1-18a^{-2}\left(\rho D\sigma^{-1}+\frac{4}{5}S_1^2\right)a_3=0\ , \tag{50}$$

$$\left\{4\pi\rho D^2-\frac{432}{35}\overline{(T_3)^2+(T_4)^2}a^{-2}\right\}a_2-a^{-2}\left\{28\rho D\sigma^{-1}+\frac{48}{5}\overline{(T_3)^2+(T_4)^2}+\frac{112}{5}S_1^2\right\}a_4=0\ . \tag{51}$$

It can be seen from (48) and (50) that $a_1=a_3=0$.

Further, the solution must satisfy the boundary condition that the magnetic field is continuous at $r=a$. The magnetic field outside the core is given as

$$\vec{h}=\begin{cases} 2a^2r^{-3}h_1P_1 \\ -a^2r^{-3}h_1\dfrac{dP_1}{d\theta} \\ 0 \end{cases} \tag{52}$$

which tends to zero at infinity. The continuity at $r=a$ gives

$$-s_{r=a}=a^{-1}h_1\ , \quad \left(r\frac{ds}{dr}+2s\right)_{r=a}=a^{-1}h_1\ ,$$

from which we have

$$\left(r\frac{ds}{dr}+3s\right)_{r=a}=0\ . \tag{53}$$

This in turn may be written as

$$3a_0+5a_2+7a_4=0\ . \tag{54}$$

In order to have a non-vanishing solution for a_0, a_2 and a_4 which satisfies the equations (49), (51) and (54), we have

$$\begin{vmatrix} 3 & 5 & 7 \\ 4\pi\rho D^2 & -10\rho D\sigma^{-1}a^{-2} & 16S_1^2a^{-2} \\ 0 & 4\pi\rho D^2-\frac{432}{35}\overline{(T_3)^2+(T_4)^2}a^{-2} & -a^{-2}\left\{28\rho D\sigma^{-1}+\frac{112}{5}S_1^2+\frac{48}{5}\overline{(T_3)^2+(T_4)^2}\right\} \end{vmatrix}=0. \tag{55}$$

If we assume that the substance in the core is perfectly conductive, (55) can be simplified as

$$D^4+4(\pi\rho)^{-1}a^{-2}\left(\frac{4}{7}S_1^2-T^2\right)D^2+\frac{1296}{245}(\pi\rho)^{-2}a^{-4}S_1^2T^2=0 \tag{56}$$

where

$$T^2=(T_3)^2+(T_4)^2 \ .$$

The assumption may be safely taken because the coefficients for D^3 and D are very small provided we adopt $\sigma \simeq 10^{-6}$ *emu* which has been accepted from various reasons.

For the magnetic field to be oscillatory, D^2 must be negative. This condition is satisfied if we have

$$\left(\frac{4}{7}S_1^2-T^2\right)^2>\frac{324}{245}S_1^2T^2 \ . \tag{57}$$

On the contrary, we have exponentially increasing solutions provided $\left(\frac{4}{7}S_1^2-T^2\right)^2\leq\frac{324}{245}S_1^2T^2$. In this case, the small oscillations of the dynamo is regarded to be unstable because a slight deviation from the stationary state will increase exponentially.

Under the condition (57), we can expect simple harmonic oscillations whose periods are given as

$$2^{\frac{1}{2}}\pi^{\frac{3}{2}}\rho^{\frac{1}{2}}a\left\{\left(\frac{4}{7}S_1^2-T^2\right)\pm\sqrt{\left(\frac{4}{7}S_1^2-T^2\right)^2-\frac{324}{245}S_1^2T^2}\right\}^{-\frac{1}{2}} \ . \tag{58}$$

7. Discussions

Thus far we see that the A-approximation of the self-exciting dynamo seems to be stable under the condition (57), otherwise its small oscillations will be unstable. In order to maintain the earth's magnetic field over long periods, the dynamo mechanism should be highly stable. Although the condition (57) is derived from a crude calculation, we may assume that such a condition approximately holds in the earth's core. It should be noticed that (57) implies smaller T_2^{2c} and T_2^{2s} magnetic field than S_1^0 field. This result does not seem to agree with Bullard's view in which he considered that the T_2^0 field is quite large and T_2^{2c} and T_2^{2s} field would be of intermediate intensity. As for the dynamo itself, however, we may take a considerable variety of velocity distribution and magnetic field distribution. It would perhaps be possible to construct a dynamo under (57). To get (57), however, we made assumptions that the stationary magnetic fields are distributed in a simple way throughout the core and the effect of the magnetic field and velocity which are expressed with higher harmonics can be ignored. The influence of the earth's rotation is also negleted in the fundamental

equation. So we do not say that the condition (57) is definitely right. It is a rough approximation for the stability condition.

It is likely, however, that S_1^0 magnetic field amounts to a few *gauss* at the surface of the core as calculated from the value at the earth's surface. Then S_1 becomes of the order of a few *gauss*. So the values in the bracket of (58) would be of the same order or a little smaller. Adopting $\rho=10\ gm/cm^3$ and $a=3.5\times10^8\ cm$, the periods amount to scores or hundreds of *years*. Therefore we can have magnetic oscillations with period of scores or hundreds of *years* which are superposed on the stationary fields of the dynamo. The secular variation in the earth's magnetic field might be interpreted in this way. The damping of these oscillations are not considered here. But it is likely that the relaxation time would be of the order of 10^4–10^5 *years* provided the conductivity is of the order of 10^{-6} *emu*.

In the above calculations we did not take into account higher powers of r^n than $n=4$. If we take them into account, we shall have many other solutions of more complicated radial distribution and of different periods. Since the distribution considered here is an approximation for the so-called ground tone of oscillation mode, the other oscillations may be considered to have shorter periods than that studied here. For shorter period oscillations the shielding due to the conducting mantle will become considerable.

The present study has nothing to do with the explanation of the reversal of the geomagnetic field which is supposed to occur during the geological time as suggested from the studies on some rocks' remanent magnetization. However, the stability condition might be broken provided something happens. For instance, the velocity distribution would change if we had changes in the rotation velocity of the earth—not necessarily the reversal of its rotation. In that case, we might have strong toroidal field which violates the stability condition. Once the stability breaks out, the field would change fairly rapidly until the system reaches another stable state. As the opposite-sign dynamo seems to be also capable of existence, we might get a reversal of the magnetic field. But we must pay attention to the fact that something must happen in this speculation. As long as the dynamo is considered stable, it is difficult to consider the earth's magnetic field to be oscillating with a period of 10^5 *years* or so. We can only expect stable oscillations whose amplitude is smaller than the stationary field, the periods of these oscillations being presumably of the order of several hundred *years*.

8. Secular change in the S_1^0 field

As far as we assume the A-approximation of the self-exciting dynamo, the equation (45) is the one which governs changes in the S_1^0 magnetic field. As for the observational side of geomagnetism, we have a number of spherical harmonic analyses of the earth's magnetic field, the change in the S_1^0 field being traced through these analyses. The coefficients for the dipole field are reproduced in the following table.

Table I. The change in the S_1^0 field

Source	Epoch	g_1^0	g_1^1	h_1^1	$\sqrt{(g_1^0)^2+(g_1^1)^2+(h_1^1)^2}$
Erman-Petersen	1829	0.3201	0.0284	−0.0601	0.3269
Gauss	1835	3235	311	625	3310
Adams	1845	3219	278	578	3282
Adams	1880	3168	243	603	3234
Fritsche	1885	3164	241	591	3228
Schmidt	1885	3168	222	595	3231
Dyson-Furner	1922	3095	226	592	3159
Bartels	1922	3090	227	586	3153
Jones-Melotte	1942	3039	218	555	3097
Afanasieva	1945	3032	229	590	3097
Vestine-Lange	1945	3057	211	581	3119

(Unit : *c.g.s.e.m.u.*)

The moment of the magnetic dipole may be used in expressing the intensity of the S_1^0 field. The moment is proportional to the root square sum of the coefficients of the first degree constituents, say $\sqrt{(g_1^0)^2+(g_1^1)^2+(h_1^1)^2}$, which is also given in Table I.

If we take the time origin at a certain epoch, say 1900, we can get the initial conditions for the change in the S_1^0 field. Starting from the initial conditions, we can obtain the change in the S_1^0 field by solving the equation (45). Although the stationary field S_1, T_3 and T_4 are not known, we may be able to choose the most probable values for these fields by comparing the calculated change with the observed one. This is what the writer would here like to do.

Here we again take the approximation

$$s=a_0+a_2(r/a)^2+a_4(r/a)^4$$

as was studied in the last section. We see that the time-change of the coefficients is given by an operational equation such as

$$\Phi(D)a_n=0 \qquad n=0,\ 2,\ 4$$

where $\Phi(D)$ denotes the operator expressed by the determinant in (55). So far as we consider the change to be within a period of some hundred *years*, we may safely assume that the electrical conductivity is infinite. In that case the intensity of the S_1^0 field at $r=a$ changes according to the following operational equation

$$\left\{D^4+4(\pi\rho)^{-1}a^{-2}\left(\frac{4}{7}S_1^2-T^2\right)D^2+\frac{1296}{245}(\pi\rho)^{-2}a^{-4}S_1^2T^2\right\}s=0$$

as was shown in the last section.

In order to solve this equation, we shall take the following initial condition

at $t=0$

$$s=s_0\,,\qquad \frac{ds}{dt}=-6.35\times10^{-12}emu\ sec^{-1} \tag{59a}$$

which is obtained from the change in the magnetic moment of the main dipole at 1900, s denoting here $\sqrt{(g_1^0)^2+(g_1^1)^2+(h_1^1)^2}$ which is proportional to the intensity of the S_1^0 field, while $\frac{d^2s}{dt^2}$ and $\frac{d^3s}{dt^3}$ are to be ignored because the moment was changing almost linearly at this epoch.

Hence we have

at $t=0$

$$\frac{d^2s}{dt^2}=\frac{d^3s}{dt^3}=0\,. \tag{59b}$$

The solution which satisfies these initial conditions is given by interpreting the following operational equation

$$\left\{D^4+4(\pi\rho)^{-1}a^{-2}\left(\frac{4}{7}S_1^2-T^2\right)D^2+\frac{1296}{245}(\pi\rho)^{-2}a^{-4}S_1^2T^2\right\}s$$

$$=D^4S_0+D^3s_0'+4(\pi\rho)^{-1}a^{-2}\left(\frac{4}{7}S_1^2-T^2\right)(D^2s_0+Ds_0')\,, \tag{60}$$

where s_0' stands for $\frac{ds}{dt}$ at $t=0$.

If we write

$$\left.\begin{matrix}\omega_1^2\\ \omega_2^2\end{matrix}\right\}=2(\pi\rho)^{-1}a^{-2}\left\{-\left(\frac{4}{7}S_1^2-T^2\right)\pm\sqrt{\left(\frac{4}{7}S_1^2-T^2\right)^2-\frac{324}{245}S_1^2T^2}\right\}\,,$$

(60) becomes

$$s=\frac{1}{\omega_1^2-\omega_2^2}\left\{(K+\omega_1^2)\frac{s_0D^2-s_0'D}{D^2-\omega_1^2}-(K+\omega_2^2)\frac{s_0D^2-s_0'D}{D^2-\omega_2^2}\right\} \tag{61}$$

where

$$K=4(\pi\rho)^{-1}a^{-2}\left(\frac{4}{7}S_1^2-T^2\right)$$

On interpreting (61) we have

$$s=\frac{1}{\omega_1^2-\omega_2^2}\left\{(K+\omega_1^2)\left(s_0\cosh\omega_1 t+\frac{s_0'}{\omega_1}\sinh\omega_1 t\right)\right.$$

$$\left.-(K+\omega_2^2)\left(s_0\cosh\omega_2 t+\frac{s_0'}{\omega_2}\sinh\omega_2 t\right)\right\} \quad \text{for} \quad \omega_1\neq\omega_2\ ,$$

$$s=s_0\cosh\omega t+\frac{s_0'}{\omega}\sinh\omega t+\frac{K+\omega^2}{2\omega^2}(s_0\omega\sinh\omega t+s_0'\cosh\omega t)t$$

$$\text{for} \quad \omega_1=\omega_2=\omega\ .$$

As already mentioned in the previous section, the solutions become infinite with $t\rightarrow\infty$ unless ω_1 and ω_2 are purely imaginary.

We see that the solutions contain an unknown constant s_0 which cannot be determined from the observed change in the S_1^0 field. However we may consider that s_0 is nearly naught provided we take the time origin at 1900. At this epoch the change is approximately symmetrical with respect to $t=0$, this condition being statisfied by taking $s_0=0$ in the above solutions which are composed of symmetrical and anti-symmetrical components. If this may be taken for granted, the change in the magnetic moment can be calculated for various combinations of S_1 and T. S_1 would be nearly 4 *gauss* as is estimated from the value at the earth's surface. Taking various values for T, we obtain

i) $T=0$ *gauss* $\quad s=-0.000635\times10^{-8}t$

ii) $T=0.5$ $\quad s=-0.0159\sin\frac{2\pi}{\Pi_1}t+0.000038\sin\frac{2\pi}{\Pi_2}t$

$(\Pi_1=492\ \textit{years},\ \Pi_2=66.5\ \textit{years})$,

iii) $T=1.0$ $\quad s=-0.00815\sin\frac{2\pi}{\Pi_1}t+0.000235\sin\frac{2\pi}{\Pi_2}t$

$(\Pi_1=233\ \textit{years},\ \Pi_2=71.8\ \textit{years})$,

iv) $T=1.5$ $\quad s=-0.00336\sin\frac{2\pi}{\Pi}t+0.000321\,t\cos\frac{2\pi}{\Pi}t$

$(\Pi=105\ \textit{years})$.

The cases for $T>1.5$ *gauss* are not taken into account because the

oscillation is not stable as well as for $T=1.5$ *gauss*.

Fig. 2 shows the changes in the S_1^0 field as calculated for the respective values of T. Any T less than 1 *gauss* seems to be acceptable judging from the values obtained from the spherical harmonic analyses which are also shown in the figure. If we can trace the change in the future, a more conclusive result will be obtainable. As was suggested by Bullard,[10] if the moment attained its minimum at about 1935 and has been recovering since then, we should be able to gain some clue for determining the magnitude of the stationary magnetic field in the earth's core sooner or later.

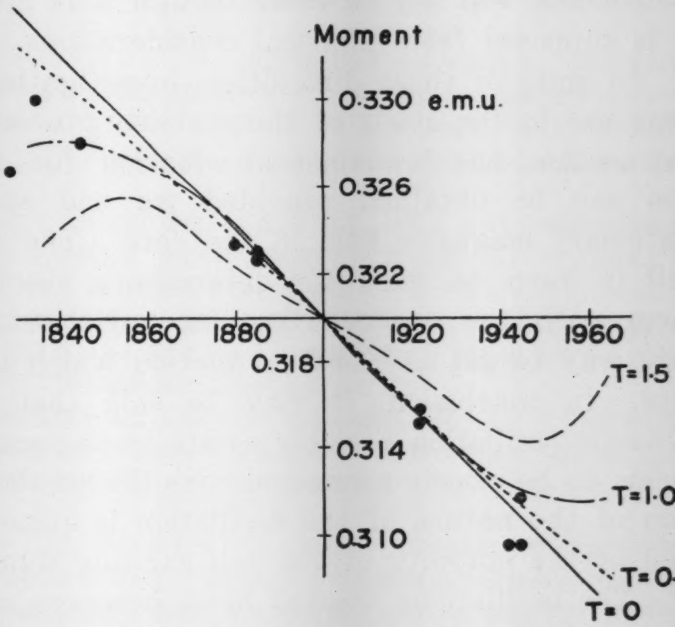

Fig. 2. Calculated and observed changes in the S_1^0 magnetic field.

9. Conclusion

The possible magneto-hydrodynamic oscillations in the earth's core are examined with their applications to the stability problem of the self-exciting dynamo and the prediction of the secular variation. In order to avoid mathematical difficulties, the writer was obliged to make some simplifications. Firstly, the earth's rotation is not taken into account. As is suggested by Bullard, the influence of Corioli's force might be appreciable. So the stability condition in this paper is not so reliable. Some further studies should be made upon this point as soon as possible. Secondly, the mutual coupling of various harmonic oscillations is ignored. In order to see to what extent one spherical harmonic component will be influenced by other components, a study on magneto-hydrodynamic oscillations of a spherical liquid body is now going on without ignoring high degree components. Although no definite result has been obtained yet, the oscillation is interpreted as

10) E. C. BULLARD, *Journ. Geophys. Res.*, **58** (1952), 277.

a coupled-oscillation of every harmonic constituent. Until we finish this sort of study the exact extent of the influence of higher degree components will not be clear though it is presumed to be not so great as is supposed from physical considerations.

In spite of those difficulties, investigations in this line would be of some use in the study of the stability problem. As is also shown in the last section, the fundamental equation for geomagnetic secular variation can be obtained provided we had sufficient knowledge on the stationary magnetic field in the core. The solutions of this equation will in turn be used for determining the internal field by comparing them with the observed secular variations. This would also be the only way to get at the fluid motion which is supposed to exist in the core. In conclusion, it may be said that a sort of magneto-hydrodynamic oscillation possibly exists in the earth's core. The oscillation seems to be closely connected with the secular variations. The examination of the nature of the oscillation is quite important for the discussion of the stability of the self-exciting dynamo.

The oscillations treated here, however, are of small amplitude. If we consider a disturbance of finite amplitude, there might be stable oscillations even though they violate the stability condition discussed here. We understand that the system of the fundamental equations, as given by (II), is not held for disturbances of finite amplitude. In that case we have to solve a system of non-linear differential equations as is done in Bullard's study on a homopolar dynamo. It should be added here that Bullard is going to mention in his unpublished study that there would be cases in which the oscillations will not depart indefinitely from their steady state even if the small oscillations are unstable.

The writer had the pleasure to talk with Sir Edward Bullard about the magneto-hydrodynamic problems while the writer was in England. The writer is very grateful to him for his helpful suggestions. The writer was encouraged by Professor A. T. Price to whom the writer's hearty thanks are also due. Professor T. Nagata and Dr. H. Takeuchi were also interested in the present study. The writer wishes to thank them for their discussions.

1. 地球核内の電磁流体振動

地震研究所 力 武 常 次

Elsasser, Bullard, 竹内等によつて研究されたように，地球核内のダイナモ作用は，現在考え得られる地磁気原因としてもつとも有力である．地球主磁場がダイナモ作用によつて維持されているという事実は，数学的表現を用いる時には，核内に於て電磁場および流体の基礎方程式が定常な解を有するということに対応する．この定常解の存在は高次の流体運動および電磁場を省略する限り確立された．

本論文に於ては定常解の存在を認めた上でそれに重なつて起り得ると考えられる電磁流体振動 (Magneto-hydrodynamic oscillation) を考察し，その地球物理学的意味を論じる．今定常解よりの小偏差を考える時は，基礎方程式を分離して，定常なものと小偏差に対応するものとの二組にすることが出来る．高次項を省略すれば小偏差に対する方程式は線形に保たれる．この方程式は適当な手続きをほどこすことにより，例えば磁場のみに関するものに帰着さすことが出来るのであるが，球函数表示をもちいる時には，あらゆる次数の振動様式の連成振動となる．

これはある型の磁場内のある型の流体運動を考える時，多くの型の電流を発生し，その電流と磁場との相互作用はさらに多くの型の流体運動をひきおこすからである．これを厳密に取扱うことは困難であるが，ここでは特に双極子磁場のみに注目して，他の型の磁場をもたらすような相互作用はすべて省略してある．

定常解として竹内―島津によつて A 近似と称されたもつとも簡単なものを採用して議論を進めた結果，小偏差を支配する積分微分方程式を求めることが出来た．定常磁場の半径方向の分布を適当に与えて，この方程式の基本振動的解を近似的に求めたところ，定常 toroidal 磁場 T_2^{2c}, T_2^{2s} があまり大きくない時には，振動性解を得た．さもない時には時間とともに極めて大きくなる解が得られ，この場合ダイナモは安定であるといえない．この toroidal 磁場の臨界値は 1.5 ガウスぐらいであり，Bullard の予想するような大きな toroidal 磁場は期待出来ないことになるが，Bullard が指摘したようにこの計算には地球廻転の影響が考慮されておらず，各種振動の相互依存性も無視されているから決定的結果であるとはいえない．しかし適当な条件のもとで核内に或種の電磁流体振動が起り得ることがあきらかになつたわけである．

また上に得た積分微分方程式に基ずいて，初期条件を与える時には，地磁気変化の予想をすることが出来る．従来の球函数分析結果をもととして 1900 年を $t=0$ とし，定常磁場をパラメーターとして，地磁気変化を計算してみたが，観測期間が短いために決定的なことはいえないけれども，上に求めた toroidal 磁場の臨界値以下なればもつともらしい様子を示すことが見られる．このような方法によつて観測の集積を待つて，内部定常磁場の大きさを推定することが可能のように思われる．ここに取扱つたことは，従来ダイナモ理論によつて地磁気永年変化が説明されるとしていた議論を定量化したものであり，今後さらに議論を精密に行うことにより核内の流体運動を永年変化からやや具体的に推察する手がかりとすることも可能であろう．

2. *On the Changes in the Heights of Mean Sea-levels, before and after the Great Earthquakes.*

By Seiti YAMAGUTI,

Earthquake Research Institute.

(Read Dec. 22, 1953.—Received Dec. 28, 1954.)

Introduction

Investigations on the changes in the heights of the mean sea-levels have been made, and the results have already been reported in my recent papers[1]. As to the sea-water temperature, which is one of the factors governing the change in the height of mean sea-level, the value at the depth of one meter from the surface was taken, assuming that those at such depths as 100 meters and 200 meters, etc. will show annual changes similar to that near the surface. If a great mass of abnormally cold water will appear in the ocean near the mareographic station, the residual correction due to the sea-water temperature, $\Delta T'$, in the equation, $\Delta L'' = \Delta L' - p\Delta b' - q\Delta T'$ will not be sufficient. Thus, in the present study, to eliminate the abnormal effects of ocean currents, the Kurosiwo (Black Current) as well as the Oyasiwo (Kurile Current) upon sea-level, the differentials between the values of mean sea-levels, corrected, $\Delta L''$, at Aburatubo and Hososima, and at Aburatubo and Osyoro were taken, and investigated respectively. The difference of the values of $\Delta L''$, between Aburatubo and Wazima was taken also during the past 10 years. The result was in close parallel to that between Aburatubo and Osyoro, so it was left for further study.

Method of Investigation, and Results

After taking the monthly mean sea-levels, corrected, $\Delta L''$, for Aburatubo, Hososima and Osyoro during the period of about 55 years, namely, from Jan. 1900 to Oct. 1954, the values of differences between Aburatubo and Hososima and between Aburatbo and Osyoro were calculated in order to eliminate the effects, if any, of abnormal ocean

1) S. YAMAGUCHI, *Bull. Earthq. Res. Inst.*, **21** (1943), and *Bull. Geog. Surv. Inst.*, **1** (1948), **2** (1950).

currents, the Kurosiwo and the Oyasiwo and diagrams were plotted with these values of differences and also with that of $\Delta L''$ at Aburatubo, as ordinates against the months taken as abscissa, and three curves were obtained. These two curves for differences are nearly parallel to that of $\Delta L''$ at Aburatubo as shown in Fig. 1, which fact may be considered as showing evidently the vertical movement of the earth's crust relative to the mean sea-level at Aburatubo. The value of difference of $\Delta L''$ between Aburatubo and Wazima during the past 10 years, is also taken and plotted similarly as before. The curve, resembling that of the difference of $\Delta L''$ between Aburatubo and Osyoro, is omitted here.

On the other hand, the mean errors of the mean sea-levels $\Delta L''$ (corrected) as well as ΔL (observed), were calculated as follows:

Successive differences, $\delta\Delta L'' = (\Delta L'')_{n+1} - (\Delta L'')_n$, where n is the number of years or months, for yearly and monthly mean sea-levels (corrected) were taken respectively, and the mean values of $\delta\Delta L''$ were calculated and denoted by m. Next, the absolute values of $|\delta - m|$ were calculated, instead of taking $(\delta - m)^2$, and the mean errors, $\varepsilon = 0.8453 \dfrac{\Sigma|\delta - m|}{n\sqrt{n}}$, were calculated. For yearly mean sea-levels, the data of the abnormally great changes at Aburatubo, in the years before and after the great Nankaido Earthquake and those at Wazima after the great Tango Earthquake were omitted here. For the values of $\Delta L''$ (corrected) and of ΔL (observed) which are the deviations from the secular mean values for 40 years, the mean errors were calculated similarly as before, $\Delta L''$ and ΔL being considered as errors.

The results are tabulated as shown in Table I.

Table I, a. The mean errors for the values of yearly mean sea-levels, during the period from 1900 to 1950

Stations	Yearly Mean Sea-levels in millimetre				Number of Years, n
	Corrected		Observed		
	$\delta\Delta L''$	$\Delta L''$	$\delta\Delta L$	ΔL	
Aburatubo	16.5±1.3	14.1±0.92	21.6±1.9	38.0±2.3	47
Hososima	23.6±1.8	20.5±1.4	26.6±2.1	27.3±2.5	51
Wazima	19.2±1.4	15.2±1.2	19.6±1.6	23.3±1.6	47
Osyoro	18.1±1.8	18.0±1.2	20.2±1.4	24.3±1.8	45
Mean of above 4 Stations	19.4±1.6	17.0±1.2	22.0±1.8	28.2±2.1	47.5

Table I, b. The mean errors for the values of monthly mean sea-levels, during the period of 10 years (1931~1940)

Stations	Monthly Mean Sea-levels in millimetre				Number of Months
	Corrected		Observed		
	$\delta\Delta L''$	$\Delta L''$	$\delta\Delta L$	ΔL	
Aburatubo	34.5±1.7	28.3±1.5	44.4±2.0	57.3±2.2	120
Hososima	43.8±2.0	31.3±1.6	64.3±2.6	90.0±3.4	120
Wazima	30.9±1.4	26.2±1.2	57.6±2.6	89.0±3.3	120
Osyoro	25.6±1.3	20.6±0.9	49.7±2.1	64.0±2.9	120
Mean of 4 Stations	33.7±1.6	26.6±1.3	54.0±2.3	75.1±3.0	120

From these tables, we may be able to say that, if the changes in the heights of mean sea-levels (corrected) amount to values greater than ±60 mm, which is double the value of the probable error in the case of the monthly mean, and ±36 mm, which is double the value of the probable error in the case of the yearly mean, those values obviously may be considered to show the vertical displacement of the earth's crust relative to the mean sea-level. Comparing these changes of mean sea-levels with the results of observations by tiltometer or of the levelling survey, we find that the former values are always larger than the latter, which fact suggests the subsidence of the earth's crust under the load of sea water at high tide, and consequently, the changes in the heights of mean sea-levels measured from the standard line fixed to the earth's crust, might apparently be exaggerated.

On the curve of the monthly mean sea-levels (corrected) $\Delta L''$ for Aburatubo, we have plotted the months of great earthquakes, which have occured in the same epoch, whose magnitudes, M in Gutenberg's or Pasadena scale, were calculated mostly by Prof. H. Kawasumi, and partly by Prof. Ch. Tsuboi, of the Earthquake Research Institute of Tokyo University, and printed by the Earthquake Section of the Central Meteorological Observatory[2]. The earthquakes with magnitude M, equal to or greater than 7, whose epicentral distance from the mareographic station at Aburatubo, d, being less than 150 kilometers, were taken. Those with magnitude M, greater than 7.3, and epicentral distance, d, greater than 150 kilometers, and less than 500 kilometers were also

2) H. KAWASUMI and C. TSUBOI, *The Magnitude Catalogue of Major Earthquakes which occurred in the Vicinity of Japan* (1885~1950).

taken separately with respect to the regions of Southwestern and Northeastern parts of Japan.

The values of $\Delta L''$ for the months of equal phase measured from the month of earthquake, were averaged for different earthquakes and plotted as ordinate against the months as shown in Fig. 2. a, b, c, d. A rather conspicuous minimum of the curve, i. e. a rather conspicuous upheaval of the earth's crust may be observed in the month immediately preceding an earthquake. In this case, we have taken the means of $\Delta L''$ for each month before and after an earthquake, omitting the months of other earthquakes in count, so that the number of months before and after the earthquakes did not exceed 43, among the total number of 54 months of the earthquakes. The mean errors, ε, of the means of $\Delta L''$, were also calculated and the values ± 4.0 mm$<\varepsilon<\pm 6.0$ mm were obtained. These values of ε are satisfactorily small when compared with the values of $\Delta L''$ in the curve, shown in Fig. 2, as was the case when we picked four stations, Aburatubo, Hososima, Wazima and Osyoro, and such destructive earthquakes, 30 in number, as have occurred in the regions within 250 kilometers from the respective mareographic stations, during the period of about 49 years (1900~1948). As already mentioned in my above cited paper,

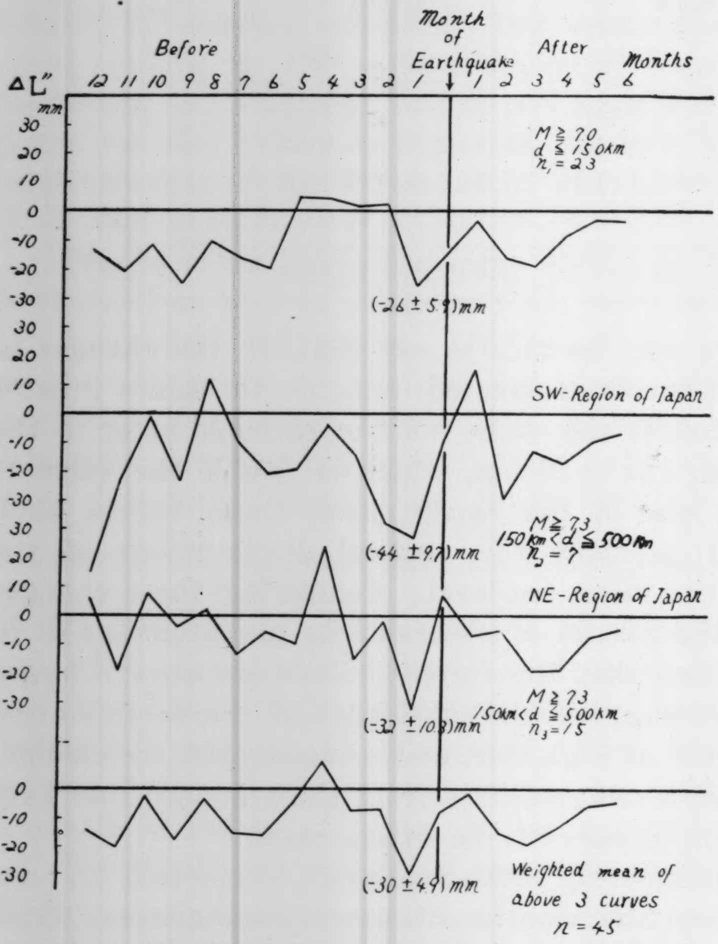

Fig. 2. Monthly mean sea-levels (corrected) $\Delta L''$ at Aburatubo before and after the Great Earthquakent, which accurred in different regions of Japan.

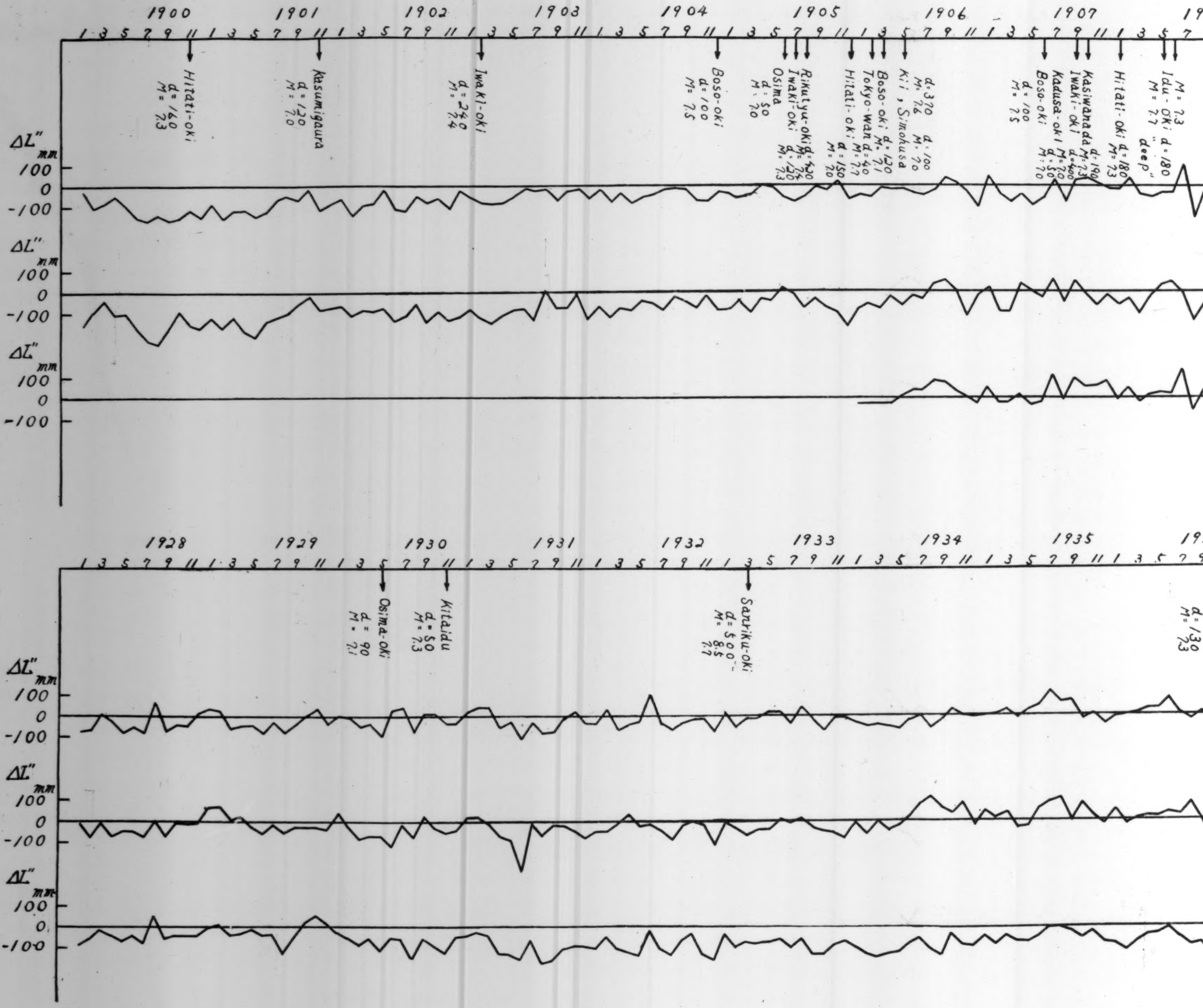

(震研彙報 第三十三号 図版 山口)

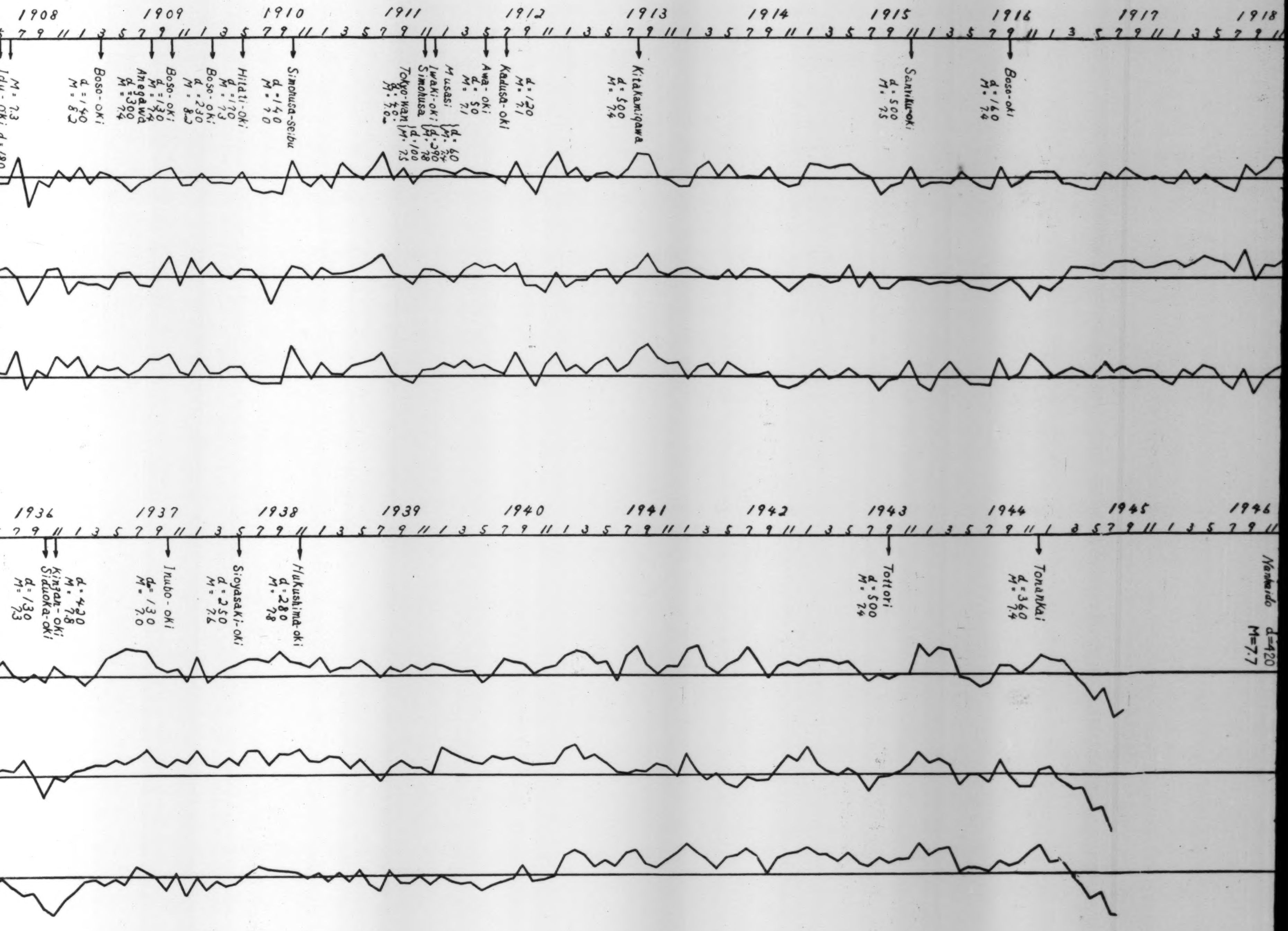

Fig. 1. Monthly mean sea-levels, corrected.

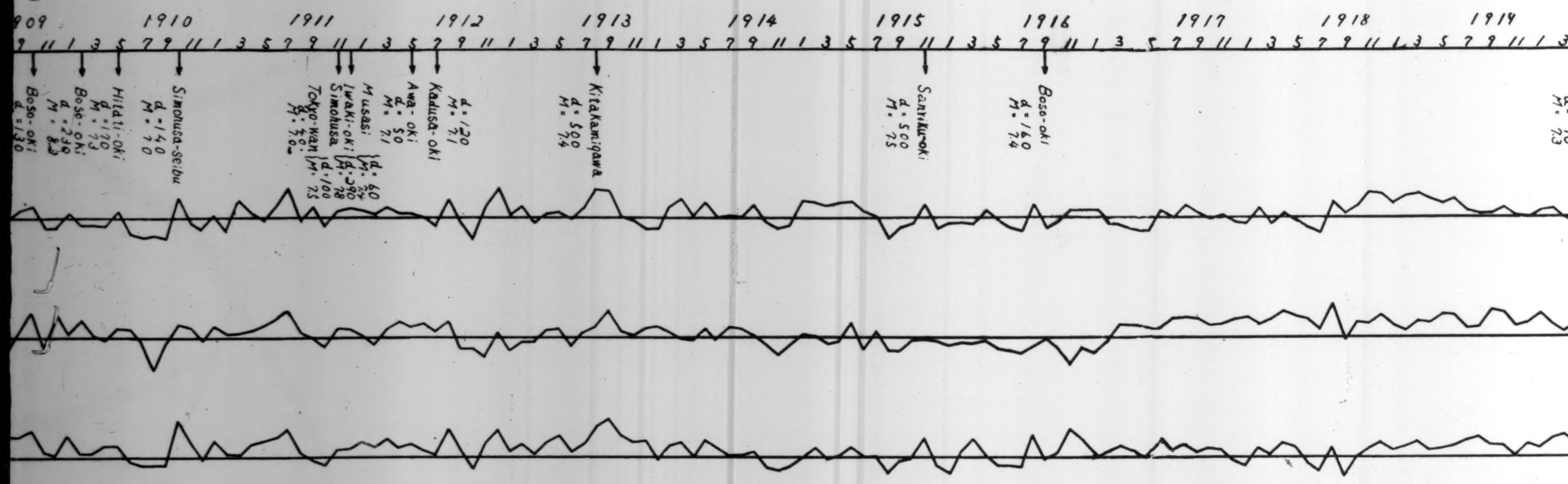

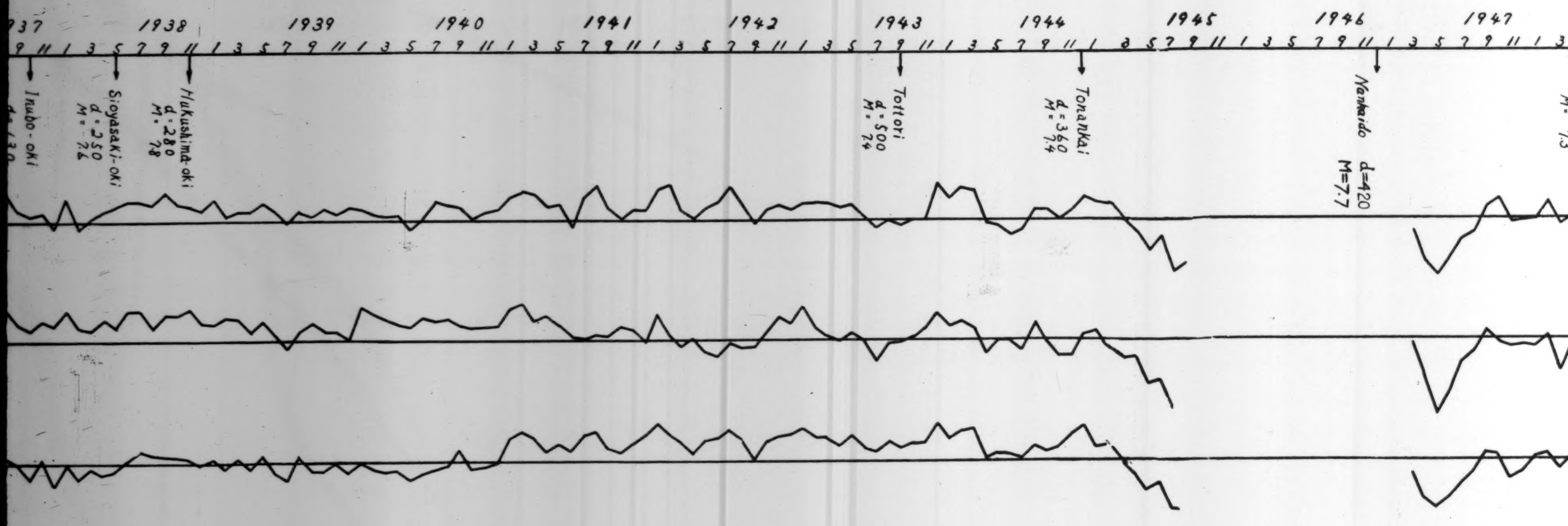

Fig. 1. Monthly mean sea-levels, corrected.

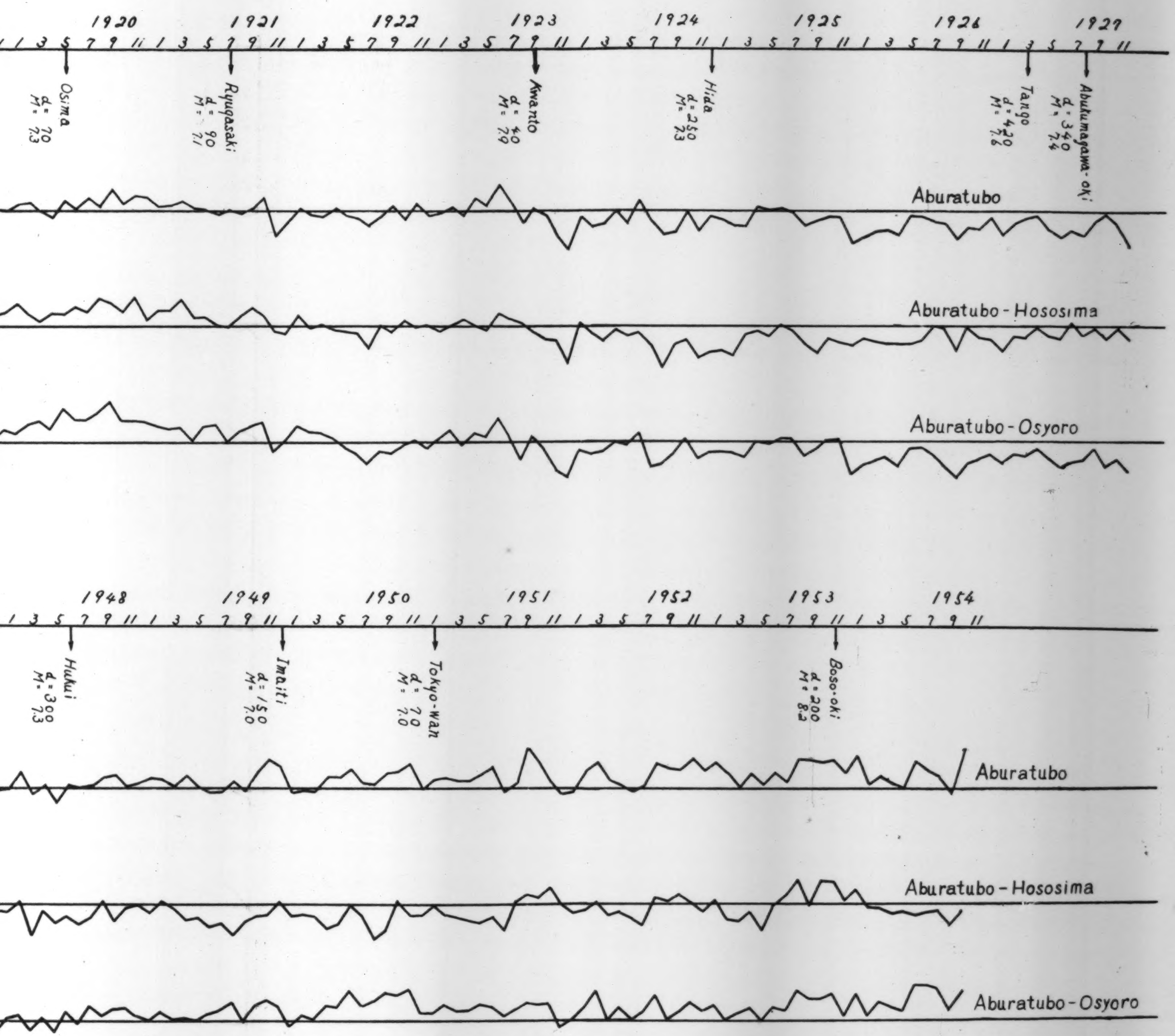
1920
1921
1922
1923
1924
1925
1926
1927
Osima d=70 M=7.3
Ryugasaki d=90 M=7.1
Kwanto d=40 M=7.9
Hida d=250 M=7.3
Tango d=420 M=7.6
Abukumagawa-oki d=340 M=7.4
Aburatubo
Aburatubo - Hososima
Aburatubo - Osyoro
1948
1949
1950
1951
1952
1953
1954
Hukui d=300 M=7.3
Imaiti d=150 M=7.0
Tokyo-wan d=70 M=7.0
Boso-oki d=200 M=8.2
Aburatubo
Aburatubo - Hososima
Aburatubo - Osyoro

these earthquakes are listed in the Scientific Chronological Table of the Tokyo Astronomical Observatory.

It is interesting to note that both two cases, the present and the preceding investigations, show nearly the same features of curves before and after great earthquakes. In the present case, we have obtained (-30 ± 4.9) mm as the mean value of $\Delta L''$ in the month immediately preceding an earthquake, and in the preceding case, it was (-38 ± 6.5) mm.

From Fig. 1, and 2, we may be able to say as follows:

The changes in the heights of mean sea-level at Aburatubo seem to have more intimate correlations with the occurrences of earthquakes in Southwestern Region than with those in Northeastern Region of Japan. The sea bed of Sagami Bay may be connected more closely with those off Tônankai and Nankai than those off Tôhoku and Sanriku, which suggests that there may exist some fault among the Fuji Volcanic Zone.

In general, the mean sea-levels, corrected, $\Delta L''$ are negative in the nearly months, before and after the great earthquakes. Especially they are greatly negative in the month immediately preceding an earthquake, and they become for one time slightly positive in the months (about four months) before the month of earthquake.

In conclusion, I wish to express my hearty thanks to the Geographical Survey Institute, as well as to the Central Meteorological Observatory of Japan for the many valuable data they put at my disposal throughout my whole investigation.

---

2. 大地震前後に於ける平均海水面の変化について

地震研究所　山　口　生　知

油壺より 150 km 以内の地点に起つた地震と 150 km 以上で 500 km 以内の地点に起つた地震とを別々に考えて,その地震前後に於ける油壺の平均海水面変化の有様を研究した. 地震の Magnitude については Pasadena scale で 7 以上のものをとり, 又 150 km 以上の所に起つたものについては 7.3 以上のものをとり, 而も場所的には西南日本と東北日本とに分類して調べて見た.

平均海水面については天体潮, 気象潮, 及び海洋潮の修正を施した値を採用したが念のため海洋潮に於て深海に冷水塊でも表はれた場合のことも考慮して油壺と細島の差並びに油壺と忍路との差をも採つて見た.

その結果大地震の 1 ケ月前には確かに平均海水面が著しく下ることが認められた. 即ち大地震の 1 ケ月前には相対的に地盤が隆起する可能性が大であることが認められた.

---

3. *Analysis of Dispersed Surface Waves by means of Fourier Transform I.*

By Yasuo SATÔ,

Earthquake Research Institute.

(Read Dec. 22, 1953.—Received Jan. 6, 1955.)

1. Introduction

From the beginning of our investigation, it has been one of the main objects of seismometry to examine the mechanism of earthquakes and the nature of media through which the waves are propagated. Of course, we have several kinds of waves available for this purpose, and P-waves have been often used successfully[1], while the surface waves are not so easily employed as the bodily waves[2]. This is due chiefly to the complex structure of the earth's crust and the dispersive nature of Rayleigh- as well as Love-waves. If the analysis of the seismograms of the dispersed surface waves is done with success, the above object will be partly accomplished. The following procedure is merely an attempt in this direction of our investigations.

The analysis has its foundation upon the very simple principle that the amplitude and the phase angle of the Fouiier transform of the curve observed at any station express the spectrum near the origin and the phase shift caused during the propagation respectively.

2. Fundamental concepts

At first we will consider the wave motion in one-dimensional space. Let us assume the movement at $x=0$ to be

$$f(t)=f(t\,;0)\ . \qquad \text{..............(2.1)}$$

This function is expressed as is well known from Fourier's double integral theorem,

---

1) We can find an enormous number of papers and reports in seismic prospecting, which all utilize the P-waves.

2) References in this branch of seismology is found, for example, in T. Akima's paper. *Bull. Earthq. Res. Inst.*, **30** (1952), 237.

$$f(t)=\frac{1}{\sqrt{2\pi}}\int_{-\infty}^{\infty} f^*(p)\exp(ipt)dp\ ,$$

in which ....(2.2)

$$f^*(p)=\frac{1}{\sqrt{2\pi}}\int_{-\infty}^{\infty} f(\tau)\exp(-ip\tau)d\tau\ .$$

The physical meaning of this expression is as follows.

An arbitrary function $f(t)$ is (if some conditions are satisfied) represented as the sum of the waves with frequency p and amplitude $f^*(p)/\sqrt{2\pi}$, while the function $f^*(p)$, which is named as Fourier transform, is also expressible in a similar form as shown in the latter expression of (2.2).

Now, if a wave $A\exp(ipt)$ is propagated by the velocity $V(p)$, it takes the form $A\exp\{ip(t-x/V(p))\}$ at the distance x. Therefore, if the disturbance at $x=0$

$$f(t)=\frac{1}{\sqrt{2\pi}}\int_{-\infty}^{\infty} f^*(p)\exp(ipt)dp$$

is propagated, the wave form at $x=x$ is

$$f(t\,;x)=\frac{1}{\sqrt{2\pi}}\int_{-\infty}^{\infty} f^*(p)\exp\{ip(t-x/V(p))\}dp$$

$$=\frac{1}{\sqrt{2\pi}}\int_{-\infty}^{\infty}[f^*(p)\exp\{-ipx/V(p)\}]\cdot\exp(ipt)dp\ . \quad (2.3)$$

The Fourier transform of this function is

$$f^*(p\,;x)=\frac{1}{\sqrt{2\pi}}\int_{-\infty}^{\infty} f(\tau\,;x)\exp(-ip\tau)d\tau\ , \quad .....(2.4)$$

which can be also expressed, by substituting the above expression, as follows.

$$f^*(p\,;x)=\frac{1}{\sqrt{2\pi}}\int_{-\infty}^{\infty}\exp(-ip\tau)d\tau$$

$$\cdot\frac{1}{\sqrt{2\pi}}\int_{-\infty}^{\infty}[f^*(p')\exp\{-ip'x/V(p')\}]\cdot\exp(ip'\tau)dp'$$

$$=f^*(p)\exp\{-ipx/V(p)\}\ . \quad ....(2.5)$$

Since $f(t\,;x)$ is the wave form observed at $x=x$, the above function can be calculated from the seismogram of that station, namely from (2.4)

$$f^*(p\,;x)=\frac{1}{\sqrt{2\pi}}\int_{-\infty}^{\infty} f(\tau\,;x)\cos(p\tau)d\tau$$

$$-i\frac{1}{\sqrt{2\pi}}\int_{-\infty}^{\infty} f(\tau\,;x)\sin(p\tau)d\tau$$

$$\equiv c(p\,;x)-is(p\,;x)\,. \qquad \ldots\ldots\ldots\ldots\ldots\ldots(2.6)$$

Now putting

$$f^*(p)=F(p)\exp\{-i\beta(p)\} \qquad \ldots\ldots\ldots\ldots\ldots(2.7)$$

we have

$$f^*(p\,;x)=F(p)\exp\{-i\beta(p)\}\cdot\exp\{-ipx/V(p)\}$$

and $$F(p)^2=c(p\,;x)^2+s(p\,;x)^2\,, \qquad \ldots\ldots\ldots\ldots\ldots(2.8)$$

where $F(p)$ and $\beta(p)$ are assumed both to be real.

From the expressions (2.6) and (2.7) we have easily

$$\begin{aligned}\mathfrak{C}(p)&\equiv-\arg f^*(p\,;x)\\ &=\arctan\{s(p\,;x)/c(p\,;x)\}\\ &=\beta(p)+px/V(p)\,,\end{aligned} \qquad \ldots\ldots\ldots\ldots(2.9)$$

where the inverse-trigonometric function does not necessarily take the principal value.

The function $F(p)$ is the spectrum of the wave observed at $x=x$, and also shows the spectrum of the vibration at the origin. The propagation velocity $V(p)$ with frequency p is from (2.9) expressed as

$$V(p)=\frac{px}{-\beta(p)+\arctan\{s(p\,;x)/c(p\,;x)\}} \qquad \ldots\ldots(2.10)$$

or, if we define ARCTAN z so as to satisfy

$$-\pi<\mathrm{ARCTAN}\,z\leq\pi\,, \qquad \ldots\ldots\ldots\ldots(2.11)$$

we have

$$V(p)=\frac{px}{-\beta(p)+\mathrm{ARCTAN}\{s(p\,;x)/c(p\,;x)\}+2n\pi} \qquad \ldots(2.12)$$

But we must add some remarks concerning the practical way of calculating the velocity. For the angle $\beta(p)$ can never be obtained from a single observation and therefore we cannot get $V(p)$ from the formula (2.12) if we do not neglect $\beta(p)$.

In order to perform an exact calculation, we are to choose at least two observations at different places, namely

$$\begin{aligned}\mathfrak{C}(p)^{(1)}&=\beta(p)+px^{(1)}/V(p)\\ \text{and}\quad \mathfrak{C}(p)^{(2)}&=\beta(p)+px^{(2)}/V(p)\end{aligned} \qquad \ldots\ldots\ldots\ldots(2.13)$$

Taking the difference of two expressions we have

$$\mathfrak{C}(p)^{(1)}-\mathfrak{C}(p)^{(2)}=p(x^{(1)}-x^{(2)})/V(p) \qquad \ldots\ldots.(2.14)$$

from which we get

$$V(p)=\frac{p(x^{(1)}-x^{(2)})}{\mathfrak{C}(p)^{(1)}-\mathfrak{C}(p)^{(2)}}\,, \qquad \ldots\ldots\ldots\ldots\ldots(2.15)$$

or

$$V(p)=\frac{p(x^{(1)}-x^{(2)})}{\mathrm{ARCTAN}\left\{\frac{s(p\,;\,x^{(1)})}{c(p\,;\,x^{(1)})}\right\}-\mathrm{ARCTAN}\left\{\frac{s(p\,;\,x^{(2)})}{c(p\,;\,x^{(2)})}\right\}+2m\pi}\,. \qquad (2.16)$$

If three or more observations are available and the dispersion formula can be assumed to be common to all of them, we can apply the method of least squares to the expressions of the type (2.13), and determine the unknown parameters $\beta(p)$ and $1/V(p)$, or $V(p)$.

3. Cylindrically-spreading waves

In the previous section we have treated the analysis of waves propagated one-dimensionally; we will now modify this theory to discuss the waves spreading in a two-dimensional space.

Cylindrically-spreading waves of course decrease their amplitude because their energy is distributed over the enlarging wave front. Since, in the two-dimensional propagation, the wave front increases proportionally to the epicentral distance, $f(t\,;r)$ must involve a factor $1/\sqrt{r}$. (Where r is the epicentral distance.) Consequently, if some wave train, whose amplitude at $r=r_1$ is A, is propagated and arrives at a point $r=r_2$, its amplitude becomes $A\sqrt{r_1/r_2}$.

Taking the above nature into consideration we will formulate expressions similar to the case of one-dimensional propagation.

Let us assume at first the movement at a point $r=r_0$, which is situated near the origin, to be

$$f(t\,;r_0)=\frac{1}{\sqrt{2\pi}}\int_{-\infty}^{\infty}f^*(p\,;r_0)\exp(ipt)dp\,, \qquad \ldots.(3.1)$$

in which

$$f^*(p\,;r_0)=\frac{1}{\sqrt{2\pi}}\int_{-\infty}^{\infty}f(\tau\,;r_0)\exp(-ip\tau)d\tau\,, \qquad ..(3.2)$$

then the expression corresponding to the equation (2.3) is

$$f(t\,;r)=\frac{1}{\sqrt{2\pi}}\int_{-\infty}^{\infty}\sqrt{\frac{r_0}{r}}\,f^*(p\,;r_0)\exp\left\{ip(t-\frac{r-r_0}{V(p)})\right\}dp$$

$$=\frac{1}{\sqrt{2\pi}}\int_{-\infty}^{\infty}\left[\sqrt{\frac{r_0}{r}}\,f^*(p\,;r_0)\exp\left\{-ip\frac{r-r_0}{V(p)}\right\}\right]\cdot\exp(ipt)dp \qquad \ldots(3.3)$$

Now the Fourier transform of this function is

$$f^*(p\,;r)=\frac{1}{\sqrt{2\pi}}\int_{-\infty}^{\infty}f(\tau\,;r)\exp(-ip\tau)d\tau$$

$$=\frac{1}{\sqrt{2\pi}}\int_{-\infty}^{\infty}\exp(-ip\tau)d\tau$$

$$\cdot\frac{1}{\sqrt{2\pi}}\int_{-\infty}^{\infty}\left[\sqrt{\frac{r_0}{r}}f^*(p'\,;r_0)\exp\left\{-ip'\frac{r-r_0}{V(p')}\right\}\right]\cdot\exp(ip'\tau)dp'$$

$$=\sqrt{\frac{r_0}{r}}\,f^*(p\,;r_0)\exp\left\{-ip\frac{r-r_0}{V(p)}\right\} \qquad \ldots\ldots\ldots\ldots\ldots(3.4)$$

If we compare (3.2) with (2.4) and (3.4) with (2.5), we find at a glance that the modification is very slight and we can immediately obtain the formula applicable to the analysis of the problem in two dimensions.

We put as before (cf. (2.6)～(2.9))

$$f^*(p\,;r)=\frac{1}{\sqrt{2\pi}}\int_{-\infty}^{\infty}f(\tau\,;r)\exp(-ip\tau)d\tau$$

$$\equiv c(p\,;r)-is(p\,;r)\,, \qquad \ldots\ldots\ldots\ldots\ldots(3.5)$$

$$F(p\,;r)^2\equiv c(p\,;r)^2+s(p\,;r)^2\,,$$

and

$$\mathfrak{C}(p)\equiv -\arg f^*(p\,;r)$$

$$=\arctan\{s(p\,;r)/c(p\,;r)\}$$

$$=\beta(p)+\frac{p(r-r_0)}{V(p)}\,, \qquad \ldots\ldots\ldots\ldots\ldots\ldots(3.6)$$

then the spectrum distribution at the place with the epicentral distance $r=r_0$ is easily obtained.

$$F(p\,;r_0)=\sqrt{\frac{r}{r_0}}F(p\,;r)\,. \qquad \ldots\ldots\ldots\ldots\ldots\ldots\ldots(3.7)$$

The following treatments concerning the velocity are quite same with the process shown in the equations (2.10)～(2.12), and the formulae (2.13)～(2.16) can be applied in this case, too.

If we neglect the phase angle $\beta(p)$ and $pr_0/V(p)$ compared with $pr/V(p)$ we have immediately the next simple formula

$$V(p)=\frac{pr}{\mathfrak{C}(p)}=\frac{pr}{\mathrm{ARCTAN}\{s(p\,;\,r)/c(p\,;\,r)\}+2n\pi}\,, \qquad (3.8)$$

while, if a more presise estimation is required, we must employ the formulae (2.15) and (2.16), where $x^{(1)}$ and $x^{(2)}$ should be replaced by $r^{(1)}$ and $r^{(2)}$ respectively. Namely

$$V(p)=\frac{p(r^{(1)}-r^{(2)})}{\mathrm{ARCTAN}\left\{\dfrac{s(p\,;\,r^{(1)})}{c(p\,;\,r^{(1)})}\right\}-\mathrm{ARCTAN}\left\{\dfrac{s(p\,;\,r^{(2)})}{c(p\,;\,r^{(2)})}\right\}+2m\pi}\,. \qquad (3.9)$$

4. Approximation formula for the integration

In the previous sections the integral of the form

$$f^*(p\,;\,r)=\frac{1}{\sqrt{2\pi}}\int_{-\infty}^{\infty}f(\tau\,;\,r)\exp(-ip\tau)d\tau$$
$$=c(p\,;\,r)-is(p\,;\,r) \qquad \ldots\ldots\ldots\ldots\ldots(4.1)$$

often appeared, which must be calculated in order to perform the treatment stated. Numerical integration by means of trapezoidal or Simpson rule can be of course utilized, but when the wave takes some simple form, we can approximate to this curve by some simple function and perform the integration more conveniently. For example, if the wave is, as shown in Fig. 1, consisted of sinusoidal curve with slowly varying amplitude and period, then we can approximate to it by

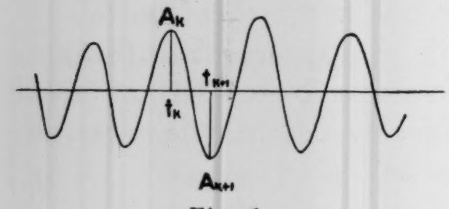

Fig. 1.

$$f(t\,;\,r)=\begin{cases}0 & \ldots\ldots\ldots t<t_0\,,\\ \dfrac{1}{2}(A_k+A_{k+1})+\dfrac{1}{2}(A_k-A_{k+1})\cos\left\{\pi\dfrac{t-t_k}{t_{k+1}-t_k}\right\} & \ldots\ldots\ldots t_k<t<t_{k+1},\ (k=0,\,1,\,..,n-1),\\ 0 & \ldots\ldots\ldots t_n<t\,. \qquad \ldots\ldots\ldots(4.2)\end{cases}$$

Hitherto, in such a case, we customarily used the method to assume the time interval $(t_{k+1}-t_k)$ as an approximate value of the period of waves, and obtained the velocity corresponding to this assumed period.

But here, we introduced the expression (4.2) into the above formula and obtained

$$\begin{cases} c(p\,;r)=\sum_{k=0}^{n-1} I_{Ck}, \quad s(p\,;r)=\sum_{k=0}^{n-1} I_{Sk} \\ I_{Ck}=\int_{t_k}^{t_{k+1}}\left[\frac{1}{2}(A_k+A_{k+1})+\frac{1}{2}(A_k-A_{k+1})\cos\left\{\pi\frac{\tau-t_k}{t_{k+1}-t_k}\right\}\right]\cos p\tau\, d\tau\,, \\ I_{Sk}=\int_{t_k}^{t_{k+1}}\left[\frac{1}{2}(A_k+A_{k+1})+\frac{1}{2}(A_k-A_{k+1})\cos\left\{\pi\frac{\tau-t_k}{t_{k+1}-t_k}\right\}\right]\sin p\tau\, d\tau\,. \end{cases} \quad \ldots\ldots(4.3)$$

Then I_{Ck} and I_{Sk} can be integrated and after a somewhat complicated but easy calculation

$$\begin{aligned} 2pI_{Ck} &= -2A_k\sin pt_k+2A_{k+1}\sin pt_{k+1} \\ &\quad -\frac{A_k-A_{k+1}}{(pc_k/\pi)^2-1}(\sin pt_k+\sin pt_{k+1})\,, \\ 2pI_{Sk} &= 2A_k\cos pt_k-2A_{k+1}\cos pt_{k+1} \qquad \ldots\ldots\ldots\ldots(4.4) \\ &\quad +\frac{A_k-A_{k+1}}{(pc_k/\pi)^2-1}(\cos pt_k+\cos pt_{k+1})\,, \end{aligned}$$

where $c_k=t_{k+1}-t_k$.

Therefore, summing up the above expressions,

$$\begin{aligned} 2p\sum_{k=0}^{n-1} I_{Ck} &= -2A_0\sin pt_0+2A_n\sin pt_n \\ &\quad -\sum_{k=0}^{n-1}\frac{A_k-A_{k+1}}{(pc_k/\pi)^2-1}(\sin pt_k+\sin pt_{k+1}) \\ 2p\sum_{k=0}^{n-1} I_{Sk} &= 2A_0\cos pt_k-2A_n\cos pt_k \qquad \ldots\ldots\ldots\ldots\ldots(4.5) \\ &\quad +\sum_{k=0}^{n-1}\frac{A_k-A_{k+1}}{(pc_k/\pi)^2-1}(\cos pt_k+\cos pt_{k+1}) \end{aligned}$$

If we can assume that

$$A_0=A_n=0 \qquad \ldots(4.6)$$

as is in the Fig. 2, the above expression may be reduced to the next simple form.

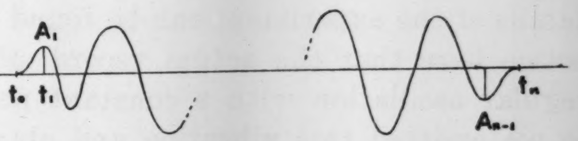

Fig. 2

$$\begin{cases} \sum_{k=0}^{n-1} I_{Ck}=c(p\,;r)=-\dfrac{1}{2p}\sum_{k=0}^{n-1}\dfrac{A_k-A_{k+1}}{(pc_k/\pi)^2-1}(\sin pt_k+\sin pt_{k+1}) \\ \sum_{k=0}^{n-1} I_{Sk}=s(p\,;r)=+\dfrac{1}{2p}\sum_{k=0}^{n-1}\dfrac{A_k-A_{k+1}}{(pc_k/\pi)^2-1}(\cos pt_k+\cos pt_{k+1}) \end{cases} \quad \ldots\ldots\ldots\ldots(4.7)$$

If

$$pt_{k+1}=pt_k+\pi, \text{ or } pc_k/\pi=1\ , \qquad \ldots\ldots\ldots\ldots\ldots(4.8)$$

$(\sin pt_k+\sin pt_{k+1})$, $(\cos pt_k+\cos pt_{k+1})$ and $\{1-(pc_k/\pi)^2\}$ all vanish and the $(k+1)$-th term in the above summation becomes indefinite. In this case we must employ the expressions

$$-(A_k-A_{k+1})\frac{\pi}{2}\cos pt_k \text{ and } (A_k-A_{k+1})\frac{\pi}{2}\sin pt_k \qquad \ldots\ldots(4.9)$$

instead of the terms

$$\frac{A_k-A_{k+1}}{(pc_k/\pi)^2-1}(\sin pt_k+\sin pt_{k+1}) \text{ and } \frac{A_k-A_{k+1}}{(pc_k/\pi)^2-1}(\cos pt_k+\cos pt_{k+1})$$

respectively. These formulae are easily obtained as the limit

$$p(t_{k+1}-t_k)\rightarrow\pi\ .$$

In some case the next formulae may be more convenient than the expression (4.7)

$$\begin{cases} c(p\,;\,r)=-\dfrac{1}{p}\sum(A_k-A_{k+1})\dfrac{\cos(pc_k/2)}{(pc_k/\pi)^2-1}\sin pt_{k+1/2}\ , \\ s(p\,;\,r)=+\dfrac{1}{p}\sum(A_k-A_{k+1})\dfrac{\cos(pc_k/2)}{(pc_k/\pi)^2-1}\cos pt_{k+1/2}\ , \end{cases} \qquad \ldots(4.10)$$

where $\qquad t_{k+1/2}=(t_k+t_{k+1})/2.$

5. Analysis of a practical record of explosion

We applied the above theory in the analysis of the practical record made by F. Kishinouye and reported some ten years ago.[3] It is a small explosion which took place on February, 1942 at Lake Haruna, and the details of the experiment can be found in the original paper. But we must notice here that the actual record of this experiment contains some regular oscillation with a constant period and amplitude, such as hum,[4] so we omitted this vibration and obtained the curves by hand-writing, which are given in Fig. 3. The epicentral distance is 141.75 m for A and 76.2 m for B respectively.

We did not integrate these curves in order to get the true vibration of the particle. For the records were obtained using an oscillograph

3) F. KISHINOUYE, "Studies on Lake-Ice," *Bull. Earthq. Res. inst.*, **21** (1943), 298.
4) F. KISHINOUYE, *ibid.* See Fig. 3 on Page 304 in this paper.

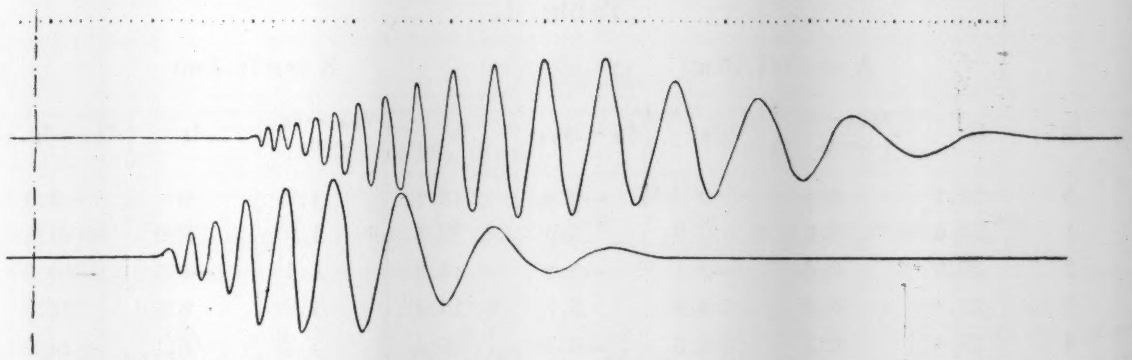

Fig. 3. The upper dotted line is the time mark. One interval is 0.01 sec. At every 0.1 sec. there is a large mark.
The middle curve shows the observation A. ($r=141.75$ m.)
The lower curve shows the observation B. ($r=76.2$ m.)
The chain line at the left indicates the shot time.

and an amplifier involving vacuum tubes, and thus their precise characteristics now cannot be clarified enough to use for the reduction of the records. Consequently we gave up such treatment and used them as they were. The results, however, seem not to contain so much error as to affect the conclusion perceptively.

We utilized the formulae introduced in the previous section for the numerical integration of the curves in Fig. 3. The data used for the calculation is given in Table I. Introducing the numerical values into (4.7), and if necessary by the aid of (4.8) and (4.9), we can obtain

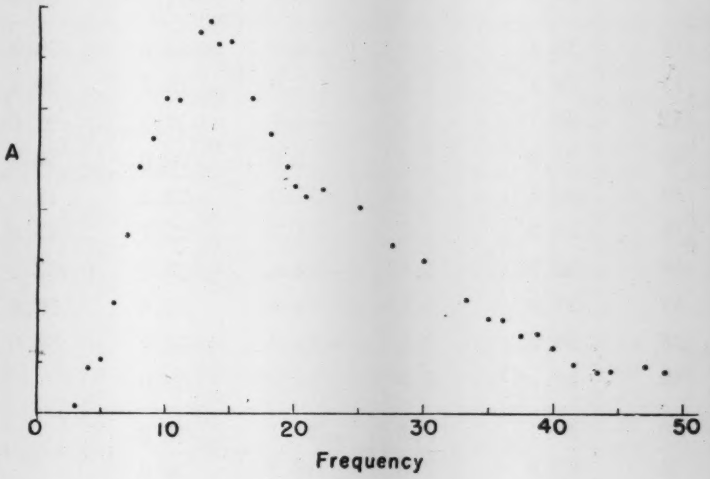

Fig. 4a.

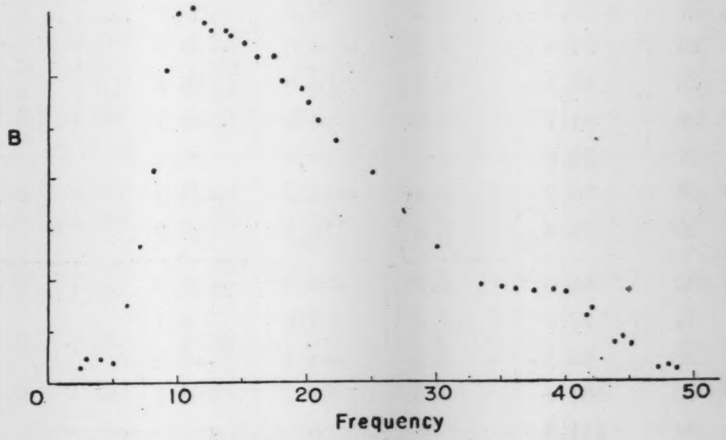

Fig. 4b. Ordinate; Amplitude in arbitrary scale.
Abscissa; Frequency per second.

Table I.

	A (r=141.75 m)				B (r=76.2 m)			
k	t_k	$t_{k+1}-t_k$ $=c_k$	A_k	A_k-A_{k+1}	t_k	$t_{k+1}-t_k$ $=c_k$	A_k	A_k-A_{k+1}
0	21.1	0.5	0	−0.9	12.1	1.2	0	−2.0
1	21.6	0.6	0.9	3.0	13.3	1.0	2.0	6.5
2	22.2	0.6	−2.1	−5.3	14.3	1.1	−4.5	−10.6
3	22.8	0.6	3.2	5.7	15.4	1.0	6.1	12.2
4	23.4	0.7	−2.5	−6.3	16.4	1.2	−6.1	−14.9
5	24.1	0.8	3.8	6.3	17.6	1.6	8.8	17.9
6	24.9	0.8	−2.5	−6.7	19.2	1.5	−9.1	−23.3
7	25.7	0.9	4.2	8.2	20.7	1.5	14.2	30.9
8	26.6	0.9	−4.0	−9.7	22.2	2.4	−16.7	−34.3
9	27.5	0.9	5.7	11.7	24.6	2.0	17.6	36.3
10	28.4	1.0	−6.0	−13.0	26.6	2.8	−18.7	−38.7
11	29.4	1.3	7.0	15.7	29.4	3.2	20.0	38.5
12	30.7	1.2	−8.7	−17.7	32.6	3.7	−18.5	−35.1
13	31.9	1.4	9.0	20.0	36.3	4.8	16.6	28.6
14	33.3	1.3	−11.0	−22.3	41.1	4.7	−12.0	−19.9
15	34.6	1.7	11.3	23.7	45.8	6.5	7.9	11.9
16	36.3	1.6	−12.4	−27.0	52.3	6.3	−4.0	−6.2
17	37.9	1.7	14.6	30.5	58.6	7.4	2.2	2.2
18	39.6	2.1	−15.9	−33.8	66.0		0	
19	41.7	2.0	17.9	36.0				
20	43.7	2.2	−18.1	−36.8				
21	45.9	2.6	18.7	38.1				
22	48.5	2.8	−19.4	−39.4				
23	51.3	3.3	20.0	39.0				
24	54.6	3.5	−19.0	−39.0				
25	58.1	3.6	20.0	36.8				
26	61.7	4.1	−16.8	−31.7				
27	65.8	4.4	14.9	29.3				
28	70.2	5.2	−14.4	−25.3				
29	75.4	5.6	10.9	20.2				
30	81.0	6.2	−9.3	−13.3				
31	87.2	7.3	4.0	8.1				
32	94.5	7.3	−4.1	−5.8				
33	101.8	9.3	1.7	1.7				
34	111.1		0					

Unit of time is 1/100 sec.
Unit of length is mm. on the original seismogram.

Table II.

		A ($r=141.75$ m)				B ($r=76.2$ m)				*
p(cycle)	T(sec)	$-p\cdot c(p;r)$	$p\cdot s(p;r)$	$\|f^*(p;r)\|$	arg $f^*(p;r)$	$-p\cdot c(p;r)$	$p\cdot s(p;r)$	$\|f^*(p;r)\|$	arg $f^*(p;r)$	
2.5	0.40	−4.80	−1.60	2.00		0.27	−0.82	0.32	−1.89	
3	0.333	0.45	0	0.17	3.14	−1.45	−0.19	0.49	−0.13	3.27
4	0.25	−2.05	4.20	1.18	1.12	2.13	−0.37	0.52	−2.97	4.09
5	0.2	6.70	2.40	1.42	2.79	0.64	1.86	0.40	1.90	1.89
6	0.167	15.5	8.2	2.91	2.65	−6.30	−7.8	1.67	−0.89	3.54
7	0.143	2.6	32.6	4.67	1.65	10.9	15.1	2.66	2.20	2.47
8	0.125	−39.2	34.5	6.52	0.72	−20.6	−23.8	4.14	−0.86	1.58
9	0.111	−55.5	−33.7	7.21	−0.55	24.2	49.0	6.08	2.03	−2.58
10	0.1	48.2	−67.4	7.28	−2.19	9.0	−71.9	7.25	−1.70	−0.25
11	0.0909	41.8	80.4	8.28	2.05	−60.1	53.9	7.34	0.73	1.32
12	0.0833					84.4	6.4	7.06	3.07	
12.5	0.08	62.4	109.1	10.05	2.09	41.4	−75.4	6.88	−1.97	4.06
13.333	0.075	−60.0	−123.8	10.31	−1.12	−86.4	−20.0	6.58	−0.23	−0.89
13.888	0.072	−61.4	120.1	9.71	1.10	−52.2	78.8	6.82	0.99	0.11
15	0.0667	−43.4	−139.6	9.75	−1.27	98.6	−14.0	6.64	−3.00	1.73
16	0.0625					−50.4	−89.4	6.42	−1.06	
16.666	0.06	45.3	−128.1	8.17	−1.91	−109.2	10.3	6.59	0.09	−2.00
18.055	0.0554	103.3	82.2	7.31	2.47	93.5	51.2	5.91	2.64	−0.17
19.444	0.0514	−116.6	46.3	6.45	0.38	−43.7	−102.2	5.73	−1.17	1.55
20	0.05	52.6	107.0	5.96	2.03	−108.3	−19.5	5.50	−0.18	2.21
20.833	0.048	14.6	−118.2	5.72	−1.69	−30.1	103.0	5.15	1.29	−2.98
22.222	0.045	65.2	114.2	5.92	2.09	101.0	−30.6	4.75	−2.85	4.94
25	0.04	134.0	−23.1	5.44	−2.97	−30.9	97.8	4.10	1.26	−4.23
27.5	0.0364	121.8	−27.4	4.40	−2.92	−10.0	−91.6	3.35	−1.46	−1.46
30	0.0333	118.5	−0.4	3.95	−3.14	35.4	71.3	2.65	2.03	−5.17
33.333	0.03	34.0	−92.6	3.34	−1.92	−62.7	7.0	1.89	0.11	−2.03
35	0.0286	0.6	86.1	2.46	1.58	24.5	59.8	1.85	1.96	−0.38
36.111	0.0277	68.4	−57.2	2.47	−2.44	64.0	5.7	1.78	3.05	−5.49
37.5	0.0267	−65.1	38.4	2.02	0.53	4.0	−66.0	1.76	−1.63	2.16
38.888	0.0257	78.9	−17.3	2.08	−2.92	−69.4	−6.1	1.79	−0.09	−2.83
40	0.025	−54.1	−41.0	1.70	−0.65	−25.6	64.2	1.73	1.19	−1.84
41.666	0.024	43.6	31.0	1.28	2.52	52.5	−5.9	1.27	−3.03	5.55
42	0.0238					56.0	−15.1	1.38	−2.88	
43.555	0.0230	−23.3	−43.7	1.14	−1.08	−37.8	−6.5	0.86	−0.17	1.74
44.444	0.0225	−0.1	52.5	1.18	1.57					
45	0.0222					−28.2	12.5	0.68	0.42	
47.222	0.0212	−56.2	18.5	1.25	0.32	2.6	10.6	0.23	1.81	−1.49
48	0.0208					6.5	13.8	0.32	2.01	
48.611	0.0206	53.4	12.0	1.12	2.92	1.5	12.8	0.27	1.69	1.23

*ARCTAN$\{s(p;r_A)/c(p;r_A)\}$ − ARCTAN$\{s(p;r_B)/c(p;r_B)\}$

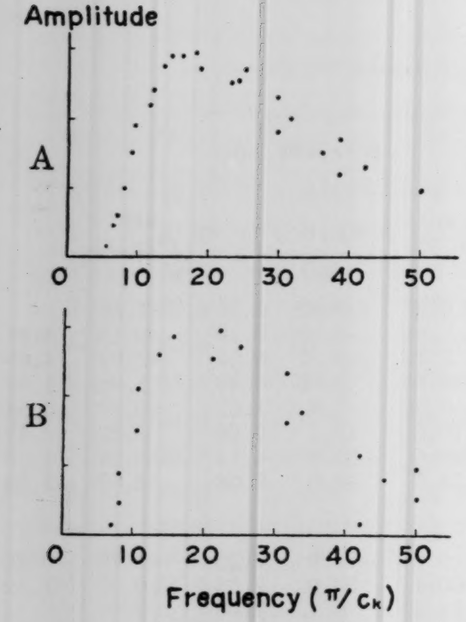

Fig. 5.

Ordinate; Amplitude in arbitrary scale.

Abscissa; Frequency per second.

Notice that the form indicated by this method is similar to that in Fig. 4.

$c(p\,;r)$ and $s(p\,;r)$, which are shown in Table II.

By means of these results, we can determine the spectrum distribution function $F(p\,;r)$ and the propagation velocity $V(p)$. $F(p\,;r)$ is obtained from (3.4) and (3.5) and is shown in Fig. 4, while in Fig. 5 the graph A_k versus π/c_k is given, which may also serve as a kind of spectrum distribution for a rough purpose. $V(p)$ is derived from (3.9). But here occures some unexpected difficulty in determining the numerical value, which is caused by the many-valuedness of the inverse trigonometric function. Although we can determine ARCTAN $\{s(p\,;r)/c(p\,;r)\}$ uniquely, there is uncertainty of $2m\pi$ in the determination of $\mathfrak{C}(p)$ which is necessary for obtaining the velocity $V(p)$. (Cf. (2.16) and (3.9). ARCTAN $\{s(p\,;r_A)/c(p\,;r_A)\}$ − ARCTAN $\{s(p\,;r_B)/c(p\,;r_B)\}$ is involved in Table II.) Hence we adopted the following method. We gave various values of m in the formula (3.9) for each p, and plotted all the points in the same figure. Thus we obtained Figs. 6a and 6b, which have same

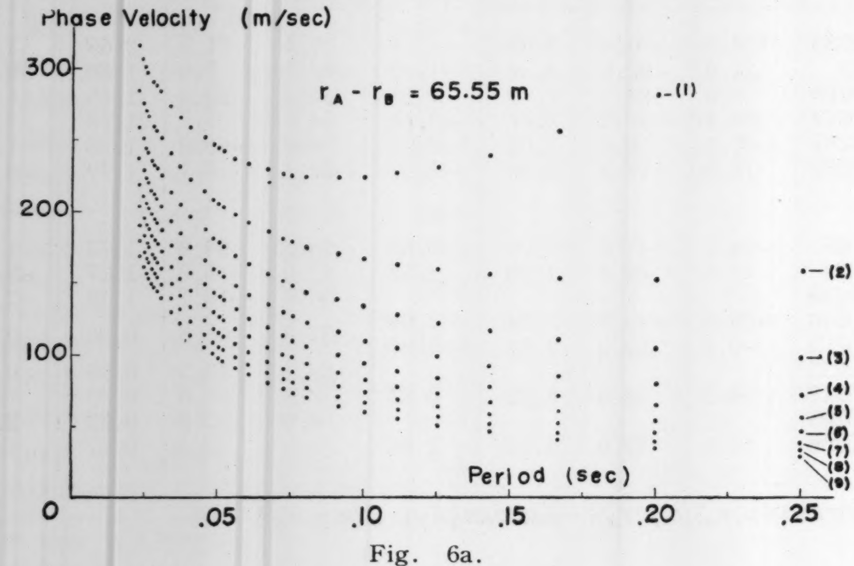

Fig. 6a.

contents, only the latter is plotted in log-log-scale. The points in this figure are naturally divided into several groups, each one describing a smooth curve. Of course, only one of them stands for the true dispersion curve, but we cannot easily determine which is the true one. To get rid of the false curves and discern the true one, we employed the following methods.

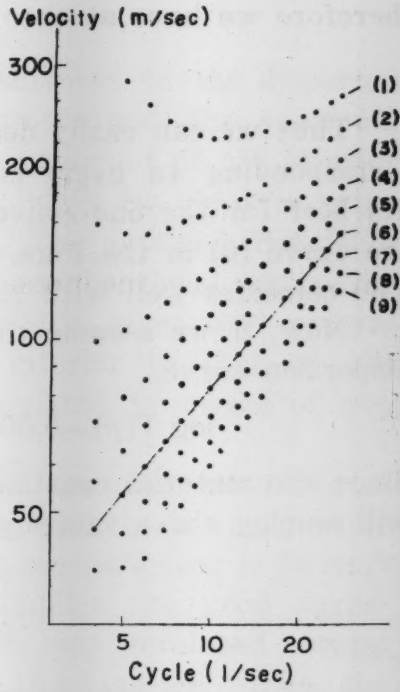

Fig. 6b.

At first we made a graph showing the relation group velocity versus period by means of a conventional way of measuring the interval of crest to crest. This is easily performed without special trouble, for we can use $2(t_{k+1}-t_k)$ as a period and r/t_k as a group velocity. Fig. 7 shows this relation. On the other hand we obtained the group velocity (U) from the data of the phase velocity. For this purpose we can conveniently use Fig. 6b. As we can notice easily in this figure $\log V(p)$ and $\log p$ are approximately connected by a linear relation, namely,

$$\log V(p)=a\log p+b\ . \qquad \ldots\ldots\ldots\ldots(5.1)$$

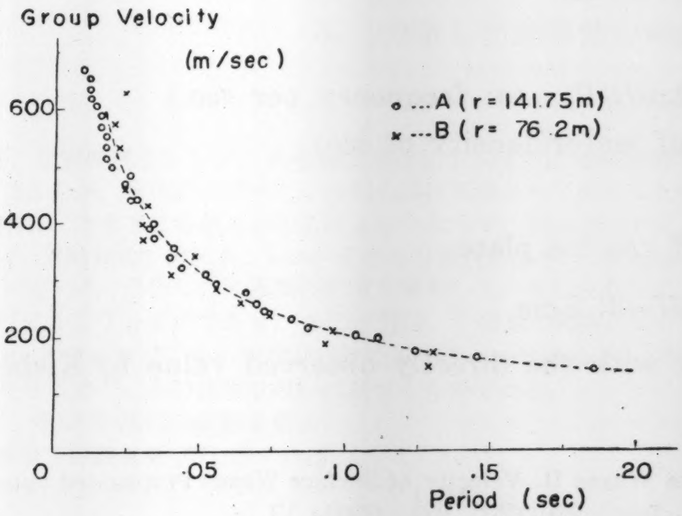

Fig. 7. Broken line is the group velocity of the curve (6) in Fig. 6a or 6b.

Now,

$$\frac{U}{V}=\frac{1}{V}\frac{dp}{df}$$

$$=\frac{1}{V}\frac{dp}{dV}\Big/\frac{d(p/V)}{dV}$$

$$=V\frac{dp}{dV}\Big/\left(V\frac{dp}{dV}-p\right)\ . \qquad \ldots\ldots(5.2)$$

On the other hand, differentiating the expression (5.1) by V, we get

$$V\frac{dp}{dV}=\frac{p}{a}\ ,$$

therefore we have at once

$$U/V=1/(1-a) \ . \qquad \dots\dots\dots\dots\dots\dots(5.3)$$

Thus we can easily deduce the group velocity from Figs. 6a and 6b corresponding to every curve in the figures. We chose a curve that fits best for the one conventionally obtained in the Fig. 7. That is the curve (6) in the Figs. 6a and 6b. Moreover the slope of this curve 0.60 coincides well with the theoretical value[5].

Now, if we assume that the curve (6) in Fig. 6b represents true dispersion curve,

$$\log V(p)=0.60 \log p+3.316 \text{ (c.g.s. unit)} \ . \qquad \dots\dots(5.4)$$

Since the material constants have been determined by Kishinouye[6], we will employ those values given in his paper, viz.,

$$V_S=1.51 \text{ km/sec} \ ,$$
$$V_P=2.82 \text{ km/sec} \ ,$$
$$\gamma^2\equiv(V_P/V_S)^2=3.49=1.87^2 \ ,$$
$$\text{Poisson's ratio}=0.30 \ ,$$
$$\mathfrak{v}_0\equiv 2\sqrt{-1+\gamma^2}/\gamma=1.69 \ .$$

Putting these values into the formula

$$\mathfrak{v}=\omega^{3/5}\left\{\frac{1}{12\Gamma}\mathfrak{v}_0^2\right\}^{1/5} \ ,$$ [7]

where
$$\begin{cases} \mathfrak{v}=V/V_S \ , \\ \omega=pH/V_S=2\pi nH/V_S \ , \ (n\text{: frequency per sec.}) \\ \Gamma=(\text{density of water/density of ice}) \\ \quad =1.09 \end{cases}$$

we have as the thickness of the ice plate

$$H=31.5 \text{ cm} \ ,$$

which is in good agreement with the directly observed value by Kishinouye (34cm.).

---

5) Y. SATÔ, "Study on Surface Waves II. Velocity of Surface Waves Propagated upon Elastic Plates," *Bull. Earthq. Res. Inst.*, **29** (1951), 237. Table VI.

6) *loc. cit.*, 3).

7) *loc cit.*, 5). Table VI or expression (7.3).

6. Conclusion

By applying the method of Fourier transform to the dispersed seismograms, we can obtain the dispersion formula and the spectrum of the vibration near the origin. For, the argument of the Fourier transform indicates the velocity of the waves, while its absolute value gives the spectrum of the given disturbance. The obtained dispersion curve agrees well with those arrived at by the conventional method of measuring the interval of crest to crest, which gives only several isolated points and its precision is decidedly inferior to that of the former. Forms of the spectrum curves calculated by means of two independent observations coincide pretty well.

Thickness of the ice plate estimated from the dispersion curve, which was obtained by the method here proposed, is 31.5 cm., while the value given by Kishinouye from the direct measurement is 34 cm.[8] The fact that the discrepancy is quite small implies the good agreement of the theory on the elastic plates, which was developed several years ago, and the observation made upon the lake ice. Also, the author believes, it assures the utility of the method here proposed.

The expense of the present study was partly defrayed from the Fund of the Scientific Research from the Ministry of Education.

---

3. 分散した地震波の解析 I

地震研究所 佐 藤 泰 夫

1. 発震機構をしらべ，地殼構造を決定する事は，地震計測学におけるもつとも重要な課題の一つであるが，実体波は従来この目的の為に利用されて見るべき成果をあげてゐる．これに反して表面波は，さまざまの試みがあるにもかかはらず，実体波ほどには用ゐられてゐないが，これは一つには，Rayleigh 波にも，Love 波にも分散性があり，取扱ひに困難があるからであらう．

本論文は，分散した表面波の記象を解析して，その分散公式，できうれば発震機構に関する推測を行はうとするものであり，その原理は，“任意の観測点において得られた波形の Fourier transform を求めれば，その振幅は震源附近での spectrum を，その位相は伝播によつて生じた位相の変りを示す”，との簡単な考へに基づくものである．

2. 先づ 1 次元の波動を扱ふ．

原点での動きを $f(t)$ とすれば

$$f(t)=\frac{1}{\sqrt{2\pi}}\int_{-\infty}^{\infty} f^{*}(p)\exp(ipt)dp \qquad \ldots.(2.2)$$

8) *loc. cit.*, 5). p. 303.

又 x の所では

$$f(t;\ x)=\frac{1}{\sqrt{2\pi}}\int_{-\infty}^{\infty}[f^*(p)\exp\{-ipx/V(p)\}]\exp(ipt)dp \qquad \ldots.(2.3)$$

であるから，その Fourier transform は

$$f^*(p;\ x)=\frac{1}{\sqrt{2\pi}}\int_{-\infty}^{\infty}f(\tau;\ x)\cdot\exp(-ip\tau)d\tau \qquad \ldots.(2.4)$$

$$=f^*(p)\exp\{-ipx/V(p)\} \qquad \ldots.(2.5)$$

従つて

$$f^*(p;\ x)=c(p;\ x)-is(p;\ x) \qquad \ldots.(2.6)$$

$$f^*(p)=F(p)\exp\{-i\beta(p)\} \qquad \ldots.(2.7)$$

とおけば

$$F(p)^2=c(p;\ x)^2+s(p;\ x)^2 \qquad \ldots.(2.8)$$

$F(p)$ は震源での spectrum をあらはし，

$$-\arg f^*(p;\ x)=\beta(p)+px/V(p) \qquad \ldots.(2.9)$$

からは速度 $V(p)$ が求められる．ここに $F(p)$, $\beta(p)$ は実数とする．(公式 (2·10))．

$\beta(p)$ は，分散公式が共通である 2 個の観測点での記録が得られれば，消去する事ができる．又 $f(t;\ x)$ から逆に $f(t)$ を求める事も可能な筈である．

3．波が 2 次元的にひろがる場合にも，上の公式をいくらか変形する事により，同様の式を導く事ができる．

即ち，震源に近い $r=r_0$ での spectrum としては，

$$F(p;\ r_0)=\sqrt{\frac{r}{r_0}}F(p;\ r) \qquad \ldots.(3.7)$$

ここに

$$F^2(p;\ r)=c(p;\ r)^2+s(p;\ r)^2$$

$$f^*(p;\ r)=\frac{1}{\sqrt{2\pi}}\int_{-\infty}^{\infty}f(\tau;\ x)\exp(-ip\tau)d\tau=c(p;\ r)-is(p;\ r) \qquad \ldots.(3.5)$$

又速度は

$$-\arg f^*(p;r)=\beta(p)+p(r-r_0)/V(p)=\arctan\{s(p;\ r)/c(p;\ r)\} \qquad \ldots.(3.6)$$

から求められる．

即ち

$$V(p)=\frac{p(r^{(1)}-r^{(2)})}{\mathrm{ARCTAN}\left\{\dfrac{s(p;\ r^{(1)})}{c(p;\ r^{(1)})}\right\}-\mathrm{ARCTAN}\left\{\dfrac{s(p;\ r^{(2)})}{c(p;\ r^{(2)})}\right\}+2m\pi} \qquad \ldots.(3.9)$$

前節の場合にも起つた事であるが，arctan の多価性の為に生ずる不確定性は，他の条件を考慮して取除かなくてはならない．

4．もし波形が Fig. 1, 2, 3 に示すやうに，振幅と周期がゆつくりと変る正弦形の波からできてゐる時には，適当な近似式で表現する事により (式 (4.2))，積分を簡単に行う事ができる (公式 (4.7)～(4.10))．

5．以上の理論を，10 年余り前に岸上が榛名湖において行つた実験の記録に適用した．Hum とおぼしき雑音を除く為，適当に曲線をならした上で，さきに求めた公式によつて数値計算を行つた．この結果を整理して，位相速度を表はす曲線としては Fig. 6a 又は 6b の曲線 (6) が得られた．この線は，以前筆者が氷の上におかれた薄い弾性板を伝はる表面波について求めた理論式とよく一致する．観測から得られた物理常数を入れて氷の厚さを求めて見ると，31.5 cm. なる値が得られる．実際に現地において測定した値は 34 cm. である．

本研究には，岸上冬彦，高橋竜太郎両先生に種々御指導を賜はつた．記して感謝を捧げる次第である．

Errata and Appendix to
Study on Surface Waves II.
Velocity of Surface Waves Propagated upon Elastic Plates.

By Yasuo SATÔ,
Earthquake Research Institute. (Published 29 (1951), 223.)

Page	Line or expression			
224, 225		$\mathfrak{B}$	read	$\mathfrak{B}$
231, 246				
227	6 from bottom	(3.10)	〃	(3.9)
231	1	farely	〃	fairly
〃	Fig. 5	u/w	〃	w/u
237	(5.4)	u^*, w^*	〃	$\dot{u}^*, \dot{w}^*$
	(5.7)	$-\rho^*\partial\phi/\partial t$	〃	$+\rho^*\partial\phi/\partial t$
	5)	$\frac{\alpha}{h^2}B$	〃	$-ip\frac{\alpha}{h_2}B$
249	(8.4)	u	〃	u^*
250	(8.6), w	$\Big[\Big\{-\xi\zeta\Big(-1+\frac{1}{2}\gamma^2\Big)+$	〃	$\Big[-\xi\zeta\Big\{\Big(-1+\frac{1}{2}\gamma^2\Big)+$
		$\mathfrak{v}^2\Big(\frac{1}{4}-\frac{1}{6}\zeta^2\Big(-1+\frac{1}{2}\gamma^4\Big)\Big/\gamma^2\Big)$	〃	$\mathfrak{v}^2\Big(\frac{1}{4}-\frac{1}{6}\zeta^2\Big(-2+\frac{1}{2}\gamma^4\Big)\Big/\gamma^2\Big)$
221	last	the reverse of	〃	same with
253	Figs. 9, 10, 11	see below		
254	last, w	$-iH\xi^2\frac{1}{2\gamma^3}$	〃	$-iH\xi\frac{2}{\gamma^3}$
255	11	same with that of	〃	reverse to
	(8.21)	$\mathfrak{v}_0^2/(-4+3\gamma^2)$	〃	$\mathfrak{v}_0^2/V(-4+3\gamma^2)$
256	Figs. 13b, 14b	see below		

The upper part of Figs. 9, 10 and 11 must be replaced by the following figure.

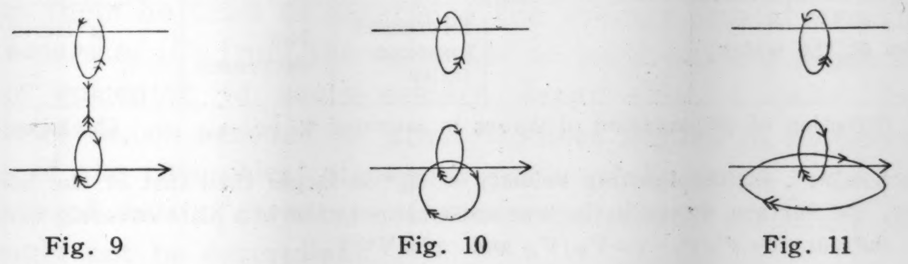

Fig. 9 Fig. 10 Fig. 11

And the upper part of Figs. 13b and 14b also must be corrected.

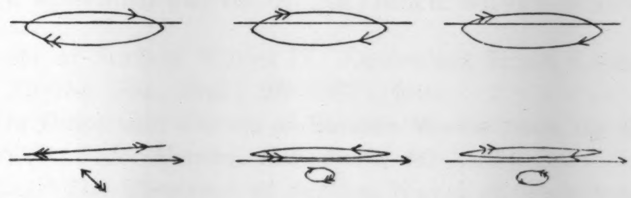

Fig. 13b Fig. 14a Fig. 14b

In the following table we will show the sense of rotation of particle orbit and the order of magnitude of displacement amplitude when the wave lengths are sufficiently long.

Π_0^- – branch

	(I) Plate	(II) Plate and infinitely deep water	(III) Plate and water with finite depth
Upper surface of the elastic plate	$u:w=O(\xi)$ ↺	$u:w=O(\xi)$ ↺	$u:w=O(\xi)$ ↺
Lower surface of the elastic plate	$u:w=O(\xi)$ ↻	$u:w=O(\xi)$ ↻	$u:w=O(\xi)$ ↻
Upper surface of the liquid		$u^*:w=O(1)$ $u^*:w=O(1)$ ↻	$u^*:w=O(1/\xi)$ $u^*:w=O(1)$ ↻
Bottom of the liquid		Decreases exponentially	$u^*:w=O(1/\xi)$ $w^*\ =0$ ⇄

Direction of propagation of waves is assumed to be →. ($\xi=2\pi$/wave length)

Π_0^+ – branch

	(I) Plate	(II) Plate and infinitely deep water		(III) Plate and water with finite depth	
		$\mathfrak{v}_0<\gamma^*$	$\mathfrak{v}_0>\gamma^*$	$\mathfrak{v}_0<\gamma^*$	$\mathfrak{v}_0>\gamma^*$
Upper surface of the elastic plate	$u:w=O(1/\xi)$ ↻	$u:w=O(1/\xi)$ ↻		$u:w=O(1/\xi)$ ↻	
Lower surface of the elastic plate	$u:w=O(1/\xi)$ ↺	$u:w=O(1/\xi^2)$ ↺	⇵	$u:w=O(1/\xi_3)$ ↺	↻
Upper surface of the water		$u^*:w$ (lower surface) $=O(1)$ $w^*:w\ =O(1)$ ↻	⇅	$u^*:w$ (lower surface) $=O(1)$ $w^*:w\ =O(1)$ ↻	↺
Bottom of the water		Decreases exponentially	Not decreases	$u^*:w=O(1)$ $w^*\ =0$ ⇄	

Direction of propagation of waves is assumed to be →. ($\xi=2\pi$/wave length)

When $\mathfrak{v}_0>\gamma^*$, or the limiting velocity of Π_0^+ is larger than that of the sound waves in water, the surface waves in the true sense cannot exist in a plate covering infinitely deep water. ($\mathfrak{v}_0^2=4(-1+\gamma^2)/\gamma^2$, $\gamma=V_P/V_S$ and $\gamma^*=V^*/V_S$.)

4. *Comparative Studies of Surface Waves Travelling Across Tibet Plateau and Sea of Japan, with Some Notes on the Method of Finding the Velocities of Surface Waves for a Limited Portion of their Path.*

By Tetsuo SANTO AKIMA,

Earthquake Research Institute.

(Read Oct. 26, 1954—Received Dec. 31, 1954.)

1. Introduction

The dispersion curve of seismic surface waves have often been utilized by many authors for determining the crustal structures in various regions of the world. Their works, however, have been done with the dispersion curves of only one of Love or Rayleigh wave. On the other hand, Y. Satô[1] made the important attention in his theoretical study that the crustal structure cannot be determined uniquely from the dispersion curve for one of these two waves alone.

Actual examples supporting Y. Satô's theoretical conclusion were shown for the first time by the present author[2]. On that occassion, the writer was able to obtain the dispersion curves of *both* Love and Rayleigh waves due to the great Assam Earthquake of August 15, 1950, and from them he tried to determine the average crustal structures of two regions, i.e. (C) from the epicenter to north-eastern Japan and (A) from the epicenter to south-western Japan (Fig. 1 (a)). In that paper, however, on account of great troubles needed in numerical calculations of the theoretical dispersion curve of Rayleigh waves for a double-layered crustal structure, the average crustal structure for (A) region could not be determined.

In 1953, N.A. Haskell[3] reduced a formula useful for numerical calculations of the dispersion curve of Rayleigh waves which travel across

1) Y. SATÔ, "Study of Surface Waves IV. Equivalent Single Layer to Double Superficial Layer." *Bull. Earthq. Res. Inst.*, **29** (1951), 519.

2) T. AKIMA, "On Dispersion Curves of Surface Waves from the Great Assam Earthquake of Aug. 15, 1950," *Bull. Earthq. Res. Inst.*, **30** (1952), 237.

3) N. A. HASKELL, "The Disperson of Surface Waves on Multilayered Media," *Bull. Seis. Soc. Amer.*, **43** (1953), 17.

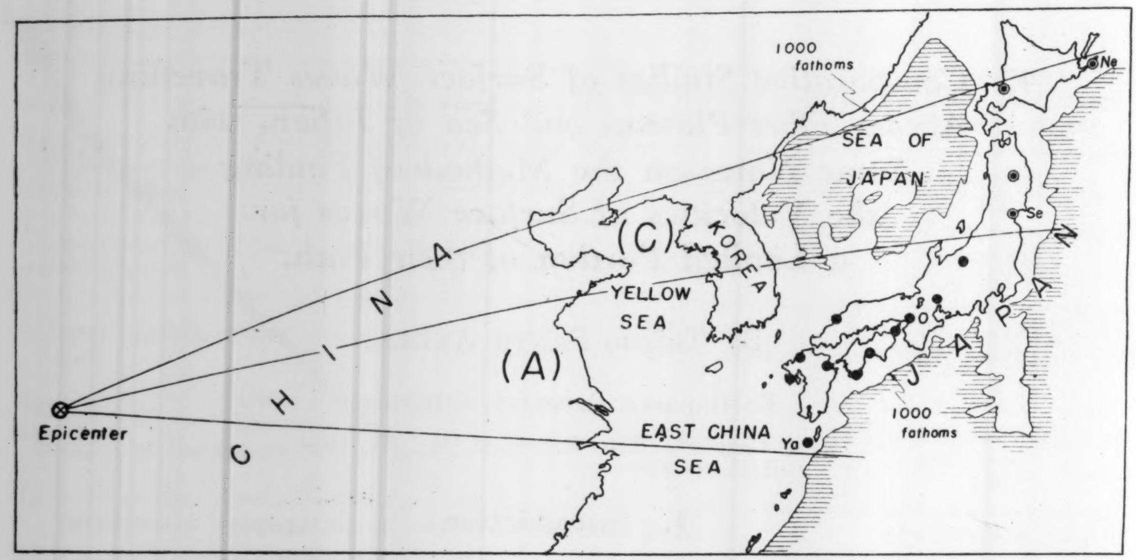

Fig. 1. (a)

Two regions (*A*) and (*C*) at Assam Great Earthquake.

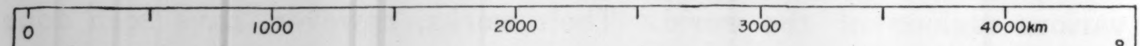

Fig. 1. (b)

Four topographical profiles for (*C*) and (*A*) regions.
Epicenter——Nemuro (marked "Ne" in Fig. 1(a)) } for (*C*) region.
Epicenter——Sendai (marked "Se" in Fig. 1(a)) }
Epicenter——Ôsaka (marked "O" in Fig. 1(a)) } for (*A*) region.
Epicenter——Yakusima (marked "Ya" in Fig. 1(a)) }
Vertical scale is 50 times as large as horizontal scale.

an n-layered crustal structure, and this formula somewhat lightened the labour of numerical calculations.

In the present paper, the writer is going to show the determined double-layered crustal structure for the above-stated (A) region applying N.A. Haskell's method at first. Secondly, another example will be added which will show that a crustal structure cannot be determined by observing only the dispersion curve of Love waves, and lastly, some notes will be given on the problem of computing the velocities of surface waves which travel across a limited portion of their path.

2. Supplements to the previous paper

It was shown in the previous paper that for (A) region, from Assam district to south-western Japan across East China Sea, a double-layered crustal structure had to be assumed[4]. In the double-layered crustal structure, β_1 and β_3, the velocities of shear waves in the uppermost and in the deepest layers respectively, can be approximately estimated from the tendencies of observed dispersion curves of both Love and Rayleigh waves. B_2, on the other hand, cannot be estimated in general from observed dispersion curves. For

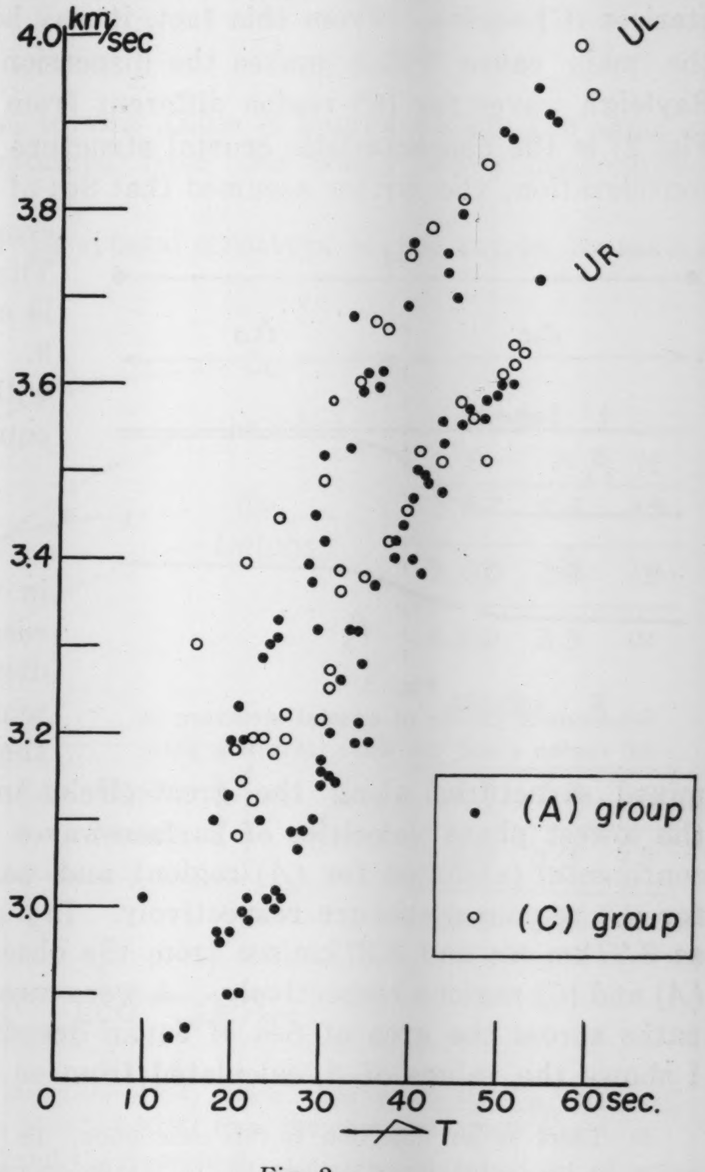

Fig. 2.
Two kinds of dispersion data for (A) and (C) regions respectively.

4) *loc. cit.*, 2)

this reason, the latter has been usually taken from data directly obtained by bodily wave observations. However, the writer here tries to estimate the value of β_2 purely from the observed surface waves data through the following considerations.

In Fig. 1(b), there are seen four topographical profiles: two for (*A*) and another two for (*C*) regions. Looking at these profiles, we find that the existence of Sea of Japan which is deep clearly characterizes (*C*) region. From this fact, it may be natural to consider that the main cause which makes the dispersion curves both of Love and Rayleigh waves for (*C*) region different from those for (*A*) region (See Fig. 2) is the characteristic crustal structure beneath this Sea. By this consideration, the writer assumed that Sea of Japan alone has "oceanic" crustal structure beneath it[5]. This assumed crustal structure is schematically shown in Fig. 3. On this assumption, β_2 will be found by the following equation,

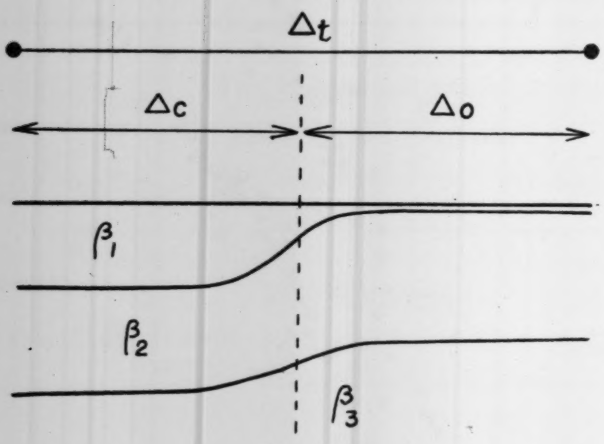

Fig. 3.
Schematical profile of crustal structure of (*C*) region along the wave-travelling path.

$$\frac{\Delta_c}{V_c}+\frac{\Delta_0}{\beta_2}=\frac{\Delta_t}{V_t} \qquad (1),$$

in which Δ_0, Δ_c and Δ_t mean respectively the travelling distances through the portions which are assumed to have the oceanic, continental and mixed structures along the great circles in (*C*) region. V_c, V_t mean the lowest phase velocities of surface waves which travel across purely continental (assumed for (*A*) region) and partly continental (assumed for (*C*) region) structure respectively. In our case, V_c and V_t are found as 3.27 km/sec and 3.37 km/sec from the observed dispersion curves for (*A*) and (*C*) regions respectively. Δ_0 were measured along the travelling paths across the area of Sea of Japan deeper than 100 fathoms. Table I shows the values of β_2 calculated from eq. (1).

5) There is an objection to this assumption. Dr. C. Tsuboi called attention to the writer by his recent investigations on the gravity anomalies throughout Japan that East China Sea, in spite of its shallowness, may have an "oceanic" crustal structure beneath it.

Therefore, the writer intends to make further investigations by collecting suitable dispersion data obtained at observatories in the south-eastern part of China.

Table I

Obs. positions	Δ_c	Δ_0	Δ_t	β_2	$k(=\Delta_t/\Delta_c)$
Morioka	3335 km	940 km	4275 km	3.76 km/sec	1.28
Sendai	3420	830	4250	3.86	1.25
Sapporo	3430	900	4330	3.82	1.26
Nemuro	3770	900	4670	3.83	1.24
mean				3.82	1.26

The mean value of β_2 in this Table is approximately the same as 3.79 km/sec which was obtained from the bodily wave observations made by E. Rozova[6].

The writer determined the crustal structure of (*A*) region by taking

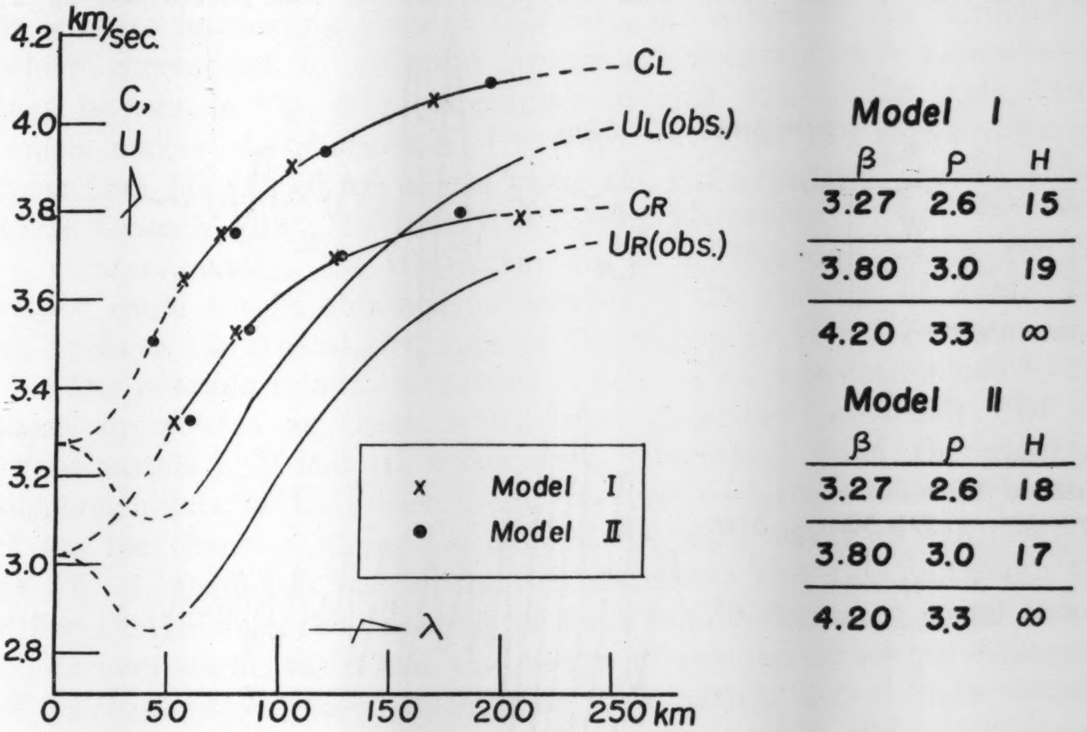

Fig. 4.

Determination for crustal structure of (*A*) region. Curves C_L and C_R were obtained by the formula $U=C-\lambda\, dC/d\lambda$ from the observed curves U_L and U_R respectively.

6) E. Rozova, "Construction of Travel-Time Curves and Determination of Principal Seismic Elements for Central Asia," *Seismol. Inst. Acad. Sci. U.S.S.R. Pub.*, No. **72** (1936), 1.

the value of β_2 as 3.80 km/sec[7] through the following procedures. From the observed dispersion curve for the group velocities U of Love waves, the dispersion curve for the phase velocities C is found with the aid of the well-known formula $U=C-\lambda dC/d\lambda$. Comparing this $C\sim\lambda$ curve with the theoretical ones which are calculated from the characteristic equation of Love waves for double-layered crustal structure, the two models I and II in Fig. 4 were obtained. Of these two models, however, model I was adopted as a suitable one because it fits the $C\sim\lambda$ curve for Rayleigh waves which was calculated from the observed dispersion curve of Rayleigh waves by means of Haskell's method. The practical procedures of calculations which was adopted by the writer in finding the $C\sim\lambda$ curve for Rayleigh waves are described in the Appendix.

The second work to determine the crustal structure by the dispersion curves of *both* Love and Rayleigh waves was performed by T.

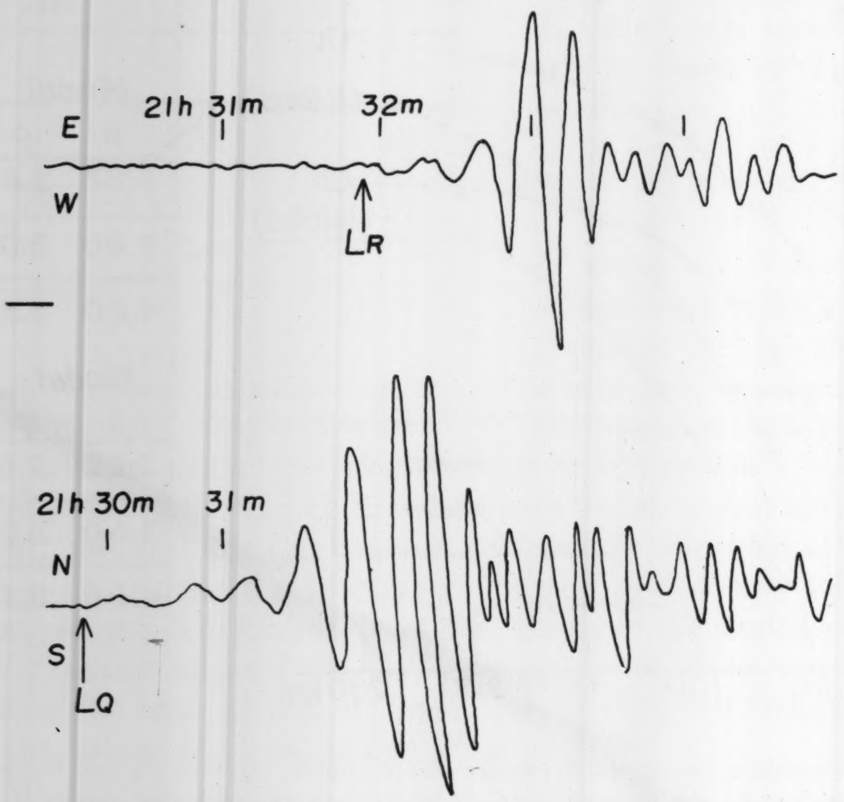

Fig. 5.
An example of seismograms obtained at Matusiro Seismological Observatory.

7) The writer's previous results of determining the double-layered crustal structure of (A) region by taking $\beta_2=3.4$ km/sec (*loc. cit.* 2)) must be corrected.

Nagamune of Matusiro Seismological Observatory. The epicenters and the dates of the seven earthquakes he used are shown in Table II. Fig. 5 shows an example of the seismograms being recorded by the long period seismograph ($T_0 \doteqdot 36$ sec, $V \doteqdot 100$). As the epicenters of these earthquakes were all located to the west of Matusiro Observatory, Love and Rayleigh waves were, as shown by this example, recorded distinctly in the NS and EW components of the seismograms respectively.

Table II

No.	Epicenters	Dates
1	Szchwan Province	Nov. 30, 1952
2	Yunnan	Dec. 21, 1951
3	〃	June 18, 1952
4	Assam	Aug. 15, 1950
5	Eastern Tibet	Aug. 18, 1952
6	〃	Nov. 18, 1951
7	Central Pakistan	Oct. 11, 1952

Re-examining the dispersion data obtained by Nagamune, the writer found that they may also be classified into two groups (See Fig. 6(a)). It is quite interesting that, in this case, epicenters of the earthquakes which correspond to different groups are geographically separated as may be seen in Fig. 6(b). According to this figure, the main cause which makes the dispersion of surface waves for (D) region different from that for (E) region seems to be the characteristic crustal structures beneath Tibet, Tsinghai and Sikang plateaus.

Unfortunately, the dispersion curve of Rayleigh waves for (E) region could not be obtained on account of the scarcity of data. For this reason, the crustal structure of this region could not be determind.

The average crustal structure of (D) region was determined by the same procedures as those which were described previously. Of the three models I, II and III which were determined from the observed dispersion data of Love waves, only the last model was adopted because it fits the observed dispersion data of Rayleigh waves as well (Fig. 7). In Fig. 7, there can be seen another noticeable fact that, although the difference between the thickness of their middle layers of model II and III is very slight, say 1 km, the results of calculation for the dispersion of Rayleigh waves based upon these two models differ quite widely. This means that the dispersion of Rayleigh waves is quite sensitive to the underground crustal structure.

4. Some notes on presuming the velocities of surface waves for a limited portion of their path.

In the study of surface wave dispersions due to the great Assam

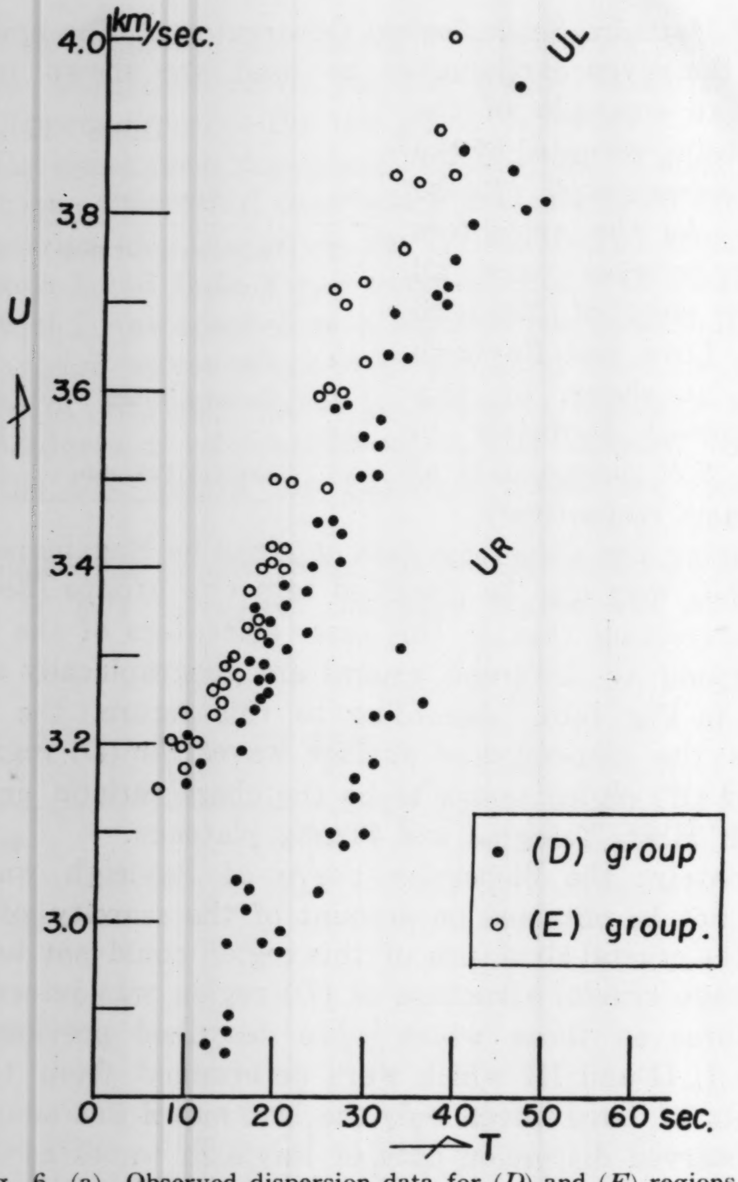

Fig. 6. (a) Observed dispersion data for (D) and (E) regions.

Earthquake, we may make another approach as follows. If we suppose that the characteristic crustal structure beneath the Sea of Japan is the main cause which makes the dispersion curves both of Love and Rayleigh waves for (C) region different from those for (A) region[8], the velocities V_0 of surface wave which travels across the characteristic part in (C) region can be obtained by the following procedures.

Replacing β_2 in eq. (1) by V_0, we obtain the expression of V_0 as follows:

8) Dr. C. Tsuboi's view referred to in the foot-note 4) has no effect upon the general conclusions of this section.

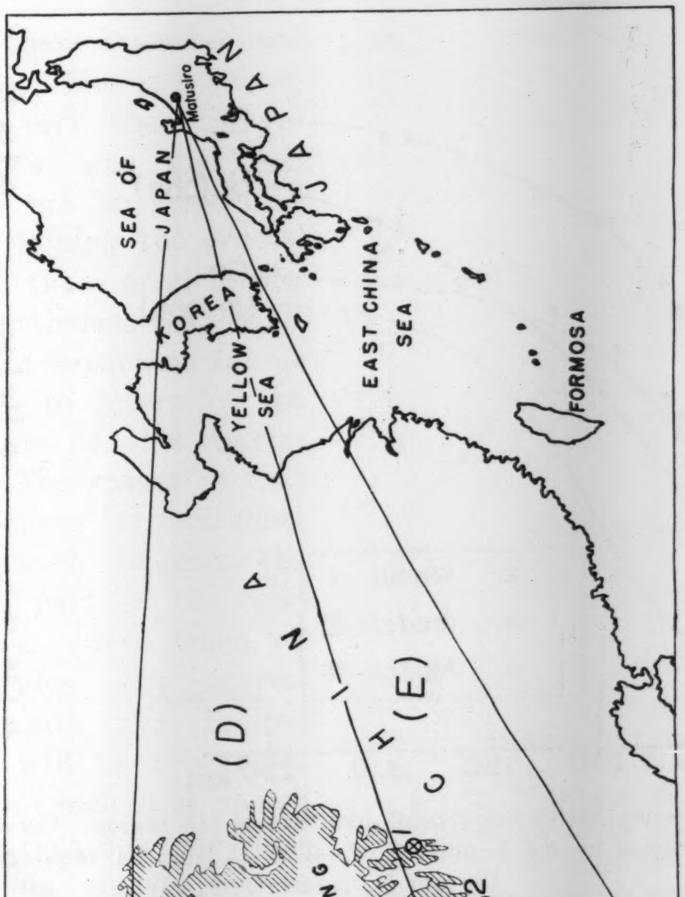

Fig. 6. (b) Two regions (*D*) and (*E*).

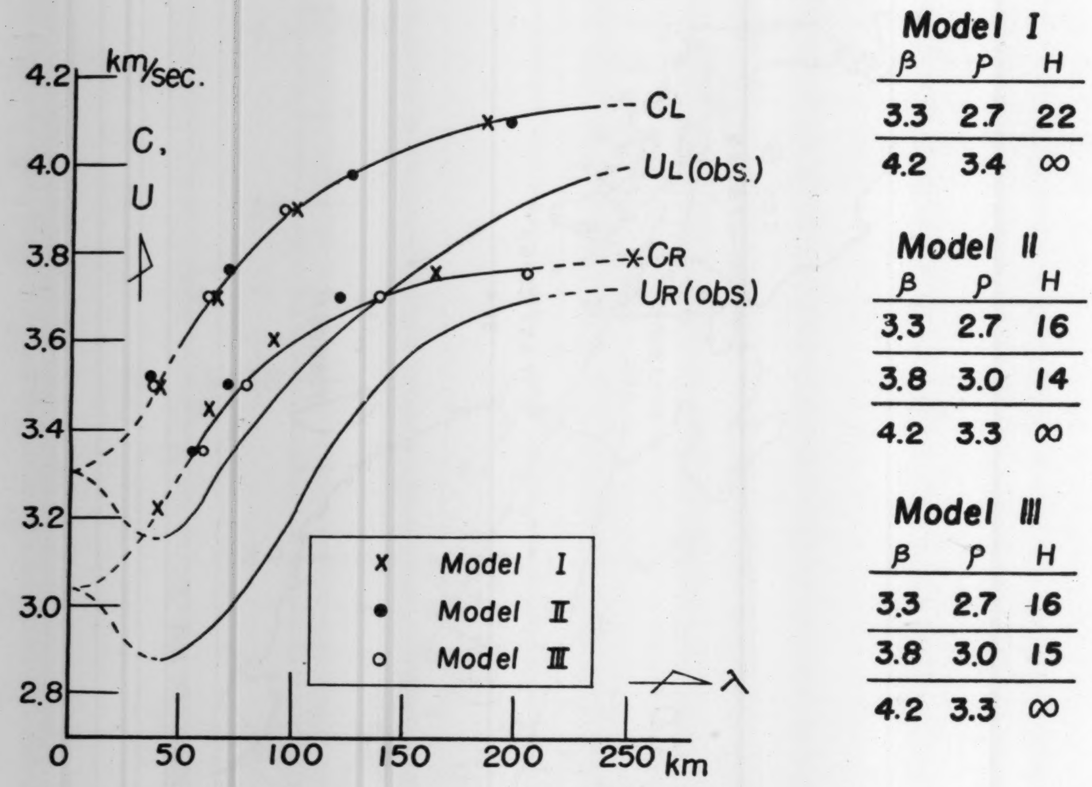

Fig. 7. Determination of the crustal structure of (*D*) region. Curves C_L and C_R were obtained by the formula $U=C-\lambda\, dC/d\lambda$ from the observed curves U_L and U_R respectively.

$$V_0=\frac{(k-1)V_c(V_c+\varDelta v)}{(k-1)V_c-\varDelta v} \qquad (2),$$

in which $k=\varDelta_t/\varDelta_c$ and $\varDelta v=V_t-V_c$.

In our case, k was calculated as 1.26 as the mean value for the four observational stations which belong to (*C*) region (See Table II). From eq. (2), value of V_0 which corresponds to each period was computed using the two dispersion curves of Love waves for (*A*) and (*C*) regions. The results are plotted by filled circles in Fig. 8, from which a demanded dispersion curve of Love waves for a characteristic part in (*C*) region was to be found.

There was, however, a difficulty in drawing this curve. In the two original dispersion curves (*A*) and (*C*) in Fig. 8, those for short wave-length branches ($\lambda\lesssim$55 km in our case) were, on account of the lack of observational data for these short wave-length surface waves, only drawn from the tendencies of those for long wave-length branches ($\lambda\gtrsim$55 km). In other words, the calculated values of V_0 based upon

the curves of these branches are quite uncertain. The lack of observation for very short wave-length branches was and has generally been not so important for us in determining the crustal structure from these original dispersion curves themselves. But, it becomes quite important for us if we are going to determine the crustal structure of this characteristic part. The reason is that the dispersion curve for such short wave-length branch becomes the most effective part of the computed dispersion curve when we try to determine the crustal structure beneath the limited portion. This will be recognized from Fig. 8, in which it is shown with dotted curves how the computed dispersion curve moves greatly in its most effective part by a slight change in the difference of the original two dispersion curves in their short wave-length branches. This fact tells us that in this case the lack of observational dispersion data in short wave-length branch at the left of the minimum group velocity becomes fatal when we wish to obtain a new dispersion curve for a characteristic part accurately enough to make the determination for the crustal structure of this part.

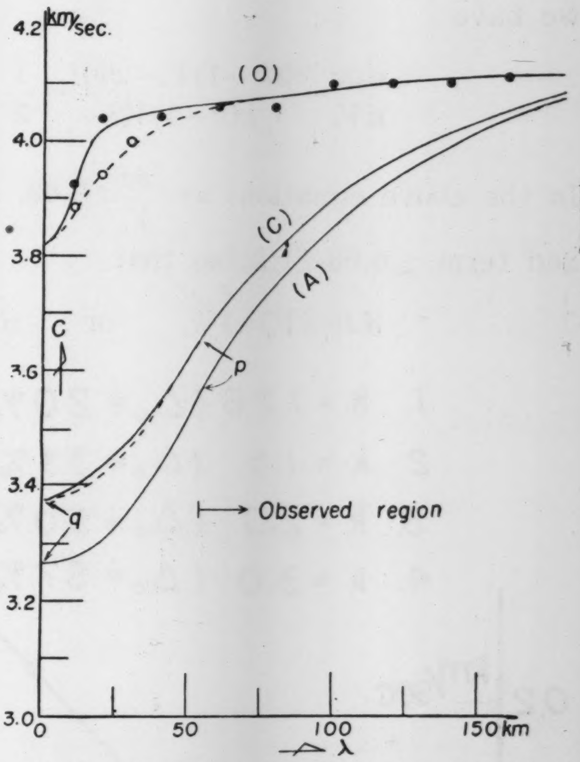

Fig. 8. Computed dispersion data (O) of Love waves for a characteristic part (Sea of Japan) from the two dispersion curves (A) and (C). If one of the original curves (C) changes slightly as is shown by a dotted curve in short period branch, for instance, the computed dispertion data move greatly as is shown by hollow circles.

These circumstances can be quantitatively indicated by numerical calculations as follows.

From eq. (2), we get

$$dV_0 = \frac{k(k-1)V_c^2}{\{(k-1)V_c - \Delta v\}^2} \cdot d\Delta v \qquad (3).$$

The relations between dV_0 and $d\Delta v$ calculated for several values of k by this equation are shown in Fig. 9. The effects of V_0 and Δv in eq. (3) upon these relations are negligible in our case at least. For, from eq. (3),

we have

$$\frac{d\Delta v}{dV_0}=\frac{\{(k-1)V_c-\Delta v\}^2}{k(k-1)V_c^2}=\frac{1}{k}-\frac{2}{k}\frac{\Delta v}{V_c}+\frac{1}{k(k-1)}\left(\frac{\Delta v}{V_c}\right).$$

In the above equation, as $\frac{\Delta v}{V_c}<0.03$, the last term is negligible and the 2nd term $\lesssim 0.03 \ll 1/k$, so that

$$d\Delta v/dV_0 \doteqdot 1/k, \qquad \text{or} \qquad dV_0/d\Delta v \doteqdot k \tag{4}$$

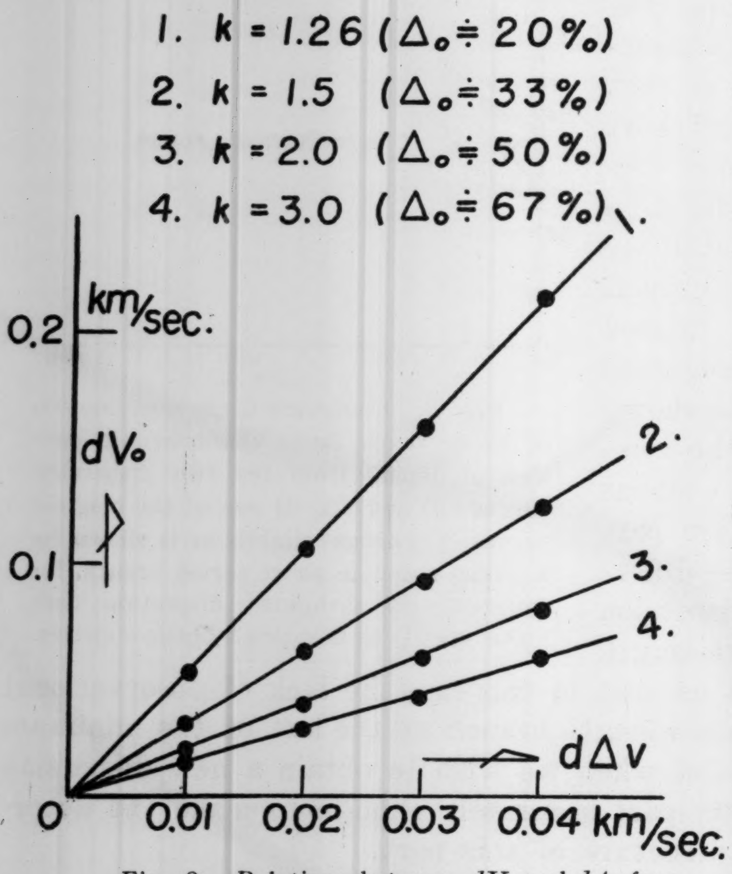

Fig. 9. Relations between dV_0 and $d\Delta v$ for several values of k.

Slopes of each curves approximately satisfy the relation $dV_0/d\Delta v=k$.

Series of filled circles with each value of k in Fig. 9 which were calculated from eq. (3), approximately satisfy the equation reduced above. Approximate equation (4) will be satisfied in general cases.

The result given above tells us that when we wish to obtain the dispersion curve which is accurate enough to be used for the determination of the crustal structure of a limited portion by computing from the two observed dispersion curves, the latter must have an accuracy inversely proportional to k. In Fig. 9, for instance, when $k=3.0$, i.e., when the characteristic part occupies approximately 67% of the total path length, errors within ± 0.04 km/sec are allowed for $d\Delta v$, but when $k=1.5$, i.e., when the characteristic part occupies approximately only 33% of the total path length, the allowed errors of $d\Delta v$ are narrowed to within ± 0.02 km/sec, if we want to keep dV_0 within ± 0.06 km/sec.

5. Conclusions

Through several investigations concerning the relation between the observed dispersion curves of seismic surface waves and the underground crustal structure, the essentials the writer would like to emphasize in this paper may be summarised as follows.

1) Some practical examples were added to the previous paper which show that the crustal structure determined only from the observed dispersion curve of Love waves cannot often satisfy the observed dispersion curve of Rayleigh waves.

2) The dispersion curves of surface waves, especially those of Rayleigh waves is quite sensitive to the underground crustal structure.

3) When we wish to compute with sufficient accuracy the velocities of surface waves which travel across a limited portion from the two dispersion curves observed for the total and for the remainder part, we must obtain the original dispersion data which have the accuracies inversely proportional to the ratio of the wave travelling path lengthes of the total and of the remainder part.

4) When the original two dispersion curves show the tendency to be separated from each other in their short period branches, observations of reverse dispersion data for very short period branches at the left of minimum group velocity[9] is quite necessary for us in performing the work mentioned here.

5) Judging from the articles 2) and 3) described above, the method of computing a dispersion curve for a limited portion from the two observed dispersion curves should not be taken, except when the limited portion occupies approximately more than two-third of the whole length of the wave travelling path.

6. Acknowledgments

In conclusion, the writer wishes to express his hearty thanks to Mr. S. Miyamura and to Mr. Y. Satô who gave him many advices in

9) In explosion seismology, L. G. Howell, etc. have recently succeeded in observing the dispersion data for this branch. cf.

L. G. HOWELL, E. F. NEUENSCHWANDER, A. L. PIERSON, "Gulf Coast Surface Waves," *Geophysics*, **18** (1953), 41.

M. B. DOBRIN, P. L. LAWRENCE and R. L. SENGBUSH, "Surface and Near-Surface Waves in the Delaware Basin," *Geophysics*, **19** (1954), 695.

But, for natural seismic waves due to continental earthquakes, no one has yet observed the dispersion data for this branch.

the course of his present works. The writer's sincere thanks are also due to Mr. T. Nagamune who placed his valuable data at the writer's disposal.

The expense of the present study was defrayed from the Grant in Aid of Miscellaneous Scientific Researches from the Department of Education.

Appendix

The practical procedures of finding a dispersion curve of Rayleigh waves assuming a double-layered crustal structure.

N. A. Haskell's method can be applied in general for finding a dispersion curve of Rayleigh waves which travel across the n-horizontally-layered structure. In practice, however, the calculations of the case when $n=3$ is most useful.

Here, the writer is going to show the practical procedures which was taken in this paper by referring to Haskell's formula.

Let us compute at first the following two values under a certain value of $k(=2\pi/\lambda)$.

$$\left.\begin{aligned} P_m &= k\gamma_{\alpha m}h_m \\ Q_m &= k\gamma_{\beta m}h_m \end{aligned}\right\}(m=1,\ 2)\ ,$$

where $k=2\pi/\lambda$

and

$$\gamma_{\alpha m}=\begin{cases} +[(c/\alpha_m)^2-1]^{1/2}, & \text{when } c>\alpha_m \\ -i[1-(c/\alpha_m)^2]^{1/2}, & \text{when } c<\alpha_m\ , \end{cases}$$

$$\gamma_{\beta m}=\begin{cases} +[(c/\beta_m)^2-1]^{1/2}, & \text{when } c>\beta_m \\ -i[1-(c/\beta_m)^2]^{1/2}, & \text{when } c<\beta_m\ , \end{cases}$$

α_1,	β_1,	ρ_1	h_1
α_2,	β_2,	ρ_2	h_2
α_3,	β_3,	ρ_3	

α : velocity of P-waves
β : velocity of S-waves
ρ : density

in which, λ and c are the wave-length and the phase velocity of Rayleigh waves.

Using these two values, we then computed the followings.

$$(a_m)_{11}=(a_m)_{44}=r_m\cos P_m-(r_m-1)\cos Q_m\ ,$$

$$(a_m)_{12}=(a_m)_{34}=i[(r_m-1)\gamma_{\alpha m}{}^{-1}\sin P_m+r_m\gamma_{\beta m}\sin Q_m]\ ,$$

$$(a_m)_{13}=(a_m)_{24}=-(\rho_m c^2)^{-1}(\cos P_m-\cos Q_m)\ ,$$

$$(a_m)_{14}=i(\rho_m c^2)^{-1}(\gamma_{\alpha m}{}^{-1}\sin P_m+\gamma_{\beta m}\sin Q_m)\ ,$$

$$(a_m)_{21}=(a_m)_{43}=-i[r_m\gamma_{\alpha m}\sin P_m+(r_m-1)\gamma_{\beta m}{}^{-1}\sin Q_m]\ ,$$

$$(a_m)_{22}=(a_m)_{33}=-(r_m-1)\cos P_m+r_m\cos Q_m\ ,$$
$$(a_m)_{23}=i(\rho_m c^2)^{-1}(\gamma_{\alpha m}\sin P_m+\gamma_{\beta m}{}^{-1}\sin Q_m)\ ,$$
$$(a_m)_{31}=(a_m)_{42}=\rho_m c^2 r_m(r_m-1)(\cos P_m-\cos Q_m)\ ,$$
$$(a_m)_{32}=i\rho_m c^2[(r_m-1)^2\gamma_{\alpha m}{}^{-1}\sin P_m+r_m{}^2\gamma_{\beta m}\sin Q_m]\ ,$$
$$(a_m)_{41}=i\rho_m c^2[r_m{}^2\gamma_{\alpha m}\sin P_m+(r_m-1)^2\gamma_{\beta m}{}^{-1}\sin Q_m]\ ,$$
$$(m=1,\ 2,\ 3)$$

where $r_m=2(\rho_m/c)^2$.

Thirdly,

$$A_{11}=(a_2)_{11}(a_1)_{11}+(a_2)_{12}(a_1)_{21}+(a_2)_{13}(a_1)_{31}+(a_2)_{14}(a_1)_{41}\ ,$$
$$A_{12}=(a_2)_{11}(a_1)_{12}+(a_2)_{12}(a_1)_{22}+(a_2)_{13}(a_1)_{31}+(a_2)_{14}(a_1)_{42}\ ,$$
$$A_{21}=(a_2)_{21}(a_1)_{11}+(a_2)_{22}(a_1)_{21}+(a_2)_{23}(a_1)_{31}+(a_2)_{24}(a_1)_{41}\ ,$$
$$A_{31}=(a_2)_{31}(a_1)_{11}+(a_2)_{32}(a_1)_{21}+(a_2)_{33}(a_1)_{31}+(a_2)_{34}(a_1)_{41}\ ,$$
$$A_{41}=(a_2)_{41}(a_1)_{11}+(a_2)_{42}(a_1)_{21}+(a_2)_{43}(a_1)_{31}+(a_2)_{44}(a_1)_{41}\ ,$$
$$A_{42}=(a_2)_{41}(a_1)_{12}+(a_2)_{42}(a_1)_{22}+(a_2)_{43}(a_1)_{43}+(a_2)_{44}(a_1)_{42}\ ,$$

and finally

$$K=r_m\gamma_{\alpha m}A_{12}+(r_m-1)A_{22}-\gamma_{\alpha m}A_{32}/\rho_m c^2+A_{42}/\rho_m c^2\ ,$$
$$L=r_m\gamma_{\alpha m}A_{11}+(r_m-1)A_{21}-\gamma_{\alpha m}A_{31}/\rho_m c^2+A_{41}/\rho_m c^2\ ,$$
$$M=-(r_m-1)A_{12}+r_m\gamma_{\beta m}A_{22}+A_{32}/\rho_m c^2+\gamma_{\beta m}A_{42}/\rho_m c^2\ ,$$
$$N=-(r_m-1)A_{11}+r_m\gamma_{\beta m}A_{21}+A_{31}/\rho_m c^2+\gamma_{\beta m}A_{41}/\rho_m c^2\ ,$$

are successively calculated.

The final purpose is to find a suitable pair of h_1 and h_2 which satisfy the following equation

$$K/L=M/N$$

by the trial and error method.

---

4. チベット高原と日本海を通過する表面波について，及びある限られた地域を通過する表面波の速度を計算で見出す場合の二，三の注意

地震研究所 三東哲夫（旧姓秋間）

アジア大陸の南部に起つた七ツの地震を気象台の松代観測所でとつた記象から，表面波の分散を調べてみると，チベット高原の根の影響と思われるものがはつきり見られた．このことは，前のアッサム大地震による表面波の分散を調べた時に，日本海の海洋的地下構造の影響とみられるものが認められたのと同じく，注目すべきことと思われる．

今度の場合にも，ラヴ波の分散からきめた地殻構造は，必ずしもレーリー波のそれとは一致しない．それで，表面波の分散の観測から地殻構造を推定するのには，どうしてもラヴ波とレーリー波の両方の分散を観測することが必要である．

次に，一般に表面波の伝播経路の中に例えば，a, b という相異つた二種の地殻構造が予想される区域があり，その中で例えば a だけに関する表面波の分散曲線と，$(a+b)$ のそれとが観測で求められて，この二つから残りの b, と云う区域に関する表面波の分散曲線を計算で出して，それにより b の地殻構造を推定しよう，と云う場合が時に起る．著者は，日本海の地下構造をこの様な方法で求めてみようと思つてやりかけたところ，この様な方法をとる場合に一般に注意しなければならない二，三の点を見出した．それは，今この $(a+b)$ 及び a の経路の長さの比を k で表わすと，

1) 求める b 地域に関する分散曲線の精度を，それによつてそこの地殻構造が十分推定されうる程度にするためには，その計算の基になる $(a+b)$ 及び a 地域の分散曲線の観測精度を，この k に比例して高めなければならないこと．

   例えば，$k=(a+b)/a=2$ つまり，表面波の分散未知の地域が全体の半分位含まれている場合には，a と $(a+b)$ についての表面波の分散の観測には，いつもの倍位の精度が要求されてくる訳である．

2) 基になる a 及び $(a+b)$ 地域に関する分散曲線が短周期の部分程互いに離れてくる様な傾向にある場合には，前記の目的のためには，之等の二つの分散曲線は，所謂「エアリー波」に相当する部分よりも周期の短い，逆分散を示す範囲迄観測されなければならないこと．

3) 之とは逆に，二つの曲線が長周期の部分で分れている時には，かなり長周期の部分迄観測されなければならないこと．

等である．

之等の点，特に 1) 及び表面波の分散が予期以上に地殻構造に敏感である点を考えると．分散未知の地域が全体の 1/3 以内である場合を除いては，二つの分散曲線から計算で未知地域のそれを出す，と云うやり方はとるべきではない．

5. *Elasticity of Marble with Special Reference to its Elastic Aeolotropy.*

By Daisuke SHIMOZURU and Isamu MURAI,

Earthquake Research Institute.

(Read Oct. 26, 1954,—Received Dec. 30, 1954.)

Introduction.

It is a well known fact that rock apparently of the same kind has considerably different velocities of propagation of elastic waves at the laboratory measurements. For example, the velocities of longitudinal waves in hard limestone are scattered within the range of 2.8 km/sec and 6.4 km/sec[1]. Rocks of other kinds also show the scattering of velocity within a considerable range. Several possible causes may be enumerated for this experimental facts. Among them, elastic aeolotropy is perhaps the most important one. If a rock specimen is aeolotropic, the velocity of elastic waves will naturally change according to the direction of propagation, and hence the fluctuation in the observed values of elastic wave velocity of the rock will occur, if the direction is not specified.

In this paper, the velocities of dilatational and rotational waves for three directions, perpendicular to each other, of cubic samples of the marble are compared and the aeolotropy is discussed taking into consideration the petrofabric analysis of the samples. Theoretical treatment on the elasticity of marble is also described.

Experimental Procedure.

Ultrasonic pulse apparatus were used for the determination of the velocities of elastic waves in the specimen. The equipment has been the same with that described in a previous paper[2] except for some little modifications. A block diagram of the apparatus is presented in Fig. 1. Trigger pulses are delayed about 10 microseconds by a variable delay line, then amplified by the pulse amplifier, and are impressed on the driving quartz crystal. The signal, transmitted through the specimen and received by a similar crystal, is amplified and displayed on the

1) F. BIRCH, *Handbook of Physical Constants*, 1942.
2) D. SHIMOZURU, *Bull. Earthq. Res. Inst.*, **32**, (1954), 271.

screen of a cathode ray oscilloscope. The sweep of oscilloscope, accurately synchronized with the trigger pulse, was adjusted to have a 100 microsecond duration. Time marks are displayed at every 2.5 microseconds.

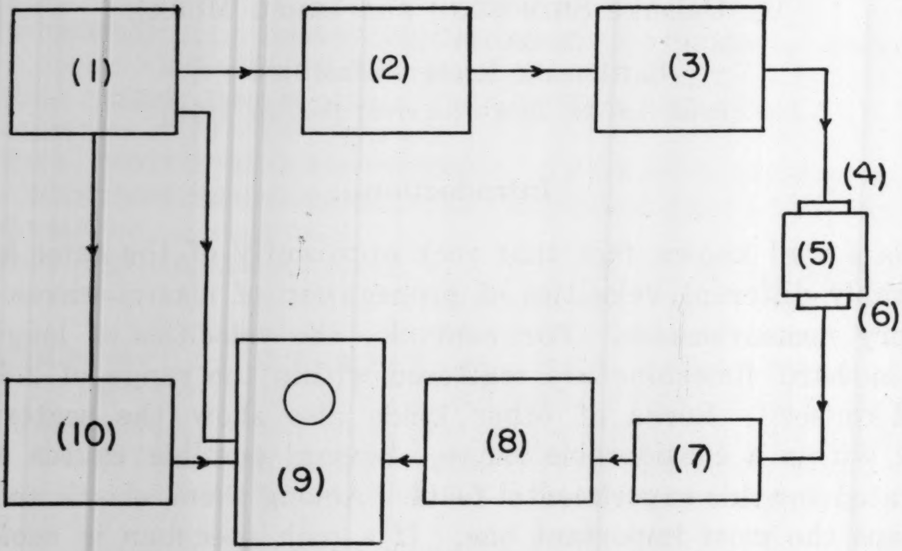

Fig. 1. Block diagram of the apparatus. (1) Main trigger pulse, (2) Variable delay line, (3) Pulse amplifier, (4) Driving crystal, (5) Secimen, (6) Receiving crystal, (7) Preamplifier, (8) Amplifier, (6) Cathode ray oscilloscope, (10) Time marker.

Each tested sample is cut into a cube of about 5 cm in one edge length. Velocities were measured along the three rectangular edges of each cubic specimen. These samples of marble were placed at the author's disposal by the kindness of Mr. T. Yabashi. These sapmles are tabulated in Table I.

Table I.

Specimen No.	Description	Origin	Commercial Name
I.	Marble	Yamaguchi Pref.	Usukumo-shirate
II.	〃	〃	Kozakura
III.	〃	〃	Mizutani
IV.	〃	Kochi Pref.	Akebono
V.	Limestone	Gifu Pref.	
VI.	〃	〃	

Experimental Results.

For determining the velocities of dilatational and rotational elastic

waves, both of the X-cut and Y-cat quartz crystals were used. Table II gives the respective values of the dilatational and rotational waves. Each specimen has six values corresponding to the combination of three directions and two sorts of elastic waves. The velocities given in the same row of the table correspond to the velocities for the same directions.

Table II.

Specimen No.	$V_p(m)$	$V_s(m)$
I	5530	3150
	5550	3200
	5390	3100
II	5450	3070
	5410	3050
	5350	3010
III	5070	2770
	5320	2810
	5390	2790
IV	5490	3250
	5470	3210
	5440	3180
V	5730	3270
	5730	3240
	5720	3250
VI	5870	3190
	5850	3200
	5860	3200

Theoretical Calculation of the Elasticity of Marble.

We will calculate the theoretically expectable value of the elasticity of marble on the assumption that marble is polycrystalline aggregate of calcite only and that the grain boundary of each crystal does not have any effect on the elasticity. Calcite is a trigonal group of the hexagonal system. So taking the axis of symmetry as z-axis, we find the strain energy function to be

$$2W=\frac{1}{2}C_{11}e_{xx}^2+C_{12}e_{xx}e_{yy}+C_{13}e_{xx}e_{zz}+C_{14}e_{xx}e_{yz}$$
$$+\frac{1}{2}C_{11}e_{yy}^2+C_{13}e_{yy}e_{zz}-C_{14}e_{yy}e_{yz}$$
$$+\frac{1}{2}C_{33}e_{zz}^2+\frac{1}{2}C_{44}e_{yz}^2+\frac{1}{2}e_{zx}^2+\frac{1}{4}(C_{11}-C_{12})e_{xy}^2 .$$

The elastic moduli of a number of minerals have been determined by W. Voigt by the twisting and bending experiments of crystal rods. According to him[3], the elastic moduli of calcite are

$$S_{11}=11.141\times10^{-10}, \quad S_{33}=17.131\times10^{-10}, \quad S_{44}=39.521\times10^{-10},$$
$$S_{12}=-3.671\times10^{-10}, \quad S_{13}=-4.241\times10^{-10}, \quad S_{14}=8.98\times10^{-10}.$$

These moduli are expressed in units of gram weight per square centimeter. Elastic constants and elastic moduli are connected with the following relations in the case of trigonal group.

3) W. VOIGT, *Abhandlungen über Elasticität.*
〃 , *Lehrbuch der Kristallphysik.* Leipzig, 1928.

$$C_{11}+C_{12}=\frac{S_{33}}{S}\,,\qquad C_{11}-C_{12}=\frac{S_{44}}{S'}\,,\qquad C_{13}=\frac{-S_{13}}{S'}\,,\qquad C_{14}=\frac{-S_{14}}{S'}\,,$$

$$C_{33}=\frac{S_{11}+S_{12}}{S}\,,\qquad C_{44}=\frac{S_{11}-S_{12}}{S'}\,;$$

where $$S=S_{33}(S_{11}+S_{12})-2S_{13}^2\,,$$
and $$S'=S_{44}(S_{11}-S_{12})-2S_{14}^2\,.$$

Therefore, the six elastic constants of calcite come to be

$C_{11}=13.97\times10^8$ gr. , $C_{33}=8.12\times10^8$ gr. , $C_{44}=3.49\times10^8$ gr. ,
$C_{12}=4.65\times10^8$ gr. , $C_{13}=4.60\times10^8$ gr. , $C_{14}=-2.12\times10^8$ gr. .

These elastic constants are isothermal values since they have been determined from the bending and twisting experiments of statical method of the crystal rods.

We must therefore derive the adiabatic elastic constants as we aim at the comparison of the theoretical value with our experimentally obtained results.

In general, the relation between the adiabatic elastic constants and the isothermal one is expressed as follows ;

$$\hat{C}_{hk}=C_{hk}+\frac{\theta q_h q_k}{\rho J C_v}\,,\qquad h=1,\,2,\,3, \tag{1}$$

where,
$\hat{C}_{hk}$ ...... adiabatic elastic constant,
C_{hk} ...... isothermal elastic constant,
θ ...... absolute temperature,
q_k ...... $\sum_h a_h C_{hk}$,
a_{kh} ...... coefficient of linear thermal expansion,
ρ ...... density,
J ...... mechanical equivalent of heat,
C_v ...... specific heat of constant volume.

In the case of hexagonal system, the following relations hold,

$$\left.\begin{aligned} q_1=q_2&=a_1(C_{11}+C_{12})+a_3C_{13}\\ q_3&=2a_1C_{13}+a_3C_{33}\end{aligned}\right\}, \tag{2}$$

and

$$\left.\begin{aligned} &\hat{C}_{11}-C_{11}=\hat{C}_{12}-C_{12}=\frac{\theta q_1^2}{\rho JC_v}\,,\quad \hat{C}_{44}-C_{44}=0\,,\quad \hat{C}_{13}-C_{13}=\frac{\theta q_1 q_3}{\rho JC_v}\,,\\ &\hat{C}_{33}-C_{33}=\frac{\theta q_3^2}{\rho JC_v}\,,\qquad \hat{C}_{14}-C_{14}=0\,.\end{aligned}\right\} \tag{3}$$

In the present case, the following values are assumed,

$$\rho=2.715\ \text{gr/cm}^3\,,\quad \theta=293^\circ\,,\quad a_1=-5.65\times10^{-6}\,,$$
$$a_3=25.26\times10^{-6}\,,\quad J=4.19\times10^7\ \text{erg/cal}\,,\quad C_p=0.175\,.$$

As the difference between the values of C_v and C_p is small, the value of C_p is used instead of C_v. Inserting the above quantities into equations (2) and (3), we obtain the adiabatic elastic constants of calcite as follows:

$$\left.\begin{aligned}&\hat{C}_{11}=13.69\times10^{11}\,,\quad \hat{C}_{33}=7.99\times10^{11},\quad \hat{C}_{44}=3.42\times10^{11}\,,\\&\hat{C}_{12}=4.56\times10^{11}\,,\quad \hat{C}_{13}=4.51\times10^{11},\quad \hat{C}_{14}=-2.08\times10^{11}\,.\end{aligned}\right\}\qquad(4)$$

These constants are expressed in units of dynes per square centimetre.

Next, we consider the longitudinal and transversal elastic constants of calcite for any direction. Taking $l_1, m_1, n_1, \ldots, n_3$ to be the direction consines between the arbitrary directed coordinate axes $x'y'z'$ and the x-y-z-axis fixed to the crystal, as given below, the longitudinal elastic constant in the direction of x' which corresponds to $(\lambda+2\mu)$ for an isotropic medium comes to be

	x	y	z
x'	l_1	m_1	n_1
y'	l_2	m_2	n_2
z'	l_3	m_3	n_3 ,

$$\begin{aligned}\tilde{C}_{11}=&\hat{C}_{11}(l_1^2+m_1^2)^2+\hat{C}_{33}n_1^4+2(\hat{C}_{13}+2\hat{C}_{44})n_1^2(l_1^2+m_1^2)\\&+4C_{14}m_1n_1(3l_1^2-m_1^2)\,.\end{aligned}\qquad(5)$$

Transversal elastic constant, wich corresponds to μ for an isotropic medium, is expressed as follows,

$$\begin{aligned}\tilde{C}_{44}=&\hat{C}_{11}\left[(l_1l_2+m_1m_2)^2+\left(\frac{l_1m_2-l_2m_1}{2}\right)^2\right]-\frac{\hat{C}_{12}}{2}(l_1m_2-m_1l_2)^2\\&+2\hat{C}_{13}n_1n_2(l_1l_2+m_1m_2)+\hat{C}_{33}n_1^2n_2^2+\hat{C}_{44}[(m_1n_2+n_1m_2)^2\\&+(n_1l_2+l_1n_2)^2]-4C_{14}m_1n_1(3l_1l_2-m_1m_2)\,.\end{aligned}\qquad(6)$$

Equations (5) and (6) give the apparent elastic constants of marble for any orientation if all composing crystals are pointed to one and the same direction. When the crystal orientation of calcite is equally probable for all directions, the elastic constants of marble will be expressed taking a space mean of equations (5) and (6) for all directions. Taking the new axis as shown in Fig. (2), direction cosines come to be

$$\begin{cases}l_1=\sin\theta\cdot\cos\varphi\\m_1=\sin\theta\cdot\sin\varphi\\n_1=\cos\theta\end{cases}\quad.$$

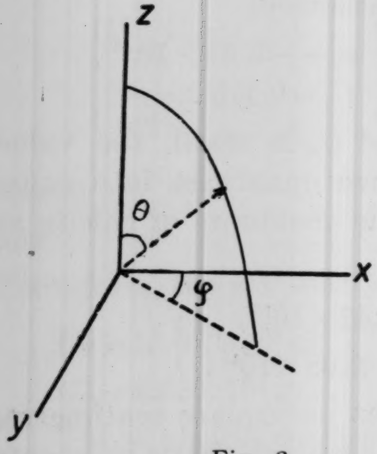

Fig. 2.

Therefore, from equation (5), the mean longitudinal elastic constant, $\bar{C}_{11}$, will be

$$\bar{C}_{11}=\frac{1}{4\pi}\int_0^{2\pi}\int_0^{\pi}\tilde{C}_{11}\sin\theta\cdot d\theta d\varphi$$
$$=\frac{1}{15}\left\{8\hat{C}_{11}+3\hat{C}_{33}+4(\hat{C}_{13}+2\hat{C}_{44})+\frac{1}{2}C_{14}\right\}. \qquad (7)$$

As for the calculation of the mean transversal elastic constant, sets of direction cosines are expressed as follows, taking the parameters θ, φ as shown in Fig. 3.

$$\left\{\begin{array}{lll} l_1=\cos\theta\cdot\cos\varphi\,, & m_1=\cos\theta\cdot\sin\varphi, & n_1=-\sin\theta\,, \\ l_2=-\sin\varphi, & m_2=\cos\varphi\,, & n_2=0\,, \\ l_3=\cos\varphi\sin\theta\,, & m_3=\sin\varphi\sin\theta\,, & n_3=\mathrm{con}\,\theta\,. \end{array}\right.$$

Inserting these direction cosines into equation (6), the mean transversal elastic constant $\bar{C}_{44}$ is calculated similarly as follows,

$$\bar{C}_{44}=\frac{1}{6}\hat{C}_{11}-\frac{1}{6}\hat{C}_{12}+\frac{2}{3}\hat{C}_{44}-\frac{1}{6}\hat{C}_{14}\,. \qquad (8)$$

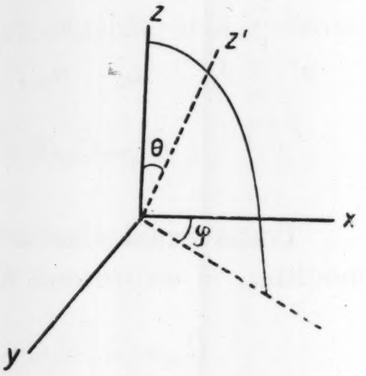

Fig. 3.

From equations (7) and (8), the apparent velocities of elastic waves is found to be

$$\bar{v}_p=(\bar{C}_{11}/\rho)^{\frac{1}{2}}=6609 \text{ m/sec},$$
$$\bar{v}_s=(\bar{C}_{44}/\rho)^{\frac{1}{2}}=3904 \text{ m/sec}.$$

where, $\bar{v}_p$, $\bar{v}_s$ are the velocities of dilatational and rotational elastic waves respectively. This is the case of macroscopically isotropic marble in which the crystal orientation is equally probable for all directions.

Discussion of the Results.

Velocities of elastic waves may be equal for all directions if the specimen is isotropic, whereas specimens I—IV show more or less aeolotropic character where the velocity of dilatational wave is scattered within significant ranges. For specimen III, the velocity is varied by such a large per cent as 6% according to the propagational direction of the wave. In order to make clear the aeolotropic character of the

specimen, the fabric analysis was made by one of the authors (I. Murai). Fig. 4 shows an example of the fabric analysis for the specimen III. Measurements were made on 211 grains in a section.

In the figure, we can see C axes of calcite is oriented somewhat predominantly to the direction almost normal to the plane of the section. This cause presumably gives rise to the said difference in velocities of elastic waves according to the propagational direction. In other words, the velocity difference can reach almost several percent according to the propagation direction, notwithstanding the slight aeolotropic behavior as has been analyzed from petrofablics. Specimens V, VI, the so-called limestone, do not show any elastic aeolotropy since the velocities for the three directions are almost equal. From the mathematical treatment given in the preceding paragraph, the velocity of dilatational and rotational waves for isotropic marble are expected to be 6609 m/sec and 3904 m/sec respectively. But, in the limestone, in which the crystal orientation is considered to be quite at random two velocities were measured and found by us to be 5860 m/sec and 3200 m/sec respectively. These discrepancies between the theory and the experiment may be considered to be the consequence of the effect of void space between each crystal boundary.

Fig. 4, Orientation diagram for c axes of calcite in specimen III. 211 grains per diagram. Contours, 0~1, 1~2, 2~4, 4~5%, per 1% area.

Acknowledgment.

We wish to express our sincere thanks to Prof. R. Takahasi who has kindly offered his some criticisms on the present study, with his deep interest in our work. Our thanks are also due to the Grant in Aid for the Miscellaneous Scientific Researches of the Department of Education for the expense of the present work.

5. 大理石の弾性，特にその異方性に就いて

地震研究所 {下 鶴 大 輔
村 井 勇

我々が実験室で岩石中を伝はる弾性波の速度を測定すると，所謂，花崗岩とか石灰岩とかの同じ種類の岩石でも速度は非常にばらつく事を経験する．この原因として，色々あると思はれるが，此の論文では，弾性の異方性の問題を取りあげた．最も取り扱いやすい試料として，大理石を選び，一辺の長さがほぼ 5 cm の長さの立方体に作り，三方向の縦波及び横波の速度を X-cut，Y-cut の水晶振動子を用いて測定した．その結果に依ると，一つの試料でも方向に依つて，少しづつ速度が違うことがわかつた．その差は数%に及ぶ．この原因は結局，大理石を構成している方解石の結晶の軸があらゆる方向に等しく向いていないからである．その有様は Fabric analysis に依つて示されてある．又，方解石の単結晶の弾性率から，その集合体としての大理石の弾性常数を，2 つの場合に就いて計算して，実験の結果と比較して見た．即ち，一つは，一斉にある方向を向いている場合の任意の方向の弾性常数と，他は，方解石があらゆる方向に等しく向いている場合の見かけ上の平均の弾性常数とである．2 つの石灰岩の試料については，三方向の速度はほぼ等しく，一応巨視的に等方性であるといへるが，その場合，計算値は実測値より，かなり大きな値を示し，これは結局，実際の大理石では結晶個体の同志間の Void space がある為めに，弾性率が小さく出るのであらうと思はれる．

6. *A Note on the Elasticity of Marble.*

By Daisuke SHIMOZURU,

Earthquake Research Institute.

(Read Dec. 21, 1954.—Received Dec. 30, 1954.)

D. S. Hughes and others have recently measured the velocities of elastic waves in some igneous and sedimentary rocks under the conditions of elevated temperatures and pressures, and their results are given in several publications. In one of their results[1], velocities both of dilatational and rotational waves in marble are tabulated as the function of pressures and temperatures. Table I shows the values of pressures, velocities and temperatures after them.

Table I.

T°C	26	
P bars	V_p (m)	V_s (m)
70	5866	2823
140	6060	3071
345	6250	3104
690	6501	3147
1035	6551	3170
1725	6621	3195
2415	6651	3118
3100	6665	3209
4140	6673	3209
5170	6660	3254

In a previous paper[2], the author calculated the mean velocities of elastic waves in marble at 20°C from the known values of elastic constants of a calcite crystal, assuming that marble is a polycrystalline aggregate of calcite crystals only and that the crystals are oriented equally likely to all directions. The average velocities of dilatational and rotational waves can be calculated using the following relations,

$\bar{v}_p=\left(\frac{\overline{C}_{11}}{\rho}\right)^{1/2}$ and $\bar{v}_s=\left(\frac{\overline{C}_{44}}{\rho}\right)^{1/2}$ respectively, where $\overline{C}_{11}$ and $\overline{C}_{44}$ are mean elastic constants, and are given by the expressions

$$\overline{C}_{11}=\frac{1}{15}\left[8\hat{C}_{11}+3\hat{C}_{33}+4(C_{13}+2C_{44})+\frac{1}{2}C_{44}\right],$$

and

$$\overline{C}_{44}=\frac{1}{6}C_{11}-\frac{1}{6}C_{12}+\frac{2}{3}C_{44}-\frac{1}{6}C_{44}\,.$$

1) D. S. HUGHES, *Bull. Geol. Soc. Amer.*, **61** (1950), 843–856.
2) D. SHIMOZURU, *Bull. Earthq. Res. Inst.*, **33** (1955), 70.

Then, assuming that $\hat{C}_{11}=13.69\times10^{11}$dynes/cm^2, $\hat{C}_{12}=4.56\times10^{11}$, $\hat{C}_{33}=7.99\times10^{11}$, $\hat{C}_{13}=4.51\times10^{11}$, $\hat{C}_{44}=3.42\times10^{11}$, $\hat{C}_{14}=-2.08\times10^{11}$ as in the previous paper, the average velocities become

$$\overline{v}_p=\left(\frac{\overline{C}_{11}}{\rho}\right)^{1/2}=6609 \text{ m/sec} \quad \text{and} \quad \overline{v}_s=\left(\frac{\overline{C}_{44}}{\rho}\right)^{1/2}=3904 \text{ m/sec} ,$$

assuming that $\rho=2.715$ gr/cm^3.
These are the theoretically computed velocities of marble from the known elastic constants of calcite crystals.

Next, we shall consider the effect of hydrostatic pressure upon the velocities of elastic waves. F. Birch[3] has given the velocities of elastic waves of an isotropic medium which is subjected to hydrostatic pressure, using Murnaghan's theory of finite strain. According to him, the dilatational and rotational waves are calculated in very convenient expressions in terms of strain and Lame's constants as follows:

$$\left.\begin{aligned} v_p^2&=(1-2\varepsilon)^{5/2}[\lambda+2\mu-\varepsilon(11\lambda+10\mu)]/\rho , \\ v_s^2&=(1-2\varepsilon)^{5/2}[\mu-\varepsilon(3\lambda+4\mu)]/\rho , \\ \text{and} \qquad -p&=(1-2\varepsilon)^{5/2}\varepsilon(3\lambda+2\mu) , \end{aligned}\right\} \qquad (1)$$

where

ε .... strain,
λ, μ .... Lame's elastic constants,
p .... pressure,
v_p .... velocity of dilatational wave,
v_s .... velocity of rotational wave.

For the purpose of comparison with laboratory measurements, it is sufficient to retain only the first powers of ε or p. Then the approximate expressions of equation (1) come to be,

$$\left.\begin{aligned} v_p^2&=v_{p0}^2\left[1+\frac{p}{3\lambda+2\mu}\,\frac{13\lambda+14\mu}{\lambda+2\mu}\right] , \\ v_s^2&=v_{s0}^2\left[1+\frac{p}{\mu}\,\frac{3\lambda+6\mu}{3\lambda+2\mu}\right] , \\ \text{and} \qquad p&=-\varepsilon(3\lambda+2\mu) , \end{aligned}\right\} \qquad (2)$$

where the subscript zero refers to the state of zero pressure. Equa-

3) F. BIRCH, *Jour. Appl. Phys.*, **9** (1938), 279–288.

tion (2) gives the velocities of dilatational and rotational waves as a function of hydrostatic pressures as tabulated in Table II, where $v_{p}0$, $v_{s}0$ and λ, μ were taken to be 6609 m/sec, 3904 m/sec and 3.58×10^{11} dynes/cm², 4.14×10^{11} dynes/cm² respectively. The theoretically computed velocities as given above, as well as the values of laboratory measurements by Hughes are shown in Fig. 1 and Fig. 2.

Table II.

P (bars)	V (m)	V (m)
0	6609	3904
1000	6624	3913
2000	6639	3922
3000	6655	3930
4000	6670	3939

It seems that theoretical and experimental values agree pretty well when the pressure is above 2000 bars. For pressures below 2000 bars, the discrepancy between the theory and the laboratory measurements is great. This discrepancy may be attributed to the pore space between crystals in the measured specimens. Owing to the existence of pore space, the velocity of dilatational wave at ordinally pressure must be much less in laboratory measurements than in the theory, in which pores are not taken into consideration. As the environing pressure becomes large, such void spaces tend to vanish being accompanied by the large increase in apparent elasticity. Therefore, the velocities of elastic waves increase in consequence of vanishment of such void spaces. Above 2000 bars, pore space seems to vanish completely and the compres-

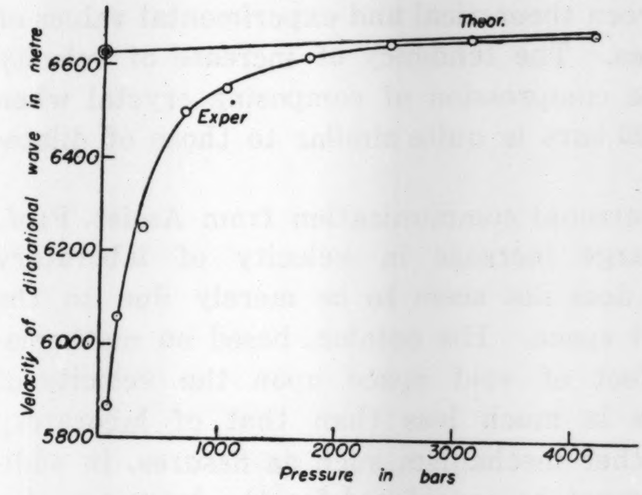

Fig. 1.

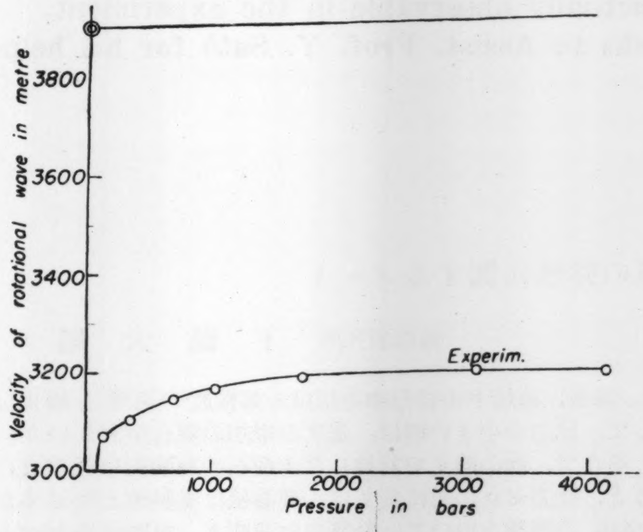

Fig. 2.

Velocities of dilatational and rotational waves versus pressure, after D. S. Hughes.
Description ; Danby marble, Origin ; Rutland.

sion of calcite itself begins to set in. In other words, agreement of velocity of dilatational wave between theory and experiment above 2000 bars indicates that crystal grains themselves are being compressed in such manner as assumed in the theory.

As for rotational wave, the propagation velocity obtained by laboratory measurements is much less than the theoretical one. Theoretical value, however, does not assume the effect of grain boundary such as cited in a previous paper, whereas such grain boundary is considered to affect the propagation velocity, especially in the case of shear. In the author's opinion, the reason cited above may be the cause of the discrepancy between theoretical and experimental values of propagation of rotational waves. The tendency of increase of velocity of rotational wave due to the compression of composing crystal when the pressure is more than 2000 bars is quite similar to those of dilatational wave.

N.B. According to the personal communication from Assist. Prof. Y. Satô of the Institute, large increase in velocity of laboratory measurement at low pressure does not seem to be merely due to the effect of disappearance of void space. His opinion, based on mathematical studies, is that the effect of void space upon the velocity of elastic wave up to 2000 bars is much less than that of laboratory measurement, accordingly another mechanism such as fissures, in addition to the above-cited effect, must be considered for the interpretation of large increase of velocity actually observable in the experiment.

I express my hearty thanks to Assist. Prof. Y. Satô for his helpful criticisms offered me.

---

6. 大理石の弾性に関するノート

地震研究所 下 鶴 大 輔

最近 Hughes 一派は，超音波を用いて，高温，高圧下の岩石中を伝はる弾性波の速度を測定している．その結果によると一般的傾向として，圧力の小さい間は，速度の増加の割合が大きいが，次第に高圧になると，割合が少なくなる．そこで，前の論文で計算した大理石の理論的な速度と，Hughes の大理石の実験値を比較して見ると，圧力ゼロの所に於ては，理論値は実験値よりはるかに大きい．圧力が次第に増すと，Murnaghan の理論を用いて，計算した速度と，実験値を比べると，縦波の場合は，2000 bar あたりから，非常に良く一致する様になる．2000 bar 以下の圧力の低い所の理論値と実験値との差は実験に使用した大理石中の空隙が原因と考へられる．圧力が次第に高くなると，その様な空隙が次第に圧縮されて，見掛上，速度が急激に増すのであらうと考へら

れる．2000 bar になると，その様な空隙は完全に押しつぶされて，それ以上は，結晶の実体の圧縮が始まるのである．故に，2000 bar 以上では有限歪の理論を用いた理論値と良く一致する様になる．横波の場合は，理論値は実験値よりも非常に大きい値を示している．これは，実際の試料中の結晶の境界が，縦波に対しては，効果を現はさないが，横波に対しては大いに効いて来るためであらうと思はれる．

7. *The 1950-1951 Eruptions of Mt. Mihara, Oshima Volcano, Seven Izu Islands, Japan. Part II. The 1951 eruption.*

B. Activity of the third period.

By Hiromichi TSUYA, Ryōhei MORIMOTO and Joyo OSSAKA,

Earthquake Research Institute.

(Read March 18, 1952.—Received Dec. 30, 1954.)

IX. Course of the activity of the third period, April—June, 1951.

(*1*) *Changes in activity of Mihara crater early in April, 1951* :

Early in April, 1951, there was a sudden decrease of eruptive activity in Mihara crater. The explosive eruption at the main cinder cone had become quite small on April 1, and by 11 h 30 m the cone was seen ejecting only a few bombs repeatedly, together with puffs of white vapours. The next day, between 10 h and 14 h, the only activity seen from Goshinkajaya was white vapour clouds rising from the cone, without any audible explosion. In the evening of the same day, for about one hour (19 h to 20 h), explosions were heard at Motomura repeatedly about twice a minute, and the cloudy sky above the mountain was seen glowing, with the glow waxing and waning. On April 3, about 10 h 50 m, explosions were again heard at Motomura several times in five minutes, and in the next morning neither explosions nor hissing noises were heard even at a short distance from the crater. During the last two days it was raining hard and the mountain was shrouded with thick clouds, so that just what occurred within the crater was quite vague, being invisible from near the rim of the crater. But volcanic manifestations of the crater must have changed in those days from the preceding continuous eruption (the second period Feb.–March, 1951) into the present intermittent eruption.

Red-hot lava was seen running over the northern rim of the crater and flowing downhill northerly on April 1 and 2, and the flows were found to have become almost dead on April 5. Therefore, the lava outpouring must have ceased some time or other between April 2 and 5, although the slower moving fronts of the flows continued to advance

for some time after the diminishing activity at the source vent cut off the supply of lava.

The above-mentioned changes of activity both at the explosive vent on the cinder cone and the lava vents on the floor of Mihara crater were accompanied by remarkable subsidence of the crater floor. Thus the crater floor, which during the activity of the second period had kept rising with intervening local and temporary subsidences, began to subside early in April, as though the subsidence were a definite reaction from the cessation of the continuous eruption. On April 7, the subsidence was seen going on with the central upthrusted mound as the centre of subsidence; the lava ground was breaking down with cracks around the mound; the top of the mound was found to have subsided several metres since the end of March, while the top of the cinder cone only a few metres in the same period. As the subsidence advanced, new cracks and slump scarps appeared noticeably in the bottom lavas of the crater outside the site of the former central pit, on the upthrusted mound and also on the cinder cone (Fig. 170). Most of the larger cracks and slump scarps run nearly concentrically around the central upthrusted mound and parallel with the rim of the crater. The most striking one of the slump scarps was concentric with the crater-rim to the west and northwest within about 50 m distance. On April 9, the crater floor inside this slump scarp was found to have subsided about 10 m relative to the floor on the other side near the crater rim, which seemed to have been left almost undisturbed. The western section of the slump scarp appeared close to the line of spatter cones (Fig. 72a, g–l), breaking down some of the cones, and its southeastern extension traversed the cinder cone from west to east, marking the southern limit of the subsiding crater floor.

The subsidence of the crater floor may have been caused locally at least by contraction due to solidification of the new fill, particularly of the lavas outside the former central pit, but it must have been due largely to the withdrawal of active lava from the bottom of the former central pit, subsequent to the voluminous outflows of Feb.—March, seeing that the site of the centre of the subsidence was identical with the former central pit (now occupied by the central upthrusted mound) and that the new slump scarps and cracks were dominantly concentric as though they were guided by the circular rim of the former central pit.

While the subsidence of the crater floor was in progress, small

Table XIV. Volcanic activity of Mihara crater during April-June, 1951.

Date	Activity	Location	Duration (approx.)
April 2, 10^h	Cessation of continuous explosive eruption.	Main cinder cone.	
2, 19^h	Explosive eruption.	Do.	1 hour.
3, 10^h 50^m	Explosions.	?	5 minutes.
5,	Cessation of advance of the lava flows.	North and northeast slopes of the mountain.	
5, 6^h	Explosions.	Main cinder cone.	1 hour.
5, 14^h 15^m	Explosions.	Do.	2–3 minutes.
8, $^h5$	Explosions.	Do.	2 minutes.
8^h 30^m	Explosions.	Do.	2 minutes.
9, 0^h 30^m	Small explosive eruption.	Do.	
12, 10^h	Small explosive eruption.		
13, 10^h	Explosion ?	?	
April 16, 8^h | 19, 17^h	Explosive eruption. Lava spattering, fountaining and outpouring.	Main cinder cone. Crater floor to the east and west of the central upthrusted mound.	3.5 days.
April 20, 14^h	Explosions.	Main cinder cone.	5 minutes.
April 30, 0^h 30^m | May 1, 19^h	Explosive eruption. Lava spattering and outpouring.	Main cinder cone. Crater floor to the east and northeast of the main cinder cone.	43 hours.
May 3, 0^h 40^m 1^h 40^m	Explosions. Explosions.	Main cinder cone. Do.	5 minutes. 30 minutes.
May 6, 0^h 25^m | May 7, 7^h	Explosive eruption. Lava fountaining and outpouring.	Main cinder cone. Temporary vents on the crater floor to the northeast of the central upthrusted mound.	30 hours.
June 9, 12^h 35^m | 10, 15^h	Explosive eruption. Lava spattering and outflowing.	Main cinder cone. Crater floor to the east and west of the central upthrusted mound.	27 hours.
June 14, 22^h 30^m | 15, 18^h	Explosive erution. Lava outpouring.	Main cinder cone. Northeast wall of the central sink of the crater floor.	15 hours.
June 17, 11^h 15^m | 18, 6^h	Explosive eruption. Lava outpouring. Lava spattering.	Main cinder cone. East wall of the central sink. Southwest rim of the central sink.	19 hours.
June 19, 2^h 30^m | 19, 16^h	Explosive eruption.	Main cinder cone.	14 hours.

(to be continued.)

Table XIV. (Continued.)

Date	Activity	Location	Duration (approx.)
June 21, 7^h 35^m – 22, 4^h 30^m	Explosive eruption.	Main cinder cone.	21 hours.
June 22, 21^h 30^m	Explosions.	Main cinder cone.	
23, 4^h	Explosions.	Do.	40 minutes.
27, 12^h 30^m – 28, 12^h 30^m	Explosions.	Do.	24 hours.

explosive activity occurred intermittently on April 5, 8, 9, 12 and 13, as shown in Table XIV. Though small and short-lived, this activity was rather high in explosive power every time as compared with the eruption of the preceding period, Feb.-March[33]. Thus the explosions now became so powerful that a number of bombs, about the size of man's head, were thrown out as far as the observation point on the west rim of the crater, about 500 m to the west of the summit of the active vent, and black ash clouds were of usual occurrence vomiting with detonations from the vent. Presumably these explosions were due to clogging of the gases in the lava that had retreated within the vent down to levels below the depth where appreciable vesiculation could occur to cause eruption with free welling action. The pressure of gases clogged within the lava was released by an occasional breaking through, hence came the explosions.

(2) *Explosive eruption, lava spattering, fountaining, and outpouring, Aprill 16–19:*

On April 16, about 8 h, bluish fume was seen rising in quantity from the cinder cone, besides white vapour clouds, and by 8 h 45 m black ash clouds began to vomit with detonations from the cone, continuously up to a height of 300 m to 400 m above its summit (Fig. 125-a), and a few minutes later, the explosive vent began to repeat emission of red-hot lava about ten times a minute, flinging up bombs up to a height of about 150 m. The same day, in the afternoon, red-hot lava was found pouring out of two new vents, one on the west side of the central upthrusted mound and the other in a great chasm to the east of the same mound, and spreading over the previously subsided

33) Eight girl-students were wounded by the explosion of April 8, about 9 h 30 m, while observing it from or near the observation point.

craterfloor to the west and north (Fig. 121 a-map). Besides, lava fountainings and spatterings were going on at the source vents and building up spatter cones several matres high, breached like an armchair niche with lava overflows.

Beginning on April 16, the activity continued in almost the same manner as the one just mentioned, but with some ebb and flow in its intensity, for three and a half days until April 19. Thus, on April 18 the new lava flows were found to have spread out into the depression that surrounded the north and west of the central upthrusted mound, forming a temporary semi-circular pool of red-hot lava (Fig. 126 a–b); about a dozen small vents could be counted near the lava source on the west of the mound, vying with each other in lava spattering (Fig. 127); and explosions were being reported with loud detonations about twenty times a minute at the summit crater of the cinder cone, which was now funnel-shaped and about 70 m in diameter, displaying columns of black ash clouds more than 200 m high (Fig. 125 b) and lava flings up to about 130 m high, and adding cinders and bombs continually to the cone which had already grown by the activity of the preceding two days to be a perfect conical hill surmounting the height of Kengaminé (755 m), the crest on the east wall of Mihara crater. The next morning, the explosive activity was as in the preceding days, the lava flows were found to have spread over about two-thirds of the inside of the crater, running over the crater rim to the north and northwest, and a small part of the flows descended the mountain slopes in these directions (Fig. 129).

The activity become weak early in the afternoon of April 19, the explosions stopped about 17 h, and soon after that the glow died out both from the surface of the new flows and from the vents which had just subsided into inactivity. From that time on, the crater continued to be virtually quiet until April 30, when it started another remarkable activity, although it showed small explosions on April 20, about 14 h, and kept on emitting white vapour clouds, sometimes accompanied with bluish fume (Fig. 128).

Almost simultaneously with the activity of April 16–19, the central upthrusted mound and the northern part of the cinder cone was upheaved suddenly and to an appreciable amount, together with the adjoining part of the crater floor, and besides being covered with new ejecta to a depth up to several metres, the upheaving continued for about two weeks, until the beginning of May, thus covering the two

periods of activity, April 16–19 and April 30-May 1. The lava column to which the activities of these periods were due must have had a gas pressure high enough to cause bifurcated and piecemeal extrusions on the one hand, and to keep pushing up the overlying fill of the former central pit on the other hand.

(3) *Explosive eruption, lava spattering and outpouring, April 30-May 1:*

On April 28, when in the morning two of the writers (H. T. and R. M.) visited Mihara crater, the cinder cone was seen emitting continuously only white vapour clouds. The southwestern brink of the throat of the cone could be reached without danger by way of its southern slope, but the inside of the throat was quite invisible because of the thick vapour clouds rising from within. There was no sound of internal noises, although small vibrations of the ground underfoot were felt almost incessantly (Figs. 130–132). No fuming or steaming areas were found upon the southern slope of the cone, but the cinders were distinctly warm underfoot, and also considerable heat was felt in places so that in climbing the slope we had to choose large lava boulders cool enough for us to step on with safety. Upon the southeast and northeast slopes of the cone were several steaming cracks radiating from the summit, and on the adjoining crater floor were found countless steaming areas. On the contrary, there were no fuming or steaming areas on the west and northwest slopes of the cone, and also on the adjoining crater floor, the greater part of which was now covered with cinders and bombs ejected from that cone. Immediately adjacent to the same cone and to the west of it were the remains of the spatter cones (c and d) formed by the activity in March (Fig. 132).

The next day the crater seemed to remain quiet as on the day before without reports of any explosion, although nobody could see just what occurred there on that day, because of the stormy weather which shrouded the mountain.

On April 30, about 0 h 30 m, an eruptive activity was confirmed to have started at the cinder cone, throwing up flings of red-hot lava to the night sky which had just cleared up. The same day, by daylight, we were surprised by a magnificent view of lava spattering and effusion going on in the eastern half of the floor of the crater, besides the explosions of the cinder cone (Fig. 133). Thus on the crater floor to the east of the central upthrusted mound were several spatter cones

(Figs. 134, 138), the largest of which was about 10 m in height and 15 m in diameter at its base, and most of these cones were active, emitting red-hot lava pieces intermittently with bluish fume, and ranged northeast, presumably along a fissure in the crater floor. Immediately adjacent to the cinder cone and to the northeast of it was a lava vent (Fig. 121 b-map) pouring a lava flow into the near-by depression to form a lava pool, about 50 m in length and 20 m in width. As nearly as could be ascertained, this vent seemed to be located approximately at the same spot as one of the lava vents of April 16–19 (Fig. 121 a, vent A) and on/or close to a zone of fissures which demarcated the central upthrusted mound toward the east wall of the former central pit and which, now being represented by a long curved line of white steaming vents, was traceable southeast to the northeast slope of the cinder cone.

On the crater floor east of the cinder cone and close to the east bluff of the crater were seen small tongues of red-hot lava oozing out very quietly and slowly from holes in the crust of an older lava and spreading over the older lava along the bluff. They were measured with the eye to have a speed of about 10 cm a second for a short distance near their outlets, but became sluggish in a few minutes with a darker scum continually forming on the surface, and at last became stagnant, being crusted over with a skin of wrinkled and ropy *pahoehoe* after travelling a distance of 20 m to 30 m from their sources (Fig. 136).

As other irregularities which added interest to the scene, several small spatter heaps and steaming vents were found on the crater floor adjacent to the southwest of the vent area of the lava flows just referred to. They were in line with the latter, generally in a SW-NE line radial from the top of the main cinder cone, suggesting a line of cracks in the crater floor (Fig. 137).

The cinder cone continued throughout the day to throw out cinders and bombs up to a height of about 200 m with explosions at intervals of several seconds.

The same day, at night, all the active vents attracted attention by their illumination, and in addition to these vents, glowing spots could be seen at several places, where in day time only vapours could be seen rising quietly (Fig. 138).

Early in the morning of May 1, in cloudy weather, observations from Goshinkajaya showed dense vapour clouds rising from the cinder

cone and from the crater floor northeast of it. The cinder cone was entirely enveloped in the clouds, and the central upthrusted mound visibly became a few metres higher than on the preceding day (Fig. 139). Small explosions were heard at the rate of five times a minute.

In the afternoon of the same day, when the sky cleared with the wind changing from northeast to southwest, the cinder cone was found to be active as in the preceding day, enjecting cinders and bombs, together with puffs of black ash clouds, up to a height of a few hundred metres. The spatter cones on the crater floor adjacent to the northeast of the central mound had stopped spattering lava, although some of them were emitting bluish fume with small jets of flame (Figs. 141, 142). The lava vents near the base of the east bluff of the crater had also become dead with no further issue of red-hot lava, and the surrounding *pahoehoe* flows had cracked and broken down in places (Fig. 143). At the same time, close to the base of the southeast bluff of the crater and on the crater floor to the southeast of the cone, were found several lava vents still sending forth small flows of pasty lava (Fig. 137). Located on or near the southeastern extension of a steaming fissure on the southeast slope of the cinder cone, these lava vents seemed to have been supplied with material through the fissure from the main lava source at the depths, in spite of their being opened in the heap of cinders and bombs ejected from the cinder cone.

The same day, about 16 h, on crossing the lava flows under which the north and northwest crater rim had been buried deep, we found a red-hot lava flowing out of a crevice in one of the older flows on the crater floor northeast of the central upthrusted mound and cascading northward into a deep chasm in streams, about 20 m in breadth, at a speed of about 20 cm a second (Fig. 144). The rock under our feet was in places so hot as to be uncomfortable, easily breaking and dangerous, and was still moving very slowly. On the northwest crater rim, where the overlying lava flows were dominantly of *pahoehoe* and ropy, was found the spatter cone (l in Figs. 73 a, 74) about 3 m high, remaining active as it was in March (Fig. 169).

By the evening of the same day, when we were observing the activity of the cinder cone from the crest of the west crater rim, explosions of the cone became suddenly less frequent but more or less louder than in daytime, and about 19 h they occurred only once every

twenty minutes, and the explosion, observed from Goshinkajaya about 20 h, marked the end of the present activity (April 30-May 1), displaying fire jets twice in succession, first obliquely upward and then vertically upward (Fig. 140).

The crater was generally quiet during the following four days May 2–5, although there occurred small explosions twice on May 3. During these days, however, the central upthrusted mound had subsided markedly, together with the surrounding crater floor, as an after-effect of the preceding eruption, and in the similar way as observed immediately after the Feb.-March eruption. Thus the central mound, which during the eruptive periods used to stand at levels high enough to be visible from Goshinkajaya, had subsided so much that, viewed from the same place, its top was now hidden from sight behind the higher, lava-covered crater rim. An eye-measurement showed the subsidence to be more pronounced than in the previous occasion, amounting to several score metres, and bringing the top of the mound down to a level only abut 20 m above the general surface of the surrounding crater floor. A semicircular depression had appeared once again surrounding the central mound on the west, north and northeast. It was about 50 m in average breadth and in some places was walled by slump scarps several metres high. Besides, during the same period, the series of subsidences in the crater was breaking down the cinder cone. Thus on May 4 the cone was found subsiding at its central part every moment at a speed of about 6 m a day, and at the same time its summit vent was seen to be enlarged by avalanches of the surrounding walls, sending up cauliflower clouds of dust.

(4) *Explosive eruption, lava fountaining and outpouring, May 6–7* :

In the early morning of May 6, about 1h25m, Mt. Mihara resumed its eruption which was to last well over thirty hours. At 2 h explosions were heard more than twenty times every minute at Motomura village (Fig. 145). With each detonation a spectacular fling of red-hot lava shot up like a column of flame, sometimes more than 300 m high, to the glowing sky above the mountain. It was the first time in the present activity that the fling of red-hot lava became visible from the village.

On the same day, about 10 h 30 m, lava bombs were thrown every few seconds from the vent on the cinder cone with greater than

average violence and accompanied by booming, explosive noises. This explosive activity continued with little change until about 17 h on the same day, adding bombs, cinders and spatters to the cone and increasing cinder accumulations on the crater floor to the east and west. Showers of small cinders fell outside of the crater, and within a range of about 800 m to the northwest of the vent. They lay more than 1 m deep on the ground adjacent to the west base of the cinder cone (Fig. 146).

A small amount of lava was spilling from a fissure on the east side of the central upthrusted mound, and a reddish fume was seen rising from the ground thereabout, already during the earliest hours of the eruption. By the noon of the same day, according to an observer from Nomashi village, red-hot lava was gushing out of three or four vents on fissures on the east side of the central mound, and was flowing north in the direction of Kakôjaya, tea-house on the northern crater rim now buried beneath older lava flows.

At 17 h there came a comparative lull in the explosive eruption from the vent on the cinder cone, and the explosion for a time died down. With occasional small explosions lava pieces were thrown up to a height of less than 50 m above the top of the cone, while ash and vapour clouds were discharged faintly. On the contrary, at that time, lava spouting was taking place with increasing violence on the east side of the central mound. Here two big lava fountains (Fig. 148) were developed, besides a few smaller ones. One of the big fountains appeared just like a kettle full of melting slag. It was a pool of incandescent lava, 50 m or more in diameter, bordered by high ramparts built up by overflow and by splashing fountains. The lava in the pool was running high vigorously and was being spouted once every minute or two up to a height of about 15 m above the lip of the pool. The other fountain, situated about 100 m south of the preceding one, was a big surface saucer full of rushing golden melt, building up a high spatter rampart at one side, with a gap on the opposite side. A very powerful continuous fountaining was displayed all over the saucer-like opening, about 40 m in diameter, sending incandescent jets 20 to 30 m high, and at the same time a torrential flow of lava was pouring out through the gap in the rampart on the east side of the fountain and spreading over the crusts of previous flows in the northeastern part of the crater floor. The flow which at first spread eastward like a fan showed the usual bright-line pattern radiating from the source fountain (Fig. 149). Approaching to the eastern crater wall, the flow

divided into three streams with two branches heading toward the southeast and east crater walls respectively, and the rest toward north. The former two branch flows were stopped by the crater wall, and thus dammed, was prevented from moving farther to the southeast and east and consequently caused a filling in of all the low areas, while the northern branch flow became a great feature, advancing to surround the northern half of the central mound and filling the semi-circular belt of depression in the crusts of previous flows on the crater floor. This northern branch flow appeared like a mighty river of fire, winding its way round the central mound, with a width varying from 100 m to 40 m (Fig. 122 a-map).

The eruption continued almost steadfastly during the evening hours of the same day, with explosive activity at the cinder cone and fountaining activity at the big fountains in the crater floor, accompanied by gush of lava. At 20 h the explosive vent on the cinder cone was sending incandescent jets a few hundred metres high, almost continuously like a jet from a hose, swinging around the central vertical position. The molten lava that gushed out of one of the big fountains spread over more than half of the northern part of the crater floor, giving spectacular glowing cloud effects over the mountain. At Kengaminé, the eastern crest of the crater rim, even small printed letters could be read by the glow of the lava, while the heat from the lava was almost unbearable.

On May 7, about 8 h, the exlosive activity at the cinder cone subsided, although white vapour cloud was rising continuously from its vent. The lava activity at the fountains also became less pronounced than on the preceding day, but it continued throughout the day, giving a glowing cloud effect to the evening sky above the mountain.

On May 9, after the daylong rainfall of the preceding day, the hot lava fill in the crater was seen to have crusted over, the fountains became completely inactive, and on the new lava flow adjacent to the west of the central mound were found two spatter cones, of which one 3 m high and 15 m wide was inactive and the other 4 m high and 15 m wide was giving vent to a glowing flow about 20 m long, with hissing noises. The crater floor was steaming from hundreds of small vents all over the surface, the cinder cone was ringed by steam, and moreover there was steam on the Feb.-April flows on the northwest outer slope of the volcano (Fig. 147). During the activity on May 6–7, there was no visible surface flow overrunning the crater and descending

the outer slope, but judging from the heavy steaming from the older flows, it seemed likely that some of the hot lava accumulated on the crater floor on May 6–7 had found its way down the outer slope through tunnels and crusts in the older flows.

From then on throughout the remainder of May and the first week of the next month, the volcano was very quiet, some steam and a little fume rising from both the cinder cone and the surrounding crater floor being the only surface activity observed every day.

(5) *Explosive eruption, lava spattering and outflowing, June 9–10:*

After the eruption of May 6–7, no very marked topographical change occurred on both the crater floor and the cinder cone until June 7, almost exactly one month later, suggesting continued upward pressure of the underlying magma column without sufficient gas potential to make it break out with visible lava flowing and spattering during this interval. But on June 7, about 17 h, the crater floor was found to have settled down several metres, leaving again a terrace-like lava ledge around its outer margin adjacent to the crater rim, and the central mound was now subsiding steadily and magestically, maintaining its identity as it went down. The site of the centre of the new sink was identical with the old central pit, which had merely been enlarged. The subsidence of the central mound caused engulfment of the northern side of the cinder cone into the new sink (Fig. 122 b-map).

On June 8, about 2 h, a bright red glow, illuminating the sky over the mountain, was visible from Motomura, not because an eruption might take place in the crater, but because glowing lava was exposed on the newly-formed cracks and slump scarps in the subsiding crater floor. The same day, by 14 h 30 m, the central mound had sunk more than 40 m, in company with the new cauldron subsidence at the site of the old central pit, thus the top of the central mound was now several metres lower than the general level of the crater floor outside of the new cauldron (Fig. 150 a). The northern half of the cinder cone was seen to have slided down 20 m or more toward the cauldron, and the sliding was still going on with clattering noises, while the other half of the cone seemed to be standing almost stable, as in the preceding days. (Fig. 171 a).

At 15 h 30 m the breakdown of the rim of the central cauldron was

going on in succession with clattering noises. Several small cascades of glowing lava were seen hanging over the walls of the slump scarps around the cauldron. Apparently these flows oozed out from under the lava sheets cut off sharply by slump scarps around the cauldron. Presumably they arose from some of still-molten feeders of the lavas which had poured out when the cauldron was filled with lava to the level of the top of the present scarps.

On June 9, at 10 h, nothing could be seen of the crater, because of a dense fog shrouding the mountain, but clattering noises were heard from near the crater as on the day before, indicating the collapse of the central part of the crater.

At 12 h 35 m, the same day, when it was still very foggy, a heavy explosive eruption began with almost continuous detonations like a thunder and so loud that they could be heard at Goshinkajaya on the somma. At 13 h, the fog lifted considerably for a while to give a better view of the eruption taking place continuously with explosions. Thus, as seen from Shiroishiyama, the highest peak of the southern somma, a vortical column of ash cloud was rising into the air up to a height of more than 1,000 m above the top of the cinder cone that was in eruption within the crater, and through the cloud of rising ash, clots of incandescent lava were flung repeatedly up to a height of about 300 m, dropping several hundred metres away. The area surrounding the crater was found to have been covered with ash and scoria to an appreciable depth. At the northwest crater rim the depth was as much as 15 cm; on the western slope of the central cone (Mt. Mihara), about 600 m away from the active vent on the cinder cone, it was about 3 cm; on the flat of the Sabaku (desert) adjoining the west base of the central cone, about 1 km away from the active vent, it decreased to about 1.5 cm. It was the first time since the beginning of the present eruption of the volcano that so much ash fell on the west side of the central cone to such a distance. The southern slope of the central cone was covered with falling bombs and lava blocks, up to 30 cm in diameter, as far as its base. The heavy explosions in progress were presumably due to clogging of the gases in the lava conduit closed by the subsidence of the central part of the crater floor, and to the confinement in the lava standing at a lower level in the conduit.

The same day, at 20 h–21 h, observation from the western rim of the crater showed the central mound rising again in its former shape, after having sunk into the cauldron about 50 m deep formed by the

subsidence of the surrounding crater floor on the day before; incandescent lava oozing out and spattering from several temporary vents opened on or near the boundary between the rising mass and the surrounding crater floor; and the cinder cone displaying explosive ejection of bombs in succession and growing again into a perfect conical mound with the accumulation of new ejecta on its northern side which had largely slumped on the day before.

The early part of June 10 was cloudy on the mountain, but later the sky cleared up, and the cinder cone was seen continuing its explosive eruption as on the day before, but rather decreasing in intensity. Accompanied by continuous noises like the roar of the sea, explosion was repeated ten to twelve times every minute, flinging up lava about 150 m, and emitting brownish puffs. Lava was oozing out from the fissures at the base of the steady-risng central mound (Figs. 150 b, 151 a; Fig. 123 a-map). On that day, about 15 h, the explosive eruption of the cinder cone stopped, while the upheaval of the central mound was still going on, together with the oozing out of lava from the fissures on the surrounding crater floor, and there activity continued during the evening hours. Possibly at that date the upper part of the lava column came again to stand at levels high enough to permit vesiculation and also enough for a large proportion of the gas bubbles to escape freely without causing any explosive eruption, but supplying the gas for the fume cloud.

(6) Explosive eruption and lava outpouring, June 14–15:

Early in the morning of June 13, the central part of the crater floor, including the central mound and the north side of the cinder cone, began to subside again in the form of a cauldron. By 11 h the subsidence was found to have amounted to more than 40 m at the centre, and continued to increase during the remainder of that day and on the following day was accompanied by larger and larger collapse of the cinder cone (Fig. 123 b-map). Thus at 13 h 30 m, June 14, the subsiding cauldron was found to be about 350 m across and 80 m deep below the average level of the surrounding crater floor. Its walls were cut off sharply by slump scarps in their upper parts, giving to debris slopes below, and the central mound was engulfed into the cauldron, together with the north side of the cinder cone, although the apical part of the mound was seen at the bottom of the cauldron, maintaining its identity (Fig. 151 b). Both on the walls of the cauldron

and on the north side of the cinder cone, slumping was still going on with occasional avalanches sending up brownish cauliflower clouds of dust. Besides, on the northeast wall of the cauldron was seen a small flow of red-hot lava spilling over the debris slope (Fig. 171 b).

About 22 h 30 m, June 14, a tremendous column of ash cloud was seen from Motomura village, rising into the air above the mountain and overcasting the sky above the village. A short time later small explosions were heard, glowing clouds were seen over the mountain, and from 22 h 40 m on, loud explosions were heard almost incessantly.

The next day, at 3 h 40 m, volcanic ashes were found falling in the village of Motomura, and explosions occurred in succession with detonations like thunders. Judging from the heights of the columns of black ash cloud and glowing cloud, which amounted to about 5,000 m and 1,000 m above the crater respectively, the explosions at this time were the largest of the explosive eruption since last year. At 4 h 30 m, when it began raining, the eruption still going on was reported by detonations travelling through the rain clouds that shrouded the mountain, and at about 15 h the detonation become so faint that could be heard only by those villagers who were listening with attention. The eruption came to an end at 18 h, when it was raining hard on the mountain, and a lull of the activity continued during that day and on the following day.

(7) *Explosive eruption, lava outpouring and spattering, June 17–18:*

June 17, at 11 h, the cauldron subsidence was found still going on at the centre of the crater floor, where no marked change in the general feature had occurred by the previous eruption. At that time the cauldron retained its general circularity with the approximate diameter of 350 m, but avalanching from the surrounding walls were of frequent occurrence, and a small gush of lava was breaking out through a fissure in the sloping part of the northeast wall and flowing down to the bottom of the cauldron, which was full of jagged and tilted blocks of lava. Blue fume was seen rising from the bottom of the half-demolished crater bowl on the subsiding side of the cinder cone.

The same day, at 11 h 15 m, explosive eruption began again, sending up a great billowing ash cloud, which arose from the crater with a counterclockwise rotating movement (Fig. 152 a). At 12 h 30 m, observations from the west rim of the crater showed the explosive

eruption going on at two vents, one in the half-demolished crater bowl on the cinder cone and the other outside of the northwest base of the cinder cone and near the west rim of the central cauldron (Fig. 152b). As illustrated in the picture, the former was by far the more active of the two, throwing up jets of bombs and scoriae, sometimes 350 m high, together with emission of black ash cloud. The latter acted like a fountain, flinging up lava clots to a height near 100 m. The lava jets from both vents, taking place side by side, were turned from time to time, like a lawn sprinkler, first in one direction and then in another, scattering the fragments about the surrounding ground. The ash cloud was bent by the southwesterly wind, and there was a light but steady fall of ash in the northeast and outside of the crater (Fig. 153). This general type of activity continued with little change for about 19 hours until 6h on June 18, adding cinders, bombs and spatters to the cinder cone and gradually increasing accumulation of these fragmentary ejecta on the crater floor to the east and west.

(8) *Explosive eruption, June 19:*

On June 19, at 2h 30 m, S. Watanabe and some others in Motomura who were awakened by a big explosion saw incandescent lava jets towering like a column of fire and shining brilliantly on the clouds above the crest of the mountain. From that time on, the explosive eruption occurred continuously but with varying intensity for about 13.5 hours, ejecting both ash clouds and lava pieces from the vent on the cinder cone. The activity was heaviest at about 8h, when a number of bombs were seen falling on the slope outside of the west rim of the crater, in company with explosions being repeated every several seconds (Fig. 154). At 9h 40 m, observation from Goshinkajaya showed a small mound rising above the crest line of the crater rim and in the direction of the south side of the central cauldron in the crater.

The same day, at 15h 57 m, the eruption stopped, and the subsidence of the central crater floor was all that had happened during the rest of that day and on the following day. Thus by the early morning of June 20, the small mound mentioned above had subsided so that it was no longer seen from Goshinkajaya.

(9) *Explosive eruption, June 21–22:*

At 7h 35 m, June 21, preceded by emission of a thick cloud of whitish vapours for a few minutes, an explosive eruption began at the

vent on the cinder cone, with emissions of volumes of ash cloud. Big explosions occurred intermittently four times in the morning hours, at 7 h 40 m, 8 h 30 m, 9 h 32 m, and 12 h 10 m, each lasting for five to ten minutes, and sending forth a large mass of ash cloud (Fig. 155). But smaller explosions occurred almost continuosly during these hours, with ejections of cinders and bombs to heights 100 m to 170 m above the top of the cinder cone.

In the afternoon the eruption went on steadily, but without emittıng any considerable mass of ash cloud, and after attaining the height of its activity at midnight, June 22, 1 h, when continuous jets of incandescent lava, in company with explosions, attracted attention by their illumination like daytime, the eruption dwindled to stop at 4 h 30 m of the some day. Since then an apparent lull of the activity continued until 21 h 30 m when a single, moderate explosion occurred.

The eruption added much cinders and bombs to the cinder cone, building up large heaps of these ejecta around the east and north sides of the explosive vent (Fig. 156 d), and immediately after the eruption, avalanches of new cinders were observed falling from the steep walls of the vent showing glow beneath.

(10) Explosive eruption, June 27–28:

On June 23, explosions occurred four times at 4 h, 4 h 10 m, 4 h 30 m and 4 h 40 m, each lasting for a few minutes and sending forth volumes of black ash cloud to a height as far as 3,000 m. The new heap of cinders and bombs which had been built up around the north side of the vent by the eruption of June 21–22 was seen subsiding during that day, and on the following day, observation from Goshinka-jaya showed that it disappeared below the level of the crest line of the crater rim. This incident, being quite similar to that observed during June 19–20, seemed to indicate that since June 13 the cauldron subsidence in the middle of the crater had been going on to break down the north side of the cinder cone, but with intervening local and short-lived rises by the intermittent explosive eruptions.

In the morning of June 27, the crater showed blue fume rising from the vent on the cinder cone and dust from avalanches rising in brownish clouds from the slump scarps around the central cauldron, but otherwise was clear as in the preceding three days. At 12 h 30 m, a thick vapour cloud mixed with some ash was seen rising from the cinder cone for about twenty minutes, at 14 h 30 m there was again

an emission of a thick vapour cloud up to a height of about 500 m above the top of the cinder cone. At 15 h 50 m, observation from Motomura showed a tremendous column of black ash cloud rising into the sky above the somma, and a few minutes later, detonations like a terrific peal of thunder were heard indicating the resumption of a big explosive eruption. At about 16 h, volcanic ash began to fall in Motomura where the sky had been overcast with the ash clouds carried by the then prevailing easterly wind. The eruption reached its maximum violence at 18 h 30 m, when explosions were heard so loud and ash fall became so heavy in Motomura that a feeling of uneasiness prevailed among the villagers. But soon afterward, the explosions became less violent and the ash fall died down. The eruption continued with intermittent explosions until 12 h 30 m, June 28, when a moderate explosion was heard.

This eruption was the largest of the explosive activity observed since the beginning of the 1950–51 eruptions of the volcano. Thus the area surrounding the crater was covered with ash, scoriae and bombs ejected by the eruption to an appreciable depth. The crater floor, except a small part near its northern rim, was covered with these ejecta so thickly that its former rugged surface of the crater-filling lava flows became quite flat and passable without trouble. At the west crater rim the depth of the ejecta was as much as 2 m in places; at the east crater rim, it was less than 1 m. The greater depth at the west was due to the easterly wind that had been prevailing during the eruption. That violent explosions had taken place during the eruption was indicated by the large number of bombs, some of which were as large as 5 m in diameter, scattered not only over the cinder cone and the adjoining crater floor but also over the slopes outside the crater rim (Fig. 157). Northwest of the central cone a blanket of ash and scoriae covered a wide area including the new lava field on the northwest caldera floor and the northwest slope of the somma (Fig. 158). It reached a depth of as much as 30 cm at the south margin of the lava field on the caldera floor and near the west base of the central cone (Fig. 159), about 3 cm at Goshinkajaya, 1.5 cm on the halfway of the trail from Goshinkajaya to Motomura village, and only 0.5 cm in the village.

X. Mihara crater as observed in July and August, 1951.

Following the end of the big explosive eruption on June 28, the

area of the central mound underwent a rapid subsidence of more than 50 m in a few days, turning into a long-lived central pit, and at the same time, the northern sector of the cinder cone was cut off, in the form of a pyramid, from the rest of the cone and partly slid down toward the bottom of the subsiding central pit. Both fume and vapour rising from clefts in the walls of the vent of the cinder cone were visible, together with dust clouds caused by slumping of the walls, during the first half of July, but they became scarcely visible afterwards.

About the middle of August the crater was visited ; no further sign of activity could be detected, except a slight emission of fume and vapour. There was no further sign of subsidence of the central pit, which by that time had a diameter of about 300 m at its upper rim and a depth of 50 m below the average level of the surrounding crater floor (Figs. 160, 173, 174). The central pit had its bottom sealed with the subsided central mound and covered with a pile of lava pieces ejected by the last eruptions, so that no liquid lava was now observable there (Fig. 160). The lava flows exposed in the walls of the pit also appeared to be lifeless except for some heat felt at places, particularly at small secondary fumaroles.

During the foregoing activity, repeated changes in the configuration of the crater floor had occurred not only with the rise and fall of the central pit area, but also with the appearance and disappearance of miniature volcanic forms such as spatter and driblet cones, and at the end the only mound left after the activity was the main cinder cone itself on the south rim of the central pit. This cone, about 300 m in diameter at the base on the adjoining crater floor and 50 m in height above the same floor, had a funnel-shaped vent, about 50 m deep, 150 m across and surrounded by a steep wall on all sides but the north where there was a deep gap through which it opened to the central pit (Fig. 161). The only small fumarole that was steaming was halfway up the west wall of the vent (Fig. 163), while faint fume was seen rising from the northeast wall and the debris-covered bottom of the vent (Fig. 164). The northern slope of the cone, facing the central pit, showed many slides and slump scarps, besides the above-mentioned deep gap, while the slopes in the other directions were kept undisturbed by the subsidence of the central pit, showing a smooth conical surface and an inclination of about 30°, the natural angle of repose of cinders and bombs (Fig. 166). The cone, which had been banked against the southern crater wall and which eventually

over-topped it, projected approximately 35 m above the old rim of the crater at that point, resting partly on the outer slope of the mountain. Upon the northwest slope of the cone was an area of solfataric yellow deposit associated with white salts, but there was not so much heat as to cause danger to walkers (Fig. 165).

The crater floor outside the central pit showed an irregularity of height within a limit of only about 20 m, its average elevation being only a few metres higher than the level of the crest of the northern crater rim, 678 m above the sea, locally left uncovered with new flows, and accordingly being about 35 m above the corresponding floor before the present eruptions. The whole area of the southern half of the floor, which was covered with a pile of cinders and bombs, was nearly flat without any notable irregularities, although it showed many marks of larger bombs (Figs. 165, 174). The rest of the floor, which was left uncovered with these fragmentary ejecta, showed pressure ridges, irregular piles of broken lava and irregular hardened flow patterns, with cracks, slump-scarps and chasms. In this part of the floor were found two features particularly worthy of notice: the one is a lava tunnel and the other a fissure-filling lava dike.

The lava tunnel, situated at the northeast margin of the crater floor and just above the lowest part of the former crater rim, was apparently the location of a very active liquid stream which had fed the lava flows far below the mountain to the north and northeast. There was an incline, probably formed by collapse of the roof of the tunnel, and through which the floor of the tunnel could be reached. The tunnel was about 5 m in diameter, and its floor was 6 m to possibly 8 m below the surface of the lava flow, being covered with slabs of lava which had fallen from the ceiling. The roof was cracked in all directions and its slabby portions seemed most precariously perched and ready to fall at any minute. Thus, in the roof about 10 m away from the entrance, there was a hole, about 2 m in diameter, like a skylight, which was the result of the cave-in of the weak portion of the roof and through which the interior was lighted enough to be seen clearly. Neither lava stalactites nor stalagmites were found, while complex patterns of parallel grooves, folds, slicken-sides and foliations were found as usual on the side walls of the tunnel (Fig. 167).

The dike, located near the northwest margin of the crater floor, was just on the line of the first spatter cones that had been active in

March, 1951, and where the line of the spatter cones had been buried by subsequent flows and fragmentary ejecta. It stood like a stone-wall, about 1 m in thickness, 20 m in length and 1–3 m in height above the surrounding cinder-covered ground of the crater floor, trending S 20°E toward the west base of the cinder cone. The sides of the protruding dike showed grooves and slicken-sides conforming to the walls of the fissure through which it had risen (Fig 168). Apparently the dike was a part of the fissure-filling lava which had fed both the line of the first spatter cone and some of the March flows on the west side of the mountain. Its protrusion into the air might be the result of squeezing-up, in a plastic condition, of the fissure-filling lava, possibly due to the settling of the surrounding crater floor. About 30 m north-west of the dike and at the outer edge of the former crater rim was a spatter cone (or a lava chimney), about 2 m in height and 1 m in diameter at the base, which was the only one preserved as it had been in the line of the first spatter cones (Fig. 169).

The principal effects of the present eruptions, between July, 1950 and June, 1951, were to fill up the Mihara crater with new lava flows and fragmentary ejecta, and at the same tme to make new lava fields covering altogether a large area to the north and west of the crater. The lava fields and the crater floor, as left by the 1950–51 eruptions, were mapped as shown in Fig. 124, and the masses of the new ejecta were calculated with the results as shown in Table XV. The figures in the table are not of high accuracy, indicating only an order of magnitude, but any error in thickness and volume is believed to be on

Table XV. Area, volume and mass of the 1950–51 ejecta.

Division of the ejecta	Area 10^6 m^2	Volume 10^6 m^3	Mass 10^6 tons	Remark
Lava flows outside the crater:				
(1) North and northeast (Senzu) flows	0.75	2.25	5.625	Average thickness = 3 m Density = 2.5
(2) West (Nomashi) flows	1.01	5.05	12.625	Average thickness = 5 m Density = 2.5
New fill of the crater:				
(1) Cinder cone		3.62	6.154	Density = 1.7
(2) All fill but the cinder cone	0.437	15.44	41.688	Average thickness = 30 m* Density = 2.7
Total		26.36	66.092	

* Excluding the area of the new central pit about 50 m deep, 300 m across, and where there was a deeper central pit about 165 m deep and 290 m across.

the conservative side. Furthermore, the total volume and mass of the new ejecta must be a little above the corresponding figures in the table, because the latter do not contain the amount of the fragmentary ejecta that fell in the area outside the crater.

On the whole the 1950–51 eruptions of the volcano appear to have been rather quiet, leaving various features in and about the crater, inherent to basaltic volcanoes, and the activity seems to come nearer to the Hawaiian type than anything else in Japan. So far as the amount of ejecta is concerned, the present activity of the volcano is about one thousand times greater than its 1910–12 eruption, and is comparable to the 1940 eruption of the neighbouring volcano Miyake-shima, both being placed in the fifth grade of the writer's (Tsuya's) provisional scale which divides the intensity of volcanic activity into ten grades from 0 (the smallest) to IX (the greatest) according to the volume of ejecta.

XI. Review of the activity of April 2—June 28, 1951.

The activity of Mihara crater of April 2—June 28, 1951, was of the third and the last period representing the declining phase of the 1950–51 eruptions of the volcano. The activity of this period may be divided, according to its course, into three stages, i. e., (1) the first stage: April 2–20, (2) the second stage: April 30–May 7, and (3) the third stage: June 9–28.

The activity of the first stage was first of all the intermittent explosive eruptions of April 2–13 at the cinder cone, then it culminated in the continuous explosive eruptions of April 16–19 at the same cone, in company with lava fountainings and outpourings from several vents on the west and east sides of the central mound, and lastly stopped with a short-lived explosive eruption on April 20 at the cinder cone. Following the tremendous overflowing of the crater rim in March, a remarkable lowering of the entire circle of the crater floor had become visible already by the beginning of the activity of this stage, and continued until the activity attained its culmination on April 16. The central mound subsided more than 20 m, together with the northern slope of the cinder cone, and there appeared a number of new cracks and slumps on their surface. At the same time the surrounding crater floor settled down several metres, leaving border slump scarps along its margin near the crater wall. Apparently the subsidence of the crater floor was occasioned by the back-flow of the crater-filling

lava, still fluid below, into a void left at the depth of the lava conduit by the Feb.-March eruption, although some slumping of the crater floor might be accounted for by the release of gas pressure from the underlying liquid lava and/or by contraction due to solidification of the lava. The central mound was lowered most remarkably by the back flow, because it was most sensitive to the movement of the underlying lava, being the fill of the former central pit, which during the eruptions of the preceding periods had been lifted as a wedge-shaped plug covering the top of the lava conduit.

The activity of April 2–13 was intermittent and purely explosive, sending forth black ash clouds from the vent on the cinder cone, probably owing to clogging of the gases in the liquid lava which had retreated into the depth of the conduit. Meanwhile, the conduit lava had been recharging itself with gases until it could lift the plug, the central mound, as much as 20 m during April 16–20. At the same time, the lava forced its way up to break out of the margin of the plug, displaying fountainings, spatterings and outflowings from several temporary vents on the west and east sides of the central mound, besides erupting explosively from the main vent on the cinder cone.

After the activity of the first stage April 2–20, the central mound and the surrounding crater floor kept standing nearly at the same level brought about by that activity, suggesting continued upward pressure of the underlying lava, though the lava had not sufficient gas potential to make it break out until April 30.

The activity of the second stage consisted of two continuous eruptions, one during April 30-May 2 and the other May 6–7, with an intervening lull but being accompanied with short-lived explosions on May 3. The April 30-May 2 eruption was the formation of flaming and puffing chimneys, spatter ramparts and driblet cones built up over fissures in the eastern half of the crater floor, besides the explosive eruption of the main cinder cone and the gushing of lava from cracks on the east side of the central mound and near the buried wall of the former central pit. Trickle lavaflows were oozing out of the floor close to the northeast and east walls of the crater. It was noticed that most of the active vents in the crater floor were arranged in lines suggestive of fissures radiating from the region of the main cinder cone. The effect was as though a strain of uplift were in progress with that cone as its centre, possibly suggesting that the radial fissures thus formed were receiving the underlying drainage

from the underlying lava conduit and welling up a little of it in the local eruptions in the crater floor. During the activity the cinder cone and the central mound were rapidly rising together, besides getting a little higher by the accumulation of new ejecta. But shortly after the activity, they began to undergo a big subsidence accompanied with collapses of the northern half of the cinder cone and concentric cracking and slumping of the crater floor around the central mound. These changes of the crater floor were indicative of the process of creating a destructive funnel (cauldron) of subsidence at the site of the former central pit.

The May 6–7 eruption was characterized by spectacular lava fountainings on the east side of the central cone, besides the explosive lava ejections from the main cinder cone. Lava gushed out from one of the two larger fountaining vents, spreading in torrents over the crater floor around the central mound. In company with this activity, the area of the former central pit, including both the central mound and the northern half of the cinder cone, rose again as much as 30 m, and the cinder cone became a perfect cone increasing its height with new addition of cinders and bombs.

The volcano had been quiet without displaying any eruptive activity until June 9, almost exactly one month later, when the activity of the third stage began. During almost the whole length of this interval, no remarkable change had occurred in the feature of the inside of the crater, although the central mound and the cinder cone appeared subsiding and breaking down little by little, and shortly before the beginning of the third stage, these parts subsided suddenly as much as 50 m to form a cauldron at the site of the former central pit.

The activity of the third stage was characterized by repetition of explosive eruptions at the cinder cone during June 9–28, sending forth volumes of black ash clouds, with intermission of varying durations. Neither fountaining nor outpouring of lava, accompanied these explosive eruptions, indicating that this activity was no more than an explosive liberation of gases from the liquid lava in the depth of the lava conduit. But a remarkable up-and-down movement of the central mound and the adjoining slope of the cinder cone occurred in concurrence with the rise and fall of the activity, while the apical part of the central mound maintained its identity as it moved. Possibly during the activity, liquid lava stood at a low level in the conduit, but its gas potential

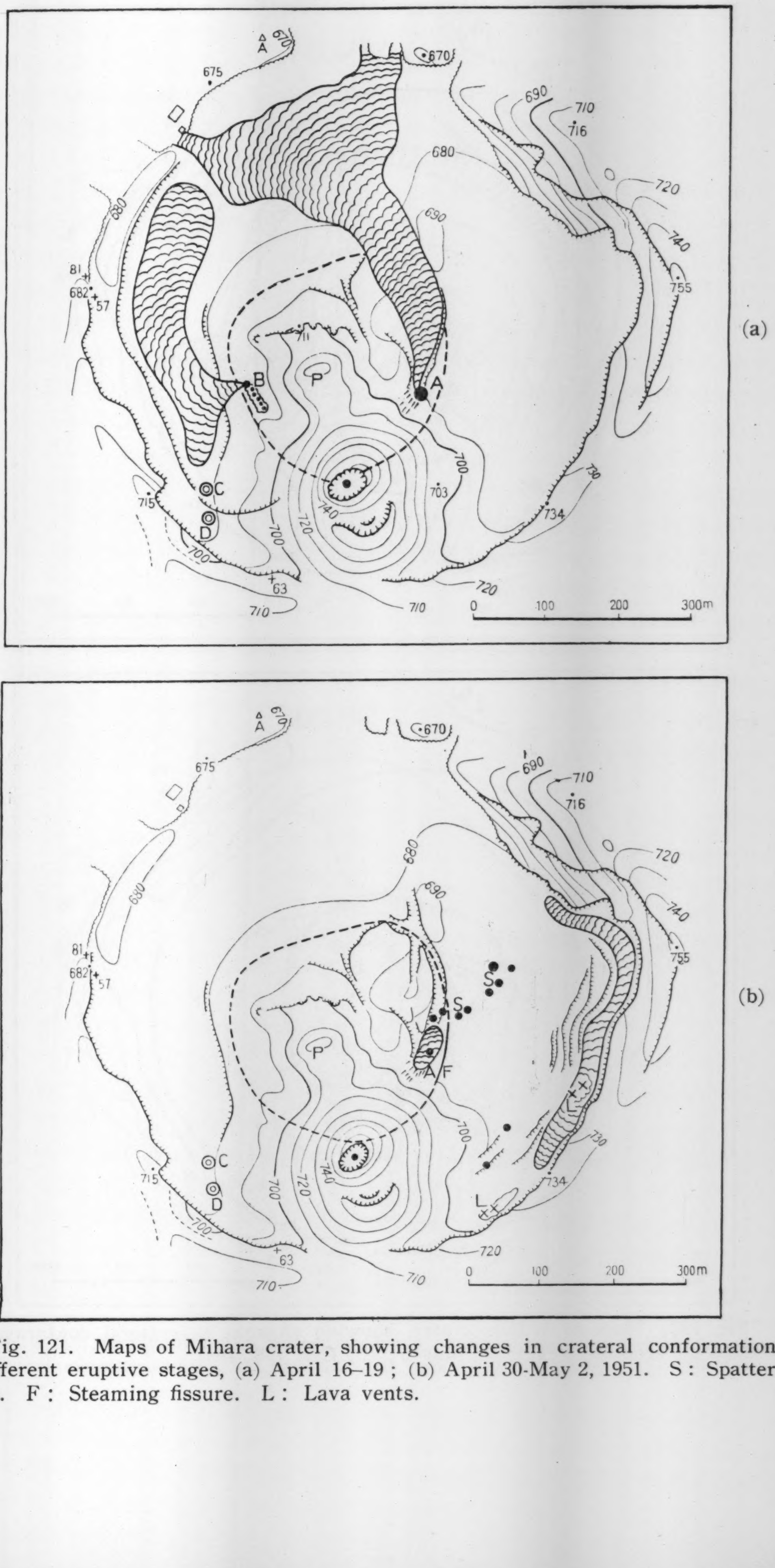

Fig. 121. Maps of Mihara crater, showing changes in crateral conformation in different eruptive stages, (a) April 16–19; (b) April 30-May 2, 1951. S: Spatter cones. F: Steaming fissure. L: Lava vents.

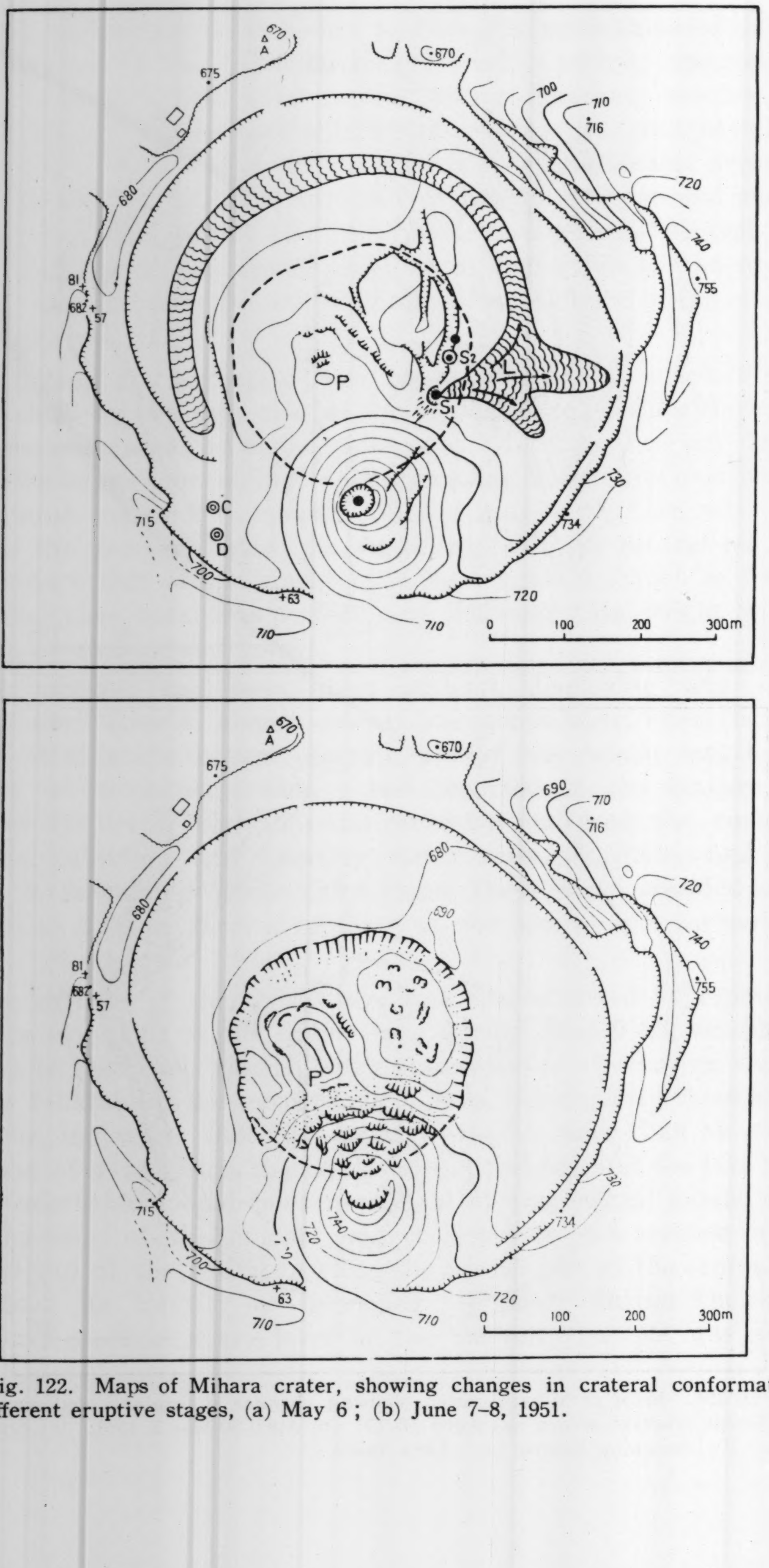

Fig. 122. Maps of Mihara crater, showing changes in crateral conformation in different eruptive stages, (a) May 6 ; (b) June 7–8, 1951.

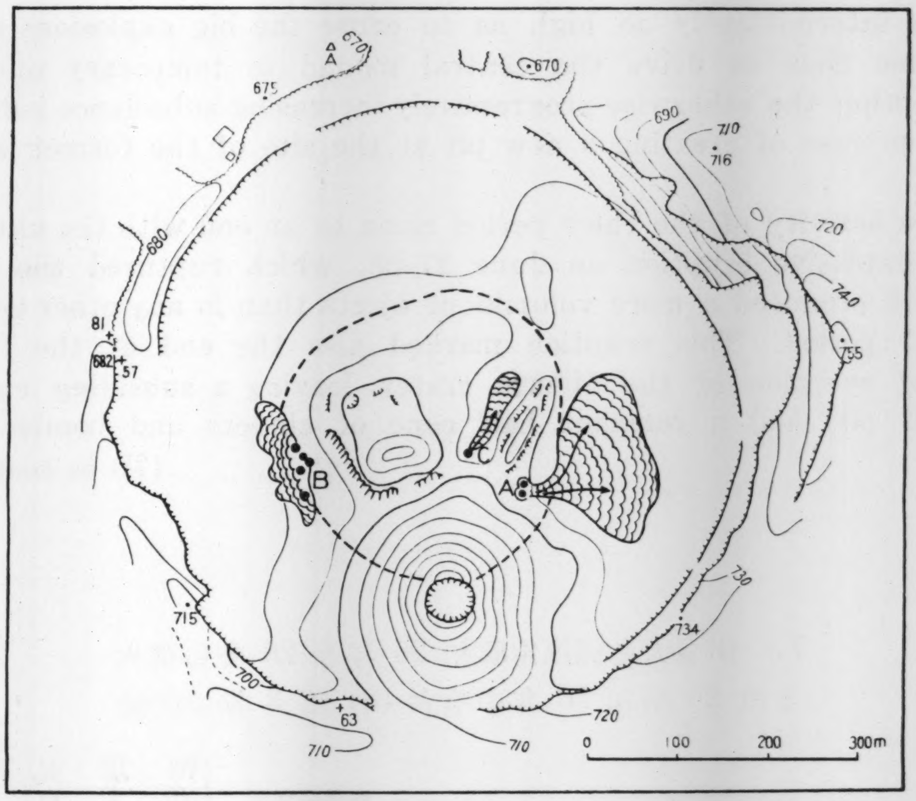

(a)

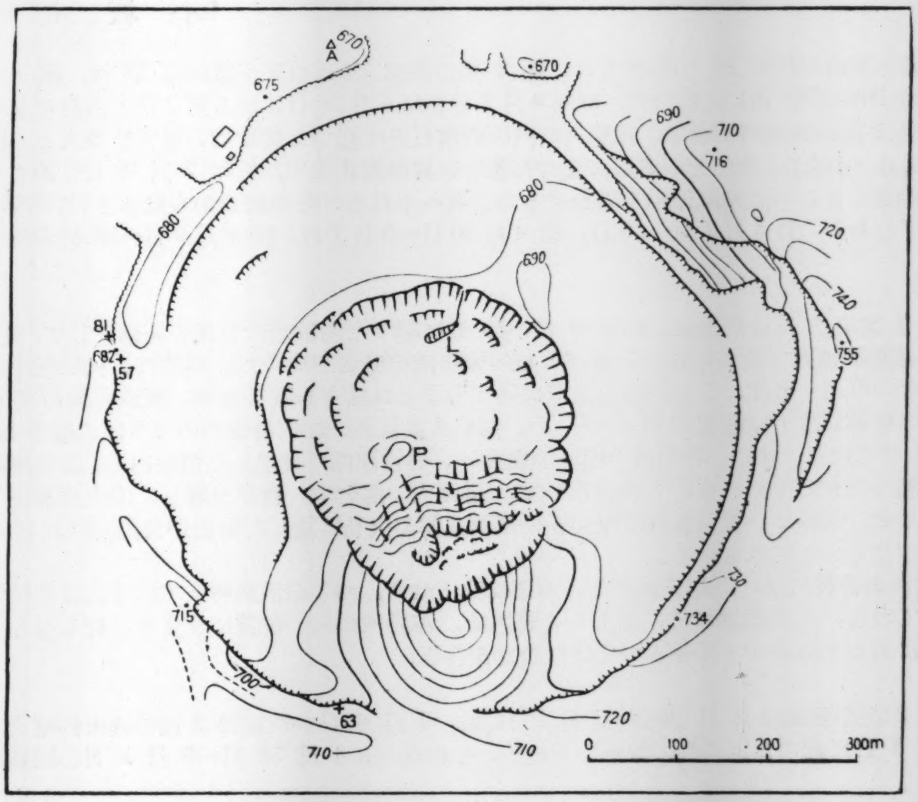

(b)

Fig. 123. Maps of Mihara crater, showing changes in crateral conformation in different eruptive stages, (a) June 10 ; (b) June 14, 1951.

became intermittently so high as to cause the big explosions and at the same time to drive the central mound to temporary upthrust, interrupting the otherwise progressively increasing subsidence indicative of the process of creating a new pit at the site of the former central pit.

The activity of the third period came to an end with the unusually heavy explosive eruption on June 27–28, which ruptured the cinder cone and produced a more voluminous ejecta than in any other eruption of that period. This eruption marked also the end of the 1950–51 cycle of eruption of the Mihara crater, leaving a subsiding cauldron (central pit) and a remnant half cone of cinders and bombs in the crater.

(To be continued)

7. 伊豆大島三原山昭和 25 年及 26 年の噴火
その 2 昭和 26 年の噴火 (B) 第 3 期の活動

地震研究所 津屋弘逵 森本良平 小坂丈予

伊豆大島三原山の昭和 26 年の噴火は，第 2 期の活動［地震研究所彙報第 32 号，第 3 冊，昭和 29 年 9 月 290—312 頁］に続いて，同年 4 月 2 日以降 6 月 28 日に至る第 3 期の活動をもつて終つた．この第 3 期の活動の特徴は，三原火口内の新噴石丘に起つた間歇的の爆発性噴火と，同火口中央部の隆起丘（中央丘）及びその周辺に起つた著しい昇降変化とで，前年 7 月 16 日に始まつた，今回の噴火輪廻のうちの活動減退相を表わすものと考へられる．その経過から見ると，この活動は，更に 3 次，すなわち (1) 4 月 2 日—20 日，(2) 4 月 30 日—5 月 7 日，(3) 6 月 9 日—28 日の各活動に分たれる．

(1) 第 3 期第 1 次の活動は，4 月 2 日—13 日に起つた間歇的の爆発を先駆として，4 月 16 日—19 日の連続的噴火で頂点に達し，翌 20 日の短時間の爆発で終つた．同時に，火口底中央部の隆起丘及びその周辺一帯は，この活動が頂点に達するまでは沈下し続けたが，頂点に達して再び上昇した．この最初の沈下は前期（2 月—3 月）の，熔岩大溢流後の熔岩導管内のガス圧の低下（熔岩源の後退）によつて起り，また，その間の間歇的爆発は，導管源部に後退した熔岩内の，ガス集積の反復によつて起つたものであろう．これに次いで，導管内の熔岩は，再び上昇し，中央丘及びその周辺を隆起せしめ，同時に，噴石丘及び隆起丘の東西両側の火孔に達した熔岩の自由面における連続的噴火が起つたものと考へられる．

第 1 次活動直後には，隆起丘及びその周辺は沈下せず，つぎの活動時まではとんどそのままの状態を保つていた．この期間には，おそらく熔岩は，導管内の高い位置に止まり，間もなくつぎの噴火を起すに足る十分のガス圧をもつていたのであろう．

(2) 第 2 次の活動は 4 月 30日—5 月 2 日及び 5 月 6 日—7 日の 2 回の連続的噴火と，その間，5 月 3 日に起つた短時間の爆発とである．そのうち，4 月 30 日—5 月 2 日の活動は，噴石

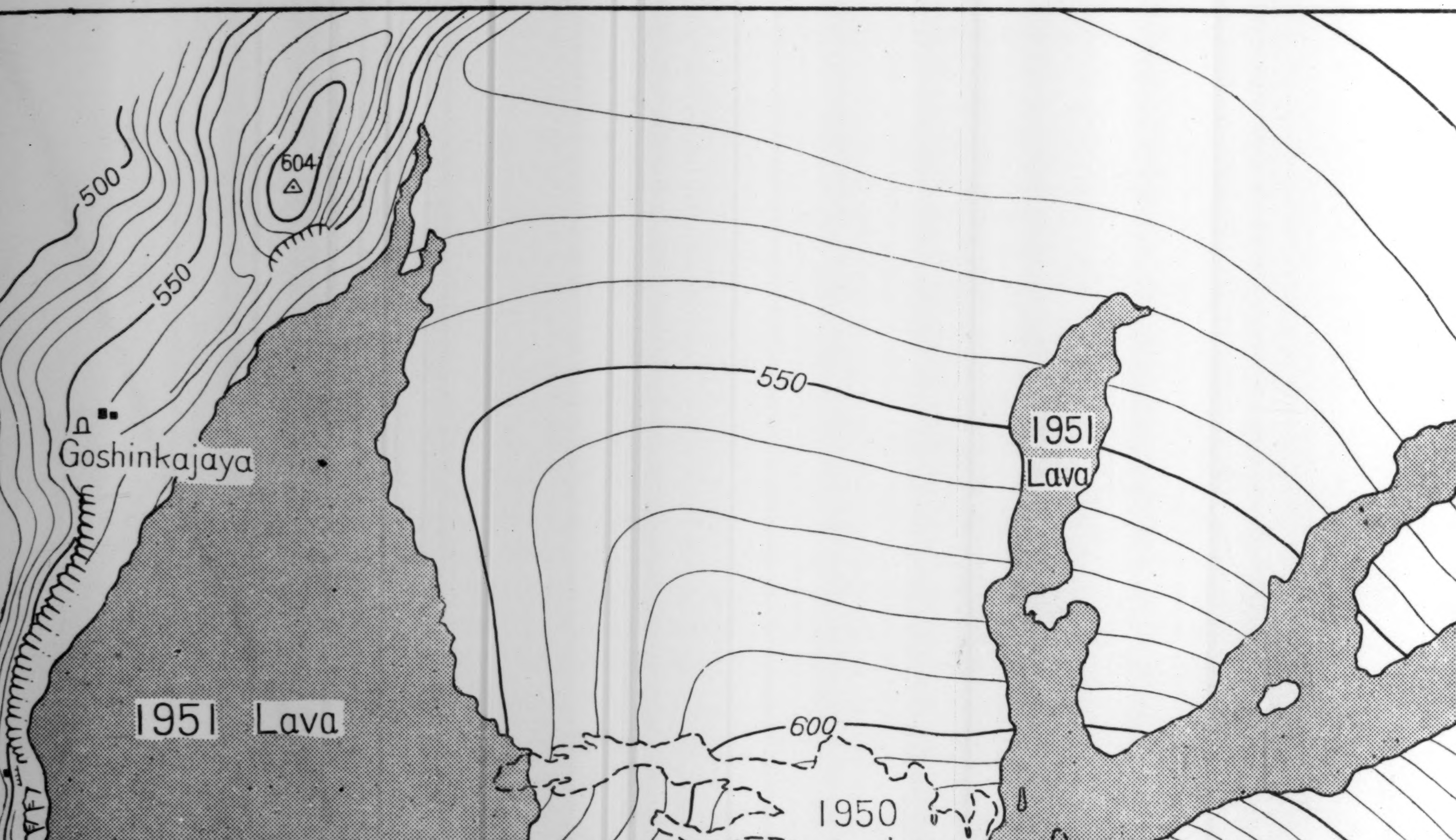

Fig. 124. Topographical map showing the 1950-51 lava flows and the feature of Mihara crater, as observed in A
former Kakôjaya at the northern crater rim had been buried be

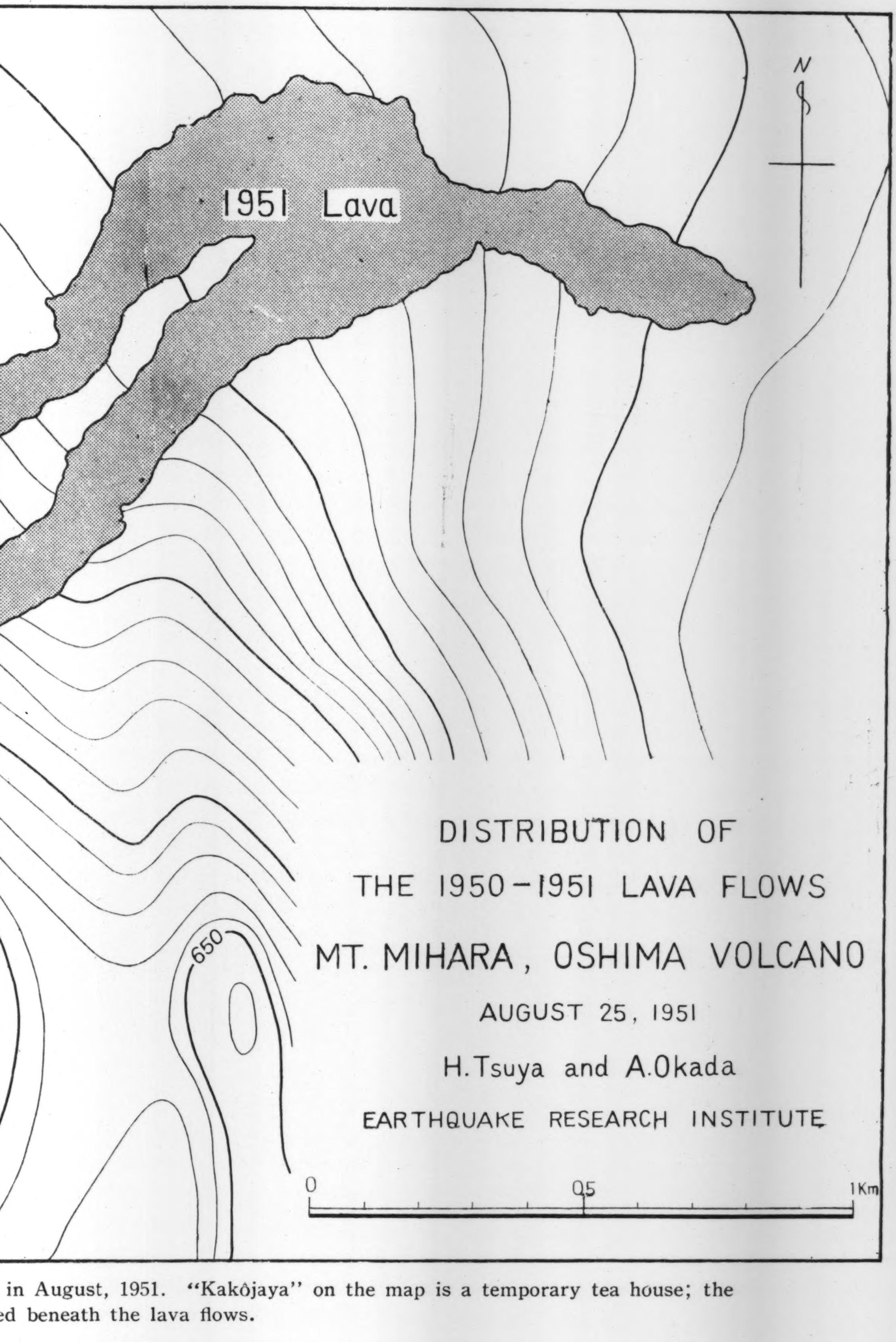

in August, 1951. "Kakôjaya" on the map is a temporary tea house; the
ed beneath the lava flows.

(a)

(b)

Fig. 125. Black ash clouds rising with explosions from the active vent on the cinder cone, as seen from Go-shinkajaya, (a) April 16; (b) April 18, 1951.

Photo. S. Watanabe.

(a)

(b)

Fig. 126. Lava fountain and flow on the crater floor east of the central mound, and the cinder cone in eruption at left, (a) as seen from the southeast crater rim; (b) from Kengaminé, the east crater rim, April 18, 1951. Photo. S. Watanabe.

(震研彙報 第三十三号 図版 津屋・森本・小坂)

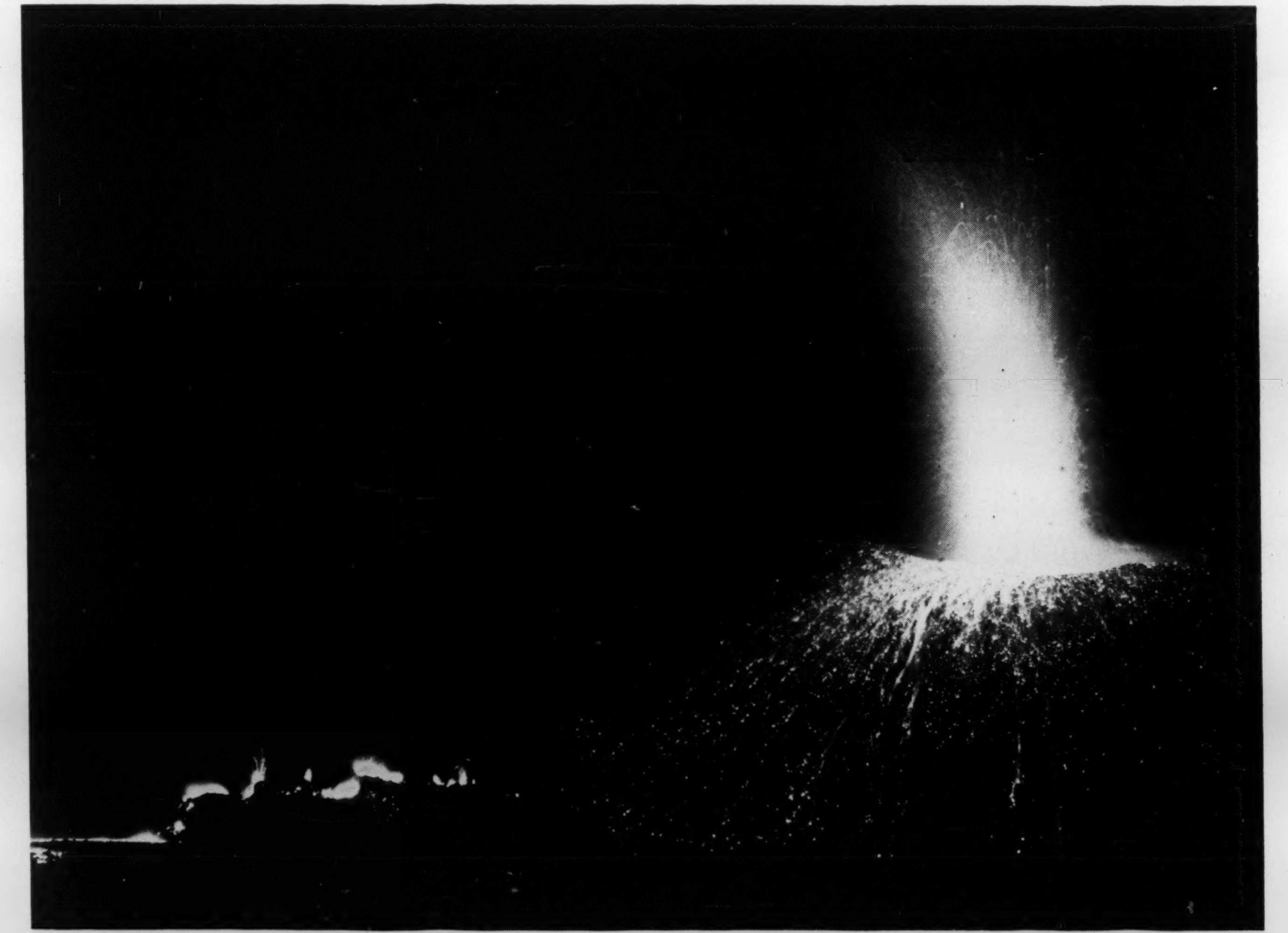

Fig. 127. Explosive eruption at the cinder cone (right) and lava fountaining and spattering at the northwest base of the cone (left), as seen from the west crater rim, April 18, 1951.

Photo. S. Watanabe.

Fig. 128. The cinder cone, as seen from the west crater rim, showing a quiet phase just after the eruption of April 16–19. April 22, 1951. Photo. S. Watanabe.

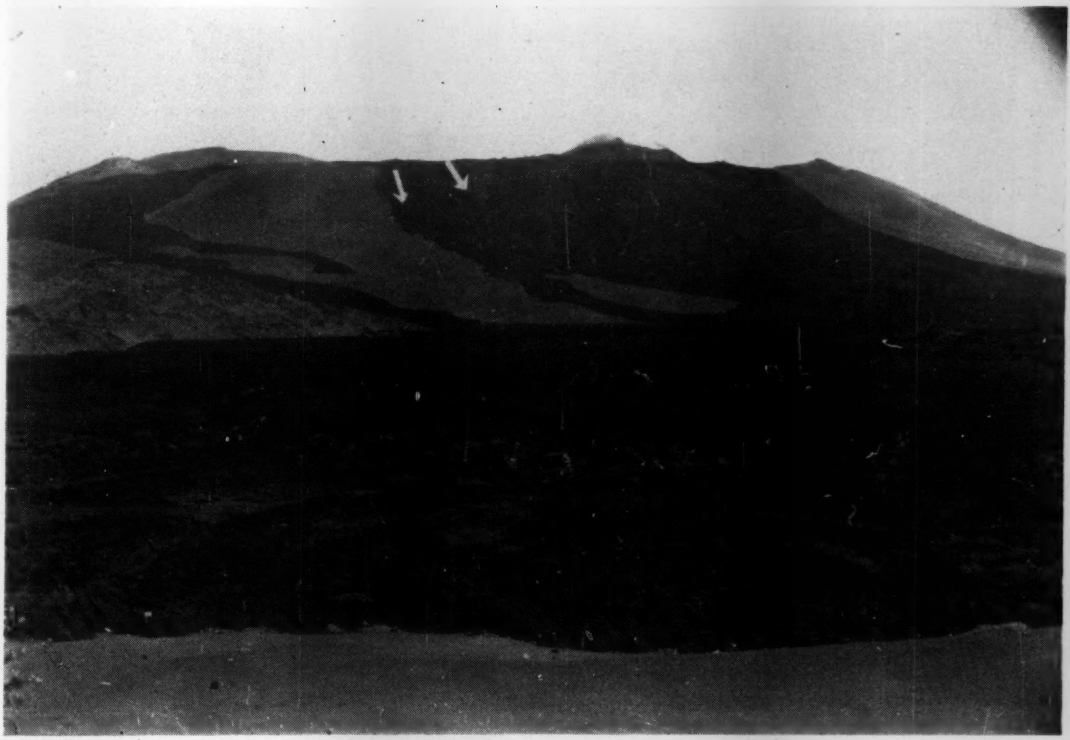

Fig. 129. New lava flows of April 19, shown at arrows, on the northwest slope of Mt. Mihara. Cf. Fig. 125 b. April 27, 1951. Photo. S. Watanabe.

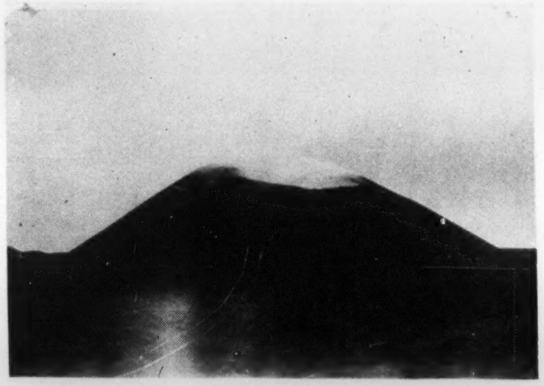

Fig. 130. View of the finished cinder cone from the northwest, April 28, 1951.

Fig. 131. Closer view of the cinder cone from the west, April 28, 1951.

Fig. 132. Two spatter cones (c, d), now extinct and covered with cinders. At left, the west rim of the crater, at extreme right, the west base of the main cinder cone, April 28, 1951.

Fig. 133. Mihara crater, showing the cinder cone in eruption (right) and the central upthrusted mound (centre). Kengaminé, the east crater rim, at distant left. April 30, 1951.

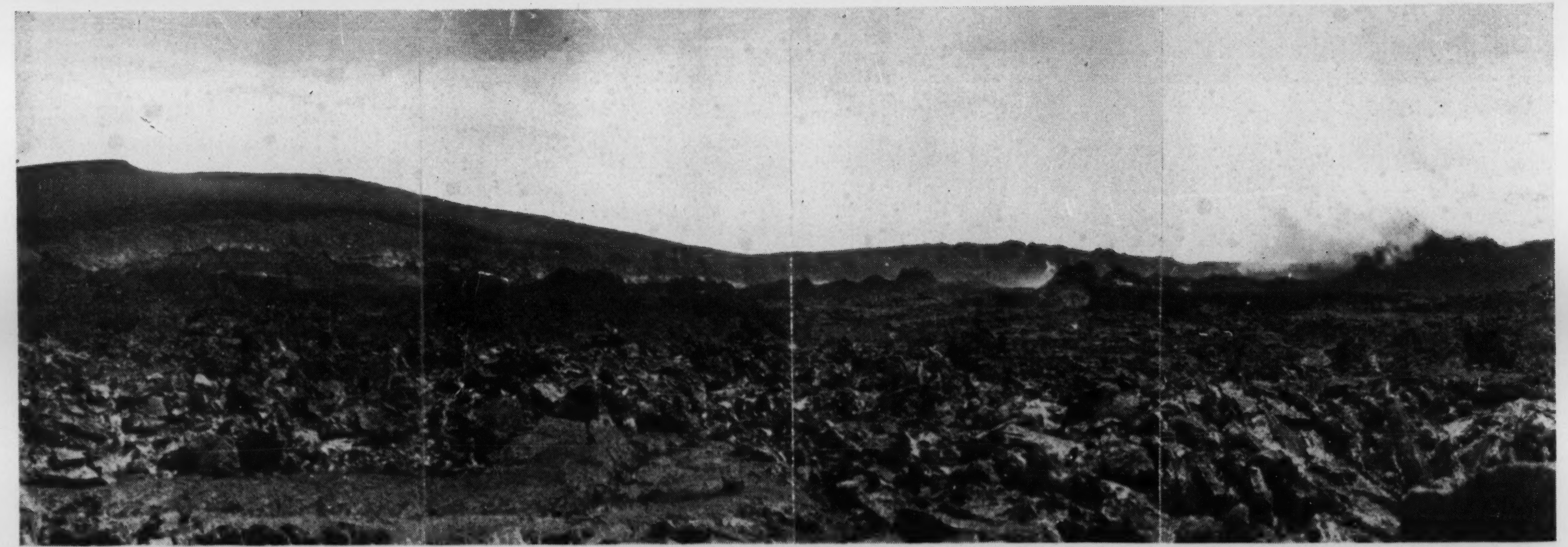

Fig. 134. General view of the crater floor northeast of the cinder cone, showing new spatter cones ranging northeast toward the bluff of the east crater rim (Kengaminé) from the base of the main cinder cone (in vapour clouds at extreme right). April 30, 1951.

(a)

(b)

Fig. 135. General view of the crater floor east and northeast of the main cinder cone, showing the new spatter cones and steaming fissures, (a) looking down from Kengaminé ; (b) from the southeast crater rim, May 1, 1951.

(a)

(b)

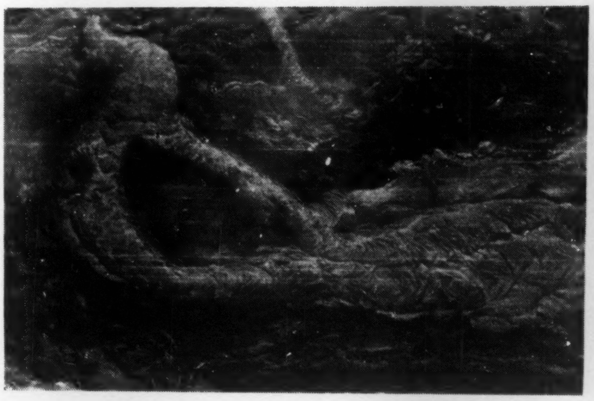

(c)

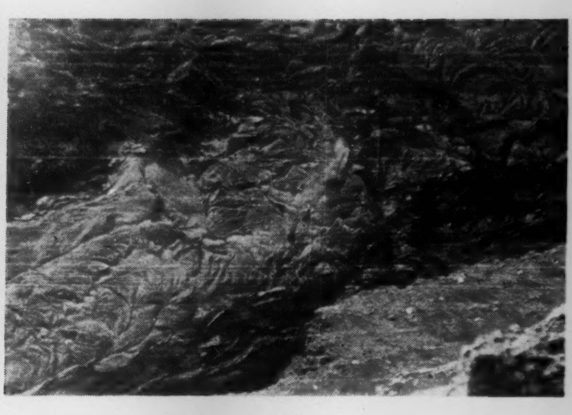

(d)

Fig. 136. Lava oozing out of temporary vents in the crater floor near the base of the east crater wall, May 1, 1951.

(a) General view, looking down from the upper edge of the crater wall.
(b) Closer view of the flows.
(c) Showing one of the flows and its source vent (upper left).
(d) Front of the same flow, showing a skin of wrinkled and ropy pahoehoe.

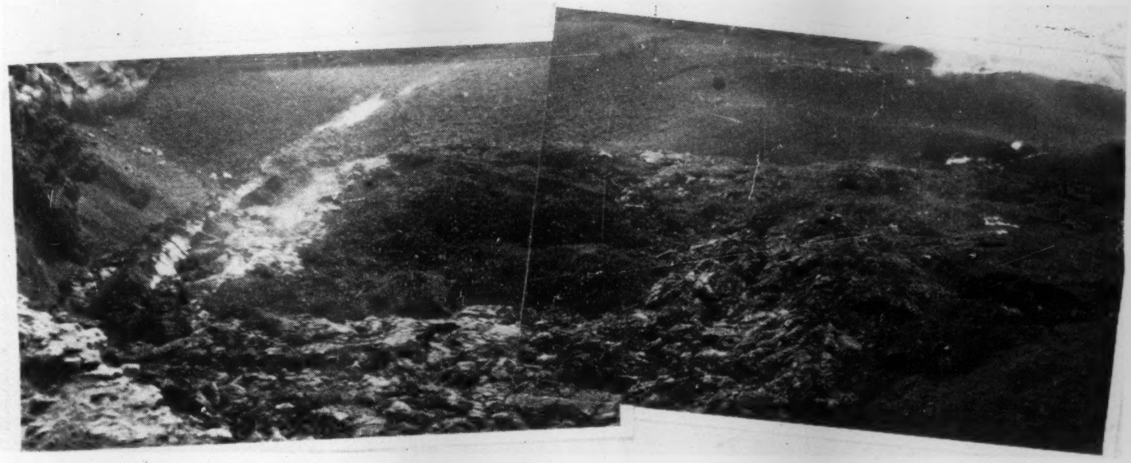

(a)

(b)

(c)

Fig. 137. Lava oozing out of small vents in loose pile of cinders at the east base of the cinder cone, April 30, 1951.

(a) General view, with the bluff of the southeast crater rim at extreme left and the east base of the cinder cone in background.

(b) One of the lava flows by day.

(c) The same by night.

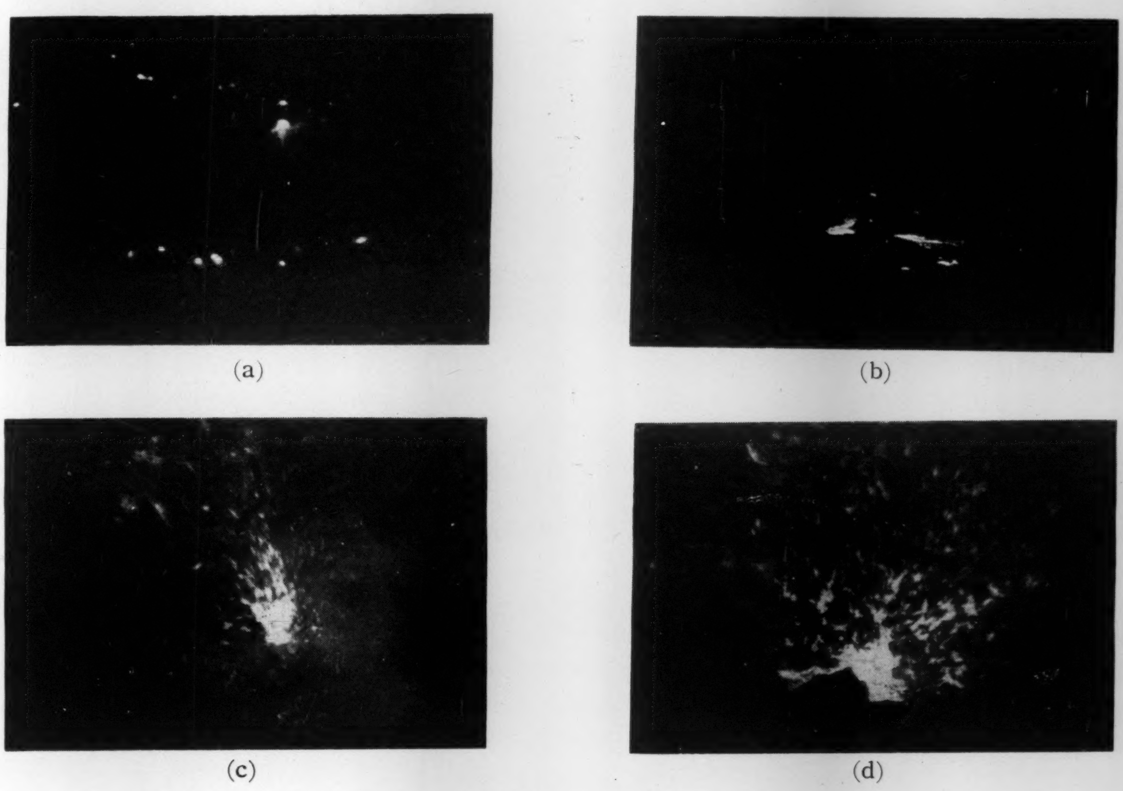

Fig. 138. Night view of the acivity in the crater floor northeast and east of the cinder cone, April 30, 1951.

(a) General view slowing glow of the active spatter cones and lava vents, as seen from the southeast crater rim.

(b) Glow of a small lava flow and a near-by spatter vents.

(c), (d) Telephoto night views of one of the active vents, showing lava spattering.

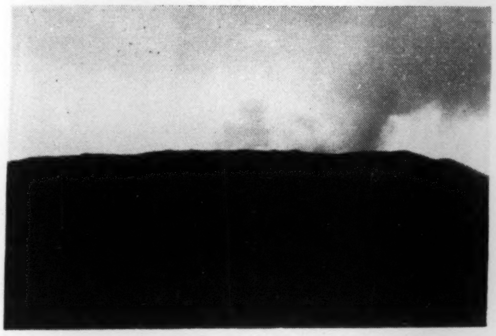

Fig. 139. Vapour clouds rising from both the cinder cone and the crater floor, as seen from Goshinkajaya, May 1, 1951.

Fig. 140. Night view of the last explosion of the activity of April 30-May 1, as observed from Goshinkajaya, May 1, 20h, 1951.

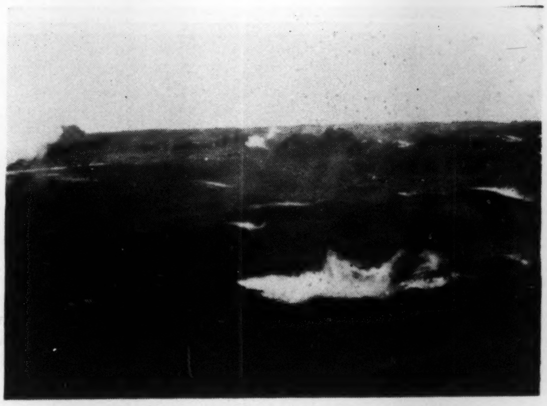

Fig. 141. The crater floor northeast of the central mound, as seen northward from the edge of the southeast crater rim, showing spatter cones now dormant, and steaming fissures, May 1, 1951.

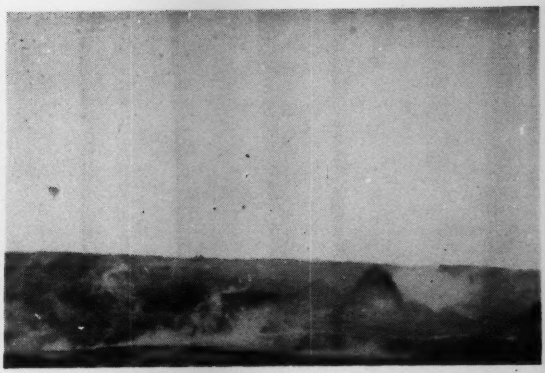

Fig. 142. Telephoto view of the upper left part of Fig. 141, showing a steaming fissure, with two spatter cones in the opposite side of the fissure, May 1, 1951.

Fig. 143. Pahoehoe flows of April 30, showing ropy, wrinkled structure of their skin, May 1, 1951.

Fig 144. Lava tongue (centre) flowing out of a crevice in one of the older flows. At upper right, the central mound. May 1, 1951.

Fig. 145. Black ash clouds, showing explosive eruption at the cinder cone, May 6, 1951. Photo. S. Watanabe.

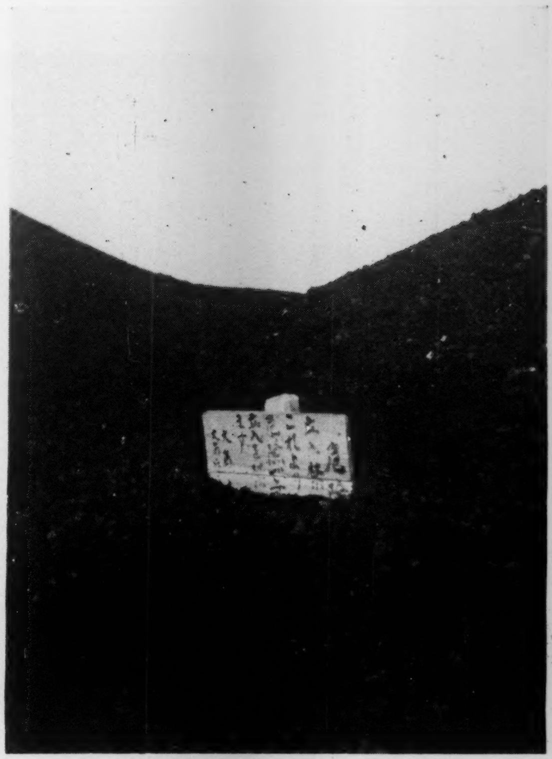

Fig. 146. A wooden board with notice "Keep off ! Danger ! ", buried deep in the new pile of cinders and bombs. At upper left, the southwest slope of the cinder cone. May 1, 1951. Photo. S. Watanabe

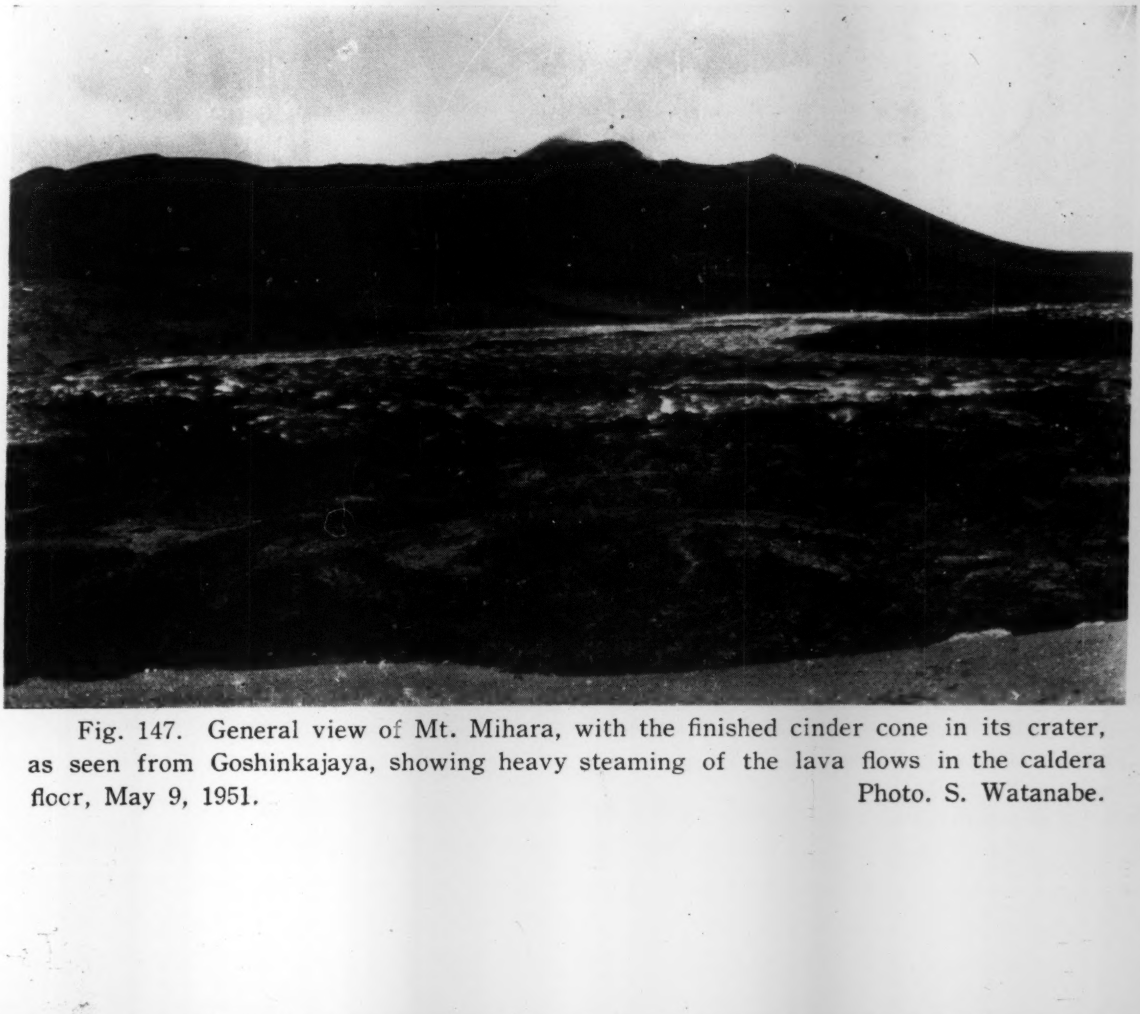

Fig. 147. General view of Mt. Mihara, with the finished cinder cone in its crater, as seen from Goshinkajaya, showing heavy steaming of the lava flows in the caldera floor, May 9, 1951. Photo. S. Watanabe.

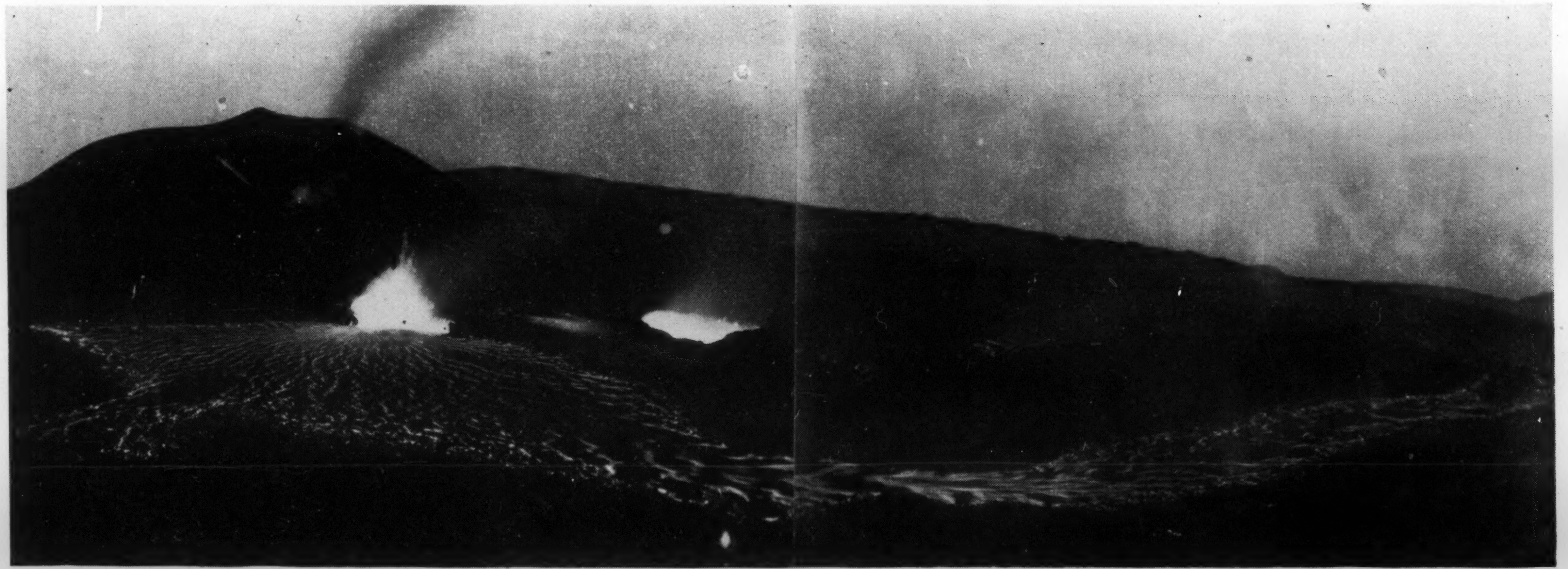

Fig. 148. Mihara crater as seen westward from Kengaminé, the east rim of the crater, showing lava fountains and flow. At upper left, the cinder cone in explosive eruption, May 6, 1951. Photo. S. Watanabe.

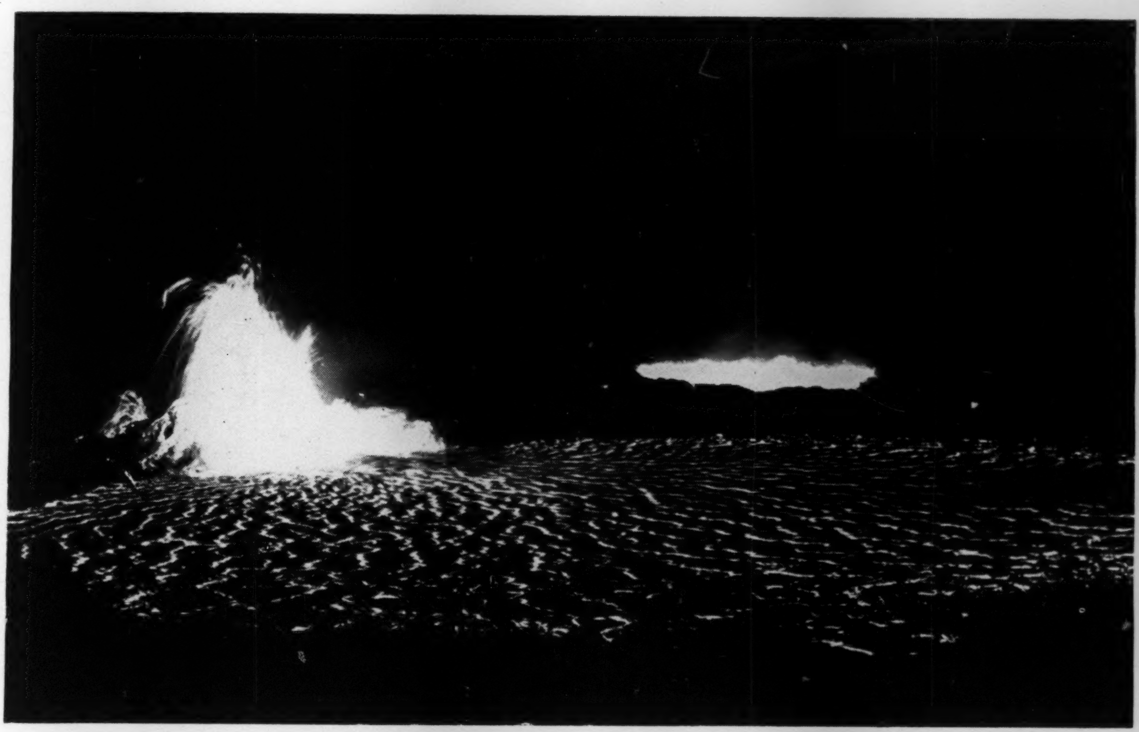

(a)

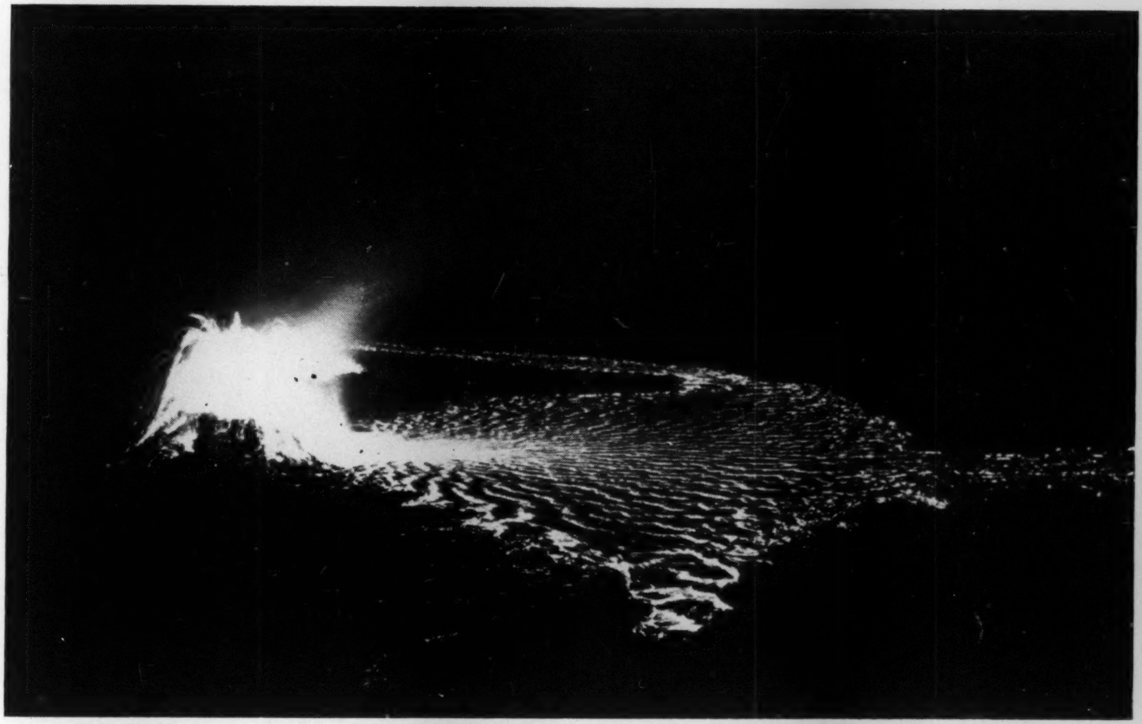

(b)

Fig. 149. Lava flow and fountains, (a) as seen from Kengaminé; (b) from the southeast rim of the crater, May 6, 1951. Photo. S. Watanabe.

(a)

(b)

Fig. 150. View of the crater, showing great changes in feature by the ups and downs of the fill of the former central pit. Photo. S. Watanabe.

(a) New cauldron formed by subsidence, June 8, 1951. Cf. Fig. 171 a.

(b) The central mound rising again above the general level of the surrounding crater floor, June 10, 1951. Cf. Fig. 171 b.

(a)

(b)

Fig. 151. View of the cinder cone and the central mound, showing great changes in conformation, (a) June 10 ; (b) June 14, 1951. Cf. Fig. 172 a. Photo. S. Watanabe.

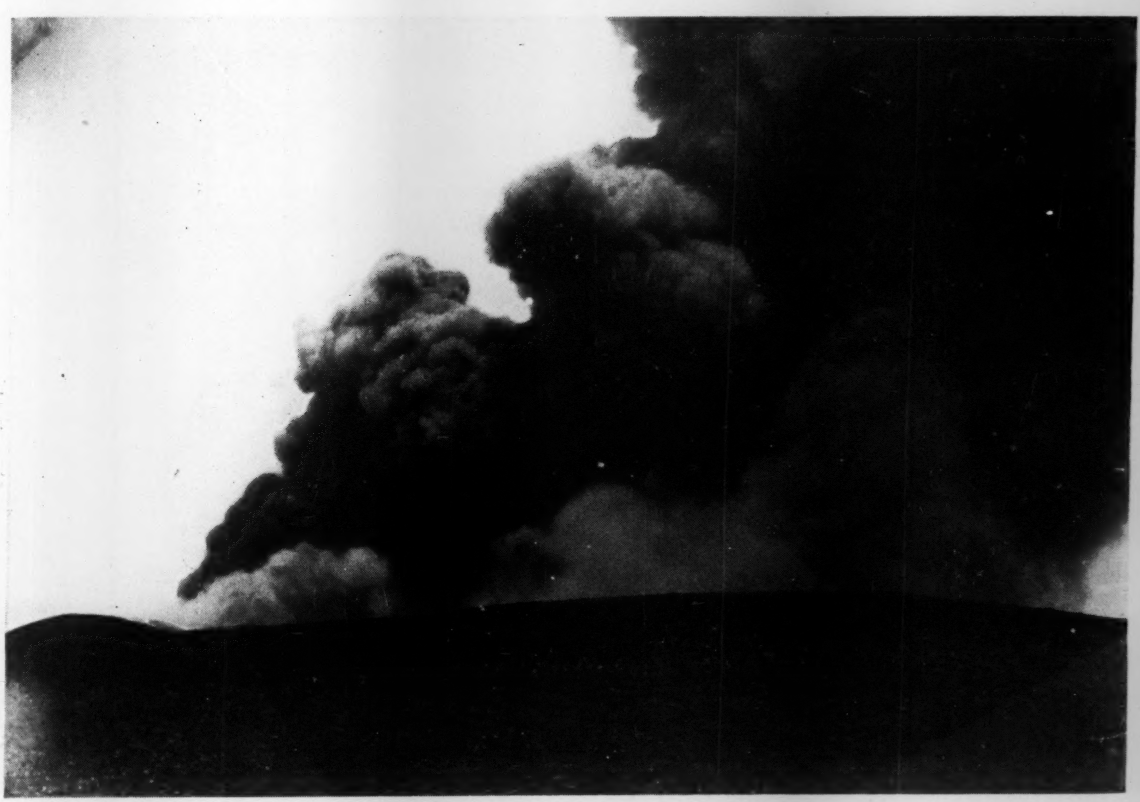

(a)

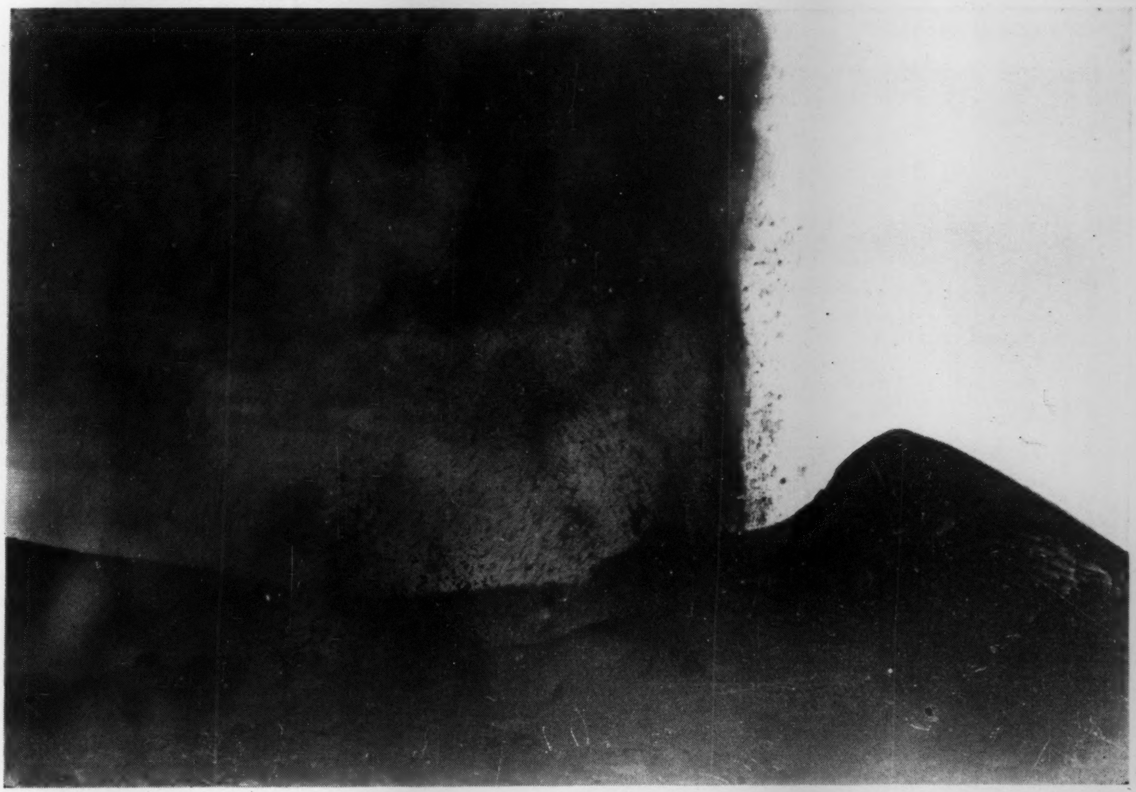

(b)

Fig. 152. Explosive eruption, June 17, 1951. Photo. S. Watanabe.
(a) Volumes of black ash clouds rising from the cinder cone, as seen northwestward from halfway down the outer slope of the southeast rim of the crater; (b) Explosive emission of bombs and cinders both at the main vent on the cinder cone and at a subsidiary vent at the northwest base of the cone.

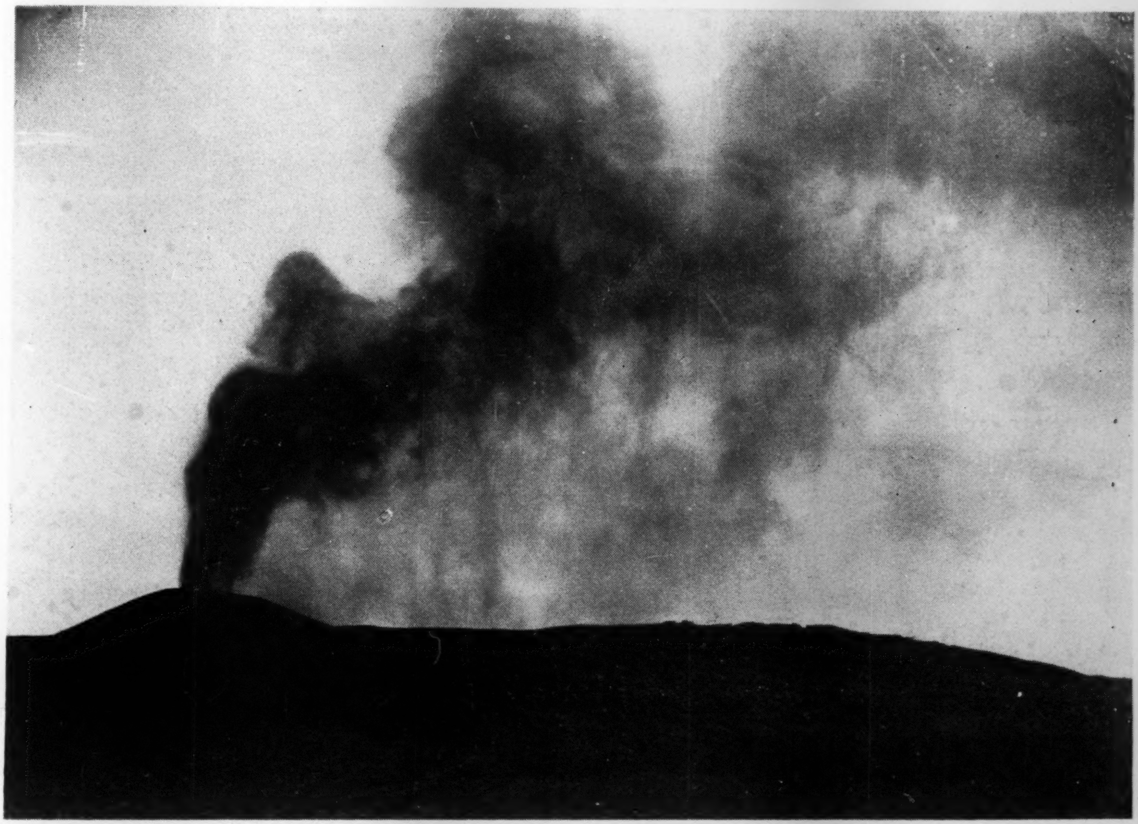

Fig. 153. The cinder cone (left), as seen from the south base of the central cone (Mt. Mihara), showing a phase of explosive eruption, June 17, 1951. Photo. S. Watanabe.

Fig. 154. Explosive eruption, as seen from Goshinkajaya, showing a column of fire accompanied by ash cloud, June 19, 1951. Photo. S. Watanabe.

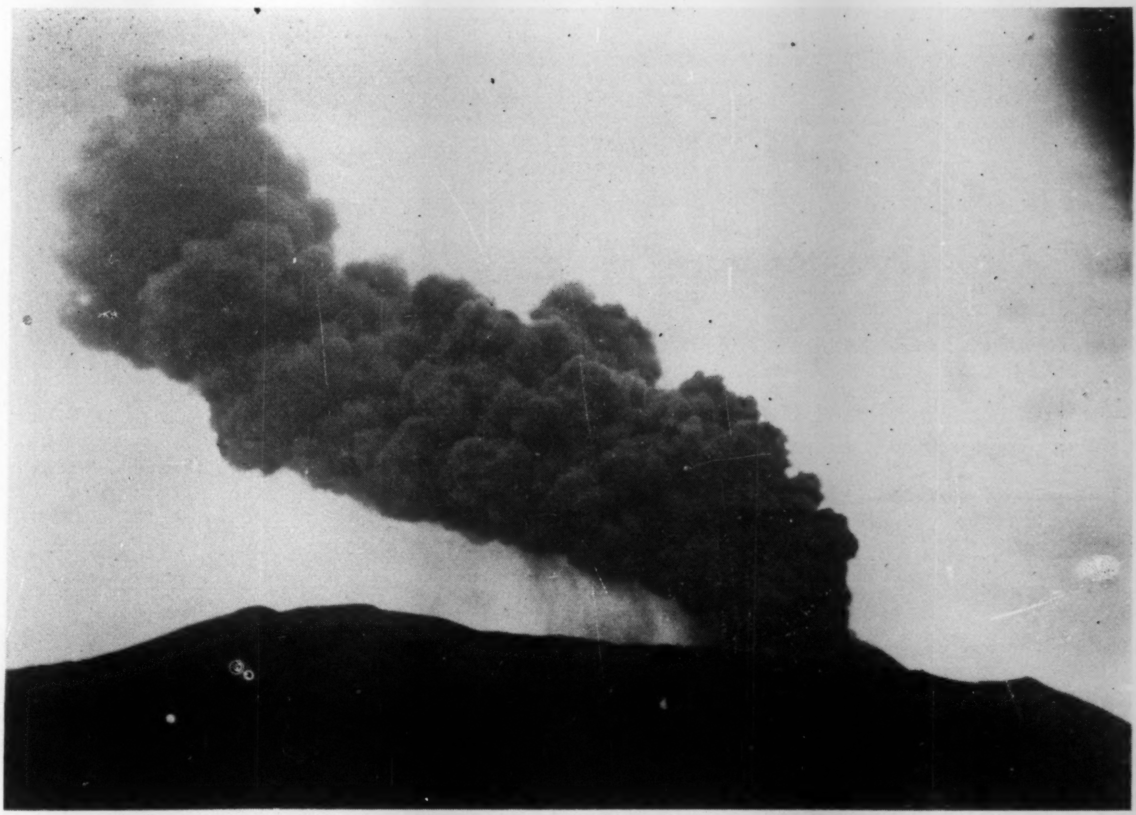

(a)

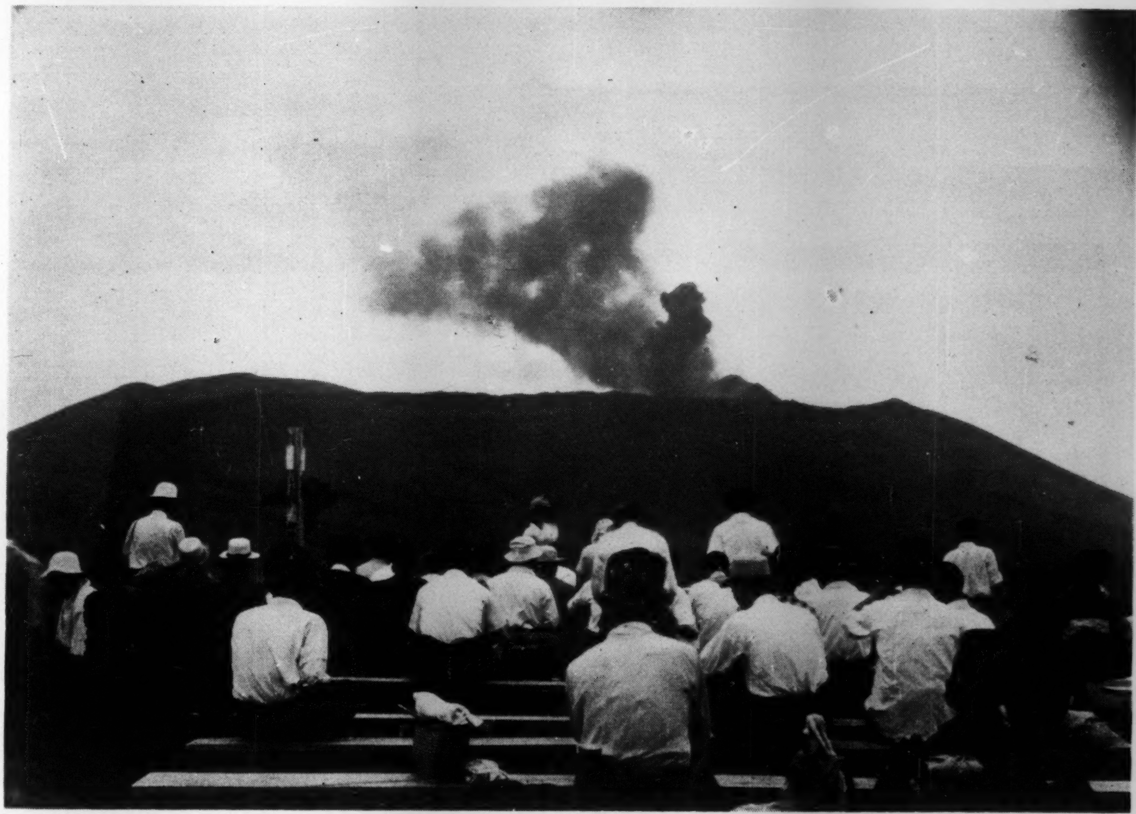

(b)

Fig. 155. Explosive eruption, as seen from Goshinkajaya, showing (a) continuous spouting of ash cloud ; (b) intermittent puffs of ash cloud, June 21, 1951.

Photo. S. Watanabe.

（震研彙報 第三十三号 図版 津屋・森本・小坂）

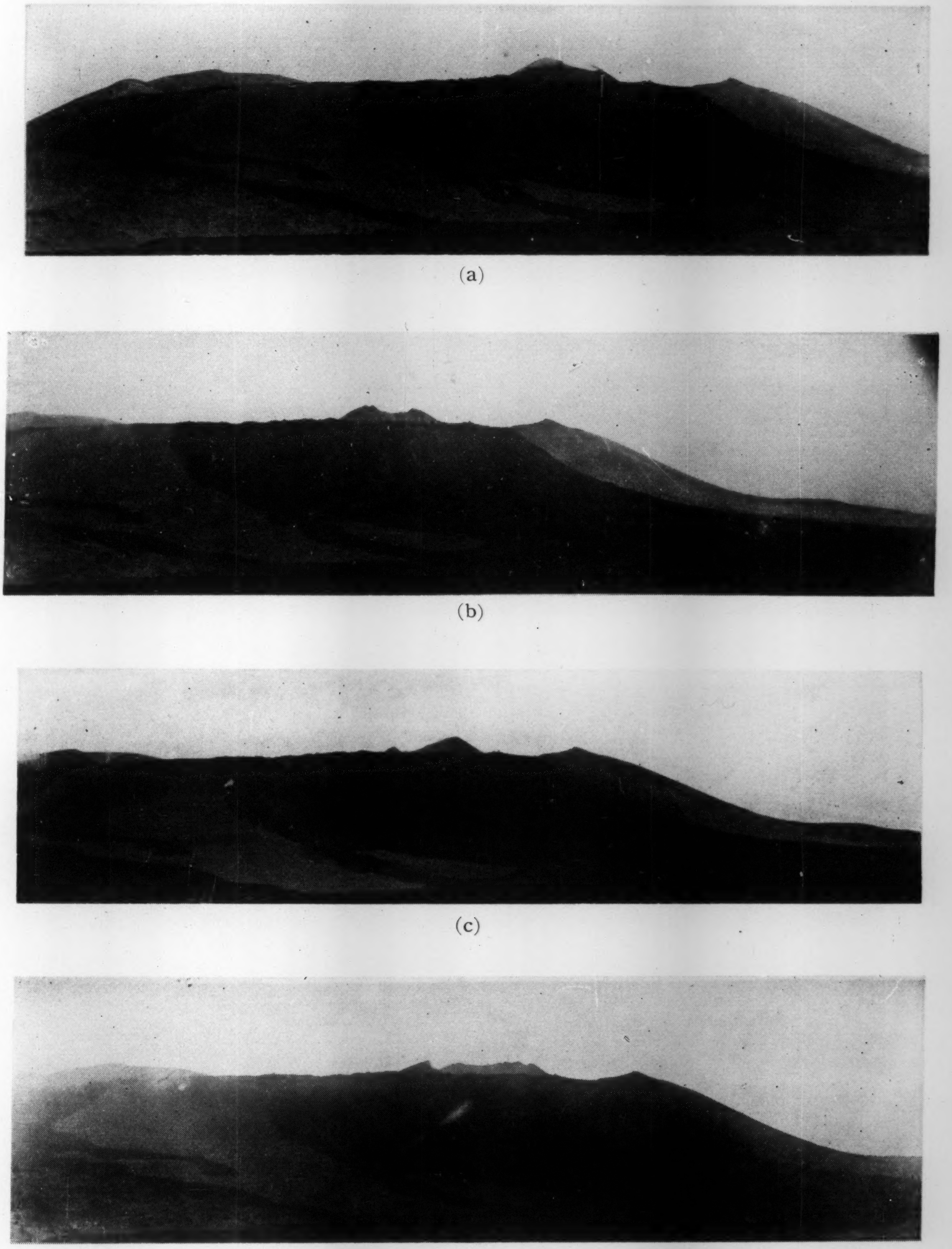

(a) (b) (c) (d)

Fig. 156. View of Mt. Mihara, as seen from Goshinkajaya, showing successive changes in conformation of the cinder cone during the third period of eruption, (a) April 26; (b) May 4; (c) June 13; (d) June 22, 1951. Photo. S. Watanabe.

Fig. 157. Bombs and cinders on the west rim of the crater, ejected by the eruption of June 27–28, 1951.

(震研彙報 第三十三号 図版 津屋・森本・小坂)

Fig. 158. General view of the new lava flows in the west caldera floor, showing their surface covered with later ejecta (ash and cinders). August 15, 1951.

(a)

(b)

Fig. 159. The deposit of ash and cinders that has covered the southwest margin of the new flows (Fig. 158, at left), (a) View as seen east toward the mountain; (b) View as seen west toward the caldera wall. August 15, 1951.

Fig. 160. The central cauldron (new central pit), as seen from its west rim. At right, the north slope of the cinder cone. August 15, 1951.

Fig. 161. The cinder cone, as seen from its northwest base, showing collapses of its north slope. August 15, 1951.

(震研彙報 第三十三号 図版 津屋・森本・小坂)

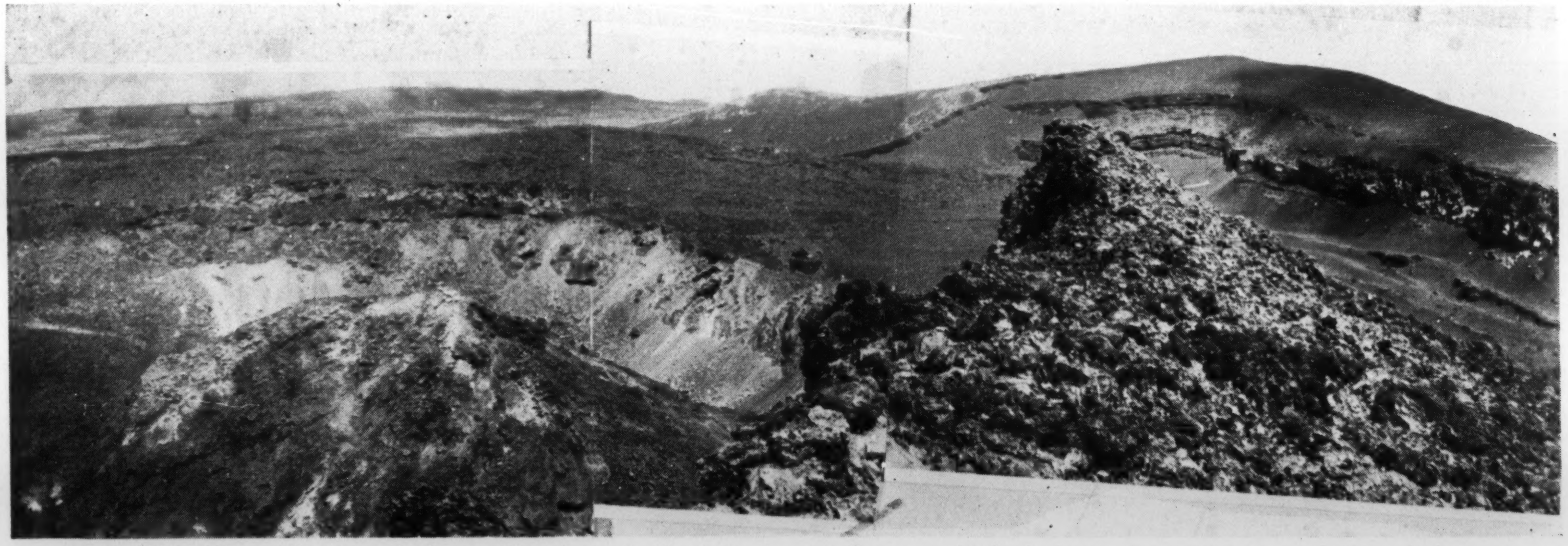

Fig. 162. General view of the northeastern half of the crater floor, as looked down from the top of the cinder cone, August 15, 1951.

Fig. 163. Southwest wall of the vent on the cinder cone, showing a fumarole, August 15, 1951.

Fig. 164. Bottom of the vent on the cinder cone, August 15, 1951.

Fig. 165. General view of the northwest part of the crater floor, now buried deep with new ejecta. At extreme right, the cinder cone ; at centre, the new central pit. August 15, 1951.

Fig. 166. The cinder cone showing perfect conical slopes on its south and west sides. At extreme left, the west rim of the crater. August 15, 1951.

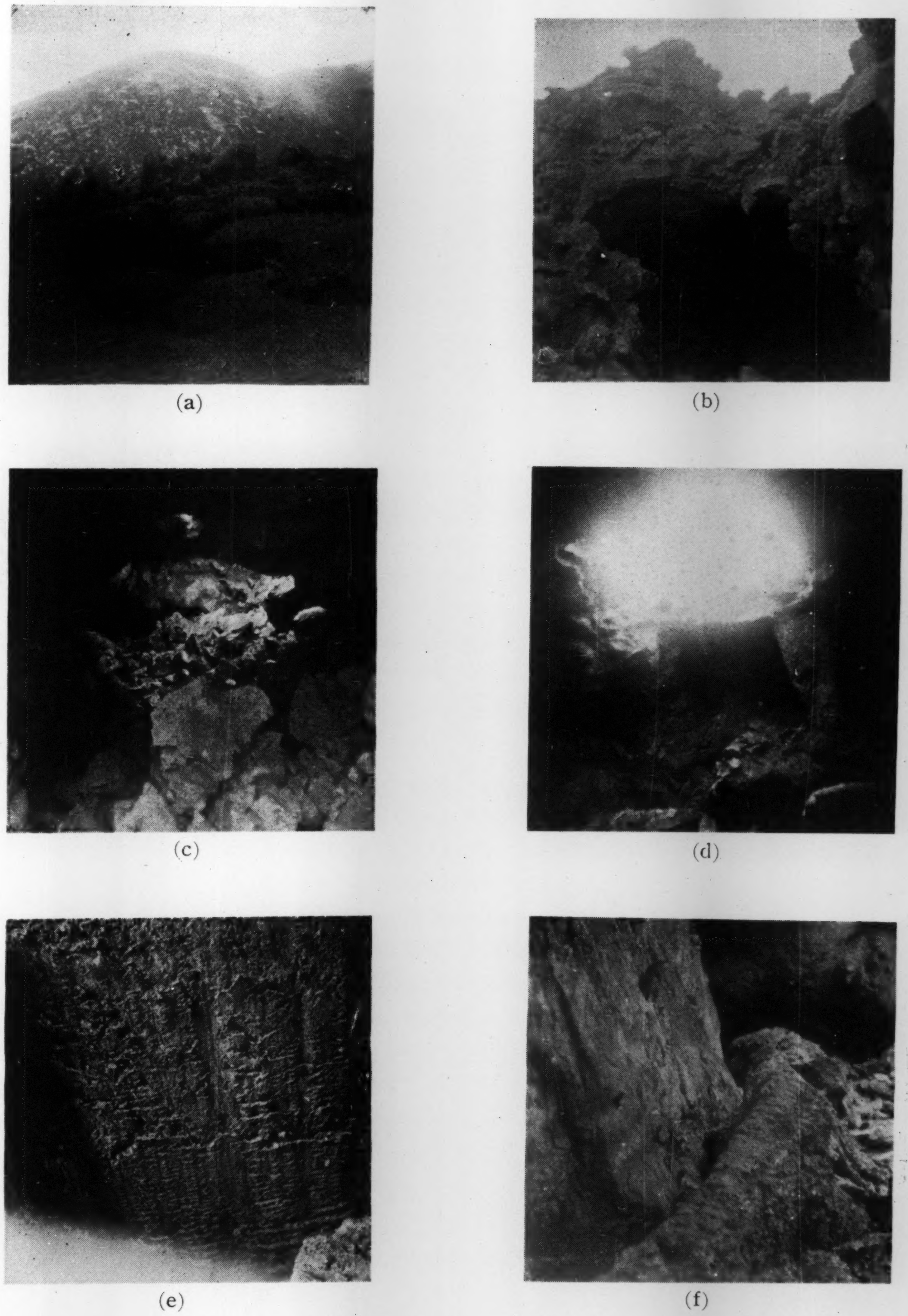

Fig. 167. Lava tunnel, (a) a hole in the roof; (b) entrance to the tunnel; (c) interior of the tunnel; (d) the hole in the roof, as seen from the interior; (e) parallel grooves in the side wall; (f) a low ridge of lava running alongside the wall.

(震研彙報 第三十三号 図版 津屋・森本・小坂)

(a)

(b)

(c)

Fig. 168. Lava dike, possibly representing a part of solidified feeder of the first spatter cones which were active in March, 1951. (a) Longitudinal view of the dike; (b) side view; (c) slickenside on the wall of the dike.

Fig. 169. The only spatter cone left uncovered with later ejecta. August 15, 1951.

[H. TSUYA, R. MORIMOTO and J. OSSAKA.]

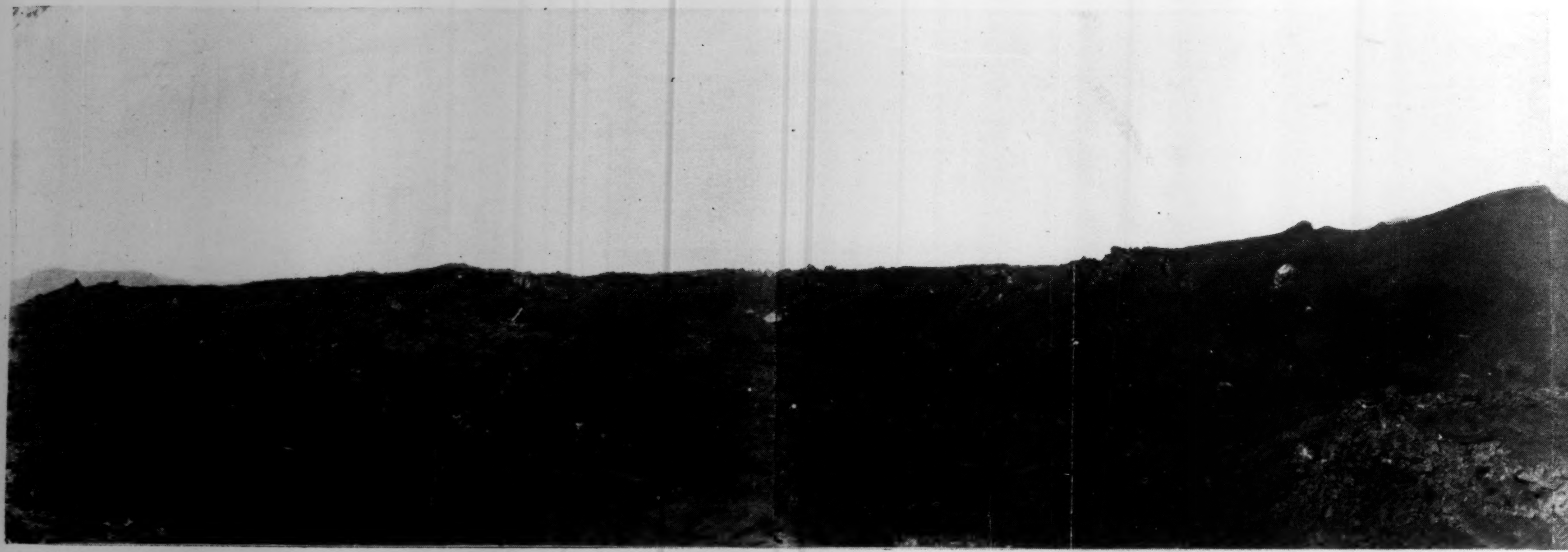

Fig. 170. General view of the western half, c
The half demolished spatter cone (c) show a stea
east rim of the crater, in the centre back ; the r

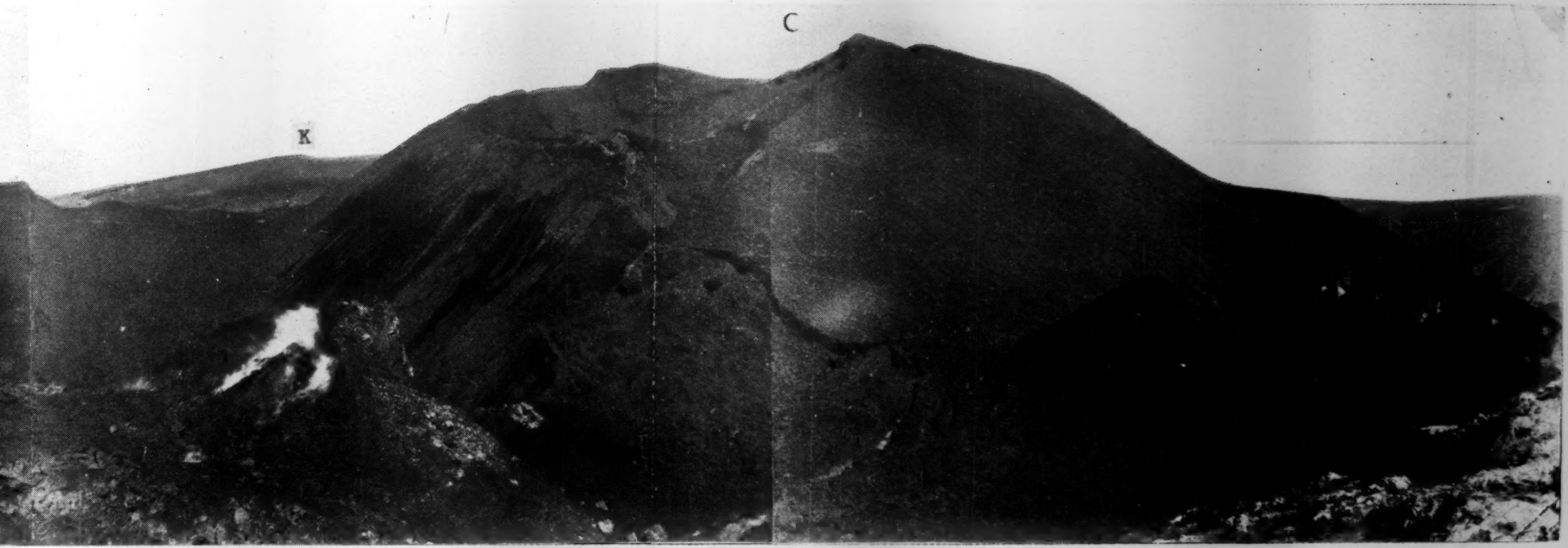

lf, of Mihara crater. The cinder cone (C) and the central upthrusted mound (P), both showing fissures and slump scarps. steaming activity, and the spatter cone (d) has become extinct, being covered entirely with cinders. Kengaminé (K), the the northwest somma (S) at distant left. April 9, 1951. Photo. S. Watanabe.

(震研彙報 第三十三号 図版 津屋・森本・小坂)

(a)

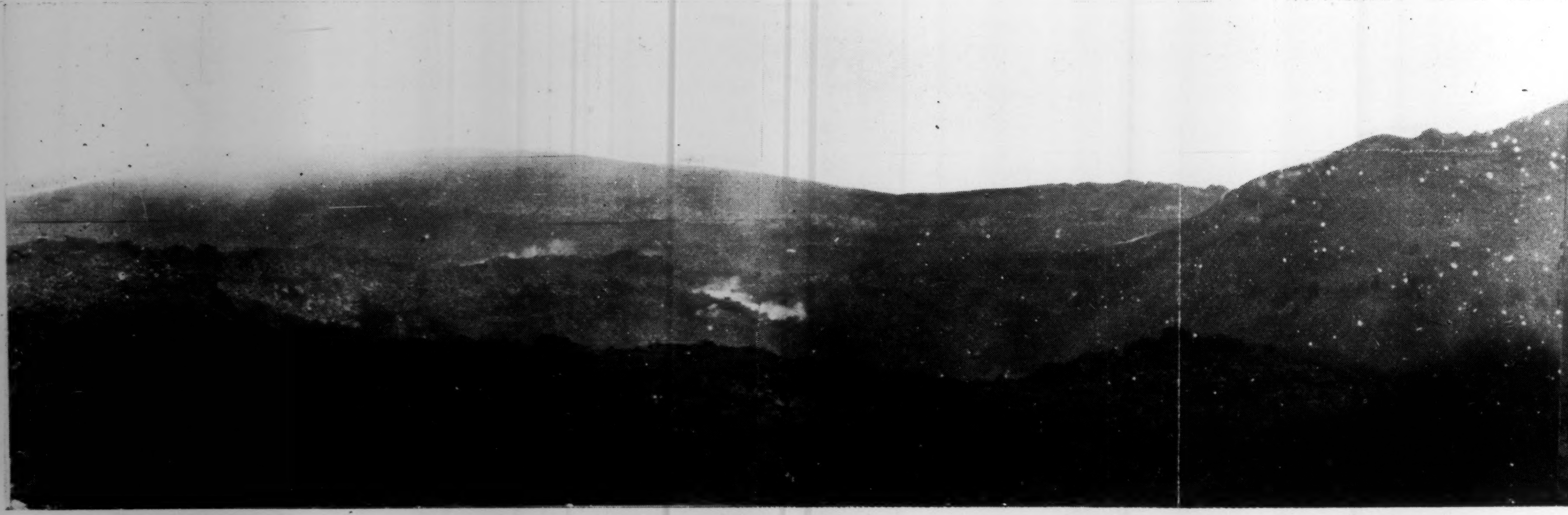

(b)

Fig. 171. General view of the northwest part of Mihara crater, showing changes in conformation of its central part, (a)

(a) June 8 ; (b) June 14, 1951. Photo. S. Watanabe.

(a)

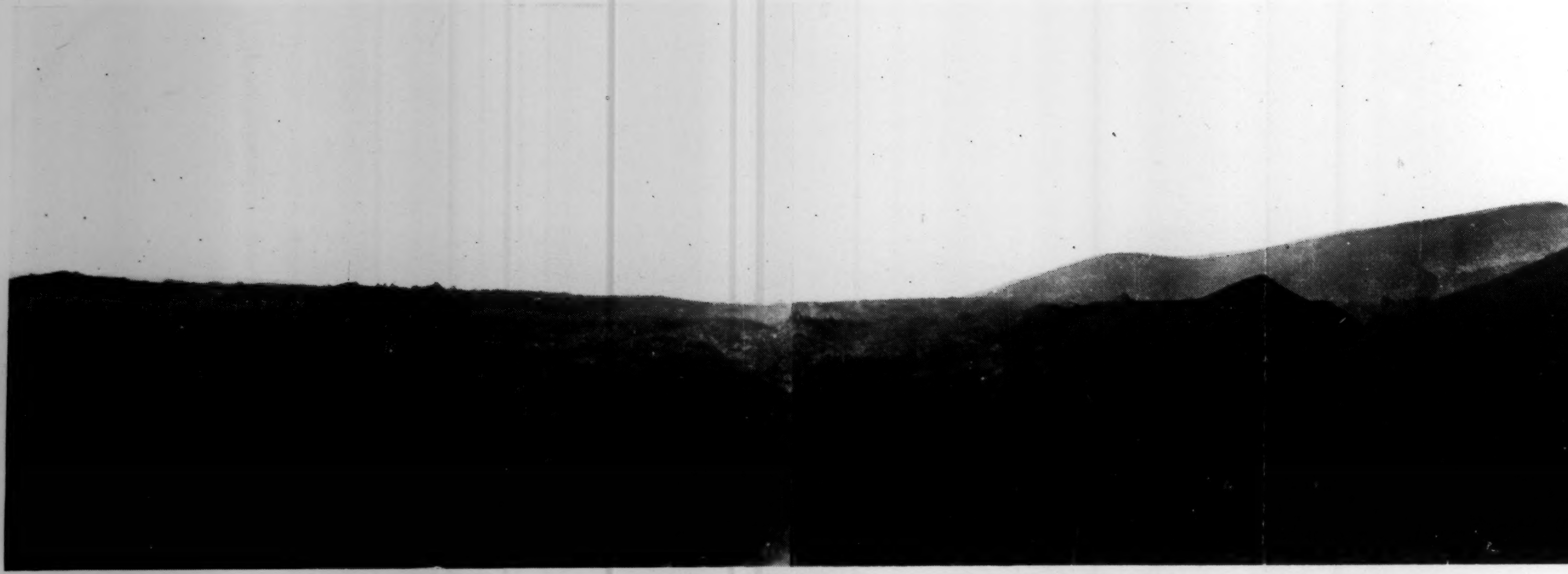

(b)

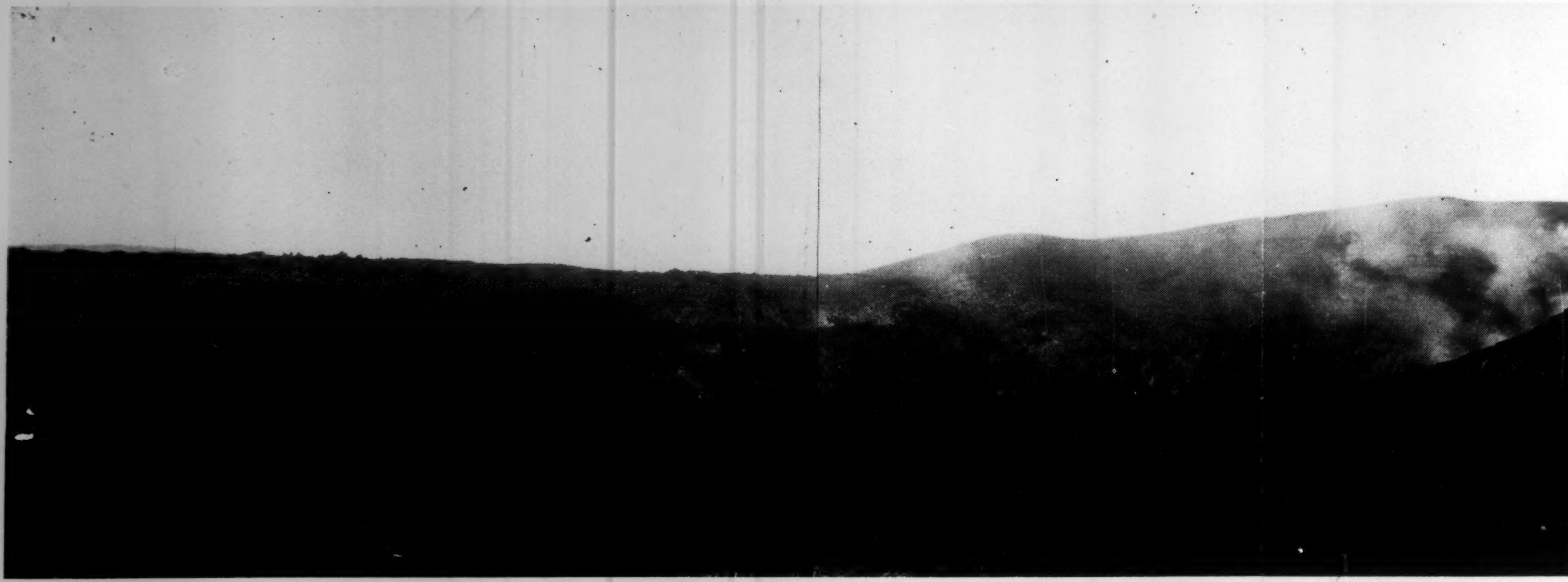

Fig. 172. General view of the northwest part of Mihara crater, showing changes in conformation of its central part,

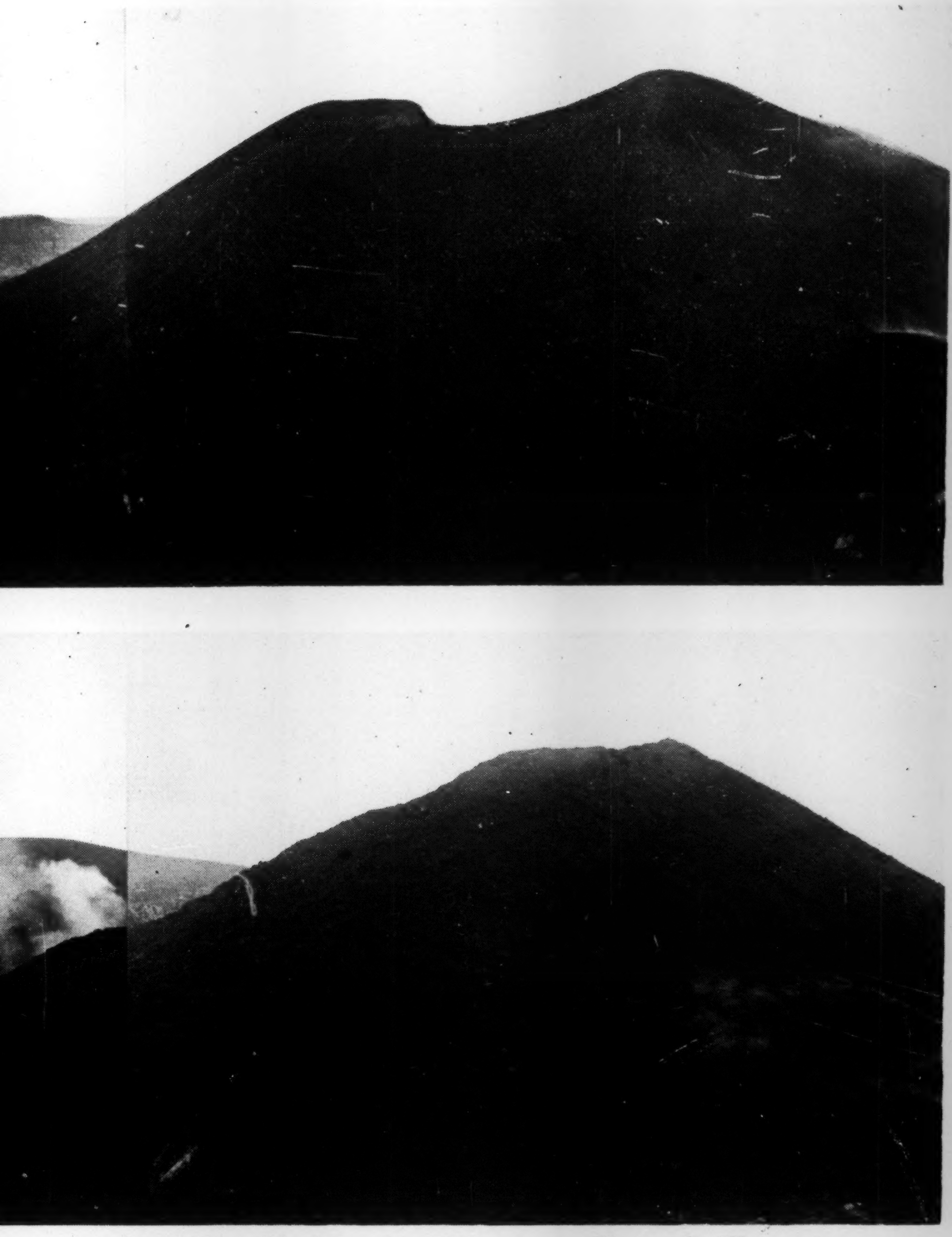

cart, (a) June 10 ; (b) June 25, 1951. Photo. S. Watanabe.

Fig. 173. General view of the northwest part of Mihara crater, as seen from the

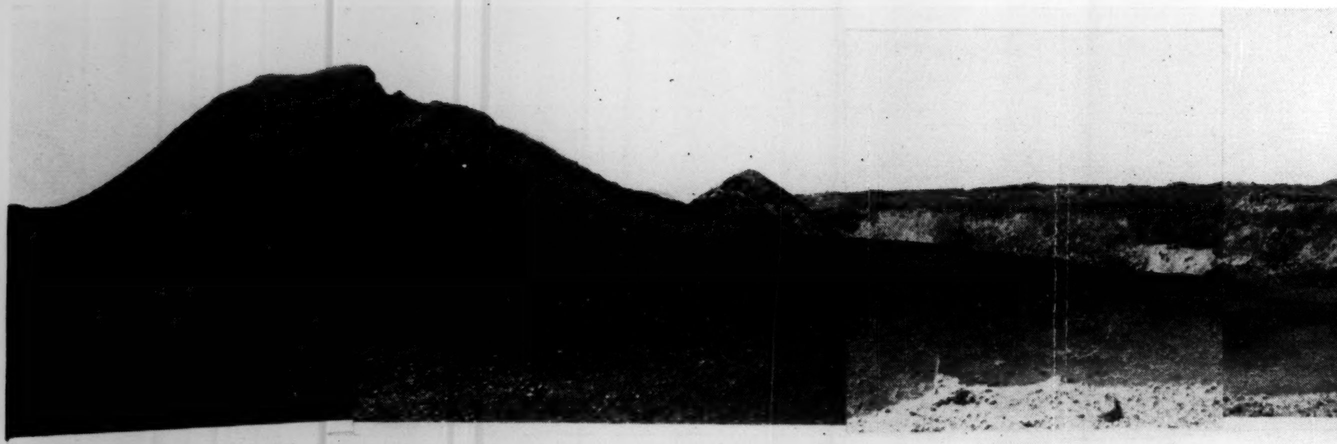

Fig. 174. General view of the northeastern half of the crater, with the cinder co
middle, August 15, 1951.

n the top of the cinder cone, August 15, 1951.

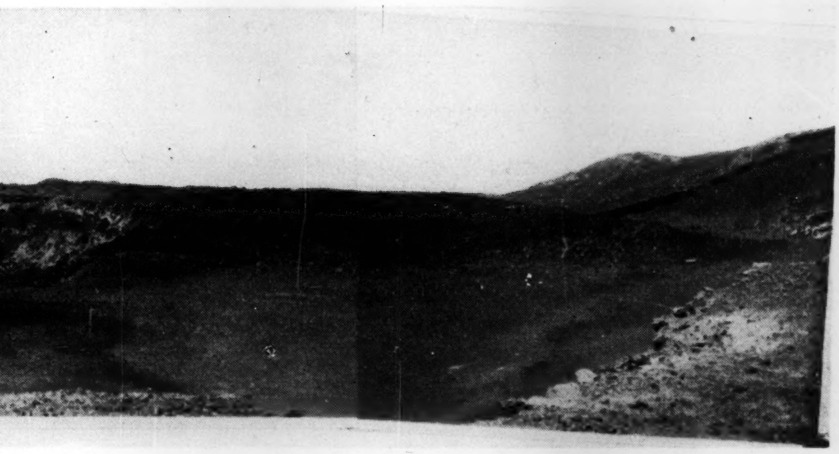

r cone at left and the new central pit in the

丘における爆発性噴火のほかに，火口底東半部に，10 個以上の大小の熔岩々滴丘が新しく生じて熔岩滴やガスを噴出し，また，東側火口壁近くの数ケ所から熔岩が湧出したことが，もつとも著しい現象である．この熔岩々滴丘や熔岩湧出孔の多くは，噴石丘を中心とする火口底の放射状割目の上に配列されており，あたかも地下の導管内の熔岩が，噴石丘を中心として，火口底を押し上げ，そのために生じた放射状割目に沿つて迸入し，さらに，その一部が火口底に噴出するに至つたことを示すもののようである．この第 2 次前半の活動に伴つて，噴石丘及び隆起丘は，急激に隆起したが，その活動休止直後に，再び沈下し，隆起丘周辺の火口底に，同心円状の割目や陥落崖が現れ，また，噴石丘の北半に崩壊が起つた．これらの変動は，火口中央にあつた旧中央孔の位置に，それと同様の桶状陥落孔を再現しようとする作用のあらわれであつたと考へられる．5 月 3 日の短時間の爆発は，この沈下の進行中に起つたもので，第 1 次の活動の場合と同様に説明される．

第 2 次後半 (5 月 6 日—7 日) の連続的活動は，噴石丘における爆発性噴火のほかに，隆起丘東側の旧中央孔東壁辺りの割目上に，二つの大きい熔岩噴泉を現出した．この噴泉の一つからは，熔岩が連続的に噴騰すると同時に，孔外に溢れ出て東部火口底上に扇状に拡がり，さらに，中央丘の北側を廻つて，帯状の流れとなつて西に進み，同丘西側の火口底にまで達した．この噴火に伴つて，先に沈下した隆起丘及びその周辺は再び隆起し，同時に噴石丘は，新噴出物の堆積によつて，完全な円錐丘となり，その高さを増した．

そのごの 1 箇月間，噴火活動は全く停止し，火口内の形状に著しい変化は起らず，隆起丘及び噴石丘に多少沈下する傾向が認められたのみであつたが，6 月 9 日に第 3 次の活動が始まる直前に至つて，これらに急激な沈下が起り，旧中央孔の位置に陥没孔が現れた．

(3) 第 3 次の活動は，6 月 9 日から同月 28 日までの間，噴石丘において繰返された爆発性噴火である．その間，隆起丘及びその周辺が，著しい隆起沈降運動を行つたが，最後には桶状陥落孔として停止した．この期間中，おそらく活動性熔岩はその導管内の深部に後退しており，そのガス圧が間歇的に十分高まつて爆発を起し，また隆起丘及びその周辺を押上げたものと考へられる．

第 3 次の活動は，6 月 27 日—28 日の異常な大爆発をもつて終り，これがまた昭和 25 年—26 年の三原火口噴火輪廻の終末を告げるものとなつた。その結果，同火口中央部には旧中央孔に匹敵する桶状陥落孔が残り，その南縁には同孔に向つて欠潰した噴石丘が残つた．(未完)

Errata

H. Tsuya, R. Morimoto, and J. Ossaka, *Bull. Earthq. Res. Inst.*, **32** (1954), 36–66.
Page 50, Foot-note. ....from the 2nd vent into a continued....:
Read ....from the 2nd vent continued.....
Page 63, Table VII, 3rd column, 6th line, 75 seconds: Read 65 seconds.
Pl. XXII. Fig. 20. Scale of the map being *1/3,000*.

Errata

H. Tsuya, R. Morimoto, and J. Ossaka, *Bull. Earthq. Res. Inst.*, **32** (1954), 289–312.
Page 295, Fig. 72. Map of....: Read Maps of.....
Page 296, Fig. 73. Map of....: Read Maps of.....
Pl. XXXIII, Fig. 64. Photo. Miyajima.: Read M. Miyajima.
Pl. XLIII, Fig. 36. ....and filowing away....: Read Fig. 86.....flowing away.....
Pl. XLVII, Fig. 97. downsteam: Read downstream.
Pl. LIII, Fig. 113. vLaa: Read Lava.

8. *Relation between the Property of Building Vibration and the Nature of Ground.*

(Observation of Earthquake Motion at Actual Buildings.) II.

By Kiyoshi KANAI and Tomisaburo SUZUKI,

Earthquake Research Institute.

(Read May 25, 1954 and Sept. 28, 1954.—Received Dec. 31, 1954.)

1. Introduction

The property of earthquake-motion is varied according to the ground property. Therefore the value of earthquake force, which has to be taken into consideration in calculation of earthquake-proof construction, depends on the ground property. In order to get the standard of estimation of such a value, we made a simultaneous observation by installing seismographs both at the basements and the roof-floors of buildings of the same structure standing on ground of different properties.

The results of the comparative observations made at two places in Tokyo and two places in Hyōgo Prefecture, have already been given in the previous paper[1]. The main points revealed in that paper are; (i) natural vibrations of buildings are apt to be caused by earthquake-motion, (ii) the damping of building in case of earthquake is larger on softer ground, and (iii) the latter phenomenon is explained from the damping caused by the dissipation of vibrational energy of the building into the ground.

In the present paper, besides the results of comparative observation made at two places in Tokyo which the previous paper contains, the results of two times of comparative observations which include in each the observations made at three spots in Tokyo are given. Observations in eight places in total were made at the basements and roof-floors of the buildings of the same structure.

2. The method of earthquake observation

The observations were made in the four-storied apartment-houses

1) K. KANAI and T. SUZUKI, *Earthq. Res. Inst.*, **31** (1953), 305.

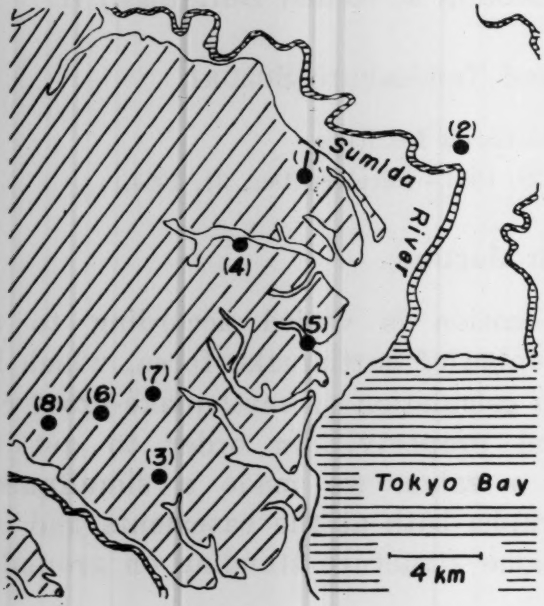

Fig. 1. The positions of the buildings.

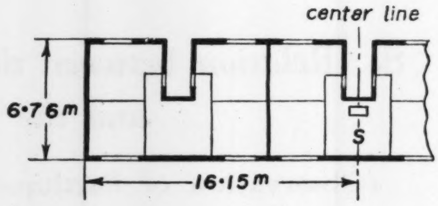

Fig. 2a. Plan view of the building of called 46-type.

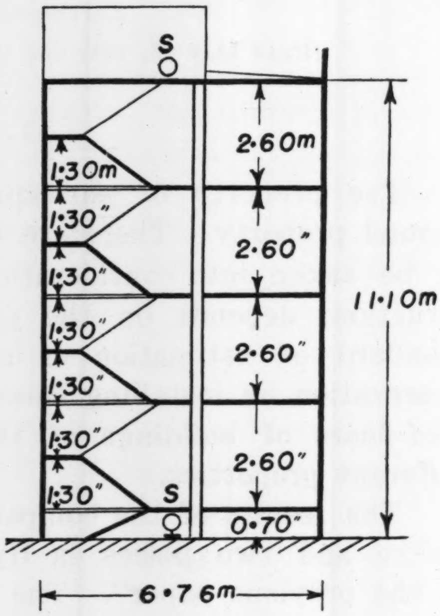

Fig. 2b. Side view of the building of called 46-type.

Table I. The names and positions of the buildings.

No.	Name	Position
(1)	Komagome Apertment	Komagome, Toshima-ku
(2)	Senju 〃	Senju-hashido-chō, Adachi-ku
(3)	Ishikawa-chō 〃	Ishikawa-chō, Ōta-ku
(4)	Totsuka 〃	Totsuka-machi, Shinjuku-ku
(5)	Honmura-chō 〃	Azabu-honmura-chō, Minato-ku
(6)	Gōtokuji 〃	Setagaya, Setagaya-ku
(7)	Taishidō 〃	Taishidō-machi, Setagaya-ku
(8)	Kyōdō 〃	Kyōdō-machi, Setagaya-ku

of reinforced concrete called "Tokyo-to Residential Association 46-type". The positions and the rough sketches of the buildings are shown in Figs. 1 and 2 respectively. The names and positions of the buildings are given in Table I.

The seismograph was installed on about the center of the basement and the roof-floor of each building and the component of beam direction of earthquake-motion was observed. The constants of seismographs used in the observation and the natural period of building obtained in the preliminary experiment are shown in Table II.

Fig. 3 illustrates the epicenters of earthquakes treated here and in Table III the date and position of the origins are shown.

Table II. The constants of seismographs and the natural period of building.

Building		Seismograph			
No.	Period (sec)	Position	Period (sec)	Damp. ratio	Magnif.
(1)	0.32	Roof	1.0	13:1	138 102
		Ground	〃	〃	174 98
(2)	0.28	Roof	〃	〃	198 117
		Ground	〃	〃	233 146
(3)	0.22	Roof	〃	〃	400
		Ground	〃	〃	400
(4)	0.33	Roof	〃	〃	100
		Ground	〃	〃	100
(5)	0.23	Roof	〃	〃	100
		Ground	〃	〃	100
(6)	0.32	Roof	〃	〃	92
		Ground	〃	〃	234
(7)	0.32	Roof	〃	〃	104
		Ground	〃	〃	212
(8)	0.32	Roof	〃	〃	100
		Ground	〃	〃	190

Table III. The date and position of the origin.

Earthq. No.	Date (1954)		Origin φ	Origin λ	Origin Depth(km)	Observation Building Number
1~8						(1), (2)
9	II	4	35.5	140.4	60	(3), (4), (5)
10	〃	5	35.6	140.5	60	
11	〃	14	35.6	139.9	40	
12	〃	20	35.4	140.1	40	
13	〃	21	35.7	140.9	40	
14	〃	22	34.3	141.7	60	
15	〃	〃	34.1	141.7	60	
16	〃	25	35.7	140.2	80	
17	〃	〃	36.0	139.9	40~50	
18	〃	26	36.1	139.2	70	
19	〃	〃	34.2	141.1	30	
20	〃	27	36.1	139.7	50	
21	III	3	37.8	140.5	50~60	
22	〃	4	36.2	139.8	50~60	
23	〃	6	36.0	139.9	50~60	
24	〃	8	36.1	140.1	65	
25	〃	11				
26	〃	〃	36.6?	139.9?	—	
27	IV	3	34.7?	140.5?	—	
28	〃	〃	35.4	139.3	50~60	
29	〃	8	36.2	140.0	50	
30	〃	10	35.5	139.7	35	
31	〃	〃	35.5	139.7	40	
32	〃	12	36.2	140.0	65	
33	〃	16	37.1	141.3	40	
34	〃	25	34.0	141.0	80~90	
35	V	3	36.2	140.0	40~50	
36	〃	4	36.4	141.2	40	
37	〃	14	37.3	141.7	50	
38	VII	10	40.7	139.3	300	(6), (7), (8)
39	〃	18	36.4	140.9	40	
40	〃	〃	35.5	141.0	50	
41	〃	〃	35.6	141.0	40	
42	〃	19	35.6	140.9	40	
43	〃	〃	35.7?	139.7?	—	
44	〃	21	35.5	141.0	40	
45	〃	〃	33.8	140.3	—	
46	〃	〃	33.7	141.2	40	
47	〃	22	35.5	141.0	—	
48	〃	〃	35.6	140.2	60~70	
49	〃	27	35.6	141.0	40	
50	VIII	1	34.0	141.0	—	
51	〃	2	37.6	141.7	50~60	
52	〃	5	36.1	140.0	50	
53	〃	10	30.2	139.4	430	

(to be continued.)

(continued.)

Earthq. No.	Date (1954)		Origin			Observation Building Number
			φ	λ	Depth(km)	
54	VIII	11	35.7?	139.7?	—	(6), (7), (8)
55	〃	12	35.8	140.9	50	
56	〃	〃	36.6	140.7	40~50	
57	〃	19	35 ?	140 ?	—	
58	〃	25	36.1	140.4	60	
59	〃	28	36.7	138.7	140	
60	〃	〃	36.7	141.1	40	
61	〃	30	37.2	140.7	80~90	
62	〃	31	42.8	143.8	60~80	
63	IX	1	35.7	141.0	40	
64	〃	2	35.6	140.9	30	
65	〃	6	35.8	141.0	Shallow	
66	〃	〃	36.8	139.3	20	
67	〃	11	36.2	139.9	40~50	
68	〃	12	36.1	140.0	70	
69	〃	〃	29.5	139.5	450	

3. Results of observations

In Table IV the maximum amplitude of the building at roof-floor and both the amplitude and the period at the basement in the time when the amplitude of roof-floor becomes maximum regarding each earthquake are shown. The representative seismograms are shown in Fig. 4.

Figs. 5~10 represent the relation between the values of the maximum amplitude of building at the roof-floor divided by the amplitudes at the basement in the time when the amplitude of roof-floor became maximum and the period of the buildings at the basement in the same time concerning each earth-

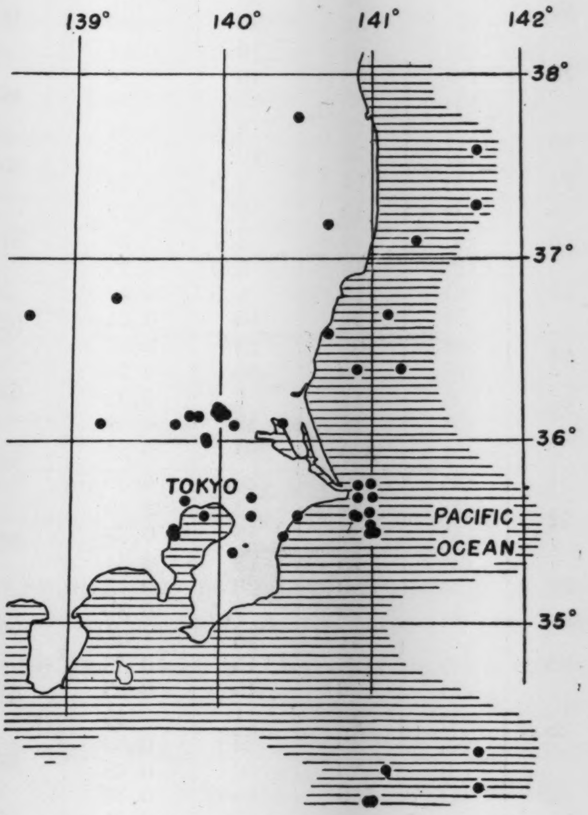

Fig. 3. The epicenters of earthquakes.

Table IV. The maximum amplitude of building and the period of earthquake-motion.

Earthq. No.	Position	Amplitude (micron) Roof	Amplitude (micron) Ground	Period (sec)
9	(5)	54	21	0.30
10	(5)	75	55	0.38
11	(4)	260	140	0.34
12	(4)	300	130	0.34
	(5)	270	110	0.24
13	(4)	60	30	0.42
	(5)	40	38	0.68
14	(4)	130	75	0.75
	(5)	63	63	0.84
15	(4)	95	55	0.60
	(5)	45	35	1.04
16	(3)	23	19	0.37
	(4)	75	25	0.34
	(5)	35	13	0.23
17	(4)	500	370	0.36
18	(3)	11	5.6	0.30
19	(3)	41	37	0.81
	(4)	100	70	0.95
	(5)	65	70	0.86
20	(5)	23	15	0.45
21	(4)	85	33	0.42
	(5)	38	30	0.59
22	(3)	28	19	0.51
	(4)	108	40	0.34
	(5)	35	18	0.38
23	(3)	13	5.6	0.34
	(5)	20	10	0.39
24	(3)	14	5.0	0.33
25	(3)	13	3.1	0.22
26	(3)	9.4	3.1	0.26
27	(3)	19	5.0	0.25
	(4)	15	5.0	0.27
	(5)	25	10	0.31
28	(4)	55	23	0.37
	(5)	90	45	0.31
29	(3)	11	6.3	0.33
	(5)	15	13	0.49
30	(5)	350	280	0.35
31	(5)	250	220	0.39
32	(3)	28	13	0.39
	(5)	30	15	0.39
33	(3)	15	13	0.54
	(4)	50	20	0.42
	(5)	20	7.5	0.39
34	(3)	11	10	1.06
	(4)	25	13	0.35
	(5)	30	15	0.65
35	(3)	38	11	0.25
	(4)	45	20	0.33
36	(3)	73	50	0.88
	(4)	180	65	0.39
	(5)	90	60	0.71
37	(3)	19	10	0.40
	(4)	50	25	0.36
	(5)	25	15	0.46
38	(8)	18	13	0.72
39	(8)	118	85	0.38
40	(8)	175	120	0.50
41	(8)	115	78	0.48
42	(8)	40	26	0.42
43	(8)	25	12	0.34
44	(7)	27	13	0.33
	(8)	22	13	0.43
45	(6)	38	13	0.38
	(8)	30	18	0.36
46	(6)	170	66	0.32
	(7)	63	33	0.46
	(8)	110	75	0.34
47	(6)	54	24	0.38
	(7)	29	17	0.48
	(8)	38	26	0.40
48	(6)	120	36	0.36
	(7)	48	21	0.36
	(8)	95	66	0.34
49	(6)	160	52	0.35
	(7)	100	37	0.36
	(8)	83	54	0.46
50	(6)	47	18	0.40
	(8)	21	12	0.34
51	(6)	51	17	0.35
	(7)	33	11	0.38
	(8)	28	16	0.38
52	(6)	75	31	0.34
	(7)	52	21	0.29
	(8)	47	26	0.38
53	(6)	32	11	0.38
	(8)	15	11	0.38
54	(6)	40	20	0.38
	(7)	19	12	0.32
	(8)	20	12	0.33
55	(6)	38	15	0.43
	(7)	41	17	0.41
	(8)	50	33	0.38
56	(6)	59	29	0.38
	(7)	41	14	0.33
	(8)	22	14	0.33
57	(6)	26	12	0.38
	(7)	23	9.4	0.44
58	(6)	71	45	0.32
	(7)	100	35	0.31
	(8)	74	46	0.42
59	(8)	20	13	0.36

(to be continued.)

(continued.)

Earthq. No.	Position	Amplitude (micron)		Period (sec)	Earthq. No.	Position	Amplitude (micron)		Period (sec)
		Roof	Ground				Roof	Ground	
60	(6)	410	170	0.38	65	(6)	24	10	0.29
	(7)	290	170	0.48		(8)	20	12	0.38
	(8)	250	160	0.76	66	(6)	40	15	0.44
61	(6)	63	22	0.35		(8)	27	18	0.56
	(7)	43	15	0.46	67	(6)	96	41	0.36
62	(6)	60	24	0.34		(8)	84	50	0.33
	(7)	49	14	0.33	68	(6)	200	75	0.43
	(8)	25	16	0.36		(7)	310	150	0.38
63	(6)	64	24	0.35		(8)	150	90	0.43
	(8)	26	14	0.36					
64	(6)	24	11	0.38	69	(8)	26	16	0.38

quake. In these figures the strips indicate the natural period of the buildings.

From Figs. 5~10 it is found that in each building the period wherein the ratio of amplitude of the roof-floor to that of the basement becomes maximum nearly corresponds to the natural period of the building. It seems that the principal reason why the amplitude ratio of roof-floor to basement varies even when the period of the

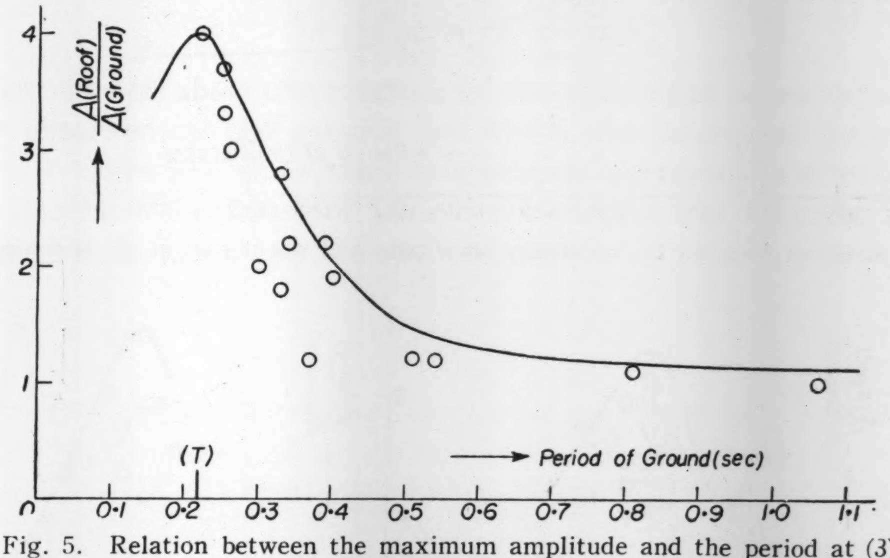

Fig. 5. Relation between the maximum amplitude and the period at (3) Ishikawa-chō.

ground vibration coincides with the natural period of building is correlated to the succession number of the earthquake-motion of the same period. This is explained from the fact that if the earthquake-motion of the period which coincides with the natural period of building occurs more than several times in succession, the amplitude of building vibration may become larger up to the value of resonance, while if the succession number of earthquake-motion of the same period is less

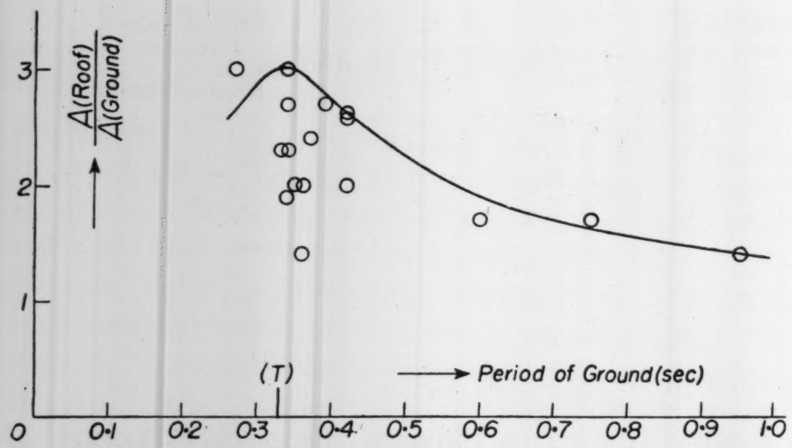

Fig. 6. Relation between the maximum amplitude and the period at (4) Totsuka.

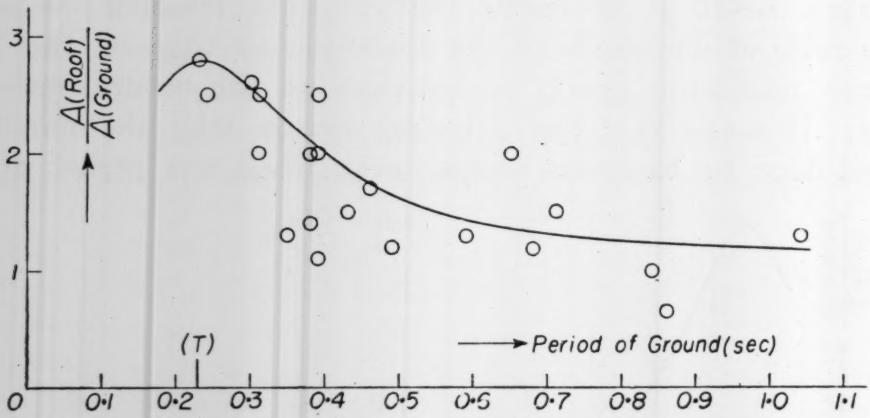

Fig. 7. Relation between the maximum amplitude and the period at (5) Honmura-chō.

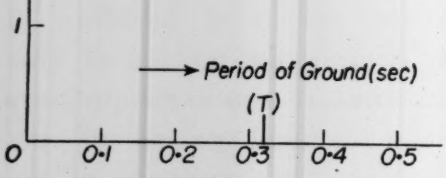

Fig. 8. Relation between the maximum amplitude and the period at (6) Gōtokuji.

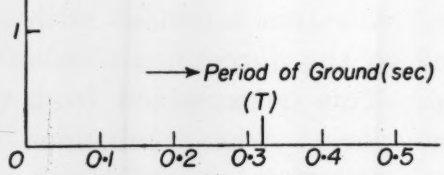

Fig. 9. Relation between the maximum amplitude and the period at (7) Taishidō.

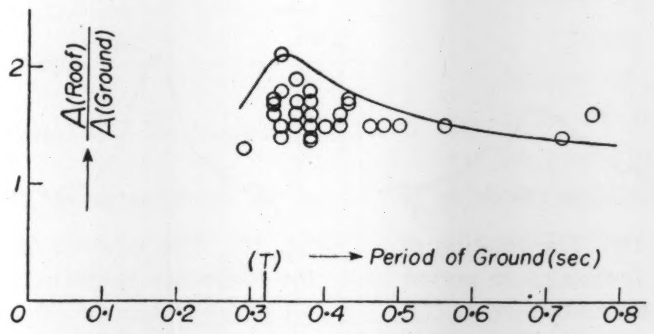

Fig. 10. Relation between the maximum amplitude and the period at (8) Kyōdō.

than several times, the increase rate of amplitude of building vibration may be smaller in proportion to the succession number.

Therefore, it may be assumed that the amplitude ratio of the roof-floor to the basement becomes maximum when the building vibration comes near to the resonance phenomenon by the earthquake-motion. In other words, the value of the maximum ratio of the amplitude of roof-floor to that of basement corresponds to the amplitude of roof-floor in case the building resonates by the simple harmonic ground motion of unit amplitude.

4. The relation between the property of building vibration and the property of ground

Figs. 11∼16 show the relation of the frequency to period of micro-tremor observed on the ground on which the buildings treated here stand. If there are more than two periods corresponding respectively to the maximum frequency of period, the largest one of them is called, for convenience sake, the natural period.

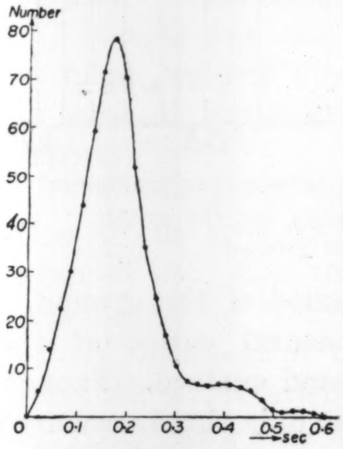

Fig. 11. The relation of the frequency to period of micro-tremor at (3) Ishikawa-chō.

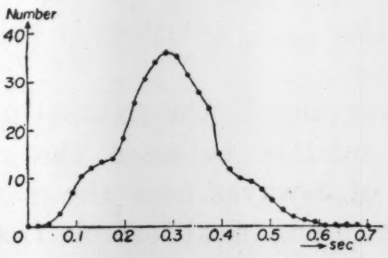

Fig. 12. The relation of the frequency to period of micro-tremor at (4) Totsuka.

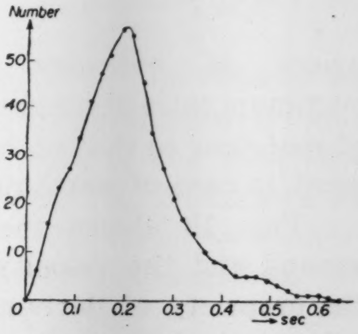

Fig. 13. The relation of the frequency to period of micro-tremor at (5) Honmura-chō.

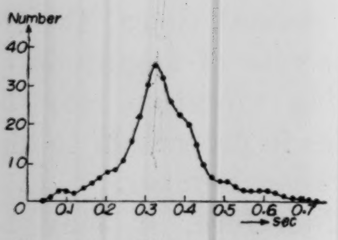

Fig. 14. The relation of the frequency to period of micro-tremor at (6) Gōtokuji.

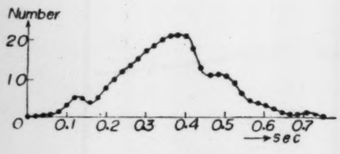

Fig. 15. The relation of the frequency to period of micro-tremor at (7) Taishidō.

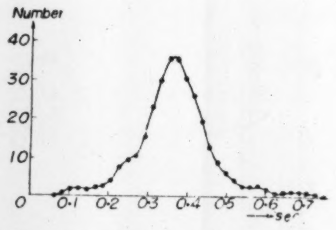

Fig. 16. The relation of the frequency to period of micro-tremor at (8) Kyōdō.

The relation between the maximum ratio of the amplitude of roof-floor to that of basement in case of earthquake and the natural period of the ground on which the building stands is derived from Figs. 5–10 and Figs. 11–16 as shown in Fig. 17. From Fig. 17, it is found that as the natural period of the ground is longer, the building standing on the place has the smaller maximum ratio as mentioned above, that is the damping of building vibration at the time of earthquake is larger. From Fig. 17 the empirical formula can be written as follows:

$$M \propto T_0^{-0.5} \qquad (1)$$

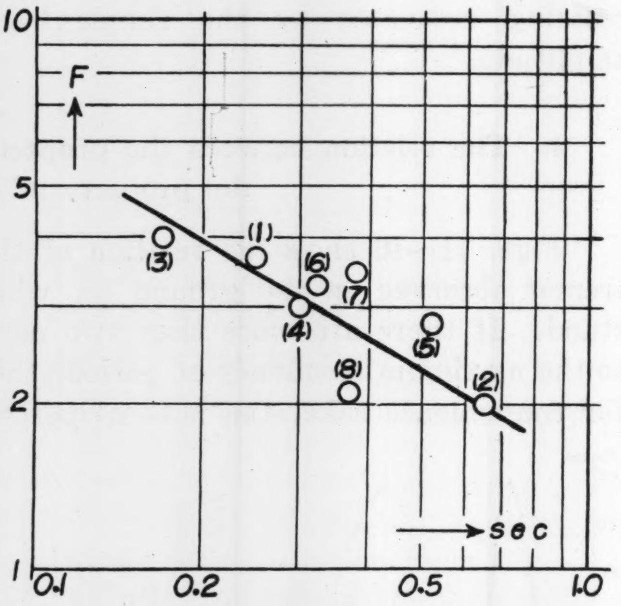

Fig. 17. The relation between the maximum amplitude of building and the proper period of ground.

where M indicates the maximum ratio of amplitude of roof-floor to that of basement in case of earthquake and T_0 the natural period of the ground.

Fig. 18 shows the relation between the natural period of the ground and the velocity of S-waves near the ground surface. Though the propriety of deriving an empirical formula from only three measured values of the velocity of S-waves may be questioned, the following empirical formula may be given for convenience sake;

$$T_0 \propto V_s^{-1.6} \qquad (2)$$

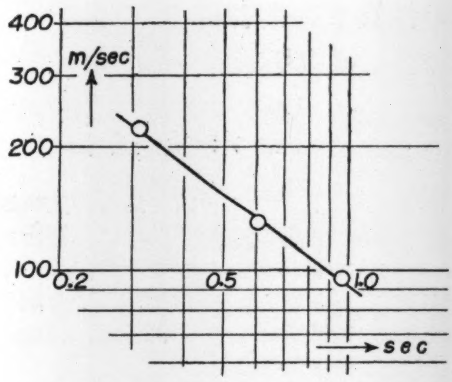

Fig. 18. The relation of the proper period of the ground and the velocity of S-waves.

where V_s is the velocity of S-waves.

From equations (1) and (2), the relation of the maximum ratio of amplitude of roof-floor to that of basement at the time of earthquake to the velocity of S-waves near the ground surface may be expressed in the following formula:

$$M \propto V_s^{0.8} \qquad (3)$$

The data concerning the velocity of S-waves is so few that we cannot expect much reliability from that formula, but at least qualitatively it can be said that the smaller the rigidity of the material around the ground surface is, the larger the damping of the building standing on that spot in case of earthquake will be.

5. Conclusion

It is found from the results of observations made at eight buildings of the same structure standing on ground of different properties that the maximum ratio of roof-floor to that of basement becomes smaller as the rigidity of the ground on which the building stands becomes smaller. In other words, the smaller the rigidity of the ground, the greater the damping of the building standing on that place in case of earthquake.

Having yet only a few data concerning the rigidity of the ground at hand, we will discuss quantitatively about the damping of buildings in case of earthquake and the property of the ground in our next report.

In conclusion, we wish to express our thanks to the Science Section of the Educational Ministry, for the financial aid (Research Funds) granted us. Also thanks are due to the members of the Residential Association of Tokyo-to for their help and to Mr. K. Nakagawa and others, members of the Architectural Institute of Construction Ministry, for their cooperation in the course of these observations and to Miss S. Yoshi zawa who assisted us in preparing this paper.

8. 建物の振動的性質と地盤の性質との関係
(実在建物における地震動観測) 第2報

地震研究所 {金 井 清
鈴木富三郎

異種地盤上に建つ同種の 8 建物 (4 階建鉄筋コンクリートのアパート) において, 地震の比較観測を行つた. その結果として, 地盤の剛性が小さい程, その上に建つ建物の地震時における振動減衰性が大きいことがわかつた. ここで云う地盤の剛性とは, 建物の基礎が接している土地附近の平均剛性にあたる. 従つて, ここでは, 地盤の地表面にごく近いところの性質が直接問題になる訳である. いづれにしても, 本研究において, 地震時における建物の振動減衰性の主要部分は, 建物の震動勢力が基礎から地中に逸散するために生ずることが, いよいよ明かになつた.

今後は, 地表面附近の物質の剛性の資料の数を何とかふやして, 地震時における建物の振動減衰性と地盤の剛性との関係を定量的にきめて, 地盤の性質を耐震設計上に有効に導入する道をひらいてゆきたい.

なお, 坑打ちなどの基礎部分の構造上の条件は, 建物の振動減衰性の本質を支配する因子とはならないものと考えられるが, その影響についての詳しい検討を行いつつあるから, 次の機会に報告する.

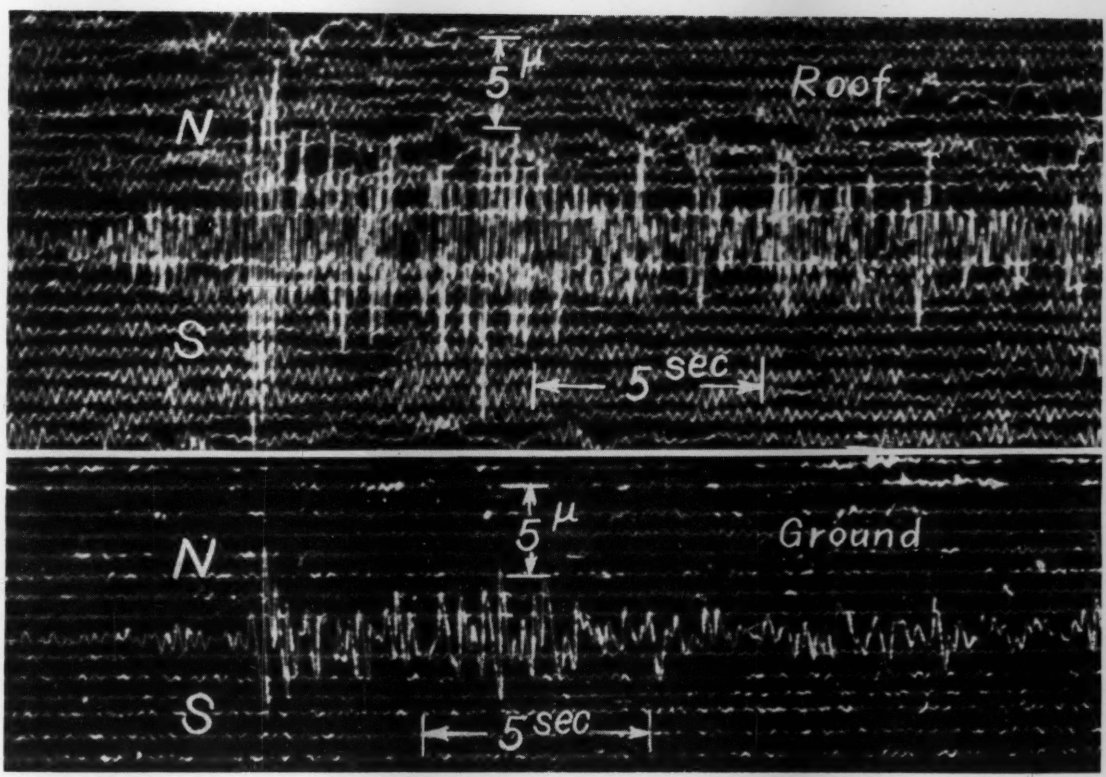

Fig. 4a. The representative seismograms at (3) Ishikawa-chō.
(Earthquake No. 29)

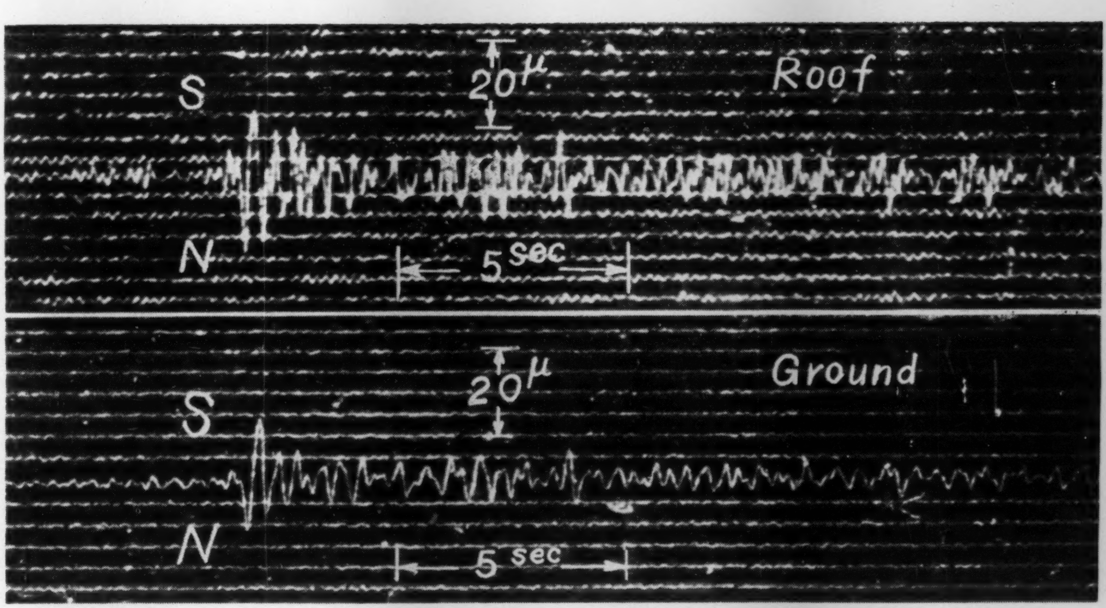

Fig. 4b. The representative seismograms at (5) Honmura-chō.
(Earthquake No. 29)

(震研彙報 第三十三号 図版 金井・鈴木)

9. 福井平野周辺地域の地質構造解析

地震研究所　村　井　　勇

(昭和 29 年 12 月 21 日発表—昭和 29 年 12 月 28 日受理)

I. 序　　言

1948 年 7 月の福井地震に際して，筆者は地震に伴つて起きた地変の調査にあたつたが，同時に福井平野周辺地域において地質構造の調査を行う機会を得た．この調査の結果はすでに簡単に報告してある[1]．この際行つた地質構造の調査とは，本地域に分布する新第三系及びそれを貫いて噴出している火成岩類の諸構造，特に内部に発達する節理及び断層の統計的調査である．調査資料を綿密に検討したところ興味ある結果が得られたので，その詳細を更めてここに報告する．

II. 福井平野周辺地域の地質概観

7 万 5 千分 1 地質図大聖寺図幅及び福井図幅[2]等によれば，本地域の地質は大体次の通りである．本地域は主として第三系，第三紀中に噴出したと思われる石英粗面岩類及び粒状安山岩等，第三紀末あるいはそれ以後に噴出したと思われる安山岩類よりなる．第三系は手取統（ジユラ系）を貫く花崗岩類を覆つて広く分布している．その構造については，断層の発達は多く認められるが，褶曲は著しくなく，一部の断層地塊を除けば，概して単斜構造をなす．断層は北東—南西性のものと，これにほぼ直交するものとあつて，後者は前者を切つている．これらの断層は第三系を切るが，輝石安山岩類により被覆されている．第三紀中に噴出したと思われる火成岩類には石英粗面岩類，玢岩，粒状安山岩があり，いずれも第三系の下部層を貫いている．第三紀上部層との関係は明らかでない．いずれもはなはだしく変質している．第三紀末あるいはそれ以後に噴出したと思われる安山岩類には Hornblende-Andesite, Hornblende-Biotite-Andesite, Trachytic Andesite, Dacite, Augite-Andesite, Two-Pyroxene-Andesite, Olivine-bearing Augite-Andesite があり，第三系を貫いて噴出し，熔岩流及び岩脈となつて分布している．

本地域の第三系は大聖寺図幅及び福井図幅では，不整合の存在及び岩相の差異に基づいて第 I 表に示すように細分されている．いずれも新第三紀に属する地層で，そのうちの福井県丹生郡国見村附近に分布する「凝灰岩及び凝灰質頁岩互層」（竹山俊雄による大丹

1) 村井勇「福井県坂井郡及び丹生郡附近の地質構造，その他」昭和 23 年福井地震調査研究速報 (1949), 100–103.

2) 薗部竜一 7 万 5 千分 1 地質図大聖寺図幅及びその説明書，1939.
7 万 5 千分 1 地質図福井図幅及びその説明書，1940.

生層[3]) より産出する化石は石川県下に分布する八尾層の化石と同類のものであつて[4]，このことより富山・石川県下の余川層群にあたる地層が本地域に存在することが認められる．下部の「緑色凝灰岩層」・「粒状安山岩質集塊岩層」は岩稲層群に相当するものであろう．福井県下ではこれらの中新統に相当する地層が広く分布している．石川県江沼郡大聖寺町附近に分布する地層は新第三系の上部にあたるものと思われ，あるいはそのなかに鮮新—更新統に相当するものがあるかもしれない．第四系は日本海沿岸，平野内部及び各河川の沿岸に広範囲にわたつて分布している．福井平野北方の日本海沿岸の台地上には更新統の砂層が新第三系及び輝石安山岩を覆つて広く分布している．(第 31 図参照)

本地域の地質構造及び層序に関しては不明の点が多く，今後の調査に待たねばならぬ問題が多く残されている．

第 I 表　第三系の細分 (薗部竜一による)

(福井図幅)	(大聖寺図幅)
	浮石質砂岩層
	粗鬆砂岩層
凝灰質頁岩層 ………	凝灰質頁岩層
	砂岩層
灰色頁岩層	頁岩及び砂岩互層
凝灰岩及び凝灰質頁岩互層	凝灰質砂岩層
	凝灰質頁岩層
緑色凝灰岩層 ………	緑色凝灰岩層
粒状安山岩質集塊岩層	

III. Fracture の統計的研究法

筆者は上に記した新第三系及びそれを貫いて噴出している火成岩類にたいして，その内部に発達する各種の割れ目 (節理・断層等) の統計的調査を行つた．その調査結果を述べるに先だち，どんな方法によつて調査を実施したかを次に説明する．

まず 7 万 5 千分 1 地質図大聖寺図幅及び福井図幅に従つて，地質学的単元として新第三系の各層，石英粗面岩類及び粒状安山岩等の第三紀火成岩類，各種の安山岩類を区分し，調査を行うべき地区としてその各単元の代表的な露出地を数個所選定した．この選定地区は全地域にわたつてあまり不均一に配置されることのないように留意した．

調査にあたつては，一定地区内の露頭にみられる岩石中の各種の割れ目 (fracture) より，数十個以上の標本を無作為的に抽出した．そして，その標本の方位性をシュミット網 (正積投影網) を用いて 1 図型内に投影し，そこに現われる投影点 (割れ目の面の極を投影した点) の集合の模様をもつて，その地区内における fracture の発達状態を代表させ

3) 竹山俊雄「越前丹生山地北部の第三紀層」地球 **20** (1933).
4) *Vicarya verneuili yokoyamai* Tak. 等の貝化石を産す．

た．このようにして認識される fracture の発達状態を筆者は fracture system と呼んでいる．

ここに説明したような方法をとつたのは，野外で fracture を測定するにあたつて，無数にある fracture のすべてを測定することは不可能であり，又少数個の標本をもつて fracture の全体の発達状態を代表させる場合には抽出の際の主観的な選択による誤差の影響が大きく，かつ局部的な変異を除却することもできないという理由による．200 個前後の無作為標本を抽出すれば，それをもつてその場所における fracture system をほぼ正確に代表させうるが，抽出操作を十分慎重に行う場合は数十個の標本で足りる．

一般に岩石中に発達する fracture はある程度の規則性をもつて配列している．したがつて，上に述べたようにして得られた図型は，投影点の局部的集中を示すのが普通である．この集中が偶然的なものであるかどうかを検定するためには，WINCHELL, H. 及び CHAYES, F. 等が述べているような方法を用いればよい[5]．多くの場合，検定の結果はこの集中が偶然的なものではないことを示す．このことが明らかになれば，図型内の投影点の集合状態の上に反映されている岩石中の fracture の発達状態の規則性が確認される．fracture system はこのようにして認識される．

WINCHELL, H. の述べている方法によれば次のようにする．今ここに相等しい大きさの空間の区劃が多数あつて，そこにある種の事象が起る場合を考える．その起り方が全くでたらめであつて，常に一定の条件のもとにすべての区劃に分配される，すなわちどの区劃においてもその事象の起る確率が相等しいならば，その確率が十分小さいとするときは，その実際に起つた事象の回数の 0, 1, 2, 3, ... という数によつて分類された区劃の数の分布は Poisson 分布に従うはずである．したがつて，無作為的に抽出された標本より作つた fracture の図型における投影点の集中が全く偶然的なものであれば，言いかえれば各 fracture の方位になんら規則性がないならば，図型の全面積を幾つかの等面積の区劃に分けて，それらの区劃内の点の数 (k) によつて各区劃を分類し，その数 (f) の分布を調べれば，$f=e^{-m}\dfrac{m^k}{k!}$ に近い分布を示すはずである．ここに $m=\dfrac{\Sigma k}{N}$ (N は区劃の数) である．もし実際に得られた分布と予測された分布との差が有意であれば，図型の示す投影点の局部的集中が全く偶然的なものであるという帰無仮説を捨てることができる．Poisson 分布との喰いちがいの有意性の検定には χ^2-検定法を用いればよい．第 II 表にその実例を示す．なお筆者は図型を 156 個の区劃に分けて検定している．

---

5) H. WINCHELL, "A New Method of Interpreting Fabric Diagrams," *Am. Min.*, **22** (1937), 15–37.
I. MURAI, "Notes on the Fracture System developed in the Setogawa Group," *Bull. Earthq. Res. Inst.*, **26** (1948), 49–53.
H. W. FAIRBAIRN and F. CHAYES, *Structural Petrology of Deformed Rocks*, (Addison-Wesley Press, Cambridge, 1949) pp. 308–326.
J. PINCUS, "Statistical Methods Applied to the Study of Rock Fractures," *Geol. Soc. Am., Bull.*, **62** (1951), 101–105.

第 II 表　第 4 図の資料により，投影点の集中の有意性を検定した例.

k	実測度数 f	予測度数 F	$(f-F)^2/F$
0	82	53.5	15.18
1	32	57.2	11.11
2	17	30.6	6.04
3	12	10.9	
4	7	2.9	
5	3	0.6	
6	1 [3–9 combined: 25]	0.1 [3–7 combined: 14.5]	7.61
7	1	0.1	
8	0		
9	1		
Σ	156	155.8	39.94

$\chi_0^2=39.94$　　$\nu=2$　　$Pr.\{\chi^2>\chi_0^2\}<0.0001$

得られた図型の各々についてこのような検査を行つてみると，いずれも $Pr.\{\chi^2>\chi_0^2\}$ は非常に小さく，各図型の示す投影点の集中性は偶然的なものではないことが確かめられた．第 III 表にその結果を示す.

第 III 表　第 1, 2, 3, 4, 5, 13 図の資料について投影点の集中の有意性を検定した結果

第 1 図	$Pr.\{\chi^2>\chi_0^2\}<0.001$
第 2 図	<0.001
第 3 図	<0.01
第 4 図	<0.0001
第 5 図	<0.01
第 13 図	<0.01

以上に説明したようにして認識される fracture system は，それがもつ色々な性質，たとえば層理面との立体的な幾何的関係，地理的方位，均質性，褶曲・断層構造との関係，fracture system を構成する各要素の相互関係等の点に，その生成当時の造構造的条件を反映させている．したがつて，それらの点を注意深く解析することにより，fracture system の形成機構にたいして構造地質学的な解釈を下すことができ，ひいては造構造運動の過程の解析を行うことも可能となる.

IV. fracture system の統計的調査の結果

上に述べたような方法によつて調査を行つた結果，本地域の新第三系中及び火成岩類中に発達する fracture system について次のような事実を認めることができた.

1. 新第三系中の fracture system

本地域に分布する新第三系の各層中には，すべて同一型の fracture system の発達が認められる．最下層の「粒状安山岩質集塊岩層」より最上層の「浮石質砂岩層」に至るまでの各層について調査した結果，それぞれの層より得られた fracture system の図型(第 2, 3, 4, 6, 7, 8, 9, 12, 13, 15, 16, 17, 22, 23, 24, 25, 26 図)の間にはなんら本質的な差異は認められなかつた．各図型はそれぞれ顕著な投影点の集中を示し，その集中模様は相互に著しく類似している．図型はいずれも，投影点の集合状態を等集中度曲線によつて表現してある．これは，図型内の各点について，図型の全面積の 1/100, 2/100 又は 3/100 の面積をもつ円を周囲に描き，その中に入る投影点の数が全投影点の数の何 % になるかを調べ，等しい%を示す点を結び合わせて描いたものである[6]．描いた円の面積が図型の全面積の 1%，2% 又は 3% にあたることより，それぞれ 1% 図型，2% 図型，3% 図型とよぶ．

新第三系中の fracture system の特徴は第 4 図 b に見られるとおりで，層理面 S にほぼ垂直な 3 つの要素 M, N 及び K が認められ，そのうちの M と N は層理面 S の走向の方向をほぼ等角にはさむ位置に現われ，特に著しい発達を示す．M, N と層理面の走向とのなす角は 45° より大きい．K は M と N とのなす面角のうちの鈍角の方を 2 等分する面にほぼ相当し，したがつてその走向は層理面 S の走向とほぼ一致する．その他の図型もすべて，M, N, K の 3 つの極大区，あるいはそのうちの 1, 2 を示す．M と N は常に尖鋭に現われるが，K はあまり明瞭でない場合もある．M 及び N の投影点の集中度は常に同じ程度とはかぎらず，一方が他方より優越する場合も多い．

2. 石英粗面岩類及び粒状安山岩等の第三紀火成岩類中の fracture system

石英粗面岩類及び粒状安山岩等の第三紀火成岩類についても，調査の結果新第三系中に発達する fracture system と非常によく一致するものが認められた．たとえば，石川県江沼郡西谷村において，「緑色凝灰岩層」とそれを覆う粒状安山岩の熔岩流とについて fracture system を調査したところ，この両者から得られた図型（第 8, 9 図及び第 2 図が緑色凝灰岩層，第 10, 11 図及び第 1 図が粒状安山岩）は相互に著しい一致を示した．同様の関係は，福井県坂井郡竹田村南部に露出する「緑色凝灰岩層」及び「粒状安山岩質集塊岩層」とそれらを覆う粒状安山岩の熔岩流との間にも認められる．坂井郡坪江村川上に露出する粒状安山岩の小岩脈中にも，周囲の新第三系中の fracture とほぼ一致する方位性をもつものが発達している．石英粗面岩類についても同様であつて，たとえば竹田村上竹田の南東方に露出する流紋岩の岩脈中の fracture が周囲の粒状安山岩質集塊岩層中のものと一致することが認められる．

火成岩類相互の間においても同様である．福井県大野郡遅羽村比島に相接して露出し

6) H. W. Fairbairn and F. Chayes, *Structural Petrology of Deformed Rocks*, (Cambridge, 1949), pp. 285–291.
E. B. Knopf and E. Ingerson, *Structural Petrology*, Geol, Soc. Am., Memoir 6, (1938), pp. 245–252.

ている粒状安山岩の熔岩流及び斜長石英粗面岩の貫入岩体について，両者の中に発達する fracture system を調査したところ，同一の方位をもつものが共通に存在することが知れた (第 14 図 a, b). 同様な関係は，西谷村九谷附近に露出する粒状安山岩と斜長石英粗面岩との間についても確かめられた.

第三紀火成岩類中の fracture system の特徴は第 1 図 b に見られるとおりで，新第三系中の fracture system と同様に，流動面 F にほぼ垂直な 3 つの要素 M, N 及び K が認められる. K は新第三系の図型におけるよりも比較的明瞭に現われる傾向を示す. また，後に述べるように，M と N との間の角 (鋭角の方) は，火成岩類の場合の方が新第三系の堆積岩層の場合よりも大きいように思われる.

以上に説明したように，第三紀火成岩類と新第三系との間，及び火成岩類相互の間に，fracture system の著しい一致が認められる. この事実は，本地域の地質構造を解釈する場合極めて重要な意味を持つと考えられる.

3. 安山岩類中の fracture system

本地域に分布する安山岩類の熔岩流はいずれも顕著な柱状節理の発達を示す. 坂井郡雄島村東尋坊附近に露出する Augite-Andesite 中のものは特に有名である. 数ケ所においてこの安山岩類中の節理の統計的調査を行い，同時に周囲の新第三系中，及び第三紀火成岩類中の fracture system との関係を検討したところ，興味ある結果が得られた.

本地域の安山岩類の熔岩流より得られた fracture の図型は，いずれも先に記した新第三系の各層の図型とある程度類似した集合模様を示す. 各図型は，先に説明した新第三系の図型における M, N 及び K にほぼ相当する極大区を示し，この 3 つの要素の相互関係及び流動面 F にたいする関係，ならびに fracture system 全体の地理的方位も，周囲の新第三系の fracture system とほぼ一致する. たとえば，坂井郡鷹巣村に分布する Trachytic-Andesite の熔岩流より得た fracture の図型 (第 18, 19 図及び第 5 図) は，周囲の新第三系より得た図型 (第 15, 16, 17, 23, 24 図等，及び第 4 図) とよく類似しており，fracture system の各要素の現われかた，及びその地理的方位もほぼ一致している. 雄島村東尋坊附近の Augite-Andesite の熔岩流中の柱状節理についても同様なことが認められる (第 21 図参照). 又，国見嶽を中心とする地域に広く分布する Augite-Andesite の熔岩流についても，fracture system が周囲の新第三系中のものと一致することが坂井郡本郷村河内附近で確かめられた (第 22 図参照). 更に，丹生郡殿下村白滝附近に露出する Two-Pyroxene-Andesite についても，fracture の発達状態が周囲の新第三系中の fracture とやや類似することが認められる.

安山岩類の fracture system と第三紀火成岩類のそれとの関係はあまり判然としないが，新第三系にたいするとほぼ同様の関係があるのではないかと思われる. 新第三系と第三紀火成岩類との間には，fracture system の著しい一致が認められるのであるから，このように期待してまちがいないであろう. 雄島村雄島に露出する流紋岩より得た fracture の図型 (第 20 図) は，東尋坊附近の Augite-Andesite の図型 (第 21 図) とやや

類似している．

以上に説明したように，本地域に分布する安山岩類中の fracture system は，先に説明した新第三系中の fracture system と，個々の要素の現われかたの点でも，地理的方位の点でも，ほぼ一致している．しかし細部については，やや相異する点も認められる．たとえば，鷹巣村の Trachytic Andesite の図（第 18 図）と東尋坊附近の Augite-Andesite の図（第 21 図）では，K の現われ方がやや異常で，単一の極大区を示さず，ある角度をもつて交わる 2 つの要素に分かれる傾向を示している．

ここに述べた事実は，おもに広範囲にわたつて分布する熔岩流について認められるのであつて，小岩脈中の fracture についてはかならずしもこのとおりでない．たとえば，国見村五太子ノ滝に露出する Augite-Andesite の岩脈の場合では周囲の新第三系中の fracture とかなりよく一致する fracture が認められるが（第 24 図参照），殿下村大矢の岩脈では，岩脈中の fracture と周囲の新第三系中の fracture とが全く喰い違つてはいないにしても，よく一致していると見ることもできない（第 26 図参照）．ただし，後者の場合は，周囲の新第三系の構造自体が乱れており，局部的擾乱の著しい個所にあたつている．

4. fracture system の地域的変化

これまで述べてきたように，本地域に分布する新第三系，第三紀火成岩類及び安山岩類は相互にきわめてよく類似する fracture system を持ち，fracture の図型は常にほとんど同様の集合模様を示す．このことは本地域内のすべての地区について言えることで，図型の示す投影点の集中度に多少の差はあるが，どの地区で調査してもほぼ同様の図型が得られる．すでに説明したように，本地域の fracture system は，層理面 S（あるいは流動面 F）に垂直な 3 つの要素 M，N，K よりなり，各図型ともこの 3 つの要素に相当する極大区を示す．そのうちのどれかが極大区として現われない場合もあるが，やはりその位置に投影点の低度の集中を認めることができる．局部的に構造の乱れた個所では，図型はやや異常となり，特異な要素が混入する．しかしその場合でも，綿密に調べれば 3 つの要素が依然としてあるのを確認できる．本地域内では，fracture system は概して均質な発達を示し，乱れた様相を示す個所はほとんどないといえる．

fracture system 自体の様相には全地域にわたつてなんら変化は認められないが，その地理的方位には著しい地域的変化が見られる．福井平野東方の富士写ケ岳山塊においては地理的方位はほぼ一定に保たれているが，西方の丹生山地においては，方位に著しい変化が現われ，fracture system 全体がそのまま逆時計方向に廻転する傾向を見せ，西部の海岸沿いの地域において特にこの傾向が著しい（第 29 図 a，b 参照）．ただし，このような方位の変化があるにもかかわらず，fracture system 自体の様相にはなんらの変化もない．fracture system の方位の変化は層理面（あるいは流動面）の方位の変化と完全に並行して起つており，fracture system の各要素と層理面（あるいは流動面）との立体的な関係は常にほぼ一定に保たれている．すなわち，M，N，K の 3 つの要素は層理

面（あるいは流動面）に垂直であり，M と N との間の角（鈍角の方）を 2 等分する面の走向は層理面（あるいは流動面）の走向とほぼ一致するという関係が常に保持されている．

本地域内の各地区において fracture system の発達状態を調査した結果を地図上に記入すれば第 32 図のようになる．

5. M と N との間の角

本地域の fracture system の 3 つの要素のうち，K は層理面（あるいは流動面）と走向を共通にするような位置に現われ，一方 M と N はその方向を等角にはさむような位置に現われる．この M と N とのなす角度は必ずしも一定していない．本地域内でこの角度を測定した資料を第 IV 表に示す．

第 IV 表 M と N のなす角度（鋭角の方）

	第三系									火成岩類					
J	A_1	A_2	B_1	B_2	C_1		C_2	C_3	D†	E_1		E_2†	E_3†	F_1	F_2†
	67°	74°	41°	62°	41°	28°	39°	37°	61°	84°	48°	75°	59°	62°	53°
	64	72	40	56	40	27	38	32	59	80	46	57	45	61	53°
	63	68	39	48	37	25	32	31	58	78	45	56	36	60	
	62	66	34	40	36	25	31	25	53	71	44	55	36	45	
	51	64	30	38	36	24	31	24	52	68	41	33	34	44	
	40	58	25	36	34	22	30	23	34	63	39		23	41	
	37	52	25	28	33		30	22	30	58			22	39	
	36	43	21		30		27	22		57				34	
		38	18		30		20			57					
平均	52.5	59.4	30.3	44.0	31.2		29.8	27.0	49.6	58.6		55.2	36.4	48.3	53.0

A: 粒状安山岩質集塊岩層，*B*: 緑色凝灰岩層，*C*: 凝灰岩及び凝灰質頁岩互層，*D*: 浮石質砂岩層及び粗鬆砂岩層，*E*: 粒状安山岩，*F*: 安山岩類，

A_1: 福井県坂井郡竹田村，　A_2: 福井県吉田郡志比谷村及び松岡町．

B_1: 福井県丹生郡国見村，　B_2: 石川県江沼郡西谷村．

C_1: 福井県丹生郡越廼村，　C_2: 国見村，　C_3: 福井県坂井郡本郷村．

D_1: 石川県江沼郡大聖寺町及び三谷村．

E_1: 西谷村，　E_2: 竹田村，　E_3: 福井県大野郡遅羽村．

F_1: 福井県坂井郡鷹巣村，　F_2: 福井県坂井郡雄島村．

註: 表中 † を付した部分の資料は局部的な露頭について測定したもの．

この角度を露頭面で直ちに測定することはなかなか困難で，（実際には M と N に相当する fracture の方位を個々に測定して，ステレオ投影によつて，その間の角度を出す），資料を十分な数得ることが容易でない．したがつて統計的処理をするための標本抽出が完全に行えぬ場合が多い．ここに掲げた表中の資料もその意味で不完全なものである．

一見して知れることは，A (粒状安山岩質集塊岩層) の内部，C (凝灰岩及び凝灰質頁岩互層) の内部，及び F (安山岩類) の内部では地区ごとの差異があまりないこと，A と C との間には著しい差が認められること，A と E (粗状安山岩) 及び F との間の近似等である．資料が不完全で確実なことは言えないが，概して，岩石の質的な相異によつて角度の差が現われ，岩質の類似する場合には近似する値を示すように思われる．たとえば，A と C との間の著しい差は，A が安山岩質集塊岩よりなる地層であるのにたいして，C は砕屑性細粒堆積岩よりなるという相異に基づくのかもしれない．又，E, F の間の近似は，いずれも安山岩よりなるということによるのかもしれない．ただし，同一系統の岩層群の内部において差が認められることがあり，たとえば B (緑色凝灰岩層) の内

第 V 表 第 IV 表の検定 (平均値の一様性の検定)

i) A の 内 部

	SS	f	V
A	193.14	1	193.14
$R(A)$	2519.33	15	167.96
AR	2712.47	16	

ii) B の 内 部

	SS	f	V
B	735.44	1	735.44*
$R(B)$	1448.00	14	103.43
BR	2183.44	15	

iii) C の 内 部

	SS	f	V
C	35.79	2	17.89
$R(C)$	1046.09	29	36.07
CR	1081.88	31	

iv) E の 内 部

	SS	f	V
E	2400.56	2	1200.28**
$R(E)$	4976.10	24	207.34
ER	7376.66	26	

v) F の 内 部

	SS	f	V
F	36.10	1	36.10
$R(F)$	859.50	8	107.44
FR	895.60	9	

vi) A と C との間の差

	SS	f	V
J	7570.92	1	7570.92**
$R(J)$	3794.35	47	80.73
JR	11365.27	48	

vii) A, E (E_3 を除く), F 間の差

	SS	f	V
J	505.03	2	252.52
$R(J)$	7649.82	44	173.86
JR	8154.85	46	

viii) C と D との間の差

	SS	f	V
J	2186.00	1	2186.00**
$R(J)$	2015.59	37	54.48
JR	4201.59	38	

*: 危険率 5% 以下で有意 **: 危険率 1% 以下で有意

部，及び E の 1 部 (E_3) にそれが認められる．この差はあるいは，地域的な変化を表わしているのかも知れぬし，又は標本抽出が不完全なため局部的変異が強く現われた結果かも知れない．B は岩質の変化の著しい地層であり，あるいはその影響が現われているのかもしれない．

いずれにせよ，これだけの資料から確実な結論をだすことはできないが，M, N 間の角は各地区ごと，各地質単元ごとに必ずしも一定しないことは事実であり，筆者の感じでは，地域的な変化は，(一部の特殊な個所における局部的変異を除けば)，むしろ著しくないと考えられ，岩石の質的な相異に基づく差の方が顕著に現われていると思われる．数値上の検定の結果は第 V 表に示すとおりである．

6.　基盤の構造との関係

本地域の第三系の基盤をなす岩石は古生層，領家変成岩類及び中生代花崗岩類等であるが，その分布はきわめて限られ，しかも散在しているので，その構造を明らかにすることは相当困難である．筆者はごく一部の露頭を調査したにすぎないので，第三系の構造と基盤の構造との関係については，ほとんど資料を持たない．ここではただ，西谷村生水に露出する領家変成岩の fracture を調査した結果だけを示すにとどめておく (第 27 図参照)．附近に分布する斜長石英粗面岩，粒状安山岩，緑色凝灰岩層等の構造との関係は，この資料だけでは論ずる手がかりがない．

V.　調査結果にたいする解釈

先に説明したような統計的調査によつて認識される fracture system は，地方地質誌の研究上の一素材として興味を引くばかりでなく，その形成の機構という面から取りあげる場合には，構造地質学上の重要な問題を提供する可能性を持つと考えられる．すなわち，岩石中に発達する各種の fracture は，過去に起きた岩石の破断性変形の痕跡であり，いわばその変形作用の記録であるから，これを綿密に解析することにより，当時の色々な造構造的条件，変形作用の様相，fracture の形成機構及びその発達の過程等を判読することも可能となるであろう．上に記載した福井平野周辺地域の fracture system の資料について，このような面から検討を加えると，いくつかの興味ある問題を見いだすことができる．そのうちの 2, 3 をここに取りあげて，それにたいする筆者の見解を少し附け加えたいと思う．

1.　新第三系の層序・構造及び fracture system について

先に述べたように，本地域の新第三系の層序については，その下部に中新世中期ないし後期に相当する地層があること以外は不明な点が多い．層厚は非常に厚く，おそらく全体としては 3000 m 以上となるであろう．特に発達の著しいのは下部の「粒状安山岩質集塊岩層」と「緑色凝灰岩層」で，熔岩流・集塊岩・凝灰岩等の火山性物質よりなり，火山作用が激烈に行われたことを物語つている．中部の地層は砂岩・頁岩よりなり，凝灰岩・火山砕屑物を豊富に含む．中部層の下部 (凝灰岩及び凝灰質頁岩互層) には植物化石が含

まれ，石炭を産することがあるが，又 *Ostrea, Barbatia, Arca, Vicarya* 等の浅海棲貝化石を産する．中部層上部の「凝灰質頁岩層」中には *Clementia, Cardium, Arca* 等の浅海棲貝化石が発見される．上部層の「粗鬆砂岩層」は細粒ないし粗粒の砂よりなり，石灰質砂層をはさむ．又「浮石質砂岩層」は炭質物を含み，亜炭を産することがある．（第I表参照）各層の間には著しい不整合はないが，丹生山地の「緑色凝灰岩層」と「凝灰岩及び凝灰質頁岩互層」との間，及び大聖寺町附近の「粗鬆砂岩層」と「凝灰質頁岩層」との間に平行不整合が認められる．最下部の「粒状安山岩質集塊岩層」より最上部の凝灰質頁岩層にいたるまでは全体として一連のもので，一つの大きな堆積輪廻を示すものと見ることができる．

以上のような層序関係を，石川・富山県下の第三系の標準層序に対比すれば，池辺展生の加越累層群に大体相当し，下部の「粒状安山岩質集塊岩層」と「緑色凝灰岩層」は岩稲層群（あるいはさらにこれより下部に続くもの）に当り，中部の「凝灰岩及び凝灰質頁岩互層」より「凝灰質頁岩層」までは余川層群に，又上部の「粗鬆砂岩層」は氷見累層（大桑層）に，「浮石質砂岩層」は卯辰山累層に当ると見ることができよう．池辺展生によれば，岩稲層群は F_1，余川層群は F_2 より H_1，氷見累層は H_2，卯辰山累層は I にそれぞれ相当する[7)]．

なお，本地域の南方では新第三系は姿を消し，敦賀湾，若狭湾より琵琶湖に至る地域には古生層が広く分布している．しかしその西方の東舞鶴地域には新第三系に相当する地層があるらしく，特に最近福井県大飯郡内浦村の海岸において *Vicarya yokoyamai* が発見され，その地層は京都府との境に聳える青葉山の南麓に分布する下部松尾寺層に続くものであろうとされている．

地質構造については，断層の発達は著しいが，褶曲構造は局部的な小褶曲を見るのみである．部分的に見ると一見単斜構造をなすといえるが，しかし本地域全体を通じて見ると，大きなドーム構造の1部分あるいは大規模な撓曲のような感がある．すなわち，大聖寺町南東方山地においては層理面の走向・傾斜はだいたい一定であるが，西方の丹生山地においては，海岸に近づくにつれて走向は逆時針回りに回転し，同時に傾斜が急になっており，全体としてはドーム構造あるいは撓曲のように見える．このことは層理面の方位をシュミット網上に投影してみれば明瞭に認められる．第28図 a, b はそれぞれ大聖寺町南東方山地及び丹生山地で測定した層理面の極をシュミット網に投影して得た図型である．第28図 a では1つの顕著な極大区が認められ，その方位は (N 75° E, N 15°) であるが，第28図 b では (N 70° E, N 17°) より (N 10° E, W 30°) に至る帯状の極大区が認められる．

新第三系は石英粗面岩類・玢岩・粒状安山岩及び安山岩類等によつて貫かれている．これらのうち安山岩類は最も新しい時期のもので，新第三系を貫く岩脈として，又は不整合

7) 池辺展生「富山県西部及石川県東部の第三紀層（富山県及石川県の地質学的研究 1)」地学 **1** (1949), 14–26.

に覆う熔岩流として分布している．新第三系上部層の堆積中，及びその後に噴出したものである．石英粗面岩類は新第三系下部層の「緑色凝灰岩層」を貫き，岩脈・熔岩流として，あるいは「凝灰質砂岩層」中の逆流岩床として現出する．上部層との関係は明らかでないが，おそらくそれ以前に噴出したものとされている．粒状安山岩類の噴出時期は一定していないようである．

本地域の新第三系の層序及び構造については大体以上のような事実が認識される．これらの資料を基にし，石川・富山県下の第三系に関する知識を参照すれば，本地域の中新世以降の地史の輪郭を知ることができる．その要点を略記すれば次の通りである．

1) 中新世前期ないし中期に堆積作用が開始され，その当初には激烈な火山活動が行われ，基盤上に火山噴出物よりなる厚層が広範囲にわたつて発達した．次の時期には火山活動はやや勢を減じ，海侵は全般的に進行して浅海成堆積物よりなる地層の堆積が続いた．この海侵は鮮新世中頃まで続き，ついでいつたん海退の時期に入る．この海侵の期間中及びその後に石英粗面岩類の噴出があつた．鮮新世後期には再び海侵が起り，浅海成の地層が堆積した．鮮新世末には海退期に入り，本地域の大半は陸化したが，洪積世初めにはなお局地的に残つた海岸の沼沢地内で堆積作用が行われた．これは中新世より継続した一連の堆積輪廻の最後の時期に当る．鮮新世末以降安山岩類の噴出があいついで起つた．洪積世よりは大体隆起の傾向が続き，河川の沿岸や海岸に段丘が形成された．

2) 造構造運動の時期については，石川・富山県下の場合と大体同時期と考えて矛盾ないと思われる．金沢附近においては，褶曲運動の時期は卯辰山層堆積前より堆積後にわたり，相当長期間と考えられ，しかもその運動のきざしは大桑層堆積前よりすでに現われていると見られる．断層運動は褶曲運動に随伴して起り，同様に長期間にわたり，更に後期にも活動し，高位段丘を切るものもあるとされている[8]．本地域においてもほぼ同様で，粒状安山岩や安山岩類の分布状態又び新第三系との関係より見て，新第三系のドーム構造（ここではかりにこう述べておく）を生ぜしめた運動はおそらく「粗鬆砂岩層」の堆積前より始まり，「浮石質砂岩層」の堆積後まで続いたものと思われる．断層運動はこれに随伴して起り，「浮石質砂岩層」の堆積後にほぼその構造は完成したが，洪積中にもなお活動したようである[9]．

以上に記したように本地域では，中新世より鮮新世にわたつて堆積輪廻の時期があり，その最後の時期に当る鮮新世末を中心として造構造運動が起つたものと見ることができる．

ところで，新第三系の各層中に発達する fracture system についてみると，それらは全く相互に一致した様相を示しており，同一の機構で形成された，一連の系統のものと考

8) 小野山武文「高岡市並に石川県津幡町附近の第三紀層」地球 **24** (1935), 338–358, 405–427.
市原実　石尾元　森下晶　中川衷三　津田禾粒「富山県及石川県の地質学的研究（其の 2）金沢・石動・福光地域」地学 **2** (1950), 17–27.

9) 雄島村浜地附近においては洪積層を切る小断層が認められ，又この附近の洪積層中には細かなひびわれが見いだされる．

えられる．かつ，fracture system の発達状態が上に述べたドーム構造と密接な関係をもち，地層面の方位の変化に完全に並行して fracture system の地理的方位も変化すること，又断層構造との間にも傾向の一致が見られることなどより，fracture system の発達は鮮新世末の造構造運動に伴つて起つたものとすることができよう．新第三系の各層の fracture system の発達状態は，下部の地層ほど密な発達を示すという相異は見られるが，fracture system 全体の型，及び各要素の現われかたは各層を通じて全く共通である．このことはある一定の時期に発達したことを物語るものであろう．

この fracture system の形成にあたり，堆積岩層の各々に同一系統の fracture が生じたばかりでなく，その層内にはさまれる火成岩類にも同様な fracture system が生じたものと考えられる．たとえば，丹生郡越廼村殿下村境附近に露出する輝石安山岩の逆流岩床中には，周囲の「緑岩凝灰岩層」中の fracture と共通な要素のあることが認められる．(第 25 図参照) このような関係は，その他の第三紀火成岩類についても期待できる．

2. 第三紀火成岩類の fracture system について

本地域の火成岩類と新第三系との関係は上に述べた通りである．各種火成岩類のうち，石英粗面岩類・玢岩・粒状安山岩は，噴出の時期より便宜上第三紀火成岩類として一括されるが，これらの中に発達する fracture system は新第三系の各層中の fracture system とよく一致している．この関係は，上にあげた輝石安山岩の逆流岩床の例と同様，新第三系の fracture system と共通のものが火成岩類に現われていることを物語るものと考えられる．第三紀火成岩類は熔岩流・逆流岩床・岩脈として現出する．一般に火成岩中の割れ目，特に熔岩流中のものについては，柱状節理等の顕著なものがあり，岩漿の固結の際の収縮によつて生ずるものとされている．しかし，本地域の第三紀火成岩類の場合は，fracture system の各要素は層理面に垂直で，一見柱状節理のようではあるが，一般の柱状節理とは異る発達状態を示している．したがつて，たとえその 1 部に収縮節理があるとしても，主要部はすべて第三紀末の造構造運動に伴つて形成したものと考えてよいと思われる．新第三系はすべて鮮新世末を中心とする造構造運動に際して強烈な変形作用を受けて，顕著な fracture system を生じたのであり，したがつて当然，同じ時期に同じ系統の構造が第三紀火成岩類中にも発達したと考えられる．すでに説明したように，石英粗面岩類と粒状安山岩類のいずれもが，新第三系の fracture system と同一の構造をもち，この関係が本地域全般にわたつて認められる．さらに，この関係は火成岩類の現出状態に関係なく認められる．すなわち，熔岩流でも岩脈でも，すべて周囲の新第三系の fracture system と同一のものが見られる．これらの事実は，第三紀火成岩類中の fracture system が新第三系中のものと同一系統のものであることを示すものと思われる．

3. 安山岩類の fracture system について

本地域に分布する安山岩類の熔岩流はいずれも顕著な柱状節理状の割れ目を示す．上に述べたように，火成岩の柱状節理は一般に固結の際の収縮により生ずるものとされている．本地域の安山岩類のものも大体そのようにして生じたものと考えられる．特に熔岩

流の表面に近い部分に顕著に現われているものは，節理面が著しく彎曲し，節理の密度が表層ほど高く，一見して収縮によるものと認められる．雄島村安島附近の輝石安山岩の節理及び鷹巣村和布附近の粗面岩質安山岩の節理はその例である．

しかし本地域の安山岩類の fracture system 全般について，すべて単なる収縮節理として片づけてしまうには多くの疑問が残される．まず熔岩流の表面附近と，内部や底部では節理の発達状態がやや異なり，内部では節理面が平面状となり，長く続き，各節理面の間隔は大きくなる．又破砕状の割れ目や小断層が部分的に認められる．さらに注意すべきことは，安山岩類の fracture system と周囲の新第三系中の fracture system との間の一致が本地域の各所において認められ，しかもこの関係は熔岩流についてばかりでなく岩脈の場合にも見られることである．この点については，安山岩類の噴出時期と造構造運動の時期との関係を合わせて考える必要がある．前に述べたように，「浮石質砂岩層」の堆積時より安山岩類の噴出が始まつており，「浮石質砂岩層」には下部の新第三系の各層中に発達する fracture system と同一系統の fracture system が見られる．したがつて，安山岩類の 1 部のものは明らかに，鮮新世末を中心として起つた造構造運動の影響を受けたはずであり，その内部に新第三系の fracture system と同一系統の構造を示すことは当然期待できる．しかも，安山岩類は段丘堆積物に被覆され，あるいはその堆積物中に礫として含まれることより，その噴出時期は洪積世初期より後れるとは考えられず，したがつて安山岩類のほとんどすべてが，鮮新世末の造構造運動の余波の影響を受けたであろうと想像される．

4. fracture system の形成機構

本地域に発達する fracture system の特徴についてはすでに詳しく説明した．その主な点を再びここに記せば次の通りである．

1) fracture system は比較的単純な様相を示し，層理面（あるいは流動面）に垂直な 3 つの要素 M, N 及び K からなる．K は層理面（あるいは流動面）と走向を共通にし，一方 M 及び N はこの走向の方向を等角にはさむような位置に現われる．M と N とのなす角度は一定せず，それは地域的な相異よりむしろ岩石の質的相異に基づくもののようである．層理面（あるいは流動面）の傾斜の方向に開いた角が常に鋭角をなす．安山岩類の場合は，K の現われ方は少し異なり，2 つの要素に分れようとする傾向を示す．

2) fracture system の発達状態は全地域にわたつて良好な均質性を示す．かつ，fracture system の各要素と層理面（あるいは流動面）との間の立体的な関係は常に一定に保たれ，地域全体を通じて見れば，層理面（あるいは流動面）の方位の変化に完全に並行して fracture system 全体がそのまま地理的方位を変えている．

これまで述べてきた通り，本地域の fracture system は主として第三紀末に起つた造構造運動によつて形成されたものと考えられる．新第三系中の fracture system がこの運動に伴つて発達したことに疑いはないと思われ，また第三紀火成岩類中のものも，その主要部分はこれと同時期に形成されたものと考えられよう．さらに安山岩類中の節理に

ついても，その形成は洪積世まで続いた造構造運動の余波の影響の下で行われたであろうと考えたい．

このように解釈した場合，上にあげたような本地域の fracture system の特徴は，構造地質学的な見地から見てどのような意味をもつものであろうか．またその形成の機構をどのように考えたらよいであろうか．この点については，まず火成岩類の場合を一応除外して，新第三系中の fracture system のみについて考えてみたい．

新第三系中の fracture system については，明らかに造構造運動に際して生じた破断性変形によるものと考えられる．一般に破断作用はその箇所における応力の分布状態に支配されて起る．したがつて fracture system の発達状態を通じて当時の応力状態を間接的に知り得るものと思われる．

破壊という現象については，工業材料の破壊試験の結果と関連させて多くの理論が出されており，岩石の破断作用を解釈する場合にはこれらの理論が適用される．Anderson, E. M. はこの問題について詳しく検討を行い，断層の形成機構については，地殻の上部においては Navier の説が適用されるとしている．これによれば，断層はある面に沿う剪断応力 $\tau=\dfrac{\sigma_1-\sigma_3}{2}\sin 2\theta$ が，その面に働く 1 種の抵抗力（垂直応力に関係） $C+\mu\sigma$ $=C+\mu(\sigma_1\sin^2\theta+\sigma_3\cos^2\theta)=C+\mu\left(\dfrac{\sigma_1+\sigma_3}{2}-\dfrac{\sigma_1-\sigma_3}{2}\cos 2\theta\right)$ に打ち勝つた場合に生ずる．ただし σ_1, σ_3 は最大，最小主応力，θ はその面（中等主応力軸を含む面）と最大主応力軸との角，C は常数，μ は内部摩擦係数に相当するものである．したがつて $\dfrac{\sigma_1-\sigma_3}{2}\sin 2\theta\pm\mu\left(\dfrac{\sigma_1+\sigma_3}{2}-\dfrac{\sigma_1-\sigma_3}{2}\cos 2\theta\right)$ が極値をもつような面に断層が生じ得るわけで，その面は最大主応力軸に $\theta=\pm45°\mp\dfrac{\omega}{2}$, $(\tan\omega=\mu)$ なる角度をなし，中等主応力軸を含む面である[10]．

この Navier の説は Tresca 及び Guest の最大剪断応力説を発展させたものであるが，Mohr はこの説をさらに一般化し，μ が一定でなく垂直応力の任意函数であるとした．Leon が指摘したように，Mohr の説では脆性物質の屈伏の際の引裂破壊に相当する場合も含まれるわけで，脆性物質では $\theta=0°$，展延性物質では $\theta=45°$ に近くなる．Guest 説，Navier 説，Mohr 説はいずれも，破壊条件に最大，最小主応力のみが入つていて，中等主応力は無関係としている．この点については多くの議論があるが，Seigel, H. O. は中等主応力も条件に入れて解き，一定の面に沿つて破断の起る可能性はその面に作用する垂直応力と剪断應力とのある函数によつて表わされ，この値が最大値をとる面が破断面となると考え，それは結局中等主応力軸を含み最大主応力軸と $\theta<45°$ なる角度をなす 2 組の面であるという結果を出している[11]．

---

10) E. M. Anderson, *The Dynamics of Faulting and Dyke Formation with Applications to Britain*, (Edinburgh, Oliver and Boyd, 1942), Sec. Ed. Revised 1951, pp. 7–11.

いずれにせよ，岩石の破断変形，特に成層岩の破断を解釈するに当つては，最大剪断応力説及びそれを修正，一般化した説を適用するのがよいようであり，NADAI も MOHR 説が適用し得ることを指摘している[12]．すなわち，岩石中の断層や節理の形成は，その部分における応力分布によつて支配され，中等主応力軸を含み最大主応力軸に $\theta<45°$ なる角度をなす 2 組の面に生ずるものと一般に認められている．

このような理論に基づいて本地域の fracture system を眺めた場合，その主要素をなす M と N とは層理面（あるいは流動面）の走向方向に最小主応力軸，傾斜方向に最大主応力軸があつたような応力状態のもとに形成されたと解釈することが可能となる．これはすなわち，走向方向に張力が，傾斜方向に圧縮力が働いたような状態である．丹生山地の数ケ所において認められる局部的な小褶曲は，この傾斜方向に働いた圧縮力によつて随伴的に生じたものと見ることができる．このような応力状態のもとで生ずる fracture system の主要素，N 及び M が断層系として現われる場合は，ANDERSON のいう wrench fault となり，その実例は大聖寺町南方の山地において認められる．他の地区においても，綿密な調査を行えば，これと同じ構造を見いだしうるであろう．

fracture system の別の要素 K については，その発達状態より見て tension fracture であるように思われる．すなわち，地層の傾斜方向に張力が働き，それに垂直に生じたものと考えられる．これは，M, N を生ぜしめた応力状態とは全く逆で，前の場合の地層の走向方向の張力が消え，傾斜方向の圧縮力が張力に変つた状態である．この M, N の場合と K の場合の関係については簡単に解決しにくいような問題が残されているが，しかし決して矛盾した関係ではない．一般に造構造運動の同一時相に生じた fracture system に幾組かの相異る fracture の要素が含まれるのは普通に見られることである．この K については，M, N を生ぜしめた応力が取去られたあとに生じた release fracture のようなものと解釈したい．造構造運動の末期にあたつて，これまで M, N を生ぜしめた地層の走向方向の張力，傾斜方向の圧縮力という応力状態が消え，地盤の隆起運動が起ると共に，今度は傾斜方向に張力が働きはじめ，その結果 K が生じたと想像したい．この場合地層に垂直な方向には圧縮力が働いているから，この方向に最大主応力軸が，傾斜方向に最小主応力軸がきたことになる．MOHR 説を適用すれば，M, N の場合と K の場合の応力状態の関係は第 30 図のように考えられ，K は地層の走向方向を含み，傾斜方向に垂直あるいは垂直に近い面として現われることになる．fracture system の各図型における K の現われかたはこれとよく一致している．この要素は常に副次的なものとして現われ，変形作用の特に強く行われたと見られるような箇所に比較的顕著な発達を示すものである．断層系として重要な意味を持つこともおそらくないと思われる．

火成岩類の fracture system の形成機構については一応除外して考えてきた．これに

11) Harold O. SEIGEL, "A Theory of Fracture of Materials and Its Application to Geology" *Trans. Amer. Geophys. Union*, **31** (1950), 612-615.

12) A. NADAI, *Theory of Flow and Fracture of Solids*, Vol. I, Sec. Ed., Engineering Societies Monographs, (New York, Mcgraw-Hill, 1950), pp. 223-224, 229-230.

ついては疑問の点もあるが，すでに説明したように，火成岩類のほとんどすべてが造構造運動の影響を受けたはずであり，新第三系中の fracture system を形成せしめたと同一の条件の下に，それぞれ M, N 及び K に相当する fracture が発達したものと考えたい．ただ新第三系の場合と異なり，固結の際の収縮節理が混入する可能性があり，あるいは，収縮節理の形成自体が，新第三系の fracture system の形成を支配した応力状態の影響を受けたのかもしれない．

次に fracture system の主要素 M, N のなす角度について少し考えてみたい．ANDERSON は 2 組の正断層の場合では $2\times18°\sim2\times25°$ であると言つている．NAVIER 等の説では，この角度は物質固有の力学的性質によつて決まるものと解されるが，MOHR 説ではさらに限界応力にも関係するとしている．SEIGEL の説くところも同様である．本地域の例では，すでに説明した通り，かなり広範囲にわたる変異を示し，大体において同一種類の岩石についてはほぼ同一の平均値が得られるようであるが，そうならない場合もある．MOHR 説では脆性物質の破壊では 2 面間の角度が 0 になり，つまり引裂破壊となり，展延性物質の破壊では $2\times45°$ になるとしている．堆積岩の場合では一般に砂質のものはこの角度が大，シルト質のものは小である．砂質の未凝固堆積岩は変形の際シルト質のものよりも可塑的な性質を示すものであるから，この点では MOHR 説と一致する．又 M, N と K の関係について見ると，上に示した通り，両者は別の応力状態で形成されたと解釈され，K が単一組の要素として現われるのは，引裂破壊を生ぜしめるような応力条件の下で形成された為と見られるのであつて，MOHR 説を適用するとよく説明できるように思われる．

次に本地域の火成岩類の場合では，M, N のなす角は一般に堆積岩層の場合よりも大きいように思われる．MOHR 説に従えば，この場合は堆積岩層の fracture の場合よりも展延性物質の破壊に近い状態で形成されたことになり，これは火成岩の力学的性質に関する一般の常識とは相反するようである．このことはあるいは，火成岩類が完全に冷却固結する迄の間に造構造運動の影響を受けて潜在的な剪断面を生じ，それがやがて収縮節理状の fracture となつて現われたことを物語るのかもしれない．特に安山岩類の fracture system が明らかに収縮節理のようでありながら，周囲の新第三系の fracture system と全く一致しているという事実は，こうした事情を想像させるものである．なお安山岩類では fracture system の要素 K が比較的顕著に現われ，かつ 1 面としてよりはむしろ 2 面に分れようとする傾向が見られる場合があるが，この点についても同様なことが考えられる．すなわち，K を生ぜしめた応力状態が現われたのは造構造運動の末期にあたり，ちようど安山岩類の噴出時期頃であろうと想像されるからである．ただし，ここに述べた事柄は，基準とする資料が不十分，不完全であるので，単なる想像の域をでないものである．

最後に，fracture system の発達状態を本地域全体にわたつて眺め，これがどのような運動によつて形成されたかを考えてみたい．fracture system は極めて良好な均質性を示し，これは当時の応力状態が全地域にわたつて均質であつたことを物語つている．第

三紀末の造構造運動に際しては，本地域全体が1つの構造的単位として変形作用を受けたことが明らかである．fracture system は層理面（あるいは流動面）と常に一定の幾何的関係を保つて発達しているが，このことは層理面（あるいは流動面）の変位と fracture system の発達とが全く並行して行われたことを示している．すでに説明した通り，本地域の新第三系の構造は大きなドーム構造の1部分あるいは大規模な撓曲のようなものである．この構造ができ上がるに際して，その各部分において，層理面の走向方向に張力が，傾斜方向に圧縮力が作用して，fracture system の要素 M, N が発達し，構造完成の末期に，地域全体が隆起，伸張の傾向をとつた時に要素 K が発達したのであろう．この構造の特徴として注目すべき点は，丹生山地西部の海岸沿いの地区において，層理面の走向が急廻転して海岸線と一致するような傾向をとり，傾斜角が増し，同時に fracture system の顕著な発達を示すという点である．以上のような構造がどのような運動によつて形成されたかを考えるには，さらに広範囲にわたる地質構造の調査・解析が必要となる．この問題について議論を進めるにたるだけの資料を現在持たないので，ここでは単に筆者の抱いている想像的な考えを附記するにとどめたいと思う．本地域の周囲の地質構造として特に注意すべきことは，西南方の敦賀湾より伊勢湾に至る地帯が，日本においては本州弧を横断する断層帯としてフオツサ・マグナについで重要であるという点である．本地域西南隅の越前崎南方干飯崎より北陸線杉津駅附近に至る海岸線は典型的な断層海岸としてよく知られている．又その南方日野川上流部より栃木峠を越えて椿坂峠・柳ケ瀬・中之郷・木之本へ延びる線は断層谷の典型的な例として有名であり，柳ケ瀬断層と呼ばれる．これはさらに伊吹山附近より関ケ原地溝以東へと續いている[13]．この断層線の西側は琵琶湖を中心とする陥没地帯であるが，又これを境として古生層の走向が急曲することより，水平移動が暗示される．新第三系は断層線の西側においては姿を消し，西方の東舞鶴地域に至つて再び現われる．筆者はこの敦賀湾より伊勢湾に至る断層帯の存在を福井平野周辺地域の地質構造と関係あるものと考えている．すなわち，この断層帯は第三紀末を中心として活動し，西側に敦賀湾，琵琶湖等の陥没地帯を生じたが，この際に福井平野周辺地域の新第三系が断層運動により引きずられて，現在見るような構造をとるに至り，同時に前述の fracture system を生じたものと考えたい．丹生山地において，新第三系の走向が越前崎に近づくにつれて急廻転して E–W より N–S となり，傾斜もまし，同時に fracture system の発達状態が著しくなるという事実は，越前崎南方より SSE へ延びる断層線に沿つて起つたと考えられる水平移動性の断層運動によつて引きずられた結果と解釈するとよく説明できるようである．

5. 地震断層との関係

福井地震に際しては，福井平野を横ぎつて NNW–SSE の地震断層を生じたような形跡が認められた．断層面は地上に現われなかつたが，水準測量及び三角測量の結果は明ら

13) 山崎直方，多田文男「琵琶湖附近の地形と其の地体構造につきて」地震研究所彙報 **2** (1927), 85–108.

かに断層運動の起つたことを示していた．かつ，その断層線に当る沖積平野上には著しいひびわれが発達した．断層運動は，西側が落ち，かつ南方に移動したような型のものであつた．那須信治はこれを福井断層と名づけ，根尾谷断層の延長と考えた[14]．この断層線は，本地域の構造と密接な関係をもつと筆者が考えた敦賀湾より伊勢湾に延びる断層線に平行するものであり，運動の型式も同一である．第三紀末の造構造運動の終焉以後も，おそらく本地域においては，地盤の安定化と同時に断層運動がひき続いたと考えられ，それはあるいは敦賀湾—伊勢湾断層線と平行し，同一の運動型式のものが主であつたろうと想像される．たとえば，本地域より濃尾平野にかけて認められる NNW–SSE の断層谷列がそれを暗示している．本地域の新第三系の構造を見ると，層理面の走向が急曲する箇所が局部的に認められる．この傾向は層理面の方位を投影した図型を見ると明らかで，福井平野東方山地の図型（第 28 図 a）では層理面はほぼ一定の方位を示してはいるが，同時にその走向が E–W より，NE–SW，N–S へと変化する傾向も認められる．これは丹生山地の層理面の図型（第 28 図 b）における走向の廻転と，程度こそちがえ，全く同じ傾向を示すものである．この事実は，本地域の主構造完成後，洪積世に入つてから，敦賀湾—伊勢湾断層線に平行する断層が本地域内に発達したことを示すものと見ることができよう．そして福井断層も又これと同一系統のものと想像できないこともないと思われる．

VI. 結　　語

以上に福井平野周辺地域の fracture system の発達状態について詳しく説明し，それがどのような機構で形成されたかを考えてみた．何分資料が不十分なので決定的なことがいえないのはやむをえない．本地域及びその附近は日本島弧の地質構造上重要な地域に当つており，地震の頻りに起る場所でもあるので，さらに広範囲にわたる詳細な調査を進めることが望ましい．この研究がその捨石として多少の意義を持ちうれば幸である．

この研究を進めるに当つて色々お骨折りをいただいた津屋弘達教授に厚く感謝の意を表する．また御指導を賜わつた坪井誠太郎教授，故大塚弥之助教授に深謝する．

---

14) N. Nasu, *The Fukui Earthquake of June 28, 1948 Report of Special Committee for the Study of the Fukui Earthquake,* "Chapter V, Crustal Deformation." 93–130.

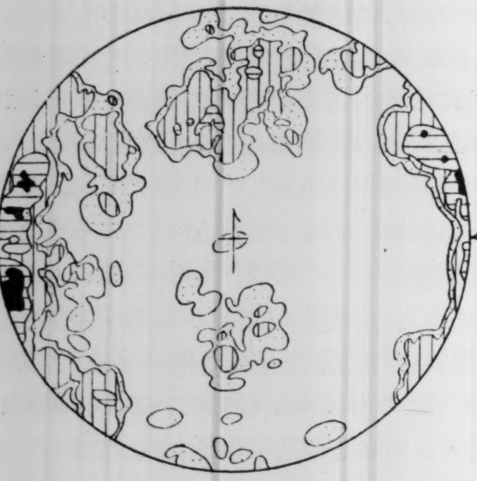

第 1 図a Propylite の熔岩流中の fracture.
石川郡江沼西谷村で測定した fracture の極 150 個の 1% 図型. 集中の度合: (8–6)–4–2–1–0%. 第 10 図と第 11 図を集合したもの.

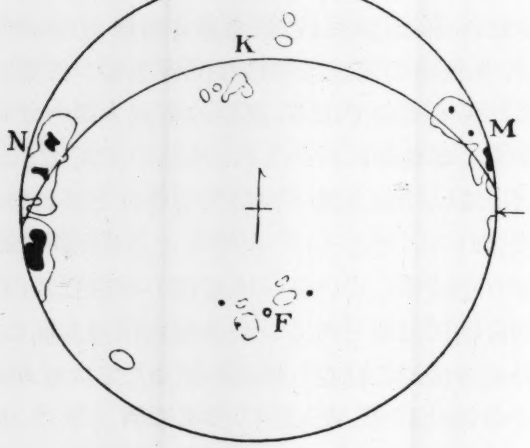

第 1 図b a 図における，流動面 F と fracture の 3 つの要素 M, N, K との関係を示す図.

第 2 図 緑色凝灰岩層中の fracture.
石川県江沼郡西谷村で測定した fracture の極 124 個の 1% 図型. (9–7)–5–3–1.5–0%. 第 8 図と第 9 図を集合したもの.

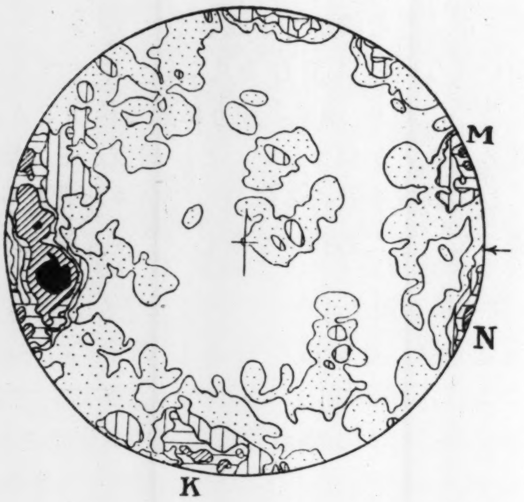

第 3 図 粒状安山岩質集塊岩層及び緑色凝灰岩層中の fracture.
福井県坂井郡竹田村で測定した fracture の極 196 個の 1% 図型. (8–6)–4–3–2–1–0%. 第 6 図と第 7 図を集合したもの.

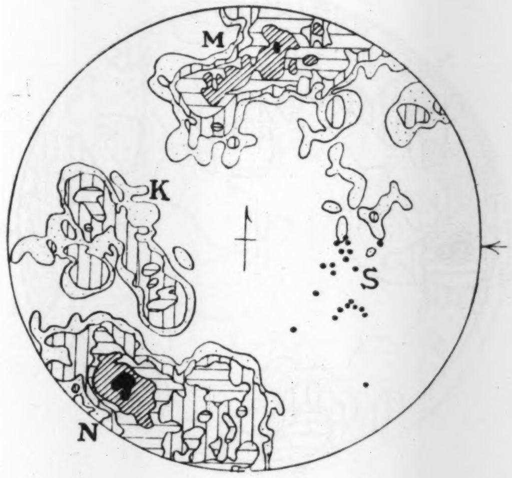

第 4 図 a　凝灰岩及び凝灰質頁岩石互層及び緑色凝灰岩層中の fracture.
福井県丹生郡越廼村及び図見村で測定した fracture の極 167 個の 1%図型. (8.5–7)–5–3–2–1–0%. ・は層理面の極. 第15図, 第16図及び第17図を集合したもの.

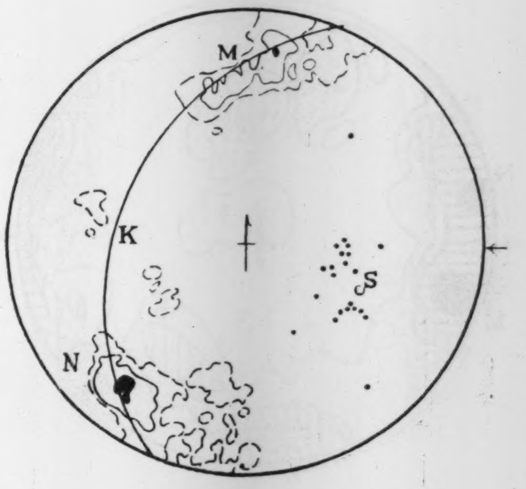

第 4 図 b　a 図における, 層理面 S と fracture の 3 つの要素 M, N, K との関係を示す図.

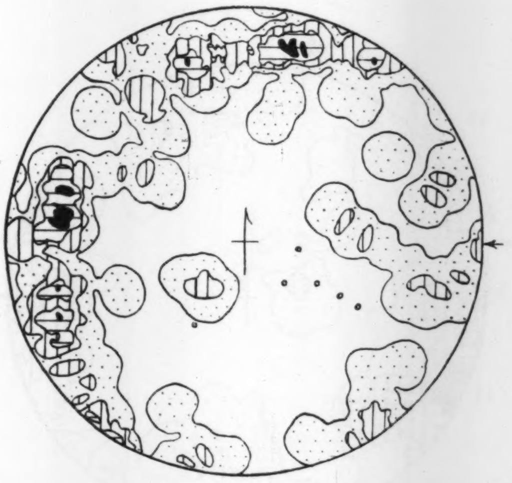

第 5 図 a　Trachytic Andesite の熔岩流中の fracture.
福井県坂井郡鷹巣村で測定した fracture の極 107 個の 1% 図型. (7–6)–5–3–1–0%. ∘ は流動面の極. 第 18 図 と第 19 図を集合したもの.

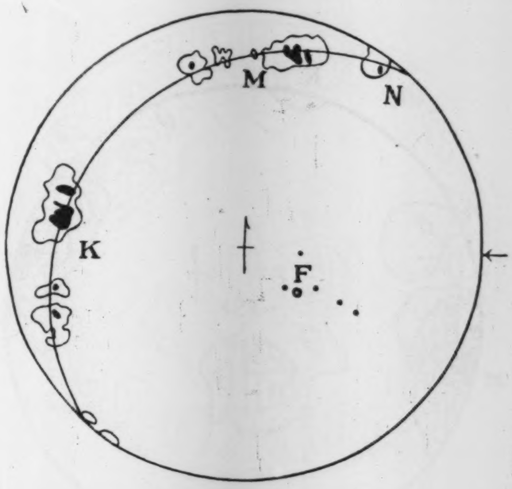

第 5 図 b　a 図における, 流動面 F と fracture の 3 つの要素 M, N, K との関係を示す図.

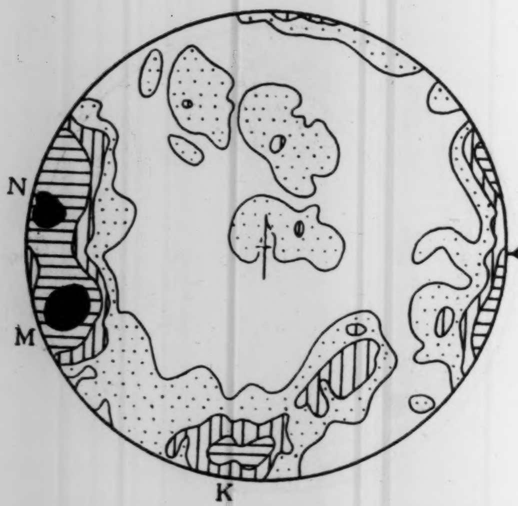

第 6 図 粒状安山岩質集塊岩層中の fracture. 福井県坂井郡竹田村山竹田より長畝村川上に至る間で測定した fracture の極 96 個の 2% 図型. (13.5–10)–6–4–2–0%.

第 7 図 粒状安山岩質集塊岩層及び緑色凝灰岩層中の fracture. 福井県坂井郡竹田村上竹田附近で測定した fracture の極 99 個の 2% 図型. (13–10)–6–4–2–0%. ∘は層理面の極.

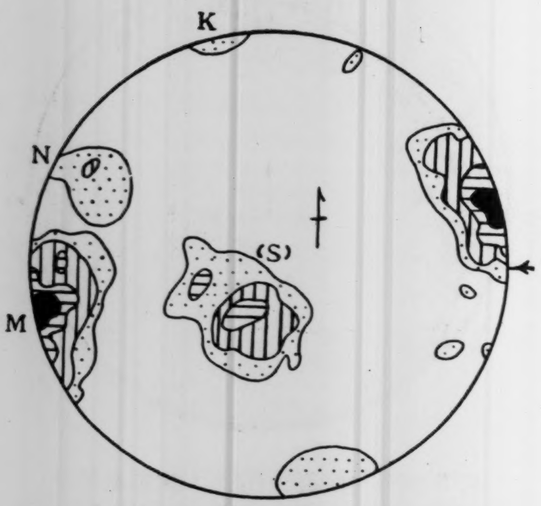

第 8 図 緑色凝灰岩層中の fracture. 石川県江沼郡西谷村栢野で測定した fractnre の極 31 個の 3% 図型. (23–19)–16–10–7–0%

第 9 図 緑色凝灰岩層中の fracture. 石川県江沼郡西谷村で測定した fracture の極 87 個の 2% 図型. (11.5)–7–4.5–2.5–0%

第 10 図 Propylite の熔岩流中の fracture.
石川県江沼郡西谷村栢野一我谷間で測定した
fracture の極 93 個の 2% 図型.
(16–11)–7.5–4.5–2–0%.

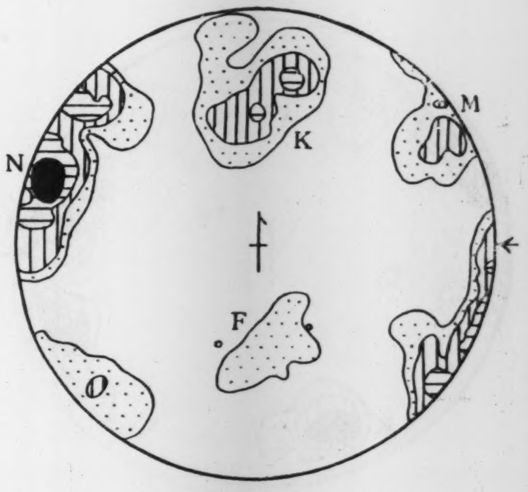

第 11 図 Propylite の熔岩流中の fracture.
石川県江沼郡西谷村九谷一真砂間で測定した
fracture の極 59 個の 2% 図型. (15–13.5)–
10–7–3.5–0%. ∘は流動面の極.

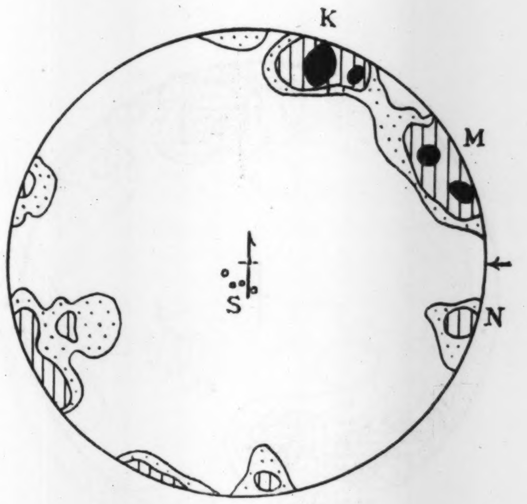

第 12 図 浮石質砂岩層及び砂岩層
中の fracture.
石川県江沼郡大聖寺町三つ俣及び三谷村百々
で測定した fracture の極 30 個の 2% 図型.
(20–17)–10–7–0%. ∘は層理面の極.

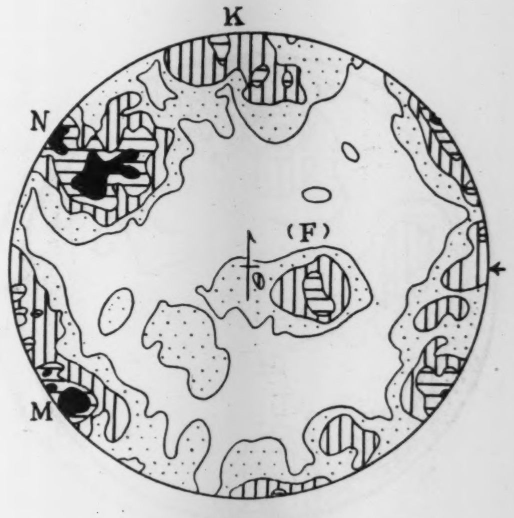

第 13 図 粒状安山岩質集塊岩層
中の fracture.
福井県吉田郡志比谷村及び松岡町で測定した
fracture の極 104 個の 2% 図型.
(9–8)–6–4–2–0%.

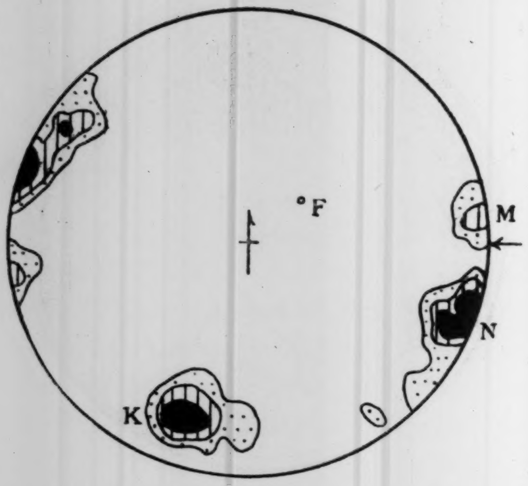

第 14 図 a Propylite の熔岩流中の fracture. 福井県大野郡遅羽村比島で測定した fracture の極 25 個の 2% 図型. (20–16)–12–8–0%. ◦ は流動面の極.

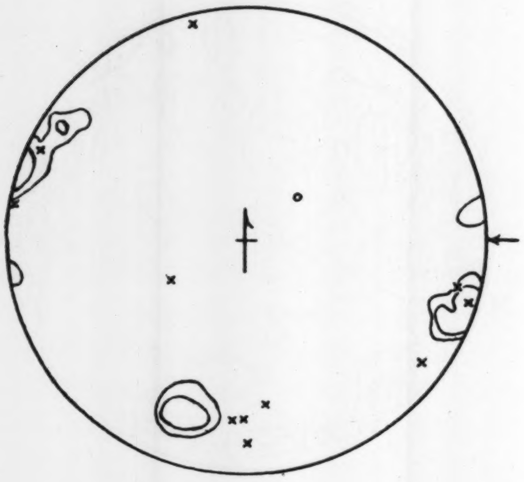

第 14 図 b a 図の Propylite 中の fracture とそれを貫く Plagiolipalite の岩脈中の fracture との関係を示す図. × で示すものは福井県大野郡遅羽村比島で測定した Plagiolipalite 中の fracture の極. 等集中度曲線は a 図の16%, 12% の線を転写したもの.

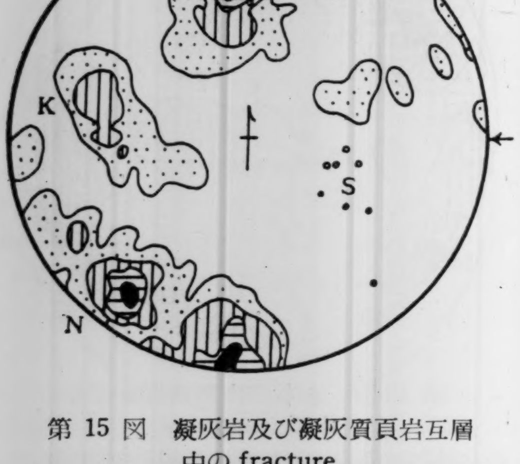

第 15 図 凝灰岩及び凝灰質頁岩互層中の fracture. 福井県丹生郡越廼村大味で測定した fracture の極 71 個の 2% 図型. (13–11)–9–6–3–0%. ◦ は層理面の極.

第 16 図 緑色凝灰岩層中の fracture. 福井県丹生郡国見村小丹生で測定した fracture の極 56 個の 2% 図型. (18–14.5)–11–7–4–0%. ◦ は層理面の極.

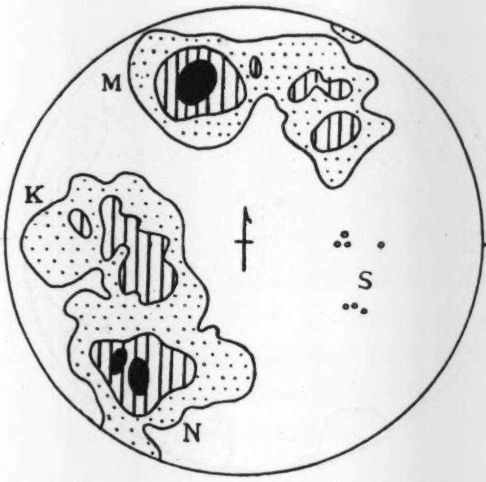

第 17 図 凝灰岩及び凝灰質頁岩互層中の fracture.
福井県丹生郡越廼村茱崎で測定した fracture の極 40 個の 3% 図型. (17.5–15)–10–5–0.
○ は層理面の極.

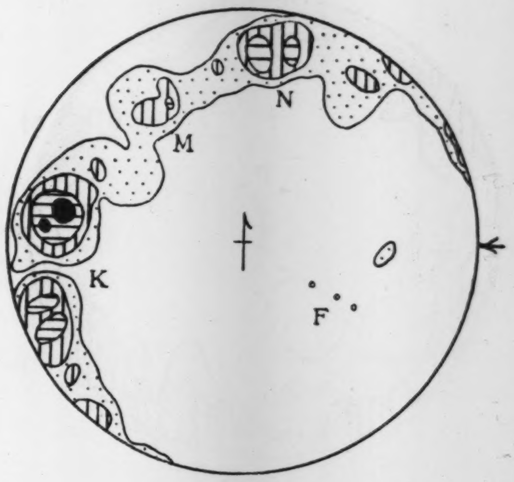

第 18 図 Trachytic Andesite の熔岩流中の fracture.
福井県坂井郡鷹巣村菅生より国見村鮎川に至る間で測定した fracture の極 47 個の 2% 図型. (19.5–17)–13–8.5–4–0%.
○ は流動面の極.

第 19 図 Trachytic Andesite の熔岩流中の fracture.
福井県坂井郡鷹巣村で測定した fracture の極 67 個の 2% 図型. (12–9)–6–3–0%.
○ は流動面の極.

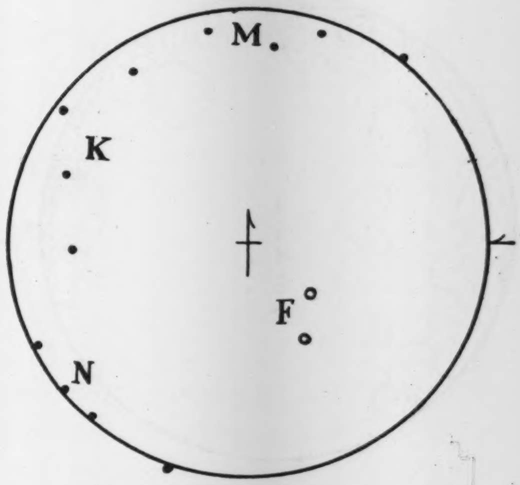

第 20 図 Ryolite 中の fracture.
福井県坂井郡雄島で測定した fracture の極の散点図型. ・が fracture の極.
○ は流動面の極.

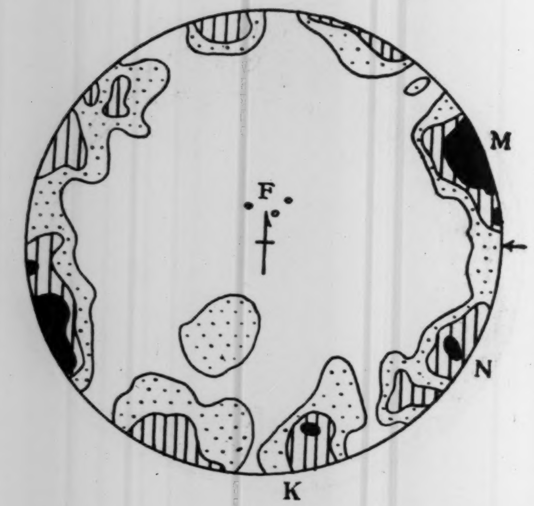

第 21 図a Augite-Andesite の熔岩流中の fracture.
福井県坂井郡雄島村東尋坊で測定した fracture の極 35 個の 3% 図型.
(16–10.5)–8–5–0%. ◦ は流動面の極.

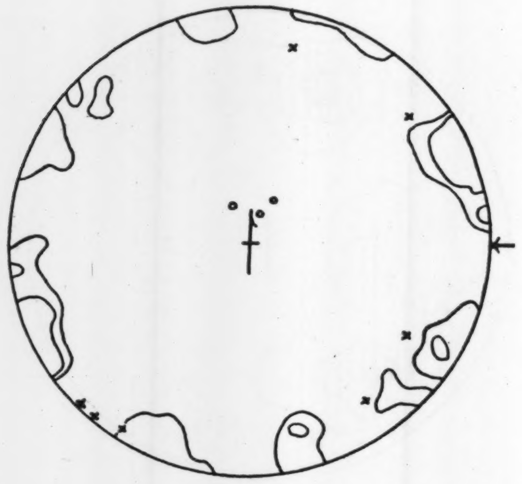

第 21 図b a 図の Augite-Andesiste 中の fracture とその下に覆われる凝灰質頁岩層中の fracture との関係を示す図. × は福井県坂井郡雄島村米ケ脇で測定した凝灰質頁岩層中の fracture の極. 等集中度曲線は a 図の 10.5%, 8% の線を転写したもの.

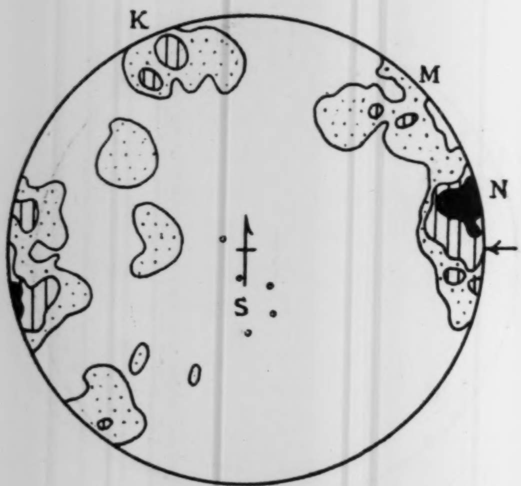

第 22 団a 凝灰岩及び凝灰質頁岩互層中の fracture.
福井県坂井郡本郷村で測定した fracture の極 42 個の 2% 図型. (19–14)–9.5–5–0%.
◦ は層理面の極.

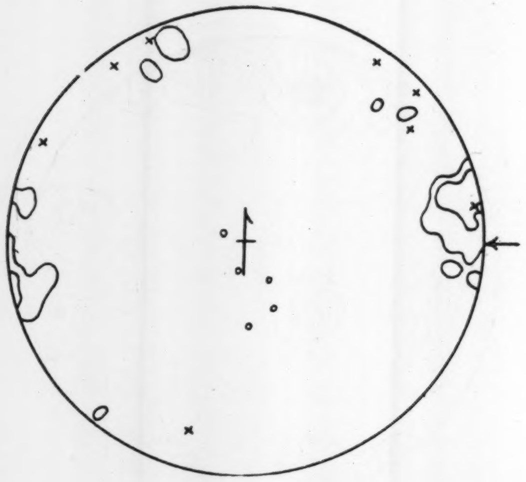

第 22 図b a 図の凝灰岩及び凝灰質頁岩互層中の fracture とその上を覆う Augite-Andesite の熔岩流中の fracture との関係を示す図. × は福井県坂井郡本郷村河内で測定した Augite-Andesite 中の fracture の極. 等集中度曲線は a 図の 14%, 9.5% の線を転写したもの.

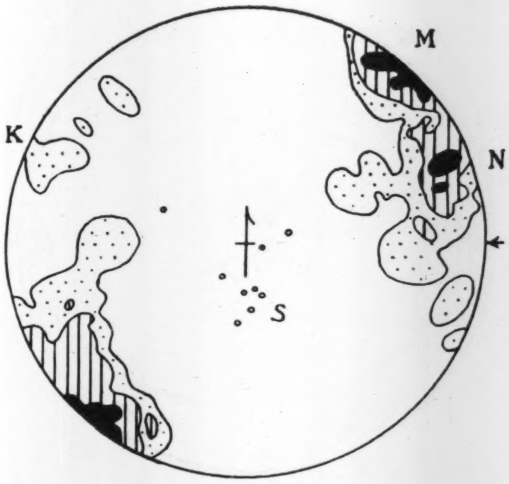

第 23 図　凝灰岩及び凝灰質頁岩互層中の fracture.
福井県丹生郡国見村で測定した fracture の極 45 個の 2% 図型. (18–13.5)–9–4.5–0%.
◦ は層理面の極.

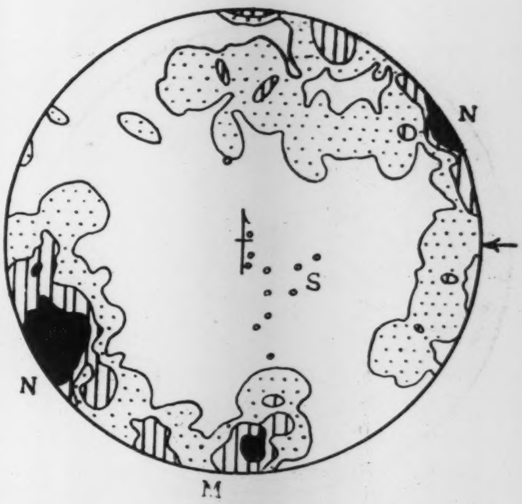

第 24 図 a　緑色凝灰岩層中の fracture.
福井県丹生郡国見村大丹生～西完居村下一光間で測定した fracture の極 73 個の 2%図型.
(15–8)–5.5–3–0%. ◦ は層理面の極.

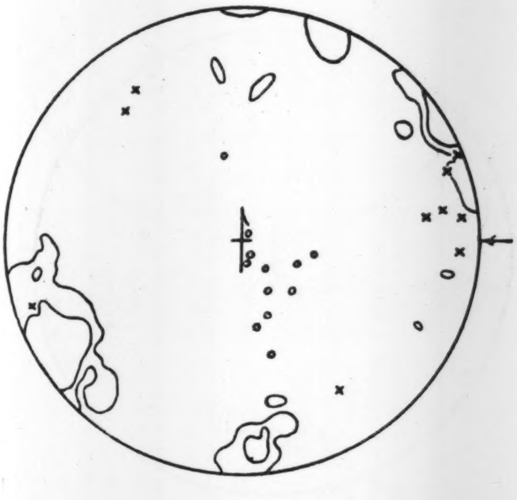

第 24 図 b　a 図の緑色凝灰岩層中の fracture とそれを貫く Augite-Andesite の岩脈中の fracture との関係を示す図. ×は福井県丹生郡西完居村五太子ノ滝で測定した Augite-Andesite 中の fracture の極. 等集中度曲線は a 図の 8%, 5.5% の線を転写したもの.

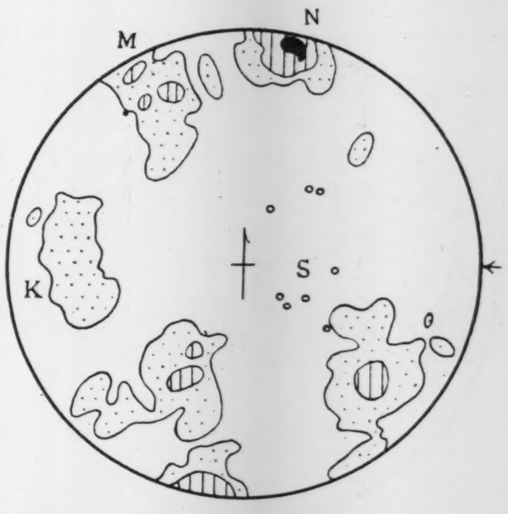

第 25 図 a　緑色凝灰岩層中の fracture.
福井県丹生郡殿下村で測定した fracture の極 46 個の 2% 図型. (15–13)–9–4.5–0%.
◦ は層理面の極.

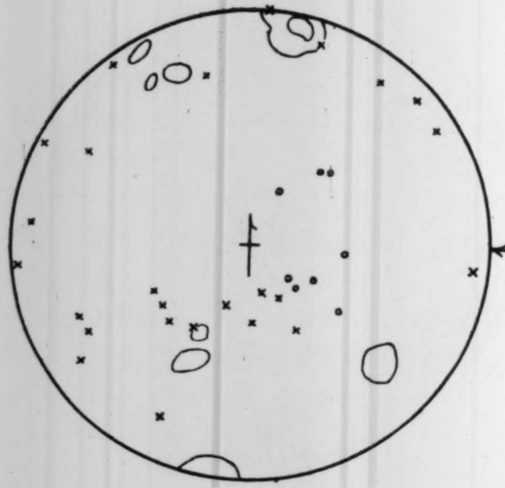

第 25 図 b a 図の緑色凝灰岩層中の fracture とその間にはさまれる Augite-Andesite の迸流岩床中の fracture との関係を示す図. ×は福井県丹生郡越廼村大味東方, 殿下村との境附近で測定した Augite-Andesite 中の fracture の極. 等集中店曲線は a 図の 13%, 9% の線を転写したもの.

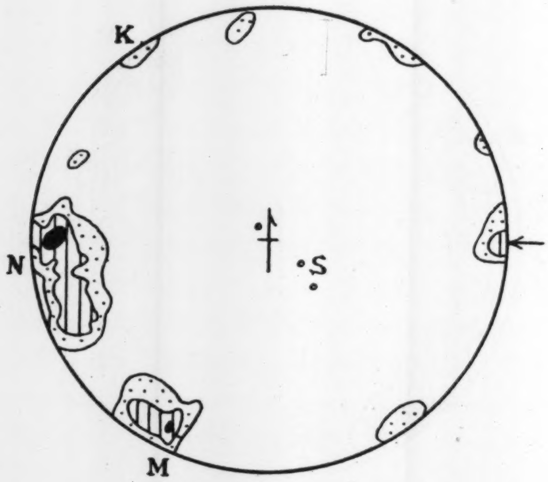

第 26 図 a 緑色凝灰岩中の fracture. 福井県丹生郡殿下村大矢で測定した fracture の極 20 個の 2% 図型. (25–20)–15–10–0%. ◦ は層理面の極.

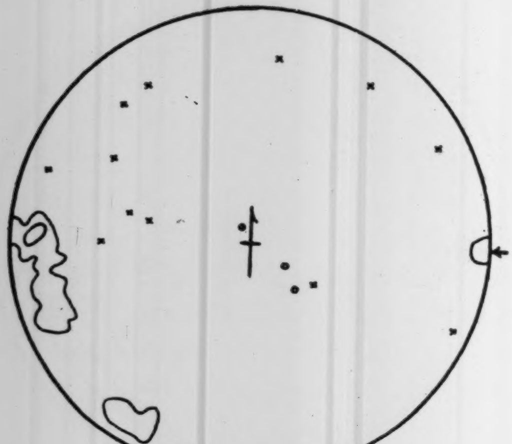

第 26 図 b a 図の緑色凝灰岩層中の fracture とそれを貫く Augite-Andesite の岩脈中の fracture との関係を示す図. × は福井県丹生郡殿下村大矢で測定した Augite-Andesite 中の fracture の極. 等集中度曲線は a 図の 20%, 15% の線を転写したもの.

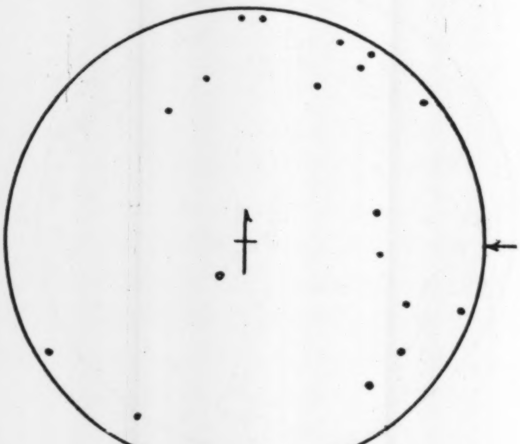

第 27 図 領家変成岩中の fracture の 1 例. 石川県江沼郡西谷村生水で測定. • : fracture の極, ◦ : 片理面の極.

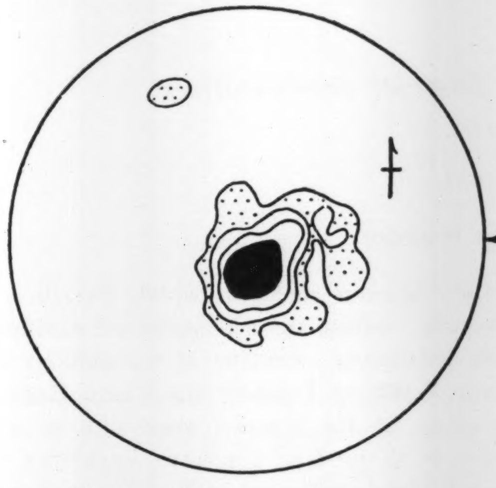

第 28 図 a　新第三系の層理面の方位性．石川県江沼郡大聖寺町南東方の山地で測定した層理面の極 102 個の 1% 図型．(55–20)–8–4–2–0%.

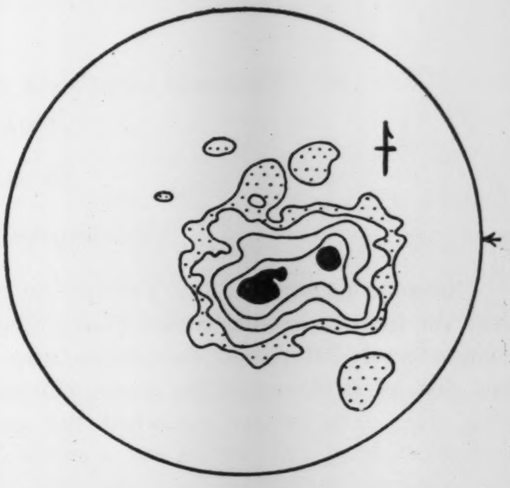

第 28 図 b　新第三系の層理面の方位性．福井平野西方丹生山地で測定した層理面の極 140 個の 1% 図型．(18–14)–11–5.5–3–1.5–0%.

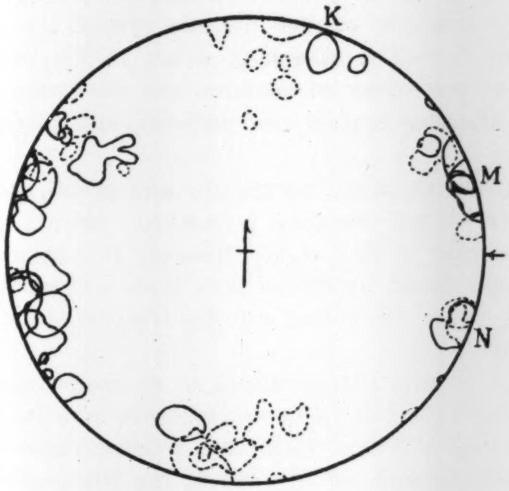

第 29 図 a　第 6～14 図の極大区，副極大区の複合図型．実線は極大区，点線は副極大区．(福井平野東方山地)

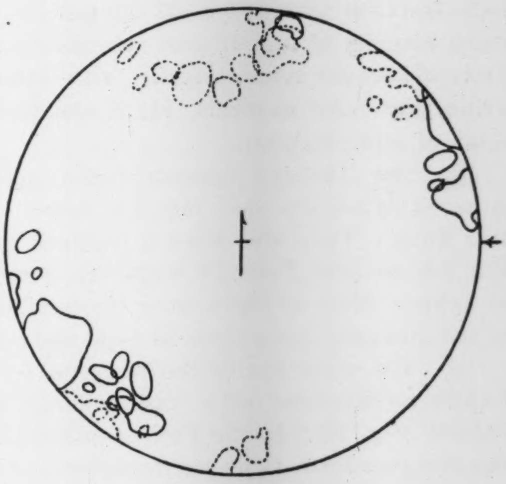

第 29 図 b　第 15～17 図，及び第 22～26 図の極大区の複合図型．実線は N, 点線は M に相当する極大区．(丹生山地)

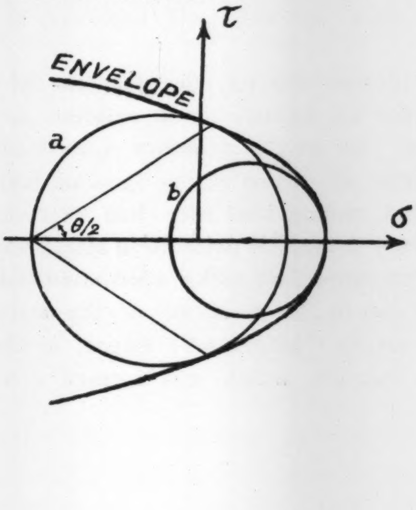

第 30 図　fracture system の要素 M, N の場合と K の場合の応力状態の関係を Mohr 説に基づき説明する図．a は M, N の場合，b は K の場合．

9. *Tectonic Analysis of the District Surrounding Fukui Plain.*

By Isamu MURAI,

Earthquake Research Institute.

Neogene formations and Tertiary or post-Tertiary igneous rocks are widely distributed over the district around Fukui Plain, Fukui Prefecture, resting upon a basement complex composed of Palaeozoic formations and Mesozoic intrusives. Outline of the geology of this district is shown in the geological map, scale 1:75,000, of Daishôji and Fukui Region (Fig. 31). The writer classified the geological units of the district according to the geological map, and carried out a statistical survey of all sorts of fractures developed in the Neogene formations and the igneous rocks of each geological unit. He analyzed statistically the fracture systems in each unit, with the results as follows.

1) Every Neogene formation in the district, from the lowermost member of the formations, "Propylitic Agglomerate Beds", to the uppermost one, "Pumiceous Sandstone Beds", has a similar fracture system, and no essential difference can be detected between each fracture system of all formations. Every diagram of the fracture system shows sharp maxima M and N, and submaximum K, the former representing a set of diagonal joints orientated symmetrically with reference to the strike of stratum, and the latter a strike joint. All elements, M, N and K, of the fracture system are perpendicular to the plane of stratification.

2) The Tertiary igneous rocks (plagioliparite, rhyolite, porphyrite and prophylite) occur as dykes intruded into the lower members of the Neogene formations, besides as lava flows. They also show a fracture system similar to that of the Neogene formations. The late or post Tertiary eruptives (andesites) are found mostly as lava flows and partly as dykes. Most of them show distinct columnar joints, coinciding with the fracture system of the Neogene formations in type and orientation.

3) The structure of the Neogene formations in the district seems to be monoclinal, locally accompanied with small foldings, but it may be a part of dome structure or a large flexure (Fig. 32). In the Fujisha-ga-take region, east of Fukui Plain, the bedding plane of the Neogene formations are monoclinal, with about (N 80° E, 10° N), but in the Niu region, west of the plain, they rotate suddenly, changing in strike from E—W to N—S and increasing in dip angle, especially along the shoreline of the Japan Sea (Fig. 28). The orientation of the fracture system in the formations rotate in accordance with the rotation of the bedding planes (Fig. 29, 32). The fracture system itself, however, is homogeneous throughout the whole area (Fig. 30).

4) Referring to the geological history of the district, development of the fracture system mentioned above may be interpreted as having some relation to the tectonic movement at the end of the Tertiary period. As to the fracture system of the Neogene formations, it may be reasonable to consider so. Most of the igneous bodies also must have been subjected to the tectonic movement, seeing that they had extruded before the movement ceased. According to Mohr's theory it may be possible to interpret the elements of M and N of the fracture system as having developed under such condition, as the axis of minimum principal stress (tensile stress) lies in the direction of the strike of bedding plane and the axis of maximum principal stress (compressive stress) in the direction of the dip. Element of K map be the release fracture which was formed after such stress

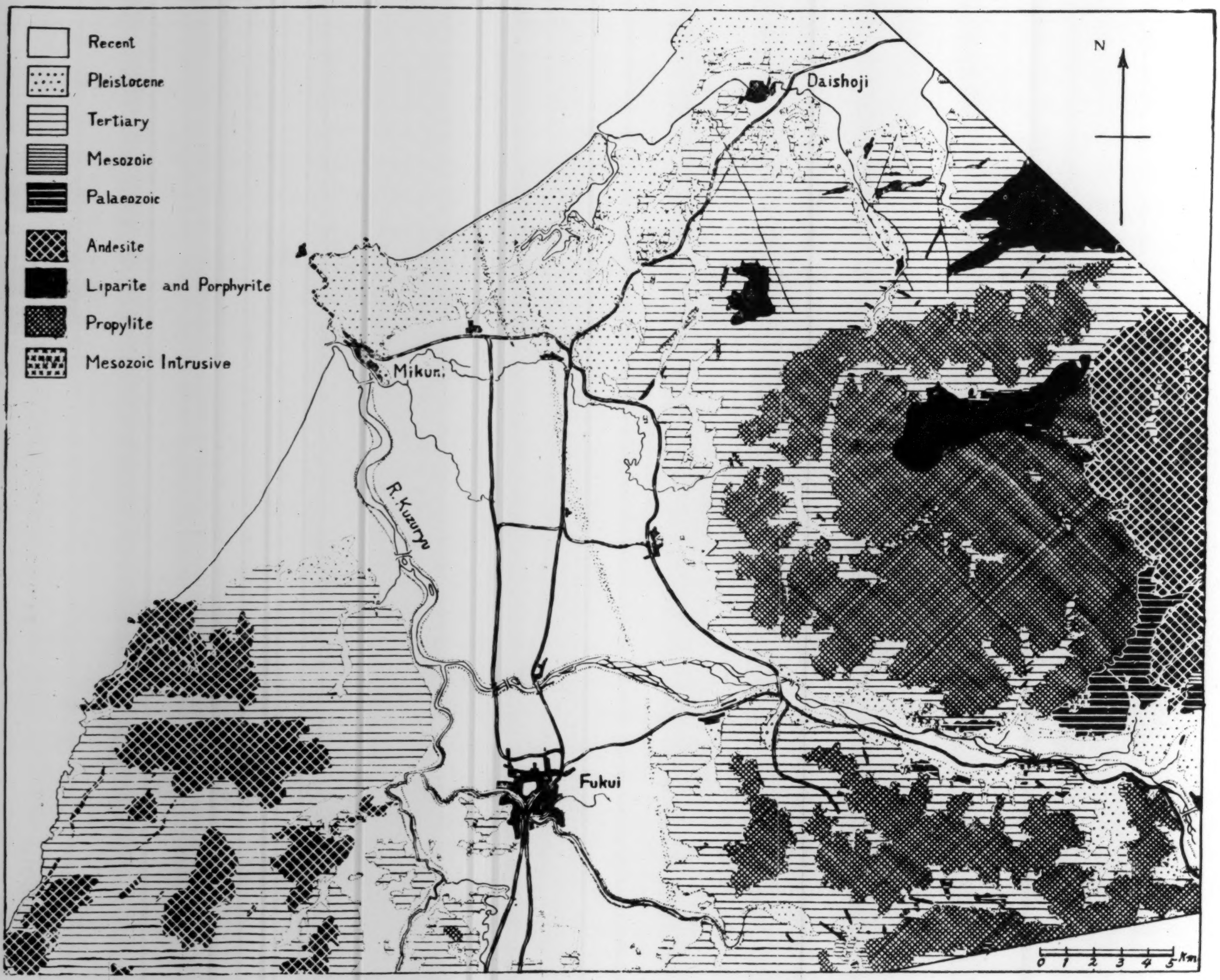

第 31 図　福井平野周辺地域の地質概略図.
図中福井平野を横ぎる NNW-SSE の線は，福井地震の際生じたひびわれの線.

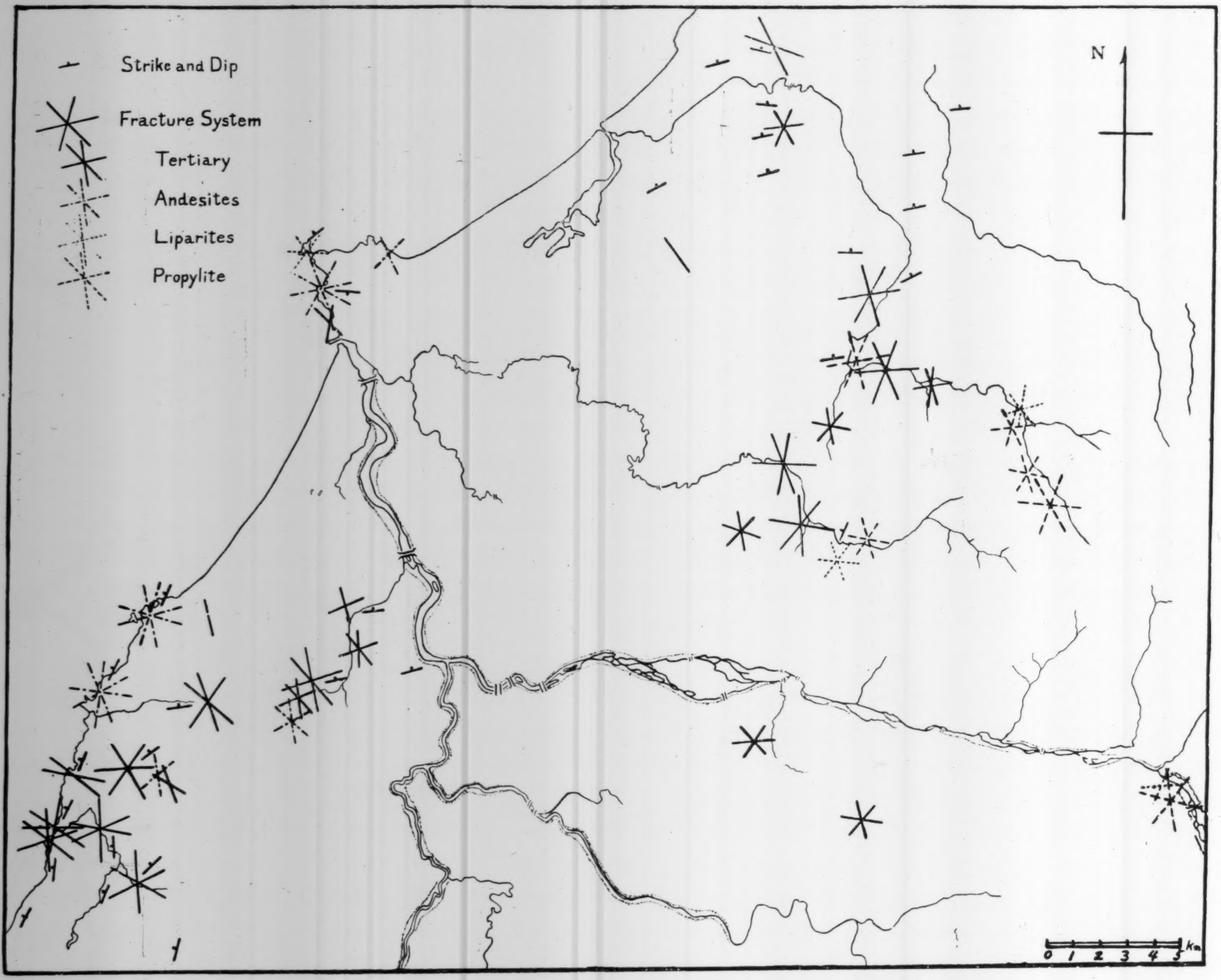

第 32 図　福井平野周辺地域の fracture system の分布図.

condition had disappeared. As regards the fracture system of the igneous rocks, however, matters may not be so simple. But the writer considers that the fracture system was formed under the same stress condition as in the case of the sedimentary formations. He regards even the columnar joints of the andesites as fractures formed during the cooling of the rocks under the influence of the tectonic movement.

5) The geologic structure of the Neogene formations and igneous rocks in the district may have an intimate connection with the "Tsuruga Bay—Ise Bay Fault Zone" in the southwest adjoining area. The Tsuruga Bay is bounded in the east with a typical fault shoreline running SSE from the Echizen Promontory, and at the south of the bay the "Yanagase Fault" in the Palaeogoic formations runs along the east shore of the Lake Biwa, extending SE to the east of Sekigahara. On the west side of this fault there lies the depression of the Lake Biwa, which seems to have been displaced southward along the fault line, as may be inferred from the sudden change of strike of the Palaeozoic formations from N—S to E—W. It is suggested that the fault zone was formed by that tectonic movement which caused folds, faults and fractures of the Neogene formations in the Fukui district at the close of the Tertiary period. The fault movement of the "Tsuruga Bay—Ise Bay Fault Zone" seems to have been active even after the Pleistocene epoch. In the Fukui district, there are several faults running parallel to this fault zone, and the "Fukui Fault" which appeared at the time of the Fukui Earthquake of 1948 may represent one of these faults.

10. 1953年7月26日の早雲山山津波の調査

地震研究所 {岸上冬彦
小坂丈予

(昭和28年11月24日発表—昭和29年12月28日受付)

1953年7月26日箱根早雲山において山津波が発生し，人員及び建造物に対して相当の損害をあたえた(第1図)．我々は7月29日，31日，8月5日及び11月11日に現地を調査する機会を得たので，その結果を報告する．

1. 当時の概要

相当長びいていた1953年の梅雨期が終つて数日後の8月24日，25日頃から小規模な地辷りが頻発して居た模様で，下流の強羅附近においても雷鳴の如きひびきが時々きかれていたが，26日午前10時20分頃突然大音響とともに早雲溪谷(須之沢)上流から大量の湿潤粘土及び岩石塊よりなる山津波が起つた．これ等の土石流は上流地域に設けられていた地辷防止用の砂防堤数箇を一挙に破壊して流れ下つたが，途中でその一部が分流して須之沢溪谷北岸の崖上にたてられていた寺院の本堂並びに附属建物を全半壊し，死者10名，負傷者16名を出したのを始め，強羅水道の浄水池，同送水管等の施設を破壊した．一方溪谷沿いに流下した土石流の本流は，更にその下流の道路約150mと，その中間にかけられた早雲橋とを埋没し，さらに流れ下つて宮城野村二ノ平部落近くまで達した．土石流の総延長約2km，最大幅約150m，流出岩石粘土流の容量は約700,000m³と推定された(第2図，第3図)．

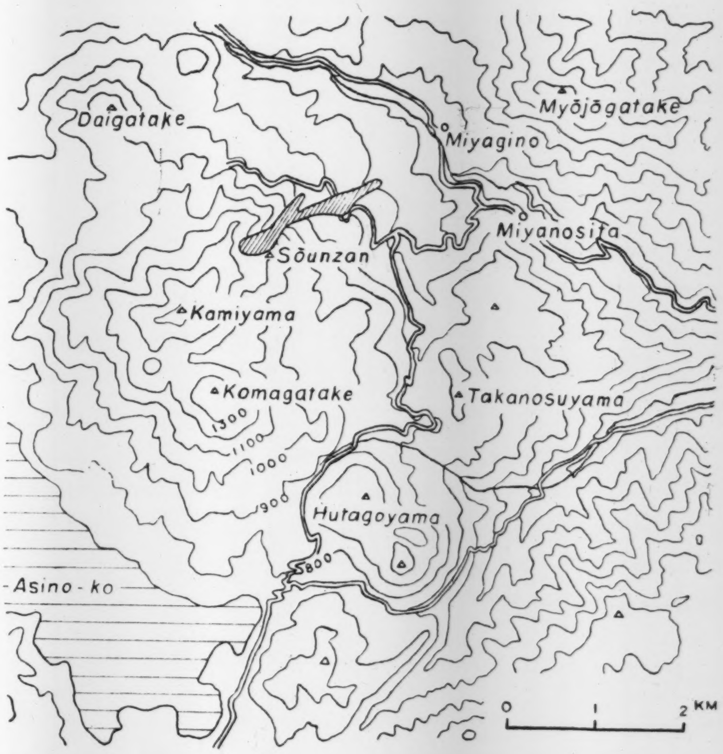

Fig. 1. Map of Sounzan and environ earth-flow.

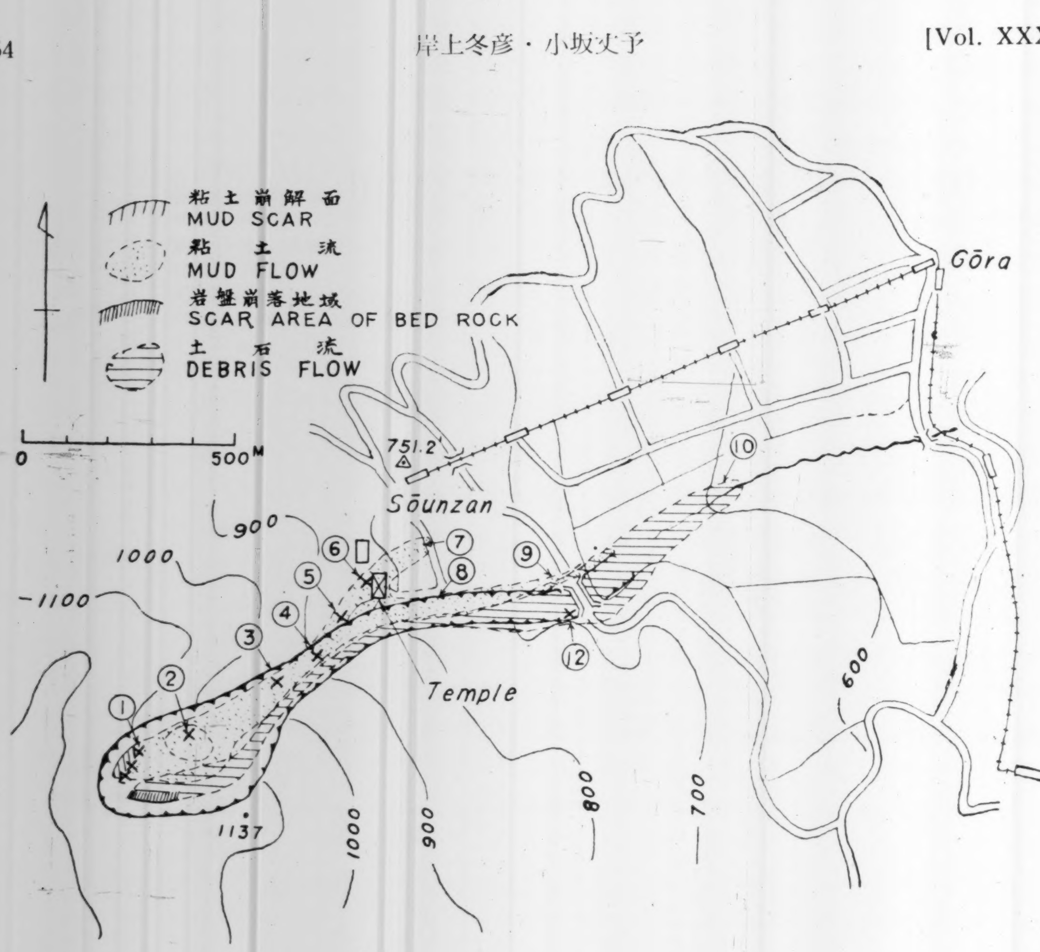

Fig. 2. Map of Sounzan earth-flow.

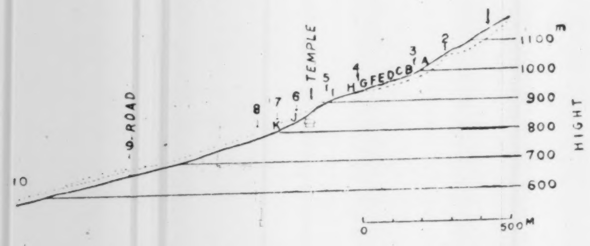

Fig. 3. The Profile of the earth-flow.

2. 被 災 地 域 の 地 形 変 化

今回の山津波は早雲山の最頂部に近い，東側斜面，須之沢と呼ばれている溪谷の最奥の標高約 1150 m の地点の絶壁における粘土塊及び岩盤の崩落にその端を発した様である．これらの結果は灰青色の火山性粘土よりなる粘土流と，安山岩の大塊を主体としてこれにわづかの赤褐色の泥土を混じた岩石流との 2 つの流れになつて，溪谷に沿つて東方に流下したのである．崩落起点は早雲地獄と称せられ，相当活発な噴気孔もあり，温泉も湧出している荒廢地帯で，崩落前にはかなりの量の火山性粘土の堆積があつたと考

えられる．その上この附近は山腹傾斜も甚だ大きく，約 40° にも達している所もある．発生したこれ等土石流は，この急斜面を約 700 m（高さにして約 300 m）流下し，寺院の上手の溪谷の狭隘な曲折部にぶつかつて溢出し，その溢出支流は，ちようどその真下にあつた寺院の建物の大部分を破壊し去つて，その約 200 m 下の道路上で停止した．末端の幅約 10 m，厚さ約 3 m であつた（第 2 図 ⑦，第 11 図）．

一方溪谷の狭隘部を通過した岩石粘土流の本流は次第にその幅を増し，溪谷をうづめて流れ下りその約 500 m 下流を横切る道路とコンクリート橋梁とを押流しこれを全く埋没してしまつた（第 2 図⑨）．その少し下流において土石流は最大の幅（約 140 m）を示している．

さらに流下した土石流は，次第に密になつて来た森林中で停止した．その末端の幅は約 20 m，厚さ 6〜8 m であつた（第 2 図⑩）．

事件発生 3 ケ月後の 11 月 11 日の調査の際はこれ等の様子が大分変化した（第 4 図）．即ち前回には溪谷上流地域に多量に堆積していた粘土流，岩石塊などがほとんど流

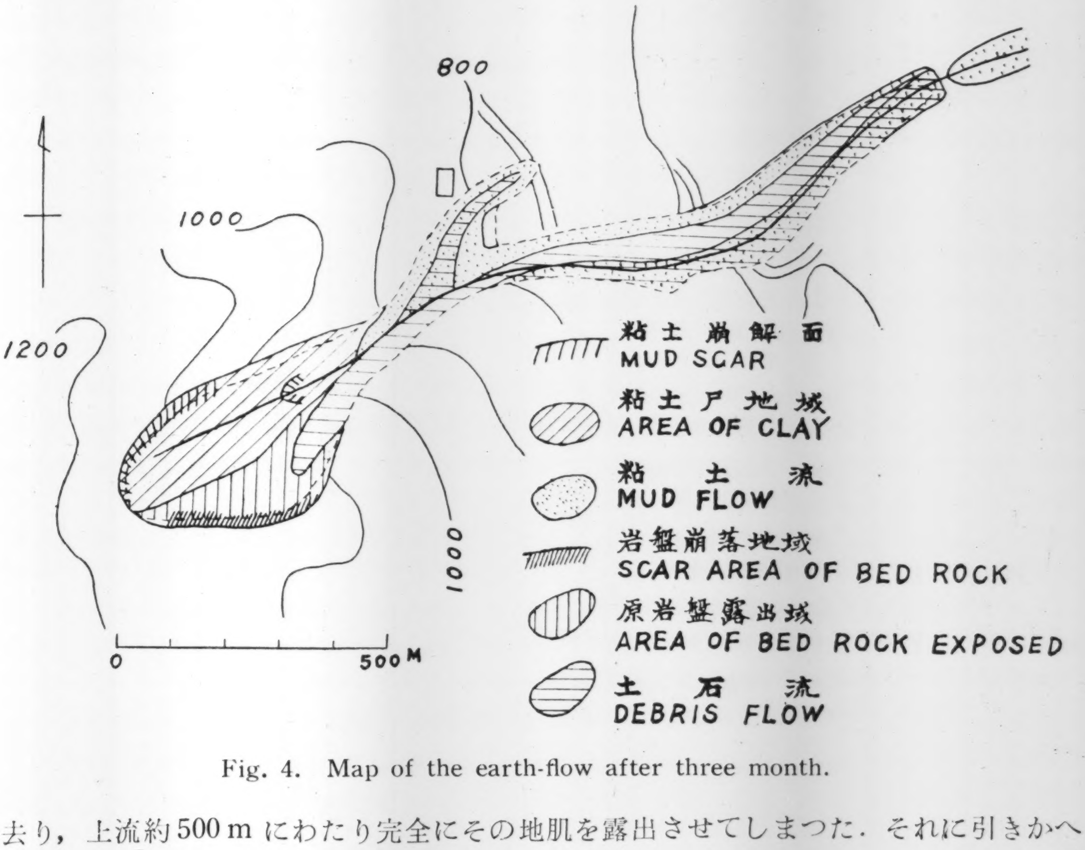

Fig. 4. Map of the earth-flow after three month.

れ去り，上流約 500 m にわたり完全にその地肌を露出させてしまつた．それに引きかへて下流の土石流は次第にその厚さを増し，末端附近において約 3〜4 m の増加を示している．又，粘土流の移動により，その青灰色粘土の大量が岩石塊を覆い，両者の区別をほとんどなくしてしまつた．地変当時土石流により分断されてしまつて，その流路も判然しなかつた溪谷沿いの水流も次第にまとまつて大きな流れとなり，土石流中を深く解析

して，新しい渓谷を形成しつつあつた．更に，この流水は，土石流末端部からその下流にむかつてさかんに粘土粒子を運び去り，この 2 次的の灰色の粘土流は 600 m 下流の早川にまで達していた．

7 月より 11 月に至る間のこのような変化は急激に行われたものではなく，最初の大山津波以後は，その後数次にわたりくりかえされた小規模な崩落，及びその間の雨水や流水による運搬により行われたもので，最初のような大規模な山津波はもはやくりかえされなかつた．

次に多少問題を含む個々の地点につき詳述する．

a. 崩落起源地点（須之沢最上流部）（第 2 図①，第 5 図）

早雲渓谷最上流部にあたり，早雲山山頂の直下にすり鉢状の絶壁でかこまれた噴気孔のある地区があり，東側だけが下り斜面になつている．この絶壁の北半部が青灰色粘土層の新しい削面を露出して居り，大量の粘土塊の崩落が想像された．この絶壁の下にはかつてその上部に繁茂していた樹木が根こそぎになつて，折り重なつて落下している．なおこの粘土崩落跡の絶壁中腹のわれ目からは，相当高温，酸性の温泉水が湧出している．（後述）

噴気孔は数個所あり，弱く水蒸気を噴出しているが，その噴気温度は最高 92°C であつた．

絶壁の南側正面には大量の岩石塊の落下が見られ，附近に散乱する巨大な岩塊の表面には崩落の激しさを物語る多数の擦痕を残していた（7 月 29 日）．

これら 2 つの崩落地点のそれぞれから明瞭に 2 つにわかれた北側の青灰色粘土流と，南側の茶褐色岩石流とが東方下流に向つて延びている．

当地点の傾斜は 7 月 29 日には約 40° であつた．

b. 途中のテーブル状台地（第 2 図②，第 6 図）

最上流起源から約 50 m 下つたところで，勾配のゆるやかなところを生じた．この部分に崩れた土砂を一時せきとめた形で，多量の粘土層の堆積が見られ，わづかに平坦な地形を作つていた．堆積している粘土は灰青色，灰緑色，白色など各種の色を呈し，かつ多量の水分がこれと混和して，泥ねい状となつていた．この泥沼のところどころに噴気孔があり，そのうちのあるものは噴気温度 85°C，微量の H_2S を検出した．

この堆積は 3 個月後には全く辷り落ちていた．

c. 渓谷中流の噴気孔（第 2 図③，第 7 図）

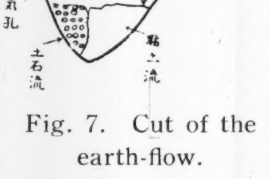

Fig. 7. Cut of the earth-flow.

前の地点より更に約 250 m 下流の，渓谷南側斜面の赤褐色岩石流の辺縁部に 2—3 箇所の相当強い噴気孔があり，盛んに水蒸気を噴出していた（7 月 29 日，31 日）．この噴気孔は 11 月調査の際は，その附近に堆積していた岩石流の下方移動によつて，気孔を覆つていた岩石塊が総て除去されて，完全に露出したためか，前にも増して強力な噴気音とともに水蒸気を放出していた（11 月 11 日）．又 7 月，8 月調査の際は，この附近ではその時の粘土流の表面より約 10 m 程高い両岸の面に粘土流のはつきりした通過あとが印されて居り，山津波当時の粘土流の厚さの如何に大きかつたかを推察することが出来た．なおこの附近でも依然として粘土流と岩石流との区別は明瞭であつたが，11 月にはそのいづれもが全く流し去られて，渓谷底の岩盤を露出していた．テーブル状台地からこの附近までの傾斜は大体 35° で，相当大きなものであつた．同地点の流

水は大分稀釈されてはいるが，なおやや温度が高く酸性であつた．(後述)

d. 急崖途中の地辷り現場 (第2図④)

それより約100m下流の寺院上手の溪谷北岸において，岩塊を含む粘土層からなる壁面が，その中腹に通じている小道を載せたまま，溪谷中に辷り落ちつつあるところを目撃することが出来た (第8図). 7月29日現在．しかしその2日後の7月31日には，その道路はすつかり崩落し去り，そこは全く通行が出来なくなつていた．この地点で採取した粘土からは後述するMontmorillonite の特に多量の含有を認めることが出来た．辷り面から湧出している水はいくらか酸性であつたが，温度は低かつた．

e. 寺院裏の急崖 (第2図⑤)

更に約100m下ると寺院裏の高い崖に達する．この附近は溪谷上流からほとんど真直ぐに下つて来た谷が曲折する部分であり，その上両岸の崖がせまつてこの溪谷中最も狭隘な地形を呈しているので，上流から直線的に急速度で流れ下つて来た粘土流，岩石流の両者がこの地点を通過するにあたつて，互にはげしくぶつかり合つて混和し谷に満ち，溢れた部分が20mある崖を乗り越して寺院を襲つたものと考えられる (第9図). それ故寺院を破壊した土石流は灰青色粘土流の中に巨大な岩石塊を多数含んでいた．

f. 寺院破壊現場 (第2図⑥)

寺院本堂はその屋根を残してほとんど原形をとどめないまでに破壊された．この附近の土石流の厚さは3～5mあつて，遭難者の発掘作業は困難していた．寺院北西にあつた水道浄水池は約半分埋没し，送水管が切断された (第10図).

g. 寺院裏崖下の土石流本流 (第2図⑧)

この附近の粘土は7月29日調査の時は未だ多分に湿潤して居り，青灰色を呈し，しかも相当高温であつたため，その表面から立ちあがる水蒸気によつて附近一帯が煙つて見透しが悪いほどであつた．それが7月31日にはすでに非常に乾燥して居つて，そのため粘土はほとんど白くなつてしまつていた．それ故津波発生当時の粘土流は8月5日採取測定した粘土の含水率よりもはるかに多いものであつて，その流動限界を充分越えていたであろうと想像される．

3. 地中温度

粘土流は，流下3日後の7月29日に至つても，広範囲にわたつて未だ相当高温であつた．またその後の粘土流の乾燥の速いことや，その温度の降下工合などから見て，事

第I表 粘土流内の地中温度
Ground temperature in mudflow.

(気温 22°C)　　July 29

測定場所	A	B	C	D	E	F	G	H	I	J	K
地中温度 °C	50	51	36	44	53	72*	53	64	49.5	58	24
崩落起点よりの距離 m	250	310	340	380	410	450	480	540	600	720	940

* 深さ約30cmで測定

件当日の粘土流の温度は更に一層高温であつたと考えられる．これは今回の地変の原因を考察する上からも，重要な一つの事柄と思う．測定の場所は現在の噴気孔や温泉から与えられる熱の影響をさけ，粘土流そのものの温度を計るため，これらの周辺を出来るだけよけて，上流より早雲橋附近までを約 50～100 m おきに測定した。結果を第 I 表にかかげる．測定点 A～K は第 3 図に示す．温度は粘土層内深さ約 15 cm で，値は同一点で得た最高値である．

粘土流内のところどころに，その表面が階段状になつているところがあるが，その地域の地中温度をこまかく測定したところ，その突出部は比較的低温であり，低くくぼんだ部分はこれにくらべて高い温度であつた．第 12 図に E，F 両地点間における測定の結果を示す。これは粘土流冷却のさい，突出部から放熱されたための現象ではないかと考えられる．

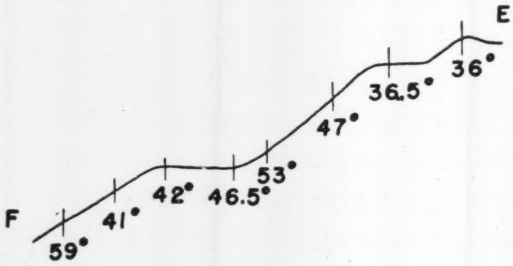

Fig. 12. Temperature observation under the surface of earth-flow.

4. 本地域の流水の pH 及び温度

当地区内における湧出水，流水を数ケ所で採取調査した結果，上流では相当高温酸性であつたが，土石流下方ではすでにほとんど稀釈されていた．測定し得た水温及び pH を次表に示す．

第 II 表 当地区内地気温度及び pH
Temperature and pH of surface water in the vicinity.

採　水　地	1	3	4	12
pH	2.4	3.4	6.1	5.6
水　温　C	52	30	9	11

5. 本地域に分布する粘土

今回の事件において，この地域一帯に分布する火山性粘土が山津波の原因の有力な一つとして挙げられる．現地において特に地ご，山津波の発生にあづかつたと思われる数ケ所の粘土を採取して帰り，2～3 の方法を用いて同定をこころみ，Montmorillonite の存在を確認した．その結果を簡単に記述する．

a. X 線粉末写真

得られた廻折線は微弱で，かつ背面のかぶり強く，甚だ不鮮明であつたが，これから読みとり得た値は次表の如きものであつた（第 III 表）．

第 III 表　青灰色粘土の X 線粉末写真
Xray powder photograph of bluish-gray clay.

d Å	I
16.2	6
4.38	10
4.02	8
2.50	4
1.49	5

d:　格子面間距離
I:　廻折線比強度

b.　示差熱分析

下図の如き示差熱分析曲線を得られた。500°C附近の発熱ピークは不純物として混入している硫化鉄のためと考えられる（第 13 図）.

c.　化学成分

採取粘土の原土の化学分析を行つた。その総化学成分は次の如くである（第 IV 表）.

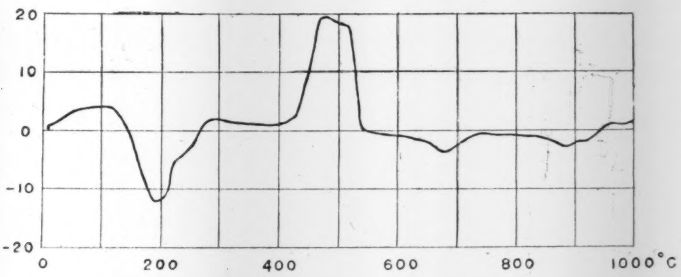

Fig. 13.　青灰色粘土の示差熱分析曲線
Differrential thermal curve of bluish-gray clay.

第 IV 表　青灰色粘土の総化学成分
Chemical composition of bluish-gray clay

成　分	SiO_2	Al_2O_3	Fe_2O_3	FeO	MgO	CaO	Na_2O	K_2O
量　重 %	46.65	18.32	7.79	n.d.	3.11	2.58	0.50	0.25

H_2O+	H_2O-	TiO_2	P_2O_5	MnO	Total
6.66	13.54	0.27	n.d.	0.05	99.72

6. あとがき

a.　山津波発生の地形的環境

当地域は火山噴気による荒廢地帯で，多量の火山性粘土と巨大な岩石塊が混在し，その上，山腹の傾斜も甚だ急であつて，もとより非常に不安定なところで，この地形的な条件が今回の山津波発生の大きな原因の一つに数えられる.

b.　直接の誘因

この年の異状に長くかつ大雨の多かつた梅雨も今回の地変の有力な原因の一つであろ

う．長雨によつて山津波発生点附近の安山岩の大塊を膠着して支えていた青灰色粘土が，多量の水を得て膨潤し滑り易くなつていたにちがいない．この様な山崩れや地辷りに，降水量の多かつたことは，しばしばその原因として挙げられている[1]．

又，現地は末期的ではあるが火山活動を継続している地域で，ことに崩落発生地附近では，温泉の湧出や，噴気孔もあり，また粘土流が広い範囲にわたつて高温であつたことなどは，今回の地変が普通の荒廢地山崩れにより発生した山津波とは趣をことにして居り，これらの火山活動が地変発生の原因と全く無関係であるとは考えにくい様に思われるのである．

しかし一部に伝えられた様な，鳴動をともなう微動が当時頻発しこれが今次崩解の一因となつたと言う説については，前年の 1952 年 11 月頃箱根附近一帯にこの様な現象があつたことが報告されているが[2]，今事件の前後にはその様な事実は確認されていない．

なお最近 1～2 年の間に，早雲山裏側の大涌谷一帯の噴気，温泉などの活動が一般に活発になつて来ていたことは事実である．

c 当地域に分布する粘土の鉱物組成

調査試験の結果，当地方に分布する粘土中には相当量の Montmorillonite を含有していることが解つた．Montmorillonite は粘土鉱物中でも特に膨潤度が高く，その存在は地辷発生の要因として甚だ有力である．従来までも我が国の大きな地辷地域の幾つかでこの Montmorillonite を主体とする粘土を産していることが知られている．

終りに本研究を実施するにあたつては援助された那須信治所長，森本良平助教授，國府谷盛明氏，並びに示差熱分析の装置の使用をゆるされた東京教育大学の須藤俊男教授に感謝申上げる。なお調査研究にあたつては，筆者等にそれぞれ交付せられた文部省科学研究費に負うところ大であつた．

---

10. Earth-flow on July 26, 1953, at Sōunzan, Hakone.

By Fuyuhiko KISHINOUYE and Jōyo OSSAKA,

Earthquake Research Institute.

The earth-flow of 1953 at Sōunzan was studied, and the results are summarized as follows:

1. The earth-flow reached about 2 km distant eastward from its source with a maximum width of nearly 140 m, and the total volume of flowed earth and stones was estimated at 700,000 m³.

1) 飯田汲事 地震研究所彙報 **16** (1938) 658.
R. P. Sharp and L. H. Nobles, "Mudflow of 1941 at Wrightwood, Southern California," *Bull. Geol. Soc. Amer.*, **64** (1953), 547–560.

2) 中央気象台地震課 横浜測候所発表の速報印刷物による．

Fig. 5. The Scarp of the earth-flow.

Fig. 6. Step-like deposition of the earth-flow photographed from the scarp.

(震研彙報 第三十三号 図版 岸上・小坂)

Fig. 8. Earth-flow in progression.

Fig. 9. The grey mud flow (right) and the debris flow (left).

Fig. 10. The collapsed temple (wooden building).

Fig. 11. The end of the flow below the temple.

2. Damage done was 4 buildings totally- or half-destructed (including a temple, 1 bridge and 1 service-water line), a road buried under the flow over a length 120 m and 26 persons killed and wounded.

3. The flow was originated by copious earth-fall at the head of Sōun Valley, and turned downstream into bluish-gray mudflow and reddish-brown debris flow.

4. The destruction of the temple was caused by mud and rocks flooded at the turning point of the valley.

5. Remarkable changes were found through further surveys carried out three months later. Most parts of the mudflow had been shoved far down by the river current of the valley.

6. As late as two days after the event, the flow mud to a great extent stayed at high temperatures.

7. Running water on the flow had a temperature as high as 52°C and an acidity of pH 2.4 soon after the event.

8. Existence of a considerable amount of montmorillonite in the flow mud was corroborated by X-ray, thermal and chemical analyses.

9. From topographical and geological points of view this locality seems to be subject to frequent land-slides.

10. The immediate cause of the earth-flow may be contributed to the abundant amount of the seasonal rainfall that year, as well as to volcanic phenomena, such as gas exhalation and gushing of hot springs.

11. 青森県天間林地域における磁気探鉱

地震研究所 横 山 泉

(昭和29年12月21日発表——昭和29年12月31日受理)

§1. ま え が き

昭和 29 年 3 月，青森県上北郡天間林（てんまばやし）地域において，砂鉄層を対象とした磁気探鉱を行つた．この地域は奥羽山脈の北端に位置する八甲田山塊の東側山麓であり，太平洋に面する平地からの立ち上りに相当する地域である（第 1 図）．このほぼ南北に走る山麓線を境として，西側山地は安山岩及び集塊岩からなり，東側は第三紀層の上を洪積層，冲積層が被つているようである．概して第三紀層は割合浅い沢に露出しているが，その傾斜は約 E 60° あるいは更に大きいことが認められていて，主として脆軟な砂岩，泥岩，砂鉄層からなつている．

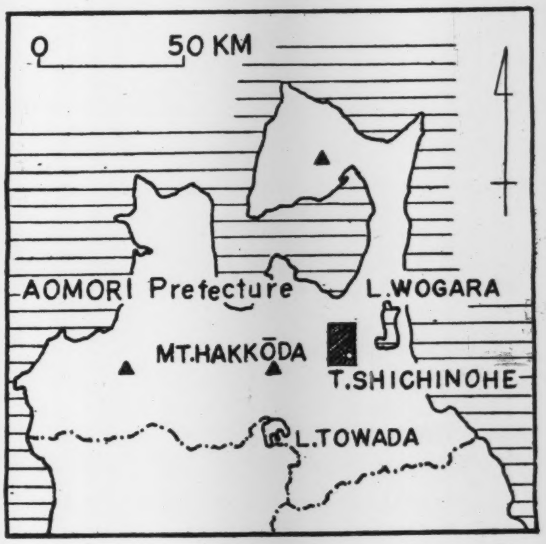

Fig. 1. Temmabayashi District.

この地域内南北約 10 km にわたる間に，点々として砂鉄層の露頭がほぼ一直線上に発見されている．現在，この地域の中央に位置する底田(そこた)地区（第 2 図）においては，地下 32 m 及び 45 m の坑内掘によつて砂鉄が稼行されているので，少くともこの部分に存する砂鉄層の状況は幾らか想像出来るわけである．

今回行なつた磁気探鉱の目的は，上記のほぼ南北の一直線上に点在する露頭をよりどころとして，砂鉄層の存在区域を確め，更に出来得ればその存在状況を量的に検討することであつた．勿論，そのためには現在迄に行われた地質調査等をもなるべく利用するように努めた．地下探査法としての磁気探鉱は鉄鉱床に対しては最も有力な方法と考えられているが，その測定成果の解析に際しては，その原理上それ相当の限界があり，又一般に幾多の仮定を採用せねばならぬ故，その結論には当然制限及び條件が伴うことを念頭におかねばならぬ．本報文において筆者は，従来から広く用いられている，地下磁化鉱体の適当な模型を設定して，実測結果と調和させようとする方法を避けて，なるべく実測結果から解析的に出発して手数を省くように試みた．但しその方法は特に新しいというものではなく，既知のものを応用したに過ぎない．

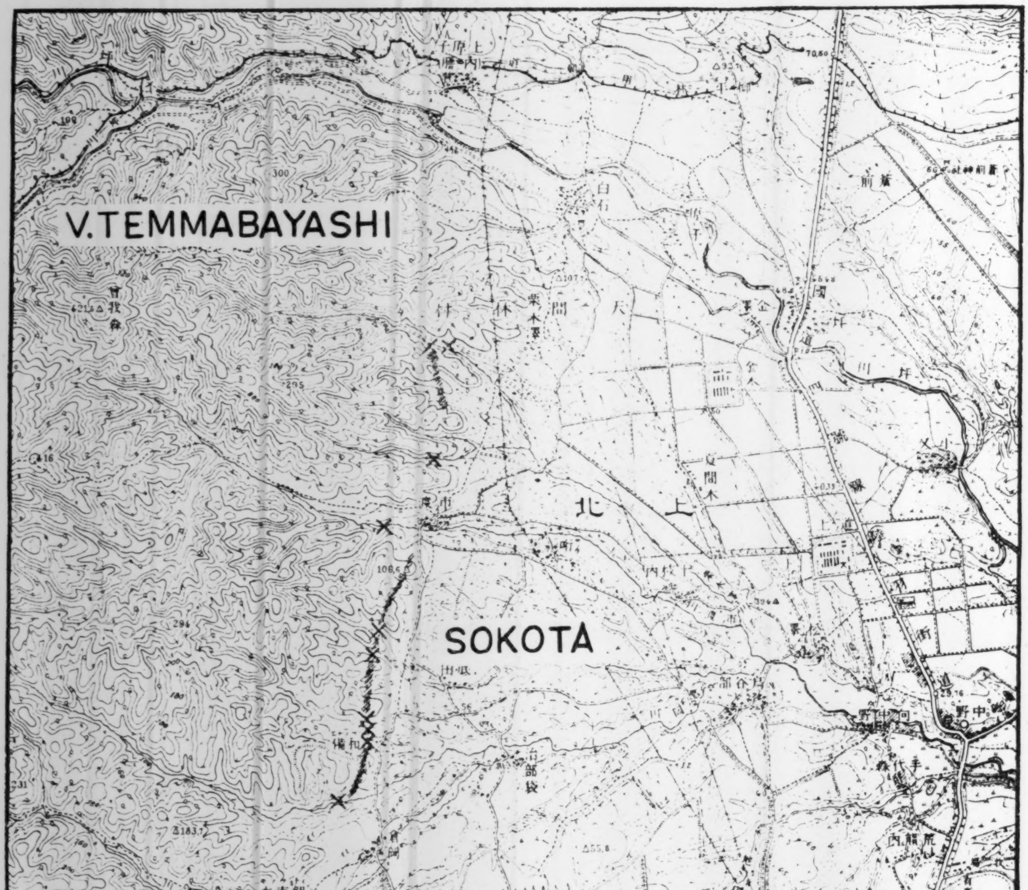

Fig. 2. Topographical map of Temmabayashi District.
× Out-crop of sand-iron
▨ Geomagnetically anomalous region

§2. 使用器械

磁気探鉱の全期間を通じて，底田にある基地に地磁気変化連続記録装置を設け，偏角及び鉛直分力の変化を観測し，磁気測量結果の補正に利用した．幸にして著しい擾乱には遭遇しなかつた．偏角変化計の感度は $0.55'$/mm，鉛直分力変化計 (Watson type) のそれは 2.68^{γ}/mm で，記録の送りは毎時 11 mm であつた．

既報[1]のように地磁気鉛直分力の短周期変化には著しい地域性があるので，これは現地において観測したが，水平分力は柿岡及び女満別の値を参考にした．

直接，磁気探鉱に用いた器械は次の三つである．

a)　小型磁気感応儀[2]　地磁気伏角の測定に用い，精度は $1'$ である（第 3a 図）．

b)　地理調査所型二等磁気儀[3]　偏角，伏角及び水平分力をそれぞれ $0.1'$, $0.1'$ 及び 1γ の精度で絶対測定をなし得る（第 3b 図）．

c)　地磁気鉛直傾度計　鉱体による異常磁場の鉛直傾度を測定するために，先年永田武教授[4]が試作したものを参考として，次のような要目のものを作り，今回の探鉱に用いた（第 3c 図）．

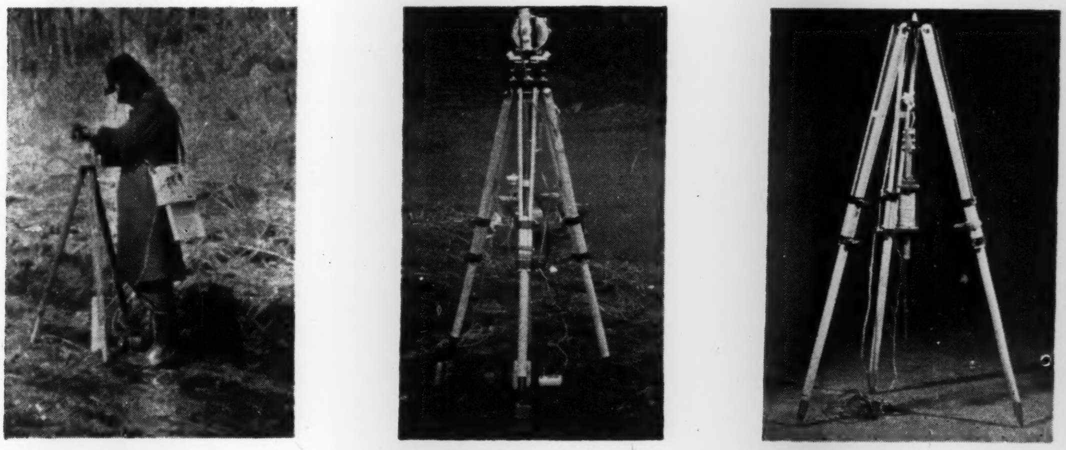

a　　　　b　　　　c

Fig. 3 Instruments used in the survey.

線輪　線輪の上下移動をなるべく短時間に，しかもその間における傾斜変化をなるべく少くするために，線輪の自重を大きくしてこれを安定に自然落下させる方式を用いた．高導磁率芯は直径 15 mm，長さ 330 mm のセンダスト棒で，見かけの導磁率は約 200 である．捲線は直径 0.27 mm のエナメル線を用い，総捲数 27000，全抵抗 1200 Ω で線輪長は 150 mm である．

1) T. RIKITAKE, I. YOKOYAMA and Y. HISHIYAMA, *Bull. Earthq. Res. Inst.*, **31** (1953), 89.
2) T. RIKITAKE, *Bull. Earthq. Res. Inst.*, **29** (1951), 147.
3) I. YOKOYAMA, *Bull. Earthq. Res. Inst.*, **31** (1953), 211.
4) 永田武・渡辺健　地質鉱床と物理探鉱　下巻 (1950), 106～118.

検流計　横河製函型 L-2 検流計で感度 3.7×10^{-8} Amp/mm，外部臨界制動抵抗 1200 Ω で周期は 2.8 sec である．

この装置によつて，高低両位置における磁束変化を弾動法によつて測定するのであるが，その感度は検流計の読みについて 40.5 γ/mm を得た（第 3c 図）．

探鉱に際しては先ず，小型地磁気感応儀を用いて伏角測量を全地域にわたつて行い磁気異常の存在を調べた．今の場合伏角の異常は近似的に鉛直分力の異常に換算出来るものである．次に代表的な鉱床と見做されている底田鉱山において，地理調型二等磁気儀を用いて地磁気三成分の精密測定を行い，伏角測量の成果を吟味する場合の参考にした．最後に，地磁気鉛直傾度計を用いて異常磁場の鉛直傾度を直接測定して鉱体の深さの決定に利用した．

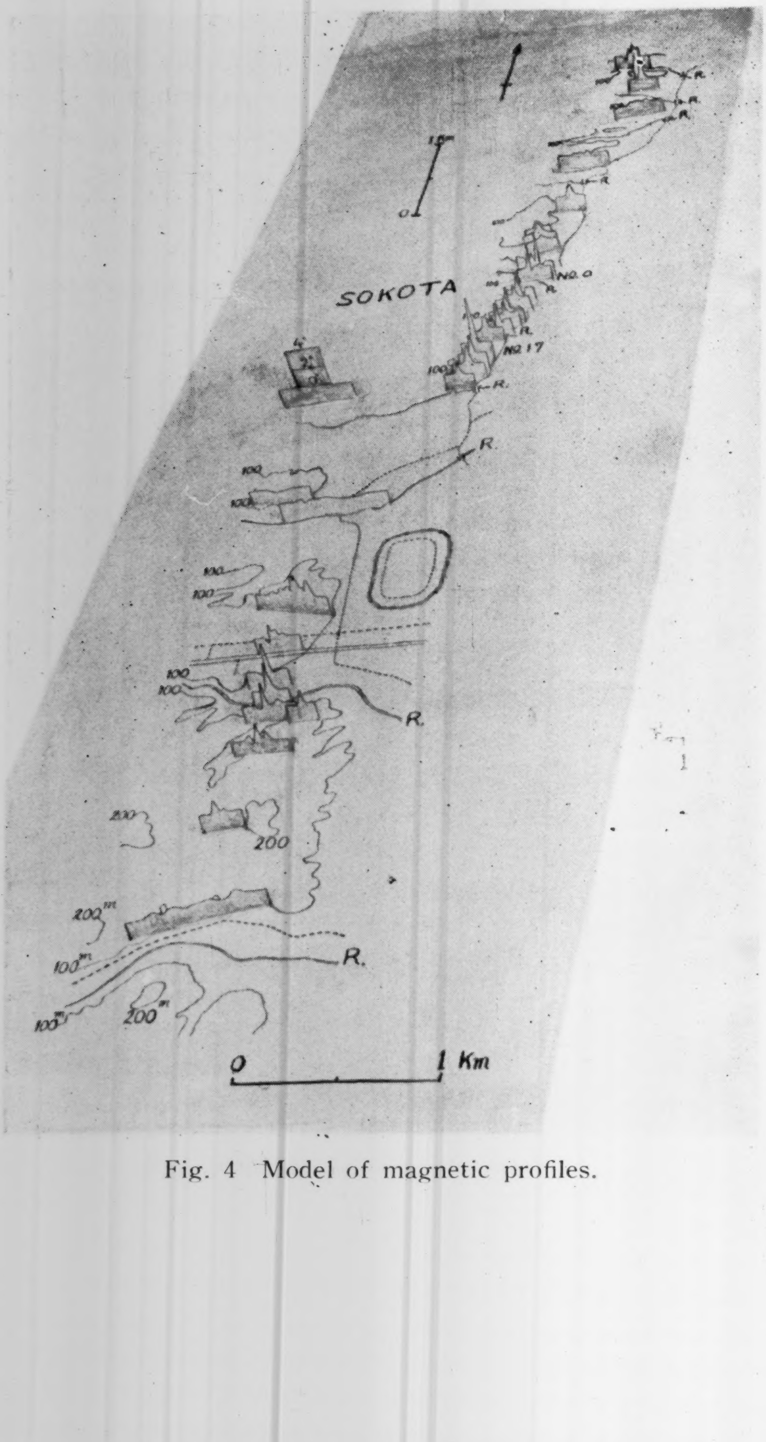

Fig. 4　Model of magnetic profiles.

§3. 全地域の伏角測定結果

露頭の走向がほぼ南北なる故，これを東西にきる測線を適当に設け，この測線に沿つて 2～10m 毎に，小型地磁気感応儀を用いて伏角の測定を行つた．測線の数は約 40 に達し，測定回数は 500 を越した．この結果を東西方向のプロファイルとして，この地域の略図上に表現したものが第 4 図である．1～5° に及ぶ著しい伏角異常が数 10 m の狭い帯状をなしてきれいに南北に断続している．そしてこの帯は必ずしも 1 本ではなく場所によつては数本から成るもののようである．この結果から判断して，磁気異常の存在する地区を示すと第 2 図のようである．露頭の見出されるその場所に磁気異常の存

在しないこともある．

前述のように，この地域においては伏角の異常 1′ が鉛直分力の異常約 15γ に対応するものである故，この伏角のプロファイルは近似的に鉛直分力のそれと見做し得るものである．

§4. 底田地区における地磁気三成分及び鉛直傾度の測定結果

底田地区において現在稼行されている鉱脈をほぼ東西に横切る測線番号 [0] について，二等磁気儀を用いて地磁気三成分の絶対測定を行つた．測線を平地になるべく長くとるために，その方向は約 N66°W とならざるを得なかつた（第 5 図参照）．測定結果はそれぞれ第 6 図及び第 7 図に示す．この結果よりすれば，この測線下の鉱体は [0] 点から約 10 mW の地下にあり，ほぼ南北に走り殆ど直角に立つている底の深い鉱脈の示す代表的磁気異常を伴つているようである．第 8 図は全磁力の異常及び東西の鉛直面内の異常ベクトルを示すものである．これから見ると，鉱体は僅かながら東へ傾いているようである．なおこの鉱脈から東へそれぞれ約 500 m（底田部落）及び 1000 m（鳥谷部）はなれた二点の地磁気成分を示すと第 I 表のようである．

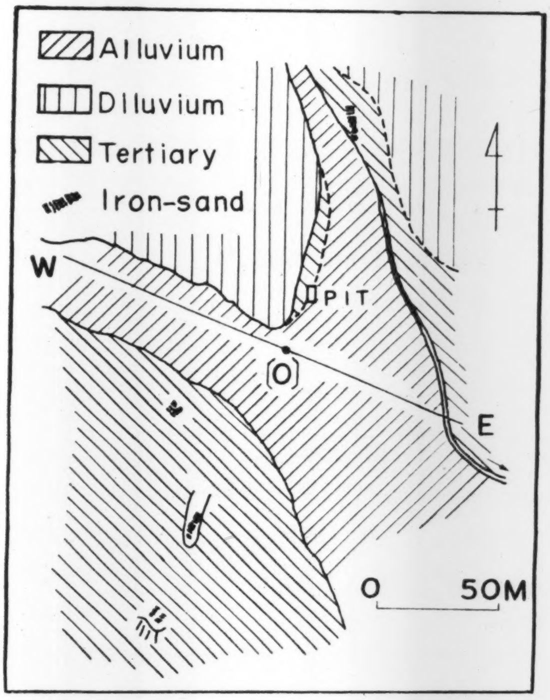

Fig. 5. Geological sketch-map of Sokota.
[0] denotes the survey-line No. [0].

鉛直傾度の測定結果を底田地区の測線 [0] 及び古和備地区の測線 [17] について示すと第 9 図の通りである．測点 [17] は

第 I 表

	500 m（底田部落）	1000 m（鳥谷部）
時刻 1954 年 3 月 30 日	14h 09m	10h 23m
伏　　角	54° 32.′4	54° 34.′2
水平分力	28388 γ	28197 γ
鉛直分力	39857 γ	39648 γ

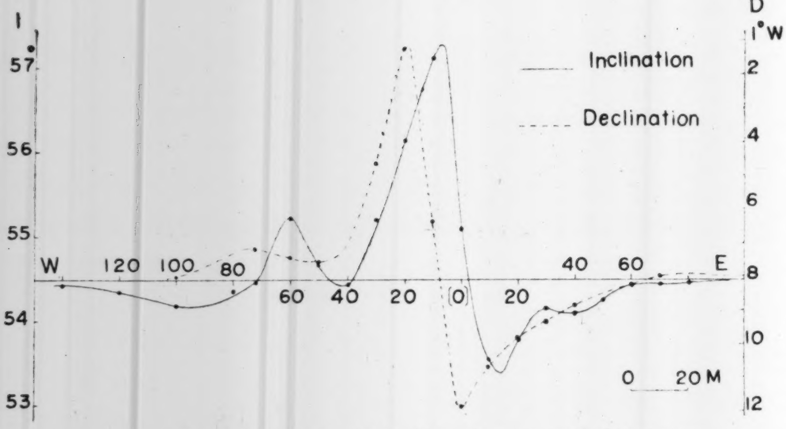

Fig. 6. Distributions of inclination and declination.

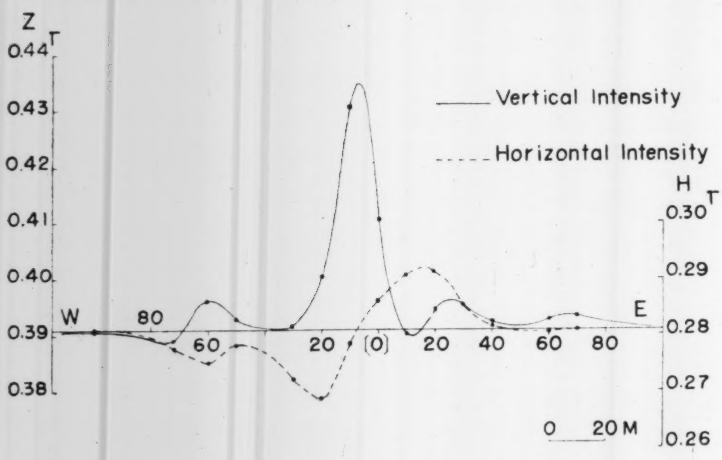

Fig. 7. Distributions of vertical and horizontal components.

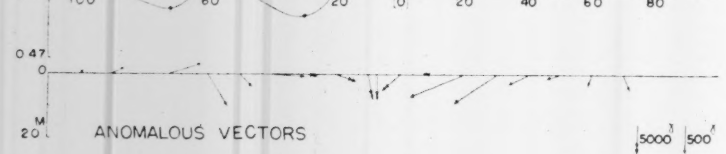

Fig. 8. Distributions of total intensity and anomalous vectors in vertical plane along the survey-line No. [0].

砂鉄層の露頭の直上であり，余りに大き過ぎて測定不可能であつた．磁気異常が最大と考えられる測点において，鉛直傾度と高さとの関係を調べると第 10 図に示す通りである．測線 [17] についてはその値が余りに大きいので，最高位置の一点しか求められなかつた．

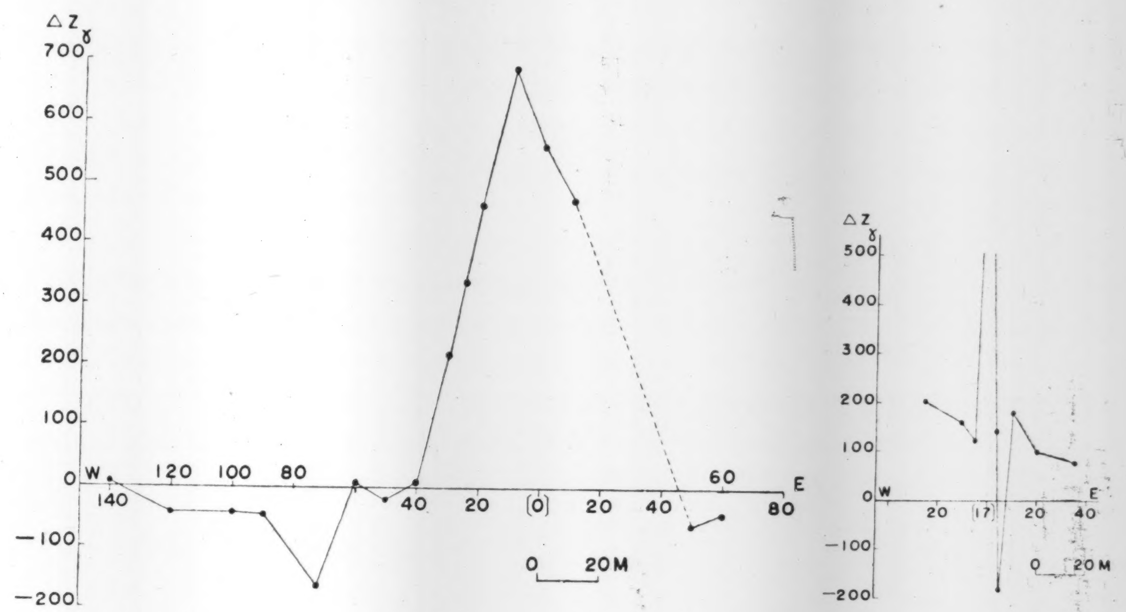

(a) $\Delta Z=\int_{0.15}^{0.95}\frac{dZ}{dz}dz$　　(b) $\Delta Z=\int_{0.15}^{0.95}\frac{dZ}{dz}dz$

Fig. 9

§5. 測定成果の解析

この地域では鉱脈がほぼ南北に連つていることが予想されたので，これを直角にきる多数のプロファイルを作つたわけであるが，果して前述のような成果が得られた．いま底田地区の測線 [0] について解析をすすめよう．

a) 地磁気分力を距離の冪級数に展開することにより，磁化鉱体までの深さの決定．磁化物質の存在は，地磁気分力 ΔX, ΔY, ΔZ, あるいは ΔF を距離 r の函数と見做した場合，その特異点に対応するという事実に基づくものである．いま磁気異常の最大なる地点を原点として，これから地表に r を測る．$\Delta F(r)$ を原点において r に関する冪級数に展開すると，

$$\Delta F(r)=\sum_{n=0}^{\infty}A_n r^n\,, \qquad \text{.............. (1)}$$

$$\text{但し}\quad A_n=(1/n!)\left(\frac{d^nF(r)}{dr^n}\right)_{r=0}. \qquad \text{.............. (2)}$$

函数論より，この級数の収斂域は

$$d=\lim_{n\to\infty}\left[\frac{1}{(|A_n|)^{1/n}}\right], \qquad \cdots\cdots\cdots\cdots\cdots (3)$$

すなわち半径 d なる収斂円周上に求める特異点が存在することになる.

第 8 図の ΔF を 10mW なる点を原点としてその両側に平均し，この曲線を $h=2$ m 毎に読取つて，展開係数を求める．このとき次の数値微分の公式を用いる.

$$\left.\begin{aligned}
hF'(0)&=\delta F(0)-(1/6)\delta^3F(0)+(1/30)\delta^5F(0)-(1/140)\delta^7F(0)+\cdots\cdots,\\
h^2F''(0)&=\delta^2F(0)-(1/12)\delta^4F(0)+(1/90)\delta^6F(0)-(1/560)\delta^8F(0)+\cdots\cdots,\\
h^3F'''(0)&=\delta^3F(0)-(1/4)\delta^5F(0)+(7/120)\delta^7F(0)+\cdots\cdots,\\
h^4F^{\mathrm{IV}}(0)&=\delta^4F(0)-(1/6)\delta^6F(0)+(7/240)\delta^8F(10)+\cdots\cdots,\\
h^5F^{\mathrm{V}}(0)&=\delta^5F(0)-(1/3)\delta^7F(0)+\cdots\cdots,\\
h^6F^{\mathrm{VI}}(0)&=\delta^6F(0)-(1/4)\delta^8F(0)+\cdots\cdots,\\
h^7F^{\mathrm{VII}}(0)&=\delta^7F(0)+\cdots\cdots,\\
h^8F^{\mathrm{VIII}}(0)&=\delta^8F(0)+\cdots\cdots.
\end{aligned}\right\} \quad (4)$$

いまの場合の展開係数は次のように求まる.

$n=0$	2	4	6	8
$d=0$	0.2	1.6	2.4	2.8

すなわち測定点から約 3 m——地表から約 2 m——の所に磁化鉱体の上端があるということになる.

b) 鉛直傾度の高さに対する分布から，磁化鉱体までの深さの決定.

磁化鉱体による異常磁場の傾度はそれからの距離が増加するに従つて急激に減少する．故に地下の鉱体の上端と地表測点との距離が鉱体の大さと同程度以上の範囲では，上端附近の磁化だけが大きく効き，下端の磁化は無視出来て，単磁極と見做して解析出来るわけである.

強さ m の単磁極の直上 D なる点における異常磁力は

$$(\Delta Z)_{x=0}=\frac{2m}{D^3}$$

なる故

$$\left(\frac{dZ}{dz}\right)_{x=0}=-\frac{6m}{D^4}. \qquad \cdots\cdots\cdots\cdots\cdots (5)$$

地表面から単磁極までの距離を d とすれば

$$D=d+h$$

第 10 図に示した実測結果から最少自乗法によつて d を求めると $d=3.8$ m を得る.

c) 磁気異常が単磁層によると考えた場合のその強さの分布の決定.

前述の結果から考えて，測線 [0] の最大の磁気異常は 10 mW の地点，地表下約 2～3 m の深さから下に存在する底の深い鉱体によるものである．次にこの測線上の他の小

さな磁気異常を考察するために，これらも地表面に平行な一水平面上の単磁層によるものと仮定してその強さの分布を調べる．

プロファイルの方向を x 軸にとると，磁気異常ポテンシャルは

$$\Delta W=\sum e^{nz}(A_n\cos nx+B_n\sin nx), \qquad \cdots\cdots\cdots\cdots\cdots (6)$$

これより，$z=0$ においては

$$\Delta Z=\sum n(A_n\cos nx+B_n\sin nx), \qquad \cdots\cdots\cdots\cdots\cdots (7)$$

観測された ΔZ をフーリエ分析して

$$\Delta Z=\sum(\alpha_n\cos nx+\beta_n\sin nx), \qquad \cdots\cdots\cdots\cdots\cdots (8)$$

上の両式から係数 A_n 及び B_n が決定され，単層の強さは次の式で与えられる．

$$\sigma=(1/2\pi)e^{nz}(A_n\cos nx+B_n\sin nx). \qquad \cdots\cdots\cdots\cdots\cdots (9)$$

いま地表下 2 m 及び 10 m に単磁層を考えると，その強さの分布はそれぞれ第 11 図に示すようになる．元の観測の分布密度を越える議論は出来ないが，30 mE 及び 60 mW の両地点附近においても，幾分深いところに鉱体の存在を認めるようである．厳密にいえば今迄の解析をプロファイルの山のそれぞれについて行うべきである．

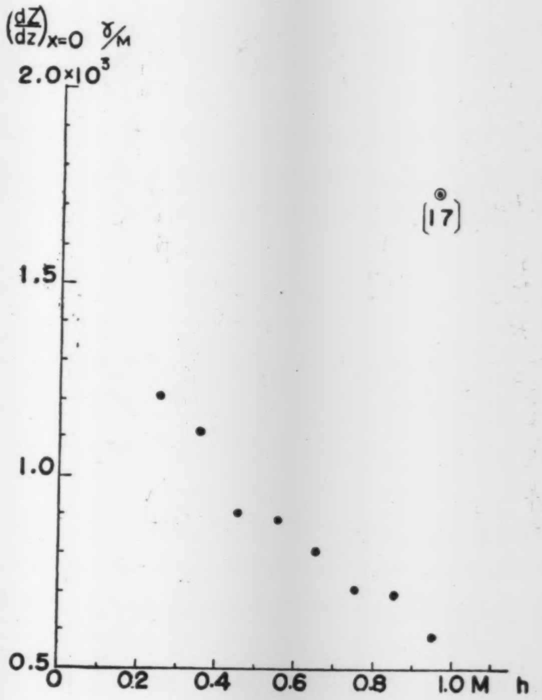

Fig. 10. Observed values of $\left(\frac{dZ}{dz}\right)_{x=0}$ at various heights.

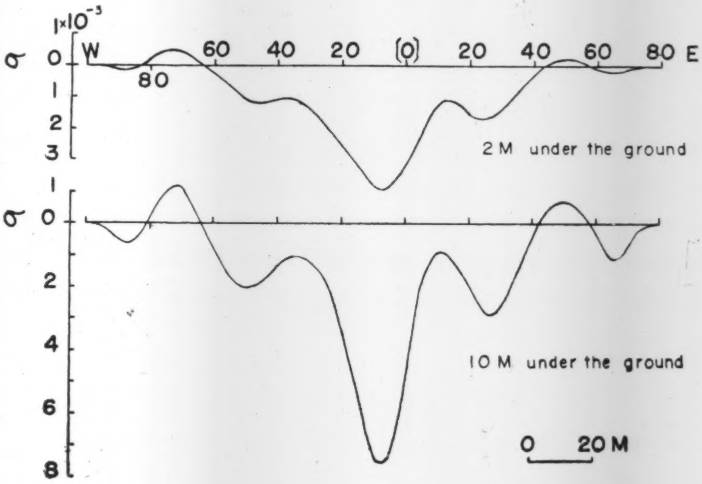

Fig, 11. Distribution of strength of single layer.

d） 地表近くに存在すると推定される鉱体の量の概略的推算

今回の磁気探鉱だけでは鉱脈の深い底を決定することは原理的に不可能と考えられる．然し地下の坑道内での測定というような資料が得られれば，議論は更に進む可能性もあるわけである．ここでは，前述の解析結果を利用して，地表近くに存在する分だけの鉱体の量を概算しよう．

底田地区の砂鉄についての分析結果は第II表に示す通りである．その磁気的性質に関しては，良品質の試料1箇について東京大学理学部地球物理学教室永田研究室の測定した結果によれば，帯磁率は $\chi=3.74\times10^{-2}$ emu/gr であり，$Q=J_n/\chi F$（J_n は自然残留磁気の強さ，F は全磁力）の値は約 0.1 である．すなわちこの砂鉄の帯磁の大部分は現在の地球磁場により誘導されたものである．

第 II 表

試料分析表（%）

T.Fe	FeO	Fe_2O_3	SiO_2	TiO_2	P	S	Cu	V	Co
56.03	28.90	47.99	3.75	13.70	0.040	0.020	0.019	0.26	0.02

（東北電化株式会社八戸工場分析）

この地区の磁気異常の殆どが誘導によるものであるとすると，その鉱体の形の影響を考えねばならぬ．然るに形は勿論，その深さも未知で，ただ鉱体の上端が 2～3 m の深さにあることを確めただけである．そこで測点の直下に球状の鉱体を仮定して，観測された磁気異常が磁気誘導によつて生ずるには，その半径が幾何であればよいかを検討する．この際，帯磁率の値としては上記のものを用いる．

$$\Delta Z=2\frac{\frac{4}{3}\pi R^3\kappa}{1+\frac{4}{3}\pi\kappa}\frac{Z_0}{d^3}, \qquad \cdots\cdots\cdots\cdots\cdots (10)$$

$$\begin{cases}\Delta Z=0.04,\ Z_0=0.48,\ \rho=2.7,\\ \kappa=1.01\times10^{-1}\ \text{emu/cc}\\ d=300+R\end{cases}$$

これより $R=3.5$ m すなわち質量にして 500 t を得る．

底田地区においては，この程度の磁気異常が南北に殆ど 200 m 続いていると考えられるので，概算して約 1.5 万 t となる．これは勿論，地表近くに存在すると推定される鉱体の量を非常に粗な仮定の下に概算したものであるが，同地区に関して地質調査所の宮本弘道，丸山修司両氏[5)]は地質調査から 5.2万 t の鉱量を推定している．

5） 宮本弘道・丸山修司 東北のチタン砂鉄資源（1953），78.

§6. 結　語

地下探査の一つの方法としての物理探査，そしてその中の一部門である磁気探査を行つただけであり，これだけで独立してその目的を達することは不可能であるが，一応測定成果を種々解析した．

なお，現地調査の後に，本地域の一部に関しては，既に昭和19年地質調査所早川正巳氏[6]により磁気探鉱が行われたことを知つたが，勿論，測定成果は両者殆ど合致していることを附記する．

最後に種々御指導を賜つた永田武教授，力武常次博士に深甚なる謝意を表すものである．又測定に終始協力して戴いた堀尾舟三君並びに絶大なる便宜を供与された東北電化工業株式会社佐々川清博士に深く感謝する次第である．

---

11. Magnetic Survey in Temmabayashi District, Aomori Prefecture.

By Izumi YOKOYAMA,

Earthquake Research Institute.

For the purpose of exploration of iron-sand body in Temmabayashi District on the foot of Mt. Hakkōda, magnetic surveys were carried out in 1954. Several outcrops of iron-sand had been discovered along a straight line running almost northward through this district and there is a vertical pit 45 *meters* depth under the ground for mining at Sokota (Fig. 2).

In order to verify the distribution of magnetized bodies, about 40 magnetic profiles running almost EW-direction were obtained by a miniature earth-inductor by which we can measure dip-angle with an accuracy of 1 *minute* of arc (Fig. 4).

To study the geomagnetic anomalies in detail, absolute measurements of three geomagnetic components with high accuracies—0.1 *minute* of arc and 1 γ—were made by the 2nd Order G.S.I. Type Magnetometer at Sokota. The results are shown as profiles in Figs. 6, 7 and 8. In addition to those measurements, vertical gradients of geomagnetic vertical components were observed along the survey-lines Nos. [0] and [17] (Fig. 9).

The analyses of the results obtained at Sokota were made as follows:

a) Determination of the depth from the earth's surface to the magnetized body by expanding the distribution of a particular geomagnetic component in power-series of distance.

b) Determination of the depth from the earth's surface to the magnetized body by using the observed values $\left(\frac{dZ}{dz}\right)_{x=0}$ at various heights under the assumption of the single pole (Fig. 10).

c) Estimation of the strength of the single layer which is assumed to be responsible for the anomaly from potential-theory using the observed $\varDelta Z$-distribution (Fig. 11).

d) Rough estimation of the extent of the magnetized body.

---

6) 早川正巳　地質調査所月報　**2**　(1952), 120～122.

昭和30年6月20日印刷
昭和30年6月25日發行

東京都文京區本富士町一番地
東京大學構內
編纂兼發行者 東京大學地震研究所

東京都千代田區富士見町一丁目十番地
印刷者 笠井康頼

東京都千代田區富士見町一丁目十番地
印刷所 株式會社 國際文献印刷社

賣捌所 東京都千代田區神田一ツ橋通
岩波書店

東京都中央區日本橋通二丁目六番地
丸善株式會社

Sold by
Iwanami Shoten,
Hitotsubashi dôri, Chiyoda-ku, Tôkyô,
and
Maruzen Co., Ltd.,
Nihonbashi dôri, Chûô-ku, Tôkyô.
Price of this copy: 728 Yen. (Postage exclusive.)

BULLETIN OF

THE EARTHQUAKE RESEARCH INSTITUTE

TOKYO UNIVERSITY

Vol. XXXIII, Part 1. March, 1955.

30TH ANNIVERSARY VOLUME

Contents.

Papers and Reports.

Page

1. T. RIKITAKE, Magneto-hydrodynamic Oscillations in the Earth's Core. (in English) 1
2. S. YAMAGUTI, On the Changes in the Heights of Mean Sea-levels, before and after the Great Earthquakes. (in English) 27
3. Y. SATÔ, Analysis of Dispersed Surface Waves by means of Fourier Transform I. (in English) 33
4. T. SANTÔ AKIMA, Comparative Studies of Surface Waves Travelling Across Tibet Plateau and Sea of Japan, with Some Notes on the Method of Finding the Velocities of Surface Waves for a Limited Portion of their Path. (in English) 49
5. D. SHIMOZURU and I. MURAI, Elasticity of Marble with Special Reference to its Elastic Aeolotropy. (in English) 65
6. D. SHIMOZURU, A Note on the Elasticity of Marble. (in English) 73
7. H. TSUYA, R. MORIMOTO and J. OSSAKA, The 1950–1951 Eruptions of Mt. Mihara, Oshima Volcano, Seven Izu Islands, Japan. Part II. The 1951 eruption. B. Activity of the third period. (in English) 79
8. K. KANAI and T. SUZUKI, Relation between the Property of Building Vibration and the Nature of Ground. (Observation of Earthquake Motion at Actual Buildings.) II. (in English) 109
9. I. MURAI, Tectonic Analysis of the District Surrounding Fukui Plain. (in Japanese) 121
10. F. KISHINOUYE and J. OSSAKA, Earth-flow on July 26, 1953, at Sōunzan, Hakone. (in Japanese) 153
11. I. YOKOYAMA, Magnetic Survey in Temmabayashi District, Aomori Prefecture. (in Japanese) 163

(For the papers written in Japanese or in occidental languages, the abstracts are given in occidental languages or in Japanese respectively.)

BULLETIN OF THE EARTHQUAKE RESEARCH INSTITUTE,
TOKYO UNIVERSITY. Vol. XXXIII, Part 2. June, 1955.

東京大學
地震研究所彙報

第33號　第2册
昭和30年6月

創立30周年記念号

目　次

論文及報告

			頁
12.	一様磁場内の導電流体球の電磁流体振動（英文）	力武常次	175
13.	震源決定の精度について（第2報）（英文）	浅野周三	199
14.	衝撃による地動に対する人体感覚（英文）	岸上冬彦	207
15.	震度と震央距離との関係（2）（英文）	佐藤泰夫	211
16.	明神礁の昭和27—28年の噴火（1）（英文）	森本良平 小坂丈予	221
17.	三原山の地球磁気学的研究　第6報（1951～1954年間の偏角変化の連続観測）（英文）	横山泉	251

所　報

(The titles in occidental languages are given on the back cover.)

本彙報ハ年4回 (但シ第1號ヨリ第6號マデハ不定期ニ，第7號ハ3冊トシテ發行セリ)，彙報別冊ハ不定期ニ發行ス.

本彙報掲載ノ論文及ビ報告ノ內容ニ關シテハ著者ノミニ共責任アルモノトス.

本彙報ニ關スル照會通信ハ東京大學地震研究所長ヘ宛テラレタシ.

The Bulletin is published quarterly. (Vols. I–VI were published at irregular intervals and Vol. VII consisted of three parts.)
Supplementary Volume is published at irregular interval.

The authors of the papers alone are responsible for the statements and opinions contained in their respective papers.

All communications relating to this Bulletin should be addressed to the Director of the Earthquake Research Institute, Tokyo University.

12. *Magneto-hydrodynamic Oscillations of a Conducting Fluid Sphere in a Uniform Magnetic Field.*

By Tsuneji RIKITAKE,

Earthquake Research Institute.

(Read March 22, 1955.—Received March 30, 1955.)

Summary

In order to examine the couplings between poloidal or toroidal magnetic fields of different type, magneto-hydrodynamic oscillations of a fluid sphere under the influence of a uniform magnetic field are studied. A set of simultaneous differential equations for the oscillation is obtained in a general form which contains harmonic constituents of successive degrees. Although the writer can not solve the equation rigorously, some features of the coupling are qualitatively examined. A simple normal mode of the free oscillation is also studied by taking into account only the S_1^0 and S_3^0 type magnetic fields.

1. Introduction

The writer[1] has studied magneto-hydrodynamic oscillations in the earth's core. It seems likely that the possible magneto-hydrodynamic oscillations play an important role for the explanation of the secular geomagnetic variations. In the previous study, only the S_1^0-type magnetic field was examined ignoring the mutual dependence of various harmonic constituents. In order to study the problem in more detail, however, we have to refine the theory by taking into account the mutual dependence because the interaction between certain fluid motions and magnetic fields would cause many types of electric currents which in turn give rise to many other types of magnetic field. Therefore we have to study oscillations of every harmonic constituent which is coupling with each other.

This sort of oscillations has also been a topic in astrophysics. M. Schwarzschild[2] discussed, in an approximate way, the magneto-hydrodynamic oscillation of a highly conducting star in a uniform magnetic field. His study was the first approach to the possible magneto-

1) T. RIKITAKE, *Bull. Earthq. Res., Inst.*, **33** (1955), 1.
2) M. SCHWARZSCHILD, *Ann. d'Astrophys.*, **12** (1949), 148.

hydrodynamic oscillations in a celestial body. Though interesting, he did not study the behaviour of a particular harmonic constituent. Accordingly, his result can not be applied to the examination of the mutual coupling of each harmonic constituent which is the main object of the present paper. V. C. A. Ferraro[3] and his colleagues also studied the oscillation of a magnetic star in which the steady magnetic field is considered as due to a magnetic pole at the centre. In that case, there was no coupling between harmonic constituents. The oscillations of this kind seem to be related with the reversal of magnetic field of magnetic variable stars though, as was pointed out by T. G. Cowling[4], no satisfactory explanation between the observed reversal and oscillations has been made yet.

The writer is going to study magneto-hydrodynamic oscillations of a liquid sphere in a uniform magnetic field as was studied by Schwarzschild. But the boundary conditions are different from those in his study because the writer would like to apply the result to the earth's core. As may be seen in the writer's previous paper[1], we may presume that the steady magnetic field would be of the S_1^0, T_2^0, T_2^{2c} and T_2^{2s} type provided we adopt the simple dynamo which would maintain the earth's permanent magnetic field. However, it is not easy to take into account all of these magnetic fields because of mathematical complexity. So we may here take into account only the S_1^0-type steady field for the purpose of examining the mutual coupling of various harmonics. The steady fluid motions are also assumed to be non-existing in the present model. Thus the problem becomes identical to the magneto-hydrodynamic oscillations of a spherical liquid body under the influence of an external uniform magnetic field. It is the purpose of this paper to study the mutual coupling of each oscillation in terms of poloidal and toroidal fields.

Starting from the fundamental equations for electromagnetism and fluid motion, the writer obtains a differential equation for the pressure, the velocity of the fluid motion being obtained from the solutions of this equation. The magnetic field produced by the interaction between the motion and the permanent magnetic field is also calculated. If we take a typical type of the magnetic field, poloidal or toroidal, we can construct an equation for the radial part of the magnetic field. The

3) V. C. A. FERRARO and D. J. MEMORY, *M.N.R.A.S.*, **112** (1952), 361. C. PLUMPTON and V. C. A. FERRARO, *M.N.R.A.S.*, **113** (1953), 647.
4) T. G. COWLING, *M.N.R.A.S.*, **112** (1952), 527.

general form of the equation suggests that the coupling occurs between five constituents of successive degrees. It is also shown that we have the coupling between fields of poloidal and toroidal types in general cases.

A more detailed study is made for magnetic fields of zonal distribution. In that case, there is no coupling between poloidal and toroidal fields. It is also shown that there is no coupling between constituents of odd degree and those of even degree. Although the writer can not solve the coupling equation quite rigorously, a normal mode of the oscillation is approximately obtained by taking into account only the S_1^0 and S_3^0 type magnetic fields.

2. Fundamental equations

As we assume that there are no fluid motion and no electric current at the equilibrium state, the fundamental equations can be written as

$$\vec{i}=\sigma(\vec{e}+\vec{v}\wedge\vec{H}_0) \ , \tag{1}$$

$$\mathrm{curl}\,\vec{e}=-\partial\vec{h}/\partial t \ , \tag{2}$$

$$\mathrm{curl}\,\vec{h}=4\pi\vec{i} \ , \tag{3}$$

$$\rho\partial\vec{v}/\partial t=\vec{i}\wedge\vec{H}_0-\mathrm{grad}\,p \ , \tag{4}$$

where $\vec{i}$, $\vec{e}$, $\vec{h}$, $\vec{H}_0$, σ, ρ, p and $\vec{v}$ denote respectively the electric current density, electric field, magnetic field, steady magnetic field applied from outside, electrical conductivity, density, pressure and velocity. It is also assumed (1) that the magnetic permeability is unity, (2) that there is no non-electromagnetic force that depends on time and (3) that the inertia term of fluid motion can be neglected. The fluid is also assumed to be incompressible, so that we have the following relation ;

$$\mathrm{div}\,\vec{v}=0 \ . \tag{5}$$

By taking curl of (1) and eliminating $\vec{e}$ with the aid of (2), we obtain

$$\mathrm{curl}\,\vec{i}=\sigma\{-D\vec{h}+\mathrm{curl}(\vec{v}\wedge\vec{H}_0)\} \tag{6}$$

where we write D in place of $\partial/\partial t$. On the other hand we have from (3)

$$4\pi\,\mathrm{curl}\,\vec{i}=\mathrm{curl}\,\mathrm{curl}\,\vec{h}=-\nabla^2\vec{h} \ . \tag{7}$$

From (6) and (7), we obtain

$$\{D-(4\pi\sigma)^{-1}\nabla^2\}\vec{h}=\text{curl}(\vec{v}\wedge\vec{H}_0)\ . \tag{8}$$

We also have from (4)

$$\rho D\vec{v}=(4\pi)^{-1}(\text{curl}\,\vec{h}\wedge\vec{H}_0)-\text{grad}\,p\ . \tag{9}$$

If we make div of (9), we obtain

$$\nabla^2 p=-(4\pi)^{-1}(\text{curl}\,\vec{h}\,\text{curl}\,\vec{H}_0-\vec{H}_0\,\text{curl}\,\text{curl}\,\vec{h})\ .$$

As $\vec{H}_0$ is applied from outside, we have the relation

$$\text{curl}\,\vec{H}_0=0\ . \tag{10}$$

Therefore the above expression becomes

$$\nabla^2 p=-(4\pi)^{-1}(\vec{H}_0\nabla^2\vec{h})\ . \tag{11}$$

3. Poloidal magnetic field

In general, $\vec{h}$ can be expressed as

$$\vec{h}=\sum_{n,m}\vec{h}^m_{s,n}+\sum_{n,m}\vec{h}^m_{t,n} \tag{12}$$

where $\vec{h}^m_{s,n}$ is of the poloidal type, the r, θ and ϕ components in the spherical coordinate being written as

$$\vec{h}^m_{s,n}=\begin{cases}-n(n+1)s^m_n(r)r^{n-1}Y^m_n\ , \\ -\left[r\dfrac{ds^m_n}{dr}+(n+1)s^m_n\right]r^{n-1}\dfrac{\partial Y^m_n}{\partial\theta}\ , \\ -\left[r\dfrac{ds^m_n}{dr}+(n+1)s^m_n\right]r^{n-1}\dfrac{\partial Y^m_n}{\sin\theta\partial\phi}\ ,\end{cases} \tag{13}$$

and $\vec{h}^m_{t,n}$ is of the toroidal type which is written as

$$\vec{h}^m_{t,n}=\begin{cases}0\ , \\ -t^m_n(r)r^n\dfrac{\partial Y^m_n}{\sin\theta\partial\phi}\ , \\ t^m_n(r)r^n\dfrac{\partial Y^m_n}{\partial\theta}\ ,\end{cases} \tag{14}$$

where

$$Y^m_n=P^m_n(\cos\theta)\frac{\cos}{\sin}m\phi\ . \tag{15}$$

In the first place, we shall take a poloidal field and calculate p, $\vec{v}$,

$\vec{v}\wedge\vec{H}_0$ and curl $(\vec{v}\wedge\vec{H}_0)$.

From (13), we obtain

$$\operatorname{curl}\vec{h}^m_{s,n}=\begin{cases} 0\ , \\ \left[r\dfrac{d^2s^m_n}{dr^2}+2(n+1)\dfrac{ds^m_n}{dr}\right]r^{n-1}\dfrac{\partial Y^m_n}{\sin\theta\partial\phi}\ , \\ -\left[r\dfrac{d^2s^m_n}{dr^2}+2(n+1)\dfrac{ds^m_n}{dr}\right]r^{n-1}\dfrac{\partial Y^m_n}{\partial\theta}\ , \end{cases} \tag{16}$$

and

$$\nabla^2\vec{h}^m_{s,n}=\begin{cases} -n(n+1)\left[\dfrac{d^2s^m_n}{dr^2}+\dfrac{2(n+1)}{r}\dfrac{ds^m_n}{dr}\right]r^{n-1}Y^m_n\ , \\ -\left[r\dfrac{d^3s^m_n}{dr^3}+3(n+1)\dfrac{d^2s^m_n}{dr^2}+\dfrac{2n(n+1)}{r}\dfrac{ds^m_n}{dr}\right]r^{n-1}\dfrac{\partial Y^m_n}{\partial\theta}\ , \\ -\left[r\dfrac{d^3s^m_n}{dr^3}+3(n+1)\dfrac{d^2s^m_n}{dr^2}+\dfrac{2n(n+1)}{r}\dfrac{ds^m_n}{dr}\right]r^{n-1}\dfrac{\partial Y^m_n}{\sin\theta\partial\phi}\ . \end{cases} \tag{17}$$

If we assume that the external field is uniform and parallel to the $\theta=0$ axis, $\vec{H}_0$ is given as

$$\vec{H}_0=\begin{cases} H\cos\theta\ , \\ -H\sin\theta\ , \\ 0\ . \end{cases} \tag{18}$$

From (17) and (18), we obtain

$$\vec{H}_0\cdot\nabla^2\vec{h}^m_{s,n}=H\Big[-n(n+1)\left\{\frac{d^2s^m_n}{dr^2}+\frac{2(n+1)}{r}\frac{ds^m_n}{dr}\right\}Y^m_n\cos\theta$$
$$+\left\{r\frac{d^3s^m_n}{dr^3}+3(n+1)\frac{d^2s^m_n}{dr^2}+\frac{2n(n+1)}{r}\frac{ds^m_n}{dr}\right\}\frac{\partial Y^m_n}{\partial\theta}\sin\theta\Big]r^{n-1}\ .$$

Taking into account the following recurrence formulae for Neumann's spherical surface harmonics

$$\cos\theta P^m_n=\frac{1}{2n+1}\{(n-m+1)P^m_{n+1}+(n+m)P^m_{n-1}\}\ ,$$

$$\sin\theta\frac{dP^m_n}{d\theta}=\frac{1}{2n+1}\{n(n-m+1)P^m_{n+1}-(n+1)(n+m)P^m_{n-1}\}\ ,$$

the above expression can be written as follows ;

$$\vec{H}_0\cdot\nabla^2\vec{h}^m_{s,n}=\frac{Hr^{n-1}}{2n+1}\Big[n(n-m+1)\Big(r\frac{d^3s^m_n}{dr^3}+2(n+1)\frac{d^2s^m_n}{dr^2}-\frac{2(n+1)}{r}\frac{ds^m_n}{dr}\Big)Y^m_{n+1}$$
$$-(n+1)(n+m)\Big(r\frac{d^3s^m_n}{dr^3}+(4n+3)\frac{d^2s^m_n}{dr^2}+\frac{4n(n+1)}{r}\frac{ds^m_n}{dr}\Big)Y^m_{n-1}\Big]. \tag{19}$$

Putting (19) into (11), we obtain a differential equation for the pressure which can be written as

$$\nabla^2 p=f_{n+1}Y^m_{n+1}+f_{n-1}Y^m_{n-1}, \tag{20}$$

where

$$\left.\begin{aligned}-4\pi f_{n+1}&=H\frac{n(n-m+1)}{2n+1}r^{n-1}\Big(r\frac{d^3s^m_n}{dr^3}+2(n+1)\frac{d^2s^m_n}{dr^2}-\frac{2(n+1)}{r}\frac{ds^m_n}{dr}\Big),\\ 4\pi f_{n-1}&=H\frac{(n+1)(n+m)}{2n+1}r^{n-1}\Big(r\frac{d^3s^m_n}{dr^3}+(4n+3)\frac{d^2s^m_n}{dr^2}+\frac{4n(n+1)}{r}\frac{ds^m_n}{dr}\Big).\end{aligned}\right\} \tag{21}$$

The solution of (20) can be given as

$$p=q^m_{n+1}Y^m_{n+1}+q^m_{n-1}Y^m_{n-1} \tag{22}$$

where q^m_{n+1} and q^m_{n-1} are respectively the solutions of the following differential equations:

$$\left.\begin{aligned}\frac{1}{r^2}\frac{d}{dr}\Big(r^2\frac{dq^m_{n+1}}{dr}\Big)-\frac{(n+1)(n+2)}{r^2}q^m_{n+1}&=f_{n+1},\\ \frac{1}{r^2}\frac{d}{dr}\Big(r^2\frac{dq^m_{n-1}}{dr}\Big)-\frac{(n-1)n}{r^2}q^m_{n-1}&=f_{n-1}.\end{aligned}\right\} \tag{23}$$

It is easily seen that the solutions of (23) which remain finite at $r=0$ are given as

$$\left.\begin{aligned}q^m_{n+1}&=a^{-(n+1)}r^{n+1}k^m_{n+1}+\frac{1}{2n+3}\Big(r^{n+1}\int_0^r r^{-n}f_{n+1}dr-r^{-n-2}\int_0^r r^{n+3}f_{n+1}dr\Big),\\ q^m_{n-1}&=a^{-(n-1)}r^{n-1}l^m_{n-1}+\frac{1}{2n-1}\Big(r^{n-1}\int_0^r r^{-n+2}f_{n-1}dr-r^{-n}\int_0^r r^{n+1}f_{n-1}dr\Big).\end{aligned}\right\} \tag{24}$$

where k^m_{n+1} and l^m_{n-1} are constants which are to be determined later.

Putting (21) into (24), we obtain, after some calculations, the following expressions:

$$\left.\begin{aligned}4\pi q_{n+1}^m&=a^{-(n+1)}r^{n+1}\alpha_{n+1}^m-H\frac{n(n-m+1)}{2n+1}r^n\frac{ds_n^m}{dr}\,,\\4\pi q_{n-1}^m&=a^{-(n-1)}r^{n-1}\beta_{n-1}^m+H\frac{(n+1)(n+m)}{2n+1}\left\{r^n\frac{ds_n^m}{dr}+(2n+1)r^{n-1}s_n^m\right\}\,,\end{aligned}\right\}\tag{25}$$

where

$$\alpha_{n+1}^m=4\pi k_{n+1}^m\,,\qquad \beta_{n-1}^m=4\pi l_{n-1}^m\,.$$

These constants are to be determined by the boundary conditions.

Thus the solution for the pressure is given by (22) together with (23).

Now we are in a position to calculate the velocity according to (9). From (16) and (18), we have

$$\operatorname{curl}\vec{h}_{s,n}^m\wedge\vec{H}_0=\left|\begin{aligned}&-H\left[r\frac{d^2s_n^m}{dr^2}+2(n+1)\frac{ds_n^m}{dr}\right]r^{n-1}\sin\theta\frac{\partial Y_n^m}{\partial\theta}\,,\\&-H\left[r\frac{d^2s_n^m}{dr^2}+2(n+1)\frac{ds_n^m}{dr}\right]r^{n-1}\cos\theta\frac{\partial Y_n^m}{\partial\theta}\,,\\&-H\left[r\frac{d^2s_n^m}{dr^2}+2(n+1)\frac{ds_n^m}{dr}\right]r^{n-1}\cos\theta\frac{\partial Y_n^m}{\sin\theta\partial\phi}\,.\end{aligned}\right.\tag{26}$$

We also calculate grad p from (22) and (23). Putting (26) and grad p thus obtained into (9), the velocity can be calculated. Taking into consideration (5), we see that the velocity can be expressed as a sum of poloidal and toroidal velocity fields, this expression being thought to be convenient. After some lengthy calculations using the recurrence formulae of spherical surface harmonics, we arrive at

$$\vec{v}=\vec{v}_1+\vec{v}_2+\vec{v}_3\tag{27}$$

in which

$$4\pi\rho D\vec{v}_1=\left\{\begin{aligned}&-(n+1)(n+2)A_{n+1}^m r^n Y_{n+1}^m\\&-\left[r\frac{dA_{n+1}^m}{dr}+(n+2)A_{n+1}^m\right]r^n\frac{\partial Y_{n+1}^m}{\partial\theta}\,,\\&-\left[r\frac{dA_{n+1}^m}{dr}+(n+2)A_{n+1}^m\right]r^n\frac{\partial Y_{n+1}^m}{\sin\theta\partial\phi}\,,\end{aligned}\right.$$

$$A_{n+1}^m=\frac{a^{-(n+1)}\alpha_{n+1}^m}{n+2}+H\frac{n(n-m+1)}{(2n+1)(n+1)}r^{-1}\frac{ds_n^m}{dr}\,,\tag{28}$$

$$4\pi\rho D\vec{v}_2=\begin{cases}-(n-1)nB_{n-1}^m r^{n-2}Y_{n-1}^m\ ,\\ -\left[r\dfrac{dB_{n-1}^m}{dr}+nB_{n-1}^m\right]r^{n-2}\dfrac{\partial Y_{n-1}^m}{\partial\theta}\ ,\\ -\left[r\dfrac{dB_{n-1}^m}{dr}+nB_{n-1}^m\right]r^{n-2}\dfrac{\partial Y_{n-1}^m}{\sin\theta\partial\phi}\ ,\end{cases}$$

$$B_{n-1}^m=\frac{a^{-(n-1)}\beta_{n-1}^m}{n}+H\frac{(n+1)(n+m)}{(2n+1)n}\left\{r\frac{ds_n^m}{dr}+(2n+1)s_n^m\right\}\ , \qquad (29)$$

$$4\pi\rho D\vec{v}_3=\begin{cases}0\ ,\\ -C_n^m r^n\dfrac{\partial\tilde{Y}_n^m}{\sin\theta\partial\phi}\ ,\\ C_n^m r^n\dfrac{\partial\tilde{Y}_n^m}{\partial\theta}\ ,\end{cases}$$

$$C_n^m=-\frac{H}{n(n+1)}\left\{\frac{d^2s_n^m}{dr^2}+2(n+1)r^{-1}\frac{ds_n^m}{dr}\right\}\ , \qquad (30)$$

where

$$\tilde{Y}_n^m=\partial Y_n^m/\partial\phi\ . \qquad (31)$$

So it becomes clear that we have two types of poloidal velocity ($S_{n+1}^{m,c}$ and $S_{n-1}^{m,c}$) and one toroidal velocity ($T_n^{m,s}$ type) through the interaction between $\vec{H}_0$ and $\vec{h}_{s,n}^{m,c}$. c and s, which are attached to the shoulders of the symbols here, denote respectively that those velocities or magnetic fiields contain $\cos m\phi$ or $\sin m\phi$. When we take $\vec{h}_{s,n}^{m,s}$ instead of $\vec{h}_{s,n}^{m,c}$, we get velocities of the $S_{n+1}^{m,s}$, $S_{n-1}^{m,s}$ and $T_n^{m,c}$ types.

Since we have obtained the velocities, the next step is to calculate $\operatorname{curl}(\vec{v}\wedge\vec{H}_0)$. Applying the recurrence formulae as before, we obtain

$$4\pi\rho D\operatorname{curl}(\vec{v}_1\wedge\vec{H}_0)=\begin{cases}-(n+2)(n+3)E_{n+2}^m r^{n+1}Y_{n+2}^m\ ,\\ -\left[r\dfrac{dE_{n+2}^m}{dr}+(n+3)E_{n+2}^m\right]r^{n+1}\dfrac{\partial Y_{n+2}^m}{\partial\theta}\ ,\\ -\left[r\dfrac{dE_{n+2}^m}{dr}+(n+3)E_{n+2}^m\right]r^{n+1}\dfrac{\partial Y_{n+2}^m}{\sin\theta\partial\phi}\end{cases}$$

$$E_{n+2}^m=H\frac{(n+1)(n-m+2)}{(2n+3)(n+2)}r^{-1}\frac{dA_{n+1}^m}{dr}$$

$$+\begin{cases} -n(n+1)F_n^m r^{n-1}Y_n^m \\ -\left[r\dfrac{dF_n^m}{dr}+(n+1)F_n^m\right]r^{n-1}\dfrac{\partial Y_n^m}{\partial\theta} \\ -\left[r\dfrac{dF_n^m}{dr}+(n+1)F_n^m\right]r^{n-1}\dfrac{\partial Y_n^m}{\sin\theta\partial\phi} \end{cases}$$

$$F_n^m=H\frac{(n+2)(n+m+1)}{(2n+3)(n+1)}\left\{r\frac{dA_{n+1}^m}{dr}+(2n+3)A_{n+1}^m\right\}$$

$$+\begin{cases} 0 \\ -G_{n+1}^m r^{n+1}\dfrac{\partial\tilde{Y}_{n+1}^m}{\sin\theta\partial\phi} \\ G_{n+1}^m r^{n+1}\dfrac{\partial\tilde{Y}_{n+1}^m}{\partial\theta} \end{cases}$$

$$G_{n+1}^m=-\frac{H}{(n+1)(n+2)}\left\{\frac{d^2A_{n+1}^m}{dr^2}+2(n+2)r^{-1}\frac{dA_{n+1}^m}{dr}\right\}, \quad (32)$$

$$4\pi\rho D\,\mathrm{curl}(\vec{v}_2\wedge\vec{H}_0)=\begin{cases} -n(n+1)H_n^m r^{n-1}Y_n^m \\ -\left[r\dfrac{dH_n^m}{dr}+(n+1)H_n^m\right]r^{n-1}\dfrac{\partial Y_n^m}{\partial\theta} \\ -\left[r\dfrac{dH_n^m}{dr}+(n+1)H_n^m\right]r^{n-1}\dfrac{\partial Y_n^m}{\sin\theta\partial\phi} \end{cases}$$

$$H_n^m=H\frac{(n-1)(n-m)}{(2n-1)n}r^{-1}\frac{dB_{n-1}^m}{dr}$$

$$+\begin{cases} -(n-2)(n-1)I_{n-2}^m r^{n-3}Y_{n-2}^m \\ -\left[r\dfrac{dI_{n-2}^m}{dr}+(n-1)I_{n-2}^m\right]r^{n-3}\dfrac{\partial Y_{n-2}^m}{\partial\theta} \\ -\left[r\dfrac{dI_{n-2}^m}{dr}+(n-1)I_{n-2}^m\right]r^{n-3}\dfrac{\partial Y_{n-2}^m}{\sin\theta\partial\phi} \end{cases}$$

$$I_{n-2}^m=H\frac{n(n+m-1)}{(2n-1)(n-1)}\left\{r\frac{dB_{n-1}^m}{dr}+(2n-1)B_{n-1}^m\right\}$$

$$+\begin{cases} 0 \\ -J_{n-1}^m r^{n-1}\dfrac{\partial\tilde{Y}_{n-1}^m}{\sin\theta\partial\phi} \\ J_{n-1}^m r^{n-1}\dfrac{\partial\tilde{Y}_{n-1}^m}{\partial\theta} \end{cases}$$

$$J_{n-1}^m = -\frac{H}{(n-1)n}\left\{\frac{d^2B_{n-1}^m}{dr^2} + 2nr^{-1}\frac{dB_{n-1}^m}{dr}\right\}, \tag{33}$$

$$4\pi\rho D\,\mathrm{curl}(\vec{v}_3\wedge\vec{H}_0) = \begin{cases} -n(n+1)K_n^m r^{n-1}Y_n^m \\ -\left[r\dfrac{dK_n^m}{dr} + (n+1)K_n^m\right]r^{n-1}\dfrac{\partial Y_n^m}{\partial\theta} \\ -\left[r\dfrac{dK_n^m}{dr} + (n+1)K_n^m\right]r^{n-1}\dfrac{\partial Y_n^m}{\sin\theta\partial\phi} \end{cases}$$

$$K_n^m = -\frac{Hm^2}{n(n+1)}C_n^m$$

$$+\begin{cases} 0 \\ -L_{n+1}^m r^{n+1}\dfrac{\partial \tilde{Y}_{n+1}^m}{\sin\theta\partial\phi} \\ L_{n+1}^m r^{n+1}\dfrac{\partial \tilde{Y}_{n+1}^m}{\partial\theta} \end{cases}$$

$$L_{n+1}^m = -H\frac{(n-1)(n-m+1)}{2n+1}\left\{r^{-1}\frac{dC_n^m}{dr} + (n+2)r^{-2}C_n^m\right\}$$

$$+\begin{cases} 0 \\ -M_{n-1}^m r^{n-1}\dfrac{\partial \tilde{Y}_{n-1}^m}{\sin\theta\partial\phi} \\ M_{n-1}^m r^{n-1}\dfrac{\partial \tilde{Y}_{n-1}^m}{\partial\theta} \end{cases}$$

$$M_{n-1}^m = H\frac{(n+2)(n+m)}{2n+1}\left\{r\frac{dC_n^m}{dr} + (n+2)C_n^m\right\}. \tag{34}$$

Therefore the interaction between the fluid motions and $\vec{H}_0$ induces the electric currents which give rise to the magnetic fields of the $S_{n+2}^{m,c}$, $S_n^{m,c}$, $S_{n-2}^{m,c}$, $T_{n+1}^{m,s}$ and $T_{n-1}^{m,s}$ types for the first case which corresponds to $\vec{h}_{s,n}^{m,c}$. If we take $\vec{h}_{s,n}^{m,s}$, the final magnetic fields become of the $S_{n+2}^{m,s}$, $S_n^{m,s}$, $S_{n-2}^{m,s}$, $T_{n+1}^{m,c}$ and $T_{n-1}^{m,c}$ types.

On the other hand, putting $\vec{h}_{s,n}^m$ in place of $\vec{h}$, the left-hand side of (8) becomes

$$\{D-(4\pi\sigma)^{-1}\nabla^2\}\vec{h}^m_{s,n}=\begin{cases} -n(n+1)\gamma^m_n r^{n-1}Y^m_n\,, \\ -\left[r\dfrac{d\gamma^m_n}{dr}+(n+1)\gamma^m_n\right]r^{n-1}\dfrac{\partial Y^m_n}{\partial\theta}\,, \\ -\left[r\dfrac{d\gamma^m_n}{dr}+(n+1)\gamma^m_n\right]r^{n-1}\dfrac{\partial Y^m_n}{\sin\theta\partial\phi}\,, \end{cases}$$

$$\gamma^m_n=Ds^m_n-(4\pi\sigma)^{-1}\left\{\frac{d^2s^m_n}{dr^2}+2(n+1)r^{-1}\frac{ds^m_n}{dr}\right\}. \tag{35}$$

4. Toroidal magnetic field

A similar calculation will be made for the toroidal magnetic field $\vec{h}^m_{t,n}$ which is given in (14). From (14), we have

$$\operatorname{curl}\vec{h}^m_{t,n}=\begin{cases} -n(n+1)t^m_n r^{n-1}Y^m_n\,, \\ -\left[r\dfrac{dt^m_n}{dr}+(n+1)t^m_n\right]r^{n-1}\dfrac{\partial Y^m_n}{\partial\theta}\,, \\ -\left[r\dfrac{dt^m_n}{dr}+(n+1)t^m_n\right]r^{n-1}\dfrac{\partial Y^m_n}{\sin\theta\partial\phi}\,, \end{cases} \tag{36}$$

and

$$\nabla^2\vec{h}^m_{t,n}=\begin{cases} 0\,, \\ -\left[\dfrac{d^2t^m_n}{dr^2}+2(n+1)r^{-1}\dfrac{dt^m_n}{dr}\right]r^n\dfrac{\partial Y^m_n}{\sin\theta\partial\phi}\,, \\ \left[\dfrac{d^2t^m_n}{dr^2}+2(n+1)r^{-1}\dfrac{dt^m_n}{dr}\right]r^n\dfrac{\partial Y^m_n}{\partial\theta}\,. \end{cases} \tag{37}$$

Corresponding to (19), it becomes

$$\vec{H}_0\cdot\nabla^2\vec{h}^m_{t,n}=H\left[\frac{d^2t^m_n}{dr^2}+2(n+1)r^{-1}\frac{dt^m_n}{dr}\right]r^n\tilde{Y}^m_n\,. \tag{38}$$

The differential equation for the pressure is given as

$$\nabla^2p=g_n\tilde{Y}^m_n \tag{39}$$

where

$$-4\pi g_n=H\left(\frac{d^2t^m_n}{dr^2}+2(n+1)r^{-1}\frac{dt^m_n}{dr}\right)r^n\,. \tag{40}$$

The solution of (39) can be given as

$$p=\bar{q}_n^m \tilde{Y}_n^m \tag{41}$$

where $\bar{q}_n^m$ satisfies the following differential equation

$$\frac{1}{r^2}\frac{d}{dr}\left(r^2\frac{d\bar{q}_n^m}{dr}\right)-\frac{n(n+1)}{r^2}\bar{q}_n^m=g_n\ . \tag{42}$$

(42) can be solved as

$$\bar{q}_n^m=a^{-n}r^n\bar{k}_n^m+\frac{1}{2n+1}\left(r^n\int_0^r r^{-(n-1)}g_n dr-r^{-n-1}\int_0^r r^{n+2}g_n dr\right) \tag{43}$$

which is written as

$$4\pi\bar{q}_n^m=a^{-n}r^n\bar{\alpha}_n^m-Hr^n t_n^m \tag{44}$$

where

$$\bar{\alpha}_n^m=4\pi\bar{k}_n^m\ .$$

After calculating grad p and curl $\vec{h}_{t,n}^m\wedge\vec{H}_0$, we obtain the velocities as before. They are given as

$$\vec{v}=\vec{v}_1+\vec{v}_2+\vec{v}_3 \tag{45}$$

in which

$$4\pi\rho D\vec{v}_1=\begin{cases} -n(n+1)\bar{A}_n^m r^{n-1}\tilde{Y}_n^m\ , \\ -\left[r\dfrac{d\bar{A}_n^m}{dr}+(n+1)\bar{A}_n^m\right]r^{n-1}\dfrac{\partial\tilde{Y}_n^m}{\partial\theta}\ , \\ -\left[r\dfrac{d\bar{A}_n^m}{dr}+(n+1)\bar{A}_n^m\right]r^{n-1}\dfrac{\partial\tilde{Y}_n^m}{\sin\theta\partial\phi}\ , \end{cases}$$

$$\bar{A}_n^m=\frac{a^{-n}\bar{\alpha}_n^m}{n+1}+\frac{H}{n(n+1)}t_n^m\ , \tag{46}$$

$$4\pi\rho D\vec{v}_2=\begin{cases} 0\ , \\ -\bar{B}_{n+1}^m r^{n+1}\dfrac{\partial Y_{n+1}^m}{\sin\theta\partial\phi}\ , \\ \bar{B}_{n+1}^m r^{n+1}\dfrac{\partial Y_{n+1}^m}{\partial\theta}\ , \end{cases}$$

$$\bar{B}_{n+1}^m=H\frac{n(n-m+1)}{(n+1)(2n+1)}r^{-1}\frac{dt_n^m}{dr}\ , \tag{47}$$

$$4\pi\rho D\vec{\bar{v}}_3=\begin{cases} 0\,, \\ -\bar{C}^m_{n-1}r^{n-1}\dfrac{\partial Y^m_{n-1}}{\sin\theta\partial\phi}\,, \\ \bar{C}^m_{n-1}r^{n-1}\dfrac{\partial Y^m_{n-1}}{\partial\theta}\,, \end{cases}$$

$$\bar{C}^m_{n-1}=H\frac{(n+1)(n+m)}{n(2n+1)}\left\{r\frac{dt^m_n}{dr}+(2n+1)t^m_n\right\}. \tag{48}$$

Thus we have got the velocities of the $S^{m,s}_n$, $T^{m,s}_{n+1}$ and $T^{m,c}_{n-1}$ types for $\vec{h}^{m,c}_{t,n}$ and of the $S^{m,c}_n$, $T^{m,s}_{n+1}$ and $T^{m,s}_{n-1}$ types for $\vec{h}^{m,s}_{t,n}$ respectively.

We also obtain

$$4\pi\rho D\,\mathbf{curl}(\vec{\bar{v}}_1\wedge\vec{H}_0)=\begin{cases} -(n+1)(n+2)\bar{D}^m_{n+1}r^n\tilde{Y}^m_{n+1} \\ -\left[r\dfrac{d\bar{D}^m_{n+1}}{dr}+(n+2)\bar{D}^m_{n+1}\right]r^n\dfrac{\partial\tilde{Y}^m_{n+1}}{\partial\theta} \\ -\left[r\dfrac{d\bar{D}^m_{n+1}}{dr}+(n+2)\bar{D}^m_{n+1}\right]r^n\dfrac{\partial\tilde{Y}^m_{n+1}}{\sin\theta\partial\phi} \end{cases}$$

$$\bar{D}^m_{n+1}=H\frac{n(n-m+1)}{(2n+1)(n+1)}r^{-1}\frac{d\bar{A}^m_n}{dr}$$

$$+\begin{cases} -(n-1)n\bar{E}^m_{n-1}r^{n-2}\tilde{Y}^m_{n-1} \\ -\left[r\dfrac{d\bar{E}^m_{n-1}}{dr}+n\bar{E}^m_{n-1}\right]r^{n-2}\dfrac{\partial\tilde{Y}^m_{n-1}}{\partial\theta} \\ -\left[r\dfrac{d\bar{E}^m_{n-1}}{dr}+n\bar{E}^m_{n-1}\right]r^{n-2}\dfrac{\partial\tilde{Y}^m_{n-1}}{\sin\theta\partial\phi} \end{cases}$$

$$\bar{E}^m_{n-1}=H\frac{(n+1)(n+m)}{(2n+1)n}\left\{r\frac{d\bar{A}^m_n}{dr}+(2n+1)\bar{A}^m_n\right\}$$

$$+\begin{cases} 0 \\ -\bar{F}^m_n r^n\dfrac{\partial Y^m_n}{\sin\theta\partial\phi} \\ \bar{F}^m_n r^n\dfrac{\partial Y^m_n}{\partial\theta} \end{cases}$$

$$\bar{F}^m_n=H\frac{m^2}{n(n+1)}\left\{\frac{d^2\bar{A}^m_n}{dr^2}+2(n+1)r^{-1}\frac{d\bar{A}^m_n}{dr}\right\} \tag{49}$$

$$4\pi\rho D\,\mathrm{curl}(\vec{\bar{v}}_2\wedge\vec{H}_0)=\left\{\begin{array}{l} -(n+1)(n+2)\bar{G}^m_{n+1}r^n\tilde{Y}^m_{n+1} \\ -\left[r\dfrac{d\bar{G}^m_{n+1}}{dr}+(n+2)\bar{G}^m_{n+1}\right]r^n\dfrac{\partial\tilde{Y}^m_{n+1}}{\partial\theta} \\ -\left[r\dfrac{d\bar{G}^m_{n+1}}{dr}+(n+2)\bar{G}^m_{n+1}\right]r^n\dfrac{\partial\tilde{Y}^m_{n+1}}{\sin\theta\partial\phi} \end{array}\right.$$

$$\bar{G}^m_{n+1}=\frac{H}{(n+1)(n+2)}\bar{B}^m_{n+1}$$

$$+\left\{\begin{array}{l} 0 \\ -\bar{H}^m_{n+2}r^{n+2}\dfrac{\partial Y^m_{n+2}}{\sin\theta\partial\phi} \\ \bar{H}^m_{n+2}r^{n+2}\dfrac{\partial Y^m_{n+2}}{\partial\theta} \end{array}\right.$$

$$\bar{H}^m_{n+2}=-H\frac{n(n-m+2)}{2n+3}\left\{r^{-1}\frac{d\bar{B}^m_{n+1}}{dr}+(n+3)r^{-2}\bar{B}^m_{n+1}\right\}$$

$$+\left\{\begin{array}{l} 0 \\ -\bar{I}^m_n r^n\dfrac{\partial Y^m_n}{\sin\theta\partial\phi} \\ \bar{I}^m_n r^n\dfrac{\partial Y^m_n}{\partial\theta} \end{array}\right.$$

$$\bar{I}^m_n=-H\frac{(n+3)(n+m+1)}{2n+3}\left\{r\frac{d\bar{B}^m_{n+1}}{dr}+(n+3)\bar{B}^m_{n+1}\right\}, \tag{50}$$

$$4\pi\rho D\,\mathrm{curl}(\vec{\bar{v}}_3\wedge\vec{H}_0)=\left\{\begin{array}{l} -(n-1)n\bar{J}^m_{n-1}r^{n-2}\tilde{Y}^m_{n-1} \\ -\left[r\dfrac{d\bar{J}^m_{n-1}}{dr}+n\bar{J}^m_{n-1}\right]r^{n-2}\dfrac{\partial\tilde{Y}^m_{n-1}}{\partial\theta} \\ -\left[r\dfrac{d\bar{J}^m_{n-1}}{dr}+n\bar{J}^m_{n-1}\right]r^{n-2}\dfrac{\partial\tilde{Y}^m_{n-1}}{\sin\theta\partial\phi} \end{array}\right.$$

$$\bar{J}^m_{n-1}=\frac{H}{(n-1)n}\bar{C}^m_{n-1}$$

$$+\left\{\begin{array}{l} 0 \\ -\bar{K}^m_n r^n\dfrac{\partial Y^m_n}{\sin\theta\partial\phi} \\ \bar{K}^m_n r^n\dfrac{\partial Y^m_n}{\partial\theta} \end{array}\right.$$

$$\bar{K}_n^m = -H\frac{(n-2)(n-m)}{2n-1}\left\{r^{-1}\frac{\bar{C}_{n-1}^m}{dr} + (n+1)r^{-2}\bar{C}_{n-1}^m\right\}$$

$$+\left|\begin{array}{l} 0 \\ -\bar{L}_{n-2}^m r^{n-2}\dfrac{\partial Y_{n-2}^m}{\sin\theta\partial\phi} \\ \bar{L}_{n-2}^m r^{n-2}\dfrac{\partial Y_{n-2}^m}{\partial\theta} \end{array}\right.$$

$$\bar{L}_{n-2}^m = -H\frac{(n+1)(n+m-1)}{2n-1}\left\{r\frac{d\bar{C}_{n-1}^m}{dr} + (n+1)\bar{C}_{n-1}^m\right\}. \quad (51)$$

In this case, the induced electric currents produce magnetic fields of the $S_{n+1}^{m,s}$, $S_{n-1}^{m,s}$, $T_{n+2}^{m,c}$, $T_n^{m,c}$ and $T_{n-2}^{m,c}$ types when we take $\vec{h}_{t,n}^{m,c}$. We also have $S_{n+1}^{m,c}$, $S_{n-1}^{m,c}$, $T_{n+2}^{m,s}$, $T_n^{m,s}$ and $T_{n-2}^{m,s}$ types for $\vec{h}_{t,n}^{m,s}$.

The left-hand side of (8) becomes

$$\{D-(4\pi\sigma)^{-1}\nabla^2\}\vec{h}_{t,n}^m = \left\{\begin{array}{l} 0\,, \\ -\bar{\gamma}_n^m r^n\dfrac{\partial Y_n^m}{\sin\theta\partial\phi}\,, \\ \bar{\gamma}_n^m r^n\dfrac{\partial Y_n^m}{\partial\theta}\,, \end{array}\right.$$

$$\bar{\gamma}_n^m = Dt_n^m - (4\pi\sigma)^{-1}\left\{\frac{d^2t_n^m}{dr^2} + 2(n+1)r^{-1}\frac{dt_n^m}{dr}\right\}. \quad (52)$$

5. The differential equations for the radial parts

The results in the sections 4 and 5 can be summarized as shown in Table I.

Now we go back to the general case (12). Putting the relations from (32) to (35) and those from (49) to (52) into (8) and equating the coefficients of the corresponding surface harmonics, we obtain the following relations for respective types of the magnetic field;

$$\left.\begin{array}{l} 4\pi\rho D\gamma_n^{m,c} = E_n^{m,c} + m(\bar{D}_n^{m,c} + \bar{G}_n^{m,c}) + F_n^{m,c} + H_n^{m,c} + K_n^{m,c} + m(\bar{E}_n^{m,c} + \bar{J}_n^{m,c}) + I_n^{m,c}\,, \\ 4\pi\rho D\gamma_n^{m,s} = E_n^{m,s} - m(\bar{D}_n^{m,s} + \bar{G}_n^{m,s}) + F_n^{m,s} + H_n^{m,s} + K_n^{m,s} - m(\bar{E}_n^{m,s} + \bar{J}_n^{m,s}) + I_n^{m,s}\,, \\ 4\pi\rho D\bar{\gamma}_n^{m,c} = \bar{H}_n^{m,c} + m(G_n^{m,c} + L_n^{m,c}) + \bar{F}_n^{m,c} + \bar{I}_n^{m,c} + \bar{K}_n^{m,c} + m(J_n^{m,c} + M_n^{m,c}) + \bar{L}_n^{m,c}\,, \\ 4\pi\rho D\bar{\gamma}_n^{m,s} = \bar{H}_n^{m,s} - m(G_n^{m,s} + L_n^{m,s}) + \bar{F}_n^{m,s} + \bar{I}_n^{m,s} + \bar{K}_n^{m,s} - m(J_n^{m,s} + M_n^{m,s}) + \bar{L}_n^{m,s}\,. \end{array}\right\} \quad (53)$$

Table I.

Magnetic field.	Velocity (Interaction with $\vec{H}_0$)	Magnetic field caused by the induced currents (Interaction with $\vec{H}_0$)
		$S_{n+2}^{m,c}$
	$S_{n+1}^{m,c}$	$S_n^{m,c}$
		$T_{n+1}^{m,s}$
		$S_n^{m,c}$
$S_n^{m,c}$	$S_{n-1}^{m,c}$	$S_{n-2}^{m,c}$
		$T_{n-1}^{m,s}$
		$S_n^{m,c}$
	$T_n^{m,s}$	$T_{n+1}^{m,s}$
		$T_{n-1}^{m,s}$
		$S_{n+2}^{m,s}$
	$S_{n+1}^{m,s}$	$S_n^{m,s}$
		$T_{n+1}^{m,c}$
		$S_n^{m,s}$
$S_n^{m,s}$	$S_{n-1}^{m,s}$	$S_{n-2}^{m,s}$
		$T_{n-1}^{m,c}$
		$S_n^{m,s}$
	$T_n^{m,c}$	$T_{n+1}^{m,c}$
		$T_{n-1}^{m,c}$
		$S_{n+1}^{m,s}$
	$S_n^{m,s}$	$S_{n-1}^{m,s}$
		$T_n^{m,c}$
		$S_{n+1}^{m,s}$
$T_n^{m,c}$	$T_{n+1}^{m,c}$	$T_{n+2}^{m,c}$
		$T_n^{m,c}$
		$S_{n-1}^{m,s}$
	$T_{n-1}^{m,c}$	$T_n^{m,c}$
		$T_{n-2}^{m,c}$

(to be continued.)

(continued.)

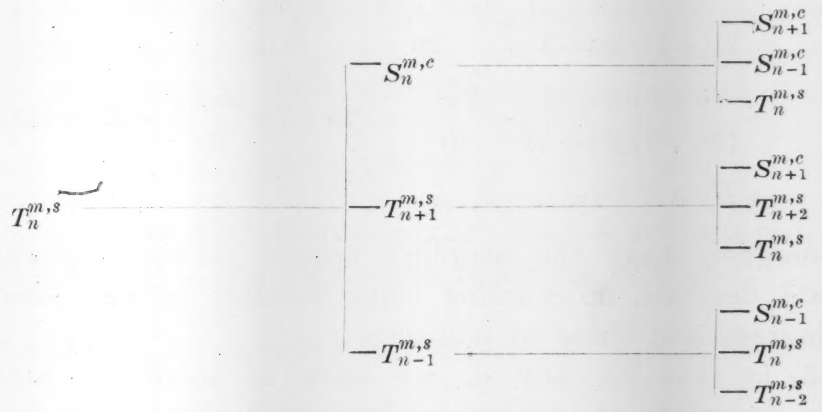

These equations can be regarded as the simultaneous differential equations for $s_n^{m,c}$, $s_n^{m,s}$, $t_n^{m,c}$ and $t_n^{m,s}$. It should be noticed that five terms having respectively $n+2$, $n+1$, n, $n-1$ and $n-2$ as their degrees come out at the same time. Therefore those terms are coupling each other. This feature is quite different from electromagnetic, elastic or hydrodynamic oscillation problems of a spherical body. If we can solve (53) somehow, we would be able to make clear the magneto-hydrodynamic oscillation problem. But it seems quite difficult to solve the general case as given by (53) because of mathematical complexity.

6. Zonal harmonic oscillations

Taking the simplest case, the writer would here like to study only the zonal oscillations because we have, as can be seen in (53), no coupling between zonal and tesseral harmonic constituents.

In that case, (53) becomes

$$\left.\begin{aligned} 4\pi\rho D\gamma_n &= E_n + F_n + H_n + I_n \ , \\ 4\pi\rho D\overline{\gamma}_n &= \overline{H}_n + \overline{I}_n + \overline{K}_n + \overline{L}_n \ , \end{aligned}\right\} \tag{54}$$

from which we find out that there is no coupling between poloidal and toroidal modes. As the toroidal field does not appear outside the sphere, we are in the main interested in the poloidal field. Putting the relations given by (32), (33), (34) and (35) into (54) and taking into account the relations (28), (29) and (30), the first equation of (54) can be written as

$$4\pi\rho DH^{-2}\left[Ds_n - (4\pi\sigma)^{-1}\left\{\frac{d^2s_n}{dr^2} + \frac{2(n+1)}{r}\frac{ds_n}{dr}\right\}\right]$$

$$= \frac{(n-1)(n-2)}{(2n-1)(2n-3)}\left(r\frac{d^2s_{n-2}}{dr^2} + \frac{ds_{n-2}}{dr}\right)r^{-3}$$

$$+\frac{1}{2n+1}\left(\frac{n(n+2)}{2n+3}+\frac{(n-1)(n+1)}{2n-1}\right)\left(\frac{d^2s_n}{dr^2}+\frac{2(n+1)}{r}\frac{ds_n}{dr}\right)$$
$$+\frac{(n+2)(n+3)}{(2n+3)(2n+5)}\left(r^2\frac{d^2s_{n+2}}{dr^2}+(2n+7)r\frac{ds_{n+2}}{dr}+(2n+5)s_{n+2}\right)$$
$$+H^{-1}a^{-(n+1)}(\alpha_{n+1}+\beta_{n+1})\ . \qquad (55)$$

(55) suggests that the coupling occurs between constituents of even or odd degrees, no coupling being possible between constitutents of even degrees and those of odd ones.

As (55) is true for any n, we have to solve the simultaneous differential equations of infinite numbers with infinite unknowns.

It seems to be almost impossible to obtain rigorous solutions of (55). So the writer would here like to obtain the solutions for the S_1^0 and S_3^0 type magnetic fields in an approximate way neglecting the S_5^0, S_7^0, $\cdots\cdot$ type fields. From (55), we have

$$K^2s_1=\frac{1}{5}\left(\frac{d^2s_1}{dr^2}+4r^{-1}\frac{ds_1}{dr}\right)+\frac{12}{35}\left(\frac{d^2\bar{s}_3}{dr^2}+5r^{-1}\frac{d\bar{s}_3}{dr}-5r^{-2}\bar{s}_3\right)+a^{-2}H^{-1}(\alpha_2+\beta_2)\ , \qquad (56)$$

$$K^2\bar{s}_3=\frac{2}{15}\left(\frac{d^2s_1}{dr^2}+r^{-1}\frac{ds_1}{dr}\right)+\frac{7}{15}\left(\frac{d^2\bar{s}_3}{dr^2}+4r^{-1}\frac{d\bar{s}_3}{dr}-10r^{-2}\bar{s}_3\right)+a^{-1}H^{-1}(\alpha_4+\beta_4)r^2\ , \qquad (57)$$

where

$$K^2=4\pi\rho D^2H^{-2}\ ,\qquad \bar{s}_3=r^2s_3$$

in which σ is taken to be infinity for the sake of simplicity. If we take a rigid boundary at $r=a$, α_2, β_2, α_4 and β_4 are determined by (28) and (29) as

$$\left.\begin{aligned}
a^{-2}H^{-1}\alpha_2&=-a^{-1}\left(\frac{ds_1}{dr}\right)_{r=a}\,,\\
a^{-4}H^{-1}\alpha_4&=-\frac{15}{7}a^{-1}\left(\frac{ds_3}{dr}\right)_{r=a}=-\frac{15}{7}a^{-3}\left(\frac{d\bar{s}_3}{dr}-2r^{-1}\bar{s}_3\right)_{r=a}\,,\\
a^{-2}H^{-1}\beta_2&=-\frac{12}{7}\left(r\frac{ds_3}{dr}+7s_3\right)_{r=a}=-\frac{12}{7}\left(r^{-1}\frac{d\bar{s}_3}{dr}+5r^{-2}\bar{s}_3\right)_{r=a}\,,\\
\beta_4&=0\ ,
\end{aligned}\right\} \qquad (58)$$

because $v_r=0$ at $r=a$.

As was done in the writer's previous paper, (56) and (57) may be

approximately solved by putting

$$\left.\begin{aligned} s_1 &= \sum_{s=0}^{4} a_s(r/a)^s \ , \\ \bar{s}_3 &= \sum_{s=0}^{4} b_s(r/a)^s \ , \end{aligned}\right\} \tag{59}$$

in which the terms with powers higher than 4 are ignored. Putting (59) into (56) and (57), we obtain the following relations:

$$\begin{aligned} K^2 \sum_{s=0}^{4} a_s(r/a)^s &= \frac{1}{5}a^{-2} \sum_{s=2}^{4} s(s-1)a_s(r/a)^{s-2} + \frac{4}{5}a^{-2} \sum_{s=1}^{4} sa_s(r/a)^{s-2} \\ &\quad + \frac{12}{35}a^{-2} \sum_{s=2}^{4} s(s-1)b_s(r/a)^{s-2} + \frac{12}{7}a^{-2} \sum_{s=1}^{4} sb_s(r/a)^{s-2} - \frac{12}{7}a^{-2} \sum_{s=0}^{4} b_s(r/a)^{s-2} \\ &\quad - a^{-2} \sum_{s=1}^{4} sa_s - \frac{12}{7}a^{-2} \sum_{s=1}^{4} sb_s - \frac{60}{7}a^{-2} \sum_{s=0}^{4} b_s \ , \end{aligned} \tag{60}$$

$$\begin{aligned} K^2 \sum_{s=0}^{4} b_s(r/a)^s &= \frac{2}{15}a^{-2} \sum_{s=2}^{4} s(s-1)a_s(r/a)^{s-2} + \frac{2}{15}a^{-2} \sum_{s=1}^{4} sa_s(r/a)^{s-2} \\ &\quad + \frac{7}{15}a^{-2} \sum_{s=2}^{4} s(s-1)b_s(r/a)^{s-2} + \frac{28}{15}a^{-2} \sum_{s=1}^{4} sb_s(r/a)^{s-2} - \frac{14}{3}a^{-2} \sum_{s=0}^{4} b_s(r/a)^{s-2} \\ &\quad - \frac{15}{7}a^{-2} \sum_{s=1}^{4} sb_s(r/a)^2 + \frac{30}{7}a^{-2} \sum_{s=0}^{4} b_s(r/a)^2 \ . \end{aligned} \tag{61}$$

Equating the coefficients of the corresponding terms of the two sides of (60) and (61), we obtain the relations between a_0, a_1, a_2, a_3, a_4, b_0, b_1, b_2, b_3 and b_4, the relations being simplified as follows:

$$\left.\begin{aligned} & a_1 = a_3 = b_1 = b_3 = 0 \ , \\ & a^2K^2a_0 = -4a_4 - \frac{60}{7}b_0 - \frac{48}{5}b_2 - \frac{108}{7}b_4 \ , \\ & a^2K^2a_2 = \frac{28}{5}a_4 + \frac{324}{35}b_4 \ , \\ & a^2K^2b_0 = \frac{8}{15}a_2 \ , \\ & a^2K^2b_2 = \frac{32}{15}a_4 + \frac{30}{7}b_0 + \frac{144}{35}b_4 \ . \end{aligned}\right\} \tag{62}$$

However, it is easily seen from (29) and (30) that we should make $b_0=0$ in order to have finite velocities at $r=0$. As can be obtained from (62), this condition also gives $a_2=0$.

Further, the solutions must satisfy the boundary condition that the magnetic field is continuous at $r=a$. The magnetic field outside the sphere is generally given as

$$\vec{h}=\begin{cases} (n+1)(r/a)^{-n-2}h_nP_n\ , \\ -(r/a)^{-n-2}h_n\dfrac{dP_n}{d\theta}\ , \\ 0\ . \end{cases} \tag{63}$$

The continuity at $r=a$ gives

$$-n(\bar{s}_n)_{r=a}=h_n$$

$$\left(r\frac{ds_n}{dr}+\overline{n+1}\,s_n\right)_{r=a}=\left(r\frac{d\bar{s}_n}{dr}+2\bar{s}_n\right)_{r=a}=h_n$$

where

$$\bar{s}_n=r^{n-1}s_n\ .$$

Eliminating h_n, we obtain

$$\left(r\frac{d\bar{s}_n}{dr}+\overline{n+2}\,\bar{s}_n\right)_{r=a}=0\ . \tag{64}$$

For the present case, (64) can be written as

$$\left.\begin{aligned} 3a_0+5a_2+7a_4=0\ , \\ 5b_0+7b_2+9b_4=0\ . \end{aligned}\right\} \tag{65}$$

In order to have non-vanishing solutions for a_0, a_4, b_2 and b_4 which satisfy the equations (62) and (65), we obtain

$$\begin{vmatrix} 3 & 7 & 0 & 0 \\ 0 & 0 & 7 & 9 \\ a^2K^2 & 4 & \dfrac{48}{5} & \dfrac{108}{7} \\ 0 & -\dfrac{32}{15} & a^2K^2 & -\dfrac{144}{35} \end{vmatrix}=0\ , \tag{66}$$

the condition $b_0=a_2=0$ being taken into account here. (66) is the equation from which we can determine the period of the oscillation considered here. The stable oscillation is specified by one of the roots of (66) which is calculated as

$$(aK)^2=-2.70\ . \tag{67}$$

The other roots do not give oscillatory motions. As $K^2=4\pi\rho D^2H^{-2}$, by taking into account the relation $D^2=-\left(\frac{2\pi}{T}\right)^2$ for periodic cases, the period of the oscillation T becomes

$$T=2.4\pi^{3/2}\rho^{1/2}aH^{-1} . \tag{68}$$

Thus we have got an oscillating magnetic field with a period given by (68). The mode of the oscillation is a superposition of the S_1^0 and S_3^0 type fields. Outside the sphere, the magnetic field has a potential composed of the two spherical harmonic constituents, $(r/a)^{-2}P_1$ and $(r/a)^{-4}P_3$, the proportion of both constituents being obtained by determining the coefficients a_1, b_2, $\cdots$ from the simultaneous equations in (62).

If we ignore all the couplings between each constituent and pick up only the S_1^0 type magnetic field, the characteristic equation becomes

$$\begin{vmatrix} 3 & 5 & 7 \\ a^2K^2 & 0 & 4 \\ 0 & a^2K^2 & -\frac{28}{5} \end{vmatrix} =0 \tag{69}$$

which gives

$$(aK)^2=-\frac{16}{7} \tag{70}$$

for the oscillating case. Hence, the period is given as

$$T_0=2.6\pi^{3/2}\rho^{1/2}aH^{-1} . \tag{71}$$

Comparing (68) with (71), it is seen that the period of the oscillating magnetic field becomes a bit shorter by the coupling between the two spherical harmonic constituents. In any case, the period is proportional to the radius of the sphere, the square root of the density and the inverse of the intensity of the external magnetic field. Suppose we take a sphere, the density of which is assumed to be $10\,g/cm^3$, the radius $10\,cm$, and the applied magnetic field 10 *gauss*, the period is found to be 42 *sec.* from (68). However, an experiment for such a small sphere would be almost impossible because of low conductivity of fluid even if we use mercury.

Although the writer can not obtain rigorous solutions because of the mathematical complexity, the general differential equation as given in (55) seems to be useful for studying the couplings between the

spherical harmonic constituents of the magnetic field. An approximate solution for the magnetic fields composed of the S_1^0 and S_3^0 type ones tells us that the period of the oscillation is estimated at about 90 per cent of that for the S_1^0 field when we ignore the coupling of the two fields. But it is not clear how far the period will be affected when we take into account the couplings with the other higher harmonics.

The relative magnitudes of the coefficients a_0, a_4, b_2 and b_4 can be obtained from (62) into which the eigen-value of aK obtained in (67) should be put. We obtain

$$a_4=-0.428a_0\ , \quad b_2=-1.83a_0\ , \quad b_4=1.43a_0\ .$$

With these coefficients, the magnetic fields can be calculated as follows:

$$\vec{h}=\left\{\begin{array}{l} -\{2.00-0.856(r/a)^4\}a_0P_1 \\ -\{2.00-2.57(r/a)^4\}\,a_0\dfrac{dP_1}{d\theta} \\ 0 \end{array}\right. + \left\{\begin{array}{l} \{22.0-17.2(r/a)^2\}(r/a)^2a_0P_3 \\ \{7.32-8.52(r/a)^2\}(r/a)^2a_0\dfrac{dP_3}{d\theta} \\ 0 \end{array}\right. \quad \text{for } r<a\ ,$$

$$\vec{h}=\left\{\begin{array}{l} -1.14(r/a)^{-3}a_0P_1 \\ 0.572(r/a)^{-3}a_0\dfrac{dP_1}{d\theta} \\ 0 \end{array}\right. + \left\{\begin{array}{l} 4.80(r/a)^{-5}a_0P_3 \\ -1.20(r/a)^{-5}a_0\dfrac{dP_3}{d\theta} \\ 0 \end{array}\right. \quad \text{for } r>a\ .$$

We can also obtain the velocity. From (28), (29) and (30), it is found that

$$A_2=0.571\{1-(r/a)^2\}Ha^{-2}a_0\ , \quad B_2=A_4=0\ ,$$

so that the velocity is of the S_2^0 type and it is given as

$$4\pi\rho DH^{-1}a\vec{v}=\left\{\begin{array}{l} -3.43\{1-(r/a)^2\}(r/a)P_2 \\ -\{1.71-2.86(r/a)^2\}(r/a)\dfrac{dP_2}{d\theta} \\ 0\ . \end{array}\right.$$

The distribution of the magnetic field and the velocity are respectively shown in Figs. 1 and 2.

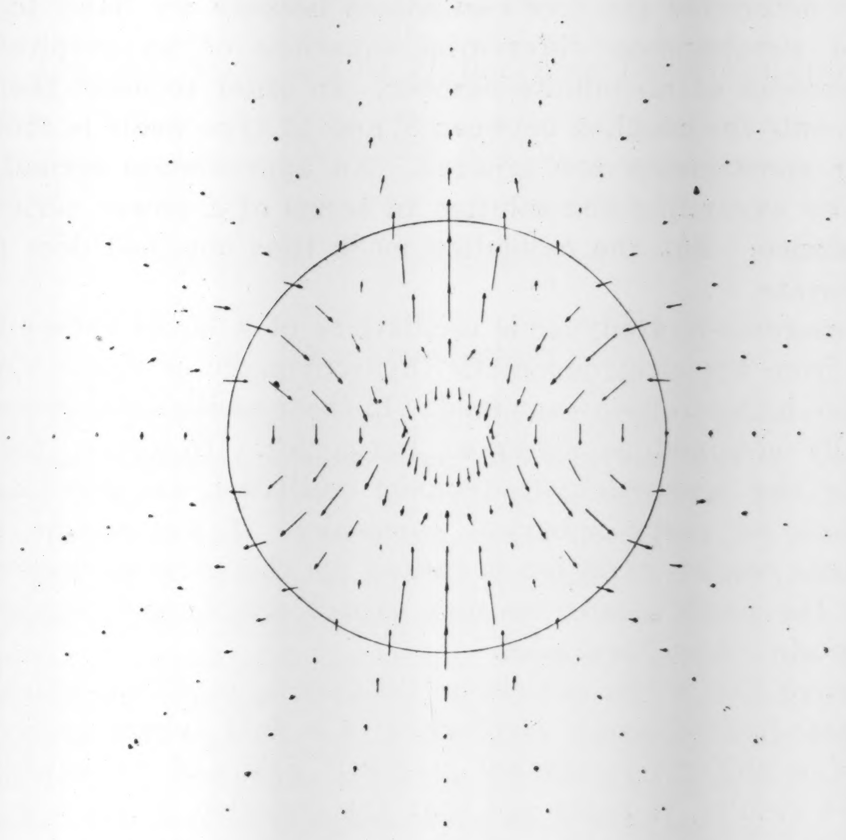

Fig. 1. The distribution of the oscillatory magnetic field.

7. Conclusion

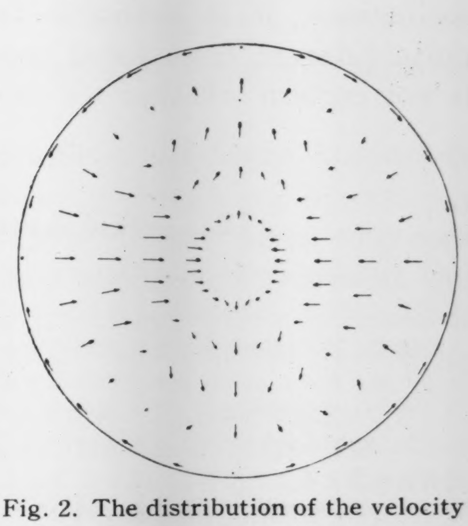

Fig. 2. The distribution of the velocity of the oscillatory motion.

For the purpose of examination of the mutual coupling between spherical harmonic constituents of different degrees, the general theory of the magneto-hydrodynamic oscillation of a liquid sphere is developed in this paper. The general differential equation is obtained as shown in (53) from which we can deduce some useful results concerning the coupling. It is made clear that there are couplings between poloidal and toroidal magnetic fields except for the case of zonal oscillations. As is closely examined in the case of zonal oscillation, it is no easy

matter to determine the free oscillations because we have to solve a system of simultaneous differential equations of an infinite number with unknowns of an infinite number. In order to make the problem tractable, only the coupling between S_1^0 and S_3^0 type fields is studied and the other constituents are ignored. An approximate normal mode is obtained by expanding the solution in terms of a power series of the radial distance. But the oscillation mode thus obtained does not seem to be accurate.

The magneto-hydrodynamic oscillations of a liquid sphere are quite different from the electromagnetic, hydrodynamic or elastic oscillations which have hitherto been examined. In those oscillations, normal modes are usually obtained as spherical harmonics. However, the normal modes for the magneto-hydrodynamic oscillation are given as certain combinations of every spherical harmonic. If we assume that the geomagnetic secular variation is caused by the magneto-hydrodynamic effect in the earth's core, we may expect complicated magnetic fields which contain many harmonics.

Although the writer can obtain the general equation, which governs the magneto-hydrodynamic oscillations of a fluid sphere under the influence of a uniform permanent magnetic field and consequently some qualitative results, it turns out that the equation is not adequate for studying the normal modes of the oscillation because it contains unknowns of an infinite number. In order to study the free or forced oscillations, it is desirable to develop a new method which would be quite different from usual treatment with spherical harmonics. But it is not certain whether we can construct such a method or not.

---

12. 一様磁場内の導電流体球の電磁流体振動

地震研究所 力 武 常 次

前論文に於て地磁気永年変化に対応すると考えられる地球核内の電磁流体振動を論じる際に，ことなつたデグリーのポロイダルまたはトロイダル磁場間の相互の影響を無視した．この影響を見るために，もつとも簡単な場合として外部から一様な磁場を与えた時の導電流体球の電磁流体振動を論じた．その結果一般的方程式を求め得たが，各デグリーの成分が互に関係しあう連成振動となり，その固有値を求めることは容易でないことがわかつた．そこで比較的簡単な帯状振動について特に考察したところ，定性的には有意義な結果を得た．また第5次以上の振動を省略した場合について，近似的に基準振動を求めた．

---

13. *On the Accuracy of Hypocentre Determination II.*

By Shūzō ASANO,

Earthquake Research Institute.

(Read Nov. 16, 1954.—Received March 31, 1955.)

1. Introduction

In the first paper[1], the writer made use of the accurate observations in a small scale explosion seismic experiment carried out by the Seismic Exploration Group, and tried to gain some clue to the accuracy of hypocentre determination. There he assumed the actually known position and time of shot as unknowns and solved them by the usual method of least squares using the arrival times of *P*-wave just as in the studies of natural earthquakes, and the results were compared with the actual items. Although the span covered by the spread was only 180 m. the velocity in the soil was low while the time accuracy was high correspondingly, so the similitude with the case of a natural earthquake was not so bad. The results obtained were as follows:

in the least square solutions

(1) the epicentre and the value of velocity are relatively well-determined,

(2) the shot time and focal depth affect each other and seem to be sensitive to a superficial layer,

(3) the larger the number of observations, the more accurately is the hypocentre determined,

(4) when the effect of superficial layer is not taken into consideration, the probable error does not always represent the extent of discrepancy between the actual and determined values.

In this report the author made the same trial as in the first paper by using the data obtained by the Research Group for Explosion Seismology (abbreviated to R. G. E. S. in this paper) which in respect of scale are close to those of natural earthquake and in respect of accuracy ten times as good as in the observations of natural earthquake. Of course, the results obtained furnish only one example under special conditions,

1) S. ASANO, *Bull. Earthq. Res. Inst.*, **32** (1954), 371.

but if those conditions are taken into consideration, we can infer the accuracy of hypocentre determination in case of a natural earthquake.

2. Materials used

Materials used are the data obtained by R. G. E. S. in cases of the second[2)] and third[3)] Isibuti explosions. As these explosions were carried out at almost the same position (the third one being situated as close as 20 m. south of the second[4)]), the data are here regarded as obtained from one explosion. A consistent analysis has been made by R. G. E. S. to cover all the data of the six explosions within the error of 0.1 sec. with the remarkable result of the crustal structure as shown in Fig. 1[5)]

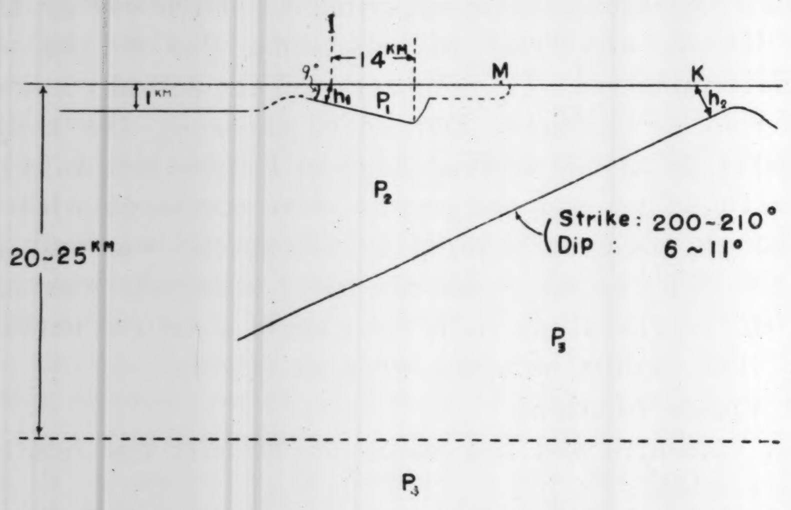

Fig. 1. Underground structure of the north-eastern part of Japan obtained by R. G. E. S.
I: Isibuti shot point; M: Mizusawa; K: Kamaisi; $h_1=630$m.; $h_2=0.5$–2.0 km.;
Velocity of P_1 layer: $V_{P_1}=2.51$ km./sec.;
〃 P_2 〃 : $V_{P_2}=5.75$–5.85 km./sec.;
〃 P_3 〃 : $V_{P_3}=6.10$–6.20 km./sec.;
〃 P_4 〃 : $V_{P_4}=7.5$–8.0 km./sec.;
Strike 200–210° is measured clockwise from north direction.

2) The Research Group for Explosion Seismology, *Bull. Earthq. Res. Inst.*, **30** (1952), 279.
The Research Group for Explosion Seismology, *Zisin*, [*ii*], **6** (1953), 7.
3) The Research Group for Explosion Seismology, *Bull. Earthq. Res. Inst.*, **31** (1953), 281.
The Research Group for Explosion Seismology, *Zisin*, [*ii*], **6** (1953), 84.
4) *Ibid.*, 3).
5) The Research Group for Explosion Seismology, "Crustal Structure in North-East Japan by Explosion-Seismic Observations," Read at the meeting of the Seismological Society of Japan on April 23, 1954 and the general assembly of I.U.G.G. at Rome on Sept. 22, 1954.

which gives the section along the nearly east-west direction of the north-eastern part of Japan. Most of the first arrivals observed within about $\Delta=90$ km. are shown to be the waves passing through the second layer, while those between $\Delta=90$ km. and $\Delta=150$ km. are the waves propagated through the third layer. The shot point and the 18 observation points within about $\Delta=90$ km. are given in Fig. 2. In the above

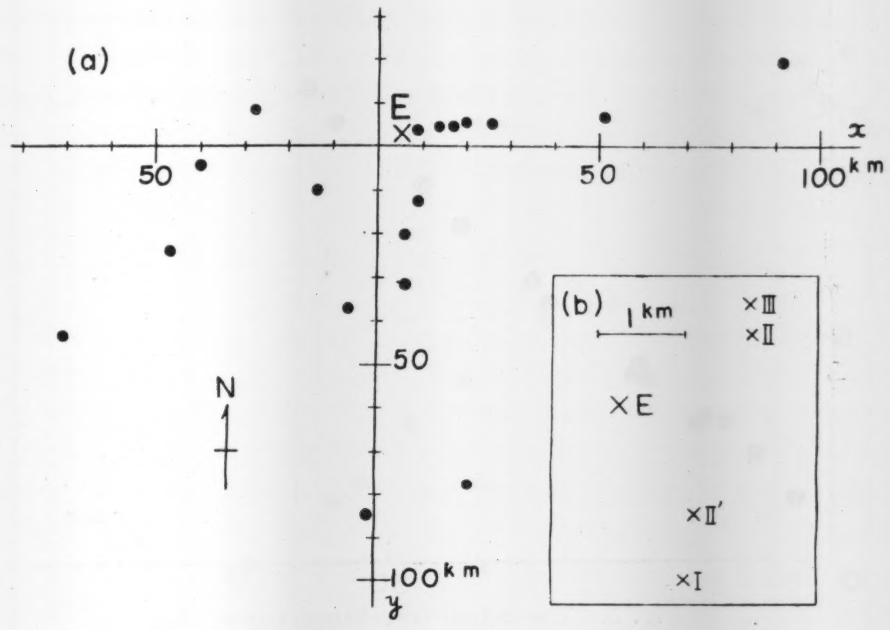

Fig. 2. (a) Shot and observation points.
E: Shot point.
(b) Relative positions of the determined epicentres.

analysis made by R. G. E. S., deviations of the observed travel-times from the calculated one with the velocity of 6 km./sec., that is, the values ($T_{\text{obs.}}-\Delta/6$) were analysed instead of the usual travel-time curve with the result that the waves traveled through not only the first and the second layers but also the second and the third ones were distinguished from each other very easily. On the other hand, from the usual travel-time curve (Fig. 3), the waves related to the second and the third layers cannot be distinguished so clearly. This usual travel-time curve gives the velocity of about 6.1 km./sec. The deviations of observed travel-time from the calculated time for the wave traveled with the velocity of 6.1 km./sec. are within ± 0.5 sec. Therefore, as the effect of the shot depth and the height of observation points on the travel-time is less than observational errors, those quantities were not taken into

consideration in this paper as in the analysis made by R. G. E. S.

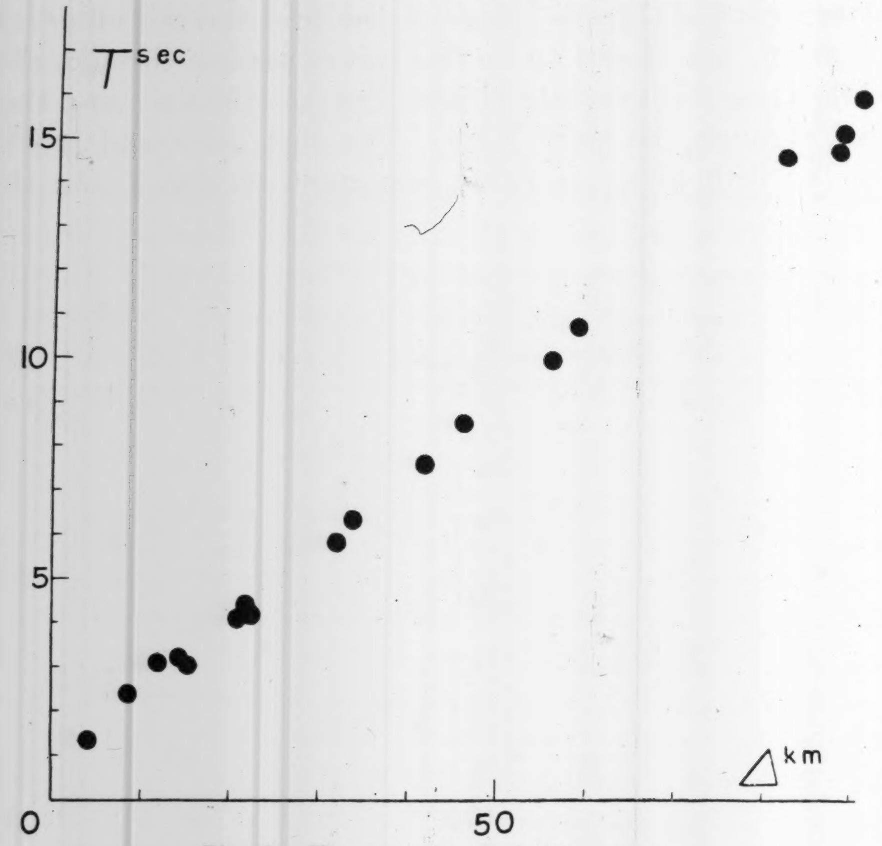

Fig. 3. The actual travel-time curve.

3. The results of hypocentre determination and discussions

In the first place, the coordinates of epicentre of the first approximation were determined as $x_0=6.00$ km. and $y_0=-0.50$ km. by using the time of commencement of *P*-waves, and the travel-time curve derived from the determined epicentre is given in Fig. 4. Although, as may be seen from this travel-time curve, there are some indications of the effect of the layer with velocity of 2.51 km./sec. in the travel-times within $\Delta=15$ km. a uniform structure was assumed for the first approximation, and the velocity and origin time were taken to be 6 km./sec. and 0.8 sec. respectively. These values of the first approximation are tabulated in the column I of Table I. Using the formula

$$(x_0-x_i)\delta x_0+(y_0-y_i)\delta y_0+z_0\delta z_0+v_0^2(t_i-t_0)\delta t_0-v_0(t_i-t_0)^2\delta v_0=v_0^2(t_i-t_0)\delta t_i\ ,$$

the corrections δx_0, δy_0, δt_0 and δv_0 were obtained by the method of least squares. In this calculation 18 observation points were used discarding those at Δ over 90 km. where the first arrivals are presumed

to be the waves passing through the layer with a velocity of 6.2 km./sec. The results obtained are given in the column II of Table I and the position of epicentre relative to the actual one is shown in Fig. 2-(b). The distance between the epicentre of the first approximation and the actual one, Δ_I, is 2.16 km., while that of the second approximation, Δ_{II},

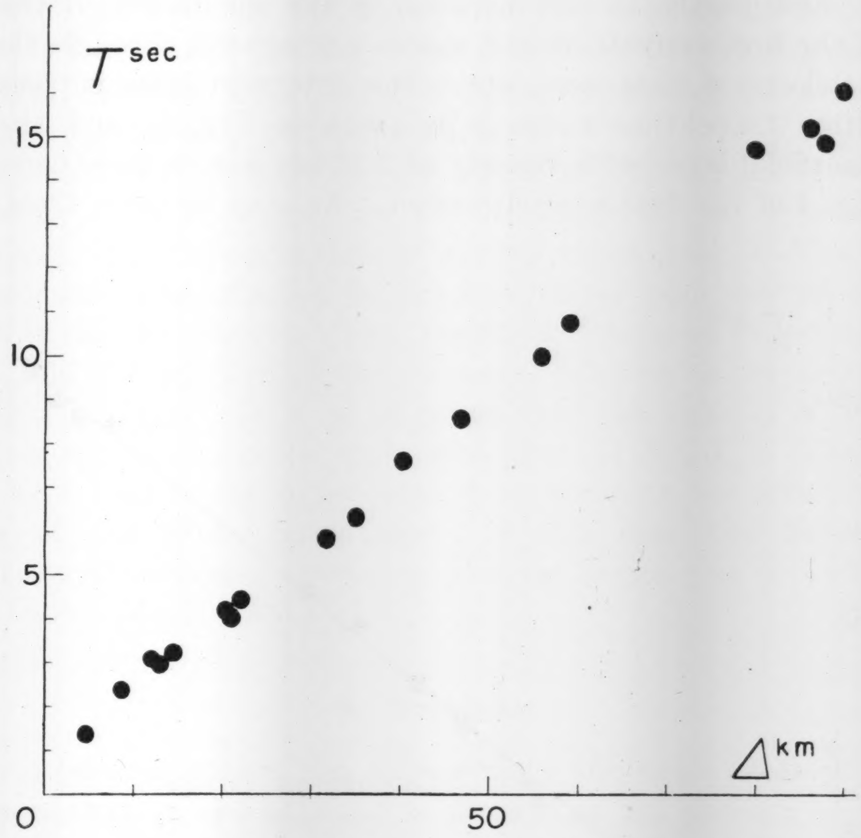

Fig. 4. The travel-time curve of the first approximation.

Table I. The comparison of quantities of successive approximation.

	Actual	I	II	III	II'
x_0	5.26 km.	6.00	6.75±0.37	6.73±0.41	6.11±0.20
y_0	−2.53 km.	−0.50	−3.34±0.57	−3.70±0.66	−1.27±0.38
t_0	0 sec.	0.80	0.51±0.15	0.51±0.19	0.53±0.09
v_0	5.75–5.85 km./sec.	6.00	5.93±0.07	5.94±0.09	5.83±0.07
Δ	0 km.	2.16	1.70	1.88	1.52

is 1.70 km. Thus we see that the epicentre of the second approximation really moved towards the actual one. Furthermore both the position of the origin time and the value of velocity were improved in comparison with those of the first approximation. But as to the velocity, the determined value is larger than the value 5.75–5.85 km./sec. as obtained by R.G.E.S. This difference seems to be due to the simplified assumption of a uniform structure, and partly to the inclusion in the calculation of the observations of the first arrivals of the waves propagated through the lower layer of velocity 6.2 km./sec., etc. The intercept time is reasonable. The resulting travel-time curve is as given in Fig. 5, and the effect of the superficial layer with velocity of 2.51 km./sec. is more clearly seen than in Fig. 4 of the first approximation. As may be seen from Fig. 5,

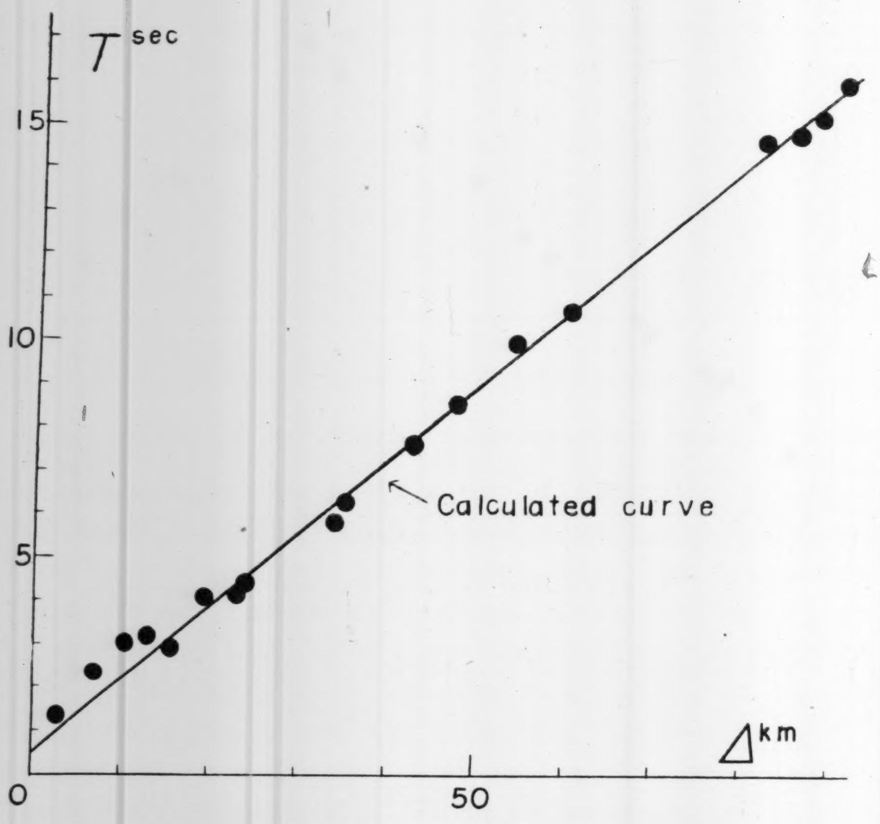

Fig. 5. The travel-time curve of the second approximation.

the observation points where the travel-time was affected by the layer of 2.51 km./sec. show large deviations, $(O-C)$. Therefore, as in the natural earthquake study, five observations with larger $(O-C)$ values were omitted in the following calculation, and the unknowns were again

determined. The results are tabulated in the column III of Table I, and the determined position of the epicentre is shown in Fig. 2-(b). These results agree very well with the values of column II of the same table within the mean errors. The fact that we had almost the same results in the third approximation as those of the second approximation, notwithstanding the neglect of the five observations of the arrival times much affected by the layer with the velocity of 2.51 km./sec., seems to indicate that the discrepancy between the velocity determined in this trial and the actual value obtained by R. G. E. S. was not due to the assumption of a uniform structure.

Next we have to consider the effect of the subjacent layer with the velocity of 6.2 km./sec. on the accuracy of the hypocentre determination. Four observations of arrival times near $\Delta=80$ km. which are presumed to be affected by the lower layer were omitted out of the eighteen in the calculation. The results are entered in column II′ of Table I, and the position of the epicentre relative to the actual one is shown in Fig. 2-(b). It is to be noted that the velocity is well-determined this time and agrees well with that of R.G.E.S. Therefore it may be said that in the hypocentre determination the identification of phase is of the prime importance. In this case the distance ($\Delta_{II'}$) between the determined epicentre and the actual one is 1.52 km. and smaller than $\Delta_{II}(=1.70$ km.).

4. Summary

In the present paper, the author made the same attempt as in the first paper, that is, the attempt to determine the position of shot and shot time assumed to be unknown and compare them with the actual known values. The data used were those obtained by R. G. E. S. on the occasions of the second and third Isibuti explosion. Through this trial we could confirm the results obtained in the first paper, so actually the epicentre and velocity are relatively well determined, while the shot time seems to be sensitive to the nature of the superficial layer. Besides these results, the identification of phase is considered to be much more important in the hypocentre determination than the superficial layer. As to the velocity, when only a certain phase was used, it was determined very well in comparison with the actual one.

5. Acknowledgements

The present author wishes to express his sincere thanks to the members of the Research Group for Explosion Seismology who placed the data at the author's disposal. His hearty thanks are also due to Professor H. Kawasumi for his helpful suggestions and encouragements throughout this study.

---

13. 震源決定の精度について (第2報)

地震研究所　浅　野　周　三

第 1 報に於いて地震探鉱の利点を応用し，実際は既知である爆破点，爆破時刻を未知と仮定し，自然地震に於けると同様に最小自乗法により，それ等の量を定め，実際の値と比較し自然地震に於ける震源決定の精度に関する目安を得る事を試みたが，本報に於いては，その規模に於いて，より自然地震に近い爆破地震動研究グループの石淵第 2 回，第 3 回大爆破地震動観測の資料を用いて，第一報と同様な取扱いを試みた．この 2 回の爆破は殆んど同一地点で行われてゐるので，一つの爆破と見做し，又爆破点の深さ，観測点の高度に関しては，震源決定の精度に及ぼす効果の考察は省略したが，得られた結果と爆破地震動研究グループによつて決定された地殻構造とを比較すると，震央と速度はよく定まり，震源発震時は，比較的表面層の影響をうけ易い等，第一報の結果を実際に確かめるを得た．更に震源決定に於いては，表面層よりも位相の対応が，より重要であると云う結果が得られた．勿論以上の結果は，地殻構造，観測点の配置，震源決定の方法等の点で，特別な条件の下で得られたもので，これ等についての考察は将来の機会を待ちたいと思つてゐる．

貴重な資料の使用をお許し下さつた爆破地震動研究グループの方々に記して感謝の意を表する．

C

14. *Human Susceptibility to Shock Vibrations of the Ground.*

By Fuyuhiko KISHINOUYE,

Earthquake Research Institute.

(Read March 22, 1955.—Received March 31, 1955.)

Earth-vibrations caused by the dropping of a heavy mass or by hammerring shocks are used for the seismic method of examining underground geology. But these vibrations frequently incur complaints from townspeople owing to noises and unpleasant shocks. It thus becomes necessary not only to study the vibrations from seismometry but also to lessen the disturbance. The writer measured such vibrations and investigated human susceptibility or the lower limit of feeling earthquake motions.

The human susceptibility was studied, on the other hand, from medical or physiological points. Recently M. Oshima published a paper "Vibration and Human Being"[1]. He drew a graph of the relation between the susceptibility and the amplitude and frequency of harmonic vibrations which is reproduced in Fig. 1.

Firstly, the relation obtained by K. Suyehiro[2] was added in the graph as white circles, the values of which he got from a seismologist point of view. The values may fit the line drawn by Oshima as shown in Fig. 1.

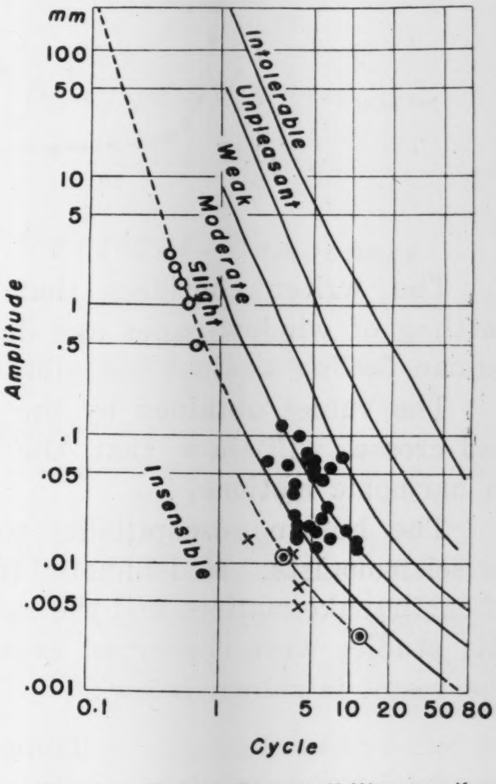

Fig. 1. Human Susceptibility to vibrations. (cross = insensible)

The writer, as mentioned above, had several occasions to measure

1) M. OSHIMA, *Tekkō-Rōdō-Eisei* **2** (1953), Nos. 1, 2 and 3–4.
2) K. SUYEHIRO, *Proc. Imp. Acad. Japan* **5** (1929), 411.

the ground vibrations caused by heavy failling mass, and some of the results were reported before[3]. The writer compares here his results with Oshima's, after describing his observed results briefly.

The acceleration of ground motions caused by fallen mass decreases rapidly with the distance from the source of the shock (Fig. 2). The shock was not felt at a greater distance than about 200 m. The vertical component was larger than the horizontal component within 200 m from the source both in amplitude and acceleration (Fig. 3), while at a distance beyond 200 m, the relation becomes contrary.

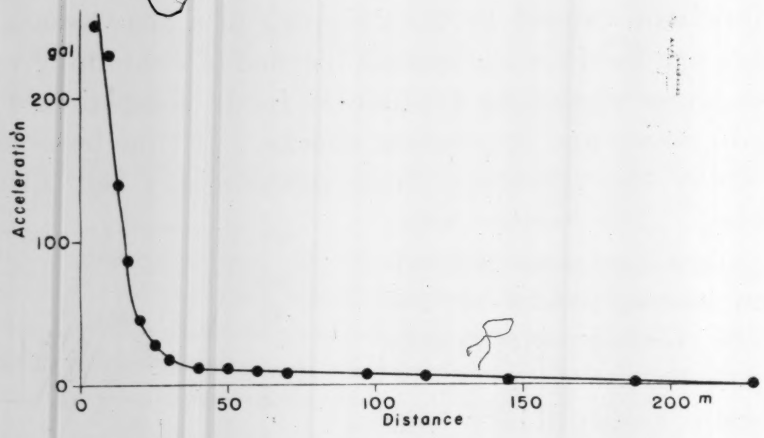

Fig. 2.

The writer considers that vertical motions of the ground and rattling of window-panes and doors caused by the shock aggravate the human feeling against the vibrations.

The values obtained by the writer plotted in Fig. 1 by black dots and crosses will show that the susceptibility to shocks is lower than to harmonic motions.

The human susceptibility to earthquake motions had been studied by seismologists. M. Ishimoto[4] found a relation between the acceleration of earthquake motions and the seismic intensity scale adopted in Japan. His studies were concerned especially with earthquakes at Tōkyō, and the result is shown below:

Ishimoto's Scale

Intensity scale	0	I	II	III	IV	....
Acceleration (gal)	0–0.5	0.5–2	2–8	8–32	32–128	....

3) F. KISHINOUYE, *Bull. Earthq. Res. Inst.*, **30** (1952), 59.

4) M. ISHIMOTO, *Bull. Earthq. Res. Inst.*, **10** (1932), 614.

Similar relations were published by W. Inouye[5], whose study was carried out at Tukuba on the bed of granite of Mt. Tukuba about 60 km N of Tōkyō.

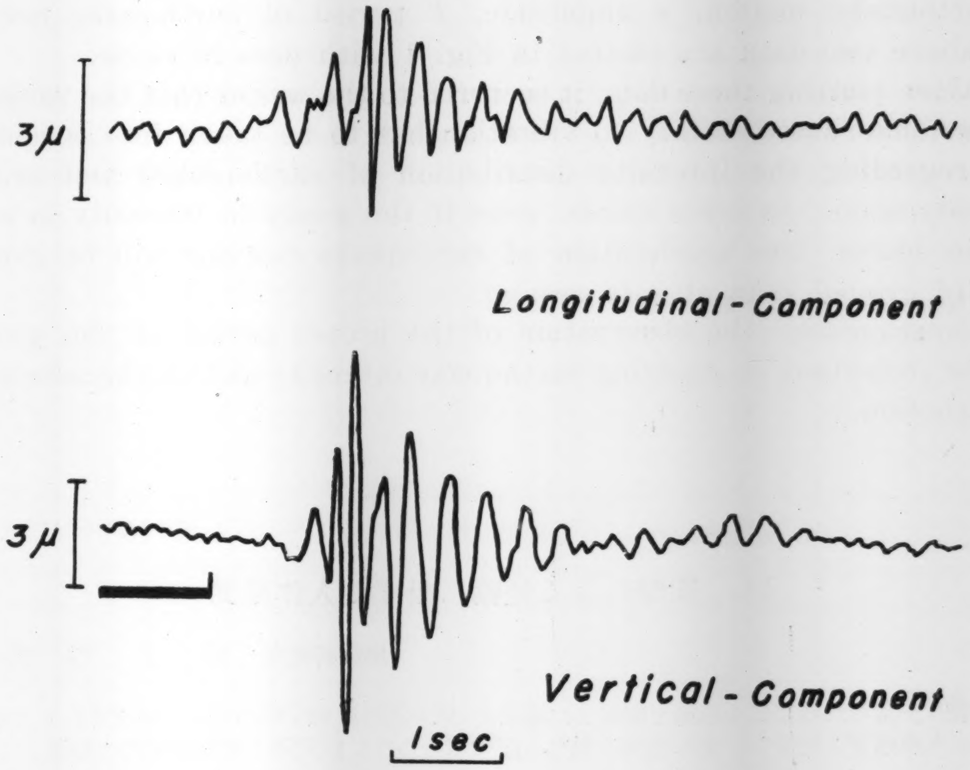

Fig. 3. Earth-vibration by falling of a mass recorded at 130 m distance.

Inouye's Scale

Intensity scale	0	I	II	III	....
Acceleration (gal)	0–1.7	1.7–6.9	6.9–35	35–	....

Both investigations failed to determine the relation to earthquakes of high grades because such strong earthquakes did not occur during their observations.

The lower limit of human susceptibility obtained by the two investigators may be moderately different from each other. It will be due to the difference in the periods of earthquake motions at the two places. Ishimoto's observations were carried out at Hongō, Tōkyō, on loam, and Inouye's on granite. The periods at the two places were

5) W. INOUYE, *Bull. Earthq. Res. Inst.*, **11** (1933), 69.

obtained as 0.3 sec (3.3 c/s) and 0.08 sec (12.5 c/s) respectively. The writer must mention here that their results were given in terms of acceleration of motions. So the relation between period and amplitude was reduced by the formula $\alpha=4\pi^2a/T^2$, where α denotes acceleration of earthquake motion, a amplitude, T period of earthquake motion. The above two data are plotted in Fig. 1 with dots in circle.

After plotting these dots, it occurred to the writer that the variation of the human susceptibility to vibration has to be taken into consideration regarding the intensity distribution of earthquakes and seismic intensity scale. In other words, even if the grade in intensity is equal at two places, the acceleration of earthquake motions will be greater at hard ground than at soft ground.

Consequently, the observation of the proper period of the ground will be important in studying earthquake intensity and earthquake-proof construction.

---

14. 衝撃による地動に対する人体感覚

地震研究所 岸 上 冬 彦

重い物体が落ちた時に起る地動を測定した結果を，医学又は生理学的の方から研究された正弦振動に対する人体感覚と比較し，更に地盤の異なる所で求められた震度階と地動加速度の関係とも比べた．

その結果，衝撃性地動は正弦振動よりも人体には激しく感ずることと，震度階も土地の固有振動周期によつて加速度との関係は変はることを求め得た．

ŏ

15. *Relation between Seismic Intensity and Epicentral Distance.* (2)

By Yasuo SATÔ,

Earthquake Research Institute.

(Read Dec. 21, 1943 to April 15, 1952.—Received March 31, 1955.)

Several years ago we made a report concerning the relation between the seismic intensity and the epicentral distance[1]. It was the result of the investigation by means of the post-card method. The seismic intensity scale employed in it is the one made by H. Kawasumi[2] of the Earthquake Research Institute and does not much differ from that of Mercalli-Sieberg.

In the previous report we have shown only the average value of the intensity of the observations made at certain epicentral distance. In the present report, however, we will show all the intensity values observed at each point. Therefore, the number of points in the figure

Table II

Fig.	Name	Day of Occurrence[3]	Epicentre		*a*	*b*
8	Mino-Owari (Nôbi)	Oct. 21, 1891	136.6°E	35.5°N	8.4	−0.94
2	Tottori	Sept. 10, 1943	134.2	35.5	6.3	−0.94
5	Noziriko	Oct. 13, 1943	138.2	36.8	3.5	−0.95
1	Tô-nankai	Dec. 7, 1944	136.2	33.7	8.3	−1.04
6	Mikawa	Jan. 13, 1945	137.0	34.7	5.7	−0.76
3	Hatinohe-Oki	Feb. 10, 1945	142.1	40.9	6.6	−0.75
4	Nankai	Dec. 21, 1946[4]	135.6	33.0	8.0	−0.71
7	Hukui[5]	June 28, 1948	136.3	36.2	7.5	−1.40
9	Akikai	July 12, 1949	132.5	34.0	5.7	−1.11
10	Imaichi	Dec. 26, 1949	139.7	36.7	6.4	−1.78
11	Tokati-Oki	Mar. 4, 1952	143.9	42.2	8.6	−0.885
12	Daishoji	Mar. 7, 1952	136.2	36.5	6.5	−1.10

1) *Bull. Earthq. Res. Inst.*, **26** (1948), 91.
2) H. KAWASUMI, "Seismic Intensity and Seismic Intensity Scale," *Zisin* [**i**], **15** (1943), 187, (in Japanese).
3) In J.S.T.
4) "1936" in the previous report is a misprint.
5) Or Fukui.

indicates the effective number of the observations or post-cards sent to our institute. New data concerning the recent earthquakes which occurred after the first report are also included in this report. (They, as well as the former ones, are shown in the Table II.)

Empirical formula connecting the seismic intensity I' and the epicentral distance Δ (unit 100 km) is

$$I'=a+b\Delta \qquad \cdots\cdots\cdots\cdots(1)$$

The coefficients a and b are given in the Table II.

In the figures 1a～12a and 9～12, the ordinate is the seismic intensity, and the abscissa is the epicentral distance in km.

This investigation was guided by Prof. H. Kawasumi as before, to whom the author's hearty thanks are due.

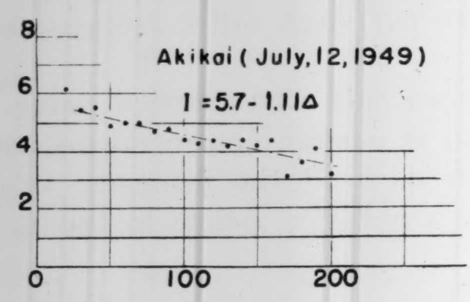

Fig. 9.

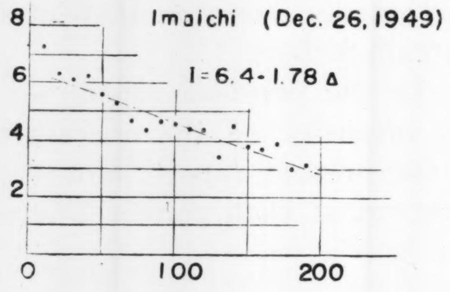

Fig. 10.

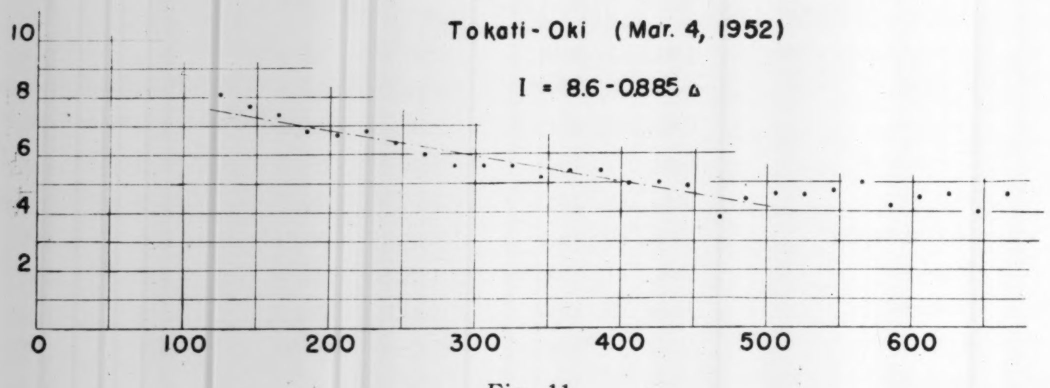

Fig. 11.

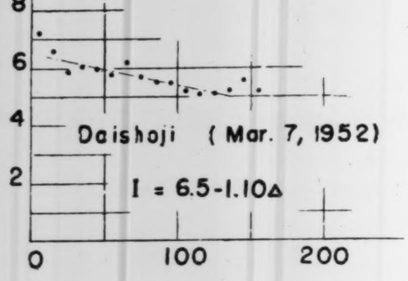

Ordinate; Seismic intensity.
Abscissa; Epicentral distance in km.

Fig. 12.

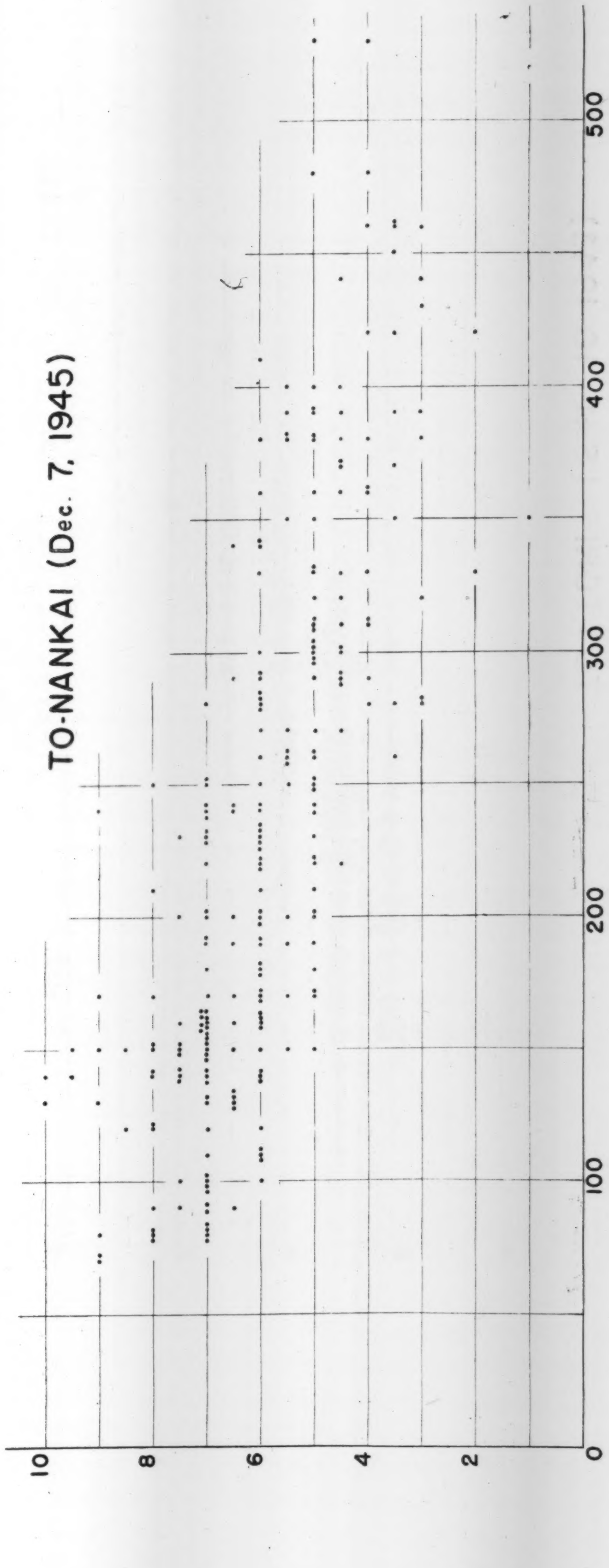

Fig. 1 a.

Ordinate; Seismic intensity. Abscissa; Epicentral distance in km.

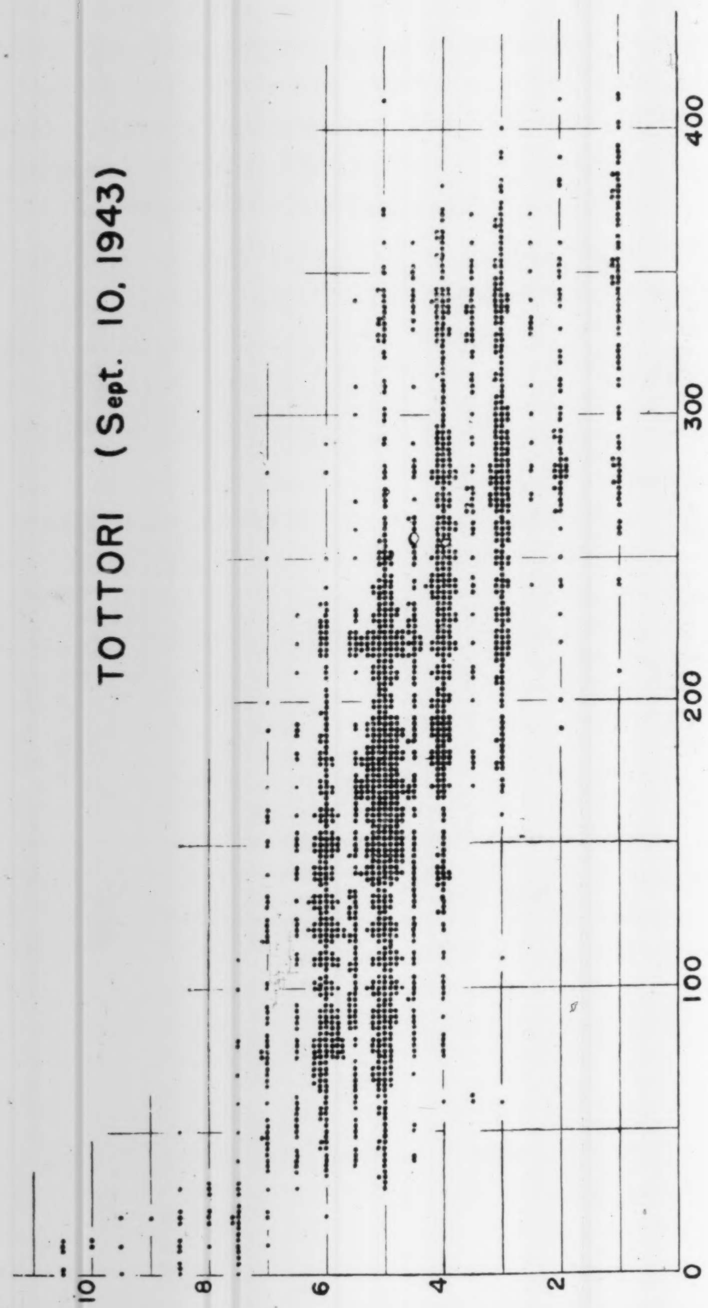

Fig. 2a.

Ordinate; Seismic intensity. Abscissa; Epicentral distance in km.

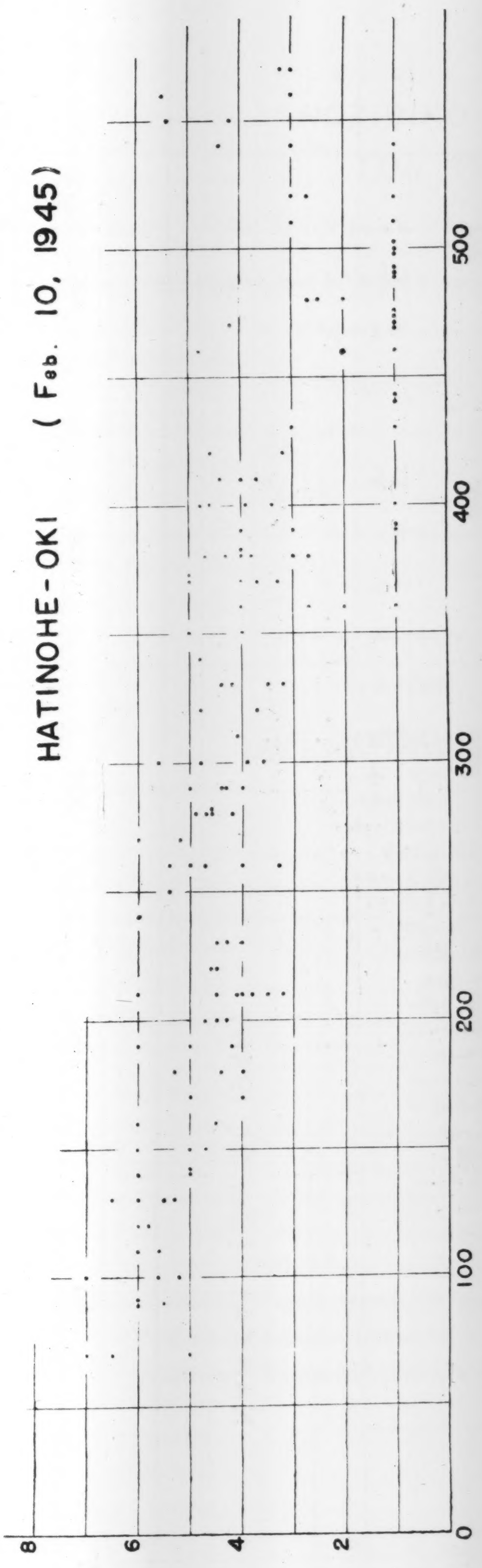

Fig. 3a.

Ordinate; Seismic intensity. Abscissa; Epicentral distance in km.

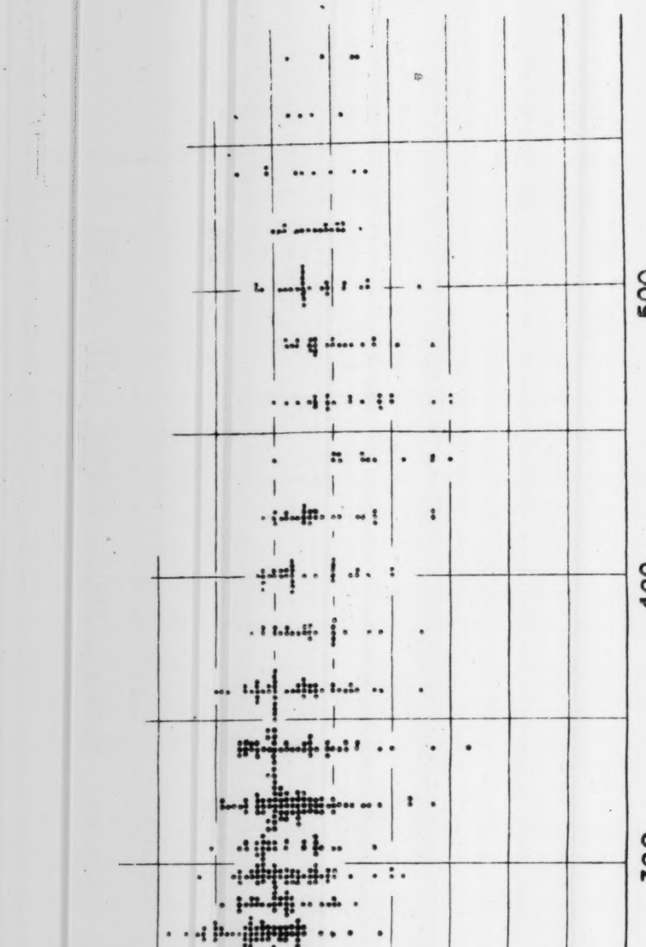

Fig. 4 a.

Ordinate; Seismic intensity. Abscissa; Epicentral distance in km.

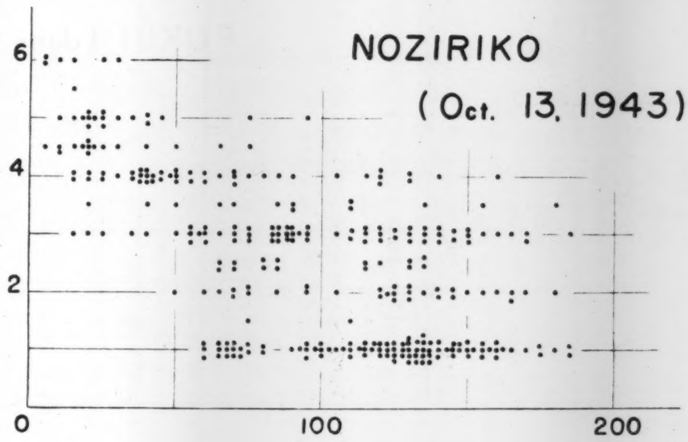

Fig. 5 a.

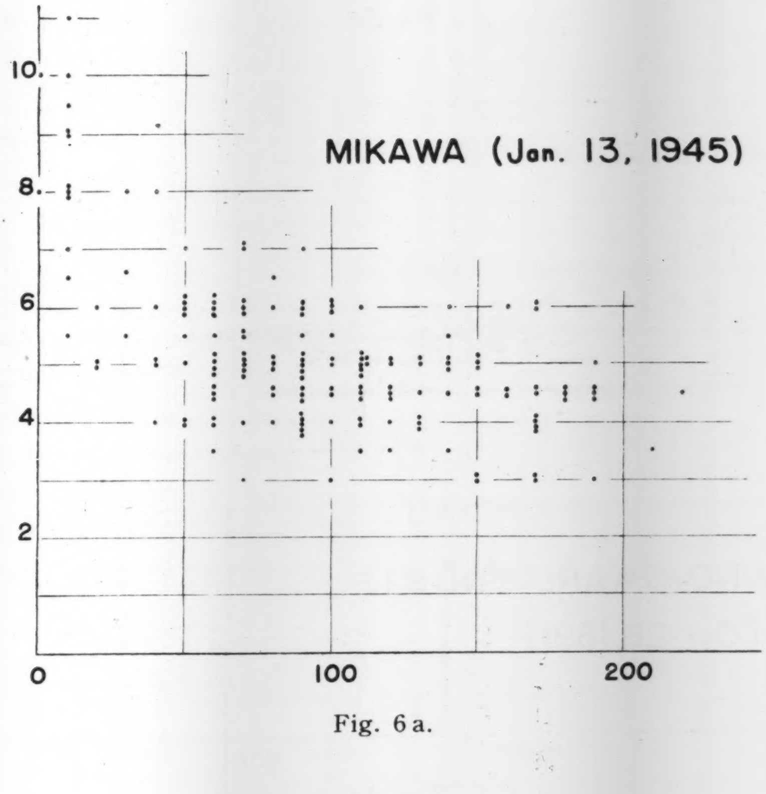

Fig. 6 a.

Ordinate; Seismic intensity.
Abscissa; Epicentral distance in km.

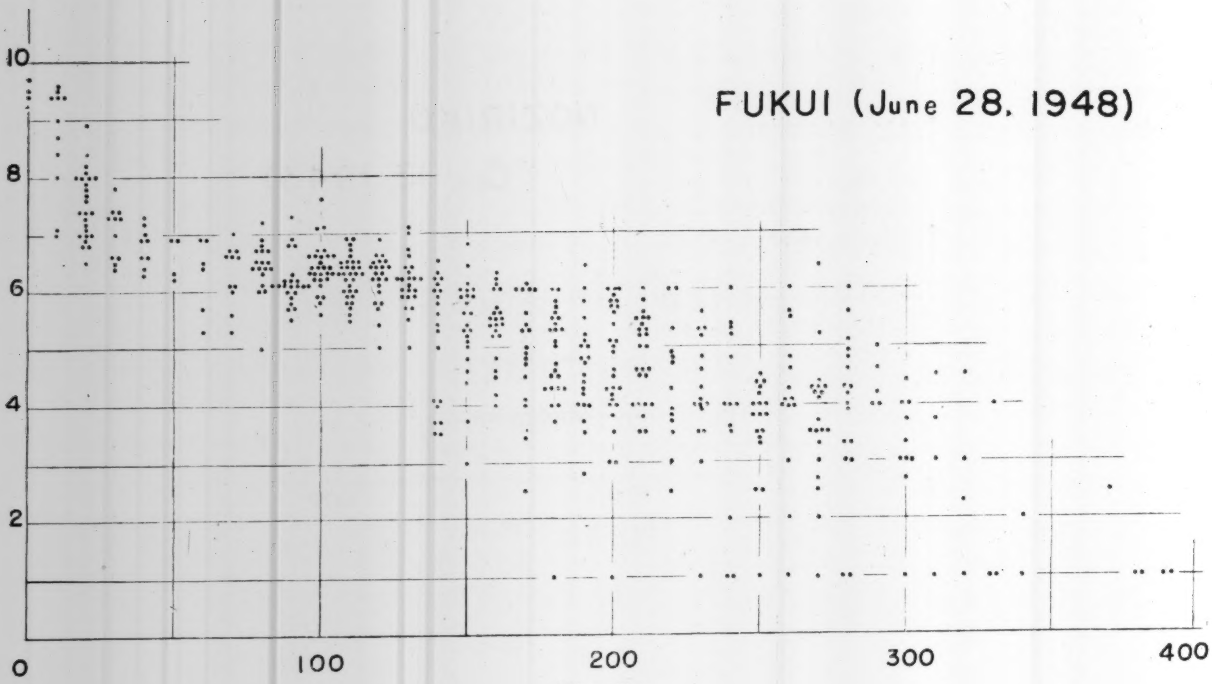

Fig. 7 a.

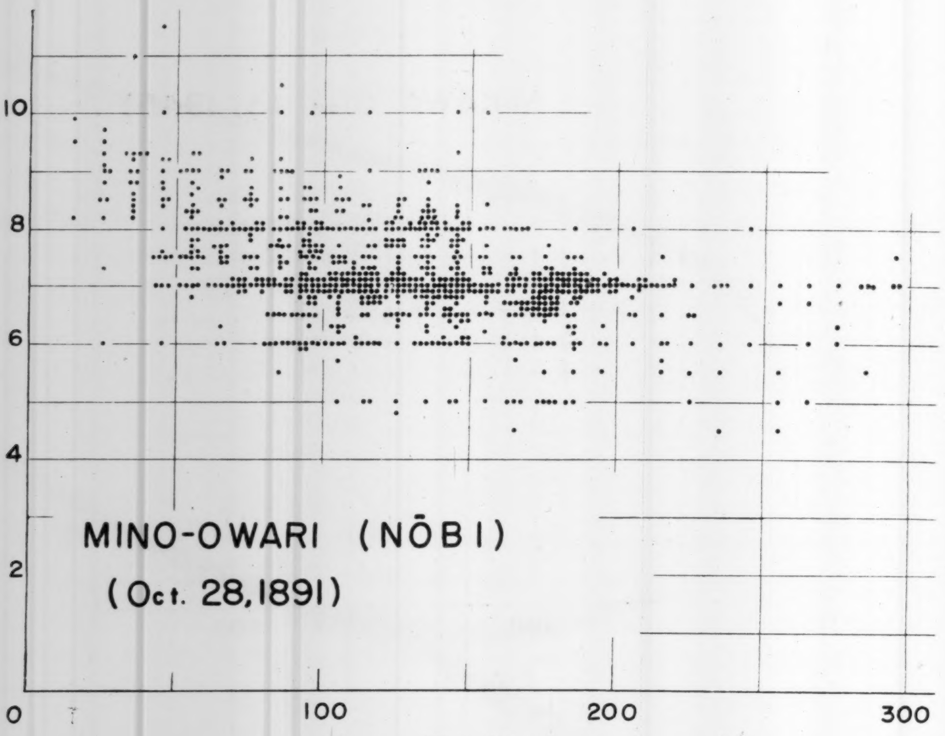

Fig. 8 a.

Ordinate; Seismic intensity.
Abscissa; Epicentral distance in km.

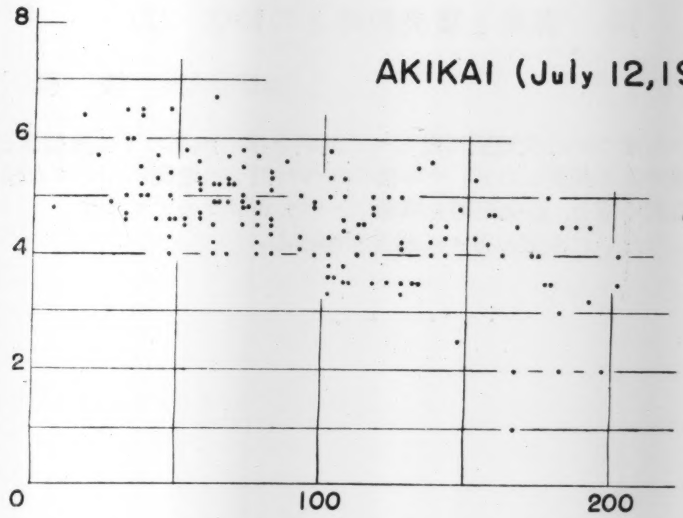

Fig. 9 a.

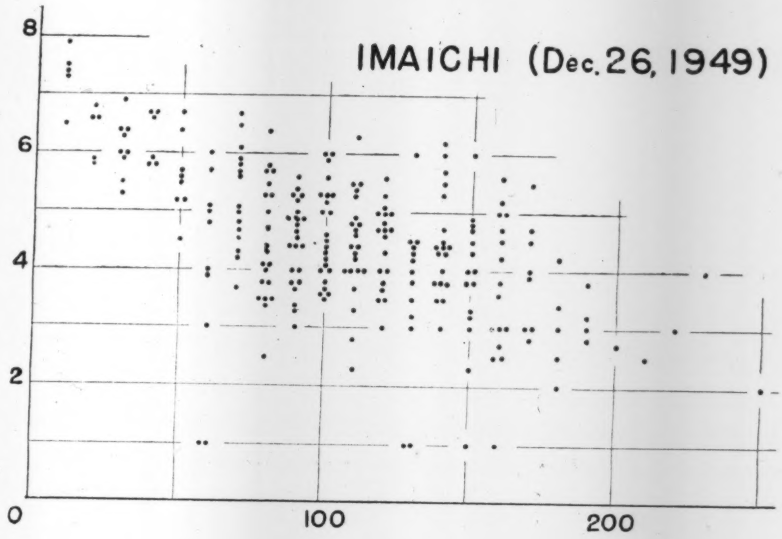

Fig. 10 a.

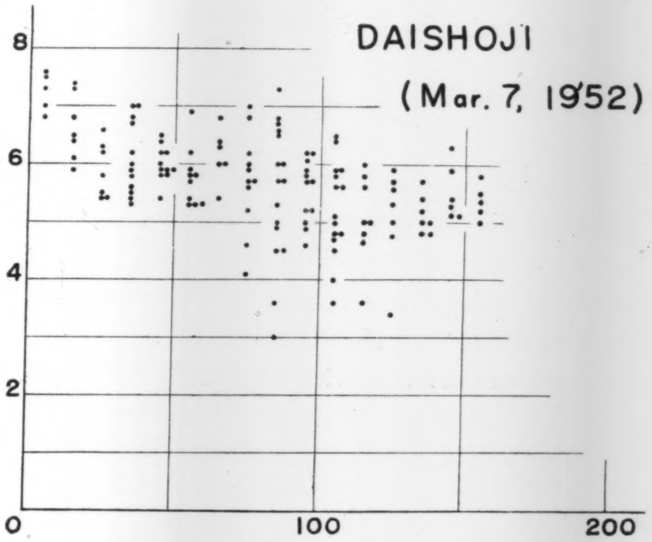

Fig. 12 a.

15. 震度と震央距離との関係 (2)

地震研究所 佐 藤 泰 夫

筆者は最近日本に起つた幾つかの大地震に際して，河角教授の指導の下に通信調査を行つて来た．その結果の一部は既に数年前に発表したが，その後に起つた四つの地震についての結果と，先には発表し得なかつた個々の震度の値を，震央距離を横軸にとつたグラフとして示す．

河角教授及び御協力いただいた多数の方々に感謝を捧げる．

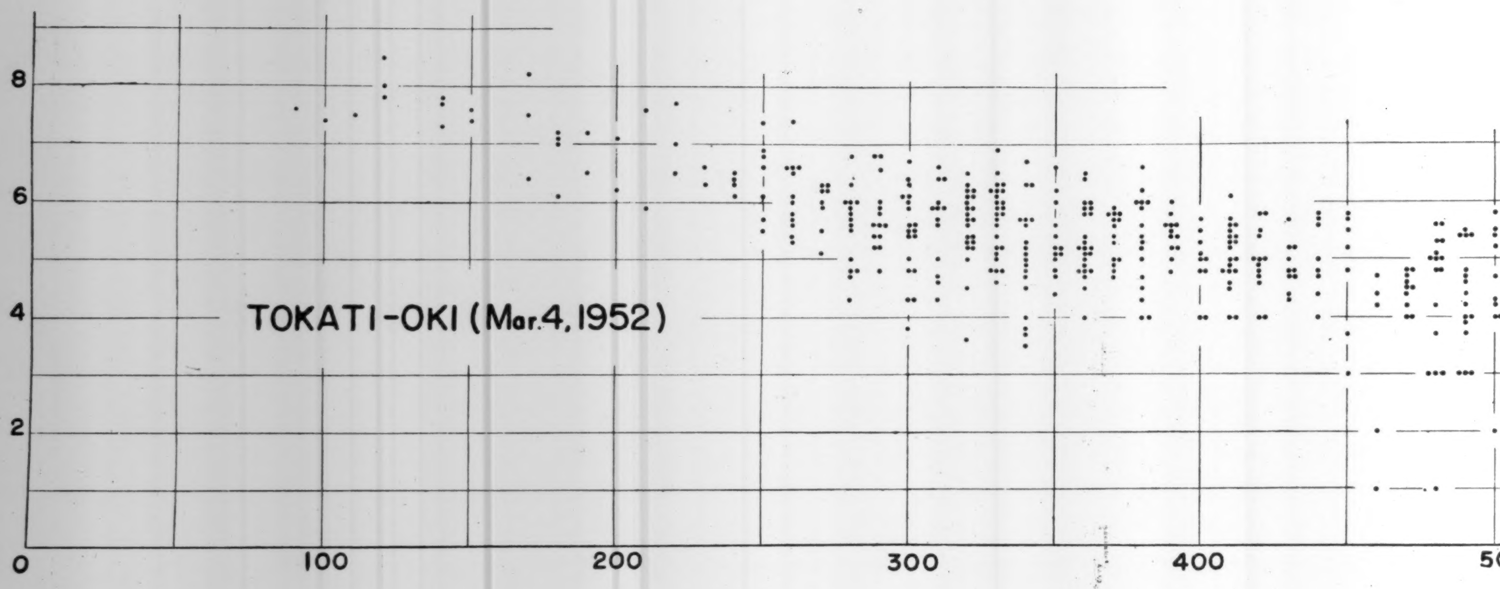

Fig. 11 a.

Ordinate; Seismic intensity. Abscissa; Epicentral distance in km.

（震研彙報 第三十三号 図版 佐藤）

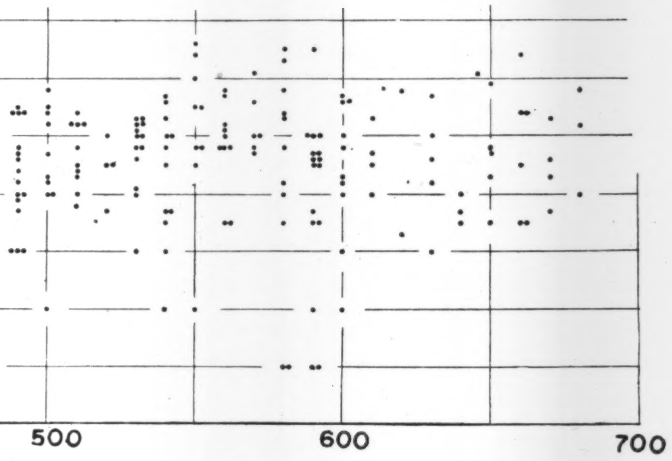

km.

16. *The 1952-1953 Submarine Eruption of the Myôjin Reef near the Bayonnaise Rocks, Japan (I)**.

By Ryôhei MORIMOTO and Joyo OSSAKA,

Earthquake Research Institute.

(Read Oct. 21, 1952, Mar. 17, 1953, and Feb. 22, 1955.—Received Mar. 31, 1955.)

Contents:

I. Introduction
II. History of the eruption
III. Submarine explosions of September 23, 1952
IV. Petrography of the ejecta
V. Summary and conclusion

I. Introduction

The present eruption was first found by the crew of the No. 11 Myôjin-maru, a fishing boat of Yaizu port, Shizuoka Prefecture early in the morning of September 17, 1952, at the sea about 10 km. east of the Bayonnaise rocks, about 420 km. south of Tokyo (Fig. 1). Thereafter, the eruption was recognized by the coastal patrol ship named "Shikiné" of the Marine Safety Board of the Japanese Government. The reef formed by the submarine eruption was named officially as "Myôjin-shô (Myôjin reef)" after the name of the boat of the first eyewitnesses, by the Hydrographic Office of the same Board in September 18.

The Bayonnaise rocks, less than 10 m. in height above sea level, are situated at 31°55.3′N in latitude and 139°54.5′E in longitude (Fig. 52). The rocks rest on the submarine ridge elongating southward from Izu peninsula to the Pacific Ocean, with many other Quaternary insular volcanoes, active or dormant, belonging to the so-called Fuji volcanic zone (Figs. 1 and 2). Near the Bayonnaise rocks, volcanic activities were recorded in our historic times, which are enumerated in the following table (Table I), though we have had no information on the petrographic characters of the rocks except the pumice collected at the time of the submarine eruption near the rocks in 1906[1].

* Dedicated to the Memories of Dr. Risaburô Tayama and thirty other persons who had met with their unfortunate deaths owing to the shock of a severe submarine explosion of the Myôjin reef.

1) T. WAKIMIZU, "The ephemeral volcanic island in the Iwôjima Group," *Bull. Earthq. Invest. Committee*, **22**c (1908), Appendix 31–33.

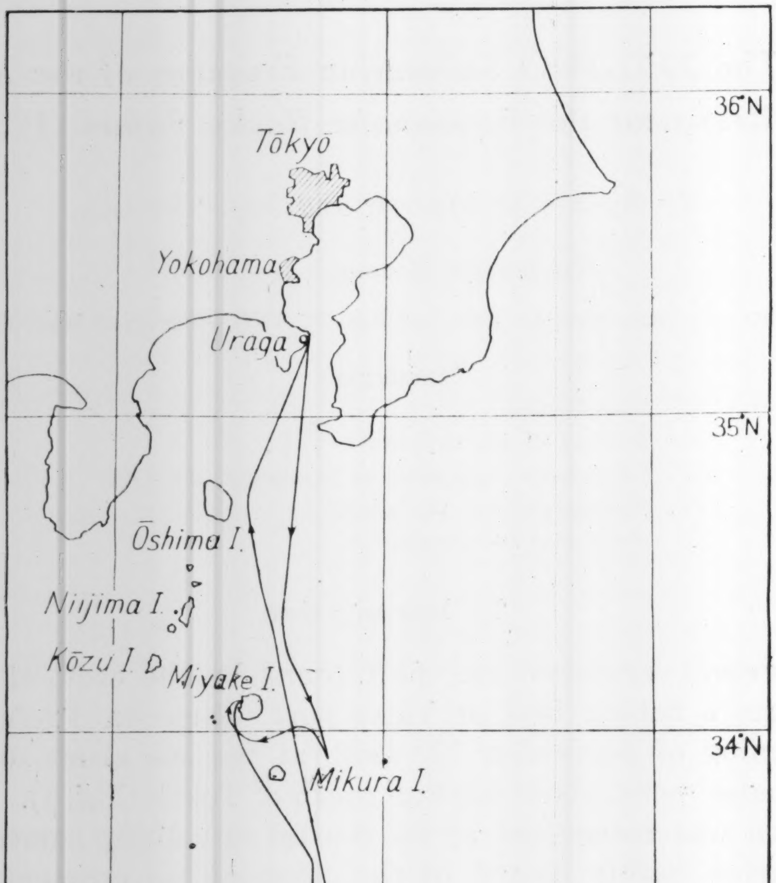

Fig. 1. Geographical situation of the Myôjin reef and the course of voyage of the S. S. Shinyô-maru, Sept. 21–24, 1952.

Table I. Volcanic activities recorded near the Bayonnaise rocks before 1952.

Date of report	Eyewitness	Localities	Remarks
Apr. 14, 1906	Okinawa-maru,*** a submarine-cable vessel of the Department of Communication.	5–8 M southeast of the rocks.	The eruption began abruptly on a day between Apr. 7 and 14. Ash clouds 130–330 m. in heights, 100 m. in dia. Large amount of pumice ejected were floating eastwards with the current covering the sea over an area of two miles in diam[1].
Feb., 1915	Tôtômi-maru	About 6 M east of the rocks****	Bank, 10 m. in depth[2].
Apr., 1915	Ditto	Ditto	Submarine eruption[2].
June 19, 1915	Daikoku-maru, a fishing boat	32°00′N., 140°05′E., about 10 M. northeast of the rocks.	1st belching of smoke at 08h33m. Activity became remarkable at 10h25m in its 6th explosion ejecting mixtures of rock fragments with water blowing up cauliflower clouds, came to a climax at 11h55m, and declined at 12 h 30 m. No evidence of eruption on the next day[3].
	No. 3 Takané-maru, a fishing boat of Yaizu port.	Ditto	Belching of smoke and spray every 20–25 minutes around 09 h. Toward noon activity became larger in scale, high wave due to explosion attacked the deck and the bulwark was broken but the ship could escape the jaws of death. The high wave washed over the Bayonnaise rocks three times[4].
July 1, 1915	Ashitaka-maru, a fishing boat	Southwest of the rocks.	Around 17 h, yellowish smoke spread over 20 km. westwards. Smoke and water spray were rising at about 4 km. southwest of the rocks[3].
May, 1934	No. 2 Shôwa-maru	About 5 M east of the rocks.	Colour of the sea water changed into yellow over an area of 180m. in diam., sulphur-smell[2].

(to be continued.)

Table I. (continued.)

Date of report	Eyewitness	Localities	Remarks
Feb., 1946	British Navy Uranus	31°57′N., 140°01′E.	Birth of an island, 200 m. long, 150 m. in width[2].
Apr., 1946	Arimasan-maru	31°57′N., 140°01′E.	Several islets, including 2 spines about 36 m. in height, appeared[2].
Oct., 1946	No. 80 Sinkô-maru	Ditto	An island 100 m. high was observed[2].
Dec., 1946	U. S. Force broadcasting	Ditto	The island disappeared. Waves break on the bank[2].

On the "Izu Shichitô Shi" and "Hachijô Senkyô Shi", it is described that in May, 1870, an islet was born about 25 "ri" (probably nautical miles) southeast of Aogashima (Personal communication from Mr. Y. Tsukamoto of the Hydrographic Office and F. OMORI, *op. cit.*, 120).

In 1896, British S. S. Linjisfahrn* found the reef on which the waves broke at the sea about 7.5 M** north of the Bayonnaise rocks[2]. * Rewritten in occidental spelling from the Japanese literature. ** M: Nautical mile. *** A suffix "-maru" in Japanese means ship or boat. **** According to the survey of the Hydrographic Office in 1925, no reef or bank was recognized thereabout[2].

1) T. WAKIMIZU, *loc. cit.*, 2) R. MITA, *Hydrographic Bulletin* **12** (1946), 57–62, (in Japanese), 3) F. OMORI, *Rep. Imp. Earthq. Invest. Committee*, **86** (1918), 114, (in Japanese), 4) Y. TSUKAMOTO, "On the No. 3 Takané-maru attacked by the submarine explosion at the 1915-eruption near the Bayonnaise rocks", *Monthly Meeting of the Earthq. Res. Inst.*, (May 24, 1955).

It is still fresh in our memory that an ephemeral island was found in February, 1946 owing to the submarine eruption which took place at approximately the same position as the locality of the present eruption.

Bottom configuration in the vicinity of the Bayonnaise rocks according to the bathymetric chart No. 81 of the Hydrographic Office is shown in Fig. 2. Ryôichi Mita, a geographer of the Hydrographic Office who embarked on the missing boat "No. 5 Kaiyô-maru", had already pointed out that the Bayonnaise rocks were a portion of the wall of the crescent-shaped caldera of large scale, up to 10 km. in its diameter, and that the island ephemerally formed at the 1946-eruption might be one of the two or more tholoides built on the submarine double volcano[2]. However, we have still no satisfactory data on the submarine topography of the volcano, leaving room for further discussions on the shape and structure of the submarine volcano.

Submarine eruptions had often been observed in Japan, such as the

2) R. MITA, "The submarine volcanic activities near the Bayonnaise rocks", *Hydrographic Bulletin*, **12** (1946), 57–62, (in Japanese).

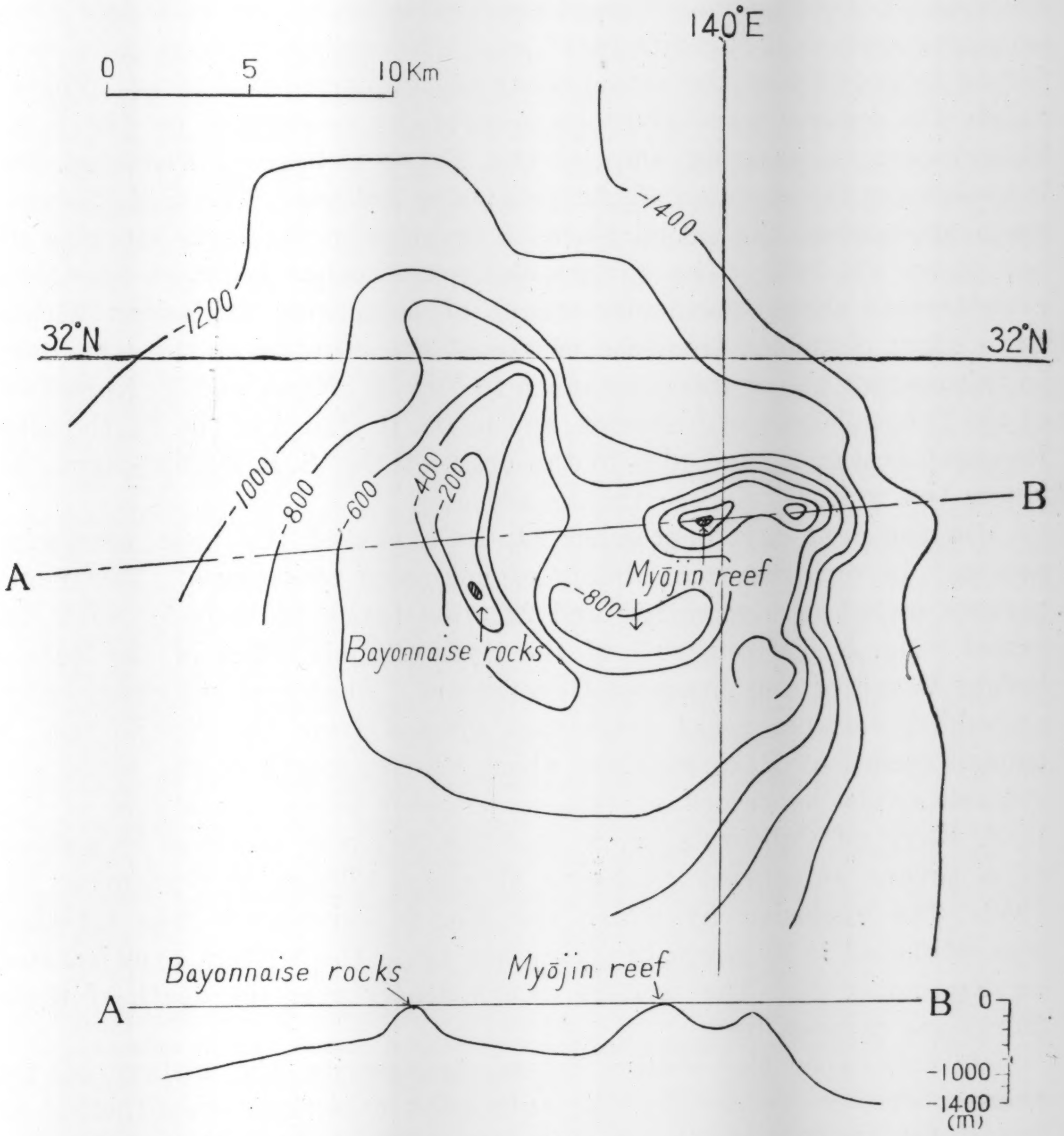

Fig. 2. Bottom configuration near the Bayonnaise rocks (after the bathymetric chart No. 81 of the Hydrographic Office, Marine Safety Board, the contour lines being drawn by the writers.)

1904 and 1914 eruptions east of South Sulphur Island[3], **the 1934–1935**

3) T. WAKIMIZU, *op. cit.*, 1–30.

T. OGURA, "The eruption of Shin Iwô-jima", *Rep. Imp. Earthq. Invest. Commitee*, **79** (1915), 4–15, (in Japanese).

T. TERADA, "On the recently appeared islands near South Sulphur Island", *Tôyô Gakugei Zassi*, **31** (1914), 149–158, (in Japanese).

eruption of Iwôgashima, Kagoshima Prefecture[4], the 1870 and 1916 eruptions southwest of Smith reef[5], etc. Nevertheless, it is quite rare for us to eyewitness the actual scene of submarine explosions. Fortunately the writers were given an opportunity to embark on the S. S. Shinyô-maru, a training ship of the Tokyo College of Fisheries, for investigating the eruption of the submarine volcano. The S. S. Shinyô-maru approached the actual place of eruption in the early morning of September 23, 1952. The writers along with other Japanese scientists eyewitnessed three spectacular scenes of submarine explosions within quite short distances from the centre of the eruption on the same day. In this matter, the writers owe much to Drs. H. Niino and T. Kumakori of the Tokyo College of Fisheries, and to Dr. H. Tsuya of the Earthquake Research Institute, and also to the crew of the S. S. Shinyô-maru, to whom the writers' sincere thanks are due.

On the next day, September 24, 1952, one of the most sorrowful accident in our research history of volcanoes took place: Thirty-one persons including 9 scientists and 22 crew threw in their lot with the vessel "No. 5 Kaiyô-maru" of the Hydrographic Office of the Marine Safety Board of the Japanese Government. Shattered wreckage with embedded volcanic rocks fragments ejected from the Myôjin reef, a tunami record at Hachijô Island about 130 km. north of the volcano, a volcanic explosion record at two underwater listening stations of the U. S. Navy off California, show that the ship was attacked by a shock of a severe submarine explosion at about 12h20m on September 24, 1952. The explosion by which the No. 5 Kaiyo-maru was attacked was estimated to be larger in scale than those the writers eyewitnessed on September 23. The writers mourn deeply over the death of these thirty-one persons here.

In this paper the writers intend to describe the history of the present eruption especially the submarine explosions eyewitnessed on September 23, 1952 and the petrography of the ejecta, a new petrological information on the submarine volcano.

In collecting the data on the history of the eruption, the writers owe much to the staff of the Hydrographic Office. The writers express their cordial thanks to Dr. Kanji Suda, Director of the Hydrographic Office and to Mr. Yûshirô Tsukamoto, Chief of the Astronomical Section

4) H. TANAKADATE, "Preliminary note on the volcanic eruption of Iwôgashima, Kagoshima Prefecture, Japan", *Bull. Volcanological Soc. Japan*, **2** (1935), 188–209, (in Japanese).

5) R. MITA, *loc. cit.*

of the same Office. In estimating the depths of the underwater explosions, the writers were kindly instructed by Professor Fuyuhiko Kishinouye of the Earthquake Research Institute to whom their sincere thanks are due. To Messrs. S. Hanzawa, K. Osawa, J. Kusaka, and R. Sugano of the Asahi Press, and to Messrs. F. Kojima, D. Miwa, Z. Ishii, T. Takei, T. Isoyama, C. Haraikawa, and T. Isa of the Yomiuri Press. The writers owe much for the use of their fine photographs. A part of the expenditure necessitated for the investigation was defrayed from the Funds for Scientific Researches of the Ministry of Education.

II. History of the eruption

In cases of submarine eruptions the opportunities for observations at sea are quite restricted. The present eruption, as well as other ones of this sort, is not an exceptional case: it occurred near a remote uninhabited islet always washed by the ocean current[6]—the Bayonnaise rocks; continuous and systematic observation of the actual scene of the activity could not be expected under such surcumstances. Indeed, the only thing the writers could do was to collect scatttering data on the activities obtained by many different eyewitnesses in describing a course of the present submarine eruption. The following table (Table II) concerning the history of the eruption was compiled by the present writers from the data chiefly collected at the Hydrographic Office of the Marine Safety Board[7], the Central Meteorological Observatory[8], and the Tokyo College of Fisheries[9], with other random observations by aeroplanes, regular liners, fishing boats, etc., in addition to the writers' own data.

It was reported by Dietz and Sheehy that the U.S. Navy SOFAR

6) Kuro-shio counter current.

7) MARINE SAFETY BOARD, Memoir of the investigations on the causes of disaster of the No. 5 Kaiyô-maru, 1953, (in Japanese).

Y. TSUKAMOTO, "Record of the eruptions of Myôjin-sho (1952–1953)", *Hydrographic Office, Tokyo, Japan*, April 14, 1954.

8) A. SUWA, "Submarine eruption of Myôjin reef", *Jour. Geography*, **62** (1953), 102–104; (in Japanese).

WADATI and SUWA, "The observation of the 1952 eruption of the Myôjin reef aboard aeroplanes", *Quart. Jour. Seismology*, **17** (1953), 71–77. (in Japanese)

S. MIURA, "The observation of the eruption of the Myojin reef aboard the weather ship, Chikubu-maru", *Ditto* 79–82 (in Japanese).

T. HOSHI, "Observation of Myojin reef aboard weather ship, Shiga-maru", *Ditto* **18** (1953), 41–42 (in Japanese).

9) TOKYO COLLEGE OF FISHERIES, "Report on the submarine eruption of Myôjin-sho", *Jour. Tokyo Coll. Fisheries*, **40** (1953), Special Number.

Table II. History of the 1952–1953 eruption of the Myôjin reef.

Date of observation	Eyewitness or author	Remarks
Sept. 16, 1952	SOFAR Tsunami record at Hachijô island	(0040, 0912, 1031, 1152, 1410, 1752, 1940) (1152)
Sept. 17, 1952	No. 11 Myôjin-maru	(0715) The eruption was first found, 32°10′N, 140°00.5′E, 17′ NNE of the Bayonnaise rocks. Ash clouds rose up to 500 m. Colour of the sea water near the reef changed into yellow.
	"Mercury" an aeroplane of Japan Air Line	(1839–1857) A new island, 120 m. long, 80 m. wide, 30 m. high was observed. 2 vents, several explosions every minute, ash cloud rose 200–1,000 m., red-hot lava was recognized.
	No. 5 Syôsei-maru, a fishing boat	(1829, 1830, 1840) Explosions every 3–5 minutes, ash columns 200 m high, were observed, red-hot lava flowed down into the sea.
	SOFAR	(0304, 0611, 1951, 2230)
Sept. 18, 1952	"Shikiné," a coastal patrol ship	(0900) Minor explosion. New island 150 m. in NS, 100 m. in EW, 30 m. in height was situated at 31°56.7′N, 140°00.5′E. Yellow sea current runs toward SSW. (Ca. 1000) Minor explosions repeated every 0.5–2.0 minutes (Fig. 8).
	"Wakakaze" an aeroplane of Asahi Press	(Ca. 1100) Ash cloud rose remarkably. Size of new island was larger than the Bayonnaise rocks (Fig. 9).
	"Venus" an aeroplane of Japan Air Line	(Ca. 1800) Minor explosions several times every minute, ash cloud rose 3,000–4,000m. high, 2 vents, with several ventlets, size of the island was same as above (Fig. 10).
	SOFAR	(0120, 0323, 0327, 0444, 0526, 0621, 0704, 0803, 0920, 1712, 1735, 1844, 1946, 2005, 2131)
Sept. 19, 1952	SOFAR	(0029, 0425, 0902, 1015, 1240, 1436, 1639, 1805, 2048, 2057)
Sept. 20, 1952	Ditto	(0613, 1312, 1400, 1649, 1819, 1850)
Sept. 21, 1952	Chikubu-maru of Central Meteorological Observatory	(Ca. 1700) Explosions every 3–5 minutes. (1734) Large explosion. Island could not be recognized.
	SOFAR	(0111, 0213, 0447, 0529, 1400, 1433, 1507, 1737, 2324)
Sept. 22, 1952	Soyokaze, aeroplane of Asahi Press	(Ca. 0900) Great explosion (Figs. 11–12).

(to be continued.)

Table II. (continued.)

Date of observation	Eyewitness or author	Remarks
Sept. 22, 1952	US Air Force	(Ca.1200) Several small rocks, several metres in diam. and in heights, were observed on the sea.
	Shinyô-maru	(1505) An explosion was observed from Hachijô island. (2345) Night view of an explosion was observed during voyage to the Myôjin reef.
	SOFAR	(0341, 0653, 0914, 1237, 1530, 1931, 2027, 2345)
Sept 23, 1952	Shinyô-maru	(0834, 1312, 1340, 1900) Severe submarine explosions. Cf. Chapter III of this paper. Volcanic island had almost collapsed down into the sea. Only 2 or 3 small rocks, 1–2 m. high were left appearing on on the sea (Fig. 13–51).
	SOFAR	(0025, 0828, 1143, 1308, 1335, 1901, 1914, 2233)
	Wave recorder at Hachijô island	Tsunami ? considered to have been related to the explosion of (1312) was recorded during (1350–1425).
Sept. 24, 1952	No. 18 Umikata-maru	(0540) Great explosion, 10'E of the Bayonnaise rocks. Island had disappeared.
	Inhabitants in Aogashima island	Explosion was heard early in the morning. At noon, two columns of ash cloud rising from the Myôjin reef were observed, east one continuosly and other west one intermittently.
	Wave recorder at Hachijô island	A conspicuous tsunami was recorded (1253–1408), related to the explosion which presumably occurred between (1219–1231).
	SOFAR	(0148, 0539, 0552, 1221)
Sept. 25, 1952	Weather station at Hachijô island	(0500) Ash fell.
	No. 3 Nisshô-maru, a fishing boat	(1330?, 1830) Severe explosions.
	SOFAR	(0618, 1316, 1823)
Sept 26, 1952	Muroto and Shikiné, coastal patrol ships	(1235) Quite severe explosion with ash fall over wide area (Fig. 53 a–b).
	Weather station at Hachijô island	Tsunami-record (1303–1438) related to the explosion (1235).
	SOFAR	(0104, 1234)

(to be continued.)

Table II. (continued.)

Date of observation	Eyewitness or author	Remarks
Oct. 3, 1952	Muroto, a coastal patrol ship	(0545) Explosion. (0800) Explosion.
Oct. 11, 1951	Ditto	(0700) Island, 150 m. wide, 200 m. long, with three peaks, 80 m. above sea level at the highest point. Ash cloud rose up to 105m.
Oct. 21, 1952	No. 5 Shôsei-maru	(2150) Minor explosion. Island 30 m. high above sea level was observed.
Nov. 7, 1952	US Air Force	(Ca. 1200) Remarkable ash cloud. Island 30 m. high was recognized.
Nov. 12, 1952	Tonan-maru of Tokyo Metropolice	Two islands were observed.
Nov. 17–18, 1952	Awaji-maru of Tôkai-kisen Co.	Ash cloud and vapour emission. Ash cloud rose up to 500–600 m.
Nov. 24, 1952	No. 12 Daikoku-maru, a fishing boat	Emission of black cloud in the early morning. An island 300 m. long and 100 m. high was observed at 31°54′N., 140°02′E.
Dec. 9, 1952	Tonan-maru of the Fisheries Experiment Station, Tokyo Metropolitan Government	White vapours were emitted from whole island of 200 m. in diam., 50 m. in height. Small rock several metres above sea level was found 100? m. south of the island.
Dec. 13–14, 1952	Inhabitants of Aogashima island	Smoke-like ash cloud was found far above the Myôjin reef.
Dec. 16, 1952	Kyôei-maru, Fisheries Experiment Station, Chiba Prefecture	A volcanic island about 50 m. high emitting smoke was recognized.
Dec. 27, 1952	Aeroplane (No. 103) of Yomiuri Press	A volcanic island was recognized (Fig. 54).
Jan. 19, 1953	Genkai, a coastal patrol ship	An island was observed whose north and south peaks were 94m. and 56m. in heights respectively. Vapours were emitted along the shore of the island.
Feb. 1, 1953	Umitaka-maru, a training ship of Tokyo College of Fisheries.	A volcanic island surrounded by steep cliff, 220 m. in NW–SE, 151 m. in NE–SW was recognized. It consisted of two peaks, north spine (93.8 m) and south dome (54.8 m). Vapours were emitted from the summits of the island. The sea water was not so stained with the volcanic materials (Fig. 55).
Feb. 6, 1953	No. 2 Seiju-maru, a fishing boat	(1500) Explosion. Column of dark ash cloud 100 m. in dia. rose up to 200 m. high.
Feb. 7, 1953	Asakaze, an aeroplane of Asahi Press	The island about 90 m. above sea level was found. The sea water east of the island changed into yellowish green over an area of 1 mile in diam.

(to be continued.)

Table II. (continued.)

Date of observation	Eyewitness or author	Remarks
Feb. 8, 1953	No. 103 aeroplane of Yomiuri Press	(1020–1040) The island elongating in N–W direction had two peaks and no crater. North one was higher. Vapours were emitted between the two peaks (Fig. 56).
Mar. 3, 1953	Aogasima island	Emission from the Myôjin reef became remarkable.
Mar. 6, 1953	"Muroto", a coastal patrol ship	(Ca. 1200) Height of the island was 120 m. Vapours were emitted from whole island.
Mar. 9, 1953	Temporary observatory at Aogashima (Telescope) by the Hydrographic Office	Successive explosions began.
Mar. 10, 1953	No. 1 Kinsei-maru	Remarkable ash cloud probably at the great explosion of the Myôjin reef.
Mar. 11, 1953	No. 103 aeroplane of Yomiuri Press	(Ca. 1500) The island had disappeared into the sea. No subaerial emissions of ash or vapour. The sea water changed into yellowish colour over an area of 2 km. wide, 4 km. long (Fig. 57).
Mar. 17–18, 1953	Temporary observatory at Aogashima	Great explosion.
Mar. 18, 1953	No. 6 Sumiyoshi-maru and Enoshima-maru, fishing boats	(Ca. 1510, 0750, 1020) Submarine explosions with large water columns and explosion clouds.
	No. 5 Shôsei-maru and Kan'ei-maru, fishing boats	(1000–1540) Several great submarine explosions. Column of water with ash up to 1 km. in diam. (Ca. 1900) Explosion.
Mar. 17–25, 1953	Wave recorder at Hachijô island	Tsunamis were recorded intermittently.
Mar. 25, 1953	US Air Force	(1400) Submarine explosion, explosion cloud 900 m. high, 100 m. in diam.
Mar. 28, 1953	Tonan-maru, Fisheries Experiment Station, Tokyo Metropolitan Government	(1530) Remarkable rising of white smoke. No explosion, no island.
Mar. 30, 1953	Temporary observatory at Aogashima island	Explosion of quite large scale.
Apr. 1, 1953	Kuro-shio-maru, a regular liner of Tôkaikisen Co.	(0540–1700) Explosion clouds were seen in the long distance south of Aogashima from Hachijô island.
	A lighthouse at Hachijô island.	(Ca. 1500) Clouds rising every several minutes were observed.

(to be continued.)

Table II. (continued.)

Date of observation	Eyewitness or author	Reference
Apr. 1, 1953	Horawazawa, Hachijô island.	Three columns of clouds of which easternmost one was largest, were visible.
Apr. 2, 1953	Torishima Weather Station	(1100–1500) Successive emissions of ash and vapour.
	A lighthouse at Hachijô island.	(1300–1600) Ash clouds were recognized in the same direction as preceding day.
Apr. 3, 1953	Hachijô Meteological Observatory	(Ca. 0100–0700) Weak tsunamis were recorded intermittently at the island.
Apr. 5, 1953	U. S. Air Force	An island about 1/4 sq. mile in area, 200 ft. in height, was recognized at 31°53′N., 140°10′E. (0941) Ash cloud was seen. Dark-reddish sea water containing pumice ran from the Myôjin reef.
Apr. 14, 1953	Shikiné and Genkai, coastal palrol ships	At 31°56.7′N., 140°10′E., an island 200 m. long in NE, with three peaks of equal heights 46 m above sea-level was recognized (Fig. 58 a).
	U. S. Air Force	Water stained into yellowish colour with volcanic material are drifting southwestward from the Myôjin reef (Fig. 58 b).
May 3, 1953	Shiga-maru of the Central Meteorological Observatory	An island, about 70 m. in height, about 250 m. in long diameter, 150 m. in short diameter was found. Fumarolic action was observed at the SSE margin of the islet.
May 9–21, 1953	Temporary observatory at Hachijô island, of the Hydrograhic Offiice.	An island with two peaks about 43 m. high, 151 m. wide, was seen. A western half of the island was covered by vapours. Situation of the Northeastern peak was at 31°56′40″N., 140°0′26″E.
May 14, 1953	U. S. Air Force	A volcanic island was recognized.
May 26, 1953	Temporary observatory at Aogashima of the Hydrographic Office	Weak sounds of explosion were heard.
July 17, 1953	Ryôfû-maru of the Central Meteorological Observatory	A volcanic island with dome was recognizable. No explosion cloud was observed.
July 18, 1953	Sakaé-maru, a fishing boat	Five rocks were visible on the sea surface.
July 23, 1953	Nikkô-maru, a fishing boat	A lava spine associated with two rocks on its southern side. Vapour was rising between the two.
Aug. 12, 1953	Temporary observatory at Aogashima of the Hydrographic Office	Size of the island became small, about half compared with that in May. Clouds were visible at the vent.

(to be continued.)

Table II. (continued.)

Date of observation	Eyewitness or author	Reference
Aug. 17, 1953	Ditto	Amount of the vapour rising from the reef increased.
Aug. 18, 1953	U. S. Air Force	The reef was in its eruption: ash cloud rose up to about 500 m. high.
Aug. 24, 1953	Temporary observatory at Aogashima of the Hydrographic Office.	(0600–0700, 1000) Ash clouds rose in a great scale from the reef. The island was invisible. (1400) Cloud rising from the island became white vapour.
Aug. 24, 1953	Tomihisa-maru, a fishing boat	(1300) Large explosion.
Aug. 26, 1953	Umitaka-maru, a training ship of the Tokyo College of Fisheries	(2200) Red-hot lava was pouring into the sea and the ash of andesitic composition was falling.
Aug. 27, 1953	Ditto	(Ca. 0100) Explosive cloud rose up to several thousand metres into the sky. An island about 200m. in width, unknown height, was visible.
	Kongô maru, a fishing boat	An island showed explosive action.
Aug. 27–28, 1953	Temporary observatory at Aogashima of the Hydrographic Office	Explosive ash cloud arose on a large scale.
Aug. 30, 1953	Eikichi-maru, a fishing boat	(Ca. 0515) Great explosion with remarkable ash column.
Sept. 1, 1953	Temporary observatory at Aogashima of the Hydrographic Office	(0730) Explosion. (1300–1400) Explosion ejecting remarkable ash and sand. Ash columns being 250m. in diameter, 500m. in height.
Sept. 3, 1953	No. 12 Tomihisa-maru, a fishing boat	Explosion clouds were visible, no island was seen except breakers observed at two points thereabout. Water changed into yellowish colour being stained with volcanic material drifted SSW-wards.
Sept. 16, 1953	Temporary observatory at Aogashima of the Hydrographic Office	N o island was visible.
Sept. 17, 1953	No. 5 Sansha-maru, a fishing boat	Ash cloud was rising from the sea, no island being found. Sea water changed into yellow in colour owing to drifting volcanic material.
Sept. 27, 1953	Hakuyô-maru, a fishing boat	The water was anged into white in colour, NNE of the Bayonnaise rocks.
Oct. 5, 1953	S. F. Baird, research vessel of Scripps Inst. of Oceanography	No projecting rock or evidence of euption. Presence of a bank at slight depth.

(Sound Fixing and Ranging) Stations at Point Sur and Point Arena, California had received 76 signals due to submarine explosions at the Myôjin reef during the 11 days from September 16 to September 26, 1952[10]. According to the records at the underwater listening stations off California, the Myôjin reef had already been in her active state since the early morning of September 16, 1952 before the first discovery of the present eruption by the crew of the No. 11 Myôjin-maru at about 07h25m on the next day.

Several tsunamis which must have been derived from submarine explosions at the Myôjin reef were recorded by a wave recorder installed near Yaené port on Hachijo island, about 130 km north of the reef[11]. The wave recorder caught the tsunami of this sort at 12h20m during its operation from 10h55m to 15h33m on September 16, already. On the same day at 11h52m, a microseism whose maximum amplitude being 5 μ and mean period being 4.1 seconds was felt at the island. The microseism was said to have travelled from the same source of the above-mentioned tsunami, therefore Nakano estimated a travel time of these tsunamis being 28 minutes[12]. A tsunami corresponding to the explosion observed by the crew of No. 11 Myôjin-maru was eyewitnessed by some fishers at Hachijo island in the morning of September 17[13]. The wave recorder was not in continuous operation unfortunately. Dietz assumed the transpacific travel time of the underwater sounds being 1 hour 37 minutes 32 seconds in obtaining the origin time from the SOFAR records[14]. In the foregoing table (Table II), each "time" indicated by a number of the four figures bracketed such as (0834), (1312), etc., means a time of explosion or of observation at or near the Myôjin reef shown by the Japanese Standard Time, the above-mentioned travel times being taken into consideration.

As revealed in the above table (Table II), the submarine volcano repeated three times its emergence and submergence during the present eruption. Appearance and disappearance of the ephemaral island is fur-

10) MARINE SAFETY BOARD, *Ibid.*, 107–110.

R. S. DIETZ and M. J. SHEEHY, "Transpacific detection of Myojin volcanic explosions by underwater sound", *Jour. Oceanogr. Japan*, **9** (1953), 53–83. *Bull. Geol. Soc. Amer.*, **65** (1954), 941–956.

11) MARINE SAFETY BOARD, *op. cit.* 74–77.

12) MARINE SAFETY BOARD, *op. cit.* 74.

S. UOKI and M. NAKANO, "On the Cauchy-Poisson waves caused by the eruption of a submarine volcano", *Oceanogr. Mag.*, **4** (1953), 119–141.

13) MARINE SAFETY BOARD, *op. cit.* 75.

14) DIETZ R. S. and M. J. SHEEHY, *Bull. Geol. Soc. Amer.*, **65** (1954), 947.

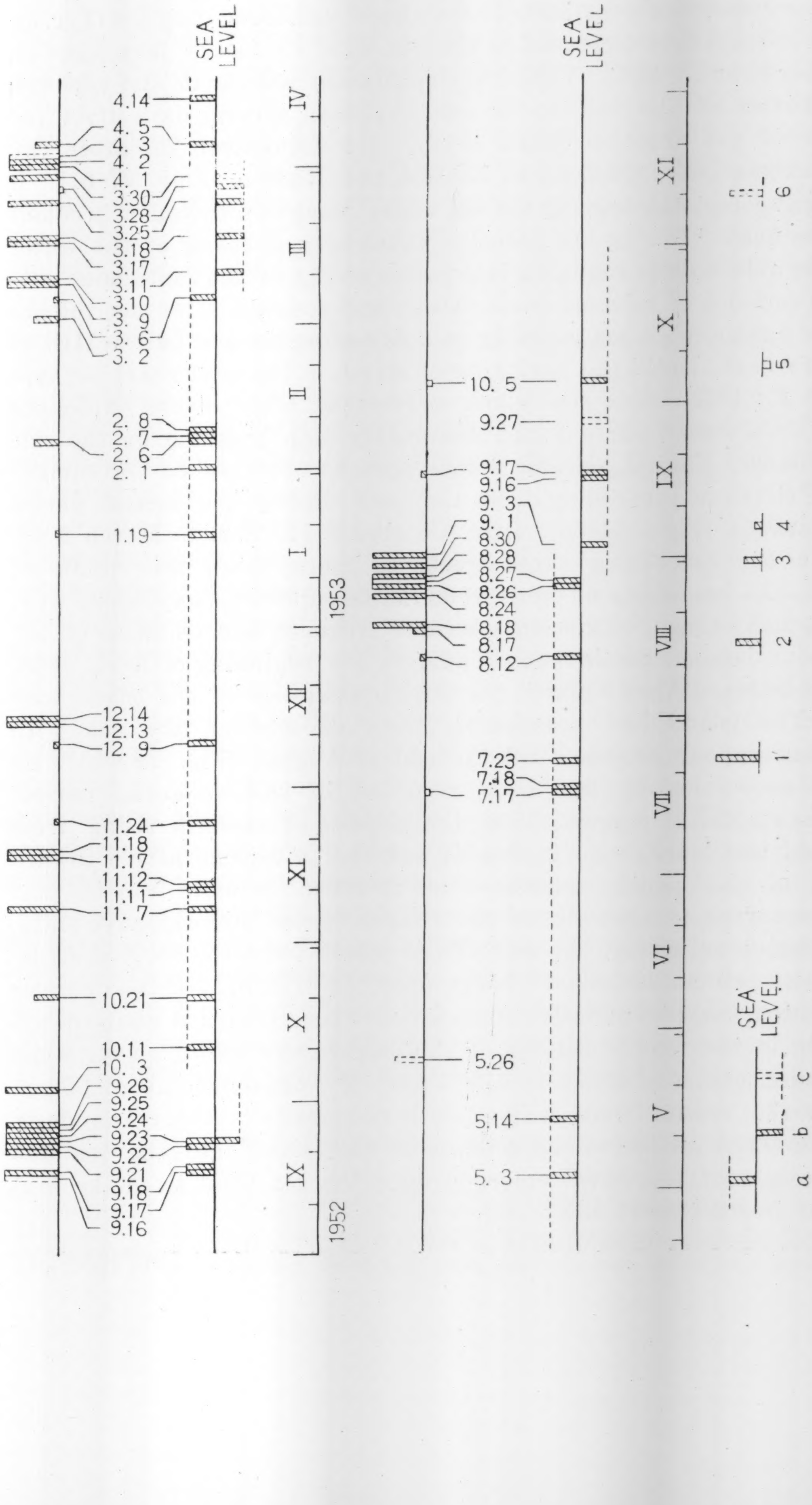

Fig. 3. Schematic representation of the 1952–1953 eruption of the Myôjin reef. a–c indicate whether the volcano being submerged or emerged; a: island visually recognized on the sea, b: the volcano completely submerged, and c: the volcano supposed to be submerged. 1–5 show a state of eruption visually observed; 1: major explosions, 2: vomiting of ash cloud and vapour with moderate explosive action, 3: remarkable vapour emission without visible explosion, 4: vapour emission only without visible explosion, and 5: no visible activity. 6 shows activities presumed from tsunami, sound, underwater listening, etc.

ther clearly shown schematically in the above-mentioned diagram (Fig. 3).

The volcano first appeared on the sea with its blocky lava head on September 16 or 17, 1952. Vomiting continuously ash clouds and vapours, the activities of the volcano became explosive several days after the outburst of the eruption (Figs. 8–12). On September 23, after two severe submarine explosions at 13h12m and 13h40m (Figs. 27–51), it submerged completely leaving the sea water changed into yellow in colour above its head. During the period of submergence, colour of the water above the volcano was changing into yellow owing to the continuous subaqueous emission of volcanic dusts. About half a month later the volcano appeared again on the sea probably on a day after 3rd and before 11th of the next month. Untill the beginning of March in the next year, perhaps March 9–10, 1953, when the island submerged after severe explosions (Fig. 57), the ocean current had presumably been breaking on the side of the island. Typical volcanic spines such as observed on the summit of Mt. Pelé were protruding from the vent during the second period of appearance (Figs. 54–56), from October 3–11, 1952 to March 9–10, 1953. In the succeeding three weeks or more, from the middle of March to the beginning of April, remarkable submarine explosions were reported many times. Explosions became frequent and emission of ash and vapour became continuous. Thus, at the beginning of April, 1953, probably between April 3 and 5, the third appearance of the island took place. The island had presumably been exposed on the sea with continuous vapour emission till the end of August (Fig. 58 a-b). No conspicuous explosions had been recorded in this subaerial period. Since the middle of August, 1953, the amount of vapours rising from the island had increased. Puffing of ash clouds became active toward the end of the month, sometimes up to 500 m. or more into the air. In the last week of that month the volcano turned into explosive state. The explosive actions at the end of the month were the most destructive of the present eruption. Large amounts of ash, sand, and pumice were ejected. Ash of andesitic composition whose chemical analysis will be shown in the fourth chapter of this paper were blown away, while the pumice grains drifted to the shore of Aogashima, about 50 km. north of the volcano were exclusively white dacite. About ten days' explosive activities led to the collapse of the island into the sea and the Myôjin reef has never emerged upon the sea level since the first few days in September 1953[15].

15) Two explosions during 14h–15h on Nov. 4, 1954 at the Myôjin reef were reported by the fishing boat Eikichi-maru of Yaizu port. But it was not recognized by the Hydro-

It is clearly shown also by the above-mentioned diagram (Fig. 3) that the successive explosive activites accompanied with outbursts of large amount of pumice continuing for several days or more always preceded the collapse of the island into the sea. The repetition of gradual formations of dome or spines followed by violent collapses owing to severe explosive activities were displayed by the Myôjin reef through the 1952–1953 eruption. Had the eruption occurred on the land, severe avalanche of domes or spines, pumice shower, nué ardente, phenomena characteristic to the Peléan eruption would have been observed.

III. Submarine explosions on September 23, 1952

The training ship Shinyô-maru, 229 tons, of the Tokyo College of Fisheries on which the writers embarked with other scientists left Uraga port, Kanagawa Prefecture, southwards for the Myôjin reef at 05h in the morning of September 21, 1952. At 17h30m of the same day the ship touched at Funato Bay of Miyake-jima, an active insular volcano of basaltic nature about 170 km. south of Tokyo, to avoid a centre of an atmospheric depression. On the next day at 05h, the ship left the island and at 14h30m of the same day cast her anchor at Horawazawa Bay of Hachijo island about 290 km. south of Tokyo to avoid arriving her destination at midnight. There, at 15h05m a white cloud (cumulonimbus formed by an explosion) was seen in far distance in the direction of the Myôjin reef. Leaving the bay at 19h15m of the same day, she continued to voyage southwards through the night at a speed of 10 knots every hour. At 23h45m of the same day after passing off Aogashima, a volcanic islet about 350 km. south of Tokyo, a night scene of an explosion was viewed far to the south.

On the next morning, at 04h, September 23, the ship first approached the Bayonnaise rocks and, next, at 06h05m, the Myôjin reef eastwards. The newly-born island had almost disappeared leaving three rocks on the sea. The three rocks, about 1.5 m. in height above sea level at the time of low water, were submerged completely at the time of full tide, where the difference between sea levels at high and low tides was about 2 m. at that time. It was quite clear and the sea was calm. There was nothing to predict any tremendous events except the breakers over

graphic Office. Activity at the Bayonnaise rocks was found by the No. 2 Hôshin-maru of the Fisheries Experiment Station of Aichi Prefecture on June 25, 1955 at 16h. (Personal communication from Mr. H. Katô, an eyewitness, of the Prefectural Fisheries Experiment Station at Gamagôri, Aichi Prefecture).

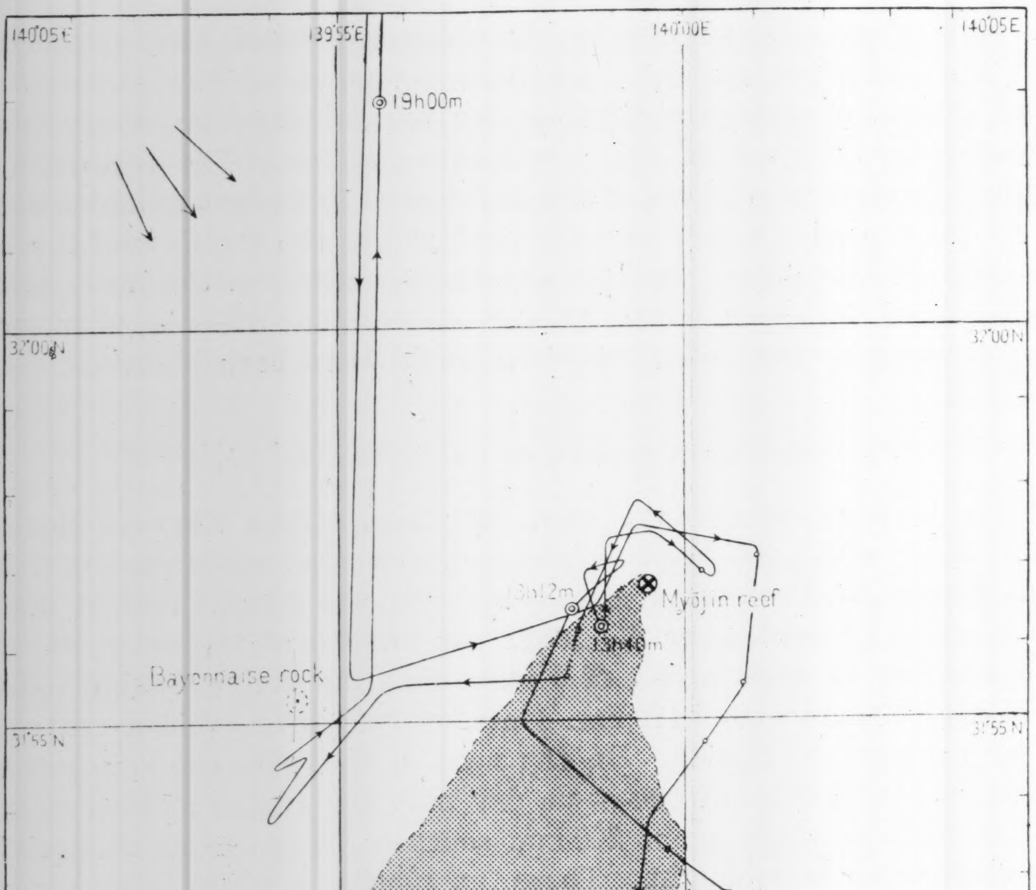
140°05'E
139°55'E
140°00'E
140°05'E
19h00m
32°00'N
32°00'N
13h12m
Myôjin reef
13h40m
Bayonnaise rock
31°55'N
31°55'N
08h34m
31°50'N
31°50'N
0
5Km
31°45'N
31°45'N
139°50'E
139°55'E
140°00'E
140°05'E

Fig. 4.

an area of 1–2 km. in diameter near and around the above-mentioned three rocks, and the stationary SSE-ward Kuroshio counter current with a speed of 1.5–0.8 km every hour changing into yellow in colour being contaminated with volcanic dusts owing to the subaqueous emission of the volcano. The turbid current, starting from the Myôjin reef, suspended minute grains of white pumice, volcanic dusts, volcanic hairs, etc. Amounts of the suspensoids in the water were measured as 3–30 mg. per litre including traces of sulphur[16]. The yellowish-stained water[17] was clearly bounded by the non-contaminated water (Figs. 13–15) of the Kuroshio[18]. Smells of hydrogen sulphide were sometimes felt on the deck of the ship. The water deeper than 25 m. was not stained with volcanic ejecta.

During the half-a-day's stay near the reef that day, four explosions were witnessed of which the three submarine explosions at 08h34m, 13h12m, and at 13h40m were observed at short distances from the centre of the eruption and the last one at 19h00m exhibiting a spectacular night scene was viewed on our way back to Uraga.

Situations of the ship when each explosion took place are shown by double circles in the map prepared by the members of the first investigation of the Myôjin reef under the auspices of the Tokyo College of Fisheries on September 23, 1952 (Fig. 4). The locus of the sailing ship during the present investigation, the drift of the ship during oceanographical observations (Fig. 16), the direction of the wind of that day, the distribution areas of the floating fine pumice or ash and of the contaminated water are shown in the same figure by real lines or curves,dotted lines, arrows, dotted area, and shaded area respectively. Locality of the reef was estimated as 31°56.8′N in latitude and 139°59.5′E in longitude by the officer of the ship. Actual scenes of the submarine explosions are described in the following sections.

(1) *Narative of the explosions*

Features of the phenomena displayed by the underwater explosions are in general similar to those reported about the geyser activities[19] and

16) H. HAMAGUCHI and M. TATSUMOTO, "Chemical investigation on the sea water and the pumice stone", *Jour. Coll. Fisheries*, **40** (1953), Special Number, 20–21.

17) Transparency 3 m., pH 7.5–7.7 in surface 8.5 deeper than 25 m., olive yellow or olive green in colour after *Wada's Colour Chart*.

18) Transparency 23 m., pH 8.5, deep lyons blue in colour after *Wada's Colour Chart*.

19) C. A. COTTON, Volcanoes as Landscape Forms. Wellington 1944. p. 280. In the geysers verfical belches are predominating.

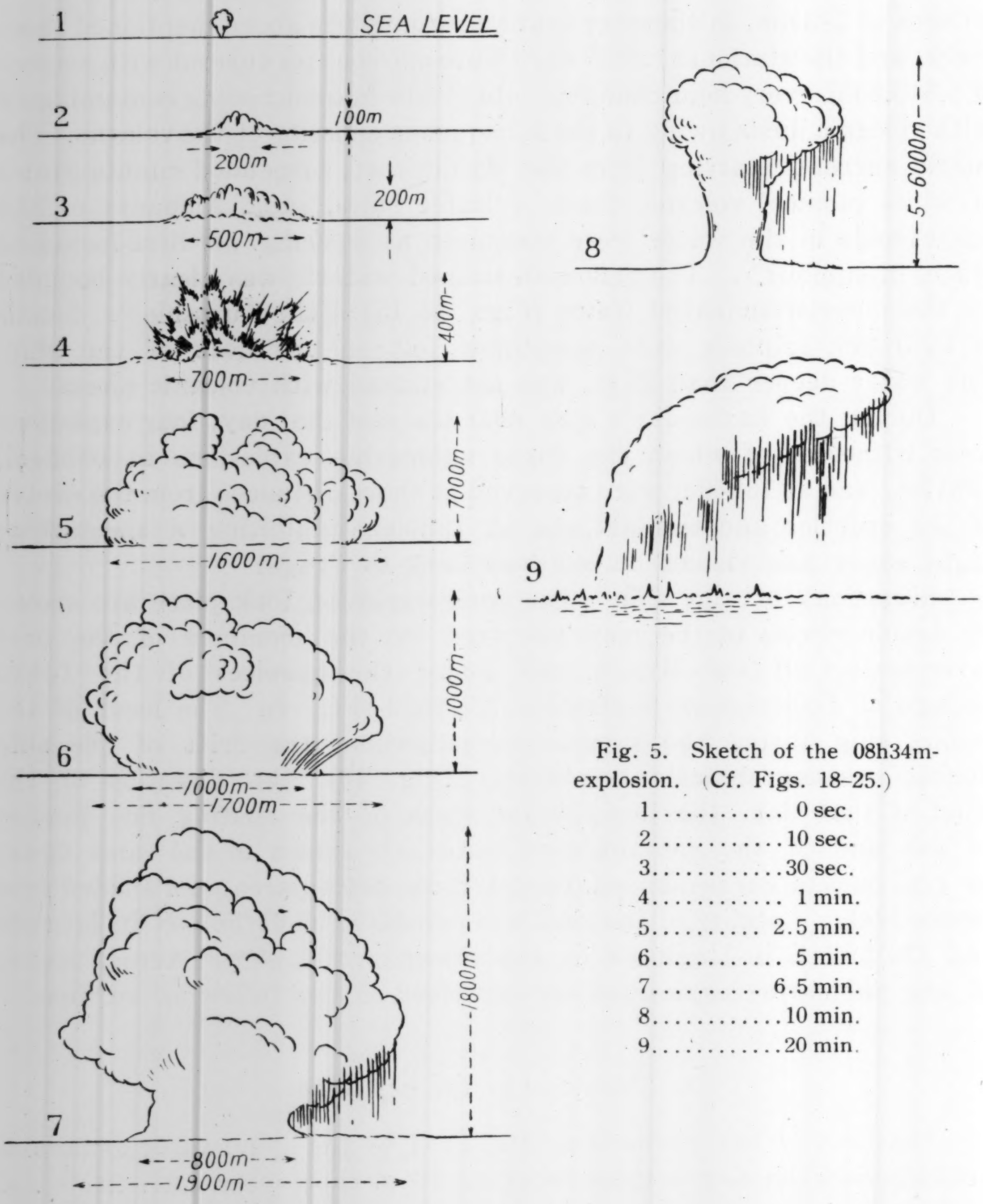

Fig. 5. Sketch of the 08h34m-explosion. (Cf. Figs. 18–25.)

1. . . . . 0 sec.
2. . . . . 10 sec.
3. . . . . 30 sec.
4. . . . . 1 min.
5. . . . . 2.5 min.
6. . . . . 5 min.
7. . . . . 6.5 min.
8. . . . . 10 min.
9. . . . . 20 min.

those of the eruption of Anak Krakatau in 1938[20]. But in detail, the Myôjin reef behaved in different ways from them, and was different even in each explosion as described below.

20) R. W. van BEMMELEN, The Geology of Indonesia IA General Geology. Haue 1949 pp. 200–201, Fig. 63 (Stehn's photographs).

a) The 08h34m-explosion:

Several minutes before the explosion, bluish dark smokes rising were seen two or three times far from the centre of the eruption (1 in Fig. 5). At 08h34m, the water, dark purplish in colour, domed up abruptly, then dark plumes like a bush of swords broke through the surface of the dome followed by greyish white water columns. The sharp tops of plumes were led by the blocks ejected. The plumes grew larger and larger with great speed before our eyes in all directions and then turned downwards. White smokes which appeared among these plumes increased in volume accelarately and completely enveloped them (Figs. 19–20). The smokes, ash clouds and vapours, gushed out widely to form a large cabage-like group (Figs. 20–21), which began to rise as a whole. The upward movement increased its speed more and more to exhibit a cauliflower with a major leg such as is often seen on the occasion of an atomic bomb explosion. It reaches up to several thousands metres (Figs. 5, 17, 22, and Table III) changing its

Table III. Spreading of the ash cloud with time at the 08h34m-explosion on September 23.

Fig. No.	Diameter of the cloud or vapour at the sea surface	Maximum diameter of the cloud in the air	Height of the cloud above sea level	Time-lapse after the first manifestation at the sea surface of the explosion
18	780 m.	780 m.	390 m.	40—50 sec.
19	1,100 m.	1,100 m.	470 m.	1.5 min.
20	1,440 m.	1,800 m.	820 m.	2.5 min.
21	1,050 m.	1,830 m.	1,170 m.	5 min.
22	860 m.	2,110 m.	1,990 m.	6.5 min.
25	2,200 m.	2,220 m.	140 m.	30 min.

colour variously (e.g. white, pinkish, yellowish brown, and light purple) under the bright sun-shine. Vapours continued to rise from the sea surface. Ash began to fall leewards. The cauliflower-cloud diverged gradually in the sky leaving white horizontal cloud below (Figs. 23–24). The colour of the sea surface was dark greyish and boubling, vapour emission still continued even after the cloud separated itself upwards from the sea. All things dissolved into the blue sky at about 08h55m leaving the floating ejecta on the sea. No explosion sounds were heard on the ship even when the ship was drifting with her engine stopped. Temperatures of the surface water and of the atmosphere were estimated at 27.8°C and 25°C respectively. The atmospheric

pressure was 1014.5 millibars, the weather was fine, the force of the wind was 2 in Beaufort's scale and its direction southwestward at that time, and the full-tide at the Bayonnaise rocks was 07h45m of that day. Observation station of the explosion is shown in the Fig. 4.

After the 08h34m-explosion and before the next explosion described below, no submarine explosion was felt on the ship. But during this calm period, the SOFAR stations off California was said to have recorded one remarkable Myôjin explosion at about 11h43m (JST)[21]. According to Dietz and Sheehy, an intensity of the 11h43m-explosion was stronger than those of the three submarine explosions witnessed at 08h34m, 13h12m, and at 13h40m. Every witnessed explosion was displayed in a visual field so clear that the Island of Aogashima about 60 km. north of the Bayonnaise rocks and even Smith reef about 55 km. south of the rocks could be seen distinctly. The weather was fine and the sea was calm. Large amounts of ejecta and of volcanic gas

21) R. S. DIETZ and M. J. SHEEHY, *Bull. Geol. Soc. Amer.*, **65** (1954), 948, Table 5:

Date	1	2	3	Corresponding explosion witnessed by the writers
	..	..	..	
	..	..	..	
	..	..	..	
Sept. 22	23h45m	4	1 explosion, 1 min.	23h45m-explosion
Sept. 23	00h25m	2	1 min.	
	08h28m	2	—	08h34m-explosion
	11h43m	3	10 min.	
4 {	13h08m	2	—	13h12m-explosion
	13h35m	2	—	13h40m-explosion
	19h01m	3	2 explosions, 1 min.	19h00m-explosion
	19h14m	2	4 explosions, $1\frac{1}{2}$ min.	
	22h33m	2	1 min.	
	..	..	..	
	..	..	..	
	..	..	..	

1. Calculated explosion time (nearest minute) in Japanese Standard Time after Dietz and Sheehy.

2. Intensity of explosion after Dietz and Sheehy.

3. Number of explosions and duration of received singnal or interval covered by series of signals after Dietz and Sheehy.

4. Time interval during which the writers stayed near the Myôjin reef in their present investigation.

were belched at every explosion witnessed by the writers. It was quite strange that under such preferable circumstance the writers should have found no manifestations on the sea of the explosion which ought to have taken place at about 11h43m according to the records of Dietz and Sheehy. When and where did the gas which should have been emitted at the time of the explosion in question escape? Did it dissolve into the water? Or did the 11h43m-explosion take place at other different vent opened at deeper place. It has never been assured that every Myôjin explosion had always taken place at the same vent. Two separate water columns arising simultaneously were observed from Aogashima in September, 1952 and three were from Hachijô island in April, 1953[22].

b) The 13h12m-explosion:

The 13h12m-explosion was witnessed at 31°56.5′N in latitude and 139°58.4′ E. in longitude about 1,800m. distant from the centre of the eruption, when the ship was sailing northeastwards along the western boundary between the turbid water and the non-contaminated "Kuroshio" counter current for observing the three projecting rocks, one in the east and two in the west about 200m. apart from the former (Fig. 4). The rocks were dark brown or sometimes brownish purple in colour under sun-shine and the waves were breaking on a bank over an area of 500–1,000 m. in diam. around the rocks.

The explosion was brought about on the sea at 13h12m without any visible forerunning phenomena except slight belching of dark smokes one or two times from the sea near the above-mentioned rocks. The sea surface of an area of 290 m. in diam. near the rocks suddenly domed up nearly to 20 m. in height (Fig. 27). Then the summit of the water dome of glassy lustre became dark purplish in colour as the dome increased its height. A number of blocks followed by dark water tails, mixtures of water and rock fragments, broke through the crest of the dome like plumes (Figs. 27–29). These numerous plumes of dark mixture of water and rocks were ejected to the heights of 400 m. or more and then turned downwards (Figs. 29–30). Some of the large blocks tailed with these dark plumes separated themselves from the tops of these plumes and flew farther away. As these ejecta turned downwards, white smokes, brown or grey ash clouds began to gush out successively (Fig. 30) to form a large mass of clouds about 600 m. high covering the sea over

22) Y. TSUKAMOTO, *Monthly Meeting of the Earthq. Res. Inst.*, (May 24, 1955).

an area of 1.5 km. in diam. (Figs. 31–34). Then the clouds moved rapidly upwards in a body (Fig. 35) to make a cauliflower cloud (Fig. 36) several thousands metres high, with an huge leg of one kilometre in diameter. Ash began to fall leewards, spouts of dark smokes rose from the dark bubling sea, and the cauliflower cloud faded into the sky leaving floating pumice blocks from 5–10m. to 30cm. in diameters on the sea, where white vapours were still rising. Low explosion sounds were slightly heard. Waves 2–3 m. high seemed to have been brought about by the explosion. Ten minutes later all things returned to their calm state. There was nothing left except the floating pumice blocks—some of them had already sunk into the sea—to show that such a conspicuous phenomenon had just been displayed there[23]. Fortunately the changing scenes of the activity were photographed successively as shown in Figs. 26–40, on which some measurements were tried as follows (Tables IV and V):

Table IV. Spreading of the ash cloud with time at the 13h12m-explosion, Sept. 23*.

Fig. No.	Diameter of the ash cloud at the sea surface	Height of the cloud above sea level	Time-lapse after the first manifestation at the sea surface due to the explosion.
27	290 m.		1 sec.
28	320 m.	290 m.	3 sec.
29	570 m.	410 m.	5 sec.
30	870 m.	430 m.	8 sec.
31		440 m.	12 sec.
32		450 m.	15 sec.
33		460 m.	20 sec.
34		650 m.	30 sec.
35	880 m.		1 min.
36			2 min.
37	520 m.		3 min.
38			4 min.
39	310 m.		5 min.

* MARINE SAFETY BOARD, *op. cit.*, 88–96.

23) Weather was fine, atmospheric pressure was 1,010 millibars, direction of the wind was southwestward, force of the wind was 2, in Beaufort's scale and the atmospheric temperature was 24.5°C, while temperature of the surface water being 27.7°C. Lower tide at the Bayonnaise rocks was 13h25m of that day.

Table V. Comparison of the observed lapse of time and height of the plume with those calculated.*

Fig. No.	Time photographed	Height of the plume above sea level read on the photograph	Time calc.	Height of the plume above sea level calc.
27	1 sec.	44 m.	1 sec.	86.₉ m.
28	3 sec.	290 m.	4 sec.	289 m.
29	5 sec.	410 m.	7 sec.	403 m.
30	8 sec.	430 m.	9.4 sec.	430 m. **

* Every "time" on the table is represented exclusively by the "time-lapse" after the first manifestation of the underwater explosion at the sea surface.

** Maximum height of the plume to which a bomb was ejected was assumed as 430 m. reading on the Fig. 30.

c) *The 13h40m-explosion*:

When we entered into the contaminated sea current southwest of the centre of the eruption in order to collect the floating pumice blocks ejected by the 13h12m-explosion, the next 13h40m-explosion suddenly took place. It occurred so shortly after the previous explosion we had just observed that we were surprised to meet such a thrilling explosion. Situation of the ship at this event was 31°56.2′N., 139°58.8′E., about 1,500 m. southwest of the explosion point. Emerald blue sea water covering an area of about 210 m. in diameter was upheaved nearly to 40 m. in height to form a water dome of sharp curvature (Fig. 41). Simultaneously the water around the dome seemed to sink slightly. Rapid darkening in colour of the summit of the transparent bluish green water dome, successive belching of a number of dark plumes breaking through the crest of the dome, and the rolling down of water particles along the surface of the dome with the bending down of the plumes (Figs. 41–42) were clearly observed. Successive scenes of the explosion and the scale of the spreading ash clouds are shown in the following photograghs and table (Figs. 41–51 and Table VI). The succeeding processes of this explosion were similar to those displayed by the previous one, though the water dome formed by the 13h12m-explosion was flat and broader compared with that of the present explosion. The shape of the domes will be discussed in later pages. Sometimes exceptionally, bombs were ejected whose trajectories of flying were flat and close to the sea surface (Fig. 49). Further observation of the spreading explosion clouds was almost impossible, for they soon scaled out from our field of view (Figs. 48–50). Waves

Table VI. Spreading of the explosion-cloud with time at the 13h40m-explosion on sept. 23.

Fig. No.	Diameter of the cloud at the sea surface	Height of the cloud above the sea level	Time-lapse after the first manifestation at the sea surface of the explosion
41	210 m.	83 m.	5 sec.
42	300 m.	150 m.	7 sec.
43	450 m.	160 m.	10 sec.
44	540 m.	160 m.	12 sec.
45	680 m.	270 m.	15 sec.
46	860 m.	340 m.	17 sec.

50 m. long and 2 m. high[24] brought about by local impulse of the underwater explosion attacked the side of the ship slightly when she was going to turn for a safer place[25]. Low explosion sounds were heard faintly. Stimulating smell of sulphurous anhydride was felt on the deck. No remarkable change was found in the temperatures of the surface water before and after the explosion. Floating pumice block was picked up on the deck in hot state still about 60–80°C. The white two pyroxene-dacite containing porphyritic crystals of quartz, our first petrographic information on the volcano, warned us of the dangerous character of the eruption. By this explosion one of the three projecting rocks was blown off. The situation off.

After some oceanographical observations, the ship left the Bayonnaise rocks at 18h10m. On the way back to Uraga an explosion was witnessed from a point, 32°04.3′N., 139°55.3′E., about 13 km. NNW of the centre of the eruption. An acute pyramid of fire was seen on the horizon. It grew larger and larger and was enclosed by the spreading cloud at the periphery of which sparkings were seen. Lightnings were also observed around and above the cauliflower cloud. The scale of the explosion seemed to be larger than the 13h12m and 13h40m explosions. But all things occurred too remote to be observed in detail. The weather was fine, atmospheric pressure was 1,014.5 millibars, force of the wind was 2 in Beaufort's scale and northeastward, temperatures of the air and of the surface water were 24°C and 25.7°C respectively,

24) TOKYO COLLEGE OF FISHERIES, *op. cit.* 11. H. MIYOSHI and Y. AKIBA, "The tsunamis caused by the Myôjin explosions," *Jour. Oceanogr. Soc. Japan*, **10** (1954), 50.

25) Order of energy of the 13h40m-explosion was estimated to be 10^{18} erg by S. Murauchi (S. MURAUCHI, "Explosive activities of Myôjin reef, 1952", *Jour. Scis. Soc. Japan*, **5** (1952), 162. in Japanese).

and the full tide at the Bayonnaise rocks was 19h05m of that day. The S. S. Shinyô-maru returned to Uraga port on September 24 at 17h30m where we heard that the No. 5 Kaiyô-maru had missed.

(2) Depths of the submarine explosions.

Methods of estimating the depths of underwater explosions have been under much discussion. Recently Pekeris, relying upon his analysis of photographs of the dome of spray from some fifty statically-fired charges, proposed some methods of estimating the depth of an underwater explosion from the shape of dome of spray formed by the explosion[26]. One of his methods, a modification of Shaw's method (i.e. the distance from the centre of the dome to a radius where the dome-height has decreased to half of the central height is equal to the depth of the explosion, or in other words, half width of the dome is equal to the depth of explosion) may be applied to the present submarine explosions. Of course, strict accuracy cannot be expected in the estimations of the depths of the Myôjin explosions by this method, though Pekeris says that his estimates can be made with an accuracy of about 10 per cent in error in cases of controlled artificial explosions. Pekeris's method, as well as Shaw's, assumes that the initial rate of rise of spray is equal to the acoustic velocity imparted to particles of water in the superficial layer by the peak of shock wave from an explosive. According to the estimations at many active volcanoes, gas pressure at a volcanic explosion is not so great; 450-500 atmospheres at greater ones[27]. So in analysis of the mechanism of the dome formation, e.g. motion of the surface water, it may be treated as an effect of pressure waves due to the submarine volcanic explosions, as Pekeris did in his paper where he used the term "shock wave".

As the data available for this estimation, the writers have a series of photographs of the scene taken by a 35 mm. camera only, for unfortunately the movie cameras of other observers could not catch the complete scene of the explosion during the investigation. As to the explosions at 13h12m and at 13h40m, shapes of the water domes representing the initial states of the manifestations of the underwater explosions were

26) C. L. PEKERIS, "Determination of the depth of an underwater explosion from measurements of the dome of spray", *Annal. New York Acad. Sci.*, **51** (1949), Art 3, 442–452.

27) T. MATUZAWA, "Gasdruck bei einigen vulkanischen Ausbruchen in Japan", *Bull. Earthq. Res. Inst.*, **11** (1933), 347–349.

Table VII. Estimations of depths of the 13h12m and 13h40m explosions.

	13h12m-explosion	13h40m-explosion
Central height of the dome	18.5 m.	39.2 m.
Half-width of the dome (right)	56.6 m.	45.6 m.
Hals-width of the dome (left)	77.3 m.	37.0 m.
Average of the above two (depth)	66.9 m.	41.3 m.

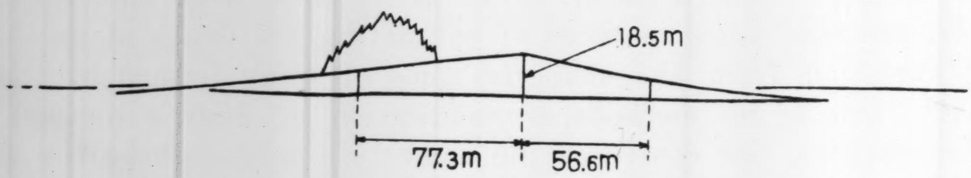

Fig. 6. (enlarged from Fig. 27.)

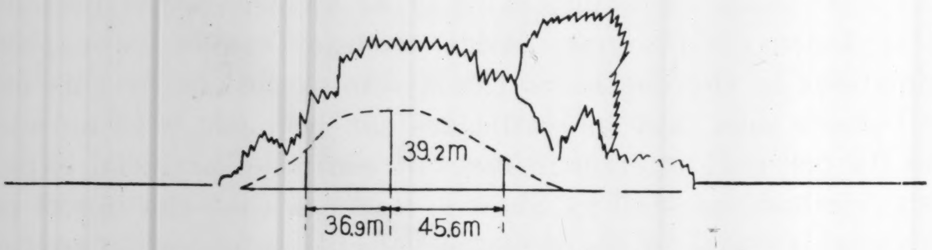

Fig. 7. (enlarged from Fig. 41.)

caught by the cameras. Applying the above-mentioned method to the photographs shown in Figs. 27 and 41, we obtained the depths of the explosions from Pekeris's formula as diagramatically shown in the Figs. 6–7, focal lengths of the cameras, and the distances to the objects from the observation stations being given. Such estimations on the photographs are subjected to more uncertainities than Pekeris's estimation on his artificially controlled underwater TNT-explosion[28]. The continuous changes in shape of the domes could not be checked by the writers' camera so successively as by a movie camera. Nevertheless, in the above estimations, it is assumed that an explosion took place always in the water which is distributed infinitely horizontally and also downwards. In fact, however, the Myôjin explosions never took place in free water but must have taken place at the submarine vent where the solid rocks are situated beneath the water. On the other hand the depths of the submarine explosions may be estimated as

28) C. L. PEKERIS, *op. cit.*, 445.

scores of metres judging from the submarine topography near the volcano before the eruption[29] and from the appearance of the activity after the outburst of the present eruption. As to the writers' estimations on the depths of the explosions of the Myôjin reef, the above-mentioned values themselves cannot indicate the actual depths but they accord with the values estimated geographically and geologically in order of their values.

(To be continued)

29) R. MITA, *op. cit.*, Text-fig. 2.

8. 明神礁の昭和 27—28 年の噴火 (1)

地震研究所 {森 本 良 平
小 坂 丈 予

昭和 27 年 9 月 17 日午前 7 時 15 分頃，ベヨネイズ列岩 (31°55.3′N，139°54.5′E) の東方約 10km. の海面に，漁船「第十一明神丸」によつて海底噴火が発見報告された．この噴火によつて出現した島は，発見した船の名を取つて「明神礁」と命名された．明神礁は，第五海洋丸と共に殉職した三田亮一氏によれば，ベヨネイズ列岩を外輪山の一角とする複式火山の中央火口丘の一つといわれ，この附近には明治 29 年，39 年，大正 4 年，昭和 9 年，21 年に噴火の記録がある．しかし，海底地形の概略と，明治 39 年噴出安山岩質浮石の簡単な記載のほか，火山の詳細は知られていなかつた．今回の噴火は，9 月 24 日，調査に派遣された海上保安庁水路部測量船第五海洋丸の遭難という，火山研究史上未曽有の事件勃発のため，各方面の注目を惹くに至つた．第五海洋丸が海底爆発によつて遭難したと信じられる 9 月 24 日の前日，筆者らは，東京水産大学（旧水産講習所）練習船「神鷹丸」に乗船して現場に臨み，海底爆発を目撃観察する機会を得たので，(1) 今回の噴火の活動経過，(2) 昭和 27 年 9 月 23 日の海底爆発の情況，(3) 各種抛出物の岩石記載を詳細に述べることにした．本篇では，噴火の発見から活動が休止したと思われる昭和 28 年秋までの明神礁の活動の経過を，各方面の資料を集めて記載し，昭和 27 年 9 月 23 日の海底爆発の情況を詳述した．

この活動期間に，明神礁は 3 回，海面に出現しては海没した．すなわち，昭和 27 年 9 月 17 日に，その熔岩ドームの頭端を海面上に現わして数日後から，活動は爆発的となり，9 月 23 日の相続く水中爆発によつて水没し，10 月 3 日から 10 日の間に水面上に出現してそのご翌年 3 月 9 日まで，熔岩尖塔を海面上に見せていた．昭和 28 年 3 月に入つて，また爆発をくりかえし 3 月 10 日に水没した．第 3 回目に海面上に現れたのは 4 月のはじめで，このときの熔岩尖塔や熔岩円頂丘も，8 月下旬のひきつづいた爆発で崩壊水没し，そののちも，浮石，火山塵で海水を黄濁させる水中噴火を続けていたが，そのごは確実な消息なく，噴火活動を終息したものと思われる．明神礁はこのように，徐々に熔岩円頂丘或ひは熔岩尖塔を突出させたのち，大量の浮石抛出を伴う烈しい爆発活動をつづけて円頂丘や尖塔を崩壊するという過程を，今回の活動期間中に，3 回くりかえしたことになり，あとで述べる抛出岩石の岩石学的性質も，このような Pelé 式噴火の活動型式を裏づけている．

昭和 27 年 9 月 23 日の午前 8 時 34 分，午后 1 時 12 分，同 40 分の爆発は，爆発地点より，それぞれ南方約 9 km.，西南西 1.8 km.，西南方 1.5 km. の距離から目撃することができた．爆発は，まず，水中爆発の圧力波による海水ドームの形成，海水ドームを突き破つて火山岩塊の抛出，

ついで，水中を上昇してきた火山放出ガスの逸出による，原子爆弾の爆発に際して見られるような茸状雲の形成とその逸散，少量の降灰，抛出浮石の漂流，といつた順序で行われる．各爆発実況の規模とその経過時間は，写真（第 28–52 図）及び図表(第 5 図，第 III–VII 表）によつて示した．なお，海水ドームの盛り上りの写真から，推定計算した爆発点の深さは，海底地形その他から推測される値と矛盾しない程度の値（40–70 m.）が得られた．（未完）

CORRIGENDUM

In the Bulletin of the Earthquake Research Institute, Vol. 33, Part 2 (June 1955), the order in the following report, i.e., 16. R. Morimoto and J. Ossaka, The 1952–1953 Submarine Eruption of the Myôjin Reef near the Bayonnaise Rocks, Japan (I). (in English), has been reversed owing to some mistake in book-binding. Pl. XLI—Pl. XLIX (from Fig. 8 to Fig. 33) should have been placed before Pl. L—Pl. LVII (from Fig. 34 to Fig. 55).

正　　誤

地震研究所彙報第 33 号第 2 冊（昭和 30 年 6 月）の論文 16. 明神礁の昭和 27–28 年の噴火 (1) (英文) 森本良平，小坂丈予の Pl. XLI から Pl. XLIX まで（第 8 図から第 33 図まで）と，Pl. L から Pl. LVII まで（第 34 図から第 55 図まで）とが，製本屋の手違ひで，前後して居ますから，御了承下さい．

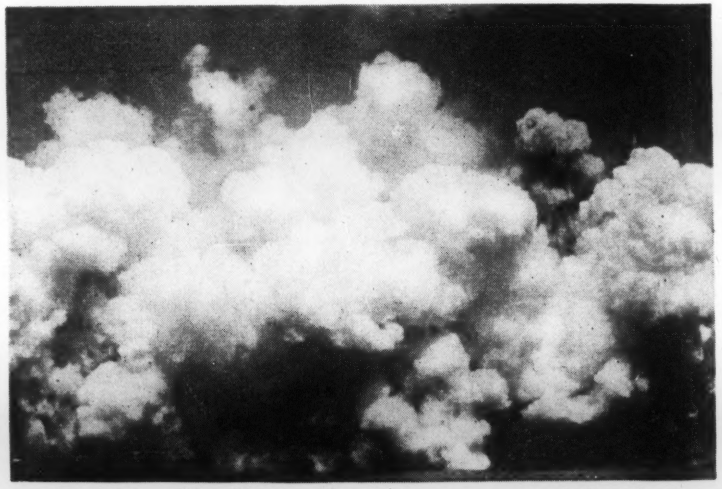

Fig. 34. Dito 30 sec. Upward movement of the cloud.

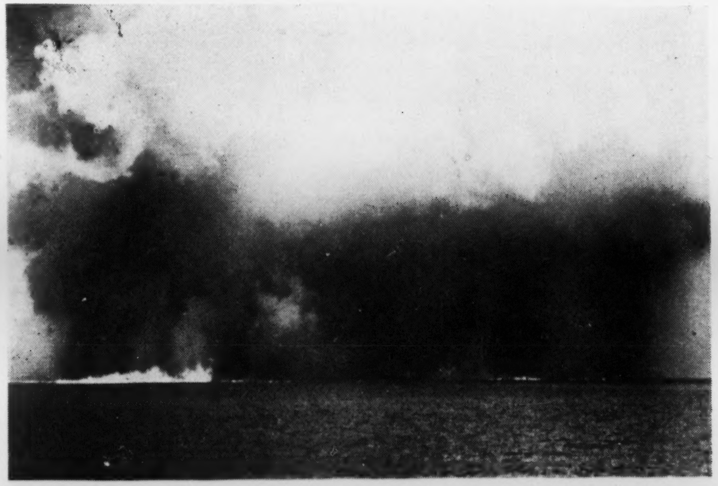

Fig. 35. Ditto 1 min. Head of the cauliflower cloud moved out of the camera field and the neck column of the cloud appeared.

Fig. 36. Ditto 2 min. Lower part of the northern half the cauliflower cloud.

(震研彙報 第三十三号 図版 森本・小坂)

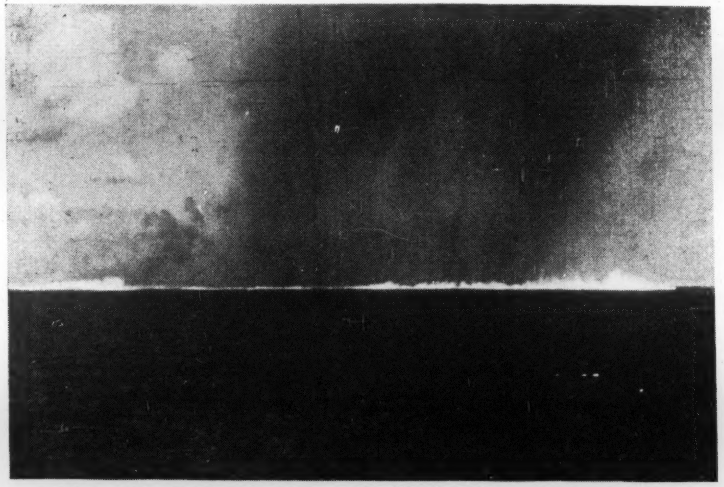

Fig. 37. Ditto 3 min. Vortical ash columns arose after the cauliflower cloud moved away.

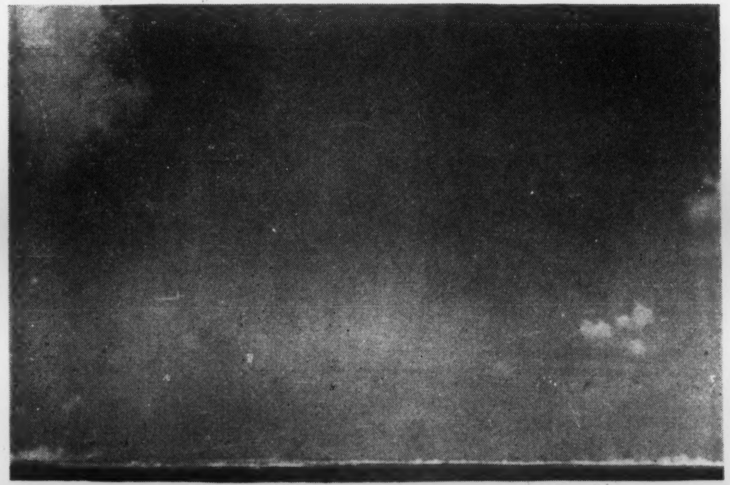

Fig. 38. Ditto 4 min. Ash began to fall and the explosion cloud became translucent gradually.

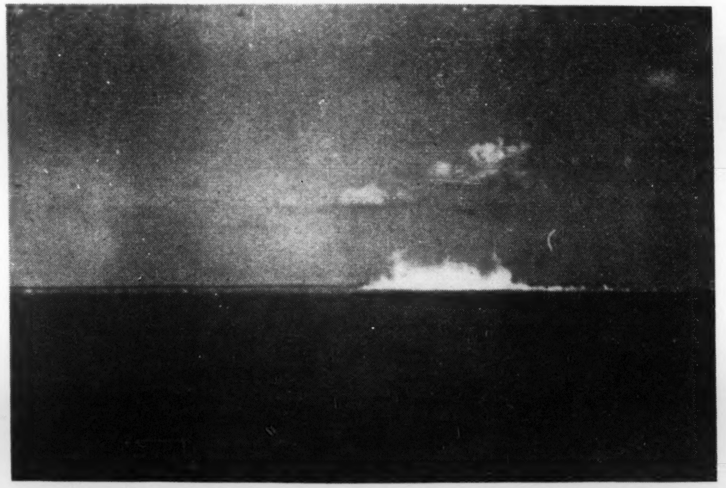

Fig. 39. Ditto 5 min. The explosion cloud dissolved into blue sky leaving only many floating pumice blocks on the sea from which white vapours were rising.

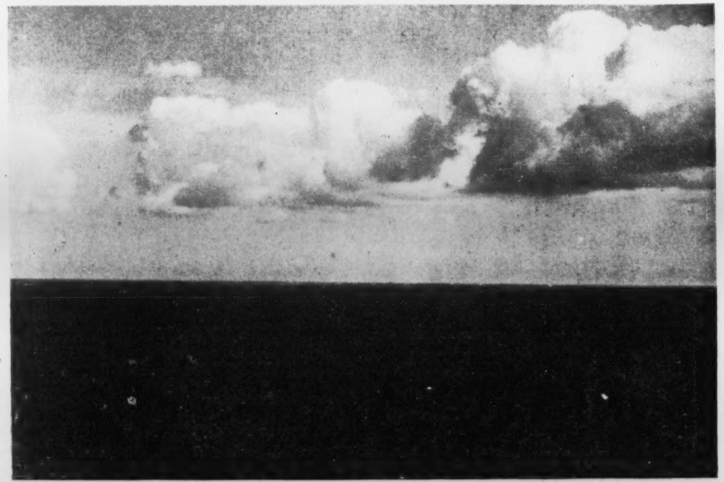

Fig. 40. Ditto 15 min. There was nothing to show any evidence of severe explosion. Yellowish turbid current only shows the continuous subaqueous emission from the volcano.

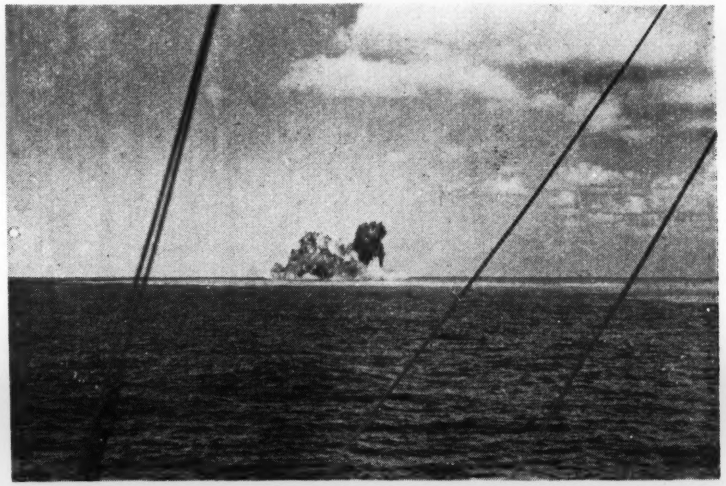

Fig. 41. 5 sec. after the first manifestation of the 13h12m-explosion on the sea.

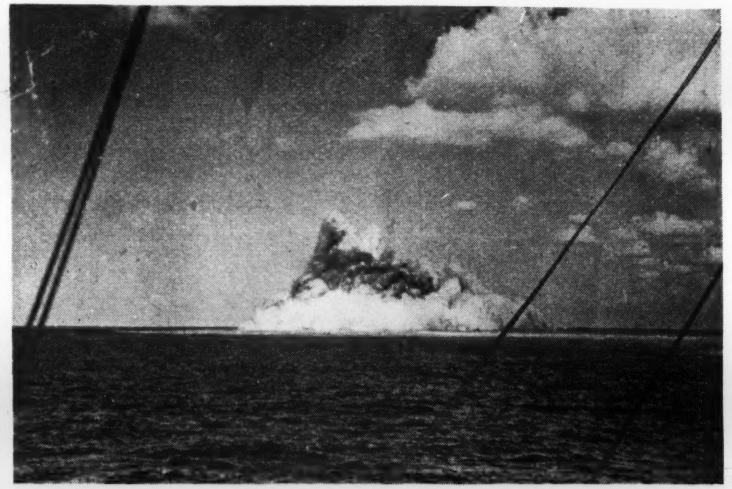

Fig. 43. Ditto 10 sec.

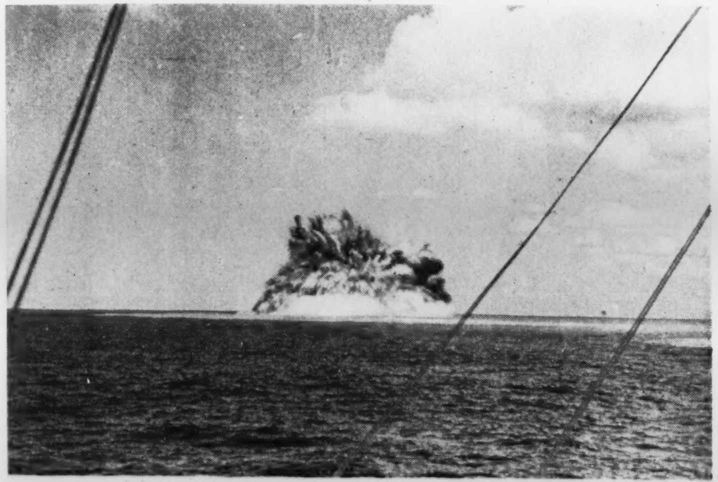

Fig. 42. Ditto 7 sec.

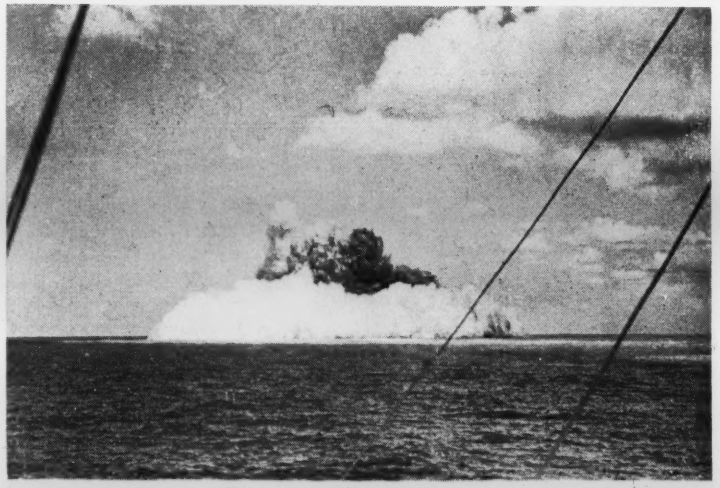

Fig. 44. Ditto 12 sec.

Figs. 41–51. Chaging scene of the 13h40m-explosion. Cf. p. 245 and Table VI. One millimetre on each photograph corresponds to about 12.5 m. in actual distance, i.e., 8.0 mm. on the photographs to 100 m. in actual distance (Figs. 41–46. were photogaraphed by R. Sugano of Asahi Press).

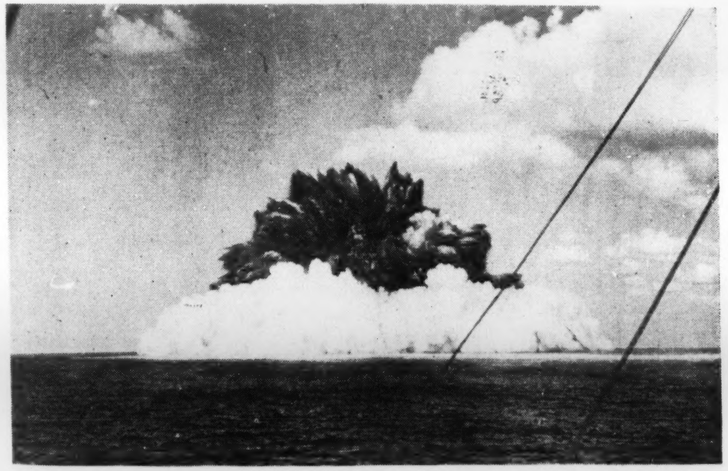

Fig. 45. Ditto 17 sec.

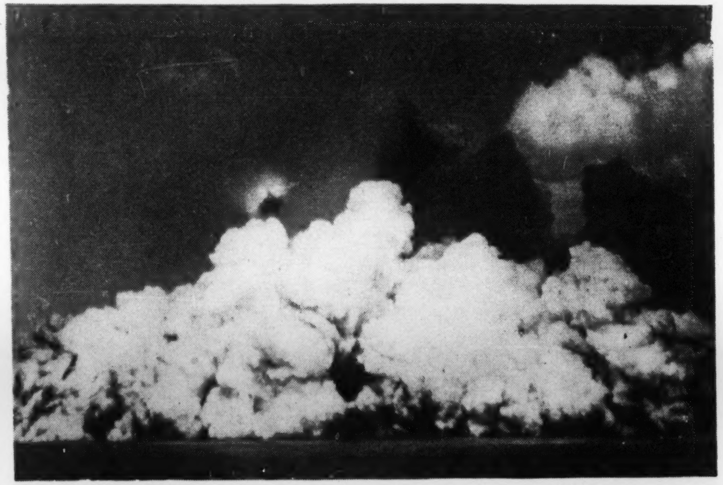

Fig. 47. Ditto 30 sec. Photo. by H. Hamaguchi

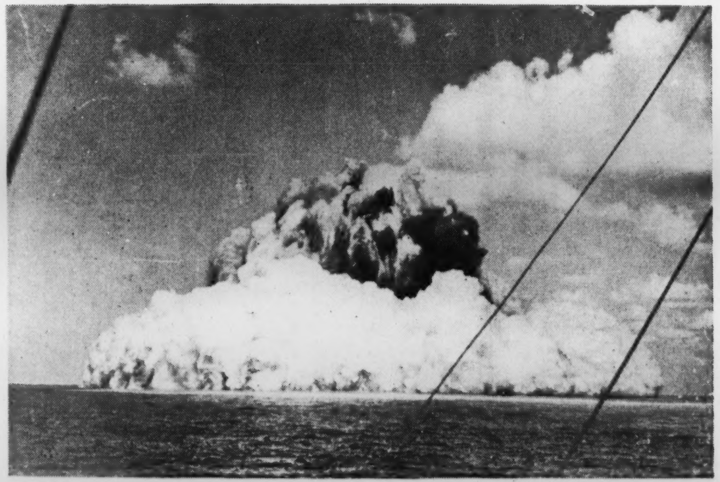

Fig. 46. Ditto 15 sec.

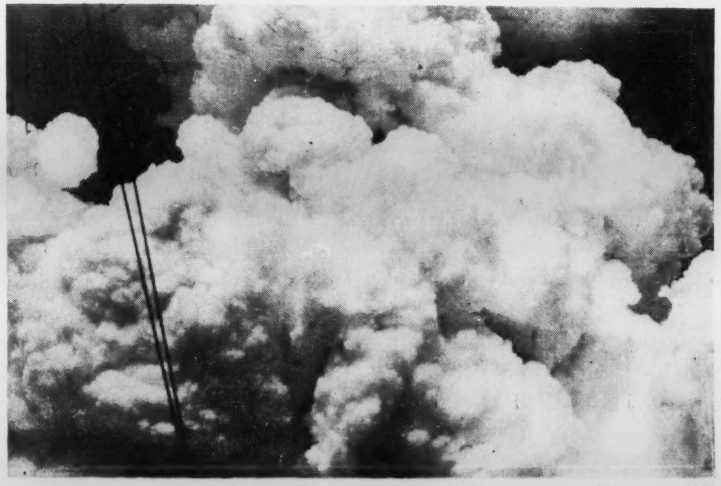

Fig. 48. Ditto 1 min.

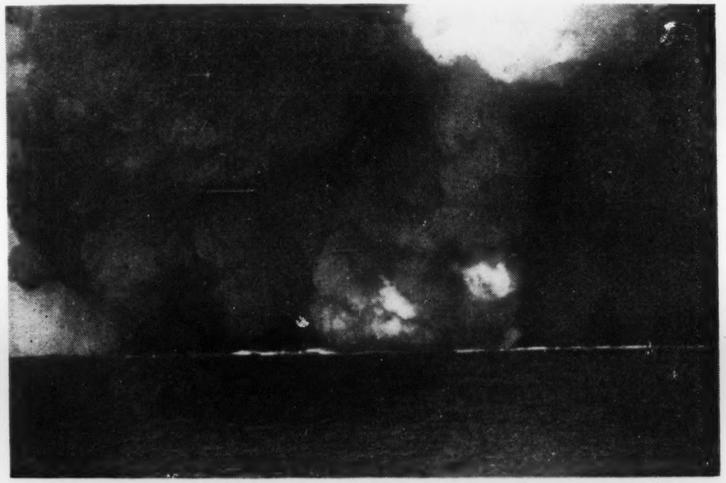
Fig. 49. Ditto 3 min.

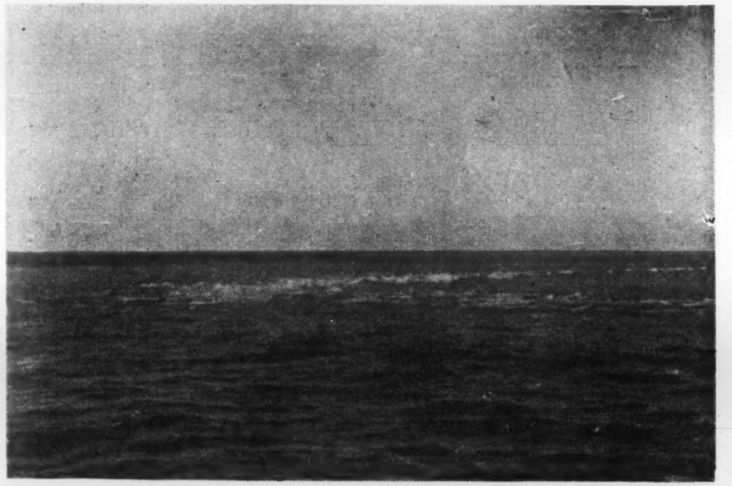
Fig. 51. Ejected pumice drifting southwestwards.

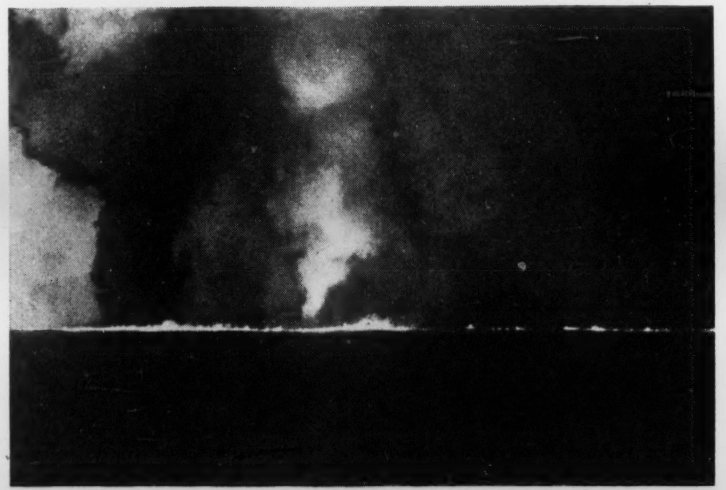
Fig. 50. Ditto 4 min.

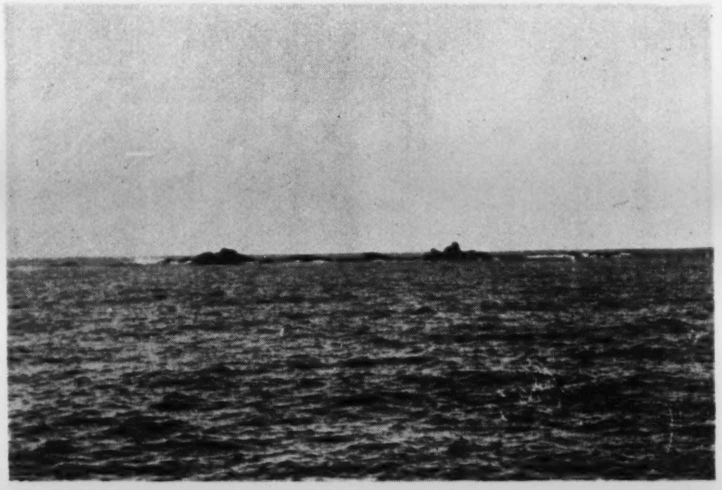
Fig. 52. The Bayonaise rocks.

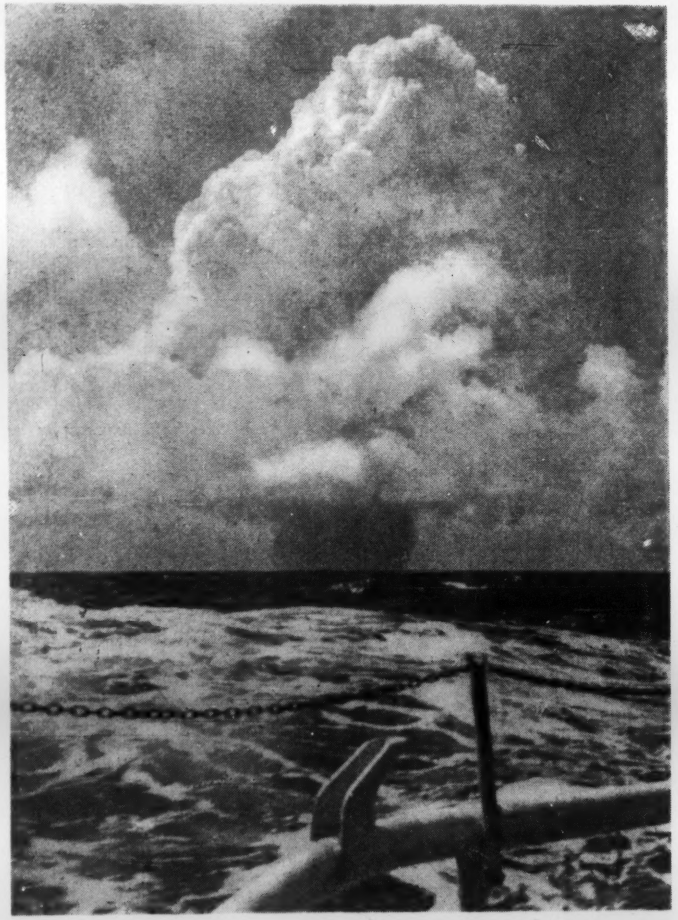

Fig. 53. A major submarine explosion at 12h35m on Sept. 26, 1952, viewed from the patrol ship "Shikiné". Left: Diameter of the cloud at sea surface was about 2,300 m. Right: A succeeding stage of the explosion shown in left.

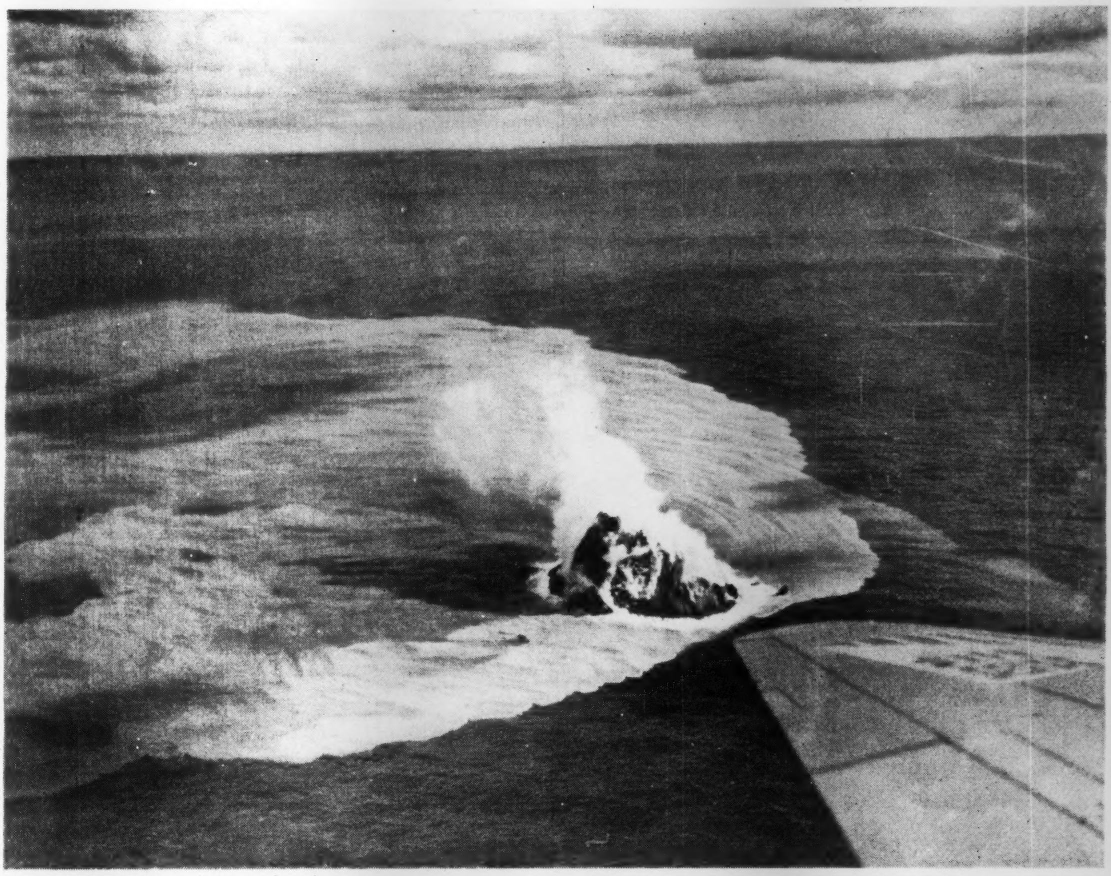

Fig. 54. An aerial view of the Myôjin reef in activity after its 2nd appearance from under the water. December 27, 1952. Photo. by Z. Ishii of Yomiuri Press.

(震研彙報 第三十三号 図版 森本・小坂)

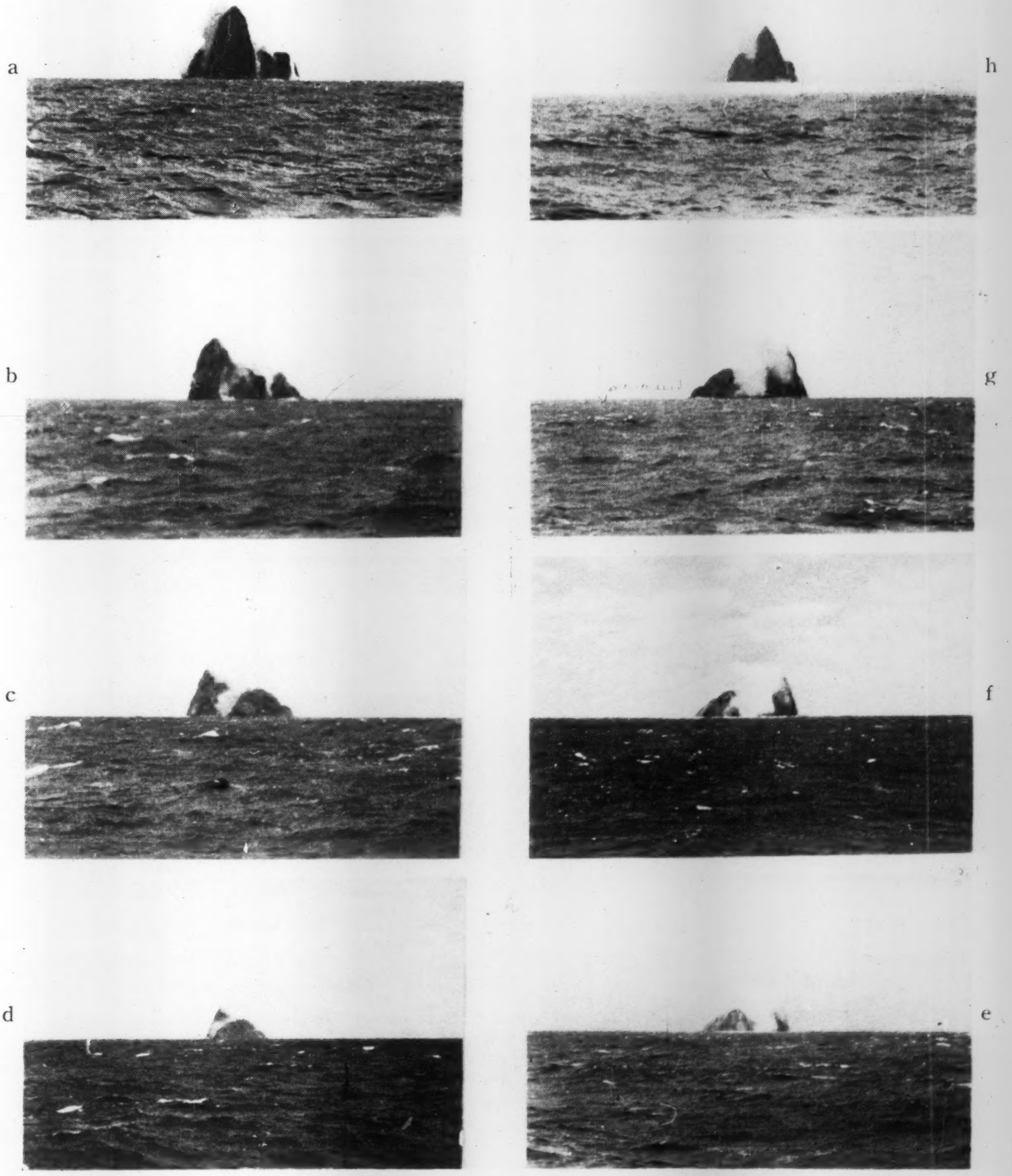

Fig. 55. Volcanic spines of the Myôjin reef after its second appearance on the sea: a, b,....h are southeastward, eastward, northeastward, northward, northwestward, westward, southwestward, and southward views respectively. Compiled by the writers from many photographs of J. Kusaka of Asahi Press. 07h–10h in the morning of February 1, 1953. Highest peak being estimated as about 94 m above sea level (Cf. TOKYO COLLEGE OF FISHERIES, *op. cit.* 39.)

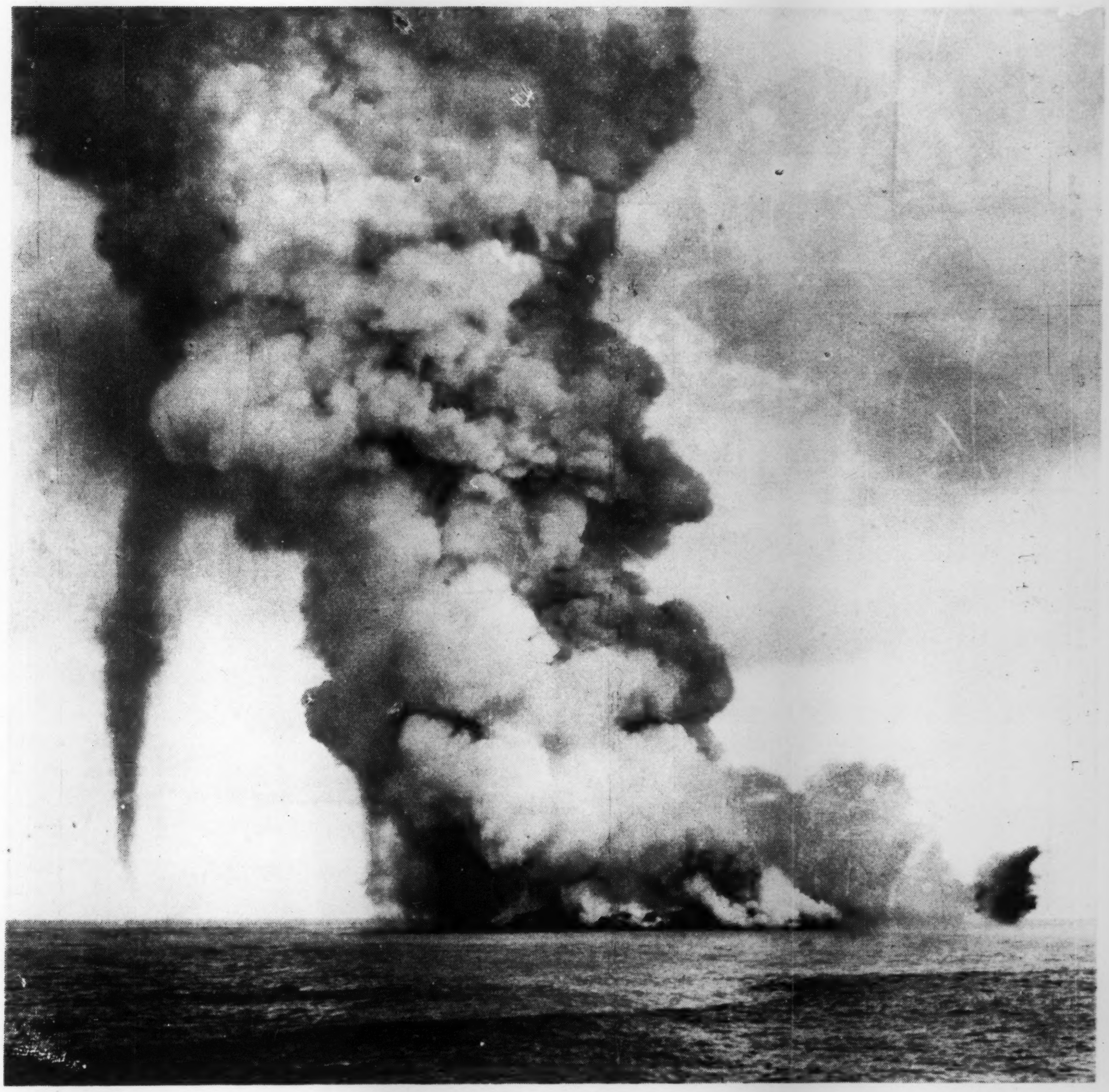

Fig. 8. Ash fall and emission of ash and vapour. The Myôjin reef viewed from the patrol ship "Shikiné", about 09h, September 18, 1952.

Photo. by C. Haraikawa of Yomiuri Press.

（震研彙報 第三十三号 図版 森本・小坂）

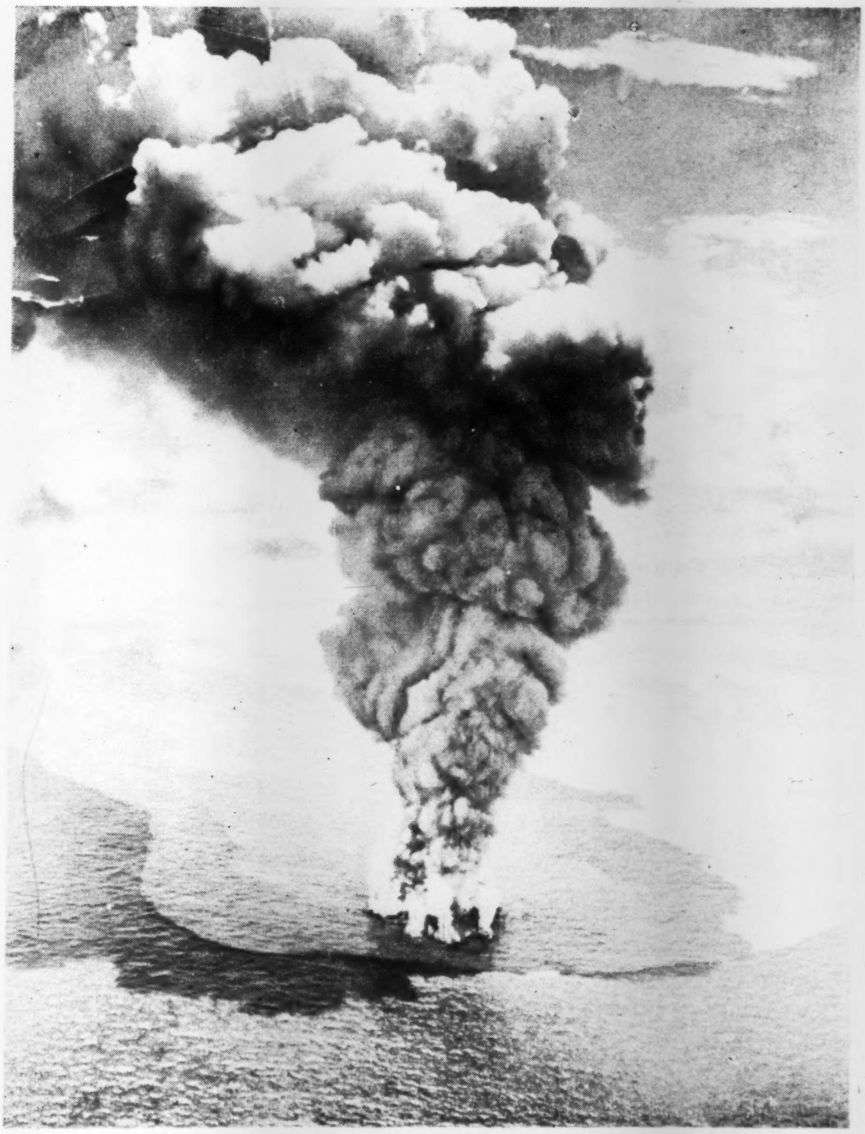

Fig. 9. An aerial view (southwestward) of the Myôjin reef in eruption, about 11 h, September 18, 1952. The sea water around the reef changes its colour into yellow being stained with volcanic material, and moves toward the background of the photograph.

(Asahi Press)

（震研彙報 第三十三号 図版 森本・小坂）

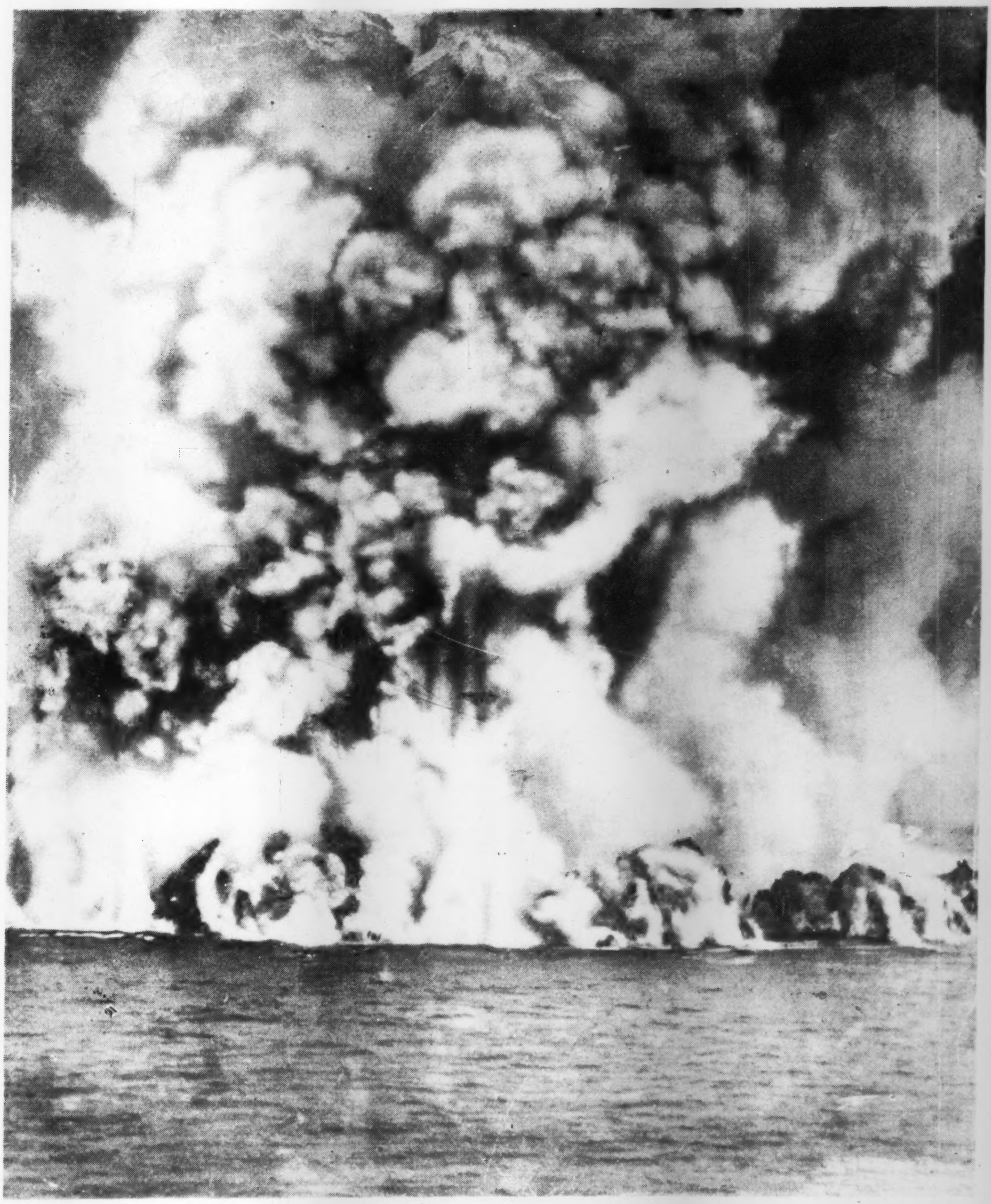

Fig. 10. Blocky head of the lava dome vomiting ash cloud and vapour, the Myôjin reef at its first appearance from the sea viewed down from an aeroplane about 70 m. above sea level. At about 18 h, September 18, 1952.

Photo. by T. Takei of Yomiuri Press.

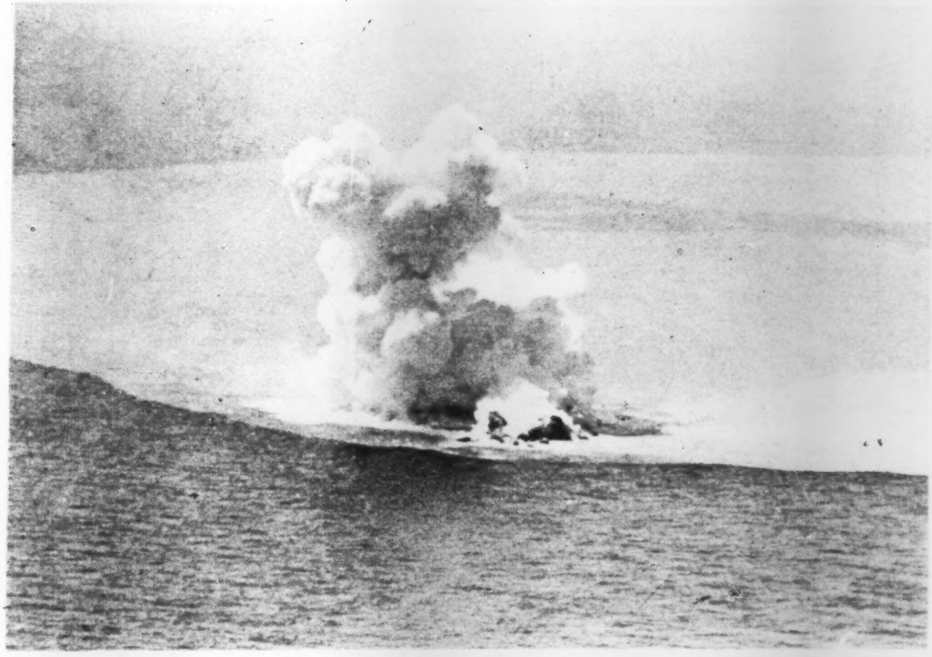

Fig. 11. An aerial view of the Myôjin reef in activity, about 09 h, Sept. 22, 1952 (Asahi Press).

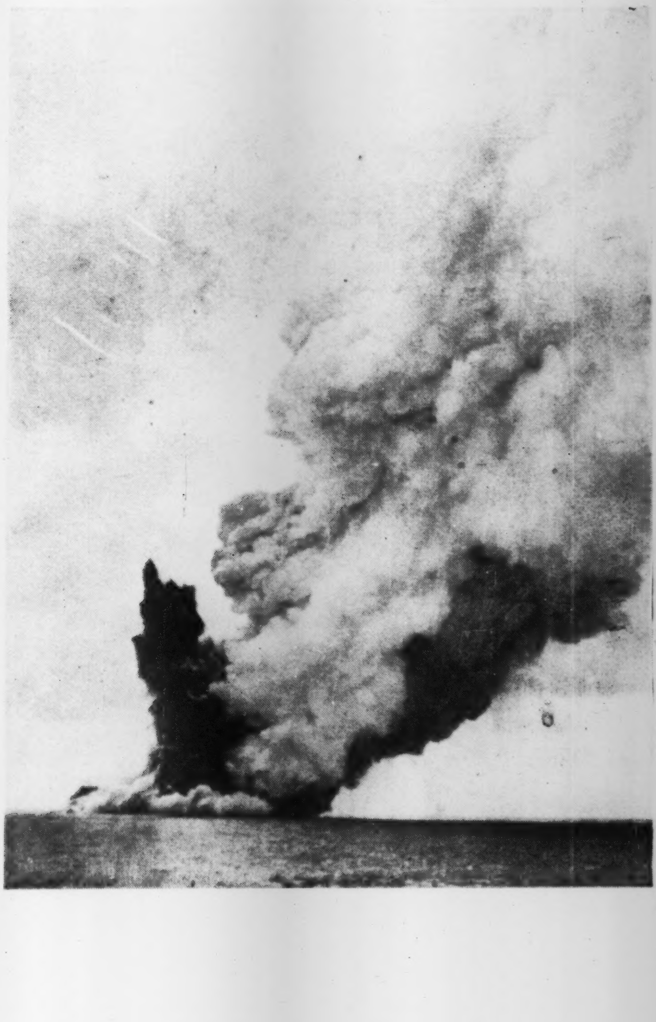

Fig. 12. An explosive activity of the Myôjin reef, about 09 h, Sept. 22, 1952 (Asahi Press).

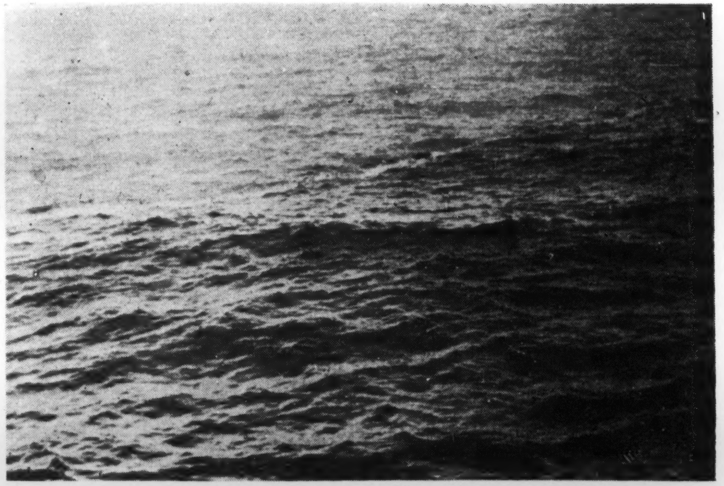

Fig. 13. Non-contaminated Kuroshio counter current (here) and the contaminated yellowish sea water (there). Along the boundary between the two, grains of white pumice were drifted.

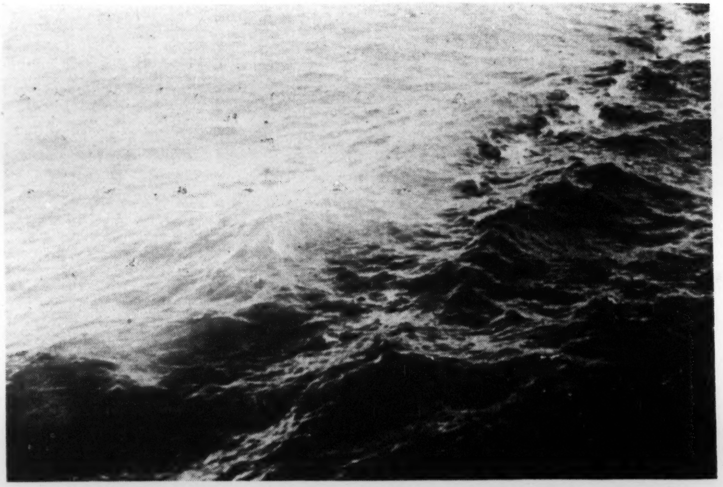

Fig. 15. A close view of the boundary between the contaminated sea water (left) and the non-contaminated water (right).

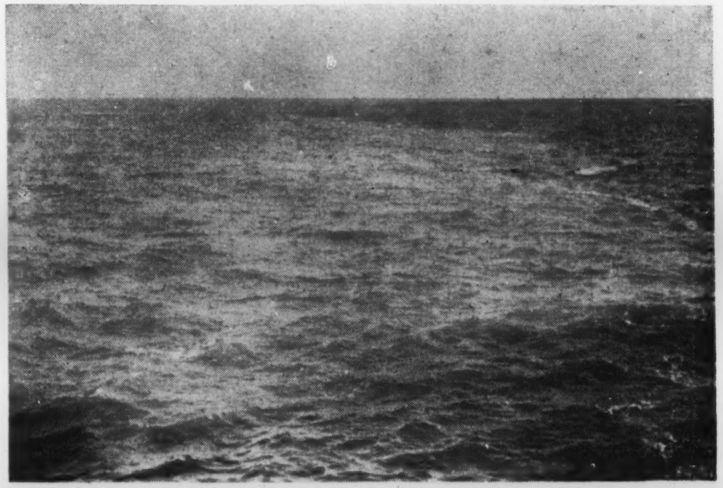

Fig. 14. The boundary between the yellowish sea water stained with volcanic dust (left) and the non-contaminated sea water (right). White drifting material in the foreground are pumice grains.

Fig. 16. Oceanographical observation of the yellowish sea water.

(震研彙報 第三十三号 図版 森本・小坂)

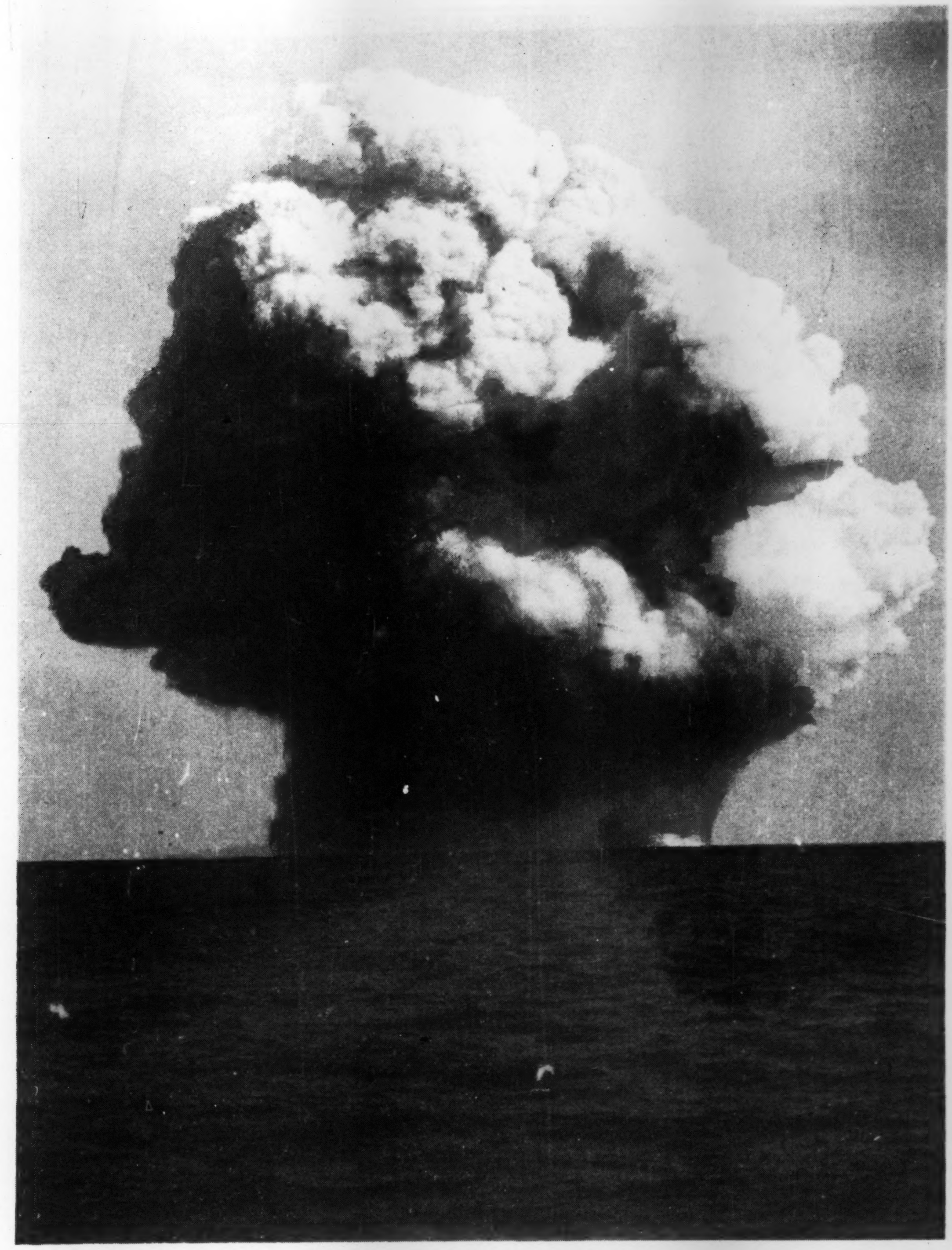

Fig. 17. A phase of a submarine explosion of the Myôjin reef which took place at 08h34m on Sept. 23, 1952. Cauliflower-shaped explosion cloud was rising about 1,800 m. high, neck column of the cauliflower being about 800 m. in diameter. A phase about several seconds after its first manifestation on the sea.

Fig. 18.

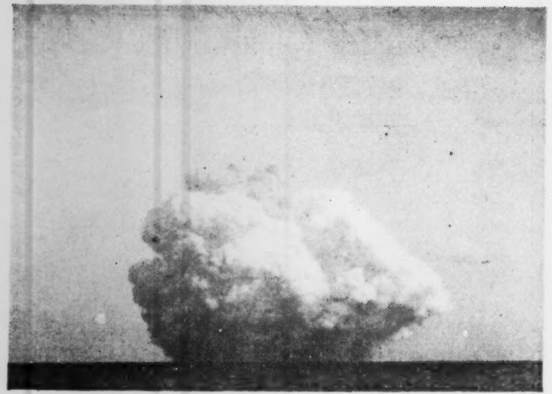
Fig. 21.

Fig. 23.

Fig. 19.

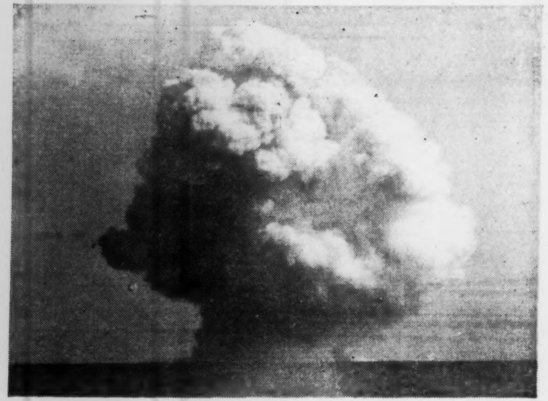
Fig. 22.

Fig. 20.

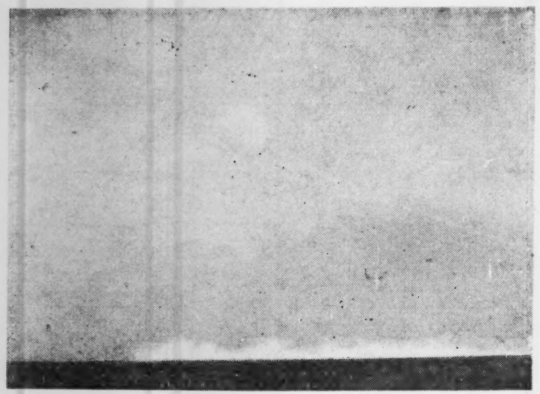
Fig. 25.

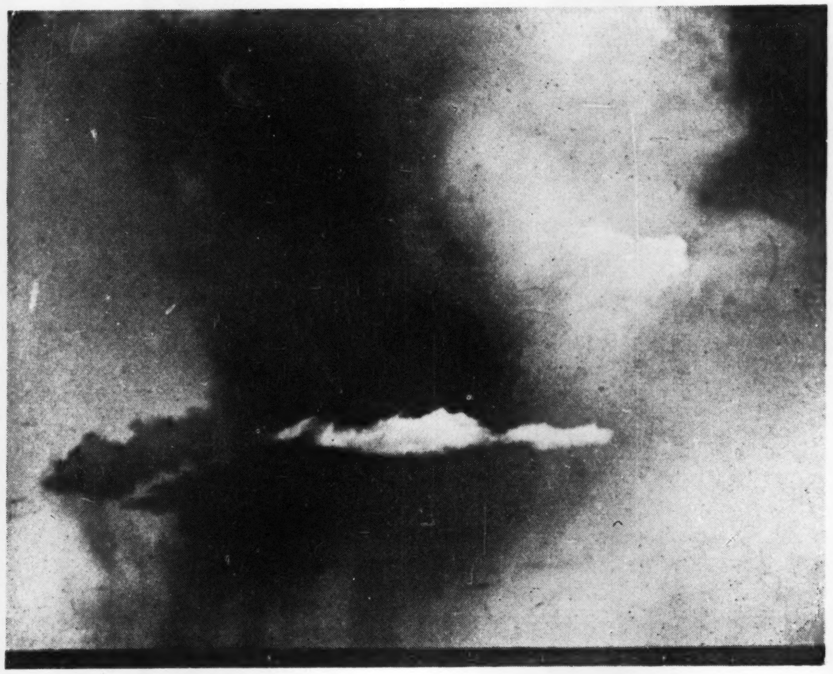
Fig. 24.

Figs. 20–27. The 08h34 m-explosion of the Myôjin reef on Sept. 23, 1952. Cf. pp. 241–242 and Table III.
One millimetre on the photographs corresponds to about 30 m. in actual distance, i.e., 3.3 mm. on the photographs to about 100 m. in actual distance.

[Bull. Earthq. Res. Inst., Vol. XXXIII, Pl. XLVIII.]

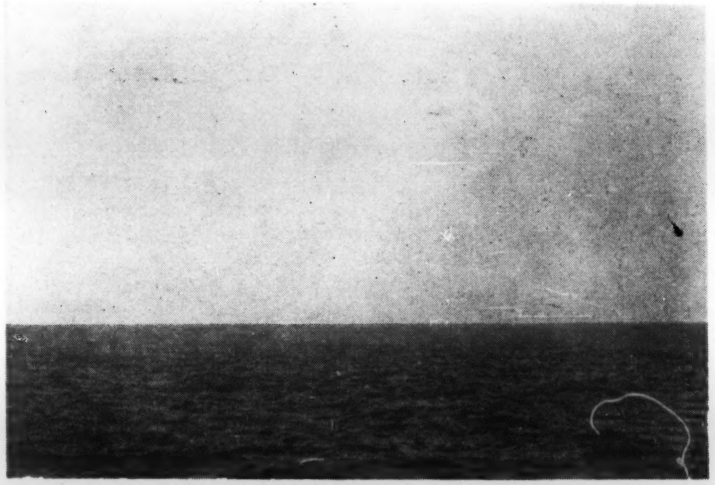

Fig. 26. Before the explosion.

Fig. 28. Ditto 3 sec.

Fig. 27. 1 sec. after the 1st manifestation of the explosion on the sea.

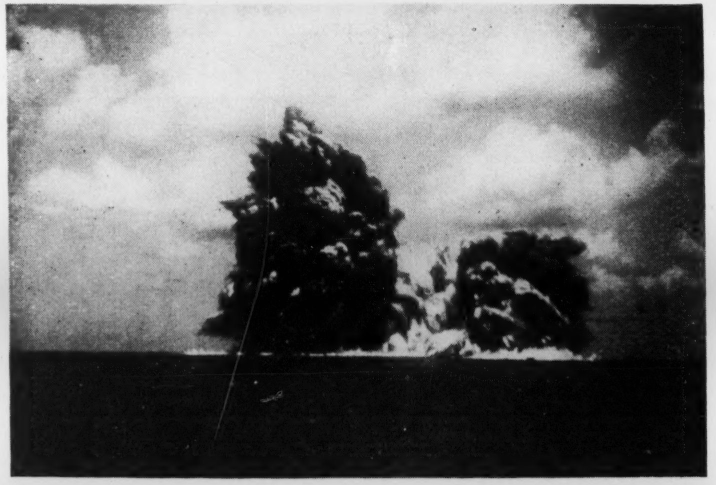

Fig. 29. Ditto 5 sec.

Figs. 26–40. Changing scene of the 13h12m-explosion. Cf. pp. 243–244 and Table IV. One millimetre on each photograph corresponds to about 138 m. in actual distance, i.e., 7.2 mm. on the photographs to 100 m. in actual distance.

(震研彙報 第三十三号 図版 森本・小坂)

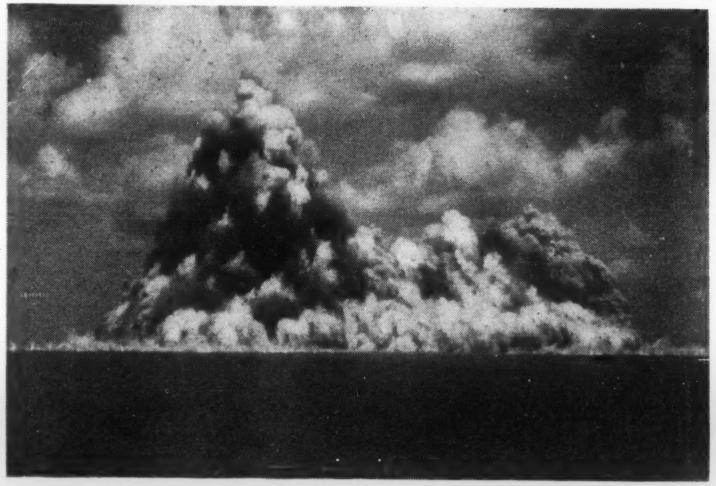

Fig. 30. Ditto 8 sec.

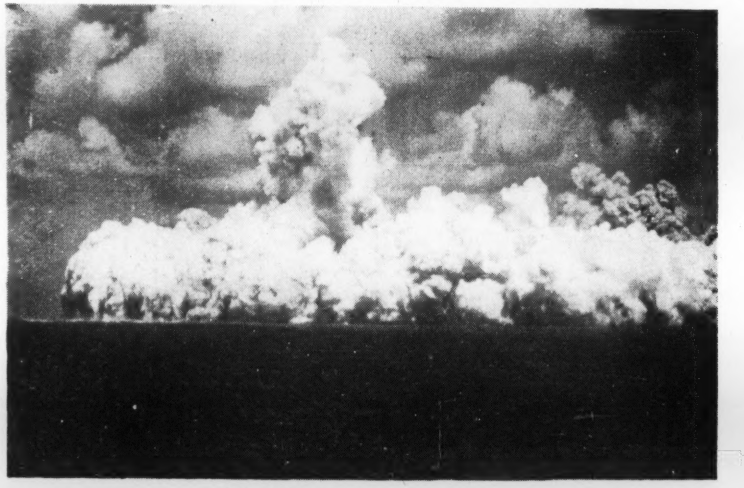

Fig. 32. Ditto 15 sec.

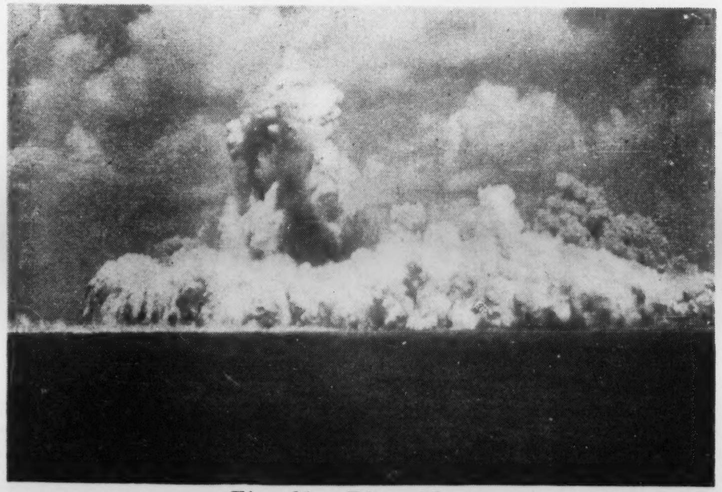

Fig. 31. Ditto 12 sec.

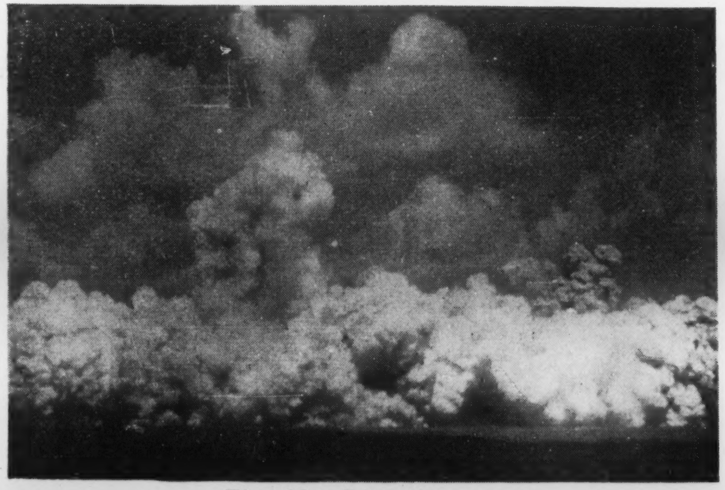

Fig. 33. Ditto 20 sec.

(震研彙報 第三十三号 図版 森本・小坂)

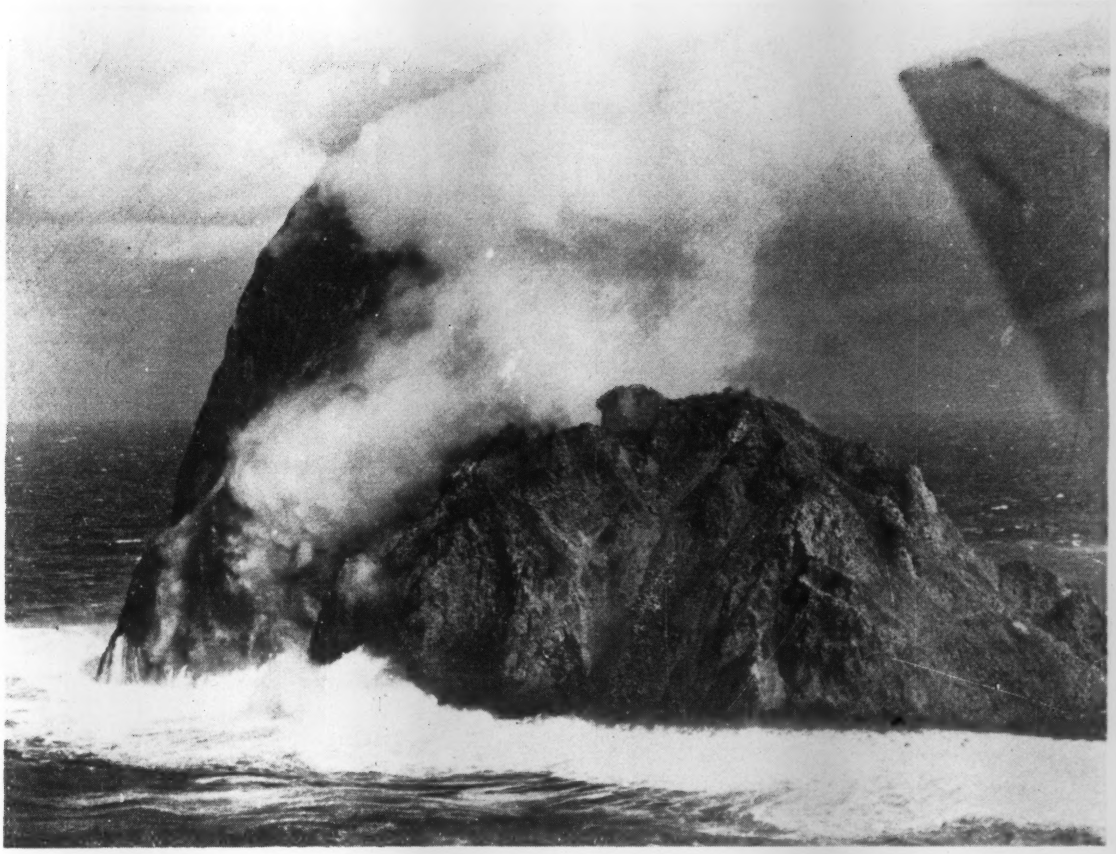

Fig. 56. Details of features of the lava dome and spine an aerial view of the Myôjin reef, February 8, 1953. Photo. by Z. Ishii of Yomiuri Press.

Fig. 57. After its second appearance on the sea since the beginning of October, 1952, the Myôjin reef submerged completely into the sea leaving the water stained with volcanic dusts on March 10, 1953.

Photo. by T. Isoyama of Yomiuri Press, March 11, 1953.

a)

b)

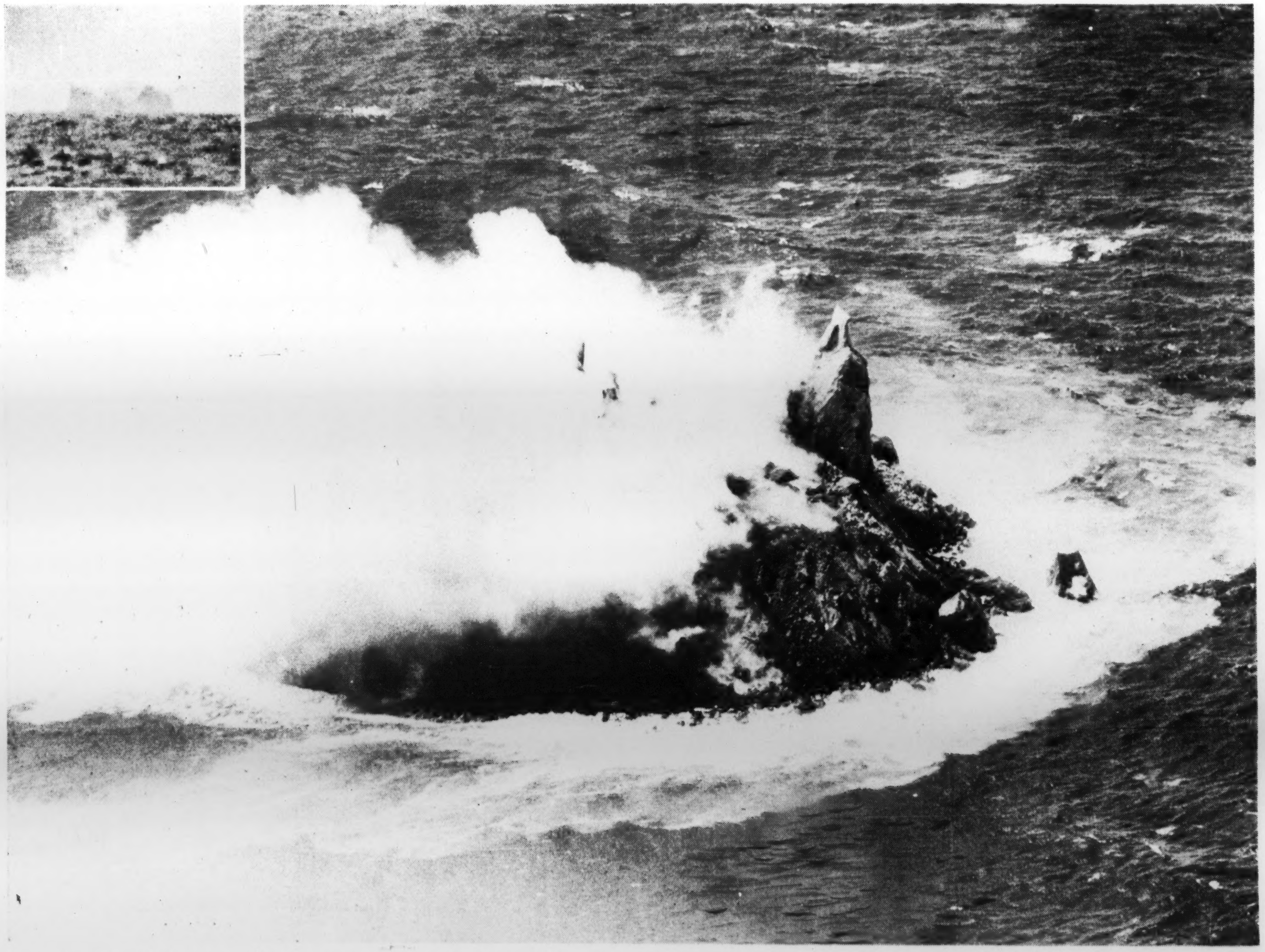

Fig. 58. Volcanic spine of the Myôjin reef in its third appearance on the sea, April 14, 1953. a) Southward view of the island from the patrol ship "Shikiné" of the Japanese Marine Safety Board, b) An aerial view (westward) from U. S. Air Force. By courtesy of the Hydrographic Office, Marine Safety Board of the Japanese Government.

17. *Geomagnetic Studies of Volcano Mihara. The 6th Paper.*

(Continuous Observation of Changes in Geomagnetic Declination during the Period from 1951 to 1954)

By Izumi YOKOYAMA,

Earthquake Research Institute.

(Read Feb. 22, 1955.—Received March 31, 1955.)

The studies on the changes in the geomagnetic field have been conducted in relation to the activities of Volcano Mihara since the 1950 eruption as has been reported in the previous papers[1]. On repeating dip surveys over the volcano, T. Rikitake found out a remarkable decrease in the geomagnetic dip-angle amounting to as much as 30 *minutes* of arc at its maximum during the early stage of the eruptions. Under the assumption that the changes are caused by the demagnetization of the volcano probably due to the temperature rise in the interior of the volcano, the demagnetized region was obtained as a sphere with a radius of 2 *km* at a depth of 5 *km* under the volcano for the first approximation. Since the discovery of strong magnetization of volcanic rocks, this sort of change in the geomagnetic field has been deemed to occur on occasions of volcanic eruptions especially on volcanoes composed of basaltic rocks which contain a large amount of titano-magnetite. For example, a local anomalous change was observed at the time of the 1940 eruption of Volcano Miyakeshima[2] though we have not yet been able to examine the changes in detail. In the case of Volcano Mihara, however, we could carry out many sorts of geomagnetic study from which we can say something about the general feature of local anomalous change in regard to volcanic activities.

In order to trace rigidly the changes in the geomagnetic field in

1) T. RIKITAKE, *Bull. Earthq. Res. Inst.*, **29** (1951) 161, 499.
T. RIKITAKE, I. YOKOYAMA, A. OKADA and Y. HISHIYAMA, *Bull. Earthq. Res. Inst.*, **29** (1951), 583.
I. YOKOYAMA, *Bull. Earthq. Res. Inst.*, **32** (1954), 17, 169.

2) R. TAKAHASHI and K. HIRANO, *Bull. Earthq. Res. Inst.*, **19** (1941), 82, 373.
T. NAGATA, *Bull. Earthq. Res. Inst.*, **19** (1941), 335.
T. MINAKAMI, *Bull. Earthq. Res. Inst.*, **19** (1941), 356.
Y. KATO, *Proc. Imp. Acad. Japan*, **16** (1940), 440.

relation to activities of Volcano Mihara, a continuous recording of declination has been carried out at the station No. 37 Nomashi village since April, 1951. Judging from the declination chart, this part of the island seems to be sensitive to changes in geomagnetic declination provided the changes are caused by the increase or decrease in magnetization of the volcano.

From the weekly record, hourly values are read off with which daily means are obtained and the semi-monthly means are calculated in order to see the gradual changes. The elimination of the errors due to transient magnetic disturbances such as magnetic storms is made by comparing the observation with that of Kakioka Magnetic Observatory, the standard observatory in Japan. The differences between them are tabulated in Table I and plotted in Fig. 1 together with their original

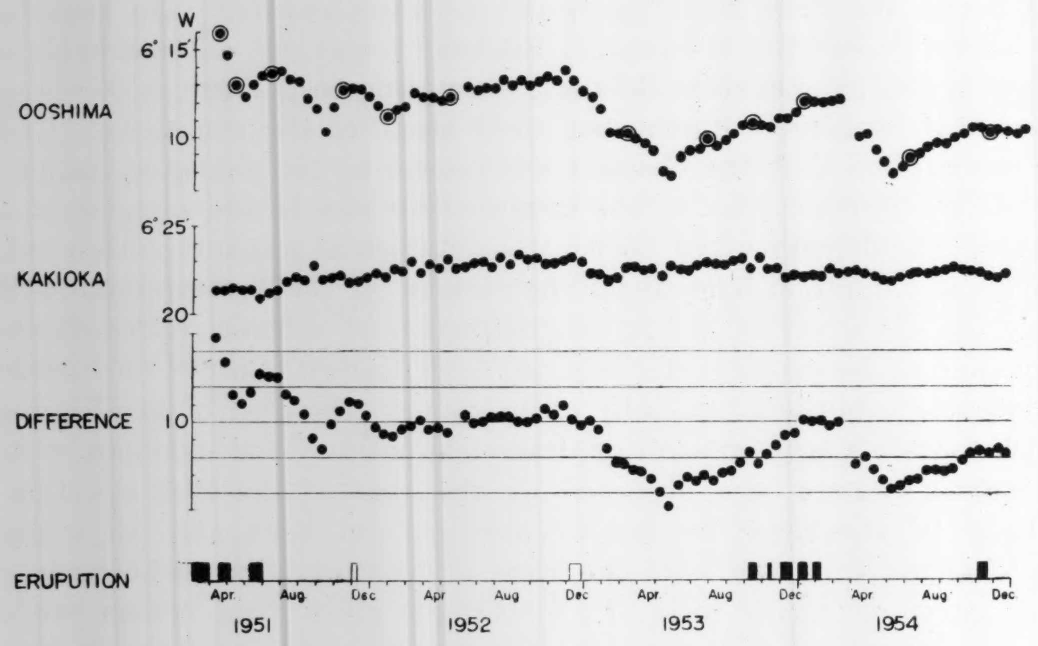

Fig. 1. The semi-monthly means of the westerly declination and activities of Volcano Mihara.

values. Those points surrounded with big hollow circles in the figure show that the base-line value of the magnetogram is checked at that epoch by absolute measurements with the aim of avoiding artificial drift. The sensibility of the variometer is usually 0.78 *minute* of arc per *mm* and the absolute values of declination are measured with an accuracy of 0.1 *minute* of arc for a single observation[3]. This degree

3) I. YOKOYAMA, *Bull. Earthq. Res. Inst.*, **31** (1953), 211.

Table I. The semi-monthly means of the westerly declination at Ooshima and Kakioka.

(Difference values for the periods of no observation are suitably corrected.)

Period	Ooshima	Kakioka	Difference
1951			
Apr.	6° 15′.8w	6° 21′.4w	−5′.4
	14.8	21.4	6.6
May	13.1	21.6	8.5
	12.4	21.4	9.0
June	13.1	21.4	8.3
	13.6	20.9	7.4
July	13.7	21.2	7.5
	13.9	21.4	7.5
Aug.	13.4	21.9	8.5
	13.3	22.2	8.9
Sept.	12.4	22.0	9.6
	11.8	22.8	11.0
Oct.	10.4	22.0	11.6
	12.1	22.1	10.2
Nov.	12.6	22.2	9.4
	12.8	21.8	8.9
Dec.	12.9	21.8	9.0
	12.4	22.1	9.7
1952			
Jan.	11.9	22.3	10.4
	11.3	22.1	10.8
Feb.	11.7	22.6	10.9
	11.6	22.4	10.6
Mar.	12.6	22.9	10.3
	12.4	22.4	10.0
Apr.	12.6	22.9	10.5
	12.2	22.6	10.4
May	12.7	23.1	10.7
	....	22.6	....
June	13.0	22.7	9.7
	12.8	23.0	10.2
July	12.9	23.0	10.1
	12.9	22.7	9.8
Aug.	13.4	23.2	9.8
	13.1	22.9	9.8
Sept.	13.4	23.4	10.1
	13.2	23.1	10.1
Oct.	13.4	23.2	9.9
	13.5	22.9	9.3
Nov.	13.4	22.9	9.6
	13.9	23.0	9.1
Dec.	13.3	23.3	10.0
	12.7	23.0	10.2

(to be continued.)

(continued.)

Period	Ooshima	Kakioka	Difference
1953 Jan.	6° 12′.4w	6° 22′.4w	−10′.0
	11.8	22.3	10.5
Feb.	10.3	21.9	11.6
	10.7	22.6	12.3
Mar.	10.3	22.7	12.4
	9.8	22.7	12.7
Apr.	9.8	22.5	12.8
	9.2	22.6	13.3
May	8.1	22.2	14.0
	7.9	22.8	14.9
June	9.0	22.6	13.6
	9.3	22.5	13.2
July	9.5	22.8	13.4
	10.1	23.0	13.0
Aug.	9.5	22.9	13.4
	9.9	22.9	13.0
Sept.	10.2	23.0	12.8
	10.8	23.2	12.4
Oct.	11.0	22.7	11.7
	10.8	23.2	12.4
Nov.	10.7	22.6	11.9
	11.0	22.6	11.4
Dec.	11.1	22.1	10.8
	11.5	22.2	10.7
1954 Jan.	12.1	22.1	9.9
	12.1	22.2	10.1
Feb.	12.1	22.2	10.0
	12.1	22.6	10.3
Mar.	12.3	22.4	10.1
	....	22.5	....
Apr.	10.8	22.5	12.4
	10.3	22.4	12.0
May	9.4	22.2	12.8
	8.8	22.0	13.4
June	8.2	22.0	13.9
	8.3	22.1	13.6
July	9.1	22.4	13.4
	9.2	22.4	13.2
Aug.	9.6	22.4	12.8
	9.8	22.5	12.8
Sept.	9.7	22.5	12.8
	10.0	22.8	12.7
Oct.	10.3	22.6	12.3
	10.5	22.5	11.9

(to be continued.)

(continued.)

Period	Ooshima	Kakioka	Difference
Nov.	6° 10′.7w	6° 22′.4w	−11′.7
	10.4	22.2	11.8
Dec.	10.6	22.1	11.6
	10.4	22.3	11.9

of accuracy is perhaps the highest one under the circumstances. The results shown in Fig. 1 are thought to be quite reliable because of the frequent absolute measurements. The activities of the volcano are shown in an arbitrary scale at the bottom of the figure. The period when eruptions were observed on the summit is marked with a black column, while the white one shows the period when we observed groups of earthquakes or tremors of volcanic origin and topographical deformations in the crater though no eruption was reported. The 1951 eruption had reached its final stage when the continuous observation was commenced. The volcano did not show any apparent activities in 1952, though it erupted again in October, 1953. This activity continued intermittently until February, next year and about 1.5×10^6 *tons* of new lava welled up on Jan. 27. A minor eruption, which turned to be the last activity, was observed in November, 1954.

As is clearly shown in the figure, the declination at Nomashi Station tends towards the west whenever the volcano becomes active and returns eastward after the subsidence of activity. As for the general tendency during the whole period, a gradual eastward drift of several *minutes* of arc is noticeable. The change observed here firmly supports the physical interpretation concerning the relation between magnetization and internal temperature of the volcano as discussed in the previous papers. It has also been proved that the changes in the declination observed at the station harmonize with those in any geomagnetic components which are obtained by examining the repeated geomagnetic surveys over the volcano.

The proposed theory suggests that the change at another station on the east side of the island should be in the opposite direction. Although it is not easy to add a new station owing to unavoidable circumstances in Ooshima Island, it is possible to compare the changes at the two stations on both sides of the island using the results of absolute measurements. A few observations at the same epoch on both sides of the island have been made. The changes at the two stations compared with Kakioka, the semi-monthly means for Nomashi and the instant

values for Zoo (east side), are plotted in Fig. 2. Black circles in the figure show the values corrected by the difference of secular variation between Kakioka and Ooshima Island. It is noticeable that the declination has been drifting to the opposite direction on both stations. Thus the proposed physical theory seems to be approximately acceptable.

Summarizing the results mentioned above, we can definitely say that local anomalous changes of a particular type take place in relation to the volcanic activities of Volcano Mihara. But we can not say that the geomagnetic phenomena related to active volcanoes are wholly understood at the present stage of investigation. Further considerations, especially concerning the mechanism of apparent demagnetization or magnetization in the interior of volcanoes should be made in future studies.

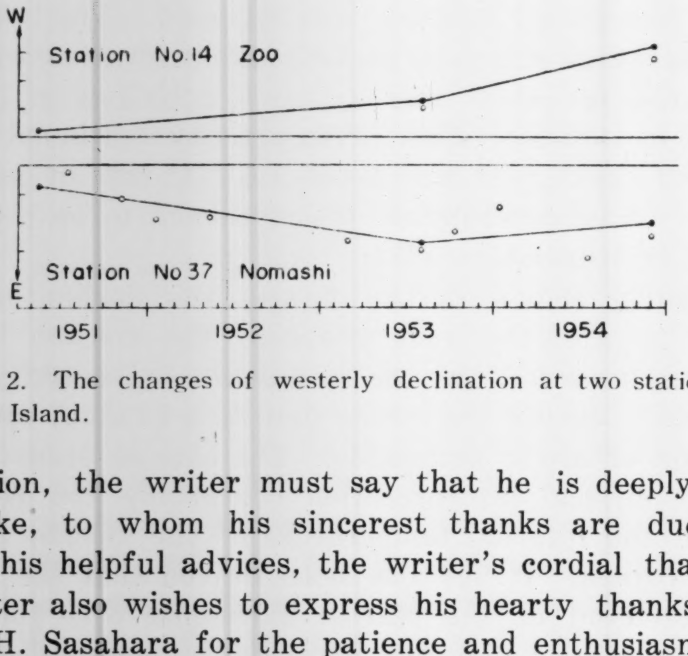

Fig. 2. The changes of westerly declination at two stations in Ooshima Island.

In conclusion, the writer must say that he is deeply indebted to Dr. T. Rikitake, to whom his sincerest thanks are due. To Prof. T. Nagata for his helpful advices, the writer's cordial thanks are also due. The writer also wishes to express his hearty thanks to Messrs. T. Yanai and H. Sasahara for the patience and enthusiasm with which they assisted the writer in the observations.

17. 三原山の地球磁気学的研究 第 6 報
(1951～1954 年間の偏角変化の連続観測)

地震研究所 横 山 泉

火山活動にともなう地球磁場の変化に関する研究は，三原山の 1950–51 噴火を契機として第二段

階に入つた．全島伏角測量および三成分絶対測定と平行して，この変化の推移を詳細に吟味するために，偏角変化の連続観測を 1951 年 4 月から大島西海岸の野増村で始めた．この結果の一部は既に報告してあるが，1951–54 年間の結果をまとめてこゝに報告した．また西側の変化に対する東側の変化を吟味することは有意義であるので，野増村と動物園との絶対測定の値を比較した．まだ資料は少いが，大体両者は反対方向に変化するとみなされる．

以上の結果から，三原山の火山活動にともなう地球磁場の変化が確認され，それはまた火山内部の状態に関する吾々の物理学的解釈を一応支持するものである．しかしながら火山内部の帯磁の変化と熱的状態との関係は簡単なものではないようである．この議論は今後行う予定である．

所　報

◎談話会記事

第317回談話会（昭和29年12月21日）

1. デイジタル方式による振動の記録（その1）　笠原慶一
2. 長週期地震計の試作　田望（松沢所員紹介）
3. 福井平野周辺地域に発達する割れ目系　村井勇
4. 青森県天間林地区における磁気探鉱
   附話　震研型アース・インダクターの製作　横山泉
5. 大理石の弾性と高圧実験に就いて　下鶴大輔
6. 地球核内の電磁流体振動　力武常次
7. 湖氷中に発生する自然震動の研究　表俊一郎・山崎良雄・小林直吉・村内必典

第318回談話会（昭和30年1月25日）

1. 応力と岩石の弾性
   1 軸圧に対する破壊領域を中心として　下鶴大輔・川原誠一郎・小林直太
2. 懸濁液中の音波の速さ
   附　静水圧を受けた多孔質媒質中の弾性波の速さ　佐藤泰夫
3. 二上山の地質（補遺）　森本良平・藤田和夫・笠間太郎・市原実
4. 二上山及びその近接地域の新生代火山活動　森本良平

第319回談話会（昭和30年2月22日）

1. 三原山の地球磁気学的研究
   （第6報）1954年観測結果概報　横山泉
2. 周期的加力による地盤振動に対する一つの解釈　金井清
3. 地震動振幅と地表層の性質との関係　第4報　金井清
4. 明神礁の海底噴火（補遺）　森本良平・小坂丈予
5. 富士山の宝永4年噴火について　津屋弘逵
6. 開口耐震壁の研究（其の1）
   1 層の場合　武藤清・大沢胖

第320回談話会（昭和30年3月22日）

1. 物体の落下によつて起される土地の衝撃とその人体感覚について　岸上冬彦
2. 一様磁場内に置かれた導電流体球の電磁流体振動　力武常次
3. 通信理論の振動学的応用（その1）　河角広

4. 浅間火山の活動と微小地震の研究（続報）　水上　武，内堀貞雄，茂木清夫，平賀士郎，宮崎　務，高橋智子

追加　開口耐震壁の研究（其の 2）
　　高層の場合　武藤　清，大沢　胖

第321回談話会（昭和30年4月26日）

1. 弾性波の発生機構に関する実験（第7報）　笠原慶一
2. 続応力と岩石の弾性　特に1軸圧に対する破壊領域について　下鶴大輔
3. 表面層を持つ媒質内の Rayleigh 波と妹沢波の存在限界　佐藤泰夫，山口林造
4. 妹沢波（M_2 波）について（補遺）　金井　清
5. 地震動振幅と地表層の性質との関係（第5報）　金井　清，吉沢静代
6. 地震動による建物振動の観測結果（第4報）　金井　清，鈴木富三郎

第322回談話会（昭和30年5月24日）

1. ラブ波の速度を求める計算図表　佐藤泰夫
2. 大型構造物試験機の衝撃振動　武藤　清
3. 大正4年第3高根丸の明神礁における遭難について　塚本裕四郎（那須所員紹介）
4. 大阪市内における常時微動の測定（序報）　金井　清，田中貞二，森下利三
5. 振動解析器の理論について　河角　広
6. レスポンスアナライザーによる地震動の研究（其の1）　高橋龍太郎，相田　勇
7. ゴム模型による耐震壁の剛性実験　武藤　清，大沢　胖

第323回談話会（昭和30年6月28日）

1. Love 波の分散曲線の解析について　高橋健人
2. 高周波有線搬送式遠隔記録地震計　宮村摂三，松本英照
3. 超短波無線搬送式遠隔記録地震計　宮村摂三，辻浦　賢
4. 超短波無線電話震研 1～6 号機使用成績報告　辻浦　賢，松本英照
5. 日本に於ける地磁気短周期変化の異常と地下構造（第6報）
　　新らしい観測結果について　力武常次，横山　泉
6. 日本に於ける地磁気短周期変化の異常と地下構造（第6報）
　　海の影響について　力武常次，横山　泉
7. 地殻内電磁誘導に関する模型実験
　　（力武，横山の研究に対する1補遺）　永田　武，小口　高

8. 地震動振幅と地表層の性質との関係（第 6 報） 金井 清 / 吉沢 静代

9. 東京都地盤調査結果（第 3 報） 地盤研究会

10. 地盤振動性能の図式解法 高橋龍太郎

昭和30年8月5日印刷
昭和30年8月10日發行

東京都文京區本富士町一番地
東京大學構內
編纂兼發行者　東京大學地震研究所

東京都千代田區富士見町一丁目十番地
印刷者　笠井康頼

東京都千代田區富士見町一丁目十番地
印刷所　株式會社 國際文献印刷社

賣捌所　東京都千代田區神田一ツ橋通
岩波書店

東京都中央區日本橋通二丁目六番地
丸善株式會社

Sold by
Iwanami Shoten,
Hitotsubashi dôri, Chiyoda-ku, Tôkyô,
and
Maruzen Co., Ltd.,
Nihonbashi dôri, Chûô-ku, Tôkyô.
Price of this copy: 388 Yen. (Postage exclusive.)

BULLETIN OF

THE EARTHQUAKE RESEARCH INSTITUTE

TOKYO UNIVERSITY

Vol. XXXIII, Part 2. June, 1955.

30TH ANNIVERSARY VOLUME

Contents.

Papers and Reports.

Page

12. T. RIKITAKE, Magneto-hydrodynamic Oscillations of a Conducting Fluid Sphere in a Uniform Magnetic Field. (in English) ... 175
13. S. ASANO, On the Accuracy of Hypocentre Determination II. (in English) ... 199
14. F. KISHINOUYE, Human Susceptibility to Shock Vibrations of the Ground. (in English) ... 207
15. Y. SATÔ, Relation between Seismic Intensity and Epicentral Distance. (2) (in English) ... 211
16. R. MORIMOTO and J. OSSAKA, The 1952–1953 Submarine Eruption of the Myôjin Reef near the Bayonnaise Rocks, Japan (I). (in English) ... 221
17. I. YOKOYAMA, Geomagnetic Studies of Volcano Mihara. The 6th Paper. (Continuous Observation of Changes in Geomagnetic Declination during the Period from 1951 to 1954) (in English) ... 251

Institute Notes.

(For the papers written in Japanese or in occidental languages, the abstracts are given in occidental languages or in Japanese respectively.)

BULLETIN OF THE EARTHQUAKE RESEARCH INSTITUTE,
TOKYO UNIVERSITY. Vol. XXXIII, Part 3. September, 1955.

東京大學
地震研究所彙報

第33號　第3册

昭和30年9月

創立30周年記念号

目　次

論文及報告

			頁
18.	地盤のスペクトル応答を求める図式解法（英文）	高橋龍太郎	259
19.	表面層をもつ媒質内の Rayleigh 波と妹沢波の存在限界（英文）	山口林造 佐藤泰夫	265
20.	妹沢波（M_2 波）について（第2報）（英文）	金井清	275
21.	周期的加力による地盤振動に対する1つの解釈（英文）	金井清	283
22.	Love 波の分散曲線の解析（英文）	高橋健人	287
23.	日本に於ける地磁気短周期変化の異常と地下構造（第6報）（その後の観測結果及び地磁気変化におよぼす海の影響）（英文）	力武常次 横山泉	297
24.	北海道・海岸湖の鹹度変化（独文）	湊正雄 北川芳男	333
25.	富士火山の地質学的並びに岩石学的研究（V） 5. 富士山の宝永4年噴火について（英文）	津屋弘逵	341
26.	筑波地方産花崗岩の副成分重鉱物（英文）	市村毅	385
27.	地震観測用磁気テープ利用ひきがね式遅延記録装置（英文）	表俊一郎 宮村摂三 山崎良雄	397
28.	弾性波の発生機構に関する実験（第5報）（英文）	笠原慶一	411
29.	月山火山の活動（英文）	市村毅	419
30.	北海道・第四紀火山の時代的分類（独文）	湊正雄	433
31.	応力と岩石の弾性，特に破壊領域に就いて（英文）	下鶴大輔	437
32.	静川層群について（附　第三紀地殻運動の一考察）（邦文）	大塚彌之助	449
33.	東京都地盤調査報告（邦文）	地震研究所地盤研究会	471

(The titles in occidental languages are given on the back cover.)

本彙報ハ年4回（但シ第1號ヨリ第6號マデハ不定期ニ，第7號ハ3冊トシテ發行セリ），彙報別冊ハ不定期ニ發行ス．

本彙報掲載ノ論文及ビ報告ノ內容ニ關シテハ著者ノミニ其責任アルモノトス．

本彙報ニ關スル照會通信ハ東京大學地震研究所長ヘ宛テラレタシ．

The Bulletin is published quarterly. (Vols. I–VI were published at irregular intervals and Vol. VII consisted of three parts.)

Supplementary Volume is published at irregular interval.

The authors of the papers alone are responsible for the statements and opinions contained in their respective papers.

All communications relating to this Bulletin should be addressed to the Director of the Earthquake Research Institute, Tokyo University.

18. *A Short Note on a Graphical Solution of the Spectral Response of the Ground.*

By Ryûtaro TAKAHASI,

Earthquake Research Institute.

(Read June 28, 1955.—Received June 30, 1955.)

1. When an infinite train of harmonic elastic waves of unit amplitude is propagated from beneath to a stratified ground, the amplitude of oscillation at the surface of the ground is a function of the wave length, and is called the spectral response of the ground.

The spectral response is a very important function because it enables us to calculate, in the Fourier manner, the response of the ground to an arbitrary disturbance. Another important point is that the spectral response explains the dominant periods of the ground which appear on occasions of earthquakes and microtremors.

2. The layers are numbered from top to bottom, so the quantities related to the uppermost layer are denoted by the suffix 1. The semi-infinite bedrock is denoted by the suffix n. The amplitude of the incident wave is u_0, and the amplitude of the ground motion at the surface is $2u$. v, τ and c mean respectively the particle velocity, the shearing stress and the propagation velocity of the elastic waves.

Since the incident wave train is infinite in length, waves propagated respectively upwards and downwards result in a stationary oscillation of the layer, because we assume the dissipation of the wave energy in the layers to be negligibly small.

In the layer i, we have

$$v_i = \frac{v_{i0}}{\cos\theta_i}\cos\left(\frac{\omega x_i}{c_i}+\theta_i\right), \qquad (1)$$

$$\tau_i = \frac{v_{i0} z_i}{\cos\theta_i}\sin\left(\frac{\omega x_i}{c_i}+\theta_i\right), \qquad (2)$$

in which v_{i0} is the value of v_i at the upper boundary of the layer from which x_i is measured downwards. z_i is equal to $jc_i\rho_i$, ρ_i being the density of the soil and $j=\sqrt{-1}$. ω is the circular frequency of the waves. θ_i is the angle which is determined by the relation

$$z_i \tan\theta_i = z_{i-1}\tan\left(\frac{\omega H_{i-1}}{c_{i-1}}+\theta_{i-1}\right). \qquad (3)$$

This relation must hold at the upper boundary of the layer i, because v_i, τ_i must be continuous respectively with v_{i-1}, τ_{i-1} at the boundary. Since τ_1 must vanish at the ground surface $x_1=0$, we must have $\theta_1=0$.

3. As can be seen in the expressions (1) and (2), τ_i/z_i and v_i are proportional to the sine and cosine of $\left(\frac{\omega x_i}{c_i}+\theta_i\right)$, so they can be represented by the ordinate and abscissa of a point which moves on a circle of radius

$$v_{io}/\cos\theta_i=|v_i+j\tau_i/z_i|\,. \qquad (4)$$

As for the phase angle at the lower boundary of the layer i, we have the relation

$$\frac{\omega H_i}{c_i}+\theta_i=2\pi\frac{H_1}{L_1}\left(\frac{H_i}{c_i}\Big/\frac{H_1}{c_1}\right)+\theta_i\,. \qquad (5)$$

We can therefore determine in turn the values $v_{20}/\cos\theta_2,\cdots\cdot v_{n0}/\cos\theta_n$,—the maximum amplitudes of the stationary oscillation in each layer—, provided that we know ρ_1, $\rho_2\cdots\cdot\rho_n$; c_1, $c_2,\cdots\cdot c_n$ and the thickness of each layer H_1, $H_2\cdots\cdot H_{n-1}$. v_{10} is assumed to be unity.

Since $v_{n0}/\cos\theta_n$ is the maximum velocity amplitude of the stationary oscillation in the bedrock, the velocity amplitude due to the incident wave is a half of this value. We have therefore

$$\frac{2u}{u_0}=\frac{v_{10}}{\frac{1}{2}(v_{n0}/\cos\theta_n)}=\frac{2}{\frac{v_{n-1,0}}{\cos\theta_{n-1}}\left|\cos\varphi_{n-1}+j\frac{z_{n-1}}{z_n}\sin\varphi_{n-1}\right|} \qquad (6)$$

$$=2\Big/\left|\cos\varphi_{n-1}+j\frac{z_{n-1}}{z_n}\sin\varphi_{n-1}\right|\cdots\cdot\left|\cos\varphi_1+j\frac{z_1}{z_2}\sin\varphi_1\right|, \qquad (7)$$

where $\varphi_i=\frac{\omega H_i}{c_i}+\theta_i$. The last expression can easily be obtained from (1), (2) and (3).

4. Instead of seeking $2u/u_0$ directly, we will find out u_0/u, which is by (6) equal to $v_{n0}/\cos\theta_n$. The construction for getting this value is as follows: Referring to Fig. 1,

i) Take OA equal to unity on the x-axis.

ii) Give H_1/L_1 a convenient value. Draw a circular arc AB such that the angle $\angle AOB=360°\times H_1/L_1$. Drop a perpendicular BC on OA. Then $OC=v_{20}$ and $BC=\tau_{20}/z_1$.

iii) Find a point D on BC such that $CD=\frac{c_1\rho_1}{c_2\rho_2}BC$. Then $\angle DOC=\theta_2$, and OD is equal to the maximum amplitude of the stationary waves in the layer 2.

iv) Draw a circular arc DE and let $\angle EOD=\angle AOB\times\frac{H_2/c_2}{H_1/c_1}$. Drop a perpendicular EF on OC. The coordinates of the point E are v_{30} and τ_{30}/z_2.

v) Find a point G on EF such that $GF=\frac{c_2\rho_2}{c_3\rho_3}EF$. Then

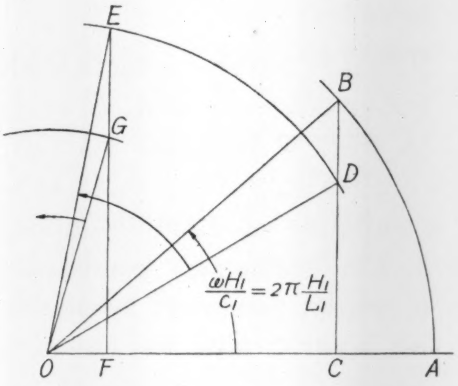

Fig. 1. $OA=1$
$DC: BC=c_1\rho_1 : c_2\rho_2$
$GF: EF=c_2\rho_2 : c_3\rho_3$
$\angle AOB=\varphi_1=2\pi H_1/L_1$
$\angle AOD=\theta_2$
$\angle DOE=2\pi\frac{H_1}{L_1}\left(\frac{H_2}{c_2}\Big/\frac{H_1}{c_1}\right)$
$\angle AOE=\varphi_2$
$\angle AOG=\theta_3$

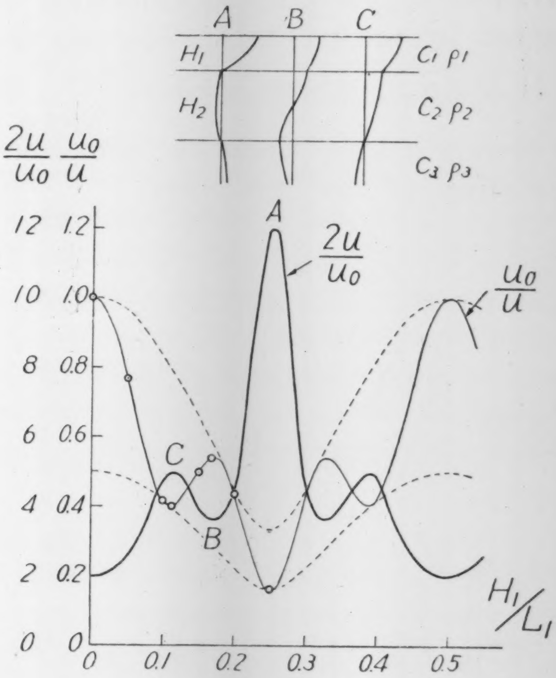

Fig. 2. $\rho_1=\rho_2=\rho_3$
$c_1 : c_2 : c_3=1 : 3 : 6$
$H_1 : H_2 : H_3=1 : 6 : \infty$
u_0: Amplitude of the incident waves
$2u$: Amplitude at the ground surface

$\angle GOF=\theta_3$ and the segment OG is equal to the maximum amplitude of the stationary oscillation in the layer 3.

vi) The procedure will be repeated until we get the amplitude of the stationary waves in the bedrock n. Then the amplitude gives us the value of u_0/u.

vii) The above procedures, i) to vi), are repeated, giving H_1/L_1 different values.

5. In Figs. 2–4 are shown spectral responses of grounds of various structures. In Fig. 2, the constants of layers are

$$\rho_1 : \rho_2 : \rho_3 = 1 : 1 : 1,$$
$$c_1 : c_2 : c_3 = 1 : 3 : 6,$$
$$H_1 : H_2 : H_3 = 1 : 6 : \infty.$$

In this case the spectral response is symmetric about the value of $H_1/L_1=0.25$ and has the period of $H_1/L_1=0.5$. Small circles in the Figure is the point obtained by the present method. Two dotted curves are envelopes of the u_0/u curve. As can be seen from Fig. 1, the upper envelope represents the radius vector OD of the ellipse which is described by the point D. This envelope can therefore be expressed as $\sqrt{1-k^2 \sin\varphi}$, where $k^2=1-\left(\frac{c_1\rho_1}{c_2\rho_2}\right)^2$ and $\varphi=2\pi\frac{H_1}{L_1}$. The lower envelope is merely $c_2\rho_2/c_3\rho_3$ times the upper envelope. These envelopes represent the effect of the first layer.

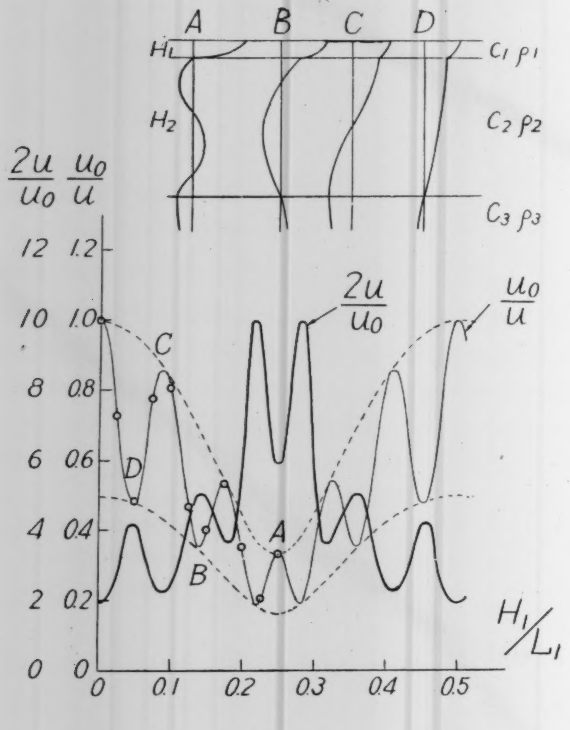

Fig. 3. $\rho_1=\rho_2=\rho_3$
$c_1 : c_2 : c_3=1 : 3 : 6$
$H_1 : H_2 : H_3=1 : 15 : \infty$
u_0: Amplitude of the incident waves
$2u$: Amplitude at the surface.

The u_0/u curve contacts with the upper envelope as at B when OG in Fig. 1 is equal to OE. This occurs only when φ_2 is zero or a multiple of 180°. This is when the stationary oscillation has a loop at the lower boundary of the layer 2 and we have $\tau_{30}=0$ there.

When the u_0/u curve contacts with the lower envelope as at C, we have $OE=\frac{z_2}{z_3}\times OG$, so the angle φ_2 must be a multiple of 90°. We have then $v_{30}=0$ which shows that there occurs a node at the inter-surface between the layers 2 and 3.

A in Fig. 2 is the special point where we have a node at each boundary between layers. This case occurs only when φ_1 and φ_2 are mutiples of 90° at the same time.

The points A, B, C do not generally coincide with the extremums of the u_0/u curve but are very near to them.

In the upper part of Fig. 2, modes of oscillation of the ground are shown for cases *A*, *B* and *C*, but they are not to scale.

In Fig. 3, the structure of the ground is as follows:

$$\rho_1 : \rho_2 : \rho_3 = 1 : 1 : 1$$
$$c_1 : c_2 : c_3 = 1 : 3 : 6$$
$$H_1 : H_2 : H_3 = 1 : 15 : \infty$$

Since H_2/c_2 is large in this case, the u_0/u curve oscillates more frequently between the envelopes, which are entirely the same curves with the envelopes in Fig. 2. Results shown in Figs. 2 and 3 agree with K. Kanai's.[1]

Fig. 4 deals with the case in which

$$\rho_1 : \rho_2 : \rho_3 : \rho_4 : \rho_5 = 1 : 1 : 1 : 1 : 1$$
$$c_1 : c_2 : c_3 : c_4 : c_5 = 1 : 2 : 3 : 4 : 8$$
$$H_1 : H_2 : H_3 : H_4 : H_5 = 1 : 3 : 6 : 6 : \infty$$

In this case curves are symmetric about the ordinate $H_1/L_1=0.5$ and have the period of $H_1/L_1=1.0$. *A* in the Fig. 4 indicates a special case in which there is a node at each boundary between layers. Even in such case, the value of $2u/u_0$ will never exceed $2c_n\rho_n/c_1\rho_1$.

6. The propagation of elastic waves in the ground normally to layers is similar to the propagation of electric waves in a transmission line with one end open. The soil particle velocity and stress due to the elastic wave corres-

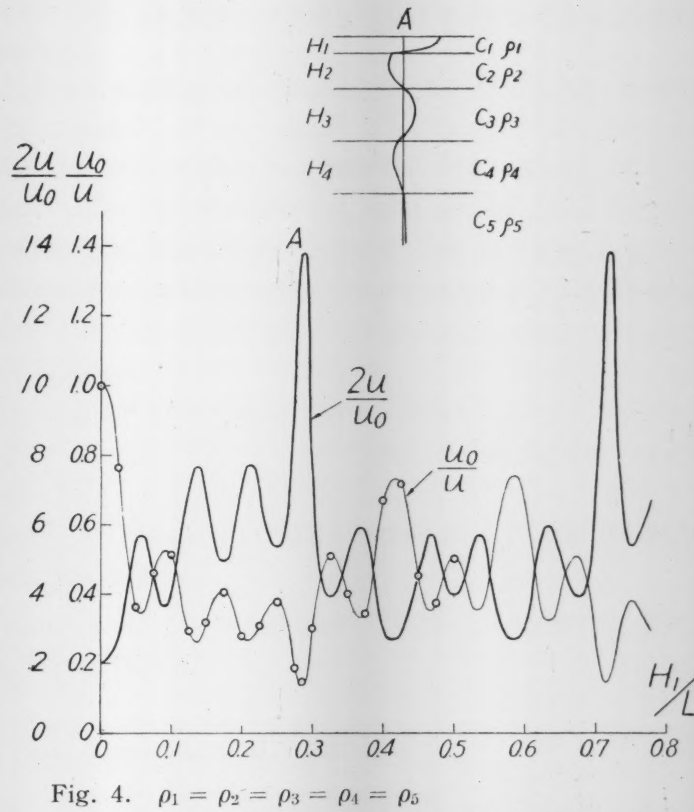

Fig. 4. $\rho_1 = \rho_2 = \rho_3 = \rho_4 = \rho_5$
$c_1 : c_2 : c_3 : c_4 : c_5 = 1 : 2 : 3 : 4 : 8$
$H_1 : H_2 : H_3 : H_4 : H_5 = 1 : 3 : 6 : 6 : \infty$

1) K. KANAI, "Relation between the Nature of Surface Layers and the Amplitude of Earthquake Motions. Part II.", *Bull. Earthq. Res. Inst.*, **31** (1953), 219.

pond to the current and voltage in the line. The present method is, in effect, a modification of the well-known method of the position angle but it has its own merit in that it furnishes a quick and intuitive solution of the problem.

18. 地盤のスペクトル応答を求める図式解法

地震研究所　高橋龍太郎

多数層から成る地盤に下方から垂直に無限長の単色弾性波が伝つて来る場合は分布常数線路に交流電圧が伝わる場合と同等であつて位置角の方法によつて計算することができる.

特に地盤内の粘性による減衰が省略できる場合には地盤内には定常波ができ，且つ同一層内の速度振巾と応力振巾/特性インピーダンスとは余弦と正弦の関係になるから，コンパスと分度器による簡単な作図によつて地表の振幅を単位とした地層内の振巾を次々に求めることができる．その方法は第1図によつて見うる．第 2~4 図には二三の例題を示した.

減衰を考えないから，短周期の振動や高次の振動に対しては次第に実際と喰違つてくるが，地盤の大体の振動特性を簡単に早く推察しうる所に利点がある.

19. *Range of Possible Existence of Rayleigh- and Sezawa-Waves in a Stratified Medium.*

By Rinzo YAMAGUCHI and Yasuo SATÔ,

Earthquake Research Institute.

(Read April 26, 1955.—Received June 30, 1955.)

1. Introduction

The problem of the possible existence of surface waves in a stratified medium was investigated by a number of authors and its nature was elucidated pretty well.

Of the various kinds of surface waves which are propagated upon the stratified medium, Love-waves have very simple property and will require no explanation today.

However, the range of existence of Rayleigh- as well as Sezawa-waves (M_2-waves), which consist of P- and SV-waves has not been clarified enough to satisfy us and make it possible for us to see into the details of the subject. The investigation was given this direction by K. Kanai[1] some years ago, and his graphs show the critical boundary of existence and non-existence of surface waves under a given condition of L/H, μ'/μ and $(v/v')^2$.

(Where L; wave length
H; thickness of the layer
μ', μ; rigidity of the layer and the substratum respectively
v', v; velocity of S-waves in the layer and the substratum respectively.)

Now, we will calculate this critical boundary more precisely, giving the parameters with smaller intervals.

2. The fundamental equation

Here, we will follow the investigation performed by K. Sezawa and K. Kanai.

1) K. KANAI, "On the M_2-waves (Sezawa waves)," *Bull. Earthq. Res. Inst.*, **29** (1951), 39.

The equation of dispersion curves of surface waves transmitted through a stratified body is, as presented originally by the above two authors[2)]

$$\frac{4r's'}{f^2}\left(2-\frac{k'^2}{f^2}\right)\eta-\frac{r's'}{f^2}\left\{4\vartheta+\left(2-\frac{k'^2}{f^2}\right)^2\zeta\right\}\cosh r'H\cosh s'H$$

$$+\frac{r'}{f}\varphi\left\{\frac{s}{f}\left(2-\frac{k'^2}{f^2}\right)^2-\frac{4rs'^2}{f^3}\right\}\cosh r'H\sinh s'H$$

$$+\frac{s'}{f}\varphi\left\{\frac{r}{f}\left(2-\frac{k'^2}{f^2}\right)^2-\frac{4sr'^2}{f^3}\right\}\sinh r'H\cosh s'H$$

$$+\left\{\left(2-\frac{k'^2}{f^2}\right)^2\vartheta+\frac{4r'^2s'^2}{f^4}\zeta\right\}\sinh r'H\sinh s'H=0\,, \qquad \ldots.(1)$$

where

$$\varphi=\frac{\mu'k^2k'^2}{\mu f^4}\,,\qquad \zeta=\frac{4rs}{f^2}\left(\frac{\mu'}{\mu}-1\right)^2-\alpha^2\,,\qquad \eta=\frac{2rs}{f^2}\left(\frac{\mu'}{\mu}-1\right)\beta-\alpha\gamma,$$

$$\vartheta=\frac{rs}{f^2}\beta^2-\gamma^2\,,\qquad \alpha=\frac{2\mu'}{\mu}-\left(2-\frac{k^2}{f^2}\right),\qquad \beta=\frac{\mu'}{\mu}\left(2-\frac{k'^2}{f^2}\right)-2,$$

$$\gamma=\frac{\mu'}{\mu}\left(2-\frac{k'^2}{f^2}\right)-\left(2-\frac{k^2}{f^2}\right),$$

$$r^2=f^2-h^2\,,\qquad s^2=f^2-k^2\,,\qquad r'^2=f^2-h'^2\,,\qquad s'^2=f^2-k'^2,$$

$$h^2=\rho p^2/(\lambda+2\mu)\,,\quad k^2=\rho p^2/\mu\,,\quad h'^2=\rho'p^2/(\lambda'+2\mu')\,,\quad k'^2=\rho'p^2/\mu',$$

ρ and ρ' are the density and $f=2\pi/L$. ....(2)

The critical condition of the existence of surface waves is that one of the functions $\exp(rz)$ and $\exp(sz)$, which give the vertical distribution of amplitude, fails to be a real function that decreases exponentially and becomes a circular function[3)]. Since k^2 is larger than h^2, the above condition is given by the relation

$$s=0\,,\qquad \text{or}\qquad f^2=k^2\,.$$

Putting this into the equation (1), we have[4)]

2) K. SEZAWA and K. KANAI, "Discontinuity in the Dispersion Curves of Rayleigh Waves," *Bull. Earthq. Res. Inst.*, **13** (1935), 237.

3) In the semi-infinite part the type of waves must be [E]. (Cf. Y. SATÔ, "Definition and Classification of Surface Waves," *Bull. Earthq. Res. Inst.*, **32** (1954), 161.)

4) K. KANAI, *loc. cit.*, 1).

$$\frac{4r's'}{f^2}\left(2-\frac{k'^2}{f^2}\right)\eta-\frac{r's'}{f^2}\left\{4\vartheta+\left(2-\frac{k'^2}{f^2}\right)^2\zeta\right\}\cosh r'H\cosh s'H$$

$$-\frac{4rr's'^2}{f^4}\varphi\cosh r'H\sinh s'H+\frac{rs'}{f^2}\varphi\left(2-\frac{k'^2}{f^2}\right)^2\sinh r'H\cosh s'H$$

$$+\left\{\frac{4r'^2s'^2}{f^4}\zeta+\left(2-\frac{k'^2}{f^2}\right)^2\vartheta\right\}\sinh r'H\sinh s'H=0\ , \qquad \ldots.(3)$$

where

$$\varphi=\frac{\mu'k'^2}{\mu f^2}\ ,\qquad \zeta=-\alpha^2\ ,\qquad \eta=-\alpha\gamma\ ,\qquad \vartheta=-\gamma^2\ ,$$

$$\alpha=\frac{2\mu'}{\mu}-1\ ,\qquad \beta=\frac{\mu'}{\mu}\left(2-\frac{k'^2}{f^2}\right)-2\ ,\qquad \gamma=\frac{\mu'}{\mu}\left(2-\frac{k'^2}{f^2}\right)-1\ ,$$

$$\frac{k'^2}{f^2}=\left(\frac{v}{v'}\right)^2,\qquad \frac{r^2}{f^2}=1-\frac{1}{\lambda/\mu+2}\ ,\qquad \frac{r'^2}{f^2}=1-\frac{1}{\lambda'/\mu'+2}\left(\frac{v}{v'}\right)^2,$$

$$\frac{s'^2}{f^2}=1-\left(\frac{v}{v'}\right)^2. \qquad \ldots.(4)$$

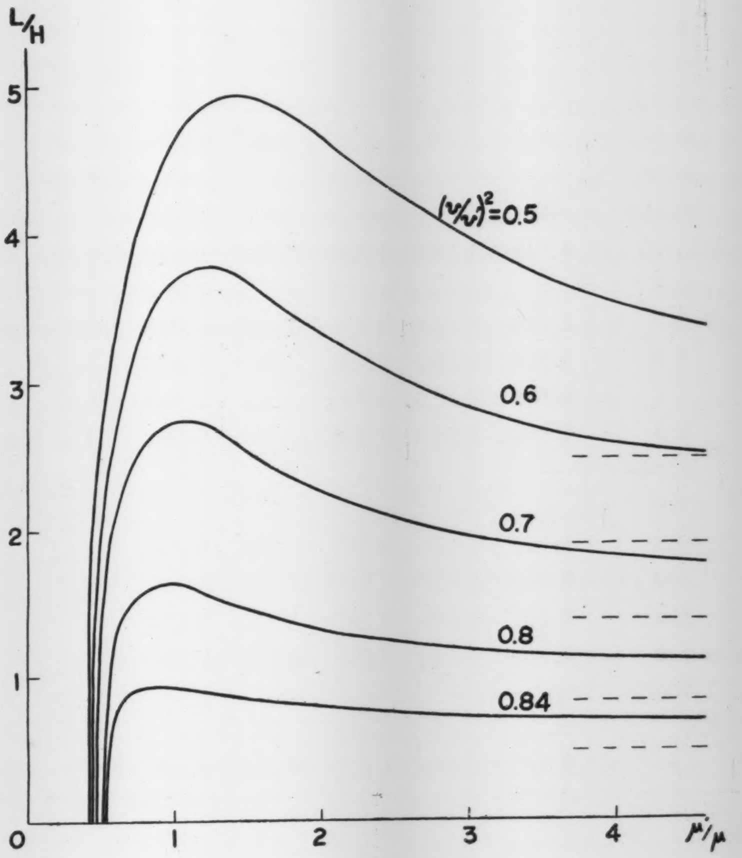

Fig. 1. Critical lines separating the existence and non-existence of Rayleigh waves. Above the curves Rayleigh waves are allowed to exist, while below them they cannot exist. Sezawa waves are not allowed to exist throughout the domain.

Table I. The values of L/H that give the critical boundary conditions μ'/μ and $(v/v')^2$

$(v/v')^2$ / μ'/μ	0.5	0.6	0.7	0.8	0.84	0.8453···	0.85	0.90	0.985	1.0
0						Critical value that separates two conditions. When $(v/v')^2>0.8453\cdots$, Rayleigh waves always exist and Sezawa waves also have the chance of existence, while if $(v/v')^2<0.8453\cdots$, no Sezawa waves are allowed to exist and only Rayleigh waves have the chance of existence.	0.795	1.274	1.606	1.651
0.25							–	–	–	1.648
0.30							0.800	1.264	–	–
0.40							–	–	1.458	1.497
0.419	0						–	–	–	–
0.443	–	0					–	–	–	–
0.472	–	–	0				–	–	–	–
0.5	2.574	2.033	1.417				0.654	0.990	1.246	1.282
0.512	–	–	–	0			–	–	–	–
0.532	–	–	–	–	0		–	–	–	–
0.537	–	–	–	–	–		0	–	–	–
0.555	–	–	–	–	–			0.735	–	–
0.572	–	–	–	–	–			0	–	–
0.60	–	–	–	1.275	0.774				–	–
0.65	–	–	–	–	–				0.677	0.765
0.698	–	–	–	–	–				0	–
0.75	4.012	3.288	2.508	1.562	0.910					0.385
0.9	–	–	–	–	–					0.049
1.0	4.652	3.713	2.739	1.629	0.919					0
1.25	4.909	3.785	2.681	1.543	0.877					0.128
1.5	4.936	3.677	2.533	1.449	0.839					0.296
2.0	4.654	3.321	2.259	1.313	0.781					0.513
2.048	–	–	–	–	–				0	–
2.2	–	–	–	–	–				0.403	–
2.5	4.254	3.021	2.072	1.229	0.745				0.525	–
3.0	3.949	2.811	1.949	1.171	0.712				0.648	0.700
3.5	3.700	2.665	1.863	1.130	0.702				–	–
4.0	3.519	2.558	1.801	1.099	0.690				0.731	0.780
8.47	–	–	–	–	–			0	–	–
114.	–	–	–	–	–		0	–	–	–
∞	2.471	1.895	1.372	0.812	0.469		0.450	0.738	0.946	0.972

lines of the existence of Rayleigh and Sezawa waves, when are given. ($\lambda=\mu$, $\lambda'=\mu'$).

1.1	1.2	1.4	1.6	1.8	2.0	2.2	2.4	2.5	2.6	3.0
1.899	2.098	2.418	2.683	2.913	3.120	3.310	3.479	3.570	3.652	3.957
1.883	2.069	2.368	2.618	2.843	3.055	3.263	3.475	3.581	3.688	4.150
–	–	–	–	–	–	–	–	–	–	–
–	–	–	–	–	–	–	–	–	–	–
–	–	–	–	–	–	–	–	–	–	–
–	–	–	–	–	–	–	–	–	–	–
–	–	–	–	–	–	–	–	–	–	–
1.491	1.666	1.970	2.246	2.513	2.786	3.072	3.384	3.548	3.722	4.479
–	–	–	–	–	–	–	–	–	–	–
–	–	–	–	–	–	–	–	–	–	–
–	–	–	–	–	–	–	–	–	–	–
–	–	–	–	–	–	–	–	–	–	–
–	–	–	–	–	–	–	–	–	–	–
–	–	–	–	–	–	–	–	–	–	–
–	–	–	–	–	–	–	–	–	–	–
–	–	–	–	–	–	–	–	–	–	–
0.945	1.195	1.563	1.878	2.185	2.513	2.868	3.279	3.508	3.752	4.852
–	–	–	–	–	–	–	–	–	–	–
0.811	1.056	1.405	1.701	1.997	2.324	2.704	3.182	3.466	3.779	5.254
–	–	–	–	–	–	–	–	–	–	
0.836	1.046	1.348	1.604	1.859	2.146	2.511	3.036	3.393	3.824	
0.888	1.076	1.353	1.588	1.821	2.081	2.418	2.941	3.336	3.862	
–	–	–	–	–	–	–	–	–	–	
–	–	–	–	–	–	–	–	–	–	
–	–	–	–	–	–	–	–	–	–	
0.960	1.123	1.375	1.591	1.801	2.035	2.338	2.835	3.260	3.919	
–	–	–	–	–	–	–	–	–	–	
1.000	1.152	1.392	1.598	1.799	2.019	2.304	2.787	3.213	3.961	
–	–	–	–	–	–	–	–	–	–	
–	–	–	–	–	–	–	–	–	–	
1.127	1.252	1.460	1.640	1.814	2.000	2.231	2.622	3.037	4.260	

3. Numerical calculation

Assuming various values of $(v/v')^2$ and putting them into the above equation, we have calculated that relation between L/H and μ'/μ which gives the critical condition of the existence of Rayleigh and Sezawa waves. (In this calculation λ and λ' are always assumed to be equal to μ and μ' respectively.)

The result is illustrated in Figs. 1, 2 and 3 and the numerical values are found in Table I. (In Fig. 3 the unit of abscissa is reciprocal to that of Fig. 2.)

4. Discussion of the result

Three of the curves in the Figs. 1 and 2 (curves corresponding to

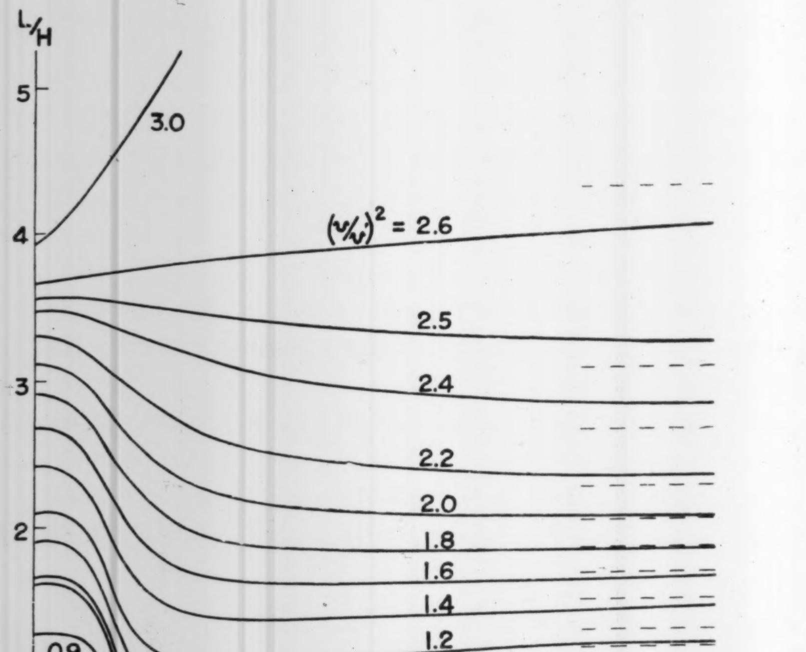

Fig. 2. Above the critical lines only Rayleigh waves can exist, while below the curves both Rayleigh and Sezawa waves are allowed to exist.

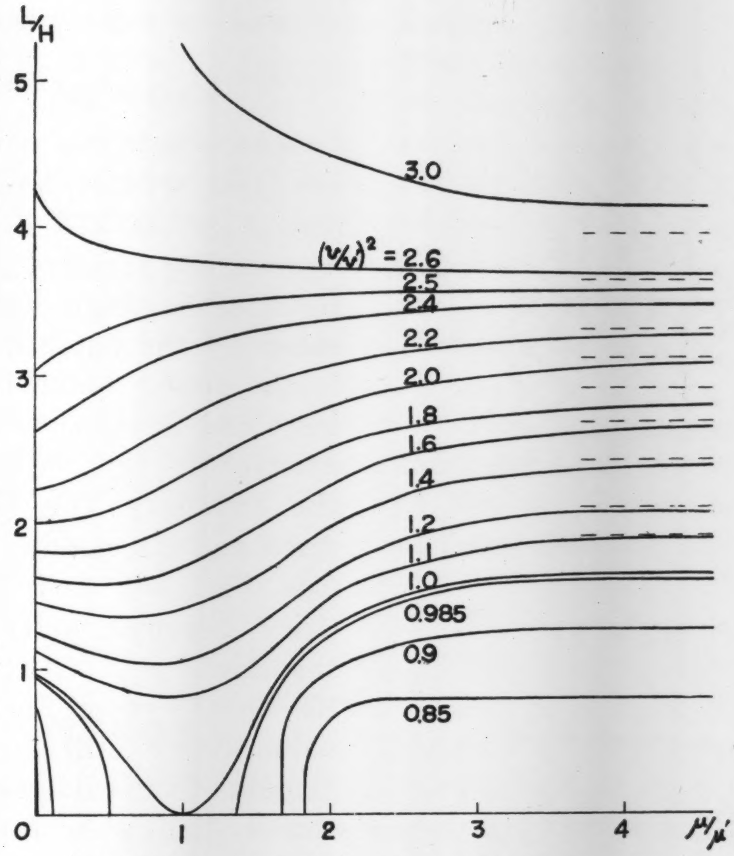

Fig. 3. Above the critical lines only Rayleigh waves can exist, while below the curves both Rayleigh and Sezawa waves are allowed to exist. This figure has the same content with the former one, but the abscissa is reversed.

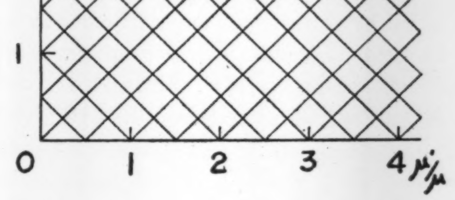

Fig. 4a.

$(v/v')^2=0.5,\ 1,\ 2)$ were already given by K. Kanai[5], but in that case three curves were isolated and the connection between them was somewhat difficult to grasp. Now, however, the tendency of the shift of curves has been made fairly clear.

At first, when the parameter $(v/v')^2$ is large, namely the velocity of S-waves is much higher in the substratum than in the upper medium, the Rayleigh waves is

5) *ibid.*

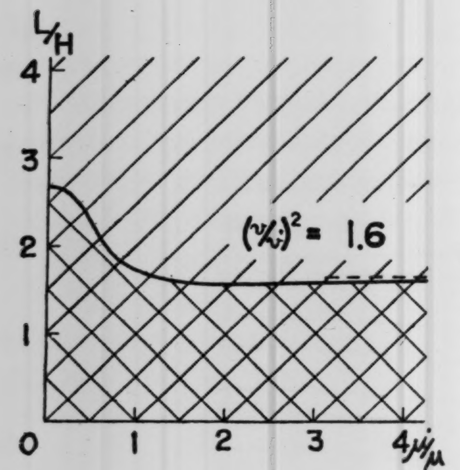

Fig. 4b.

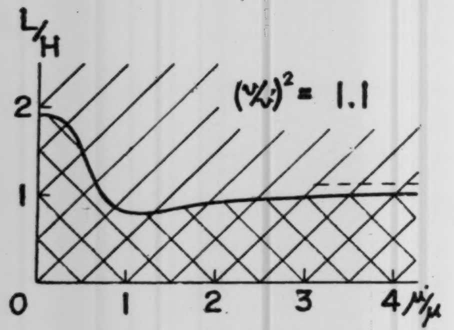

Fig. 4c.

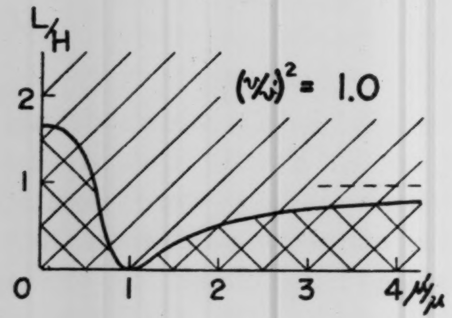

Fig. 4d.

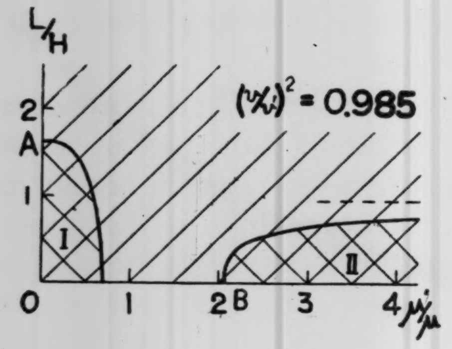

Fig. 4e.

allowed to exist throughout the domain of $\frac{\mu'}{\mu}$, $\frac{L}{H}$-plane while the Sezawa waves can exist only below the critical boundary line. (See Figs. 4a and 4b. In these figures, the range of possible existence of Rayleigh waves is indicated by the hatched area, while in the double hatched area Rayleigh and Sezawa waves can both exist.) As the value decreases, the boundary line shifts downward and its middle part droops (see Fig. 4c), and finally when $(v/v')^2$ becomes unity it touches the axis of μ'/μ. (Cf. Fig. 4d and K. Kanai's paper Fig. 9.) If the value $(v/v')^2$ still decreases, the domain of the existence of Sezawa waves diminishes further and is separated into two areas (see Fig. 4e) until it vanishes when $(v/v')^2$ takes the value $0.8453\cdots$[6]. And in this case the tendency of the shift of curves can be seen better in Fig. 3 than in Fig. 2.

If $(v/v')^2$ is smaller than $0.8453\cdots$, no Sezawa waves are allowed to exist, and even the existence of Rayleigh-waves is somewhat

6) This condition implies that the velocity of Rayleigh waves in the layer is equal to that of S-waves in the substratum.

As the value $(v/v')^2$ diminishes, the point A in Fig. 4e approaches to 0 and the area I vanishes, while the point B tends to $+\infty$ and thus the area II becomes null. This property may be proved from the expression (3) by a little calculation.

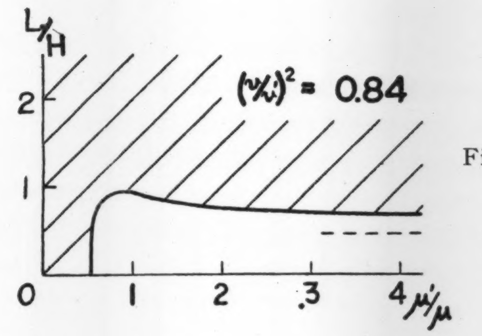

Fig. 4f.

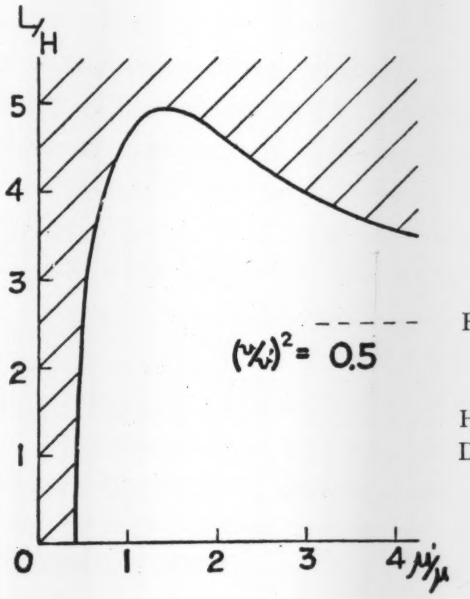

Fig. 4g.

limited. If $(v/v')^2$ decreases further, the domain of the existence of Rayleigh waves above the critical boundary line diminishes, namely the blank area (domain without surface waves) increases. (Cf. Figs. 4f and 4g.) The details of the nature of this matter will be found in Fig. 1.

This investigation was performed under the kind guidance of Dr. K. Kanai, to whom the authors' heartiest thanks are due.

Hatched area; Rayleigh waves only can exist.
Double hatched area; Rayleigh and Sezawa waves can both exist.

19. 表面層をもつ媒質内の Rayleigh 波と妹沢波の存在限界

地震研究所 {山口林造, 佐藤泰夫}

表面層をもつ媒質内を伝わる分散性 Rayleigh 波と妹沢波（M_2 波）の存在限界をしらべた．

v, v' をそれぞれ下層，表面層の S 波の速度とすると，$(v/v')^2=0.5$, 1.0, 2.0, の代表的な場合については，$\lambda/\mu=\lambda'/\mu'=1$ としたときの計算が既に金井によつて報告されている[1)]．

ここではその方法に準じて，より精しく数値計算を行い図で見られるような結果を得た．

これによつて存在限界の変動を明確に把えるとともに，上の代表的な場合をも充分に結びつけて理解することが出来た．

特に注意すべきは下層の S 波の速度が上層の Rayleigh 波の速度に等しくなる（すなわち $(v/v')^2=0.8453\cdots$）ときである．Rayleigh 波について言えば，これを境にして $(v/v')^2\geqq 0,8453\cdots$ では常に存在するが，$(v/v')^2<0.8453\cdots$ のときは比較的短波長の範囲に存在しない部分が出来る．妹沢波については $(v/v')^2>0.8453\cdots$ の場合は比較的短波長の範囲に存在するようになるが，$(v/v')^2\leqq 0.8453\cdots$ のときは常に存在しない．

御指導をたまわつた金井博士に厚く御礼申し上げる．

20. *On Sezawa-waves (M_2-waves). Part II.*

By Kiyoshi KANAI,

Earthquake Research Institute.

(Read Apr., 26, 1955.—Received June 30, 1955.)

1. Introduction

Assuming that there is a surface layer in the earth, two kinds of surface waves seem to originated from it and one of them newly discovered was named Sezawa-waves (or M_2-waves).

Ordinary Rayleigh-waves are transmitted with an orbit of sense opposite to that of gravitational waves, while Sezawa-waves are transmitted with an orbit of the same sense as that of gravitational waves.

Sezawa-waves which can exist are limited. They are only of short wave length. This limit of existence depends on the relation between the property of the material of surface layer and that of the lower layer.

Sezawa-waves appear when the velocity in the surface layer is smaller or slightly larger than the velocity in the lower layer[1], while they do not appear when the velocity in the surface layer goes beyond a certain degree.

The conditions which determine the range of possible existence and the displacement distribution in the surface layer as for Sezawa-waves have close relation to the range of possible existence of Stoneley-waves.

The above-stated is the outline of the properties of Sezawa-waves which have been known till now[2].

In this paper we will describe precisely the condition which determines the range of possible existence of Sezawa-waves and the condition of the displacement distribution in the surface layer.

1) *Corrigenda* to paper 4, "On the M_2-waves (Sezawa-waves)", *Bull. Earthq. Res. Inst.*, **29** (1951). Page 44, lines 2–3 and page 47, 4th line from the bottom.
Read v_s/v_s' is slightly less than 1, for $v_s/v'_s, < 1$.

2) K. SEZAWA and K. KANAI, *Bull. Earthq. Res. Inst.*, **13** (1935), 237, 471, **15** (1937), 845, **16** (1938), 683, **17** (1939), 1, **18** (1940), 1.
K. SEZAWA, *ditto*, **16** (1938), 1, 225.
K. KANAI, *ditto*, **26** (1948), 57, **29** (1951), 39, 49.

2. The relation between the property of Sezawa-waves and the range of possible existence of Stoneley-waves

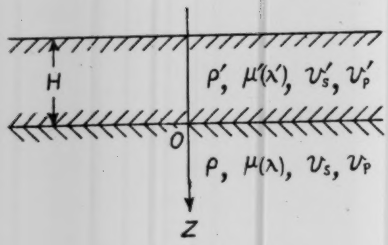

Fig. 1.

Let the densities of the lower medium and surface layer, the elastic constants and the velocities of S- and P-waves be ρ, ρ', $\mu(\lambda)$, $\mu'(\lambda')$, v_s, v_s', v_p and v_p' respectively. Also assume H and L to be the thickness of the surface layer and the wave length respectively.

The equation of dispersion curves of the surface waves transmitted through a stratified body originally obtained by us is

$$\begin{aligned}\frac{4r's'}{f^2}\left(2-\frac{k'^2}{f^2}\right)\eta-\frac{r's'}{f^2}\left\{4\vartheta+\left(2-\frac{k'^2}{f^2}\right)^2\zeta\right\}\cosh r'H\cosh s'H\\+\frac{r'}{f}\varphi\left\{\frac{s}{f}\left(2-\frac{k'^2}{f^2}\right)^2-\frac{4rs'^2}{f^3}\right\}\cosh r'H\sinh s'H\\+\frac{s'}{f}\varphi\left\{\frac{r}{f}\left(2-\frac{k'^2}{f^2}\right)^2-\frac{4sr'^2}{f^3}\right\}\sinh r'H\cosh s'H\\+\left\{\left(2-\frac{k'^2}{f^2}\right)^2\vartheta+\frac{4r'^2s'^2}{f^4}\zeta\right\}\sinh r'H\sinh s'H=0,\end{aligned}\qquad(1)$$

where

$$\varphi=\frac{\mu'k^2k'^2}{\mu f^4},\quad \zeta=\frac{4rs}{f^2}\left(\frac{\mu'}{\mu}-1\right)^2-\alpha^2,\quad \eta=\frac{2rs}{f^2}\left(\frac{\mu'}{\mu}-1\right)\beta-\alpha\gamma,$$

$$\vartheta=\frac{rs}{f^2}\beta^2-\gamma^2,\quad \alpha=\frac{2\mu'}{\mu}-\left(2-\frac{k^2}{f^2}\right),\quad \beta=\frac{\mu'}{\mu}\left(2-\frac{k'^2}{f^2}\right)-2,$$

$$\gamma=\frac{\mu'}{\mu}\left(2-\frac{k'^2}{f^2}\right)-\left(2-\frac{k^2}{f^2}\right),$$

$$r^2=f^2-h^2,\quad s^2=f^2-k^2,\quad r'^2=f^2-h'^2,\quad s'^2=f^2-k'^2$$

$$h^2=\rho p^2/(\lambda+2\mu),\quad k^2=\rho p^2/\mu,\quad h'^2=\rho' p^2/(\lambda'+2\mu'),\quad k'^2=\rho' p^2/\mu'.\qquad(2)$$

If there is a surface layer, the amplitude distribution of P- and S-waves contained in surface waves in the surface layer may be expressed as follows:

$$e^{\sqrt{1-\left(\frac{V}{v_P'}\right)^2}\,\frac{2\pi z}{L}},\qquad e^{\sqrt{1-\left(\frac{V}{v_S'}\right)^2}\,\frac{2\pi z}{L}},\qquad(3)$$

And the distribution in the lower medium is

$$e^{-\sqrt{1-\left(\frac{V}{v_P}\right)^2}\,\frac{2\pi z}{L}}, \qquad e^{-\sqrt{1-\left(\frac{V}{v_S}\right)^2}\,\frac{2\pi z}{L}}, \tag{4}$$

where V represents the velocity of the surface waves.

It holds that $v'_P > v'_S$ and $v_P > v_S$. Therefore Equation (3) shows that there are no surface waves in case of $V > v_S$. In case of $V < v'_S$, however, the amplitude distribution in the surface layer is exponential concerning both P- and S-waves. In case of $v'_P > V > v'_S$, the distribution of P-waves is exponential, while that of S-waves is sinusoidal. With $V > v'_P$, it is sinusoidal concerning both P- and S-waves, as shown in Equation (2).

In this paper, all the numerical calculations are carried out under the case in which Poisson's ratio $\sigma = 1/4$, that is to say, $\lambda = \mu$, $\lambda' = \mu'$.

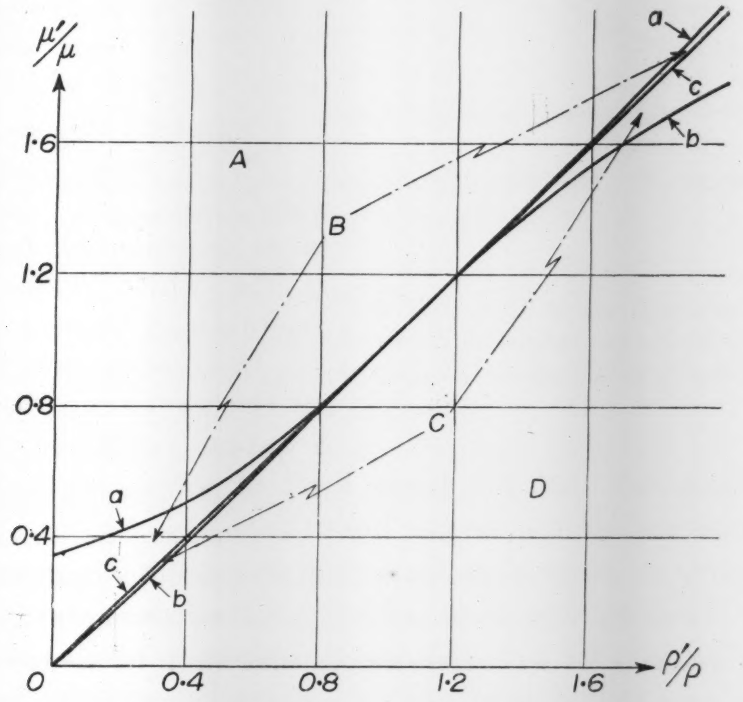

Fig. 2. Range of existence of Stoneley-waves ($\lambda = \mu$, $\lambda' = \mu'$), as shown by the narrow parts between a- and b-line.

Fig. 2 shows the range of existence of Stoneley-waves, which was studied before[3]. In this figure a- and b-line satisfy the condition of

3) K. SEZAWA and K. KANAI, "The Range of Possible Existence of Stoneley-waves, and Some Related Problems," *Bull. Earthq. Res. Inst.*, **17** (1939), 1.

$V=v_S$ and $V=v'_S$ respectively. The area lying between *a*- and *b*-line corresponds to the existence-range of Stoneley-waves.

Therefore in the area represented by *A*, as it holds that no surface waves can be seen, (It goes without saying that no Sezawa-waves can exist.) *c*-line satisfies the condition of $v_S=v'_S$. The area represented by *C* satisfies the conditions of $v_S>v'_S>V$, as it holds that $v_S>v'_S$ and $v'_S>V$. Therefore at the lower limit of wave length, it holds that $V<v'_S$, while at the largest limit of wave length, it holds that $V=v_S$. Between those limits there may be the value of wave length which corresponds to $V=v'_S$. In other words, though in *C* area the amplitude distribution of Sezawa-waves of shorter wave length takes the exponential function form, that of the waves of which the wave length exceeds a certain value is sinusoidal. In Fig. 3 full lines show the exponentail type while the dotted line represent the sinusoidal type.

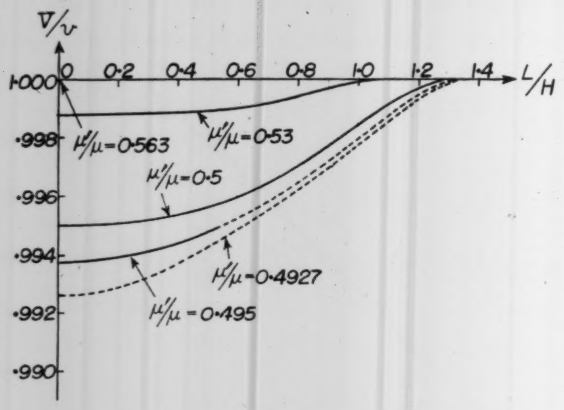

Fig. 3. Dispersion curves of Sezawa-waves within the range where the conditions to originate Stoneley-waves is satisfied. $\lambda=\mu$, $\lambda'=\mu'$, $\rho=2\rho'$.

In *B* area, the amplitude distribution of Sezawa-waves takes exponential function form in the whole range of possible existence of those waves.

In *D* area, as $V>v'_S$ holds, all the amplitude distribution of *S*-waves contained in Sezawa-waves are sinusoidal. At the lower limit of wave length in *D* area $V=v'_S$ holds true and at the larger limit $V=v_S$.

The velocity of Sezawa-waves within the range where the conditions to originate Stoneley-waves is satisfied, is of the intermediate value between the velocity of Stoneley-waves and that of S-waves in lower medium. In case the velocity of the lower medium is larger than that of the surface layer, the value of velocity of Sezawa-waves under the condition which does not permit Stoneley-waves to exist is between the velocity of S-waves in the surface layer and that of S-waves in the lower medium. In case the velocity of the lower medium is smaller than that of the surface layer, Sezawa-waves can not exist under the condition which does not allow the existence of Stoneley-waves.

3. The amplitude distribution of Sezawa-waves in the surface layer

Fig. 4 shows the relation among μ'/μ, the range of possible existence and the amplitude distribution of Sezawa-waves in case of $\rho=2\rho'$.

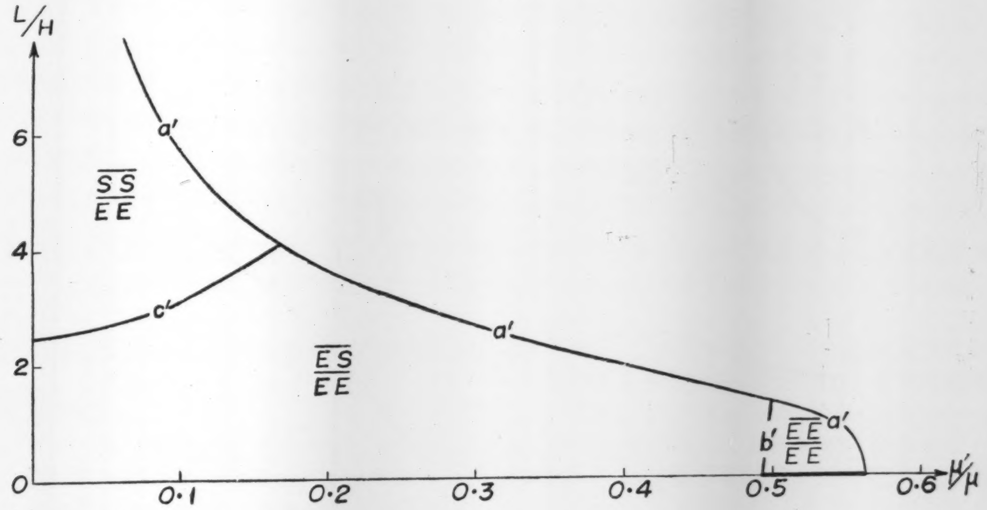

Fig. 4. Relation among μ'/μ, the range of existence and the amplitude distribution of Sezawa-waves. $\lambda=\mu$, $\lambda'=\mu'$, $\rho=2\rho'$.

In Fig. 4, a'-, b'- and c'-line satisfy $V=v_S$, $V=v'_S$ and $V=v'_P$ respectively. Therefore, concerning any value of μ'/μ, L/H in the upper part separated by a'-line does not permit Sezawa-waves to exist, as $V>v_S$ holds true there. In the area enclosed by a'- and b'-line, the displacement distribution concerning both P- and S-waves are exponential, since $V<v_S$ and $V<v'_S$ hold true there. As to the area enclosed by b'-, a'- and c$'$-line, since $v'_P>V>v'_S$ and $V<v_S$ holds true, the displacement distribution of P-waves in the surface layer is exponential, but that of S-waves is sinusoidal. In the area enclosed by a'- and c'-line, P- and S-waves in the surface layer takes the displacement distribution of sinusoidal function, since $v_S>V>v_P'$ holds true.

The limit of $L/H\to 0$ in the range of $\mu'/\mu=0.5\sim 0.635$ (indicated by a big horizontal line) corresponds to the range where Stoneley-waves exist. From this conception, it may be said that Stoneley-waves are special cases of Sezawa-waves.

As to Sezawa-waves there is a region where the displacement distribution of exponential function exists in the surface layer. This

shows, as stated before, that Sezawa-waves are not of the higher order of Rayleigh-type waves.

In Fig. 5, the amplitude distribution of Rayleigh-type waves in the surface layer in case of $\rho=2\rho'$ is shown for reference.

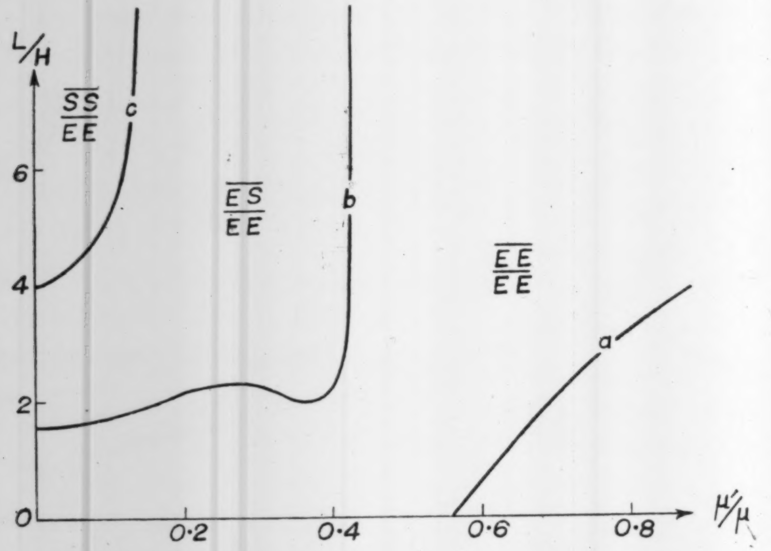

Fig. 5. Relation between the wave length and amplitude distribution of Rayleigh-type waves. $\lambda=\mu,\ \lambda'=\mu',\ \rho=2\rho'$.

4. Conclusion

By studying precisely the displacement distribution of Sezawa-waves in the surface layer, it was found that there exists a region where the distribution can be exponential. In other words it is made clear that Sezawa-waves is not of the higher order of Rayleigh-type waves.

Moreover, though Sezawa-waves cannot be seen when the wave-length exceeds a certain limit, the reason why Sezawa-waves are rarer than Rayleigh-type waves in case of shorter wave length of actual seismic disturbance is hard to find. Also there is no reason why the amplitude of Sezawa-waves is smaller than that of Rayleigh-type waves, but in some cases, it seems that the amplitude of Sezawa-waves becomes larger than that of Rayleigh-type waves[4].

Generally speaking, in case of forming a dispersion curve from seismograms, the largest of actually read wave length is properly de-

4) K. SEZAWA, "Amplitudes of Rayleigh-waves with Discontinuities in their Dispersion Curves", *Bull. Earthq. Res. Inst.*, **16** (1938), 1.

veloped into the form of a dispersion curve of Rayleigh-type waves which has been known for a long time. In such cases, we are led to consider that surface waves of wave length exceeding a certain limit cannot exist actually.

In conclusion the corrections in footnotes 1) are due to Mr. Y. Satô and Mr. R. Yamaguchi, to whom I wish to express my deep gratitude.

---

20. 妹沢波 (M_2 波) について (第2報)

地震研究所　金井　清

妹沢波の実在範囲と表面層内における変位分布を詳しくしらべた．その結果として，妹沢波が，半無限体の上に表面層がある場合のレーレー型の波の高次の波にあたるものではないことが一層はっきりした．

実際の地震記象から分散曲線を作る場合には，読みとられた最大の波長から先は適当にひきのばされる．この場合に，古くから知られているレーレー型の波の分散曲線の形になるように処理されるのが普通である．

妹沢波は，長い波長のものは存在しない．しかし，短い波長については，妹沢波がレーレー型の波よりも起りにくいという条件は見出せない．むしろ，妹沢波の振巾がレーレー型の波の振巾よりも大きくなるのではないかという場合さえある．

それ故，実際の記象から分散曲線を作る場合には，読みとり得た最大の波長以上の長い波は存在し得ないのではないかと，一応は考えて見る必要があろう．

---

21. An Explanation for the Ground Vibration caused by Periodically Exerted Force.

By Kiyoshi KANAI,

Earthquake Research Institute.

(Read Feb. 22, 1955.—Received June 30, 1955.)

Figs. 1 and 2 illustrate the relation between the distance from the vibration origin and the amplitude of the actual ground vibration generated by a vibrator[1]. As seen in these figures, in Fig. 1 the amplitude decreases in accordance with the distance from the origin but in Fig. 2 it does not decrease in such a simple way.

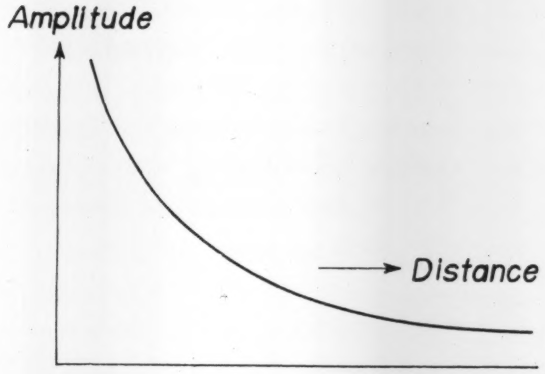

Fig. 1

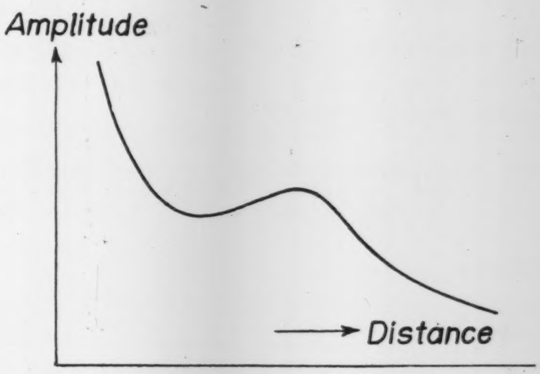

Fig. 2

The relation of the distance to the amplitude which is shown by a sinuate curve is considered to be a superposition of two waves of different velocity. For instance, it has been considered that if there exists a surface layer, the relation of the distance from the origin to the amplitude is an superposition of the direct waves and the refracted waves which run under the surface layer[2].

But when the relation curve scarcely waves, as in Fig. 1, or when it has waves of finite number, the explanation mentioned above does not clarify the phenomena.

1) K. KANAI and T. SUZUKI, *Monthly Meeting of the Earthq. Res. Inst.*, (June 1952), K. KANAI, T. TANAKA, T. SUZUKI and K. NAKAGAWA, *ditto*, (May 1953), K. KANAI and N. NASU, *ditto*, (Nov. 1954).

2) T. WATANABE, *Journ. Seism. Soc., Japan*, [ii], **3** (1951), 31, (in Japanese).

Now, let us assume the amplitude at the vibration origin to be a, the phase difference ϕ, the constant concerning the attenuation of amplitude in case of wave-propagation α, the constant of damping due to solid viscosity k, the propagation velocity v, $p=2\pi/T$, the period T, the thickness of the surface layer H, the time t, the distance from the origin x, and the index of reflection $R(x)$. Then the amplitude of direct wave A_D and the amplitude of reflected wave A_R can be expressed as follows:

$$\left.\begin{aligned} A_D &= ax^{-\alpha}e^{-kx}\sin\left\{\phi+p\left(t-\frac{x}{v}\right)\right\}, \\ A_R &= aR(x)(4H^2+x^2)^{-\alpha}\, e^{-k(4H^2+x^2)^{1/2}}\cdot\sin\{\phi+p(t-\sqrt{4H^2+x^2}/v)\}. \end{aligned}\right\} \tag{1}$$

And the condition necessary for the amplitude to become the maximum or the minimum at a certain point will be

$$\frac{d}{dx}(A_D+A_R)=0, \tag{2}$$

from which we get

$$\left\{\alpha\frac{d\alpha}{dx}+\beta\frac{d\beta}{dx}+\cos(X-Y)\frac{d(\alpha\beta)}{dx}\right\}+\alpha\beta\frac{d\cos(X-Y)}{dx}=0. \tag{3}$$

where

$$\left.\begin{aligned} \alpha &= \frac{e^{-kx}}{x}, & \beta &= R(x)\frac{e^{-k\sqrt{4H^2+x^2}}}{\sqrt{4H^2+x^2}}, \\ X &= \frac{px}{v}, & Y &= \frac{p\sqrt{4H^2+x^2}}{v}. \end{aligned}\right\} \tag{4}$$

Here, in order to find the outline of the problem, the term put in { } of Equation (3) is omitted by considering the derivatives of the terms of damping and the index of reflection to be negligible. Therefore, roughly speaking, the maximum and the minimum of the amplitude-distance curve will appear under the following condition:

$$\alpha\beta\frac{d\cos(X-Y)}{dx}=0. \tag{5}$$

From Equation (5) the condition finally becomes

$$\frac{p}{v}(\sqrt{4H^2+x^2}-x)=n\pi. \quad [n=1, 2, 3, \cdots] \tag{6}$$

Equation (6) can be rewritten as follows:

$$x=\frac{(4H)^2-(nvT)^2}{4nvT}. \qquad (7)$$

As a practical question, x must be greater than 0. Therefore,

$$4H>nvT. \qquad (8)$$

Equation (8) may be the necessary condition for the amplitude-distance curve to be wavy. In other words, if $4H$ is smaller than vt, the curve will not be sinuate. The larger the value of $4H$ is than vt, the greater the value of n can be, that is, the number of wave becomes greater.

From Equation (8) it can be said qualitatively that the number of waves of the amplitude-distance curve becomes larger as H (the thickness of surface layer) gets thicker and the wave length gets shorter (the velocity of propagation v is smaller or the period T is shorter).

Equation (8) explains qualitatively the following experimental results: At the up-town of Tokyo, where the ground is firm, non-wavy curves of amplitude-distance are observed, while at the down-town where the ground is rather soft, there are many spots where we obtained sinuate curves[3].

Next, we can rewrite Equation (6) as follows:

$$v=\frac{2\{\sqrt{x^2+4H^2}-x\}}{nT} \qquad (9)$$

from which we can obtain the propagation velocity v if the values of H, x and T are known. If, the thickness of the surface layer H are found by means of the ordinary seismic prospecting, and the distance x which corresponds to the maximum and the minimum of the amplitude-distance curve are also found from the ground vibration caused by the periodically exerted force, the propagation velocity v will be obtained, since the period of exerted force T is already known.

When an amplitude-distance curve has more than two waves, the unknown values of H and v can be obtained at the same time. As a practical question, there still exists the effect of the terms neglected in the course of the derivation of Equation (5) from Equation (3). Therefore there are some cases where v or H obtained from Equation (9) may include a considerable error. Since the error can be

2) *loc. cit.*, 1).

estimated from the amplitude-distance curve, by taking Equation (3) into consideration, the error may be lessened.

Conducting one or two experiments on the actual ground and applying the method stated above, the plausible value of the velocity of S-waves was obtained. As to some examples of its application, we will report in the next paper.

---

21. 周期的加力による地盤振動に対する1つの解釈

地震研究所 金 井 清

地表面で周期的加力を与えたときの，地表面の振巾は，震動源からの距離とともに単純には減少しないで，波を打つて減少することは，古くから氣付かれていた事柄である．

その理由としては，普通，速度のちがう2つの波の合成が考えられて来た．2つの波としては，地表面に沿つて伝わる直接波と表面層と下層との境界面を伝わる屈折波を考える場合，或は表面波と実体波を考える場合などがあつた．

ところが，ここ数年来，各種地盤上に建つ建物の振動実験を行うにあたつて，建物の振動にともなう地盤の振動を測定した結果，振巾と距離の間にはいろいろ変つた関係が見られ，その関係は地盤の性質に左右されることがわかつた．すなわち，一般に東京の山手のような地盤では Fig. 1 のようになり，下町のようなところでは Fig. 2 のような形になる傾向があることがわかつたわけである．

このような現象は，従来の考え方だけで解釈することは容易でない．

それで，地表面に沿つて伝わる直接波と表面層と下層との境界面で反射してくる波との合成を考えてみると，この現象が，定性的には一応説明できることになつた．

そして，もし，これらの現象が，直接波と反射波との合成で起るものならば，地震波地下探査法で表面層の厚さを求めた後，周期的加力を与える方法で表面層内の S 波の速度を求めることが可能なことになる．又，やり方によつては，周期的加力の方法だけで，表面層の厚さと S 波の速度を求めることも必ずしも不可能ではない．

22. *Analysis of the Dispersion Curves of Love-Waves.*

By Takehito TAKAHASHI*,

Earthquake Research Institute.

(Read June 28, 1955.—Received June 30, 1955.)

1. Introduction

A characteristic feature of Love-wave is that it shows dispersion owing to the stratified structure or more generally to the heterogeneity of the medium. It is usual to assume two or more homogeneous layers and choose the values of their density and elastic constants so as to explain best the observed dispersion curve.

But it must be remarked that within the errors of observation the result can not be unique—we can suppose different structures which equally fit the observations[1]. In other words, we can conclude only with ambiguity where and how the discontinuities exist in the earth's crust.

It seems, then, rather natural to assume that the density and elastic constants vary continuously in the medium. This might be looked upon as the result of averaging over various surface layers which the Love-wave encounters while travelling long distance from its source to the place where it is observed.

In this paper, we shall first develop the general theory of dispersion under the assumed heterogeneity, next the inverse problem—given the dispersion curve to determine the structure of the medium—will be treated.

2. Dispersion of Love-type waves propagated over heterogeneous medium

We shall treat the problem in a two-dimensional form. The x-axis indicates the surface and z-axis is taken vertically downward. Density ρ and rigidity μ are thought to be the analytic positive functions of z. The displacement v occurs in the vertical direction both to x- and z-axes.

Then the equation of motion is expressed as

---

* Assistant Professor of the Seizyo University, Setagaya, Tokyo.

1) Y. SATÔ, *Bull. Earthq. Res. Inst.*, **29** (1951), 519.

$$\rho(z)\frac{\partial^2 v}{\partial t^2}=\mu(z)\frac{\partial^2 v}{\partial x^2}+\frac{\partial}{\partial z}\left(\mu(z)\frac{\partial v}{\partial z}\right). \qquad (1)$$

Assuming now $v=\exp(ipt-ifx)V(z)$,
the equation (1) reduces itself to

$$\frac{d}{dz}\left(\mu\frac{dV}{dz}\right)+\mu s^2 V=0 \qquad (2)$$

with

$$\left.\begin{aligned} s^2&=(\rho/\mu)p^2-f^2=f^2\{(v_Q/v_s(z))^2-1\} ,\\ v_Q&=p/f , \qquad v_s(z)=\sqrt{\mu/\rho} . \end{aligned}\right\} \qquad (3)$$

Let the variables be changed by the substitution

$$\left.\begin{aligned} \theta&=\int_0^z s dz ,\\ Z(\theta)&=\sqrt{\mu s}\,V(z) , \end{aligned}\right\} \qquad (4)$$

then the equation (2) is transformed into

$$d^2Z/d\theta^2+\{1+Q(\theta)\}Z=0 , \qquad (5)$$

with

$$Q(\theta)=-(\mu s)^{-1/2}(d/d\theta)^2(\mu s)^{1/2}=-(\mu s)^{-1/2}(d/sdz)^2(\mu s)^{1/2} . \qquad (6)$$

We now make following assumptions:

(i) $v_s(z)$ is a increasing function of z.

(ii) $v_Q>v_s(0)$. Then s^2 has only one zero-point $z=H$, and $v_s(H)=v_Q$. (7)

(iii) $|Q(\theta)|\ll 1$, if $|z-H|$ is large.

It is easy, then, to observe that the asymptotic solutions of the equation (5) are

(a) sinusoidal, if $z\ll H$ ($v_Q>v_s(z)$ and θ is real),

or

(b) exponential, if $z\gg H$ ($v_Q<v_s(z)$ and θ is imaginary).

We need the solution which converges to zero as $z\to\infty$. To obtain the corresponding sinusoidal function, we must remark that, owing to the many-valued character of s, the so-called Stokes' phenomenon happens. H. Jeffreys was the first who showed how to connect the above

two asymptotic solutions each belonging to different regions[2]. According to him, the sinusoidal solution at $z \ll H$, which decreases exponentially for large z, is expressed as

$$Z(\theta) \sim \cos\{\pi/4-(\theta_H-\theta)\} \,, \tag{8}$$

or

$$V(z) \sim (\mu s)^{-1/2} \cos\left(\pi/4-\int_z^H s dz\right) . \tag{9}$$

In case the assumption (iii) is fulfilled near the surface, we can apply to the expression (9) the boundary condition

$$(dV/dz)_{z=0}=0 \,, \tag{10}$$

and obtain

$$\tan\left(\int_0^H s dz-\pi/4\right)=\left\{-\frac{\mu}{2}\frac{d}{dz}\left(\frac{1}{\mu s}\right)\right\}_{z=0} , \tag{11}$$

or

$$\int_0^H s dz=n\pi+\frac{\pi}{4}-\mathrm{Tan}^{-1}\left\{\frac{\mu}{2}\frac{d}{dz}\left(\frac{1}{\mu s}\right)\right\}_{z=0} , \quad (n=0,1,2,\cdots) . \tag{12}$$

This equation gives the relation between the velocity v_Q and the wave-length $L(=2\pi/f)$ of the n-th Love-wave, if the functions $\rho(z)$ and $\mu(z)$ are known satisfying the conditions (i)-(iii).

Substituting in (12) the expression (3), we have

$$\int_0^H \{(v_Q/v_s(z))^2-1\}^{1/2} dz=\frac{L}{8}\left\{4n+1-\frac{4}{\pi}\mathrm{Tan}^{-1}\left(\frac{\mu}{2}\frac{d}{dz}\left(\frac{1}{\mu s}\right)\right)_0\right\} , \tag{12'}$$

from which we can observe that

$$\begin{cases} \text{if } L\to 0, \text{ then } H\to 0 \text{ and } v_Q\to v_s(0). \\ \text{if } L\to\infty, \text{ then } H\to\infty \text{ and } v_Q\to v_s(\infty). \end{cases}$$

To derive the formula (12), it was necessary to assume that $Q(\theta)$ becomes negligibly small near the surface; this condition may be fulfilled when H is of several wave-lengths, that is, when n differs from 0. But the only case $n=0$ being practically observed, we must next obtain the corresponding formula to (12) which is valid when L is not small compared with H.

2) Now called as W.K.B. method:
E. KEMBLE, *Fundamental Principles of Quantum Mechanics* (1937).
M. MOOSE and H. FESHBACH, *Methods of Theoretical Physics* (1953), chap. 9.

2.1. Near the zero point $z=H$, taking the first term of the expansion, s^2 is proportional to $(H-Z)$, then

$$\varphi\equiv\theta_H-\theta=\int_z^H sdz \propto \int_0^s s^2ds=s^3/3 \ . \tag{13}$$

Putting this relation into (6), we get as the first approximation

$$Q(\theta)=-\varphi^{-1/6}(d^2/d\varphi^2)\varphi^{1/6}=(5/36)\varphi^{-2} \ . \tag{14}$$

Then the solutions of (5) are expressed as Bessel functions of order $\pm 1/3$ multiplied with $\varphi^{1/2}$. We choose the linear combination of them so as to converge to zero when $z\to\infty$, and obtain

$$V=(\varphi/\mu s)^{1/2}\{J_{1/3}(\varphi)+J_{-1/3}(\varphi)\} \ . \tag{15}$$

This procedure is due to R. E. Langer[3].

We can rewrite the expression (15) in the following form

$$V=(\varphi/\mu s)^{1/2}\cos(\pi/6)\{\exp(i\pi/6)\cdot H^{(1)}_{1/3}(\varphi)+\exp(-i\pi/6)\cdot H^{(2)}_{1/3}(\varphi)\}$$
$$=2\cos(\pi/6)(\varphi/\mu s)^{1/2}|H^{(1)}_{1/3}|\cos(\pi/6+\arg H^{(1)}_{1/3}) \ . \tag{16}$$

If we apply the boundary condition (10) to (16), we have

$$\tan(\pi/6+\arg H^{(1)}_{1/3}(\varphi_0))\{(d/dz)\arg H^{(1)}_{1/3}(\varphi)\}_{z=0}$$
$$=\{(d/dz)\log((\varphi/\mu s)^{1/2}|H^{(1)}_{1/3}(\varphi)|)\}_{z=0} \ . \tag{17}$$

On utilizing the relations

$$\arg H^{(1)}_{1/3}=\tan^{-1}(Y_{1/3}/J_{1/3}) \ ,$$
$$|H^{(1)}_{1/3}|=(J_{1/3})^2+(Y_{1/3})^2 \ ,$$
$$J_{1/3}\cdot\frac{d}{d\varphi}Y_{1/3}-Y_{1/3}\cdot\frac{d}{d\varphi}J_{1/3}=\frac{2}{\pi\varphi} \ ,$$

we get

$$y\equiv(d/dz)\arg H^{(1)}_{1/3}=-2s(\pi\varphi)^{-1}|H^{(1)}_{1/3}|^{-2} \ . \tag{18}$$

Then the equation (17) is written as

$$\arg H^{(1)}_{1/3}(\varphi_0)+\pi/6=n\pi+\mathrm{Tan}^{-1}\{(\mu/2)(d/dz)(\mu y)^{-1}\}_{z=0} \ . \tag{19}$$

When $\varphi\to\infty$, we have $\arg H^{(1)}_{1/3}\to\varphi-(5/12)\pi$, $\sqrt{\varphi}\ |H^{(1)}_{1/3}|\to\sqrt{2/\pi}$ and $y\to -s$. This shows that (19) coincides with (12) when $z\ll H$.

3) R. E. LANGER, *Phys. Rev.*, **51** (1937), 669.
MOOSE and FESHBACH, *loc. cit.*
I. Imai extended the result of Langer:
I. IMAI, *Phys. Rev.* **74** (1948), 113; **80** (1950), 1112.
His formulas are available when a more precise knowledge about the behaviour of the solution is needed.

We next try to bring the expression (19) to a more convenient form, under the condition which reads

$$1 \gg |\{(\mu/2)(d/dz)(\mu y)^{-1}\}_{z=0}| = |-(\mu/2)\{(d/dz)(\mu s)^{-1}\}(\pi\varphi/2)|H^{(1)}_{1/3}|^2$$
$$+(\pi/4)(d/d\varphi)(\varphi|H^{(1)}_{1/3}|^2)|_{z=0} \, . \tag{20}$$

For a small quantity ε compared with φ, we have

$$\arg H^{(1)}_{1/3}(\varphi+\varepsilon) \doteqdot \arg H^{(1)}_{1/3}(\varphi) + \varepsilon(d/d\varphi)\arg H^{(1)}_{1/3}(\varphi)$$
$$= \arg H^{(1)}_{1/3}(\varphi) + 2\varepsilon(\pi\varphi)^{-1}|H^{(1)}_{1/3}(\varphi)|^{-2} \, .$$

Then the equation (19) is reduced into

$$n\pi - \pi/6 = \arg H^{(1)}_{1/3}[\varphi_0 - (\pi\varphi_0/2)^2|H^{(1)}_{1/3}(\varphi_0)|^4\{(\mu_0/2)(d/dz)(\mu s)^{-1}\}_0$$
$$+(\pi^2/8)\varphi_0|H^{(1)}_{1/3}(\varphi_0)|^2(d/d\varphi)\{\varphi_0|H^{(1)}_{1/3}(\varphi_0)|^2\}] \, . \tag{21}$$

To solve this equation we can utilize the numerical tables[4] of $\arg H^{(1)}_{1/3}$. In the case $n=0$, the relation

$$\arg H^{(1)}_{1/3}(0.835) = -\pi/6$$

shows that we can take 0.835 for the first approximation value of φ_0.

Again from the tables[4] of $|H^{(1)}_{1/3}|$

$$|H^{(1)}_{1/3}(0.835)| \doteqdot 0.85 \, ,$$
$$(d/d\varphi)|H^{(1)}_{1/3}(0.835)| \doteqdot -0.475 \, .$$

With these values the equation (21) becomes

$$\varphi_0 - 0.035 + 0.9 \times \{(\mu/2)(d/dz)(\mu s)^{-1}\}_{z=0} = 0.835$$

or

$$\varphi_0 \equiv \int_0^H s\,dz \doteqdot 0.87 - 0.9\{(\mu/2)(d/dz)(\mu s)^{-1}\}_{z=0} \, . \tag{22}$$

Comparing this formula with (12), we see that the principal term $(\pi/4)$ is augmented about 11 per cent.

When the condition (20), or

$$[(\mu/2)(d/dz)(\mu s)^{-1}]_{z=0} \ll 1$$

does not hold, we must use the equation (19). In this case the equation (12) of the former section may be used as the first approximation formula.

2.2. In case the equation (2) has an explicit solution satisfying the

4) G. N. WATSON, *Theory of Bessel Functions* (1922), p. 714.

boundary condition, W.K.B. solution (9) or (15) proves to be an asymptotic function of it.

Sezawa[5] and later Satô[5] treated the case when ρ is constant and μ increases linearly. In this case the solution of (2) which tends to zero for large z is given using Whittaker's function

$$V=\zeta^{-1/2}W_{\kappa,0}(\zeta)\ , \tag{23}$$

where

$$\zeta=2f\mu/\beta\ , \qquad \kappa=\rho p^2/2f\beta\ , \tag{24}$$

and

$$\mu=\mu_0+\beta z\ .$$

When $\kappa\gg 1$ and $\kappa\gg\zeta$, the expression (23) becomes, disregarding the constant factor, asymptotically[6]

$$V\sim\zeta^{-1/4}\cos\left(\kappa\pi-2\sqrt{\kappa\zeta}-\pi/4\right)\ . \tag{25}$$

Meanwhile our calculation goes on as follows:

$$s=f\{\rho p^2/\mu f^2-1\}^{1/2}=f(4\kappa/\zeta-1)^{1/2}\ ,$$

$$\mu s=\beta\zeta(4\kappa/\zeta-1)^{1/2}\ ,$$

$$\int_z^H s dz=(1/2)\int_\zeta^{4\kappa}(4\kappa/\zeta-1)^{1/2}d\zeta$$

$$=-(1/2)(4\kappa\zeta-\zeta^2)^{1/2}+\kappa\ \mathrm{Cos}^{-1}(\zeta/2\kappa-1)\ .$$

Putting these results into (9), we have

$$V=\beta^{-1/2}(4\kappa\zeta-\zeta^2)^{-1/4}\cos\{\pi/4+(1/2)(4\kappa\zeta-\zeta^2)^{1/2}-\kappa\ \mathrm{Cos}^{-1}(\zeta/2\kappa-1)\}\ .$$

We can easily verify that this expression approaches to (23) when $\kappa\gg\zeta$.

We can also observe that with these values equation (15) expresses the asymptotic form of Whittaker's function when κ and ζ are large and $\zeta/\kappa\approx 4$[6].

Y. Satô newly calculated the greatest roots of $dV/d\zeta=0$, according to his formulation of reference 5). His result is shown in Table I and Fig. 1 (dispersion curve).

In our method, we first reduce the expression of φ_0 to the following form:

5) K. SEZAWA, *Bull. Earthq. Res. Inst.*, **9** (1931), 310.
Y. SATÔ, *Bull. Earthq. Res. Inst.*, **33** (1952), 1.

6) A. ERDÉLYI, *Higher Transcendental Functions*, I. (1953), pp. 279 and 281.

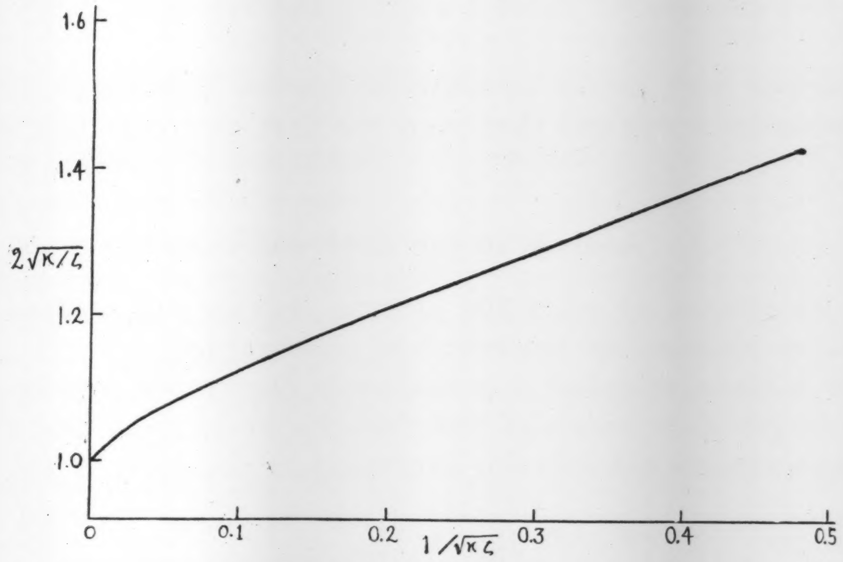

Fig. 1. Ordinate; Phase velocity of surface waves.
Abscissa; Period of surface waves.
Unit of velocity is that of S-waves at the free surface.

Unit of length is the distance from the free surface to the depth where the rigidity is twice that of the surface. Unit of time is determined by the ratio of above two quantities. If we assume, say, the velocity of S-waves at the surface to be 4.0 km/sec and the rate of change of rigidity adequately, the unit of time becomes nearly 1 minute.

$$\varphi_0=\kappa(\omega-\sin\omega)\ ,$$

$$\zeta=2\kappa(1+\cos\omega)\ , \qquad (\pi\geqq\omega\geqq0)$$

Then the equation (22) is expressed as

$$\omega-\sin\omega=0.87/\kappa-\varepsilon\ ,$$

with

$$\varepsilon=0.9/\kappa\,\{\mu/2\cdot d/dz(\mu s)^{-1}\}_0$$
$$=0.9(4\kappa^2)^{-1}\cot\omega(1-\cos\omega)^{-1}\ .$$

Neglecting the small quantity ε, we can solve this equation by help of the numerical table of trigonometric functions. The second approximation is obtained by iteration, on making use of the relation

$$\delta\zeta=-2\kappa\sin\omega\cdot\delta\omega=2\kappa\sin\omega(1-\cos\omega)^{-1}\cdot\varepsilon$$
$$=0.9(2\kappa)^{-1}\cos\omega(1-\cos\omega)^{-2}\ .$$

Table I.
[S] Satô's result
[I] First approximation
[II] Second approximation

κ	ζ[S]	ζ[I]	ζ[II]
1.5	3.00	2.97	2.97
2.5	6.45	6.27	6.35
3.5	10.0	9.73	9.9
4.5	13.7	13.3	13.5
5.5	17.4	16.9	17.2
6.5	21.1	20.6	20.9
7.5	24.9	24.4	24.7
8.5	28.8	28.1	28.5
9.5	32.5	31.8	32.2
11.5	40.2	39.4	39.9
13.5	47.8	47.1	47.6
16.5	59.3	58.5	59.1
19.5	71.1	70.1	70.8
∞	4κ	4κ	4κ

The last two columns of Table I contain the values of ζ calculated in this way.

Comparison with Satô's accurate calculation shows that our method gives satisfactory result and that even the first approximation is capable of use.

3. Analysis of the dispersion curve

Now we proceed to solve the inverse problem—to analyse the dispersion curve obtained as the result of observation.

If the surface values of ρ, μ and their derivatives are known, and the wave-length L is given as the function of v_Q from the dispersion curve, equations (12) and (22) are expressed in the form of the integral equation

$$\varphi_0/f \equiv \int_0^H \{(v_Q/v_s(z))^2-1\}^{1/2}dz = I(v_Q) \ . \tag{26}$$

For instance, if we can neglect the last term of the right side of (22), we have for $n=0$

$$I(v_Q)=(1.\,11/8)L(v_Q) \ . \tag{27}$$

We now set

$$\left.\begin{aligned} &(v_s(0)/v_Q)^2=t \ , \\ &(v_s(0)/v_s(z))^2=\tau \ , \quad (0 \leqq t,\ \tau \leqq 1) \end{aligned}\right\} \tag{28}$$

and write $I(v_Q)$ merely as $I(\tau)$, then the equation (26) is transformed into the following integral equation of Abel's type

$$-\int_\tau^1 \{(t-\tau)/\tau\}^{1/2}(dz/dt)dt = I(\tau) \ , \tag{29}$$

whose solution is obtained in the usual manner as

$$z(t) = -(2/\pi)(d/dz)\int_t^1 \{t/(t-\tau)\}^{1/2}I(\tau)d\tau \ . \tag{30}$$

Integrating the right side of (30) by parts, we get

$$z(t)=(2/\pi)\int_{\tau=1}^{\tau=t} (\tau-t)^{-1/2}d(\tau^{1/2}I(\tau)) \ . \tag{31}$$

We then reduce the variables to v_Q and $v_s(z)$ by (28) and have finally

$$z=(2/\pi)\int_{v_Q=v_s(0)}^{v_Q=v_s(z)} v_s(z)\{(v_s(z)/v_Q)^2-1\}^{-1/2}d(I(v_Q)/v_Q) \ . \tag{32}$$

When the expression (27) is used, this formula is written as

$$z(v_s)=(1.\,11/4\pi)v_s\int_0^{T_s} \{(v_s/v_Q(T))^2-1\}^{-1/2}dT \ , \tag{33}$$

with

$$\left.\begin{aligned} T &= L/v_Q\,, \\ v_Q(T_s) &= v_s\,. \end{aligned}\right\} \qquad (34)$$

3.1. It is difficult to determine the surface values of the derivatives of ρ and μ. They are zero when the earth's crust has actually homogeneous surface layer. Moreover, Love-waves of short wave-length being hardly observed, we assume for the present that derivatives are all zero at the surface. Then we may be allowed to use the equation (33).

As an example of numerical calculation, we took up one of the dispersion curves of Love-waves from the Assam earthquake of 1950 gained by Akima (Fig. 2)[7].

Using the values read from his curve we performed the numerical integration of the right side of the equation (33). (Fig. 3 and Table II).

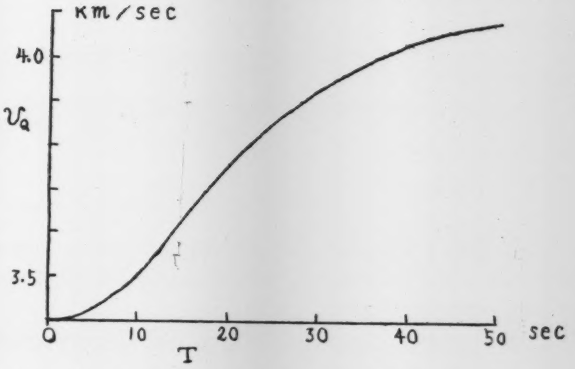

Fig. 2. Dispersion curve gained by Akima.

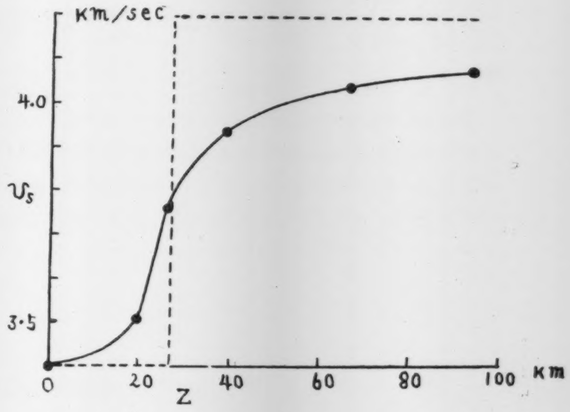

Fig. 3. Full line indicates our result. Dotted line shows the structure employed by Akima.

Table II.

T_s sec	0	10	20	30	40	50
v_s km/sec	3.40	3.51	3.76	3.94	4.04	4.08
z km	0	19.9	26.0	39.0	66.0	94.0

The result seems to give us information about the structure of the earth's crust, at least in the sense inferred in the introduction. In the next stage we should like to treat Rayleigh-waves.

7) T. AKIMA, *Bull. Earthq. Res. Inst.*, **30** (1952), 237.

Finally the author wishes to express his thanks to Mr. Y. Satô who kindly took the labour of troublesome numerical calculation to be compared with our result, and, still more, whose knowledge on surface waves has been of great aid to the author.

---

22. Love 波の分散曲線の解析

地震研究所 高 橋 健 人

Love 波の分散曲線から地殻の構造を定めるとき観測誤差内で一意的に定められないことが知られている. そこで平均的な意味で ρ 及び μ が連続的に変化するものとして所謂 W.K.B. 法の考えによつて近似的な分散公式を求めた.

ρ が一定で μ が深さの一次函数である場合の厳密解を使つて佐藤泰夫が数値計算を行つた結果に対して我々の方法が良好な近似値を与えることを確めた (第I表).

次に分散公式を積分方程式と考えてそれを解くことによつて分散曲線から地殻の構造を求める公式を得た. 計算例として秋間の分散曲線の解析を行つた (第3図).

23. *The Anomalous Behaviour of Geomagnetic Variations of Short Period in Japan and Its Relation to the Subterranean Structure. The 6th report. (The results of further observations and some considerations concerning the influences of the sea on geomagnetic variations.)*

By Tsuneji RIKITAKE and Izumi YOKOYAMA,

Earthquake Research Institute.

(Read June 28, 1955.—Received June 30, 1955.)

Summary

New results of the recent observations are described in regard to the anomalous distribution of short-period geomagnetic variations in Japan. The possible influence of the sea on the variations is also studied from the standpoint of the electromagnetic induction theory. It is made clear that the observed results can not be explained by the effect of the electric currents induced in the sea. An interpretation concerning a possible cause of the phenomenon is also attempted.

Introduction

The anomalous behaviour of geomagnetic variations of short period in Japan has been investigated by the writers. As has been published in a series of papers in this bulletin[1),2),3),4),5)] and elsewhere[6),7)], the characteristic features of the anomaly were examined in detail by all available means. As a result of these investigations, it becomes clear that the anomalously large amplitudes of the vertical component of

---

1) T. RIKITAKE, I. YOKOYAMA and Y. HISHIYAMA, *Bull. Earthq. Res. Inst.*, **30** (1952), 207.
2) T. RIKITAKE, I. YOKOYAMA and Y. HISHIYAMA, *Bull. Earthq. Res. Inst.*, **31** (1953), 19.
3) T. RIKITAKE, I. YOKOYAMA and Y. HISHIYAMA, *Bull. Earthq. Res. Inst.*, **31** (1953), 89.
4) T. RIKITAKE, I. YOKOYAMA and Y. HISHIYAMA, *Bull. Earthq. Res. Inst.*, **31** (1953), 101.
5) T. RIKITAKE, I. YOKOYAMA and Y. HISHIYAMA, *Bull. Earthq. Res. Inst.*, **31** (1953), 119.
6) T. RIKITAKE and I. YOKOYAMA, *Journ. Geomagn. Geoelectr.* **5** (1953), 59.
7) T. RIKITAKE and I. YOKOYAMA, *Naturwissenschaften*, **41** (1954), 420.

geomagnetic variations as observed in central Japan on occasions of bays and storms have nothing to do with things outside the earth but must be explained by some agencies inside the earth. So there must be a complicated distribution of the induced electric currents at the time of geomagnetic variations. On the basis of this fact, we are now inclined to imagine a peculiar distribution of the electrical conductivity underneath Japan.

It is also of interest that an anomalous phenomenon of the same character concerning short-period geomagnetic variations has been recently discovered in Germany[8),9)]. It seems likely that the anomaly is caused by a concentrated distribution of the induced electric currents underneath the northern part of Germany, though the distribution of the electric currents seems somewhat simpler than that in Japan.

Although we still know very little about the cause of the phenomenon, there was no knowledge of this kind in the past. Consequently, an intensive study in this line may throw some light on the study of the earth's crust or deeper interior. It might be possible to obtain some knowledge on the physical property of the substances at a depth of about 100 *km* and its relation to the geological structure, seismic and volcanic activities, provided we can carry out sufficient observations for detailed analyses.

In the light of the importance of the phenomenon, it is quite desirable to make further observations for the three geomagnetic components at as many places as possible, especially observations on the islands in the southern sea of Japan being of special interest in order to determine the southern boundary of the area in which we observe the large amplitude of the vertical component. The writers set up a temporary station in Ooshima Island, about 100 *km* south of Tokyo, as the first step. As will be stated in this paper, the behaviours of short-period variations there do not differ much from those observed at Aburatsubo and Kakioka, the observations at the latter two observatories being already reported in the previous papers.

In the cases of bay disturbances in Japan, which are mostly used in the previous analyses, the magnetic vector in the horizontal plane is directed towards the north. This is due to the fact that bays occur during nights when the magnetic vectors are necessarily directed towards approximately the north as has been made clear by the statistical

8) U. FLEISCHER, *Naturwissenschaften*, **41** (1954), 114.
9) H. WIESE, *Zeits. f. Meteorologie*, **8** (1954), 77.

studies of geomagnetic bays[10),11)]. Accordingly, the results discussed in the writers' previous papers are based on geomagnetic variations which change nearly in one direction. If there is a special distribution of the electrical conductivity in the earth, the magnetic field caused by the induced electric currents might show an apparent anisotropy, the analyses of which would be useful for the present study. Some examinations are carried out with regard to the observations at a few observatories from this point of view though there are not many favourable cases because of the above-mentioned characters of bays. The writers have got an empirical law between the vertical force and the north and east forces, the relation thus made clear being sometimes useful in inferring the distribution of the induced currents.

One might suspect that the electric currents induced in sea water play an important role in the interpretation of the anomaly because of the high conductivity of sea water. The writers have been of the opinion that the anomalous distribution of geomagnetic variations in Japan are not to be explained by the influence of the sea judging from the duration-time or period of the variations and the mode of distribution. However, it will be useful to study the possible influence of the sea so as to keep at the same question from cropping up all the time. So the writers would here like to describe the possible influence of the sea on the basis of the theory of the electromagnetic induction in a sheet. In the study, the effect of the self-induction, which is important for rapid variations, is fully taken into account.

In the final part of this paper, a speculation about the cause of this anomalous phenomenon is added. Although we have to accomplish many more observations and analyses in order to establish a physical picture of the origin which is situated underneath the earth's crust, it would be of some use to construct a possible model of the electrical state for future studies. But it seems somewhat puzzling to accept the model thus constructed from both the geological and geophysical stand-points because the model is not simple.

Chapter I. Results of the new observation

1. The observation on Ooshima Island

In order to bring out more clearly the anomalous characteristics

10) H. HATAKEYAMA, *Geophys. Mag.*, **12** (1938), 16.
11) N. FUKUSHIMA, *Journ. Faculty Sci. Tokyo Univ.* Sec. II, **8** (1953), 291.

of geomagnetic variations in the central part of Japan, a temporary station for a continuous observation of three geomagnetic components has been set up in Ooshima Island (34°44′ N, 139°22′ E) in July and August, 1954, while the routine observations at Aburatsubo (35°09′N, 139°37′ E) and Maze (37°44′ N, 138°48′ E) were going on as usual. It is not easy to keep the observation of this kind in good condition over a long period on Ooshima Island, because we have no commercial electric supply there except for a few hours in the evening.

The magnetic variometers were installed in a cave where the changes in geomagnetic declination in connection with the activities of Volcano Mihara have been continuously recorded since 1951. The sensibility of the D (declination)-variometer is $0.58'/mm$ with a $3\,m$ optical lever, a magnet being suspended with a quartz fibre of $10\,\mu$. The H (horizontal intensity)-variometer has a suspending quartz fibre of $60\,\mu$ with a sensibility of usually $1.5\gamma/mm$. The Z (vertical intensity)-variometer is the one of the Watson type with a sensibility of $0.7\gamma/mm$ as a rule. At this station, absolute measurements of the three components have often been carried out with a G.S.I. type magnetometer. The values at the epoch of 1954.0 are given in the foot-note[12]. In the magnetograms obtained here, we can see that the strong parallelism between the short period changes in the horizontal (ΔH) and vertical (ΔZ) components is very conspicuous.

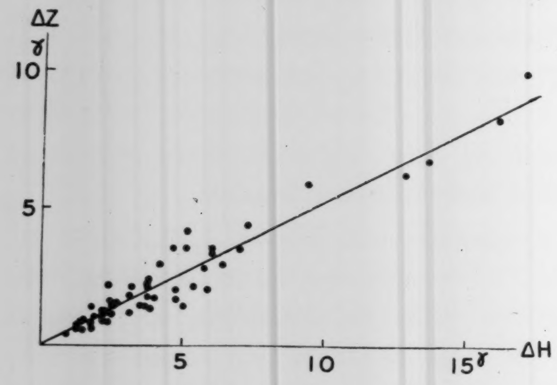

Fig. 1. The relation between ΔZ and ΔH for short period variations obtained by the observation on Ooshima Island.

The relation between ΔH and ΔZ for short period variations are shown in Fig. 1. The mean value of $\Delta Z/\Delta H$ is estimated at 0.52. Judging from the value of $\Delta Z/\Delta H$ and the above-mentioned parallelism between ΔZ and ΔH, we may presume that Ooshima Island belongs to the same district as Kakioka and Aburatsubo where the anomalous behaviours of geomagnetic variations have been observed.

With the aid of the value of $\Delta Z/\Delta H$ newly obtained by the con-

12)

D	H	I
6°11′.9W	30045γ	47°18′·7

tinuous observations on Ooshima Island and Shimosato (33°34′ N, 135°55′ E) of Hydrographic Office, Maritime Safety Agency, the preliminary chart showing the statistical distribution of $\Delta Z/\Delta H$ for short-period variations in Japan is modified as shown in Fig. 2.

In Fig. 3 the relation between the ratio $\Delta Z/\Delta H$ and the duration-time of geomagnetic variations is shown. The shorter the period is, the more dispersive the value of $\Delta Z/\Delta H$ becomes (the variations whose duration-time is shorter than 5 *min.* are omitted in the figure). This phenomenon is caused by small and irregular fluctuations, especially in Z-component, which seem to be always observed except for a few hours during midnight. It is probable that the disturbances are caused by the stray electric currents from electric railways in Tokyo district.

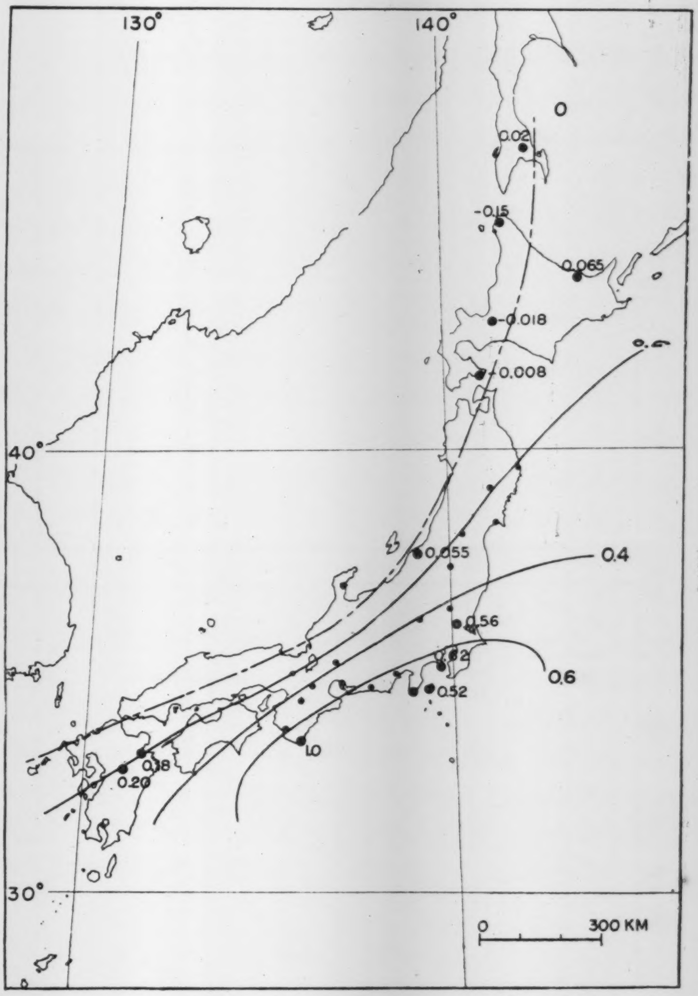

Fig. 2. The revised distribution of $\Delta Z/\Delta H$ for short period variations in Japan.

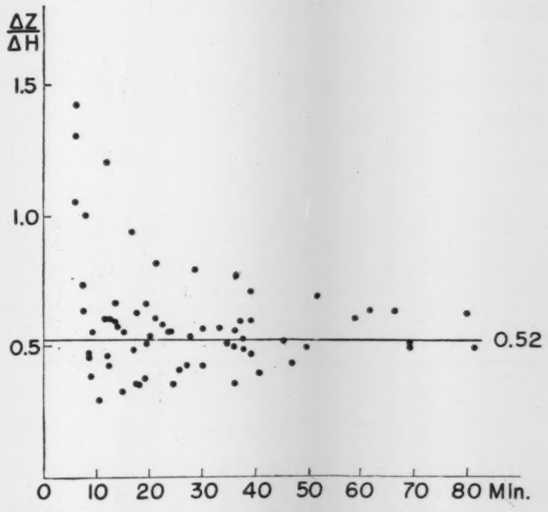

Fig. 3. The relation between $\Delta Z/\Delta H$ and the period of geomagnetic variations at Ooshima Island.

2. Apparent anisotropy of geomagnetic variations in the central part of Japan

The accumulation of the observations enables

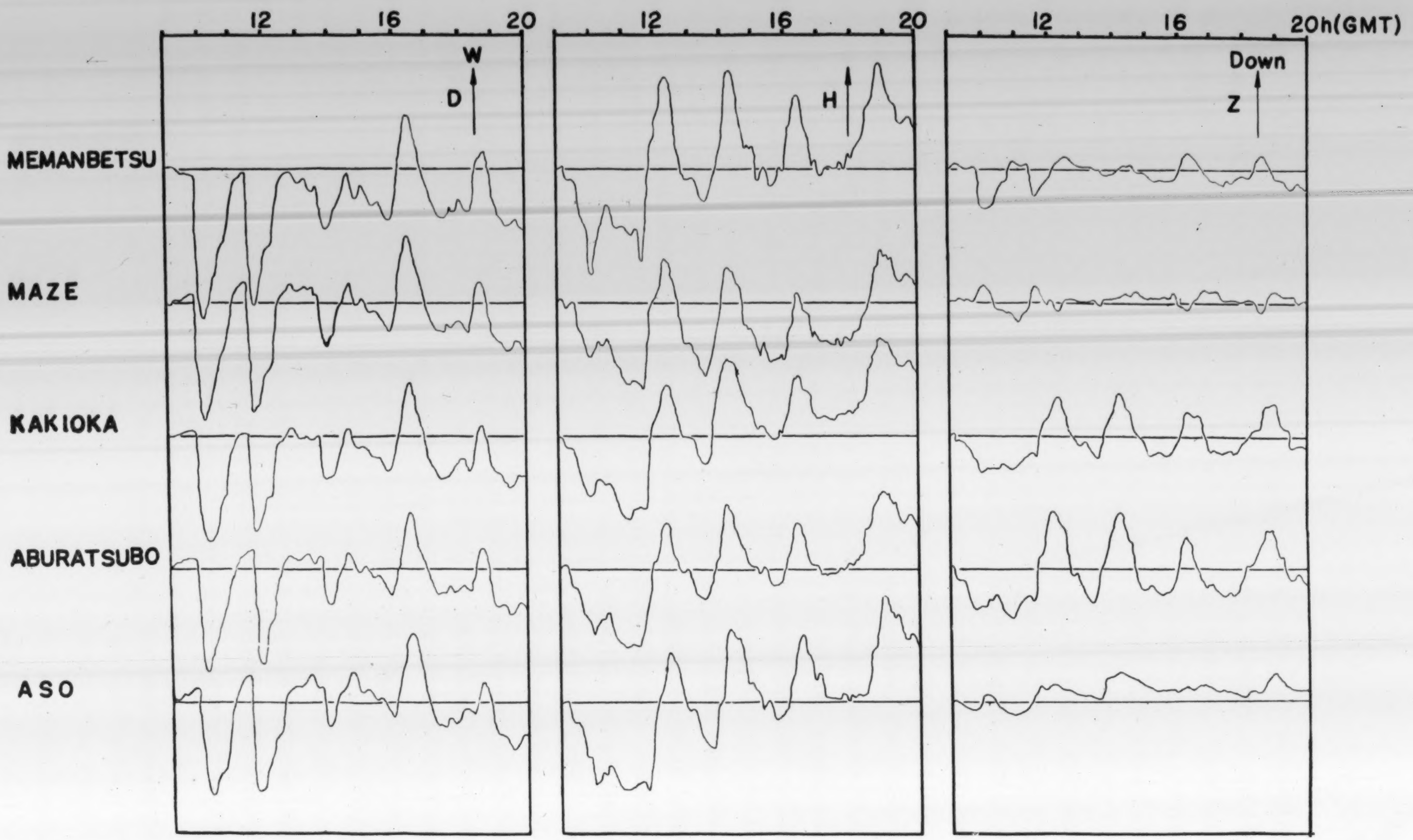

Fig. 4. The changes in the three components observed at the five stations in Japan at the time of the repeated occurrences of bays on Sept. 23 and 24, 1953. The distance between two datum lines corresponds to 40 *gammas*.

us to examine some further characteristics of geomagnetic variations of short period in the central part of Japan. At Maze, it is found out that ΔZ is fairly large whenever the magnetic vector is directed towards approximately east or west, though ΔZ is quite small for usual variations whose magnetic vectors lie nearly in the north-south direction. This tendency has been only recently discovered in spite of three years of observation, because bay disturbances, which were mostly

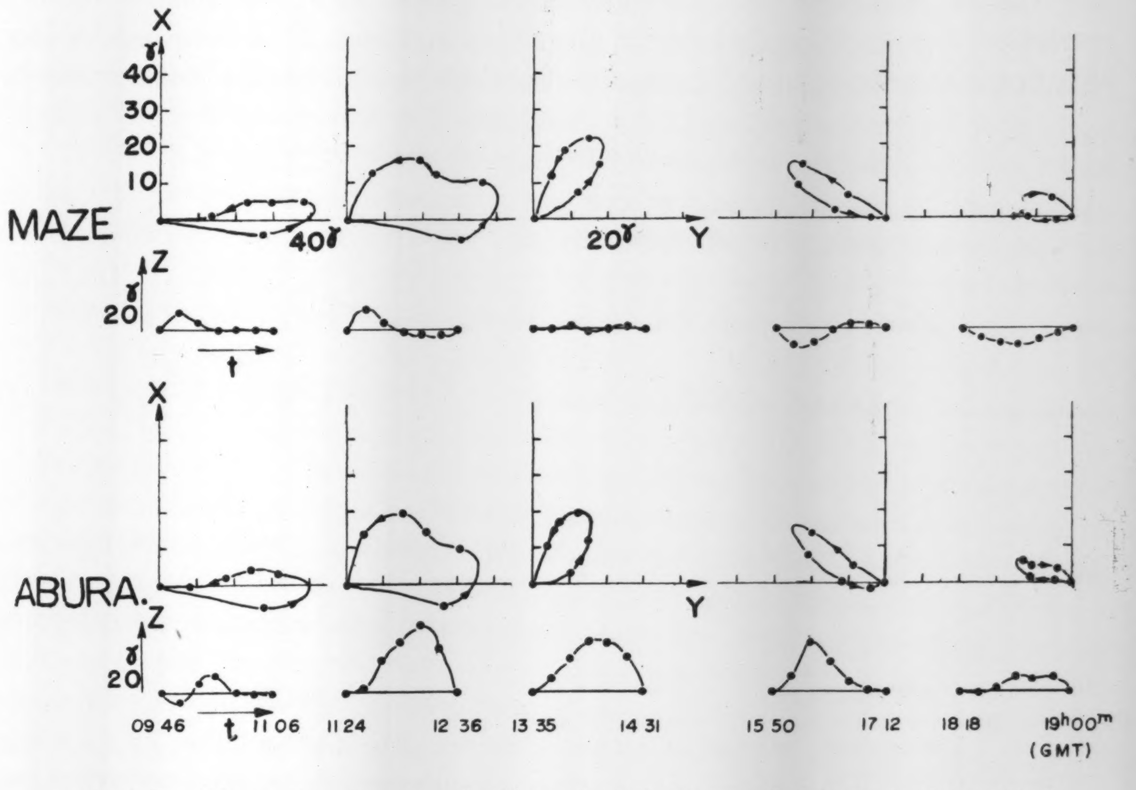

Fig. 5. The vector diagrams in the horizontal plane and changes in the vertical component respectively for Maze and Aburatsubo on occasions of the repeated occurrences of bays on Sept. 23 and 24, 1953.

analysed before, often occur during nights when the magnetic vector of the disturbance mainly points to the north[10),11)]. By a similar examination in regard to the observation at Aburatsubo, a quite different characteristics has been found there. ΔZ is quite small for the east-west changes of the magnetic vector though we observe an anomalously large ΔZ when the vector changes in the north-south direction. So we may say that there is a sort of anisotropy of geomagnetic variations. In order to make clear the underground structure, it will be of importance to study the anisotropy or the dependency of ΔZ on the direction

of the inducing magnetic field.

The characteristics stated above is well demonstrated by the following examples. We found a successive occurrence of several bay disturbances during one evening on Sept. 23 and 24, 1953. Copies of the magnetograms at that time from five stations in Japan, Memanbetsu (43°54′ N, 144°12′ E), Kakioka (36°14′ N, 140°13′ E), Aso (32°55′ N, 131°04′ E) and our two stations, are shown in Fig. 4. Fig. 5 shows the vector diagrams in the horizontal plane and the modes of ΔZ-variation for each bay at Maze and Aburatsubo. It is noteworthy that an apparent anisotropy of geomagnetic variation exists at both stations.

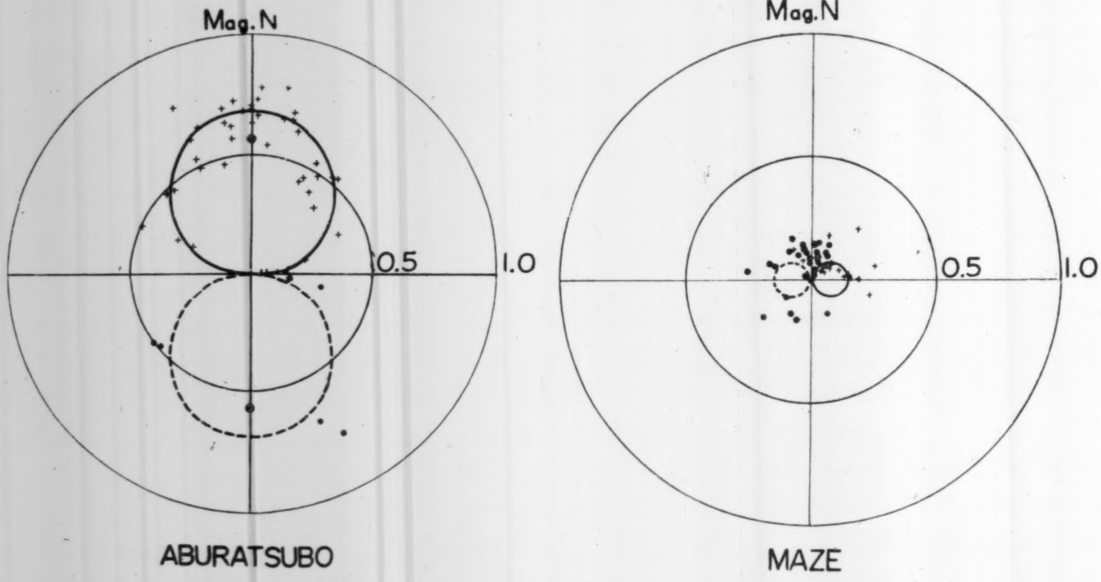

Fig. 6a. The relation between $\Delta Z/\Delta R$ and the direction of the magnetic vector in the horizontal plane at Aburatsubo.

Fig. 6b. The relation between $\Delta Z/\Delta R$ and the direction of the magnetic vector in the horizontal plane at Maze.

+ : positive value of ΔZ,
● : negative value of ΔZ.

In the following discussion, we will examine ΔZ in relation to ΔR (changes of the resultant component in the horizontal plane) in place of ΔH. At Aburatsubo, large amplitude of ΔZ becomes smaller in the cases of east- or westward variations, while slight parallelism between ΔZ and ΔR can be seen at Maze during the same variations.

The values of $\Delta Z/\Delta R$ at both stations are plotted in the diagrams as shown in Fig. 6. The radial distance gives the value of $\Delta Z/\Delta R$ while the direction of the magnetic vector is given by the azimuth. In the figures the small circle and the cross denote respectively the

positive and negative values of ΔZ. If we express $\Delta Z/\Delta R$ by empirical formulae, we get the following expressions by means of the least square method:

$$\frac{\Delta Z}{\Delta R}=0.68\frac{\Delta X}{\Delta R}+0.01\frac{\Delta Y}{\Delta R} \quad \text{for Aburatsubo,} \tag{1}$$

$$\frac{\Delta Z}{\Delta R}=-0.01\frac{\Delta X}{\Delta R}+0.15\frac{\Delta Y}{\Delta R} \quad \text{for Maze,} \tag{2}$$

where ΔX and ΔY denote respectively the north and east components of variations. These formulae are shown in the figures with full and broken lines respectively for positive and negative values of ΔZ.

Here, we shall consider normal distribution of $\Delta Z/\Delta R$ in the cases of bay type variations assuming the uniform core model of the earth. As has been studied by one[13] of the writers, the distribution of the magnetic potential of a bay type disturbing field in low and middle latitude may be expressed approximately by the expression

$$W=\left(er+i\frac{R^3}{r^2}\right)\sin\phi Q_1^1(\cos\theta), \tag{3}$$

where ϕ, θ, R, e and i denote respectively the geomagnetic longitude, co-latitude, the radius of the earth, external and internal parts of the coefficient of the magnetic potential. ϕ is equivalent to the local time. Then the magnetic components at $r=R$ become as follows:

$$\left.\begin{aligned} X&=(e+i)\sin\phi\frac{dQ_1^1}{d\theta}, \\ Y&=-(e+i)\cos\phi\frac{Q_1^1}{\sin\theta}, \\ Z&=(e-2i)\sin\phi Q_1^1. \end{aligned}\right\} \tag{4}$$

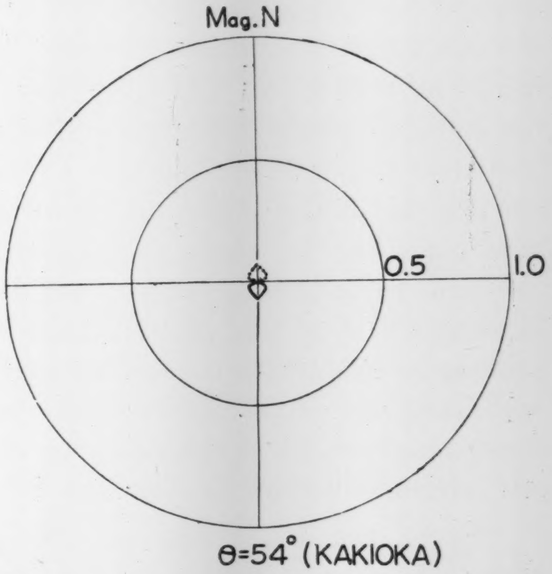

Fig. 7. The calculated relation between $\Delta Z/\Delta R$ and the direction of the magnetic vector in the horizontal plane at a point for $\theta=54°$, the relation being obtained with respect to an idealized uniform earth.

On taking the uniform core model which has been accepted from various reasons, the relation between $i(t)$ and $e(t)$ is given by

13) T. RIKITAKE, *Bull. Earthq. Res. Inst.*, **28** (1950), 45.

$$i(t)=\frac{q^3}{2}e(t)=0.415e(t) \quad (q=0.94)\ . \tag{5}$$

Calculating each magnetic component by (4) and (5) for various values of ϕ, the distribution of $\Delta Z/\Delta R$ is shown in Fig. 7 where θ is taken as 54° (Kakioka).

Comparing Fig. 7 with Fig. 6, we find that the distributions of $\Delta Z/\Delta R$ at both Aburatsubo and Maze are quite different from those theoretically derived from the uniform core model of the earth. So we may say that the variations at the two stations are of the type which can not be explained by assuming a uniform conducting earth. The subterranean structure by which we can explain the anomalous behaviour of geomagnetic variations in the central part of Japan should be such as can account for these observed results.

Chapter II. The influences of the sea on geomagnetic variations

1. Review of the problem

Although the characteristic features of geomagnetic variations in Japan as well as in Germany have been considered to be caused by the induced electric currents flowing in the earth's interior, the question that the induced electric currents in the sea might be responsible for the particular distribution of geomagnetic variations has constantly been discussed by some geomagneticians. J. Coulomb[14] suggested that the sea surrounding Japan might have an appreciable influence. K. Burkhart[15] is of the opinion that all the characteristic distribution of geomagnetic variations can be explained by a particular distribution of the electrical conductivity near the surface of the earth. In view of these opinions, it is desirable to clarify the possible effect of the electric currents flowing in the sea on short-period geomagnetic variations.

From the beginning of the quantitative studies of geomagnetic variations, the influence of the seas or oceans has often been considered in relation to the interpretation of the relation between the external and internal parts of geomagnetic variations. However, no definite results were obtained because of the irregularities of the distribution of land and sea.

14) J. COULOMB, Discussion to the writers' paper at the Rome Assembly of IUGG ATME (1954).

15) K. BURKHART, Personal communication.

S. Chapman and T. T. Whitehead[16] made a mathematical study on the possible effect of a hypothetical ocean covering the whole surface of the earth with a uniform depth. They found that the internal origin part of a geomagnetic variation would be considerably affected even by a shallow ocean. It is not likely, however, that the influence of the real ocean will be as great as studied by them because the land areas will greatly reduce the said effect. The same kind of investigation was also made by B. N. Lahiri and A. T. Price[17] with special application to the electromagnetic induction within a non-uniform earth.

Since an appreciable effect of an ocean which is supposed to spread all over the earth can be expected as stated above, it becomes important to see to what extent geomagnetic variations will be influenced by the real distribution of the seas though a rigorous estimate would be of great difficulty to make. J. M. de Wet[18] calculated the induced electric current by solar diurnal variation in the oceans. On the basis of the distribution of ocean depth, he constructed a world-map of the distribution of the electrical conductivity over the earth's surface, the boundaries between the lands and seas being approximated with suitable meridians and parallel circles of every 15°. Ignoring the effect of self-induction, he calculated the induced electric currents by means of the relaxation method. So he got the induced currents whose distributions change according to the universal time. As may be expected, current vortices were obtained in large oceans such as the Pacific, Atlantic and Indian Oceans, so that we may suppose that a comparatively large magnetic field due to the induced currents exists there. T. Rikitake[13] also investigated the possible influence of a sea which is bounded by two meridians $\pi/2$ apart. According to his study it was concluded that the induced currents by S_q variation would produce a magnetic field of several *gammas* as its maximum. Near the boundaries between lands and seas, the field would become smaller. Since, however, the self-induction is ignored in the two studies mentioned above, the results can not be applied to rapid variations. A. A. Ashour[19] studied the induction of electric currents in a uniform circular disk. He applied the result to the problem of the induced current in the ocean which is regarded as a large disk.

In spite of all the studies reviewed here, the question of whether or

16) S. CHAPMAN and T.T. WHITEHEAD, *Trans. Cambr. Phil. Soc.*, **22** (1922), 463.
17) B.N. LAHIRI and A.T. PRICE, *Phil. Trans. Roy. Soc. London A*, **237** (1939), 509.
18) J.M. DE WET, *Thesis*, *London University*, (1949).
19) A.A. ASHOUR, *Quart. Journ. Mech. and Applied Math.*, **3** (1950), 119.

not the anomalous behaviour of short-period geomagnetic variations as observed in Japan can be explained as being the effect of the electric currents induced in the sea still remains unsolved. Although it seems unlikely that the anomalous behaviour is caused by the electric currents in the sea judging from the duration-time of variations and also from the mode of the distribution of the anomaly, we have to prove that the sea is not responsible for the phenomenon, otherwise no rigorous conclusion can be obtained. The writers would here like to investigate the behaviour of time-dependent magnetic field in the neighbourhood of the boundary between land and sea.

The present investigations will be divided into two parts. In the first part, the electromagnetic induction in a hemi-spherical shell of uniform conductivity will be investigated for the purpose of examining the effect of ocean of a world-wide scale. A similar study will be made in regard to a plane sheet in the second part, the sheet having different conductivities respectively for idealized land and sea. The plane sheet model may be applied to a smaller scale distribution of land and sea.

2. Electromagnetic induction in a hemi-spherical shell of uniform conductivity[20]

We will examine here the electromagnetic induction in a hemi-spherical shell of uniform conductivity, the shell being placed in a time-dependent uniform magnetic field. Although the model differs from the real distribution of oceans over the earth, the hemi-spherical shell can, as a rough approximation, be regarded as an ocean of world-wide extent. Since no exact examination has hitherto been undertaken, the following study might be of some use for studying rapid changes in geomagnetic field because the effect of self-induction is fully taken into account.

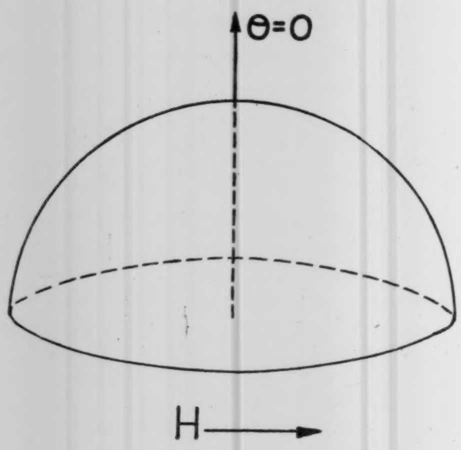

Fig. 8.

Let us take a hemi-spherical shell as shown in Fig. 8 where the

20) A part of this study was carried out by one of the writers (T.R.) under the direction of Professor A.T. Price in relation to the screening effect of the ionosphere which had been suggested by Professor S. Chapman. He is very grateful to Professor Price for the guidance given by him.

external magnetic field is applied in a direction as shown by the arrow. The centre of the sphere is taken as the origin of a spherical polar coordinate whose $\theta=0$ axis is also shown in Fig. 8.

The magnetic potential of the external field is given as

$$W_e = -rHP_1^1(\cos\theta)\cos\phi\ . \tag{6}$$

It is readily seen that we can express the current function of the induced electric currents in a form as

$$\Psi = \sum_n a_n P_n^1(\cos\theta)\cos\phi\ , \tag{7}$$

the expression being effective not only on the shell but on the whole surface of the sphere whose radius is denoted by a. The current function is to be determined by the following differential equation which is true only on the conductor, the equation being written as

$$\frac{1}{a^2}\left\{\frac{1}{\sin\theta}\frac{\partial}{\partial\theta}\left(\sin\theta\frac{\partial}{\partial\theta}\right)+\frac{1}{\sin^2\theta}\frac{\partial^2}{\partial\phi^2}\right\}\Psi = K\frac{\partial H_r}{\partial t} \tag{8}$$

in which K and H_r denote respectively the integrated conductivity which is uniform on the hemi-sphere and the normal component of the magnetic field. The magnetic permeability is assumed to be unity in electromagnetic unit.

Let us now suppose that the external magnetic field changes as

$$\begin{aligned} H&=0 & t&<0 \\ &=H_0 & t&\geqslant 0\ . \end{aligned} \tag{9}$$

In that case, a particular distribution of the induced currents takes place in the shell at $t=0$. Since there is no change in the external field after that, the currents thus excited will decay freely. So the first task is to obtain the initial current distribution.

In the case of a sudden change in the external field, the self-induction is so large that we can neglect the lefthand-side of (8). Hence we have

$$H_r=0 \qquad \text{for} \quad t=0 \tag{10}$$

from which we see that the magnetic field produced by the initial currents cancels the normal component of the applied magnetic field. Hence the problem becomes equivalent to that of a hemi-spherical shell moving in an ideal fluid, the stream lines corresponding to the magnetic lines of force.

If we take into account (6) and (7), the relation (10) may be written as

$$\frac{aH_0}{4\pi}P_1^1+\sum_n\frac{n(n+1)}{2n+1}a_nP_n^1=0 \tag{11}$$

which is true only for $0<\theta<\pi/2$. (11) can be also written as

$$\sum_n a_nP_n^1=-\sum_n\left\{\frac{n(n+1)}{2n+1}-1\right\}a_nP_n^1-\frac{aH_0}{4\pi}P_1^1 \qquad 0<\theta<\pi/2. \tag{12}$$

On the other hand, the current function should be zero on another half of the sphere, so that we have

$$\sum_n a_nP_n^1=0 \qquad \pi/2<\theta<\pi\,. \tag{13}$$

Table I. R_{nN} $(=R_{Nn})$.

n \ N	1	2	3	4	5	6
1	0.666667	0.433013	0	−0.131762	0	0.071603
2		0.400000	0.176778	0	−0.034939	0
3			0.2857143	0.181546	0	−0.058463
4				0.222222	0.114820	0
5					0.181818	0.115549
6						0.153846
7						
8						
9						
10						
11						
12						

n \ N	7	8	9	10	11	12
1	0	−0.046876	0	0.033798	0	−0.025875
2	0.014321	0	−0.0075646	0	0.0045805	0
3	0	0.033490	0	−0.022809	0	0.016946
4	−0.027235	0	0.012430	0	−0.0070562	0
5	0	−0.037823	0	0.022090	0	−0.015311
6	0.084573	0	−0.021890	0	0.010604	0
7	0.133333	0.067344	0	−0.027944	0	0.016473
8		0.117647	0.066878	0	−0.018223	0
9			0.105263	0.066957	0	−0.022150
10				0.095238	0.055287	0
11					0.086957	0.055325
12						0.076923

From (12) and (13), we can determine the coefficients in the following way. After multiplying by $P_N^1(\cos\theta)\sin\theta$, we shall integrate (12) and (13) with respect to θ from $\theta=0$ to $\theta=\pi$. In that case (12) is true between 0 to $\pi/2$ while we have to take (13) between $\pi/2$ to π. So we obtain

$$2a_n R_{nN} + \sum_n \left\{\frac{n(n+1)}{2n+1} - 1\right\} a_n R_{nN} = -\frac{aH_0}{4\pi} R_{1N}\,, \qquad (14)$$

where

Table II. The coefficients and the right-hand members of the simultaneous equations.

a_1	a_2	a_3	a_4	a_5	a_6	a_7
1	0.077942	0	−0.144606	0	0.143757	0
−0.164020	1	0.143488	0	−0.068578	0	0.044480
0	0.045590	1	0.285462	0	−0.168171	0
0.061391	0	0.181258	1	0.277213	0	−0.104053
0	−0.010311	0	0.206604	1	0.380357	0
−0.036669	0	−0.064158	0	0.306633	1	0.355055
0	0.004538	0	−0.052623	0	0.298937	1
0.025369	0	0.038839	0	−0.106070	0	0.298861
0	−0.002505	0	0.025100	0	−0.080865	0
−0.018963	0	−0.027423	0	0.064222	0	−0.128565
0	0.001563	0	−0.014863	0	0.040367	0
0.015487	0	0.021734	0	−0.047485	0	0.080848

a_8	a_9	a_{10}	a_{11}	a_{12}	right-hand member*)
−0.136493	0	0.128917	0	−0.122140	0.600000
0	−0.032122	0	0.024668	0	0.492060
0.139714	0	−0.124650	0	0.114499	0
0	0.064925	0	−0.046742	0	−0.184173
−0.180569	0	0.138111	0	−0.118384	0
0	−0.125676	0	0.077210	0	0.110008
0.345230	0	−0.187656	0	0.136773	0
1	0.405758	0	−0.140218	0	−0.076107
0.358301	1	0.469912	0	−0.192640	0
0	0.421150	1	0.441024	0	0.056890
−0.100609	0	0.399844	1	0.494705	0
0	−0.148620	0	0.470790	1	−0.046461

*) The right-hand members should be multiplied by $-\frac{aH}{4\pi}$.

$$R_{nN}=\int_0^1 P_n^1(x)P_N^1(x)dx\ . \tag{15}$$

R_{nN}'s are constants which can be evaluated by (15) as given in Table I up to the 12th degree of the spherical surface harmonics. With the aid of these values we can obtain a set of simultaneous equations for a_n's. On taking a_n up to $n=12$, the coefficients of a_n's and the righthand members are calculated as given in Table II. Since

Table III. The solutions of the simultaneous equations. $\left(\text{Unit}: -\dfrac{aH}{4\pi}\right)$

a_1	a_2	a_3	a_4	a_5	a_6
0.4737	0.5549	0.0922	−0.2210	−0.0403	0.1498
a_7	a_8	a_9	a_{10}	a_{11}	a_{12}
−0.0025	−0.1025	0.0074	0.0813	−0.0312	−0.0417

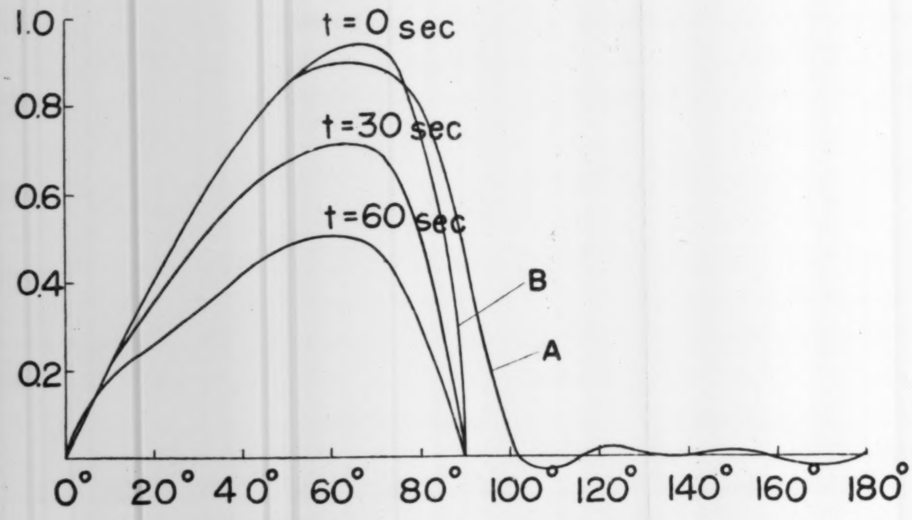

Fig. 9. The distribution of the current function on $\phi=0$. $\left(\text{Unit}: -\dfrac{aH}{4\pi}\right)$ Curve A shows the distribution for $t=0$ as obtained by (7). Curve B corresponds to that obtained by (16). The decay of the initial distribution is also shown for $t=30$ *sec.* and $t=60$ *sec.*

the coefficients of the diagonal terms are relatively large, we may solve the equations though the rigorous proof of convergency of the solution is disregarded here. The solutions which are solved by the relaxation method are given in Table III.

With these a_n's the current function is obtained from (7), the distribution on $\phi=0$ being shown in Fig. 9. It is clearly seen that the current function is nearly zero between $\theta=\pi/2$ and $\theta=\pi$. The fact that the current function is not exactly zero is due to the procedure of calculation in which we take harmonics of $n=1, 2, \cdots, 12$ only. This is also the cause of small fluctuations between $\theta=\pi/2$ and $\theta=\pi$.

If we take into consideration the fact that the normal component of the electric currents should vanish at $\theta=\pi/2$, we may have an alternative expression for the current function

$$\Psi=\sum_m c_{2m}P^1_{2m}(\cos\theta)\cos\phi \tag{16}$$

which is true only for $0<\theta<\pi/2$. So we have

$$\left.\begin{aligned}&\sum_n a_nP^1_n=\sum_m c_{2m}P^1_{2m} && 0<\theta<\pi/2\,,\\ &\sum_n a_nP^1_n=0 && \pi/2<\theta<\pi\,,\end{aligned}\right\} \tag{17}$$

from which we deduce the following relation between a_n and c_{2m} by means of a procedure similar to the determination of a_n, the relation being given as

$$2R_{NN}a_n=\sum_m c_{2m}R_{2m,N}\,. \tag{18}$$

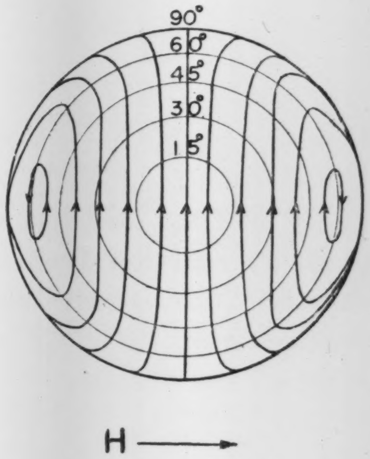

Fig. 10. The distribution of the initial currents, the same amount of the electric current flowing between two adjacent lines.

Since $a'_n s$ are given in Table III, we can solve $c'_{2m}s$ from (18). The current function thus obtained is also shown in Fig. 9 while the current system viewed from a point on $\theta=0$ axis is shown in Fig. 10. Although we see some difference between the two curves, it would be meaningless to discuss the difference unless we take into account many more harmonics.

Now we are in a position to investigate the decay of the induced electric currents which are excited at $t=0$. We shall start again from (8) which can be written as

$$-\sum_n n(n+1)a_nP^1_n=a^2KpH_0P^1_1+4\pi aKp\sum_n\frac{n(n+1)}{2n+1}a_nP^1_n \quad \text{for} \quad 0<\theta<\pi/2 \tag{19}$$

where p denotes $\partial/\partial t$.

It is also obvious that

$$\sum_n n(n+1)a_nP^1_n=0 \qquad \text{for} \quad \pi/2<\theta<\pi\,. \tag{20}$$

After multiplying by $P_N^1(\cos\theta)\sin\theta$ and integrating (19) and (20) with respect to θ from $\theta=0$ to $\theta=\pi$, we obtain

$$-2a_N R_{NN} N(N+1) = a^2 K p H_0 R_{1N} + 4\pi a K p \sum_n \frac{n(n+1)}{2n+1} a_n R_{nN} \,. \tag{21}$$

If it is assumed that a_n can be expressed as

$$a_n = \sum_s a_n^s p^{-s} \,, \tag{22}$$

(21) becomes

$$-\frac{R_{NN}N(N+1)}{2\pi a K}\sum_s a_N^s p^{-s-1} = \frac{aH_0}{4\pi}R_{1N} + \sum_s\sum_n \frac{n(n+1)}{2n+1} a_n^s R_{nN} p^{-s} \,. \tag{23}$$

On equating the coefficients of the corresponding powers of p, we obtain

$$\left.\begin{aligned}
&\sum_n \frac{n(n+1)}{2n+1} a_n^1 R_{nN} = -\frac{R_{NN}N(N+1)}{2\pi a K} a_N^0 \,,\\
&\sum_n \frac{n(n+1)}{2n+1} a_n^2 R_{nN} = -\frac{R_{NN}N(N+1)}{2\pi a K} a_N^1 \,,\\
&\cdots\cdots\cdots\cdots\cdots\cdots\cdots\cdots\cdots\cdots\\
&\sum_n \frac{n(n+1)}{2n+1} a_n^s R_{nN} = -\frac{R_{NN}N(N+1)}{2\pi a K} a_N^{s-1} \,.
\end{aligned}\right\} \tag{24}$$

By solving the first set of the equations in (24), therefore, we can obtain a_N^1 starting from a_N^0 obtained in the preceding paragraph. On repeating the successive operations, the coefficients a_N^2, a_N^3, $\cdots$ can be obtained from (24). If we interpret the operational equation (22) term by term, we obtain

$$a_n = \sum_s \frac{a_n^s}{s!} t^s \,, \tag{25}$$

so that it is possible to estimate the change in the current function with lapse of time provided the series (25) are convergent. Actually, the coefficients of the first three harmonics can be written as

$$\left.\begin{aligned}
c_2 &= (1.16 - 7.67\omega t + 32.0\omega^2t^2 - 124\omega^3t^3 + 468\omega^4t^4 \cdots)\left(-\frac{aH_0}{4\pi}\right),\\
c_4 &= (-0.458 + 6.07\omega t - 41.7\omega^2t^2 + 206\omega^3t^3 - 840\omega^4t^4 \cdots)\left(-\frac{aH_0}{4\pi}\right),\\
c_6 &= (0.260 - 6.49\omega t + 68.5\omega^2t^2 - 456\omega^3t^3 + 2240\omega^4t^4 \cdots)\left(-\frac{aH_0}{4\pi}\right),
\end{aligned}\right\} \tag{26}$$

where

$$\omega = \frac{1}{4\pi a K}. \tag{27}$$

In this case, the second way of expression for the current function which is true only for $0<\theta<\pi/2$ as given in (16) is adopted. $c_2^s, c_4^s, \cdots$ are readily obtained from $a_1^s, a_2^s, \cdots$.

If we assume $K=10^{-7}emu$[21], the distribution of the current function becomes like the curves which are also shown in Fig. 9 respectively for $t=30$ *sec.* and $t=1$ *min.* It is seen that the centres of the current

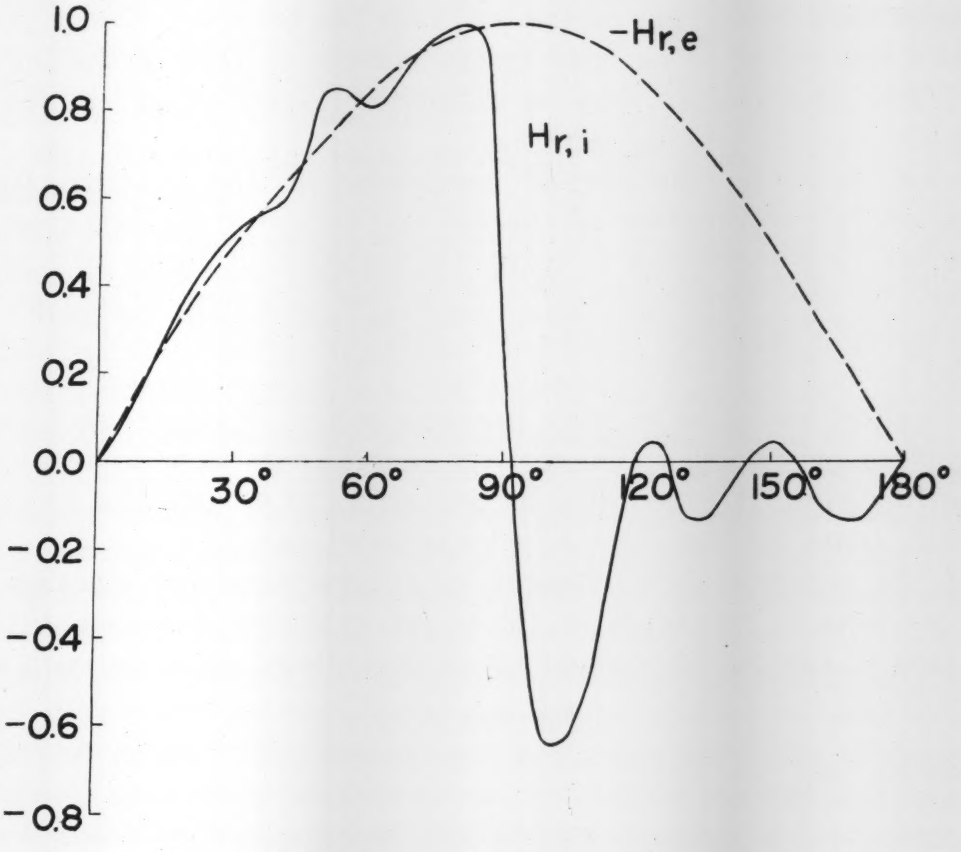

Fig. 11. The initial distribution of the normal component of the inducing and induced magnetic field on $\phi=0$. (Unit: H_0)

vortices move towards $\theta=0$ point while the intensity of the currents is decreasing. However, it seems difficult to obtain the current function for large t because the series as given by (25) does not converge for that case.

The normal component of the magnetic field produced by the induced

21) The electrical conductivity of sea water is about $10^{-11}emu$. So this value corresponds to an ocean whose depth is about $100m$.

electric currents at $t=0$ are easily calculated with the coefficients given in Table I, its distribution on $\phi=0$ being shown in Fig. 11 in which the reversed external field is also shown. It is clearly seen that the induced field nearly cancels out the inducing one on the conducting shell though there are some fluctuations due to the method of approximation using spherical harmonics of finite number. On the other half of the sphere, we obtain a remarkable intensity of the normal component of the magnetic field which is of the same sign as that of the inducing one. We can therefore expect a large vertical field which intensifies the external one on the land near the boundary, the magnitude of which amounting to as much as 60 percent of that of the inducing field. This phenomenon may be called the "coast effect" in the case of rapidly varying geomagnetic field.

Since, however, the normal component of the external field is intensified by the presence of the sea on the land in the neighbourhood of the sea, the anomalous geomagnetic variation in Japan can not be ascribed to the "coast effect". If so, on occasions of sudden commencements of magnetic storms, the external vertical field should be upward in Japan, but we usually observe downward vertical field there as the writers examined in their previous paper. Even if we take into account not only sudden changes but general ones as will be mentioned in the following, it would still be impossible to explain the anomalous chage in Japan by the coast effect examined here.

If the external field changes in an arbitrary way starting from $t=0$, we have to regard H in (1) as an arbitrary function $H(t)$. In that case a_n can be determined by an operational equation such as

$$a_n(t)=\Phi_n(p)H(t) \ . \tag{28}$$

On solving (28), we obtain

$$a_n(t)=h_n(0)H(t)+\int_0^t H(t-u)h'_n(u)du \ , \tag{29}$$

where h_n denotes a_n when $H(t)$ changes as given by (9), so that we have

$$h_n(0)=a_n^0 \tag{30}$$

and also

$$h_n(0)h'_n(t)<0 \ . \tag{31}$$

When the sea is to be regarded as a perfect conductor, there is no decay of the induced currents whence we have always $h'_n(t)=0$. In

that case, the $a_n(t)$'s are always proportional to $H(t)$. Even in the case of a sea of finite conductivity, the second term in the righthand-side of (29) is fairly small provided the depth is around hundreds or thousands of meters. So $a_n(t)$ is nearly equal to $h_n(0)H(t)$ even for this case. Furthermore, we see that the second term is of opposite sign to the first one except in cases for very small $H(t)$ because of (31). So we see that

$$|a_n(t)| \leq |a_n^0 H(t)| \tag{32}$$

together with

$$a_n(t) a_n^0 H(t) > 0 \tag{33}$$

for general cases provided $H(t)$ is of proper magnitude. For very small $H(t)$, however, the relations do not hold good, but such cases are not important here.

Thus far we see that the coefficients of the spherical harmonic constituents will not usually exceed their initial values multiplied by $H(t)$. Roughly speaking, therefore, the distribution of the current function as well as the magnetic field which are expressed by a sum of these spherical harmonic constituents will change proportionally to $H(t)$ provided the conductivity of the sea is assumed to be high. If it is so, the behaviour of the magnetic field is almost the same as that for sudden changes, its anomalous distribution such as has been observed in Japan being impossible. Even if we take into account the effect of finite conductivity, as is discussed in (32) and (33), we obtain current systems and magnetic fields whose distributions differ very little from the initial ones because the difference between $a_n^0 H(t)$ and $a_n(t)$ is not great. However, the discussions can not be applied to cases in which $H(t)$ is very small. They are also not applicable for parts of the sphere where we have very small amount of electric current and magnetic field because the zero point of the current function or magnetic field is likely to be displaced appreciably when we have slight changes in the amplitudes of the various spherical harmonic constituents. But those unfavourable cases are not important because of the small magnitude of electric currents and magnetic fields. Summarizing all the discussions stated here, it is unlikely that the tendency of the distribution which is observed for a sudden change would be seriously altered for variations of arbitrary shape.

So long as we consider the effect of an ocean as examined here, there is no possibility to explain the fact that the vertical component

of the induced magnetic field overcomes the inducing one as has been observed in Japan.

3. Electromagnetic induction in a plane sheet having a special distribution of the electrical conductivity

The magnetic effect of the electric currents induced in an ocean of world-wide scale becomes clear in the last section. It is of interest to see how the effect will change if we take into account a distribution of land and sea of a smaller scale. For instance, we may regard the coast of the main island of Japan as a straight line. If we ignore the curvature of the earth's surface, we may imagine an idealized distribution of the electrical conductivity on a plane sheet as shown in Fig. 12 where the conductivity on the land $(-a<x<0)$ is much smaller than that on the sea $(0<x<a)$. For the purpose of mathematical convenience, it is assumed that the same distribution is repeated periodically along x-axis. In so far as the magnetic effects in the neighbourhood of the boundary between the land and sea are concerned, the present model would be useful. Furthermore, the distribution is assumed to be constant in the y-direction, while z-axis is taken to be upward.

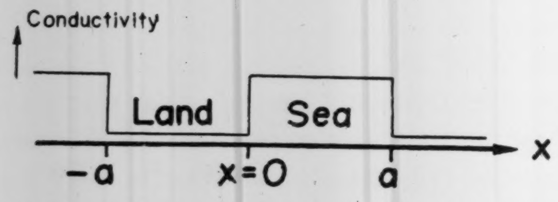

Fig. 12. The supposed distribution of the electrical conductivity on the land and sea.

We are now going to investigate the electromagnetic induction in a thin sheet having a distribution of the conductivity as shown in Fig. 12, the medium underneath the sheet being regarded as non-conducting. The theory of the electromagnetic induction in sheets or shells was fully studied by A.T. Price[22]. The following study will be made in a way similar to his study.

i) In the first place, we shall ignore the conductivity on the land while the integrated conductivity on the sea is denoted by K_s. In that case we have the boundary condition on the positive face of $z=0$ as follows;

$$\left.\begin{aligned} &W_i=0 && \text{for the land or} \quad -a<x<0\,, \\ &\frac{1}{K_s}\left(\frac{\partial^2 W_i}{\partial z^2}\right)=2\pi\frac{\partial}{\partial t}\left(\frac{\partial W_i}{\partial t}+\frac{\partial W_e}{\partial t}\right) && \text{for the sea or} \quad 0<x<a\,. \end{aligned}\right\} \quad (34)$$

22) A.T. PRICE, *Quart. Journ. Mech. and Applied Math.*, **2** (1949), 283.

In (34), W_e and W_i denote respectively the magnetic potential of the inducing and induced field, so that W_e and W_i must satisfy the differential equations

$$\nabla^2 W_e = 0 , \qquad \nabla^2 W_i = 0 \tag{35}$$

in the space. Hence we may assume that W_e and W_i are given by the following expressions for $z>0$;

$$W_e = E(t)e^{qz} \cos qx , \tag{36}$$

$$W_i = \sum_m e^{-mqz}\{I_m(t) \cos mqx + J_m(t) \sin mqx\} . \tag{37}$$

If we assume that W_e is caused by inducing electric currents on a sheet $z=h$, the currents should flow in a direction parallel to the coast line.

If we denote the electric current function by Ψ, Ψ can be expressed as

$$\Psi = \frac{1}{2\pi} W_i \tag{38}$$

on the positive face of the sheet.

Before we investigate the decay-mode of the induced field, we seek the initial state for $t=0$ by solving the following equations in place of (34).

$$\left.\begin{array}{lll} W_i = 0 & \text{for the land or} & -a<x<0 , \\ \dfrac{\partial W_i}{\partial z} + \dfrac{\partial W_e}{\partial z} = 0 & \text{for the sea or} & 0<x<a , \end{array}\right\} \tag{39}$$

in which we take into account only the self-induction effect ignoring the diffusion effect because of the sudden change considered. On introducing (36) and (37) into (39), we obtain

$$\sum_m \{I_m \cos mqx + J_m \sin mqx\} = 0 \qquad \text{for } -a<x<0 , \tag{40}$$

$$\sum_m m\{I_m \cos mqx + J_m \sin mqx\} + E \cos qx = 0 \qquad \text{for } 0<x<a . \tag{41}$$

Similarly as in the last section, (41) can be transformed as

$$\sum_m m\{I_m \cos mqx + J_m \sin mqx\}$$
$$= - \sum_m (m-1)\{I_m \cos mqx + J_m \sin mqx\} - E \cos qx \tag{42}$$

From (40) and (42), we can determine the coefficients I_m and J_m as follows. After multiplying by $\cos Mqx$ and $\sin Mqx$ where M is an integer, we shall integrate (40) and (42) with respect to x over the

whole range and obtain the following two relations respectively.

$$\left.\begin{aligned} 2\sum(m-1)g(M,m)J_m &= \pi(M+1)I_M - \pi E \qquad \text{for} \quad M=1 \\ &= \pi(M+1)I_M \qquad\qquad \text{for} \quad M>1\ , \end{aligned}\right\} \quad (43)$$

$$2\sum(m-1)h(M,m)I_m = \pi(M+1)J_M + 2k(M)\ , \qquad (44)$$

where q is taken to be π/a for simplifying the calculations and $g(M, m)$, $h(M, m)$ and $k(M)$ are given by the following integrals.

$$\left.\begin{aligned} g(M,m) &= \frac{1}{q}\int_{-a}^{0} \cos Mqx\cdot\sin mqx dx\ , \\ h(M,m) &= \frac{1}{q}\int_{-a}^{0} \sin Mqx\cdot\cos mqx dx\ , \\ \text{and} \qquad k(M) \quad &= \frac{1}{q}\int_{-a}^{0} \sin Mqx\cdot\cos qx dx\ . \end{aligned}\right\} \quad (45)$$

Table IV.

m	1	2	3	4	5	6
I_m	0.2995	0	−0.0339	0	−0.0090	0
J_m	0	0.2693	0	0.0767	0	0.0406

m	7	8	9	10	11	12
I_m	0.0008	0	0.0064	0	0.0115	0
J_m	0	0.0265	0	0.0275	0	0.0089

(Unit: E)

Solving the simultaneous equations (43) and (44), the coefficients I_m and J_m are evaluated as given in Table IV up to the 12th degree of the trigonometric harmonics. Using these values, we obtain the distribution of magnetic potential from (36) and (37) as shown in Fig. 13 (a) in which we see that the internal part is approximately zero on the land.

The vertical (downward) component of the magnetic field produced by the induced electric currents at $t=0$ are easily obtained with the coefficients given in Table IV. Fig. 13 (b) shows the distribution of the downward component. We see that the induced field nearly cancels out the inducing one for the sea region and the "coast effect" is existing as well as in the last section.

To investigate the decay of the induced electric currents which are excited at $t=0$, we go back to the equations (34). On introducing (36)

and (37) into (34), we obtain the following two relations by the same procedure as before. We have

$$\left.\begin{aligned} &2\left(\sum\frac{m^2-1}{\pi}+\frac{2\pi K_s p}{q}\sum\frac{m}{\pi}\right)g(M,\, m)J_m-\left(M^2+1+\frac{2\pi K_s p}{q}M\right)I_M \\ &\qquad =-\frac{2\pi K_s p}{q}E\,, \\ &2\left(\sum\frac{m^2-1}{\pi}+\frac{2\pi K_s p}{q}\sum\frac{m}{\pi}\right)h(M,\, m)I_m-\left(M^2+1+\frac{2\pi K_s p}{q}M\right)J_M \\ &\qquad =\frac{2\pi K_s p}{q}\frac{2k(M)}{\pi}E\,, \end{aligned}\right\} \quad (46)$$

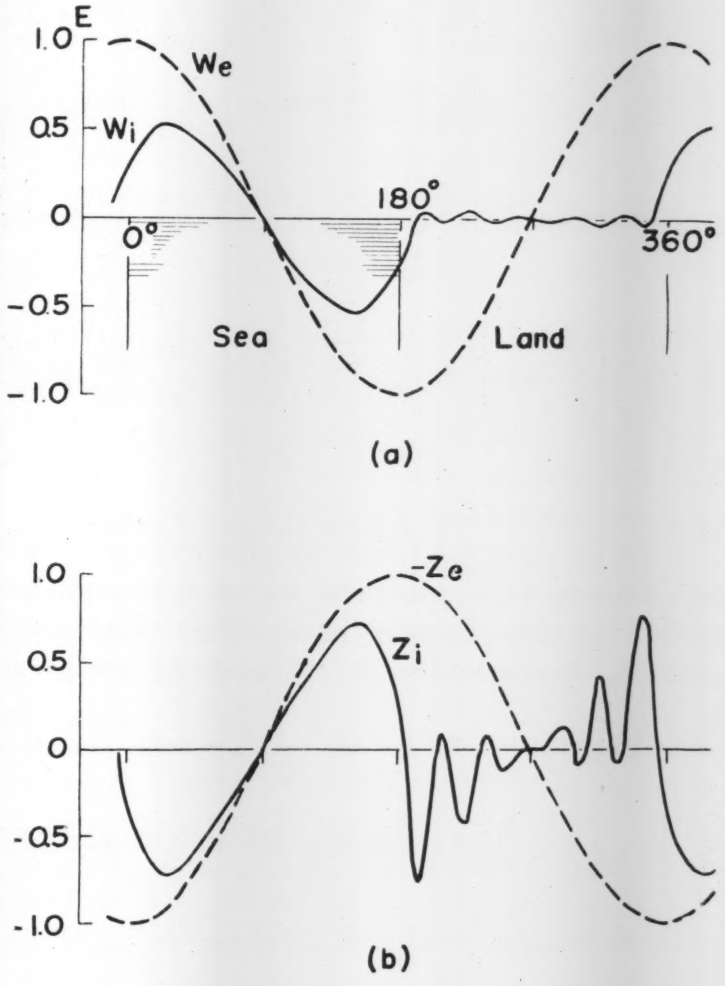

Fig. 13. (a) The inducing and induced magnetic potential or current function. (b) The vertical component of the inducing and induced field. $\left(\text{Unit: } \frac{\pi}{a}E\right)$

where p denotes $\partial/\partial t$.

On assuming the following expressions

$$I_M = \sum_{s=0} I_M^s p^{-s} \quad \text{and} \quad J_M = \sum_{s=0} J_M^s p^{-s} , \tag{47}$$

we obtain the following sets of simultaneous equations from (46),

$$\left.\begin{aligned}
&\begin{cases}
2\sum \frac{m^2-1}{\pi} g(M,m) \frac{q}{2\pi K_s} J_m^0 + 2\sum \frac{m}{\pi} g(M,m) J_m^1 - \frac{q}{2\pi K_s}(M^2+1) I_M^0 - M I_M^1 = 0 , \\
2\sum \frac{m^2-1}{\pi} h(M,m) \frac{q}{2\pi K_s} I_m^0 + 2\sum \frac{m}{\pi} h(M,m) I_m^1 - \frac{q}{2\pi K_s}(M^2+1) J_M^0 - M J_M^1 = 0 ,
\end{cases} \\
&\cdots\cdots\cdots\cdot \\
&\begin{cases}
2\sum \frac{m^2-1}{\pi} g(M,m) \frac{q}{2\pi K_s} J_m^{s-1} + 2\sum \frac{m}{\pi} g(M,m) J_m^s - \frac{q}{2\pi K_s}(M^2+1) I_M^{s-1} - M I_M^s = 0, \\
2\sum \frac{m^2-1}{\pi} h(M,m) \frac{q}{2\pi K_s} I_m^{s-1} + 2\sum \frac{m}{\pi} h(M,m) I_m^s - \frac{q}{2\pi K_s}(M^2+1) J_M^{s-1} - M I_M^s = 0 .
\end{cases}
\end{aligned}\right\} \tag{48}$$

Here, we can obtain the decay-mode starting from I_m^0 and J_m^0 which are given in Table IV.

Next, we assume that the inducing electric currents on $z=h$ flow perpendicularly to the coast line. In this case W_e and W_i take the following forms for $z>0$;

$$W_e = E(t) e^{rz} \cos ry , \tag{49}$$

$$W_i = \cos ry \sum_m e^{-z\sqrt{r^2+m^2q^2}} \{ I_m(t) \cos mqx + J_m(t) \sin mqx \} . \tag{50}$$

On introducing (49) and (50) into (39), we seek the initial state by the same procedure as in the former case. The relations between the coefficients I_m and J_m corresponding to (43) and (44) are given as follows;

$$\left.\begin{aligned}
\sum(\sqrt{1+m^2}-1) g(M,m) J_m &= \frac{\pi}{2}(\sqrt{1+M^2}+1) I_M - 2aE \quad \text{for } M=0 \\
&= \frac{\pi}{2}(\sqrt{1+M^2}+1) I_M \qquad\quad \text{for } M>0
\end{aligned}\right\} , \tag{51}$$

$$\sum(\sqrt{1+m^2}-1) h(M,m) I_m = \frac{\pi}{2}(\sqrt{1+M^2}+1) J_M - E\frac{2}{M} , \tag{52}$$

where q and r are both taken to be π/a for mathematical simplicity. Solving the simultaneous equations (51) and (52), we can evaluate the coefficients I_m and J_m as given in Table V. With the aid of these

values, the distributions of magnetic potential and vertical (downward) component of the magnetic field are obtained as shown in Fig. 14. In the figure we also notice the "coast effect" which intensifies the vertical component of the external field.

Table V.

m	0	1	2	3	4	5	6
I_m	0.3770	0	−0.0619	0	−0.0101	0	−0.0053
J_m	—	0.5099	0	0.1095	0	0.0443	0

m	7	8	9	10	11	12
I_m	0	−0.0049	0	−0.0055	0	−0.0088
J_m	0.0230	0	0.0139	0	0.0095	0

(Unit : E)

ii) In the second case, we deem the sea to be perfectly conductive while the conductivity on the land is finite. The differential equations become

$$\left.\begin{aligned} \frac{1}{K_l}\left(\frac{\partial^2 W_i}{\partial z^2}\right) &= 2\pi\frac{\partial}{\partial t}\left(\frac{\partial W_i}{\partial z}+\frac{\partial W_e}{\partial z}\right) \quad \text{for the land or } -a<x<0\,, \\ 0 &= 2\pi\frac{\partial}{\partial t}\left(\frac{\partial W_i}{\partial z}+\frac{\partial W_e}{\partial z}\right) \quad \text{for the sea or } \quad 0<x<a\,, \end{aligned}\right\} \tag{53}$$

where K_l denote the conductivity on the land.

For brevity, we confine the later discussion to cases in which the inducing electric currents flow in a direction parallel to the coast line. In that case we have

$$\left.\begin{aligned} W_e &= E(t)e^{qz}\cos qx\,, \\ W_i &= \sum_m e^{-mqz}\{I_m(t)\cos mpx + J_m(t)\sin mpx\}\,. \end{aligned}\right\} \tag{54}$$

By the procedure similar to the previous one, we obtain the following relations.

$$\left.\begin{aligned} \left(\frac{M^2}{2}+\frac{2\pi K_l}{q}pM\right)I_M + \sum\frac{m^2}{\pi}g(M,m)J_m &= \frac{2\pi K_l}{q}pE \quad \text{for } M=1\,, \\ &= 0 \quad \text{for } M>1\,, \\ \left(\frac{M^2}{2}+\frac{2\pi K_l}{q}pM\right)J_M + \sum\frac{m^2}{\pi}h(M,m)I_m &= 0\,. \end{aligned}\right\} \tag{55}$$

On assuming that the coefficients I_m and J_m are expressed by a power series of the operator p, the internal part of magnetic potential W_i is

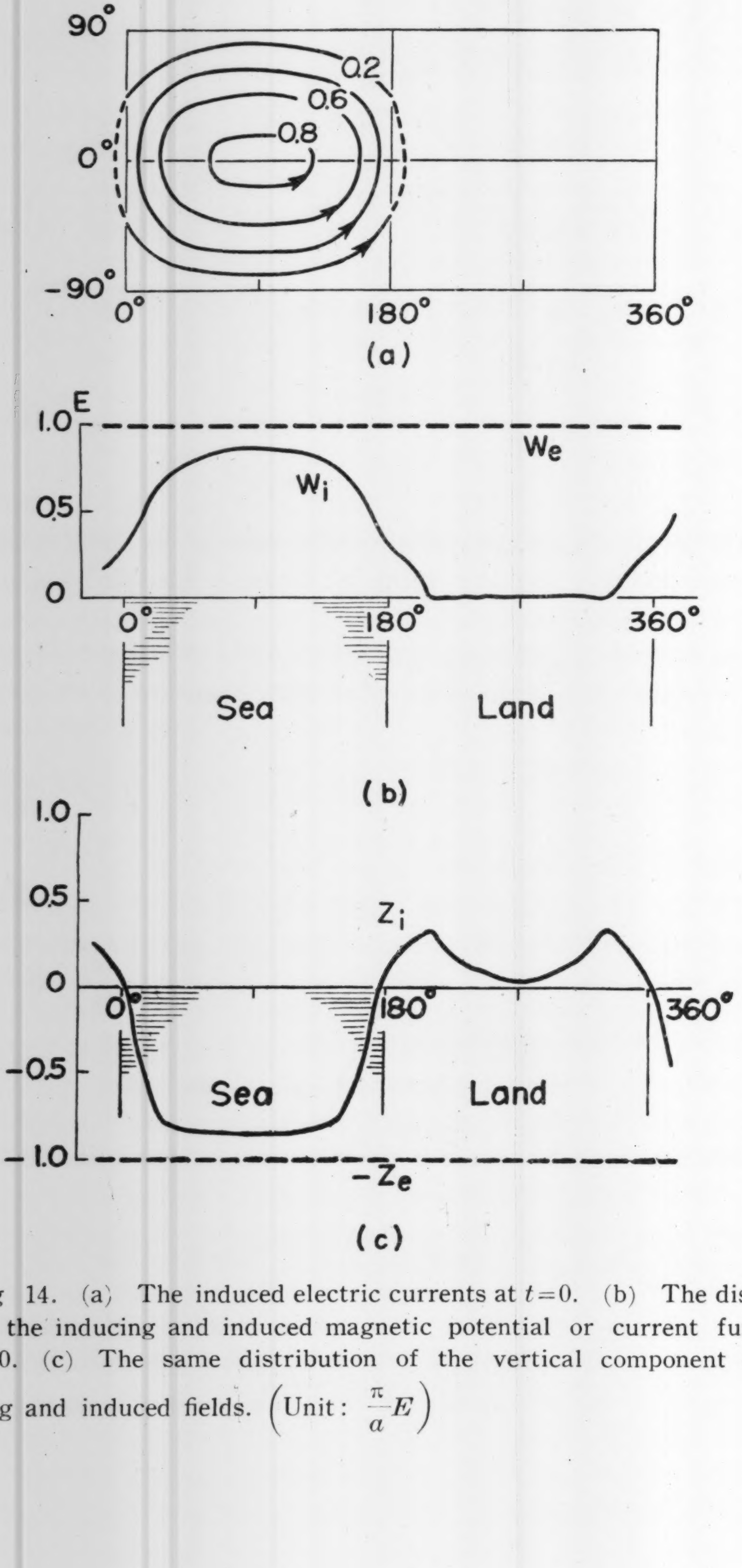

Fig 14. (a) The induced electric currents at $t=0$. (b) The distribution ot the inducing and induced magnetic potential or current function on $y=0$. (c) The same distribution of the vertical component of the inducing and induced fields. $\left(\text{Unit}: \dfrac{\pi}{a}E\right)$

obtained as follows.

$$W_i=\left\{1-0.2501\frac{t}{aK_l}+0.0849\left(\frac{t}{aK_l}\right)^2+\cdots\cdots\right\}E\cos px$$
$$+\left\{0.1062\frac{t}{aK_l}-0.0400\left(\frac{t}{aK_l}\right)^2+\cdots\cdots\right\}E\sin 2px$$
$$+\left\{0.0054\left(\frac{t}{aK_l}\right)^2+\cdots\cdots\right\}E\cos 3px$$
$$+\left\{0.0214\frac{t}{aK_l}-0.0133\left(\frac{t}{aK_l}\right)^2+\cdots\cdots\right\}E\sin 4px$$
$$+\left\{-0.0005\left(\frac{t}{aK_l}\right)^2+\cdots\cdots\right\}E\cos 5px$$
$$+\left\{0.0091\frac{t}{aK_l}-0.0079\left(\frac{t}{aK_l}\right)^2+\cdots\cdots\right\}E\sin 6px$$
$$+\cdots\cdots\cdots\cdots\cdots \quad . \tag{56}$$

Fig. 15 shows one example of the decay-mode.

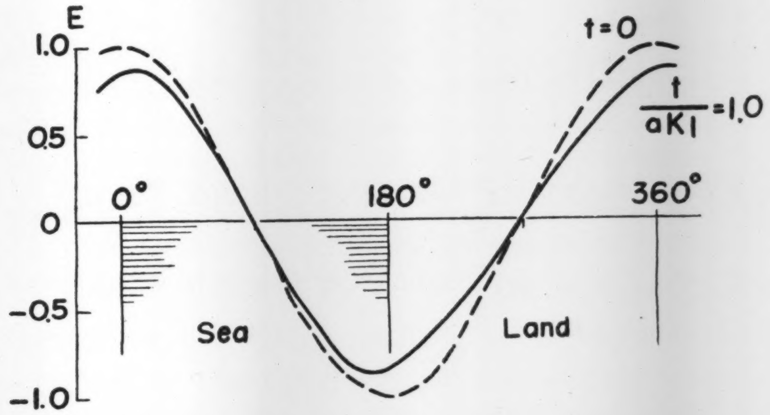

Fig. 15. The induced (broken line) magnetic potential or current function at $t=0$, while that at $t=0.1$ *sec.* is shown by the full line. The conductivity on the sea is taken to be infinity, while that on the land is assumed to be 10^{-9} *emu* and a to be 10^8 *cm*.

iii) In the third case, we take the conductivities both on the sea and on the land to be finite. Then the fundamental equations become as follows.

$$\left.\begin{aligned}\frac{1}{K_l}\left(\frac{\partial^2 W_i}{\partial z^2}\right)&=2\pi\frac{\partial}{\partial t}\left(\frac{\partial W_i}{\partial z}+\frac{\partial W_e}{\partial z}\right) \quad \text{for the land or} \quad -a<x<0\,,\\ \frac{1}{K_s}\left(\frac{\partial^2 W_i}{\partial z^2}\right)&=2\pi\frac{\partial}{\partial t}\left(\frac{\partial W_i}{\partial z}+\frac{\partial W_e}{\partial z}\right) \quad \text{for the sea or} \quad 0<x<a\,.\end{aligned}\right\} \tag{57}$$

We assume the following form for magnetic potential following the examples of the former cases.

$$\left.\begin{aligned} W_e &= E(t)e^{qz}\cos qx\ , \\ W_i &= \sum_m e^{-mqz}\{I_m(t)\cos mqx + J_m(t)\sin mqx\}\ . \end{aligned}\right\} \tag{58}$$

By the method similar to the previous cases, we obtain

$$\left.\begin{aligned} &\{M^2+aM(K_l+K_s)p\}I_M+2p\sum mJ_m g(M,m)\frac{a}{\pi}(K_l-K_s) \\ &\qquad\qquad = a(K_l+K_s)pE \qquad \text{for} \quad M=1\ , \\ &\qquad\qquad = 0 \qquad\qquad\qquad \text{for} \quad M>1\ , \\ &\{M^2+aM(K_l+K_s)p\}J_M+2p\sum mI_m h(M,m)\frac{a}{\pi}(K_e-K_s) \\ &\qquad\qquad = 2\frac{a}{\pi}(K_l-K_s)k(M)pE\ . \end{aligned}\right\} \tag{59}$$

Introducing the expressions (47) to (59), we get

$$\left.\begin{aligned} &I_1^0=E\ , \qquad I_2^0=I_3^0=\ldots\ldots\ldots=0\ , \\ &J_1^0=J_2^0=J_3^0=\ldots\ldots\ldots\ldots\ldots=0\ , \end{aligned}\right\} \tag{60}$$

and

$$\left.\begin{aligned} 2(K_l-K_s)\sum mJ_m^s g(M,m)\frac{a}{\pi} &= -M^2I_M^{s-1}-aM(K_l+K_s)I_M^s\ , \\ 2(K_l-K_s)\sum mI_m^s h(M,m)\frac{a}{\pi} &= -M^2J_M^{s-1}-aM(K_l+K_s)J_M^s\ , \end{aligned}\right\} \tag{61}$$

where $s>0$.

Although we are to obtain the decay-mode of the induced field by solving the simultaneous equations (61), the power series (47) become divergent when K_s much exceeds K_l. Assuming that the series (47) are convergent, the magnetic potential of the induced field is given as

$$\begin{aligned} W_i = &\left[1-3.7602\frac{t}{a(K_s-K_l)}+0.7062\left\{\frac{t}{a(K_s-K_l)}\right\}^2+\ldots\ldots\right]E\cos px \\ &+\left[\qquad\qquad\qquad\qquad 0.0049\left\{\frac{t}{a(K_s-K_l)}\right\}^2+\ldots\ldots\right]E\cos 3px \\ &+\left[\qquad\qquad\qquad\qquad 0.0089\left\{\frac{t}{a(K_s-K_l)}\right\}^2+\ldots\ldots\right]E\cos 5px \\ &+\ldots\ldots\ldots\ldots \end{aligned}$$

$$+\left[\quad 0.0531\frac{t}{a(K_s-K_l)}-0.1194\left\{\frac{t}{a(K_s-K_l)}\right\}^2+\ldots\ldots\right]E\sin 2px$$

$$+\left[\quad 0.0107\frac{t}{a(K_s-K_l)}-0.0281\left\{\frac{t}{a(K_s-K_l)}\right\}^2+\ldots\ldots\right]E\sin 4px$$

$$+\left[\quad 0.0066\frac{t}{a(K_s-K_l)}-0.0247\left\{\frac{t}{a(K_s-K_l)}\right\}^2+\ldots\ldots\right]E\sin 6px$$

$$+\left[\qquad\qquad -0.0128\left\{\frac{t}{a(K_s-K_l)}\right\}^2+\ldots\ldots\right]E\sin 8px$$

$$+\ldots\ldots\ldots\qquad . \quad (62)$$

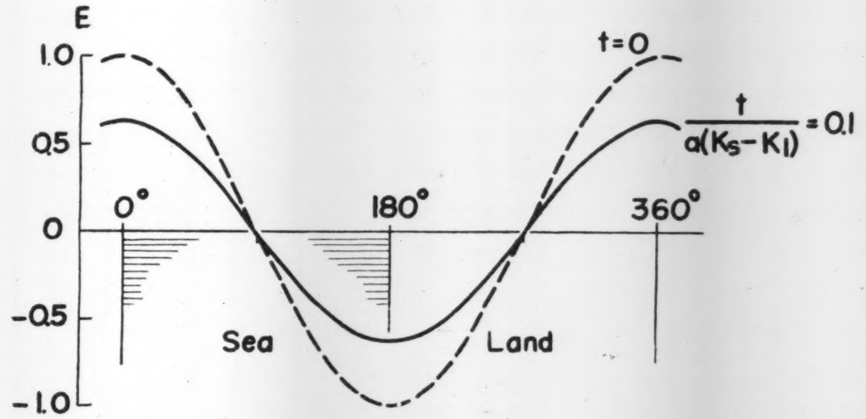

Fig. 16. The distribution of the induced (broken line) magnetic potential or current function at $t=0$, while that at $t=1$ *sec.* is shown by the full line. The conductivities are taken to be 2×10^{-7} and 10^{-7} *emu* respectively and a is assumed to be 10^8 *cm*.

One example of the decay-mode is shown in Fig. 16 in which we see that the effect of the difference of conductivity is very small.

Summarizing all the results for various cases, we see that the initial distribution of the induced field is exactly the same as that for a uniformly conducting sheet, provided there is a finite conductivity on the land. As far as a finite conductivity is concerned, however small it is, we have the same distribution. But if we put the conductivity on the land absolutely zero, the situation becomes greatly different. Physically speaking, the initial state of the induced field should soon decay changing into the pattern of the distribution which is described in the case of the absolutely non-conducting land, though it is difficult to trace the process of such a rapid change because of mathematical difficulties. It is also found that the general feature of the effect of the sea is almost the same in the neighbourhood of

the boundary between sea and land both for the semi-spherical and plane models.

Discussions and conclusions

The results of the observations newly added do not materially change the statistical distribution of $\Delta Z/\Delta H$ which was already reported in the third paper. In spite of the observation on Oosoima Island, we could not determine the southern extent of the anomalous area in which we observe anomalously large ΔZ. We have to wait for the coming observations that will be carried out on other islands farther in the south. After those observations we might be able to say something definite about the southern boundary of the area.

Almost all the variations used in the statistics, however, are bay disturbances whose magnetic vector is directed approximately towards the north. In this paper, the writers are specially interested in cases in which the changing vectors are in a direction perpendicular to the above-examined direction. Although those cases are not many because bays usually occur during nights when the vectors lie in the north and south direction, we sometimes observed a different distribution in these cases. It is surprising that we should have observed fairly large amplitude for ΔZ at Maze (a station at the coast of Japan Sea) while ΔZ at Aburatsubo (at the coast of the Pacific Ocean) is practically zero, the direction of the magnetic vector being nearly east- or west-wards in these cases. For the intermediate cases when we have the directions of the magnetic vectors that deviate from the above two directions, we observed ΔZ of either the same or the opposite sign respectively at the two stations. Thus we found that the distribution of the vertical component depends on the magnetic field applied from the outside.

In Germany, a similar anisotropy has been found. For instance, we have to suppose an induced electric current flowing in a direction from the west to the east underneath North Germany whenever the ionospheric current which is regarded as the origin of the inducing field flows from the south to the north. In the case of uniformly conducting earth, the induced currents should flow from the north to the south in this case. So it is obvious that there is an apparent anisotropy. However, the mode of distribution is not clear when the inducing field is perpendicular to the above-mentioned direction.

For the purpose of discussing the cause of the phenomenon, it becomes of importance to know all the behaviours of the magnetic field

for the inducing field of any direction. Through the investigations carried out in Chapter I of this paper, the characteristics can be expressed by empirical formulae which are obtained for respective stations. The possible cause of the phenomenon should be presumed on the basis of these considerations.

Since the observations are not enough for presuming the cause, we can only speculate a possible model from the observed facts which have been hitherto accumulated. First of all, we have to imagine a roughly circular circuit under central Japan in order to understand the large ΔZ observed there. The electric current flowing along the circuit should be clockwise when it is viewed from above while the inducing magnetic field is directed to the north. In order to give rise to a vertical magnetic force of 20 *gammas*, the intensity of the current must be about 5,000 *amperes*, the diameter of the circuit being roughly a few hundred *kilometers*. It is not possible to suppose the induced currents in the specified direction from the electromagnetic induction theory even if we have good conductors along the circuit. Suppose the circuit is a ring-shaped conductor in the horizontal plane and the inducing field has some upward component such as is the case for usual bays, there will be some electric currents induced in the circuit. But we can not expect such an intense electric current required here. The only plausible interpretation is to suppose that the electric currents come from the conducting part of the deep interior along paths which are connected with the above-mentioned circuit. It is well known that the earth is conducting under the depth of several hundred *kilometers*. Therefore the electric currents induced there might come up near the earth's surface provided there is a conducting passage. Although it is rather artificial to suppose such a distribution of the conductivity, it is difficult to find any other explanation.

If we assume a suitable size and position of the circuit, the magnetic field due to the current in this hypothetical circuit may be consistent with the anisotropy examined in this paper. From the quantitative standpoint it is still unknown whether or not we have enough electric currents accounting for the anomalous magnetic field. T. Nagata and T. Oguti[23] made a preliminary experiment in order to examine the possibility of the present model. It is tentatively concluded that there is such a distribution of the conductivity as considered here from which we might expect an anomalous magnetic field as has been observed in

23) T. NAGATA and T. OGUTI, Unpublished.

Japan. It would perhaps be necessary to suppose a low conducting region wedged into the deep earth, at a depth of several hundred *kilometers*, just under the above-considered circuit, in order to make intense current flow along the circuit.

The speculation stated above should be criticized from geological and geophysical standpoints. The high conducting passage and circuit may correspond to some high temperature belts distributed in a special way. But there seems no serious objection to that sort of distribution though it is rather an extraordinary phenomenon. Until we carry out many more observations, we can not say anything definite about the cause of the anomaly considered here.

In Chapter II of this paper, the influence of the electric currents induced in the sea has been examined in detail. Since the effect of self-induction is fully taken into account, the result can be applied to rapid variations. It has been found that the influence of the sea is not of the type that reinforces the anomalous distribution of the magnetic variation in Japan. On the contrary, it diminishes the amplitude of ΔZ in the central part of Japan. So we need not hereafter worry about the influence of the sea.

In conclusion, the writers are grateful to Professor T. Nagata and Mr. T. Oguti who discussed this problem on the basis of their experiments. The writers are also indebted to Professor J. Bartels, Dr. U. Fleischer, Dr. H. Wiese, Sir Edward Bullard, Professor A.T. Price, Professor C. Tsuboi, and Professor H. Kuno with whom the writers had the pleasure of discussing the problem through personal talk or communication. A part of this study was carried out with the financial aid of the Research Grant from the Ministry of Education. The writers would like to extend their thanks to the Ministry.

---

23. 日本に於ける地磁気短周期変化の異常と地下構造 (第6報)
(その後の観測結果及び地磁気変化におよぼす海の影響)

地震研究所 {力 武 常 次
横 山 泉}

日本における地磁氣短周期変化の異常に関連して，伊豆大島に臨時観測所を設けて約2ヶ月連続観測を行つた．大島においても ΔZ の ΔH に対する著しい相似性と，大きな比を認めた．即ち大島も油壷，柿岡を含む異常地域に属するものである．

油壷，間瀬においてその後えられた観測結果を加えて，新たに統計的に調べると，その地磁氣変化にそれぞれ異方性が認められる．両者とも，理論的に求められた正常分布からそれぞれの様相を以て偏倚している．

地磁氣変化に対する海の影響を，次の2つの場合に分けて論じた．すなわち地球が半球殼の海を有するとして，大洋の電磁感応的影響を球殼に関して論ずると同時に，陸，海と周期的に電氣伝導度が分布するとして，小規模な海岸線の電磁感応的影響を平板に関して論じた．両者とも明らかに陸地の海岸周辺にいわゆる“海岸線効果”とも稱すべき異常を生ずることを知つたが，この異常は吾々が日本中部において観測する異常とは正に反対向きのものである．以上からして，海の影響として観測事実を説明しようとする説は否定されるが，現段階において一応吾々が日本中部の地下構造に関して抱きうるであろう推測の一つを述べた．

24. *Die Veränderung des Salzgehaltes in den küstennahen Seen Hokkaidos.*

Von Masao MINATO und Yoshio KITAGAWA.

Hokkaido Universität, Sapporo.

(Vorgelegt den 14. April 1955.—Eingegangen den 30. Juni 1955.)

Es ist eine schon festgestellte Tatsache, dass die küstennahen Seen am ochotskischen Meere in Hokkaido Spuren von alte Meeresbuchten aus dem Beginne des Alluviums sind. Besonders kann man nicht mehr zweifeln, dass die Wasserbezirke des Abashiri-Sees[1] paläogeographisch etwa während dieser 10000 Jahre einen Wechsel vom *Paphia*-Meer durch die *Ostrea*-Meerbucht und durch die *Corbicula*-See zum *Anodonta*-See durchgemacht haben. (Abb. 1) Dabei sieht man, dass diese Wasserbezirke seit dem Anfange des Alluviums allmählich versüsst geworden sind, z. B. waren sie früher so salzig, dass *Paphia*-Arten dort lebten; dann begann das Gewässer dort sich zu versüssen, und die *Ostrea gigas*-Fauna kam in diese Bezirke. Im Laufe der Zeit änderte sich der ökologische Zustand dieser Bezirke; das Gewässer wurde noch viel mehr versüsst, und es war nunmehr für die *Ostrea*-Fauna unmöglich, noch länger darin zuleben, sie wurde von der *Corbicula*-Fauna abgelöst. Gegen Ende der *Corbicula*-Zeit, als die Wasserbezirke noch stärker versüsst wurden, konnte die *Corbicula*-Fauna sich dieser neuen Wasserbeschaffenheit nicht anpassen und wechselte mit der *Anodonta*-Fauna.

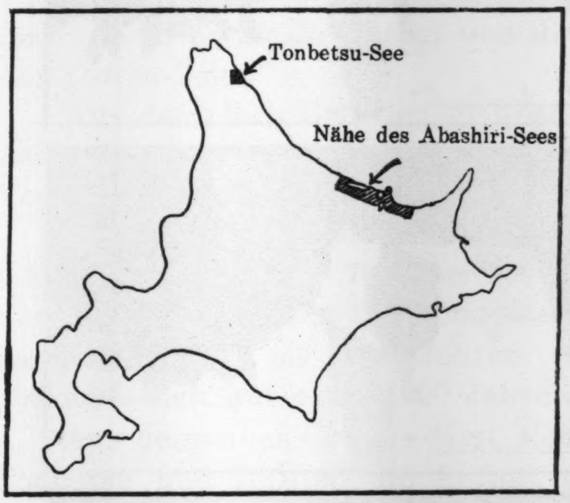

Abb. 1.: Die küstennahe Seen am ochotskischen Meer.

Wir erreichten die oben erwähnte Schlussfolgerung aus den stratigraphischen Untersuchungen der Schalenzonen, die aus verschiedenen Zusammensetzungen wie *Corbicula* bzw. *Ostrea* bestehen, den ökologis-

1) M. MINATO, Y. KITAGAWA, S. KUMATO und S. SUGIYAMA, *Jour. Fac. Sci. Hokkaido Uuiv.* (IV), **8** (1953), 259–266.

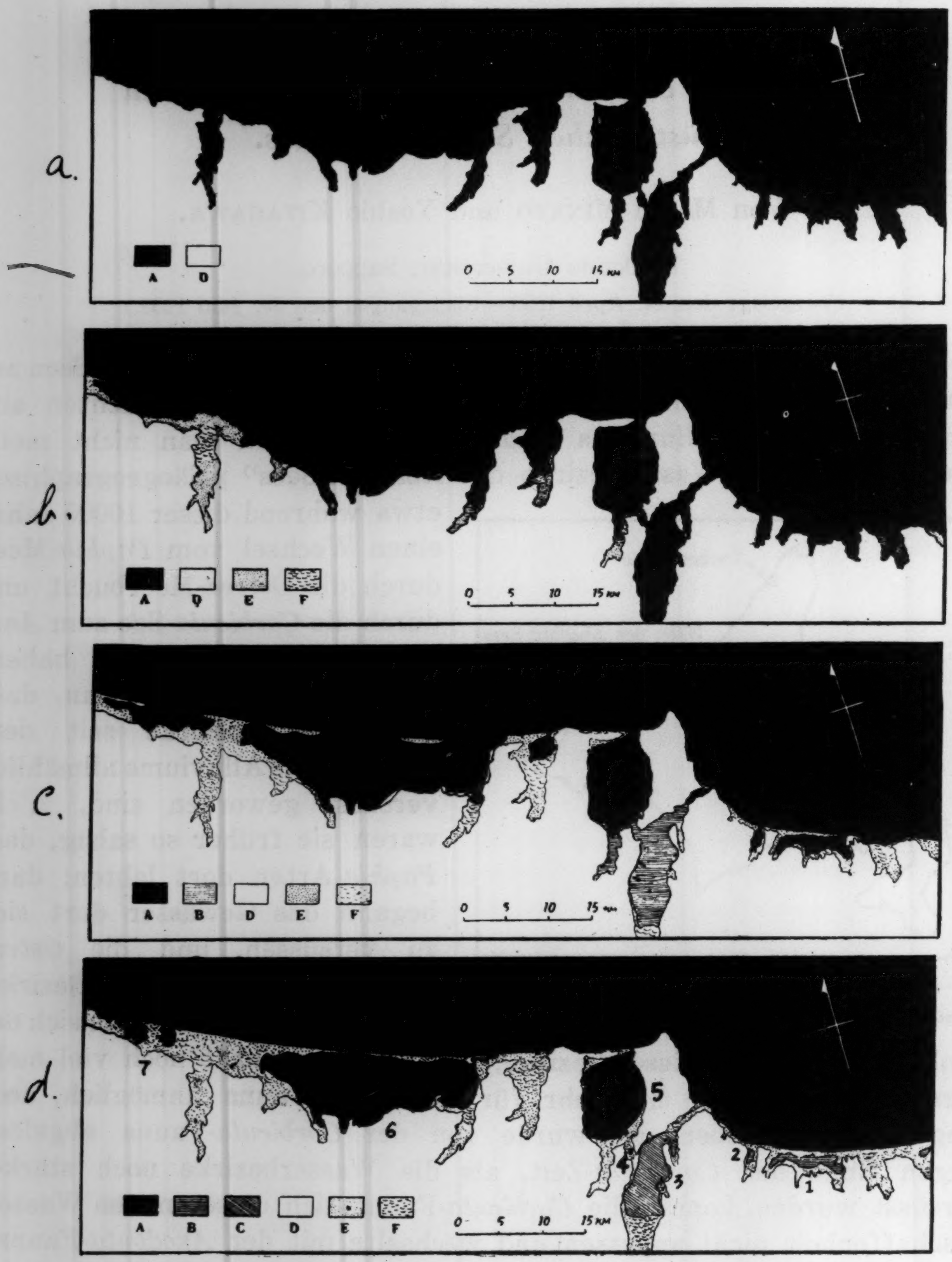

Abb. 2. Paläogeographische Entwicklung des küstennahen Sees

Abb. 2a:	*Paphia* Zeit	(Vor ca 10000–7000 Jahren)
2b:	*Ostrea* Zeit	(Vor ca 7000–3000 Jahren)
2c:	*Corbicula* Zeit	(Vor ca 3000–1000 Jahren)
2d:	*Anodonta* Zeit	(Vor ca 1000 Jahre bis heute)

A:	Meerwasser-polyhalinisch	D:	Land
B:	mesohalinisch	E:	Sanddünen und Nehrung
C:	oligohalinisch-Süsswasser	F:	Moor

1: Tofutsu-See, 2: Mokoto-See, 3: Abashiri-See, 4: Riyaushi-See,
5: Notoro-See, 6: Saroma-See, 7: Komuke-See.

chen Studien über die gegenwärtigen Faunen, die dem verschiedenen Salzgehalt entsprechen, und aus topographischen Untersuchungen in der Gegend des Abashiri-Sees.

Ferner haben wir jede einzelne Periode vom *Paphia*-Meer bis zum *Anodonta*-See mit den verschiedenen Kulturlagerungen, welche man in der Nähe des Abashiri-Sees findet, untersucht. Die älteren Muschelhaufen dort, welche Tongefässe vom ältesten Typ enthalten, bestehen meistens aus *Ostrea gigas* THUNBERG, dagegen bestehen die jüngeren Muschelhaufen in den Tongefässen neueren Typs, ausschliesslich aus *Corbicula*.

Diese Tatsache zeigt mit Sicherheit, dass anfangs nur polyhalinische Arten wie *Ostrea* in den Gewässern gelebt haben, unweit der Wohnungen der Urbewohner, die jene Gefäss-Überreste des älteren Typs in den Muschelhaufen hintersassen haben. Damals lebten dort noch keine *Corbicula* Arten, und diese Periode entspricht vollkommen der *Ostrea*-Zeit.

Aus denselben Gründen glauben wir die darauf folgende *Corbicula*-Zeit erkennen zu können, da die Urbewohner, ihre während dieser zeit, Tongefässe des neueren Typs anfertigten.

Die Archäologen sind der Ansicht, dass die älteren Tongefässe auf eine Zeitspanne von 7000 bis 3000 Jahren, von heute an gerechnet, zurückgehen, dagegen die Tongefässe des neueren Typs auf eine Zeitspanne von 3000 bis 1000 Jahren. Daher haben wir den Anfang der *Anodonta* Zeit auf etwa 1000 Jahre zurückzudatieren.

Aus demselben Grunde lässt sich schliessen, dass die heutigen Seen Tonbetsu und Tofutsu am Anfang des Alluviums ein Teil der Meeresbucht gewesen sind und seither allmählich verkleinnert wurden; das Gewässer ist auch allmählich versüsst geworden.

Zum Schluss, lässt sich die paläogeographische Entwicklung der küstennahen Seen am ochotskischen Meer entlang veranschaulichen, wie die folgenden Tabelle I und beiliegenden Abbildungen zeigen.

Im Gegensatz hierzu ist das Wasser des Abashiri-Sees in neuester zeit in der Tiefe viel salzhaltiger als früher geworden, wie Tabelle II zeigt. Vergleicht man den Salzgehalt von 1950 mit jenem von 1933, so hat sich der Salzgehalt um mehr als das zehnfache vermehrt. Beinahe dieselb Erscheinung wurde im Tonbetsu-See beobachtet.

Diese Erscheinung ist keine zufällige und vorübergehend, m.a.W. der Salzgehalt dort nimmt nicht etwa zufällig nur einige Tage durch Einströmen von Meerwasser zu, sondern er ist neuester Zeit sicher

Tab. I. Entwicklung des Abashiri-Sees

DATIERUNG	ZEIT	KULTURABLAGERUNG (von Dr. Kono)	GEOGRAPHIE	SALZGEHALT	CHARAKTERISTISCHE ART
Vor ca 10000–7000 Jahren	Pahia-Zeit		Meeresstrasse	Meerwasser	*Paphia* sp.
Vor ca 7000–3000 Jahren	Ostrea-Zeit	Muschelhaufen mit Tongefässen älteren Typs	Meeresstrasse Meeresbucht	Polyhalin	*Ostrea gigas* THUNBERG
Vor ca 3000–1000 Jahren	Corbicula-Zeit	Muschelhaufen mit Tongefässen neueren Typs	See	Mesohalin	*Corbicula japonica* PILSBRY
Vor ca 1000 Jahre bis heute	Andonta-Zeit		See	Oligohalin Süsswasser	*Anodonta iwakawai* SUZUKI
Entwicklung des Notoro-Sees			GEOGRAPHIE	SALZGEHALT	CHARACTERISTISCHE ART
			Meeresstrasse	Meerwasser	
			Meeresstrasse Meeresbucht	Polyhalin	*Ostrea gigas* THUNBERG
			Meeresbucht-See	Polyhalin	*Ostrea gigas* THUNBERG
			See	Polyhalin	*Ostrea gigas* THUNBERG
			GEOGRAPHIE	SALZGEHALT	CHARACTERISTISCHE ART
			Meeresstrasse	Meerwasser	

Entwicklung des Mokoto-Sees		Meeresstrasse Meeresbucht	Polyhalin	*Ostrea gigas* THUNBERG
		Meeresbucht-See	Mesohalin	*Soletellina* (*N.*) *nuttallii* CONRAD
		See	Mesohalin	*Corbicula japonica* PILSBRY
Entwicklung des Tofutsu-Sees	KULTURABLAGERUNG	GEOGRAPHIE	SALZGEHALT	CHARACTERISTISCHE ART
		Meeresstrasse	Meerwasser	
	Muschelhaufen mit Tongefässen älteren Typs	Meeresstrasse Meeresbucht	Polyhalin	*Ostrea gigas* THUNBERG
	Muschelhaufen mit Tongefässen neueren Typs	Meeresbucht-See	Mesohalin	*Macoma* sp.
		See	Mesohalin	*Corbicula japonica* PILSBRY
Entwicklung des Tonbetsu-Sees	KULTURABLAGERUNG	GEOGRAPHIE	SALZGEHALT	CHARAKTERISTISCHE ART
		Meeresstrasse	Meerwasser	*Dosinia* sp.
	Tongefässe älteren Typs (Oshigatamon) (Jomon)	Meeresstrasse Meeresbucht	Polyhalin	*Ostrea gigas* THUNBERG
	Tongefässe neueren Typs (Satsumon)	Meeresbucht-See	Mesohalin	*Corbicula japonica*
		See	Mesohalin	*Corbicula japonica* PILSBRY

stetig vergrössert worden, wenn auch die Ursache dieser Tatsache noch unbekannt ist.

In dieser Hinsicht vermuten wir, dass in der Nähe des Abashiri-Sees und des Tonbetsu-Sees in neuester Zeit eine allmähliche Senkung stattgefunden hat, sodass das Meerwasser mehr als früher in diese Seen einfliessen kann[2]. Aus diesem Grunde ist das Wasser dieser Bezirke salzhaltiger geworden, m.a.W. die Veränderung des Salzgehaltes in küstennahen Seen mag auf lokaler Krustenbewegung beruhen, obgleich diese Bewegung etwas verschieden von jener Krustenbewegung ist, welche von Beginne des Alluviums in diesen weiten Bezirken sich im allgemeinen fortgesetzt hat.

Tab. II. Veränderung des Salzgehaltes im Abashiri-See

Salzgehalt	Tiefe	Zeitangabe	Observator
85mg/1	14m.	1923, (11)	Takayasu & Tobijima
302mg/1	13m.	1927, (6)	Takayasu & Tobijima
7610mg/1	15m.	1933, (11)	Takayasu
8700mg/1	16m.	1936, (8)	Yoshimura
8030mg/1	15m.	1938, (3)	Hada
9000mg/1	15m.	1947, (8)	Ishida
9720mg/1	16m.	1949, (8)	Ishida

Tab. III. Veränderung des Salzgehaltes im Tonbetsu-See

Salzgehalt	Tiefe	Zeitangabe	Observator
200–1000mg/1	0.–1.5m.	1942	Asahina
9000–13000mg/1	0.–1.5m.	1953, (10)	Kitagawa

Um die gegenwärtige kleine Krustenbewegung zu erkenen, benutzt man im allgemeinen in Japan die Methode, durch wiederholtes genaues Nivellieren ein Jahr um das andere sämtliche Höhenunterschiede festzustellen.

Aber wenn die Veränderung des Salzgehaltes der küstennahen Seen eine Krustenbewegung beweist, dann kann man auch sicherlich sie nutzbar verwenden, um geringe Krustenbewegungen zu erkennen.

2) Es bestehen keine Anzeichen dafür, dass die Topographie an den Mündungen des Sees in das Meer in neuster Zeit verändert geworden sei.

24. 北海道・海岸湖の鹹度変化

北海道大学 { 湊 正 雄
北 川 芳 男

北海道オーツク海沿岸の海岸湖は，いわゆる海跡湖に属し，その水質は沖積世初葉以来，次第に稀釈され，海水→高鹹水→中鹹水→低鹹水と変化した．これは湖岸に残された貝殻層の層位学的研究や，湖岸の地形から明らかである．

しかるに最近に至つて，アバシリ湖ートンベツ沼では，いちぢるしく鹹度をましてきている．この原因は必ずしも明らかではないが，そのひとつとしてこの附近の一般的な地殼の沈降により，海水が湖内に流入しやすくなつたことが考えられる．

もしもこの推定が正しいとすれば，海岸湖の水質，特に鹹度の変化は，その附近の微小な地殼運動を推定するのに役立つであろう．

25. *Geological and Petrological Studies of Volcano, Fuji, V.** 5. On the 1707 eruption of Volcano Fuji.***

By Hiromichi TSUYA,

Earthquake Research Institute.

(Read Feb. 22, 1955.—Received June 25, 1955.)

Introduction

Volcano Fuji (Fuji-san or Fuji-yama), situated near the shore of Suruga Bay, central Japan, was in a state of eruptive activity thirteen times, at least, in historic times. Its earliest recorded eruption occurred in 781 A.D., being followed by the eruptions of 800, 826, 864, 870, 937, 999, 1033, 1083, 1511, 1560, 1700 and 1707[1]. Of these, according to all the historical materials ever found, the eruptions in 800, 864, and in 1707 were more violent than the rest which have been mentioned only as being eruptions of the volcano.

The eruption of 800 (19th year of the Enryaku era) occurred at the summit crater of the volcano, the activity continuing for thirty five days from April 15 to May 19. Lava was poured out of the crater, flowing down on all sides. In the daytime the smoke covered the mountain under a pall of darkness, and at night the fire showed up against the sky. The noises that accompanied the eruption were like thunder, and the ashes fell like rain, causing the rivers at the base of the mountain to be of a reddish color.

The eruption of 864 (6th year of the Teikan era) occurred in June[2] at the parasitic cone Nagao-yama[3] on the northwest flank of the volcano. The eruption was quite violent with the fire covering the mountain for

* Parts I-IV of this paper have been published by the author in Japanese, respectively in the *Bull. Earthq. Res. Inst.*, **16** (1938), 452; *ibid.*, 638; *ibid.*, **18** (1940), 419; and *ibid.*, **21** (1943), 376.

** The investigation was aided by the Grant-in-Aid for Scientific Research from the Ministry of Education.

1) F. OMORI, "History of Volcanic Eruptions in Japan," *Report Earthq. Invest. Com.*, **86** (1918), 90 (in Japanese).

The Earthquake Investigation Council, *Historical Data on the Earthquakes in Japan*, **1** (1941); **2** (1943).

2) Definite date and duration of the eruption are not mentioned.

3) H. TSUYA, *Bull. Earthq. Res. Inst.*, **16** (1938), 639 (in Japanese).

a space of several kilometers square and the flame shooting up to a height of scores of meters. The land was shaken three times in succession with noises like thunder. During the eruption which lasted for more than ten days, red-hot stones broke loose from the mountain, and sand and stones fell like rain. Red-hot lava flowed down northwestwards falling into the two lakes, Motosu-ko and Seno-umi, which at that time stood side by side at the northwest foot of the volcano. Parts of the lakes were filled up with the lava, together with a number of farm-houses on the shores, and the lake water became so hot as to cause the death of many fish and tortoises. The lava field now called "Aokiga-hara marubi"[4] is the product of the eruption, and the two lakes, Shôji-ko and Sai-ko, situated 2 km and 8 km northeast of another lake

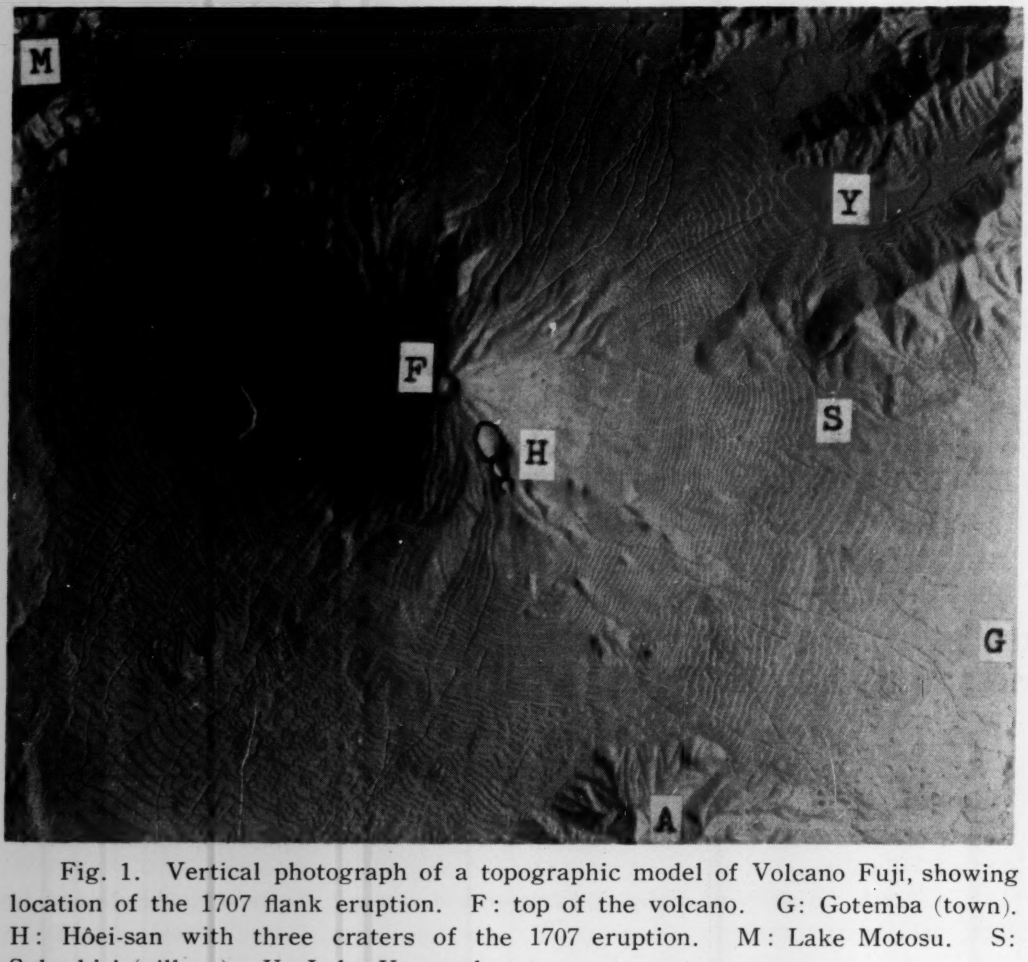

Fig. 1. Vertical photograph of a topographic model of Volcano Fuji, showing location of the 1707 flank eruption. F: top of the volcano. G: Gotemba (town). H: Hôei-san with three craters of the 1707 eruption. M: Lake Motosu. S: Subashiri (village). Y: Lake Yamanaka.

4) "Marubi" means recent bare *aa* flows (identical with the Mexican "malpais") on the lower slopes of the volcano.

Motosu-ko respectively, are evidently those parts of the historical lake Seno-umi left intact by the lava. At present the three lakes are separated from each other with broad belts of the Aokiga-hara marubi.

The eruption of 1707 (4th year of the Hôei era) occurred half way up the southeast flank of the volcano (Fig. 1). It was not only the most violent eruption ever recorded in the history of the activity of the volcano but a severe explosive eruption—quite unusual for basaltic volcanoes. Moreover, the eruption deserves special mention from the fact that prior to the ejection of a large volume of basaltic material (scoriae and bombs) ejection of acid andesite or dacitic material (pumice and obsidian) occurred for a few hours at the beginning of the activity. This material, though small in quantity compared with the basaltic ejecta, was juvenile in origin, and was new to the basaltic Fuji, its occurrence being absolutely unexampled in the history of the volcano. The fact that the 1707 eruption was a violent explosive activity attended by successive ejection of acidic and basic materials has been mentioned in some old writings on the eruption, and can be actually proved by investigating both the distribution and the mode of occurrence of the ejecta of that time. The purpose of this paper is to give an account of this eruption by referring to some authentic writings and at the same time studying the geological data obtained by field observations.

Volcanic and seismic activities in Japan within ten years before the 1707 eruption of Fuji

The volcanoes that erupted in Japan during the ten years from 1697 to 1707 are Fuji-yama, Asama-yama, Kirishima-yama and Sakura-jima[5]. The twelfth eruption of Fuji in historic times occurred in 1700, but it might have been of a small scale, seeing that the only historic record of the eruption to which reference can be made mentions nothing about the activity but the word "eruption". Neither ejecta nor craters which may be assigned to that eruption can be traced at the present time. Asama-yama, situated about 117 km north of Fuji, had a big eruption in 1704 lasting for several days, and another eruption in 1706; Kirishima-yama and Sakura-jima, both in southern Kyushu, had an eruption each in 1706. But further details of these eruptions are quite unknown. Asama, Kirishima aud Sakura-jima, together with Aso-zan in Kyushu and Ô-shima in Izu, all rank among the leading active

5) F. OMORI, *loc. cit.*

volcanoes in Japan, having records of many eruptions in historic times. Their activity culminate in eruptions repeatedly in recent years, although Kirishima alone has been quite without any eruptive activity since the beginning of the present century. It may be said therefore that volcanic activity in Japan had never become exceptionally violent in the ten years' period 1697–1707, at the end of which the 1707 eruption of Fuji occurred, and during which volcanic activity was about as normal as in recent years.

As to the seismic activity of Japan in the period 1697–1707, two big earthquakes may be specially mentioned, besides a number of smaller ones[6]. One of the big earthquakes occurred on Dec. 31, 1703, with its epicentre in Sagami Bay off the southern tip of the Bôsô Peninsula. Tokyo and the provinces on the shore of the bay suffered heavily from the shocks and associated fires, the damage including the loss of 5233 lives and 20,161 houses destroyed. The other occurred on Oct. 28, 1707, with its epicentre in the sea off the southern tip of the Kii Peninsula, causing serious damage to life and houses in the provinces on the shore of the Pacific in Southwest Japan[7]. Among the damage were included 4900 lives lost and 29,000 houses destroyed. In addition to these big earthquakes, a local but destructive one occurred in 1704 on the shore of the Japan Sea, in Noshiro district north of Akita City, Northeast Japan, with the loss of 58 lives, 435 houses destroyed and 759 houses burned. Taking into account another earthquake of the same district in 1694, together with some others[8], it may be said that the seismic activity of Japan got to a peak around the beginning of the 17th century in the fluctuation of its rise and fall, so far as earthquakes of destructive nature are concerned. But it could have had no positive correlations with the volcanic activity of Japan at that time, if the latter, as inferred above, was not deviating from the normal course of the intermittent volcanic activities through centuries.

6) Rika Nempyo (the Annual Science Table) compiled by the Tokyo Astronomical Observatory, 1954 (in Japanese).

7) The earthquake might well be compared with the Nankai earthquake of 1946 in various aspects, i.e., loci of the epicentres, extent of the stricken provinces, and nature and scope of the damage wrought.

8) An earthquake occurred in 1710 in the provinces to the west of Tottori City, another in 1711 in the same provinces, and the third one in 1714 at Omachi City and vicinity, all being local but destructive ones on or near the shore of the Japan Sea.

Course of the 1707 eruption[9)]

Although an eruption of Fuji occurred in 1700, the volcano must have recovered immediately from its effects and entered into a dormant state, thus keeping it from being noticed by those who lived nearly. Thus no smoke or other signs of activity of the volcano have been mentioned in any of the writings of the time. Nothing unusual of the volcano has been mentioned also on the occasion of the big 1707 (Oct. 28) earthquake in Southwest Japan, while considerable damage done by the shocks to the district adjacent to the south of the volcano has been reported. Only fifty days later, on Dec. 16, came the present eruption accompanied with great havoc wrought by a heavy ash-fall in the countries adjoining the east of the volcano.

Preliminary symptoms of the eruption. During the first half of December, 1707, light shocks were felt at times at Mito, a fishing village on Suruga Bay, near the southeast foot of the volcano[10)]. From Dec. 3, unusual rumblings as coming from the mountain became audible three or four times a day at Yoshida on the northeast foot of the volcano. These shocks and rumblings might be indications that, within about two weeks preceding the eruption, the volcanic activity beneath Fuji-yama was drawing nearer to the surface of the volcano where, however, no change was yet noticed in its surface features.

From the evening of Dec. 15 to the next morning, earth-shocks were felt more than thirty times at Yoshiwara on the south foot of the volcano, and more than fifty times at Yoshida, becoming almost countless by the same morning. Being followed soon by the eruption, these shocks must have occurred as premonitory symptoms warning that the volcanic activity was approaching the surface of the volcano. At Yoshiwara, some houses which narrowly escaped being destroyed by the big earthquake of Oct. 28, 1707, were destroyed by the present shocks. At Subashiri on the east side of the volcano, too, some of the precursory shocks were strong enough to demolish some houses.

9) Of many writings about the eruption, two may be mentioned as the most authentic descriptions: *Ito Shimanokami Nikki* (a diary written by Ito, the then Lord of Shima Province) and *Motokiko-ki* (a description by Prince Konoe Motoki, one of the five regent houses at the time, including several official and private reports of the eruption). The course of the eruption here outlined has been traced mainly through these descriptions, as well as by referring to some other writings.

10) Previous to that, earthquakes were felt at times, but they might have been after-shocks of the earthquake of Oct. 28, or otherwise shocks from sources other than the volcano Fuji.

In Tokyo and vicinity, the weather continued to be calm without rain for two weeks from Dec. 3 to the day of the eruption, although from Dec. 13 on it was cloudy and cold with occasional snow-falls.

Beginning of the eruption, Dec. 16, 1707. Subsequent to some rather strong earth's shocks at dawn on Dec. 16, 1707, rumblings like thunder were heard at about 8h at Subashiri and the neighbouring village Ômika, and at the same time black clouds were seen rising in the west and overcasting the entire sky. Everything in and about the villages was shrouded in the clouds so thickly that the people there could barely distinguish the difference between day and night. About 10h there came a heavy fall of volcanic sand and stones. They were white to yellow in color, more or less salty and ill-smelling, and looked like a pumice stone. On falling on the ground, the bigger stones, which were of the size of footballs, broke flamingly into pieces. Some houses and vegetation were burnt by heat from the hot stones with which they came in contact. A violent eruption of Fuji was seen taking place half way up the mountain and near the Subashiri-guchi trail[11], causing avalanches of the snow thereabout. The eruption continued throughout the day with heavy explosions, besides the thunder and lightning that occurred from time to time in different quarters of the sky overcast with the eruption clouds. By the evening of the day the country roundabout had been covered with the sand and stones ejected by the eruption.

The eruption was witnessed for the first time at about 10h of the same day by those who lived in Yoshiwara and Fujimiya, respectively situated on the south and southwest foot of the mountain. At that time they saw a rolling cloud rising from the southeast side of the mountain, at about eight tenth of its height and near the upper limit of the zone of vegetation, with rumblings resounding through the country roundabout. The vomiting clouds in a moment spread high in the sky to the south and southeast of the mountain, but a few hours later, about 14h, blown by the westerly wind, they spread over the provinces east of the mountain. In the evening, a great fire was seen on the mountain, with black smoke repeatedly drifting to the east. Fire balls shot up into the night air and broke to pieces on falling on the ground, and flashes of lightning crossed in all directions through the clouds of black smoke. Owing to the fire, the villages to the west

11) There are five old trails leading to the top of the mountain, the Subashiri-guchi trail being on its east side.

of the mountain were light as day in the night. Concussions accompanied with noises of rattling doors were felt almost continuously.

At Yoshida the eruption was seen first at 10h with gigantic clouds of black smoke rising from the south side of the mountain and fire-balls falling from the clouds, accompanied with rumblings and thundering noises. From that time on the eruption continued far into the night with shooting flames and fire-balls, and repeated thunders and lightnings.

At Mito on Suruga Bay, subsequent to several earthquakes in the early morning (6h–9h), houses were shaken by rumblings like thunder and the noises of the doors and windows rattling were loud enough to make conversation impossible. The clouds with which the sky had been overcast broke at 15h, and variegated clouds were seen drifting from Fuji to the east. The villagers were informed of the eruption of the mountain by a message from Numazu.

In Tokyo and vicinity, at about 10h on the same day, pale and dark clouds were seen spreading high in the air southwest, and shocks were felt shaking houses with noises of rattling doors and windows, but without accompanying any sensible earth-shocks. From that time on rumblings kept occurring frequently, forerun by house-shaking shocks, and at noon, accompanied with thunder, flashes of lightning were seen in the black clouds overcasting the southern sky. Shortly afterward, as the heavens suddenly became overcast with black clouds, it darkened outdoors as well as indoors like a moonless night, so that nothing could be seen clearly without lighting a candle. About 13h ashes of white to grayish color began to fall like snow, everything on the ground was coated with the ashes, and people found difficulty in walking outdoors because the ashes got into their eyes and noses. After 15h volcanic sand also fell and by 20h they accumulated to a depth of several centimeters. The sand-fall was heavy particularly during the evening hours, and late in the evening black sand began to fall instead of the whitish sand and ashes that fell during the preceding hours. About 22h the sky cleared a little, and at midnight the moon was seen in the star-strewn sky, but the southwest part of the sky continued to be overcast with black clouds. House-shaking shocks also kept occurring frequently through the night, together with distant thunders and lightnings.

The above-mentioned description of the first day of the eruption indicates that the mountain Fuji started an explosive eruption at about 8h (or 10h) on Dec. 16, 1707, with some forerunning earth's shocks,

and that for the first several hours of the eruption it ejected whitish ashes, sand and stones, turning soon after into longer-continued and more violent ejection of black sand. That the eruption was taking place on Fuji naturally became known from the first to those who lived in the provinces near the mountain, while in Tokyo and vicinity it became known first by a courier's message which arrived from Yoshiwara two days later (Dec. 18). Till then many people in Tokyo, knowing nothing of the eruption, were very fearful of the ash-fall and shocks which were strange features they never met with before, and some hastily ascribed these phenomena to Asama-yama, which at that time was known as an active volcano causing occasional ash-fall in Tokyo and the neighbouring provinces, as it still does in recent years.

Continuous eruption, Dec. 16–20, 1707. The eruption which began on Fuji Dec. 16, 1707, displayed itself almost continuously for five days until Dec. 20, without any daylong or longer lull in the activity as shown by the fact that ash-fall, rumblings and shocks, all occurred frequently every day during that period. However, the eruption seems to have reached its most violent explosions on the first day and then to have declined day by day, seeing that the largest piece of the ejecta that fell in Subashiri and vicinity was of the size of a football on the first day, then decreasing into the size of a peach, a pea, and of fine dust, successively on the second, third, and fourth days. The main events relative to the eruption in these days are as follows:

Dec. 17. At Subashiri and Ômika ashes and stones were seen falling as on the preceding day, but the eruption clouds with which the sky was overcast became a little thinner, and through a rift in the clouds the sun shone at intervals in the daytime and the stars would be seen at night. Viewed from Subashiri, Fuji was found for the first time to have formed a new mound (Hôei-san)[12] halfway up the southeast side of the mountain. At Yoshida, about 20h, a rather strong earth-shock was felt, and more violent rumblings and flashes were still coming from the mountain.

At Tokyo, for the most part of the day, the northern sky was clear, while in the southwestern sky pale and black clouds were occasionally giving out thunders and lightnings. Shocks were felt at times, particularly at 3h and 16h, with a short lull between 10h and 16h. A rather strong earth's shock was felt at about 20h, and smaller ones at

12) Who named the new mound after the era Hôei (in which the eruption occurred) and when it was so named is quite unknown.

18h, 23h and 24h. Volcanic ashes rained off and on while it was blowing from the west, and they continued to fall during the evening hours after sunset when the wind had died down.

Dec. 18. At Subashiri and Ômika the weather continued to be gloomy with ash-fall, although the latter had abated somewhat and most of the ash grains had become smaller than the size of a pea. In the villages a number of animals, domestic and wild, were struck to death by the ash-fall, and the people without a drop of water to drink faced starvation; the wells in the neighbourhood had all dried up, and the rivers had become muddy with the ashes. Leaving their household effects, these people sought safety in the southwestern villages.

This day, in Tokyo, it was almost windless, the northern sky was clear, while there were black clouds in the southern sky. Rumblings like thunder kept occurring frequently in the south, as well as shocks which caused the houses to repeat rattling noises. At 14h it became so gloomy with the overhanging clouds that one could hardly recognize his neighbouring houses. At 16h black sand began to fall, and during the evening hours they continued falling heavily.

Dec. 19. This day, at Ômika, the sun shone a little, and the new mound (Hôei-san) could be viewed at intervals through a rift in the thin clouds of smoke emitted by the eruption which was still going on. The ashes that fell in the village on this day were for the most part of the size of fine dusts, although sandy pieces of pea size came down at times.

In Tokyo, though rumblings like thunder were heard, they were much slighter and of less frequent occurrence than those on the preceding day. Early in the morning black clouds hang in the southern sky, about 9h and afterward they were blown by the south wind and spread over Tokyo and vicinity, and black sand continued falling till late in the evening, making a noise like heavy showers. After falling on the ground the sand drifted here and there accumulating to a depth of 5 to 10 mm.

Dec. 20. This day, at Yoshida, the weather was fine, but black clouds of smoke were seen rising from the mountain. At Subashiri, ashes, sand and stone were found to have accumulated to a depth of 3–4 m within the last five days.

In Tokyo, volcanic sand stopped falling at 1h, and rumblings like distant thunder were heard only at long intervals all through the night but they died down towards morning. In the morning it was overcast

with white clouds, but about noon black clouds were seen again rising to the southern sky and spreading to the north, and at the same time there came a fall of black sand, together with rumbling noises and shocks. The sand fell at intervals in the afternoon, rather heavily in the evening hours, but stopped falling at 23h. At midnight there were occasional shocks and noises like thunder.

Intermittent eruptions, Dec. 21–31, 1707. Subsequent to the daily eruption which continued for five days till Dec. 20, eruptions continued to occur intermittently and at intervals of a few days through the latter part of the month of December, although the intensity of the eruptions gradually diminished toward the end of the month[13].

Dec. 21. In Tokyo, rather strong shocks were felt at about 9h, black clouds were seen in the southern sky for the most part of the day, and noises like distant thunder were heard in the south several times at midnight. Viewed from Yoshida, both rumblings and flashes had greatly calmed down.

Dec. 22. At Yoshida nothing new was seen in the direction of the volcano. But in Tokyo, black clouds which were seen in the southern sky in the morning came to spread overhead in the afternoon, and volcanic sand began to fall at 23h.

Dec. 23. About 3h at Tokyo, shocks were felt at times, and noises like distant thunder were of frequent occurrence with flashes like lightning in the southern sky. The volcanic sand continued to fall through the night, but stopped falling at 4h in the morning. An hour later, when it was raining, both shocks and noises like thunder had stopped. The rain continued for hours in the morning, and after it stopped falling at noon, the sky cleared, but black clouds spread overhead in the evening and volcanic sand continued to fall for an hour from 22h to 23h. At Yoshida, about 20h, an earth-shock was felt, and at the same time Fuji was seen emitting a tremendous column of smoke in company with fire-balls.

Dec. 24. In Tokyo, the sky was overcast with black clouds and volcanic sand continued falling for four hours from 2h to 6h. The sand stopped falling afterwards, while in the sky were black clouds all day, hanging like a thick fog over Tokyo toward the evening.

Dec. 25. This day, in the daytime, the sky had cleared up in all

13) How and when eruptions occurred on and after Dec. 21 must be inferred from the course of events observed in Tokyo at that time, because in the writings found, only brief mention has been made about the eruptions as observed from a shorter distance.

directions, for the first time since the beginning of the present eruption, but after 16h, in Tokyo, a line of black clouds was seen running from the southwestern sky to the east, and volcanic sand continued to fall for six hours from 22h to 4h the next morning.

Dec. 26. After the volcanic sand stopped falling at 4h, in Tokyo, there was no fall of volcanic material throughout the rest of the day, while the sky was overcast with white clouds and in the southwestern sky was a black cloud of volcanic smoke rising all day. At Yoshiwara, by this day, it had become calm without any audible volcanic noise.

Dec. 27. At Yoshida, this day from 10h to midnight, earth-shocks were felt at times, and fire-balls were seen shooting up violently from the volcano. In Tokyo, there was a dense vapor in the early morning as during the preceding few days, a roaring sound like that caused by running water was heard from 10h to 19h, earth-shocks were felt for some time about 12h, and volcanic sand came down at 13h and at midnight.

Dec. 28. At Yoshida, from morning to evening (17h), rumblings were heard, and at the same time, Fuji was seen to emit a clouds of smoke. In Tokyo, earth-shocks were felt at about 4h, and black clouds were seen in the southern sky throughout the day.

Dec. 29, 30. Throughout these days, the weather was fine at Yoshida, while in Tokyo it was cloudy for the most of the time, the southern sky being dark with black clouds. There was no falling of volcanic ashes and stone in the least.

Dec. 31. This day, at midnight, heavy rumblings were heard at Yoshida, and Fuji was seen to emit both flames and fire-balls to the southern sky. According to a report from the province of Suruga on the south side of the mountain, a number of shocks were felt there at about 21h. In Tokyo black clouds were seen rising in the southern sky throughout the day, but there was no falling of volcanic ashes or sand.

The end of the present eruption was practically complete on the last day of the year; volcanic ashes stopped falling and rumblings like thunder became inaudible even at Ômika on the east foot of Mt. Fuji and the weather returned to its normal condition. Thus early in the morning of Jan. 1, 1708, the mountain as viewed from Yoshida was covered with fresh snow from its top to half way down. The same day, in Tokyo, the black clouds which continued to rise to the southern sky during the eruption became invisible, the sky was overcast with

the snow clouds, and about 20 cm of snow fell in twelve hours ending at 10h the next day.

Judging from the events that have been followed thus far in their chronological sequence, the present eruption may be regarded as an activity of purely explosive type, occurring in two successive stages: (1) the activity of the first stage from Dec. 16 to Dec. 20, during which the eruption attained its culmination with continual explosions accompanied with ejections of incandescent material, and (2) the activity of the second stage from Dec. 21 to Dec. 31, representing a declining phase of the eruption, with intermittent explosions becoming less intense and of shorter duration towards the close of the activity.

Since this eruption which was the last of its activities in historic times, the volcano Fuji has kept dormant for 250 years. An eruption of the volcano on Feb. 24, 1708, is mentioned by Omori in his "History of Volcanic Eruptions in Japan", and another one on Jan. 16, 1709, together with that, are mentioned in the "Historical Data on the Earthquakes in Japan"[14]. But there remains the question whether the volcano really had these eruptions or not, because there is no reliable document describing the events. Even if these eruptions really occurred to the volcano, they might have been an aftermath of the big eruption of 1707.

Within ten years after the cessation of the present eruption of Fuji, some certain eruptions occurred to the volcanoes Miyaké-shima (1712–14), Asama-yama (1708–11), Iwaki-san (1709), Aso-zan (1708–09) and Kirishima-yama (1716–17). But these eruptions were of usual occurrence and do not suggest that volcanic activity in Japan had exceptionally increased at the time. Of the afore-mentioned volcanoes, Miyaké-shima is an active insular volcano in the Seven Islands of Izu and, together with Ôshima in the same island group, are members of the Fuji Volcanic Zone. Although the eruption of Miyaké-shima in 1712–14 was of the bigger ones of its twelve eruptions[15] in historic times since 1085 A.D.[16], there is no reliable basis for inferring that the Miyaké-shima eruption occurred in response to the foregoing Fuji eruption, much less is it likely that the latter occurred in response to

14) *Loc. cit.*

15) H. TSUYA, "Geological Observation of the Miyaké-shima Eruption of 1940. (I)," *Bull. Earthq. Res. Inst.*, **19** (1941), 163.

16) In addition an eruption of Miyaké-shima on April 23, 1709, is mentioned in the "Historical Data on the Earthquakes in Japan".

the eruption of Ôshima in 1684–1690. Seeing that either Ôshima and Miyaké-shima had several eruptions during the last 250 years, the latest being the eruptions of 1950–54 and 1940 respectively, these volcanoes seem to have no correlation in activity with Fuji, which has kept dormant since 1707.

Damage caused by the 1707 eruption

Little is known definitely of the damage caused by the 1707 eruption of Fuji, because they are not given in detail in any of the writings ever found. But from a few fragmentary and unconnected references to the damage in the writings describing the eruption, together with the distribution and volume of the ejecta as stated below, it is conceivable that considerable damage must have been done in the provinces adjacent to the east of the volcano[17]. Thus the eastern foot of the volcano, together with the country adjoining the east, had been devastated, everything within 20 km of the scene of the eruption being buried in a pile of volcanic ashes and sand more than 1 m deep[18]. The villages of Subashiri and Ômika were totally destroyed; of 75 houses in Subashiri, 37 were burnt and the rest collapsed. Most of the rivers and wells in and around the town of Gotemba, which took their rise on the eastern foot of the volcano, were temporarily dried up. The river Sakawa also ran dry temporarily on its lower course near the town of Odawara where it flowed into Sagami Bay, as a result of the stoppage of its middle and upper courses owing to the ejecta accumulated deep in the area through which the river was running.

During the eruption, in Tokyo, the falling of volcanic ashes and sand was occasionally so heavy that the towns people were kept indoors, and not a few of them had sore throats. But it is not known for certain whether any epidemic or infectious desease spread on that occasion in the district stricken by the eruption or not.

---

17) As the damage done to houses, cultivated land, roads and bridges in the stricken district was enormous, repairs were carried out with a very large sum of money raised by the then government (the Tokugawa Shogunate) from all the feudal lords in Japan.

18) The report that the towns of Yoshiwara, Hara and Numazu had been buried and Mishima burnt by the eruption, as told in one of the writings dealing with this, is incorrect and may be a miscopy from a report of the disasters caused by the big earthquake of Oct. 28, 1707.

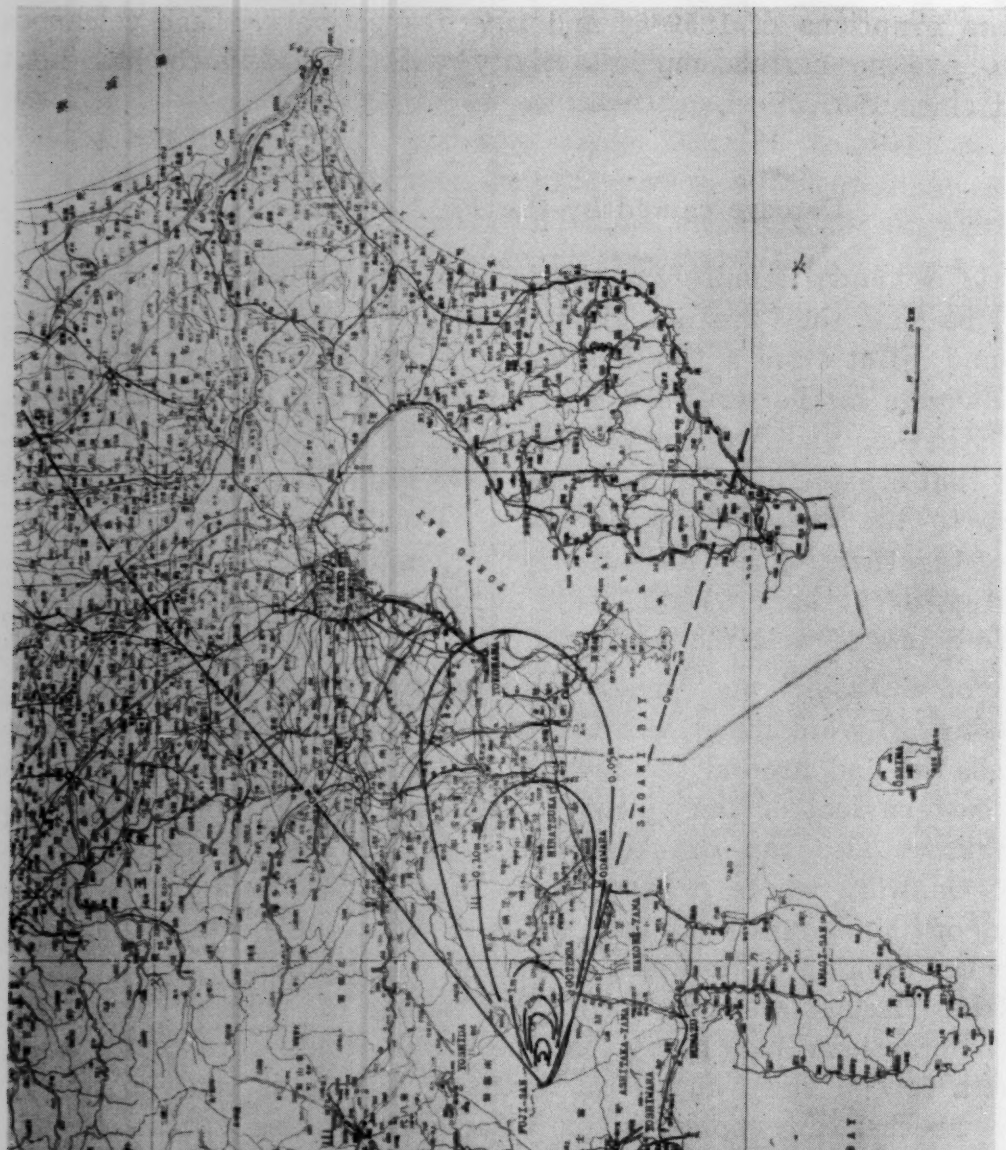

Fig. 2. Map of the southern Kantô, showing the distribution of the ejecta in the 1707 eruption.

The 1707 craters

That the present eruption took place in the vicinity of Hôei-san halfway down the southeast slope of the volcano is evident from the above-mentioned course of the eruption, and it can be proved by tracing the distribution of the material ejected at the time. Thus as mentioned below, the ashes and sand which, distributed on the eastern foot of the volcano and in the adjacent country, are regarded unmistakably as the material in question, cover a fan-shaped area becoming narrow westwards towards the vicinity of Hôei-san. Moreover, when an attempt is made in the field to follow the ejecta to their source, it is easily accomplished by finding out the actual connection of the ejecta with craters lying close to the side of Hôei-san.

There are three craters, namely the first, second and third craters, which have survived from the eruption of 1707. Although these craters must have been greatly deformed through the unceasing erosion after the eruption, their crateriform features are quite evident even now, as shown in the topographic map (Fig. 3). They are situated on the mountain slope with an inclination of about 25°, between the heights of 3100 m and 2100 m above the sea, and form a crater chain running straight as a line in the direction of the summit of the volcano (Fig. 6). Thus the second crater, lying at the middle of the chain, is linked with the first and third craters on its upper (northwest) and lower (southeast) sides respectively. The first crater, which is by far the largest of the three, is popularly known as the one which was opened by the eruption of 1707; hence the name "Hôei Crater" (Fig. 6). It is really the main crater which must have played leading roles in 1707 in repeating heavy explosions with the ejection of a large quantity of basaltic materials. The other two craters, though small in dimension and liable to escape notice of casual observers, are worth noticing too, particularly in that

Table I. Dimensions of the 1707 craters.

Crater	Major axis (m)	Minor axis (m)	Depth* (m)	Height of the floor** (m)	Volume (m^3)
The first	1400	750	650	2400	77,742,000
The second	550	400	235	2265	12,141,000
The third	500	400	195	2155	5,273,000

* From the highest point of the crater rim.
** Above the sea.

they are the source of the pumice and obsidian which, prior to the ejection of basaltic materials from the first crater, had been ejected for a few hours at the beginning of the eruption of 1707 (Fig. 8). The dimensions of the three craters as measured in the topographic map (1 : 25,000) are shown in Table I.

The ***first crater***, which is recognizable at a glance as the largest of the scars that break the regularity of the conical outline of the volcano,

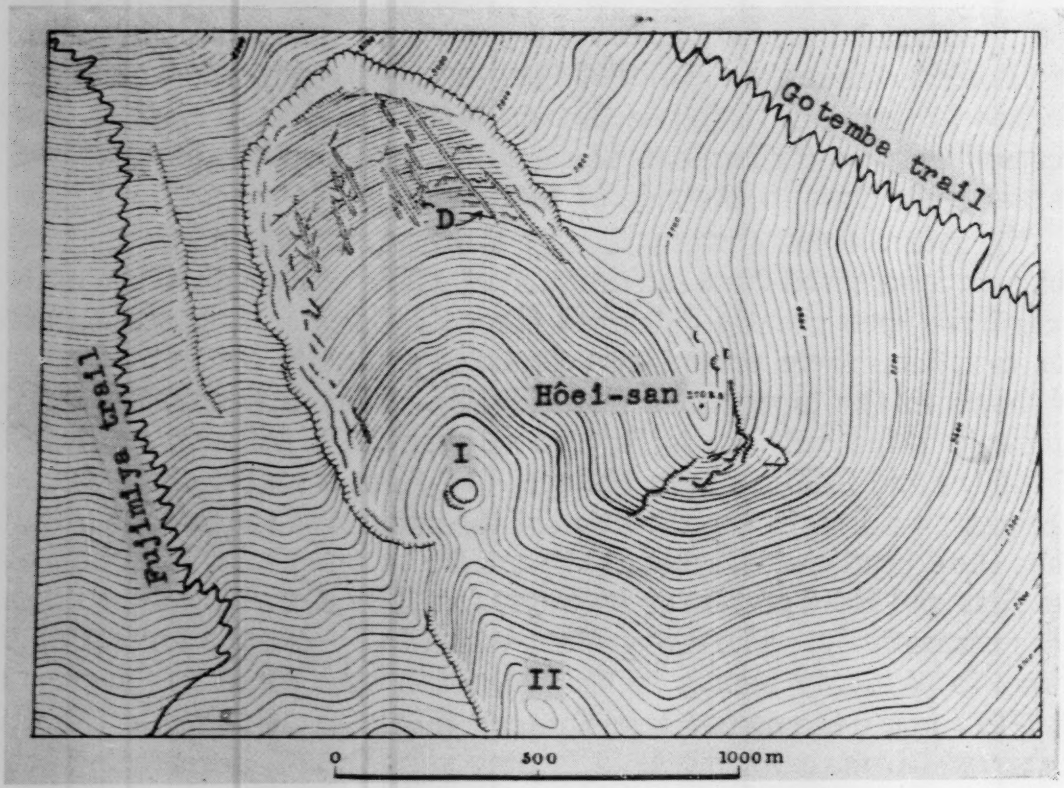

Fig. 3. Topographic map of the first crater of 1707 and Hôei-san. I: the first crater. II: the second crater. D: parallel dikes in the northwestern wall of the first crater. See Fig. 12.

is an opening of the form of a shallow vessel in section and oval in plan with its longer axis running NW.-SE. in the direction of the summit of the volcano. It is surrounded with an unbroken stretch of crater-wall on all sides except on the southeast side where there is a great gap in the wall, through which the crater opens to the second crater (Fig. 9). The crater-wall is highest on the northwest side, lowering gradually towards the southeast and southwest sides, in accordance with the slope outside the crater. In the upper half of the wall are exposed alternating layers of basaltic lava flows and frag-

mentary ejecta, besides a number of lava dikes (Fig. 12). These dikes run nearly parallel to each other and in the same direction with the longer axis of the crater, showing that the volcano is cut with a number of nearly vertical fissures radiating from its central conduit and through which the dikes have intruded into its flank. So far as have been observed, the dikes are exclusively of basaltic composition, though there are some petrographic varieties among them, and each stands like a partition-wall, a few meters or less in thickness, protruding from the general slope of the crater wall. Some of the dikes each merge upward into their contemporaneous lava sheets, showing that the former are the feeders through which the latter erupted to the surface. Thus, for example, the youngest of the dikes, which is exposed at the northwest wall of the crater, merges at its upper end into the uppermost lava sheet which forms a bluff several meters high at the northwest brim of the crater. However, all the dikes and flows exposed in and around the crater are older than the products of the 1707 eruption, and they have no direct relation with the latter.

The eastern half of the southeast side of the first crater is walled with the back slope of the knob of Hôei-san, the top of which is 2700 m above the sea but only 300 m above the floor of the crater. This part of the crater wall is covered thickly with the ejecta of 1707, neither lava dikes nor sheets nor anything else being exposed in the part. As to Hôei-san, particular mention will be made presently.

The lower half of the wall of the first crater is covered everywhere with a gently sloping talus of the detritus that fell from the cliffs above. Originally, the crater floor must have been wider and deeper than it is now, seeing that the talus extends from the surrounding wall down to near the centre of the floor. Thus the floor is nearly flat only within a radius of a few scores of meters in its lowest part lying about 650 m below the upper edge of the crater wall on the northwest side and 2400 m above the sea[19]. This part of the floor is surrounded on its south side with a crescentic heap of basaltic ejecta (scoriaceous lapilli, bombs, and lava blocks), remnant of a cinder cone formed within the crater during the later stage of the 1707 eruption (Fig. 13). The northern side of the heap is a cliff about 10 m higher than the adjoining crater floor and suggestive of the demolished wall of a small

19) The diary written by Ito already referred to, mentions that some people went to see the crater immediately after the 1707 eruption and that they failed in their attempt to measure the whole depth of the still rumbling crater with a rope about 550 m long.

crater on the cinder cone, while the back of the same heap descends with an almost imperceptible slope to the flat ground[20] on the boundary between the first and second craters.

The ***second crater*** is rather oblong in plan with its longer axis running northwest and southeast and in the direction of the summit of the volcano, and shows a V-shaped outline in transversal section. On the west the crater is bordered with a steep wall running nearly straight from northwest to southeast for a distance of about 700 m, while on the east it is hemmed in with the southwestern slope of the knob of Hôei-san (Fig. 10). The western wall exposes in its upper half a number of basaltic lava sheets, which are concordant with each other and parallel to the upper rim of the wall. These lava sheets, like those exposed in the walls of the first crater, are not of the 1707 eruption, but belong to older eruptions either at the summit or on the flank of the volcano. The eastern wall is covered everywhere with the ejecta (basaltic lapilli and bombs) of 1707, besides being studded with blocks of basaltic tuffs that have tumbled down from a high bluff near the top of Hôei-san; lava sheets like those of the opposite wall are exposed nowhere in the wall.

Although the second crater opens out of the first crater, there is a difference of about 135 m in level between their floors. Thus the second crater is walled on its northwest side with a gentle slope ascending from its bottom to the floor of the first crater (Fig. 9). This slope is covered with the ejecta of 1707 and other detritus.

On the southeast side of the crater there is a wall separating it from the third crater. The lowest part of the wall is probably not more than 30 m in height above the bottom of the second crater, and forms a saddle between the adjoining higher walls. This part of the crater wall also is covered with the ejecta of 1707 and other detritus.

The ***third crater*** ranks in size with the second crater, although its longer axis from northwest to southeast is a little shorter than that of the latter. It is surrounded with a wall on all sides except the southeast side where it opens into the head of a large valley (Fig. 11). As the bottom of the crater lies about 110 m below that of the second crater, it naturally follows that the northwest side of the former rises

20) The flat ground, together with the deep part of the crater floor, are studded with a number of huge lava blocks that fell from the surrounding walls, besides the ejecta of 1707, and are popularly known as "Botanbatake" (peony-garden). Large bombs lie broken on the ground, showing a feature suggestive of the flowers of peony, hence the name, according to a common view.

as a high but gently sloping wall up to the crest of the southeast wall of the latter. The west and east walls of the crater become higher as they approach the corresponding walls of the second crater; the west wall exposes in its upper part a number of lava sheets probably continuing from those on the west side of the second crater[21]; while the opposite wall is covered with the ejecta of 1707, besides being studded with various detritus.

The second and third craters are evidently of the 1707 eruption, to say nothing of the first crater, seeing that the ejecta thrown out by the eruption are distributed in a fan-shaped area widening out eastwards from these craters, as will be mentioned presently. Besides, there is a horseshoe-shaped, crater-like hollow on the slope adjacent to the east of the third crater. It can hardly be supposed, however, that the hollow is the fourth crater of the 1707 eruption; it may be the ruin of an older crater instead.

Each of the above-mentioned three craters is nothing but an opening bored in the flank of the volcano by the 1707 eruption. Although these craters may be regarded morphologically as explosion craters, they are not merely of phreatic origin, but are magmatic in the sense that their explosions have been accompanied by ejections of juvenile incandescent materials. The volumes of the crater bowls are as shown in the last column of Table I, being calculated on the assumption that before the eruption the site of the craters was a smooth slope representing that part of the conical surface of the volcano. Although the crater bowls must have been shallowed to some extent with detritus accumulated by weathering, their present volumes all told may represent the minimum amount of the old materials which occupied the bowls before being blown away by the eruption.

Distribution and volume of the solid ejecta of 1707

The solid ejecta thrown out by the 1707 eruption are exclusively of fragmentary materials, consisting of volcanic ash, sand, lapilli, bombs and lava blocks. They as a whole are distributed in a fan-shaped area widening out eastward from the crater region, their deposit decreasing in thickness as well as in grain size with the increase of distance from their source. Thus they are actually traceable as a mantle deposit

21) The west and south sides of the crater are grown with alpine flora, representing the upper limit of the vegetation zone on the southeast flank of the volcano.

more than 1 m thick within about 25 km east of the point of outbreak on the volcano, and beyond this distance their thinner deposit is identified only locally as it was. The northern limit of the ejecta-covered area is represented by a nearly straight line running from the northeast margin of the first crater northeastwards in the direction of the village of Hirano on the east shore of Lake Yamanaka, while the southern limit is represented by two different lines according to the kind of the ejecta distributed thereabout. One of these lines represents the southern limit of the area covered with basaltic ejecta, running from the southern margin of the first crater southeastwards in the direction of the south of Gotemba, a town in the intervale between Fuji and Hakone, and the other represents the southern limit of the area covered exclusively with acidic ejecta (pumice and obsidian), running from the southern margin of the third crater southeastwards in the direction of the same town. Beyond this town, however, no definite demarcation can be made out in the areal distribution of the two different kinds of ejecta. There is also no remarkable discrepancy between the northern limits of distribution of the two. Thus in the area covered with the basaltic ejecta, even very close to its northern limit, their deposit is seen accumulated always on a whitish bed of the acidic ejecta, the former being over ten times as thick as the latter. Their stratigraphic relation, together with the thickness of their deposits, may be seen almost everywhere where a thick bed of the basaltic ejecta is exposed in a vertical section either natural or of artificial cuttings (Fig. 18).

The thickness of deposition of the ejecta was measured by the writer at a number of places both near the craters and on the eastern foot of the volcano, with the results shown in Table II in which it is compared with that measured by some people just after the eruption. So far as data are available, the writer's measurements are approximately comparable with the old ones, which proves that the latter are reliable, although they all include both the basaltic ejecta and the underlying acidic ejecta, in the thickness of the deposit. As to the ejecta that fell in the area far distant from the volcano, the thickness of their deposit at several places is shown in the table, as deduced from some old writings of the eruption. But in the area where the ejecta might have lay less than 1 m deep, the thickness of their deposit can hardly be confirmed by actual measurement, because they are not found as such at present. Thus the volcanic ash and sand which must have fallen fairly deep at the time of the eruption in

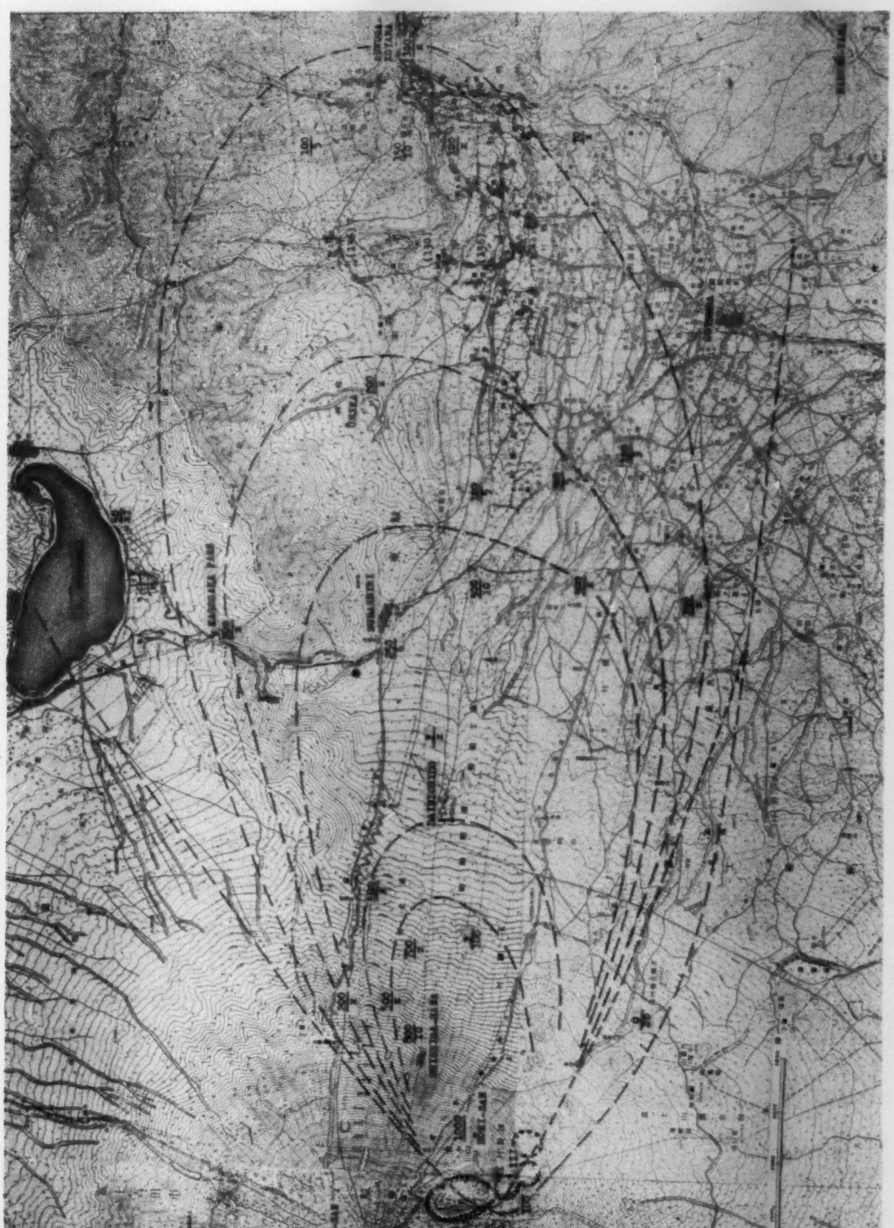

Fig. 4. Map of a portion of Volcano Fuji and the country adjoining the eastern foot of the volcano, showing the distribution of the ejecta in the 1707 eruption. Cf. Table I.

Table II. Thickness of the deposit of the 1707 ejecta.

	Locality*	Thickness** (cm)	Diameter of one of large-sized ejecta (cm)
(1)	Hôei-san	**1000** / —	**100**
(2)	West side of the second and third craters	— / 100	30
(3)	Shishiga-hana	**800** / 10	10
(4)		**500** / x	30
(5)		**700** / x	
(6)		$\boldsymbol{y}$ / 100	
(7)		**200** / x	
(8)		**400** / x	
(9)	Dainichidô	$\boldsymbol{y}$ / x	**5**>
(10)	Subashiri	**250** / 6 (400)	
(11)		**300** / 10	
(12)		**300** / x	
(13)		**0** / 2	
(14)		**200** / 5 (210)	
(15)		**100** / 5	
(16)	Ômika	**200** / x (150)	
(17)	Kagosaka	**200** / x	**10**>
(18)	South shore of L. Yamanaka	**50** / x?	
(19)		**150** / x	
(20)		**100** / 3 (100)	3
(21)		(136)	
(22)		(130)	
(23)		(136)	
(24)		**100** / x (106)	

(to be continued.)

Table II. (continued.)

Locality	Thickness (cm)	Diameter of one of large-sized ejecta (cm)
(25)	**150** / 10	0.5
(26) Suruga-Koyama	**100** (110) / x	
(27)	**100** (110) / 5	2>
(28)	**70** / x	
(29)	(40)	
(30) Ôiso	(6–12)	(coarse sand)
(31) Fujisawa	(9–12)	(coarse sand)
(32) Kawasaki	(5)	(fine sand)
(33) Tokyo	(3?)	(fine sand and ash)

* See Fig. 2.
** Thickness of the deposit of the basaltic ejecta is shown by Gothic letters, that of the acidic ejecta by Roman; the deposit whose thickness was not measured is shown by x for the acidic ejecta and by y for the basaltic ejecta; the figures in brackets in the column of thickness give the thickness of the deposit of the ejecta, as deduced from old writings of the eruption.

southern Kantô including Tokyo and the neighbouring prefectures Kanagawa, Chiba, Saitama and Ibaragi, have been washed away, or otherwise have been decomposed into soil in the course of two and a half centuries after the eruption.

The thickness data are plotted in Figs. 2, 4, together with several contour lines, each of which passes through the places where the deposit of the ejecta has a certain equal thickness. Thus seven contour lines are shown representing their respective grades of the thickness of the deposit, namely, 5 cm, 10 cm, 100 cm, 200 cm, 300 cm, 400 cm, and 500 cm. Of these, the 5 cm and 10 cm lines may be rather uncertain for lack of reliable data, while the rest are considered to be nearly accurate, being based on a number of reliable data checked by actual measurements in the field. Table III shows the areas enclosed with the two successive contour lines and the volumes of the ejecta distributed in the respective areas.

The calculated total volume of the ejecta comes approximately to 847×10^6 m^3, which is nearly comparable with that of the 1914 eruption of Sakura-jima (918×10^6 m^3)[22], but is far larger than that of the

22) B. KOTO, "The Great Eruption of Sakura-jima in 1914," *Jour. Coll. Sci., Tokyo Imp. Univ., Japan.*, **38** (1916), Art. 3, 103.

1950–51 eruption of Ôshima (26×10^6 m³)[23].

Table III. Areas covered with the ejecta and volumes of the ejecta.

Division	Mean thickness (m)	Area (m²)×10³	Volume (m³)×10³
I	7	11,830	82,810
II	4.5	8,738	39,321
III	3.5	42,668	149,338
IV	2.5	28,505	71,262
V	1.5	76,450	114,675
VI	0.3	601,250	180,375
VII	0.07	1,129,250	79,047
VIII*	0.03	4,345,060	130,352
Total			
I–V		168,191	457,406
VI–VIII		6,075,560	389,774
I–VIII		6,243,751	847,180

* Division VIII represents the area outside the 0.05 m line, limited on the east by the meridian of Tokyo.

In the volume calculation, no distinction has been made between the basaltic ejecta and the underlying acidic ejecta. But the acidic ejecta are expected to occupy only a small part of the above-mentioned total volume, since the thickness of their deposit is far smaller than that of the basaltic ejecta throughout the area covered with them. Thus the deposit of the acidic ejecta, which reaches to about 1 m in thickness at the western margin of the second and third craters, thins out rapidly southeastwards, becoming less than 20 cm thick within a distance of about 5 km and near the southern boundary of its distribution. In the area covered with the basaltic ejecta, so far as the observed exposures are concerned, the underlying acidic ejecta are about 10 cm or less in the thickness of their deposit everywhere but one place (locality No. 6, Table III, Fig. 2) where they lie about 100 cm deep. Assuming that the acidic ejecta lie 10 cm deep all over the area enclosed with the 100 cm line shown in Fig. 4, their volume in all amounts to $7{,}645\times10^3$ m³, occupying only a little more than 6% of the total volume of both the basaltic and acidic ejecta in the same area. Even

23) H. TSUYA, R. MORIMOTO, and J. OSSAKA, "The 1950–51 Eruptions of Mt. Mihara, Oshima Volcano, Seven Izu Islands, Japan. Part III," *Bull. Earthq. Res. Inst.*, **33** (1955), 99.

if the acidic ejecta distributed outside that area are taken into account, the whole amount of the ejecta of this kind is not likely to run much over ten millions in cubic meters. The acidic ejecta of this amount at the most were thrown out from the second and third craters in a few hours at the beginning of the 1707 eruption.

The basaltic ejecta, which occupy more than 90% in volume of the 1707 ejecta, are of the main eruption which, immediately after the preceding short eruption of the acidic ejecta, took place at the first crater with repeated explosions for about two weeks ending on Dec. 31, 1707. The basaltic ejecta are mostly scoriaceous and of the size of lapilli, but as a matter of course there is, in general, a gradual increase in the size of the ejecta with decrease in distance from the crater, and larger lava blocks and bombs are met with, besides the lapilli, particularly in and about the crater. Thus a large number of well-formed volcanic bombs[24], together with something like lava spatters, are distributed within a few hundred meters from the crater bottom, suggesting, as has been noticed on some other volcanoes, that the ejection of the volcanic bombs took place mainly at a later stage of the eruption[25].

Formation of the knob of Hôei-san

The first crater of 1707 is walled on its east side with a knob called Hôei-san, the top of which rises about 300 m above the bottom of the crater and 2702.3 m above the sea (Fig. 14). As already mentioned, some old writings of the 1707 eruption give the knob this name as it was formed by the eruption occurring in the fourth year of Hôei era. However, granting that the knob was a new appendix to the volcano at the time, it is neither a usual parasitic cone nor a simple pile of the ejecta thrown out of any of the three 1707 craters. An inquiry into the morphological and structural features of the knob suggests how it was formed by the eruption.

Morphologically, Hôei-san is a ledge on the steep slope of the main volcano; its summit reach forms a flat ridge about 500 m long from NNW. to SSE. and about 100 m wide; its west side is a steep slope looking on the bottom of the first crater, its back side decends eastwards with a little gentler slope merging downwards into a far gentler

24) H. TSUYA, "On the Form and Structure of Volcanic Bombs, with Special Reference to the Origin of the Basaltic Bombs from Volcano Fuji," *Bull. Earthq. Res. Inst.*, **17** (1939), 809.

25) H. TSUYA, The Eruption of Miyaké-shima in 1940. *Loc. cit.*

part of the eastern flank of the main volcano; the ridge ends on the south abruptly with a bluff up to 100 m high and about 500 m long from NE. to SW., and from the foot of the bluff a rather steep slope extends southwards and southeastwards until it merges into the adjoining gentler slopes of the main volcano (Fig. 15). Supposing that Hôei-san is a knob formed by the 1707 eruption on the proper slope which the main volcano might have had in that place before the eruption, the volume of the knob above the supposed slope amounts to about 68×10^6 m^3, which is a little less than the total volume of the adjoining three craters (95×10^6 m^3, cf. Table I).

Although Hôei-san is covered for the most part with the deposit more than 10 m thick of the 1707 ejecta, a small part of its summit reach is entirely devoid of that deposit, being occupied by confusedly dislocated strata of older ejecta (Figs. 16, 17). Thus, well-bedded volcanic breccia and tuffs, which *en masse* may be termed Hôei-san tuffs, are exposed in the bluffs at the southern end of the summit ridge of Hôei-san and also in patches adjacent to the top and bottom edges of the bluffs, being unconformably surrounded by the deposit of the 1707 ejecta. They are cut by numerous faults and fissures running in various directions, resulting in fault-blocks large and small (Fig. 5); the bluffs in which the tuffs are best exposed, are simply ruins of certain major fault scarps along which the eastern hanging side has slid down. The strata of the tuffs show different dips and strikes in different fault-blocks, their dips being often as large as 90°. Their disposition suggests nothing of a usual volcanic cone whose ejecta are formed in layers showing a quaquaversal dip, or of a deposit of the ejecta thrown out either from the summit crater of the main volcano or one of the 1707 craters.

The Hôei-san tuffs are certainly basaltic in composition, but they are quite different in petrographic features from the basaltic ejecta of 1707. Thus the latter, which are for the most part black scoriaceous lapilli, form a loose deposit without any remarkable stratification, while the former consist of well-bedded tuff-breccia and fine tuffs, both of which have become hard enough to be easily trimmed with a hammer. The tuff-breccia, which stratigraphically lie on the fine tuffs, are composed of angular rock-fragments, mostly smaller than 10 cm in diameter, and interstitial sandy materials. The rock-fragments are various in petrographic characters, and as far as have been examined, they differ very much from the younger lavas that form the upper part of the volcano, that is, a few of them are of the foreign rocks which seem

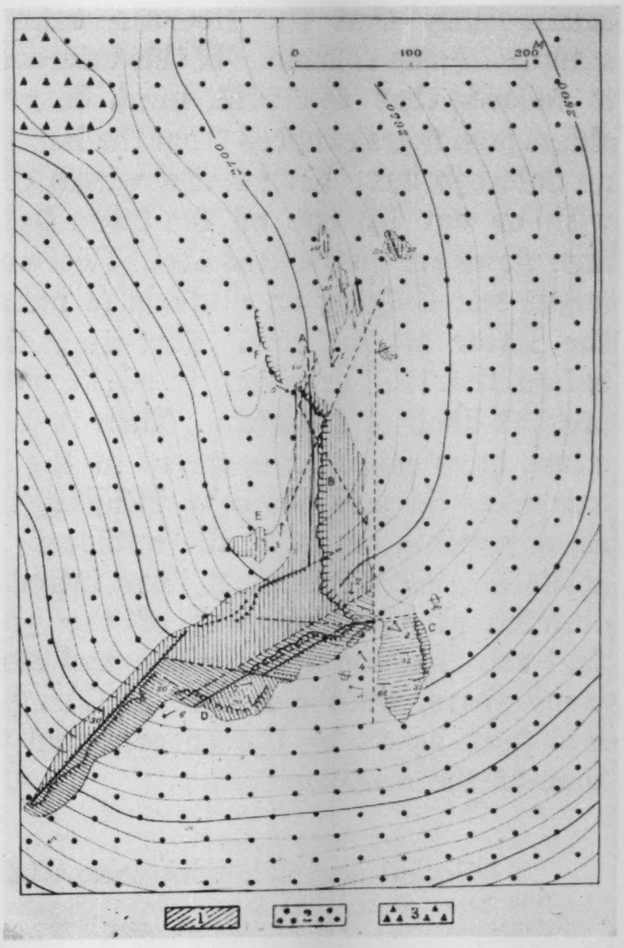

Fig. 5. Geologic sketch-map of the top of Hôei-san. 1. Hôei-san tuffs. 2. 1707 ejecta (basaltic bombs and lapilli). 3. Detritus.

to underlie the volcano. The fine tuffs are pale brown or gray in color, bearing a resemblance to the Pleistocene volcanic tuffs which, distributed extensively in the Kantô region, are collectively called the Kantô loam. They consist exclusively of angular pieces less than 5 mm in diameter of basaltic lavas containing microphenocrysts of lath-shaped plagioclase and irregularly shaped olivine, besides a few grains of augite, in a groundmass composed either almost wholly of brown glass or of aggregate of minute mineral grains (plagioclase, pyroxene, and magnetite) and interstitial glass; while the material with which the tuffs are cemented hard is a colorless, scaly mineral, isotropic with the refractive index lower than Canada balsam and probably of a kind of clay minerals (Fig. 30). Besides, only a few basaltic bombs are found imbedded in the tuffs, together with fragments of some foreign rocks.

The Hôei-san tuffs have their equivalents nowhere in the inner walls of the 1707 craters nor on the upper slopes of the volcano; on the contrary, they resemble in many respects the tuffs and tuff-breccia which, distributed on the eastern and southwestern skirts of the volcano, are regarded as products of the old Fuji volcano[26]. It is inferred

26) According to the writer's geological study, Volcano Fuji is a composite volcano consisting of three parts, andesitic Komitake, basaltic Ko-Fuji (old Fuji), and basaltic Fuji proper, which began their activities in lower Pleistocene, upper Pleistocene, and in the uppermost Pleistocene or the lowest Recent, respectively. The products of the old Fuji are older than the oldest visible lava flows from the Fuji volcano proper, the former being unconformably covered with the latter (H. Tsuya, *Bull. Earthq. Res. Inst.*, **16** (1938), 452; **18** (1940), 419).

consequently that the Hôei-san tuffs may have their origin in the activity of this volcano. If this inference may be provisionally accepted, it follows that the tuffs must be geologically older than any of the oldest lava flows erupted from the Recent Fuji volcano proper. Although no outcrops have been found where the tuffs are seen either covered with or cut by one of the lavas from the Recent Fuji, a number of lava flows are distributed about Hôei-san in such a way that the former might run dodging an obstacle (a mass of the tuffs) at the site where the latter stands now. Supposing that this obstacle existed already before the 1707 eruption, it might not have been so prominent as the present knob of Hôei-san. Then it is inferred that the 1707 eruption might have caused a upthrust of the Hôei-san tuffs which had already existed as the said obstacle, bringing the latter to its present position. As a possible cause of the upthrust, we may mention an intrusion of acidic magma which must have introduced the ejection of pumice and obsidian at the beginning of the present eruption. Thus it may be that the Hôei-san tuffs, which had stood as a "kipuka"[27] for a great many years, were upheaved to their present position and were broken into fault-blocks by the underground intrusion of acidic magma at the time of the eruption[28].

Mineral and chemical compositions of the ejecta of 1707

Ejecta from the first crater. There are three kinds of the ejecta thrown out of the first crater, viz., juvenile, accessory, and accidental ones. Of these, the juvenile ejecta occupy by far the greater part of the total mass of the three. The accessory ejecta, which must exceed the first crater in volume, do not occur by themselves, but are found embedded scatteringly in the deposit of the juvenile ejecta, together with the accidental ejecta.

The juvenile ejecta, which occur as volcanic sand, lapilli, bombs and blocks, are all basalt of one and the same composition. Thus the rock has been identified as an augite-bearing olivine basalt containing microphenocrysts of plagioclase (anorthite and bytownite), olivine and augite, in a groundmass composed of plagioclase laths and dark-brown

27) "Kipuka" is an Hawaiian term meaning an "island" of older rock in a sea of younger lava flows.

28) Shallow-seated intrusion of a stiff, acidic magma might cause a dome-shaped swelling of the ground above it, as has been actually observed on Showa-Shinzan, a new volcano born in 1944 at the north-eastern foot of Volcano Usu in Hokkaido.

glass packed with dust materials (Fig. 24)[29]. It does not differ much in chemical composition from basalt lavas of the volcano, as shown in Table IV.

Table IV. Chemical analyses of basalts from Fuji*.

	1	2	3	4	5	6
SiO_2	51.09	51.30	50.80	50.25	50.12	50.80
Al_2O_3	17.62	18.74	17.59	16.96	16.26	16.92
Fe_2O_3	2.64	1.83	3.48	2.81	3.05	2.92
FeO	8.42	8.34	7.26	9.64	10.10	8.36
MgO	5.09	4.80	5.34	5.34	4.67	5.12
CaO	9.68	9.76	9.75	9.25	8.60	9.78
Na_2O	2.80	2.55	2.67	2.46	2.78	2.65
K_2O	0.76	0.71	0.67	0.76	0.96	0.76
H_2O+	0.28	0.22	0.40	0.36	0.44	0.21
$-$	0.06	0.06	0.12	0.07	0.20	0.16
TiO_2	1.38	1.43	1.26	1.59	1.91	1.37
P_2O_5	0.26	0.29	0.18	0.21	0.29	0.29
MnO	0.21	0.28	0.24	0.22	0.23	0.24
Total	100.29	100.31	99.76	99.92	99.61	99.58

* By S. Tanaka, the late analyst of the Earthquake Research Institute. For further analyses of Fuji rocks, see the papers in the footnote (29).

1. Augite-bearing olivine basalt. Scoriaceous lava-block, one of the ejecta of 1707.
2. Two-pyroxene-olivine basalt. Aokiga-hara lava of 864 eruption on the northwestern foot of the volcano.
3. Olivine basalt. Lava from Ômuro-yama, the largest parasitic cone, situated on the northwestern foot of the volcano.
4. Aphyric basalt carrying a few microphenocrysts of bytownite. Lava on the southwest side near the top of the volcano.
5. Aphyric basalt consisting of bytownite, olivine, monoclinic pyroxene, iron ores, and a little interstitial glass. One of the oldest lava flows from the volcano, in the valley of Kise-gawa, about 6 km south of the town of Gotemba.
6. Olivine basalt. One of the bombs embedded in the Hôei-san tuffs.

The accessory ejecta, representing rock-fragments torn off and ejected from the crater bottom and surrounding walls at the time of the eruption, are mostly olivine basalt with or without augite and/or hypersthene. Besides, numbers of blocks up to about 20 cm across of coarse-grained, crystalline rocks are found among the ejecta, especially

29) H. TSUYA, "On some lavas of Volcano Huzi (Fuji), *Bull. Earthq. Res. Inst.*, **13** (1935), 645; On the Volcanism of the Huzi Volcanic Zone," ibid., **15** (1936), 216.

around the top of Hôei-san[30]. They occur not only as isolated blocks embedded in the deposit of the ejecta but occasionally as cores of the juvenile basaltic bombs. Of the specimens examined under the microscope, the following types of crystalline ejecta are distinguishable according to their mineral composition, the constituent minerals of each type being mentioned in order of increasing amount.

1. Magnetite-plagioclase-hypersthene-augite-olivine-rock.
2. Magnetite-augite-olivine-plagioclase-rock (Fig. 27).
3. Magnetite-hypersthene-augite-olivine-plagioclase-rock (Fig. 26).
4. Magnetite-olivine-hypersthene-augite-plagioclase-rock (Fig. 28).
5. Hornblende-magnetite-olivine-augite-hypersthene-plagioclase-rock (Figs. 25, 29).
6. Magnetite-augite-bearing plagioclase-rock.

Of these, the rock type (3) is more frequently met with than the rest, including some varieties which differ from each other in granularity and other textural characters. A little brown glass is present in every one of the rocks either in the form of small drops occluded in the constituent minerals or as interstitial filling of the mineral grains. Hypidiomorphic granular texture is common in all the rock types but the type (3) in which there is a variety showing an ophitic texture (Fig. 32).

As shown in the above-mentioned list, plagioclase predominates over the rest of the constituent minerals in all the rock types but (1), and in the type (6) it forms more than 95% of the rock. The plagioclase, usually devoid of any remarkable zoning, has a composition of bytownite, as the plagioclase phenocrysts in many of the lavas of the volcano have. The bulk analysis of plagioclase pieces collected from a crystalline block belonging to the type (3) is shown in column 1, Table V, in which it is compared with the analyses of anorthite from Volcano Miyaké-shima, Izu[31].

The analyses (1) and (2) contain several oxides which may be regarded as impurities derived mostly from minute, inseparable inclusions of mafic minerals in the analyzed plagioclase crystals. Because of the notable amount of the impurities, particularly iron oxides and magnesia, the actual molecular composition of the analyzed plagioclase

30) T. HIRABAYASHI has mentioned some of these crystalline ejecta under the name of "phanerocrystalline bombs". "Geology of Volcanoes Fuji and Ashitaka", *Report Earthq. Invest. Com.*, **24** (1899), 1-74 (in Japanese).

31) Anorthite, together with olivine, are found as crystal bombs among the ejecta of the eruption in 1940 and 1874, besides occurring as phenocrysts in some lava flows.

cannot be computed with accuracy from either of the analyses. However, the analysis (1) gives a bytownite approximately of the composition $Ab_{15}An_{85}$, and the analysis (2) an anorthite of the composition Ab_3An_{97} which is comparable with the anorthite Ab_5An_{95} analyzed by H. S. Washington[32].

Table V. Chemical analyses of plagioclase crystals from Fuji and Miyaké-shima.

	1	2	3
SiO_2	45.65	42.98	44.49
Al_2O_3	33.46	35.31	36.00
CaO	17.29	19.46	19.49
Na_2O	1.88	0.35	0.59
K_2O	0.31	0.04	0.03
Fe_2O_3	0.60	0.96	0.08
FeO	0.36	0.57	
MgO	0.79	0.35	0.04
H_2O+	0.24	0.01	
−	0.16	0.02	
TiO_2			
P_2O_5	tr.	0.02	
MnO	tr.	tr.	
Total	100.74	100.07	100.72

1. Bytownite from a phanerocrystalline block (magnetite-hypersthene-augite-olivine-plagioclase-rock) ejected from the first Hôei crater, Volcano Fuji, in 1707. S. Nakajima, analyst.
2. Anorthite bomb ejected from Hyôtan-yama, the 1940 parasitic cone, Miyaké-shima. S. Nakajima, analyst.
3. Anorthite bomb ejected in 1874, Miyaké-shima.[32] H. S. Washington, analyst.

Olivine leads all other minerals in the rock type (1), and is next to plagioclase in (2) and (3) in abundance, thus it can be collected easily from specimens of these types. An analysis of the olivine which, together with the analyzed plagioclase (column 1, Table V), was made on a specimen of the type (3), is shown in column 1, Table VI , besides two analyses of olivine from Miyaké-shima.

The analyses show that the Fuji olivine is a little more ferric than the Miyaké-shima olivine, the former being approximately of the com-

32) S. Kozu, "Optical, chemical and thermal properties of anorthite from three localities in Japan," *Sci. Rep. Tohoku Univ.*, **2** (1914), second series (geology).

position $Fo_{76}Fa_{21}$ as against $Fo_{85}Fa_{15}$ (analysis 2) or $Fo_{83}Fa_{17}$ (analysis 3) of the latter.

Table VI. Chemical analyses of olivine crystals from Fuji and Miyaké-shima.

	1	2	3
SiO_2	37.53	38.48	38.82
MgO	37.50	44.37	42.51
FeO	21.53	14.65	14.93
MnO	0.83	0.12	0.23
Fe_2O_3	2.66	1.76	1.65
TiO_2	tr.	tr.	—
P_2O_5	tr.	tr.	
Al_2O_3	tr.	0.43	0.20
CaO	tr.	tr.	0.40
Na_2O	tr.	tr.	
K_2O	tr.	tr.	
H_2O+	0.03	0.14	0.90*
−	0.07	0.36	
Total	100.15	100.31	99.64

* Ignition loss.
1. Olivine from a crystalline block ejected in 1707, Fuji. S. Nakajima, analyst.
2. Olivine from an allivalite block ejected in 1940, Miyaké-shima. S. Nakajima, analyst.
3. Olivine ejected in 1874, Miyaké-shima.[33] K. Seto, analyst.

Pyroxenes (augite and hypersthene) are next to plagioclase in abundance in the two rock types (4) and (5), and are common in (1), (2) and (3), while a little augite is the only pyroxene met with in (6). The pyroxenes show neither zoning nor twinning; the augite is pale brown in color, and the hypersthene is greenish brown with distinct pleochroism. Crystallization of the pyroxenes around olivine is seen to have advanced further in the rock types (4) and (5) than in (1), (2) and (3). Furthermore, a greenish brown hornblende is present in the rock type (5) in which hypersthene surpasses augite in quantity; the hornblende develops around the periphery of the pyroxenes and along their cleavages, besides occurring as small rods scattered in the rock.

Full account of their petrographic characters being set aside for

33) S. KOZU, "Studies on Ejecta from Volcano Miyaké-shima," *The Globe* (*Chikyu*), **9** (1928), 246 (in Japanese).

the present, the above-mentioned phanerocrystalline ejecta may be all regarded as being genetically related to each other and to the magma which underlies Mt. Fuji as the source of basaltic lavas of the volcano. It is likely that some of them, especially those having ophitic texture, are immediate products of crystallization of the basaltic magma either at the periphery of its reservoir or in its offshoots (dikes) which intruded into the surrounding rocks. But some others, especially those of the rock type (6), seem to have been derived either from a composite mass or separate masses of different mineral assemblages formed by local accumulation of the minerals that were crystallizing out of the magma under deep-seated conditions[34].

A few fragments of pumice and obsidian are found among the 1707 ejecta at the top of Hôei-san. Petrographically, they are similar to those ejected from the second and third craters, so that it is quite uncertain whether they are juvenile ejecta thrown out from one of these craters or accessory ejecta from the first crater.

Besides the juvenile and accessory ejecta, there are rock fragments which, being quite unfamiliar to the volcano, may be regarded as accidental ejecta from the first crater. Altered tuffs are most frequently met with among them, especially at the top of Hôei-san, being not only scattered as ejected blocks but also enclosed as xenoliths in the juvenile basaltic ejecta. They are usually light gray to white in color, consist of granular aggregate of quartz and feldspar (albite) with an amorphous matrix, either colorless or clouded with dust materials, and some of them show a vesicular structure like that of pumice (Fig. 35). Their original character is obscured by secondary changes, so that they can not be traced back to any particular kind of unaltered rocks; some of them are silicified tuffs, but some others may be highly altered igneous rocks, originally of the composition of acidic andesite or allied rocks. One of these rocks is hornblende andesite, the only specimen of which was found among the accidental ejecta collected at the top of Hôei-san. The rock is partly altered, but its original structure is clearly seen under the microscope. Thus the rock contains phenocrysts of labradorite and brown hornblende in a groundmass consisting of lath-shaped crystals of plagioclase, minute grains of monoclinic pyroxene and magnetite, with a little interstitial glass. The hornblende is usually

34) Hirabayashi has mentioned two kinds of phanerocrystalline blocks (two-pyroxene diabase and olivine-pyroxene diabase) from the Hôei crater, considering them as fragments torn by the eruption from a deep-seated dike. *Loc. cit.*

bordered with minute granular aggregate of pyroxene and iron ores (Fig. 33).

The altered tuffs and andesites mentioned have their equivalents among the Miocene volcanics distributed in the Izu region adjacent to the southeast of the volcano. Therefore, it is inferred that they have come from a basal formation which, underlying the volcano at some depth below the first Hôei crater, may be correlated with one of the Tertiary volcanic formations of Izu[35].

Ejecta from the second and third craters. The most important of the ejecta from these craters are fragments of pumice and obsidian. As already stated, the pumice occurs in a thin bed at the bottom of the deposit of the 1707 ejecta (Fig. 18), while the obsidian is found locally accumulated in the vicinity of the craters (Fig. 19). Thus angular blocks less than 1 m across of obsidian, together with grayish pumice and other rock fragments, are found on the ground close to and outside of the western rims of the second and third craters. They are also exposed forming a bed of volcanic breccia in the walls of the valley through which the third crater opens to the south. Whitish pumice is of rare occurrence in the vicinity of the craters, but it becomes predominant instead of the obsidian within a distance of several hundred meters to the southeast.

The pumice is commonly light gray to white in color, but it is sometimes yellowish brown or dark gray. There are also varieties in which variously colored bands are mixed with each other, revealing a flow structure (Figs. 20, 21). Vesiculation of the pumice is exhibited in various degrees in different specimens; alternation of highly vesiculated parts with denser layers, exhibiting flow bands, is met with in some specimens. The pumice is sometimes so extremely vesiculated as to resemble a mass of "soap-bubbles", and in other cases it is fibrous with silky luster, possessing a structure like "thread-lace scoria". Regardless of its various structures, the pumice consists essentially of glass; in the whitish pumice the glass is colorless, while in the dark grayish one it is clouded with very minute microlites and dust materials. Microscopic phenocrysts of plagioclase (andesine Ab_{55}) and small prismatic crystals of monoclinic pyroxene are found very sparingly in the pumice,

35) According to the core-boring carried out at Obuchi (700 m above the sea) on the southern flank of the volcano, there is a mass of altered andesite (propylite) at the depth from 620 m down to more than 1000 m below the surface. This rock is also similar to one of the representatives of the Miocene volcanics distributed around the volcano. H. TSUYA, *Bull. Earthq. Res. Inst.*, **18** (1940), 417.

besides a few larger crystals of more calcic plagioclase and augitic pyroxene. These larger crystals are regarded as xenocrysts, seeing that the pumice often carries basaltic xenoliths, from which they might have come. Among the xenoliths is a phanerocrystalline rock consisting of plagioclase, augite, hypersthene, magnetite and olivine, with a little interstitial glass. Some xenoliths occur as nucli in the vesicular cavities of the pumice (Fig. 26), being either attached to the walls of the cavities, or entwined with glass thread spinned out of the enclosing pumice material. None of the xenoliths show such thermal alteration as might have been caused by the host material.

The obsidian is dull-black in color with a pitchy luster and has a perfect conchoidal fracture (Figs. 22, 23). It contains only a few microscopic phenocrysts of lath-shaped plagioclase and small prismatic crystals of monoclinic pyroxene in a groundmass packed with plagioclase and pyroxene microlites, although, like the pumice mentioned, it often carries xenocrysts and xenoliths. The xenocrysts are of plagioclase, olivine, augite, hypersthene and green hornblende. Pyroxene-bearing biotite-hornblende dacite and olivine-two-pyroxene andesite are present among the xenoliths, besides various basalts and phanerocrystalline rocks like those mentioned above in regard to the accessory ejecta from the first crater. The dacite xenolith is white in color and pumiceous with abundant vesicular cavities, but differs from the pumice ejected in quantity together with the obsidian, in that it contains phenocrysts of strongly zoned plagioclase (andesine—oligoclase Ab_{65-80}), bipyramidal quartz, dark-brown biotite, deep-green hornblende, hypersthene, augite and magnetite in a colorless glassy groundmass (Fig. 34). The olivine-two-pyroxene-andesite xenolith resembles petrographically certain lavas from Volcano Komitaké underlying the northeastern flank of Fuji or from Volcano Ashitaka-yama abutted upon by the southeastern flank of Fuji.

The pumice, together with the obsidian, are undoubtedly of juvenile origin, occupying the greater part of the ejecta from the second and third craters. Among the rest of the ejecta are found rock fragments similar to the xenoliths contained in either the pumice or the obsidian. Thus, for example, the pyroxene-bearing biotite-hornblende dacite occurs not only as xenoliths in the obsidian but also as isolated fragments among the ejecta, suggesting the existence of a mass of the rock at some depth beneath the volcano as a member of late Tertiary or early Pleistocene volcanic formations. Naturally there are also among the

ejecta fragments of basalt lavas which, formerly occupying the site of the second and third craters, were blown away by the 1707 eruption. There are also ejected fragments of basaltic tuffs, and one of these (Fig. 31) is worthy of special mention in that it is petrographically quite similar to the Hôei-san tuffs (Fig. 30) already referred to. Compared with the latter, the former is harder and more colored, suggesting a baking effect possibly due to volcanic heat to which it might have been subject at the time of the eruption. Supposing that both are the same, it follows that the Hôei-san tuffs had been in exsistence as such already before 1707 and were fragmented partly by the eruption of the year.

Table VII. Chemical analyses of pumice and obsidian, juvenile ejecta from the second and third craters of 1707, Volcano Fuji.

	1	2	3	4
SiO_2	63.84	63.93	67.22	68.25
Al_2O_3	15.82	14.74	13.40	14.28
Fe_2O_3	0.95	1.44	2.71	2.43
FeO	5.02	5.32	2.30	1.74
MgO	1.67	1.82	1.18	1.41
CaO	4.88	5.10	4.57	3.15
Na_2O	3.88	3.15	3.62	3.68
K_2O	2.12	2.30	2.66	2.82
H_2O+	0.45	0.75	0.98	1.30
−	—	0.36	0.91	0.26
TiO_2	0.87	0.50	0.40	0.44
P_2O_5	0.22	0.36	0.19	0.16
MnO	0.17	0.16	0.12	0.09
Total	99.89	99.93	100.26	100.01

1. Obsidian.[36] An ejected block about 10 cm across collected at Nagamine on the west side of the second crater. S. Tanaka, analyst.
2. Obsidian. Locality, same as (1). S. Nakajima, analyst.
3. Pumice. An ejected piece about 5 cm across collected from the pumice bed underlying the basaltic scoria bed, about 4 km northeast of the second crater and 1800 m above the sea, on the eastern flank of the volcano. S. Nakajima, analyst.
4. Pumice. Locality, same as (3). J. Ossaka, analyst.

36) In an earlier paper dealing with the volcanism of the Fuji Zone, the writer used the name "pitchstone" for the rock. But, seeing that the rock is small in water content, it may be called obsidian rather than pitchstone whose water content is usually as high as 8–10%. H. TSUYA, *Bull. Earthq. Res. Inst.*, **15** (1937), 307.

Chemical analyses of the obsidian and pumice are shown in Table VII. The two analyses of the obsidian, one by S. Tanaka and the other by S. Nakajima, are very much alike, showing that the obsidian is an andesite of intermediate to acidic composition. Thus the norm of the analysis (1) contains 18% quartz, 65% feldspars ($Or_{20}Ab_{51}An_{29}$) and 13% pyroxenes ($Wo_{10}En_{33}Fs_{57}$), and that of the analysis (2) 21% quartz, 60% feldspars ($Or_{22}Ab_{45}An_{33}$) and 14% pyroxenes ($Wo_{9}En_{33}Fs_{58}$). But compared with the obsidian, the pumice is more acidic as shown in analysis (3), Table VII. Its norm contains 26% quartz, 58% feldspars ($Or_{27}Ab_{52}An_{21}$) and 8% pyroxenes ($Wo_{47}En_{34}Fs_{19}$). For comparison, another specimen of the pumice, collected at the same locality as the said pumice (3), was analyzed by J. Ossaka, with the result as shown in (4), Table VII; it is likewise higher in silica content than the obsidian, although its analysis slightly differs from the analysis (3). The norm of the pumice (4) consists of 27% quartz, 62% feldspars ($Or_{27}Ab_{50}An_{23}$) and 4% pyroxenes ($Wo_{6}En_{82}Fs_{12}$), besides a small amount of magnetite, ilmenite and apatite.

The pumice can not be regarded as a highly frothed equivalent of the obsidian, so far as their chemically analyzed specimens are concerned. But, among the ejecta scattered about the craters are fragments intermediate in appearance between pumice and obsidian, and also those in which pumiceous and obsidian-like parts are accompanied with each other, sometime showing a flow structure with their alternating layers. Therefore, it is inferred that both the pumice and the obsidian have come from one and the same underground mass, more or less heterogeneous in chemical composition and which was vesiculated in various degrees in its different parts.

As already stated, both the pumice and the obsidian contain not a few xenocrysts and xenoliths of basaltic composition, besides those of some other rocks. Petrographically, the basaltic xenoliths are quite similar to the proper basalts of the host volcano, Fuji. Therefore, supposing that both the pumice and the obsidian have come from one and the same magma mass, this latter must have been intruded into the basaltic body of the volcano as a fluid capable of capturing the basaltic xenoliths from the surrounding. It is inferred that, on the eve of the 1707 eruption, this magma of acid andesitic composition was located close to the basaltic magma at some depth below the south-eastern flank of the volcano, both having become so high in gaseous tension as to be explosively ejected in succession and in the form of acid andesitic pumice and obsidian on the one hand and of basaltic lapilli and bombs on the other.

It is possible that the acid andesitic magma represents a foreign mass accidentally intruded into the basaltic mass of the volcano, or that the former is a palingenetic magma originated from a rock of quartz-dioritic composition under the influence of heat from the basaltic magma of the volcano. But, under such circumstances as mentioned above, it may be more natural to consider that the acid andesitic magma is genetically related with the basaltic magma of the volcano, the former having been derived from the latter through a process of crystallization-differentiation. Assuming that the two magmas are represented respectively by (A) and (B) of Table VIII, the composition of the material to be subtracted from (B) to yield (A) is obtained graphically by means of the addition-and-subtraction diagram. It is shown in (C) of the same table, together with its norm, and represents the smallest amount (57%) removed without yielding nepheline in the norm.

Table VIII.

	A	B	C		
SiO_2	65.0	53.0	44.0	Norm:	
Al_2O_3	16.1	15.1	14.4	Or	1.6
Fe_2O_3	1.0	4.6	7.4	Ab	16.8
FeO	5.1	9.3	12.5	An	29.5
MgO	1.7	5.3	7.9	Wo	11.7
CaO	5.0	8.8	11.6	En	6.1
Na_2O	3.9	2.8	1.9	Fs	5.3
K_2O	2.2	1.1	0.3	Fo	9.5
				Fa	8.9
				Mt	10.6

A. Analysis of the obsidian (Table VII, 1), calculated as free of water and other minor oxides.
B. Average of calculated groundmass compositions of four Fuji basalts. H. Tsuya, *Bull. Earthq. Res. Inst.*, 13 (1935), 655.
C. Composition of a material subtracted from (B) to yield (A).

The norm of the subtracted material (C) consists of feldspars ($Or_3Ab_{35}An_{62}$), pyroxenes ($Wo_{51}En_{26}Fs_{23}$), olivine ($Fo_{51}Fa_{49}$) and magnetite. This mineral assemblage is comparable with some of the phanerocrystalline rocks found among the 1707 ejecta.

Although Fuji proper is a young basaltic volcano born at a late date, probably later than the uppermost Pleistocene, it seems likely that part of the basalt magma underlying the volcano has been subjected to crystallization-differentiation so advanced as to bring about

only a little residual liquid of acid andesitic composition, and that this residual liquid has been squeezed out of the parent body to make the only source of the acid andesitic pumice and obsidian of the volcano.

Table IX. Intensity of volcanic activity, classified according to the volume of solid ejecta.

Intensity scale		Volcano	Year of eruption	Ejecta	
Grade	Limit of volume of ejecta (km³)			Kind*	Volume (km³)
IX	>100	Tambora, Soembawa	1815	B	150
VIII	100~10	Krakatau, Sunda Str.	1883	B	18
VII	10~1	Kljutschewskaja Ssopka, Kamchatka	1829	A	3.7
		Shtyubelya, Kamchatka	1907	B	3.0
		Sakurajima, Japan	1914	A B	>1.5
		Bandaisan, Japan	1888	D	1.2
VI	1~0.1	**Fujisan**, Japan	1707	B	0.8
		Taal, Luzon	1911	D	0.5
		Komagataké, Hokkaido, Japan	1929	B	0.1
		Asamayama, Japan	1783	A B	0.2
		Sakurajima, Japan	1946	A	0.1
V	0.1~0.01	Torishima, Japan	1939	A B	0.09
			1902	B	0.03
		Ôshima, Izu, Japan	1950–51	A	0.03
		Miyakéshima, Izu, Japan	1940	A B	0.02
		Lemongan, Java	1877	A	0.01
IV	0.01~0.001	Goentoer, Java	1843	B	0.008
		Adatarasan, Japan	1900	B	0.004
		Keloet, Java	1901	B	0.002
III	0.001~0.0001	Azumasan, Japan	1893	B	0.0005
II	0.0001~0.00001	Ôshima, Izu, Japan	1912	A	0.00002
		Tokachidaké, Japan	1926	D	0.00001
I	0.00001>	Yakéyama, Niigata, Japan	1949	D	small
		Kusatsu-Shiranésan, Japan	1932	D	small
0	0	Volcanoes displaying fumarolic activity only		0	0

* A: essentially lava-flows, B: fragmentary ejecta only, D: essentially ejected old detritus.

Summary and conclusions

The last eruption of Volcano Fuji began in the morning of Dec. 16, 1707, continued for four days with explosions coming in succession,

and thenceforward was repeated with intermittent and smaller explosions until the last day of the year, when it virtually stopped, being followed by its long dormancy lasting up to the present. During the eruption, explosions were frequently heard in Tokyo and vicinity, where at the same time the sky was overcast with eruption-clouds blown by the westerly wind and volcanic ashes fell to lie several centimeters deep.

The eruption occurred halfway down the southeastern flank of the mountain, with ejection of incandescent fragmentary materials from three new craters. Of these craters, the first one, situated on the northwest side of a knob called Hôei-san, is by far the largest, forming the only bowl-shaped hollow which has fatally broken the regularity of symmetrically curved slopes of the volcano. The two other craters, the second and the third, are much smaller and, situated on the southwest side of Hôei-san, they are in a NW.-SE. line, together with the first crater. This crater line represents one of the radial fissures in the volcano, as a number of parallel dikes exposed in the walls of the first crater do.

Hôei-san is mentioned in some of the historic records of the 1707 eruption (Hôei era in the Japanese history) as having been formed for the first time by the eruption, hence the name. But, so far as the writer's geological observations are concerned, the knob is neither a new cinder cone having its own crater nor a pile of ejecta thrown out of either one of the new craters mentioned. Although the knob is really veneered with the ejecta of 1707, its main mass is composed of loosely-coherent beds of volcanic ashes and breccia, both of which altogether are called Hôei-san tuffs. These beds, which are well exposed in the steep cliffs on the southeast side near the top of the knob, are divided into numerous minor blocks with both minor faults and fissures mostly striking in the NE.-SW. direction and less so in the N.-S. direction. They are basaltic in composition, but differ petrographically as well as structurally from any that are exposed in and around the new craters. Admitting that Hôei-san was formed by the 1707 eruption, its formation was not due to accumulation of new ejecta, but probably resulted from the upthrust of the older mass (Hôei-san tuffs) yielding to a magmatic intrusion which was advancing from the heart of the volcano to break out into the eruption.

The solid materials thrown out by the eruption are exclusively fragmentary ejecta including juvenile bombs, lapilli, pumice and obsidian,

besides some accessory and accidental ejecta. The juvenile pumice and obsidian were ejected from both the second and the third craters only in the first several hours of the eruption, causing the first falling of whitish ashes in the ash-covered area. Subsequent to the pumice and obsidian, the juvenile lapilli and bombs of basaltic composition began to be ejected from the first crater, and their ejection was repeated for the rest of the eruption.

The ejecta were accumulated in a fan-shaped area widening out eastward from the crater region, their deposit attaining a thickness of more than one meter within about 25 km of the craters and several centimeters even in Tokyo and vicinity, about 100 km distant. The total volumes of the ejecta which were accumulated within 25 km and 100 km of the craters, amounted respectively 0.5 km^3 and 0.8 km^3, both inclusive of small amounts of the pumice and obsidian. The volume of these ejecta puts the 1707 eruption at grade VI of the intensity scale of volcanic eruption (Table IX), which classifies the intensity of volcanic activity into ten grades, 0–IX, on the assumption that the intensity is proportional to the potentiality of volcanic gases to drive their container (lava), either fluent or fragmentary, hence proportional to the total volume of ejecta. Generally speaking, volcanic activity of grade VI is usually big explosive eruptions of the Vulcanian type; these are common in andesitic volcanoes, but quite unusual for such a young basaltic volcano as Fuji. The 1707 eruption, in this sense, may be specially worth noticing.

The basaltic ejecta of the 1707 eruption are augite-bearing olivine basalt, while the pumice and obsidian are andesite of intermediate to acid composition. The andesite is interpreted as having been derived through a process of crystallization-differentiation from the basaltic magma underlying the volcano. Be that as it may, it is almost an unheard-of occurrence in the world volcanoes that the juvenile ejecta of two rock types, wide apart in chemical composition, were thrown out in succession by one and the same eruption. In company with the juvenile ejecta were thrown out not a few fragments of foreign rocks, which must have come from the foundation of the volcano, suggesting that the 1707 eruption had its origin at a large depth, possibly more than 2 km below the 1707 craters. The highly explosive character of the eruption might have been an inevitable consequence of the large depth of its origin and also of the incorporation of basaltic magma with more viscous andesitic magma in the eruption. Exhaustion of an enormous

mass of volcanic gases by the eruption may have brought forth the dormancy in which the volcano has lain for 248 years since 1707.

---

25. 富士火山の地質学的並びに岩石学的研究 (V)

5. 富士山の宝永4年噴火について

地震研究所 津 屋 弘 逵

富士山の最新の噴火は 1707 年 12 月 16 日（宝永4年 11 月 23 日）の朝に始まり，4 日間にわたつて殆ど休みなく続き，その後も同月 31 日まで間歇的に爆発を行つたが，同日に至つて事実上止んだものである．この2週間にわたる噴火中，その爆音は東京及びその附近においてしばしば聞かれ，また西風になびいた噴煙は黒雲となつて空をおおい，そのため東京では昼間に灯を用いるほど暗くなつた時があり，火山灰は数センチメートルの厚さまで降り積つた．

この噴火は富士山の東南側中腹に起つたもので，三つの新噴火口から白熱の抛出物を噴出した．その第一火口は宝永山という小山の北西側にでき，富士山の規則正しい外形を損う唯一の大きい窪みとして残つているものである．他の二つ，すなわち第二及び第三火口は宝永山の南西側にできたもので，第一火口よりはるかに小さいが，明かに噴火口の跡として現在も認められる．これらの3火口は北西–南東方向に相接して並び，第一火口の火口壁に露出する多数の同方向の平行岩脈と共に，同火山の頂上火口から出る放射状割目の一つを表わすものである．

宝永山はこの宝永4年噴火によつて初めてできたものと伝えられ，そのためこの名が与えられている．しかし，この小山は新しい噴火口をもつ噴石丘でなく，また上記の3火口からの噴出物が積つてできたものでもない．すなわち，この小山はこれらの火口からの噴出物で大部分がおおわれてはいるが，その主体は宝永山凝灰岩層とよぶ黄灰色の一見ロームに似る凝灰岩と灰色凝灰角礫層とからできている．そしてこの地層は宝永山東南側の断崖でよく見られるように，割目や小断層によつて切断され，いくつかの小地塊の集まりになつており，宝永4年噴出物には不整合的に接している．岩質上，この地層はやはり玄武岩質であるが，よく固まつており附近の富士山腹を構成する火山灰や角礫層のどれにも対比できず，むしろ富士山麓の一部に見られる古い富士火山の噴出物に類似するものである．それ故，もし宝永山が宝永4年の噴火によつて現れたものとすれば，それは新噴出物の堆積によつて小山になつたのではなく，以前からその附近の富士山腹の一部にかくれていた古い凝灰岩層が，噴火を起そうとする岩漿の地下貫入によつて，推し上げられて小山となり，断層や割目で切断されたものと見ることができよう．

宝永4年の噴出物は熔岩流を伴わず，すべて抛出物で，新しく生じた火山弾，火山礫，軽石，黒曜石等の他に，同火山を構成する古い火山岩の破片や火山基盤の岩石の破片などをふくむ．軽石と黒曜石とは噴火の初めの数時間の間に第二及び第三火口から抛出されたもので，これらが白い火山灰となつて噴火の最初に降つたことが記録に残つており，また，これらが全噴出物の最下位に堆積していることは，降石地域内の各地で現在も認められる．次いで玄武岩質の火山礫や火山弾が第一火口から抛出されはじめ，その抛出が噴火の終るまでくり返された．

噴出物は噴火口附近から東方に次第に拡がる扇状地域内に堆積し，駿河駅附近に至る 25 km 以内では厚さ 1 m 以上に達し，現在でもよく追跡される．古記録によると，それより遠くでは，平塚附近で 10 cm 内外，川崎附近で 5 cm 内外，東京でも同程度の厚さの火山灰が堆積した．噴火口から 25 km までの地域内に堆積した噴出物の全容積は約 0.5 km^3，東京附近（約 100 km）までのそれを加えると約 0.8 km^3 となる．この量は宝永4年噴火が噴火強度階の VI に相当することを示す．ここに噴火強度階というのは，噴火の強さが噴出物の総量に比例するものと仮定して，噴出物の多少を 10 階級，0–IX，に区分したものである．火山噴出物は，熔岩流も抛出物も共に，それに伴うガスの圧

Fig. 6. Volcano Fuji as seen from the top of Volcano Hakoné, showing the 1707 craters (I, II, III) and Hôei-san (H). S: Subashiri. G: Gotemba. Part of the somma and caldera of Hakoné volcano in the foreground.

Fig. 7. The southeast flank of the mountain where the 1707 eruption occurred. Right, top of Hôei-san (H) showing cliffs of the Hôei-san tuffs. Left, the first crater (I) with the eastern wall of the second crater (II) in the foreground and the snow-covered top of the mountain in the background.

Fig. 8. All three 1707 craters (I, II, III), looking downward.

Fig. 9. The first crater with the northwestern wall of the second crater in the foreground.

Fig. 10. The second crater and its western wall.

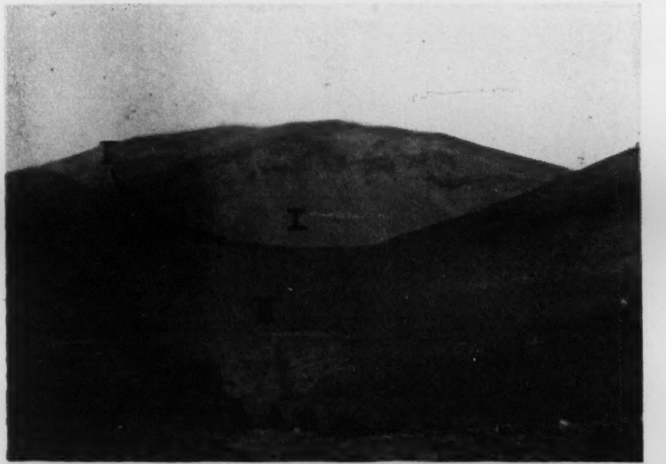

Fig. 11. The third crater with the northwestern wall of the first crater in the background.

（震研彙報　第三十三号　図版　津屋）

Fig. 12. The northwestern wall of the first crater, showing strata of lava flows and parallel dikes. Top of the mountain in upper right.

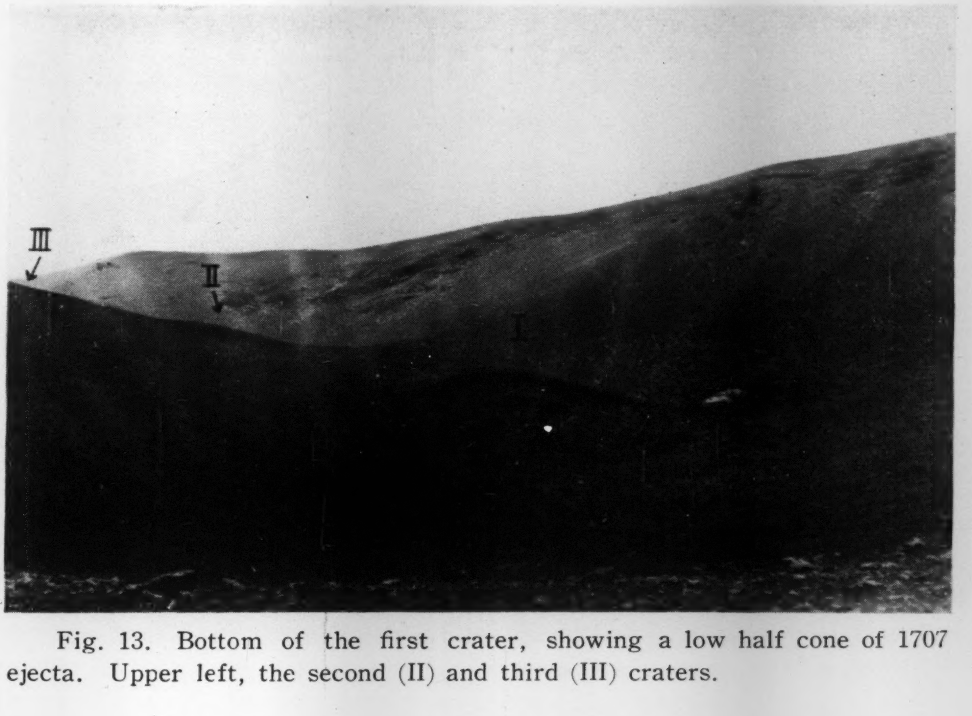

Fig. 13. Bottom of the first crater, showing a low half cone of 1707 ejecta. Upper left, the second (II) and third (III) craters.

（震研彙報 第三十三号 図版 津屋）

Fig. 14. Hôei-san, looking downward from near the eighth stage of Gotemba trail. I: the first crater.

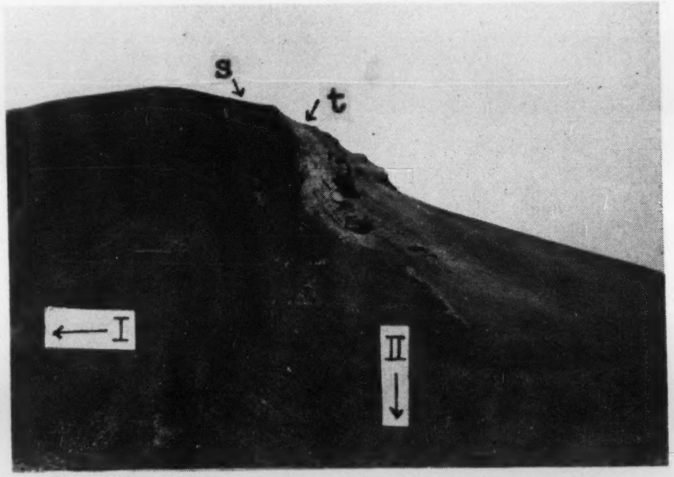

Fig. 15. Hôei-san seen from the west. I: the first crater. II: the second crater. S: 1707 ejecta. t: Hôei-san tuffs.

Fig. 16. Cliff of the Hôei-san tuffs. II: the second crater.

Fig. 17. Hôei-san tuffs showing minor faults and cracks.

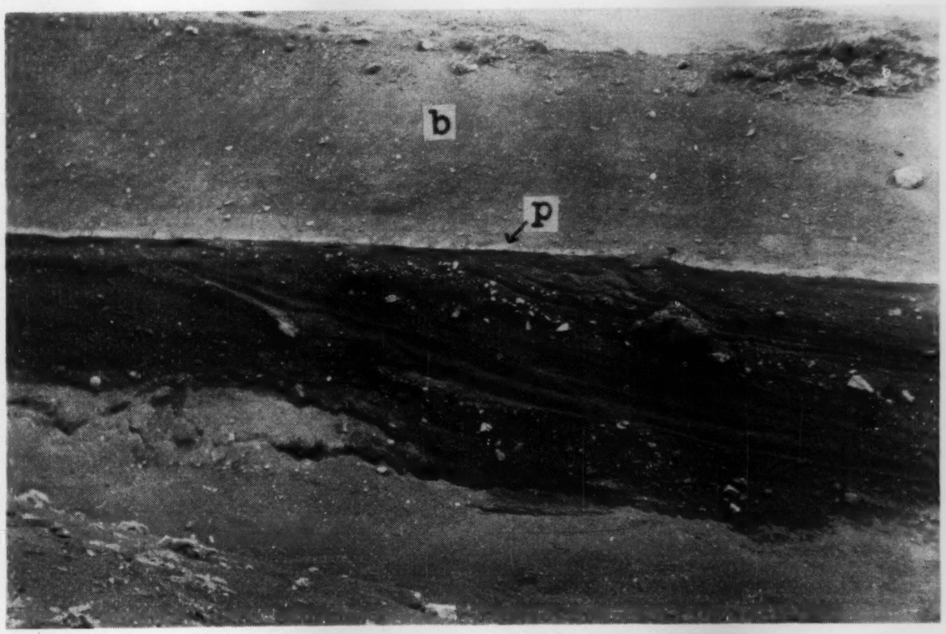

Fig. 18. Wall of a gully, showing the deposit of 1707 ejecta with underlying old ejecta. b: basaltic lapilli. p: acid andesite pumice. Locality: Shishiga-hana on the eastern flank of the volcano.

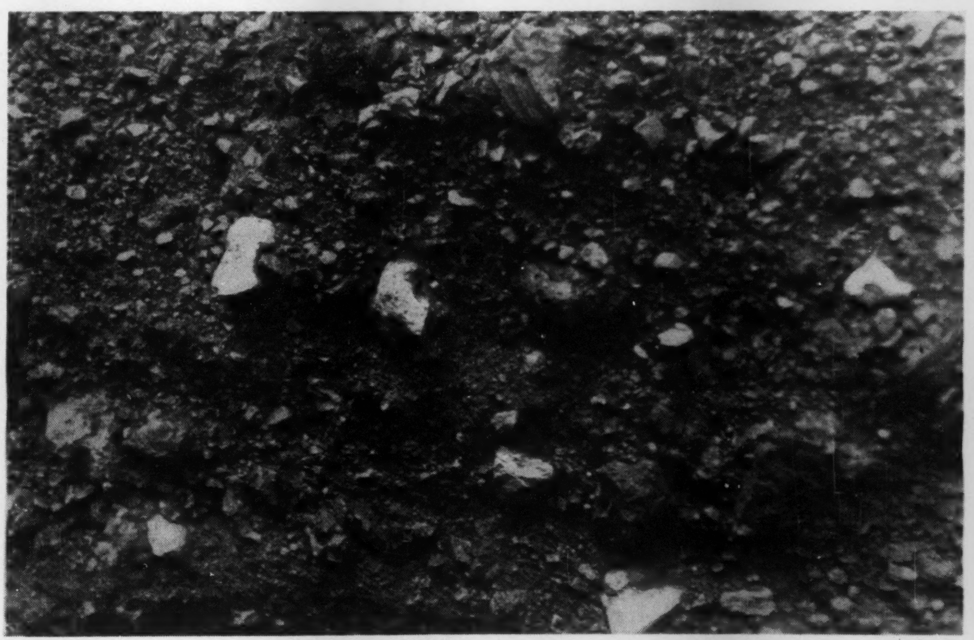

Fig. 19. Volcanic breccia composed essentially of fragments of acid andesite obsidian. Locality: Head of a gully in the gap of the southern wall of the third crater.

（震研彙報 第三十三号 図版 津屋）

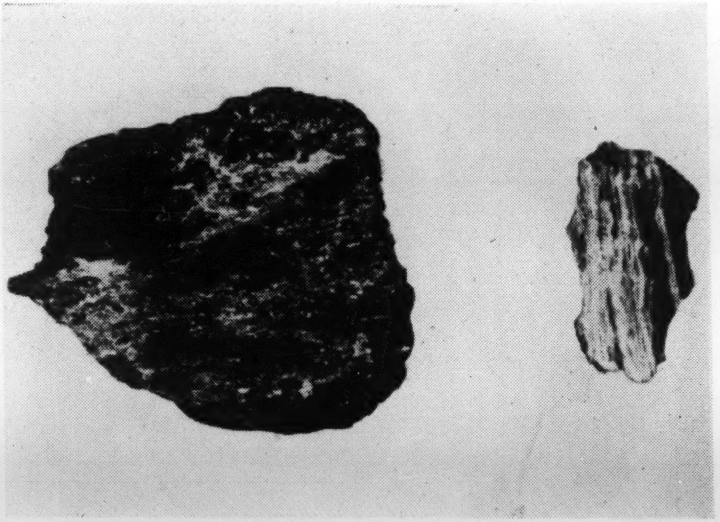

Fig. 20. Acid andesite pumice of 1707, from Shishigahana on the eastern flank of the mountain. 2/3 natural size. Right, a light-grayish specimen. Left, a specimen showing flow bands of whitish and grayish pumice.

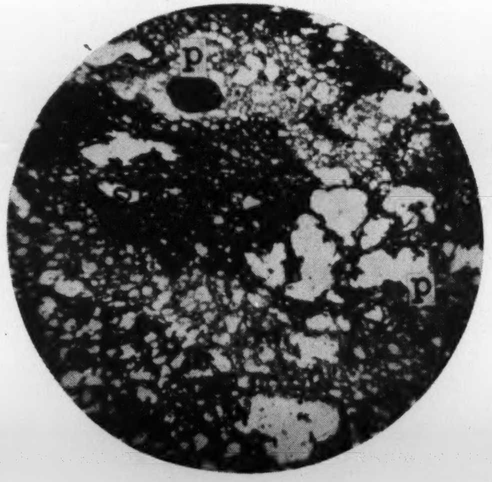

Fig. 21. Microphotograph of the pumice (Fig. 20, left). ×15. p : augite xenocryst.

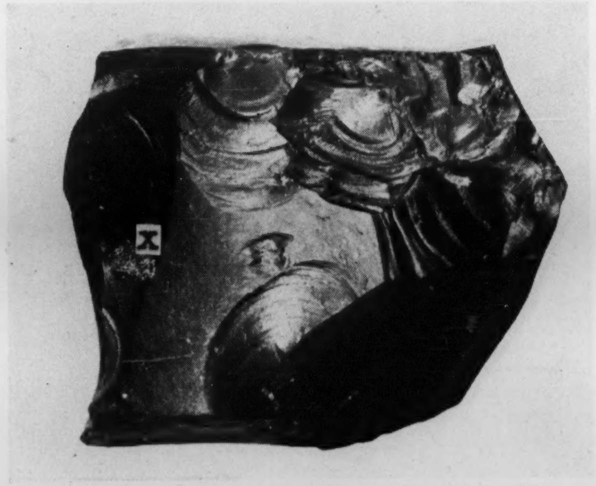

Fig. 22. Andesite obsidian of 1707, from the west side of the second crater (II, Fig. 2). 2/3 natural size. Showing conchoidal fracture. x : xenolith.

Fig. 23. Microphotograph of the obsidian (Fig. 22). ×15. x : xenolith (augite-plagioclase-rock). x′ : xenolith (olivine-basalt).

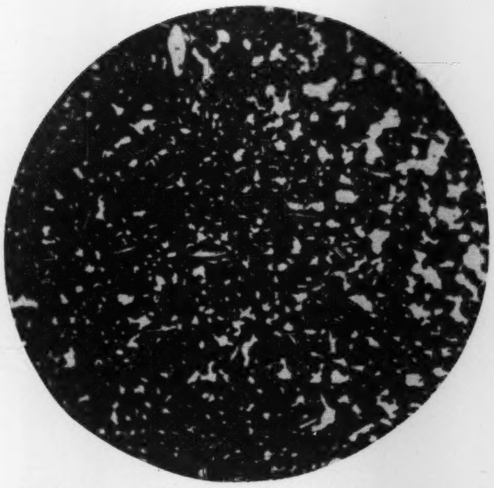

Fig. 24. Augite-bearing olivine basalt. 1707 ejecta (scoriaceous lapilli). ×15.

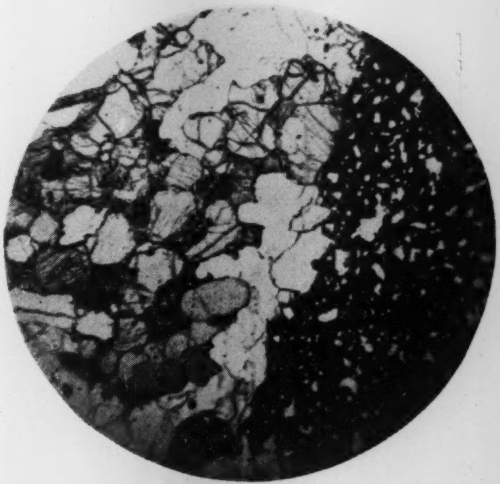

Fig. 25. Magnetite-hornblende-olivine-hypersthene-augite-plagioclase-rock (left) enclosed in the basalt (right). ×15.

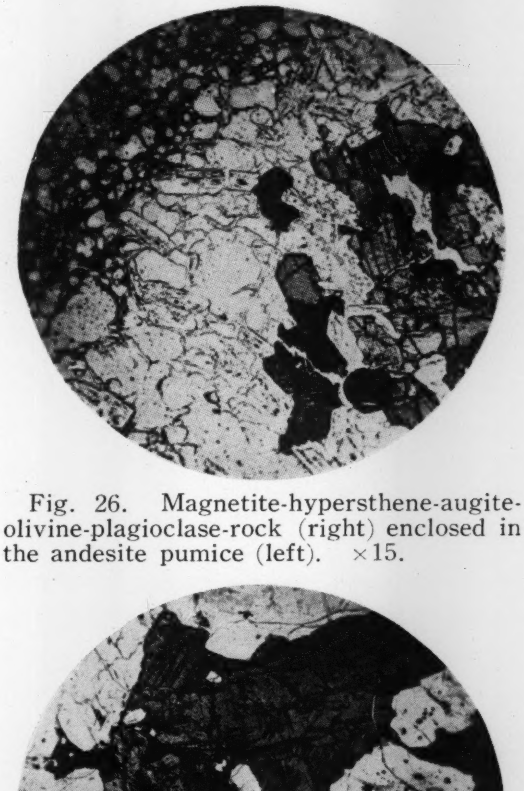

Fig. 26. Magnetite-hypersthene-augite-olivine-plagioclase-rock (right) enclosed in the andesite pumice (left). ×15.

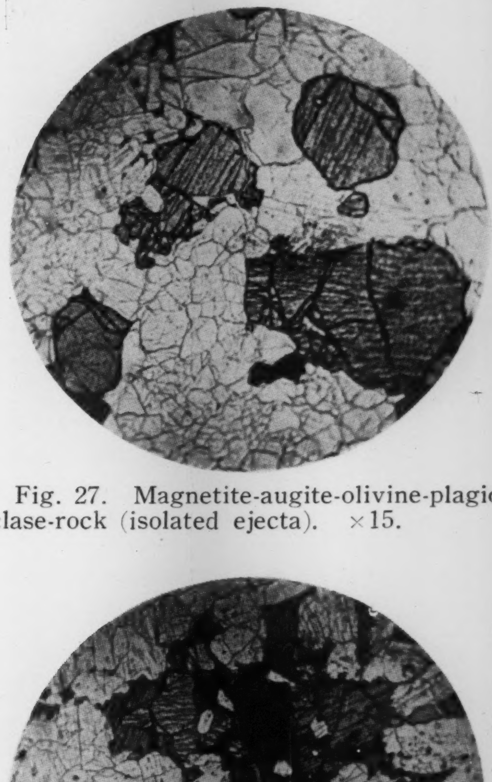

Fig. 27. Magnetite-augite-olivine-plagioclase-rock (isolated ejecta). ×15.

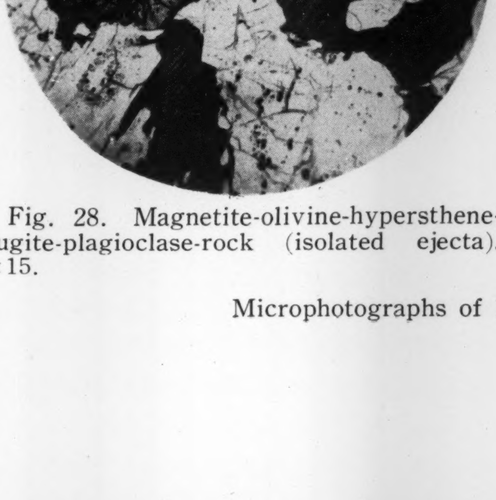

Fig. 28. Magnetite-olivine-hypersthene-augite-plagioclase-rock (isolated ejecta). ×15.

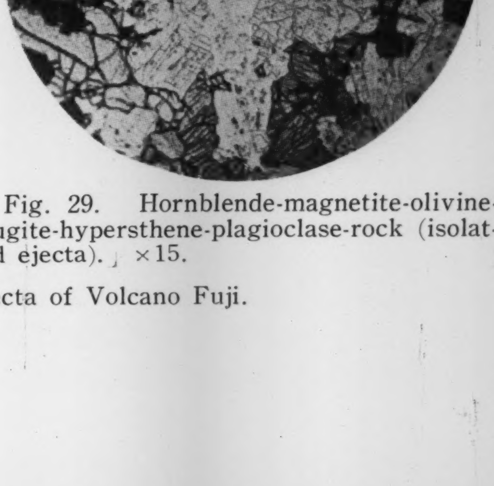

Fig. 29. Hornblende-magnetite-olivine-augite-hypersthene-plagioclase-rock (isolated ejecta). ×15.

Microphotographs of 1707 ejecta of Volcano Fuji.

(震研彙報 第三十三号 図版 津屋)

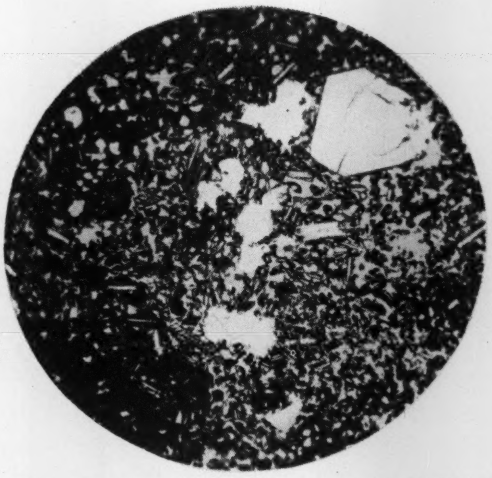

Fig. 30. Augite-olivine-basalt tuff (Hôei-san tuffs). ×15.

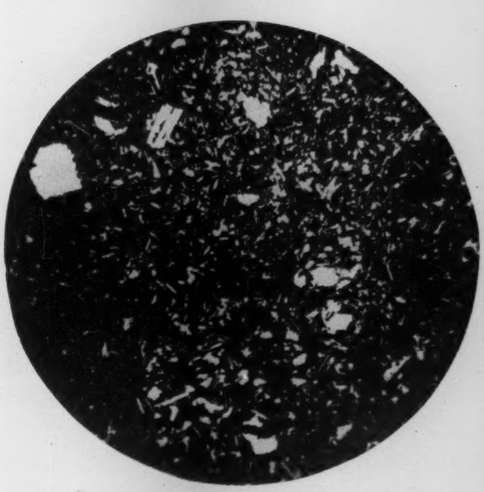

Fig. 31. Augite-olivine-basalt tuff (ejected block). ×15.

Fig. 32. Magnetite-olivine-hypersthene-augite-plagioclase-rock (isolated ejecta), showing an ophitic texture. ×15.

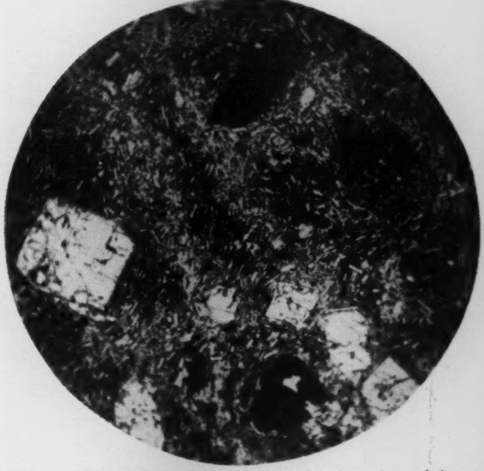

Fig. 33. Hornblende andesite (accidental ejecta). ×15.

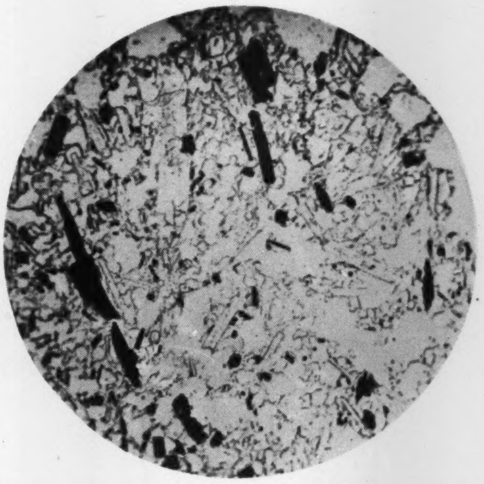

Fig. 34. Augite-biotite-hornblende-dacite pumice (accidental ejecta). ×15.

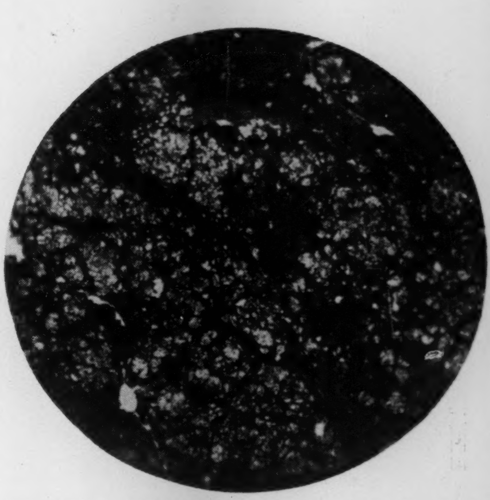

Fig. 35. Silicified tuff (accidental ejecta). ×15.

Microphotographs of 1707 ejecta of Volcano Fuji (Fig. 30 excepted).

力によつて地表に噴出されるものであるとすれば，噴出物の量が多い事はその噴出に与つたガスの総圧力が大きく，したがつてその噴火の強さが大きいと考えられるだろう．強度 VI の噴火といえば，ヴルカノ式の大きい爆発的噴火の例が多く，安山岩或はこれより一層酸性火山岩を噴出する火山で普通に行われ，富士山のような玄武岩火山ではまれである．この意味で，宝永 4 年の噴火は，同火山はもちろん一般玄武岩火山の活動として，注目に値する稀有の爆発的噴火であつた．

この噴火で抛出された玄武岩質火山礫や火山弾は一様に含普通輝石橄欖石玄武岩である．それに反して，軽石及び黒曜石は僅少の斜長石斑晶のみを有するガラス質の中性乃至酸性安山岩である．軽石は標本によつては多少異なる化学成分を示し，黒曜石も軽石と多少異なる化学成分をもつ．しかし，軽石と黒曜石との中間的構造を示すもの，両者が流理構造をもつて混つているものなども，同時の抛出物として見出されるので，これらは全体として一つの多少不均質な岩漿から生じたものと考えられよう．そして，この岩漿は富士山本来の玄武岩々漿から結晶分化作用によつて生じたと解釈される．昭和 14 年の三宅島噴火の際の無斑晶玄武岩と灰長石の巨晶，橄欖石などを多くふくむ斑状玄武岩との例のように，同一噴火で多少異なる岩質のものが同時或は相次いで噴出されることは知られているが，玄武岩と酸性安山岩とのように著しく異なる岩石が相次いで噴出された例は他には知られていない．富士山自体においても宝永 4 年の噴火のみがその例で，同火山の他のどの部分にも軽石，黒曜石などのような噴出物は発見されない．これらの新抛出物の他に，愛鷹山火山の熔岩に類似する岩片，第三紀火山岩と考えられる岩片などが上記の 3 火口の何れからも抛出され，また火山弾や軽石，黒曜石などの中に捕獲岩として包まれている．したがつて，宝永 4 年の噴火は富士山基盤の岩石を通して，少くとも地下 2 km 以上の深さの所から起つたものと考えられる．この噴火が玄武岩火山の活動として稀有の大爆発であつた事は，その爆発源が地下深くにあつた事，粘性の大きい酸性安山岩々漿が玄武岩々漿と共に噴火に与かつた事などによる必然の結果であろう．また，この噴火によつて岩漿内のガスの大量が一時に失われ，岩漿温度の著しい低下を来たした事はその後現在に至る 248 年の永い休眠を富士火山にもたらしたものと考えられる．

26. *Some Heavy Accessory Minerals in Granitic Rocks from the Tsukuba District, Ibaraki Prefecture.**

By Takeshi ICHIMURA,

Yamagata University.

(Received June 28, 1955.)

Introduction

The Tsukuba district includes the southern end of the Abukuma Range and is geologically a well-known area which has already been investigated by H. Yamada[1], B. Suzuki[2], R. Ōhashi[3], S. Shimizu[4], Y. Ōdaira[5], H. Satō[6], K. Sugi[7], H. Fujimoto[8], H. Tsuya[9], G. Kojima[10], H. Shibata[11], K. Kawada[12], S. Okada[13] and others. It is mainly built up of granitic rocks and various kinds of metamorphosed sediments assigned to the Upper Paleozoic in association with such basic or ultrabasic rocks as gabbro, norite and gabbro pegmatite as well as anorthosite. The most important rock exposed here is represented by biotite granite traversed by many dykes of pegmatite and aplite. It affected greatly the Paleozoic sediments distributed extensively on the hilly land near Mt. Tsukuba, resulting in the contamination of sediments due to the intrusion, formation of ball granite, *lit par lit* injection of

---

* Communicated by N. Nasu.

1) H. YAMADA, *Geol. Map, Mito, 1:200,000 and Its Explanatory Text*, (1888).

2) B. SUZUKI, *Bull. Geol. Surv. Japan*, **18** (1905).

3) R. ŌHASHI, *Jour. Geol. Soc. Tokyo*, **18** (1911).

4) S. SHIMIZU, *Jour. Geogr.*, **25** (1913).

5) Y. ŌDAIRA, *Ms. Geol. Inst. Tokyo Univ.*, (1925).

6) H. SATŌ, *Geol. Map, Tsukuba, 1:70,000 and Its Explanatory Text*, (1927).

7) K. SUGI, *Jour. Geol. Soc. Tokyo*, **34** (1927), 358–375: *Jour. Geol. Soc. Tokyo*, **35** (1928): *Jap. Jour. Geol. & Geogr.*, **8** (1930), 29–112.

8) H. FUJIMOTO, *Jour. Geol. Soc. Japan*, **45** (1938), 377.

9) H. TSUYA, *Bull. Earthq. Tokyo Univ.*, **17** (1937), 517–534.

10) G. KOJIMA, *Kagaku*, **13** (1943), 167–168.

11) H. SHIBATA, *Stud. Geol. & Min. Inst., T. K. D.*, 1944: *Jour. Geol. Soc. Japan*, **57** (1951): *Sc. Rept. T. K. D.*, [C], **3** (1954), 159–161.

12) K. KAWADA, *Jour. Geol. Soc. Japan*, **53** (1947), 622–627: *Jour. Geol. Soc. Japan*, **54** (1948), 639: *Sc. Rept. T. B. D.*, [C], **2** (1953), 217–307.

13) S. OKADA, N. SHIMODA & H. SHIBATA, *Stud. Geol. & Min. Inst. T. K. D.*, (1954), 197–203.

igneous materials, etc. Such geological features attracted the writer's attention to the granitic rocks of this district. In addition, the writer was born in this district and was, therefore, in a favourable position to examine these granitic rocks from place to place. During his repeated field works, various specimens were collected from many localities of this granitic area. They were mineralogically investigated, and some of them were chemically analysed. In the former case, the writer had a special interest in heavy accessory minerals which had almost been neglected formerly in the microscopical investigation of such granitic rocks, because they have quite a similar character in the same granitic body except for its contaminated part.

The writer crushed various specimens obtained from different parts of granitic bodies including the contact aureole, and the heavy accessory minerals extracted in this way were crystallographically and optically investigated to confirm whether there are dissimilarities or not in different kinds of granitic rocks. The results are summarized in this paper.

General Features of Mother Rocks

The granitic rocks under consideration begin to be exposed at the southern periphery of the hilly land adjoining Mt. Tsukuba, Mt. Ashio, Mt. Kaba, Mt. Amabiki and the surrounding area. They are mostly biotite or two-mica granites with varying petrographical and chemical characters. These granites are traversed by pegmatite or aplite and intruded through with the Upper Paleozoic sediments, giving striking contact effects and capturing their fragments as well as the big gabbroic xenoliths which are composed of uralite gabbro, hornblende gabbro, olivine gabbro, norite, gabbro pegmatite in association with amphibolite and anorthosite. Most of such granites are being quarried at many places of the area extending over Hōjō, Oda, Shichiku-mura, Makabe, Yubukuro, Minedera-san, Yamanoo, Amabiki, Nishiyama, Mito, Inada, etc. Of these, the so-called "Inada granite" is very famous as a building stone of high quality.

In Okada's recent paper[14], the granites exposed in this district are divided into such three types as the Tsukuba-type granite, Inada-type granite and Kamishiro-type granite. In these cases, The Tsukuba-type granite consists of biotite or two-mica granite and is well exposed at the

14) S. OKADA, *op. cit.*, (1954), 217–307.

southern part of this granitic area, passing northwards into the Inada-type granite which surrounds the Kamishiro-type granite near Nishiyama, Mito and Kitanakayama.

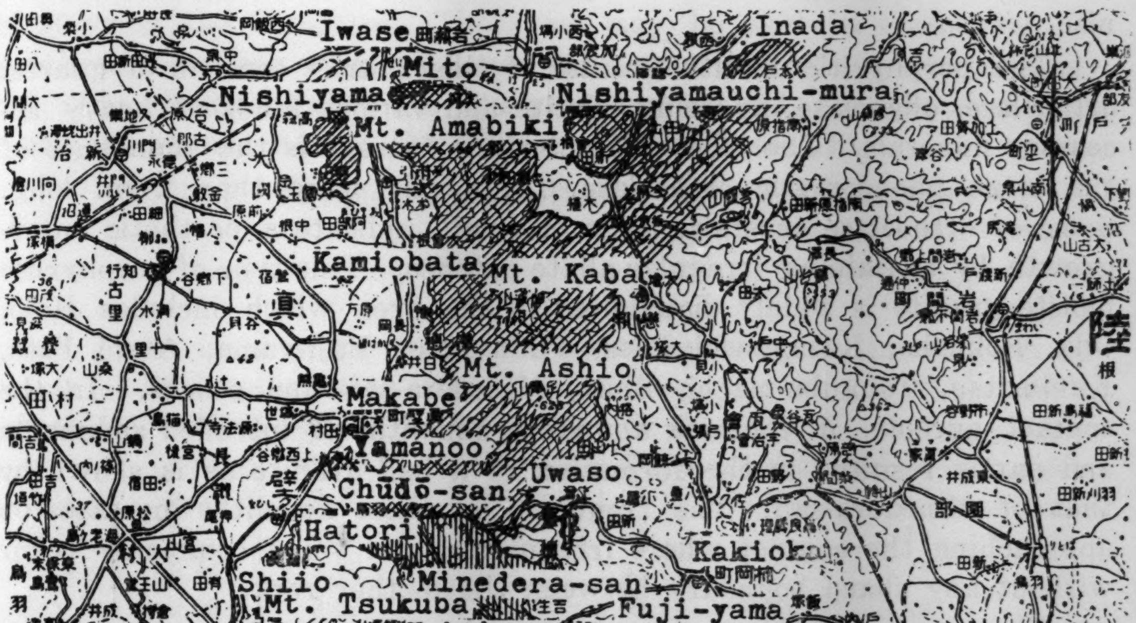

Fig. 1. Map showing the distribution of granitic rocks in the Tsukuba district.
1 = Kamishiro-type granite, 2 = Inada-type granite, 3 = Tsukuba-type granite.

The Tsukuba-type granite is partly represented by a porphyritic biotite granite which are in contact with metamorphosed sediments characterized by the occurrence of various kinds of contact minerals such as andalusite, cordierite, diopside, hornblende, garnet and sillimanite.

The porphyritic biotite granite of this district consists of quartz, orthoclase, oligoclase, andesine, biotite and various kinds of heavy accessory minerals. The most characteristic feature is the abundance of the large phenocrystic orthoclase, frequently more than 2 cm. long. Some of orthoclase crystals, large or small, indicate a perthetic intergrowth by containing irregular albite patches. This type of porphyritic biotite granite is widely distributed in the area which includes Hōjō, Oda, Rokusho, Kazagaeshi Pass, Fudō Pass, Fuji-yama, Asahi Pass, Kunimatsu, Tsukuba-machi, Shiio, Minedera-san and others. In the contact aureole, it contains abundant xenoliths of intruded sediments and partly resulted in the formation of a ball granite as is shown by that of Minedera-san. The frequency of these xenoliths increases on approaching the contact where irregular aplitic veins commonly occur without any sharp boundary between the mother rock.

The porphyritic biotite granite, on the other hand, grades into the non-porphyritic variety with a minor amount of muscovite at Shichiku-mura and Oda as well as on Jō-yama or elsewhere. It is also very noteworthy that the foundation of Mt. Tsukuba is built up of the porphyritic biotite granite on which a large mass of gabbroic rock is found as an erosion remnant.

The Inada-type granite is largely exposed at the mountainous area situated at the north of the line connecting Uwaso to Hatori. It is non-porphyritic granite with some features different from the Tsukuba-type granite, being composed of quartz, orthoclase, oligoclase, andesine, biotite, muscovite and its accessory minerals. The specimens collected on Chūdō-san, Mt. Ashio and Mt. Kaba as well as at the Kamiobata quarry of Amabiki-mura indicate different textures from coarse to fine. Some of these have dark colors due to the abundance of minute biotite flakes and are rich in xenoliths. They can be obtained at the Chūdō-san quarry and its vicinity. The boundary between the Inada-type granite and Tsukuba-type granite could not be confirmed exactly by the writer. As to the Kamishiro-type granite, the writer is unfortunately not acquainted with its mode of occurrence. It is, therefore, eliminated from the writer's present paper.

Chemically speaking, the silica percentage of the porphyritic biotite granite shows a tendency to become lower than the non-porphyritic variety. For instance, the biotite granite obtained from Jō-yama shows a high percentage of silica as compared with the porphyritic variety of Jō-yama and Hirasawa. The same may be said in comparing the porphyritic variety with the Inada-type granite which is non-porphyritic. The results of chemical analyses carried out on several mother rocks are summarized in the following table (Table I).

Table I. Chemical composition of some granites from the Tsukuba district.

	(1)	(2)	(3)	(4)	(5)	(6)	(7)
SiO_2	74.48	65.88	64.23	66.63	70.91	74.38	71.80
Al_2O_3	14.00	17.48	18.09	16.28	14.38	14.33	15.11
Fe_2O_3	0.15	0.49	0.58	0.15	0.40	0.26	0.28
FeO	1.52	4.02	4.11	4.47	2.54	1.40	2.03
MgO	0.35	0.75	1.38	1.24	0.28	0.17	0.20
CaO	2.57	4.01	4.99	3.33	2.60	1.80	2.27
Na_2O	3.44	3.55	3.04	3.53	3.30	3.10	3.24
K_2O	2.99	2.59	2.83	2.59	2.59	3.48	2.93
H_2O+	0.25	0.73	0.39	0.66	0.89	0.65	0.77
H_2O-	0.06	0.06	0.09	0.12	0.25	0.26	0.32
TiO_2	0.13	0.47	0.35	0.58	0.36	0.18	0.34
P_2O_5	0.09	0.16	0.12	0.21	0.32	0.15	0.24
MnO	0.28	0.20	0.27	0.09	0.30	0.11	0.18
S					0.11	0.03	0.05
ZrO_2						0.05	
Total	100.34	100.19	100.47	99.88	99.23	100.35	99.78
				Norm			
Q	36.12	23.94	20.22	24.18	34.68	38.34	35.94
or	17.79	15.57	16.68	15.57	15.57	20.57	17.24
ab	28.82	28.30	25.68	29.87	27.72	26.20	27.25
an	11.95	19.18	23.91	15.57	11.12	8.06	9.73
C	0.71	2.04	1.22	1.94	2.04	2.45	2.45
Fs	2.90	6.60	7.00	7.26	4.09	2.24	3.30
En	0.90	1.90	3.50	3.10	0.70	0.40	0.50
mt	0.23	0.70	0.93	0.23	0.70	0.46	0.46
il	0.30	0.91	0.61	1.06	0.76	0.30	0.60
ap	0.34	0.34	0.34	0.34	0.67	0.34	0.67

(to be continued.)

Table I. (continued.)

Niggli's value

	(1)	(2)	(3)	(4)	(5)	(6)	(7)
si	405.54	268.46	238.52	277.75	369.35	433.56	383.63
al	44.77	41.81	39.42	40.00	44.06	48.95	47.44
fm	11.77	20.54	23.16	24.00	16.25	9.44	12.82
c	15.03	17.60	19.82	14.75	14.38	11.19	13.14
alk	28.43	20.05	17.60	21.25	25.31	30.42	26.60
mg	0.25	0.23	0.34	0.32	0.13	0.07	0.13
k	0.37	0.34	0.37	0.67	0.35	0.43	0.37
c/fm	1.28	0.86	0.86	0.61	0.88	1.19	1.03
or : ab : an in norm							
or	30.38	24.69	25.17	25.52	28.61	37.51	31.80
ab	49.21	44.89	38.75	48.96	50.95	47.79	50.26
an	20.41	30.42	36.06	25.52	20.44	14.70	17.94

(1) Two-mica granite from the Jō-yama quarry, Analysed by K. Azuma.
(2) Porphyritic biotite granite from the Jō-yama quarry, Analysed by K. Azuma.
(3) Porphyritic biotite granite from the Hirasawa quarry, Analysed by K. Azuma.
(4) Porphyritic biotite granite from the Hirasawa quarry, Analysed by S. Tanaka.
(5) Biotite granite from the Kitaishi quarry, Kabaho-mura, Analysed at Geol. Surv.
(6) Biotite granite from the Hikage-yama quarry, Nishiyamauchi-mura, Analysed at Geol. Surv.
(7) Hornblende biotite granite from the Fujita-yama quarry, Kabaho-mura, Analysed at Geol. Surv.

Mineralogical and Optical Characters of Heavy Accessory Minerals

The writer crushed many specimens collected from the Tsukuba district to extract heavy accessory minerals from granitic rocks. For this purpose, he used Thoulet solution and could concentrate such heavy accessory minerals as zircon, monazite, apatite, garnet, titanite, allanite and magnetite. Of these, zircon is the commonest accessory mineral in all kinds of granitic rocks. It occurs as colorless or pink crystal with a long or short prismatic habit. Mostly, the crystals have a well-defined form which is composed of prism and pyramid, although there are sometimes rounded crystals. They are simple or complicated combination of $a(100)$, $m(110)$, $p(111)$, $x(311)$ and $u(331)$. So far as has been examined by the writer, the commonest form is represented by such combinations as p and a, p and m or p, a and m, but various types of crystal form associated with x or u can be seen in biotite or two-mica granites from the Oda quarry and the Kamiobata quarry, although u is rather rare as compared with the frequent occurrence of x.

Sometimes, both the colorless and pink zircon are found together, as is shown by several cases of the Hirasawa quarry (Fig. 2) and also in the specimen from the hill near Sugimoto. In such cases, the colorless zircon is more abundant than that with a pink color, and it seems that there is a transition stage of color between them. The colorless variety is always very clear and transparent, taking usually a long and sharp prismatic form in contrast with the short prismatic habit of the pink crystal. Frequently, it contains microlites with unknown characters, and the amount of such colorless zircon is increased in the specimens from Hirasawa, Kankyosandaishi (Fig. 3) and Rokusho where the Tsukuba-type granite is exposed at or near the contact with Paleozoic sediments. The same may be said of the specimens rich in xenoliths. This is one of the chief points different from the Inada-type granite obtained on Mt. Amabiki, Mt. Kaba and Mt. Ashio, in which beautiful zircon crystals are scarcely present and those with a short prismatic habit are rather abundant. The combination of *a*, *p*, *m* and *x* is frequently seen in the specimens obtained from the Kamiobata quarry (Fig. 4) and the Oda quarry.

The length of these crystals shows a wide range. The largest crystal is 0.35 mm. long in the colorless variety, whereas it is 0.25 mm. long in the pink one. The beautiful crystal with a sharp outline was found in the specimens from the Hirasawa quarry and the Kankyosan quarry (Fig. 4). The zircon crystals mentioned above are generally enclosed in biotite flakes to which they afford a pleochroic halo along the contact between them.

The occurrence of monazite is also known occasionally in granitic rocks of the Tsukuba district. It has a stout prismatic or somewhat rounded form, being composed of *a*(100), *m*(110), *b*(010), *u*(021), *w*(101), $v(\bar{1}11)$ and $x(\bar{1}01)$. As is indicated by many crystals, *a*, *b*, *m* and *w* are easily recognized when compared with *u*, *v* and *x*. The mineral is weakly pleochroic, viz., x=light greenish yellow and z=light yellow. The extinction angle, $Z \wedge c$, is 2°. Some of the crystals enclose minute particles undetermined.

It is very noteworthy that monazite is found in almost all specimens including the Tsukuba-type granite and Inada-type granite, although its amount is variable from place to place. The high frequency of this mineral is shown by various specimens from the Hirasawa quarry (Figs. 5–6). Jō-yama quarry, Kamiobata quarry, Oda quarry and Mt. Ashio as well as from the pass between Uwaso and Makabe.

In these cases, granitic rocks of the Hirasawa quarry reveal the highest frequency of monazite crystals. The writer also examined biotite-rich granite near the contact and transition part between such a granite and aplitic rock. Occasionally, they contain good crystals suitable for determining such faces as *a*, *m*, *b*, *u*, *v*, *x* and *w*. The largest crystal is 0.27 mm. long and 0.19 mm. across. The aplitic rock exposed here is similarly rich in minute crystals of monazite as compared with the ordinary porphyritic biotite granite.

A characteristic feature is also shown by the abundance of apatite crystal (Fig. 7). It is a common mineral in the porphyritic biotite granite of the Tsukuba-type, particularly in the specimens from near the contact, where biotite is remarkably increased. Most of the apatite crystals are contained in such biotite flakes, but isolated crystals may also be seen in these specimens. The apatite crystals examined by the writer generally assume a short prismatic or rounded form. The largest crystal with an elongated form is 0.37 mm. long. They are colorless and mostly very clear in appearance. Rarely, such prismatic crystals have a dark grey core which seems to be a decomposed part. They may be a combination of several forms, viz., pyramid, prism and base, but there is no distinct face exactly determined except prism. Sometimes, enclosures of unknown character are to be seen.

The specimens collected from the direct contact have a tendency to be rich in this mineral. It is, however, quite or almost absent in the Inada-type granite and in the specimens from the quarry situated at the south of Kankyosandaishi.

Besides these, garnet is also a well-known mineral in granitic rocks of this district. The most important locality is represented by Yamanoo where beautiful crystals with icositetrahedral habit were found from pegmatites. They are, however, nearly exhausted at present. In other localities, garnet is only an accessory mineral which is about 2 mm. across in the large crystals. The mineral is pink or rarely colorless and commonly assumes a rounded form without showing any well-defined crystal faces. Such garnet crystals can be seen in the specimens from Jō-yama, Hirasawa, Negoyashinden and others. Of these, the pink variety shows some similarities to almandite.

In the specimens from near Rokusho, the writer noticed the frequent occurrence of titanite, which is found together with zircon, apatite and monazite, although its crystal can not be recognized with the naked eye. It has a light brown color and occurs in an anhedral

form, being not infrequently associated with biotite flakes. Titanite is, however, a scanty ingredient of the granitic rocks under consideration, and it is nearly or entirely absent in the writer's specimens from other localities except when secondarily derived from biotite in its chloritization.

Similarly, allanite may be seen to a very small extent. It is a black or dark brown mineral with a subhedral or anhedral form. In thin sections, this mineral is distinctly pleochroic from brownish yellow (X) to reddish brown (Y) or light yellow (Z), and its absorption is $Y > X > Z$. When the crystal is in contact with biotite flake, the former gives a striking pleochroic halo to the latter. Such optical characters can be determined in the specimens from near Rokusho where the porphyritic biotite granite frequently contains allanite crystals. Sometimes, they enclose minute apatite crystals and are occasionally characterized by a zonal structure. The writer similarly found allanite in the porphyritic biotite granites from Hirasawa and Jō-yama.

Geological Significance Suggested by Some Heavy Accessory Minerals

As has already been stated, granitic rocks of this district contain various kinds of heavy accessory minerals which have some features differing from place to place. One of these is indicated by zircon. This mineral is characterized by the occurrence of two different crystal habits, long prismatic or stout prismatic. Such types of crystals are to be commonly found in the Tsukuba-type granite including biotite or two-mica granite. In this case, long and sharp prismatic crystals are abundantly present as compared with those of another type. The Inada-type granite, on the other hand, is nearly free of elongated forms, although colorless and pink zircon crystals are co-existing as in the case of the Tsukuba-type granite.

As to the dissimilarities in crystal habits and colors indicated by zircon, the writer has already noticed them in several granites and associated gold placers in Hainan Island[15]. A similar idea has been proposed recently by Karakida[16] who discussed on the zircon zone at the contact of the Cretaceous granodiorite and granite. The same may be said of the zircon crystals contained in the Tsukuba-type and Inada-type granites which were supposed by Shibata to have successively

15) T. Ichimura, *Mem. Fac. Sc. Taihoku Imp. Univ.* [iii], **1** (1944), 126–128.
16) Y. Karakida, *Jour. Geol. Soc. Jap.*, **60** (1954), 517–532.

been intruded. Such difference of crystal habit as mentioned above is, however, unavailable in confirming the order of intrusion between these two types of granite.

As to the geological age of granitic intrusion in this district, there are some different opinions. Tomita applied his zircon method to the Inada-type granite exposed in the Toriashi district farther north, and he fixed its geological age as the Miocene. This had, however, already been discussed by Kawada[17] who supposed that its intrusion had taken place after the deposition of the Toriashi Group (Permian) and before that of the Torinoko Group (Jurassic).

Monazite is not a mineral so significant as in the case of zircon, because it shows the same crystallographical and optical characters in all the specimens of granitic rocks obtained from various localities of the Tsukuba district. It is, however, noteworthy that this accessory ingredient is more abundantly present in the contact aureole, particularly in the granitic rocks of the Hirasawa quarry, where they had remarkable contact effects on the Paleozoic sediments.

A quite similar tendency is shown by the distribution of apatite crystals whose amount is proportional to that of biotite. It is clearly indicated in the porphyritic biotite granite. The high frequency of monazite and apatite, therefore, suggests that these granites were once found close to the contact, if metamorphosed sediments were already eroded away from the contact aureole.

Garnet, titanite and allanite are, however, unimportant heavy accessory minerals having little bearing on the writer's present idea, because they are contained in quite neglible amount.

Summary

(i) Biotite granite or two-mica granite is extensively exposed in the Tsukuba district, where the Upper Paleozoic sediments were intensely metamorphosed by their large intrusive bodies. They are represented by the Tsukuba-type, Inada-type and Kamishiro-type granites which were successively intruded.

(ii) Of these, the Tsukuba-type and Inada-type granites were selected to investigate their heavy accessory minerals. These granites were crushed, and heavy accessory minerals were separated by using Thoulet solution.

17) K. KAWADA, *op. cit.* (1953), 256, 304.

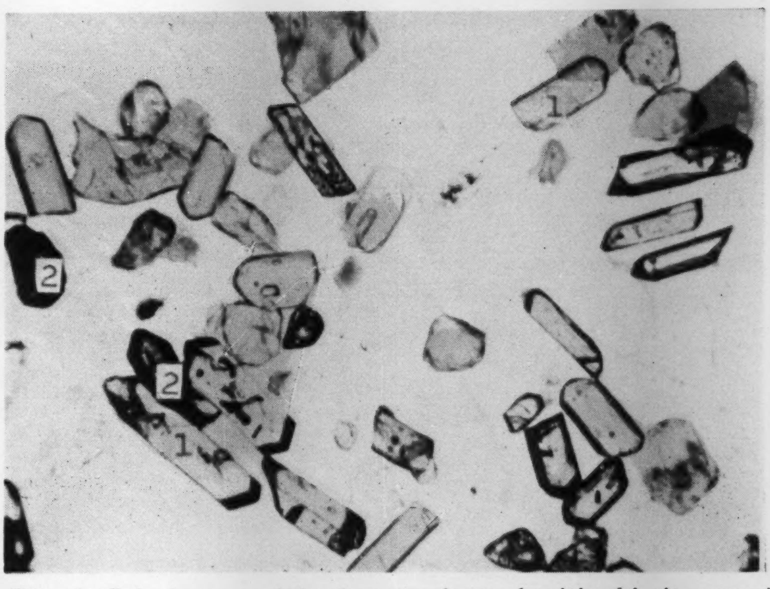

Fig. 2. Colorless or pink zircons of porphyritic biotite granite. (Hirasawa). ×100. 1=Colorless zircon, 2=pink zircon.
Tsukuba-type granite.

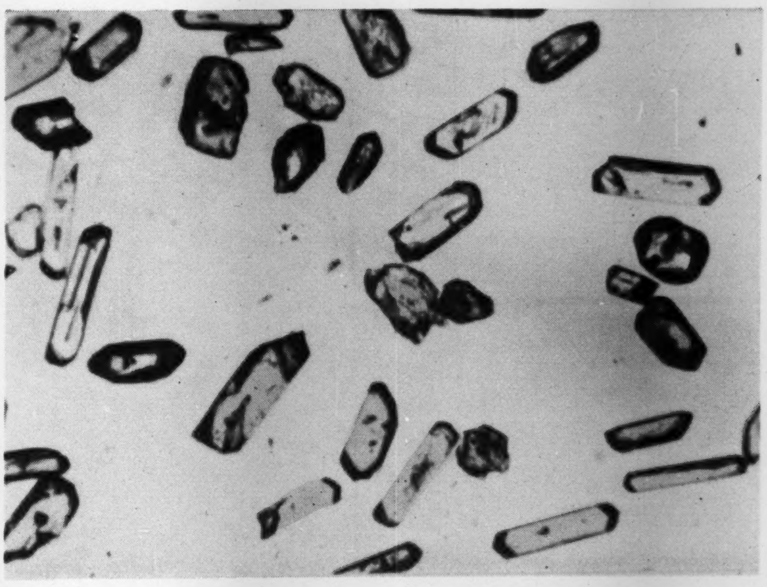

Fig. 3. Zircon crystals of two-mica granite. (Kankyosandaishi). ×100.
Tsukuba-type granite.

（震研彙報 第三十三号 図版 市村）

Fig. 4. Zircon crystals of biotite granite. (Kamiobata quarry). ×100. Inada-type granite.

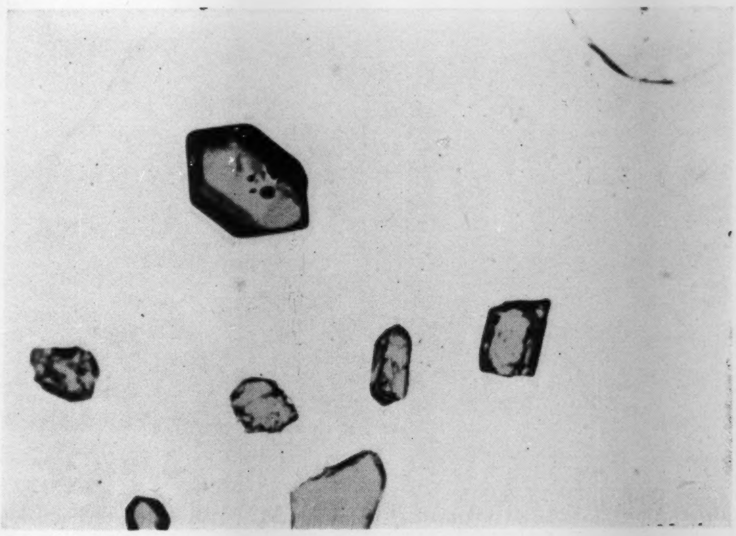

Fig. 5. Monazite crystal of porphyritic biotite granite. (Hirasawa). ×100. Tsukuba-type granite.

（震研彙報 第三十三号 図版 市村）

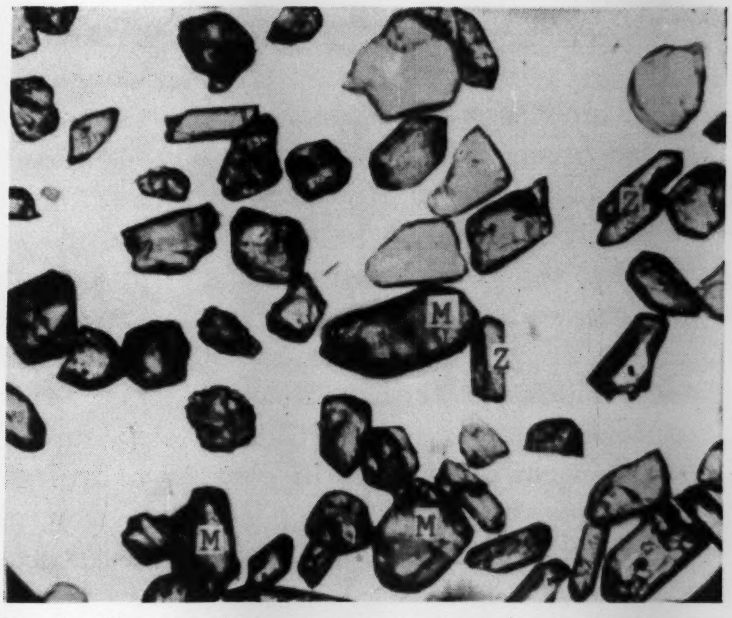

Fig. 6. Zircon and monazite crystals of porphyritic biotite granite. (Hirasawa). ×100. M=Monazite, Z=Zircon.
Tsukuba-type granite.

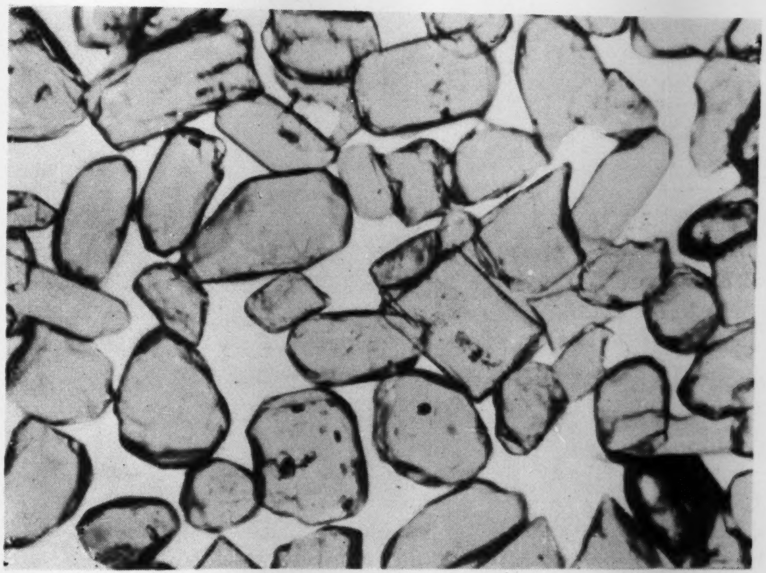

Fig. 7. Apatite crystals of porphyritic biotite granite. (Hirasawa). ×100.
Tsukuba-type granite.

（震研彙報 第三十三号 図版 市村）

(iii) The heavy accessory minerals thus obtained and examined are zircon, monazite, apatite, garnet, titanite and allanite. The amount of these minerals varies from place to place.

(iv) The commonest one is shown by zircon which has different crystal habits and colors even in the same specimen. The zircon taken out from the Tsukuba-type granite is characterized by the abundance of sharp and long prismatic forms. It is colorless and has a very clear appearance. On the contrary, that of the Inada-type granite is mostly represented by stout prismatic crystals which are occasionally rounded. Such difference in crystal form may be of use in clarifying the distinction between these two types of granite.

(v) Moreover, it is noteworthy that the same specimens contain colorless and pink zircon crystals together in various proportions. This is a common feature to be seen in the biotite or two-mica granite of the Tsukuba district. In such a case, it is, however, uncertain whether there are zircon crystals derived from Paleozoic sediments subjected to contamination.

(vi) Monazite and apatite are also important accessory minerals of granitic rocks exposed in the contact aureole. They are especially concentrated near the contact, where Paleozoic sediments are highly metamorphosed. In such a case, the frequency of apatite seems to increase in proportion to the amount of biotite.

---

26. 筑波地方産花崗岩の副成分重鉱物

山形大学　市　村　　毅

筑波地方に産する2種の花崗岩（稲田型花崗岩と筑波型花崗岩）に含まるる副成分重鉱物の中，ジルコン，モナヅ石，燐灰石，クサビ石，柘榴石，褐簾石などについて，顕微鏡下の研究を行つた．この結果，ジルコンは，貫入期を異にするこれ等両種の花崗岩を区別するに役立ち，又モナヅ石や燐灰石には，両花崗岩共，秩父系との接触部やそれに近い場所，或はその捕獲岩に富む場合に殊更集中する傾向があることを確めた．然し柘榴石とかクサビ石とか褐簾石には，斯る特徴が認められない．

(iii) The heavy accessory minerals thus obtained and examined are zircon, monazite, apatite, garnet, magnetite and ilmenite. The amount of these minerals varies from place to place.

(iv) The commonest one is shown by zircon which has different crystal habits and colors even in the same specimen. The zircon taken out from the Tsukuba-type granite is characterized by the abundance of sharp and long prismatic forms. It is colorless and has a very clear appearance. On the contrary, that of the Inada-type granite is mostly represented by stout prismatic crystals which are occasionally rounded. Such difference in crystal form may be of use in clarifying the distinction between these two types of granite.

(v) Moreover, it is noteworthy that the same specimens contain colorless and pink zircon crystals together in various proportions. This is a common feature to be seen in the Inada as the same granite of the Tsukuba district. In such a case, it is, however, uncertain whether there are zircon crystals derived from Paleozoic sediments subjected to contamination.

(vi) Monazite and apatite are also important accessory minerals of granitic rocks exposed in the contact aureole. They are especially concentrated near the contact, where Paleozoic sediments are widely metamorphosed. In such a case, the frequency of apatite seems to increase in proportion to the amount of zircon.

[illegible]

27. *Triggered Magnetic Tape Recorder for Routine Seismic Observations.*

By Syun'itiro OMOTE, Setumi MIYAMURA and Yoshio YAMAZAKI,

Earthquake Research Institute.

(Read June 22, 1954.—Received June 30, 1955.)

1. Introduction

Until recently, mechanical recording system using a smoked paper has been prevailingly adopted in most Japanese seismological stations, owing to its simple treatment and its cheap expense for routine operations.

As it became more necessary to have sensitive seismographs and to put more accurate timemarkings on the record, optical recording systems had to be introduced also in our routine observations. Needless to say, high sensitivity is easily obtained by using the mechano-optical seismographs, and much more higher sensitivity is attained by electromagnetic and electronic seismogaphs with oscillograph recorders. By means of these systems, it is expected that much more informations on the nature of earthquake motions can be obtained than by the former methods of recordings.

However, large amount of photographic films or bromide papers must be consumed when these methods are introduced in the routine observations. Of course, some techniques can be introduced to minimize these defects by focussing the light spot on the film as sharply as possible and recording it on the standard film of 35 mm width. T. Hagiwara and his collaborators have already succeeded in developing this standard film recording device in their routine observations.

On the other hand, also for the purpose of economizing the expense of bromide papers, it is suggested to introduce the trigger device in the recording system. But by the ordinary way of recordings with a starter attached to the seismometer, it is inevitable to miss the very beginning part of the earthquake motions, even if the sensitivity of the starter may be extremely sensitized. These disadvantages will be put aside if we introduce a memory device in the recording of earth-

quake motions. Since 1949 we have adopted the idea of taking up the commercial magnetic tape recorder for the triggered seismograph.

This method has more excellent characteristics than the mechanical and mechano-optical recording method. Mechanical seismographs heretofore in use were limited either in their frequency ranges capable of being registered or in their amplitude ratio of the smallest to the largest. The electro-magnetic type seismographs were somewhat improved in these characteristics, but anyhow these seismographs heretofore in use can supply only a record which was almost irrepeatable. As compared with these circumstances the case becomes quite different if we use the magnetic tape recorder as a new means for the registration of earthquake waves. Magnetic recordings can cover these defects by storing the seismic energy in broad-band frequency ranges, and by playing back the recorded tape we can have a nearly perfect facsimile of the seismic signals repeatedly.

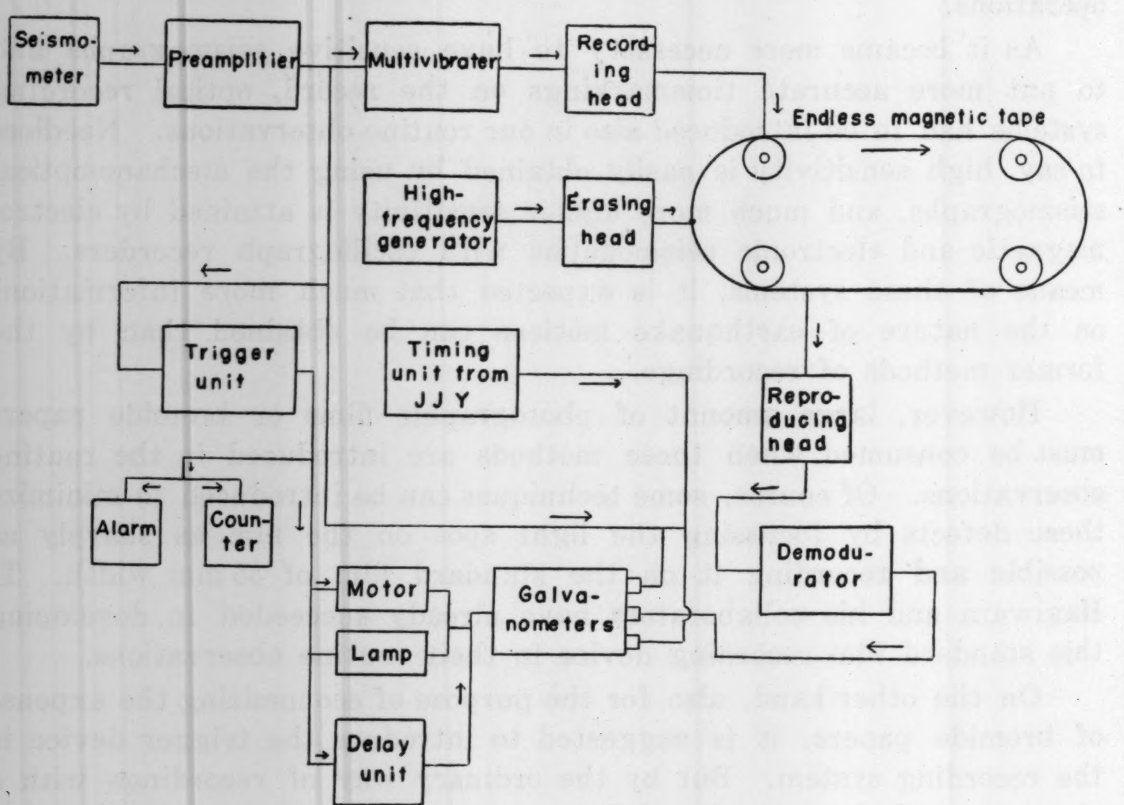

Fig. 1. Block diagrams of the equipment.

The play-back from the tape is electrical in form and can be led

into the differential, integral, bandpath filter circuits or combinations of these circuits, and makes it possible for the analyst to repeat more detailed analysis.

In Johannesburg, South Africa, Gane and others[1] have devised and constructed a new equipment with a long endless magnetic wire as a delay unit. With this equipment they succeeded as early as in 1948 in getting a good recording of the earth tremors in the vicinity of Witwatersrand. In our country, Tomoda and Aki[2] have constructed a seismometer which can record earthquake motions on a magnetic tape by means of the area type recording device. We have constructed a seismometer that records on the magnetic tape by means of the density type recording device. It was possible for us to construct the equipment in portable size, because it used magnetic type, not wire. The equipment has been in use for more than one year smoothly, and it seems very adequate for the routine observations of earthquake motions. So somewhat detailed descriptions of the equipment shall be given here.

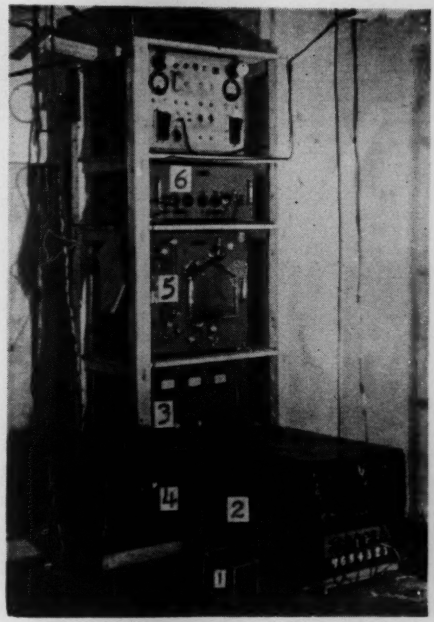

Fig. 2. General appearance of the equipment. 1, seismometer. 2, recording oscillograph. 3, power supply. 4, stabilizer. 5, endless magnetic tape. 6, preamplifier modulator and demodulator. 7, alarm and counter units.

2. Details of the equipment and its working characteristics

a. Introduction. The general idea of the equipment is illustrated schematically by the block diagram in Fig. 1 and its appearance is shown in Fig. 2. Input signals from a seismometer, being amplified by the preamplifier, modulate the frequency of the carrier waves of 800 c/s. Then the frequency modulated carriers are led to the recorder head. These signals are here recorded on the endless magnetic tape which runs with the velocity of 3.75 ips (9.53 cm/s). The tape that passes through the recording head reaches some times later to the reproducing head where the seismic

1) P. G. Gane, H. J. Logie and J. H. Stephen, *Bull. Seis. Soc. Amer.*, **39** (1949), 117.
2) Y. Tomoda, K. Aki, *Zisin* (*Jour. Seism. Soc. Japan*), [ii] **5** (1952), 132.

signals are picked up and led to the demodulation circuit. The circuit diagrams of these electronics parts are shown in Figs. 3–a, b, c. The demodulated current is conducted to a low resistance galvanometer, and rotates the mirror attached to the string of the galvanometer. Thus the record of seismic signals is reproduced on a photographic paper. The endless magnetic tape that passed through the reproducing

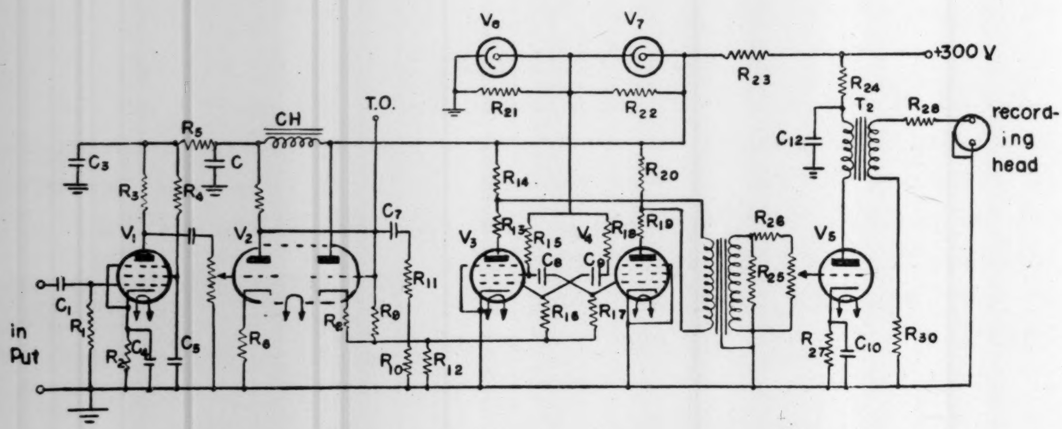

Fig. 3–a. Circuit diagrams of preamplifier and modulator.

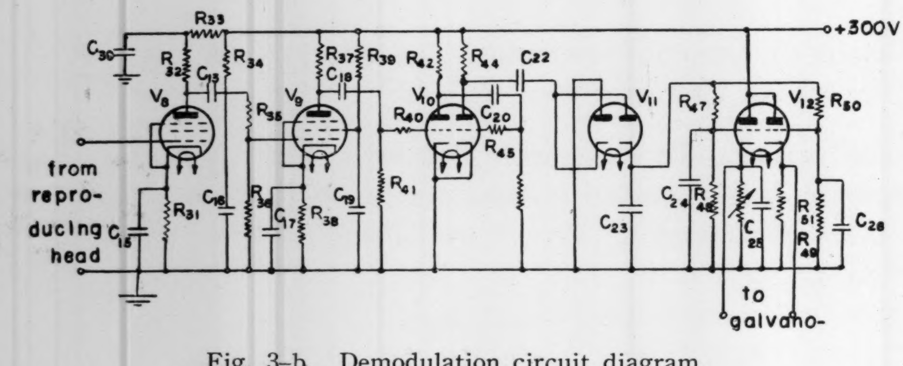

Fig. 3–b. Demodulation circuit diagram.

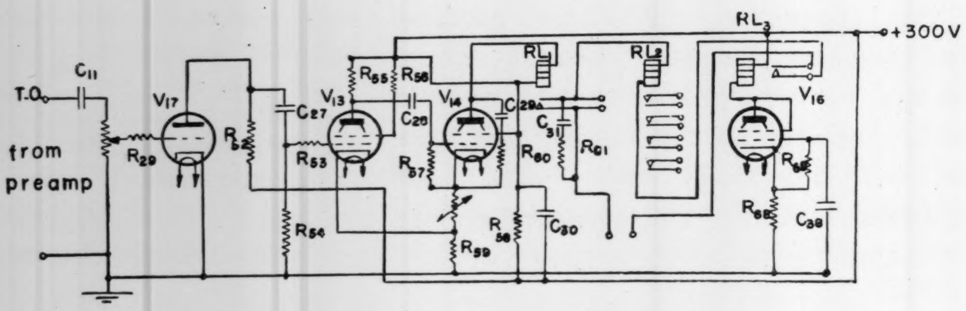

Fig. 3–c. Trigger circuit diagram.

head goes round and just before coming back again to the recording head, the tape passes through an erasing head where it is cleaned out and a new tape is supplied always to the recording head.

The galvanometer and recording camera assemblage is not in operation continuously. The trigger circuit which is connected to the preamplifier, is operated by the seismic signals and starts on one hand the driving of the recording camera, and on the other hand operates a delay circuit, which after a lapse of about three minutes, plays automatically the role of a stopper for the recording assemblage.

Thus the routine observations of earthquakes are carried on.

b. Preamplifier. As seen in Fig. 3-a, this part of the equipment is an ordinary low frequency amplifier, the characteristic curves of which are illustrated in Fig. 4. When a known voltage of a constant frequency is applied to the input of the preamplifier, the output current from it will deflect the recording galvanometer, provided the latter is directly connected to the former. In Fig. 4, which shows the relation between the input voltage and the amplitude of the deflection of the galvanometer, we see also that the difference of frequencies exerts little effect on the output amplitude within the range from 5 to 50 cycles.

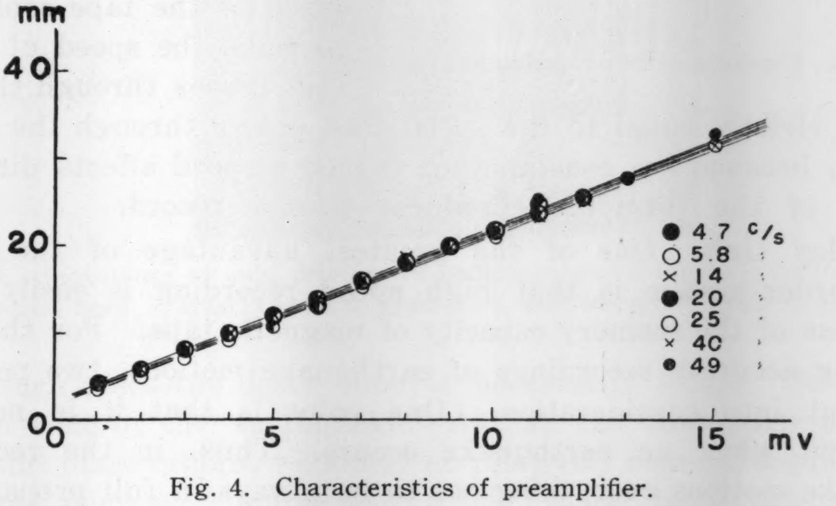

Fig. 4. Characteristics of preamplifier.

c. Modulation Circuit. As the frequencies of the seismic waves are extremely low, it cannot be clearly recorded directly on the magnetic tape, so we must introduce a system to modulate high frequency carrier waves by the input signals. As the frequencies of ground movement to be handled range from one to fifty cycles, the center frequency of

the carrier wave was taken at 800 cycles. As seen in the circuit diagram in Fig. 3, 800 c/s carrier wave is generated by the V_3 and V_4 multivibrators and in turn the frequency of this carrier wave is modulated by the output voltage from the preamplifier that is led to R_{12}. The characteristic curve of this modulation circuit is seen in Fig. 5. We see from Fig. 5, that the input voltages less than 30 mV are modulated without distortion, and that the deviation of frequency that is deduced from the input voltage of 3 V to V_2 amounts to 200 cycles.

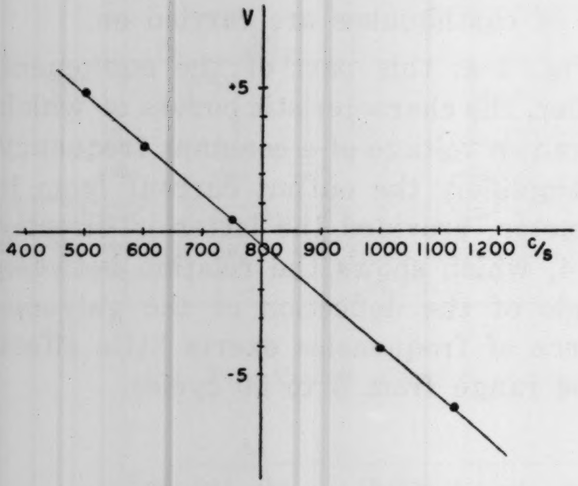

Fig. 5. Characteristics of modulator.

d. Recording Head and Reproducing Head. The carrier waves from the multivibrator are modulated in frequency by the signals to be recorded, and are recorded on the magnetic tape through recording head, then they are picked up by the reproducing head. With respect to these frequency modulation systems it becomes a factor of great importance to keep the speed of the tape constant and to make the speed of the tape that passes through the recording head strictly equal to the speed that passes through the reproducing head, because the constancy of the tape speed affects directly the accuracy of the form of reproduced seismic record.

e. Delay Unit. One of the greatest advantage of the magnetic tape recorder system is that high speed recording is easily obtained by the use of the memory capacity of magnetic tape. For the purpose of making accurate recordings of earthquake motions, two points have to be put into consideration. One point is that it is not known beforehand when an earthquake occurs. Thus, in the recording of earthquake motions everything has to be always in full preparation for recording. The second point is that the record of the earthquake motions has to be taken in a form fit for higher analyses. From this reason the paper speed of the seismic record becomes a matter of great importance.

In order to settle the first point, we adopted an endless tape system, in which the tape is running all day long and everything stands ready

for the recording, and to settle the second point, the magnetic delay system was introduced. One of the final products of our system is a seismic record, photographed on a bromide paper that was driven at the highest possible paper speed. After the trigger operation of the trip circuit it takes only a few seconds for the whole apparatus to become ready for the recording, including the stationary running of a photographic paper. The next problem is to adjust the start of the trigger circuit. The very beginning part of the P waves is, in some cases, very small in their amplitude, so that if we adjust the trigger level so high as to start with the week beginning waves of P, a false start may frequently be caused by the ordinary background noises. To make them free from these false starts the trigger levels have to be made somewhat lower, but then it happens that the trigger circuit misses the week P and starts at the beginning of the large S phase.

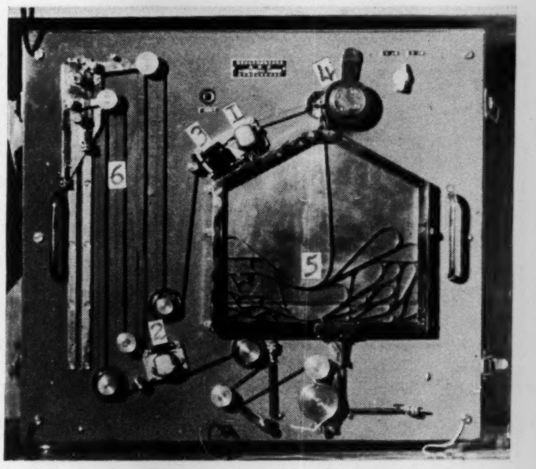

Fig. 6. Appearance of unit, driving the endless magnetic tape. 1, recording head. 2, reproducing head. 3, erasing head. 4, capstan. 5, tape storage. 6, endless magnetic tape.

In such cases the delay time is necessarily longer than the P–S duration time of the earthquake. As, at the first step of our experimental observations, we aimed at relatively near earthquakes, it was considered that one minutes and a half would be sufficient for such delay time. As is mentioned above, the tape speed is 3.75 in/sec (9.53 cm/sec) in order to give the delay time of 90 sec., it is necessary to have the store of the magnetic tape as long as eight meters.

To devise a mechanism capable of storing such a long tape was a difficult point. We succeeded in overcoming this difficulty by constructing a device as seen in Fig. 6. This is a box twenty centimeters

square with a thickness of about one centimeter, that is to say, just a little wider than the width of the magnetic tape. As shown in the figure, this box, having its surface made of plane glass and facing vertically, has two slits, one at the upper side and the other at the lower side and through them the tape goes in and out. The magnetic tape that has passed through the recording head is driven into the box from the upper slit and goes down by its body weight piling up in the box as may be seen in the photograph in Fig. 6. The thickness of the box is so constructed as to be only a little wider than the width of the magnetic tape, so the tape piles up in good order and never becomes entangled in the box, going out in turn from the down (lower) slit very smoothly. In the box, the tape piles on succesively showing a natural curve as seen in the photograph, and through the lower slit the tape goes out from the box.

By means of this mechanism it is easy to store up a tape of more than ten meters.

f. Demodulation system. The output voltage picked up from the reproducing head is amplified by the square wave amplifier. Then passing through the differential circuit the numbers of waves are counted and thus the output current from the recording head is demodulated and as the time constant of the grid of V_{12} is 0.5 sec. these demodulated current produces the deflection of galvanometer that is proportional to the output current from the seismometer. As is illustrated in Fig. 7, 200 cycles of deviation of modulated frequencies generates an output of 1.5 mA.

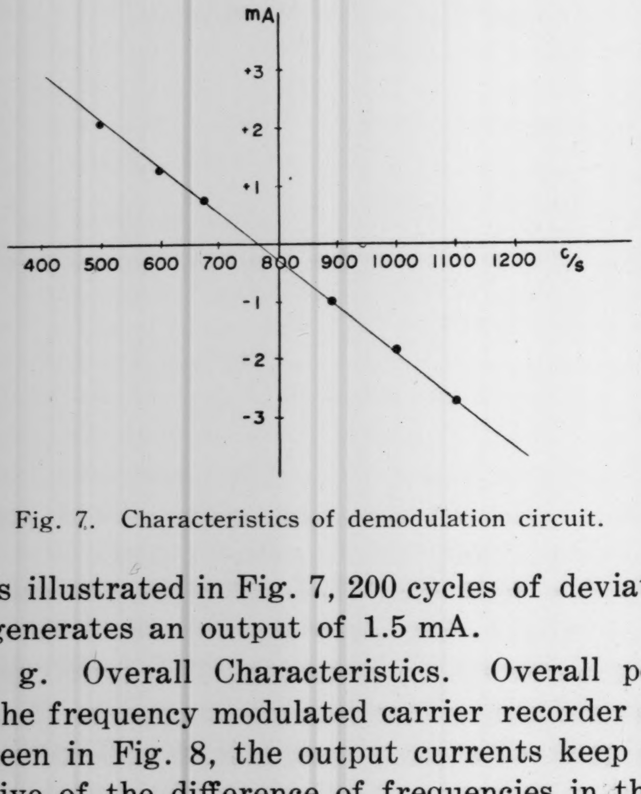

Fig. 7. Characteristics of demodulation circuit.

g. Overall Characteristics. Overall performance characteristics of the frequency modulated carrier recorder are illustrated in Fig. 8. As seen in Fig. 8, the output currents keep up a constant value irrespective of the difference of frequencies in the low frequency range, while they decrease in the somewhat higher frequencies.

h. Erasing circuit. After passing through the reproducing head the tape is erased at the erasing head that is placed just before the recording head. In this endless system of ours, the tape may be erased and re-recorded on each cycle and thus it can continue recording even if the duration of an earthquake motion happens to be longer than the whole cycle of the tape. Erasure is done magnetically.

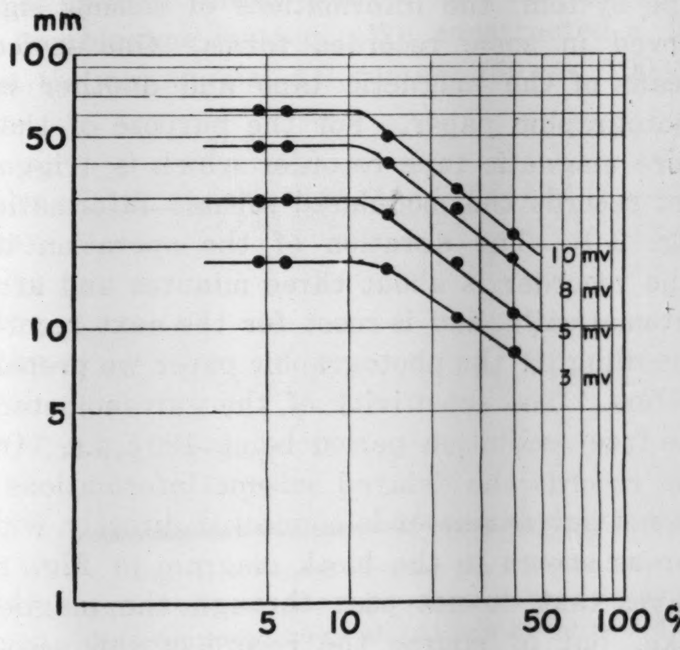

Fig. 8. Over-all frequency characteristics.

i. Trigger Circuit. A part of the output current of the low frequency amplifier is led to the trigger circuit. In Fig. 3–c, V_{14} is normally conducting a current, while by the input signals from a seismometer, the plate current of the tube V_{13} will be increased and this in turn causes V_{14} to be cut off and at the same time this makes work the relay RL_2, which works on the recording circuit. The relay RL_1 will be reset in about 10 seconds. The sensitivity of the trigger circuit that makes the trip on will be adjusted by VR_3 as shown in Fig. 9. In the frequency range from 3 to 30 c/s, differences in frequency hardly affect the voltage that makes the trip on. The minimum input voltage for the trigger circuit is 0.5 mV.

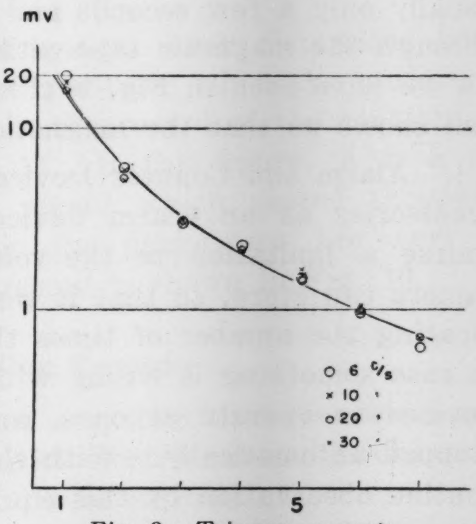

Fig. 9. Trigger current
Abscissa represents the scale number of the input dial plate of the trigger unit.

j. Timing. In the routine observation timing is an important factor. Our equipment is not yet constructed so as the time signals and seismic signals can be recorded on the tape simultaneously. One of the galvanometers of the oscillograph records

the JJY time signals. This timing device will be improved in the near future.

k. Recording Devices. So long as we use the endless magnetic tape system, the informations of seismic signals will have to be preserved in some recorded forms. One device is to preserve them by means of the magnetic tape and another is to record them on the photographic paper. For the purpose of the former, we prepared one more magnetic tape recorder which is triggered by the seismic pulse and records the modulated seismic informations from the amplifier in Fig. 3-b. The duration of the operation time of this 2nd magnetic tape recorder is about three minutes and after that it stops operation automatically, and is reset for the next recordings. For the purpose of recording on the photographic paper we prepared three-element galvanometers. The sensitivity of the galvanometers is about 6.7×10^{-6}A/mm, the free oscillation period being 100 c.p.s. Of the three galvanometers one records the delayed seismic informations mentioned above, and the second galvanometer is connected directly with the output of preamplifier as shown in the block diagram in Fig. 1, and records the seismic waves that do not pass through the magnetic tape for comparison's sake, but of course the record of this second galvanometer lacks the beginning part of the earthquake motion. But the missing part is usually only a few seconds and we can compare the record that passed through the magnetic tape with the record that did not pass through it. As we have seen in Fig. 10 (Plate) the two is quite similar to each other and shows us that the magnetic tape does not distort the seismograms.

l. Alarm and Counter Device. It is also important to prepare such accessories as an alarm device and a counter device. There is of course a limitation to the volume of bromide paper the oscillograph camera can store, so that it would be effective to device a circuit indicating the number of times the trigger circuit had operated. Next, in case something is wrong with the equipment, the alarm circuit is deviced to operate at once, and all the runnings of the equipment is stopped automatically. With these devices we are able to continue the routine observation by this equipment.

m. Power Supply. Our equipment was designed and constructed to carry out the routine observation of earthquakes. Thus, excepting the galvanometers and their recording parts, all other parts, for examples, the driving part of endless magnetic tape, the low frequency amplifiers, the modulation and demodulation circuits etc., are in operation all day

long unceasingly. It becomes a very important requirment to have a power supply without batteries. Needless to say it is very useful to have a battery as the heat source of the first-stage tube of the amplifier and some dry batteries as high-voltage sources, but the maintenance of these batteries is a troublesome matter. We constructed a power supply, fed wholly from the commercial AC current (50 cps, 100 volts). In the case when we use the AC 100 volts as a heater source of the tubes, however we may rectify them, some ripples remain and become the source of hums, and the fluctuations of the voltages of the source power generate some disturbances. We used balast tubes and other means to get rid of these undesirable effects as much as possible.

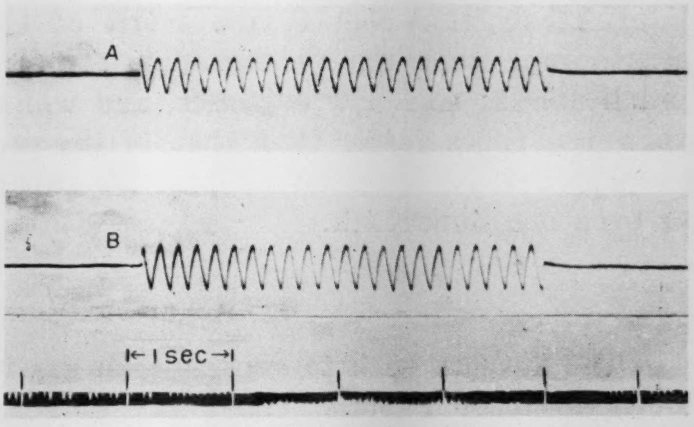

Fig. 11. Record showing the fidelity of the tape recorder system. An alternating voltage is applied to the seismometer terminal. (A) is a direct record through the preamplifier. (B) is a record passing through the entire channel, including the magnetic delay unit.

n. Recordings obtained. So long as we adopt the F–M system some distortions between the input and output wave forms is inevitable when the uniformity of tape seed is disturbed. To check this, the record of the constant input from an oscillator is shown in Fig. 11. In this figure, A is a record from the preamplifier and B is a record which passed through the magnetic tape. As may be seen in the figure two are very much alike. An example of the seismic record is shown in Fig. 10.

3. Concluding Remarks

We have described in this report a system that connects a seismometer and a magnetic tape recorder with electric cables. In the comming report the wireless linked systems will be reported.

The equipment here described is easy to maintain and the operating expenses are negligibly small, except for the bromide paper. Magnetic tape is replaced once a week but the expense is very light, the consumption of vacum tubes is negligible, the magnetic heads are not yet worn at all.

Through this mangetic tape recorder seismograph we obtain two sorts of records of earthquake motions. One is the magnetic tape in which the seismic signals are converted into the variation of the magnetic density of a layer of iron oxide on a recording tape, and the other is the bromide paper on which the seismic wave is photographed as an oscillation curve.

Setting aside the magnetic tape on which are recorded the seismic informations, it is still to the merit of this magnetic tape recorder seismograph that the photographic recording of the seismic waves is practicable at such low expenses, and while the paper speed is more than ten times faster than that of the ordinary photographic seismographs, the consumption of bromide paper is only about one tenth or even one hundredth.

4. Acknowledgement

The authors wish to express their gratitude to Professor M. Hirata, Department of Physics, University of Tokyo for his kind advices and encouragements offered in the course of this study. Our best thanks are due to the Tokyo Tsushin Kogyo Co. Ltd. for the hearty cooperation given in the construction of this equipment. We also appreciate the valuable advices from Mrs. T. Asada and N. Den given to us in the course of this study. To Dr. N. Nasu and Dr. H. Tsuya, the director and the ex-director of our Institute our hearty thanks are also due for their encouragements. A part of the expense of the present study was defrayed from the budget of the Observation Branch of our Institute, and we express our indebtedness to Professor Takahiro Hagiwara, the Head of this Branch. The other part of the expense of the present study was defrayed from the Fund of the Experimental Scientific Research from the Ministry of Education.

---

27. 地震観測用磁気テープ利用ひきがね式遅延記録装置

地震研究所 表 俊一郎
宮村摂三
山崎良雄

南アフリカの GANE らが Witwatersrand の rock-burst を研究するために長い磁氣録音鉄線の無終端ループをはりめぐらして，ひきがね式の遅延記録装置をつくり，無線方式による遠隔記録をもちいて，画期的な局地的地震観測網の運転に成功したのは数年前のことである．われわれも時をおな

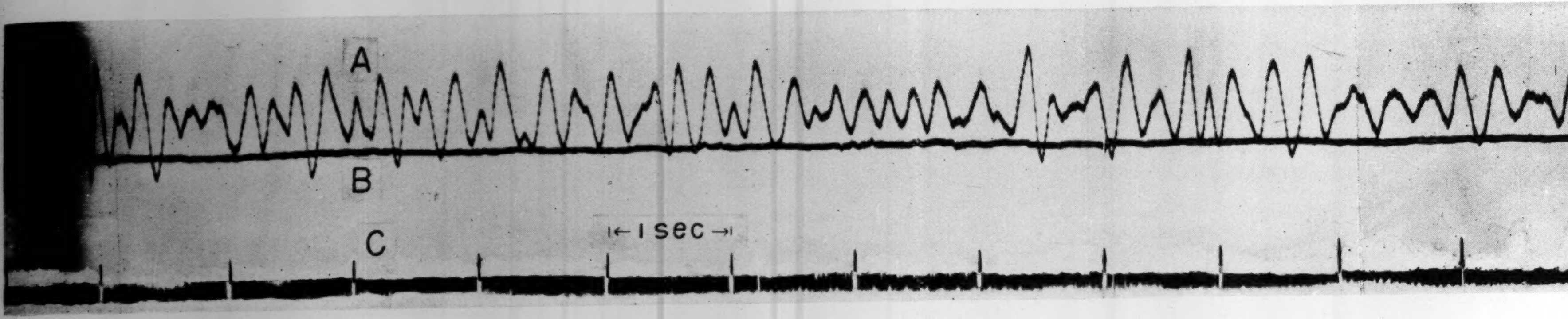

(震研彙報 第二十三号 図版 表・宮村・山崎)

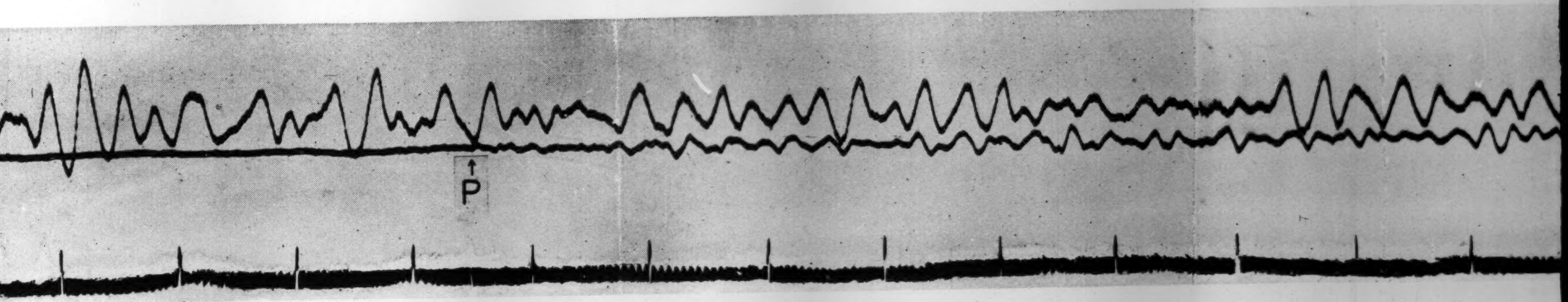

Fig. 10. An example of the typical seismog
including the magr

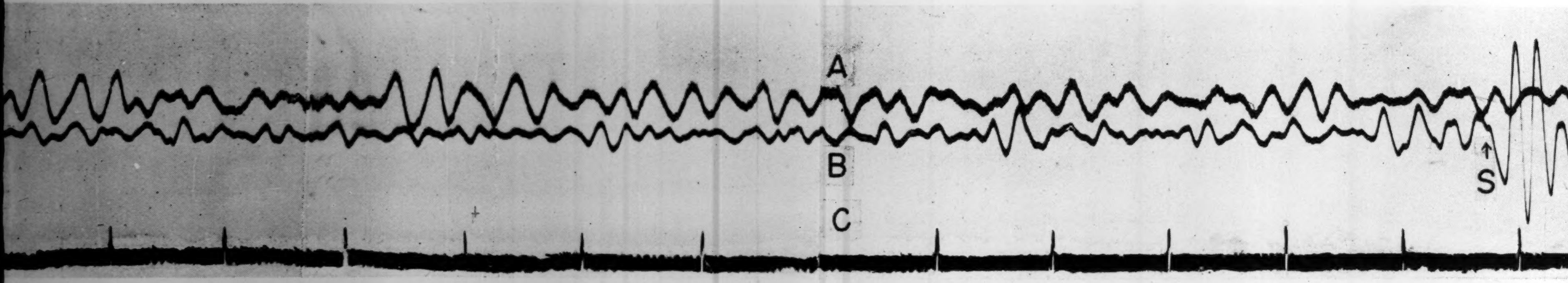

Fig. 10. An example of the typical seismogram. (A) is a direct record through the preamplifier, (B) is a record including the magnetic delay unit, (C) is a timemarking from the JJY time signal. (1/2

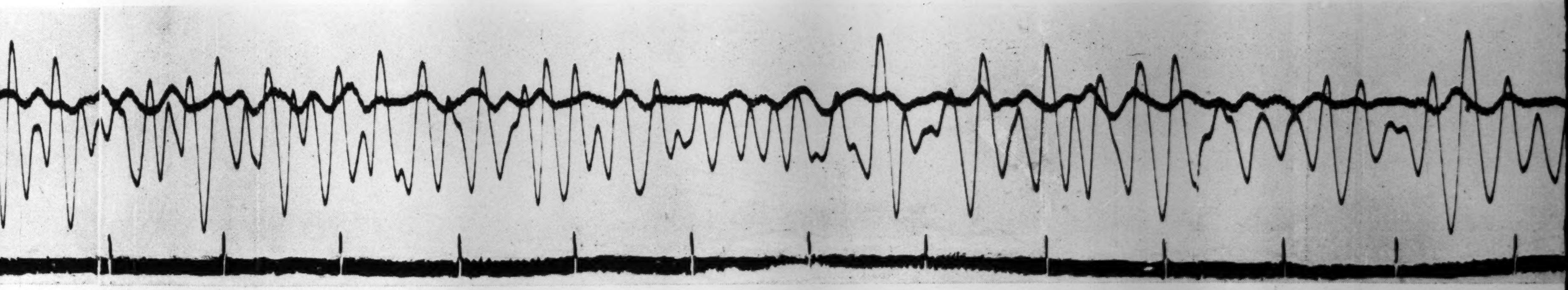

cord passing through the entire channel,
1/2 the actual)

[I

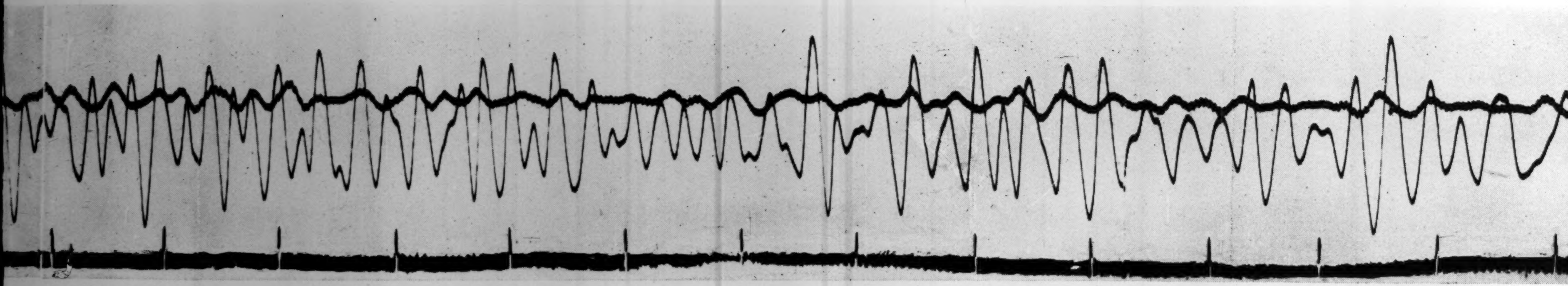

passing through the entire channel,
he actual)

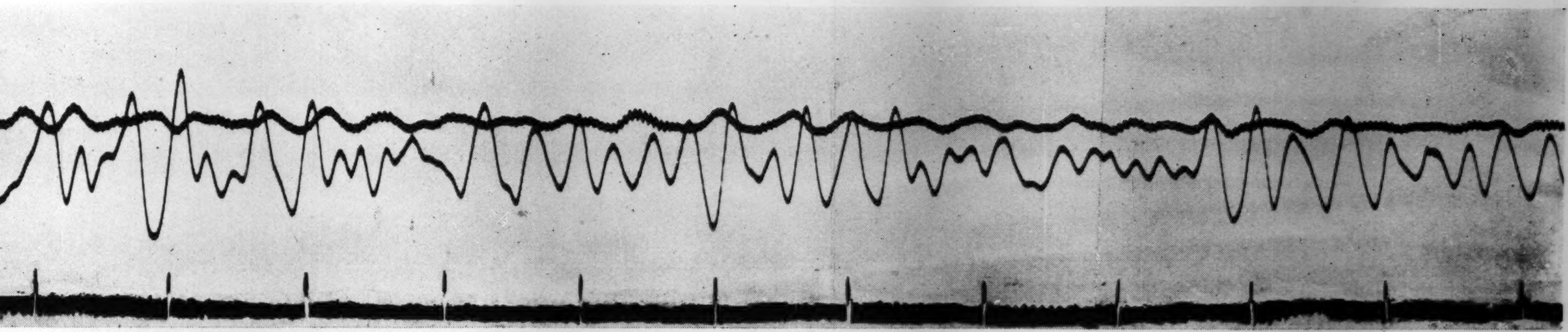

じくして，同様の方式により観測装置の研究をはじめたが，ここには無線及び有線搬送による遠隔記録の部分は，別に報告することとし，約1年あまりまえから常時的観測業務にたえる装置として働くようになつたひきがね式遅延記録装置の部分についてその大要をのべることとした.本装置がGANEらのものとことなる要点は，磁氣録音鉄線の長いループをはりめぐらす代りに，市販の磁氣録音テープを無終端のループとして小さくまとめ，箱の中にためてうまく流し，遅延の目的を達するようにして全体を可搬型にしたことにある．遅延時間の調整もある程度自由に出来て便利になつている．また地震計としては GANE らが容量変化型の換振器をもちいているのに対し，可動線輪動電型換振器をもちいているので，低周波増幅部はおのづからことなつている．録音方式は，補助搬送波 800 c./s をもちいて，ほぼ同様の回路によつている.

装置の構成は第1図の模式図にまたその外観は第2図の写真にみられるとおりである.磁氣テープの速度は 3.75 i.p.s.，遅延時間すなわちテープが録音ヘッドと再生ヘッドとの間を通るに要する時間は 30 秒から 90 秒まで自由に調節できるので希望の遅延時間を与えて観測を行いうる.

ひきがね式遅延記録装置の地震観測装置としての特徴は，記録紙速度のはやい，従つて時間精度のすぐれた記録を経済的にとることができることであり，又特に本機においてはたとえ P 振巾が小さくて S あるいはその他かなり大きい振巾の位相の地動で始めてひきがねがひかれても，その地震動の P が始まる少しまえからの記録がとれるので，一定の規準以上の振巾のものだけを記録することが出来るという便がある．本所において1954年3月以降ほぼ連続運転しており，記録の1例は，第10 図の写真にかかげてある.

本装置の開発については，東京通信工業株式会社の努力におうところが多いので，特にしるして感謝の意を表したい．また東大地球物理教室浅田敏，田望両氏にも御協力を得たので感謝する．本装置試作の経費は主として (1) 筆者らに与えられた文部省試験研究費および (2) 地震研究所に対する国際的地震観測網に寄与する特別事業の施設整備費によるものであり，前者については東大理学部平田森三教授，後者に関しては本所観測部長萩原尊礼教授に対し厚くその御配慮を感謝するものである.なお，終りに本研究に対し終始支持と激励を与えられた那須所長および津屋前所長に感謝する.

28. *Experimental Studies on the Mechanism of Generation of Elastic Waves V.*

By Keichi KASAHARA,

Earthquake Research Institute.

(Read Apr. 26, 1955.—Received June 29, 1955.)

1. Introduction

There are many problems in the practical field of seismology which may be idealized as the generation of elastic waves from an origin embedded deep (or not so deep) in a semi-infinite elastic body. Theoretical and experimental works carried out on the origin lying on the surface or embedded quite deep in the body are of much use in these cases. However, the existence of the seismic origin beneath—but not so far apart from—the free surface of the body must have some special effects, which can not be interpreted by the above-stated works only.

Since the well-known work of Nakano[1)], several studies have been made mathematically[2)] from the above-mentioned standpoint, while we have few experiments made either to prove the results of mathematical ones or to find the correspondences between theories and practical fields[3)]. Model experiments on the laboratory scale seemed to be quite useful for the present purpose, and that was the reason why the author undertook laboratory studies, a part of which will be shown in this paper.

2. Systems of experiments

Generation of elastic waves were made in the block of the low velocity material—solution of agar-agar[4)], and observations were carried out on its free surface in vertical component. The whole system of the experiment is shown in Fig. 1. In the inside of the block (90cm long, 30 cm wide, and 30 cm deep) is embedded a cylindrical cavity as

1) H. NAKANO, *Jap. Journ. Astron. Geophysics*, **2** (1925), 233.
2) K. SEZAWA, *Bull. Earthq. Res. Inst.*, **6** (1929), 1, *etc.*
E. R. LAPWOOD, *Phil. Trans. Roy. Soc. London, Ser. A*, **242** (1949), 63.
M. NEWLAND, *Phil. Trans. Roy. Soc. London, Ser. A*, **245** (1952), 213.
3) *f.i., Research Group Explo. Seis. Report,* No. 9 (1954), 14.
4) K. KASAHARA, *Bull. Earthq. Res. Inst.*, **30** (1952), 259.

the origin. The cavity has the dimension of 20 cm in length and 0.6 cm in radius, and is bounded from the surrounding solution of agar-agar by a thin film of rubber. The compliance of the film is high enough

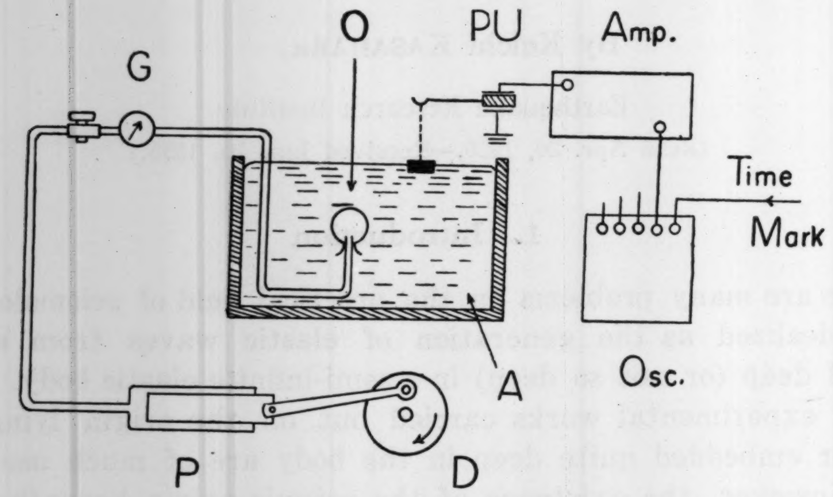

Fig. 1. System of experiments.

A: block of agar--agar, O: origin of disturbances (cylindrical shape), G: pressure gauge, P: air pump, D: driver PU: pick-up Amp.: amplifier Osc.: oscillograph

not to obstruct transmission of the inside pressure of the cavity to the surrounding medium. The pressure in the cavity is excited impulsively with an air pump, and its change in time can be measured with a piezo-electric gauge attached to the connecting pipe.

Fig. 2. Travel time curve.

Displacements of the surface are detected by piezo-electric pick-ups connected with thin fibre to marks placed on the surface. Out-puts from pick-ups are amplified by low frequency amplifiers and recorded by a multi-elements oscillograph, with the pressure change and time marks at the same time. Calibrations

of electronic systems show that recorded traces of oscillograms can be considered as indicating the velocity of vertical movements of the surface.

3. Results and discussions

We have to know, first of all, the elastic properties of the material under our test, which was so prepared as to have the lowest possible velocities. The travel time curve, Fig. 2, was obtained by applying impulsive pressure to the origin (focal depth: 1 cm). This and other tests[5] indicate the properties of the material being as follows:

	velocity of longitudinal wave	275 cm/sec,
	velocity of free surface wave	102 cm/sec,
and	density of the solution	1.0 g/c.c.

In the course of experiments, observations were made only at points of epicentral distances, 0, 5, 10, 15, 20, 25, and 30 cm. In some cases, disturbances of velocity 102 cm/sec showed remarkable reflection at the side wall of the vessel (Fig. 13), and travel times of these reflected events observed at the said points were used supplementally to draw Fig. 2.

Experiments were made by changing the depth of the origin from 8 to 0 cm. That is, when one set of experiments was finished for a certain focal depth, the surface layer of the block of 2 cm in thickness was taken off before the next step. In this way, effects of changing focal depths could be investigated without changing any of the other conditions.

To the cavity in the block is applied an impulsive pressure of the same duration and of the same maximum value in each experiment (Fig. 13). We know that generations of disturbances are so reproducible that recorded traces can be compared with each other, and Figs. 3 and 4 show representative ones which were obtained by arranging several sheets of oscillograms recorded under the corresponding condition of the origin, respectively. In each case, the epicenter showed a simple impulsive movement followed by slight oscillatory movements, while at points somewhat apart from the epicenter appeared more complicated features, which may be explained as the combination of two series of events: one corresponds to a phase propagating from the origin with the velocity of 275 cm/sec and dissipates rapidly with distance,

5) K. KASAHARA, *loc. cit.*.

while the other appears to be a phase with the velocity of 102 cm/sec and is still remarkable at distant places. The former can be considered as the longitudinal wave from the origin and the latter as the free surface wave of Rayleigh type. The fact that the phase of 102cm/sec shows the linear travel-time curve running from the origin of the coordinates will confirm this interpretation. Figs. 5 and 6 illustrate this result more clearly.

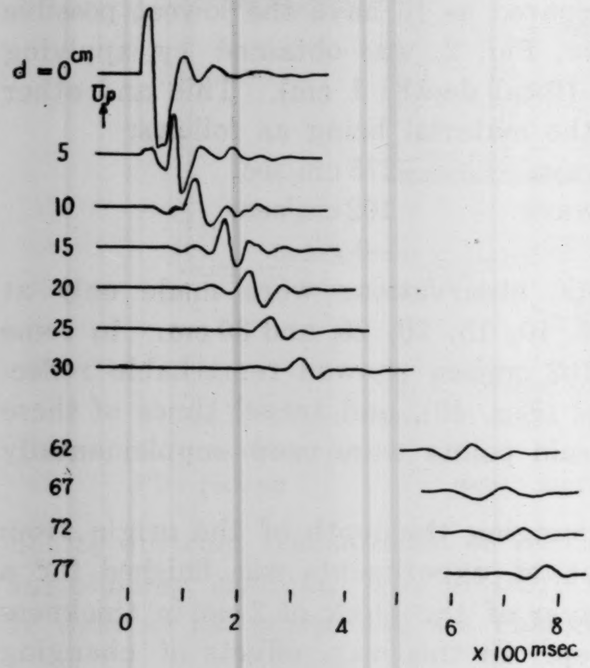

Fig. 3. Traces of disturbances on the surface. Focal depth: 2 cm.

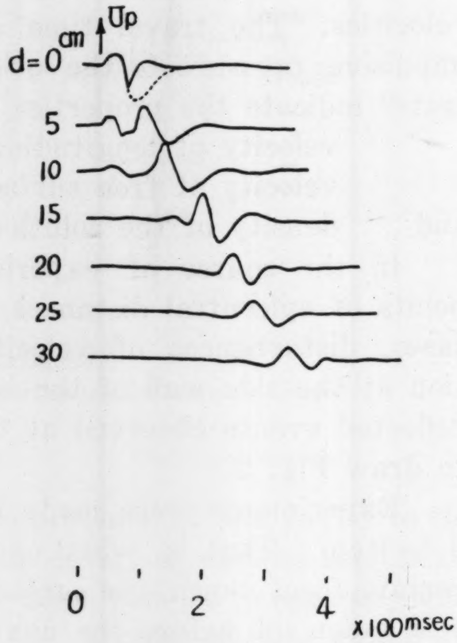

Fig. 4. Traces of disturbances on the surface. Focal depth: 6 cm.

According to the theory of Lapwood, the main shock will show downward initial movement at surface points distant from the origin, when the pressure in the origin increases suddenly (initial P-pulse)[6]. The present result seems to agree with his prediction as well as with the theory of Takeuchi and Kobayashi[7], who carried their study to the phenomena at surface points very close to the epicenter. They showed how the phase of the main shock develops from its primitive form (non-periodic) at the epicenter to its final form (Rayleigh wave) at distant places. From their results, we can easily infer the time derivative of

6) E. R. LAPWOOD, *loc. cit.*

7) H. TAKEUCHI and N. KOBAYASHI, *Annual Meeting of Seis. Soc. Japan*, 1955. (unpublished).

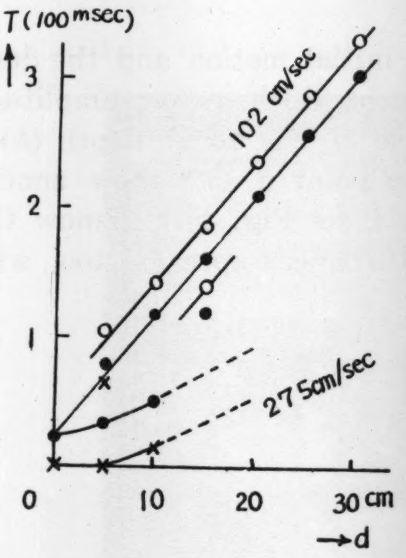

Fig. 5. A part of travel time curves.
Focal depth: 2 cm.

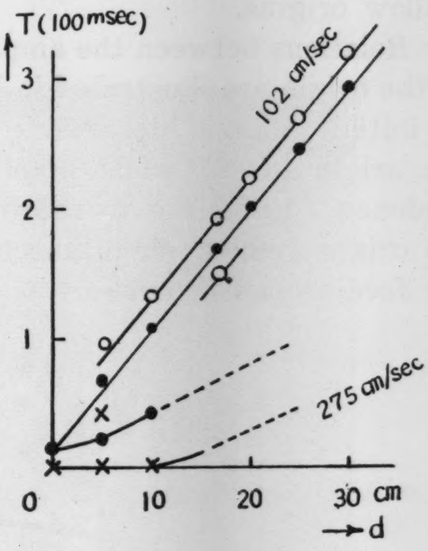

Fig. 6. A part of travel time curves.
Focal depth: 6 cm.

movements corresponding to impulsive pressure changes at the line source, which is to be compared with the present experiment.

Nakano has predicted that the event corresponding to free surface waves will be clearly observed only at places where epicentral distances exceed the critical distance, which depends on the depth of the origin[8]. Fig. 7 is offered to illustrate the fact predicted by him. The amplitude of the main disturbance, which forms the surface wave at distant places, shows its maximum value at a critical distance, which becomes larger for deeper origin. Besides this, the fact that the amplitude of this event shows smaller values for deeper origins seems to agree with the theory. We have to notice, however, that remarkable disturbances which show incomplete type of Rayleigh waves exist in the epicentral area of

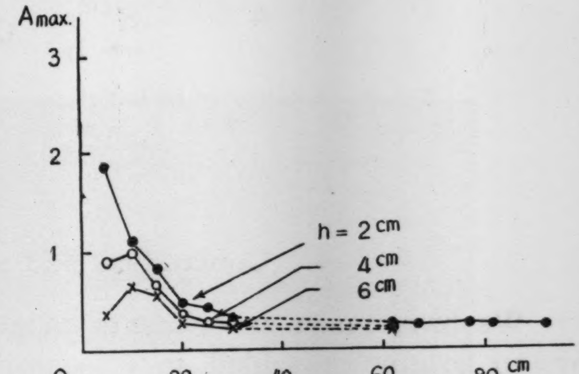

Fig. 7. Amplitudes of main disturbances and epicentral distances.

8) H. NAKANO, *loc. cit.*

shallow origins.

Relations between the amplitude of the initial motion and the depth of the origin are illustrated in Figs. 8 and 9, in which we see amplitudes of initial motions decreasing with increase of the focal depth (h) at the origin ($d=0$) while amplitudes at the point $d=5^{cm}$ show another tendency. Referring to recorded traces (*f.i.* see Fig. 4) we know that the origin area of simultaneous initial disturbances spreads, too, when the focal depth increases.

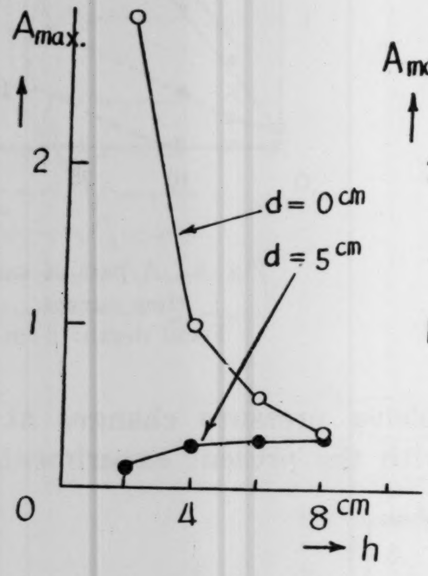

Fig. 8. Amplitudes of initial motions. Short duration of pressure impulses.

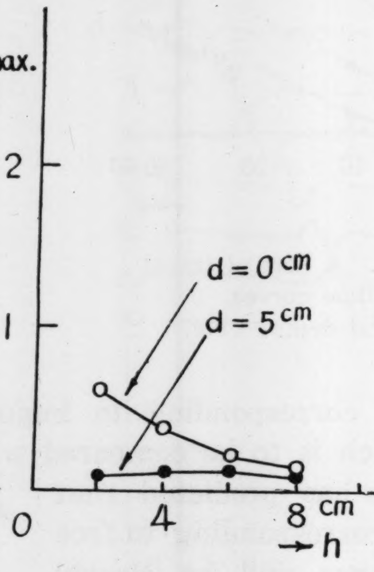

Fig. 9. Amplitudes of initial motions. Longer duration of pressure impulses.

4. Conclusions and acknowledgements

We have made experiments on generation of elastic waves caused by an origin embedded in a semi-infinite elastic body, with a two-dimensional model. Results obtained in this study may be summarized as follows:

1. The initial motion at the epicenter shows an impulsive form, the amplitude of which decreases when the focal depth increases. This tendency appears more clearly when the duration time of pressure impulses becomes shorter.

2. When the shock arrives from the origin, the surface points close to the epicenter commence their motion simultaneously. This area of simultaneous motions spreads when the origin goes deeper in the body.

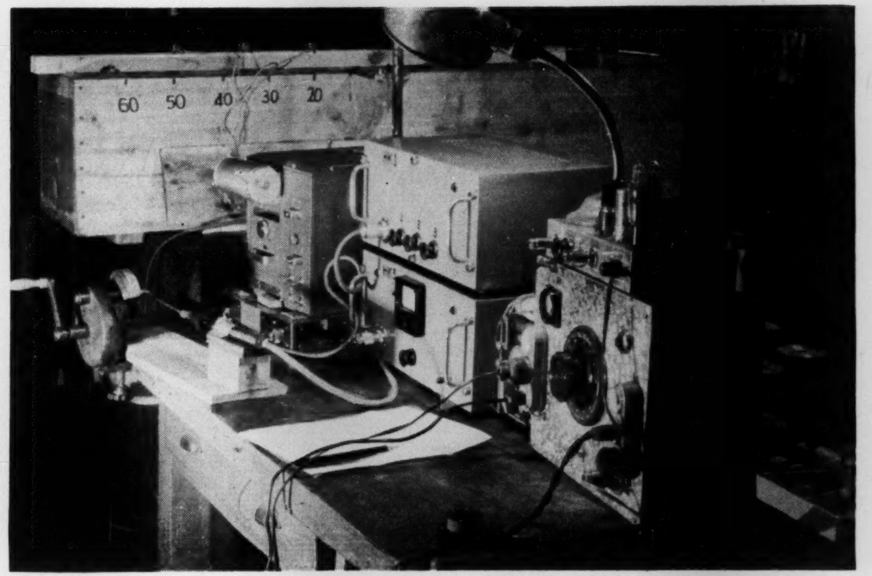

Fig. 10. General view of the laboratory.

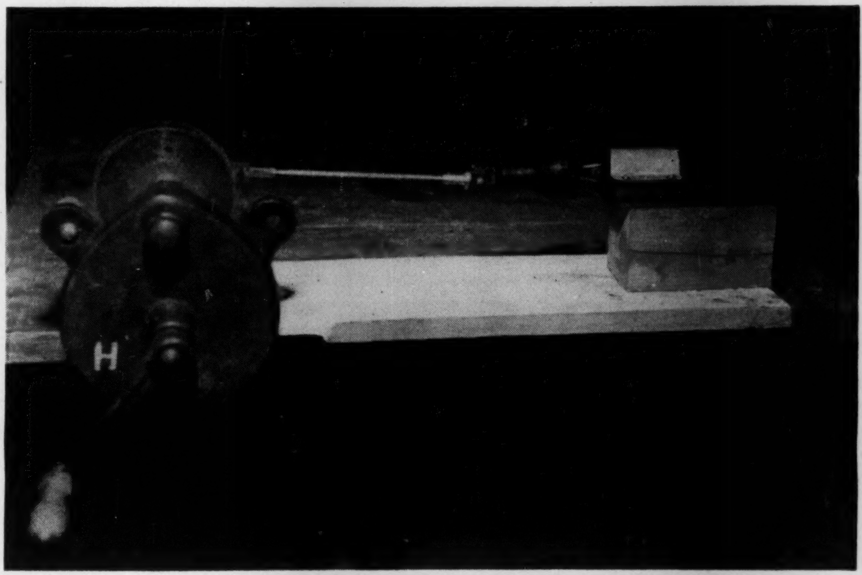

Fig. 11. Air pump and driver.

（震研彙報 第三十三号 図版 笠原）

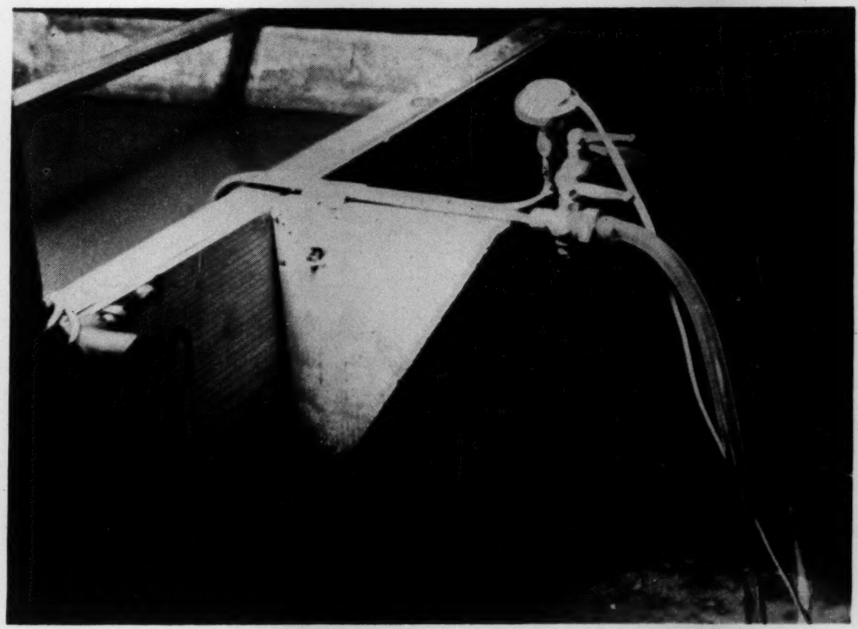

Fig. 12. Pressure gauge.

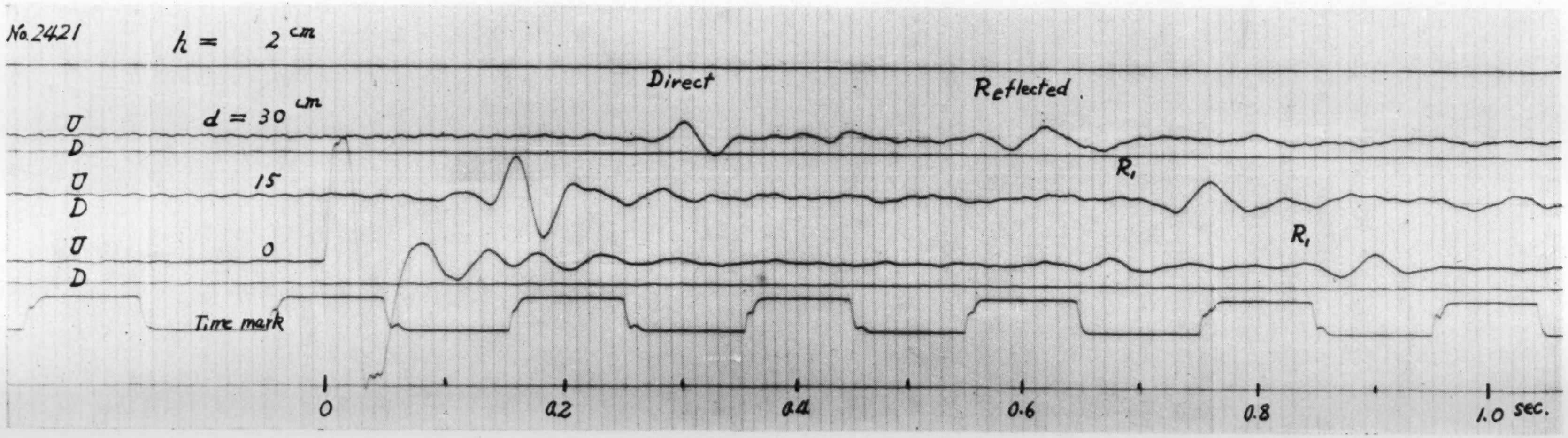

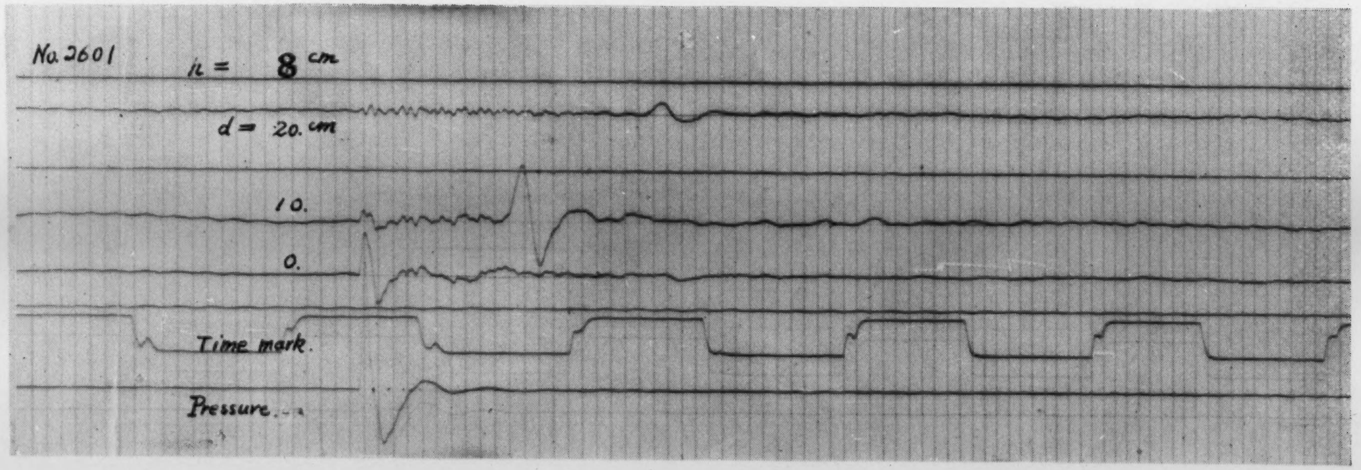

Fig. 13. Examples of oscillograms.

3. The amplitude of main disturbances gets to its maximum value at a critical point on the surface, whose distance from the epicenter depends on the focal depth.

4. The magnitude of main disturbances at the same surface point decreases when the origin goes deeper. This tendency is less remarkable at distant places.

5. The free surface wave shows the linear travel time curve as coming from the epicenter at the origin time of pressure changes.

In the course of this study the author owes very much to encouragement given by Prof. Hagiwara and Dr. Rikitake, both of this institute. He wishes to express his hearty thanks to them as well as to Dr. Takeuchi and Mr. Kobayashi who offered valuable suggestions to him. Mr. Saito and other colleagues kindly helped the author in the laboratory.

The series of experiments was supported by the Grant in Aid from the Department of Education, to whom the author express his thanks, too.

---

28. 弾性波の発生機構に関する実験 (第5報)

地震研究所 笠 原 慶 一

二次元的模型を用いて，波動源が半無限媒質内部 (余り深くない) にある場合の弾性波発生機構を実験した．方法は大体において前報迄のものと類似する．結論されるところは次の諸点である．

1. 波動源に衝撃的圧力変化が起ると，表面上その真上の点は単純な衝撃的運動を行う．その大きさは波動源の深さに伴つて減少する．
2. 衝撃が表面に到着すると，震央部は一斉に運動を開始する．そしてそのひろがりは，波動源が深い程大きくなる．
3. 主要動の振巾はある特定の震央距離において最大となり，この臨界点が波動源の深さに応じて震央を遠ざかることは，理論の結果と比較して興味深い．
4. 同一地点における主要動は波動源が深い場合程少さいが，その傾向は震央を離れた点においては余り明瞭でない．
5. 自由表面波は，あたかも原点時 (origin time) に震央を出発したかのような走時曲線を示している．

---

3. The amplitude of main disturbance gains its maximum value at a certain point on the surface, whose distance from the epicenter depends on the focal depth.

4. The amplitude of main disturbance at the same surface point decreases when the origin goes deeper. The tendency is less remarkable at distant places.

5. The free surface wave shows the Rayleigh travel time curve as coming from the epicenter at the origin time of the [illegible].

In the course of this study the author owes much to encouragement given by Prof. Hagiwara and Dr. Kishinouye, both of this institute. He wishes to express his hearty thanks to them as well as to Dr. Takeuchi and Mr. Kobayashi who offered valuable suggestions to him. Mr. Saito and other colleagues kindly helped the author in the laboratory.

The series of experiments was supported by the Grant in Aid from the Department of Education, to whom the author expresses his thanks, too.

[illegible]

[illegible]

29. *Activities of the Gassan Volcano**.

By Takeshi ICHIMURA,

Yamagata University.

(Received June 28, 1955.)

Introduction

At the southern part of Northeast Japan, there are several important volcanoes almost neglected for a long time without receiving any detailed geological investigation. One of these is the Gassan Volcano which belongs to the Chōkai volcanic zone and rises up on the eroded surface of large granitic masses and overlying Tertiary sediments.

This volcano had geologically and petrologically been unexplored until the field and laboratory works were recently started by the writer and his colleagues[1]. Moreover, it is noteworthy in its characteristic topographical features from which an aspite-type of volcano may be supposed.

In 1954, the writer spent about three weeks in the vicinity of this volcano and was able to make clear the number of activities which took place after its first eruption. It was also confirmed that the present form of the Gassan Volcano with its very gentle slope was not caused by the fluidity of overlapped lavas, but resulted from the destruction of its upper part due to the big explosion which happened at the final stage of activities. These problems are summarized in this paper, with a brief description of some lavas and ejecta.

Location

The Gassan Volcano extends over three counties of Yamagata Prefecture, namely Mogami-gun, E. Tagawa-gun and W. Murayama-gun. The main peak is respectively accessible from Hijiori, Hondōji, Iwanezawa (Tsunatori), Shizu, Yudono-san and Tōge. Of these, the Hijiori course, passing through Ōmori-yama, Akasuna-yama, Ko-take and Nenbutsugahara, is longest and hard of access when compared

* Communicated by N. Nasu.

1) The Gassan Volcano has been investigated by N. Jimbo and T. Konda. The details of this volcano are to be published before long by Konda.

with others. It is about 27 km. from Hijiori to the summit. The Yudono-san course, on the other hand, is the shortest and is the most easy approach to the highest point.

Topographical and geological features of the Gassan Volcano

The Gassan volcano consists of the main peak of Gassan (1979.5 m.), Ubaga-take (1669.7 m.), Kenga-mine (1402.7 m), Shinakura-yama (1210.9 m) and others. It has quite different topographical features at its eastern and western sides. The eastern side slopes down gently to the deep valley of the Tachiyazawa-gawa where it abruptly ends and forms a sharp cliff, whereas the western side is much deformed by erosion and explosion, and is characterized by the formation of a horse-shoe-shaped hollow opening northwestwards and an exposure of quartz diorite at its bottom.

The adjacent district of this volcano is almost unexplored and thickly forested. It is, therefore, difficult to approach such a highly mountainous area consisting of Waradahage-yama (1217.1 m.), Shimo-yanagizawa-yama (1178.4 m.), Senbonmatsu-yama (1260 m.), etc. which are deeply dissected by several rivers, viz., the Tachiyazawa-gawa, Karasu-gawa, Yotsuya-gawa, Tamugi-gawa, Sasa-gawa and their tributaries (Fig. 1).

The area mentioned above is extensively covered by lavas and ejecta. Besides these, it is composed of granite (granodiorite) and its associated intrusives, Tertiary sediments, liparite, felsophyre, dacite, propylite, basalt and Quaternary fluviatile deposits, as well as of talus deposits. Most of the lavas and ejecta exposed here rest upon the eroded surface of granite and Tertiary sediments (Fig. 2).

(1) Granite (granodiorite) and associated intrusives :—Granite is the most predominant intrusive of this area. It is not only found at the foundation of the Gassan Volcano, but is widely exposed at its adjacent area, being partly overlain by the Tertiary formation and being traversed by many dykes of liparite, felsophyre, propylite and basalt. The surface of the granitic mass is remarkably undulated, and its highest point rises up to about 1400 m.[2] above the sea-level at the uppermost course of the Yotsuya-gawa and Sasa-gawa where the Gassan lavas and ejecta directly cover this rock. So far as is

2) Granitic rocks elevated to a height of about 1400 m. are similarly seen on the Zaō volcanoes and Azuma volcanoes.

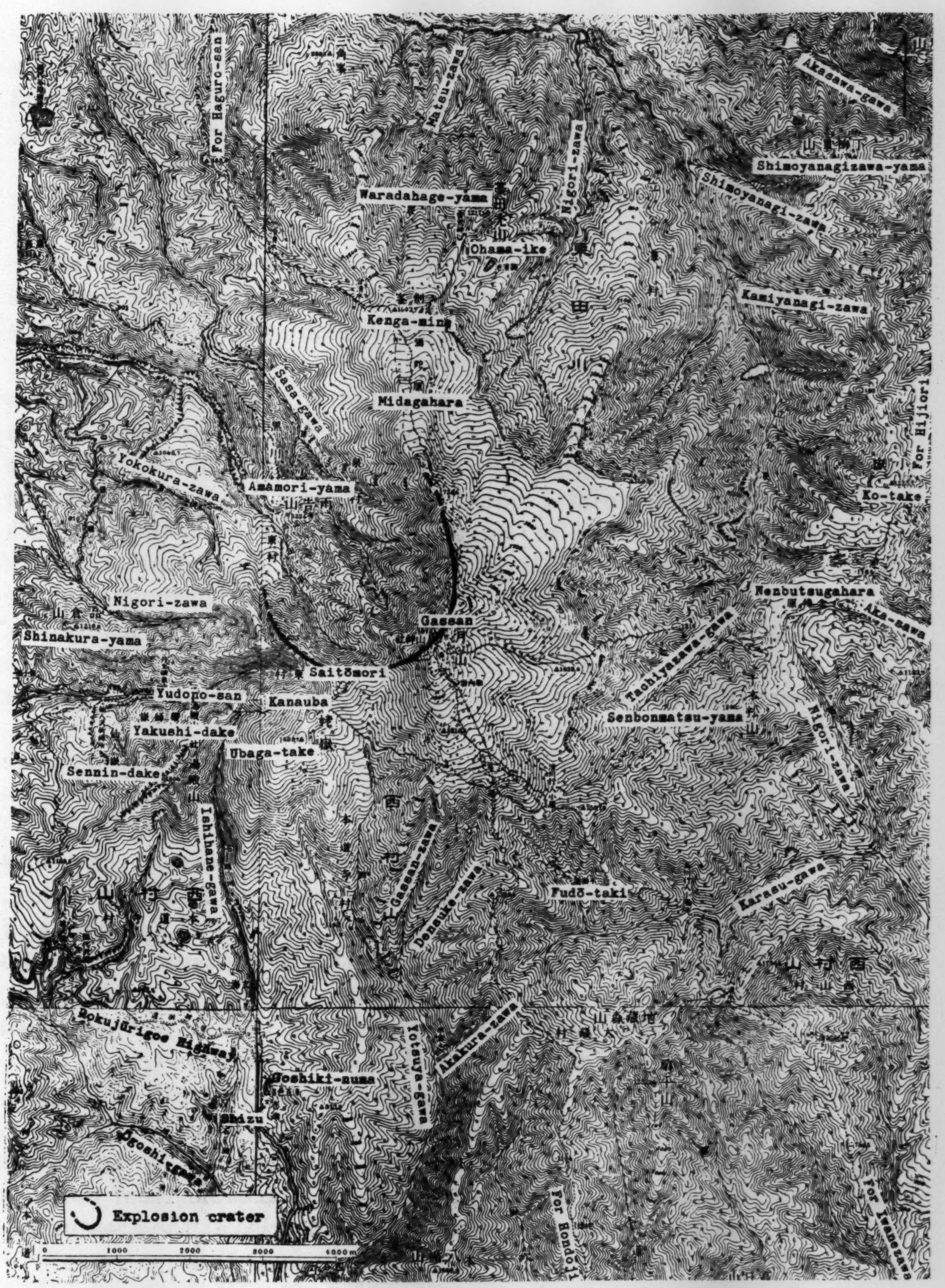

Fig. 1. Topographical map of the Gassan Volcano and its vicinity.

known at present, such a granite is mostly distributed at the area including Ko-take, Nenbutsugahara, Senbonmatsu-yama as well as at the upper courses of the Tachiyazawa-gawa, Karasu-gawa (Dōzan-gawa) and their tributaries such as the Akasawa-gawa, Aka-sawa, Nigori-zawa, etc.

Though usually a coarse or medium-grained biotite granite or granodiorite, the occurrence of some leucocratic varieties with a very coarse texture is also known along the Tachiyazawa-gawa and Karasu-gawa or elsewhere. They are composed of quartz, orthoclase, andesine or labradorite, biotite, magnetite, apatite, zircon, pyrite, chlorite, titanite, epidote and leucoxene.

One of characteristic features indicated by this granitic rocks is the abundance of xenoliths, large and small. As can be seen at the upper course of the Tachiyazawa-gawa and Karasu-gawa, they are mostly found in a state of gradual transition to the mother rock and are represented by dioritic or lamprophyric rocks consisting of such primary or secondary minerals as plagioclase, quartz, hornblende, biotite, magnetite, apatite, chlorite, epidote, titanite, leucoxene, pyrite and calcite. Moreover, the granite under consideration has a tendency to pass into quartz diorite or diorite southwards, particularly at the area between the Hondōji-zawa and Yotsuya-gawa, where they may be supposed to have been formed by the contamination of foreign rocks.

These intrusives are strikingly subjected to the tectonic disturbance and frequent impregnation of pyrite, as is indicated by liparite, felsophyre and the Tertiary green tuff.

(2) Tertiary sediments:—The Tertiary formation covers the eroded surface of biotite granite and associated intrusives mentioned above, disappearing partly beneath the accumulation of lavas and ejecta of the Gassan Volcano as well as beneath the talus deposits. It is also found in close association with such extrusives as liparite, felsophyre, propylite and basalt. This undoubtedly suggests that it was deposited during repeated volcanic activities in the Upper Miocene.

The formation exposed here is mainly composed of tuff and shale. It is represented by green tuff at its lower horizon, but is rich in shale at the upper half, being occasionally intercalated by tuffaceous rocks. The exposures of these sediments are traceable from north to south across the Tachiyazawa-gawa and its tributaries at the area including Waradahage-yama, Shimoyanagizawa-yama and Akasuna-yama.

(3) Extrusives independent of the activities of the Gassan Vol-

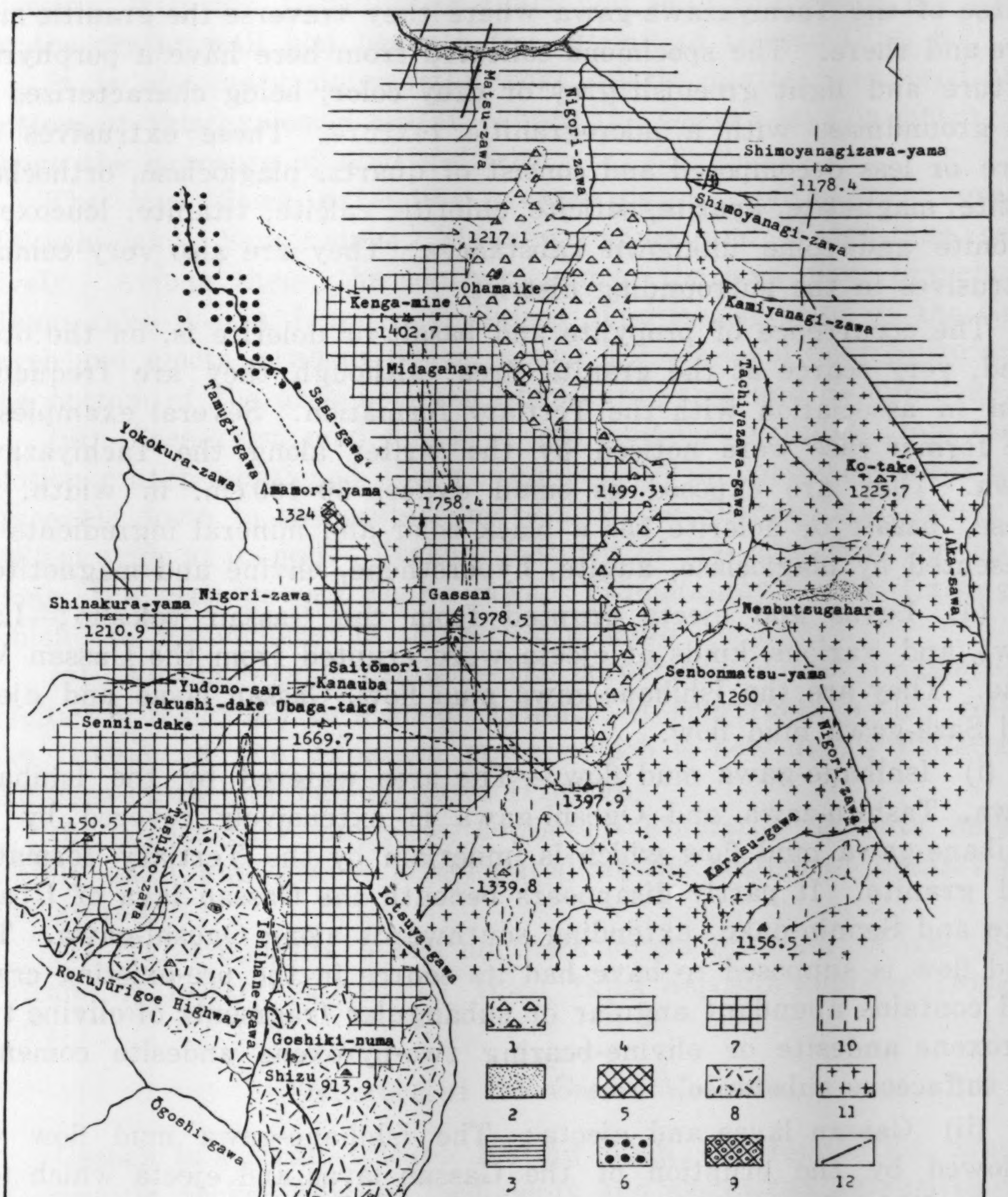

Fig. 2. Geological map of the Gassan Volcano and its vicinity. 1. Talus deposits, 2. Fluviatile deposits, 3. Shale and tuff (U. Miocene), 4. Green tuff (U. Miocene), 5. Dacite, 6. Sasa-gawa mud flow, 7. Gassan lavas and ejecta (Ol. two-pyroxene andesite), and Ol.-bearing or Ol.-hornb.-bearing two-pyroxene andesite), 8. Ishihane-gawa mud flow, 9. Ol. basalt or dolerite, 10. Liparite and felsophyre, 11. Biot. granite (granodiorite), quartz diorite and diorite, 12. Fault.

cano:—Liparite and felsophyre are well exposed at the uppermost course of the Tachiyazawa-gawa where they traverse the granitic mass here and there. The specimens collected from here have a porphyritic texture and light greenish grey or grey color, being characterized by the groundmass with a microgranitic texture. These extrusives are more or less decomposed and consist of quartz, plagioclase, orthoclase, biotite, magnetite, apatite, sericite, chlorite, calcite, titanite, leucoxene, limonite and some unknown substances. They are also very common extrusives in the surrounding district.

The occurrence of propylite and basalt or dolerite is, on the other hand, very scarce at the granitic area, although they are frequently seen in association with the Tertiary formation. Several examples of the former case were noticed by the writer along the Tachiyazawa-gawa. They are exposed as small dykes, 30–100 cm. in width. Of these, basalt or dolerite has a black color and mineral ingredients represented by plagioclase, augite, hypersthene, olivine and magnetite.

(4) Lavas and ejecta erupted from the Gassan volcano:—Lava flows and various kinds of ejecta were erupted from the Gassan Volcano. They are the Ishihane-gawa mud flow, Gassan lavas and ejecta and Sasa-gawa mud flow.

(i) Ishihane-gawa mud flow:—The area watered by the Ishihane-gawa, Tashiro-zawa and Ōgoshi-gawa is extensively covered by the Ishihane-gawa mud flow which is underlain by the Tertiary formation and granite. It partly disappears beneath the Gassan lava of Ubaga-take and Sennin-dake, extending southwards along Ōgoshi-gawa. This mud flow is supposed to have had its source in the pre-existing crater and contains abundant angular or subangular fragments of olivine two-pyroxene andesite or olivine-bearing two-pyroxene andesite comented by tuffaceous substance.

(ii) Gassan lavas and ejecta:—The Ishihane-gawa mud flow was followed by the eruption of the Gassan lavas and ejecta which took place within the same crater. It spreads over the area including the summit of Gassan, Kenga-mine, Midagahara, Ubaga-take, Yakushi-dake and Sennin-dake. The eastern half of this lava flow is intercalated with thin beds of ejecta and is represented by gently sloping flank, where it gradually decreases its height (Fig. 3). The terminal cliff is frequently estimated to be 100 m. or more along the valley of the Tachiyazawa-gawa and its tributaries (Fig. 4).

The western half is, on the other hand, remarkably subjected to

the dissection due to erosion and deformation resulting from the explosion. It forms, therefore, a sharp cliff here and there, particularly on the crater wall just beneath the summit of Gassan (Fig. 6.).

It is also very noteworthy that quartz diorite is exposed at the bottom of this explosion crater, where the Gassan lava is 400 m. thick above the exposure of quartz diorite.

The lava flows extending westwards or southwards construct Yakushi-dake, Sennin-dake, Shinakura-yama and Ubaga-take respectively. Among them, the southern end of the lava flow branched on Ubaga-take is now found near Shizu. The lowest point of the Gassan lavas and ejecta is about 800 m. above the sea-level near Shizu and at the bottom of the area between Shinakura-yama and Sennin-dake.

(iii) Sasa-gawa mud flow:—A big mud flow erupted from the explosion crater mentioned above extends 18000 m. northwestwards and is traceable down to the eastern margin of the Shōnai Plain, where it is 7000 m. wide at its end. Various features of the mud flow can be seen along the Sasa-gawa, Konno-gawa, Tsumeta-gawa and Harai-gawa, which are not included in the writer's map.

(5) Amamori-yama dacite:—The occurrence of the Amamori-yama dacite[3)] is restricted to a small extent. It constructs a tiny relief at the bottom of the explosion crater which is now deeply dissected by the Sasa-gawa and Tamugi-gawa (Fig. 5).

(6) Quaternary fluviatile deposits:—Fluviatile deposits here are mainly sand and gravel accumulated at the bottom of present rivers and swamps.

(7) Talus deposits:—The northern or eastern end of the Gassan volcano is mostly skirted by thick talus deposits supplied from high cliffs.

Structure of the Gassan Volcano

Gassan is a strato-volcano resting upon the foundation composed of granitic rocks, Tertiary sediments and associated extrusives which are exposed at the maximum elevation of 1300 m.–1400 m. above the sea-level. The structure of this volcano is much complicated by the successive eruption of the Ishihane-gawa mud flow, Gassan lavas and ejecta, Sasa-gawa mud flow and Amamori-yama dacite. It can be investigated along the Tachiyazawa-gawa, Yotsuya-gawa, Ishihane-gawa, Ōgoshi-gawa, Nigori-zawa, Yokokura-zawa, Tamugi-gawa, Sasa-gawa and

3) Personal Communication by T. Konda.

their tributaries. The best example is indicated on the wall of explosion crater just beneath the summit, Saitōmori and Kanauba, where the exposures of lavas and ejecta are highly cliffed. These lavas and ejecta have a thickness of about 400 m. above the surface of quartz diorite and spread out from here with several trends and an inclination of 10°–13°. The structure of this area is also complicated by the exposure of the Amamori-yama dacite.

So far as has been confirmed by the writer, the main part of the Gassan Volcano is built up of the Gassan lavas and ejecta underlain by the Ishihane-gawa mud flow. They are supposed to have been supplied from the pre-existing crater which seems to have been opened somewhere near the present explosion crater. At that time, the Gassan Volcano was probably a homate, but it is probable that it increased its height by erupting lavas and ejecta successively, passing into a konide (?) higher than the present volcanic body. Moreover, it is inferable that such a konide (?) lost its upper part and lowered its height in the subsequent explosion. This is the reason why the Gassan Volcano now looks like an aspite on its eastern half with an inclination of 10°–13° (Fig. 3). This idea may be supportable from the large explosion associated with the eruption of the Sasa-gawa mud flow.

Explosion Crater

One of important events which happened on the Gassan Volcano is the formation of explosion crater opening northwestwards (Figs. 6～7). It is a horse-shoe-shaped hollow with a diameter of about 2.5 km. from east to west, and its deepest part is about 700 m. below the summit. The crater wall here is highly cliffed and is composed of the Gassan lavas and ejecta resting upon the eroded surface of quartz diorite exposed at the bottom.

The crater wall is represented by an exposure of thick lava flows intercalated with ejecta, showing some disturbances due to explosion on its southern cliff. The highest wall is found at the southeastern corner, where the Gassan lavas and ejecta are estimated to be about 400 m. up to the summit, inclining gently eastwards.

The bottom of the crater is irregularly undulated and is partly buried with fragmental rocks which crumbled down from the wall. At such an area, Amamori-yama projects out as a small mass, about 200

m. high above the bottom of the Tamugi-gawa and Sasa-gawa (Fig. 4). It consists of biotite hornblende dacite with a light grey color and porous structure.

Besides this, Konda[4] noticed a small exposure of similar dacite somewhere near the source of the Nigori-zawa, a tributary of the Tachiyazawa-gawa.

Mineral Composition of the Gassan Lavas and Ejecta

The Gassan lavas and ejecta are a thick accumulation of lava intercalated with various kinds of ejecta. They construct the main part of this volcano.

Exclusive of decomposed specimens, these rocks have a dark grey color and are characterized by a remarkable porphyritic texture. The rocks are composed of such minerals as plagioclase, augite, hypersthene, olivine, hornblende, magnetite, apatite, quartz, tridymite, bowlingite and brown glass, being represented by olivine two-pyroxene andesite and olivine-bearing or olivine-hornblende-bearing two-pyroxene andesite. The relationship between olivine-rich and olivine-poor andesites can be investigated along several courses, where the writer collected many specimens and examined their thin sections. In these cases, the former passes gradually into the latter as the altitude increases.

One of predominant minerals in these andesite is plagioclase which occurs abundantly as phenocrysts and also in the groundmass. In general, the phenocrystic plagioclase is euhedral or subhedral and has a tabular or rectangular form. It is well zoned and occasionally turbid at its periphery or inner part. Sometimes, the crystal reveals a worm-eaten structure due to the invasion of the groundmass and encloses augite, hypersthene, magnetite and brown glass. It is also noteworthy that there are some lava flows and andesite fragments of ejecta with large phenocrysts. They are seen in the specimens from Kanauba and several places of the eastern or southern flank. In these specimens, the largest one is 1.1 cm. long and 0.7 cm. across. The indices refraction suggest that the phenocrystic plagioclase belongs to andesine or labradorite with a composition of An_{39-61}.

The plagioclase in the groundmass occurs commonly as small lath-shaped or rectangular crystals 0.02 mm.–0.16 mm. long.

The next important ingredients are augite and hypersthene. Of

4) Personal Communication by T. KONDA.

these two minerals, phenocrystic augite takes a long or stout prismatic form, the former resembling the augite crystal of the Zaō volcanoes[5]. The crystal is mostly subhedral or anhedral, but it is sometimes euhedral and is 6 mm. long and 2.5 mm. across in the largest one. Such a phenocryst is occasionally twinned on (100) or (101). It is, however, uncertain whether the crystal is twinned on $(\bar{1}22)$ or not, as in the case of the Zaō volcanoes. The maximum extinction angle, $Z \wedge c$, is 40°. When this mineral is intergrown with hypersthene, the latter is always fringed by the narrow zone of the former. The phenocrystic augite commonly encloses magnetite, but the crystal containing plagioclase and apatite is very rare.

Minute augite crystals are abundantly found in the groundmass, in which they take a prismatic or granular form, generally 0.01 mm.–0.1 mm. in length or diameter.

Hypersthene is mostly present as phenocryst in nearly the same amount as that of augite. The crystal has a long prismatic form, euhedral or subhedral. It is 1.87 mm. long and 0.51 mm. across in the largest phenocryst and contains magnetite.

Besides these, a noticeable feature is the frequent occurrence of olivine phenocryst in most of specimens collected by the writer from various parts of the Gassan lavas and ejecta, although it gradually decreases its amount at the later stage of eruption. The crystal is always subhedral or anhedral and reveals high frequency in the specimens obtained from Matsukura, Suzumekura, the ridge opposite to the Akakura-zawa, Ubaga-take and the lower part of the eastern flank. The largest one is 1.7 mm. in diameter, and the lava of the eastern flank is rich in large phenocrysts. Frequently, olivine passes into bowlingite along its periphery or crack and includes magnetite.

It is also noteworthy that hornblende occur frequently in some specimens. This mineral appears in olivine-poor lavas, as is indicated by olivine-hornblende-bearing two-pyroxene andesite of the Yake-yama Volcano[6], being represented by the occurrence of oxyhornblende with a subhedral or anhedral form, 2.07 mm. long and 0.68 mm. across in the largest crystal. Such oxyhornblende is distinctly pleochroic from light yellow (X) to yellowish brown (Y) or reddish brown (Z). The absorption is $Z > Y > X$, and its maximum extinction angle, $Z \wedge c$, is 4°. It is partly or almost wholly opacitized and changed into aggregates

5) T. ICHIMURA and H. MINATO, *Bull. Earthq. Res. Inst.*, **29** (1951), 342–348.
6) T. ICHIMURA, R. MORIMOTO & H. TSUYA, *Bull. Earthq. Res. Inst.*, **27** (1949), 110–112.

of minute magnetite and augite crystals.

Magnetite is a very common ingredient in the groundmass or as enclosure of other phenocrystic minerals. Generally, it has an octahedral or granular form and is mostly 0.01 mm.–0.85 mm. in diameter. The largest crystal is, however, 0.76 mm. across in its thin section.

Apatite and quartz are contained in a negligible amount. The former has a long prismatic form, 0.43 mm. long and 0.08 mm. across in maximum and a dark grey or grey color due to decomposition, being traversed by cracks, whereas the latter is corroded xenocryst captured probably from granite or liparite or other quartzose rocks. The writer found these minerals in the lavas exposed on the summit of Kanauba or elsewhere.

Tridymite is very scarce and fills up the interspaces of various ingredients in the groundmass. The same can be said of brown glass, and it is almost absent in the writer's specimens.

The groundmass consists of oligioclase, andesine, augite, hypersthene, magnetite, apatite, tridymite and brown glass. Commonly, it exhibits a pilotaxitic texture, but its texture is rather orthophyric in some specimens. The rocks mentioned above, furthermore, contain basaltic or gabbroic xenoliths in which mineral ingredients are plagioclase, augite, hypersthene, olivine, biotite, magnetite and brown glass. It is a non-porphyritic rock with a grey color and compact appearance, being sharply bordered against their mother rocks.

History of Volcanic Activities

The Gassan Volcano seems to have repeated its activity on the upheaved area composed of granite (granodiorite), quartz diorite, diorite, liparite, felsophyre, dacite, propylite, basalt and Tertiary sediments.

The first eruption of this volcano probably took place through the weak point of base rocks where the pre-existing crater is supposed to have been opened.

The forerunner of repeated activities is indicated by the eruption of the Ishihane-gawa mud flow which covered the southern part of the volcanic area. It is believed to have poured forth from the pre-existing crater now obscured. This activity was followed by the ejection of the Gassan lavas and ejecta. It started with the eruption of olivine two-pyroxene andesite and was succeeded by olivine-bearing or olivine-hornblende-bearing two-pyroxene andesite during the same activity.

These lavas are intercalated with various kinds of ejecta and are thickly piled up on the base rocks as well as on the Ishihane-gawa mud flow. During this activity, the Gassan volcano is inferred to have gradually increased its height above the level of the present summit. It is also supposed that the summit of this volcano was once situated at farther west.

The next activity is represented by the formation of the large explosion crater and ejection of the Sasa-gawa mud flow which is traceable north-westwards down to the Shōnai Plain. It resulted in an extensive destruction of the Gassan volcano. At that time, the upper half of konide (?) was blown off and a quite different form of volcano was left behind. This is the present Gassan Volcano which has a very gentle slope on the east, but is highly cliffed on the west.

The activities were closed by the big explosion which erupted the Sasa-gawa mud flow. Such activities were probably repeated successively at the pre-historic time. It is, however, not clear whether the first eruption took place in the beginning of the Quaternary or not, since there is no Pliocene sediment overlain unconformably by the lavas and ejecta of the Gassan Volcano at this area under consideration.

On the contrary, the relationship between the Ha-yama Volcano and Pliocene sediments of the neighbouring district has recently been investigated by Konda[7]. He concluded that the eruption of this volcano had already started in the Pliocene and had repeatedly supplied a large amount of tuffaceous or andesitic substance to construct the main part of the volcano and Pliocene sediments intercalated with lignite beds. In his paper, however, the possibility of a clino-unconformity between folded Pliocene sediments and newly erupted lavas or ejecta of the present Ha-yama Volcano seems to have been neglected without any description. To the writer, this seems to be an important key point in making clear the period of the first activity shown by the Gassan Volcano.

Summary

(i) The Gassan Volcano rises up on the boundary between W. Murayama-gun and E. Tagawa-gun or Mogami-gun of Yamagata Prefecture. It is approachable by several courses from various sides.

(ii) It is composed of the Ishihane-gawa mud flow, Gassan lavas

7) T. KONDA, *Bull. Yamagata Univ.* (*Nat. Sc.*), **3** (1954), 127–131.

and ejecta and Sasa-gawa mud flow which successively erupted on the eroded surface of granite (granodiorite), quartz diorite, diorite, liparite, felsophyre, dacite, propylite, basalt and Upper Miocene sediments elevated frequently to 1300 m.–1400 m. above the sea-level.

(iii) The lavas and ejecta including mud flows erupted successively from pre-existing crater and also from the explosion crater. Of these, the pre-existing crater is now obscure, being covered by lavas and ejecta which erupted subsequently, whereas the explosion crater opened northwestwards with a horse-shoe-shaped hollow just beneath the present summit.

(iv) Most predominant are the Gassan lavas and ejecta which consist of olivine two-pyroxene andesite, olivine-bearing or olivine-hornblende-bearing two-pyroxene andesite and their fragments. One of characteristic features indicated by these rocks is the frequent occurrence of olivine phenocryst. This mineral is sometimes found in association with oxyhornblende.

(v) The activities of this area began with the eruption of the Ishihane-gawa mud flow and ended with the formation of a big explosion crater which poured forth a large amount of the Sasa-gawa mud flow.

(vi) By this enormous explosion, the Gassan Volcano lost its upper half of konide (?) and left behind a quite different from of volcanic body. It has a very gentle slope on the east and is highly cliffed on the west.

(vii) The first activity of the Gassan Volcano is supposed to have taken place in the beginning of the Quaternary, but it will be confirmed later in connection with the activities that happened at the Ha-yama volcanic area.

In conclusion, the writer's thanks are due to Mr. N. Jimbo and Mr. T. Konda for the valuable suggestions which they offered during his field and laboratory works.

The expence of this research was partly defrayed from the fund for the Scientific Research of the Educational Ministry.

29. 月山火山の活動

山形大学 市 村 　毅

月山は，山形県の東田川郡，最上郡及西村山郡に跨り，鳥海火山帯の中でも特異な形態を有する火山である．その東側は，アスピーテを思わせる緩傾斜をみせ，西側は，大きな爆裂火口のために物凄い断崖をなしている．この火山は，花崗岩（花崗閃緑岩）石英閃緑岩，閃緑岩，石英粗面岩，珪長斑岩，石英安山岩，変朽安山岩，玄武岩，新第三紀（上部中新世）堆積岩などよりなる基盤岩の侵蝕面上に盛上り，その活動は，石跳川泥流，月山熔岩及砕屑岩，笹川泥流，順次に噴出せしめている．大爆裂火口は，月山熔岩及砕屑岩の噴出後に生じ，これがために旧月山火山の上半部が噴き飛ばされるに至つた．月山の現形態は，この際に生じたものであり，笹川泥流は，爆発に伴つて噴出したものと思われる．月山火山の活動は，恐らく第四紀の初期に始まり，大爆裂火口の生成と笹川泥流の噴出を以て，その終りを告げている．

Fig. 3. The Gassan Volcano viewed from Nenbutsugahara. This picture shows the eastern side of the volcano with a gentle slope. The lavas and ejecta exposed here rest upon the eroded surface of base rocks composed mainly of granite (granodiorite), quartz diorite, liparite, felsophyre and Tertiary sediments. 1= Gassan lavas and ejecta, 2=The terminal cliff of lavas and ejecta along the deep valley of the Tachiyazawa-gawa, 3=Base rocks.

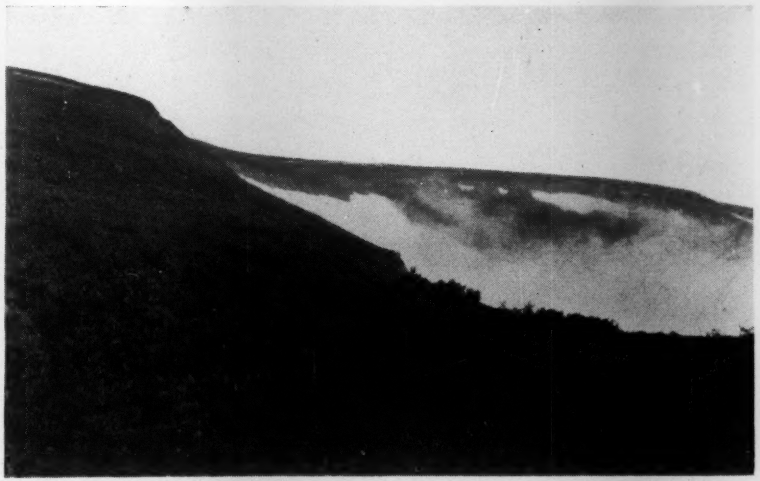

Fig. 4. The eastern end of the Gassan lavas and ejecta forming a sharp cliff along the deep valley of the Tachiyazawa-gâwa.

Fig. 5. The bottom of the explosion crater viewed from the summit. Amamori-yama is a small relief built up of dacite. x= Amamori-yama.

Fig. 6. The summit of the Gassan Volcano. The rock of the foreground is olivine-bearing two-pyroxene andesite. x=Crater wall.

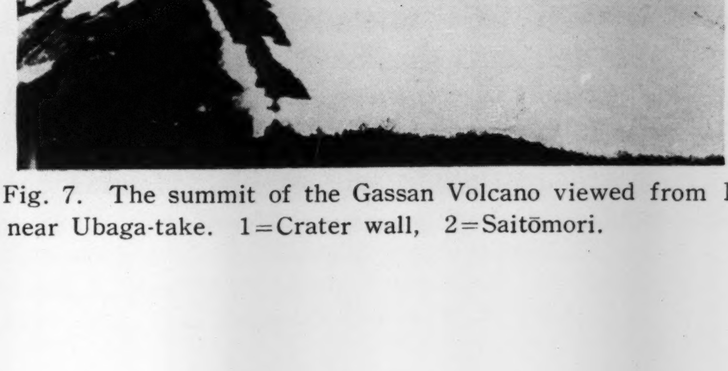

Fig. 7. The summit of the Gassan Volcano viewed from Kanaba near Ubaga-take. 1=Crater wall, 2=Saitōmori.

（震研彙報 第三十三号 図版 市村）

30. *Die zeitliche Verteilung der Vulkane im Quartär Hokkaidos.*

Von Masao MINATO,
Hokkaido Universität, Sapporo.

(Vorgelegt den 14. April 1955.—Eingegangen den 30. Juni 1955.)

Auf der Insel Hokkaido, im Chokai, Nasu und Kurilen-Bogen, befinden sich viele Vulkane. Der Verfasser ist zur Zeit der Ansicht, dass es sich dabei um die Möglichkeit dreier zeitlicher Gruppierungen handele, nämlich:

1.) Die Vulkane, die älter sind als das jüngere Pleistozän;
2.) die Vulkane des jüngeren Pleistozän;
3.) die Vulkane des Alluviums.

Die Verbreitung der Gesteine, aus denen sich jede Gruppe dieser Vulkane formiert, lässt sich aus Abb. 1 ersehen.

Die älteren Vulkane sind jetzt schon ziemlich zerstört, und es ist die Beobachtung gemacht worden, dass die Produkte solcher vulkanischer Tätigkeiten stratigraphisch unter den Ablagerungen der sogenannten mittleren bzw. höheren Terrassen liegen. Die Vulkane, die zu dieser Gruppe gehören, sind folgende: Hakodate-yama, Yokotsu-dake, Kariba-yama, Raiden-yama, Muroran-dake, Syokan-dake, Chubetsu-dake, Nupukaushi-yama, Kikin-dake, Mokoto-yama, Samakki-yama, Onnebetsu-dake und Shiretoko-yama.

Die zweite Gruppe besteht aus solchen Vulkanen, die beinahe den Niederterrassen vergleichbar sind, m.a.W. die Bildungszeit dieser Vulkane ist mit der Tottabetsu-Eiszeit[1] bzw. der Nacheiszeit vergleichbar. Es ist jedenfalls sicher, dass diese Vulkane zum jüngeren Pleistozän gehören; sie sind sicher älter als das Alluvium.

Die Vulkane dieses Zeitabschnittes sind charakteristisch in der vulkanischen Tätigkeit. So ist in dieser Zeit nur der grosse Erguss des Schmelztuffes zu sehen in Begleitung der Grossen Caldera-Bildung, bzw. der Verwerfungstätigkeit. Solche Bildungen sind: Kutcharo-Caldera, Daisetsu-Caldera, Tokachi-Caldera und Shikotsu-Caldera, usw.

Obwohl im Falle des Daisetsu und des Tokachi das Caldera durch

1) M. MINATO und S. HASHIMOTO, *Proc. Japan Acad.*, **30** (1954), 106. S. HASHIMOTO and M. MINATO, *Jour. Fac. Sci. Hokkaido Univ.*, IV, **9** (1955), 7.

die Auffüllung der Produkte neuerer Vulkane des Alluviums schon bereits verlöscht ist, so ist doch kein Zweifel mehr möglich, dass bei allen Vulkanen dieses Typus eine Caldera-Bildung nach dem Ergusse des Schmelztuffes stattgefunden hat.

Stratigraphisch ist dieser Schmelztuff beobachtete als örtlich bedeckt bzw. eingeschlossen in der Schotterablagerung der Niederterrassen.

In Hokkaido findet man örtlich die Fossilien der Fauna des *Mammonteus primigenius primigenius* (BLUMENBACH)[2] in dieser Schotterablagerung

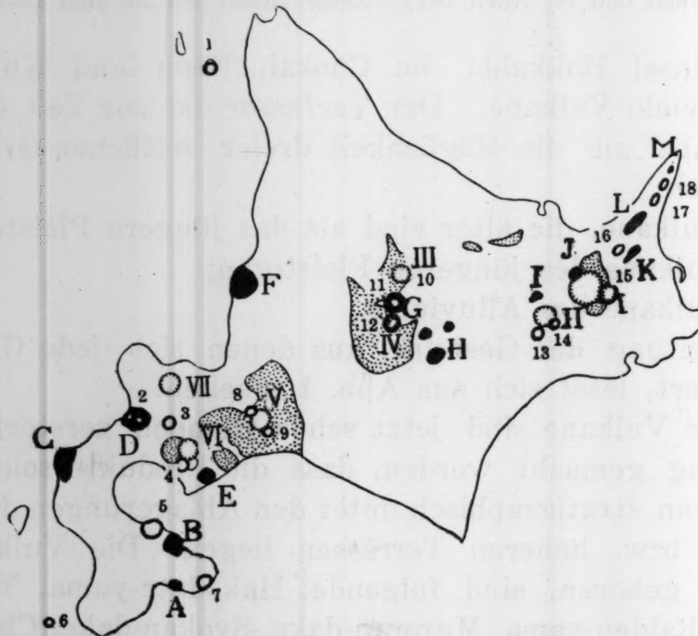

Abb. 1 Die Verbreitung der Vulkane Hokkaidos
Schwarz: Die Vulkane des älteren Pleistozänes.
Punktiert: Die Schmelztuff des jüngeren Pleistozänes. (Die zeitliche Vergleichung ist aber zum Teil noch fraglich.)
Hell. Kreis: Die Vulkane des Alluviums.
Kreis mit Dornen: Das Caldera.
A: Hakodateyama, B: Yokotsudake, C: Karibayama, D: Raidenyama, E: Murorandake, F: Syokandake, G: Chubetsudake, H: Nupukaushiyama, I: Kikindake, J: Mokotoyama, K: Samakkiyama, L: Onnebetsudake, M: Shiretokoyama.
I: Kutcharo-Caldera, II: Akan-Caldera, III: Daisetsu-Caldera, IV: Tokachi-Caldera, V: Shikotsu-Caldera, VI: Doya-Caldera, VII: Akaigawa-Caldera.
1: Rishiridake, 2: Iwaonupuriyama, 3: Yesofujiyama, 4: Usuyama, 5: Komagadake, 6: Oshima, 7: Esan, 8: Eniwadake, 9: Tarumaedake, 10: Daisetsusan, 11: Tomuraushiyama, 12: Tokachidake, 13: Meakandake, 14: Oakandake, 15: Mashudake, 16: Syaridake, 17: Rausudake, 18: Shiretokoiwaoyama.

der Niederterrassen, die man mit der Moräne der Tottabetsu-Eiszeit im Kar des Hidaka-Gebirges stratigraphisch vergleichen kann; man nimmt deshalb allgemein an, dass diese vulkanische Tätigkeit dem jüngeren Pleistozän zugehörig ist.

Die Vukane des Alluviums sind die folgenden: Rishiri-dake, Iwaonupuri-yama, Yesofuji-yama, Eniwa-dake, Tarumae-dake, Tomuraushi-yama, Meakan-dake, Oakan-dake, Mashu-dake und Shiretokoiwao-yama, usw.

Diese Vulkane sind topographisch meistens frisch und haben die ursprünglichen Formen gut bewahrt; ferner sind sie, wenigstens zum Teil, heute noch tätig. Man sieht dabei, dass die vulkanischen Produkte des Alluviums den Schmelztuff des jüngeren Pleistozän decken, bzw. auf den Ablagerungen der niederen Terrassen liegen. In Frage stehen nun folgende Punkte:

1.) Was ist eine Vulkankette? Die ältere war ja nicht immer gleichörtlich mit der neueren.

2.) Der Typ der vulkanischen Tätigkeit ist zeitlich verschieden. So sieht man z.B. in der Zeit des jüngeren Pleistozän nur den grossen Erguss des Schmelztuffes und die Caldera-Bildung.

3.) Man kann nicht die sogenannte Gesteinsprovinz allein in Betracht ziehen, ohne das geologische Zeitalter zu berücksichtigen. So charakterisiert z.B. das Vorhandensein des Hornblende-Andesit alle ältere Vulkane Hokkaidos, die dem Nasu-Bogen angehören die Vulkane des Alluviums in demselben Bogen ausschliesslich aus Pyroxene-Andesit bestehen.

Früher war Kuno[3] der Ansicht, dass der Hornblende-Andesit im Vergleich mit dem Pyroxene-Andesit die dicke Erdkruste charakterisiere. Aber es ist nicht gut glaublich, dass die Mächtigkeit der Erdkruste im Gebiete des südlichen Hokkaido, dass dem Nasu-Bogen angehört, sich vom Pleistozän bis zum Alluvium ziemlich verändert habe.

Die Veränderung der Gesteinsprovinz mag deshalb auf anderem gründe beruhen.

Jedenfalls muss man jedoch darauf achten, dass die Gesteinsprovinz sich in einer solchen kurzen Zeitspanne verändern kann.

Der Verfasser möchte es nicht unterlassen, auch an dieser Stelle den Herren Prof. T. ISHIKAWA, Dr. M. SAITO, Dr. S. DOI und Dr. T.

2) M. MINATO, *Japanese Jour. Geol. Geogr.*, **26** (1955) im Druck.
3) H. KUNO, *Tr. New York Acad. Sci.*, **14** (1952), 225.

KATSUI für die vielfache und stets bereitwilligst gewährte Hilfe seinen Dank auszusprechen.

---

30. 北海道・第四紀火山の時代的分類

北海道大学 湊 正 雄

北海道の第四紀火山は今のところ時代的に，次の3に区分するのが至当である．

1) 旧洪積世， 2) 新洪積世， 3) 冲積世

この様に分類してみると，火山活動の生じた地域の範囲は時代によつて異なり，またその活動の型式も同じでないことがわかる．したがつて火山列（脈）なるものはこの点からの吟味が必要になつてくる．

また火山噴出物の岩石学的性状によつて区別された岩石区なるものも時代的に異なることを注意しなければならない．道南の那須火山列の地域では，旧洪積世の火山に普辺的な角閃石安山岩は冲積世には認られなくなつている．

---

31. *Elasticity of Rocks under the Initial Stresses, with Special Reference to the Fracture Problem.*

By Daisuke SHIMOZURU,
Earthquake Research Institute.

(Read Jan. 25, 1955 and April 26, 1955.—Received June 30, 1955.)

1. Introduction

The occurrence of earthquakes is considered by many seismologists to be the consequence of the accumulation of stresses in the earth's interior to such an amount as to produce fracture of the earth's crust. If the earth's crust is subjected, in addition to hydrostatic pressure, to such stresses as simple tension, compression or shearing stress, the elastic properties of the crust may differ from those whithout such additional stresses. In effect, some observations in Japan of the earth tides[1] or of the velocity of seismic waves[2] seem to show the change in the elasticity of the earth's crust with time. This, in turn, may be considered to show the state of stress accumulation in the crust, which seems also to have some relations with the occurrence of earthquakes.

Some years ago, the author measured the variation of Young's modulus of some igneous rocks such as granite, basalt, andesite etc. under the uniaxial compression by the method of flexural vibrations. The purpose of the above experiment was to study how the variation due to the stresses of Young's modulus depends upon the fine petrological structure of the rocks. Results obtained are described briefly in the previous paper[3].

The purpose of the present research, which is somewhat different from the experiment cited above, is to trace the variation of elastic behaviour of rocks when subjected to the initial stress, which leads the rock to fracture eventually. Especially, as the elasticity near the fracture point is the essential point in these problems, the experiment has been undertaken with this point in view.

The change in elasticity due to pressure was measured by the

1) E. NISHIMURA, *Trans. Amer. Geophys. Union.*, **31** (1950), 357.
2) M. HAYAKAWA, *Rep. Geol. Surv. Japan., Spec. Number*, (1950).
3) D. SHIMOZURU, *Bull. Earthq. Res. Inst.*, **30** (1952), 63.

velocity of elastic waves in rock specimens. Though for geophysical applications rock samples must be subjected to a differential force under the confining hydrostatic pressures, only compressional initial stress was applied to the specimens.

2. Experimental Procedure

Specimens. White marble specimens produced from Akiyoshidai, Yamaguchi Prefecture were chosen as the test pieces. Each of them was cut into a rectangular prismatic bar of about 7 cm in length. When the length of the sample is considerably large compared with the lateral dimensions, the buckling of the sample will occur at large axial force. Therefore, the shape of the testing samples must not be too long. In order to compare the change in elasticity of polycrystalline aggregates with that of amorphous materials, methyl-methacrylate[4], a kind of plastics, was used as a testing specimen.

Hydraulic press. A thirty-ton hydraulic press of the Amsler type was used to produce the uniaxial stress. The specimens were simply kept compressed between the anvil and the piston of the press. The oil control cock was adjusted so as to compress the specimens with a uniform speed at the whole stage of each experiment. Contraction of the specimens was measured by a dial gauge as a function of the pressure.

Measurements of the velocity of elastic waves in the specimen. Ultrasonic pulse equipment was used for the determination of the velocity of dilatational wave in the specimens. The equipment has been the same with that described in a previous paper[5].

Trigger pulses, delayed about 10 microseconds by a variable delay line, are amplified by the pulse amplifier and are impressed on the driving quartz X-cut crystal. The signal, transmitted through the specimen and received by a similar crystal, is amplified and displayed on the screen of a cathode ray oscilloscope, on which time marks are displayed at every 2.5 microseconds. Velocities of dilatational waves propagated along the axis of the load and those propagated perpendicular to the axis were measured separately. Experimental arrangements for the measurements of the velocity are illustrated in Fig. 1 and Fig. 2. (cf. Figs. 11, 12)

4) Fujikasei Co. Ltd. kindly put methyl-methacrylate at the author's disposal.

5) D. SHIMOZURU and I. MURAI, *Bull. Earthq. Res. Inst.*, **33** (1955), 65.

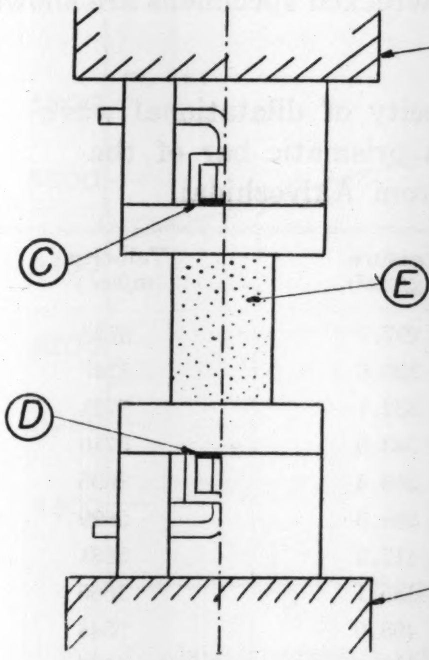

Fig. 1. Experimental arrangement for the determination of the velocity propagated parallel to the axis.

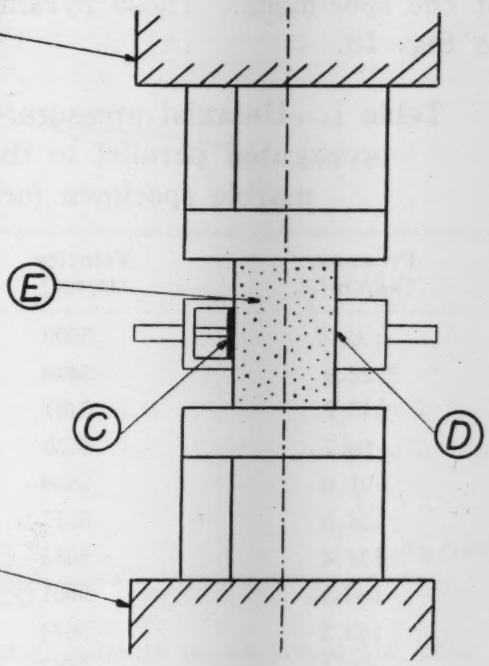

Fig. 2. Experimental arrangement for the determination of the velocity propagated perpendicular to the axis.

(A) The Anvil of the hydraulic press. (B) The piston. (C) Pulse-generating crystal. (D) Pulse-receiving crystal. (E) Specimen.

3. Experimental Results

Three marble specimens were compressed and led to fracture finally in every experiment. Velocities of dilatational waves propagated parallel to the axis were measured for one specimen and those propagated perpendicular to the axis were measured for two specimens. Every experiment was carried out at the same stress rate, that is, about 2.5 minutes per ton. Tables I, II and III are the tabulated values of the velocities and the corresponding axial loads for three marble specimens. These values are also illustrated in Fig. 3 and Fig. 4. In every case, three specimens fractured at the axial load of about 520 kg/cm^2.

Velocities of dilatational wave for methyl-methacrylate were measured only for the direction parallel to the axis of load. They are tabulated in Table IV and are illustrated in Fig. 5. Up to the critical axial load, the marble specimens keep up the resisting strength, until they suddenly fracture and break into fragments much smaller than the individual crystal grains leaving two pyramids at both the upper and lower ends

of the specimens. These pyramids of the wrecked specimens are shown in Fig. 13.

Table I. Uniaxial pressure versus velocity of dilatational wave propagated parallel to the axis of a prismatic bar of the marble specimen (originated) from Akiyoshidai.

Pressure (kg/cm^2)	Velocity (m/sec)	Pressure (kg/cm^2)	Velocity (m/sec)
0.0	5500	297.7	5732
22.9	5493	320.6	5747
45.8	5497	332.1	5721
68.7	5530	343.5	5710
91.6	5538	366.4	5695
114.5	5577	389.3	5699
137.4	5583	412.2	5681
160.3	5601	435.1	5666
183.2	5644	458.0	5544
206.1	5662	480.9	5304
229.0	5655	503.8	4987
251.9	5736	515.3	4717
274.8	5721	527.0	fractured

Tables II, III. Uniaxial pressure versus velocity of dilatational wave propagated perpendicular to the axis of a prismatic bar of the marble specimen (originated) from Akiyoshidai.

Table II.

Pressure (kg/cm^2)	Velocity (m/sec)
0.0	5578
57.5	5613
115.0	5683
172.5	5750
230.0	5822
287.5	5802
345.0	5817
402.5	5682
460.0	5304
517.5	4375
520.0	fractured

Table III.

Pressure (kg/cm^2)	Velocity (m/sec)
0.0	5455
88.2	5480
176.4	5523
264.6	5536
352.8	5505
441.0	5331
470.4	5183
499.8	4821
517.4	fractured

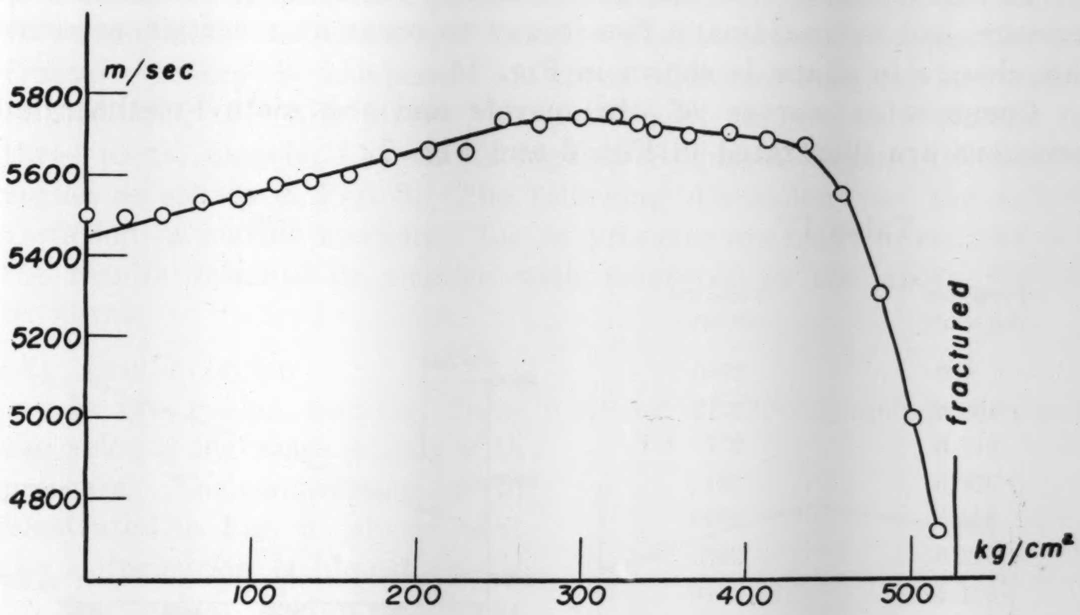

Fig. 3. Uniaxial pressure versus velocity of dilatational waves propagated along the axis of the pressure.

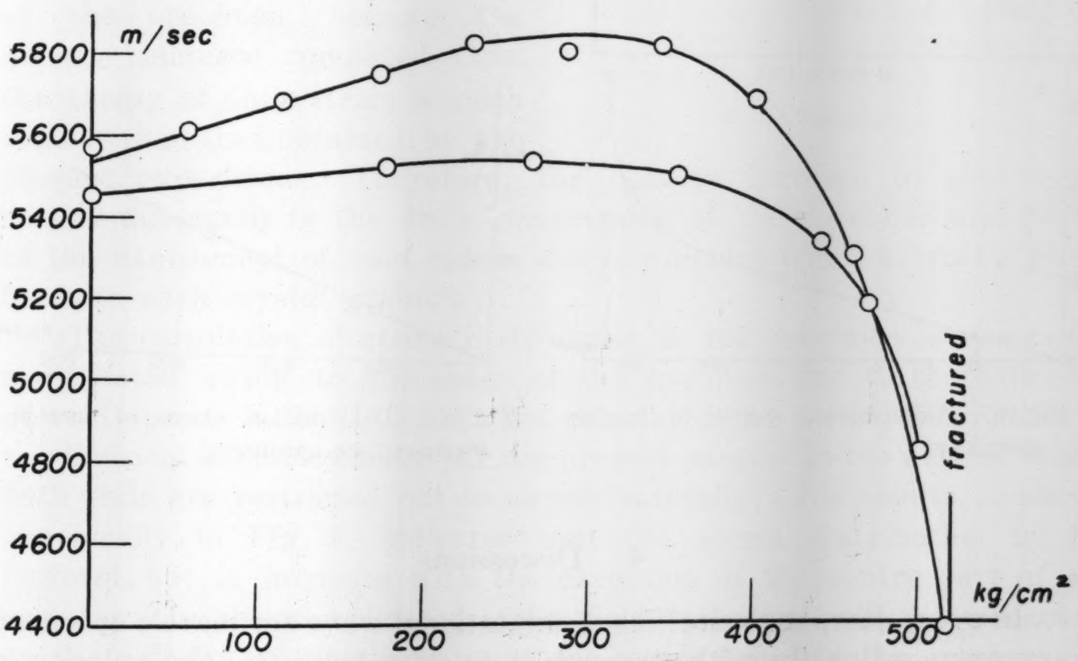

Fig. 4. Uniaxial pressure versus velocity of dilatational waves propagated parallel to the axis of the pressure.

Methyl-methacrylate did not fracture up to a considerable high pressure, but extraordinary flow began to occur at a certain pressure. This change in shape is shown in Fig. 14.

Compression curves of the marble and the methyl-methacrylate specimens are illustrated in Fig. 6 and Fig. 7.

Table IV.

Pressure (kg/cm^2)	Velocity (m/sec)
0.0	2740
108.5	2772
217.0	2777
325.5	2812
434.1	2830
542.6	2823
651.1	2876
759.7	2900
868.2	2920
976.7	2925
1085.3	2918
1193.8	2926

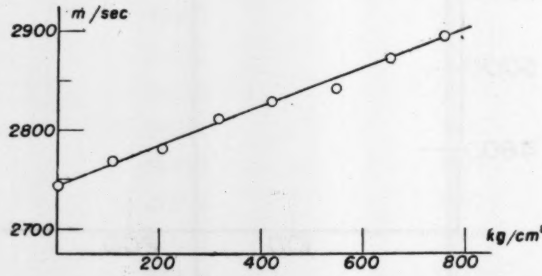

Fig. 5. Velocity of dilatational wave in methyl-methacrylate versus pressure.

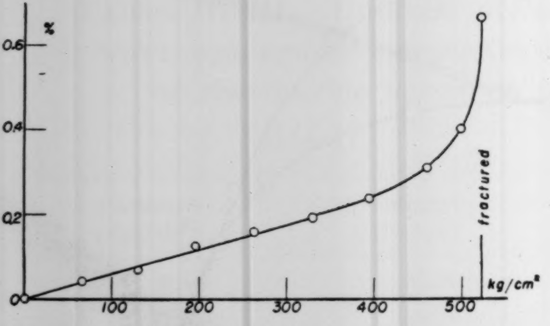

Fig. 6. Deformation curve of marble specimen.

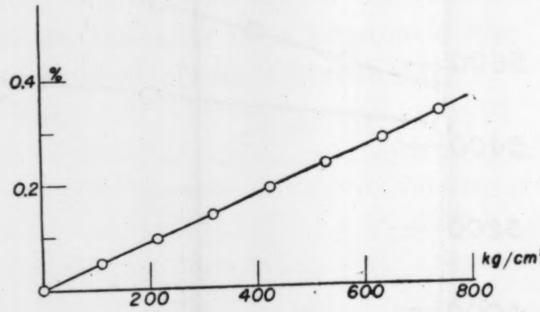

Fig. 7. Deformation curve of methyl-methacrylate specimen.

4. Discussions

In every case, the velocities of dilatational wave for marble specimens vary extraordinarily with pressure. At low pressure, the velocity increases with pressure at a considerable rate, until it ceases to increase and begins to decrease slightly with pressure. Then the velocity begins

to decrease with pressure by a considerable amount and fracture occurs. It seems that the change of velocity due to pressure in marble until fracture occurs is composed of three different regions in nature. Accordingly, we will divide the pattern of this velocity change into three parts, namely, (A) elastic region, (B) plastic region, (C) fracture region as shown in Fig. 8. The following discussions on the velocity variation in marble specimen due to pressure are made in contrast with the results obtained in plastics with reference to the above divisions by turns.

(A) Elastic region

In this region, namely, from 0 kg/cm² to 300 kg/cm² in pressure, the velocity increases largely with pressure. The compression curve, illustrated in Fig. 6, shows that the deformation is almost elastic in this region holding a linear relation between stress and strain. However, this large increase in velocity can not be considered only as the consequence of finite strain of the specimen, because the velocity increase computed from the theory of finite strain is much smaller than that obtained by the present experiment. Therefore, the velocity increase in this region may be due partly to the finite compression of the specimen and partly to the vanishment of void spaces due to pressure which existed *a priori* between each crystal grains[6].

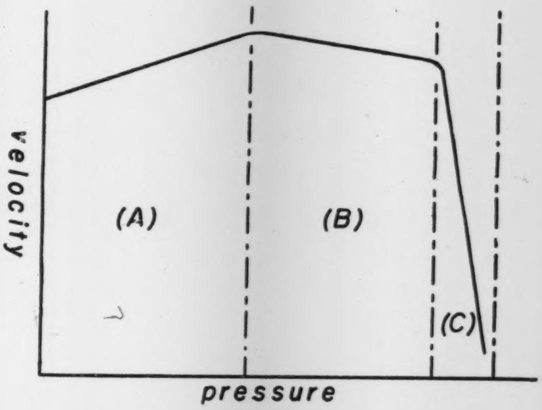

Fig. 8.

The calculation of stress distribution in the specimen is somewhat complicated owing to the shape of the specimen and to the existence of void space. L. N. G. Filon[7] has calculated the stress distribution in a cylindrical isotropic elastic bar compressed parallel to the axis of which both ends are restricted not to expand laterally. His results, as shown graphically in Fig. 9, indicates that the stress distribution is not uniform but is intricate with the exception of the centre part of the cylinder. In this complicated stress field, pressure will be efficacious on the velocity of elastic wave as the mean stress in the specimen.

6) D. SHIMOZURU, *Bull. Earthq. Res. Inst.*, **32** (1954), 73.
7) L. N. G. FILON, *Phil. Trans. Roy. Soc. London*, **198** (1902), 209.

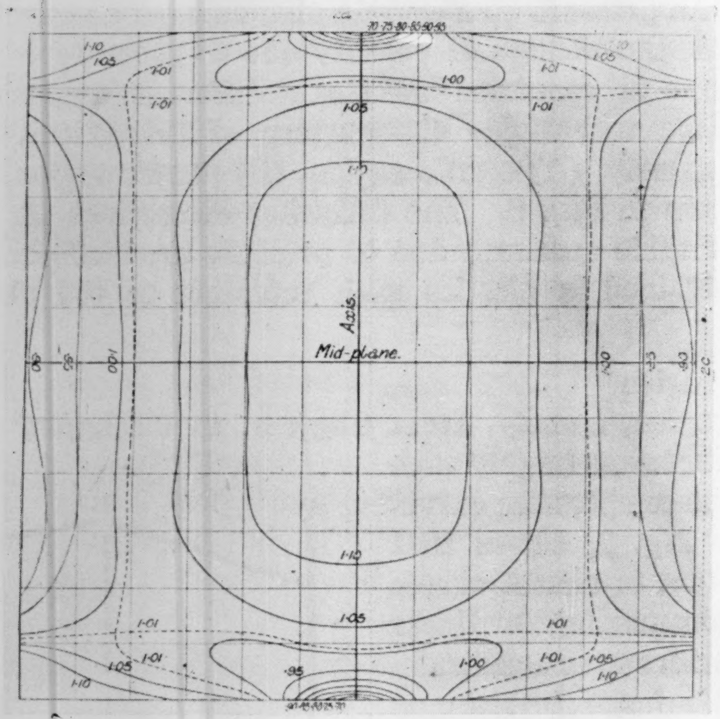

Fig. 9. Distribution of principal stress $\widehat{ZZ}$ inside the cylinder (case of compression between rough rigid plane) after Filon.

(B) Plastic Region

In this region which ranges from about $300\,kg/cm^2$ to $400\,kg/cm^2$ in pressure plastic deformation seems to have taken place. At present, metallurgists hold that many crystals deform plastically through translational slip which is caused by the movement of dislocations. According to them the critical shear stress necessary to move a dislocation is approximately

$$\sigma = \frac{2\mu}{(1-\nu)} e^{-2\pi/(1-\nu)} ,$$

where σ ...... critical shear stress,
ν ...... Poisson's ratio,
μ ...... Rigidity modulus.

If we put $\nu=0.27$, $\mu=2\times10^{11}$ dynes/cm², we obtain $\sigma=100\,kg/cm^2$ as the critical shear stress needed to move a dislocation in a calcite crystal along a crystallographic gliding plane. Considering the orientation of gliding plane in a crystal, however, the above shear stress must be multiplied by the orientation factor. Therefore, we infer that the

shear stress in this region is sufficient to move a dislocation in a composing crystal of the specimen. Then what will happen in the specimen?

If a slip plane contains an obstacle or a crystal grain boundary to the passage of dislocations, they will pile up into an equilibrium distribution against the obstacle, and thus large stress concentration will occur near a piled-up group of dislocations. The normal tensile stress σ acting on the plane making an angle θ with the slip plane is[8)9)]

$$\sigma=\frac{3}{2}\left(\frac{L_0}{r}\right)^{1/2}\sigma_0 \sin\theta\cos\frac{1}{2}\theta ,$$

where

L_0 .... length of the slip plane,

σ_0 .... applied shear stress,

r .... length of the crack.

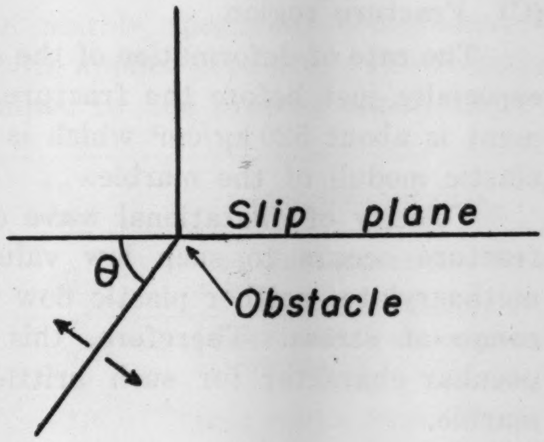

Fig. 10.

Therefore, θ is maximum when $\theta=70.5°$ of which the value is

$$\sigma_{\max}=\left(\frac{2}{\sqrt{3}}\right)\left(\frac{L_0}{r}\right)^{1/2}\sigma_0 .$$

On the other hand, according to Griffith's theory of crack of length r subjected to a tensile stress σ, the condition for the initiation of the crack is

$$\sigma^2 r > 16\gamma\mu/\pi(1-\nu) ,$$

where γ ...... surface energy per unit area,

μ ...... rigidity modulus,

ν ...... Poisson's ratio.

Thus we obtain the condition of initiation of crack as

$$n > 12\gamma/b\sigma_0 ,$$

where n ...... number of edge dislocations packed into a length L_0,

b ...... atomic spacing.

Since the approximate order of magnitude of γ, b, σ_0 are 10^3, 10^{-8} and 10^8 respectively n becomes of the order of 10^3 which is natural for many crystals. Thus, we conclude that, though it is difficult to

8) J. S. Koehler, *Phy. Rev.*, **85** (1952), 480.

9) A. N. Stroh, *Proc. Roy. Soc.*, **223** (1954), 404.

demonstrate at the present stage, large stress concentration round the piled-up group of dislocations at the end of a slip line as the consequence of plastic flow is sufficient to initiate a crack, and these cracks may reduce the velocity of dilatational wave in the specimen.

(C) Fracture region

The rate of deformation of the specimen becomes large in this region, especially just before the fracture. Fracture stress in every experiment is about 520 kg/cm^2 which is roughly of the order of 10^{-3} of the elastic moduli of the marble.

Velocity of dilatational wave decreases rapidly with stress before fracture occurs to such low value as 4300 m per second. In methylmethacrylate, neither plastic flow nor velocity decrease occur in such range of stress. Therefore, this large decrease in velocity may be a peculiar character for such brittle and polycrystalline aggregates as marble.

The cause of this large decrease in velocity in this region is considered to be quite different from that in plastic region. If the applied stress becomes considerably large, e.g. more than 400 kg/cm^2 in the present case, besides the formation of narrow cracks as a result of plastic flow, large cracks are produced along the grain boundary of the specimen which can be seen with the naked eye at the surface. As a result of formation of such cracks, which loosen the mechanical structure and reduce the resisting strength against the applied stress, the specimen begins to yield and finally breaks down. Thus these cracks which are wider than those produed by plastic flow will slacken greatly the velocity of elastic waves.

The total amount of deformation up to the fracture stress reaches to 10^{-3}, however, the actual elastic strain of the specimen will be much smaller than this value. Total work done till the specimen fractures which are obtained by the method of graphical integration of stress-strain curve is as follows:

$$\text{Total Work Done} = 10^6 \text{ ergs per unit volume.}$$

This value is much larger than that expected from the elasticity theory. In reality, the above value will depend not only on the mechanical structure of the specimen but on the rate of strain of the specimen, the temperature and the confining pressure. If we assume that rocks can store such amount of strain energy in their unit volume, the effective volume which can store a strain energy of 10^{25} ergs, which is

the energy of the earthquake of magnitude 8.7, is estimated to be approximately a sphere with a radius of about 24 km.[10]

Summary and Acknowledgment

Velocity of dilatational wave in marble specimens compressed by the hydraulic press vary markedly with applied pressure. The following table shows briefly the results obtained by the present experiment.

Pressure in kg/cm²	Region classified by the author	$\overline{dv}$ * / $\overline{dp}$	Miscellaneous facts
0–300	(A) Elastic	+0.1	void vanishes, elastic finite strain
300–400	(B) Plastic	−0.05	plastic flow, dislocations, narrow cracks
400–520	(C) Fracture	−1.6	large cracks, large flow

* Average rate of change in velocity with pressure.

It was found that symptoms of fracture of rocks could be regarded as the velocity decrease of dilatational wave starting from a point far below the fracture stress.

The author wishes to express his sincere thanks to Prof. R. Takahasi who offered him valuable suggestions regarding the present study. His thanks are also due to the members of the Department of Precise Engineering, Chûô University who accommodated him with a hydraulic press and operated it for the present experiment. He is also greatly indepted to the Grant in Aid for the Miscellaneous Scientific Researches of the Department of Education given for the series of the present work.

10) K. E. BULLEN, *Bull. Seis. Soc. Amer.* **45** (1955), 43.

31. 応力と岩石の弾性，特に破壊領域に就いて

地震研究所 下 鶴 大 輔

地殻に応力が蓄積して，或る限界を超えると遂いに破壊に至るという現象は浅い地震の発震機巧を考える場合に根本的問題となつて来る．此の実験は岩石にその様な応力が作用して遂いに破壊に至るまでの弾性的な性質の変化を超音波速度というものを媒介にして研究したものである．岩石の

試料としては，秋吉台産の大理石を角柱に切つたものを用い，材料試験機で軸圧をかけながら，軸方向及び軸に直角な方向の縦波の速度を測定した．又，岩石のように brittle な多結晶体と比較するために一種の有機ガラスについても同様な実験をした．その結果によると，速度の変化に三段階あるようにみえる．すなわち，圧力の小さいところでは速度はほぼ直線的に増加する．(弾性領域)．つぎに，速度は少しづつ減少しはじめる (塑性預域)．速度の減少の割合が急に激しくなつて遂いに破壊する (破壊領域)．この説明として，弾性預域では，void space の圧縮に伴う減少と結晶自体の finite strain による速度の増加がみられ，塑性領域では結晶中の dislocation が動いて，その結果粒界に応力集中が起きて，非常に小さい crack が沢山入るために速度が少しづつ減少する．破壊領域では結晶粒界の結合が loose になつて，大きな crack があちこちに入るため，変形も大きくなり速度の減少が甚しい．有機ガラスでは，同程度の応力ではほとんど弾性的性質を保つと考えられる．

このように，破壊は，一瞬にして起るけれども，破壊の芽生えは，破壊応力に達する相当以前から除々にでてくる．このことは，中を通る弾性波の速度に非常に鋭敏にきいてくるようであつて，応力が増すにもかかわらず速度が減少するという結果となつて表われることがわかつた．なお，大理石の変形曲線から外力のなした仕事を計算すると 10^6 ergs/cm^3 となる．つまり単位体積の中にこれだけのエネルギーを蓄えられるということである．大地震のエネルギーを 10^{25} ergs とすると，どの位の effective volume になるかというと，半径約 24 km の球となる．このこと自体も，地震の本性の研究上大変面白いが，岩石は完全弾性体ではないので，strain rate を変えたり，温度を変えたり，また，静水圧下で，軸圧を変えたりしなければ，本当の所は判らない．このことも将来に残された問題である．

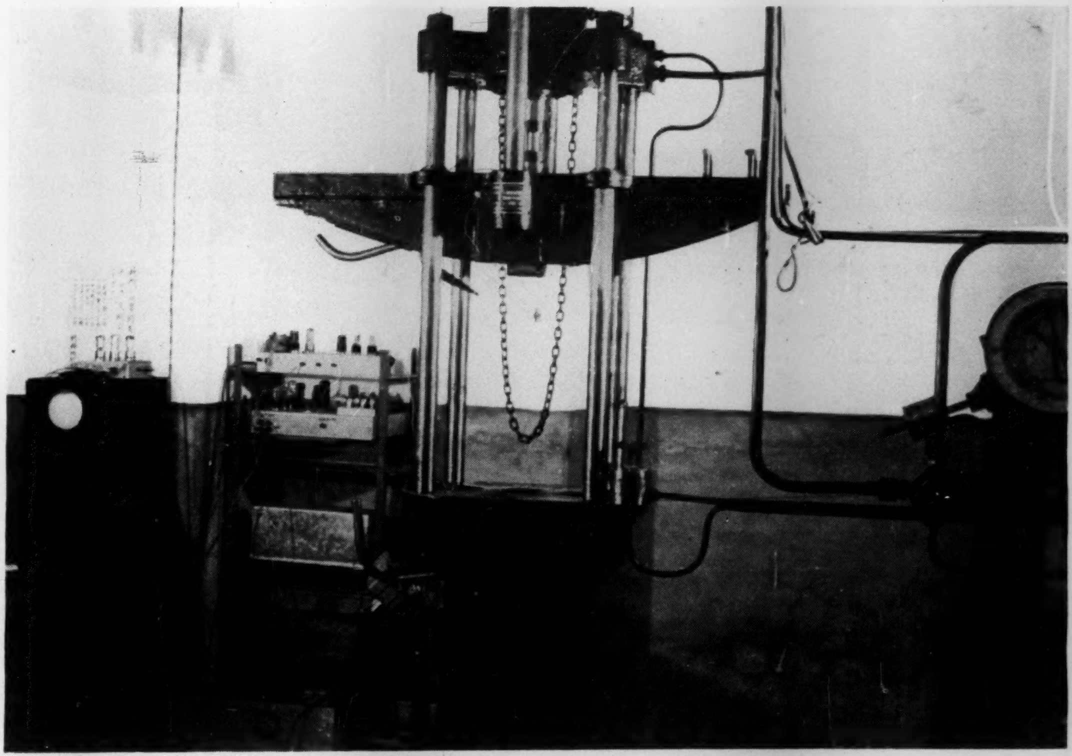

Fig. 11. General view of the experimental equipments.

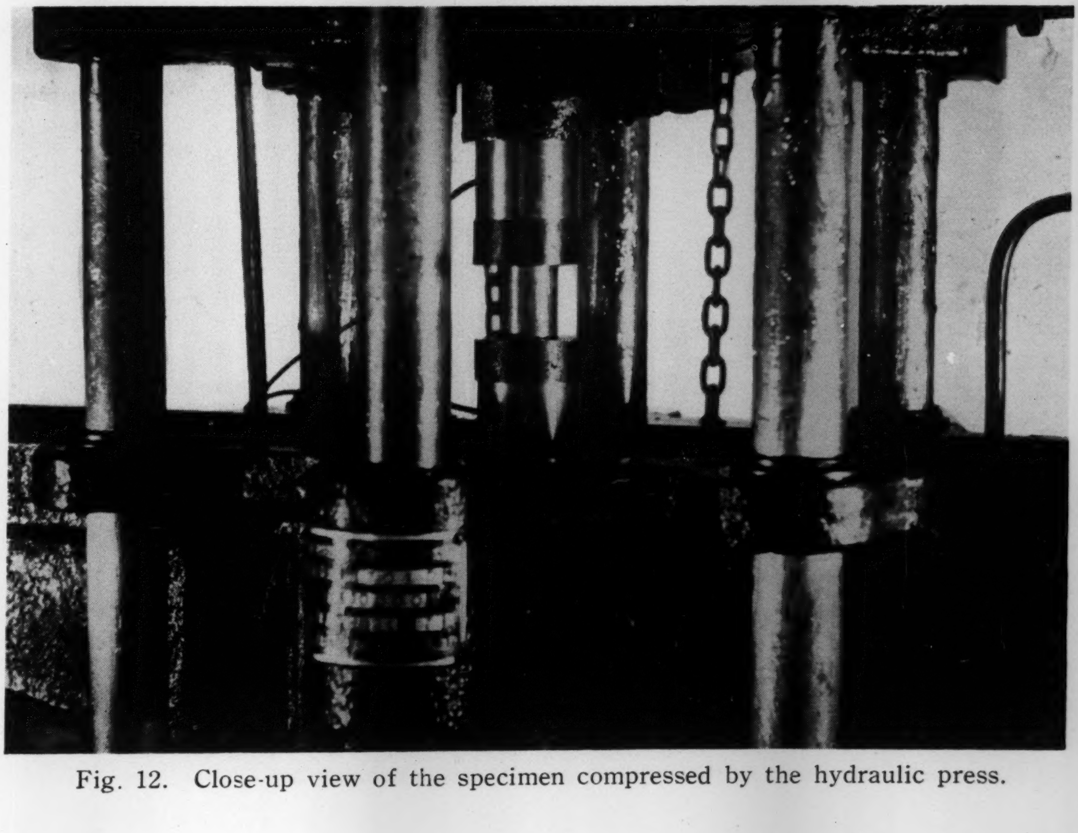

Fig. 12. Close-up view of the specimen compressed by the hydraulic press.

（震研彙報 第三十三号 図版 下鶴）

Fig. 13. Pyramids of marble specimen after fractured.

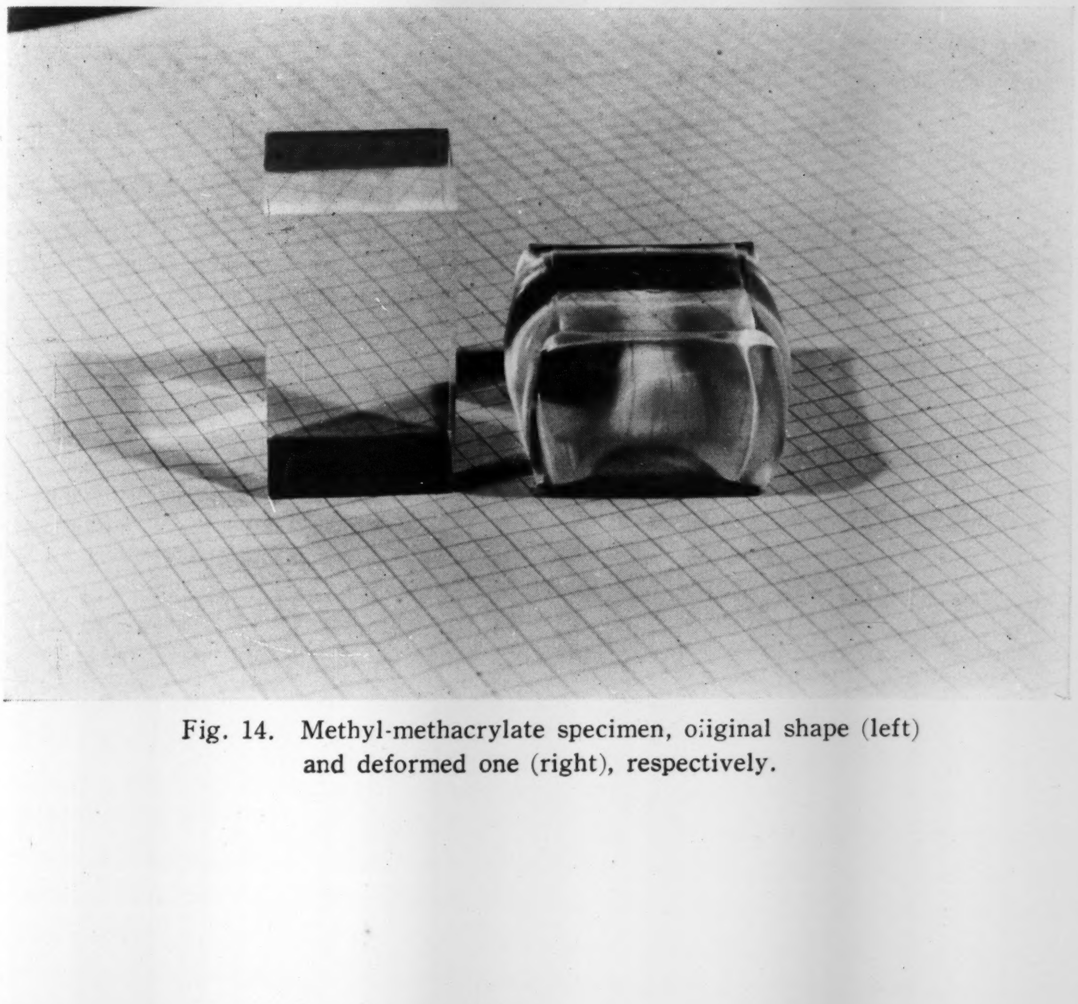

Fig. 14. Methyl-methacrylate specimen, original shape (left) and deformed one (right), respectively.

(震研彙報 第三十三号 図版 下鶴)

32. 静川層群について*
(附　第三紀地殼運動の一考察)

(昭和 14 年 12 月 21 日発表—昭和 30 年 6 月 30 日受理)

地震研究所　大塚彌之助

緒　　論

山梨県南部から静岡県庵原郡地方へかけて，富士川沿岸に広く分布する第三系は，稀に海棲貝類の化石を産し[1]，種々の岩相を呈して，その層序細分の必要に迫られてゐた．田中元之進[2] は身延山以北の巨摩山地に於いて，先ずこの第三系の層序区分を行ひ，次のやうに細分された．即ち上部から下部へ (1) 第四紀層，(2) 御坂層，(2a) 静川層，(2b) 櫛形山層，(2bi) 蘆倉層，(2bii) 大草里層，(2c) 中山層，(3) 秩父古生層で，御坂層中に静川層以下中山層迄を含めてゐる．

その後筆者[3] は富士見山断層崖の研究をした際に，その附近の第三系を曙礫層・静川層・櫛形山層・西八代統等に細分し，静川層の貝化石を研究して，静川層を，下部鮮新統と考へられてゐる下部掛川統と，略ぼ同時代の地質系統と推定した．

又筆者は地蔵岳・鳳凰山付近で，この第三系の研究[4] を行ひ，中山層を桃ノ木層と改め，桃ノ木層中から ***Lepidocyclina* (*Nephrolepidina*) *japonica*** Yabe, ***Miogypsina ozawai*** Hanzawa 等を含む泥岩を発見し，中新統下部のランギアン階の層であることを確め，少くとも桃ノ木層 (田中氏の中山層) だけは，富士山の北側に分布する，***Lepidocyclina* (*Nephrolepidina*) *japonica*** Yabe を含む御坂層に，該当させて差支えないことを明かにした．

本論に於いては，更に，その後実施した調査・研究により得られた資料を加へて，静川層の上下の層序を明かにして，之等を一纏めにして静川層群として，其の層位学的特徴を明かにして，その地質学的意義を明かにした．

静川層群の層序

静川層群とここに新たに呼ぶものは，富士川の中流域を占め，略ぼ南北に長い分布を示し，略ぼ類似の層位を示してゐる一連の地層群で，北は山梨県南巨摩郡五開村附近から，身延山東麓を過ぎ，内船南部附近に達する厚さ約 6000 m に達する大きな一海進輪廻を代表する地質系統である．

静川層群は岩相上，上部から下部へ次のやうに細分される．

---

* 故大塚弥之助博士 (1903–1950) は，1930 年から 1950 年 8 月 7 日病没されるまで地震研究所に在職された．この遺稿は，教授の没後，研究室から門下生により発見され，地質断面図 1 枚が見当らないほか原稿は完成されていた．この論文が書かれたのは 1940 年代であるが，最近再び問題になつている地方の地質に関する研究結果であり，引用文献として重要なものであるので，本記念号の発刊にあたり特に掲載することにした．(地震研究所 森本良平　記)

1) 鈴木　敏　富士図幅地質説明書 (1886), 36–37.
2) 田中元之進　小川琢治博士還暦記念地学論叢 (1930), 549–570.
3) 大塚弥之助　地質学雑誌 **41** (1934), 562–564; 地理学評論 **15** (1938), 969–984.
4) 大塚弥之助　地震研究所彙報 **19** (1941), 115–143.

静川層群	曙半凝固礫岩	(層厚 1250 m)
	静川砂岩	(層厚 1500 m)
	塩沢砂岩泥岩互層	(層厚 650 m)
	荒屋敷砂岩	(層厚 350 m)
	角打泥岩	(層厚 500 m)
	丸滝礫岩	(層厚 1000 m)
	小内船火砕岩	(層厚 700 m)

曙半凝固礫岩

山梨県南巨摩郡曙村中山附近に露出する水蝕円礫層を，曙半凝固礫岩の標準とする．遠望した場合には，この礫岩は灰白色又は灰色である．礫の大きさは全区域では一定でないが，中山附近では径 7 cm 内外の水蝕円礫が揃つてをり，円礫の長軸は層面に平行である．南巨摩郡五開村方面では，この礫岩の下半は礫の型が大きく，径 50 cm を超えるものも稀でない．それらの円礫の種類は石英閃緑岩・輝石安山岩・角閃石安山岩・玢岩・アルカリ粗面岩等を主体とし，稀に珪岩・砂岩の礫を含む．本累層の上限は欠けてゐるために本地域では明かでない．その下限は静川村手打沢の西，同村水口，同村夜子沢西部，曙村後山，同村遅沢等に確められるやうに，急斜した層面断層状の明確な境界面で静川砂岩と接してゐる．この境界の性質は，野外では，曙半凝固礫岩が静川砂岩に対して不整合の関係にあると断定するに足る資料を欠き，寧ろ整合状の層位関係で，僅に層面断層を生じたかの如く思はれる資料に豊富である．本層は西島村西部附近では，不整合の層位関係で，西島アルカリ粗面岩体その他と接してをり，その不整合面は急斜或ひは直立してゐる．又，その不整合の基底礫岩中にはアルカリ粗面岩の礫を豊富に含んでゐる．

仮に上記の境界を曙半凝固礫岩の下限とすれば，この下限から上の方へ約 150–100 m の厚さに円礫岩層の部分を横たへ，その上位に円礫を稀に持つ，厚さ約 100 m の砂岩の部分層を挾在する．この砂岩の部分層の分布は前記下限と略ぼ平行してゐるので，前記下限の境界が地層を斜断するやうな，断層でないことを示してゐる．この砂岩の部分層中には稀に海棲貝類の印痕又はその破片を含み，この砂岩の部分層が海成であることを示してゐる．この砂岩の部分層より上方は，一般に径 5–10 cm 内外の円礫からなる半凝固礫岩で，厚さ 1000 m 以上に達してゐる．

曙半凝固礫岩の層位は，地質図 (第 8 図) に示してあるやうに，略ぼ NS の層向を示し，その傾斜は急で,，殆ど垂直に近い部分さへある．併し一般には西へ傾き下り，分布区域の東部では傾斜 W 85° (西島村足平附近)，垂直或ひは E 80° (静川村水口附近)，W 65°–70° (八日市場村後山附近) であるが，五開村·大須成村大塩·石畑·間遠峠，曙村中山附近では垂直である．曙礫岩の分布区域の西部では，曙礫岩の一般層向に対して層向を異にし，五開村南方では層向 N 70° W: 傾斜 N55°–60°; 大須成村平須の南の溪谷では層向 N 20° W: 傾斜垂直; 曙村久保では層向 N 80° W: 傾斜 S 70°: 曙村腰巻の沢では層向 N 86° W: 傾斜 N 75°; 層向 N 80° W: 傾斜 N 55°; 曙村江尻窪の沢では層向 N 65° W: 傾斜 N 45° 等で層向を変へてゐる．この層向の変化する地点の分布は，曙礫岩が，後に述べる筈の，曙逆断層に接してゐる附近であるので，この逆断層によつて，曙礫岩が擾乱を受けたものと解釈することもできるが，曙礫岩が同斜褶曲構造を持ち，その向斜軸附近に沿うて層向の変換があるとも解釈できる．筆者は下位の静川砂岩の化石帯の分布が，舟形のやうな窪んだ向斜構造状の分布を示す点から判断して，後者である

と推定している．槇山次郎[5] もこの向斜構造に就いて論及されてゐる．

曙半凝固礫岩は後に述べる曙推し被せ断層のために，身延山下に没してゐるが更に南方で，波木井川の上流，豊岡村小田船原附近に，層向略ぼ南北，西へ急斜してをり，小田船原の北では層向 N 15° E: 傾斜 W 80°，小田船原の南では層向 NS: 傾斜 W 70°，相又下附近で同じく層向 NS: 傾斜 W 70° で，相又下から相又上に至る附近で，西へ傾く逆断層面を境として，古い地層で被ひ隠されてしまふ．

曙半凝固岩に類似する岩相の地層を本調査区域の附近に求めるならば，富士川—由比川間に露出する蒲原礫岩[6] が極めて類似した地層であるとして挙げることができる．蒲原礫岩の下部には砂岩相の部分があることは曙礫岩の場合とよく似てゐる．層序的に両層を同時代と見做して差支えない．本層は次の静川砂岩に比較して，岩相の点で全く別の堆積状況の下に堆積したと見られる．

静川砂岩

静川砂岩は南巨摩郡静川村夜子沢附近に露出する，主として黒色安山岩質物から構成されてゐる，砂岩および集塊岩質礫岩の地層であり，化石を豊富に含んでゐる．

夜子沢で観察した処によると，静川砂岩の最下部は，夜子沢部落の東端を劃する南北走向の不整合面[7] で，西八代層群に接するが，この不整合面の西に軟弱な鼠色又は黒色の砂岩層が，略ぼ層向 N 15° W: 傾斜 W 80°; 層向 N 15° E: 傾斜 E 70°; 層向 N 15° E: 傾斜 90° の層位で，約 250–300 m の厚さで露出する．この砂岩の西に鉄銹色に風化した安山岩質集塊岩層が約 20–30 m，更に風化せぬ黒色粗粒の安山岩質砂礫岩及び砂岩の層が 500–450 m の間に露出し，西部へ行く程細粒となり，小さな層面断層で曙礫岩と接してゐる．上に述べた風化した鉄銹色の安山岩質集塊岩は上伊沼の西の烏森山を構成してゐるものでその中には，石膏鉱床が胚胎されてゐる．筆者は之を烏森山集塊岩質部分層と呼ぶこととした．静川砂岩の風化せぬ砂岩中には貝化石を含んでゐる．

然るに，静川村大子山の南の渓谷では，次に述べる筈の鼠色の泑泥岩質からなる塩沢砂岩泥岩互層の薄層理の地層が，約 500 m の厚さに横たはり，然る後小層面断層を境として，夜子沢に見られるやうな静川砂岩の層序が追跡できる．

飯富村から早川渓谷の北岸に沿うて露出するものに就いては，飯富村部落の南端から西方へ約 600–700 m に亘つて，層向 N 45°–30° W: 傾斜 SW 50° の層位を持つ，西八代層群の砂岩・凝灰質礫岩が露出してゐるが，略ぼ南北に走る境界面を経て，その西側には鼠色の泑泥岩質の薄層理層の塩沢互層が露出し，更に三ツ石部落の東端に集塊岩質礫岩層が露出してゐる．この部分は侵蝕に対する抵抗が強いため早川河原に突出してゐる．之より西方早川釣橋附近迄は黒色の砂岩および鼠色の泥岩の互層で，早川釣橋附近は砂岩層からなつてゐる．早川釣橋の西方 300 m 附近には集塊岩及び安山岩の熔岩流の露出があり，その上位には含化石黒色砂岩層を横たへてゐる．この含化石砂岩層の上位は細く砕け易い泥岩質の層で，之は曙礫岩と接してゐる．故にこの層序では，第 1 図の柱状断面図に示したやうに，2 層の安山岩質集塊岩の部分層及び 1 枚の安山岩熔岩流（V 印）を介在してゐるが，大子山の南でみたやうな薄層理鼠色泑泥岩質の塩沢互層は静川砂岩の下に整合的に横たはるかの如く見えた．筆者は，暫く，早川の出口の北岸の露頭を以て，静川砂岩を細分する際の標準露出地と見做した．

---

5) 槇山次郎　学術研究会議構造地質学委員会講演 (1943).

6) 大塚弥之助　地震研究所彙報 **16** (1938), 428–429.

7) 大塚弥之助　前掲 (1938), 975 ではこの境界を断層と記したが斜交不整合が主体で断層は従的なものであることが明かとなつた．

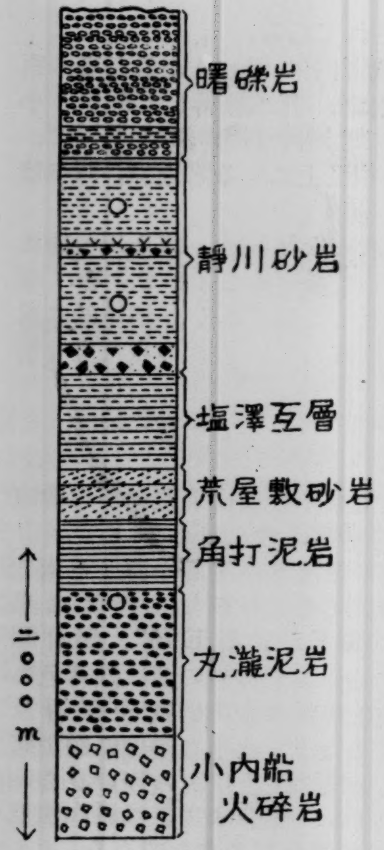

第 1 図　静川層群柱状断面図
編註：　丸滝泥岩は丸滝礫岩の誤り.

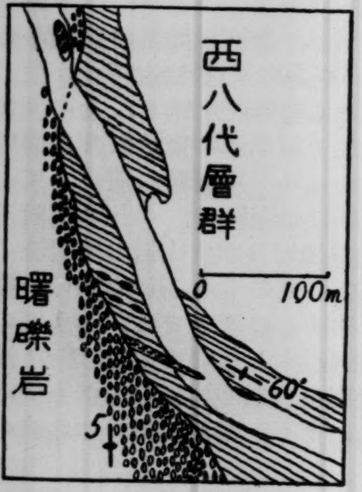

第 2 図　手打沢に露出してゐる曙礫岩と西八代層群との斜交不整合（平面図）.

静川砂岩の層位

静川砂岩はその黒色の安山岩質砂岩層と化石の豊富な点で他と容易に区別がつく．静川村附近に露出する静川層は層向略ぼ南北，曙半凝固礫岩の層位と似る．その地層の傾斜は大体に於いて西へ 60°–70°，或ひは垂直に近く，静川村手打沢で東西僅 200–300 m の間にしか露出してゐないものが，寺沢附近では約 500 m，夜子沢では 1000m 以上，鳥森山附近では 1500 m，標準露出地である早川北岸では 1500 m に達し，北へ行く程狭く南北に細長い．即ち北へ行く程地層の厚さが小さくなる特徴を示してゐる．

この静川砂岩とその東に位する西八代層群との境界は，一般に確め難いが，唯だ一ヶ所，静川村手打沢の河底で，次に述べるやうな露頭を発見でき，その境界が斜交不整合であることが明かとなつた．第 2 図はその見取図である．即ち N 60° W の層向を持ち，急に傾いた，中新統の西八代層群の泥岩層の褶曲構造の西に，略ぼ南北の層向を以て，西へ 80° 内外に急に傾く静川砂岩の基底礫岩が，断層でなしに，斜交不整合で接してゐる．この東西に近い層向の西八代層群も，南北走向の静川砂岩も，いずれも，夫々この地方の一般層向と一致してゐるので，この露頭が局部的なものとは考へられない．併しこのやうな斜交不整合関係を明かに示す露出面は，多くの場合観察できにくく，断層に移過する場合が多い．併しその断層の意義は左程重要視する必要はない．

静川砂岩は早川の南岸身延山方面へも延長分布することは，田中元之進[8] の記した如くである．併し栗倉以西，小原島に至る間の早川南岸には，曙礫岩の分布は殆ど見られぬが，静川砂岩は小原島附近に次の様な層位で露出してゐる．即ち小原島附近の静川砂岩は，層向 N 30° E：傾斜 NW 80° から西へ向つて次第に層向東西となり，更に層向 N 55°–70° W：傾斜 N70° の層位となり，曙逆断層面に沿うて楔状に分布し，曙村梨ノ子・福原附近に達する．従つて静川砂岩は舟窩状の向斜褶曲構造をしてゐるものと見做せる．小原島附近に産する貝化石は著しく歪められてゐるが，これは前に述べたやうに，曙礫岩にも見られたこの向斜褶曲構造が形成された時の変形作用のためであらう．

小原島付近の櫛形山累層は N 70° W の層向：90° に近い傾斜で走り，層序上，上位の静川砂岩と曙逆断層を境として接してゐる（第 3 図参照）.

8）田中元之進　前掲（1930），556.

下山村附近の静川砂岩は，早川橋の東方下粟倉の東北河岸に露出し，その層向 N 30°–40° W: 傾斜 WS 30° 程であるが，東へ行く程層向南北に近付き，層の傾斜垂直に近付き，遂に大子山附近から続く塩沢互層に接する．

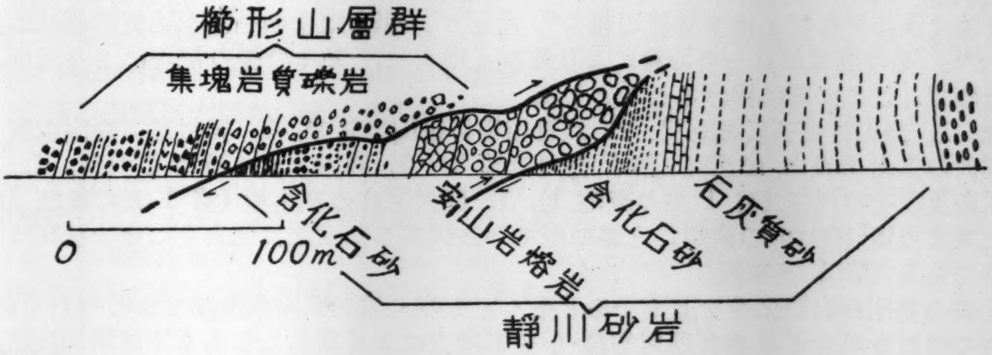

第 3 図　小原島の部落対岸の推し被せ断層露頭見取図 (正面図).

静川砂岩は更に身延町附近以南に分布し，主として砂岩質，稀に礫を交へ，身延山附近では安山岩質凝灰岩・集塊岩からなる 2 部分層を挾む．之等 2 部分層は静川村鳥森山の鳥森山集塊岩部分層その他に該当するものと言へる．

第 1 表　静川砂岩産化石

1.	*Cuculaea granulosa* (JONAS) var.	1	–	–
2.	*Glycymeris rotunda* (DUNKER)	1	2	3
3.	*Glycymeris totomiensis* (MAKIYAMA)	–	–	3
4.	*Chlamys miurensis* (YOKOYAMA)	1	2	–
5.	*Chlamys vesiculosa* (DUNKER)	1	–	–
6.	*Amussiopecten praesignis* (YOKOYAMA)	1	2	–
7.	*Limopsis tokaiensis* (YOKOYAMA)	–	–	3
8.	*Nemocardiuu sp.*	–	–	3
9.	*Meiocardia tetragona* (ADAMS et REEVE)	1	–	–
10.	*Venericardia panda* (YOKOYAMA)	1	2	3
11.	*Mercenaria chitaniana* (YOKOYAMA)	–	2	3
12.	*Dosinia sp.*	–	–	3
13.	*Dentalium yokoyamai* (MAKIYAMA)	1	2	3
14.	*Astraea sp.*	1	–	–
15.	*Lemintina muronoensis* (OTUKA)	1	–	–
16.	*Erosaria aff. boivini* (KIENER)	1	–	–
17.	*Microfusus magnificus* (LISCHKE)	1	–	–
18.	*Kelletia kelleti* ? (FORBES)	–	–	3
19.	*Siphonalia signum imai* (MAKIYAMA)	–	–	3
20.	*Polinices sp.*	1	2	–
21.	*Conus aff. tuberculosus* (TOMLIN)	–	2	–

1　下山村小原島 (産地 1)
2　曙村遅沢の東北 (産地 2)
3　下山村粟倉の東北麓 (産地 3)

本層は曙礫岩と同様に，更に南方へ分布し，匪ノ木峠の近くまで分布する．

静川砂岩の地質時代

静川砂岩は，幸，海棲貝類の化石に恵まれ，次の数ヶ所から報告されてゐる．之等の化石産地は既に平林武・鈴木敏等の報告[9] もあり，筆者はその一部を地質学雑誌に公にしたが[10]，その後徳田貞一の好意により種数も増大し，又その後の調査により産地も増大したので．ここに新に掲げることとした．

産地：1．静川村夜子沢押立沢，2．八日市場村後山東北方，3．同村烏ノ森山西麓，4．曙村遅沢の東北 500 m の沢底（第 1 表の産地 2)，5．同東北東 450 m の沢底，6．下山村小原島及びその対岸（第 1 表の産地 1)，7．同村粟倉の東北麓（第 1 表の産地 3)，8．同村上粟倉の東 500 m の崖等．之等の産地から採集した主な貝化石その他の種類は前頁の通りである（第 1 表参照)．

第1表の静川砂岩の化石を通覧すると殆んどその大部が黒潮型陸棚浅海に棲むもので，内湾性の特徴を示さず，静岡県周智郡・小笠郡地方によく露出してゐる下部掛川統に特有なもの，又は普通なものである．掛川統の地質時代は千谷好之助・槇山次郎等が鮮新世前半と考へてゐたもので，静川砂岩も略ぼ掛川統中の一部と同時代のものと思はれる．

塩沢砂岩泥岩互層

本層は身延町の東方，塩沢部落の渓谷から波木井橋附近に至る間に露出する砂質泥岩砂岩互層で，層向は略ぼ NS，傾斜 W 65°～80°，身延中学校北方には比較的厚層理の砂岩（厚さ約 100 m 以内）の立派な露出が見られる．

本層は，静川村大子山の南の渓谷で，500 m の厚さを有するが，それより以北では薄失し，以南へは連続露頭し，下山村妙見寺の谷，身延町一里松等によく観察でき，更に北清子，富士川の東岸の西八代郡大河内村平附近へ分布してゐる．

大子山附近では南北の層向の急斜した境界面によつてその連続を絶たれ，その境界面より東は礫岩を挟んだ砂岩及び泥岩の互層が略ぼ EW または N 60° E の層向で接してゐる．本層は塩沢附近では 650 m の厚さを有してゐる．

荒屋敷砂岩

荒屋敷砂岩は塩沢層の下位に整合状に横たはり，主として粗粒砂岩からなり，往々偽層理を呈し，礫岩の部分もある．本層は西八代郡大河内村和田・荒屋敷の富士川沿岸に露出する粗粒砂岩を標準とする．

この砂岩は厚層理状をなし，青味がかつた鶯色を呈し，礫岩は稀に径 5 cm 程の礫を挟み，その礫岩層の基底は不規則な面をなし，逆転相を示してをらぬ．

荒屋敷の本層は層向 NS：傾斜 W 50°，層向 N 10° E：傾斜 W 50°，層向 NS：傾斜 W 55° 等の層位を示してゐる．此の地層の厚さは約 350 m に達してゐる（第 9～12 図)．

本層は荒屋敷から北方では波木井附近に延びてゐるが，それより北方では薄く不明瞭となる．荒屋敷より南方では富士川の西岸に連り，光子沢・中村方面に露出してゐる．

本累層からは稀に化石を産し，富士川西岸の光子沢（大島部落の対岸）の出口の南の隧道南口附近から豊富に *Operculina ammonoides* (Gronovius) n. subsp. を含む砂岩を発見した．この化石は次に述べる丸滝礫岩からも産するが，両産地は同一の *Operculina*

9) 鈴木 敏 前掲 (1886), 36–37.
平林 武 震災予防調査会報告 **24**, (1898).
10) 大塚弥之助 前掲 (1934), 562–564.

帯に属するものかも知れぬ.

角打泥岩

角打泥岩は身延線身延駅の南方角打附近によく発達する泥と薄い砂岩層との互層で,砂岩層には安山岩質砂粒を含むことが多く,その上部には往々層間異常がみられる. 泥層は屡々 *Sagarites chitanii* MAKIYAMA を含んでゐる.

角打部落の西南富士川の沿岸,身延橋の西北等にこの特徴がよく示されてゐる. 層向は略ぼ NS で,傾斜は W 50°-60° を示してゐる. 本層は北方の分布が明かでなく,次第に砂相を呈してゐるもののやうである. 南方へは,大河内村大島附近迄延長し,富士川の沖積層下に没する. 上位の荒屋敷砂岩とは整合,下位の丸滝礫岩とも整合に重さなつてゐる. 本累層は北方へ向つても南方へ向つても,その分布が明かでなく,レンズ状層の疑がある. 角打泥岩の厚さは約 500 m に達する.

丸瀧礫岩

本累層は厚さ 1300 m にも達する砂礫岩で,身延線身延駅の北方,丸滝附近を標準露出地とする. 本層は主として粒径 7 cm-5 cm 内外の円礫を豊富に含む礫岩と泥質砂岩からなり,上部には細粒礫岩を横へ,下部には凝灰質岩を挾む.

身延駅の北の大崩沢では,沢の入口では砂岩・泥岩の互層であるが,奥へ入るに従つて礫岩に移化し,層向 NS,傾斜 W 55°-42° の層位を示し,更に細粒礫岩となり,厚さ 300 m で再び礫岩に移化して,大崩附近に露出する泥岩と接してゐる. (この泥岩中には大崩西部では角閃石安山岩の凝灰質砂礫岩をみることがある. 礫岩の礫には石英閃緑岩の礫が著しく目立つ.

塩ノ沢の渓谷の観察によれば,塩ノ沢入口附近は砂岩・礫岩の互層で,厚さ約 1000 m,層位は層向 N 15°-30° E: 傾斜 W 65°-70° 内外のものであるが,渓谷底に入ると石英閃緑岩の礫の目立つ礫岩層となり,その層向は NS—N 15° W,傾斜は W 50°-75° 内外である. 本礫岩は塩ノ沢部落の東方 1500 m で,下位の大崩砂・泥互層に接する. この関係は露頭面では整合状に見える. 礫の大きさは大崩の沢の場合より一般に大型である. 之等の礫岩中には稀に薄い泥質砂岩層を介在し,その層位を正しく測定できる.

西八代郡大河内村帯金も丸滝礫岩の露出区域で,下八木沢泥岩との関係が確められる. 第 11 図は帯金附近の調査図で,丸滝礫岩が層向 NS: 傾斜 W 43°, 層向 N 15° E: 傾斜 W 60°, 層向 N 20° E: 傾斜 W 35°, 層向 N 15° E: 傾斜 W 52°, 層向 N 5° E: 傾斜 W 60°, 層向 N 5° W: 傾斜 W 45°, 層向 N 10° E: 傾斜 W 47° 等を示してゐるのに,その延長上には礫岩は露出せず,西八代層群の下八木沢泥岩の泥岩が層向 N 15° W: 傾斜 90°, 層向 N 15°-38° W: 傾斜 W 30°, 層向 N 20° W: 傾斜 W 48°-32° の層位で分布してをり,両者の間が斜交不整合であることを示してゐる. (第〇図 [図紛失] の露頭 4 号では礫岩中に 1 m 以上の径の泥岩層の大礫を含んでゐるし,露頭 5 号では砂泥互層がこの礫岩の下に不整合に横はつてゐる).

本累層は南へ至るに従ひ礫相を変へ,砂質ないし泥質の相になる. 西八代郡栄村湯別当附近の本累層下部の礫層中にも下八木沢累層の砂泥互層の大礫を有し,その砂泥互層の大礫中には *Sagarites* 等を含み,八木沢累層の上に本累層が不整合に横はることを暗示してゐる. 南部町附近では本累層は砂相部が多く,礫相部は少い.

本層からは稀に化石を産し,上記湯別当の礫からは *Ostrea* 属の破片を産し,帯金 (第 11 図参照) に *Operculina ammonoides* (GRONOVIUS) n. subsp. を含む砂岩を発見した.

小内船火砕岩累層

小内船火砕岩累層は丸滝礫岩の下位に横はり，黒色の複輝石安山岩の角礫状熔岩・集塊岩質礫岩等からなり，厚さ 700 m 前後に達する部分もある．南部部落の対岸，阿層・小内船附近によく露出し，大河内村馬込の沢にもよく露出してゐる．

馬込の沢では，先づ沢の入口から大島温泉附近までは，丸滝礫岩が略ぼ南北に近い層向で，西へ 60° に傾いて発達するが，その東方 50 m 付近で小内船火砕岩累層となり，沢の入口から約 1350 m 附近で，黒色の砂岩・泥岩の互層からなる西八代層群に接してゐる．

小内船火砕岩累層は大崩方面では丸滝礫岩の下位に露出してゐない（第 9–12 図参照）．

静川層群の層位

以上に詳述したやうに静川層群は小内船火砕岩累層を基底として，曙礫岩に至る一大沈積輪廻堆積物である（第 4 図）．静川層群の大沈積輪廻は，先づその基底の火砕岩で示されるやうに火山活動に始まつて，次第に南から北へ海進して行つたものと解釈できる．即ち静川層群の基底は多くの場合斜交不整合を以て，下位の古い岩石・地層に接し，併も小内船火砕岩累層は内船から約 6 km 迄の間，静川層群の基底を占めて分布するが，丸滝礫岩は小内船火砕岩累層より更に北方で約 6 km 程の間，小内船累層を挾まず，直接に下位の地層群に斜交不整合で接してゐる．しかるに更に北方では丸滝礫岩の上に位する塩沢互層が斜交不整合に西八代層群に接し，更に北方では静川砂岩が斜交不整合で直接に西八代層群に接し，最後には曙礫岩が西八代層群或ひは西島アルカリ粗面岩体に接するに至る．このやうな層位上の関係は南から北へ進んだ一つの海進的累積（transgressive overlap）を代表する堆積状態の断面図をみてゐるやうなもので，静川層群の傾斜が西へ 90°–45° に傾いてゐるので，その地質図は，曙礫岩・静川砂岩に見られる向斜褶曲構造を除けば，略ぼ静川層群の地質断面図を見てゐるやうなものである．

静川層群は既に上に述べたやうに，静川砂岩・荒屋敷砂岩・角打泥岩・丸滝礫岩中に，化石類を含んでをり，静川砂岩のは掛川統の大日階の化石類に類似し，黒潮・陸棚浅海の特徴を示してゐる．荒屋敷・丸滝両累層のものは *Operculina ammonoides* GRONOVIUS) n. subsp. を密集含有し，下部掛川統下部（＝堀ノ内層準）に見られる *Operculina ammonoides*（＝*Op. venosa*）帯を想起せしめる[11]．又，角打泥岩中の *Sagarites chitanii* MAKIYAMA は下部掛川統下部（堀ノ内層準）にも普通に産してゐる[12]．以上の諸点から考察すれば本層群は先づ掛川統の沈積輪廻と略ぼ同時代のものと見做すことができやう．

静川層群に該当するものは富士川河口地方の浜石岳礫岩[13]，興津川上流の清見寺層群[14]等で，両者は何れもその基底に複輝石安山岩類の火砕岩を介在してゐる（又前者には掛川世を思はせる化石類を含んでゐる）ので，静川層群としても下半に近いものであらう．静川層群が南から北へ海進したと推定でき，而も，その南方にある浜石岳・清見寺

11）半沢正四郎 東北帝国大学理科報告（地質学）**18** (1935), 1 号, 6, 20. 荒屋敷・丸滝両累層産のものは径 2.5 mm 程度のもの最も多く，3 mm 以上のものは殆どない．この現生種と稍々その特徴を異にしてゐる．尚，半沢正四郎は日本地質学地理学輯報 **16** 巻 (1939), 3–4 号, 225–232 頁に於いて，*Operculinella venosa* (FICHTEL et MOLL) は *Operculina ammonoides* (GRONOVIUS) であることを明かにした．

12）J. MAKIYAMA, *Mem. Coll. Sci. Imp. Univ. Kyoto*, [B], **7** (1931), 6.

13）大塚弥之助 地震研究所彙報 **16** (1938), 429.

14）大塚弥之助 地震研究所彙報 **21** (1944), 403.

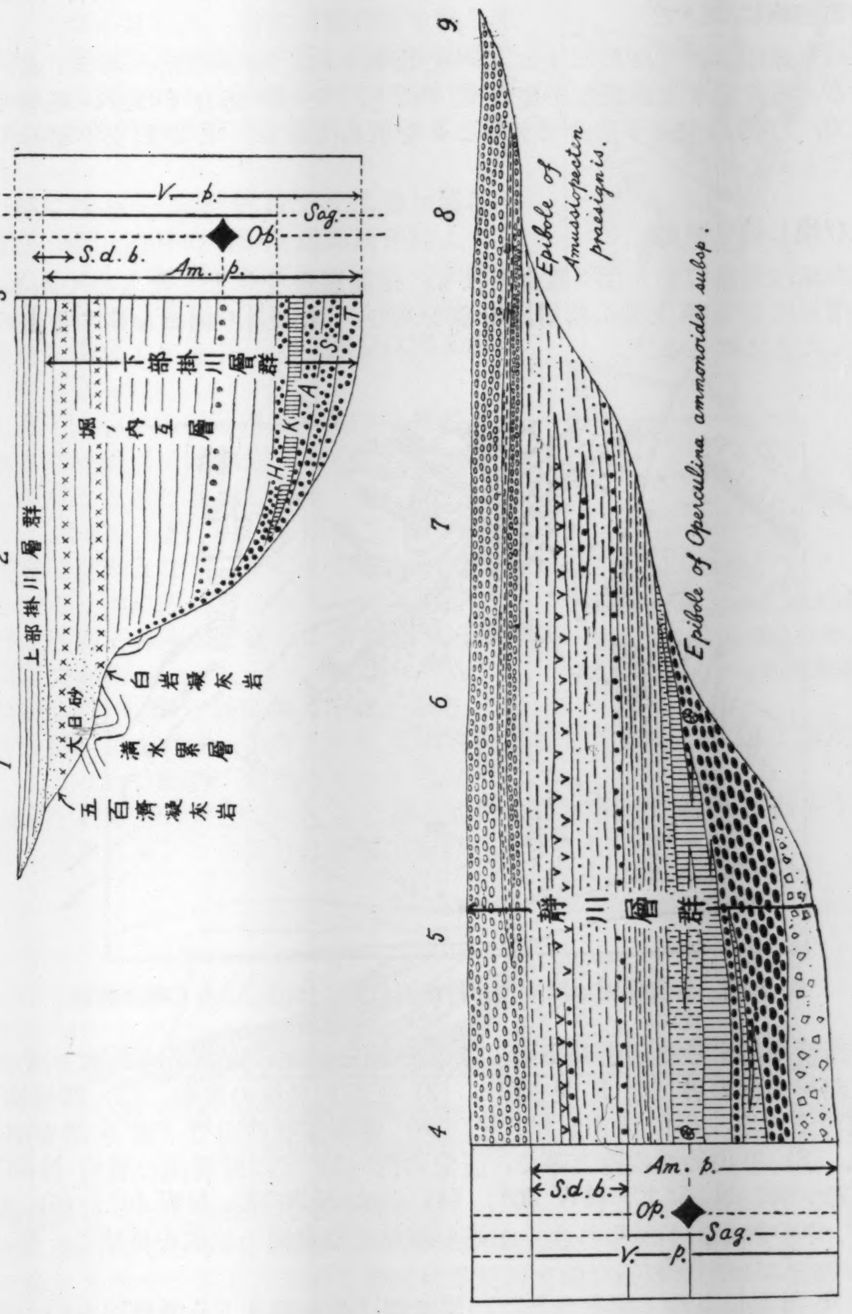

第 4 図　静川層群の海進的累積を示す堆積状態の概念図.

両層群が静川層群下半に比べられるとすれば，この静川層群の海進は比較的広範囲の海進作用であつたことを思はせる．

静川層群の西縁について

静川層群の東縁については既に上に述べた事実から，南から北へ向つて進入した海の堆積物であることを示す海進的な不整合で，而も，その不整合下の古い地層の構造は甚だ複雑なので，明瞭な斜交不整合であることを示してゐる．この斜交不整合のことは既に報告したことがある[15]．

曙衝上及び推し被せ断層

本層群の西縁は東縁のやうな不整合でなく，逆断層を主体としたものである．その内，五開村より曙村に至る富士見山断層崖の麓を走り，曙礫岩の西縁を劃するものに就いては既に報告したことがある[16]．

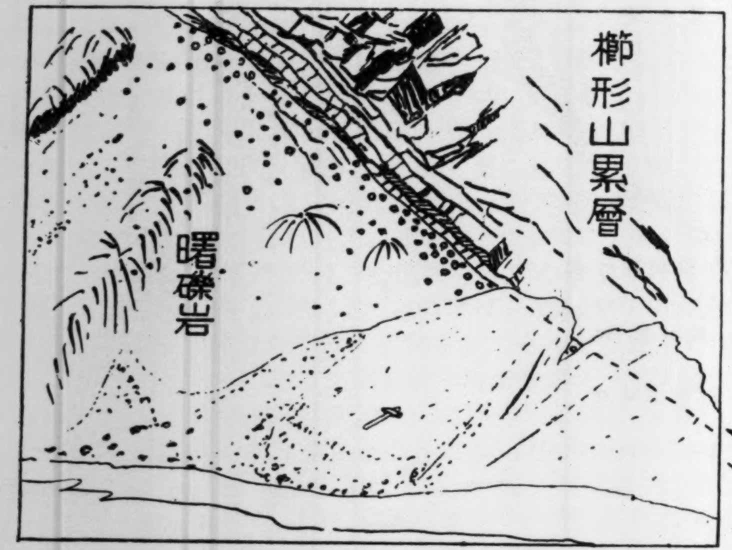

第 5 図　山梨県南巨摩郡五開村白沢の奥に露出してゐる曙逆断層．

曙礫岩の西境を劃する断層を曙断層と呼ぶ．曙断層面の露頭は次の数ケ所で確認できた．(1) 五開村白沢の奥（第 5 図参照），(2) 五開村鳥屋の東端，(3) 同村柳川の南部，(4) 大須成村上大塩，(5) 大須成村堂平，(6) 曙村腰巻の西方（第 6 図参照），(7) 江尻窪の東方，(8) 早川釣橋の西方等で，上記の内 (1) では断層面の層向 N 55° E: 傾斜 NW 60°; (2) では N 35° E: NW 40°; (4) では N 20° E: NW 40°; (6) では N 18° E: NW 62° 等の測定値が得られた．上述の露頭の他実測で位置を推定し，第 9–10 図地質図に示すやうな分布を得た．

第 3，5，6 図等によつて解るやうに，曙断層は西へ傾き下る断層面を持つ衝上及び推し被せ逆断層である．早川釣橋から下山村小原島に至る間早川の北岸には曙断層が露出してゐるが，南岸には櫛形山層群及び静川砂岩が露出し，早川の河底に逆断層が隠さ

15)　大塚弥之助　日本の地質構造 (1942), 161.
16)　大塚弥之助　前掲 (1938).

れてゐる．この逆断層は栗倉附近から下山村西部へと達し，1 つの大きな逆断層系である．

曙逆断層に接近した分岐逆断層系は腰巻部落の上流，梨ノ木等に見られ，前者は曙礫岩を截り主断層に平行，後者は主断層に平行して櫛形山層群と静川砂岩との間を走り小原島の対岸で層向 N 80° W：傾斜 S 30° の断層面を露出してゐる（第 3 図参照）．

以上の様に曙村一五開村付近では静川層群の西縁は略ぼ 45° 内外の明かな逆断層系によつて劃されてゐることが確認されてゐる．この逆断層系は更に南へ分布してゐるであらうことは静川層群の分布から推定できるが，その露頭は容易に求めることができない．

第 6 図　山梨県南巨摩郡曙村腰巻の西方に露出している曙逆断層．

南巨摩郡下山村杉山部落南方の沢での観察によれば，波木井坂附近では砂岩であるが，沢の入口附近から傾斜は次第に急斜し，泥・砂の細層理互層となる．沢口から約 100 m 附近で砂岩相に変化し，傾斜は垂直となり，更にその西方は集塊岩質礫層となる．次に泥岩層となり，急に集塊岩質の層灰岩と砂岩との互層となる．この集塊岩は複輝石安山岩である．

本層の西に西へ 60° 程に傾く断層があり，白色の鉱物の網状脈を有する破砕された安山岩が露出してゐる．本層は静川層群のものでなく，それより古い櫛形山層群のものと見做せる．

身延村東北新宿部落附近では，この静川層群の西縁附近で第 7 図のやうに甚だしく揉めた部分が見られる．この部分は櫛形山層群に属するものらしい．

第 7 図　南巨摩郡身延町の東，新宿部落北部に露出している擾乱された地層．露頭の高さ約 6 m.

南部部落附近では丸滝礫岩は砂岩相を呈し，NS に走り，傾斜は W 55° 内外に傾き，南部岩床に貫かれてゐるが，南部の西の柳島附近は砂・泥の細層理互層で，第 8 図のやうに複雑に擾乱を受けてゐる．この互層は柳島泥岩で櫛形山層群中の 1 累層で，***Sagarites chitanii*** を含んでゐる．丸滝礫岩と柳島泥岩との接触部は明かな断層で，クシャクシャに揉めた柳島泥岩中に砂岩の角礫が転在し，西へ 50° 内外に傾くが，その東は鉄銹色をした稍々明瞭な断層面を境として，整然とした砂礫岩層が横はつてゐる．この断層面は層向 N 10° W：傾斜 W 55°–50° と測定した．（この露頭は第 12 図地質図 A 地点である．）

以上の様に静川層群の西緣は各地に於いて逆斷層の層位關係を示してゐる．從つて斷層關係の確實に知られた箇所は數箇所に過ぎないが，静川層群の西緣を一般に逆斷層で境をされてゐるものと見做しても差支えあるまい．今仮に上のやうに推定すると，地質図第 9・10・11・12 図に示されてゐるやうに，北部では曙礫岩が櫛形山層群と斷層で接してゐるが，身延山附近では西側の古い地層・岩石は東へ凸出して，塩沢砂岩泥岩互層と接してゐる．それにも関はらず相又川の溪谷では，この境は西へ後退し，再び曙礫岩と接してゐる．又南へ向ふに從ひ，この境界は東へ凸出し，遂に南部部落附近では丸滝礫岩と逆斷層で接してゐるのである．從つて上述の内，東へ凸出した部分では，静川層群の上部が逆斷層を境として，古い岩石・地層のため被ひ隠されてゐるものと見做せる訳である．このやうに静川層群の西緣は大きな逆斷層系であるが，南部部落以南では静川層群が分布せぬため，その分布も稍々明瞭でない．この逆斷層は静川層群全部を地下に隠してしまふものと思はれる．併し更に南方では再び静川層群に該当する清見寺層群の西緣に沿うて分布し，中河内一袖師斷層[17]として，南は駿河湾へ向つて，連なつてゐるやうに見える．尤もその連絡はまだ確めてゐない．

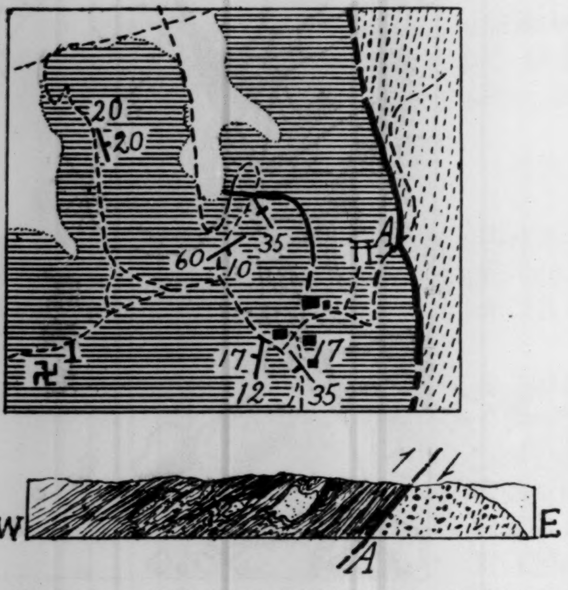

第 8 図 山梨県南巨摩郡睦合村柳島の曙逆斷層の露頭（第 12 図 A 地点）．

この逆斷層は曙逆斷層と初め呼んだので，その儘々その延長にも適用することとした．

以上述べたことによつて，静川層群の西緣は一つの大きな逆斷層系で境されてゐることが明かとなつた．しかもこの逆斷層系は種々の傾斜を示し，W 70° 近くの急傾斜から，W 20° 近い低い角度に傾くこともあり，そのために静川層群の分布は極めて不規則で，ある場合には全層群が古期岩層に被はれてしまふことがある．またこの斷層系は南方駿河湾に迄も延長することが推定される．

静川層群総括 附．第三紀地殼運動一考察

以上の静川層群に関する観察から次のやうな結論が得られる．

1．静川層群は次のやうな累層に細分される．即ち基底から上部へと，小内船火砕岩・丸滝礫岩・角打泥岩・荒屋敷砂岩・塩沢砂岩泥岩互層・静川砂岩・曙礫岩．

2．静川層群の層厚は小内船火砕岩から曙礫岩まで身延町附近の観察で 6000 m に近いが，北部では 1500 m 内外に過ぎぬ．

3．静川層群堆積期初期には既に石英閃緑岩が地表に露出してをり，円礫となることができた．

4．静川層群は南から北へ向つて累積した堆積相を示し，一つの大きな海進輪廻を代表する堆積物である．從つて静川層群が堆積した海は南から北へ向つて行はれたものであ

17） 大塚弥之助 前掲 (1944), 408–410.

る．

5．静川層群の堆積は火山活動を以つて開始されてゐる．静川砂岩の堆積中に鳥森山安山岩類の噴出があつた．

6．静川層群には古生物を含み，静川砂岩中には主として軟体動物化石を，角打泥岩中には ***Sagarites*** を，荒屋敷砂岩・丸滝礫岩中には ***Operculina*** を産する．静川砂岩の軟体動物群は基底の斜交不整合部に近附く程種類多く，陸棚浅海，黒潮型で，下部掛川統のものに類似してゐる．荒屋敷砂岩・角打泥岩・丸滝礫岩のものは下部掛川統の堀ノ内階のものに類似する．以上の古生物上の特徴は下部掛川統と同時代のものと見做すことを許してゐる．

7．静川層群と下部掛川統との海進はその規模に於いて略ぼ等しいものと見做される．

8．静川層群の基底は明かな斜交不整合である．下部鮮新統と推定できるこのやうな地層の基底に，このやうな明瞭な斜交不整合の見られる他の例は，静岡県掛川地方の下部掛川層群の基底[18]と，三浦半島の下部武蔵野累層の基底[19]と，房総半島地方の天津累層の基底[20]とである．

9．このやうな斜交不整合は奥羽地方西部の新第三系中には見られない[21]．即ち掛川・房総・三浦両半島・富士川流域地方と奥羽地方西部とは新第三紀地質構造発達史を異にするものと言へる．即ち前地方には中新世末乃至鮮新世初期に造構造運動があつたと解釈でき，後地方にはそのことがなかつたと言はねばなるまい．

10．静川層群は略ぼ南北の層向を示し，一般に西へ急斜し，直立することさへあり，その分布区域の西で，等斜向斜構造をなす．その東縁は斜交不整合，西縁は層向略ぼ南北に近い逆断層で，古い地層・岩石に被はれる．静川層群に該当する浜石岳礫岩・清見寺層群も褶曲・変位し，その特徴は静川層群のものと類似する．

11．このやうな静川層群の層位上の特徴は，同時代の地層である下部掛川統には全く見られない．後者に於いては 10° 内外で西又は南へ緩傾斜する半円皿状の構造を示すに過ぎない[22]この点に於いて富士川沿岸地方は掛川地方ともその新第三紀地質構造発達史を異にしてゐる．即ち前地方では，鮮新世末以後にも，激しい造構造運動があつた訳である．即ち，この点では奥羽地方西部の新第三紀地質構造発達史に類似してゐる．

12．富士川沿岸地方は中新世末乃至鮮新世初期には掛川地方と類似な地質構造発達史をとり，鮮新世後半以後に於いては奥羽地方西部の第三紀地質構造発達史に類似する．すなわち富士川沿岸地方は両地域の造構造運動を受けてゐる．即ち前者は大井川褶曲であり，後者は瑞穂・フォッサ・マグナ褶曲である．富士川沿岸地方は之等両褶曲が，前後して行はれた交叉褶曲地域といふことができる．

13．本論文では静川層群に就いてのみ論じ，古期層に就いては述べなかつた．之等に就いては他日詳論する機会があると思ふ．唯だ身延山付近の火山岩類は，掛川地方南方に発達する相良層群より，後期の噴出物であらうと思はれること，南部部落西方の柳島泥岩は相良層群の一部に比較されるであらうことが，最近の調査によつて稍々明かにされたことをここに述べておく．静岡県庵原郡両河内村の檜村泥岩も，この柳島泥岩に近い

18) J. MAKIYAMA, *Mem. Coll. Sci. Kyoto Imp. Univ.*, [B], **7** (1931).

19) 渡辺久吉　地学雑誌 **37** (1925), 495–501, 585–595.

20) 著者は天津累層の基底に斜交不整合を発見してゐる．その露頭は安房郡保田，富浦等にある．

21) 従来の報告類に発見されてゐない．

22) J. MAKIYAMA, *op. cit.* (1933).

第 9 図　山梨県南巨摩郡，鰍沢南方，五開村附近の地質図．凡例は第 13 図にある．

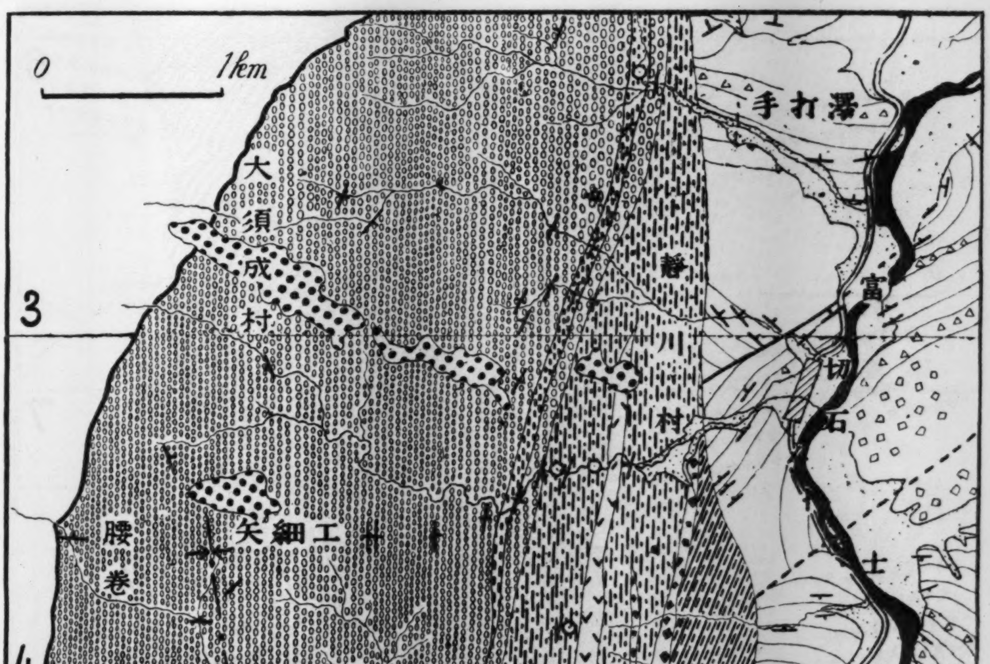

第 10 図　山梨県南巨摩郡曙村・飯富附近の地質図．凡例は第 13 図にある．

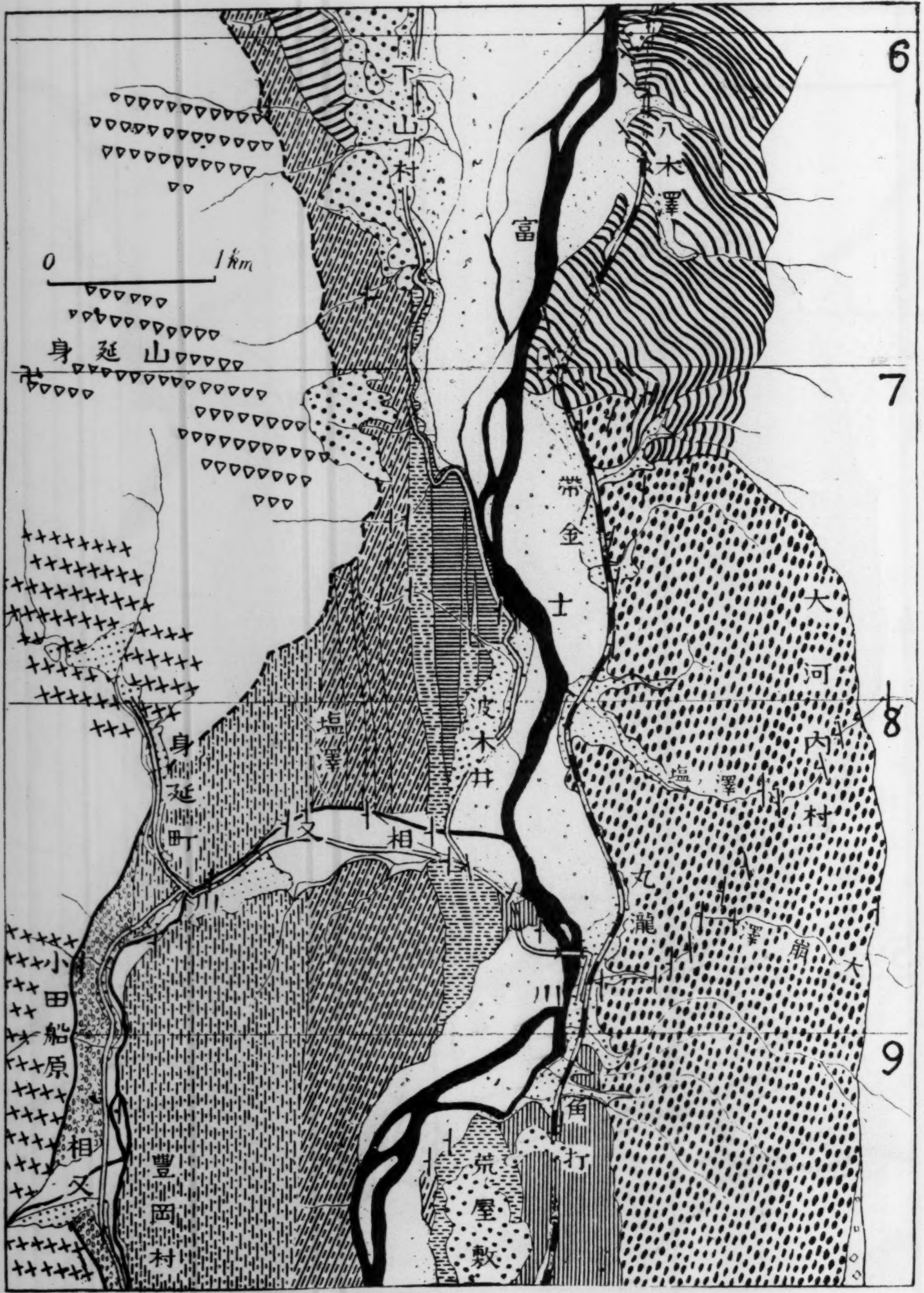

第 11 図 山梨県南巨摩郡身延町附近の地質図．凡例は第 13 図にある．

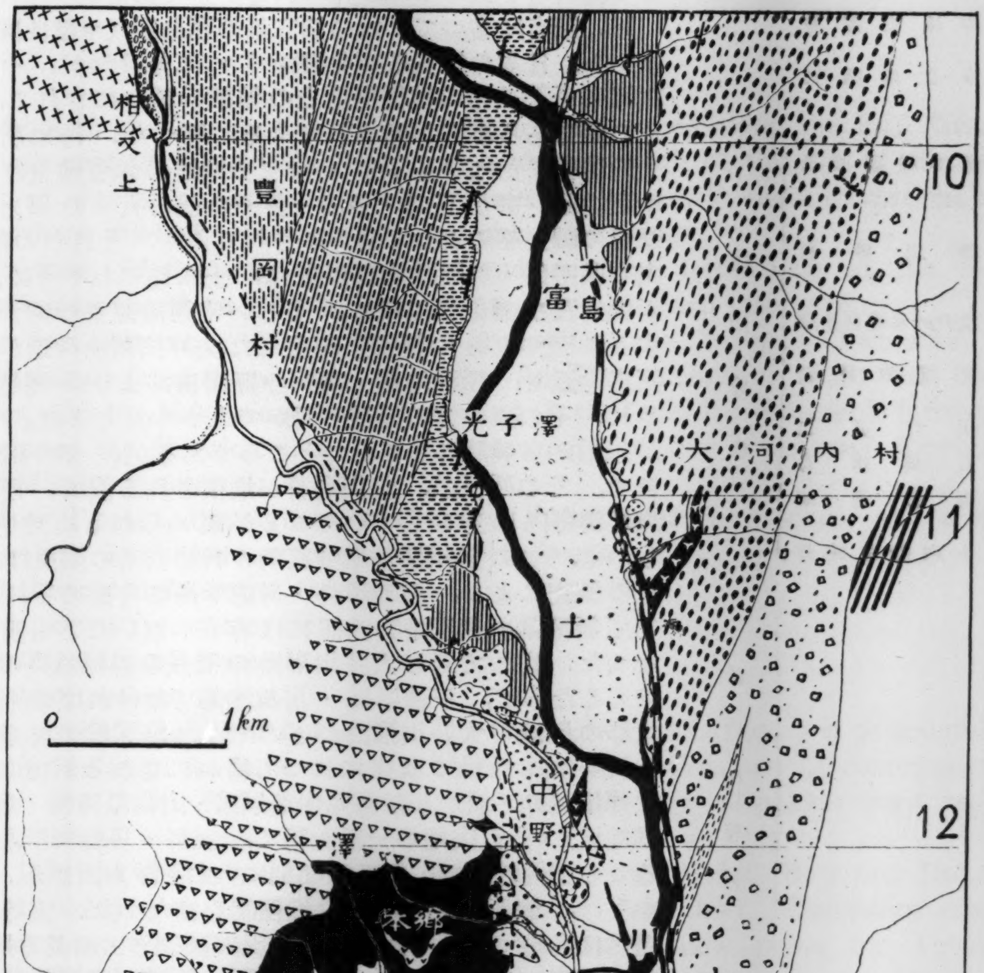

第 12 図 山梨県南巨摩郡南部附近の地質図. 凡例は第 13 図にある.

第 13 図

地質時代のものであらう．身延山附近の火山岩類には，この泥岩層を貫くものが見られるからである．

14．筆者は嘗つて日本の第三系の褶曲度（＝皺曲度）分布から，日本の第三系褶曲帯を 7 つに分けたが，その後次第に各褶曲帯の地質構造上の特徴が明かにされて，多くの興味ある事実が示されてくるに至つた．特に所謂中央地溝帯又たはフォッサ・マグナ地域の地質構造は，田中元之進・井尻正二・伊田一善その他の人々の努力及び筆者の調査等によつて明かにされてきた．それらの結果，山梨県南部・静岡県中部以東は，上に述べたやうに，中新世末及び鮮新世以後に，著しい造構造運動の舞台と化するに至つた．中新世末に生じた大井川褶曲構造が，静岡市附近で，所謂塩尻・静岡の断層線により，突然遮断され，その東の方の延長が明かでなかつたことは，筆者が以前から疑問にしてゐたところであるが，幸今回の調査で，その延長が，静川層群が堆積される前に，所謂中央地溝帯内に存在していたことが認められるに至つた．しかも，この静川層群堆積直前の新第三系の褶曲は，最近の調査により，三浦半島・房総半島にも確められ，そして新潟県や奥羽地方西部には存在しないことも明かとなつた．従つて若し大井川褶曲の延長を静岡以東の地に求めるならば，三浦半島・房総半島でなければならぬ．之等の区域で大井川褶曲がどのやうな地質構造を示してゐたかは，今後の研究によつて明かにされる訳である．大井川河口区域から静岡県中部以東・山梨県南部（南巨摩郡地域）・丹沢山地の一部を経て，三浦・房総両半島に至るこの褶曲地域は，鮮新世初期に，太平洋方面から，海進を受け，海底に没し，厚く堆積物を横たへた．之等の堆積物は各地でそれぞれ掛川統・浜石岳礫岩・清見寺層群・静川層群・足柄第三系・中津層群・下部武蔵野累層・清澄・天津累層等で代表されてゐる．この堆積時に火山活動が最も激しかつたと思はれるのは，各地の岩相からみて，現在の富士川沿岸区域及びその以東と考へられる．堆積物は大井川区域を除いて一般に厚かつたやうである．鮮新世の終末と共に，それまでとは全く走向を異にした南北走向の瑞穂・フォッサ・マグナ褶曲運動が，富士川中流に沿うて起り，宛も東西方向に収縮されたやうに，所謂塩尻・静岡断層も完成されたが，富士川中流流域，即ち，この断層線を境としてその以東が，逆断層を伴ひつつ，褶曲された．而も塩尻・静岡断層の線の西ではこのことが見られなかつた．洪積世中期以後の火山はこの褶曲構造が完成されて後に噴出した．

*32. Shizukawa Group and Tertiary Crustal Movements in Japan.**

By Yanosuke OTUKA,
Earthquake Research Institute.

Although the Tertiary formations, broadly developed along the Fuji River, in the south part of Yamanashi Prefecture and the north of the city of Shizuoka, consist of several kinds of rocks and contain many fossils[1], these formations have not yet been studied from new stratigraphic viewpoints.

At first, Motonoshin TANAKA[2] restudied these formations in the Koma mountainland, north of Mt. Minobu, and subdivided them into seven:

(1) the Quaternary, (2) the Misaka group—(2a) the Shizukawa formation, (2b) the Kushigatayama formation, (2bi) the Ashikura member, (2bii) the Oozōri member, (2c) the Nakayama formation,—and (3) the Chichibu Palaeozoic formation. He included the Shizukawa, the Kushigatayama, and the Nakayama formations in the Misaka group.

After TANAKA, the writer[3] studied the Fujimiyama fault scarp, and divided the Tertiary formations exposed there as follows:

Akebono conglomerate formation.
Shizukawa formation.
Kushigatayama formation.
Nishiyatsushiro group.

He also studied the fossil fauna from the Shizukawa formation, and palaeontologically inferred from the fauna that the Shizukawa formation may by contemporaneous with the Lower Kakegawa group, the geologic age of which may be the Lower Pliocene in Japan.

In 1939 the writer[4] studied the geologic structure of Mt. Ho'ō and Jizō, and found ***Lepidocyclina*** **(*Nephrolepidina*)** ***japonica*** YABE and ***Miogypsina ozawai*** HANZAWA from his Momonoki formation, which is the new name for Tanaka's Nakayama formation. On account of this fossil occurrence only the Momonoki formation is ascribable to the type Misaka, in which *L.* (*N.*) ***japonica*** and others are contained.

In this paper, the writer has established a new group, the Shizukawa group, and has described the stratigraphic characteristics of the group. He has also expressed his opinion on some tectonic features of the Neogene Tertiary in Central Japan.

---

* Dr. Yanosuke OTUKA, Professor in Stratigraphy at the Geological Institute of the Tokyo University and a Member of the Staff of the Earthquake Research Institute died on August 7, 1950. A complete manuscript of this paper was found by his students at his room after his death.

1) T. SUZUKI, *Expl. Text. Geol. Map.* 1/200000, "Fuji" sheet, (1886), 36–37 (in Japanese).

2) M. TANAKA, *Chigakuronsō*, (1930), 549–570 (in Japanese).

3) Y. OTUKA, *Jour. Geol. Soc. Japan*, **41** (1934), 562–564 (in Japanese); *Geogr. Rev. Japan*, **15** (1938) 969–984 (in Japanese).

4) Y. OTUKA, *Bull. Earthq. Res. Inst.*, **19** (1941), 115–143 (in Japanese).

The Shizukawa group is an aggregation of formations exposed from Gokai Village in Minamikoma District, Yamanashi Prefecture, to Nambu Village along the Fuji River. It attains to about 6000 m in thickness. The formations composing it are in descending order as follows:

The Shizukawa group.

The Akebono subconsolidated conglomerate. (Thickness: 250 m. Type locality: Nakayama in Akebono Village.)

The Shizukawa sandstone. (Thickness: 1500 m. Type locality: Yonagozawa in Shizukawa Village).

The Shiozawa alternation of sandstone and mudstone. (Thickness: 650 m. Type locality: The Shiozawa valley, east of Minobu Town.)

The Arayashiki sandstone. (Thickness: 350 m. Type locality: Along the shore of the Fuji River at Wada and Arayashiki in Ookōchi Village, Nishiyatsushiro District.

The Tsunouchi mudstone. (Thickness: 500 m. Type locality: Tsunouchi, south of Minobu Railway Station.)

The Marutaki conglomerate. (Thickness: 1000 m. Type locality: Marutaki, north of Minobu Railway Station.)

The Koutsubuna pyroclastic rocks. (Thickness: 700 m. Type locality: Asō and Koutsubuna, north of Utsubuna-Nanbu Railway Station.)

From his stratigraphic researches, the writer has obtained the following results:

1) The Shizukawa group is an independent group limited by a marked angular unconformity. It is divisible into the 7 subdivisions written above according to the rock character.

2) Thickness of the group amounts to 6000 m or so at the south of Minobu Town, but it is less than 1500 m or so in the north of Shizukawa Village.

3) The Shizukawa group shows a structure of transgressive overlap. It represents a major marine transgression in the Shizukawa epoch from the south to the north.

4) The deposition of the Shizukawa group began with volcanic activities.

5) The Miocene quartz diorite was exposed on the land surface and was eroded and disintegrated into rounded pebbles from the early epoch of sedimentation of the Shizukawa group.

6) During the deposition of the Shizukawa sandstone, the Karasumoriyama volcano was active, and extruded andestic lava and agglomerate.

7) Some formations of the Shizukawa group are fossiliferous. Fossil marine mollusca (Table I in the Japanese part) from the Shizukawa sandstone is a shallow pelagic fauna in the Kuroshio (Japan Current), and resembles the Kakegawa fauna of the Japanese Pliocene. Among of them, biozone of *Amussiopecten praesignis* (YOKOYAMA) and of *Siphonalia* and teilzone of *Venericardia panda* (YOKOYAMA) are worth considering in correlation between these two faunizones. The Tsunouchi mudstone contains *Sagarites chitanii* MAKIYAMA, which ranges from the Miocene to the Pliocene in Japan. The Arayashiki sandstone and the

Marutaki conglomerate contain epibole of *Operculina ammonoides* (Gronovius) n. subsp., which is reported from the Horinouchi formation of the lower Kakegawa group.

8) The marine transgression of the Shizukawa group is comparable with that of the Kakegawa in its scale. Accordingly the Shizukawa group may be contemporaneous with the Kakegawa.

9) The Shizukawa group rests on the Miocene formations with a decided angular unconformity. Other localities, where such decided angular unconformity is observable between the Lower Pliocene and the Miocene formations, are the basal part of the lower Kakegawa group developed in Kakegawa District, Shizuoka Prefecture and the basal part of the lower Musashino formation at Zushi in Miura Peninsula.

10) These decided angular unconformities are not seen in the Neogene of the western half of Northeast Japan. Namely the tectonic history of the Neogene Tertiary in the former three districts (Kakegawa, Shizukawa and Miura) is different from the latter district (western half of Northeast Japan). These former districts were disturbed by a tectogenetic movement, while the latter district was not disturbed by any tectogenetic movements except epeirogenetic ones, during the Late Miocene epoch or pre-early Pliocene.

11) The Shizukawa group runs in meridional direction and inclines steeply westward or vertical, and forms an isoclinal synclinal fold. The east margin of the distribution area of the Shizukawa group is bounded by a decided angular unconformity as written above, while its west margin is bounded by the Miocene formations with a remarkable reverse fault.

12) The Hamaishidake conglomerate[5] and the Seikenji group[6], which are exposed at the south part of the districts now in concern and which may be contemporaneous with the Shizukawa, are also similarly folded and dislocated. These disturbed structures written above are not seen in the Kakegawa group, the strata of which gently incline southwards in the north part and westwards in the south to form a semi-amphitheatral downwarp structure. Namely, these two regions, Shizukawa and Kakegawa, have different tectonic history of the post-Kakegawa epoch. So far as the tectonic history of the post-Kakegawa epoch is concerned, the Shizukawa region is similar to the western half of Northeast Japan. Accordingly the region along the Fuji River has similar tectonic history to that of the Kakegawa during the early Pliocene or the late Miocene, while during the post-Kakegawa epoch, it is the same as the western half of Northeast Japan.

The former tectonic disturbance is, in the writer's terms, the Ooigawa folding[7], and the latter the Mizuho-Fossa Magna disturbance[8]. The region along the Fuji River has successively been disturbed by these two crustal movements, which are different in tectonic characteristics. It is a structural type of cross-foldings, on which the Ooigawa folding meets with the Mizuho-Fossa Magna folding.

5) Y. OTUKA, *Bull. Earthq. Res. Inst.* **16** (1938), 415–451 (in Japanese).
6) Y. OTUKA, *Bull. Earthq. Res. Inst.* **21** (1944), 394–413 (in Japanese).
7, 8) Y. OTUKA, *Proc. Imp. Acad. Tokyo*, **13** (1937), 78–81.

33. 東京都地盤調査報告

（昭和 27 年 9 月 16 日，昭和 30 年 6 月 28 日発表—昭和 30 年 6 月 30 日受理）

地震研究所地盤研究会

震害と地盤に密接な関係のある事は既に古くから知られて居り，最近施行された我国の建築基準法にも設計基準震度は地盤により異つた指定がなされ，地盤調査が必要となつて来た．又更に最近では耐震構造の合理的経済的設計には地盤の知識が不可欠とまで建築家から要請される様になつた．それは建築物の振動特性にまで地盤が関係する事が知られたからである．

これ等の要請や目的の為に我々地盤研究会は研究を進めて居るが，今回ここに報告するのは地盤研究会の前身であつた有志が協力して行つた最初の研究結果であり，文部省科学研究費，建設省助成金及び東京都の委託研究費等により東京都内に於て地盤良否の物理的本性の究明と地盤種別の決定とを目的とした調査の綜合報告である．

目　次　　　　頁

第 I 章　緒　言 471
第 1 節　歴　史 471
第 2 節　調査事項 472
第 3 節　調査箇所 475
第 II 章　火薬による人工地震動測定結果 477
第 1 節　吾嬬町における地震探査 477
第 2 節　下町 11 ヶ所における地震探査結果 479
附　初動及び最大動
第 III 章　常時微動の測定結果 492
第 IV 章　起振機による周期波動測定結果 495
第 1 節　起振機 495
第 2 節　起振機による土地の振動調査 497
第 3 節　東京大学構内における測定 498
第 4 節　墨田区吾嬬町における測定 499
第 V 章　自然地震による調査結果 500
第 1 節　本郷と吾嬬町における自然地震の比較観測 500
第 2 節　本郷と下町 4 ヶ所における自然地震の比較観測 512
第 3 節　金町における地震動観測結果 530
第 VI 章　地下の振動測定結果 532
第 VII 章　結　論 538

第 I 章　緒　言

第 1 節　歴　史

震害の軽重が著しく地盤の良否に支配されることは古くから注目されて来た．東京市内の地盤良否の区分は安政地震の資料により関谷，今村により研究され，それが大正 12 年

の関東大震の際の震度分布と一致したことも周知のことである．このため地盤の調査は東京市の震災復興の基礎的事業であると認められ，時の内務省復興局によつて市内全域の試錐調査が実行され，美しい立体地質図が作製出版された．この試錐によつて知られた地盤構造と震害との関係は多くの学者の注意を惹いたが，特に北沢は試錐の難易と地盤の関係迄も検討を行つた．

また一方においては煉瓦造および土蔵造のごとき建物が地盤の硬い山手において却つて被害の大きいことも注目を惹き，単なる地盤の硬軟以外の重要な因子についても別の考察が進められた．

関東地震の直後今村，および那須は数多い余震の市内各地と本郷における比較観測をおこない，地盤毎に特殊の周期の波動に対して振幅比が増大されることのあるのを見出し，続いて末広は地震分解器を用いて本郷および丸の内のごとき下町に優勢に現われる周期に差がみられる事を発見し，石本は加速度地震計による東京および横浜市内 10 箇所の地震動の比較観測を実施して，各地毎に固有な卓越周期を定めた．この観測は斉田その他の人々によつて継続され，その卓越周期が主として地盤表層に関係することが略確められた．又妹沢は地盤固有振動の可能性に関する理論的研究を行つた．その後高橋は本郷台，上野台およびその中間谷地において地震動の比較観測を行い，地盤上層における地震波の多重反射により所謂地盤の固有振動が誘発される機構を理論と実際の両面から実証した．勿論古くから地殻表層がその基盤との境界面を節とし，自由表面を腹とする自己振動をすることについては Wiechert その他の学者に注意されていたが，上の事実は，石本により見出された所謂卓越周期がそこの冲積層の厚さとほぼ比例する事実とともに，地盤の固有振動説を支持する有力な証拠であつた．

終戦後の国情から合理的経済的建築が要望され，その為の基準法制定の根幹として，地震の危険度竝びに地盤良否を定量的に定める必要が起つた．その要請により河角は大正の関東地震による東京市内町別の木造家屋全潰率から物部公式により震度を定め，それと地質，冲積層の厚さ，埋立地の厚さ，および北沢の計算した地盤の突下数等と震度との定量的関係をさだめ，震度の地盤係数の分布図を作製した．これらの結果は建築基準法の地盤種別指定基準に参照されたが，現東京都区域は旧市内より著しく拡張されており，同法実施に伴う都区内全域の地盤種別指定には新しく地盤調査をおこなう必要があつた．そのため昭和 26～27 年度に亘り都内地盤調査が建築学会に委託され，地震研究所および建築研究所の研究者がそれを実施した．その要求は単に各地点の地盤種別の判定だけでなく，代表的地点における調査から広範囲の地盤判定に役立つ事実を見出し，都内全域の地盤指定を早急に可能ならしめることにあつたので，われわれはこれを機として文部省科学研究費，および建設省助成金等をえて地盤良否の物理的定量的解明を目的として各地で調査をおこなつた．それら諸調査の中東京都内に関する結果を次に報告する．

第 2 節　調査事項

建築基準法実施に関連して建設省告示第 1074 号によつて地盤は

第 1 種　岩盤，硬質砂礫層その他主として第 3 紀以前の地層によつて構成されているもの

第 2 種　砂礫層，砂混り硬質粘土層，ローム層その他主として洪積層にて構成されているもの，または厚さが概ね 5 m 以上の砂利層若しくは砂礫の冲積層によつて構成されているもの

第 3 種　第1，2 種および次の第 4 種に属さないもの

第 4 種　（イ）腐植土，泥土その他これに類するもので構成されている冲積層（盛土

がある場合においてはこれを含む）でその厚さが概ね 30 m 以上のもの

（ロ） 沼沢，泥海等を埋め立てた土地であつて，ごみ，泥土その他これに類するもので埋め立てた地盤の厚さが概ね 3 m 以上であり，且つこれらで埋立てられてから概ね 30 年を経過しないもの

の 4 種類に分類され，別々の設計基準震度が指定されることになつている．この種別は主として試錐調査によつて決定される事になつているが，施行令第 88 条第 5 項によつて地震力が確実に小さいことが証明される場合には設計基準震度を減らすことが許されるので，われわれは地盤の良否を決定する物理的因子を究明し，試錐その他の地質学的方法によらずに，直接地盤震度を決定する地球物理学的方法を確立し地盤種別の判定に資したいと考えた．

そのために第一に考えられることは標準地盤の地点と地震動の比較観測をおこない直接震度の比率（地盤係数）を定めることであり，その地盤係数に対する地質構造および地層の物理的性質の影響を定めることが続いて問題となる．そのために既知の地盤構造の地点で種々の地球物理学的調査をおこない，それぞれの関連性を確めることが必要となる．

如上の目的を以て選ばれた調査事項は次の通りである．

（イ） 自然地震
（ロ） 常時微動
（ハ） 火薬による人工地震動
（ニ） 起振機による周期的波動
（ホ） 地下の振動

これらは勿論上の目的に合致する最良なものばかりとは限られていないのみならず，調査も不十分な点が多く，最初の期待に反した結果を与えたものもあるが，以下簡単にその説明を記そう．

（イ） 自然地震

隣接地点間においても地形地盤の相違により地震動に差異のあることは Milne，大森，今村等の諸先輩によつて観測されたところであり，各地盤の振動性能が地震動の周期によつて異ること，又卓越周期の相違等については既に述べた．それに関する観測結果も又多い．われわれは上述の地盤係数を求め，またそれと地盤の物理的性質の比較をおこなうために，昭和 26, 27 年度の東京都よりの委託調査の一部として本郷地震研究所を標準点として 3 箇所，続いて 28～29 年に地震研究所事業として 3 箇所の比較観測をおこなつた．観測は宮村，高橋，那須の 3 研究室が担当した．

地震動を標準地点のそれと比較して，周期別に地盤係数を求め，地盤のいわゆる固有振動を明かにすることを主眼とし，そのために両地点で観測された同周期の最大動の振巾比から知られる共鳴現象と，卓越周期との関連性の有無を調査した．殊に最近周期の頻度曲線の形状が表層地層内における多重反射に起因する地面の振動特性と密接な関係を持つ可能性が示唆されたので，この方面も注意した．

卓越周期の分析にはその他に調和分析，自己相関函数による分析等が考えられるが，本報告においては後者の試みだけがおこなわれただけで，反応解析器による分析結果は別に報告されるであろう．

（ロ） 常時微動

地面は低気圧や波浪等の影響により 2～3 秒以上の周期を以つて連続的に振動し，或は火山活動に際し短周期の脈動を起すことは周知のことであるが，交通機関その他の人工

的原因により1秒以下程度の常時の微動を続けることもよく知られ，"Tagesunruhe"の名前で呼ばれている．われわれはそれを常時微動と呼んでいる．これはその周期が建築物等の固有周期に近い関係から，この常時微動にみられる地盤の振動特性が地震の際のそれと密接な関係を持つことが考えられる．この調査には金井が特に力を注いでいる．本調査には岸上も参加し，脈動計で観測した．結果の解析には周期の頻度曲線を用いた．

(ハ) 火薬による人工地震動

地盤の振動性能は地盤の構造と地層の物理的性質特にその弾性的性質と地層の厚さに密接な関係を持つ筈である．この調査に弾性波による地下探査法が有力であることはいうを要しないであろう．火薬によつて起される人工地震縦波の走時から地層の厚さおよび伝播速度を求めることは各種の目的に用いられているが，縦波の振巾，表面波の伝播速度および減衰も勿論地盤の構造に関係する筈であり，それが地盤調査に応用されてもいるが，表面波の利用については考えなければならない問題がある．今迄考えられたのは半無限体表面を伝わるレーリー波の理論であるが，層状構造をなす媒質では波動の分散が起るから，最近佐藤によつて明かにされたとおり，分散曲線の解析から地盤構造を一義的に定めることは不可能であり，また振巾の距離による減衰は単に吸収作用ばかりでなく分散も関係するので問題は実際には極めて複雑である．

それゆえ本調査においては屈折法による走時曲線の解析から地下構造を求めた外は，縦波の初動の振巾の距離による減衰，最大動の伝播の速度，および記象上において最大振巾から振巾が半減するに要する時間（半減時間）τ を調査したに過ぎない．本調査は主として表研究室および建築研究所中川技官等がおこない，一部河角研究室も分担した．本報告にそれらの結果を発表できたことに対し建築研究所竹山，中川両技官に深く感謝する次第である．

(ニ) 起振機による周期的波動

起振機を地盤調査に最初に利用したのは Deutsche Gesellschaft für Bodenforschung (Degebo) である．起振機で起された一定周期の波動の振巾—距離曲線にみられる周期性を観測し，それを異つた速度を持つ二地層内を伝播する波動の干渉の結果としてその成層構造を調査することと，起振機駆動に要する電力の回転数による変化を調査し，その極大値から地盤の固有振動数を求めようという2方法が用いられたが，われわれもそれを追試してみた．

第一の方法は後に調査結果の項で述べる如く問題は複雑で簡単に結論がだせないことが知られ，第2の方法は調査不十分で未解決のまま残された．何れ将来の再調査の日を期待している．

以上と別にわれわれは構造物の振動特性調査に起振機を利用しているが，それと同じ方法によつて地盤の振動特性，従つて固有周期が調査できないかとの問題がある．これは Degebo の第2法とも関連することであるが，偏心質量の回転を用いる起振機の回転数をできるだけ上げた所で自由にしてやれば，波動にエネルギーを奪われて起振機の回転は次第におそくなり，起振力は周期の2乗に逆比例して小さくなつてゆくが，その途中地盤の固有振動に共鳴を起すのではなかろうかという問題である．このことは当然と考えられるのであるが，起振機から少しく隔つたところにおいて地動を観測する場合には Degebo の第一法に関連する諸現象が影響し簡単には最大振巾を与える周期が固有周期とは結論でき兼ねるので，この問題も現在は未解決で残されている．

(ホ) 地下の振動

地盤の振動性能を解明するには地表における振動特性を調べるとともに地中における振動様式を測定する必要がある．周期的波動の多重反射による地下の振動様式について

は多くの理論的研究によつて明かにされており，自然地震の地下と地上の比較観測も古くから行われているがまだ必ずしも理論と実際との十分な一致が確められてはいない．

本調査に関連して河角研究室では起振機および火薬によつて地表で起した弾性波動を試錐孔底に入れた地震計によつて観測し，地盤振動の解明の一助とすることにした．地盤振動の理論に仮定されている平面波の場合とは異るが将来この方面の理論の進展と，実際観測の促進を期待しておく．(河角)

調査担当者は次の通りである

那須信治	新井信夫	森下利三	野田哲夫	
高橋竜太郎	平能金太郎	相田　勇	羽鳥徳太郎	
岸上冬彦	諸我丈吉	吉岡久義	小高美江子	
河角　広	島　悦三	柴野睦郎	柳沢馬住	
表　俊一郎	山崎良雄	小林直吉	萩原輝一	小牧昭三
宮村摂三	堀　実	辻浦　賢	松本英照	
金井　清	田中貞二	鈴木富三郎	長田甲斐男	吉沢静代
佐藤泰夫				

第3節　調査箇所

調査事項竝びに調査箇所は次の通りである．(附図参照)

1951 年度

A. 自然地震動比較観測実施箇所

1. 文京区本富士町　東京大学地震研究所内
   台東区　隅田公園事務所内

B. 弾性波試験実施箇所

1. 台東区隅田公園　東側（埋立地域）
2. 同　上　西側（自然地盤）
3. 江東区大島町　旧瓦斯会社敷地
4. 墨田区吾嬬町　吾嬬第一中学校庭
5. 江東区砂町 3 丁目　汽車会社構内
6. 文京区本富士町　東京大学運動場

1952 年度

A. 自然地震動比較観測実施箇所

1. 文京区本富士町　東京大学地震研究所内
   墨田区吾嬬町　吾嬬ポンプ場内
2. 文京区本富士町　東京大学地震研究所内
   江東区大島町　小名木川変電所内

B. 弾性波試験実施箇所

1. 江戸川区東篠崎町　ミヨシ化学会社構内
2. 江戸川区小岩 8 丁目道路上
3. 江戸川区小松川 5 丁目　大杉公園附近
4. 足立区千住橋戸町　住宅協会アパート敷地
5. 江戸川区西瑞江 4 丁目　トロリーバス終点附近
6. 葛飾区新宿 5 丁目　三菱製紙会社構内
7. 葛飾区金町 1 丁目　浄水場附近

8．足立区蒲原町　日立製作所寮敷地
9．千代田区　日比谷公園内

C．地下の振動測定実施箇所
1．墨田区吾嬬町　吾嬬ポンプ場内

1953 年度

A．自然地震動比較観測実施箇所

1．{ 文京区本富士町　東京大学地震研究所内
江戸川区東篠崎町　ミヨシ化学会社構内 }

2．{ 文京区本富士町　東京大学地震研究所内
江戸川区逆井町　小松川高等学校内 }

以上の他に常時微動の観測を上記の各地点において実施した．（平能）

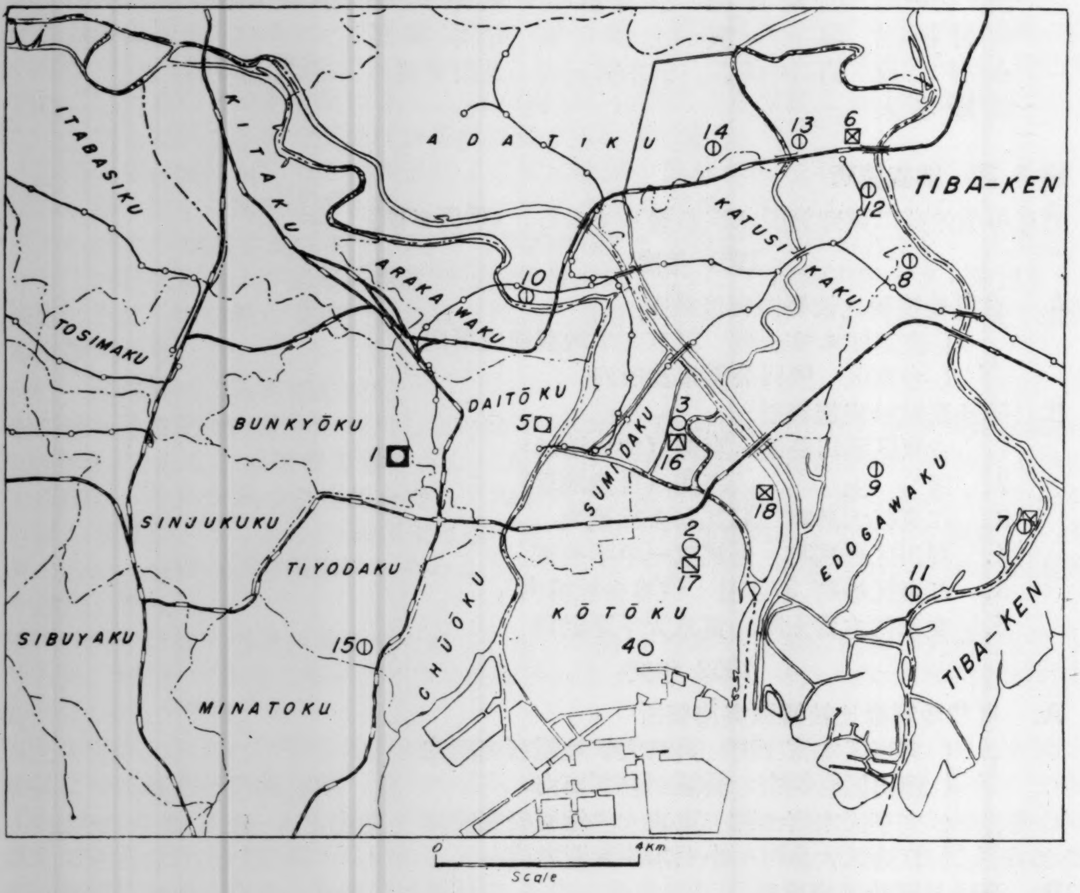

Fig. 1–1. Distribution of observation points. Various squares indicate points where earthquake observations were made. Various circles indicate those points where seismic prospectings were executed.

凡　例

■ 1951 年度以降自然地震観測及び 1951 年度人工地震，常時微動観測実施箇所
□ 1951 年度自然地震観測実施箇所
⧄ 1952 年度自然地震観測実施箇所

⍍ 1952 年度自然地震，地下振動，常時微動観測実施箇所
⊠ 1953 年度以降自然地震観測実施箇所
○ 1951 年度人工地震観測実施箇所
⦶ 1952 年度人工地震観測実施箇所

1 Hongo　文京区本富士町　東京大学地震研究所及び同大学構内運動場
2 Oshima-machi 1　江東区大島町　旧瓦斯会社敷地
3 Azumacho 1　墨田区吾嬬町　吾嬬第一中学校庭
4 Sunamachi　江東区砂町 1 丁目　汽車会社内
5 Sumida Park　台東区隅田公園　(自然地盤及び埋立地)
6 Kanamachi 1　葛飾区金町 4 丁目　東北毛織会社金町工場内
7 Higashi-shinozakicho　江戸川区東篠崎町　ミヨシ化学構内
8 Koiwa　江戸川区小岩 8 丁目道路上
9 Osugi Park　江戸川区小松川 5 丁目　大杉公園附近
10 Hashidocho　足立区千住橋戸町　住宅協会アパート敷地
11 Nishimizue　江戸川区西瑞江 4 丁目　トロリーバス終点附近
12 Kanamachi 2　葛飾区金町 1丁目　浄水場附近
13 Niijiku　葛飾区新宿 5 丁目　三菱製紙構内
14 Kambaramachi　足立区蒲原町　日立製作所寮敷地
15 Hibiya Park　千代田区　日比谷公園内
16 Azumacho 2　墨田区吾嬬町　吾嬬ポンプ場内
17 Oshimamachi 2　江東区大島町　小名木川変電所内
18 Komatsugawa　江戸川区逆井町　小松川高等学校内

第 II 章　火薬による人工地震動測定結果

第 1 節　吾嬬町における地震探査

1. 東京都の依頼に依る地盤調査の一つとして地震探査に依る各地の地下構造の決定が取り上げられ，多くの場所の探査が行われた．これはその一つとして 1952 年 4 月東京都墨田区吾嬬町東五丁目吾嬬第一中学校庭に於いて行われた．

2. 測線は現場が非常にせまく，120 m の測線[1)] が 1 本しかとれず，そのため第三紀層と思はれる基盤の深さが決定出来なかつたのは残念であつた．Pick-up の間隔は 5m おきとし，4 個の Pick-up を次々と移動して測線の両端で発破をかけ，横川製のオッシログラフを改造した 6 成分のオツシログラフに記録した．Pick-up は爆破地震動研究グループの固有振

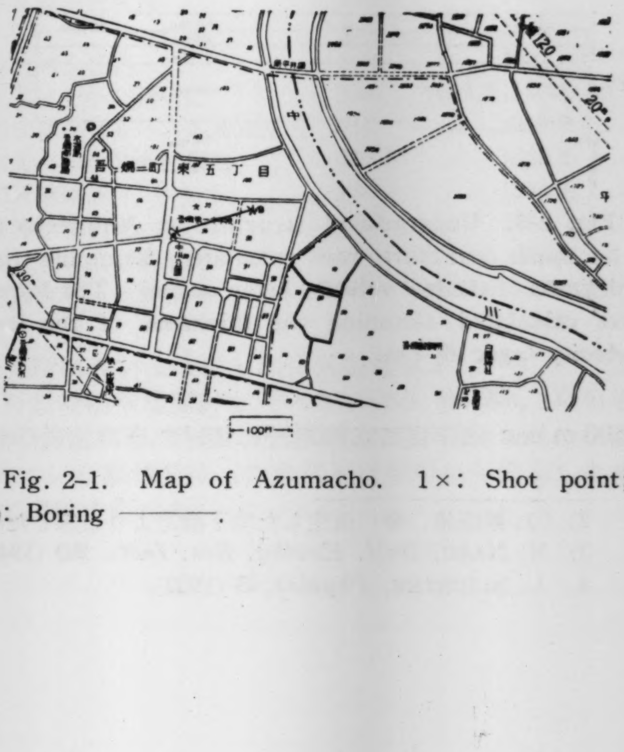

Fig. 2–1. Map of Azumacho. 1×: Shot point; ○: Boring ———.

1) 地図上 A, B で示す．

動周期 0.3 sec. のものに，横河製 D 型 Vibrator を直結使用した．爆破孔は地盤の非常に悪いと考えられているこのあたりの土地の性質として，地表数十糎の固つた部分を掘つてやれば，その下は所謂ヘドロとなり，竹の先に火薬をつけてつつくと簡単に掘れて地下の固い処まで入れることが出来る．この様にして火薬はダイナマイトを，距離に応じて，1 本から 5 本まで使用した．爆破は前にも述べた様に地下の固くなるところで行つたが，その深さは両端とも 4 m である．このことは後に地下構造を決定する際に非常に役に立つている．尚，表層の構造を知るために，爆破点近くで距離約 20 m の測線をとり 2 m おきに Pick-up を置き記録をとつた．

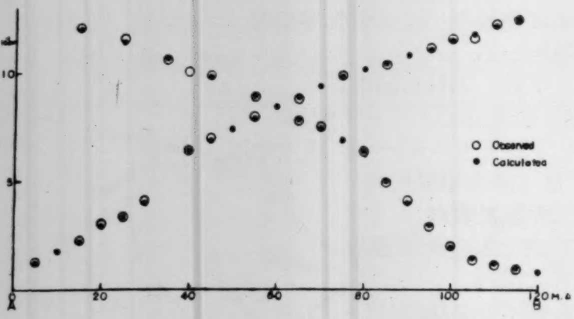

Fig. 2–2. Travel time curve. Azumacho 1.

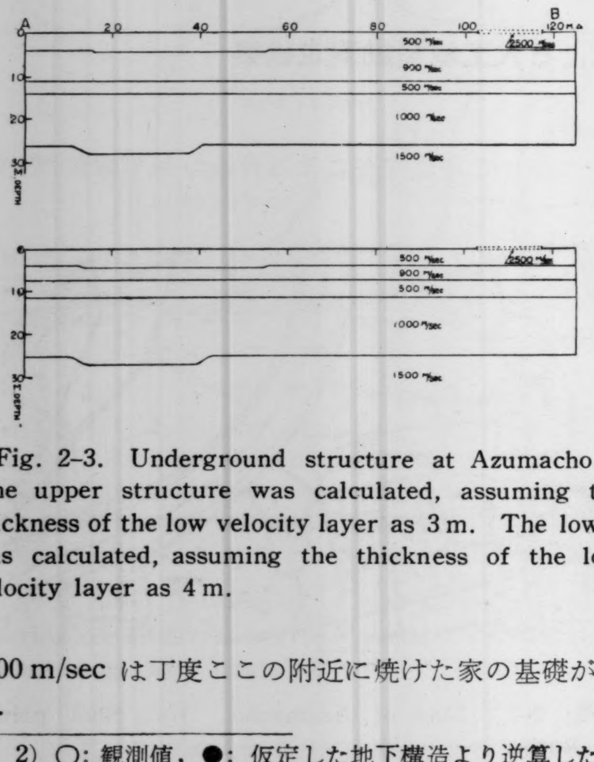

Fig. 2–3. Underground structure at Azumacho 1. The upper structure was calculated, assuming the thickness of the low velocity layer as 3 m. The lower was calculated, assuming the thickness of the low velocity layer as 4 m.

3. 得られた走時曲線は Fig. 2–2 の様なものである[2]．この様な走時曲線から推定される地下構造は，一般には次の二つの場合が考えられる．

i) 測線の中央附近で地下構造が凹になつている場合．

ii) 低速度層が高速度層の間に介在している場合．

東京の下町について考えれば，i) は考えにくいが，ii) の場合は実際に経験されて居り[3]，確からしく思われたので ii) の場合と考えて，地下構造の解析を行つた．低速度層が高速度層の間にある場合には，その層に於ける弾性波の速度及び厚さを一義的に決定することは出来ない．しかしながら我々は，与えられた走時曲線から適当な仮定[4] により，低速度層の最大の厚さと，最小の厚さを決定することが出来る．これから低速度層は 5～3 m の厚さを持つていることがわかる．低速度層中の弾性波の速度を 500 m/sec におさえると，層の厚さは 4.5 m より厚くすることは出来ない．そこで我々は，低速度層中の弾性波の速度を 500 m/sec におさへ，厚さが 3 m と 4 m の場合の地下構造を作つてみた．(第 2–1 表) 尚，地表の 2500 m/sec は丁度ここの附近に焼けた家の基礎が残つて居り，それが出たものと思われる．

2) ○: 観測値，●: 仮定した地下構造より逆算した走時．

3) N. Nasu, *Bull. Earthq. Res. Inst.*, **20** (1942).

4) L. Slichter, *Physics*, **3** (1932).

第 II-1 表

	縦波の速度 m/sec	層の厚さ H (m)	H' (m)
第1層	500	4	4
第2層	900	7	3.5
第3層	500	3	4
第4層	1000	11.5	13.5
第5層	1500	—	—

H は低速度層を 3 m として計算し，H' は 4 m として計算した.

4. この様にして得られた地下構造が Fig. 2-3 に示してある. ここに現われた 1500 m/sec のものが，我々の考えている第三紀層のものにあたるかどうかは不明であつたが，1 年後東京都により，ここから約 200 m 程離れた吾嬬ポンプ場構内[5]に，地盤沈下測定の目的でボーリングが行われたのでその data を聞くことが出来た. それによると，我々の得た低速度層の附近は非常にやわらかくて掘りやすかつたとの事であり，興味あることと思う. 又地下 26 m 附近から砂が出て来て居るが 1500 m/sec 層までの深さは，これと，およそ一致している. (島)

第 2 節 下町 11 ケ所にける地震探査結果

a. 地域及び測定器

地震探査を行つた場所及び測線の長さ等は第 2-2 表に見る通りである. この中 No. 6 〜No. 12 の地域については第 2-10〜16 図に測線附近の地図が示されている. 測定に使用した器械は No. 1〜No. 5 は地震研究所において改造した横河製電磁オシログラフ (D 型バイブレーター) 及び 10 サイクル可動線輪型地震計を用いたが No. 6〜No. 12 の地震探査を行うにあたつては建築研究所所有の SIE. P-11 型地震探鉱器が用いられた. 爆破孔は大部分 3 m 位の深さの孔を弁のついた鉄管又は，生産技術研究所から借用したハンドオーガによつてほり，水を充填して爆破を行つた.

第 II-2 表

記号	調査地点		測線の長さ	測定年度
イ	隅田公園	台東区隅田公園東側	240 m	1952
ロ	同	同 西側	200	1952
ハ	大島	江東区大島六丁目瓦斯会社敷地	200	1952
ニ	同	同	200	1952
ホ	砂町	江東区砂町五丁目汽車会社内	160	1952
ヘ	大杉公園	江戸川区小松川五丁目大杉公園附近	280	1953.2.13〜2.19
ト	今井	江戸川区西瑞江四丁目トロリーバス終点附近	350	1953.3
チ	ミヨシ化学	江戸川区東篠崎町ミヨシ化学会社構内	420	1953.5
リ	小岩	江戸川区小岩八丁目道路五	280	1953.5
ヌ	金町浄水場	葛飾区金町一丁目浄水場附近	380	1953.3
ル	三菱製紙工場	葛飾区新宿五丁目三菱製紙工場構内	450	1953.4.25〜5.4
ヲ	日立製作所	足立区蒲原町日立製作所青年寮敷地	274	1953.4.18〜4.21

5) 地図上に○印で示してある,

b. 測定結果

イ） 隅田公園東側

地形が（地下構造図で示す通り）階段的になつているので，上段に S_1，S_3，下段に S_2 の爆破点を設けて測定を行つた．表層について見ると，S_1，S_3 の shot 即ち上段に対しては 260 m/s が出ているが，S_2 の shot 即ち下段に対しては，780 m/s が出ている．尚 S_1，S_3 の shot に対して，この 780 m/s は第 2 層の速度として現われている．実際，この上段は人工的に築かれたものであることを考え合せると上のことは当然のことである．上段について，萩原の方法[1)]により第 1 層の厚さ，及び第 2 層の速度を求めた．第 3 層の見かけの速度は S_1 に対して 1310 m/s，S_2，S_3 に対して 1360 m/s であり，萩原の方法により第 2 層の厚さ及び第 3 層の速度 $V_3=1330$ m/s を決めた．第 4 層の速度は略 1800 m/s であるので，第 4 層の上面の形を graphical に決定した．（走時曲線第 2–4 図，地下構造第 2–9 図）．

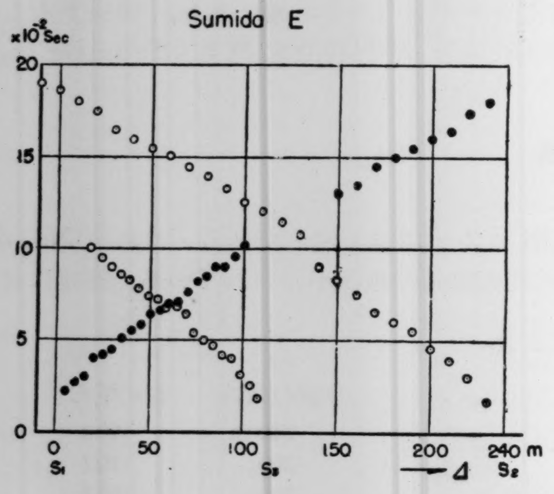

Fig. 2–4. Travel-time graph.

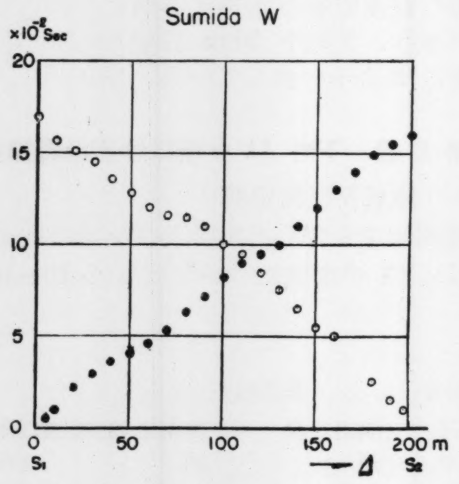

Fig. 2–5. Travel-time graph.

ロ） 隅田公園西側

S_1，S_2 の二ケ所に爆破点を設けて測定した．得られた走時曲線を見ると，表層については，S_1，S_2 の shot に対して何れも略 1000 m/s の速度が現われている．第 2 層の見掛けの速度は S_1 については 1250 m/s，S_2 については 1320 m/s が出ているので，萩原の方法により第 1 層の厚さ及び第 2 層の速度を決めた．又第 3 層の速度は略 1660 m/s で，之を用いて graphical に第 3 層の上面の形を決めた．（走時曲線第 2–5 図，地下構造第 2–9 図）．

ハ） 大 島 A

爆破点 As_1，As_2 の 2 点を設けて測定を行つた．得られた走時曲線に依ると，表層の速度は略 330 m/s である．第 2 の branch の見掛けの速度は何れも略 730 m/s となり，第 1 層の厚さ及び第 2 層の速度は，萩原の方法で求めた．更に第 3 層及び第 4 層の速度は，夫々何れも略 1150 m/s，1880 m/s を示している．これに依り，図式的に第 2 層及び第 3 層の厚さを求めた．（走時曲線第 2–6 図，地下構造第 2–9 図）．

1） 萩原尊礼 地震 **10** (1938), 463.

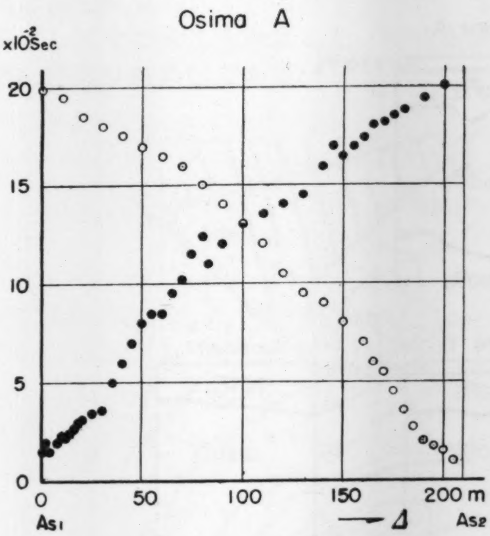

Fig. 2–6. Travel-time graph.

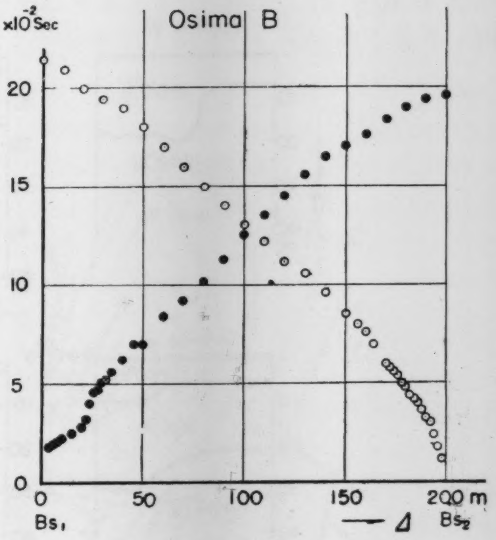

Fig. 2–7. Travel-time graph.

ニ) 大 島 B

Bs_1, Bs_2 の爆破点に依り，測定を行つた．走時曲線を見ると，爆破点の近傍では略 330 m/s の速度が出ている．第 2 層の見掛けの速度は何れも略 750 m/s が得られる．萩原の方法に依り表層の厚さと第 2 層の速度とを求めた．第 3 層の速度は，Bs_1, Bs_2 の shot に対して共に，$\Delta > 45$ m に於て，夫々略 1050 m/s, 1170 m/s となつているので，此等の平均を取り第 3 層の速度 $V_3 = 1110$ m/s と仮定し，これに依り第 2 層の厚さを graphical に求めた．更に第 4 層については，Bs_1 の shot に対して $\Delta > 170$ m, Bs_2 の shot に対して $\Delta > 160$ m に於て，速度は夫々略 2000 m/s, 1600 m/s と出ているので，これも平均をとり 1800 m/s と仮定して，第 4 層の上面の形を graphical に決定した．(走時曲線第 2-7 図，地下構造第 2-9 図).

ホ) 砂 町

2 つの爆破点 S_1, S_2 を設けて，測定を行つた．第 1 層の速度は S_1, S_2 の shot に対して夫々略 800 m/s, 600 m/s であるので，その平均値 700 m/s とした．第 2 層の見掛けの速度は夫々略 1200 m/s, 1440 m/s が得られる．萩原の方法に依り表層の厚さ及び第 2 層の速度 $V_2 = 1330$ m/s とを求めた．第 3 層の速度は略 2060 m/s を示している．之を用いて，第 3 層の上面の形を graphical に決定した．(走時曲線第 2–8 図，地下構造第 2–9 図).

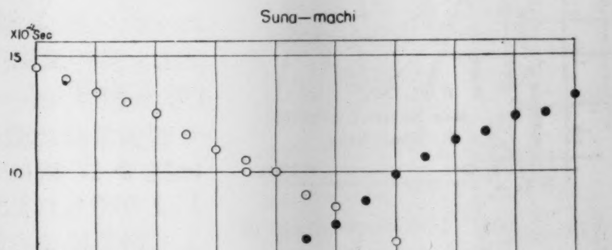

Fig. 2–8. Travel-time graph.

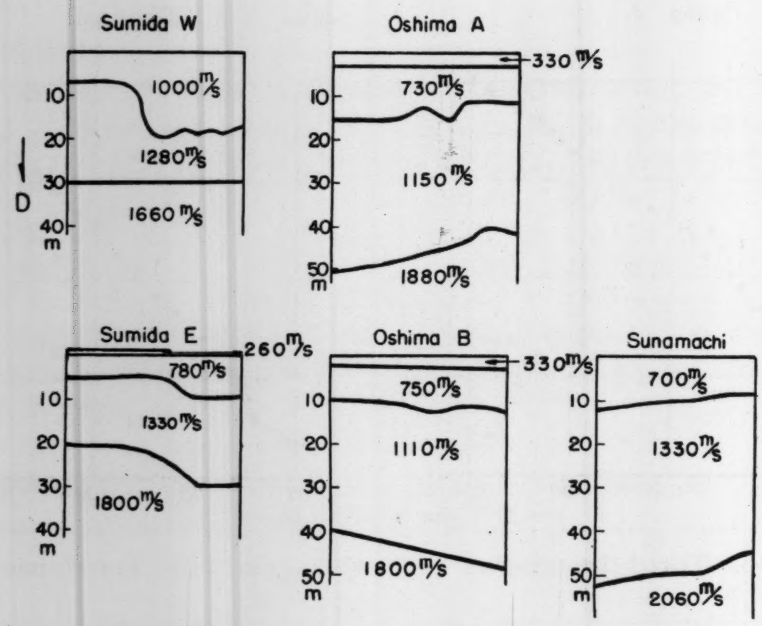

Fig. 2–9. Seismic cross-section.

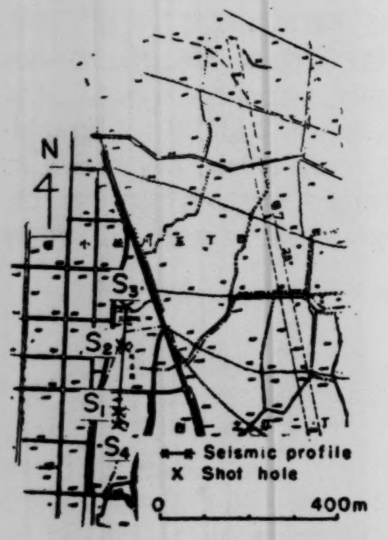

Fig. 2–10. Location map of seismic profile, Osugi Park.

へ) 大杉公園

爆破点 S_1, S_2, S_3 の 3 点を設けて測定を行つた. 得られた走時曲線を見ると爆破点に近い所には略々 750 m/s の速度が出ている. 第 2 の branch の見掛けの速度はいずれも 1500 m/s となる. 萩原の方法で第 1 層の形及び第 2 層の速度を求めた. 第 3 層の速度は S_1 shot のもの及び S_2 shot のものについて, わずか得られたにすぎないので別に, S_1 から 35 m はなして S_4 の shot hole を設けて Δ の大きい所だけ測定を行い第 3 層の速度 2000 m/s を確認することが出来た. この速度を用いて第 3 層の上部の形状を graphical に計算した.

測定された走時曲線及びこれより計算した地下構造は第 2–17 図に示されている. 走時曲線の黒丸は観測により得られた走時, 白丸は得られた地下構造を基として計算により期待される走時を示すものである. 尚, 測線地図は第 2–10 図に示す.

ト) 今 井

今井トロリーバス終点附近において地図第 2–11 図に見るように測線を道路にそつてもうけた, 道路の 1 つの側にはどぶ川がながれ他の側には水田があつたので PU. は道路上に配置した. 第 1 の branch に 1150 m/s の速い速度が見られるのはその影響であるかも知れない. 第 2 の branch は 1580 m/s の速度をあたえる. 第 1 層の厚さは萩原の方法により求めた. 第 3 層の速度は S_1 及び S_4 の shot に対し最も遠い PU. 数

点の測定に見られているにすぎない．この値をそのままとして 1900 m/s を第 3 層の速度としてその深さを計算した．走時曲線及び地下構造を示す第 2–18 図に於て黒丸は観測値，白丸は計算値である．

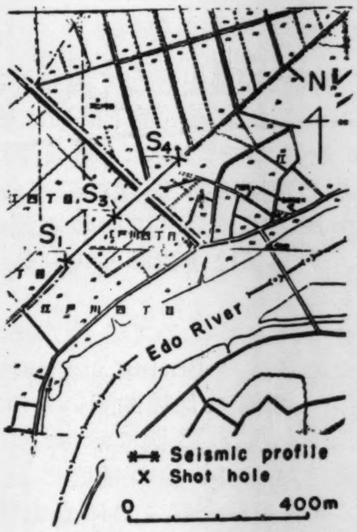

Fig. 2–11. Location map of seismic profile, Nishimizue.

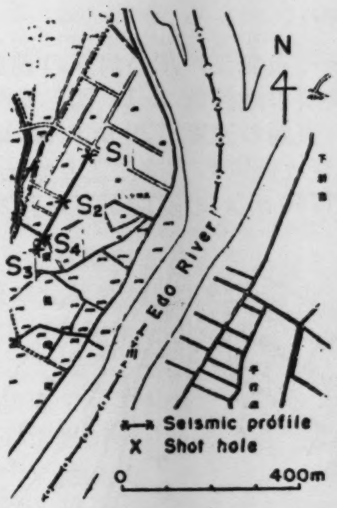

Fig. 2–12. Location map of seismic profile, Higashi-shinozakicho.

チ） 東篠崎町

爆破孔のために 3 m の穴をあけた．ここまでは非常にやわらかい泥である．走時曲線にこの表層の速度が出ていないが later phase をよんで 410 m/s の速度を得た．第 2 層の見掛けの速度は走時曲線からほぼ 1450 m/s が得られている．萩原の方法により表層の厚さと第 2 層の速度とを求めた．第 3 層の速度は S_1 及び S_3 の shot のものに出ている．夫々ほぼ 1550 m/s 及び 1750 m/s であるのでこの両者の平均 1650 m/s を第 3 層の速度として図式的にその層さを求めた．第 2–19 図に於て計算値白丸は実測値黒丸と 0.002 秒以内の精度で一致する．第 4 層の速度は S_3 の shot に対し最も遠い距離でわずかに出ている．これから第 4 層の深さをもとめれば 50 m 以上となる．尚，測線地図は第 2–12 図に示す通りである．

リ） 小 岩

第 2–13 図に示す如く，小岩 8 丁目の直線の道路上に測線を設ける，3 つの爆破孔について測定を行つた．

第 1 層の速度は later phase を読んできめた．第 2 層の速度及び第 1 層の厚さは萩原の方法による．第 3 層の速度は S_1 の shot に対し $\varDelta=220$ m より遠い所 S_5 の shot に対しては $\varDelta=170$ m 以上の所のものに出ている．夫々ほぼ 2400 m/s，1900 m/s となつているので第 3 層の速度 $V_3=2150$ m/s と仮定した．これに

Fig. 2–13. Location map of seismic profile, Koiwa.

従つて graphical に第 3 層の上面の形をきめた. S_5 shot に対し S_1 shot の位置に対する PU. の観測値がないので S_1, S_5 に対する Ts_1, Ts_5 が等しいと仮定するため第 3 層上面の形は S_1 側で特に深くなつている. 第 2-20 図に於て計算値（白丸）は観測値（黒丸）と 0.002 秒以内で一致している.

ヌ） 金 町

金町浄水場の東側江戸川の河原の運動場に南北方向に測線をとつて測定を行つた. 測定を行つた場所の地図第 2-14 図, 走時曲線及びこれより求めた地下構造は第 2-21 図の通りである. 表層の速度 720 m/s は later phase を読んできめた. 第 1 層の厚さ及び第 2 層の速度は萩原の方法により求めた. 第 3 層の速度は第 2 層に較べ余り大きな違いがないが 1750 m/s の速度が見られるのでこれを用いて図形的にその表面の形を求めた. 計算値は観測値と 0.002 秒以内で一致している.

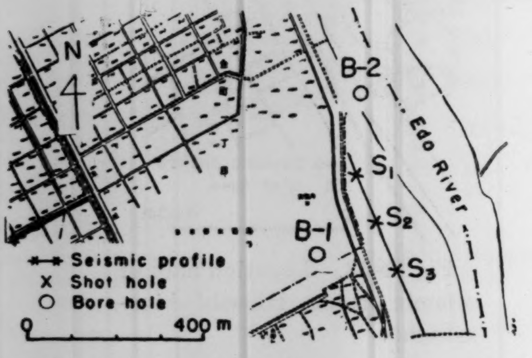

Fig. 2-14. Location map of seismic profile, Kanamachi 2.

金町浄水場に於ては浄水場建築物を作るため多数の Boring が行われていた. この中, 測線に比較的近いものの柱状図が第 2-22 及び 23 図に示されている. その位置は第 2-14 図の地図に見る通りである. 我々の結果によれば表土層の厚さは 6 m 位であるが Bore hole 1 によれば最上層のローム質の厚さはほぼ 5～6 m となつている. しかし柱状図と比較して, 地震探査で求められた層の境がどの地質に相当するかを対比させることはこの場合困難である.

ル） 三菱製紙工場

新宿五丁目の三菱製紙工場内で測定が行われたが, その場所は第 2-15 図に示されている. 測定より得られた走時曲線は第2-24図のようになり第 1 層の厚さが可なり厚いことを示している. 走時曲線に出ている第 1 層の速度を平均してその速度 560 m/s とおいた. 萩原の方法により第 1 層の厚さ及び第 2 層の速度 1400 m/s を求めた. 第 3 層の速度は S_1 及び S_3 の shot について Δ が夫々 280 m, 200 m の所から, 又 S_4 より S_1 に向うものについても $\Delta=170$ m の所から出ている. 両者の見掛けの速度を平均して $V_3=1900$ m/s とした. これより図式的に経路を計算して形をきめた. 傾向としては $S_3 \rightarrow S_1$ の方向に上り勾配に上つているが S_3 shot の $\Delta=430$ m より遠い 5 点は明らかに $\Delta=200\sim400$ m の間の点の平均傾斜の線よりは遅くなつているので地下に段違いを置いて計算した. このような地下構造にすれば S_4 の shot に対し $\Delta=170$ m～245 m の間で観測した値とも計算値は良く合致する. 走時曲線には観測値黒丸, 計算値白丸として示されて

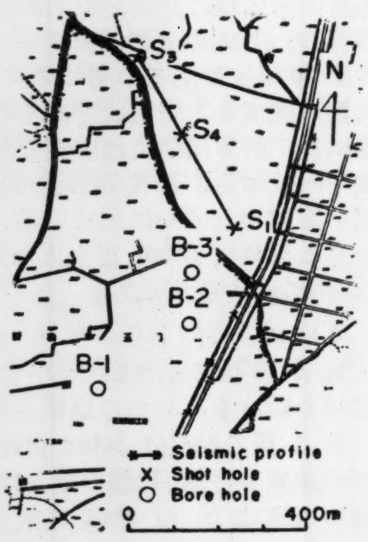

Fig. 2-15. Location map of seismic profile, Niijiku.

いるが全体としてみると計算値と観測値とは 0.002 秒以内の精度で一致する．この地域内にも 3 本の Boring が行われていた．その結果は第 2–25 図，第 2–26 図 及び 第 2–27 図に見る通りであるが場所が測線より可なり距つているので対比は困難であると思われる．表層については B–1 より B–3 に行くにつれ次第に深くなる傾向があるので地震探査より得られている表層の厚さ 12m というのは Boring *B*–2, *B*–3 等の最上層の砂の層に相当すると考えられるかも知れない．2km/s の層に相当するものは *B*–2, *B*–3 などでは深度が浅いため対比しにくい．

ヲ）日立製作所

この場所は第 2–16 図に見るように測線 S_1–S_2 間は旧工場あと，S_2–S_3 は運動場となつており，昔田甫であつた所を埋立て作られたものである．第 2–28 図の走時曲線において始めは早い速度が見られ，後，走時が遅くなり低速層の介在を思わせるものがある．特に S_1–S_2 の間では工場あとの地域でかつては簡単な補装がほどこされたものらしくアスファルトが所々残つていて表面は堅くなつていた．走時曲線を見てもほとんど delay time なしに 1600 m/s の速度の branch が見られているが上記のようなことを考慮に入れ下までずつとこの速度であると推定することは無理であると考える．解析を行うにあたり，先ず S_2–S_3 の間について表面に 1000 m/s の速度がありその下に 500 m/s の低速層が介在し更にその下に再び 1000 m/s の速度があると考えた．低速層の速度は走時曲線から推定する材料はないが先に吾嬬町で行われた時に得られている値と同様のものと仮定することとした．このようにして図式的に S_2–S_3 の間で低速層の厚さを計算した．S_1–S_2 の間については，走時曲線に 1600 m/s が出ているので intersept を合せるため shot point の附近に少し遅いものを置きその先は一様に薄い 1600 m/s の層が存在するとした．この厚さは知り得ないが人工的な原因によるものであるので極薄いものであり，その下には S_2–S_3 の場合と同様 1000 m/s 及び 500 m/s の層がありその下に再び 1000 m/s の層があると考えた．これ等の層の厚さを色々変えてみて，最も深い層（第 3 層）の上部の形が走時曲線に得られている観測値となるべく良く一致するように計算した．第 3

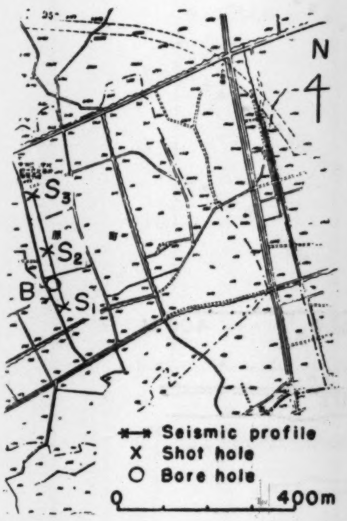

Fig. 2–16. Location map of seismic profile, Kambaramachi.

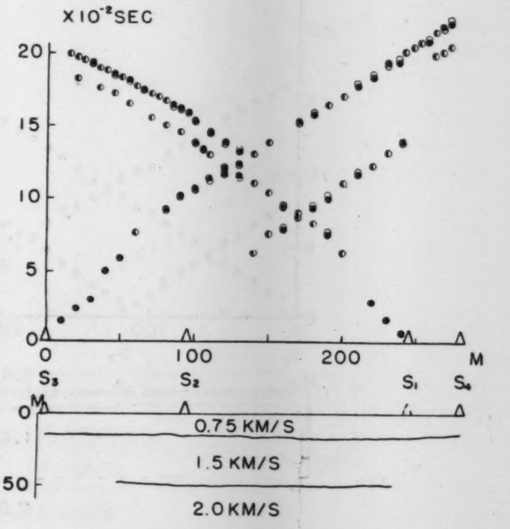

Fig. 2–17. Travel-time graph and seismic cross-section. Osugi Park.

層の速度は S_1 の shot に対しては $\Delta=250$ m の所から，S_3 の shot に対しては 170 m の所から走時曲線に出ている．傾向としては S_1 より S_3 に向つて下り勾配になつている．このようにして計算した1例が図には示されている．ここには第2–16図の測線配置に見るように測線 S_1–S_2 の中間附近に boring があるのでこれと対比することが出来る．boring の柱状図第 2–29 図に見る通りである．柱状図によれば薄い表土がありその下に

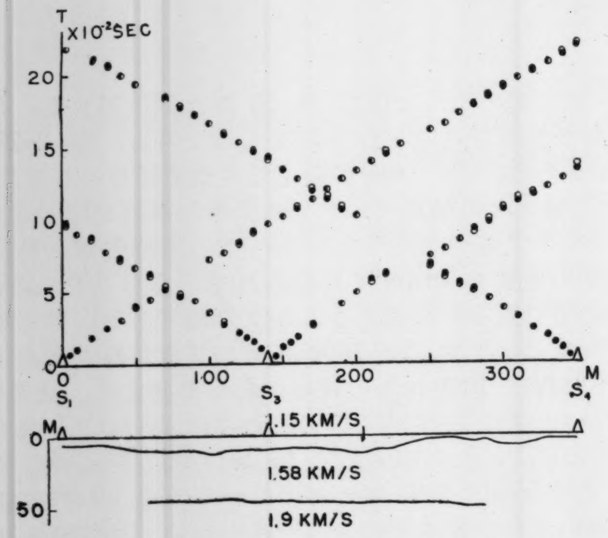

Fig. 2–18. Travel-time graph and seismic cross-section. Nishimizue.

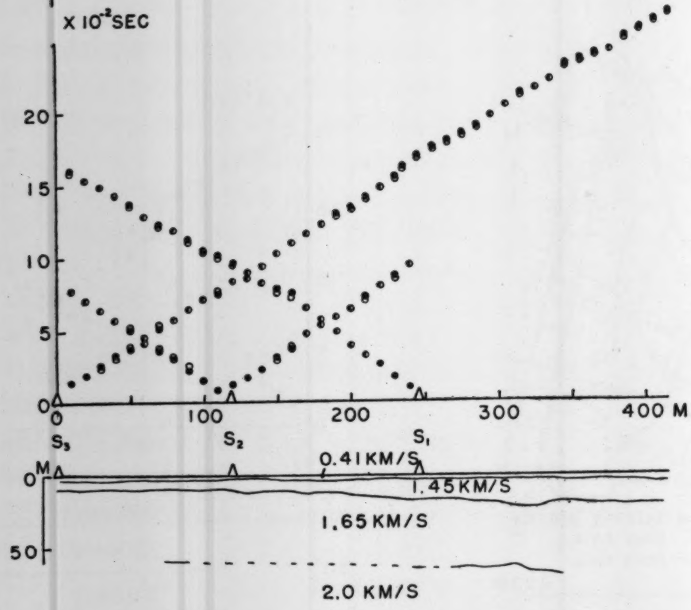

Fig. 2–19. Travel-time graph and seismic cross-section. Higashi-shinozakicho.

ほぼ 4 m 位の厚さの砂土がある．更にその下には貝殻まじりの砂が 3 m 近くある．その下，可なり厚く土砂又は土の層があり，約 40 m で堅土に当つている．我々の結果によれば，最上部には早い速度（1600 m/s）を持つ薄い表土があり，その下に 1000 m/s の速度の 2 m の厚さの層があり，その下にほぼ 500 m/s の低速層があることになつている．1000 m/s の速度を表面近い砂土の層，低速層を貝殻混りの砂層とすれば大体良く合致している．更に第 3 層の層の深さは 38 m となるのでこれが堅土の上面であるとすれば都合がよい．しかし上記低速層及び 1000 m/s の層の厚さは勿論一義的にきまらない．例

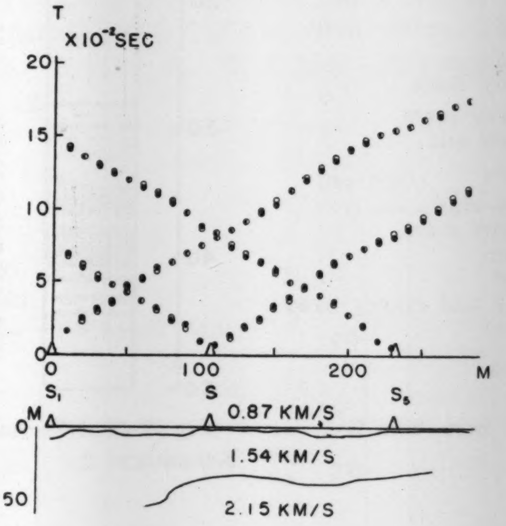

Fig. 2–20. Travel-time graph and seismic cross-section. Koiwa.

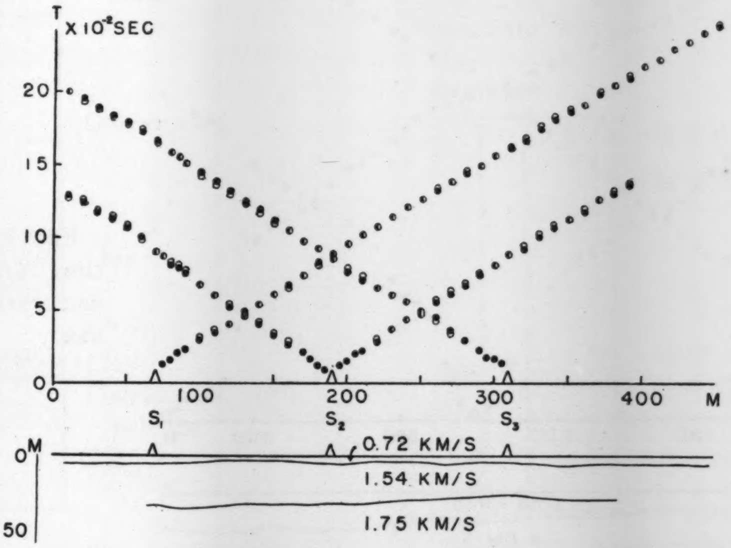

Fig. 2–21. Travel-time graph and seismic cross-section. Kanamachi 2.

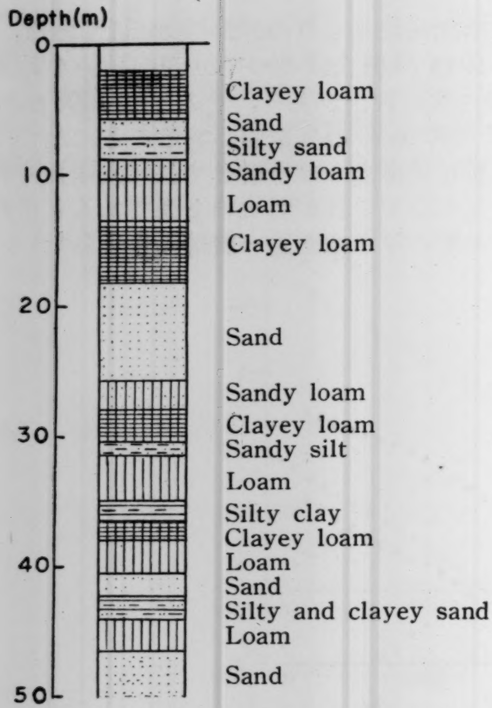

Fig. 2–22. Section of bore hole B–1, Kanamachi 2.

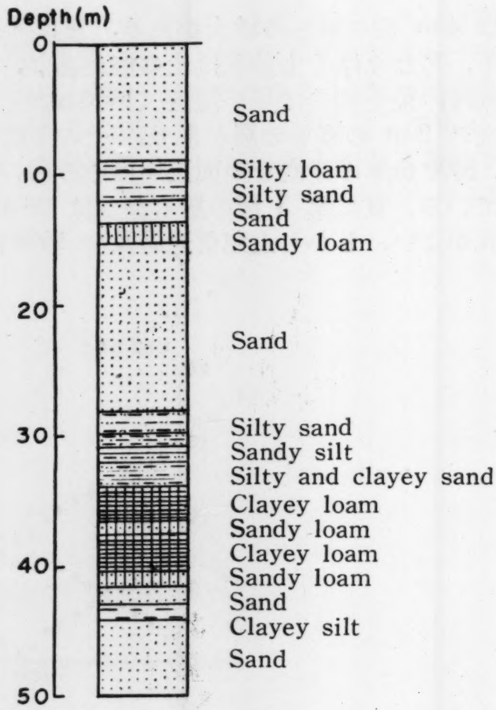

Fig. 2–23. Section of bore hole B–2, Kanamachi 2.

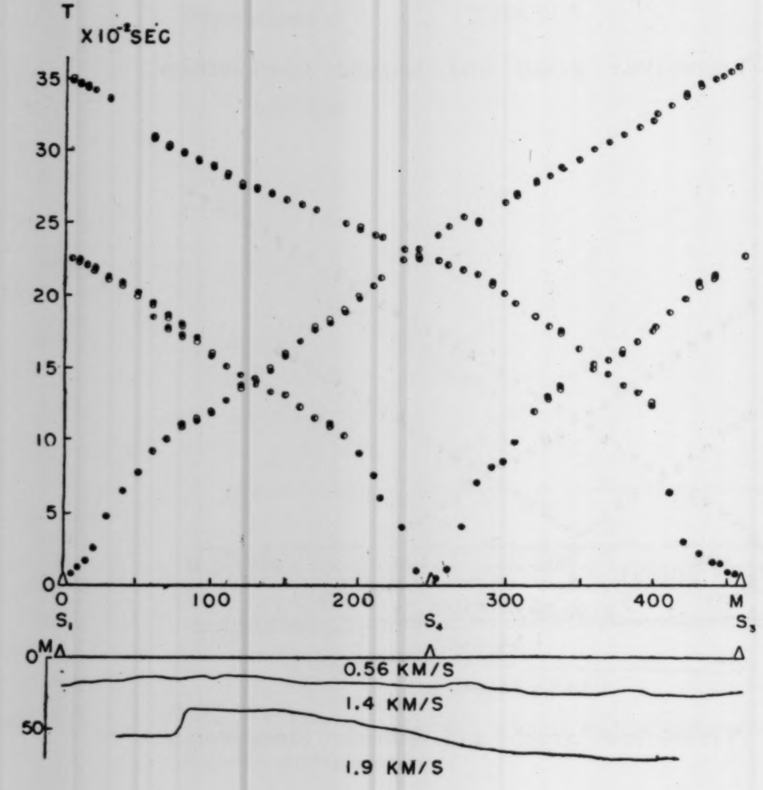

Fig. 2–24. Travel-time graph and seismic cross-section. Niijiku.

えば，第 3 層の深さが図のようであるとすれば低速層の厚さは 4～6 m の間である．低速層がないとすれば第 3 層の上面の深さは現在のものより 6 m 深くなる．以上のようにして走時曲線にみるように実測値（黒丸）と地下構造より得られた計算値は大部分 2/1000 秒のていどでよく一致しているのが見られる．

c. 結果の一覧

地震探査結果一覧

以上測定した結果によれば大体において，3 つの層に分けられるようである．第 1 層はその厚さは大よそ数米乃至十数米でその速度は略々 1000 m/s 以下である．第 2 層は 1500 m/s 又はこれに近い速度をもつ層である．第 3 層は略々 2 km/s の速度をもつものであり，この層の上面の地表からの深さは 40 m～60 m 位である．これ等の結果を一括して示せば第 2-3 表のようになる．第 3 層の上面は冲積層の下の境界面を示すものであるかも知れない．（表）

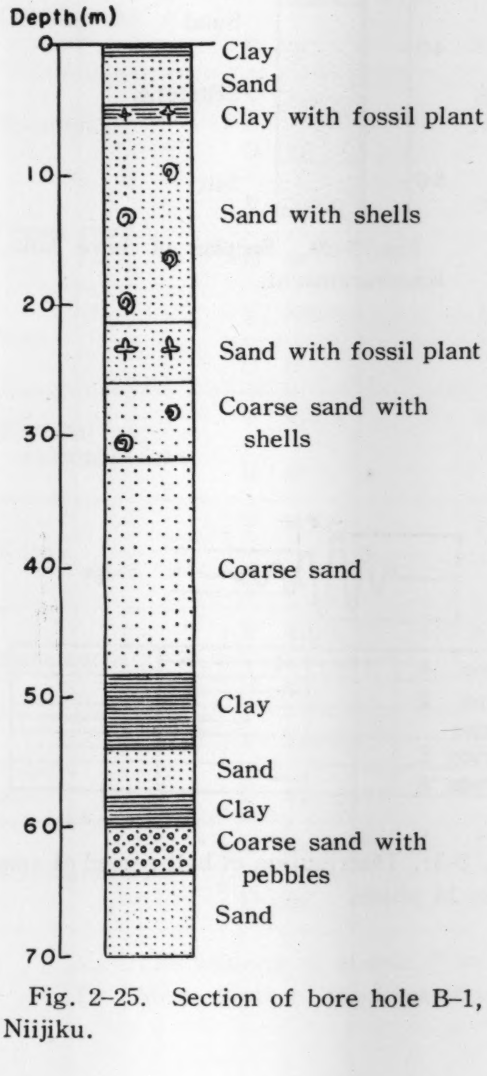

Fig. 2-25. Section of bore hole B-1, Niijiku.

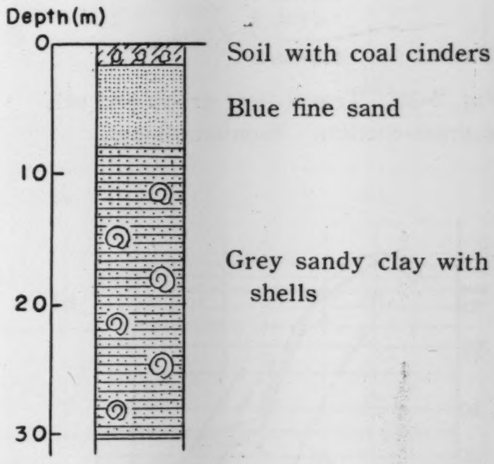

Fig. 2-26. Section of bore hole B-2, Mitsubishi Works.

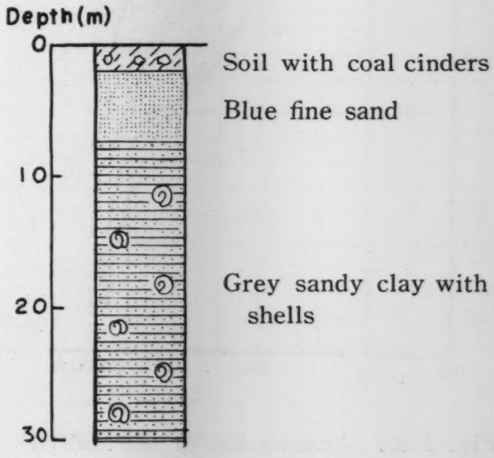

Fig. 2-27. Section of bore hole B-3, Niijiku.

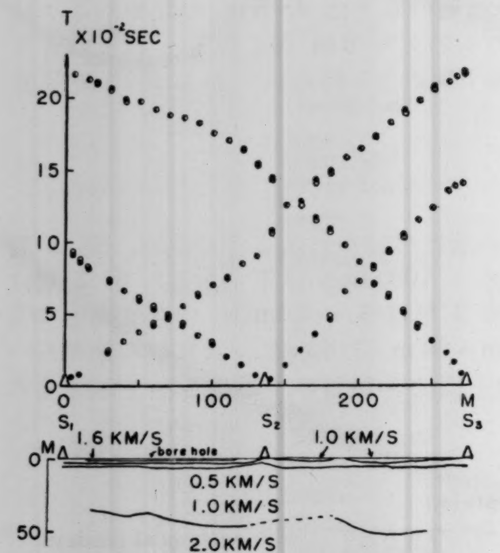

Fig. 2-28. Travel-time graph and seismic cross-section. Kambaramachi.

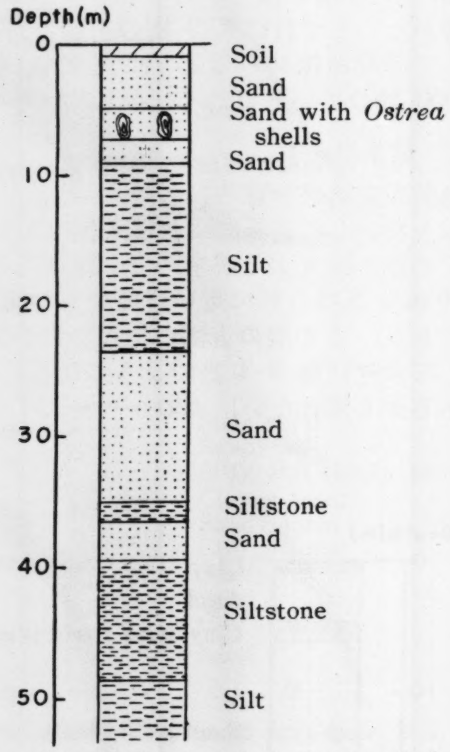

Fig. 2-29. Section of bore hole, Kambaramachi.

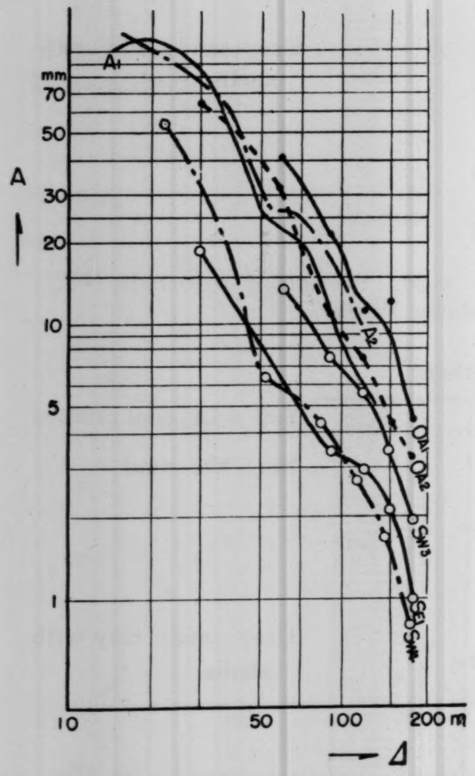

Fig. 2-30. Attenuation of the initial amplitude with distance.

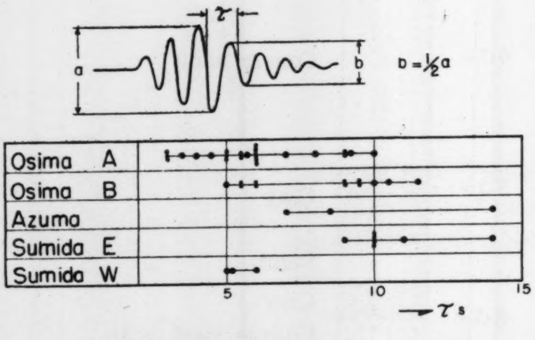

Fig. 2-31. Distribution of half-period of amplitude in M phase.

第 II–3 表

Locality \ Seismic-layer		1		2		3
Sumida Park, E.	V km/s	(0.26) 0.78		1.33		1.80
	D m	8		25		
Sumida Park, W.	V km/s	1.00		1.28	1.66	
	D m	13		30		
Oshima, A	V km/s	0.33	0.73	1.15		1.88
	D m	3	13	46		
Oshima, B	V km/s	0.33	0.75	1.11		1.80
	D m	3	11	44		
Sunamachi	V km/s	0.70		1.33		2.06
	D m	10		49		
Osugi Park	V km/s	0.75		1.50		2.00
	D m	16		50		
Imai	V km/s	1.15		1.58		1.90
	D m	7		45		
Higashi-shinozakicho	V km/s	0.41		1.45	1.65	2.00
	D m	4		16	66	
Koiwa	V km/s	0.87		1.54		2.15
	D m	5		44		
Kanamachi 2	V km/s	0.72		1.54	1.75	
	D m	4		32		
Niijiku	V km/s	0.56		1.40		1.90
	D m	19		53		
Kambaramachi	V km/s	(1.60, 1.00, 0.50)		1.00		2.00
	D m	6		43		

V: The velocity of elastic *P* waves in the seismic layer.
D: Mean depth of the lower boundary of seismic layer.

附. 初動及び最大動

集つた data の一部で，初動の振巾の減衰をしらべた．(第 2–30 図)，又最大動の振巾が半分になるまでの時間をしらべた．(第 2–31 図) これによると地盤の悪いと思われるところは，やはり時間がよけいにかかる様な傾向がある様であるが data がすくないのであまりはつきりした決論を下すことは出来ない．又最大動の走時曲線 (第 2–32 図) を作つて見たが，これに依つても，大たい，地盤の悪いところ程速度がおそい様に思われる．

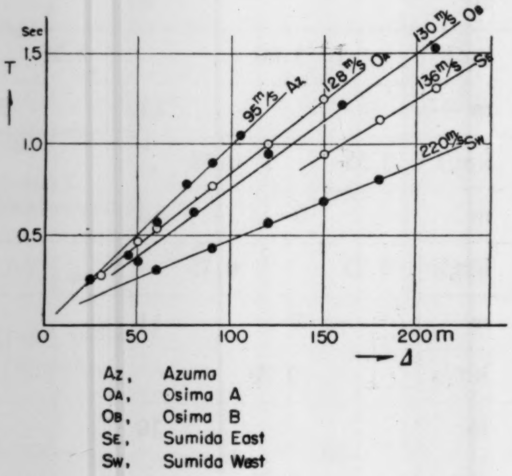

Fig. 2–32. Velocity of the maximum phase.

第 III 章 常時微動の測定結果

常時微動の周期頻度特性が，地震時における地盤の振動特性を知る上に，役立ちそうに考えられたので[1]，今回，東京都内で各種地盤上における地震動の比較観測及び弾性波地下探査が行われた場所について，常時微動の測定を行い，地震動の解析結果と照し合せてみることを試みたものである．

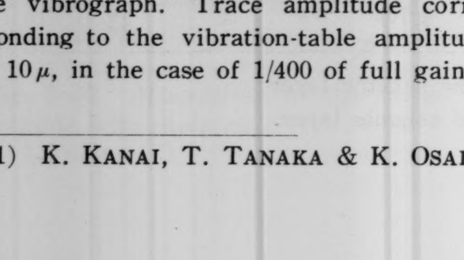

Fig. 3–1. Frequency characteristics of the vibrograph. Trace amplitude corresponding to the vibration-table amplitude of 10 μ, in the case of 1/400 of full gain.

常時微動測定装置は，電磁型煤書式で，換振器，増幅器，記録器及び記録ドラムから成る．今回使用した測定装置の構造及び特性は，既に報告したものに[1] 1，2 の改良を加えたものである．その周波数特性を第 3–1 図に示す．

(イ) 増巾器

増巾度の調整は確度 0.5% の精密減衰器を使用して 2 db 宛の変化で最大増巾度の 1/10000 迄微細に変化できるようにし，低域濾波回路や積分回路もつけ加えた．

(ロ) 記録ドラム

従来は記録器と記録ドラムは別個であつ

1) K. Kanai, T. Tanaka & K. Osada, *Bull. Earthq. Res. Inst.*, **32** (1954), 199.

たが，今回はこれを 1 つの台の上に組立て，ドラムは定位置で回転し，記録器がガイドレールの上を滑つて移動するようにした.

ドラムの 1 回転に対する記録器の移動量は 8 mm，記録紙の送り速度は 10 mm/sec で 30 分の連続記録ができる．又記録器が終端まで移動すると電源の主回路を切断して総べての動作を停止するようにしてある．これはタイムスイッチによる深夜の測定の際に使うと便利である．記録装置の写真を第 3–2 図に示す.

(ハ) 電　源

この測定装置の電源は通常は商用 100 V 電源を使用するが，インバーターを使つて 12 V の蓄電池によつて 100 V 50 c/s の交流を供給することも出来るようにした.

測定装置全体の写真を第 3–3 図に示す.

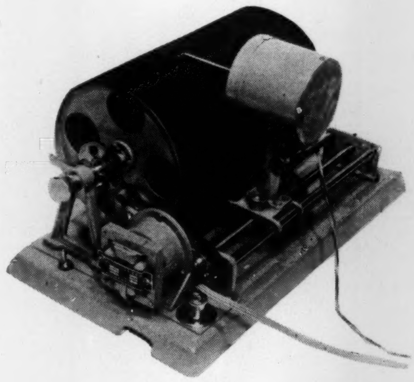

Fig. 3–2. Recording apparatus.

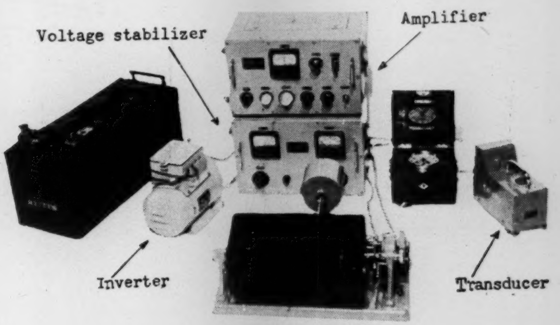

Fig. 3–3. Measuring equipment.

記録の解析方法はいつもと同じように，測定記録中の任意の 2 分間について，記録波形が零線を横切る点に着目し，この点の間隔を順次に読みとる．この相隣る 2 点間の長さに相当する時間をその波の半周期と考え，全区間のよみとりから各々の周期に対する波数を集計して周期頻度曲線を作る.

周期のよみとりは記録上の長さで 0.1 mm 迄よむから，周期の差は 0.02 sec である.

この計器を用いて前掲 8 ケ所で測定を行つた．測定記録の 1 例を第 3–4 図に示し，そ

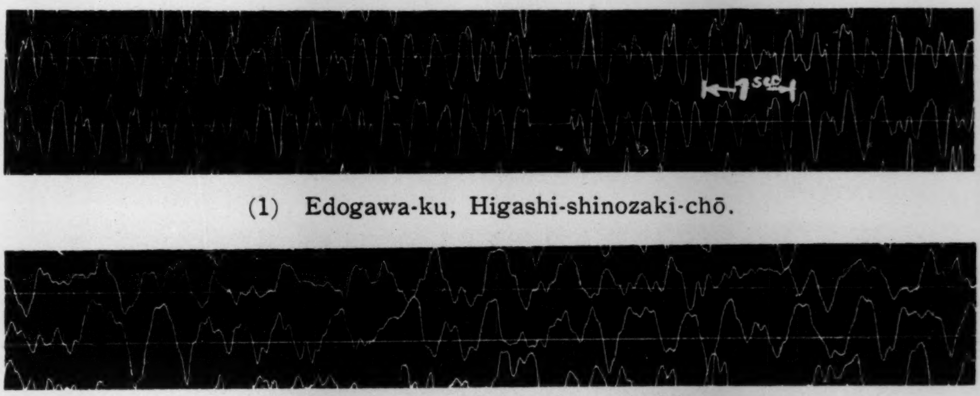

(1) Edogawa-ku, Higashi-shinozaki-chō.

(8) Edogawa-ku, Nishi-mizue, 4-chōme.

Fig. 3–4. Records of micro-tremor. Original size.

の 8 ヶ所の測定記録から周期の頻度曲線を求めたものを第 3–5 図に示す．これまでに多くの場所の常時微動について，同じような解析をした結果によると，頻度曲線は大体 4 つの型に分けられることがわかつた．即ち，第 1 の型は，0.1 sec から 0.2 sec 位の間に 1 つの鋭い山ができるもの．第 2 の型は，0.2 sec と 0.4 sec 位の間に山ができ，0.6 sec 位まで頻度の尾を引くもの．第 3 の型は，0.3 sec と 0.4 sec 位の間の頻度が卓越し，1 sec 位まで頻度がつづく．第 4 の型は，0.5 sec 附近に僅かに頻度の大きいところがあるが，全体が非常に平坦で，頻度は 1 sec 以上にまで及ぶものである．

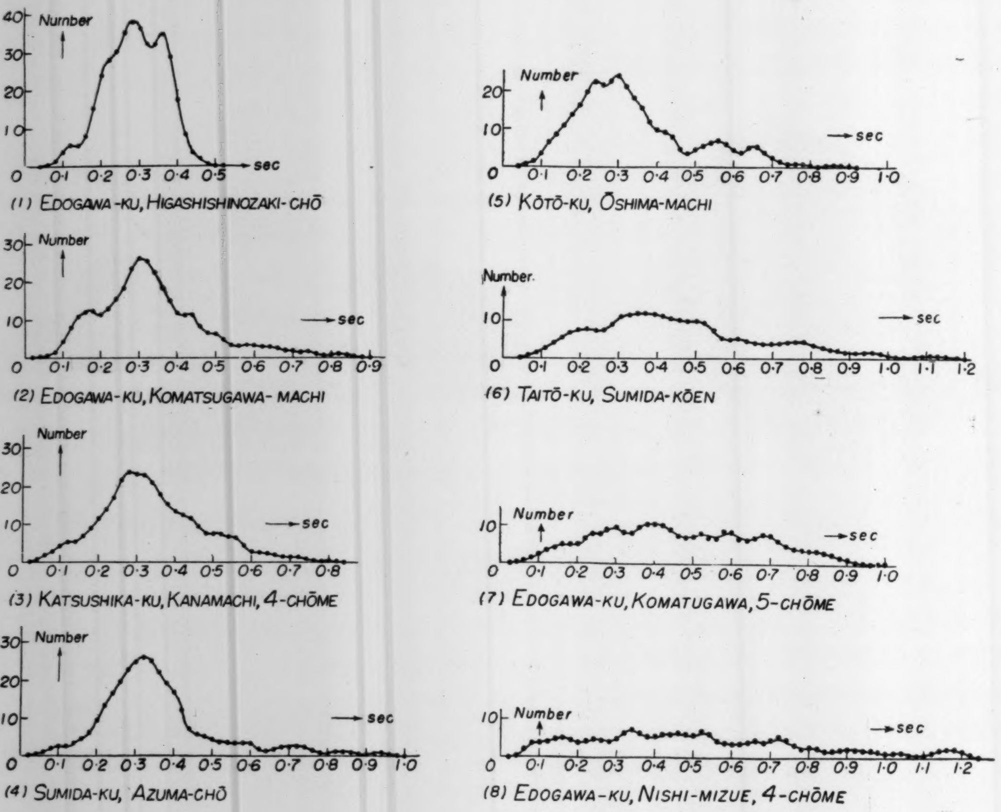

Fig. 3–5. Distribution of periods of micro-tremor.

第 3–5 図を見ると (1) の東篠崎町は第 2 の型と第 3 の型の間，(2), (3), (4), (5) の小松川町，金町 4 丁目，吾嬬町，大島町は第 3 の型，(6), (7), (8) の隅田公園，小松川 5 丁目，西瑞江 4 丁目は第 4 の型にあたる．

普通の建物の地階で測定した常時微動の周期の頻度曲線と，屋外で測定したそれとは大差ないが，一般に，屋外で測定したものでは 0.1 sec 以下の頻度が多い目である．今回の測定は，すべて，建物の地階で行つたものであるから，0.1 sec 以下の頻度は目立つ程大きくない．

今回の測定で，特に気が付いたことは，8 ヶ所のうち，隅田公園を除く 7 ヶ所において，0.3 sec 附近で頻度が特に卓越することである．隅田公園はいろいろな振動が重なつたような形で，見ただけでは，はつきりしないが，0.3 sec 附近に卓越する振動があるようにも見える．

そこで，東京都内で常時微動を測定した結果[2]のうち，第 3 の型に属するもの 12 ヶ所について見直したところ，6 ヶ所までがこの性質をもつことがわかつた．

第3の型に対しては,地震の観測結果及び地震波地下探査結果と照し合せて説明したい．

第 4 の型については，半無限弾性体の上に 2 層以上がある場合の振動問題とすれば，理論的には一応の説明がつくものである．

第 1，第 2 の型は，半無限弾性体の上に 1 層がある場合の振動問題として，理論的にも，又，週期的加力をした場合の 1，2 の実験結果からも，説明されるものである．(金井，田中，長田)

第 IV 章 起振機による周期波動測定結果

第 1 節 起振機

自然に起る地震を待つだけでは地震に関する研究は思うように進められない．そこで地中に火薬を埋め爆発させ人工的に地震を起すことが行われる．併し市街地などでは火薬を使うことは危険が多いので，重錘を落して地中に波を起すこともあるが，此の方法では大きな振動を起すことができないことと，重錘を落すときには其を吊つている台に

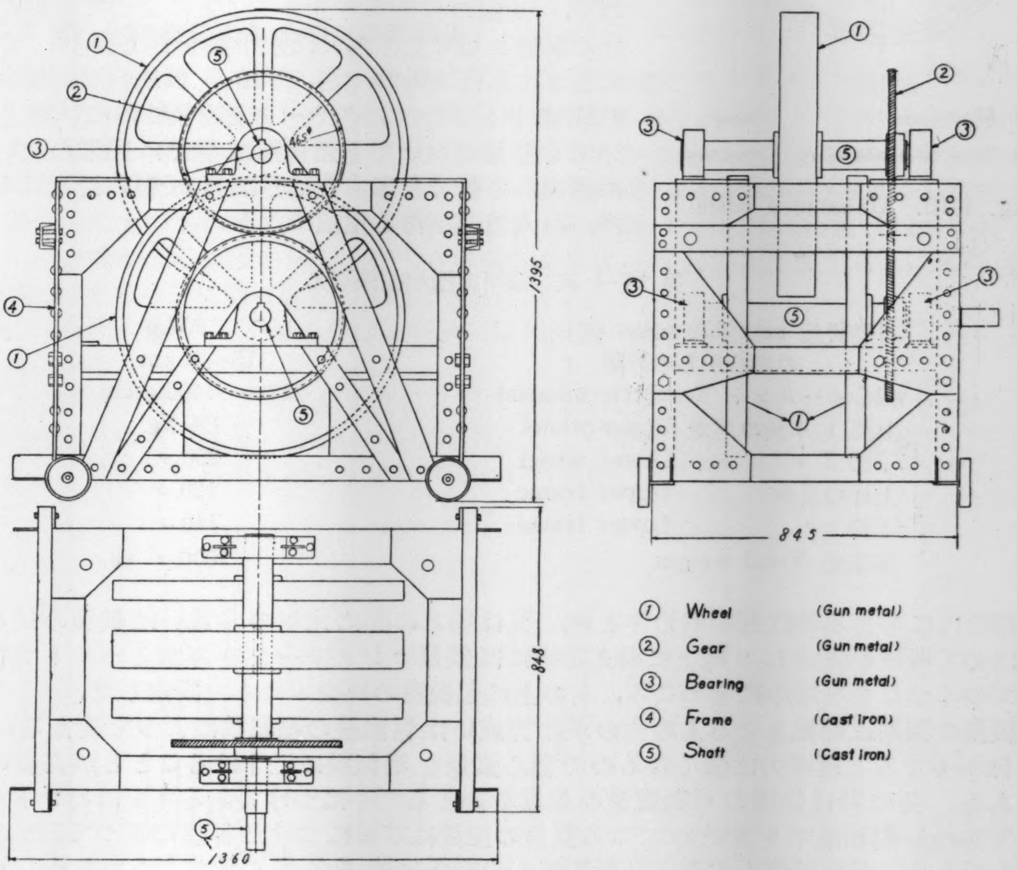

Fig. 4–1a. Vibrator

2) *loc. cit.*, (1).

反作用があつて不必要な振動が起ることなどの欠点がある．起振機は車輪に偏心荷重をつけて廻わすので，以上の欠点はなく，しかも正弦振動に近い振動を起すので実験の結果を振動理論と比べるには都合のよいという長所がある．地震研究所にはこの様な起振機が 2～3 台あつたが，普通ビルディングといわれる大きな建物内に取付けて建物全体を揺らして実験するもの，或いは地盤を大きく振動させる実験に使うものがなかつた．昭和 25 年度文部省からの研究費によつて今までよりも大きい起振機を作ることができ，それ以来大きな力の必要な振動実験には屢々使われている．

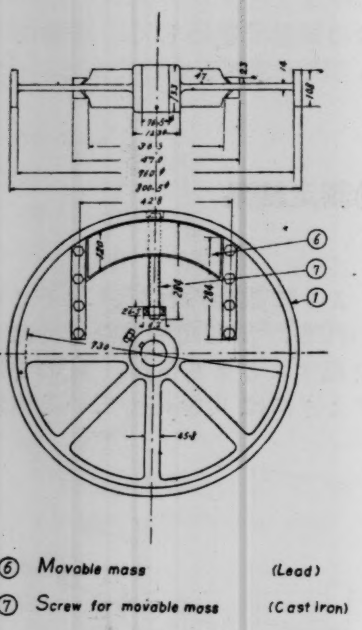

Fig. 4-1b. Unbalance wheel.

この大型起振機は第 4-1 図に示すように車輪は 3 個で，其等は 1 輪は上，2 輪は下につけられ偏心質量は下の 2 輪につけるものは等しく上の 1 輪のものは下の 2 倍とし，上と下とでは回転の向きを反対になるようにした．駆動は下の車輪の軸を人の力又は電動機によつて廻転させる．そこには自転車の駆動部分と同様に一方向きの廻転力を与えるようにした．

上下の偏心質量の回転は向きが反対で速度は等しいので，回転の位相差を変えることによつて単純の一成分の振動として上下動又は水平動を起し得る．車輪の大きさは直径 80 cm で，車輪 3 個組合せた場合普通の強度をもつたコンクリート造建築物内に大きさについても重量についても運搬及び据付に困難のないように適当に分解できる．各部分は 1 m 幅の出入口も通り得，2 人で運び得る重量になる．

第 IV-1 表 震研大型起振機諸元

可動質量	movable mass m	80 kg
〃 の中心からの距離	r	15～31 cm
偏心モーメント	Eccentric moment	2170～3440 kg-cm
上部 1 車輪の重量	Upper wheel	190 kg
下部 2 〃 〃	Lower wheel	250 〃
上枠の重量	Upper frame	120 〃
下枠 〃	Lower frame	140 〃
総重量	Total weight	1000 〃 ca.

建物内に据える時は起振機の枠と柱，又は梁との間に木材の柱或いは鉄製のジャッキをはめて機械を固定し，地上に据える時には鉄筋コンクリートの厚板とボルトでしめ合せてつくつた台を地中に埋めこみ，その上に起振機の枠をボルトで固定した．

振動の周期は廻転させる人の力のかけ方或いは電動機の廻転数によつて変える．周期が短かくなると起振力は強くなるので偏心質量を廻転軸に近ずけることとが必要のことがある．その時は鉛製の可動質量の位置をかえるためにつけてあるネジにハンドルをつけてまわし廻転能率を変える．この質量の位置は車輪につけた目盛によつてわかるようにしてある．可動質量の位置と回転能率との関係は第 4-2 図に示すようである．可動質量を回転軸に最も近ずけた場合 (a)，最も遠くにした場合 (c)，a と b との中間 (c) とに区別するとその時々に対応する力を 第 4-3 図に示す．(岸上)

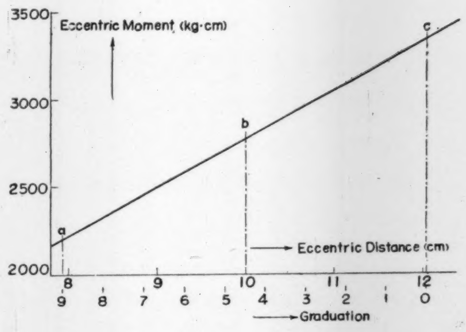

Fig. 4–2. Eccentric moment and radial distance of the mass.

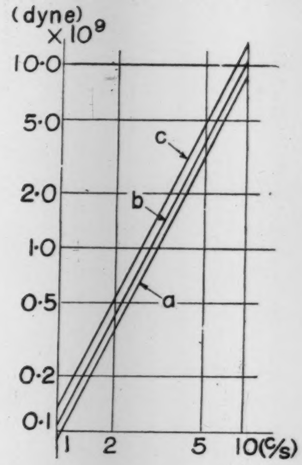

Fig. 4–3. Relation between rotation and eccentric force of the vibrator.

第 2 節　起振機による土地の振動調査

この機械を使つて測つた結果を簡単にのべると，本郷の東京大学の運動場で行つたときは距離 8 m に於て観測した記録には共振周期が見出せなかつた．これは固有周期が起振機で起し得る周期の範囲外に速いため共振を示さなかつたことによるかも知れない．

次に台東区隅田公園に於いて実験をしたその結果は第 4–4 図に常時微動を脈動計を以つて記録したものから求めた周期の頻度分布を示し，第 4–5 図には距離 10 m に於て観測した起振機による振動の周期と振巾との関係を示す．これ等を比較すると，0.17 秒から 0.20 秒までの間に固有振動があると思われる．

更に江東区大島町 2 丁目に於ける実験では起振機の起す振動は小さくなつた為に測定できなかつた．

以上の結果から機械の取付が下部だけでは機械自身が台と共にロッキングを始め，又台と共に地中に沈下する．今迄の測定は方法として不完全であるが更に改良して行きたく，ここに試験した結果を記し参考に供した．(岸上)

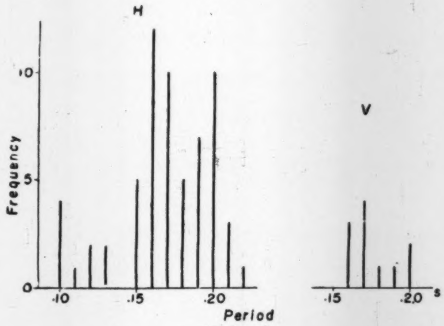

Fig. 4–4. Frequency distribution of periods of earth tremors. Sumida Park.

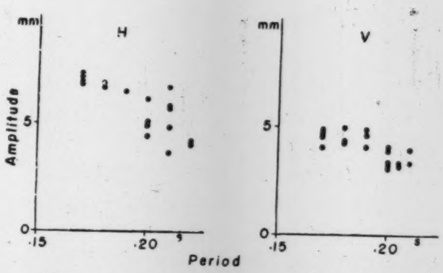

Fig. 4–5. Relation between amplitude and period of vibrations caused by the vibrator. Sumida Park.

第 3 節　東京大学構内に於ける測定

1.　東京大学運動場において，起振機に依る地震動を調べた．これによると，今までこういう調査の際に用いられた Degebo の考え方には，色々の問題があるということが解つた．

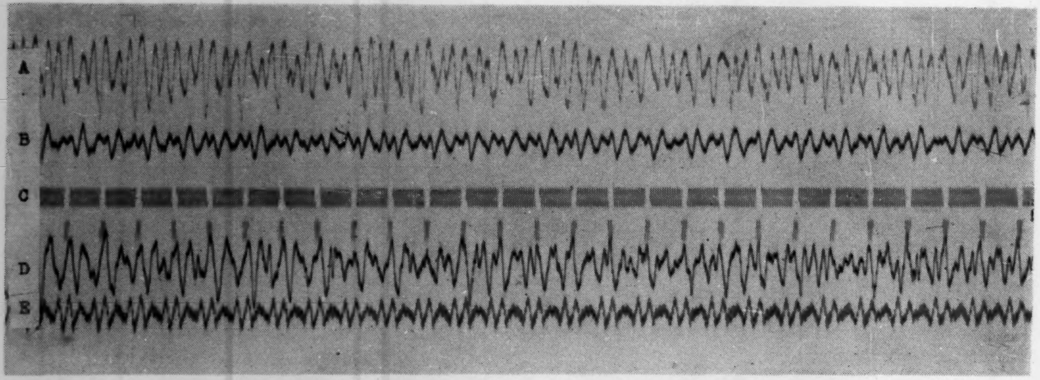

continued

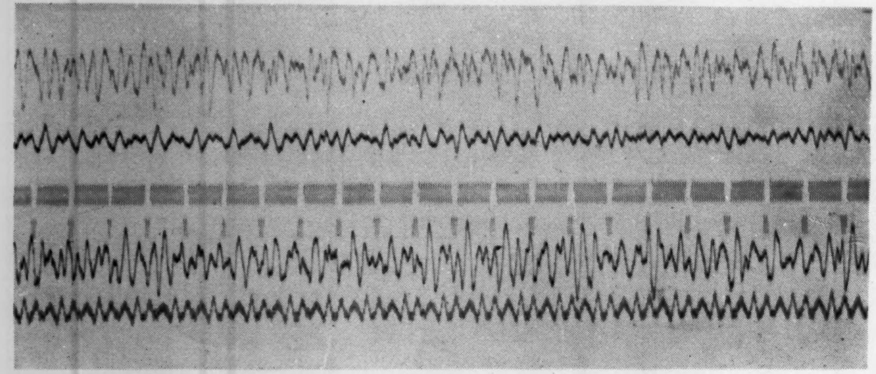

Fig. 4-6.　Example of record of the ground vibrations caused by the vibrator.　A: $\Delta=60$ m.　B: $\Delta=70$ m.　C: Time mark, 50 c/s.　D: $\Delta=80$ m.　E: $\Delta=20$ m. Hongo.

2.　Fig. 4-6 はその記象の一例であつて，中央にはいつて居るのが 50 サイクルの振動で，その零線をずらし，起振機の一回転ごとの位相を入れてある．これを見て解ることは，

i)　第一調波がはつきりせず，従つてこれから位相速度を求めることが出来ない．

ii)　同じ記象の中で，第三調波の出るところと第二調波の出るところとある．

iii)　或る周期で振巾が大きくなつて居るところがある．

3.　この観測結果を見れば，高調波がよく出るのは，起振機の Rocking が多分に影響して居ると思われるが，ともかくも起振機から種々の波が出されて居ることは想像される．今簡単のため，

$$\left.\begin{aligned} y_1 &= a_1 \sin \omega(t-\varphi_1) \\ y_2 &= a_2 \sin \omega(t-\varphi_2) \qquad \text{但し} \quad \varphi_1 = \frac{\Delta}{V_1} \\ & \qquad\qquad\qquad\qquad \varphi_2 = \frac{\Delta}{V_2} + \delta \end{aligned}\right\} \tag{1}$$

の二つの波が合成される場合を考える．そのときの振巾を a, phase を φ とすれば，

$$a=\sqrt{a_1^2+a_2^2+2a_1a_2\cos\omega(\varphi_1-\varphi_2)} \tag{2}$$

$$\varphi=\frac{a_1\sin\omega\varphi_1+a_2\sin\omega\varphi_2}{\omega(a_1\cos\omega\varphi_1+a_2\cos\omega\varphi_2)} \tag{3}$$

(2) は，$\omega(\varphi_1-\varphi_2)$ の値により $a\sim\Delta$ 曲線に山や谷が出来ることを示し，これだけでも Degebo 流の考え方をしなくともよいことが解る．又起振機の回転数が，順々に変つて行く場合，波の中に表面波の性質をもつものがあれば，当然分散のことを考えなければならず，そのことによつても振巾の山谷が出来る可能性がある．従つて，このことは起振機の回転をすこしづつ変えて行き，観測された振巾曲線の山をとつて，それを固有振動周期だと言う事ができないことを示して居る．この様に，起振機に依つておこされる震動は非常に複雑であり，その性質をよほど究明しない限り，Degebo 流に簡単に始末してしまうのは危険であると思われる．

尚昭和 27 年 4 月吾嬬ポンプ場に於て観測した振巾—距離曲線は地中の振動の項第 6–6 図，第6–7 図に示してある，（河島，角）

第 4 節 墨田区吾嬬町における測定

1. 起振機を地盤の上に据えて廻転させれば，それに要する電力は振動数の平方に比例する筈であり，もし地盤の固有振動数に相当するところがあれば，エネルギーが地盤にとられる量が大きくなり，電力も又非常に増す筈である．このことは Degebo で地盤調査に利用した所である．従つて，振動数をかえながら Wattmeter で，起振機を廻転させるに要する電力を次々に読みとつて行けば，その山の出来るところで地盤の固有振動数がわかる筈である．我々はこのことを調べるため，吾嬬ポンプ場において起振機を約 2 c/s より 20 c/s までの間の廻転数でまわし，それに要する電力を調べた．

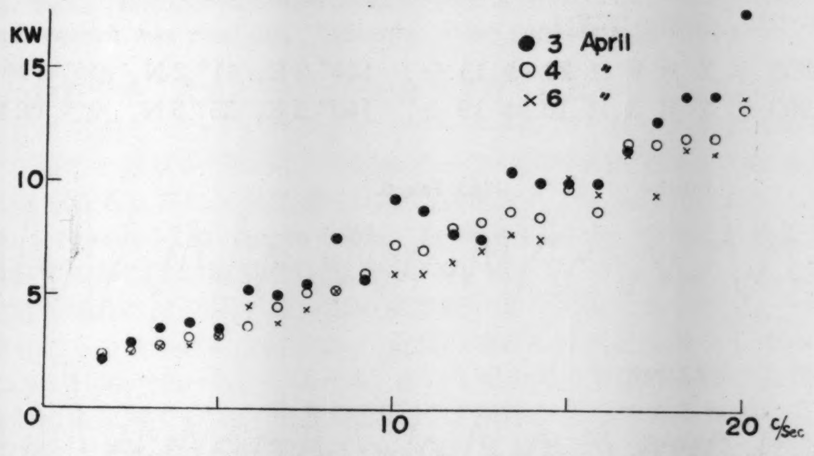

Fig. 4–7. Relation between power and frequency of the Vibrator.

2. 得られた結果は，Fig. 4–7 に示す様なものである．ここに●は 4 月 3 日，○は 4 月 4 日，× は 4 月 6 日にやつたものである．3 日にやつた際は，起震機がよく地盤について居らず，Rocking を行い，Wattmeter を読むのに苦労した．その夜雨が降り，起震機も落着いたので，4 日，6 日は Rocking も殆んどなくなり，二回ともほぼ一致した

結果を得ることが出来た.

3. これを見ると振動数に依る電力の変化は，Degebo の考え方に程遠く，この位の間ではむしろ直線的に変化して居る様である．また3日の分を除けば山になる様な場所も見受けられなかつた．（河角，島）

第 V 章　自然地震による調査結果

第 1 節　本郷と吾嬬町における自然地震の比較観測

1. **目的**　此の観測は東京都内地盤調査の一部として行われたもので，他の場所での観測と同様に，各種地盤における地震動の特徴を比較究明し，地盤の所謂良否なるものを端的適切に現すには如何なる量が適当であるか，又吾嬬町の地盤は第何種の地盤であるかを研究した.

2. **使用地震計，観測場所，期間等**．使用地震計は比較観測用として特に設計製作された逆立振子型水平動変位計[1] 2 台で，其の常数は次の通り

周期	7.0 秒	減衰比	10
基本倍率	47.5	記録速度	毎秒 2 粍

以上の地震計を文京区本郷東京大学構内地震研究所地下観測室並びに墨田区吾嬬町ポンプ場内に，何れも NS 方向に据付けた．記象の上方が S になる．観測は高橋研究室平能金太郎が担当し，昭和 28 年 1 月 28 日より同年 3 月 31 日まで行つた．此の期間内に

やゝ遠い地震:	大 1,	小 2.
比較的近い地震:	大 1,	小 10.

を観測した．上記の小というのは何れも記象紙上振巾数粍のもので，地震動の微細な点までを読取り得ない．従つて本研究には上記に大と記した遠震 1 回，近震 1 回だけしか利用出来なかつた．此等の地震は

1953 年 2 月 6 日 22 時 13 分，144°.2 E，41°.2 N，襟裳岬沖
1953 年 2 月 3 日 10 時 19 分，140°.3 E，35°.5 N，深さ 60 km

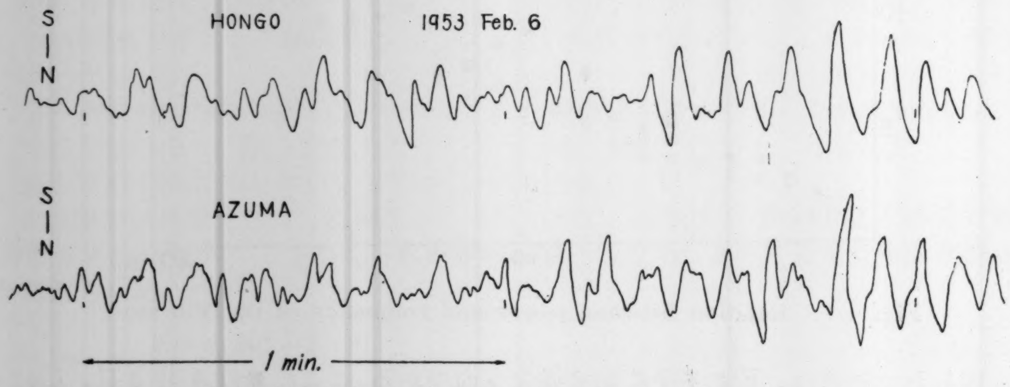

Fig. 5–1a. Records of Hokkaido earthquake obtained respectively at Hongo and Azumacho. Epicentre: Erimo Cape, Hokkaido. Δ≒1000 km.

1) 高橋龍太郎・平能金太郎　地震研究所彙報 **19** (1941), 527.

で近震の震央は房総半島中部にあたる．今後これらの地震をそれぞれ遠震及び近震と略称する．第 5-1 図 a, b にこれらの地震の記象を示した．

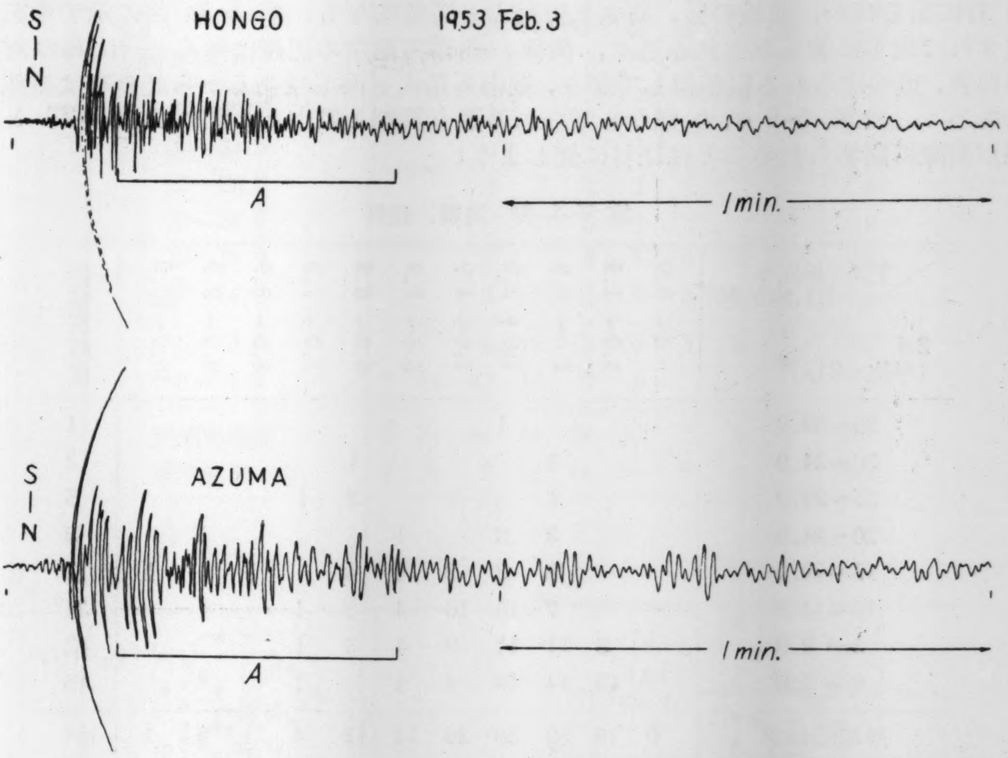

Fig. 5-1b. Records obtained respectively at Hongo and Azumacho. The part A in each record was read off. Epicente: Bôsô peninsula. $\Delta \fallingdotseq 100$ km.

3. **記象の読取方法**．遠震については記象が重なり縺れ合つているので，本郷，吾嬬両所の記象を互に参照しつつトレーシング・ペーパーに写し取り，此れから直接に地震波動の周期及び振巾の読取を行つた．今記象の一つの山の縦横坐標を (a_1, t_1)，この山に続く谷の坐標を (b_2, t_2)，更に其れに続く山谷山谷を夫々 (a_3, t_3), $(b_4, t_4)\cdots$，とするとき，$a_1-b_2=2A_1$，$t_2-t_1=\frac{1}{2}T_1$; $a_3-b_2=2A_2$，$t_3-t_2=\frac{1}{2}T_2$; $\cdots$ で与えられる A_iT_i をもつて一組の対応する振巾及び周期とした．

近震の記象の場合には周期が短いため直接読取は不可能であるので，一旦写真に撮り 4 倍に引伸したものから読取を行つた．近震の場合には遠震と違つて $\frac{1}{4}(a_1+a_3-2b_2)$ と (t_3-t_1)，或いは $\frac{1}{4}(2a_3-b_2-b_4)$ と (t_4-t_2) という組を夫々対応する振巾及周期とした．地震計の針先が円弧を画くので，記象の読取には縦線が円弧である特別の方眼板を作つて用いた．読取つた記象の部分は遠震については S の始から 5 分間，近震については S の始から算えて 5～39 秒の部分で，第 5-1b 図中 A と記した部分である．S の直後にある最大動の部分は記象がカスれ，或はヨロけているため振巾の外は読み取らなかつた．

上記のようにして決定した一組の A, T を用い，其の部分の地震動を正弦曲線と考えて，$v=2\pi A/T$ 及び $\alpha=4\pi^2A/T^2$ なる量を算出してこれを夫々速度，加速度と考えた．

4. **遠震**．遠震の周期，振巾を表示すると，震研の分は第 5-1 表の通りになる．表の数は其の周期,振巾をもつた波の数である．全体で 154 波あるが，周期別頻度を画いて

見ると第 5–2a 図に見られるような，$T=3.24$ 秒に一つの山を持つ滑らかな曲線になる．又振巾別頻度は奇麗なポアソン分布のような分布を示している．同様のことを吾嬬町の遠震記録についてすると第 5–2 表のようになり，周期別頻度の山が震研のと同様 $T=3.45$ 秒に出るほか，曲線の形，高さまで殆んど同様になる．第 5–1a 図に示す原記録を一見すれば直ちに看て取られる通り，震研，吾嬬町両所の記録は殆んど一山毎の対応が此等の表，或つけられる程相似して居り，振巾も殆んど同じであるから此の事は当然の帰結であろう．は第 5–3 a，b 図から看られる通り周期と振巾との間には $A\infty T^3$ という関係が明瞭に認められることは注目に価しよう．

第 V–1 表　遠震，震研

T/2 (単位＝1/1.845 秒) / 2A (単位＝21μ)	0～0.9	1.0～1.9	2.0～2.9	3.0～3.9	4.0～4.9	5.0～5.9	6.0～6.9	7.0～7.9	8.0～8.9	9.0～9.9	10.0～10.9	振幅別頻度
35～39.9				1								1
30～34.9			1				1					2
25～29.9			1				2	1				5
20～24.9			3	3		1				1		8
15～19.9			2	3	3	4	4		1		1	17
10～14.9			7	10	10	4	2	1				34
5～ 9.9		3	11	11	9	4	3	1				42
0～ 4.9		15	14	10	4	1		1				45
周期別頻度	0	18	39	38	26	14	12	4	1	1	1	154
優位波数	0	0	11	12	8	7	8	2	1	1	1	51

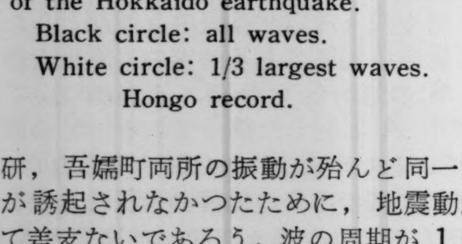

Fig. 5–2a. Distribution of periods of the Hokkaido earthquake.
Black circle: all waves.
White circle: 1/3 largest waves.
Hongo record.

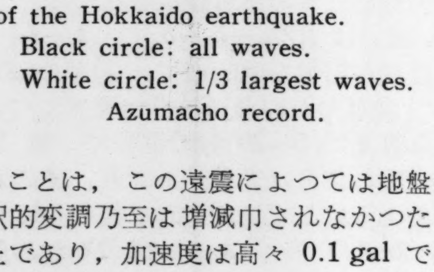

Fig. 5–2b. Distribution of periods of the Hokkaido earthquake.
Black circle: all waves.
White circle: 1/3 largest waves.
Azumacho record.

震研，吾嬬町両所の振動が殆んど同一であることは，この遠震によつては地盤の固有振動が誘起されなかつたために，地震動が撰択的変調乃至は増減巾されなかつたものと考えて差支ないであろう．波の周期が 1 秒以上であり，加速度は高々 0.1 gal であることを考えれば，地盤の振動が誘起されなかつたのも当然である．

5.　**優位波**．構築物に損害を与えるような波動は変位，速度或は加速度の大きな波であ

第 V-2 表　遠震，吾嬬町

$T/2$ (単位＝1/1.845 秒) \ $2A$ (単位＝21μ)	0 ~0.9	1.0~1.9	2.0~2.9	3.0~3.9	4.0~4.9	5.0~5.9	6.0~6.9	7.0~7.9	8.0~8.9	振幅別頻度
35~39.9			1							1
30~34.9						1				1
25~29.9			1	2	1	1	1			6
20~24.9				3	3	1	1			8
15~19.9			1		5	5	1	1		13
10~14.9			3	7	5	2	2	1	1	21
5~ 9.9			8	19	13	4	2	1		47
0~ 4.9	2	24	27	13	5	2				72
周期別頻度	2	24	40	44	32	16	7	3	1	169
優位波数	0	0	6	12	14	10	5	2	1	50

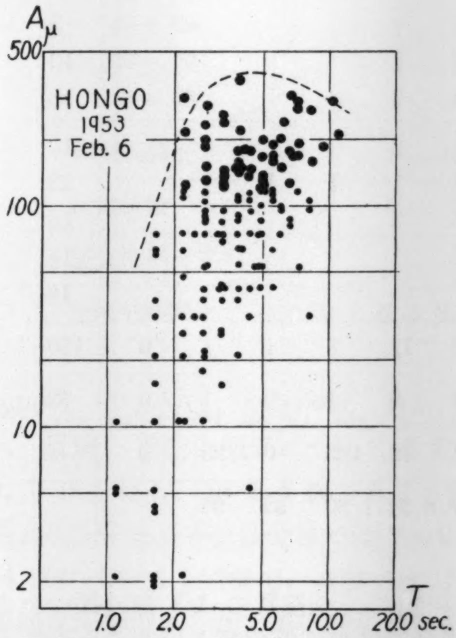

Fig. 5-3a. Amplitude-Period relation of the Hokkaido earthquake.
Large dots: 1/3 largest waves.
Hongo record.

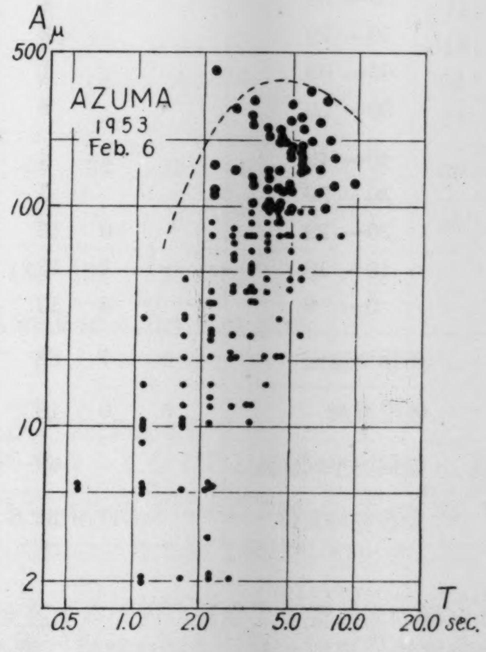

Fig. 5-3b. Amplitude-Period relation of the Hokkaido earthquake.
Large circles: 1/3 largest waves.
Azumacho record.

つて，其の何れが最も深く関係するかは構造物の性質によると思われる．何れにしても変位，速度或は加速度の小さな波は震害の点からは問題にならない．一方統計的に振巾が大きくなれば周期も延びるから，振巾の大きなもののみの周期別頻度は周期の大きい

方へ偏つて来る筈で，震害を論ずるには此の偏つた頻度分布を用いた方が合理的である．従つて今全波数の内から変位の大きい順に，総波数の 1/3 だけ採つて，其等の波を変位優位波ということにする．これは最大振巾の一山だけが特に飛び抜けて大きいような，特別な場合を除けば最大振巾の 1/3 以上の振巾を有する波だけを採るのと略々同様にな

第 V-3 表　周期—振巾別頻度表　近震，震研

$4A$ (単位=5.25μ) ＼ T (単位=1/7.85 秒)	0 ~0.9	1.0~1.9	2.0~2.9	3.0~3.9	4.0~4.9	5.0~5.9	6.0~6.9	7.0~7.9	8.0~8.9	9.0~9.9	振幅別頻度
150~159											0
140~149				1							1
130~139						1					1
120~129				1			1				2
110~119				2							2
100~109				1	1						2
90~ 99			3	0	2	1			1		7
80~ 89			2	2	1						5
70~ 79			2	1	2						5
60~ 69			1	5	3	1					10
50~ 59			8	4	3	3					18
40~ 49		2	4	1	4	2					13
30~ 39			3	9	8	1	1	1			23
20~ 29		0	10	7	6	2					25
10~ 19		1	12	2	2	1					18
0~ 9		4	13	1							18
周期別頻度	0	7	58	37	32	12	2	1	1	0	150
優位波数	0	0	16	17	12	6	1	0	1	0	53
優位波平均変位			69	83	74	76	125	0	95	0	
全波平均変位		17.9	32.6	53.1	47.8	54.1	80	35	95		

る．同様の考に従つて全波の内から加速度の大きい順に，全波数の 1/3 だけ採つたものは加速度優位波である．今後は誤解の虞のない場合には単に優位波ということがある．そして今後の色々な統計や議論は，特に断らない限り優位波について行う．

優位波の頻度の山の位置は全波の頻度の山の位置の 1.2~1.3 倍，優位波についての平均値は全波についての平均の 1.2~1.3 倍になるらしいが，此の数値は更に多数の地震記象について確められなければ確かでない．

第 5-1, 2, 3, 4 表中に点線で示したのは優位波の下限である．第 5-2 図 a, b には優位波の周期別頻度をも示してある．第 5-3 a, b 図中では優位波は大きい丸で示してある．

優位波の数を $N^1/_3$ で，又加速度，速度又は変位の優位波についての平均を夫々

第 V-4 表　周期―振巾別頻度表　近震，吾嬬町

T (単位=1/7.85 秒) / 4A (単位=5.25μ)	0 ～0.9	1.0～1.9	2.0～2.9	3.0～3.9	4.0～4.9	5.0～5.9	6.0～6.9	7.0～7.9	8.0～8.9	9.0～9.9	振幅別頻度
280～299											0
260～279							1		1		2
240～259									1		1
220～239								1			1
200～219						1					1
180～199						1	1	1			3
160～179					1						1
140～159						1			1		2
120～139						2		1			3
100～119					2		3	1			6
80～ 99				1	1	4	3	3	1		13
60～ 79			2	1	1	8		2			14
40～ 59		1	1	5	3	4	3	1			18
20～ 39		3	9	6	6	2	1	4			31
0～ 19	1	4	4	3		1					13
周期別頻度	1	8	16	16	14	24	12	14	4	0	109
優位波数	0	0	0	1	4	9	8	7	4	0	36
優位波平均変位				90	120	130	133	133	190	0	
全波平均変位	10	22.5	31.2	38.8	62.9	83.4	103.1	88.6	190		

$\sum\alpha/N^{1}/_{3}$，$\sum v/N^{1}/_{3}$，$\sum A/N^{1}/_{3}$，又は $\overline{\overline{\alpha}}$，$\overline{\overline{v}}$，$\overline{\overline{A}}$ で示すことにする．

6. **近震**．前記の近震について遠震の時と同様なことをすると第 3，4 表並に第 5-4 a，b 図を得る．第 5-3 表で見ると震研での周期別頻度は全波数では $T=0^{s}.32$，$0^{s}.57$ の両点に山があるが，優位波では $T=0^{s}.38$ のみに山のある単純な頻度分布を示している．第 4 表についても同様で，全波では $T=0^{s}.38$ 及 $0^{s}.70$ に山があるが優位波では $T=0^{s}.77$ に単純な山を示す．此の事は従来用いられている意味で，本郷では $0^{s}.32$ の波が，又吾嬬では $0^{s}.70$ の波が卓越することを示すものであり，優位波について言えば，それより少し大きい $0^{s}.38$ 及び $0^{s}.77$ の波が卓越することを示している．

振巾別の頻度分布は近震の場合にもポアソン分布的になる．第 5-4 a, b 図について見るに遠震の場合に見られた $A\infty T^{3}$ の関係は振巾の小さい波についてはかなりよく成立つているが，優位波については其の周期は振巾に無関係になる傾向を示している．即ち振巾に無関係に本郷ではほぼ $0^{s}.83$ を，又吾嬬町ではほぼ $0^{s}.77$ を中心に集つている．此のことは此等の周期に近い波が地盤によつて撰択増巾された結果．$A\infty T^{3}$ の関係から外

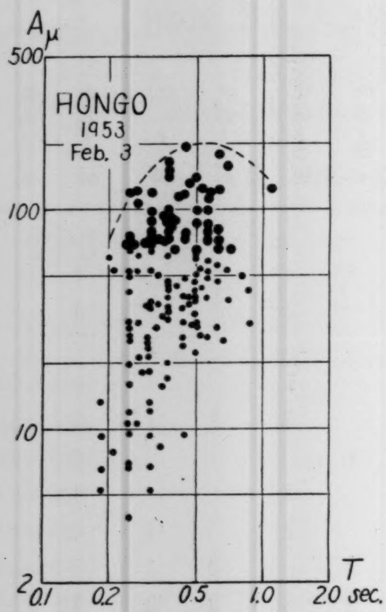

Fig. 5–4 a.

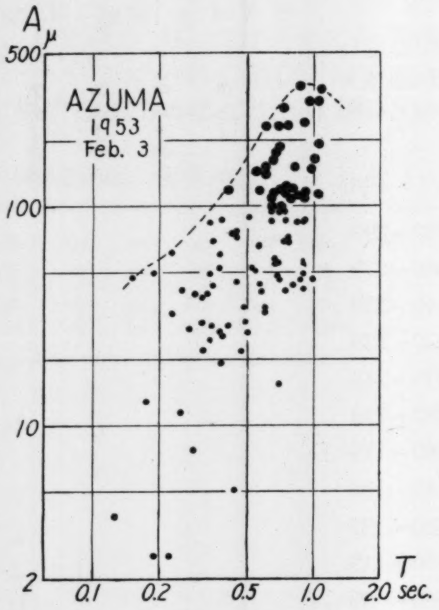

Fig. 5–4 b.

Amplitude-period relation. The Boso earthquake. Large
dots: 1/3 largest waves.

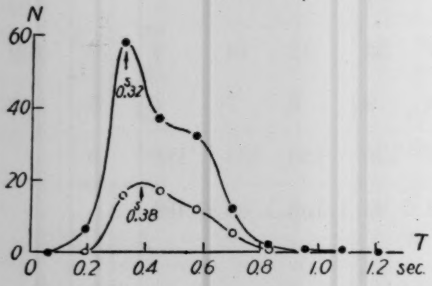

Fig. 5–5a. Distribution curve of periods of the Boso earthquake.
Black circle: all waves.
White circle: 1/3 largest waves.
Hongo record.

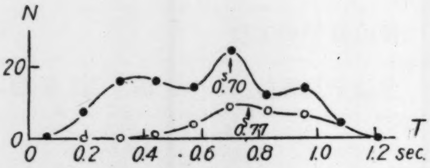

Fig. 5–5b. Distribution curve of periods of the Boso earthquake.
Black circle: all waves.
White circle 1/3 largest waves.
Azumacho record.

れて大きくなつているものと解釈してもよいであろう.

近震の優位波の頻度分布を図示すれば第 5–5 a, b 図のようになる. この図で見られるように震研における頻度分布は 0.25〜0.7 秒という比較的狭い範囲に限られ, 尖つた山を有するのに反し, 吾嬬町では頻度分布の範囲は 0.19〜1.10 秒に亘り且つ平坦である. 優位波についても同じことがいわれるが卓越する優位波が震研では 0.38 秒に吾嬬では 0.77 秒であるのが著しい対照をなしている.

第 5–6 a 図は周期別平均振巾の変化を示している. 震研, 吾嬬両所共平均振巾は周期と共に大きくなる傾向があつて, 大体のことを言えば吾嬬は震研の約 1.5 倍の振巾を持つている. 更に詳しく見るとこの比は 0.3 秒辺で小さく, 0.75 秒附近で大きくなること

は最大振巾の分布からも見られる．第 5–6b 図にそれらの様子を示した．

又第 5–1 b 図の地震記象における最大振巾の比は約 1.7 である．

第 5–4 図における波を表す各点の上限を示す線の形が，本郷のは遠震の場合のと略同様であるのに対し，吾嬬のは特異な形であるのは面白く，地盤の振動特性と関係があるらしく思われる．

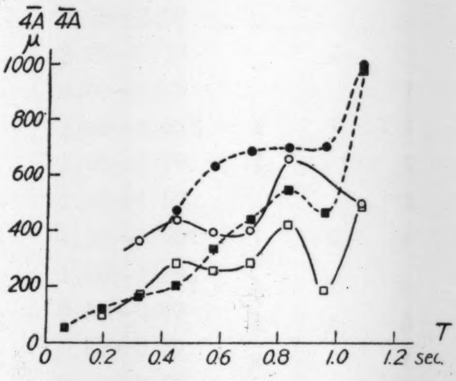

Fig. 5–6a. Mean amplitude.
Black circle: Azuma } 1/3 largest waves
White circle: Hongo
Black square: Azuma } all waves.
White square: Hongo

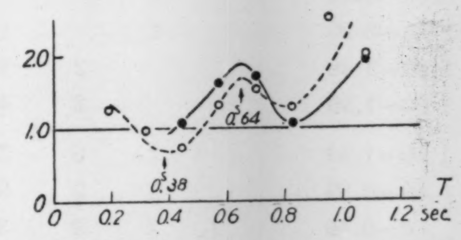

Fig. 5–6b. The ratio (the mean amplitude at Azumacho)/(the mean amplitude at Hongo).
Black circle: 1/3 largest waves
White circle: all waves.

第 V–5 表 周期—速度別頻度表 1953 年 2 月 3日 近震，震研

T (単位＝1/7.85 秒) / $2\pi A/T$ (単位 0.065 キネ)	0 ~0.9	1.0~1.9	2.0~2.9	3.0~3.9	4.0~4.9	5.0~5.9	6.0~6.9	7.0~7.9	8.0~8.9	9.0~9.9	速度別頻度
4.50~4.99		1	1								2
4.00~4.49			2	2							4
3.50~3.99			1	2							3
3.00~3.49			1								1
2.50~2.99		1	6	3	1	1					12
2.00~2.49		1	8	7	2						18
1.50~1.99			6	5	4	1	1				17
1.00~1.49			8	6	6	3			1		24
0.50~0.99		1	12	12	15	5	1				46
0.00~0.49		2	13	1	4	2		1			23
周期別頻度	0	6	58	38	32	12	2	1	1	0	150
優位波数	0	3	25	19	7	2	1	0	0	0	57
優位波平均速度		3.75	2.97	2.57	2.04	2.25	1.75				
全波平均速度	0	1.84	1.50	1.72	1.06	1.04	1.25	0.25	1.25	0	

第 V-6 表　周期―速度別頻度表　1953 年 2 月 3 日　近震，吾嬬町

T (単位＝1/7.85 秒) ＼ 2πA/T (単位＝0.065 キネ)	0 ～ 0.9	1.0～ 1.9	2.0～ 2.9	3.0～ 3.9	4.0～ 4.9	5.0～ 5.9	6.0～ 6.9	7.0～ 7.9	8.0～ 8.9	9.0～ 9.9	10.0～10.9	速度別頻度
4.00～4.49							1					1
3.50～3.99					1	1						2
3.00～3.49		1				1	1	1	2			6
2.50～2.99		2		1	1	2		1				7
2.00～2.49			2	1	2	1						6
1.50～1.99			2	4	1	4	3	1	1			16
1.00～1.49		2	5	2	1	8	3	4	1			26
0.50～0.99		1	5	5	7	6	4	5				33
0～0.49	1	2	2	3	1	1		2				12
周期別頻度	1	8	16	16	14	24	12	14	4	0	0	109
優位波数		3	4	6	5	9	5	3	3			38
優位波平均速度		2.92	2.00	2.00	2.55	2.42	2.55	2.58	2.75			
全波平均速度	0.25	1.56	1.15	1.18	1.39	1.52	1.62	1.22	2.37			

7. **速度分布**．一般に構造物の変形は地動のスペクトル中，構造物と同周期の部分強度に比例すると考えられるから，若し構造物の破壊がその変形の大きさによつてのみ定まるような場合には地震動の速度分布は最も重大な量となる．

前記のようにして読取つた A, T から $v=2\pi A/T$ なる量を計算してこれを速度とした．其の周期に対する分布は第 5 表，第 6 表に与えた．其の頻度分布，速度優位波の頻度分布は第 7 図 a, b の通りである．当然のこと乍ら全波の頻度分布は振巾の場合と

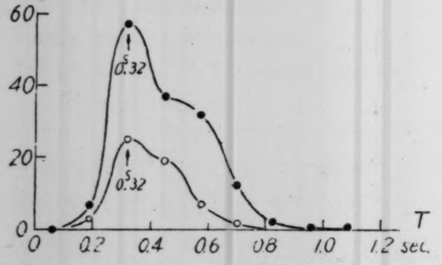

Fig. 5–7a. Distribution of periods of computed velocity. The Boso earthquake.
Black circle: all waves
White circle: 1/3 largest waves
Hongo record.

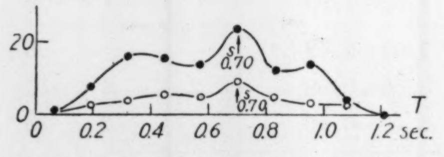

Fig. 5–7b. Distribution of periods of computed velocity. The Boso earthquake.
Black circle: all waves
White circle: 1/3 largest waves
Azumacho record.

第 V-7 表 周期—加速度別頻度表 1953 年 2 月 3 日 近震，震研

T (単位＝1/7.85 秒) ＼ $4\pi^2A/T^2$ (単位＝3.20 ガル)	0 ～0.9	1.0～1.9	2.0～2.9	3.0～3.9	4.0～4.9	5.0～5.9	6.0～6.9	7.0～7.9	8.0～8.9	加速度別頻度
2.40～2.59										
2.20～2.39			1							1
2.00～2.19			1							1
1.80～1.99		1	1							2
1.60～1.79										0
1.40～1.59		1	2	1						4
1.20～1.39			1	2						3
1.00～1.19			2	1						3
0.80～0.99			9	1						10
0.60～0.79			5	9	1					15
0.40～0.59		1	9	5	4					19
0.20～0.39		3	14	12	15	6	1			51
0.00～0.19		1	12	6	12	7	1	1	1	41
周期別頻度	0	7	57	37	32	13	2	1	1	150
優位波数	0	3	31	19	5	0				58
平均加速度		1.30	0.93	0.78	0.54					

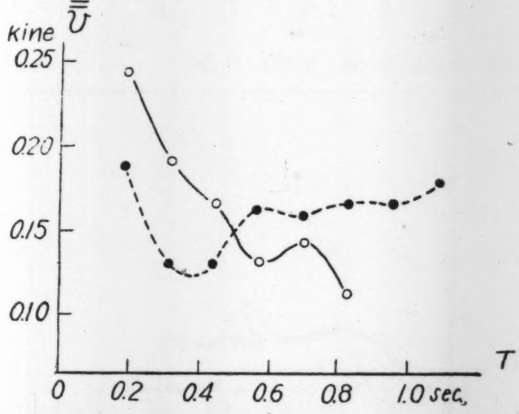

Fig. 5–8a. Mean of the 1/3 largest velocity waves of the Boso earthquake.
Black circle: Azumacho,
White circle: Hongo.

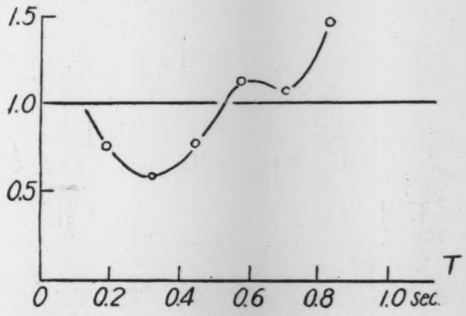

Fig. 5–8b. The ratio (the mean velocity at Azumacho)/(the mean velocity at Hongo).

全く同じである．速度優位波の分布を図について看察すると其の形が殆んど全波の形と同様であるのは著しい事柄である．震研では 0.32 秒に，吾嬬町では 0.70 秒に卓越周期

を有するが，前者では山が明瞭であるのに対し，後者では頗る平坦である．

各周期について，優位波のみの平均速度，全波の平均速度を示したのが第 5–8 a 図で，何れの平均も吾嬬では周期と共に増し，震研では減少する傾向を示しているが，吾嬬で

第 V–8 表 周期—加速別頻度度表 1953 年 2 月 3 日 近震，吾嬬町

$4\pi^2A/T^2$ (単位＝3.20 ガル) ＼ T (単位＝1/7.85 秒)	0.0～0.9	1.0～1.9	2.0～2.9	3.0～3.9	4.0～4.9	5.0～5.9	6.0～6.9	7.0～7.9	8.0～8.9	加速度別頻度
2.40～2.59		1								1
2.20～2.39										0
2.00～2.19										0
1.80～1.99										0
1.60～1.79		1								1
1.40～1.59		1								1
1.20～1.39										0
1.00～1.19										0
0.80～0.99			2	1	1					4
0.60～0.79		1	2	1	1	1	1			7
0.40～0.59		1	6	5	3	4	1	1		21
0.20～0.39	1	1	5	4	3	12	6	2	3	37
0.00～0.19		2	1	5	6	7	4	11	1	37
周期別頻度	1	8	16	16	14	24	12	14	4	109
優位波数	0	5	10	7	5	5	2	1	0	35
平均加速度		1.38	0.62	0.59	0.62	0.54	0.60	0.50		

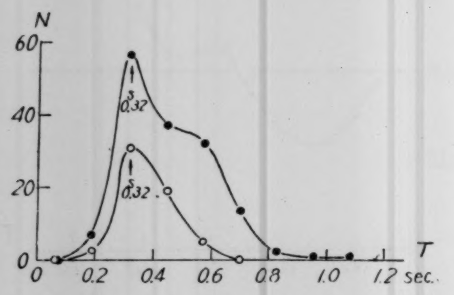

Fig. 5–9a. Distribution of periods of computed acceleration. The Boso earthquake.

Black circle: all waves.

White circle: 1/3 largest accelerations.

Hongo record.

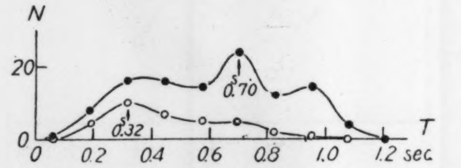

Fig. 5–9b. Distribution of periods of computed acceleration. The Boso earthquake.

Black circle: all waves.

White circle: 1/3 largest acceleration.

Azumacho record.

は余り著しくない．速度比は第 5–8b 図に示す如く 0.32 秒附近で小さく 0.6 位であるのが 0.7 秒附近では逆に吾嬬の速度が大きくなり 1.3∼1.5 倍となつている．0.5 秒附近では両者に差がない．このことは 0.5 秒以上の周期の構造物は吾嬬町では本郷よりも不利であることを示す．

遠震の速度分布については本郷，吾嬬の差は殆んどない．

8. **加速度分布**．第 5–7，5–8 表は A, T から計算した $\alpha=4\pi^2A/T$ なる値の分布を示す．吾々はこの値を加速度と見做した．第 5–9 図には近震の加速度優位波の頻度分布を示した．本郷，吾嬬とも 0.32 秒に卓越周期を有するが，吾嬬ではこの外 0.7 秒にも小さい山があり，分布曲線は頗る平坦である．

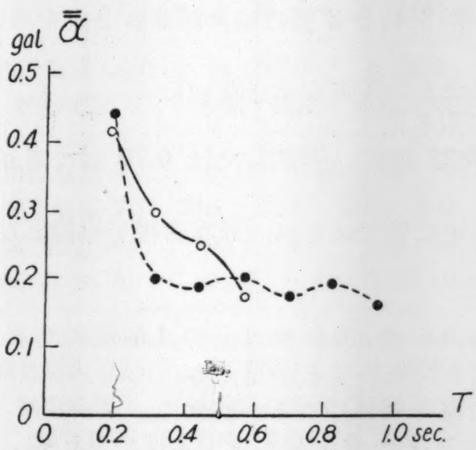

Fig. 5-10a. Mean of the 1/3 largest accelerations.
Black circle: Azumacho.
White circle: Hongo.

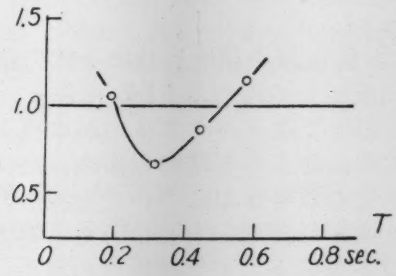

Fig. 5–10b. The ratio (the mean acceleration at Azumacho)/(the mean accelerations at Hongo).

第 5–10 図には両場所の平均加速度及び其の比を示した．本郷に比し吾嬬では 0.3 秒で加速度小さく 0.7 秒で大きい．

第 5–11 図は遠震の平均加速度を示した．前にも述べた通り遠震に対しては本郷と吾嬬とに殆んど差違がない．

第 5–10 b 図で見ると 0.32 秒附近では吾嬬町の加速度は小さく本郷の 0.65 倍位であることは前述の通りであるが，0.7 秒以上及び 0.2 秒以下において 1.5 倍以上の加速度比を示す．0.7 秒以上のものは吾嬬町での卓越振動によるものであろうが，0.2 秒以下のものは其の本態を未だ説明し得ない．然し斯様な短周期の，又そのために加速度の大きい波は時々厚い冲積層の上で観測されるも

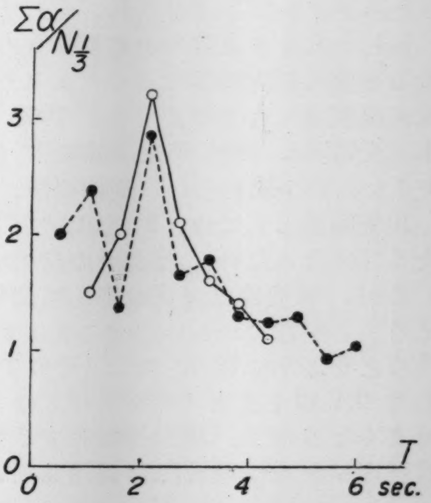

Fig. 5–11. Mean acceleration of the Hokkaido earthquake.
Black circle: Azumacho.
White circle: Hongo.

ので，石本博士[2] はこれを卓越周期の第三調波とした．然し地震波の場合には関連した波の波数がさ程多くないから第三調波は現れ難いのではないかと思われる．この波の本性については将来の研究に俟たねばならない．

9. **表層中の横波の速度**．吾嬬町の表面層の厚さはボーリングの資料[3] 並に弾性波探査[4] により 22 m と推定されているので，0.77 秒の卓越周期を表面層の剪断振動によるものとすれば[5] 横波の速度は 115 m/s となる．一方弾性波探査と地中地震計の観測[6] により横波の速度は 95 m/s と得られている．これは相当よく合致した値といえる．

10. 結論．従来の周期頻度図より一歩進んで第 5-1, 5-2 表の如き周期振巾表を用い，更にこれから速度，加速度を計算した結果，

1) 遠震の際には吾嬬町，震研の地動はあまり著しい差違を示さない．

2) 振巾と周期の間には略々 $A \backsim T^3$ の関係がある．

3) 以下近震の際について言えば，震研では 0.32 秒に，吾嬬町では 0.70 秒に卓越周期がある．

4) 1/3 優位波の頻度分布は全体の波の頻度分布に似て来るが，分布曲線が単純となり且卓越周期がやや延びる (1.2 倍位).

5) 吾嬬町ではスペクトル巾が本郷より広い．

6) 本郷に対する吾嬬町の振巾比は 0.32 秒で 0.6 位，0.6 秒以上で 1.5 位になる．

7) 速度の頻度分布についても振巾の場合と略々同様のことが言える．

8) 加速度の頻度分布についても振巾の場合と略々同様のことが成立つ．

9) 以上を総合して吾嬬町での振巾，速度，加速度は 0.3 秒附近で本郷の 0.6 倍，0.6 秒以上の周期で本郷の 1.5～2.0 倍であるから，吾嬬町の地盤は第 3 種地盤と考えられる．

（高橋，平能）

第 2 節　本郷と下町 4 箇所における自然地震の比較観測

1. 近年，大地震後の余震を激震地域内の異つた性質の地形地質をもつ近接した場所で観測して，その地震動を比較し，それによつて震害の地理的分布を説明しようというこころみが，しばしばなされ，それぞれ興味ある結果がえられている．

われわれは東京都内の地盤調査の一つとして，同様の方法を日常東京において観測される普通の近地地震によつておこなうことをこころみた．すなわち，本郷（地震研究所本館観測室）を基準点とし，1952 年度隅田（隅田公園事務所），1953 年度大島町（小名木川変電所），1954 年度東篠崎町（ミヨシ化学江戸川工場），逆井町（小松川高等学校）の 4 点をえらび調査した．観測場所，観測期間，観測計器の常数は第 5-9 表にしめした．

比較観測としては，2 点におく 1 組の地震計のそれぞれの特性が充分よくそろつていなくてはならない．地震計の常数中，自己周期は製作のときに比較的よくそろえられているが，減衰比は設置に際して調整するものであり，臨界に近くなると特にこれをそろえることがむつかしい．そのために減衰比 v を比較的小さくして，精確に 2 台の v をそろえるように努力した．（それでも，測定結果でかなりちがつた場合もあつたが h にして 0.1 以上大きくちがうことはまれであつた)．したがつて地震計の周波数特性の巾がせまくなるので，構造物に対する影響の予想される週波数帯域をおおうために，数種の自己周期をもつ地震計を使用した．直接にはまたこれによつて地震動の速度スペクトル

2) 石本巳四雄　地震研究所彙報　**13** (1935), 600.
3) 復興局　東京及横浜地質調査報告及同附図
4) 島　悦三　本論文 p. 477, p. 539.
5) 高橋龍太郎　軟弱地盤における地震動　地震研究所彙報 **19** (1941), 534.
6) 河角　広・島　悦三　本論文 p. 492, Fig. 2-32.

を記録させることをも意図したわけである．さらに考え方をかえれば，これら数種の地震計は，建物をふりこのような簡単な振動体とみなせるかぎりにおいて，それぞれと同一の週期と減衰をもつ構造物の類似物とみなしてもよいわけであり，その直接的振動比較をしたことになるとおもわれる．

観測の実施にあたつては，ミヨシ化学秋本幸一，小松川高校羽賀貞四郎両氏の協力をえた．特に記して心から感謝の意を表したい．

第 V-9 表　自然地震比較観測使用地震計常数表

地震計型式 (成分)	A (NS)		A (EW)		M (NS)		M (EW)		D (NS)		D (EW)	
観測場所	本郷	隅田	本郷	隅田	本郷	隅田	本郷	隅田	本郷	隅田	本郷	隅田
自己周期 T_0	$0^{s}.11$	$0^{s}.10$	$0^{s}.09$	$0^{s}.11$	$0^{s}.90$	$0^{s}.96$	$0^{s}.86$	$0^{s}.93$	$3^{s}.5$	$4^{s}.2$	$3^{s}.4$	$3^{s}.4$
幾何倍率 V_G	216	212	216	242	214	240	214	214	18.0	18.0	14.4	18.3
減衰比 v	10	10	9.4	14.5	10	13	10	12	10.5	12	10.5	11.2
減衰率 h	0.59	0.59	0.58	0.65	0.59	0.63	0.59	0.62	0.6	0.62	0.6	0.61

地震計型式 (成分)	A (EW)		B (EW)		C (EW)		M (EW)		D (EW)	
観測場所	本郷	大島町	本郷	大島町	本郷	大島町	本郷	大島町	本郷	大島町
自己周期 T_0	0.1	0.1	0.2	0.2	0.5	0.5	1.0	1.0	5.6	5.6
幾何倍率 V_G	210	210	168	168	168	168	168	168	8.6	8.0
減衰比 v	5.3	5.4	5.6	3.4	3.7	3.5	4.2	3.4	4.7	5.9
減衰率 h	0.47	0.47	0.48	0.36	0.38	0.37	0.42	0.37	0.44	0.49

地震計型式 (成分)	A (EW)		B (EW)		C (EW)		M (EW)	
観測場所	本郷	ミヨシ化学	本郷	ミヨシ化学	本郷	ミヨシ化学	本郷	ミヨシ化学
自己周期 T_0	—	0.10	0.2	0.21	0.5	0.5	0.95	0.87
幾何倍率 V_G	—	210	168	168	168	168	168	168
減衰比 v	—	4.3	3.5	4.1	4.1	3.8	3.7	5.1
減衰率 h	—	0.42	0.36	0.41	0.41	0.39	0.37	0.46

地震計型式 (成分)	A (EW)		B (EW)		C (EW)		M (EW)	
観測場所	本郷	小松川	本郷	小松川	本郷	小松川	本郷	小松川
自己周期 T_0	0.1	0.1	0.2	0.2	0.5	0.5	0.95	0.98
幾何倍率 V_G	210	210	168	168	168	168	168	168
減衰比 v	3.9	4.4	4.5	7.7	3.8	3.8	4.1	4.3
減衰率 h	0.4	0.42^{5}	0.43	0.54^{5}	0.39	0.39	0.41	0.42

註　地震計型式略号：A：石本式加速度地震計，B：石本式加速度計型 5 c/s 地震計，
C：石本式微動計型 2 c/s 地震計，M：石本式微動地震計，
D：萩原式小型変位地震計．

2. えられた記象について． いままでに整理できたおもなことがらをつぎにのべよう．

(a) **最大動の比較**　各点の地震動の記録上の最大動をとり，その地震の本郷の記録の

第 V–10 表　隅田公園と本郷との最大動振巾の比較

地震 地震月報 (C.M.O) による	地震計 型式	地震計 成分	本郷記録最大動 記録全振巾 A_m	本郷記録最大動 振子重心振巾 $\frac{A_m}{V_G}$	本郷記録最大動 周期 T	本郷記録最大動 速度振巾補正値	隅田記録最大動 記録全振巾 A_m	隅田記録最大動 振子重心振巾 $\frac{A_m}{V_G}$	隅田記録最大動 周期 T	隅田記録最大動 速度振巾補正値	隅田/本郷 振巾比 $\frac{A'_mS}{A'_mH}$	隅田/本郷 周期平均 T
1) 1952			*mm*	μ	*s*	μ/s	*mm*	μ	*s*	μ/s		*s*
1.29 06^h39^m	A	NS	1.0	4.6	0.2	3.1	0.7	3.3	0.1_5	2.8	0.9	0.1_8
茨城県南西部	A	EW	1.2	5.6	0.1_5	4.4	—	—	—	—	—	—
36°.1N, 140°.1E	M	NS	7.1	33.0	0.4_5	20.8	12.9	54.0	0.5_5	38.6	1.8_5	0.5
深さ 40～45 km	M	EW	8.4	39.0	0.6	33.0	12.4	58.0	0.6_5	57.0	1.7_3	0.6_3
東京震度 I.	D	NS	0.6	33.0	0.4	4.1	1.0	56.0	0.4	6.5	1.6	0.4
最遠有感 115 km	D	EW	0.7	49.0	0.4_5	7.6	1.0	55.0	0.5	9.4	1.2	0.4_8
2)												
1.31 10^h50^m	A	NS	0.6	2.8	0.2	1.9	0.9	4.2	0.1_5	3.5	1.84	0.1_8
熊谷附近	A	EW	0.8	3.7	0.2	2.2	1.0	4.1	0.1_5	3.8	1.73	0.1_8
36°.2N, 139°.6E	M	NS	7.8	37.0	0.6	32.0	10.9	45.0	0.6_5	37.5	1.17	0.6_3
深さ 115～120 km	M	EW	7.1	33.0	0.5_5	26.0	8.6	40.0	0.6_5	33.4	1.28	0.6
東京(隅田)震度 I	D	NS	0.6	33.0	0.5_5	6.3	0.9	50.0	0.6	8.5	1.35	0.5_8
最遠有感 140 km	D	EW	0.6	42.0	0.5_5	8.2	0.8	44.0	0.6_5	10.1	1.23	0.6
3)												
2.20 16^h03^m	A	NS	3.8	18.0	0.2	12.0	1.8	8.5	0.2_5	4.3	0.36	0.2_3
茨城県南西部	A	EW	4.8	22.0	0.2	13.0	3.0	12.0	0.1_5	11.0	0.85	0.1_8
36°.1N, 139°.9E	M	NS	23.7	111.0	0.3_5	54.0	33.0	138.0	0.5	90.5	1.68	0.4_3
深さ 55 km	M	EW	35.2	164.0	0.4	96.0	37.9	177.0	0.5_5	159.0	1.66	0.4_8
東京　震度 II	D	NS	1.4	78.0	0.5_5	14.8	2.3	128.0	0.4_5	16.6	1.12	0.5
最遠有感 160 km	D	EW	2.4	168.0	0.3	16.8	3.2	175.0	0.5	14.6	0.87	0.4
4)												
2.26 03^h41^m	A	NS	1.2	5.6	0.2	3.8	0.9	4.3	0.1_5	3.6	0.96	0.1_8
鹿島灘	A	EW	1.2	5.6	0.1_5	4.4	0.9	3.7	—	—	—	—
36°.2N, 141°.3E	M	NS	23.3	108.0	0.5_5	82.0	44.5	185.0	0.7_5	172.0	2.1	0.6_5
深さ ca. 40 km	M	EW	20.1	94.0	0.7_5	92.0	35.0	164.0	0.9_5	151.0	1.64	0.8_5
東京　震度 II	D	NS	2.2	122.0	1.2	51.0	3.3	183.0	1.0	53.0	1.04	1.1
最遠有感 240 km	D	EW	1.8	125.0	0.7	31.0	3.6	197.0	1.2	86.0	2.8	0.9_5
5)												
3.7 16^h32^m	A	NS	—	—	—	—	0.6	—	0.7_5	—	—	—
大聖寺沖	A	EW	0.7	3.2	1.0	3.2	0.8	3.3	1.0	3.2	1.00	1.0
36°28′N, 136°12′E	M	NS	—	—	—	—	54.3	—	1.2_5	—	—	—
深さ 20 km	M	EW	45.4	212.0	2.2	103.0	56.7	265.0	2.2	109.0	1.06	2.2
東京　震度 I	D	NS	—	—	—	—	46.5	—	4.9	—	—	—
最遠有感 770 km	D	EW	48.1	3340.0	4.9	2820.0	30.5	1670.0	5.0	1400.0	0.5	4.9_5

第 V-10 表 (つづき)

6)			*mm*	μ	*s*	μ/*s*	*mm*	μ	*s*	μ/*s*		*s*
3.8　20^h03^m	A	NS	0.8	3.7	0.1_5	3.2	0.7	3.3	0.2	2.1	0.66	0.1_8
茨城県南西部	A	EW	0.8	3.7	0.1_5	2.9	1.9	7.8	0.1_5	7.2	2.50	0.1_5
36°.1N, 139°.9E	M	NS	5.0	23.0	0.5	15.9	10.2	43.0	0.6_5	35.7	2.24	0.5_8
深さ　60 km	M	EW	6.4	30.0	0.4_5	19.8	9.2	43.0	0.5_5	38.8	1.96	0.5
	D	NS	0.3	17.0	0.5	2.9	0.7	39.0	0.7	7.8	2.7	0.6
	D	EW	0.4	28.0	0.3_5	3.4	0.7	38.0	0.4	5.3	1.56	0.3_8
7)												
3.10　02^h04^m	A	NS	0.6	2.8	0.3	1.2	0.5	2.4	0.7	0.42	0.3	0.5
襟裳岬南東沖	A	EW	0.6	2.8	0.4	0.8	0.8	3.3	0.5	0.9	1.1	0.5
41°.7N, 143°.5E	M	NS	36.3	170.0	1.1	163.0	65.6	274.0	1.3_5	242.0	1.48	1.2
深さ　0～20 km	M	EW	38.7	180.0	1.5	129.0	47.9	222.0	1.4	146.0	1.13	1.5
東京　震度 I	D	NS	16.9	940.0	5.0	817.0	14.0	780.0	3.2	710.0	0.87	4.1
最遠有感 820 km	D	EW	17.6	1220.0	5.9	875.0	12.2	670.0	4.2_5	640.0	0.73	5.1
8)												
4.8　05^h44^m	A	NS	3.4	15.7	0.2_5	8.4	3.2	15.0	0.2	9.6	1.14	0.2_3
東京湾西部	A	EW	2.9	13.4	0.2_5	6.2	3.4	14.0	0.2	10.0	1.61	0.2_3
35°.5N, 139°.7E	M	NS	43.8	204.0	0.8	200.0	66.7	278.0	0.8	268.0	1.34	0.8
深さ　110 km	M	EW	32.8	153.0	0.5_5	121.0	68.3	319.0	0.5_5	287.0	2.37	0.5_5
東京　震度 II	D	NS	3.3	183.0	0.6_5	41.2	5.8	321.0	0.7	56.2	1.36	0.7
最遠有感 170 km	D	EW	2.2	153.0	0.5	26.8	4.3	235.0	0.6	50.5	1.88	0.6

第 V-11 表　大島町と本郷との最大動振巾の比較

地　震	地震計 (EW) 自己周期	本郷最大動				大島町最大動				振巾比	周期平均
		記録全振巾 A_m	重心変位 $\frac{A_m}{V_G}$	周期 T	速度振巾補正値	記録全振巾 A_m	重心変位 $\frac{A_m}{V_G}$	周期 T	速度振巾補正値		
1) 1953	sec	*mm*	μ	sec	μ/sec	*mm*	μ	sec	μ/sec		sec
2.3　10^h19^m	0.1	12.6	60.0	0.27	22.2	22.8	108.5	0.27	40.1	1.81	0.27
千葉県中部	0.2	32.6	194.0	0.32	139.5	75.5	449.0	0.22	433.0	3.10	0.27
35°.5N, 140°.3E	0.5	58.3	347.0	0.32	227.0	72.6	432.0	0.54	423.0	1.86	0.43
深さ　50 km	1.0	>	—	—	—	65.3	389.0	0.16	—	—	—
東京　震度 III	4.0	—	—	—	—	—	—	—	—	—	—
2)											
2.11　21^h24^m	0.1	0.3	1.4	0.11	1.3^6	0.4	1.9	0.17	1.2^4	0.91	0.14
千島中部	0.2	0.6	3.6	0.16	3.2	0.5	3.0	0.17	2.7	0.83	0.17
	0.5	2.0	11.9	0.38	9.6	0.7	4.2	0.28	2.1	0.22	0.33
深さ　80 km	1.0	2.0	11.9	0.43	4.7	2.1	12.5	0.45	4.6	0.98	0.44
	4.0	0.2	23.2	0.27	1.1	0.3	35.0	0.14	0.9	0.85	0.21

第 V-11 表 （つづき）

	sec	mm	μ	sec	μ/sec	mm	μ	sec	μ/sec		sec
3) 2.13	0.1	0.5	2.4	0.11	2.3	0.6	2.9	0.11	2.8	1.22	0.11
	0.2	—		—	—	1.2	7.1	0.28	—	—	—
	0.5	2.4	14.3	0.32	9.4	1.6	9.5	0.33	6.2	0.66	0.33
	1.0	3.2	19.0	0.49	8.8	3.0	17.8	0.39	5.5	0.63	0.44
	4.0	0.3	35.0	0.16	0.9[5]	0.2	25.0	0.17	0.8	0.84	0.17
4) 2.18 03^{h}14^m	0.1	0.5	2.4	0.22	1.1	0.8	3.8	0.22	1.8	1.58	0.22
鹿島灘	0.2	1.2	7.1	0.22	6.9	2.8	16.7	0.27	12.5	1.81	0.25
36°.5N, 141°.0E	0.5	2.9	17.2	0.38	13.3	6.2	36.9	0.32	22.8	1.65	0.35
深さ 40 km	1.0	2.9	17.2	0.22		—	—	—	—	—	—
東京 震度 0	4.0	0.3	35.0	0.32	0.5[4]	0.3	35.0	0.32	0.6	1.17	0.32
5) 2.18 11^{h}01^m	0.1	0.4	1.9	0.17	1.2	0.7	3.3	0.22	1.5[5]	1.30	0.20
千葉県北部	0.2	1.3	7.7	0.22	7.5	2.8	16.7	0.28	12.0	1.60	0.25
35³/₄° N, 140°.5 E	0.5	2.7	16.1	0.39	—	—	—	—	—	—	—
深さ 約 60 km	1.0	14.1	84.0	0.77	—	—	—	—	—	—	—
東京震度 0	4.0	0.5	58.0	0.26	—	—	—	—	—	—	—
6) 2.22 17^{h}34^m	0.1	0.3	1.4	0.17	0.9	0.6	2.9	0.11	2.8	3.10	0.14
相模湾東部	0.2	0.8	4.8	0.17	4.5	1.6	9.5	0.16	8.0	1.78	0.17
	0.5	1.8	10.7	0.28	5.8	1.3	7.7	0.27	3.6	0.61	0.28
	1.0	2.2	13.1	0.33	3.8	2.6	15.5	0.43	5.4	1.43	0.38
	4.0	0.3	35.0	0.22	0.8	0.2	25.0	0.27	0.6	0.76	0.25
7) 3.1 08^{h}52^m	0.1	0.8	3.8	0.11	2.7	1.3	6.2	0.10	6.2	1.68	0.11
房総半島中部	0.2	1.4	8.3	0.21	8.2	3.0	17.8	0.20	17.8	2.16	0.21
35°.3N, 140°.2E	0.5	2.8	16.7	0.42	15.2	5.9	35.1	0.41	31.2	2.06	0.42
深さ 40～50 km	1.0	3.7	20.6	0.42	7.8	6.4	38.1	0.41	12.6	1.60	0.42
東京 震度 0	4.0	0.3	35.0	0.21	0.9	0.3	35.0	0.20	1.0	1.17	0.21
8) 3.4 01^{h}45^m	0.1	1.3	6.2	0.11	6.0	1.9	9.1	0.10	9.1	1.52	0.11
千葉県中部	0.2	2.1	12.5	0.27	10.6	2.9	17.3	0.20	17.3	1.63	0.24
35°.5N, 140°.1E	0.5	4.1	24.4	0.32	16.0	7.0	41.6	0.41	36.0	2.25	0.37
深さ 50 km	1.0	4.8	28.6	0.42	10.9	9.1	54.2	0.51	54.0	4.9[6]	0.47
	4.0	0.3	35.0	0.21	0.8[6]	0.5	58.0	0.31	1.1	1.3	0.26
9) 3.12 16^{h}45^m	0.1	0.3	1.4	0.10	1.4	0.6	2.9	0.10	2.9	2.1	0.10
茨城県北部	0.2	0.9	5.4	0.26	4.7[5]	1.5	8.9	0.26	7.1	1.5	0.26
36°.6N, 140°.6E	0.5	1.8	10.7	0.36	8.1	1.9	11.3	0.26	5.1	0.6	0.31
深さ 50 km	1.0	2.0	11.9	0.41	4.4	2.8	16.7	0.41	5.6	1.3	0.41
	4.0	trace	—	—	—	trace	—	—	—	—	

第 V-11 表 (つづき)

	sec	*mm*	μ	sec	μ/sec	*mm*	μ	sec	μ/sec		sec
10) 3.21 10^h24^m	0.1	0.3	1.4	0.31	0.4	0.3	1.4	0.40	0.3	0.73	0.36
房総半島東方沖	0.2	1.1	6.6	0.41	3.5	1.5	8.9	0.75	2.0	0.57	0.58
35°.1N, 141°.2E	0.5	—	—	—	—	8.9	53.0	0.60			—
深さ 20 km	1.0	11.2	66.7	1.02	66.0	32.1	191.0	1.00	191.0	2.90	1.01
東京　震度 0	4.0	4.2	488.0	3.32	310.0	5.3	663.0	0.50	76.0	0.25	1.91
11) 3.21 16^h58^m	0.1	0.5	2.4	0.20	1.2	0.4	1.9	0.20	0.9^7	0.81	0.20
関東南部？	0.2	1.9	11.3	1.04	2.2	2.0	11.9	1.40	1.2	0.54	1.22
	0.5	4.3	25.6	0.51	25.0	5.7	33.9	0.40	28.4	1.14	0.46
	1.0	4.8	28.6	0.61	17.6	5.9	25.1	0.45	9.3	0.53	0.53
	4.0	0.6	69.8	0.20	1.8	0.3	35.0	0.30	0.6^8	0.38	0.25
12) 2.25 22^h30^m	0.1	0.4	1.9	0.26	0.7^2	0.4	1.9	0.21	0.9	1.26	0.24
勝浦東方沖	0.2	1.0	5.9	0.21	5.8	1.5	8.9	0.26	7.1	1.22	0.24
35°.2N, 140°.7E	0.5	2.4	14.3	0.36	10.9	3.9	23.2	0.52	23.0	2.11	0.44
深さ　約 40 km	1.0	4.7	28.0	0.52	13.9	6.1	36.3	0.52	16.0	1.15	0.52
東京　震度 1	4.0	0.4	46.5	0.31	2.7	0.7	87.5	1.84	30.6	11.3	1.08
13) 3.30 13^h36^m	0.1	0.3	1.4	0.10	1.4	0.9	4.3	0.10	4.3	3.07	0.10
九十九里浜	0.2	0.4	2.4	0.10	1.3	2.6	15.5	0.25	13.0	10.0	0.18
	0.5	1.4	8.3	0.41	7.4	5.6	33.3	0.40	28.0	3.78	0.41
	1.0	1.7	10.1	0.36	3.2	4.2	25.0	0.40	8.0	2.48	0.38
	4.0	no trace	—	—	—	0.4	50.0	0.30			
14) 4.2 20^h56^m	0.1	0.5	2.4	0.16	1.7	0.6	2.9	0.10	2.9	1.70	0.13
福島県東方沖	0.2	1.7	10.1	0.21	10.0	1.3	7.7	0.26	6.2^5	0.63	0.24
37°.5N, 141°.5E	0.5	5.8	34.5	0.42	31.4	5.1	30.4	0.42	27.7	0.88	0.42
深さ　約 45 km	1.0	5.8	34.5	0.52	17.2	5.6	33.3	0.42	11.6	0.68	0.47
東京　震度 1	4.0	0.5	58.0	0.42	4.9	1.0	125.0	0.94	2.3	0.47	0.68
15) 4.4 02^h51^m?	0.1	0.5	2.4	0.29	0.84	0.4	1.9	0.29	0.67	0.79	0.29
銚子東北東沖	0.2	1.6	9.5	0.34	6.4	1.5	8.9	0.29	6.0^5	0.95	0.32
35°.9N, 141°.6E	0.5	7.0	41.6	0.49	41.0	8.4	50.0	0.39	40.5	0.99	0.44
深さ 20 km	1.0	6.3	37.5	0.49	17.2	21.8	129.0	0.64	78.7	4.57	0.57
東京　震度 0	4.0	3.7	43.0	3.62	30.8	3.7	46.2	1.32	11.5	0.38	2.47
16) 4.4 14^h52^m	0.1	2.2	10.5	0.36	2.8	2.9	13.8	2.20			1.28
銚子東方沖	0.2	8.1	48.2	0.52	20.0	13.5	80.4	0.57	22.5	1.13	0.55
35°.8N, 141°.9E	0.5	23.6	140.4	0.42	128.0	61.9	368.0	0.42	335.0	2.62	0.42
深さ 40 km	1.0	52.4	312.0	0.94	307.0	66.8	398.0	0.73	293.0	0.95	0.84
東京　震度 1	4.0	33.4	3890	3.90	3004	42.3	5288	3.12	3330	1.10	3.51

第 V-11 表 (つづき)

17) 4.6 14^h50^m	0.1	6.1	29.0	0.26	11.0	11.5	54.8	0.31	16.9	1.54	0.29
江戸川河口	0.2	15.7	93.4	0.31	69.0	49.1	292.0	0.26	231.0	3.34	0.29
35°.7N, 139°.8E	0.5	24.3	144.5	0.42	130.0	61.5	366.0	0.42	329.0	2.53	0.42
深さ 約 60 km	1.0	33.2	197.5	0.42	39.5	56.6	337.0	0.36	72.0	1.84	0.39
東京 震度 2	4.0	3.0	349.0	0.36	24.4	5.4	675.0	0.42	58.4	2.39	0.39
18) 4.10 11^h28^m	0.1	0.5	2.4	0.15	1.8	0.4	1.9	0.15	1.4	0.78	0.15
栃木県東部	0.2	1.9	11.3	0.25	10.3	1.3	7.7	0.20	7.7	0.75	0.23
36°.5N, 140°.1E	0.5	2.7	16.1	0.40	14.0	2.8	16.7	0.40	14.5	1.03	0.40
深さ 105 km	1.0	2.7	16.1	0.35	5.0	4.5	26.8	0.35	7.2	1.45	0.35
東京 震度 0	4.0	0.3	35.0	0.25	1.6	0.3	35.0	0.25	1.6	1.00	0.25
19) 4.13	0.1	0.2	0.9^{5}	0.20	—	no trace	—	—	—	—	—
	0.2	0.4	2.4	0.25	2.2	0.4	2.4	0.20	2.4	1.09	0.23
	0.5	1.6	9.5	0.40	8.3	0.7	4.2	0.30	2.3	0.28	0.35
	1.0	1.5	8.9	0.30	2.3	2.3	13.7	0.40	4.4	1.91	0.35
	4.0	0.2	23.2	0.30	1.3	0.4	50.0	0.60	5.5	4.23	0.45
20) 4.14 17^h23^m	0.1	0.4	1.9	0.16	1.3	0.4	1.9	0.21	0.9	0.67	0.38
銚子東南東沖	0.2	1.4	8.3	0.31	6.1	1.5	8.9	0.26	7.1	1.16	0.29
35°.6N, 141°.2E	0.5	4.4	26.2	0.42	23.8	4.2	25.0	0.36	18.0	0.76	0.39
深さ 約 60 km	1.0	5.7	33.9	0.52	16.7	6.6	39.3	0.52	17.2	1.03	0.52
東京 震度 0	4.0	0.5	58.1	0.36	4.1	1.0	125.0	0.94	2.3	0.56	0.65
21) 4.15	0.1	no trace	—	—	—	no trace	—	—	—	—	—
	0.2	0.4	2.4	0.20	2.4	0.5	3.0	0.30	1.9	0.80	0.25
	0.5	1.3	7.7	0.40	6.7	1.3	7.7	0.45	7.0	1.04	0.43
	1.0	2.4	14.3	0.50	6.7	3.2	19.0	0.45	7.0	1.05	0.48
	4.0	0.3	35.0	0.35	2.4	0.8	100.0	0.25	4.9	2.04	0.30
22) 4.21	0.1	0.3	1.4	0.11	1.4	0.6	2.9	0.11	2.9	2.06	0.11
	0.2	1.4	8.3	0.27	7.1	1.5	8.9	0.27	6.7	0.94	0.27
	0.5	2.8	16.7	0.27	8.7	4.0	23.8	0.32	14.5	1.67	0.30
	1.0	2.3	13.7	0.43	5.4	4.5	268.0	0.43	9.4	1.74	0.43
	4.0	0.2	23.3	0.22	0.9	0.3	37.5	0.27	1.9_{5}	2.16	0.25

第 V-12 表　ミヨシ化学と本郷との最大動振巾の比較

地　震	地震計型式	本郷記録最大動				ミヨシ化学最大動				ミヨシ化学/本郷	
		記録振巾 A_m	振子重心振巾 $\frac{A_m}{V_G}$	周期 T	土地速度振巾補正値	記録振巾 A_m	振子重心振巾 $\frac{A_m}{V_G}$	周期 T	土地速度振巾補正値	振巾比 $\frac{A'_m M}{A'_m H}$	周期平均 T
1)		mm	μ	s	μ/s	mm	μ	s	μ/s		s
1.28　12^h41^m	10 c/s	—		—		—		—	—	—	—
茨城県北部	5	1.00	5.9	0.25	5.0	2.25	13.4	0.15	10.1	2.02	0.2
36°.7N, 140°.5E	2	2.30	13.7	0.4	11.9	3.60	21.4	0.5	21.4	1.8	0.45
深さ　約 100 km	1	—		—		5.2	31.0	0.4^5	16.7	—	—
2)											
1.31　20^h47^m	10 c/s	—	—	—	—	—	—	—	—	—	—
千葉県北部	5	1.00	5.9	0.3	4.1	2.2	13.1	0.4	6.6	1.61	0.35
35°.9N, 140°.1E	2	2.00	11.9	0.4	10.1	7.2	42.8	0.4	36.4	3.60	0.4
深さ　約 120 km	1	2.5	14.9	0.45	6.6	10.9	64.9	0.5	36.6	5.54	0.48
3)											
2.1　10^h09^m	10 c/s	—	—	—	—	—	—	—	—	—	—
父島東方沖	5	0.7	4.2	0.3^5	2.3	1.5	8.9	0.4^5	4.0	1.72	0.4
25° N, 244° E	2	2.8	16.7	0.5	16.7	4.6	27.4	0.5	27.4	1.64	0.5
	1	4.9	29.2	0.6	17.2	8.4	50.0	0.5	30.7	1.78	0.5^5
4)											
2.1　10^h22^m	10 c/s	—	—	—	—	—	—	—	—	—	—
同　上	5	1.4	8.3	0.3^5	4.2	4.1	24.4	0.35	14.9	3.55	0.35
(余　震)	2	3.3	19.6	0.4	17.0	11.7	69.7	0.40	60.7	3.56	0.40
	1	4.5	26.8	0.5	12.0	13.8	82.2	0.5	50.5	4.20	0.50
5)											
2.2　17^h53^m	10 c/s	—	—	—	—	2.7	1.3	0.1	1.3	—	—
千葉県中部	5	1.5	8.9	0.25	7.5	4.2	25.0	0.3	18.8	2.5	0.28
35°.5N, 140°.4E	2	3.5	20.8	0.38	16.8	11.3	67.2	0.4	58.5	3.48	0.39
深さ　50～60 km 有感最遠 120 km	1	4.4	26.2	0.5	11.8	13.7	81.5	0.4^5	43.6	3.7	0.48
6)											
2.4　22^h28^m	10 c/s	—	—	—	—	—	—	—	—	—	—
同　上	5	1.8	10.7	0.25	9.0	7.1	42.2	0.2^5	38.2	4.25	0.25
35°.5N, 140°.5E	2	2.6	15.5	0.33	10.6	7.3	43.4	0.3^5	32.1	3.03	0.34
深さ　約 60 km	1	2.4	14.3	0.40	4.4	13.7	81.5	0.4^5	43.6	9.9	0.43
7)											
2.5　03^h34^m	10 c/s	—	—	—	—	6.6	3.1	0.1^5	2.2	—	—
千葉県北部	5	6.8	40.4	0.35	20.4	15.0	89.3	0.2^5	80.8	3.96	0.3
35°.5N, 140°.5E	2	19.6	116.6	0.5	116.5	25.6	152.3	0.4^5	148.0	1.27	0.48
深さ　約 60 km	1	35.3	210.0	0.8^5	199.5	40.1	238.7	0.6^5	200.6	1.01	0.75

第 V-13 表 (つづき)

8)		*mm*	μ	*s*	μ/*s*	*mm*	μ	*s*	μ/*s*	—	*s*
2.9 03^h38^m	10 c/s	—	—	—	—	—	—	—	—	—	—
宇都宮附近	5	1.4	8.3	0.2	8.3	2.6	15.5	0.2	15.3	1.84	0.2
	2	4.2	25.0	0.4	21.8	4.9	29.2	0.4	25.4	1.16	0.4
	1	4.9	28.2	0.5	12.7	7.0	41.6	0.5	25.6	2.01	0.5
9) 2.9 19^h41^m	10 c/s	—	—	—	—	—	—	—	—	—	—
千葉県西部	5	1.4	8.3	0.2	8.3	5.1	30.4	0.2	30.1	3.63	0.2
	2	2.3	13.7	0.3	8.2	5.1	30.4	0.25	14.3	1.75	0.28
	1	2.2	13.1	0.3	3.1	5.4	32.1	0.25	8.5	2.74	0.28
10) 2.12 07^h22^m	10 c/s	—	—	—	—	—		—	—	—	—
茨城県南西部	5	1.7	10.1	0.25	8.5	1.9	11.3	0.25	10.2	1.20	0.76
36°.1N, 140°.0E	2	2.9	17.3	0.40	15.1	2.8	16.7	0.4^5	16.2	1.04	0.43
深さ 約 50 km	1	3.0	17.7	0.45	7.0	3.3	19.6	0.5	12.1	1.73	0.48
11) 2.12 19^h03^m	10 c/s	—	—	—	—	—	—	—	—	—	—
東京湾北部	5	1.8	10.7	0.25	9.0	9.1	54.1	0.25	49.0	5.44	0.25
35°.7N, 140°.0E	2	2.8	16.7	0.4	14.5	14.6	87.0	0.45	84.4	5.81	0.43
深さ 約 80 km 有感最遠 110 km	1	2.6	15.5	0.4	5.3	17.0	101.1	0.5	62.2	11.7	0.45
12) 2.4 12^h14^m	10 c/s	4.5	2.1	0.10	2.1	11.4	5.4	0.1	5.4	2.57	0.1
同 上	5	8.7	52.0	0.17^5	48.3	7.7	45.8	0.15	34.6	0.72	0.16
35°.6N, 139°.9E	2	23.6	140.3	0.3	84.3	17.5	104.0	0.3	62.4	0.74	0.3
深さ 約 40 km 有感最遠 140 km	1	27.0	160.5	0.4	54.7	26.3	156.5	0.4	72.8	1.33	0.4
13) 2.17 05^h15^m	10 c/s	—	—	—	—	—		—	—	—	—
房総半島東海岸	5	—	—	—	—	1.0	5.9	0.25	5.3	—	0.25
	2	0.8	4.8	0.4^5	4.7	2.7	16.0	0.45	15.5	3.3	0.45
	1	1.2	7.1	0.5	3.2	3.1	18.4	0.50	11.3	3.5^3	0.5

第 V-13 表 小松川高校と本郷との最大動振巾の比較

地震	地震計型式	本郷最大動				小松川最大動				小松川/本郷	
		記録振巾 A_m	振子重心振巾 $\frac{A_m}{V_G}$	周期 T	土地速度振巾補正値	記録振巾 A_m	振子重心振巾 $\frac{A_m}{V_G}$	周期 T	土地速度振巾補正値	振巾比 $\frac{A'_mK}{A'_mH}$	周期平均 T
1) 1954		*mm*	*u*	*s*	μ/*s*	*mm*	μ	*s*	μ/*s*		*s*
5.15 07^h39^m	10 c/s	24.3	116.0	0.40	23.2	22.6	108.0	0.5	17.3	0.75	0.45
飛驒山脈	5	78.5	467.0	0.35	284.0	67.0	399.0	0.3	317.0	1.12	0.33
36°.0N, 139°.8E	2	91.0	542.0	0.30	325.0	65.8	399.0	0.3	249.0	0.77	0.30
深さ 約 75 km 有感最遠 110 km	1	95.6	569.0	0.30	156.0	106.0	632.0	—			

第 V-13 表 (つづき)

		mm	μ	s	μ/s	mm	μ	s	μ/s		s
2) 5.16 03^h39^m	10 c/s	0.6	2.9	0.15	2.0	1.4	6.7	0.15	4.7	2.32	0.15
埼玉県東部	5	2.3	14.0	0.25	12.5	2.5	15.0	0.25	14.0	1.12	0.25
35°.9N, 139°.8E	2	3.5	21.0	0.30	12.6	5.2	31.0	0.30	18.6	1.48	0.30
深さ 75 km 有感最遠 110 km	1	3.8	23.0	0.50	11.6	11.0	66.0	0.60	40.7	3.50	0.55
3) 6.5 22^h14^m	10 c/s	11.7	56.0	0.30	16.5	15.0	72.0	0.2	34.0	2.06	0.25
筑波山附近	5	49.0	292.0	0.35	178.0	29.6	176.0	0.3	140.0	0.79	0.33
36°.0N, 139°.9E	2	87.5	521.0	0.45	505.0	74.0	430.0	0.42	391.0	0.78	0.44
深さ 50〜60 km 有感最遠 340 km	1	73.5	438.0	—	—	—	—	—	—	—	—
4) 6.12 12^h26^m	10 c/s	0.3	1.4	0.12^5	1.2	1.2	5.7	0.15	4.0	3.33	0.14
霞ヶ浦附近	5	0.25	1.5	0.2	1.5	0.9	5.4	0.15	4.8	3.20	0.18
	2	2.0	12.0	0.4	10.4	2.7	16.0	0.30	9.6	0.93	0.35
	1	2.2	13.0	0.75	11.0	5.6	33.0	0.75	27.0	2.46	0.75
5) 6.13 03^h11^m	10 c/s	0.3	1.4	0.2	0.7	1.2	5.7	0.15	4.0	5.71	0.18
霞ヶ浦附近	5	0.7	4.0	0.2^5	3.6	1.8	11.0	0.4	6.5	1.8	0.33
	2	2.8	17.0	0.4	14.8	10.3	61.0	0.3	36.6	2.46	0.35
	1	3.3	20.0	0.7^5	17.0	—	—	—			
6) 6.16 00^h04^m	10 c/s	0.2	0.9^5	0.07^5	0.7^6	0.4	1.9	0.07^5	1.5	1.97	0.07^5
鹿島灘	5	0.6	4.0	0.1	2.1	2.0	12.0	0.15	9.6	4.57	0.13
36°.4N, 141°.1E	2	2.3	14.0	0.4	12.2	2.6	15.5	0.3	9.3	0.76	0.35
深さ 約 30 km 有感最遠 185 km	1	2.1	13.0	0.25	2.9	—		—			

第 V-14 表 隅田，大島町，ミヨシ化学，小松川各点の本郷に対する最大動振巾比較の要点

振巾比 / 場所	各地震計によるすべての記録された地震についての最大動振巾比の			平均振巾比の周期特性曲線における	
	最大値	最小値	平均値	最大値	最小値
隅田/本郷	2.8	0.3	1.5	1.7	0.9
大島町/本郷	4.5	0.2	1.5	1.9	0.7
ミヨシ化学/本郷	10.0	0.7	3.1	4.1	1.4
小松川/本郷	5.7	0.8	2.2	3.5	1.3

最大動との振巾比をもとめる．第 5–10～5–13 表にはこの振巾比と最大動の週期とをしめす．それぞれの最大動の週期は同一地震については大体同一であるが，ちがう場合も

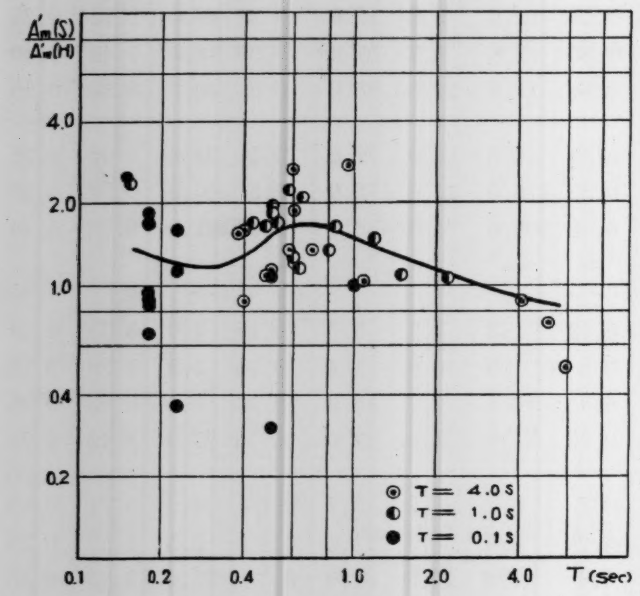

Fig. 5–12. Period characteristics of maximum amplitude ratio. A'_m(SUMIDA)/A'_m(HONGO).

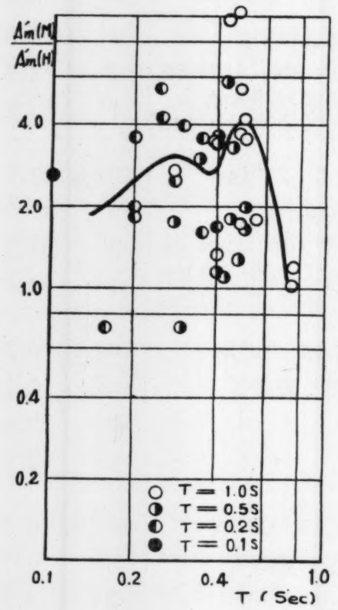

Fig. 5–14. Period characteristics of maximum amplitude ratio. A'_m(MIYOSI)/A'_m(HONGO).

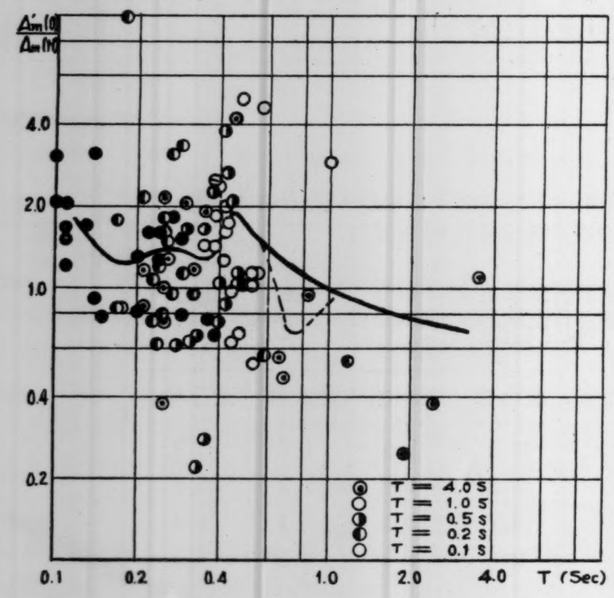

Fig. 5–13. Period characteristics of maximum amplitude ratio. A'_m(OSIMA)/A'_m(HONGO).

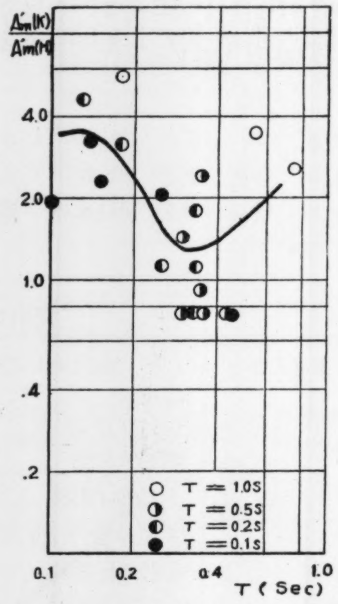

Fig. 5–15. Period characteristics of maximum amplitude ratio. A'_m(KOMATUGAWA)/A'_m(HONGO).

あるので，振巾比については速度として振動倍率の補正をおこなつてから比をとり，週期としては両方の平均を対応させた．この結果を図示したものが第 5–12～5–15 図であり，最大動に関するかぎり，これが本郷に対する各点の震動性能の週期特性をしめすものといえる．地震によつてかなりばらつきがあるが，これを適当な週期別に区分して振巾比と週期とを夫々平均すると大体点線で示すような平均的特性曲線をひくことができる．(第 5–16 図) この曲線はどの点も本郷の卓越週期と考えられる 0.3～0.4 秒附近は本郷の振巾が大きくなるため 1 に近い値の谷となつているが，それよりはやい振動もおそい振動も 1 より大きく，本郷より大きくゆれていることを示す．隅田では 0.5～0.7 秒附近に山があり本郷の 約 1.7 倍，大島町では 0.4～0.5 秒に山があり約 1.9 倍になる．隅田，大島町とも 2 秒以上で 1 以下に小さくなることは，地震例がすくないので多少問題もあるが，注目をひく．ミヨシ化学（東篠崎町）では 0.38 秒の谷の値も 2.5 もあり，これにややちかく 0.28 秒に約 3.0 の山があるし，0.48 秒の山は 4.1 に達し 4 点中でもつとも振巾比が大きい．小松川では谷は 0.31 秒で 1.3，その両方で振巾比はますが 1 秒以上の最大動をしめす地震が記録されてないので，はつきり山の位置がまだでていない．要するに第 5 図の要点をまとめると，第 5–14 表にしめすようになり，しらべられた週期の範囲において，大体すべて本郷より大きい振巾をしめし，隅田では最大 2.8，大島町で 4.5，ミヨシ化学で 10.1，小松川は 5.7 に達する．地盤の特性による最大動の増巾率は本

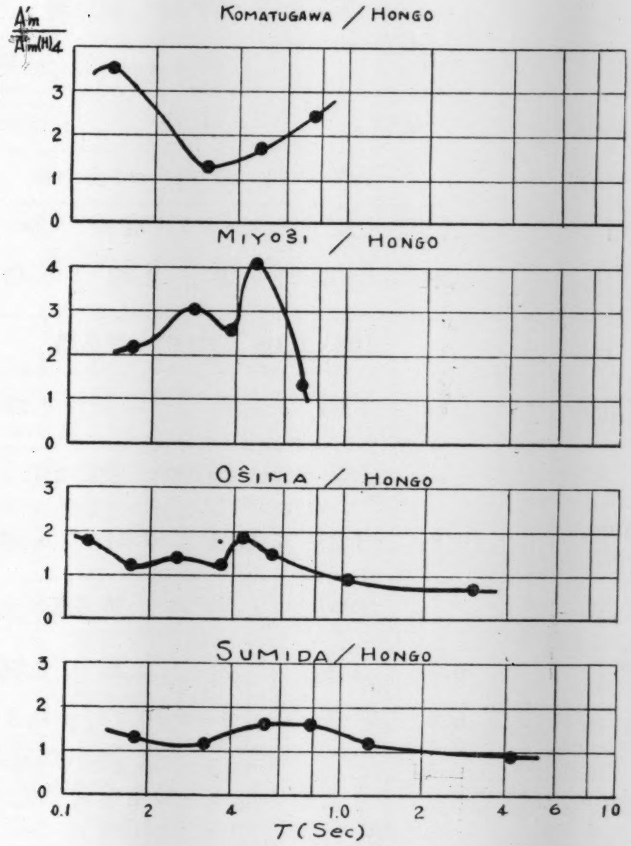

Fig. 5–16. Mean period characteristics of maximum amplitude ratios.

郷に対し，ミヨシ化学，小松川，大島町，隅田の順になつており，これは他の項の調査事項とくらべて，地盤の性質をしる重要な結果といえよう．

(b) **速度振巾の自乗和の比較** 若干の地震の S 以後について最大動の 1/5 以上の振巾の波の振巾の自乗の和をもとめ，本郷の同じ地震の同じ量との比をとつたものが，第 5-15 表第 5-17 図にしめしてある．記象は各々の振子の自己週期に近い振動をしている

第 V-15 表 振巾自乗和の比較と卓越周期

地震	1952.2.20 16^h04^m 茨城県南西部				
地震計型式	A			M	D
地震計成分	NS, EW }平均			NS, EW }平均	NS, EW }平均
振巾自乗和比 (隅田/本郷)	0.53, 0.96 }0.75			1.76, 0.93 }1.35	1.53, 1.48 }1.50
卓越週期 {本郷, 隅田	0.35, 0.2 }0.2			0.4, 0.6 }0.5	0.4, 0.6 }0.5
自己相関係数にあらわれる周期 {本郷, 隅田	0.2, 0.2 }0.2			0.5, 0.5 }0.5	0.5, 0.6 }0.5_5
地震	1953.2.26 03^h41^m 鹿島灘				
振巾自乗和比 (隅田/本郷)	0.35, —			2.39, 2.04 }2.22	3.09, —
振巾自乗和比平均	0.61			1.78	2.03
地震	1953.2.11 21^h24^m 千島中部				
地震計型式	A	B	C	M	D
振巾自乗和比 (大島町/本郷)	1.24	1.01	0.12	2.89	0.43
地震	1953.2.18 03^h14^m 鹿島灘				
振巾自乗和比 (大島町/本郷)	1.84	1.44	0.67	—	2.20
地震	1953.3.21 16^h58^m 関東南部				
振巾自乗和比 (大島町/本郷)	0.81	1.11	1.04	2.34	0.39
地震	1953.3.25 22^h30^m 勝浦南東沖				
振巾自乗和比 (大島町/本郷)	0.74	1.84	1.27	2.25	2.66
卓越周期 本郷	0.5		0.4	0.4	0.8
卓越周期 大島	0.4		0.3	0.4	1.0
卓越周期 平均	0.4_5		0.35	0.4	0.9
自己相関係数にあらわれた周期 本郷	—	—	0.5	0.7	—
自己相関係数にあらわれた周期 大島	—	—	0.5	0.5	—
自己相関係数にあらわれた周期 平均	—	—	0.5	0.6	—
振巾自乗和比平均	1.16	1.35	0.78	2.49	1.42

地震		1954.2.12 07^h22^m 茨城県南西部		
地震型式		B	C	M
振巾自乗和比 (ミヨシ/本郷)		2.77	1.73	1.84
卓越周期	本郷	0.2	0.3	0.3
	ミヨシ	0.2	0.4	0.5
	平均	0.2	0.3_5	0.4
自己相関係数にあらわれた周期	本郷	0.3	0.4	0.4_5
	ミヨシ	0.3_5	0.4_5	0.4
	平均	0.3_3	0.4_3	0.4_3

地震		1954.4.12 12^h20^m 霞ヶ浦附近			
地震計型式		A	B	C	M
振巾自乗和比 (小松川/本郷)		8.73	4.01	2.14	0.20
卓越周期	本郷	0.4	0.4	0.4	0.5
	小松川	0.2	0.2	0.4	0.5
	平均	0.3	0.3	0.4	0.5
自己相関係数にあらわれた周期	本郷	—	0.2_5	0.4_5	0.7
	小松川	—	0.3	0.3	0.7
	平均	—	0.2_8	0.3_8	0.7

地震	1954.6.16 00^h04^m 鹿島灘			
振巾自乗和比 (小松川/本郷)	1.43	2.54	1.77	—

ので，速度記象とみなせるので，これはそれぞれの振子にあたえられた運動エネルギーの合計の比とかんがえられる．

しかし，この量も地震によるばらつきがおおいが，大体平均として卓越週期をとり，週期特性をみると，最大振巾比でえられた本郷の 0.3〜0.4 秒の山の影響がないことが注目される．すなわち 0.3 秒附近の週期の震動について，最大動では本郷が他の点より大きくはないがややそれに近い振巾でゆれても，地震動全体としての運動エネルギーの総和は，問題なく下町の各点の方が大きいといえるようである．つまり 0.1 秒において隅田が本郷より小さいのをのぞき，大体どこも本郷にくらべ大きい全運動エネルギーをうけている．週期特性はむしろ比較的単調である．ただ小名木川の 0.5 秒附近もやや小さく本郷に近い．

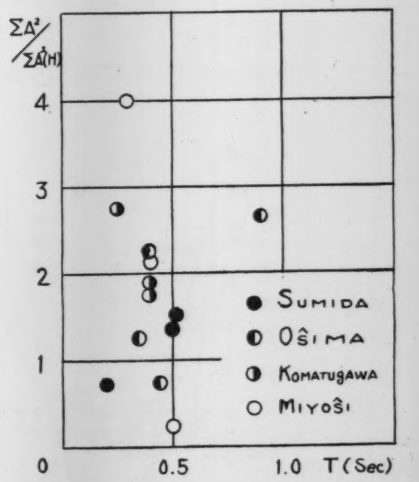

Fig. 5–17. Relation between the period and the sums of squared amplitudes at various points devided by that of Hongo.

(c) **自已相関係数の比較** 若干の地震について，記象の S 以後の主要動部分の自己相関係数をもとめてみると第 5–18 図のようになる．地震計の振動特性によつて，短週期の振子では長週期の振子でひろつていない短週期振動をふくむようになつている点をのぞけば，大体地震計による差はあまりでていない．地震による差は

本郷のものすべてをみてわかるように (Fig. 5–18c)，かなりいちぢるしく．そこにも興味ある問題点が存することはいうまでもない．しかし一方，同一地震についての観測点の差によるものもあきらかに存在しているが地震による差よりちいさいようである (Fig. 5–18a, b)．本郷においては 0.3～0.4秒および 0.6 秒週期の振動，ミヨシ化学の 0.4 秒，大島町の 0.4～0.5 秒，隅田 0.5～0.6 秒が一応注目されるがくわしい考察は後の機会にゆずりたい．なおこの計算は東大地物教室坪井研究室安芸敬一氏のつくられた計算機を利用させていただいた．氏には同時に種々の御教示をえたので，ここに感謝の意を表しておく．

(d) **週期の頻度分布** 若干の地震について，記象の S 以後の主要部分について，ゼロ線をきる点をはかつて週期の頻度分布をつくつた．これは地震計の減衰比が小さく，速度についてはせまい帯域フィルターとなつているので，減衰の大きい，ひろい週波数帯域をもつ地震計による従来の結果とかならずしも同一にはみなせない．自己相関係数からえられた卓越週期との差はあまりない．(Fig. 5–19)

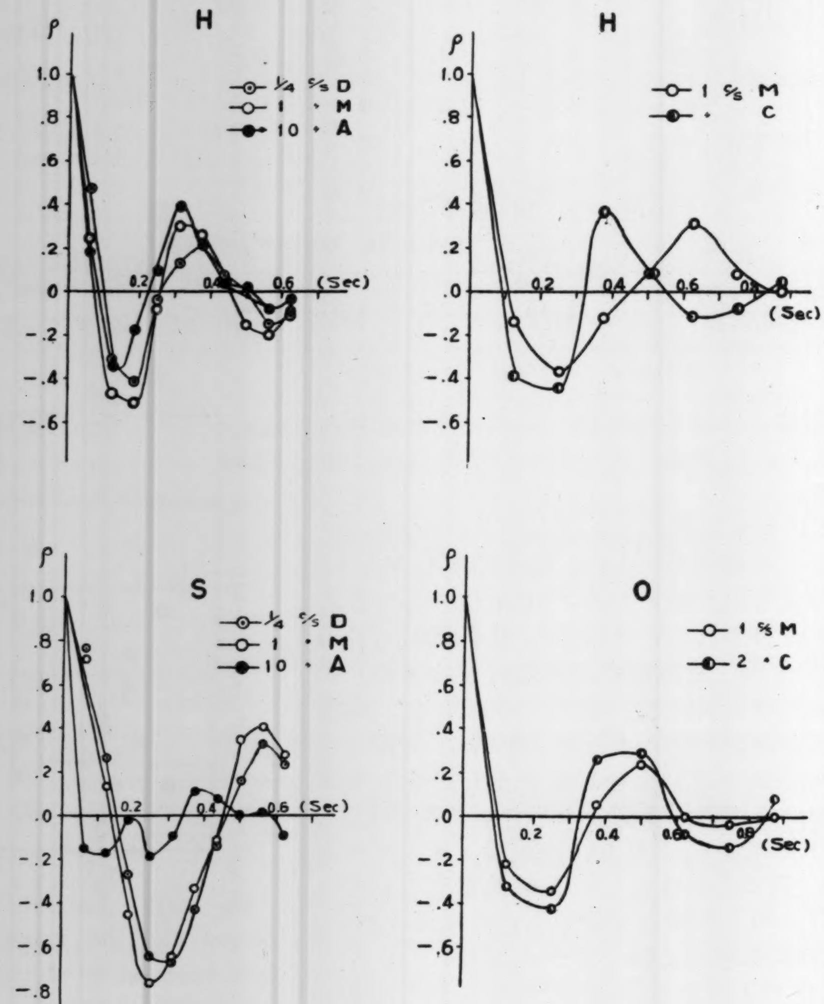

[I] 1952.2.20 16^h04^m Earthquake [II] 1953.3.25 22^h30^m Earthquake

Fig. 5–18a. Autocorrelation functions. H: Hongo, S: Sumida, O: Osima.

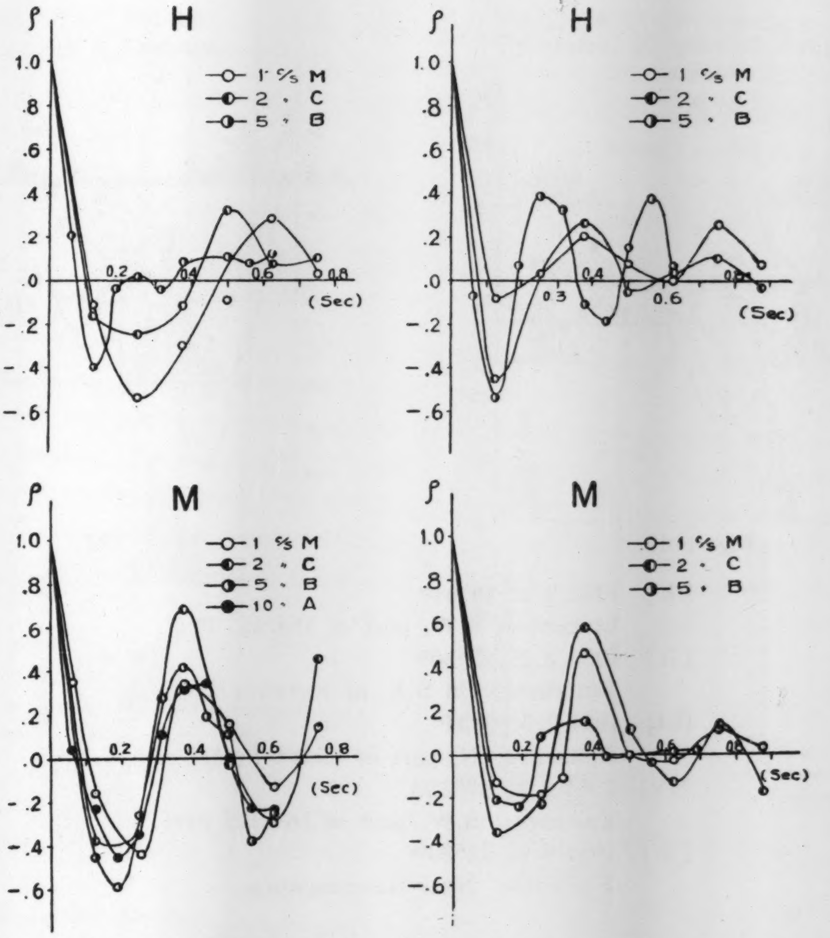

[III] 1954.2.5 03^h34^m Earthquake [IV] 1954.2.12 07^h22^m Earthquake

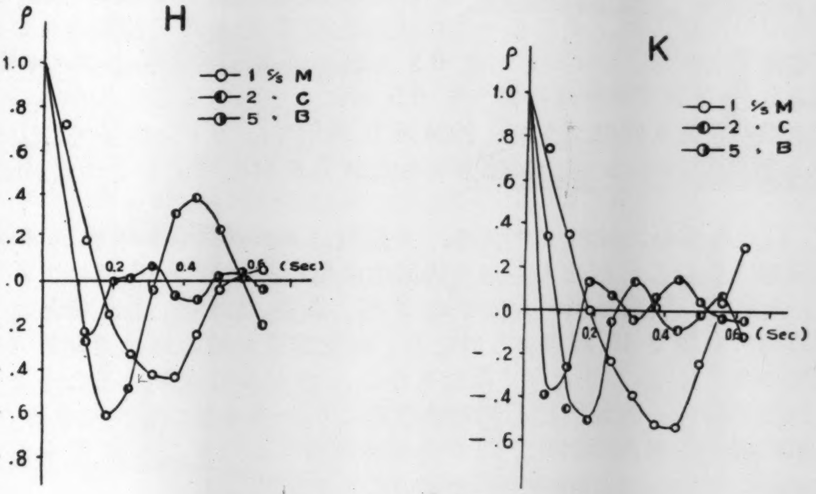

[V] 1954.6.12 12^h20^m Earthquake

Fig. 5–18b.

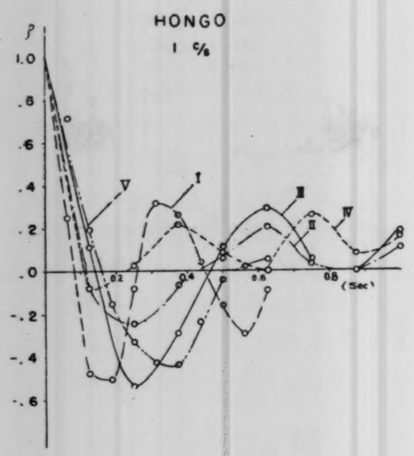

Fig. 5–18c.

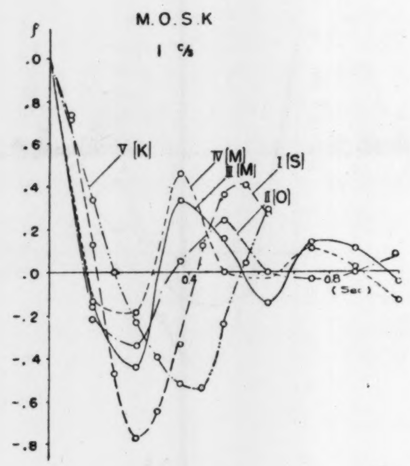

Fig. 18d.

[I] 1952.2.20 16^h04^m
Epicentre: S.W. part of Ibaraki Pref.
[II] 1953.3.25 22^h30^m
Epicentre: Off S.E. of Katuura
[III] 1954.2.5 03^h34^m
Epicentre: N. part of Chiba Pref.
[IV] 1954.2.12 07^h22^m
Epicentre: S.W. part of Ibaraki Pref.
[V] 1954.6.12 12^h20^m
Epicentre: Near Kasumigaura

しかし，とにかく地震計の自己週期よりずれて頻度の山のあることはその山を示す週期の振動のいちぢるしく強いことを示す．1953.3.25 の地震では本郷，大島ともに 0.4 秒中心の頻度の山が注意され，4 秒振子では大島町に 1 秒の山が注意される．1954 年 2 月 14 日の地震では本郷，ミヨシともに 0.5 秒振子で 0.3 秒に山があり，1 秒振子でもその山がみられ，なおミヨシはそのうえ 0.5 秒にもいちぢるしい山がある．1954.5.16 の小松川，本郷の比較も同様である．1954.6.5 地震では 0.1 秒振子での山が本郷，小松川ともに 0.2 秒にずれて 3 点，1 秒振子の山が 0.8 秒にも山をもつ点が注意される．

3. 結論 自然地震の比較により隅田，大島町，ミヨシ化学，小松川 4 点の本郷に対する地盤の振動性能をしらべると，最大動振巾の増巾比は第 5–16 表のごとく，ミヨシ化学，小松川，大島町，隅田の順で大体平均 3 倍，2 倍，1.5 倍，1.5 倍となり，それぞれの増巾比週期特性は第 5–15 図のようになり，従来本郷台地の卓越週期といわれた 0.3 秒附近でも本郷の振巾が他より大きくはならない．ただ他の週期のところよりは本郷の振巾も大きくはなるので一応増巾比週期特性曲線に 0.3〜0.4 秒に谷ができる．なお第 5–20 に各点の本郷に対する平均増巾比とその点の冲積層のあつさとの関係をあらわしてみると，大体冲積層のあついほど増巾比が大きいことが明瞭である．

地震動主要部全体の振巾自乗和についてはこのような週期特性もなく，すべて 4 点とも本郷より大きい．

1953.3.25 22^h30^m Earthq.
Epicentre: Off S.E. of Katuura.

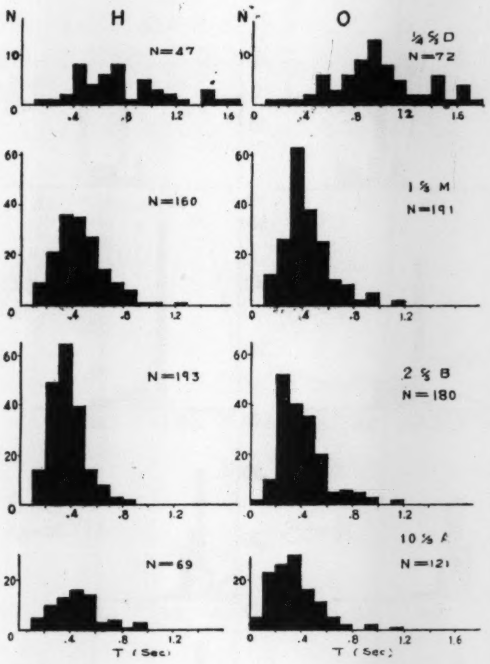

1954.2.14 12^h14^m Earthq.
Epicentre: N. part of Tokyo.

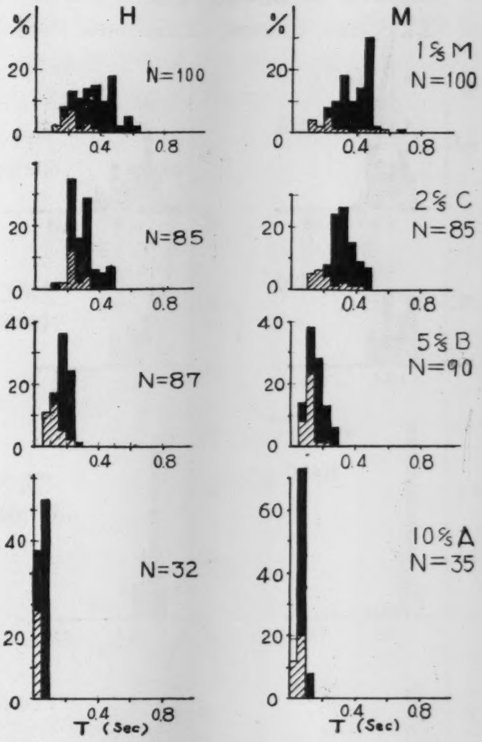

1954.2.20 16^h04^m Earthq.
Epicentre: S.W. part of Ibaraki Pref.

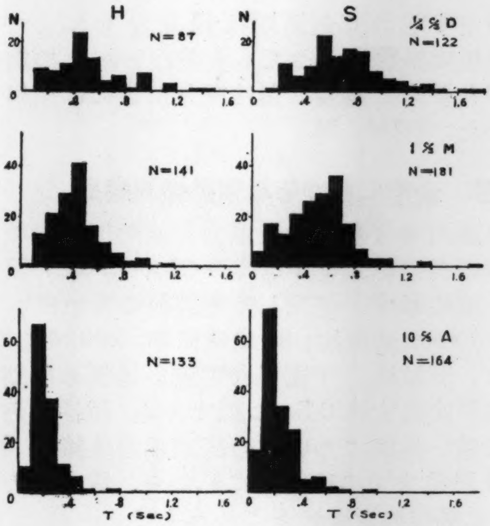

1953.3.00 00^h00^m Earthq.
Epicentre:

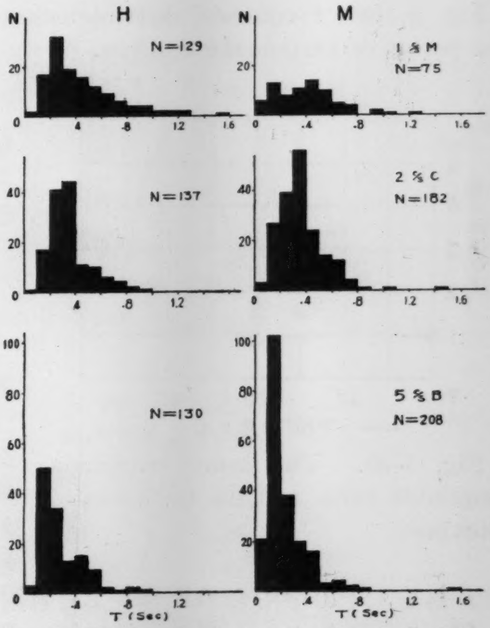

Fig. 5–19a. Frequency distribution of the periods of earthquake motions.

Fig. 5–19b. Frequency distributions of the period of the earthquake motions.

1954.5.16 03^{h}39^m Earthq.
Epicentre: E. part of Saitama Pref.

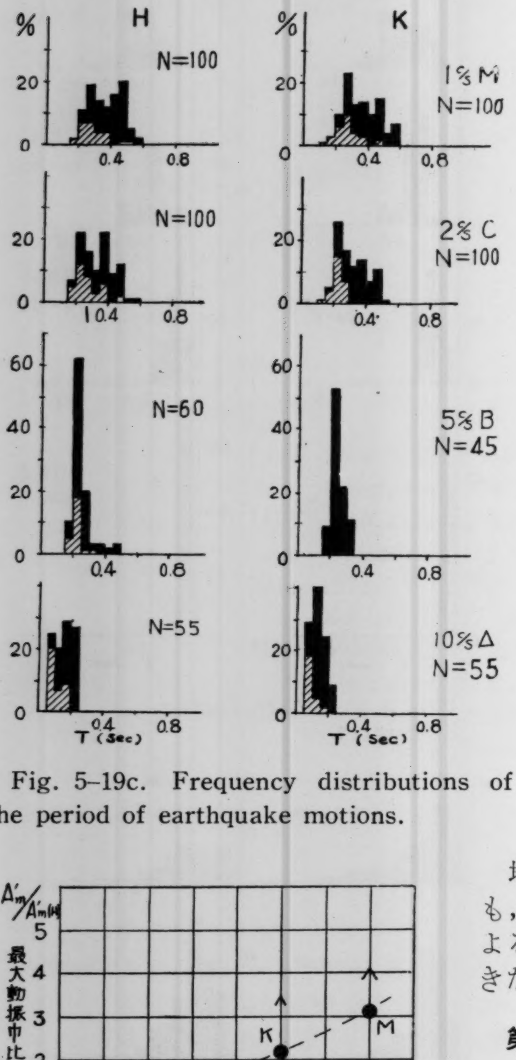

Fig. 5–19c. Frequency distributions of the period of earthquake motions.

1954.6.5 22^{h}14^m Earthquake.
Epicentre: TUKUBA.

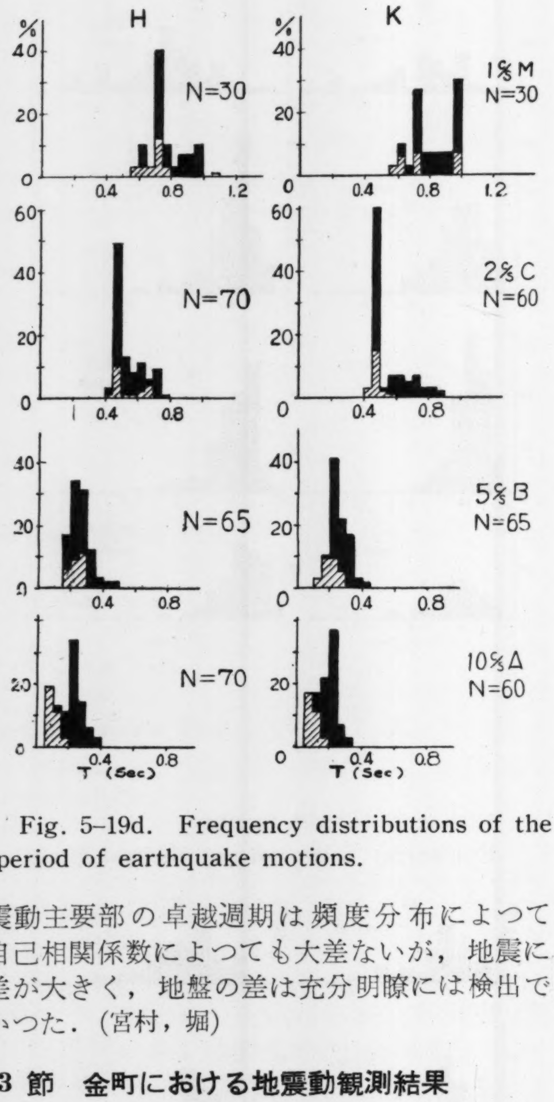

Fig. 5–19d. Frequency distributions of the period of earthquake motions.

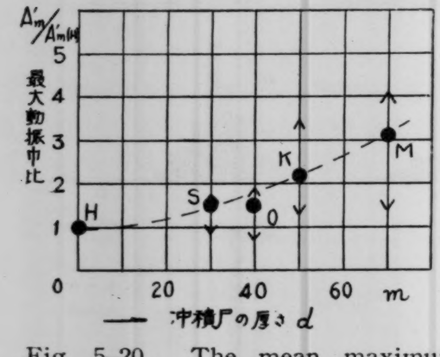

Fig. 5–20. The mean maximum amplitude ratio and the thickness of alluvium.

地震動主要部の卓越週期は頻度分布によつても，自己相関係数によつても大差ないが，地震による差が大きく，地盤の差は充分明瞭には検出できなかつた．(宮村，堀)

第 3 節 金町における地震動観測結果

葛飾区金町4丁目東北毛織会社金町工場内で行つた地震観測の結果を Figs. 5–21 a～5–21 l 及び第 5–16 表に示す．使用した地震計の常数は，自己周期; 1 sec, 減衰比; 8, 幾何倍率; 200 である．金町では，茨城県，千葉県など近い地震の周期の頻度曲線の山は大体 0.5 sec にできる．房総半島沖などの稍遠い地震についての周期頻度曲線は 0.3 秒から 2 秒位までの広範囲にわたり．数多くの凹凸がある．その中でも 0.5 秒，1.1 秒附近に特に頻度の大きいところがある．

従つて，金町のいわゆる卓越周期は 0.5 秒位と考えてよかろう．

変位振巾の最大になる波をはさむ 5 波の平均周期は第 5–16 表の通りで，大体 0.5 秒

となる．即ち，変位振巾の最大になる周期と，卓越周期とは大体一致することになつた．

なお，詳細に見ると，周期頻度曲線の広範囲にわたる稍遠い地震では，最大振巾の周期と卓越周期との差違が多少大きい，周期頻度曲線に鋭い山のできる近い地震では，最大振巾の周期は卓越周期によく合う．このことは，半無限弾性体の上に 1 層がある場合の地震波の重複反射を考えれば，一応の説明がつく．(那須，森下，新井)

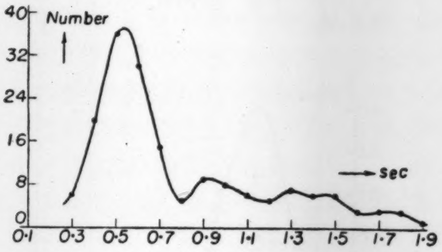

Fig. 5–21a.

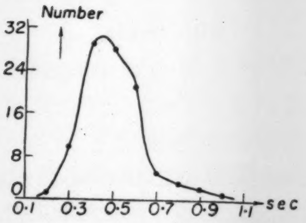

Fig. 5–21b.

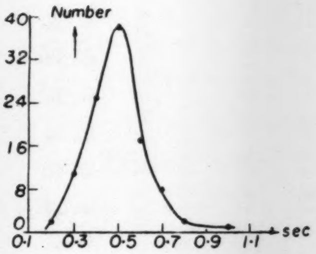

Fig. 5–21c.

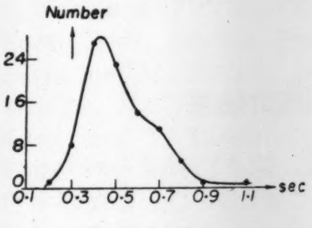

Fig. 5–21d.

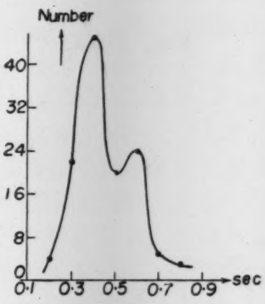

Fig. 5–21e.

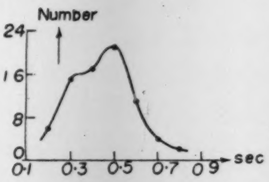

Fig. 5–21f.

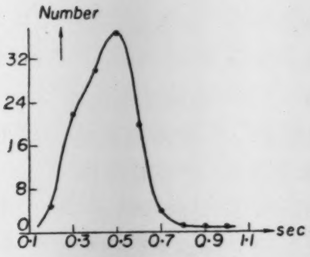

Fig. 5–21g.

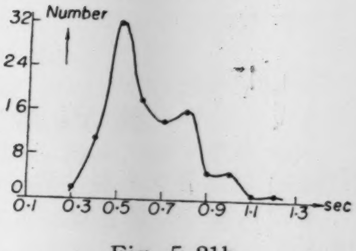

Fig. 5–21h.

Fig. 5–21i.

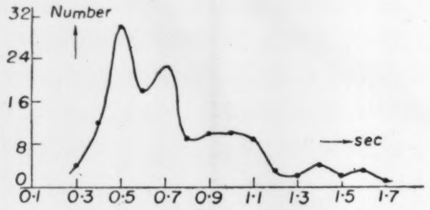

Fig. 5–21k.

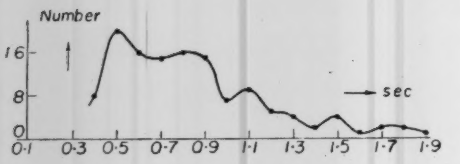

Fig. 5–21j.

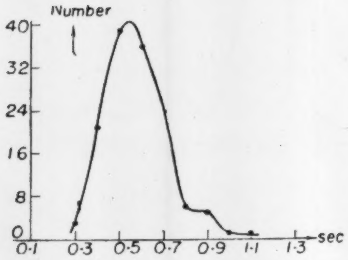

Fig. 5–21l.

第 V-16 表

年 月 日		震 央	卓 越 周 期 (sec)					最大振幅のときの周期	最大振幅 μ
1954	I.17	茨城県南西部	0.54	0.9	1.3	1.5		0.52 sec	225
	〃.19	〃	0.45					0.48	20
	II.2	千葉県中部	0.51					0.52	23
	〃.4	〃	0.48					0.58	90
	〃.9	茨城県南西部	0.40	0.6				0.56	51
	〃.14	東京湾北部	0.50					0.52	45
	〃.20	千葉県中部	0.50					0.48	20
	〃.21	銚子附近	0.50	0.8	1.0			0.54	40
	〃.22	房総半島南東部	0.50	1.1	1.4	1.7		0.67	43
	〃	〃	0.50	0.8	1.1	1.5	1.8	0.58	44
	〃.26	〃	0.50	0.7	1.0	1.4	1.6	0.48	33
	III.28	茨城県南西部	0.54					0.52	18

第 VI 章　地下の振動測定結果

1. 地震時に於ける被害を最小限度にとどめるのは，我々に課せられた一つの大きな問題であり，昔から多くの諸先輩が色々な研究を行つて来た．しかしながら今迄の研究は主に耐震構造論に集中され，建築物の基礎になる地盤については殆んど注意がはらわれ

ていなかつた．そこで我々は，地震時に於ける地盤の性質を調べるために，先ず地盤の振動様式が深さによつてどんな風に変るかを調べることにした．地表と地下の地震動を比較研究することの必要に，最初に目をつけたのは，J. Milne[1]であつた．彼は，10′の深さの乾いた固い自然の井底に地震計を据付けて30′程離れた地震計と比較した．次いで関谷・大森[2]は東大構内で全く同様なことを行つている．但しこの場合，地下の地震計は，約18′の深さに据えてあつた．その後，中村[3]が熱海附近のトンネルの中と入口との比較を行い，那須[4]は丹那トンネルの中と，その上の丹那盆地で比較観測を行つた．この際地上からトンネルまでの深さは160 m 程あつた．その後斎田・鈴木[5]は丸の内で，68尺，30尺の井底と地表との比較を行い，井上[6]は駒場で地下9 m にある地下室と地上の観測室での比較観測を行つている．最近では金井・田中・長田・吉沢[7][8]が日立鉱山の坑道を利用して，地下150, 300, 450 m の地震動の比較をして居る．これらの諸研究は，天然の地震をとらえて，その周期と振巾との関係を調べたものであつて，結果を総合すると，i) 地上の振巾は常に地下の振巾より大である；ii) 土地によつてあるきまつた周期があり，そこでは地上：地下の比は非常に大となる；iii) 洪積層の上に冲積層がある様な場合に，冲積層中では洪積層面の振動と較べると殆んど比が変らない；iv) 入射波の周期が表面層の固有周期に近いものであつても，入射波の連続する波数が極く少ない場合には，地盤の硬軟の差異は地表面の振巾にあまり影響を与えないことの4点になる．

最近の Seismometry によれば，大きな地震の場合と，小さな地震の場合では地盤の Response が違つたものになるらしいということもいわれている．であるから，我々としては，被害を生ずる程度の地震を研究するのが工学上からは理想的だと思われるが，いつ起るか全然見当もつかない地震を待つのは，労力，費用，又日時から言つても大変なものである．それに，地下室とか，直径2 m もある様な大きな井戸を利用して，その底に地震計を設置するとすれば，色々な制約を受け多くの深さで観測することも困難であり，又その施設そのものの影響を受けやすく，その中から本当に地盤の影響だけを取り出すことは困難であろう．この様な困難を避けるために，我々は Boring 孔を利用して，その底に小型の Pick-up を入れ，地上で記録する様にしたいと考えた．この様にして地震の際の様子を推定する手掛りを得るための，予備実験として起振機によつて起される地震動を試錐孔の上下で取つてみることにした．

2. たまたま，東京都土木技術研究所が墨田区吾嬬町東五丁目に於て[i]，地盤沈下測定所を設置するために Boring を行うことが分つたので，これを利用することにした．そして昼間 Boring をして居る時は，地震計を出して置き，夜間 Boring を休んでいる間に地震計を孔中に入れて測定を行つた．そして地震計は常に孔の底にあるわけであるから

1) J. MILNE, *Trans. Seis. Soc.*, **10**
2) S. SEKIYA and F. Omori, *Trans. Seis. Soc.*, **16** (1892)
3) S. T. NAKAMURA, *Proc. Physico-Mathem. Soc. Japan*, **7** (1925) 127–
4) N. NASU, *Bull. Earthq. Res. Inst.*, **9** (1931) 454–
5) T. SAITA and M. SUZUKI, *Bull. Earthq. Res. Inst.*, **12** (1934) 517
6) W. INOUYE, *Bull. Earthq. Res. Inst.*, **12** (1934) 712
7) K. KANAI and T. TANAKA, *Bull. Earthq. Res. Inst.*, **29** (1951) 107–
8) K. KANAI, K. OSADA and S. YOSHIZAWA, *Bull. Earthq. Res. Inst.*, **31** (1953) 327–

i) 地図は，Fig. 2–1.

測定の度に，より深いところの振動を調べることになるわけであるii)．孔には casing が入つていたが測定を行つたところは常に casing の外で，casing の下端から常に 50～100 cm 下であつた．この様にして，地表より地下 25.9 m の深さまで 12 点の測定を行うことが出来た．測定した日時は 1953 年 3 月 29 日より 4 月 9 日までの 12 日間である．用いた地震計は，自己振動周期公称 25 c/s の S.I.E. の地震探鉱用地震計上下動 2 台で，これを増巾器を通して電磁 Oscillograph に入れ，Bromide 紙上に振動をかかせた．起振機は建築研究所の御好意により貸して頂いたもので，回転数を連続的に 0～25

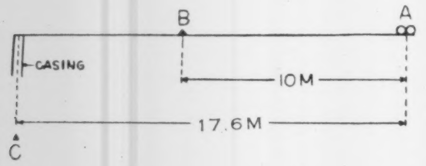

Fig. 6–1. Location of Instruments. A: Vibrator; B: Standard pick up; C: Bore hole pick-up.

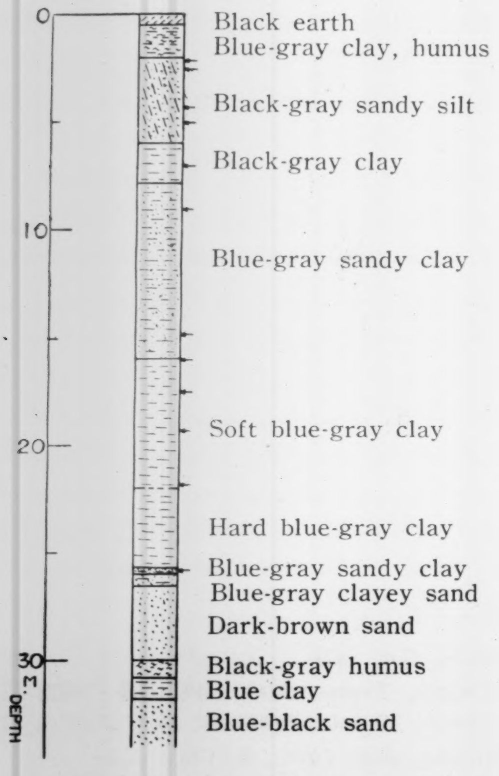

Fig. 6–2. Boring at Azumacho.
← indicates observation point.

ii) この際地震計は耐水容器に入れ，泥中につきささる様にするため，容器はさきをとがらし，かつ充分重くした．こうすると Boring 孔は小さな (6～8″ 程度) 径であり，中には泥水が一杯つまつているわけで，地震計は泥中に埋つているとみてもよいと思う．

c/s までかへられる様になつて居た．我々はこの起振機を Boring 孔より出来るだけ離れた位置に設置したかつたのであるが実際には，場所が狭かつたため，起振機と Boring 孔間の距離は 17.6 m であつた．そして 10, 15, 20 c/s の振動を取り，地表及び地下の震動を比較した．10 c/s 以下は振巾が小さくなり，又 20 c/s 以上は起振機がおどつて不正確になると思われたので実験はやらなかつた．又地上に於ける減衰もしらべた．これ等の測定の際，起振機によつておこされる振動が常に一定でないことが考えられたので

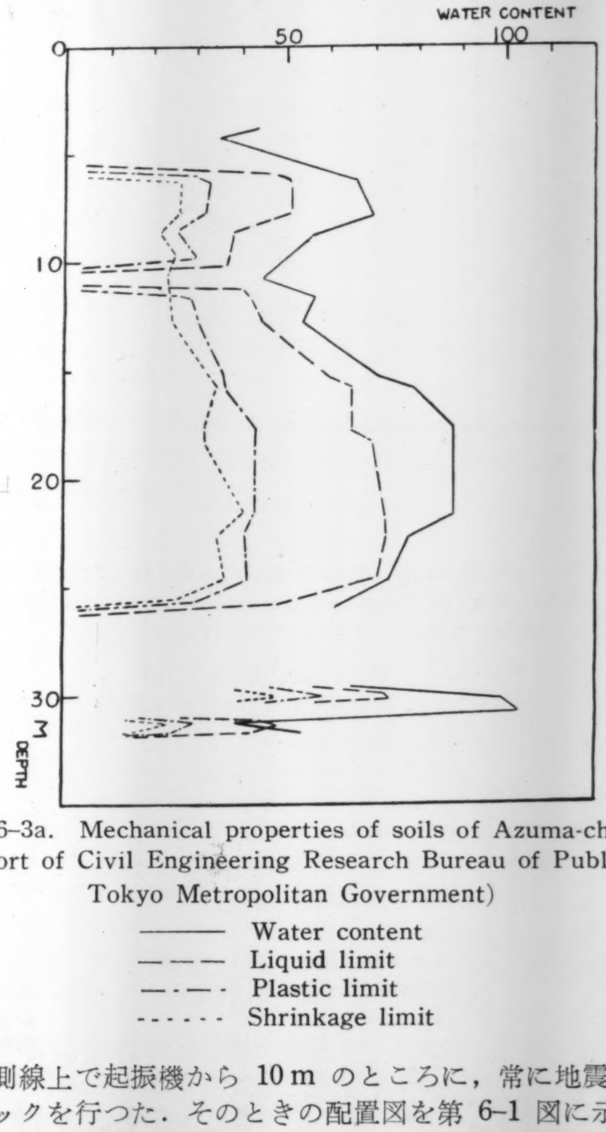

Fig. 6–3a. Mechanical properties of soils of Azuma-cho. I
(after report of Civil Engineering Research Bureau of Public Work
Tokyo Metropolitan Government)

——— Water content
— — — Liquid limit
—·—· Plastic limit
- - - - - - Shrinkage limit

起振機から孔を結ぶ測線上で起振機から 10 m のところに，常に地震計を 1 台設置しておいて，振巾のチェックを行つた．そのときの配置図を第 6–1 図に示す．

3．この附近の地下構造を明らかにして置くことは結果を論ずる上に重要であるので，利用した Boring 孔で得られた柱状図を第 6–2 図に示す．尚，図上矢印は測定を行つた場所を示す．現場で Boring 作業を見て居て，気が附いたことは 10 m 附近では非常に土が軟かく[iii]て仕事がはかどり，又 22.5 m 附近から，柱状図では 15.8～25.8 m の間は，同じ粘土で区別がないにかかわらず，急に固くなり，Boring に時間がかかる様にな

iii) 液性限界はやはり 10 m 附近で非常に小さい．

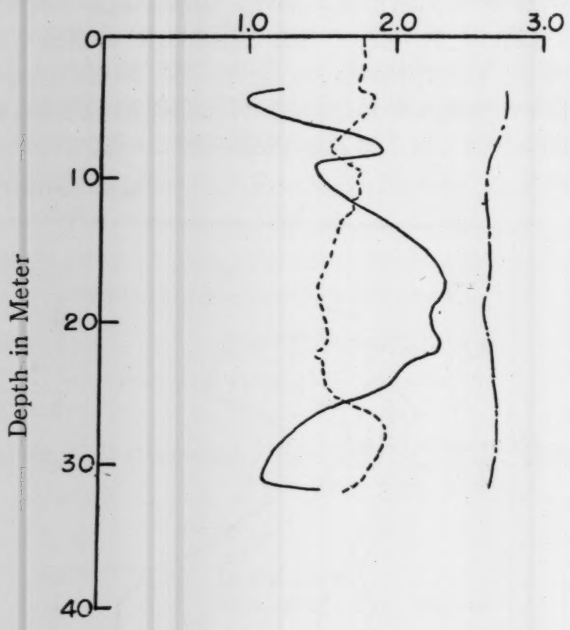

Fig. 6–3b. Mechanical properties of soils of Azuma-cho. II (after report of Civil Engineering Research Bureau of Public Work Tokyo Metropolitan Government)

—·—· True specific weight
- - - - - - Apparent specific weight
——— Void ratio

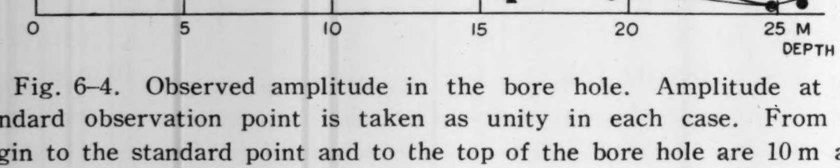

Fig. 6–4. Observed amplitude in the bore hole. Amplitude at the standard observation point is taken as unity in each case. From the origin to the standard point and to the top of the bore hole are 10 m and 17.6 m respectively.

つたことである．そして又 10 m 附近の非常に軟らかだつたところはその際にやはりみとめられた低速度層にあたるのかも知れない．参考のために，Boring の際得た core を東京都土木技術研究所が調べたデータの一部分をいただいたので，第 6-3 図にかかげて置く．

さて起振機による振巾の深さによる変化の有様を示したのが第 6-4 図，第 6-5 図である．この図の縦軸は，第 6-4 図は地下の振動の振巾と standard の地震計の振巾の比，

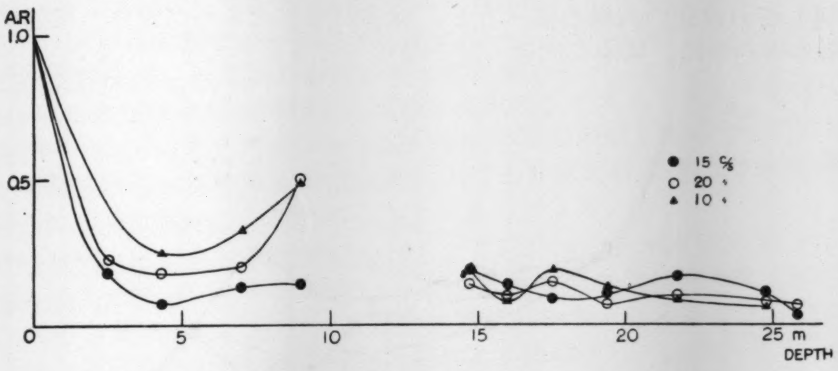

Fig. 6-5. Observed amplitude in the bore hole. Amplitude at the top of the bore hole is taken as unity in each case. From the origin to the top of the hole is 17.6 m.

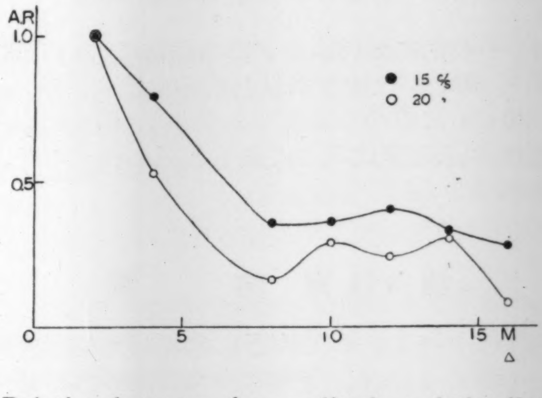

Fig. 6-6. Relation between the amplitude and the distance. (surface) Amplitude at 2 m from the origin is taken as unity.

又第 6-5 図は地下の振巾と孔の直上の振巾の比で，いずれも地表で 1 になる様に書き直してある．横軸は共に深さである．これを見るとわかる様に，地下僅か数 m で振動は既に地表の 1～2 割程度になつてしまうということである．そして 15 m より深くなると殆んど比が変つていない．そして更に注目すべきことは，10～15 m の間で少し比が大になる傾向を見せていることである．10～15 m の間に観測点がないのは Boring が終つて仕事にかかろうとした際，豪雨に襲われ，遂に観測を断念せざるを得なかつたためである．このため，この部分が本当に大きくなつたのか，又はたいして大きくならずにすぐ表面の振巾の 2 割程度に落ちてしまうのか全く不明である．しかしながら地下構造からみて，このあたりは所謂低速度層にあたつていると思われるので，地震動のエネルギ

ーが，ここに集中したと考えることも出来る．このことは大切なことであるから，同様の地質の場所で，もう一度同様の実験を操り返しどうなるものかを確かめた上で議論することにしたい．

次に地上に於ける振動の距離についての減衰曲線を示す．第 6–6 図，第 6–7 図iv) は 2 m に於ける振巾を 1 として書いてある．これを見ると，大体極端な凸凹もなく，10 m 位で 2 m のところの約 4 割位となり，あとは非常にゆるやかに減衰している．但し，16～18 m の間は Boring のため，深さ約 1 尺の泥沼になつていたことを附け加えて置く．深さに関しての減衰の有様と較べると，地表の方がはるかに減衰の状態が悪い．又深さに関するものの様に，途中で大きくなる様なこともなさそうである．

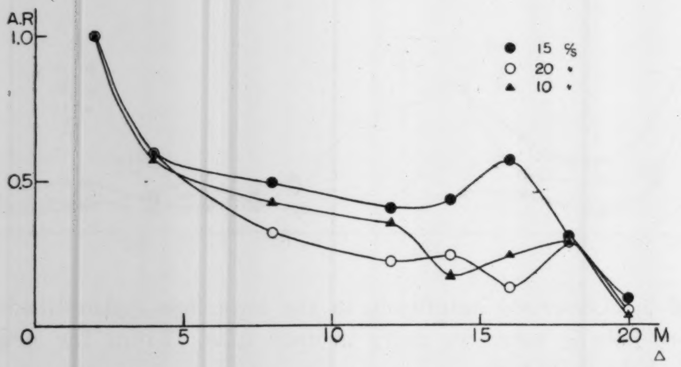

Fig. 6–7. Relation between the amplitude and the distance. (surface) Amplitude at 2 m from the origin is assumed as unity.

以上述べて来たことは，一般的には大体 3 ッの周波数について同様のことであるが，減衰曲線を見ると，10 c/s と 20 c/s は非常に似た傾向を見せて居り，15 c/s は違つている様に見える．10 c/s と 20 c/s は波形も綺麗であつたが 15 c/s のものは，波形が悪かつたので，そのための誤差もある程度は入つて来ると思われるので，15 c/s はあまり重要視しない方がよいと思われる．(島)

第 VII 章 結　　論

東京都内において地盤のよいといわれる山手，本郷の地震研究所を標準点として，地震動の比較観測を行つた結果によれば，下町よりも本郷の方が必ずしも，最大動の加速度，速度或は変位の振巾が小さいとは限らない．特に近い地震で，0.2 秒以下の短周期波動が優勢に現われる場合にはこの事が著しい．0.4～0.5 秒から 1 秒辺の波が優勢な近い地震では一般に下町の方が振巾大きく，その振巾比と周期との平均の関係を示す振巾比特性曲線には夫々特別な周期の所に極大値が現われる．(第 5–16 図) その平均曲線の極大値は冲積層のよく発達している下町の観測点においては 1.7～4.1 倍を示し，周期に無関係にとつた最大動全体についての総平均では 1.5～3.1 倍を示した．これ等の振巾比が後述の地下探査で求められた高速度層（縦波速度約 2 km/sec の層）の深さと共に大きくなつていることは注目に価するが，(第 5–20 図) 又表面層の速度の小さい程その比が大きくなつている事も見逃すことは出来ない．他方，上述の振巾比ー周期特性曲線の山の所の

iv) 第 6–6 図と第 6–7 図は同じ場所でやつたにかかわらず，違つた様子をして居る．これは前者をやつた頃起振機が充分に落着いて居らず，Rocking をしたためと思われる．

周期が周期の頻度曲線の山として現われる卓越周期に一致することが隅田公園及び吾嬬町の観測では知られた．（但し 1 秒以下の波動の弱勢である稍遠い地震に於ては標準点との差異は全く見られなかつた．）かくの如き周期特性は入射地震波の地層内の多重反射からも期待される所でその様な振巾の極大値を示す地動を地盤の固有振動と仮りに呼ぶ事とすれば（地層は力学的に閉ぢられた力学系ではないから厳密な意味で固有振動などあり得ない事はいう迄もない）上の結果は，上述の意味での固有振動誘発説に極めて有力な支持を与えるものであるが，我々の観測の内制振度の低い短周期の地震計で観測した大島，小松川及び篠崎町では必ずしも振巾比の極大になる周期が卓越周期と一致しない様に見える．この事は地震記象の自己相関函数による分析結果からも云える．これが用いられた地震計の制振度と無関係であるか否か俄に断言出来ないが，ただその様な地震計の記録において，地震計の固有周期より稍短い周期の波が著しく卓越する傾向のある事実は無視出来ないであろう．又同時に最大動の継続時間の問題も注意しなければならない．我々の考える所謂地盤の固有振動が地層内における多重反射の結果十分に発達するには入射地震動が相当回数継続しなければならないからである．

次に常時微動に現われる卓越周期を見ると著しい事は各地点に共通して 0.3 秒位の周期に頻度の極大が認められる事である．この事は今迄の観測結果によれば必ずしも到る所で見られる事実ではないから，この卓越周期が地盤と無関係と結論するのは早計かも知れないが，今はこれを問題外とする．それより周期の長い波に着目すれば，上述自然地震の観測から固有振動の存在が有力視された隅田公園及び吾嬬町については，さきに固有周期と見られる周期 0.7 秒とこの常時微動の卓越周期とが全く一致し，金町において自然地震に著しく卓越する 0.5 秒辺の波は又常時微動において 0.55 秒の所に頻度の極大値を示している．同じく東篠崎町でも常時微動及び自然地震の卓越周期は共に 0.4 秒辺に見られる．

之等常時微動に見られる卓越周期 (T) と地下探査で知られた速度の不連続面の両側に於ける速度比の一番大きくなる面の深さ H を比べると略 $T=CH$ と書け，C は H を m で表わす時 0.03～0.04 位になる．

次に火薬を用いた地震地下探査の結果は 0.4～0.5 km/sec 位から 1 km/sec 程度の速度が地表近くで見られ，その下に 1.2 km/sec，1.5～1.6 km/sec 基盤に 1.5 km/sec 或は 2 km/sec 程度の速度の層の存在が知られたが，之等の何れが如何なる時代の地層に相当するか速度だけからは不明である．

火薬で起された人工地震の初動の振巾の距離による変化も測定して見たが，走時曲線の折れる点の近傍で振巾の増大或は減衰率の低下が見られるが全体としての減衰の傾向には地盤との目立つた関係は認められなかつた．

又火薬で起された最大動の伝播速度は約 100 m/sec から 200 m/sec の間にあり，その速度の小さい所は地盤もよくはないが，これは極く表面近い層の物性に関係すると思われるし，分散現象をも考えてよく吟味する必要があると思われる．

尚最大動の表われた時から振巾の半減するまでに要する半減時間をしらべたがそれは分散現象が影響し観測距離によつて著しく変るからそれを簡単に吸収の作用にのみ帰することは出来ない．

最後に起振機を用いる地盤調査は Degebo の主張する如く簡単には利用出来ない事が知られた．それによる地下の垂直振巾分布は深さによる振巾の著しい減少を示したほか，途中に振巾の大きくなる所があると思われるが，それが地盤の物性によるのか，波長に関係したものであるかまだ判定出来ない．

以上を簡単に要約すれば最も著しい事は震度の地盤係数は地動の周期の函数である事

が知られた事で，その地盤振動特性は地層内の多重反射に起因すると見られる証拠が多く知られたが，現在までの整理された資料からはこの事があらゆる地点で確認されたとはいいかねる．併しながら上の所謂地盤の固有振動の存在を否定するのはまだ早計であると思われる．

地震動及び常時微動の卓越周期は速度の著しい不連続面までの深さに略々比例し，上の固有振動説を支持する．

地震地下探査法によつて地下構造を知つた．

起振機を用いる Degebo 流の地盤調査法には問題があり，簡単には用いられない．

地震動は地下から地表に近づくに従つてかなり大きくなる．

特に調査した冲積層 30 m 位迄の地域で隅田公園，大島町，吾嬬町，金町は本郷に比べ 1.5～2 倍振巾が大きく，軟弱な冲積地盤のさらに厚い（4～70 m）と思われる様な地点で振巾比は 3～4 倍となり，やはりその様な今迄地盤が悪いといわれた地域においてその判断を覆すような事実は認められなかつた点は注目しなければならない．（河角）

32. *Investigation into Seismic Characteristics of Subsoils in Tokyo (Abstract)*

Subsoil Research Team, the Earthquake Research Institute.

In Japan, it is a matter of common knowledge that the earthquake damage is closely related to the subsoil characteristics of the locality. In the building code recently laid down, regulations were therefore made for the seismic lateral force design according to the kind of buildings, the seismic activity of the region and the subsoil characteristics of the building site.

In designing an earthquake-proof structure, the knowledge of dynamic properties of the subsoil is very important, since the resonance of building vibrations at the proper or predominant period of the subsoil may increase the seismic damage, while the dissipation of the vibration energy of the building into the ground will prevent the resonance. Rocking vibrations of the building will also release the stresses in the building.

Efforts have been made in recent years to investigate, on one hand, the various dynamic properties of the different kinds of subsoils, and, on the other hand, to classify the subsoils of Tokyo according to the knowledge of the dynamic property thus obtained.

The present paper deals with the results of the following observations and measurements which were made as a part of the aforesaid investigation.

a) Observations of earthquakes at various places;
b) observations of micro-tremors at various places;
c) seismic prospectings;
d) dynamic tests of the subsoils with a vibrator;
e) underground distribution of amplitudes of vibration excited by a vibrator.

Observation of earthquakes

Differences in the earthquake vibrations at different kinds of subsoil have been noticed by Milne and followers. A. Imamura investigated the differences in the damage in the case of the 1923 earthquake. M. Ishimoto made an extensive observation of earthquakes with his accelerometers and found out the existence of the predominant vibration periods of subsoils. He also noticed the difference in the frequency distribution of the ground acceleration periods for different subsoils.

In 1951, S. Miyamura made earthquake observations at Sumida Park in the down town of Tokyo, and the seismograms were compared with those obtained at our Institute, which is at Hongo in the uptown of Tokyo. The comparison showed that the ratio (amplitude at Sumida)/(amplitude at Hongo) is less than 1 for the periods of 0.3 sec. or less, while the ratio is 1.7 for the periods greater than 0.5 sec. This was explained by the existence of proper periods of 0.3 sec.

at Hongo and of 0.7 sec. at Sumida.

In 1952–53, he also made earthquake observations at Sumida, Shinozakicho and other places, by means of resonance seismometers with respective periods of 2.5, 1.0, 0.5, 0.25 and 0.1 sec., and damping constants $h=0.4$ for all. Results of comparison with Hongo are given in Fig. 4–8∼4–10 in the text. The curves show that there are proper periods of 0.3 sec. at Hongo and of 0.6 to 1.0 sec. at down town. Velocity amplitudes are 1.5 to 2.0 times greater at down town than at Hongo. Since he took the average of all earthquakes without regard to their epicentral distances, the curves are rather flat. Localities of observation can be found in the map given in the text.

In Feb., 1953, R. Takahasi observed two earthquakes at Azumacho by means of a seismograph with a period of 5.0 sec. and a magnification of 47.5. Azumacho has an alluvial layer 22 m thick. One of the earthquake had its epicenter in Hokkaido, the epicentral distance being about 1000 km. The other earthquake took place in the Boso Peninsula, so the distance was about 100 km.

Seismograms of these earthquakes were compared with those obtained at our Institute, where there is a diluvial loam layer underlain by Tertiary layers.

No remarkable difference has been observed between the dynamic characteristics of Azumacho and Hongo in the case of the Hokkaido earthquake cited above. As for the Boso earthquake, photographically enlarged seismogram was read off to obtain $2A$ (from crest to trough) and $T/2$ (from trough to crest). From A and T thus obtained, we calculated $v=2\pi A/T$ and $\alpha=4\pi^2 A/T^2$ and took them for velocity and acceleration respectively.

Distribution curves of these quantities against the period of waves are shown in Figs. 5–2∼5–10 in the text in comparison with the same curves at our Institute. In these figures the lower curves show the frequencies of one third largest waves respectively in amplitude, velocity and acceleration. Figures show that spectral breadth of the earthquake vibration is much wider at Azumacho than at Hongo, and also that the predominating period is much longer at Azumacho (0.77 s) than at Hongo (0.32 s).

Amplitude ratio as a function of the period is given in Fig. 5–6, which shows that the amplitude is 0.6 times that of Hongo at the period of 0.32 sec, while the ratio becomes as large as 1.5 to 2.0 for the periods over 0.5 sec.

The same features were observed with regard to velocity and acceleration of the earthquake. These features were explained as the results of shearing vibration of the surface layers.

Earthquake observations were also carried out by N. Nasu at Kanamachi, in 1953. Period-frequency diagrams of earthquakes were prepared. They clearly showed that the predominant period lies in the range between 0.4 sec and 0.5 sec. This is according to our experience rather short, and we may perhaps infer that the seismic characteristics of the subsoil is rather good at this place.

Seismic prospectings

As the results of investigations in Japan of damage caused by the Kwanto

earthquake of 1923, the Nankai earthquake of 1946 etc., the thickness of the soft alluvial layer has been revealed to be closely related to the percentage of the demolished wooden houses.

It will therefore be of great importance to know the thickness of the alluvial layer to classify the subsoils. For this purpose, seismic prospectings were carried out by S. Omote at ten places in Tokyo, mainly in the down town, in the years 1951–53. The results are summarized in Table III–8 in the text. In the Table it is shown that in most localities a fairly clear boundary is seen at the depth of about 30 to 50 meters from the surface. At this boundary the velocity of the seismic waves jumps from about 1500 m/s to about 2000 m/s.

In the April of 1952, another seismic prospecting was carried out by E. Sima at the playground of the Azuma First Middle School. The velocity and thickness of each layer were determined as follows:

The first layer	$V_1=500$ m/sec	$H_1=4$ m	$H_1'=4$ m
The second layer	$V_2=900$	$H_2=7$	$H_2'=3.5$
The third layer	$V_3=500$	$H_3=3$	$H_3'=4$
The fourth	$V_4=1000$	$H_4=11.5$	$H_4'=13.5$
The fifth layer	$V_5=1500$	—	—

The third layer is, so to say, a low velocity layer. H_1, H_2, H_3, H_4 were calculated assuming the thickness of the low velocity layer to be 3 m and $V_3=500$ m/sec. H_1', H_2', H_3', H_4' were obtained under the assumption that the low velocity layer is 4 m thick and $V_3=500$ m/sec.

According to the results of boring made at a neighbouring site, the soil was found to become hard beyond 22 m.

Micro-tremor Observation

Micro-tremors of periods less than 0.1 sec. are supposedly minute oscillations of the surface alluvial layers excited by artificial and other distrubances. It is only natural that their spectral frequency distributions should have a close relation with the subsoil structure. Systematic measurements of the micro-tremors have been carried out by K. Kanai at various places in Tokyo. The properties of ground as inferred from the characteristics of micro-tremor are utilized for the determination of the foundation coefficient relating to earthquake-proof construction.

The distribution of periods of micro-tremors shows a definite form for respective kinds of subsoils. Generally speaking, on hard grounds a sharp peak appears at 0.1—0.2 sec. period, while on the firm diluvial ground the peak is at 0.2–0.4 sec. On the soft alluvial ground the curve is irregular in shape and a number of peaks appear in the range of 0.3–0.6 sec. On especially soft ground the curve is flat, the period ranging from 0.2 to 1 sec.

Distribution of periods of micro-tremors observed at various places in the City of Tokyo are given in Fig. 3–5 in the text.

Experimental study of the ground properties with a vibrator

Attempts to clarify ground properties with a vibrator were first made by German investigators. A large vibrator was made by K. Kanai and F. Kishinouye of our Institute to excite artificial vibrations of buildings and grounds. The vibrator is shown in Figs. 4–1a, 1b and dimensions and weights of the elements of the machine are given in Table IV–1 in the text.

Some observations were made by the members of our team to test the two methods worked out by the Degebo (Deutche Gesellschaft für Bodenforschung). In the first method the propagation of elastic waves excited by a vibrator was observed. The observed fluctuation of the wave amplitude with the distance was attributed to the interference of the direct and refracted waves. Based upon this assumption the thickness of the surface layer and the velocities in the media were obtained. But our experiment proved that such a simple assumption is not permissible. Since the vibrator emits bodily waves as well as surface waves, the phenomena must be so complicated that our cursory observations can give no definite conclusions.

The second method of the Degebo is the measurement of the power used for driving the vibrator as a function of the driving frequency. They obtained the proper period of the ground from the position of the peak in the power-frequency diagram. Kawasumi and Sima's observations, with vibrator smaller than that mentioned above, at Azumacho in the down town, showed no resonant peak in the watt-meter reading. The amplitude reading increased rather slowly and almost linearly with the driving frequency of the vibrator, but not, contrary to the expectation, with the square of the frequency. No definite explanation can be drawn from our insufficient data.

The third test was carried out by K. Kishinouye. The vibrator was set on the ground and its wheels were made to rotate as fast as possible, and the driving force was then taken away. The rotation of the free wheels becomes slower while at the same time the amplitude of the ground vibrations also decay. If the ground had its proper vibration, the amplitude will show a maximum. In other words, the resonance period can be determined from the period of the maximum amplitude on records of ground vibrations.

But many difficulties obliterated the record to such an extent that we had to defer our conclusion until more elaborate studies were made. The use of the vibrator for the dynamic ground test was thus abandoned in the present investigation.

Another experiment with the vibrator was carried out at Azumacho by Kawasumi and Sima. Tremors of the ground caused by the vibrator were observed at the top and bottom of a boring hole. They found that the amplitude of tremors becomes rapidly small with the depth of the observing point. At the depth of only few meters, it becomes almost 20% of the surface value. They also found that, in the low velocity layer, amplitude of tremors exhibits the tendency of growing large.

Conclusions

From the above investigations we could find a remarkable fact that the foundation coefficient for the enhancement of amplitude is not constant for all earthquake motions, but it is a function of their period. This vibration characteristics of the subsoil may be inferred as resulting from the multiple reflections of the seismic waves within subsoil layers. Many evidences supporting this explanation were found, although some seemingly irreconcilable data were also found at some localities. But such negative evidences are not concrete enough to put off doubts concerning the effects of instrumental conditions and methods adopted for the present analysis of the records.

On the other hand, predominant periods appearing in the seismograms of natural earthquakes and microseisms of short periods were nearly proportional to the thickness of the soil layer above the most remarkable discontinuity in the velocity log. This fact gives support to the above explanation of the vibration characteristics by the multiple reflections.

Refraction shootings were done at 11 places in the down town of Tokyo.

Vibrators were first used to generate ground vibrations for the study of the subsoil characteristics. But the two methods worked out by the Degebo were proved to be untenable, because some difficulties in principle and practice were found.

Underground distribution of the amplitude of the vibrations caused by a vibrator within the soil layers was observed. It showed a considerable decrease and regain of amplitudes with the increase in depth from the surface.

At some localities where our observations were made, as the Sumida Park, Azumachō and probably Kanamachi, the amplitudes of the earthquake acceleration, velocity and displacement were about 1.5∼2 times as large as at Hongo, while at other localities where soft alluvium develops more thickly, the amplitudes were 3∼4 times as large as at Hongo. We could not thus find in this investigation any place where seismic characteristics proved to be better than inferred from geological considerations.

2

昭和30年12月5日印刷
昭和30年12月10日發行

東京都文京區本富士町一番地
東京大學構內
編纂兼發行者　東京大學地震研究所

東京都千代田區富士見町一丁目十番地
印刷者　笠井康頼

東京都千代田區富士見町一丁目十番地
印刷所　株式會社國際文献印刷社

賣捌所　東京都千代田區神田一ツ橋通
岩波書店

東京都中央區日本橋通二丁目六番地
丸善株式會社

Sold by

Iwanami Shoten,

Hitotsubashi dôri, Chiyoda-ku, Tôkyô,

and

Maruzen Co., Ltd.,

Nihonbashi dôri, Chûô-ku, Tôkyô.

Price of this copy: 923 Yen. (Postage exclusive.)

BULLETIN OF

THE EARTHQUAKE RESEARCH INSTITUTE

TOKYO UNIVERSITY

Vol. XXXIII, Part 3. September, 1955.

30TH ANNIVERSARY VOLUME

Contents.

Papers and Reports.

Page

18. R. TAKAHASI, A Short Note on a Graphical Solution of the Spectral Response of the Ground. (in English) 259
19. R. YAMAGUCHI and Y. SATÔ, Range of Possible Existence of Rayleigh- and Sezawa-Waves in a Stratified Medium. (in English) 265
20. K. KANAI, On Sezawa-waves (M_2-waves). Part II. (in English) 275
21. K. KANAI, An Explanation for the Ground Vibration caused by Periodically Exerted Force. (in English) 283
22. T. TAKAHASHI, Analysis of the Dispersion Curves of Love-Waves. (in English). 287
23. T. RIKITAKE and I. YOKOYAMA, The Anomalous Behaviour of Geomagnetic Variations of Short Period in Japan and Its Relation to the Subterranean Structure. The 6th report. (The results of further observations and some considerations concerning the influences of the sea on geomagnetic variations.) (in English) 297
24. M. MINATO und Y. KITAGAWA, Die Veränderung des Salzgehaltes in den küstennahen Seen Hokkaidos. (im Deutschen) 333
25. H. TSUYA, Geological and Petrological Studies of Volcano Fuji, V. 5. On the 1707 eruption of Volcano Fuji. (in English) 341
26. T. ICHIMURA, Some Heavy Accessory Minerals in Granitic Rocks from the Tsukuba District, Ibaraki Prefecture. (in English) 385
27. S. OMOTE, S. MIYAMURA and Y. YAMAZAKI, Triggered Magnetic Tape Recorder for Routine Seismic Observations. (in English) 397
28. K. KASAHARA, Experimental Studies on the Mechanism of Generation of Elastic Waves V. (in English) 411
29. T. ICHIMURA, Activities of the Gassan Volcano. (in English) 419
30. M. MINATO, Die zeitliche Verteilung der Vulkane im Quartär Hokkaidos. (im Deutschen) 433
31. D. SHIMOZURU, Elasticity of Rocks under the Initial Stresses, with Special Reference to the Fracture Problem. (in English) 437
32. Y. OTUKA, Shizukawa Group and Tertiary Crustal Movements in Japan. (in Japanese) 449
33. SUBSOIL RESEARCH TEAM, THE EARTHQUAKE RESEARCH INSTITUTE, Investigation into Seismic Characteristics of Subsoils in Tokyo. (in Japanese) .. 471

(For the papers written in Japanese or in occidental languages, the abstracts are given in occidental languages or in Japanese respectively.)

BULLETIN OF THE EARTHQUAKE RESEARCH INSTITUTE,
TOKYO UNIVERSITY. Vol. XXXIII, Part 4. December, 1955.

東京大學
地震研究所彙報

第 33 號　第 4 册

昭和 30 年 12 月

創立 30 周年記念号

目　次

創立以来 30 年間の地震研究所……所長

論文及報告

			頁
34.	連続的に変る地層による地震波の反射及び屈折（独文）	松沢武雄	543
35.	Stoneley 波—その速度，軌道及び振幅の分布（英文）	山口林造 佐藤泰夫	549
36.	地球内電磁誘導現象の模型実験（英文）	永田武 小口高 前川英夫	561
37.	地磁気ダイナモに於ける磁場の生長（英文）	力武常次	571
38.	地球核内の有限振幅電磁流体振動（英文）	力武常次	583
39.	蔵王火山の地質学的研究（第 3 報）（英文）	市村毅	593
40.	地震動に含まれる短週期震動（リップル）について ——房総沖地震の余震の場合——（英文）	笠原慶一	631
41.	鳥取地震余震観測（第 2 報）（英文）	表俊一郎	641
42.	湖氷中に発生する自然震動の研究（第 1 報）（英文）	表俊一郎 山崎良雄 小林直吉 村内必典	663
43.	土地の脈動の周期と台風位置との関係（英文）	池上良平	681
44.	二層建物の非線形定常振動（英文）	久田俊彦 中川恭次	689
45.	東北日本に於ける第 5 回爆破地震動観測（英文）	爆破地震動研究グループ	699
46.	局地的地震観測網のための有線搬送式遠隔刻時装置（邦文）	宮村摂三 辻浦賢	709
47.	有線搬送式遠隔記録地震計（邦文）	宮村摂三 松本英照	715
48.	超短波無線搬送式遠隔記録地震計（邦文）	宮村摂三 辻浦賢	725
49.	携帯用石本式加速度地震計の野外実地使用に対する二三の基礎実験（邦文）	宮村摂三 堀実	733
50.	黒沢尻附近の水準測量結果（邦文）	岡田惇	749

所　報

索　引

(The titles in occidental languages are given on the back cover.)

本彙報ハ年4回 (但シ第1號ヨリ第6號マデハ不定期ニ，第7號ハ3冊トシテ發行セリ)，彙報別冊ハ不定期ニ發行ス.

本彙報掲載ノ論文及ビ報告ノ內容ニ關シテハ著者ノミニ共責任アルモノトス.

本彙報ニ關スル照會通信ハ東京大學地震研究所長ヘ宛テラレタシ.

The Bulletin is published quarterly. (Vols. I–VI were published at irregular intervals and Vol. VII consisted of three parts.)

Supplementary Volume is published at irregular interval.

The authors of the papers alone are responsible for the statements and opinions contained in their respective papers.

All communications relating to this Bulletin should be addressed to the Director of the Earthquake Research Institute, Tokyo University.

EARTHQUAKE RESEARCH INSTITUTE: PAST THIRTY YEARS SINCE ITS ESTABLISHMENT

Motivated by the Great Kwanto Earthquake of September 1, 1923, the Earthquake Research Institute was founded with the object of promoting basic research in seismology. The new Institute was the successor of the then-existing body known as the Imperial Earthquake Investigation Committee of the Ministry of Education, and it was established with its additional new aim in the Tokyo Imperial University (the present University of Tokyo) on November 14, 1925.

During the first ten years after its establishment, there were a series of calamities such as the Tango Earthquake, the Izu Earthquake, the Sanriku seismic sea-wave, the Taiwan (Formosa) Earthquake, and the Komagatake (Hokkaido) and Asama volcanic eruptions, which provided us with excellent opportunities of studying earthquake phenomena as they occurred consecutively with appropriate intervals between. As the consequence, the Institute was able to obtain gratifying results in a very short time. As early as 1931, at the time of the late Dr. Kyoji Suyehiro's visit to the U.S.A., the works of the Institute were introduced abroad and received warm approval.

Most of the research conducted in the Institute is compiled in the Bulletin of the Earthquake Research Institute, Vol. 1 to Vol. 33 (1955), the Supplementary Volumes of the same Bulletin, Vol. 1 to 4 (now being printed), and the Special Bulletins of the Earthquake Research Institute, Vol. 1 to 7. When these volumes are read in the order of their publication, one may trace the development of the research conducted in the Institute up to present. In the course of its development, the rapid progress during the first decade is especially worthy of note. In this period such instruments as a seismic vibration analyser, a tiltmeter, and an acceleration seismograph were newly invented which contributed greatly to seismometrical studies. Furthermore, crustal deformation and movement of the earth-block were studied by using the results of the triangulation and levelling surveys repeatedly carried out in the seismic regions such as the Tango and Izu districts. From the detailed investigation of distribution of after-shocks, the migration of the center of earthquake activity was made known. These studies set fine examples for the later investigations of earthquakes and volcanic eruptions.

Studies undertaken in the Institute are not limited to those arising from earthquakes and volcanic eruptions. They extend to purely theoretical studies such as earthquake motion, vibration of earthquake-resistant structures, construction of the earth's interior and others. There are other petrological and geological studies which require continuous mental and physical efforts. In the former field, a brilliant discovery was made of a new earthquake wave known as Sezawa-wave and a comprehensive theory of the energy dissipation in the seismic vibration of a building was formed. In the latter field, valuable research has been conducted on volcanoes such as Mt. Fuji and Mt. Mihara.

The earth's magnetism is another subject of study of our Institute. It is being studied with special interest in connection with volcanic activities. Recently at Mihara Volcano, volcanic activity and the change of magnetic declination were found to be correlated, the result of which may lead to the possibility of foretelling volcanic activities. On the other hand, volcano-physical study has been started on a full scale since 1931 at Mt. Asama and from its observation data for volcanic earthquakes, volcanic tremors and tilting of the earth's surface, the possibility of danger of the eruption and eruption forecast have been verified in recent years.

The period from the end of 1943 to 1945 was a difficult time to continue research, due to World War II. But these difficulties were met with great endeavour by the members of the Institute which gave rise to opening new fields of study in ground motion and air pressure caused by the blast. Calamities visited our country mercilessly during and after the war while the whole nation was suffering their worst living conditions; for example, the Tottori Earthquake, the Tonankai Earthquake, the Mikawa Earthquake, the Nankaido Earthquake and the Fukui Earthquake. Investigations of these earthquakes were carried out with extreme difficulty, but fortunately at the time of the Fukui Earthquake, research institutes were mobilized on a nation-wide scale and investigation was conducted under a well-controlled research organization. Our Insitute had participated in the program and was able to contribute greatly. After this, social conditions began to recover and research work in various fields seemed to function smoothly again. The system of scientific research shows some changes in the post-war years. There are more cooperative research works than in former years with relatively large subjects under which researchers of related fields work together. Consequently the members of this Institute work more closely

than before with outside researchers as leaders or participants in such research works. Cooperative research with the Institute is especially requested in the fields of architectural and civil engineering. As a result, research on vibration of the ground and a theory of earthquake resistant structure has been largely promoted.

Today, various scientific research grants are being given by the government to research institutes and their members throughout the country in order to encourage scientific studies. This Institute, also, is favoured with such grants for which we are very grateful and by which further study of many important research works is made possible. One of the most extensive studies of this type has been a gravity survey conducted throughout all Japan. Besides the ordinary research works, our Institute is at present engaged in the following projects, namely; preparation of the instruments to be contributed to the international network for seismic observation, investigation of the earth's crust constitution by means of seismic prospecting, construction of a seismograph registering the earthquake motion transmitted by wireless, volcanic eruption forecast, and characteristics of vibrations of various types of grounds.

Looking back at the history of our research for the past thirty years, the footprints of progress are distinctly marked in a strikingly expanded area of research and it cannot be denied that each footprint has been made with utmost efforts for the sincere pursuit of truth. At this Thirtieth Anniversary, recalling our past tradition, the members are united again to exert our utmost for the future prosperity of the Institute.

December 1955.

Dr. Nobuji Nasu
Director

創立以来 30 年間の地震研究所

地震研究所設立の動機は大正 12 年 (1923) 9 月 1 日の関東大地震にあつた．それはこの地震によつて蒙つた被害があまりにも大きかつたので，このような災害が再び起らないように地震の学理と震災予防軽減の方策の研究を従来の文部省震災予防調査会で行われてきたより一層進捗する必要を痛感したからである．そこで大正 14 年 (1925) 11 月 13 日に地震研究所と名付けられた新しい研究所が東京帝国大学の構内に設立されたのである．この頃は関東大地震の余震がまだかなり活溌に活動しており，その後も，特に 10 年間は各地で顕著な地震，火山の活動が起つた．これらは我国に取つては，不幸な出来事であつたにちがいないが，この研究所の研究成果を急速に上げるに非常によい機会が与えられたといえよう．

創立僅か 6 年間にこの研究所がおさめた研究業績は初代所長事務取扱末広恭二博士によつてアメリカに紹介され，同国の土木学会より「地震工学講義」が出版され，高く評価されたことは周知のことである．その後 20 有余年の間の業績も決してこれには劣らないものであると信ずる．

この研究所の研究は地震研究所彙報，同別册及び速報に発表される．彙報は年 4 回発行されることになつているが，創立後の 4 年間 (1925～1929) 及び第二次世界大戦中から終戦後の 5 年間 (1943～1950) は必ずしもそうではなかつた．彙報別册は特に研究事項の多い事件が起つた場合，これらの研究調査結果を集録しておくのに便利なため不定期的に出版され，速報は特別な問題を早く発表する必要な場合に出された．

当研究所の研究が如何なる過程をたどつて進展したかはこれらの出版物を年を追つて読んでゆけばわかるが以下簡単に紹介してみよう．

先ず 1926 年，土地の傾斜変化を測定する新しい計器が完成され，又この時，地震動の分解器が作られたことはその後の研究に大きな貢献をした．1927 年の丹後地震においては地殻変動が，度々繰返し行われた三角測量，水準測量によつて明らかにされ，地殻変動や地塊運動に対する我々の考えがはじめて確立された．又同地震の余震の震源分布について行われた研究が，以後起つた地震の余震調査に一種の型をなした．1929 年駒ケ岳の噴火には各種の地球物理学的な調査研究が行われ，これも亦爾後の噴火後の調査方法の範例となつた．

1930 年は，地震の調査に忙しい年であつた．即ち同年の初め頃伊東に地震群が起り，その年の 11 月 26 日には北伊豆地震が起つた．この地震のときの光り物の現象の研究結果は未だに未解決の部分を残しておるが，非常に興味あるものであつた．

1931 年中に特に記述すべきことは水平動加速度地震計の完成されたことであり，1933 年に完成された上下動加速度地震計と共に，地震動の性質を明らかにするためには実に劃期的なものといえよう．この器械の各地における観測結果から土地の固有振動や震度階と最大加速度との関係が明らかにされ，最近の地盤振動の研究の基礎がここに作られた．この地盤の問題は耐震工法に直接関係のある重大な問題であり，これはアメリカでも大いに注目されている．

1932 年には地震力の震源における分布状態，即ち四重源説が，地震の初動分布の研究から提唱され，地震の発生機構が明らかにされた．

一方地震波動の理論的研究は創立当時からずつと続けられてきたが，地震波の Rayleigh waves や Love waves の研究が特に熱心に続けられ 1935年 には M_2-wave とい

う一種の新しい形式の表面波の実在可能性が見出された．この年の 3 月 3 日には三陸地方に大津浪が起り，種々な研究分野から津浪の研究が行われ，その膨大な成果は本所彙報別冊第 1 号として発行された．

1933 年頃から浅間火山の地球物理学的研究が行われることになり，翌年新らしく設置された火山観測所を中心に現在迄続けられている．

1934 年 1 月 15 日，印度 Nepal-Bihar 大地震には本所員を派遣して調査せしめた．同年 9 月 21 日の西日本の颱風は大被害を及ぼしたので，津浪の研究に関連して各分野の研究員の手によつて調査が行われ，それらの結果は彙報別冊第 2 号に掲載されている．

1935 年には台湾中部が地震に見舞われたので，この地震についても詳細な調査が行われた．その結果は彙報別冊第 3 号にのせてある．

地質学，岩石学，地理学的な研究も本所の創立以来から続けられ，地震地域及び活火山に関連してこの方面の研究がなされたのである．1935 年頃よりは浅間及び富士の両火山の研究が本格的となつた．

一方物質，特に岩石及び土の粘性及び弾性に関する実験的な研究が 1935 年頃より開始され，大いに興味を呼んだのである．又地盤の変動として東京江東地区の沈下問題が取り上げられ，その原因を判定することができたことも記憶に残つているところである．

耐震建築の研究は当研究所の主要な研究課題であるが，先に 1934 年丸の内在の深礎建築の基礎及び地表における地震動の比較，五重の塔，名古屋城等の耐震性の問題，或は構築物の振動理論，実在建物の振動実験等この方面の研究に可成り多くの業績を上げて来たのであるが，1936 年頃には建物の振動逸散性の問題が，決定的な結論に達したように見えた．

1936 年には河内，大和の強震及び伊豆新島の地震があり，又 1939 年には男鹿地震が起り，いずれも当研究所の研究が多忙であつた．

一方地下構造の研究は，重力異常分布に関連して行われ，又地球核の熱力学的成因と地球内の粘性分布の問題がとりあげられて地球内部構造の研究が 1939 年頃から大いに興味をもたれたのである．

1940 年三宅島の噴火には各分野の研究がなされた．この頃より岩石の磁気的性質の研究が開始され，以後継続された研究により特に火山岩の磁気的性質が明らかにされたことは特筆すべきである．一方地震波動理論に基ずく地震探鉱法の研究は 1940 年以後本格的に当研究所において取り上げられ，実用方面にも貢献したのである．架構の立体的振動及び海底変動に因る津浪生成に関する研究等は 1942 年の主なものであろう．

1943 年 (昭和 18 年) より 1945 年 (昭和 20 年) 8 月に至る間，第二次世界大戦の影響により，研究継続に困難がないではなかつたが，あらゆる困難を克服して本所の研究を続ける努力が払われ，この期間に起つた鳥取地震，東南海地震，三河地震についても調査を行つた．戦時中の研究としては爆震，爆風の研究，地下資源開発のため地下探査法等の研究が重要な分野であつた．

1944 年には有珠の昭和新山の出現があり，火山学上に新しい又稀らしい現象を見た．

1946 年には桜島の噴火に関連する総合的研究，又北海道有珠山の調査，南海大地震の調査等が終戦直後の悪条件のもとに行われたことは特に記録に残すべきことであろう．

1948 年頃からは地殼変動の観測整備が開始された．この観測は従来も行つていたのであるが，水管傾斜計及び土地伸縮計等の新しい器械が考案試作され，それを油壺に設置することとなり，地殼変動が一段向上された精度で測定し得るようになつた．この年の最も大きな出来事は福井地震である．この地震の調査は殆んど全国の研究機関を動員して行われたので，地震研究所もこれに参加し，各種の研究が行われたことは今なお記憶に新らし

いところである．この地震の影響範囲が比較的狭い地域に限られており，調査し易かつたこと及び調査組織が合理的であつたこと及び調査方法が，進歩していたため，これほど詳細，且つ系統立つて調査が行われた地震は未だかつてない．

1949 年には今市地震という可成りの強さの地震が，東京の近くに起つた．これらの調査も戦後の主なもものに属する．

1950 年以後地震の表面波特に Love 波等の表面波の研究が続けられ，脈動及び地盤震動に関する研究が，理論的及び実験的に行われた．又 1951 年我国各地の地震危険度の研究結果は構築物設計震度決定に頗る有益な資料を提供した．

1950 年から 1951 年には伊豆大島三原山が活動して，地質・岩石・地球物理各方面から研究された．

1952 年の頃には表面波の分散曲線の研究や地球内の電気伝導度，津浪の太平洋における反射の現象を明らかにした研究等は頗る興味あるものであつた．

続いて 1953 年には日本における地磁気短周期変化，地震動振幅と地表層の性質，火山岩の粘性と弾性の研究等が行われた．

1954 年には理論的研究において新しい試みとして地震の場の論が現われて注目を引いた．又三原火山の地磁気的研究が永続的に行われるようになつた．

以上の他，岩石学的或は地質学的な方面から三原山の熔岩の化学成分の研究等重要な研究が勿論あつたのである．

戦後全国の研究機関或は研究者に政府から与えられた科学研究費によつて，一般の科学が振興され，当地震研究所もこの恩恵に浴したのである．そして以上に述べた研究の或るもの，及びここには省略した研究の数々がこの研究費によつて行われたのである．特に大地震危険地帯における地球物理学的研究，大爆破による地下構造の研究(目下継続中)又最近の火山噴火予知，各種地盤における地震動の研究等に対する研究費の交付は本研究所の研究成果を一層挙げさせるために大きな貢献をなすものと信ずる．

なお，当研究所の特別事業である国際的地震観測網に寄与する観測施設の整備の事業により地震及び地殻変動観測の諸設備が着々整備されている．又大爆破による地殻構造の調査も当研究所の事業として 1955 年より開始されることになつた．

重力異常分布の測定は北海道を除き，日本全国にわたつて行われ，その成果の一部は既に彙報別冊第 4 号に出版されている．

以上のべて来たことは当研究所の研究が行われた大略の過程をのべたもので，すべてのことが包含されているのではない．有益且つ重要な研究も数多くぬけていると思う．当研究所の研究分野は広いのであるが，これを要約すると最初に述べた本所の使命である地震及びそれに付随した現象の研究と地震による直接及び間接的災害の予防，軽減の研究に外ならなかつたのである．そして過去 30 年間この研究所が挙げて来た研究業績が，今後益々発展する基礎となることは疑いないことである．

1955 年 12 月 30 日

地震研究所長　那　須　信　治

34. *Reflexion und Refraktion der seismischen Wellen durch eine kontinuierlich verändernde Schicht. I. SH Welle.*

Von Takeo MATUZAWA,

Geophysikalisches Institut.

(Vorgelegt den 19. Juli 1955.—Eingegangen den 20. Sept. 1955.)

1. Einleitung.

Die Sprengseismik zeigt uns viele Eigentümlichkeiten der Wellenfortpflanzung in der komplizierten Schichten der Erdkruste. Besonders interessiert uns die Abhängigkeit der Stärke der reflektierten Wellen von der Wellenperiode[1]. Bei der Reflektion an einer Unstetigkeitsfläche im strengen Sinne des Wortes können wir nicht solches Verfahren erwarten.

In Wirklichkeit ist die Schichtgrenze nicht immer eben sondern gerunzelt. Manchmal muss die Übergang kontinuierlich sein, wenn auch er sehr stark veränderlich sei. Der letzte Fall wird hier untersucht.

2. Rechenmethode.

Im allgemeinen ist die strenge Lösung der Wellengleichung in unhomogenen Medien schwierig. Hier ist eine horizontale allmählich veränderliche Schicht vorausgesetzt. Diese Schicht wird durch Überlagerung von vielen parallelen homogenen Schichten ersetzt und nach der Rechnung wird die Grenzübergang gemacht.

3. Eine linear veränderliche Schicht, die von einer homogenen Schicht zur anderen kontinuierlich übergeht.

Der Fall ist in Fig. 1 veranschaulicht.

Wenn ein kohärenter Zug Sinuswellen in die Schichten eintritt, dann finden unendlichmaligen Refraktionen und Reflektionen an jeden Unstetigkeitsflächen statt. Wir beobachten die überlagerten Wirkungen dieser Wellen. Im folgenden bedeutet die erste Nachsilbe die Nummer

1) *Z. B.*, G. B. LOPERT and R. R. PITTMAN, *Geophysics*, **19** (1954), 104–115.

der Schicht, die zweite Nachsilbe „1" die Welle in der Richtung des Eintrittes und die zweite „2" die Welle in der Richtung der Zurückkehrung.

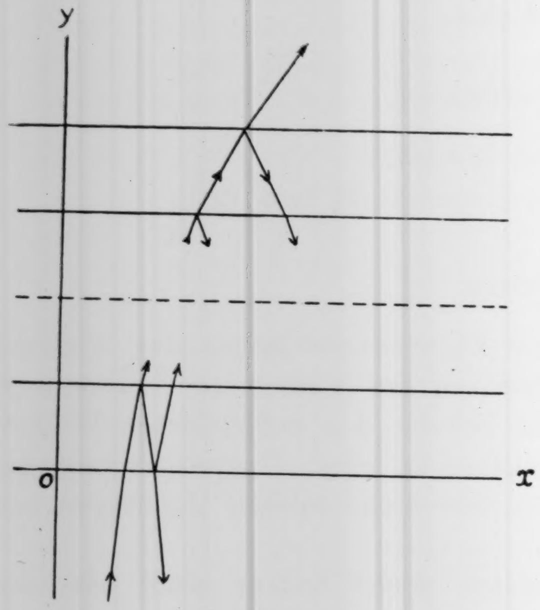

Fig. 1.

Nun

$$w_{01}=A_{01}\exp\{jk_0(l_0x+m_0y-v_0t)\}\ ,$$
$$w_{02}=A_{02}\exp\{jk_0(l_0x-m_0y-v_0t)\}\ ,$$
$$w_{11}=A_{11}\exp\{jk_1(l_1x+m_1y-v_1t)\}\ ,$$
$$w_{12}=A_{12}\exp\{jk_1(l_1x-m_1y-v_1t)\}\ ,$$
$$w_{21}=A_{21}\exp\{jk_2(l_2x+m_2y-v_2t)\}\ ,$$
$$w_{22}=A_{22}\exp\{jk_2(l_2x-m_2y-v_2t)\}\ ,$$

u.s.w.,

mit den Bedingungen

$$k_il_i=k_0l_0\ , \qquad k_iv_i=p\ .$$

Es sei

d, die Dicke der unhomogenen Schicht,

n, die Zahl der geteilten Schichten,

und

$H=\Delta d=d/n$, die Dicke der einzelnen Schicht.

Die Bedingungen an den Unstetigkeitsflächen sind wie folgt,

$$A_{01}+A_{02}=A_{11}+A_{12}\ ,$$
$$\mu_0k_0m_0(A_{01}-A_{02})=\mu_1k_1m_1(A_{11}-A_{12})\ ,$$
$$A_{11}\exp(jk_1m_1H)+A_{12}\exp(-jk_1m_1H)=A_{21}\exp(jk_2m_2H)$$
$$+A_{22}\exp(-jk_2m_2H)\ ,$$
$$\mu_1k_1m_1\{A_{11}\exp(jk_1m_1H)-A_{12}\exp(-jk_1m_1H)\}$$
$$=\mu_2k_2m_2\{A_{21}\exp(jk_2m_2H)-A_{22}\exp(-jk_2m_2H)\}\ ,$$
$$\cdots\cdots$$
$$A_{i1}\exp\{jk_im_i(iH)\}+A_{i2}\exp\{-jk_im_i(iH)\}$$
$$=A_{(i+1)1}\exp\{jk_{i+1}m_{i+1}(iH)\}+A_{(i+1)2}\exp\{-jk_{i+1}m_{i+1}(iH)\}\ ,$$
$$\mu_ik_im_i[A_{i1}\exp\{jk_im_i(iH)\}-A_{i2}\exp\{-jk_im_i(iH)\}]$$
$$=\mu_{i+1}k_{i+1}m_{i+1}[A_{(i+1)1}\exp\{jk_{i+1}m_{i+1}(iH)\}$$
$$-A_{(i+1)2}\exp\{-jk_{i+1}m_{i+1}(iH)\}]\ ,$$
$$\cdots\cdots$$

$$A_{n1}\exp\{jk_nm_n(nH)\}+A_{n2}\exp\{-jk_nm_n(nH)\}$$
$$=A_{(n+1)1}\exp\{jk_{n+1}m_{n+1}(nH)\}\ ,$$
$$\mu_nk_nm_n[A_{n1}\exp\{jk_nm_n(nH)\}-A_{n2}\exp\{-jk_nm_n(nH)\}]$$
$$=\mu_{n+1}k_{n+1}m_{n+1}A_{(n+1)1}\exp\{+jk_{n+1}m_{n+1}(nH)\}\ .$$

Die Linearität der Wellengeschwindigkeit v wird ersetzt durch

$$\frac{\Delta v}{\Delta d}=\frac{v_{n+1}-v_0}{d}\ , \qquad n\Delta d=d\ .$$

Folglich

$$\Delta l_i=\frac{k_0l_0}{p}\Delta v\ , \qquad l_i-l_0=\frac{k_0l_0}{p}i\Delta v\ , \qquad v_i=v_0+i\Delta v\ ,$$

$$l_{i+1}=l_i+\frac{l_0}{v_0}\Delta v\ ,$$

$$\mu_i=\rho v_i^2=\rho_0(v_0+i\Delta v)^2\ ,$$

unter der Voraussetzung der konstanten Dichte $\rho=\rho_0$.

Weiter

$$m_i^2=1-l_i^2=m_0^2-2\frac{k_0l_0^2}{p}(i\Delta v)-\frac{k_0^2l_0^2}{p^2}(i\Delta v)^2\ ,$$

$$m_{i+1}^2=m_i^2\left(1-2\frac{l_i\,l_0}{m_i^2}\,\frac{\Delta v}{v_0}\right),$$

$$\mu_{i+1}=\rho_0v_{i+1}^2=\mu_i\left(1+2\,\frac{\Delta v}{v_i}\right),$$

$$k_{i+1}=k_i\left(1-\frac{\Delta v}{v_i}\right).$$

Von diesen Beziehungen können wir jeden Wert am beliebigen Punkt ableiten.

Zum Beispiel, von

$$m_{i+1}-m_i=-\frac{l_il_0}{m_i}\,\frac{\Delta v}{v}\ ,$$

durch den Grenzübergang bekommt man

$$m\,dm=-l_0^2\left(1+\frac{v}{v_0}\right)\frac{dv}{v_0}\ .$$

Integriert man mit der Bedingung $m=m_0$ für $v=0$, dann ergibt sich

$$m^2=m_0^2-2l_0^2\frac{v}{v_0}\left(1+\frac{v}{2v_0}\right).$$

In ähnlicherweise bekommt man

$$km=k_0m_0\frac{v_0}{v_0+v}\exp\left\{-\left(\frac{l_0}{m_0}\right)^2\frac{v}{v_0}\left(1+\frac{v}{2v_0}\right)\right\}.$$

4. Annäherung für kleinen Eintrittswinkel.

Nun wollen wir den Fall von kleinem l_0 behandeln, und zwar l_0^2 für 1 vernachlässigen. Noch dazu beschränken wir uns auf den Fall, dass l_i immer klein bleibt.

Dann $$m \doteq 1 .$$

Folglich

$$k=k_0\frac{v_0}{v_0+v}.$$

Durch die nacheinander folgenden Iterationen bekommt man

$$A_{n1}=A_{01}-\frac{1}{2}A_{01}\left\{\sum_{i=0}^{n-1}\left(\frac{\varDelta v}{v_0+i\varDelta v}-\frac{\varDelta v}{v_0+i\varDelta v}2jk_0iH\frac{v_0}{v_0+i\varDelta v}\right)\right\}$$
$$+\frac{1}{2}A_{02}\sum_{i=0}^{n-1}\frac{\varDelta v}{v_0+i\varDelta v}\exp\left(-2jiHk_0\frac{v_0}{v_0+i\varDelta v}\right),$$

$$A_{n2}=\frac{1}{2}A_{01}\left\{\sum_{i=0}^{n-1}\frac{\varDelta v}{v_0+i\varDelta v}\exp\left(2jiHk_0\frac{v_0}{v_0+i\varDelta v}\right)\right\}+A_{02}-\frac{1}{2}A_{02}\left(\sum_{i=0}^{n-1}\frac{\varDelta v}{v_0+i\varDelta v}\right),$$

wobei Glieder von zweiten Ordnung selbst oder Summen davon vernachlässigt sind.

Durch den Grenzübergang $n\to\infty$, d.h. $\varDelta v\to 0$ bekommt man

$$A_{\infty 1}=A_{01}+\frac{1}{2}A_{01}\left\{\int_0^{v_\infty-v_0}2jk_0v_0\frac{v}{v_\infty-v_0}d\frac{dv}{(v_0+v)^2}-\int_0^{v_\infty-v_0}\frac{dv}{v_0+v}\right\}$$
$$+\frac{1}{2}A_{02}\left\{\int_0^{v_\infty-v_0}\exp\left(-2jk_0v_0\frac{v}{v_\infty-v_0}\frac{d}{v_0+v}\right)\frac{dv}{v_0+v}\right\},$$

$$A_{\infty 2}=A_{02}-\frac{1}{2}A_{02}\left(\int_0^{v_\infty-v_0}\frac{dv}{v_0+v}\right)$$
$$+\frac{1}{2}A_{01}\left\{\int_0^{v_\infty-v_0}\exp\left(2j\frac{v}{v_\infty-v_0}\frac{k_0v_0}{v_0+v}d\right)\frac{dv}{v_0+v}\right\}.$$

Die letzte Randbedingung gibt

$$A_{\infty 2}=0 .$$

Also

$$A_{02}\left(1-\frac{1}{2}\log\frac{v_\infty}{v_0}\right)+\frac{1}{2}A_{01}\left\{\int_0^{v_\infty-v_0}\exp\left(2j\frac{k_0v_0}{v_\infty-v_0}d\frac{v}{v_0+v}\right)\frac{dv}{v_0+v}\right\}=0\,.$$

Die reflektierte Welle A_{02} ergibt sich

$$A_{02}=-\frac{1}{2}I_1\frac{A_{01}}{1-\frac{1}{2}\log\frac{v_\infty}{v}}\,,$$

wo

$$I_1=\int_0^{v_\infty-v_0}\exp\left(2j\frac{k_0v_0}{v_\infty-v_0}d\frac{v}{v_0+v}\right)\frac{dv}{v_0+v}\,.$$

Hier sei es bemerkt, dass unsere Rechnung unter der Voraussetzung von kleinem $\log(v_\infty/v_0)$ ausgeführt wurde. Das ist gleichwertig, dass die Summen von Gliedern mit $(\Delta v)^2$ vernachlässigt wurden.

Die in die letzte homogene Schicht eintretende Welle ist

$$A_{\infty 1}=A_{01}+\frac{1}{2}A_{01}\left\{2jk_0v_0d\left(\log\frac{v_\infty}{v_0}-\frac{v_\infty-v_0}{v_\infty}\right)-\log\frac{v_\infty}{v_0}\right\}$$
$$+\frac{1}{2}A_{02}I_2$$

wo

$$I_2=\int_0^{v_\infty-v_0}\exp\left(-2j\frac{k_0v_0}{v_\infty-v_0}d\frac{v}{v_0+v}\right)\frac{dv}{v_0+v}\,.$$

Integrationen I_1 und I_2 enthalten

$$I_K=\int_0^{v_\infty-v_0}\cos\left(2\frac{k_0v_0}{v_\infty-v_0}d\frac{v}{v_0+v}\right)\frac{dv}{v_0+v}\,,$$

und

$$I_S=\int_0^{v_\infty-v_0}\sin\left(2\frac{k_0v_0}{v_\infty-v_0}d\frac{v}{v_0+v}\right)\frac{dv}{v_0+v}\,.$$

5. Zahlenbeispiel.

Zum Beispiel, sei

$$v_\infty=(1+0.2)v_0\,,$$

dann annäherungsweise ist das Kosinusintegral I_K gleich

$$I_K=0.1\times\frac{\sin 1.8k_0d}{k_0d}\,,$$

und das Sinusintegral I_S ist gleich

$$I_s = -0.1 \times \frac{\cos 1.8k_0d - 1}{k_0d}.$$

Nun hängt die Amplitude der reflektierten Welle ab von

$$\left\{\left(\frac{\sin 1.8k_0d}{k_0d}\right)^2 + \left(\frac{1-\cos 1.8\,k_0d}{k_0d}\right)^2\right\}^{1/2} = 2\,\frac{\sin 0.9k_0d}{k_0d}.$$

Darum können wir sehen, dass die Amplitude der reflektierten Welle von k_0d, nämlich von (Schichtdicke/Wellenlänge) abhängt. Natürlich kommt der Maximumwert vor, wenn $k_0d=0$.

Die refraktierte Welle in der letzten homogenen Schicht mag ohne weiteres ganz anschaulich sein.

---

34. Renzokuteki ni kawaru Tisô ni yoru Zisin-Nami no Hansya oyobi Kussetu.

Tikyû-Buturigaku Kyôsitu, Matuzawa Takeo.

Renzokuteki ni Seisitu no kawaru Tisô wo itiyô na usui Sô no Kasanari ni okikaete Hansya oyobi Kussetu no Nami wo keisan si, sono Kyokugen to site renzoku no Baai wo dasu.

Omona Kekka wa Hansya oyobi Kussetu no Nami no Tuyosa ga (Sô no Atusa/Hatyô) no Kansû to naru koto de aru.

---

35. *Stoneley Wave—Its Velocity, Orbit and the Distribution of Amplitude.*

By Rinzo YAMAGUCHI and Yasuo SATÔ,

Earthquake Research Institute.

(Read July 19, 1955.—Received Sept. 30, 1955.)

Introduction

About thirty years ago, Stoneley proved the possible existence of boundary waves of the Rayleigh-type being transmitted along the plane surface of separation of two solid media, and also proved that it is impossible for waves of the Love-type to be so transmitted[1].

Later, the nature of the wave, now called the Stoneley wave, was investigated by K. Sezawa and K. Kanai[2], and the range of possible existence was elucidated. But even its velocity, to say nothing of the orbit and the distribution of amplitude, has not yet been studied, although more complicated problems concerning the Rayleigh and Sezawa waves propagated in a stratified medium have been approached by a number of authors[3].

Hence, in this paper, we will give the results of our calculations concerning the said properties, and will discuss the nature and the meaning of the Stoneley wave.

Velocity

Let the axes of x and z be drawn in coincidence with and perpendicular to the surface of discontinuity, the density and elastic constants in the media on the positive and negative side of z being $\rho, \lambda, \mu; \rho', \lambda', \mu'$

---

1) R. STONELEY, "Elastic Waves at the Surface of Separation of Two Solid," *Proc. Roy. Soc. London*, **106** (1924), 416.

2) K. SEZAWA and K. KANAI, "The Range of possible Existence of Stoneley-waves and Some Related Problem," *Bull. Earthq. Res. Inst.*, **17** (1939), 1. With respect to the generation of waves in a medium consisting of two semi-infinite elastic body, K. SEZAWA and K. KANAI published another paper. "The Formation of Boundary Waves at the Surface of a Discontinuity within the Earth Crust I," *ibid.*, **16** (1938), 504.

3) e.g. K. KANAI, "On the M_2-waves (Sezawa-waves)," *Bull. Earthq. Res. Inst.*, **29** (1951), 39.

respectively. In this case the displacement potentials of the dilatational and distortional waves assume the forms

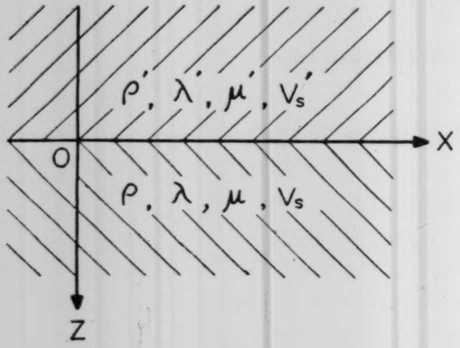

Fig. 1. We always assume the relation $\rho'<\rho$, which does not impair the generality. In the numerical calculations we also assumed the relation $\lambda=\mu$, $\lambda'=\mu'$.

$$\begin{aligned} \phi &= A \ \exp(-rz+ifx-ipt)\,, \\ \psi &= B \ \exp(-sz+ifx-ipt)\,, \\ \phi' &= A' \exp(r'z+ifx-ipt)\,, \\ \psi' &= B' \exp(s'z+ifx-ipt)\,, \end{aligned} \tag{1}$$

where

$$\begin{aligned} & r^2=f^2-h^2, \quad s^2=f^2-k^2, \\ & r'^2=f^2-h'^2, \quad s'^2=f^2-k'^2, \\ & h^2=\rho p^2/(\lambda+2\mu), \quad k^2=\rho p^2/\mu, \\ & h'^2=\rho' p^2/(\lambda'+2\mu'), \quad k'^2=\rho' p^2/\mu'. \end{aligned} \tag{2}$$

The displacements in both media are then expressed by

$$\begin{aligned} u&=\frac{\partial\phi}{\partial x}+\frac{\partial\psi}{\partial z}\,, \qquad w=\frac{\partial\phi}{\partial z}-\frac{\partial\psi}{\partial x}\,, \\ u'&=\frac{\partial\phi'}{\partial x}+\frac{\partial\psi'}{\partial z}\,, \quad w'=\frac{\partial\phi'}{\partial z}-\frac{\partial\psi'}{\partial x}\,. \end{aligned} \tag{3}$$

Since the two media are continuous, the boundary conditions which must be satisfied at the surface of separation are the continuity of the displacements and the stress, viz.,

$$\begin{aligned} & u=u', \\ & w=w', \\ & \mu\Big(\frac{\partial w}{\partial x}+\frac{\partial u}{\partial z}\Big)=\mu'\Big(\frac{\partial w'}{\partial x}+\frac{\partial u'}{\partial z}\Big)\,, \\ & \lambda\Big(\frac{\partial u}{\partial x}+\frac{\partial w}{\partial z}\Big)+2\mu\frac{\partial w}{\partial z}=\lambda'\Big(\frac{\partial u'}{\partial x}+\frac{\partial w'}{\partial z}\Big)+2\mu'\frac{\partial w'}{\partial z}\,. \end{aligned} \tag{4}$$

Putting (1) and (3) into (4), we get

$$\begin{aligned} & ifA-sB-ifA'-s'B'=0\,, \\ & rA+ifB+r'A'-ifB'=0\,, \\ & i2\mu rfA-\mu(f^2+s^2)B+i2\mu'r'fA'+\mu'(f^2+s'^2)B'=0\,, \\ & (-\lambda h^2+2\mu r^2)A+i2\mu sfB+(\lambda'h'^2-2\mu'r'^2)A'+i2\mu's'fB'=0\,. \end{aligned} \tag{5}$$

Thus the velocity equation of the wave transmitted along the boundary

surface under consideration is

$$\begin{vmatrix} if & -s & -if & -s' \\ r & if & r' & -if \\ i2\mu rf & -\mu(f^2+s^2) & i2\mu' r' f & \mu'(f^2+s'^2) \\ -\lambda h^2+2\mu r^2 & i2\mu sf & \lambda' h'^2-2\mu' r'^2 & i2\mu' s' f \end{vmatrix} = 0 \qquad (6)$$

Assuming various values of ρ'/ρ and putting them into the above equation, we calculated the relation between $(V/V_s)^2$ and μ'/μ. Here we can assume, without losing generality, that the condition $\rho' < \rho$ holds. Further, we employed the assumption that λ and λ' are always equal to μ and μ' respectively.

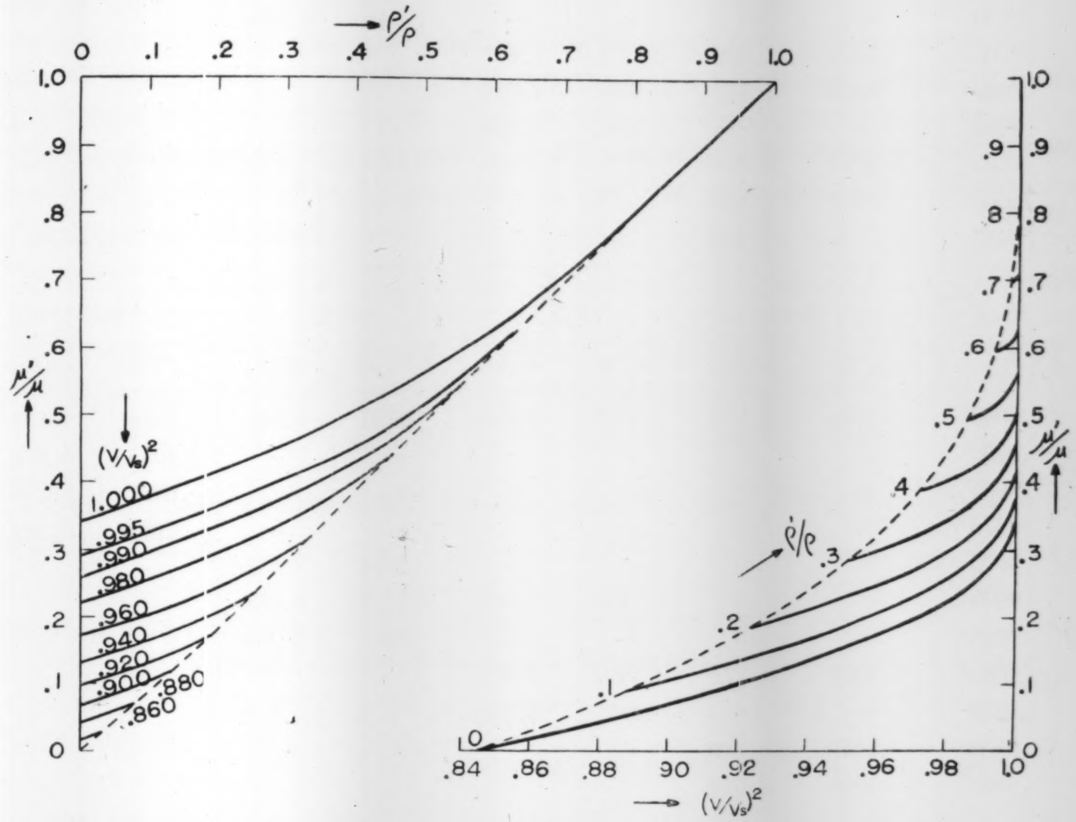

Fig. 2. The relation between ρ'/ρ, μ'/μ and $(V/V_s)^2$. V being the velocity of Stoneley wave. Above two figures have the same content, only the parameter and the abscissa are interchanged. On the broken lines V is equal to V_s'. In the right figure the parameter is ρ'/ρ, the value of which is given on the left and of the full lines. $\rho'/\rho=0$, $\mu'/\mu=0$ gives the Rayleigh wave.

The results of the calculation are given in Table I, and illustrated in Fig. 2.

Table I. The values of μ'/μ and w_0/u_0 when the conditions ρ'/ρ and $(V/V_s)^2$ are given. (w_0 and u_0 are the vertical and horizontal displacements at the plane of separation.)

ρ'/ρ → / $(V/V_s)^2$ ↓	0		0.1		0.2		0.3	
	μ'/μ	w_0/u_0	μ'/μ	w_0/u_0	μ'/μ	w_0/u_0	μ'/μ	w_0/u_0
1.0000	.3435	1.608	.3772	1.685	.4153	1.789	.4579	1.932
.9900	—	—	—	—	—	—	.3766	1.977
.9800	.2221	1.592	.2559	1.678	.2955	1.800	.3425	1.999
.9600	.1710	1.575	.2043	1.659	.2449	1.799	.2965	2.066
.9519	—	—	—	—	—	—	.2856	2.164
.9400	.1312	1.555	.1646	1.643	.2070	1.803		
.9240	—	—	—	—	.1848	1.864		
.9200	.0976	1.535	.1311	1.627				
.9000	.0680	1.517	.1024	1.619				
.8882	—	—	.0888	1.638				
.8800	.0414	1.499						
.8600	.0169	1.480						
.8453	0	1.468						

ρ'/ρ → / $(V/V_s)^2$ ↓	0.4		0.5		0.6		0.7	
	μ'/μ	w_0/u_0	μ'/μ	w_0/u_0	μ'/μ	w_0/u_0	μ'/μ	w_0/u_0
1.0000	.5065	2.138	.5625	2.458	.6290	3.011	.7088	4.104
.9990	—	—	—	—	—	—	.7005	4.805
.9980	—	—	—	—	—	—	.6987	5.220
.9978	—	—	—	—	—	—	.6984	5.389
.9975	—	—	—	—	.6046	3.432		
.9950	—	—	.5160	2.690	.5978	3.758		
.9935	—	—	—	—	.5961	3.986		
.9900	.4307	2.271	.4997	2.876				
.9854	—	—	.4927	3.139				
.9800	.4015	2.379						
.9720	.3888	2.570						

ρ'/ρ → / $(V/V_s)^2$ ↓	0.8		0.9		1.0	
	μ'/μ	w_0/u_0	μ'/μ	w_0/u_0	μ'/μ	w_0/u_0
1.00000	.8013	6.648	.90005	14.73	1.00000	∞
.99997	—	—	.89997	16.27		
.9998	.8000	7.485				
.9995	.7996	8.141				

Orbit

When the characteristic equation (6) holds, only three of the four equations in the expression (5) are independent, so we selected the upper three.

$$
\begin{aligned}
ifA - sB - ifA' - s'B' &= 0 , \\
rA + ifB + r'A' - ifB' &= 0 , \\
i2\mu rfA - \mu(f^2+s^2)B + i2\mu' r' f A' + \mu'(f^2+s'^2)B' &= 0 .
\end{aligned}
\tag{7}
$$

The amplitude constants A, B and A', B' can be then written as follows:

$$
\begin{aligned}
A &= K\Delta_A , \quad & B &= K\Delta_B , \\
A' &= K\Delta_{A'} , \quad & B' &= K\Delta_{B'} .
\end{aligned}
\tag{8}
$$

In these expressions Δ_A, Δ_B and $\Delta_{A'}$, $\Delta_{B'}$ are the minor determinants made by the coefficients of A, B and A', B' in the equation (7). They may be written as follows:

$$
\begin{aligned}
\Delta_A &= \mu(f^2 - r's')(f^2+s^2) - \mu'(f^2+r's)(f^2+s'^2) + 2\mu' r' f^2 (s+s') , \\
\Delta_B &= -if\{\mu'(r+r')(f^2+s'^2) - 2\mu r(f^2 - r's') - 2\mu' r'(f^2+rs')\} , \\
\Delta_{A'} &= \mu(f^2+rs')(f^2+s^2) - \mu'(f^2 - rs)(f^2+s'^2) - 2\mu r f^2 (s+s') , \\
\Delta_{B'} &= -if\{\mu(r+r')(f^2+s^2) - 2\mu' r'(f^2 - rs) - 2\mu r(f^2+r's)\} .
\end{aligned}
\tag{9}
$$

Using these expressions, we can describe the displacements in both media as follows:

$$
\begin{aligned}
u &= K(\Delta_A \, if \, e^{-rz} - \Delta_B \, s \, e^{-sz}) \cdot \exp(ifx - ipt) , \\
w &= K(-\Delta_A \, r \, e^{-rz} - \Delta_B \, if \, e^{-sz}) \cdot \exp(ifx - ipt) , \\
u' &= K(\Delta_{A'} \, if \, e^{r'z} + \Delta_{B'} \, s' \, e^{s'z}) \cdot \exp(ifx - ipt) , \\
w' &= K(\Delta_{A'} \, r' \, e^{r'z} - \Delta_{B'} \, if \, e^{s'z}) \cdot \exp(ifx - ipt) .
\end{aligned}
\tag{10}
$$

Taking the real part,

$$
\begin{aligned}
u &= K(\Delta_A f \, e^{-rz} + \Delta_B \, is \, e^{-sz}) \sin(pt - fx) , \\
w &= K(-\Delta_A \, r \, e^{-rz} - \Delta_B \, if \, e^{-sz}) \cos(pt - fx) , \\
u' &= K(\Delta_{A'} f \, e^{r'z} - \Delta_{B'} \, is' \, e^{s'z}) \sin(pt - fx) , \\
w' &= K(\Delta_{A'} \, r' \, e^{r'z} - \Delta_{B'} \, if \, e^{s'z}) \cos(pt - fx).
\end{aligned}
\tag{11}
$$

The ratio of the displacements u and w at $z=0$ is

$$\frac{w_0}{u_0}=\frac{r_1(1-r_1's_1')(V/V_s)^2+r_1'(1-r_1s_1)(\rho'/\rho)(V/V_s)^2}{2(1-\mu'/\mu)(1-r_1s_1)(1-r_1's_1')-(1-r_1's_1')(V/V_s)^2+(1-r_1s_1)(\rho'/\rho)(V/V_s)^2}, \tag{12}$$

where the quantities with suffix 1 have the following meaning:

$$r_1=r/f=\sqrt{1-V^2/\gamma^2V_s^2}, \qquad s_1=s/f=\sqrt{1-(V/V_s)^2},$$
$$r_1'=r'/f=\sqrt{1-(V^2/\gamma'^2V_s^2)(\rho'/\rho)(\mu/\mu')}, \quad s_1'=s'/f=\sqrt{1-(V/V_s)^2(\rho'/\rho)(\mu/\mu')}, \tag{13}$$

(when $\lambda=\mu$ and $\lambda'=\mu'$, $\gamma^2=\gamma'^2=3$)

We put various values of ρ'/ρ, μ'/μ and $(V/V_s)^2$ which satisfy the condition (6) into the above expressions and performed the calculation. The results are shown in Fig. 3. In this figure, the ordinate is the ratio w_0/u_0, the abscissa is the square of the velocity of the Stoneley wave measured by the unit V_s, while the parameter is the ratio of the densities of the two media. The numerical values are tabulated in Table I. From the sign of the ratio we can infer the direction of the rotation of orbit which is shown in Fig. 4.

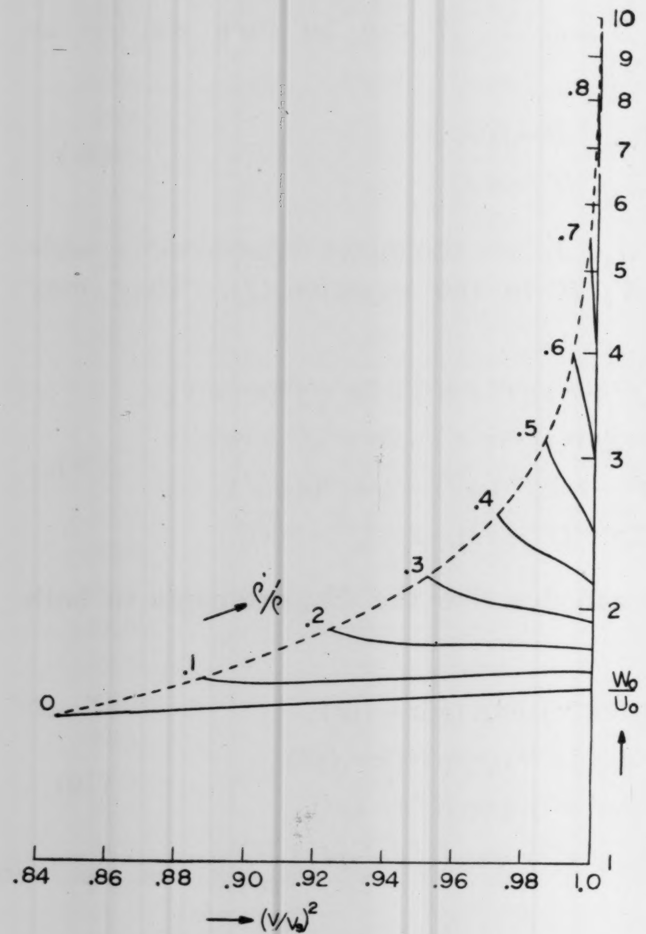

Fig. 3. Ratio of the amplitude of vertical and horizontal displacements at the boundary surface. Numbers beside the broken line are the parameter ρ'/ρ. On the broken line V is equal to V_s'.

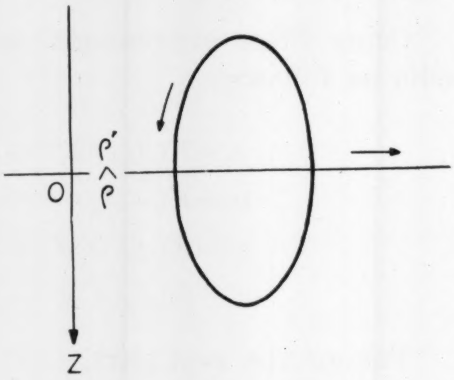

Fig. 4. The direction of the rotation of particle orbit at the surface of separation of two media.

Distribution of Amplitude

We also studied the distribution of amplitude at different depths. Using the equation (11), the horizontal and vertical displacements in both media are calculated corresponding to the given values of z/L. (L implies wave length.) The results are shown in Figs. 5–13. (In these figures the vertical displacement at $z=0$ is taken as unit.)

Conclusion

1. In the previous sections we have tried to elucidate the relation between ρ'/ρ, μ'/μ and $(V/V_s)^2$. If two of the above three quantities are given, we can obtain the remaining one using Fig. 2. This study also makes clear that the Rayleigh wave (the velocity of which is equal to $\sqrt{0.8453\cdots\cdots}\cdot V_s$) is the limiting case of the Stoneley wave in which the values ρ'/ρ and μ'/μ both tend towards zero. (See Fig. 2.)

2. We next considered the ratio of the amplitude of vertical and horizontal displacements at $z=0$. When $(V/V_s)^2=0.8453\cdots$ the ratio w_0/u_0 gives the minimum value and is equal to that of the Rayleigh wave ($1.468\cdots$). As the parameter ρ'/ρ increases, so does the ratio w_0/u_0. These properties can be seen from Fig. 3. When the parameter ρ'/ρ approaches to unity the change of the value of w_0/u_0 becomes very remarkable, because the horizontal displacement becomes small and finally vanishes when ρ' becomes equal to ρ.

3. The sence of the rotation of particle orbit at the surface of separation of two media is determined easily by means of the expression (11). With respect to the denser medium (the lower one), the sense of rotation is the same with that of the Rayleigh wave, consequently it is reverse with regard to the upper medium. (See Fig. 4.)

In the aspect of the distribution of the amplitude, we also find a feature similar to that of the Rayleigh wave in the lower denser medium, excluding the case when V/V_s is nearly equal to 1. Of course the Rayleigh wave is the limiting case of $\rho'/\rho\to 0$ and $\mu'/\mu\to 0$ (V tends towards V_s'). (See Figs. 2 and 11.) The general tendency can be seen in Figs. 5–13.

4. Lastly we will consider the significance of the Stoneley wave a little. The Stoneley wave is a wave propagated along the surface of separation of two semi-infinite medium and has the type $\left[\frac{EE}{EE}\right]$[4].

4) Y. SATô, "Study on Surface Waves XI. Definition and Classification of Surface Waves," *Bull. Earthq. Res. Inst.*, **32** (1954), 161.

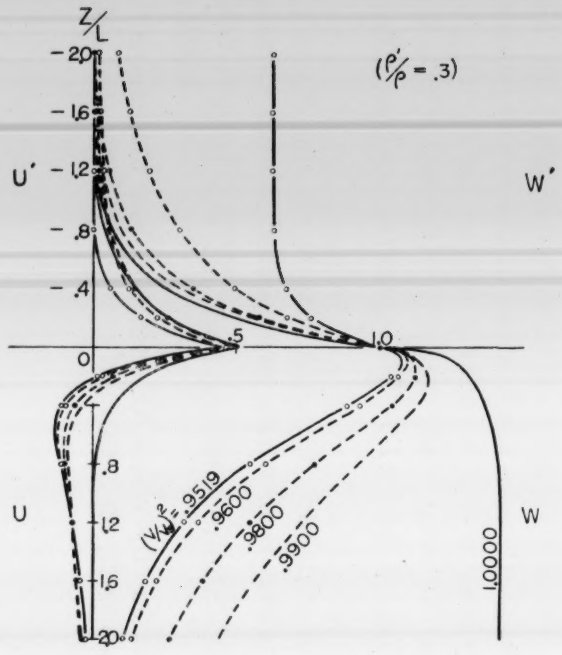

Fig. 5.

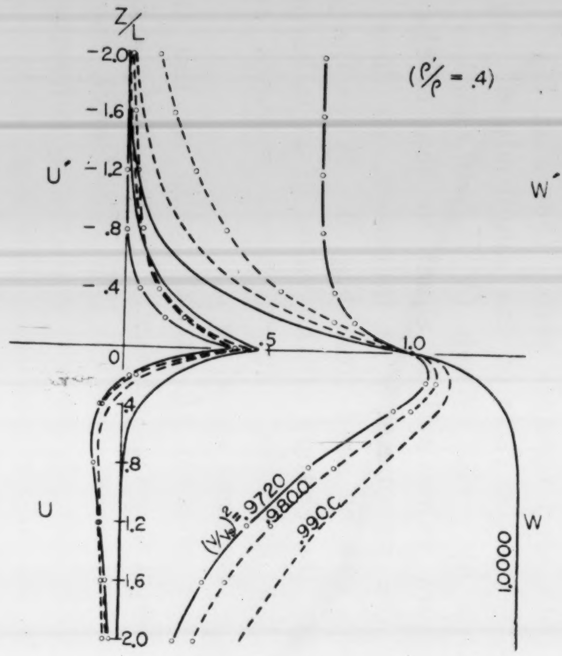

Fig. 6.

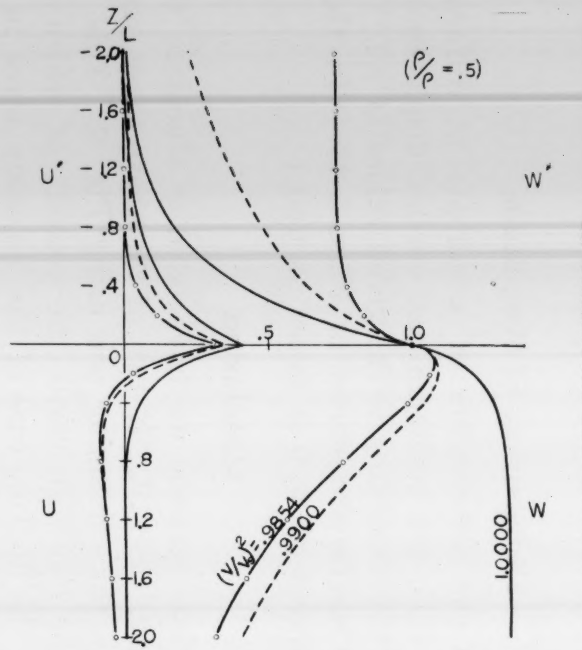

Fig. 7.

Distribution of the amplitude U, U' (horizontal component) and W, W' (vertical component) when $\rho'/\rho=0.3$, 0.4 and 0.5. In these figures the vertical displeasement at $z=0$ is taken as unit.

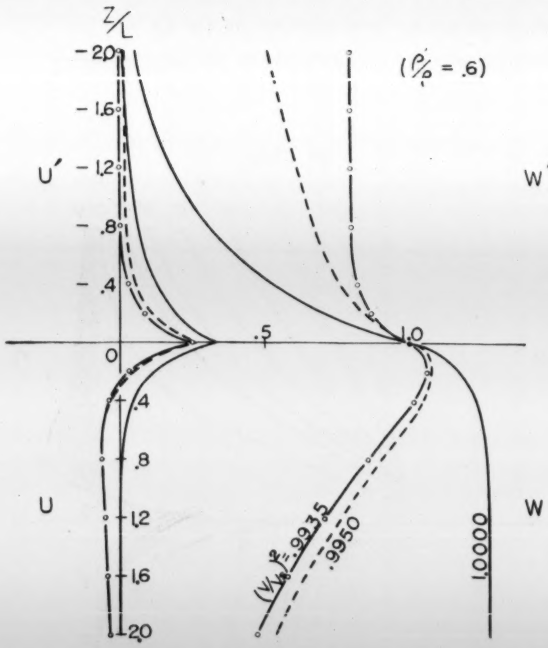

Fig. 8.

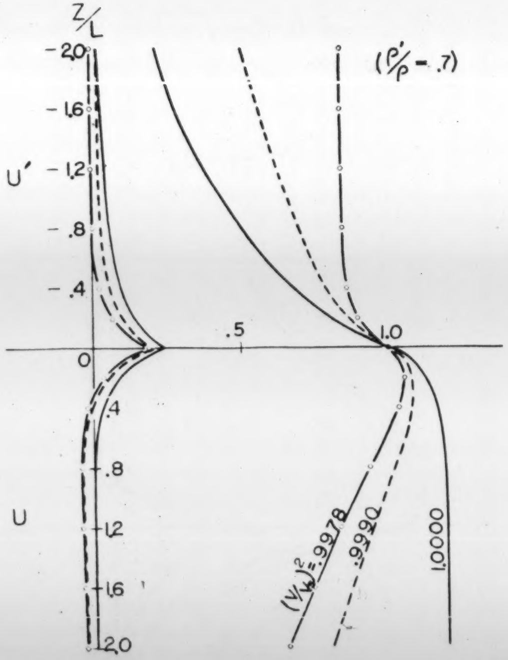

Fig. 9.

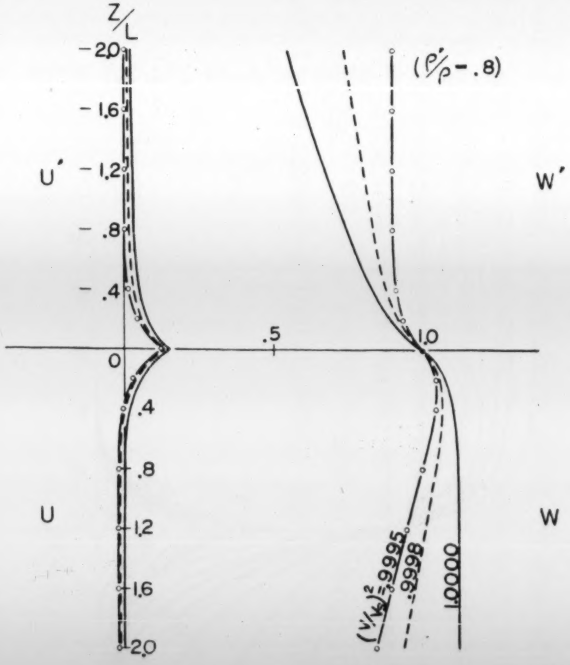

Fig. 10

Distribution of amplitude U, U' (horizontal component) and W, W' (vertical component) when $\rho'/\rho=0.6$, 0.7 and 0.8. In these figures the vertical displacement at $z=0$ is taken as unit.

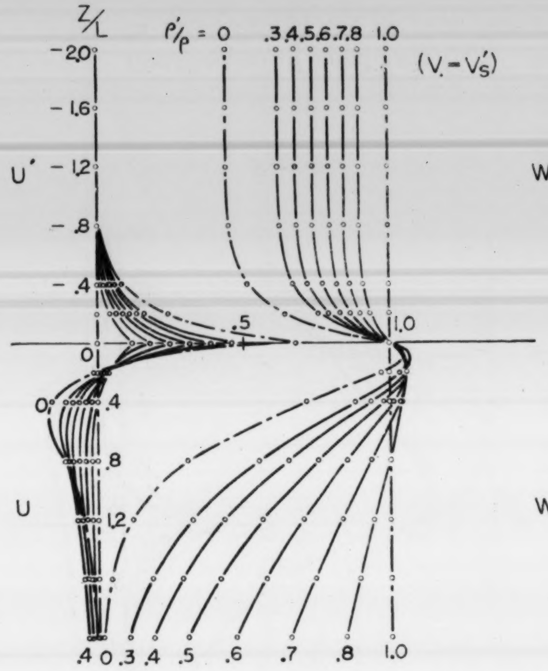

Fig. 11.

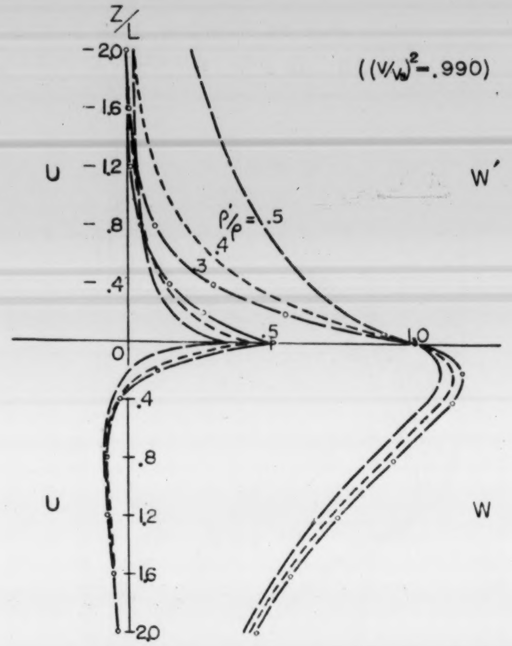

Fig. 12.

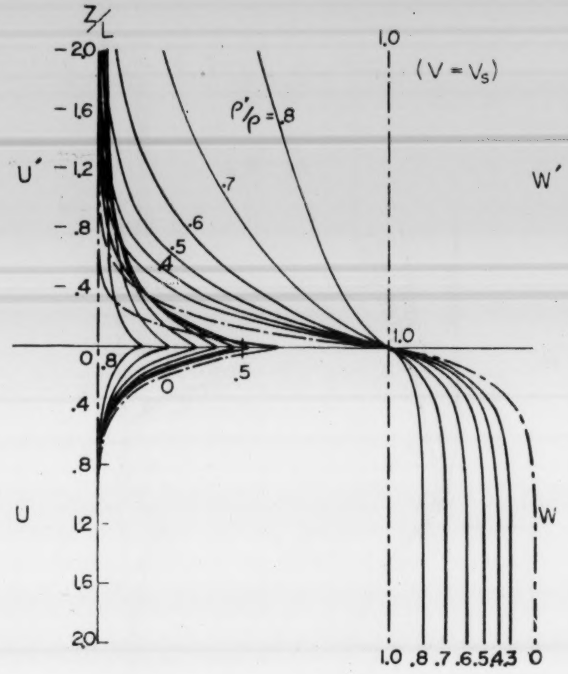

Fig. 13.

Distribution of amplitude U, U' (horizontal component) and W, W' (vertical component) when $V=V_s'$, $(V/V_s)^2=0.990$ and $V=V_s$. In these figures the vertical displacement at $z=0$ is taken as unit.

Consequently it cannot practically exist in the strict sense. Therefore, when the term "Stoneley wave" is used with reference to a stratified medium, the authors are of opinion that it should stand for the phenomenon that approximately shows the properties of the Stoneley wave, because the thickness of the layer is sufficiently large compared with the wave length. Such a wave, however, can hardly be observed unless we install the measuring instruments deeply in the ground.

---

35. Stoneley 波——その速度，軌道及び振巾の分布

地震研究所 {山口林造 / 佐藤泰夫}

1. 今日 Stoneley 波と名づけられている表面波の可能性について，初めて論文が書かれてから既に 30 年以上を経過する．

その後，妹沢・金井らによつて存在限界についての議論はなされたが，速度・軌道・振幅の分布等については未だに手が着けられていない．本研究はこの欠を補う為になされたものである．

2. 速度．速度方程式は既に得られているが，この式によつて決定される ρ'/ρ，μ'/μ と $(V/V_s)^2$ の関係を求めた．(ρ, ρ'; μ, μ'; V_s は慣用の意味を持つ． V は Stoneley 波の速さ．第 1 図参照.) 即ち，存在限界の範囲内において，ρ'/ρ と μ'/μ を与えれば V/V_s が，ρ'/ρ，μ'/μ の一方と V/V_s とを与えれば残りの一つの量が求められる．(第 2 図.)

3. 軌道．速度方程式が成立つ場合，境界面における変位は容易に計算する事ができる．上下，水平両成分の振幅を計算して，その比 (第 3 図) 及び軌道の回転方向 (第 4 図) を求めた．

上下動と水平動の比は $\rho'/\rho\to 0$, $\mu'/\mu\to 0$ の時 (即ち Rayleigh 波) が最も小さくて 1.468…,他の場合にはこれより大きくなる．ρ'/ρ が大きくなるとこの値は急激に増し，又 V/V_s の変化に伴う変動も急になる．軌道の回転方向は密度の大きい方の媒質に関して常にレーリー波と同じ，従つて軽い方の媒質に関しては逆になる．

4. 振幅の分布．既に求めた計算式によつて，境界面から離れるに伴つて振幅が変る状態をも求める事ができる．(第 5~13 図) 図に見られるように，V/V_s が 1 に極めて近い場合をのぞき重い方の媒質内の分布は，Rayleigh 波と似た点がすくなくない．当然の事ながら，$\rho'/\rho\to 0$，$\mu'/\mu\to 0$ とすると Rayleigh 波の振幅分布に近づく．(第 11 図)

5. Stoneley 波の意義．Stoneley 波は二つの半無限体の境界にそつて伝わる波であり，$\left[\frac{EE}{EE}\right]$ なる型を持つ．従つて厳密な意味で現実には成立ちがたい．時に表面層を持つ構造内に於いても "Stoneley 波" なる言葉が使用されるが，これは層が十分あつくて，自由表面の影響が無視しうる時に，近似的に成立つ現象に附せらるべき名称と解すべきであろう．但し，観測は地下深い境界面の附近に限られ，一般にはその機会に乏しいと考えられる．

36. *Model Experiments of Electromagnetic Induction within the Earth.*

By Takesi NAGATA, Takasi OGUTI and Hideo MAEKAWA,

Geophysical Institute.

(Read June 28, 1955.—Received Sept. 30, 1955).

Summary

This is a supplementary note to Rikitake-Yokoyama's paper "The Anomalous Behaviour of Geomagnetic Variations of Short Period in Japan and Its Relation to the Subterranean Structure". It is shown that model experiments are very useful for solving problems of electromagnetic induction within the earth, especially in the cases of complicated distribution of electric conductivity. By means of the model experiments, the problem of anomalous distribution of induced subterranean electric currents in the vicinity of Japan, which was pointed out by Rikitake and Yokoyama, was studied with the result that a possible subterranean distribution of electric conductivity responsible for the said anomalous currents may be something like that shown in Fig. 3.

1. Introduction

It has long been noticed that transient variations in the geomagnetic field on the earth's surface consist of the external part which originates in the outside of the earth, say the ionized upper atmosphere, and the internal part which is induced within the earth by the external part. The latter is due to electromagnetic induction within the electrically conductive earth. We may then be able to find the subterranean distribution of electric conductivity by analyzing the distribution of various geomagnetic variations over the earth's surface. Studies on the electric behaviour of the earth along this line have been developed with fruitful results by S. Chapman[1),2)], A. T. Price[3),4),5),6),7)] and their colleagues, and

---

1) S. CHAPMAN and A. T. PRICE, *Phil. Trans. Roy. Soc. London, A,* **229** (1930), 427.
2) S. CHAPMAN and T. T. WHITEHEAD, *Trans. Cambr. Phil. Soc.,* **22** (1922), 463.
3), 4) A. T. Price, *Proc. London Math. Soc., Ser.* 2, **31** (1930), 217; **33** (1931), 233.
5) B. N. LAHILI and A. T. PRICE, *Phil. Trans. Roy. Soc. London, A,* **237** (1939), 509.
6) A. T. PRICE, *Quart. Journ. Mech. Appl. Math.,* **2** (1948), 3.
7) A. A. ASHOUR and A. T. PRICE, *Proc. Roy. Soc. A,* **195** (1948), 198.

have recently been carefully revised and extended by T. Rikitake[8),9),10),11)]. The main purpose of their studies is to find the average distribution of electric conductivity along the earth's radius, though they sometimes took into account the effect of the oceans.

Thus, so far as the uppermost part of the earth about 2000 *km* thick is concerned, it seems likely that a fairly reliable knowledge of change in the average electric conductivity with depth has been obtained.

However a question still remains to be solved in connection with the problem of electromagnetic induction within the earth, namely the remarkable heterogeneity of lateral distribution of the internal parts of short period variations in the geomagnetic field. Since the internal part of the shorter period variations is subject to the conductivity of the shallower parts of the earth, the said heterogeneity ought to be mainly due to some heterogeneous distribution of electric properties of the earth's upper part. One of the most striking results of this study is that obtained recently by T. Rikitake and I. Yokoyama[12),13),14),15),16),17),18)]. In their studies, Rikitake and Yokoyama have concluded that the internal electric currents induced within the earth by eastward external electric currents of short duration are eastward in the south-east parts of Japan, though in the other parts of her neighbourhood the corresponding internal currents flow westwards as usually expected from the simple theory of electromagnetic induction.

This result may suggest the presence of a very abnormal distribution of subterranean electric conductivity in the above-mentioned area of Japan. If the reason why such an abnormal phenomenon takes place is made clear from the viewpoint of the electromagnetic induction theory, it would give us an important information as to the physical structures of the earth's upper part.

Mathematical procedures of calculating the induced electric currents in the earth having heterogeneous distribution of electric conductivity are so difficult and complicated, especially for transient phenomena, that only several problems of specially simple cases have been solved hitherto. There should be, however, an alternative method of attacking this problem with the aid of model experiments. This short note gives some

8), 9) T. RIKITAKE, *Bull. Earthq. Res. Inst.*, **28** (1950), 45; **28** (1950), 219.

10), 11) T. RIKITAKE, *ibid.*, **29** (1951), 263; **29** (1951), 539.

12)–16) T. RIKITAKE, I. YOKOYAMA and Y. HISHIYAMA, *ibid.*, **30** (1952), 207; **31** (1953), 19; **31** (1953), 89; **31** (1953), 101; **31** (1953), 119.

17) T. RIKITAKE and I. YOKOYAMA, *Bull. Earthq. Res. Inst.*, **33** (1955), 297.

18) T. RIKITAKE and I. YOKOYAMA, *Journ. Geomag. Geoelectr.*, **5** (1953), 59.

results of such experimental researches, which seem to be promising in this field of research.

The Earthquake Research Institute has been interested in electric and magnetic phenomena in the solid earth since some twenty years ago. This is because these phenomena can show us additional, and sometimes very useful, information about the physical conditions of the earth's crust and interior, even in connection with earthquake and volcanic phenomena. One of the authors (T.N.) fortunately had the honour to join the research group of geoelectricity and geomagnetism in this Institute in the earliest stage of the research. This short note is dedicated to this world-wide known research institute of solid geophysics on its 30th anniversary.

2. Model Experiments of Electromagnetic Induction within the Earth

When a phenomenon of electromagnetic induction is sufficiently slowly changing, it is considered to be quasi-stationary, the displacement currents being neglected. In such a case the general equations of electromagnetic induction within a body of σ and μ in electric conductivity and magnetic permeability are given by

$$\mathrm{curl}\,\boldsymbol{E} = -\frac{\partial \boldsymbol{B}}{\partial t}\,, \qquad \boldsymbol{i} = \sigma \boldsymbol{E}\,, \qquad \boldsymbol{B} = \mu \boldsymbol{H}\,, \tag{1}$$

where generally σ is not uniform being expressed by

$$\sigma = \sigma_0 f\,, \tag{2}$$

f being a normalized function of coordinates. Now, the coordinates are taken as the spherical ones (r, θ, φ), with which the surface of the conductive sphere concerned is expressed by $r=a$. Let us further consider such a normalized spherical coordinate system as expressed by $(r/a, \theta, \varphi)$, and let the curl with respect to this normalized coordinate system be denoted by curl_0. Then

$$\mathrm{curl} = \frac{1}{a}\,\mathrm{curl}_0 \tag{3}$$

Putting (2) and (3) into (1), we get

$$\mathrm{curl}_0(\boldsymbol{i}/f) = -a\sigma_0 \frac{\partial}{\partial t} \boldsymbol{B}\,. \tag{4}$$

It is thus shown that the relation between changes in magnetic induction $\boldsymbol{B}$ and distribution of electric currents induced into the spherical conductor of $\sigma_0 f$ in conductivity is uniquely determined, provided that $a\sigma_0 \frac{\partial}{\partial t}$ is kept constant. In other words, the law of similitude in the case of electromagnetic induction within a spherical conductor is given by

$$a\sigma_0 p = \text{invariant}\,, \tag{5}$$

where p denotes the operator of time derivative $\frac{\partial}{\partial t}$ as usual.

Thus the electrically conductive earth can be represented by a metallic sphere or spherical shell of a suitable dimension. Changes in magnetic field owing to the presence of this conductive sphere are estimated by measuring the time derivative $\frac{\partial \boldsymbol{H}}{\partial t}$ of the radial component of the field over the spherical surface by means of a search coil 9 *mm* in effective radius and 3×10^{-5} *sec.* in time constant. The change of output electromotive force of the search coil is given as a curve on a cathode ray oscilloscope. Such measurements were carried out at a large number of points over the spherical surface, and their results were compared with those of similar measurements carried out at the same point without the conductive sphere. The difference of the former curves from the latter ones represents the time derivative of the secondary magnetic field caused by the electric currents induced within the sphere. Therefore, integration of the difference curve can give the change with time of the secondary field.

3. Effect of a Semi-Spherical Ocean on the Electromagnetic Induction within the Earth

In all the experiments mentioned below, the external magnetic field is almost uniform in the space occupied by the model earth, and the intensity of uniform magnetic field $\boldsymbol{H}$ is expressed by

$$\boldsymbol{H} = \boldsymbol{H}_0(1 - e^{-t/t_0})\,,$$

where t_0 is actually 10^{-3} *sec.* That is to say, the type of change of the external magnetic field is nearly similar to that of the sudden commencement of magnetic storms.

In order to check the reliability of the model experiment, the electromagnetic induction within a spherical shell of uniform conductivity was

first measured and the result was compared with a theoretical estimation[19]. The degree of agreement of the observed changes with the theoretical ones is satisfactory so far as the charges during $t=0\sim4\,m\,sec.$ are concerned. It seems likely that the discrepancy between the experiment and the theory in the later stages ($t>4\,m\,sec.$) is chiefly due to accumulation of the errors in the process of numerical integration.

Now, one of the chief causes of the anomalous phenomenon of electromagnetic induction within the earth in the vicinity of Japan may be the effect of the electrically conductive ocean, since Japan Islands are situated at the north-western margin of the Pacific Ocean. For the purpose of demonstrating the said effect of the ocean, electromagnetic induction within a semi-spherical shell was experimentally studied.

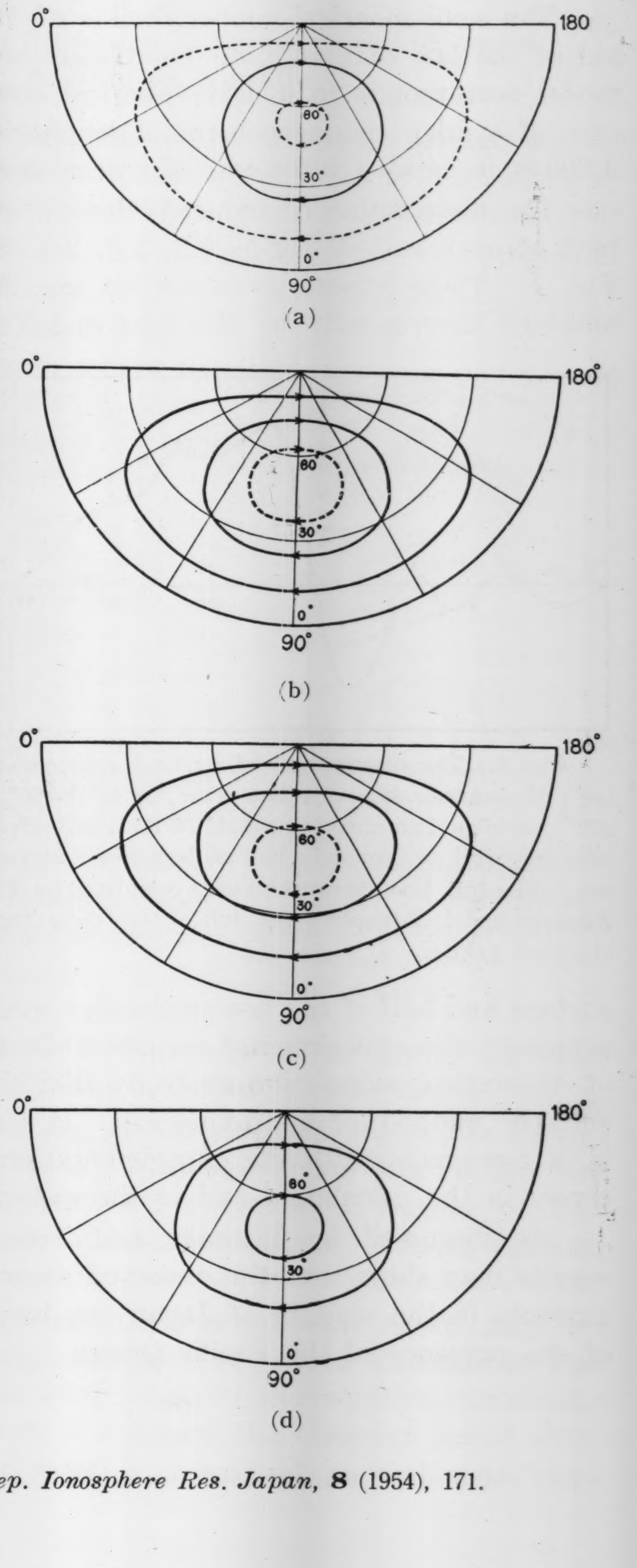

Fig. 1. The distribution of induced electric currents in the northern half part of semi-spherical shell for $t=0.3$, 1.0, 2.0 and 3.0 *m sec.*, viewed from North Pole. Electric currents of about 1 *amp.* flow between successive full stream lines and about 0.5 *amp.* between successive full and broken lines.

19) T. OGUTI and T. NAGATA, *Rep. Ionosphere Res. Japan,* **8** (1954), 171.

The semi-spherical copper shell is of 1.5 *mm* in thickness. With the aid of the law of similitude mentioned before, it was found that this model corresponds to a semi-spherical ocean of 170 *m* in depth for the case of sudden commencement of magnetic storms, and to that of about 4,000 *m* in depth for the case of a geomagnetic bay of 2 hours in duration.

The distribution of induced electric currents in the northern half part of such a shell for $t=0.3$, 1.0, 2.0 and 3.0 *m sec.* is illustrated in Fig. 1. These experimental results are in good agreement with those obtained theoretically by Rikitake and Yokoyama[17]. Our problem here is concerned with the mode of change in the magnetic field outside this spherical shell, because the continental part where we have magnetic stations may be represented by the non-conductive semi-spherical surface and the ocean by the conductive shell.

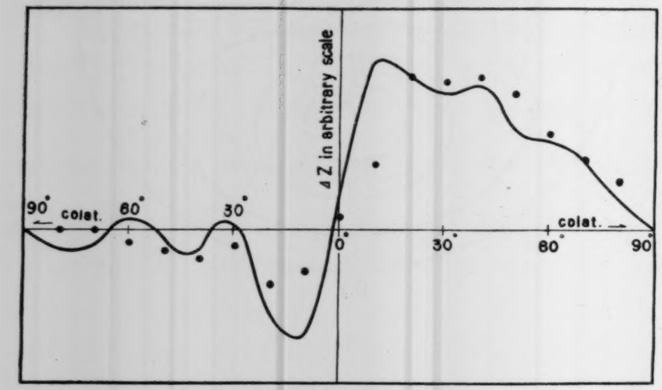

Fig. 2. The distribution of vertical component (ΔZ) of magnetic force for $t=2$ *m sec.* along the 90°–270° meridian line covering a half of the conductive semi-spherical surface and a half of the non-conductive one. The full line shows the result calculated by T. Rikitake and I. Yokoyama and full circles show the observed values.

Fig. 2 shows the distribution of vertical component (ΔZ) of magnetic force at $t=2$ *m sec.* along the 90°–270° meridian line (*cf.* Fig. 1) covering half of the conductive semi-spherical surface and half of the non-conductive one. In this figure, the full circles represent the experimental results while the full line shows the result of theoretical calculation made by Rikitake and Yokoyama[17] through a suitable method of approximation. It seems that the theoretical result is in agreement with the experimental one within the limit of probable errors in the calculation and in the experiment.

As discussed by Rikitake and Yokoyama[17] in their paper, these results may show that the observed anomaly of the subterranean electric currents in the vicinity of Japan can hardly be attributed to any effect of the presence of the Pacific Ocean.

4. Probable Subterranean Structure Responsible for Observed Geomagnetic Anomalous Variation

Under the circumstances mentioned in the preceding section, a possible explanation may be that some particular distribution of high electric conductivity in the earth's crust or the upper part of the earth's mantle is responsible for the observed anomalous distribution of geomagnetic variations. This interpretation may be justified, as pointed out by Rikitake and Yokoyama also, by considering that the region where the anomaly is observed is near the Fuji (Huzi) Volcanic Zone under which magma of high temperature and high conductivity may be distributed in a fairly complex form.

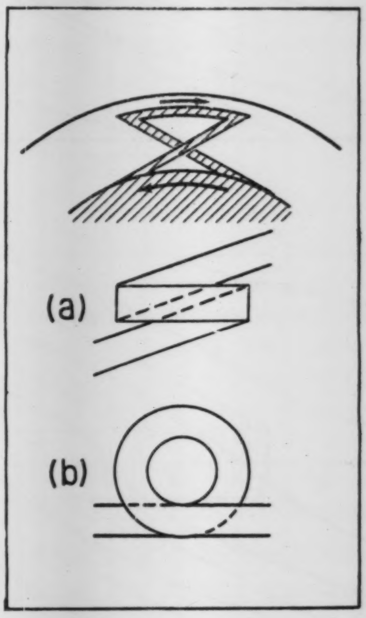

Fig. 3. Proposed subterranean structures responsible for observed geomagnetic anomalous variation.

After several trials along this line of study, we have been led to conclude so far that only a considerable distribution of high electric conductivity, from the viewpoint of electromagnetic induction, will be such as schematically illustrated in Fig. 3, namely, an upheaved zigzag circuit (a) or an upheaved loop (b). In these cases, a part of the general westward currents induced in the major parts of the earth's interior may be forced to pass through this branch circuit, and the electric currents passing through this branch in the opposite direction may have a predominant effect on the observed geomagnetic field because of its shorter distance from the earth's surface. Fig. 4 shows examples of experimental results for $t=0.3$, 1.0, 2.0, 3.0 and 4.0 *m sec.* in the case (a), where the zigzag belt of copper is 1.5 *mm* in thickness. Although in the later stages we can see slight eastward currents around the centre of locality of the upheaved zigzag belt, this tendency of local inversion of induced current is still much smaller than that actually observed in the vicinity of Japan.

It must be taken into consideration, however, that there may be some ambiguity about the absolute intensity of general currents in the case of the analysis of a regional distribution of geomagnetic variations. If so, it may be rather reasonable to compare the observed result with the experimental one in which a suitable amount of general zonal cur-

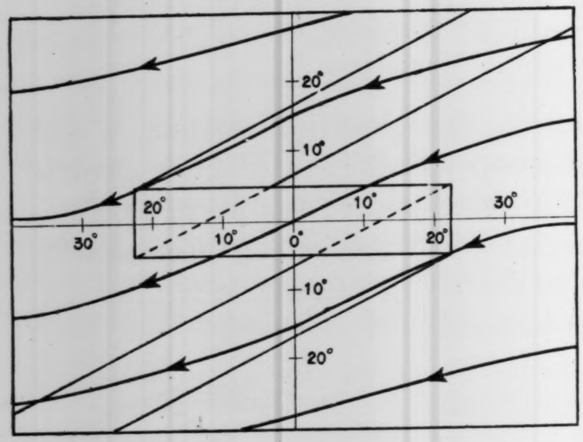

(a)

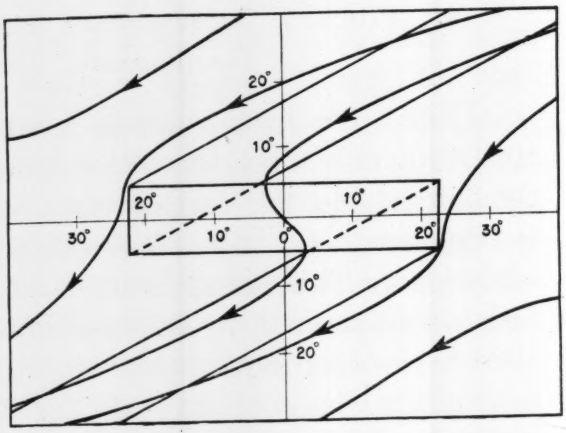

(d)

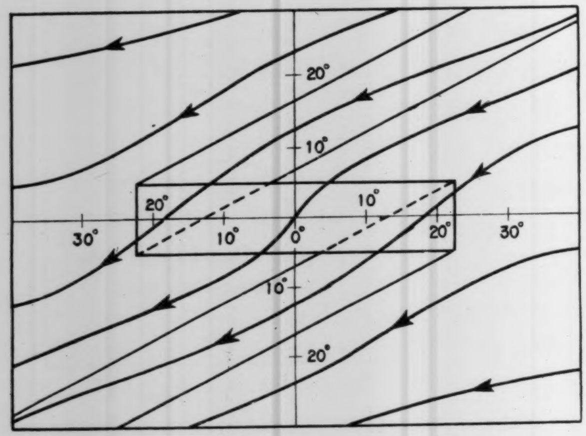

(b)

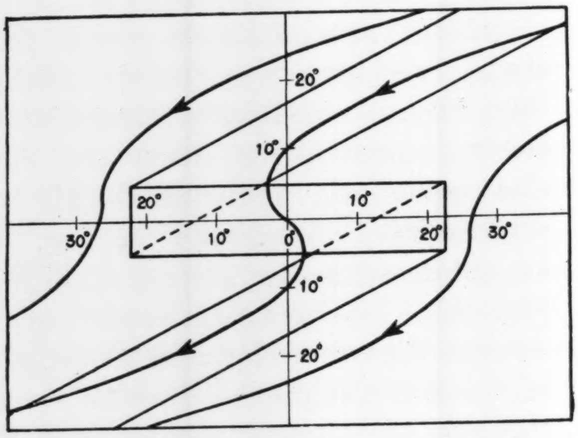

(e)

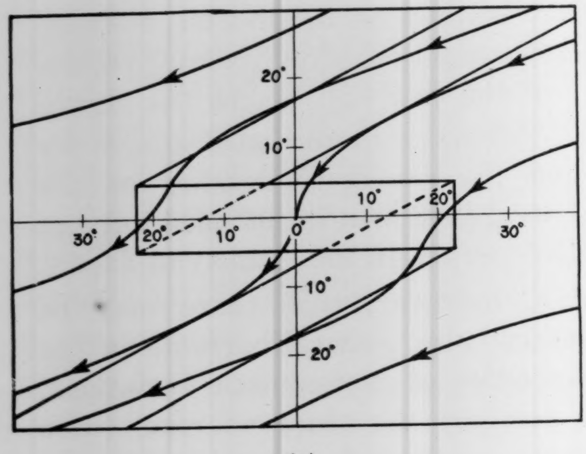

(c)

Fig. 4. The induced electric currents in the model (a). Electric currents of about 1 *amp.* flow between successive stream lines.

rent is subtracted or added. Fig. 5. illustrates an example where the intensity of zonal currents is so adjusted that the effect of the zigzag belt becomes remarkable.

Thus, the local inversion of subterranean induced currents can, at any rate, be demonstrated experimentally. But this is only the first step towards the real solution of the observed important problem.

Actual underground structures may probably be much more complicated, even from the viewpoint of electromagnetic induction, and moreover, a reliable information of the phenomenon must be obtained in relation to geological data.

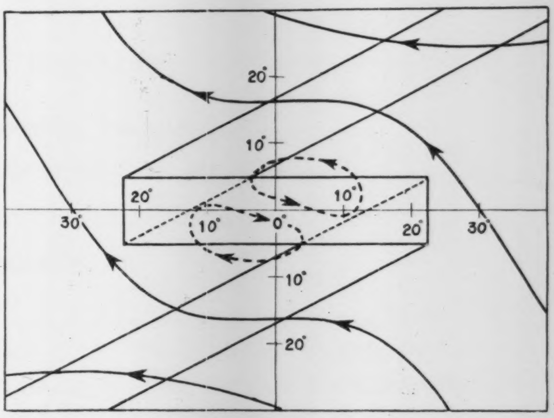

Fig. 5. An example of induced electric current where the intensity of zonal currents is so adjusted that the effect of the zigzag belt becomes remarkable. The representation of the electric current intensity is as same as that in Fig. 1.

Since the model experiments dealt with in this paper seem to be very useful in solving the problems of electromagnetic induction, especially in the cases of complicated distribution of electric conductivity, it is hoped that this kind of study will be extended in future towards the final solution of the preblem.

In conclusion, the authors wish to express their thanks to Dr. T. Rikitake and Mr. I. Yokoyama for their valuable discussion on this subject.

---

36. 地球内電磁誘導現象の模型実験

地球物理学教室 永田 武　小口 高　前川英夫

この論文は力武，横山両氏の論文に対する一補遺であつて，複雑な電気伝導度分布を持つ地球内部への電磁誘導現象を考究するに当つて，模型実験が極めて有効である事を示した．この方法を用いて力武，横山が発見した“日本近傍における地磁気短周期変化の異常分布現象”の解釈を試みたが，現在のところ第 3 図に示した様な地下の電気的構造が最も都合がよい．

---

37. *Growth of the Magnetic Field of the Self-exciting Dynamo in the Earth's Core.*

By Tsuneji RIKITAKE,

Earthquake Research Institute.

(Read Sept. 27, 1955.—Received Sept. 30, 1955.)

Summary

An investigation is attempted in order to see whether or not the earth's dynamo can grow from a state of zero field. The dynamo considered by E. C. Bullard and H. Gellman seems likely to grow, the rate of the growth being also obtained. A period of about 10^4 *years* is required in order to have a field e times of the initial one.

1. Introduction

The idea that the earth's magnetic field is maintained by a self-exciting process in the earth's core has been developed by a number of investigators[1),2),3),4),5)]. Although the theory of the self-exciting dynamo is quite difficult to establish, many difficulties of the theory have been removed, one by one, through the elaborate works of the investigators cited above. The use of powerful calculating machines has also been of great help in promoting the studies. Now we may consider that the theory is approximately applicable to the explanation of the earth's magnetic field though there will be many more problems left for dispute. One of them is the stability of the dynamo which should be highly stable in order that the earth's magnetic field may be maintained over a long period. E. C. Bullard[6)] examined the oscillation of finite amplitude of a self-exciting disc dynamo. He found that there exist oscillations of finite amplitude even though small disturbances are unstable. Making use of

1) W. M. ELSASSER, *Phys. Rev.*, **69** (1946), 106; **70** (1946), 202; **72** (1947), 821. *Rev. Mod. Phys.*, **22** (1950), 1.

2) E. C. BULLARD, *Proc. Roy. Soc. London A*, **197** (1949), 433; **199** (1949), 413.

3) H. TAKEUCHI and Y. SHIMAZU, *Journ. Phys. Earth*, **1** (1952), 1; 56, **2** (1954), 5. *Journ. Geophys. Res.*, **58** (1953), 497.

4) E. C. BULLARD and H. GELLMAN, *Phil. Trans. Roy. Soc. London A*, **247** (1954), 213.

5) E. N. PARKER, *Tech. Rep. Dept. Phys., Univ. Utah* (1954).

6) E. C. BULLARD, *Proc. Cambr. Phil. Soc.* **51** (1955), 744.

the analogies between the disc dynamo and the homogeneous one, he discussed the magnetic oscillations of celestial bodies, the reversals of the earth's magnetic field and other points. T. Rikitake[7] investigated possible oscillations of small amplitude of the earth's dynamo with the result that the small disturbances of the dynamo considered by Bullard and Gellman might be unstable. As was suggested by Bullard, however, there is no reason to believe that the earth's dynamo is utterly unstable, because some finite amplitude oscillations might be possible. S. Lundquist[8] has also studied the stability of magnetic lines of force which are twisted by the magneto-hydrodynamic action. He pointed out that the existence of a strong toroidal field is a little doubtful because instabilities may be caused by the twisting. In spite of all the investigations mentioned above, no definite conclusion concerning the stability problem has been obtained yet.

Another thing to be done is the examination of the growth of the earth's dynamo starting from the zero field. Whether an accidental field given to the system with no field grows or not is not a self-evident problem. The problem would be easier to study than the stability problem of the steady field because we start from the zero field, while the growing field can be treated as a small quantity. The rate of the growth might give some clue to the interval of the occurrence of the normal and reverse magnetization of the earth as has been suggested from the studies of palaeomagnetism of rocks. The writer would here like to investigate the growth of the magnetic field both in homopolar and homogeneous dynamos. Some discussions on the limit of the growth will also be added in the final part of this paper.

2. Growth of the magnetic field of a disc dynamo

As was fully studied by Bullard, the simplest dynamo would be like the one shown in Fig. 1. A conducting disc can rotate about an axle, while a brush is attached on the periphery of the disc. The brush is connected with a ring-shape circuit whose other end touches the axle as shown in the figure. If there is a magnetic field in the direction of the axle, an electromotive force will be induced in the rotating disc, so that we have some potential difference between the axle and the periphery. The electric current driven by the potential difference in the circuit will

7) T. RIKITAKE, *Bull. Earthq. Res. Inst.*, **33** (1955), 1.
8) S. LUNDQUIST, *Phys. Rev.*, **83** (1951), 307.

produce a magnetic field at the disc. If the rotation velocity of the disc is sufficiently large, the initial magnetic field will grow indefinitely. At a critical velocity, the magnetic field will remain unchanged while it exponentially decreases in the case of a lower rotation velocity than that of the critical one.

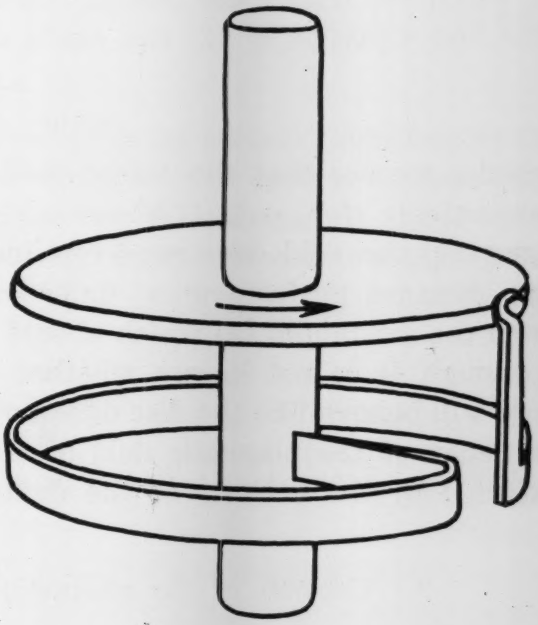

Fig. 1. Schematic view of the disc dynamo after Bullard.

Since this dynamo was investigated in detail by Bullard, the discussion in this section will have nothing new to add. But by going over his discussion, the later discussion is hoped to be better understood.

Bullard has given the differential equations which govern the electric current flowing in the circuit and the motion of the dynamo as follows:

$$\left.\begin{aligned} L\frac{dI}{dt}+RI&=M\omega I\,, \\ C\frac{d\omega}{dt}&=G-MI^2\,, \end{aligned}\right\} \qquad (1)$$

where L, R, $M/2\pi$, I, ω, C and G denote respectively the self inductance and the resistance of the circuit, the mutual inductance between the coil and the periphery of the disc, the electric current, the angular velocity, the monent of inertia of the disc, and the couple driving the disc. It is also assumed that there is no friction at the axle.

Suppose the disc is rotating with an angular velocity ω_0 for $t<0$, and a small magnetic field $\vec{h}_0$ perpendicular to the disc is given at $t=0$, the equations which hold for small values of the electric current or magnetic field will be simplified as

$$\left.\begin{aligned} L\frac{di}{dt}+Ri&=M\omega_0 i\,, \\ C\frac{d\omega}{dt}&=G\,, \end{aligned}\right\} \qquad (2)$$

in which we ignore the second order quantities writing i in place of I. The first equation of (2) can easily be integrated as

$$i=i_0 e^{\frac{M\omega_0-R}{L}t}, \qquad (3)$$

whence we see that the initial field will exponentially grow or decay respectively for $\omega_0 > R/M$ or $\omega_0 < R/M$. As was shown by Bullard, however, the field does not grow indefinitely but reaches a maximum, the dynamo performing a finite amplitude oscillation as can be seen from the solution of (1) which should be taken for large electric current. Although it is not known whether the supposed dynamo in the earth's core will behave like the disc dynamo or not, the condition of the growth or decay of the magnetic field of the earth's dynamo should be seriously affected by the velocity of the fluid motion in the earth's core.

3. Growth of the magnetic field of the earth's dynamo

In a homogeneous dynamo, whose magnetic field or electric current are regarded as the first-order small quantities, the fundamental equations are given as

$$\left.\begin{aligned} &\vec{i}=\sigma(\vec{e}+\vec{V}_0\wedge\vec{h}) , \\ &\mathrm{curl}\,\vec{e}=-\partial\vec{h}/\partial t , \\ &\mathrm{curl}\,\vec{h}=4\pi\vec{i} , \\ &\rho d\vec{v}/dt=-\mathrm{grad}\,p , \end{aligned}\right\} \qquad (4)$$

where $\vec{i}$, σ, $\vec{e}$, $\vec{V}_0$, $\vec{h}$, ρ, $\vec{v}$, and p denote respectively the electric current density, the electrical conductivity, the electric field, the steady velocity of the fluid motion, the magnetic field, the density, the disturbing velocity and pressure. It is also assumed that the system has steady motions with the velocity $\vec{V}_0$ for $t<0$ during which the non-electromagnetic force is balanced by the steady pressure gradient. In this case, the differential equations for the magnetic and electric quantities are independent of the one for the fluid motion.

On eliminating $\vec{i}$ and $\vec{e}$ from (4) and measuring times in units of $4\pi\sigma a^2$ and velocities in units of $1/4\pi\sigma a$, where a denotes the radius of the earth's core, we obtain

$$D\vec{h}-\nabla^2\vec{h}=V\,\mathrm{curl}\,(\vec{v}_0\wedge\vec{h}) , \qquad (5)$$

in which

$$\vec{V}_0 = \frac{V\vec{v}_0}{4\pi\sigma a} \tag{6}$$

and D is written in place of $\partial/\partial t$.

Now we are in a position to solve (5) under certain conditions at the boundary. As has been done in the theory of the earth's dynamo and its stability problem, the only tractable way for solving (5) would be to consider suitable combinations of spherical harmonic constituents of the magnetic field. Since the magnetic field is non-divergent, $\vec{h}$ can be expressed as

$$\vec{h} = \sum_{n,m} \vec{h}^m_{s,n} + \sum_{n,m} \vec{h}^m_{t,n} \tag{7}$$

where $\vec{h}^m_{s,n}$ is of the poloidal type, the r, θ and ϕ components of it being written as

$$\vec{h}^m_{s,n} = \begin{cases} \dfrac{n(n+1)}{r} s^m_n(r) Y^m_n \,, \\ \dfrac{1}{r}\dfrac{ds^m_n}{dr}\dfrac{\partial Y^m_n}{\partial\theta} \,, \\ \dfrac{1}{r\sin\theta}\dfrac{ds^m_n}{dr}\dfrac{\partial Y^m_n}{\partial\phi} \,, \end{cases} \tag{8}$$

and $\vec{h}^m_{t,n}$ is of the toroidal type which is written as

$$\vec{h}^m_{t,n} = \begin{cases} 0 \,, \\ \dfrac{t^m_n(r)}{r\sin\theta}\dfrac{\partial Y^m_n}{\partial\phi} \,, \\ -\dfrac{t^m_n(r)}{r}\dfrac{\partial Y^m_n}{\partial\theta} \,, \end{cases} \tag{9}$$

in which

$$Y^m_n = P^m_n(\cos\theta) \begin{matrix}\cos\\ \sin\end{matrix} m\phi \,. \tag{10}$$

As has been shown by the present writer[9] in the theory of the magneto-hydrodynamic oscillations of a spherical fluid body, it is almost impossible to take into account all the constituents, so that we shall take a combination of the constituents which seem to be important as has been done by Takeuchi, Shimazu, Bullard and Gellman in the eigen-value problem of the self-exciting dynamo. The simplest one is the so-called A-approximation in which only the S^0_1, T^0_2, T^{2c}_2 and T^{2s}_2 type fields are

9) T. RIKITAKE, *Bull. Earthq. Res. Inst.*, **33** (1955), 175.

taken into account, all other constituents being ignored. As for the fluid motion, only the S_2^{2c} and T_1^0 velocity fields are considered. They are to be expressed also in a form of (8) or (9), their radial functions being respectively denoted by Q_S and Q_T following Bullard and Gellmans' expression. In that case, it is easy to obtain the following four equations[10] from (5):

$$\left.\begin{aligned}
&-Dr^2s_1^0+r^2\frac{d^2s_1^0}{dr^2}-2s_1^0=-\frac{216}{5}VQ_St_2^{2s}\,,\\
&-Dr^2t_2^0+r^2\frac{d^2t_2^0}{dr^2}-6t_2^0\\
&\qquad=-\frac{2}{3}V\left(\frac{dQ_T}{dr}-\frac{2Q_T}{r}\right)s_1^0-\frac{72}{7}V\left\{Q_S\frac{dt_2^{2c}}{dr}+2\left(\frac{dQ_S}{dr}-\frac{Q_S}{r}\right)t_2^{2c}\right\}\,,\\
&-Dr^2t_2^{2c}+r^2\frac{d^2t_2^{2c}}{dr^2}-6t_2^{2c}\\
&\qquad=-\frac{6}{7}V\left\{Q_S\frac{dt_2^0}{dr}+2\left(\frac{dQ_S}{dr}-\frac{Q_S}{r}\right)t_2^0\right\}+2VQ_Tt_2^{2s}\,,\\
&-Dr^2t_2^{2s}+r^2\frac{d^2t_2^{2s}}{dr^2}-6t_2^{2s}\\
&\qquad=-2VQ_Tt_2^{2c}-\frac{2}{3}V\left\{3Q_S\frac{d^2s_1^0}{dr^2}+\left(\frac{dQ_S}{dr}-\frac{6Q_S}{r}\right)\frac{ds_1^0}{dr}\right.\\
&\qquad\qquad\left.+\left(\frac{d^2Q_S}{dr^2}-\frac{2}{r}\frac{dQ_S}{dr}\right)s_1^0\right\}\,.
\end{aligned}\right\}\tag{11}$$

In order to solve these equations, we have to specify the radial functions Q_S and Q_T, of which considerable varieties may be expected. One of their usual forms which have been considered in the theory of the self-exciting dynamo is

$$Q_S=r^3(1-r)^2\,,\qquad Q_T=\epsilon\, r^3\,,\tag{12}$$

where ϵ is a constant which determines the ratio of the T_1^0 and S_2^{2c} velocities. If (12) is adopted, (11) becomes

$$\begin{aligned}
&-Dr^2s_1^0+r^2\frac{d^2s_1^0}{dr^2}-2s_1^0=-\frac{216}{5}V(r^5-2r^4+r^3)t_2^{2s}\,,\\
&-Dr^2t_2^0+r^2\frac{d^2t_2^0}{dr^2}-6t_2^0\\
&\qquad=-\frac{2}{3}V\epsilon\, r^2s_1^0-\frac{72}{7}V\left\{(r^5-2r^4+r^3)\frac{dt_2^{2c}}{dr}+(8r^4-12r^3+4r^2)t_2^{2c}\right\},
\end{aligned}$$

10) See Bullard and Gellmans' paper. Expressions (25) of p. 225 and (29) of p. 236.

$$
\left.\begin{aligned}
&-Dr^2t_2^{2c}+r^2\frac{d^2t_2^{2c}}{dr^2}-6t_2^{2c}\\
&\quad=-\frac{6}{7}V\left\{(r^5-2r^4+r^3)\frac{dt_2^0}{dr}+(8r^4-12r^3+4r^2)t_2^0\right\}+2V\epsilon\, r^3t_2^{2s},\\
&-Dr^2t_2^{2s}+r^2\frac{d^2t_2^{2s}}{dr^2}-6t_2^{2s}\\
&\quad=-2V\epsilon\, r^3t_2^{2c}-\frac{2}{3}V\left\{(3r^5-6r^4+3r^3)\frac{d^2s_1^0}{dr^2}\right.\\
&\qquad\qquad\left.+(-r^4+4r^3-3r^2)\frac{ds_1^0}{dr^2}+(10r^3-20r^2+3r)s_1^0\right\}.
\end{aligned}\right\}\quad(13)
$$

A considerable variety of methods will be available for the solution of the simultaneous equations. In order to examine whether an accidental field given to the system at $t=0$ grows or not, we may choose a crude way of examination making use of power series of r for s_1^0, t_2^0, t_2^{2c} and t_2^{2s}. Let us assume the following expressions:

$$
\left.\begin{aligned}
s_1^0&=\sum_n a_nr^{n+2},\\
t_2^0&=\sum_n b_nr^{n+1},\\
t_2^{2c}&=\sum_n c_nr^{n+1},\\
t_2^{2s}&=\sum_n d_nr^{n+1},
\end{aligned}\right\}\quad(14)
$$

all of which remain finite at $r=0$. Introducing (14) into (13), we obtain

$$
\left.\begin{aligned}
&-D\sum a_nr^{n+4}+\sum n(n+3)a_nr^{n+2}\\
&\quad=-\frac{216}{5}V\sum d_nr^{n+6}+\frac{432}{5}V\sum d_nr^{n+5}-\frac{216}{5}V\sum d_nr^{n+4},\\
&-D\sum b_nr^{n+3}+\sum(n^2+n-6)b_nr^{n+1}\\
&\quad=-\frac{2}{3}V\epsilon\sum a_nr^{n+4}-\frac{72}{7}V\sum(n+9)c_nr^{n+5}\\
&\qquad+\frac{144}{7}V\sum(n+7)c_nr^{n+4}-\frac{72}{7}V\sum(n+5)c_nr^{n+3},\\
&-D\sum c_nr^{n+3}+\sum(n^2+n-6)c_nr^{n+1}\\
&\quad=-\frac{6}{7}V\sum(n+9)b_nr^{n+5}+\frac{12}{7}V\sum(n+7)b_nr^{n+4}\\
&\qquad-\frac{6}{7}V\sum(n+5)b_nr^{n+3}+2V\epsilon\sum d_nr^{n+4},
\end{aligned}\right\}\quad(15)
$$

$$
\left.\begin{aligned}
&-D\sum d_n r^{n+3}+\sum(n^2+n-6)d_n r^{n+1}\\
&\quad=-2V\epsilon\sum c_n r^{n+4}-\frac{2}{3}V\sum(3n^2+8n+14)a_n r^{n+5}\\
&\qquad+\frac{4}{3}V\sum(3n^2+7n+12)a_n r^{n+4}-2V\sum(n+1)^2 a_n r^{n+3}\ .
\end{aligned}\right\}
$$

If we ignore a_n, b_n, c_n and d_n for $n>5$, the following relations can be obtained by equating the coefficients of the corresponding terms of the left- and right-hand sides of the above equations:

$$
\left.\begin{aligned}
&a_0=a_1=a_2=a_3=b_0=b_1=b_2=b_3=c_0=c_1=c_3=d_0=d_1=d_3=0\ ,\\
&40a_5=\frac{432}{5}Vd_2\ ,\\
&-Da_4=-\frac{216}{5}Vd_2-\frac{216}{5}Vd_4\ ,\\
&-Db_2+14b_4=-\frac{504}{7}Vc_2\ ,\\
&24b_5=\frac{1296}{7}Vc_2\\
&-Dc_2+14c_4=-6Vb_2\ ,\\
&14c_5=\frac{108}{7}Vb_2+2V\epsilon d_2\ ,\\
&-Dd_2+14d_4=0\ ,\\
&14d_5=-2V\epsilon c_2\ .
\end{aligned}\right\}\qquad(16)
$$

The boundary conditions that the magnetic field is continuous at the surface of the core give the relations such as

$$
\sum(n+3)a_n=\sum b_n=\sum c_n=\sum d_n=0\ , \qquad (17)
$$

from which we have

$$
\left.\begin{aligned}
&7a_4+8a_5=0\ ,\\
&b_2+b_4+b_5=0\ ,\\
&c_2+c_4+c_5=0\ ,\\
&d_2+d_4+d_5=0\ ,
\end{aligned}\right\}\qquad(18)
$$

in which a_n, b_n, c_n and d_n for $n>5$ are neglected as before.

In order to have non-vanishing solutions for (16) and (18), the following relation should hold good:

$$\begin{vmatrix}
0 & 0 & 0 & -\frac{432}{5}V-40 & 0 & 0 & 0 & 0 & 0 & 0 & 0 \\
0 & D & -\frac{504}{7}V & 0 & 0 & -14 & 0 & 0 & 0 & 0 & 0 \\
0 & 0 & \frac{1296}{7}V & 0 & 0 & 0 & 0 & 0 & -24 & 0 & 0 \\
0 & -6V & D & 0 & 0 & 0 & -14 & 0 & 0 & 0 & 0 \\
0 & \frac{108}{7}V & 0 & 2V\epsilon & 0 & 0 & 0 & 0 & 0 & -14 & 0 \\
0 & 0 & 0 & D & 0 & 0 & 0 & -14 & 0 & 0 & 0 \\
0 & 0 & -2V\epsilon & 0 & 0 & 0 & 0 & 0 & 0 & 0 & -14 \\
7 & 0 & 0 & 0 & 8 & 0 & 0 & 0 & 0 & 0 & 0 \\
0 & 1 & 0 & 0 & 0 & 1 & 0 & 0 & 1 & 0 & 0 \\
0 & 0 & 1 & 0 & 0 & 0 & 1 & 0 & 0 & 1 & 0 \\
0 & 0 & 0 & 1 & 0 & 0 & 0 & 1 & 0 & 0 & 1
\end{vmatrix} = 0 . \tag{19}$$

(19) can be written as

$$D^3+14D^2+(588-1728V^2+4V^2\epsilon^2)D-2744-7056V^2-54V^2\epsilon^2=0 . \tag{20}$$

If V and ϵ are larger than 10, the equation has a root which is approximately given by

$$D=\frac{2744-7056V^2-54V^2\epsilon^2}{588-1728V^2+4V^2\epsilon^2} .$$

Bullard and Gellman have shown that a steady state of the self-exciting dynamo is possible, for example, for the combination of $\epsilon=100$ and $V=22.06$. Corresponding to these values of ϵ and V, the above root becomes 14.3, the other roots of (20) being complex with negative real parts. It is obvious that the complex roots whose real parts are negative specify simple harmonic oscillations superposed by exponential decays of the magnetic field. Hence the magnetic field does not grow in these cases. On the other hand, we see that the magnetic field grows exponentially when the root is positive. In that case, we obtain

$$\vec{h}=\vec{h}_0 e^{\frac{14.3t}{4\pi\sigma a^2}} \tag{21}$$

If we take $\sigma=3\times10^{-6}$ *emu* and $a=3.5\times10^{8}$ *cm*, the period during which the magnetic field increases *e* times of its initial value is calculated to be 10^4 *years* from (21). It is of importance that the magnetic field

of the dynamo, the fluid motion in which is studied by Bullard and Gellman, can grow starting from the zero field provided an accidental field is given. Therefore it might be assumed that the earth's magnetic field was generated either from the interstellar magnetic field which is supposed to amount to $10^{-6}\sim10^{-5}$ *gauss* or from an unknown accidental field given to the earth when the fluid motion in the core was arranged favourably. If the initial field were of opposite direction to the present one, the field grown from it would be the reversed one. Suppose the earth's dynamo is destroyed by some causes and the state of no magnetic field is apparently attained, the new growth of the field might take place in the above-described way, provided there are suitable fluid motions in the core. Since the probability of a large magnetic field being applied to the earth would be quite small, the period for getting a new field of appreciable strength would exceed 10^4 *years*. The above theory can not be applicable for cases in which electromagnetic forces are comparable with the mechanical forces because we assumed that the electric and magnetic quantities are the first-order small ones. A theory of finite magneto-hydrodynamic oscillations in the earth's core will be advanced later.

4. The limit of the growing field

Although it is obvious that we can have no exact understanding about the growth and other time-dependent behaviours of the earth's dynamo until we solve the fundamental equations of electromagnetism and fluid motion, which are intrinsically non-linear, a number of attempts have been made to determine the limit of the amplification of the magnetic field as well as the period needed to attain to that state from analogical and physical points of view.

G. K. Batchelor[11] studied the behaviour of the magnetic field associated with turbulent motions of a conducting liquid. Making use of the results concerning the statistical behaviour of homogeneous turbulence, he suggested that a magnetic field can grow from an initial field arriving finally at a certain steady state. The rate of the growth, the time needed for the complete growth and the magnetic energy at the steady state were approximately obtained. According to Bullard, however, the equality between the kinetic and magnetic energies at the steady state as is supposed by Batchelor for turbulent motions does not always hold

11) G. K. BATCHELOR, *Proc. Roy. Soc. London A*, **201** (1950), 405.

good for large-scale motions such as considered here, so that Batchelor's way of discussion is hardly applicable for the present case.

Elsasser[1] has pointed out that the mechanical forces produced by the magnetic field in the earth's core will become significant when they become comparable in magnitude with the purely mechanical forces which control the fluid motion. If the magneto-mechanical forces are supposed to be much larger, the motion that would be caused by the forces would modify the fluid motion in a way so as to decrease the magnetic field. He supposed that the magnetic forces can be amplified up to the same order of magnitude with the Coriolis force that seems most important for relatively slow motions in the core. If this equating is taken for granted, the limit of the amplification is obtained to be about 12 *gauss* by Elsasser, while Bullard suggested some larger values.

The writer is of opinion, however, that the steady value of the earth's magnetic field would be determined from the energetics in the earth's core. The energetics has been discussed by Elsasser, Bullard and others from time to time. The mean magnetic energy in the earth's core is estimated at 2.3×10^{3} *ergs/cm*^{3} according to Bullard's recent study. The figure might become smaller if we take the view that the toroidal magnetic field in the core is not so large as is estimated by Bullard. The rate of dissipation of magnetic energy is therefore roughly 5×10^{-9} *ergs/cm*^{3} *sec.* when we take into consideration the fact that the free decay period of the core's field amounts to 1.4×10^{4} *years*. To maintain the magnetic field, the energy of this order of magnitude should be always supplied from the fluid motion or ultimately from the thermal source. It is known that the dissipation due to fluidal friction is much smaller than the figure cited above. On the other hand, investigations of meteorites suggested that thermal energy of 0.3×10^{20} *ergs/sec.* would be generated in the whole core, whence we have 1.7×10^{-7} *ergs/cm*^{3} *sec.* as the value of generation of thermal energy. The efficiency of this heat engine then becomes about 3%. The limit of the efficiency of the thermodynamical process in the core is given by the adiabatic difference between the top and bottom of the convection currents after the second law of thermodynamics, the ideal efficiency being supposed to be of the order of 10%. The convert of the thermal energy into the magnetic energy is therefore possible.

However, the above discussions have nothing to do with the determination of the magnitude of the magnetic field in the core. On the contrary, the magnitude of the toroidal magnetic field obtained by making

the Coriolis force equal to the electromagnetic force has been adopted in estimating the magnetic energy in the earth's core. The matter would become clearer if the logical order is inverted, that is if we point out that the magnitude of the magnetic field produced by the earth's dynamo would be determined from the amount of thermal energy transferable to magnetic energy. This is equivalent to determining the efficiency of the thermodynamical engine. In order to do this, however, the detail of thermal behaviour of the dynamo should be known. The introduction of thermal energy into the system of the dynamo, which has been described by the fundamental equations of fluid motion and electromagnetism, would be quite a task, and no satisfactory results can be expected within a short time.

5. Concluding remarks

As a result of a rough examination, it is shown that the dynamo in the earth's core considered by Bullard and Gellman can grow from the state of zero field. The rate of the growth is also obtained. The time needed for getting at a field e times of the initial one is of the order of 10^4 *years*. No satisfactory result concerning the limit of the growing field is obtained from a survey of related problems.

---

37. 地磁気ダイナモに於ける磁場の生長

地震研究所　力 武 常 次

Bullard-Gellman および竹内一島津等によつて求められて来た地球核内のダイナモの零磁場状態に微小磁場を与えた時，その微小磁場が生長するか否かを検討した．ある定常ダイナモを形成し得ると考えられる流体運動に対しては，微小磁場の生長が確められ，初期値の e 倍に生長するのに 10^4年かかることがわかつた．つまりこのような流体運動は磁場を増幅する作用を有することになる．

---

38. *Magneto-hydrodynamic Oscillations of Finite Amplitude of a Conducting Fluid Sphere.*

By Tsuneji RIKITAKE,

Earthquake Research Institute.

(Read Sept. 27, 1955.—Received Sept. 30, 1955.)

Summary

Finite magneto-hydrodynamic oscillations of perfectly conducting fluid sphere are studied. No motion and no magnetic field are assumed at the equilibrium state. Ignoring higher spherical harmonic constituents, only the field that gives the dipole-like one outside the sphere is considered. Although it seems difficult to solve the non-linear integro-differential equations which are deduced from the fundamental equations of electromagnetism and fluid motion, a crude examination of the equations suggests that there exists a finite oscillation of a special type. The result also suggests that the earth's dynamo might perform a finite oscillation even though the small oscillations of the dynamo are unstable. In that case, it is of interest to note that one might expect reversals of the earth's magnetic field.

1. Introduction

Magneto-hydrodynamic oscillations of small amplitude have been investigated by M. Schwarzschild[1], V. C. A. Ferraro[2), 3)] and others with applications to magnetically variable stars, while the present writer[4), 5)] has been investigating possible oscillations of the same sort in relation to the stability of the earth's dynamo. All of these studies dealt with small oscillations about a steady state. The steady state has been assumed to be a magnetic field uniformly given from the outside to the conducting liquid body in question, or a magnetic field given by a magnetic pole at the centre of the body, or one generated by the self-exciting process with suitable fluid motions. The writer's investigation has suggested that the steady state of the earth's dynamo considered

1) M. SCHWARZSCHILD, *Ann. d'Astrophys.*, **12** (1949), 148.
2) V. C. A. FERRARO and D. J. MEMORY, *M.N.R.A.S.*, **112** (1952), 361.
3) C. PLUMPTON and V. C. A. FERRARO, *M.N.R.A.S.*, **113** (1953), 647.
4) T. RIKITAKE, *Bull. Earthq. Res. Inst.*, **33** (1955), 1.
5) T. RIKITAKE, *Bull. Earthq. Res. Inst.*, **33** (1955), 175.

by E. C. Bullard and H. Gellman[6] would be unstable for small disturbances. According to Bullard, however, the earth's dynamo might perform a finite oscillation though its steady state is unstable for small disturbances. Bullard's discussion[7] is based on possible analogies between homogeneous and homopolar dynamos, and finite oscillations of the latter are fully studied by Bullard himself. However, in order to see whether or not the supposed earth's dynamo performs oscillations of such sort, it is highly desirable to investigate the possibility of magneto-hydrodynamic oscillations of finite amplitude in the earth's core. This sort of oscillation would be, if it does occur, closely related to the hypothetical reversals of the earth's magnetic field in the past.

It will be of great difficulty to establish, in a complete form, the theory of finite magneto-hydrodynamic oscillations of a conducting body because it has been shown that even small oscillations are quite complicated. In order to render the problem tractable, it is assumed here that the fluid has no motion and no magnetic field at the equilibrium state. It is also assumed that only the S_1^0 type field may be taken into account, the fields of other types being ignored. Non-linear integro-differential equations concerning the radial part of the fluid will be obtained from Maxwell's equations and the equation of fluid motion. The equations thus obtained will be solved with rough approximation.

2. Theory

Since we assume that there are no fluid motion and no magnetic field at the equilibrium state, the fundamental equations can be written as

$$\vec{E}+\vec{V}\wedge\vec{H}=0\,, \tag{1}$$

$$\mathrm{curl}\,\vec{E}=-\partial\vec{H}/\partial t\,, \tag{2}$$

$$\mathrm{curl}\,\vec{H}=4\pi\vec{I}\,, \tag{3}$$

$$\rho\left\{\frac{\partial\vec{V}}{\partial t}+(\vec{V}\cdot\mathrm{grad})\vec{V}\right\}=\vec{I}\wedge\vec{H}-\mathrm{grad}\,p\,, \tag{4}$$

where $\vec{I}$, $\vec{E}$, $\vec{H}$, ρ, p and $\vec{V}$ denote respectively the electric current

6) E. C. BULLARD and H. GELLMAN, *Phil. Trans. Roy. Soc. London A*, **247** (1954), 213.

7) E. C. BULLARD, *Proc. Cambr. Phil. Soc.*, **51** (1955), 744.

density, electric field, magnetic field, density, pressure and velocity. It is also assumed that the magnetic permeability is unity in electromagnetic unit, that the non-electromagnetic force balancing the pressure gradient at the equilibrium state is not dependent on the time, and that the fluid is perfectly conducting. The fluid is also assumed to be incompressible, whence we have

$$\operatorname{div} \vec{V} = 0 . \tag{5}$$

If we eliminate $\vec{I}$ and $\vec{E}$ from the equations from (1) to (4), we obtain

$$\frac{\partial \vec{H}}{\partial t} = \operatorname{curl}(\vec{V} \wedge \vec{H}) , \tag{6}$$

$$4\pi\rho\left\{\frac{\partial \vec{V}}{\partial t} + (\vec{V}\cdot\operatorname{grad})\vec{V}\right\} = \operatorname{curl}\vec{H} \wedge \vec{H} - 4\pi \operatorname{grad} p \tag{7}$$

In the cases of small oscillations, as have been investigated in the writer's previous papers, the time-dependent velocity and the magnetic field are considered to be of the first order small quantities and the second order quantities are ignored. If we take the same approximation here, it becomes clear that the equation for the magnetic field is to be separated from the one for the fluid motion, coupling between the magnetic field and fluid motion being by no means possible. Hence the next step of approximation may be to take into account the electromagnetic force in the right-hand side of (7), while the second term of the left-hand side of (7) may be assumed to be smaller than the first one, so that we may take

$$4\pi\rho\frac{\partial \vec{V}}{\partial t} = \operatorname{curl}\vec{H} \wedge \vec{H} - 4\pi \operatorname{grad} p \tag{8}$$

instead of (7). If this approximation is taken for granted, we obtain the following relation by making div. of (8) and using (5).

$$\nabla^2 p = -(4\pi)^{-1}\{\vec{H}\nabla^2\vec{H} + (\operatorname{curl}\vec{H})^2\} . \tag{9}$$

We shall now assume that $\vec{H}$ is of the S_1^0 type that gives only the dipole-like field outside the sphere. In that case, the r, θ and ϕ components of $\vec{H}$ are respectively written as

$$\overrightarrow{H}=\begin{cases}-2s(r,t)P_1\,,\\ -\left(r\dfrac{\partial s}{\partial r}+2s\right)\dfrac{dP_1}{d\theta}\,,\\ 0\,,\end{cases}\tag{10}$$

from which we also obtain

$$\operatorname{curl}\overrightarrow{H}=\begin{cases}0\,,\\ 0\,,\\ -\left(r\dfrac{\partial^2 s}{\partial r^2}+4\dfrac{\partial s}{\partial r}\right)\dfrac{dP_1}{d\theta}\,,\end{cases}\tag{11}$$

$$\nabla^2\overrightarrow{H}=\begin{cases}-2\left(\dfrac{\partial^2 s}{\partial r^2}+\dfrac{4}{r}\dfrac{\partial s}{\partial r}\right)P_1\,,\\ -\left(r\dfrac{\partial^3 s}{\partial r^3}+6\dfrac{\partial^2 s}{\partial r^2}+\dfrac{4}{r}\dfrac{\partial s}{\partial r}\right)\dfrac{dP_1}{d\theta}\,,\\ 0\,.\end{cases}\tag{12}$$

With the aid of the expressions from (10) to (12), (9) can be written as

$$\nabla^2 p=f_0+f_2P_2\tag{13}$$

where

$$\left.\begin{aligned}-4\pi f_0=&\frac{2}{3}\Bigg[2\left(\frac{\partial^2 s}{\partial r^2}+\frac{4}{r}\frac{\partial s}{\partial r}\right)s+\left(r\frac{\partial^3 s}{\partial r^3}+6\frac{\partial^2 s}{\partial r^2}+\frac{4}{r}\frac{\partial s}{\partial r}\right)\\ &\times\left(r\frac{\partial s}{\partial r}+2s\right)+\left(r\frac{\partial^2 s}{\partial r^2}+4\frac{\partial s}{\partial r}\right)^2\Bigg]\,,\\ -4\pi f_2=&\frac{2}{3}\Bigg[4\left(\frac{\partial^2 s}{\partial r^2}+\frac{4}{r}\frac{\partial s}{\partial r}\right)s-\left(r\frac{\partial^3 s}{\partial r^3}+6\frac{\partial^2 s}{\partial r^2}+\frac{4}{r}\frac{\partial s}{\partial r}\right)\\ &\times\left(r\frac{\partial s}{\partial r}+2s\right)-\left(r\frac{\partial^2 s}{\partial r^2}+4\frac{\partial s}{\partial r}\right)^2\Bigg]\,.\end{aligned}\right\}\tag{14}$$

The solution of (13) becomes

$$p=q_0+q_2P_2\,,\tag{15}$$

in which q_0 and q_2 should satisfy the following differential equations.

$$\left.\begin{aligned}&\frac{1}{r}\frac{\partial}{\partial r}\left(r^2\frac{\partial}{\partial r}\right)q_0=f_0\,,\\ &\left\{\frac{1}{r^2}\frac{\partial}{\partial r}\left(r^2\frac{\partial}{\partial r}\right)-\frac{6}{r^2}\right\}q_2=f_2\,.\end{aligned}\right\}\tag{16}$$

The solutions of (16) which do not become infinite at $r=0$ are given as

$$\left.\begin{aligned} q_0 &= K_0+\int_0^r rf_0\,dr - r^{-1}\int_0^r r^2 f_0\,dr\ , \\ q_2 &= (r/a)^2 K_2+\frac{1}{5}\left(r^2\int_0^r r^{-1} f_2\,dr - r^{-3}\int_0^r r^4 f_2\,dr\right)\ , \end{aligned}\right\} \tag{17}$$

where K_0 and K_2 are constants which will be determined later. a denotes the radius of the sphere.

After some calculations, q_0 and q_2 are obtained as

$$\left.\begin{aligned} 4\pi q_0 &= 4\pi K_0-\frac{2}{3}\left[2r\frac{\partial s}{\partial r}s+\frac{1}{2}r^2\left(\frac{\partial s}{\partial r}\right)^2+3s^2+\int_0^r r\left(\frac{\partial s}{\partial r}\right)^2 dr\right]\ , \\ 4\pi q_2 &= 4\pi K_2(r/a)^2+\frac{2}{3}\left[2r\frac{\partial s}{\partial r}s+\frac{1}{2}r^2\left(\frac{\partial s}{\partial r}\right)^2-\frac{7}{5}r^{-3}\int_0^r r^4\left(\frac{\partial s}{\partial r}\right)^2 dr \right. \\ &\qquad \left. +\frac{12}{5}r^2\int_0^r r^{-1}\left(\frac{\partial s}{\partial r}\right)^2 dr\right]. \end{aligned}\right\} \tag{18}$$

Since we have calculated the pressure, the right-hand side of (8) can be obtained from (10), (11), (15) and (18). The result is as follows:

$$\vec{V}=\left\{\begin{array}{l} -6S(r)rP_2\ , \\ -\left(r\dfrac{\partial S}{\partial r}+3S\right)r\dfrac{dP_2}{d\theta}\ , \\ 0\ , \end{array}\right. \tag{19}$$

where

$$4\pi\rho\frac{\partial S}{\partial t}=\frac{4}{3}\pi K_2 a^{-2}+\frac{2}{3}\left[-r^{-1}\frac{\partial s}{\partial r}s+\frac{7}{10}r^{-5}\int_0^r r^4\left(\frac{\partial s}{\partial r}\right)^2 dr+\frac{4}{5}\int_0^r r^{-1}\left(\frac{\partial s}{\partial r}\right)^2 dr\right]. \tag{20}$$

In obtaining (19), it is easily seen that the term that does not depend on θ vanishes.

On the other hand, by putting (19) into (6), the right-hand side of (6) is obtained as

$$\operatorname{curl}(\vec{V}\wedge\vec{H})=\left\{\begin{array}{l} -2t_1P_1\ , \\ -\left(r\dfrac{\partial t_1}{\partial r}+2t_1\right)\dfrac{dP_1}{d\theta}+ \\ 0\ , \end{array}\right. \left\{\begin{array}{l} -12t_3r^2P_3\ , \\ -\left(r\dfrac{\partial t_3}{\partial r}+4t_3\right)r^2\dfrac{dP_3}{d\theta}\ , \\ 0\ , \end{array}\right. \tag{21}$$

where

$$t_1 = -\frac{6}{5}\left\{r\frac{\partial}{\partial r}(sS) + 5sS\right\}, \tag{22}$$

$$t_3 = \frac{1}{5}r^{-1}\left(6S\frac{\partial s}{\partial r} - 4\frac{\partial S}{\partial r}s\right). \tag{23}$$

If it is assumed that we can ignore the magnetic field of the S_3^0 type thus brought forth, (6), (21) and (22) give

$$\frac{\partial s}{\partial t} = -\frac{6}{5}\left\{r\frac{\partial}{\partial r}(sS) + 5sS\right\}, \tag{24}$$

whence we see that the radial parts of the magnetic field and velocity are to be determined by solving (20) together with (24) under suitable boundary conditions. This means solving a set of simultaneous non-linear integro-differential equations. It is not known whether or not we can solve them with rigorous accuracy. But the writer would here like to show a simple solution by making use of a way of rough approximation.

Let us assume that

$$\left.\begin{aligned} s &= \sum_n a_n(r/a)^n, \\ S &= \sum_n b_n(r/a)^n, \end{aligned}\right\} \tag{25}$$

in which the terms for $n > 4$ are ignored. It is also assumed that $a_1 = 0$, otherwise one of the integrals in (20) is divergent. After introducing (25) into (20) and (24), the coefficients of the corresponding terms are equated, so that we obtain

$$\begin{aligned} &a_3 = b_1 = b_3 = 0, \\ &\frac{da_0}{dt} = -6a_0b_0, \\ &\frac{da_2}{dt} = -\frac{42}{5}(a_0b_2 + a_2b_0), \\ &\frac{da_4}{dt} = -\frac{54}{5}(a_0b_4 + a_2b_2 + a_4b_0), \\ &\cdots\cdots\cdots\cdots\cdots\cdots \\ &4\pi\rho\frac{db_0}{dt} = \frac{2}{3}a^{-2}(2\pi K_2 - 2a_0a_2), \\ &4\pi\rho\frac{db_2}{dt} = -\frac{2}{3}a^{-2}\cdot 4a_0a_4, \\ &4\pi\rho\frac{db_4}{dt} = -\frac{2}{3}a^{-2}\cdot\frac{14}{9}a_2a_4, \\ &\cdots\cdots\cdots\cdots\cdots\cdots \end{aligned} \tag{26}$$

while K_2 is to be determined from the condition that the normal component of the velocity vanishes or $b_0+b_2+b_4=0$ at the boundary, that is, the right-hand side of (20) becomes zero at $r=a$. Taking into account this condition, K_2 is given as

$$2\pi K_2=2a_0a_2+4a_0a_4+\frac{14}{9}a_2a_4\,. \tag{27}$$

Further, the solutions should satisfy the boundary condition that the magnetic field is continuous at $r=a$, so that the following relation must be satisfied as has been shown in the previous papers:

$$3a_0+5a_2+7a_4=0\,. \tag{28}$$

With the aid of (27) and (28), we obtain simultaneous differential equations with respect to a_0, a_2, b_0 and b_2 as follows:

$$\left.\begin{aligned} \frac{da_0}{dt}&=-6a_0b_0\,,\\ \frac{da_2}{dt}&=-\frac{42}{5}(a_0b_2+a_2b_0)\,,\\ 4\pi\rho a^2\frac{db_0}{dt}&=-\frac{4}{21}\left(2a_0+\frac{7}{9}a_2\right)(3a_0+5a_2)\,,\\ 4\pi\rho a^2\frac{db_2}{dt}&=\frac{8}{21}a_0(3a_0+5a_2)\,. \end{aligned}\right\} \tag{29}$$

The writer is going to show a solution of (29) for the special case of $a_2=b_2=0$. In that case, b_0 may be easily eliminated by obtaining a non-linear differential equation for a_0 as

$$a_0\frac{d^2a_0}{dt^2}-\left(\frac{da_0}{dt}\right)^2-f^2a_0^4=0\,, \tag{30}$$

where

$$f^2=\frac{12}{7\pi\rho a^2}\,. \tag{31}$$

If we put $da_0/dt=\xi$, (30) can be written as

$$a_0\xi\frac{d\xi}{da_0}=\xi^2+f^2a_0^4\,, \tag{32}$$

which can be integrated as

$$\xi^2=Aa_0^2+f^2a_0^4\,, \tag{33}$$

whence we have

$$\frac{da_0}{dt} = \pm a_0\sqrt{A+f^2a_0^2}\,. \tag{34}$$

Taking the plus sign of the right-hand side of (34) and putting

$$k^2 = -Af^{-2}, \tag{35}$$

(34) can be integrated as

$$ft = \frac{1}{k}\tan^{-1}\sqrt{\frac{a_0^2-k^2}{k^2}} + c$$

that gives

$$a_0 = k \sec k(ft-c)\,. \tag{36}$$

We see therefore that the magnetic field performs a periodic oscillation given by (36). At $t=c/f$, we have

$$(a_0)_{t=f/c} = k\ , \quad \left(\frac{da_0}{dt}\right)_{t=f/c} = 0\,.$$

The period is given by

$$T = \frac{2\pi}{kf} = \sqrt{\frac{7}{3}}\,\frac{1}{k}\pi^{\frac{3}{2}}\rho^{\frac{1}{2}}a\,. \tag{38}$$

3. Discussions and concluding remarks

Under the assumption that the finite oscillations of the S_1^0 field can occur independently of those of the other harmonics, a simple mode of magneto-hydrodynamic oscillation is obtained in the last section. The oscillation, which is given by (36), is shown in Fig. 1. Since many approximations are made use of in order to get at (36), it is not known to what extent (36) can be applied for the real earth. Especially, the infinite growth of the field causes doubt. In that case, the couplings between a_0 and b_0 and the ignored quantities such as a_2, b_2, a_4, b_4, ... would become appreciable, so that the differential equation (30) would be seriously affected. For all the crude treatments, however, it is of interest to note that the study suggests possible reversals of the S_1^0 field.

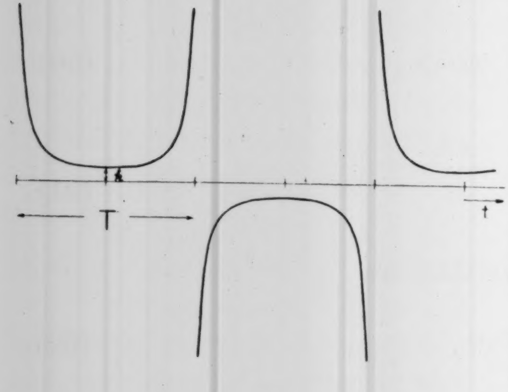

Fig. 1. The oscillation of the S_1^0 field.

The finite oscillation of a disc dynamo studied by Bullard does not give reversals after a field has once been established in a given direction. The finite oscillations of a conducting fluid sphere, however, might give rise to reversals, judging from the study, though incomplete, in this paper.

We see that the period of oscillation is proportional to the square root of the density, the radius of the sphere and the inverse of the initial field as shown in (38). This is thought to be of the right form as made clear in the studies of small oscillations of a conducting fluid sphere and finite one of a disc dynamo. Since the period depends on the initial value of the field, the period may be given any value by assuming suitable values for the initial field. In order to give a period of 10^5 *years*, k is taken to be 5×10^{-3} *gauss*, that means the initial magnetic field at the pole should be 10^{-2} *gauss*.

Since the electrical conductivity has been assumed to be infinity throughout the mathematical treatments in this paper, the effect of finite conductivity on the magneto-hydrodynamic oscillations concerned is not known. But it is clear that the loss of energy as Joule's heat will after all damp down the oscillation. If we suppose that quite a small field is given at the initial state, it is hardly likely that the field will grow without limit following the course as shown in Fig. 1, because of the ohmic dissipation. The situation would be, however, quite different if there are steady fluid motions of certain distribution at the equilibrium state. Actually, the writer[8] has shown that a small field given to a conducting fluid sphere, in which fluid motions supposed by Bullard and Gellman are existing, can grow. Once the field grows up to an appreciable magnitude, the non-linear terms would become to play an important role. In that case, we might expect finite oscillations of the system. Even reversals of the S_1^0 field might occur at this stage.

The above discussions, of course, are incomplete because the writer can not solve the problem with steady motion at the equilibrium state. It is also not known to what extent the results will be affected by the neglect of higher harmonic constituents. The investigation of the mutual couplings of various harmonic constituents are difficult even in the case of small oscillations. In spite of these defects, the fact that we might expect reversals of the earth's magnetic field when we take into account magneto-hydrodynamic oscillations of finite amplitude still seems to be of importance and interest.

8) T. RIKITAKE, *Bull. Earthq. Res. Inst.*, **33** (1955), 571.

38. 地球核内の有限振幅電磁流体振動

地震研究所　力　武　常　次

従来地球核内の微小振幅振動を取扱つて地磁気ダイナモの安定性を論じて来たが，この議論を有限振幅の場合に拡張した．数学的困難をさけるために，平衡状態に於ては磁場および流体運動がともに零であるとし，核外に双極子磁場としてあらわれるものにのみ着目し，それ以外の磁場は一切無視する．かくして流体運動の運動方程式および Maxwell の基礎方程式より，磁場ならびに速度に関する非線型連立積分微分方程式を求めた．この方程式を適当な省略をほどこして解く時は，非常に簡単な場合として振動性の解が求められる．この解は磁場が正負の両符号をとり得ることを示し，振動周期は密度の自乗根と核半径に比例し初期磁場の振幅に逆比例する．もしこのような振動が実在する時には，地球磁場の逆転も起り得ることになる．実際問題としては磁場が小さい間は非電磁的流体運動による増幅作用が行われ，磁場がかなり大きくなると本論文にのべたような電磁力の作用がいちじるしくなるものと思われる．

39. *Geological Investigations on the Zaō Volcanoes. III Byōbu Volcano.**

By Takeshi ICHIMURA,

Yamagata University.

(Received Sept. 30, 1955.)

Introduction

The western half of the South Zaō is represented by the Byōbu Volcano which includes Byōbu-dake (1817.1 m.), Sugiga-mine (1745.3 m.), Fubō-zan (1705.3 m.), Ushiro-eboshi-dake (1666 m.), Mae-eboshi-dake

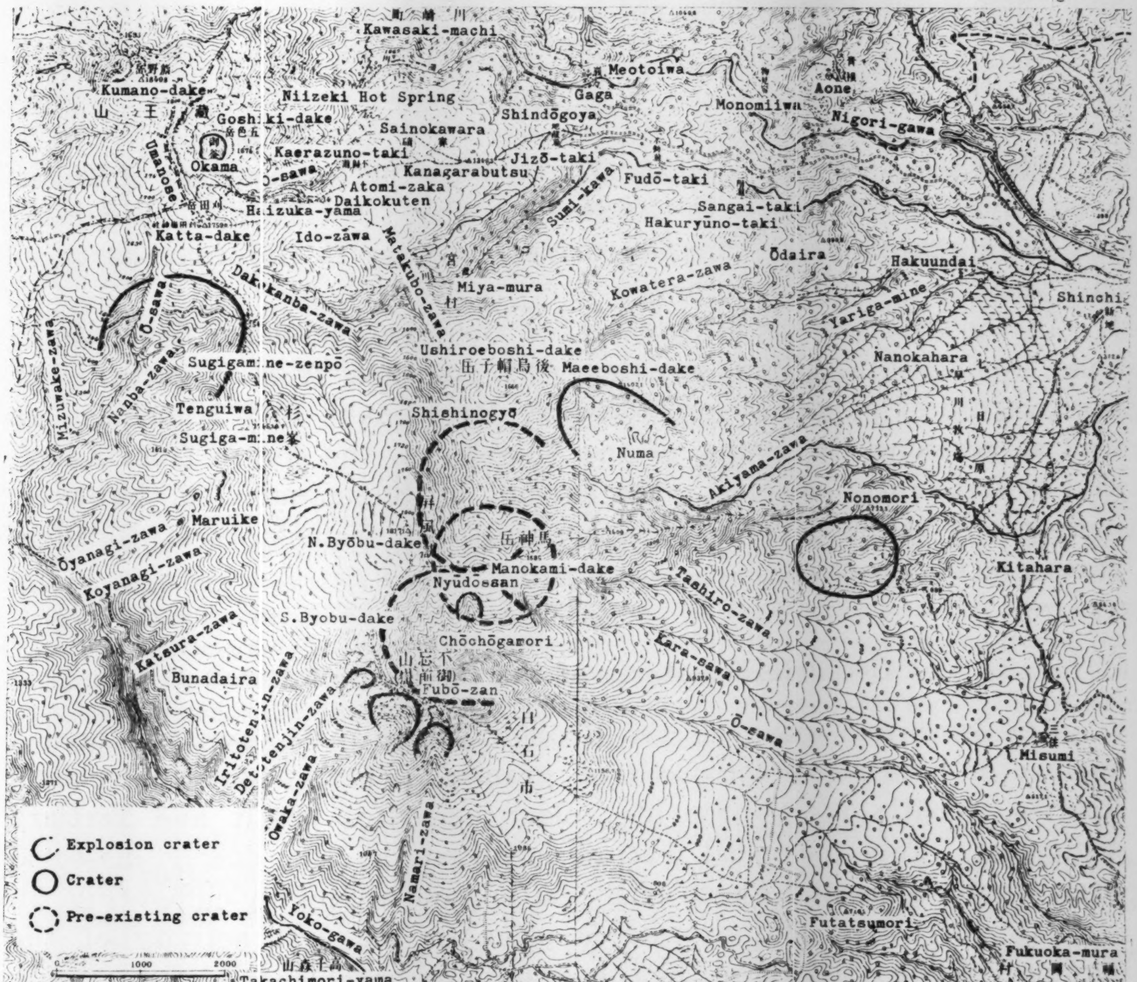

Fig. 1. Topographical map of the Byōbu Volcano and its vicinity.

* Communicated by N. Nasu.

(1402.1 m.), Nyūdō-san (1640 m.), Manokami-dake (1585 m.) and Nonomori (733.3 m.), and is separated from the North Zaō by the Sumi-kawa, and Nanba-zawa. This area is now dissected deeply along the Yoko-gawa, Sumi-kawa, Nigori-gawa and Akiyama-zawa as well as along their tributaries (Fig. 1). Moreover, it is thickly forested and almost unexplored when compared with other parts of the Zaō volcanoes. Most of its area is, therefore, not easily approached, but the first geological work was already carried out by A. Takada[1] more than 30 years ago. From that time, no further investigation had been intended until the writer's field work started in the autumn of 1947.

The results obtained in his field and laboratory works are summarized in this paper, excluding those of chemical investigations of lavas and ejecta which have not been finished.

Location

The Byōbu Volcano is situated at the northeastern corner of Katta-gun, Miyagi Prefecture. It is now accessible from Tōgatta, Kamasaki and Gaga respectively. These courses lead us to different parts of this volcano.

In the first case, Manokami-dake, Ushiro-eboshi-dake, Mae-eboshi-dake, Nonomori and Fubō-zan can be approached from Tōgatta. For the purpose of climbing up Fubō-zan, Byōbu-dake and Nyūdō-san as well as reaching the source of the Yoko-gawa, the course from Kamasaki is frequently selected. The summit of Sugiga-mine is, however, more easily attained from Gaga, crossing over Sainokawara, Haizuka-yama and Katta-dake.

Geological Features of the Byōbu Volcano

The lavas and ejecta of the Byōbu Volcano rests upon the eroded surface of base rocks composed of granite, aplite, pegmatite, plagioliparite, felsitic rock, propylite, older andesite, basalt and Tertiary sediments. This geological feature is shown at the deeply dissected area where lavas and ejecta of Byōbu Volcano are highly cliffed (Fig. 2).

(1) Intrusives and extrusives prior to the first activity of the Byōbu Volcano:—Of these, biotite granite or hornblende-biotite granite is the most predominant rock covered by the Tertiary formation and

1) H. TAKADA, The Zaō Volcano, *M.S.*, 1922.

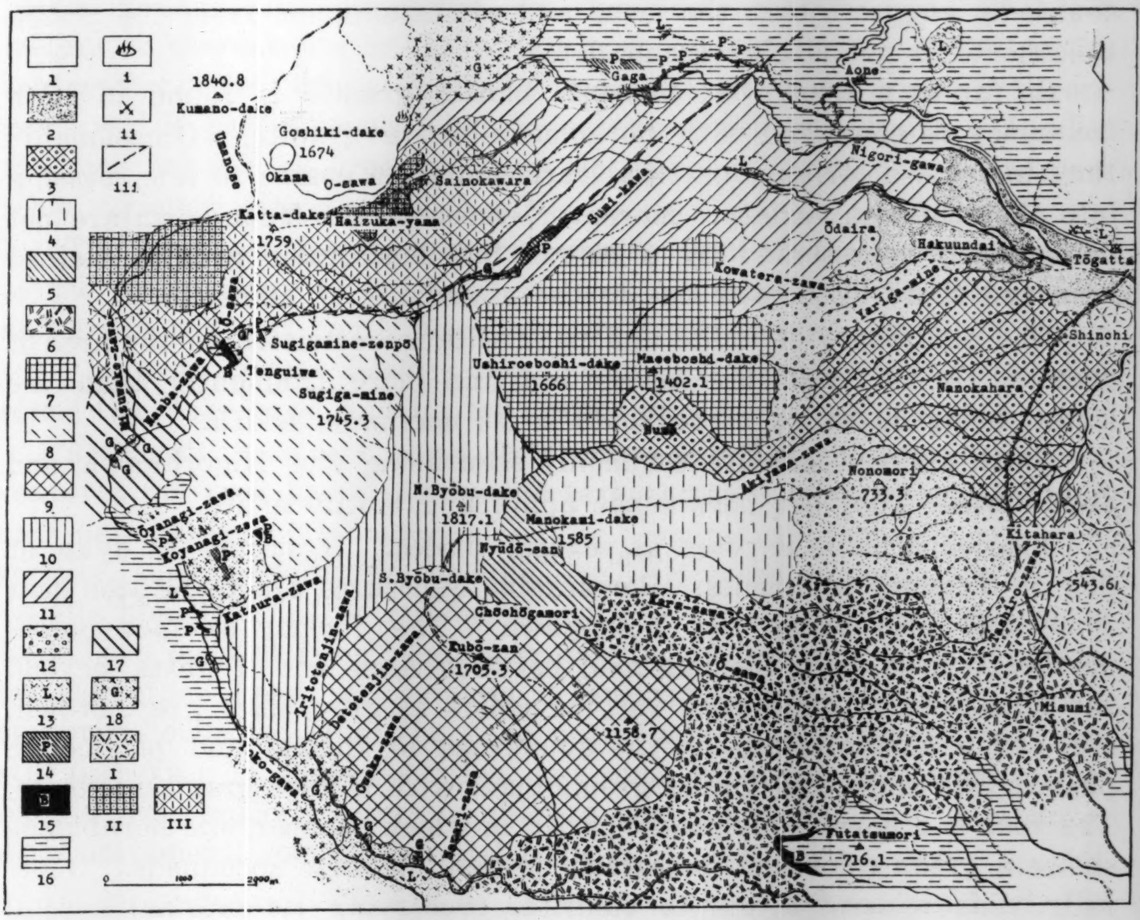

Fig. 2 Geological map of the Byōbu Volcano and its vicinity.

1. Recent fluviatile deposits, 2. Older fluviatile deposits, 3. Nanokahara mud flow, 4. Manokami-dake lava and agglomerate, 5. Nyūdō-san lava and agglomerate, 6. Kara-sawa mud flow covered partly by talus deposits, 7. Ushiro-eboshi-dake lava and ejecta, 8. Sugiga-mine lava and agglomerate, 9. Fubō-zan lava and ejecta, 10. Byōbu-dake lava, 11. Sumi-kawa lava and agglomerate, 12. Nonomori agglomerate, 13. Liparite, felsophyre and felsite, 14. Propylite, 15. Basalt, 16. Green tuff and shale (Upper Miocene), 17. Older andesite, 18. Granite or granodiorite, I. Matsu-kawa mud flow (Aoso Volcano), II. Kumano-dake lava and ejecta (Zaō Proper), III. Nanba-zawa lava and ejecta (Zaō Proper), i. Hot spring, ii. Mine abandoned, iii. Fault.

older or younger andesite, being cut by aplite, pegmatite, plagioliparite, felsitic rock, propylite and basalt. The granite here are sporadically exposed near Gaga and along the Sumi-kawa as well as along Yoko-gawa. The best exposure can be seen on the bottom of Yoko-gawa and its tributaries represented by the Ōyanagi-zawa, Koyanagi-zawa, Nanba-zawa, etc. The highest point is seen at the upper course of the Nanba-zawa more than 1300 meters above the sea-level. This fact un-

doubtedly suggests that the lavas and ejecta supplied from the Byōbu Volcano were not thickly accumulated.

So far as is known at present, biotite granite is found in high frequency as compared with hornblende-biotite granite. Occasionally, they indicate a striking textural variation from coarse to fine, passing into the schistose variety. Moreover, those of the Yoko-gawa are not infrequently represented by a coarse but leucocratic granite stained here and there by a color due to the abundance of hematite.

The occurrence of aplite and pegmatite is restricted to the area of granite. In this case, the former is found more frequently than the latter, being 50 cm. or thereabouts in its maximum width.

Small aplite dykes are commonly seen along the Nigori-gawa and Sumi-kawa. They are hornblende aplite and biotite aplite.

Plagioliparite is exposed at several places. It occurs as dyke or flow in Tertiary sediments. Remarkable exposures are to be seen near Aone and also along the Yoko-gawa. The former extends north-northeastwards from the bus road between Aone and Tōgatta beyond the Mae-kawa. It has such varying colors as grey, dark grey, brown, etc. and is characterized by the abundance of quartz and plagioclase phenocrysts embedded in the groundmass with a microgranitic texture. The rock is a hornblende plagioliparite in which phenocrystic hornblende shows a green color and is scarcely present in some specimens. Generally, this mineral alters to chlorite, preserving its original crystal form. The latter seems, on the other hand, to be underlain by granite at the southern foot of Fubō-zan. The plagioliparite here reveals a beautiful columnar joint which occasionally takes a horizontal position. It is a spherulitic liparite with a light greenish grey color due to chloritization.

Tertiary sediments are sometimes traversed by felsitic rocks, as is observed on the route between Gaga and Aone. The similar kind of rock is also found near Fudō-taki of the Sumi-kawa and at the lower course of the Namari-zawa running down southwards from near the summit of Fubō-zan. The felsitic rock is felsite or felsophyre with a light grey or light greenish grey color. The specimen obtained from the Namari-zawa is a felsophyre rich in phenocrystic plagioclase and grades into plagioliparite westwards.

A noticeable feature of base rocks is the abundance of propylite dykes, large or small, in the granitic mass and green tuff. The largest one is traceable more than 800 meters west-northwestwards from Gaga,

being bordered by green tuff on the ridge behind Gaga. It is 400 meters or thereabouts in the widest part and is highly cliffed at its southeastern end, where the dyke is deeply cut down by the Nigori-gawa and is partly covered by olivine two-pyroxene andesite. Usually, the rock has a dark greenish grey or green color, although there is some varieties with a purplish shade.

The next prominent exposure extends from northeast to southwest at the upper course of the Sumi-kawa in contact with biotite granite and green tuff. It has a black color in fresh specimens, but a green color in weathering. Besides these, many minor dykes are distributed along the Yoko-gawa and its tributaries or elsewhere.

Although there are some differences in mineral composition and texture, the rock has a porphyritic texture and consists of such ingredients as andesine or labradorite, augite, magnetite, hematite, chlorite, sericite, zoisite, leucoxene, epidote, etc. Of these minerals, chlorite is usually abundant in the specimens with a green color and seems to have been derived from plagioclase, augite, olivine, etc. Epidote occurs, on the other hand, as veinlets or incrustations of druses. In the specimens collected from the dyke near Gaga, augite phenocrysts are still preserved in fresh condition, but some phenocrystic mineral resembling olivine entirely alters to chlorite and magnetite. It exhibits a diabasic mineral composition and texture.

Older andesite begins to be exposed at the western corner of the Byōbu Volcano and extends westwards beyond the boundary between Miyagi and Yamagata Prefectures. It is a lava flow underlain by biotite granite and overlain by green tuff. Its thickness is variable from place to place, the exposure being estimated to be about 1300 meters at the highest point.

The andesite under consideration is a compact and porphyritic rock with a dark grey or dark greenish grey color which passes into a grey or yellowish grey color in intensely decomposed specimens. Under the microscope, the rock is composed of labradorite, magnetite, chlorite, leucoxene, titanite and glass. Exclusive of plagioclase, it does not contain any other phenocrystic mineral with a fresh appearance. Most of ferromagnesian minerals and a part of plagioclase change into chlorite or other secondary minerals.

Olivine basalt older than lavas and ejecta of the Byōbu Volcano are found as dykes, large or small, along the Nanba-zawa, Sumi-kawa and Koyanagi-zawa as well as near Futatsumori. Of these exposures,

dykes of the Nanba-zawa seem to extend from east to west in contact with biotite granite and older andesite. The specimens collected here have a black color and a coarse porphyritic texture due to the abundance of large plagioclase phenocrysts, 5 millimeters or more in the maximum diameter. Besides plagioclase, this type of basalt consists of olivine, augite and magnetite in fresh specimens, but usually changes to the rock with a greenish shade or grey color, resulting in the formation of such minerals as bowlingite, calcite, sericite and chlorite. These alteration products are derived from various phenocrystic minerals and the ingredients of the groundmass with an intergranular texture. Moreover, the rock has a tendency to break easily into small fragments in weathering. There are also many boulders of similar basalt on the bed of the Sumi-kawa where they are supposed to have been supplied from the dyke running across the granitic area.

The olivine basalts of the Koyanagi-zawa and near Futatsumori, on the other hand, have somewhat different features from those mentioned above. The former traverses biotite granite and is exposed about 1500 meters along the valley, whereas the latter is traceable more than 1000 meters from east to west and 700 meters or thereabouts from north to south in green tuff. They are finely porphyritic and compact rocks with a black color and contain plagioclase, olivine, augite, magnetite, apatite, bowlingite and chlorite. In some specimens, phenocrystic olivine is abundantly present in the intergranular groundmass.

(2) Tuff, conglomerate and shale beds:—The Byōbu Volcano is partly underlain by Tertiary sediments which are composed of tuff, conglomerate and shale. They are well exposed along the Yoko-gawa and its tributaries, Sumi-kawa, Nigori-gawa and Mae-kawa as well as in the surrounding district of this volcanic area. These sediments are occasionally traversed by plagioliparite, felsitic rock, propylite, basalt, etc. and rest upon biotite granite or hornblende-biotite granite of the Yoko-gawa, Nanba-zawa, Sumi-kawa and Nigori-gawa. It is noteworthy that the formation frequently has a basal conglomerate, as is shown in the vicinity of Gaga and at the upper course of the Nanba-zawa and Sumi-kawa. The basal conglomerate contains various kinds of pebbles represented by biotite granite, hornblende-biotite granite aplite, plagioliparite, felsitic rock, propylite, older andesite and shale. They are cemented with tuffaceous or sandy substances with a green or grey color different from place to place, and pebbles of older

andesite and shale are restricted to the specimens from the Nanbazawa where the fragments of petrified woods are abundant in conglomerate. In such cases, the presence of granite pebbles supplied undoubtedly from this district suggests that granite had already been intruded prior to the sedimentation of the Tertiary formation under consideration.[2)]

Green tuff is sometimes associated with conglomerate with a gradual transition between them. It is generally mottled with a green color. The writer has discovered some fossils in green sandy tuff exposed on the trail near Fudō-taki of the Sumi-kawa. They are imperfectly preserved, but there are brachiopods which can be identified with *Terebratulina*.

Grey shale is distributed in close association with green tuff. The former, however, occurs in a small extent as compared with the latter, and its exposure is to be seen along the Nigori-gawa near Aone and the upper course of the Yoko-gawa.

The Tertiary formation mentioned above is much disturbed here and there. Hence, the green tuff bed near Aone and Gaga indicates a strike of N 50°–55°E to N 20°–70° W and a dip of 40°–60° SE or 25°W–40° SSW, whereas the shale bed of the Yoko-gawa has a strike of N–S and a dip of 30°–40° W. They are always poor in fossils, but have some lithological similarities to the Upper Miocene sediments of the neighbouring district.

(3) Lavas and ejecta from the Byōbu Volcanio:—The volcanic products including lavas and ejecta of the Byōbu Volcano are complicatedly overlapped, suggesting that there were repeated eruptions of this volcanic area. They are the Nonomori agglomerate, Sumi-kawa lava and agglomerate, Byōbu-dake lava, Fubō-zan lava and ejecta, Sugigamine lava and agglomerate, Ushiro-eboshi-dake lava and ejecta, Karasawa mud flow, Nyūdō-san lava and agglomerate, Manokami-dake lava and Nanokahara mud flow.

(i) Nonomori agglomerate:—The first eruption of the Byōbu Volcano seems to have taken place at the eastern periphery of this volcanic area where the large crater of Nonomori is found on the hilly land between the Akiyama-zawa and Tashiro-zawa. The agglomerate exposed here extends northwards up to Yariga-mine and Haku'undai, being overlain by the Nanokahara mud flow on its east and by the

2) T. Ichimura, H. Minato & K. Kanehira, *Jour. Geol. Soc. Japan*, **56** (1950), 470.

Sumi-kawa lava and agglomerate, Ushiro-eboshi-dake lava and ejecta and Manokami-dake lava on its west respectively. It was undoubtedly erupted from the crater which was almost circularly hollowed at the southern foot of Nonomori (Fig. 3).

The best exposure can be seen along the middle course of the Akiyama-zawa, and it is composed of the angular fragments of two-pyroxene andesite or olivine-bearing two-pyroxene andesite, large or small, cemented with tuffaceous or sandy matrix.

(ii) Sumi-kawa lava (olivine-bearing two-pyroxene andesite or olivine two-pyroxene andesite) and agglomerate:—The Sumi-kawa lava and agglomerate are exposed at the northern part of the Byōbu Volcano dissected deeply by the Nigori-gawa, Sumi-kawa and Kowatera-zawa. Of these, the lava flow gently inclines northwards or northeastwards and is highly cliffed along the Nigori-gawa and Sumi-kawa (Figs. 4—5), where it is 150 meters or thereabouts in the thickest part and is characterized by the predominance of columnar joints (Fig. 6). Such exposures are traceable up to Kaerazuno-taki of the Nigori-gawa and the junction of the Matakubo-zawa and Sumi-kawa.

The agglomerate is, on the other hand, found only at the lower course of the Sumi-kawa. It is well exposed on the cliff near Fudō-taki and Sangai-taki, showing that it is the basal part of the thick lava flow mentioned above.

These volcanic products rest upon the eroded surface of the Nonomori agglomerate, biotite granite or hornblende-biotite granite or Tertiary sediments, but they partly disappear beneath such lavas and ejecta erupted later from the Byōbu Volcano and Zaō Proper, as is indicated by the Byōbu-dake lava, Ushiro-eboshi-dake lava and ejecta, Nanba-zawa lava and ejecta, etc.

The Sumi-kawa lava and agglomerate are supposed to have been supplied from the pre-existing crater which is now obscured by the eruption of the Manokami-dake lava and Nyūdō-san lava and agglomerate.

(iii) Byōbu-dake lava (olivine-bearing two-pyroxene andesite):—The eruption of the Byōbu-dake lava took place later than those of the Sumi-kawa lava and agglomerate, although it poured out from the same pre-existing crater. The lava flow extends down to the uppermost course of the Sumi-kawa northwards and to the Yoko-gawa southwestwards. It is bordered by the Sugiga-mine lava and agglomerate on the west, but is covered by the Ushiro-eboshi-dake lava and ejecta and Nyūdō-san lava and agglomerate on the east. The eastern side of

Byōbu-dake slopes steeply downwards and forms here a high cliff in contrast with its western gentle slope (Figs. 7–8). Such a topographic feature partly depends upon the inclination of the Byōbu-dake lava. The highest point of this lava is 1817.1 meters above the sea-level, and its thickest part is more than 400 meters. It is also known that the lava flow rests upon Tertiary sediments and biotite granite along the Yoko-gawa and Katsura-zawa.

(iv) Fubō-zan lava (olivine-bearing two-pyroxene andesite or olivine two-pyroxene andesite) and ejecta:—The southern end of the Byōbu Volcano is represented by Fubō-zan (Figs. 3, 9) which rises up to 1705.3 meters above the sea-level on the base rocks composed of biotite granite, felsophyre, olivine basalt and green tuff. The lava flows and ejecta exposed here are alternately bedded with an inclination of 20°–30° southwestwards, suggesting that they are supplied from the same source as that of the Byōbu-dake lava. Such features are confirmable on the narrow ridge extending northwestwards from the summit of this peak. It is also noteworthy that these alternate beds of lava flows and ejecta are repeatedly traversed by small basalt dykes on the cliff rising up from Chōchogamori.

(v) Sugiga-mine lava (olivine two-pyroxene andesite) and agglomerate:—The Byōbu-dake lava is covered by the Sugiga-mine lava and agglomerate which had a source on the western flank of Byōbu-dake. In this case, the lava flow, about 400 meters thick, was preceeded by the eruption of agglomerate, about 100 meters in thickness. It is well exposed on the western flank of Sugiga-mine in close association with agglomerate underlain by the Tertiary andesite and biotite granite of the Yoko-gawa and its tributaries. The relationship between lava and agglomerate can be seen at the upper course of the Ōyanagi-zawa, and the latter passes into the former upwards. The lava of this area is highly cliffed and shows a topographically characteristic feature. Such remarkable cliffs are sporadically traceable from Tengu-iwa to the upper course of the Koyanagi-zawa southwards. The northern end of these exposures are bordered by the Nanba-zawa lava of the Zaō Proper along the Nanba-zawa and Sumi-kawa.

(vi) Ushiro-eboshi-dake lava (two-pyroxene andesite) and ejecta:—As has already been explained, the Ushiro-eboshi-dake lava and ejecta partly cover the Sumi-kawa lava and agglomerate or Nonomori agglomerate, constructing here Ushiro-eboshi-dake and Mae-eboshi-dake at the northern end of the Byōbu Volcano. The former inclines 15°–20°

northeastwards on the eroded surface of the latter and is supposed to have been erupted from the crater which had similarly been the source of the Sumi-kawa lava and agglomerate. The alternation of these lava flows and ejecta, about 350 meters thick, may be well investigated by going up the Kowatera-zawa or traversing Ushiro-eboshi-dake from north to south. In this case, lava flows are usually predominant as compared with ejecta composed of agglomerate, lapilli and tuff.

(vii) Kara-sawa mud flow:—The gentle slope dissected by the Tashiro-zawa, Kara-sawa and Ō-sawa is widely covered by the Kara-sawa mud flow (Fig. 3) which seems to have poured out from the source which is supposed to have succesively supplied the Nyūdō-san lava and agglomerate. It flowed down eastwards and spreaded widely over the area including Misumi and the eastern foot of Fubō-zan, probably in contact with the Matsu-kawa mud flow of the Aoso Volcano[3] at its eastern end.

(viii) Nyūdō-san lava (two-pyroxene andesite) and agglomerate:— Nyūdō-san (Figs. 3, 10) is composed of lava and agglomerate erupted alternately from the pre-existing crater where it was borned as a central cone. The basal part of these volcanic products is agglomerate which is exposed along the uppermost course of the Akiyama-zawa and passes into lava flow intercalated by agglomerate upwards. They have mostly an inclination of 20°–30° to the south.

(ix) Manokami-dake lava (two-pyroxene andesite):—It extends from east to west and builds up Manokami-dake (Figs. 3, 10), being bordered by the Akiyama-zawa at the north and the Kara-sawa at the south. The best exposure of this lava is seen on the northern flank of Manokami-dake where the lava flow is deeply dissected and highly cliffed here and there by the Akiyama-zawa. It is considered to have poured out from the pre-existing crater after the eruption of the Nyūdō-san lava and agglomerate, since there are some evidences that the former rests upon the latter.

(x) Nanokahara mud flow:—The activities of Byōbu Volcano was closed with the eruption of the Nanokahara mud flow (Fig. 3). The source of this mud flow is the explosion crater of Numa just beneath the summit of Mae-eboshi-dake. The mud flow which rushed down from here to northeast through the narrow between the southern branch of Mae-eboshi-dake and eastern end of Manokami-dake, formed a large fan-shaped slope now called Nanokahara. Topographically, it

3) T. ICHIMURA, *Bull. Earthq. Res. Inst.*, **31** (1953), 134.

shows a characteristic feature easily distinguishable easily from its surrounding district.

(4) Quaternary fluviatile deposits:—Younger or older fluviatile deposits are seen along the present river course where they consist of clay, sand and gravel.

Structure of the Byōbu Volcano

The Byōbu Volcano consists of two homates. One of these includes the hilly land between the Akiyama-zawa and Tashiro-zawa where a large but shallow crater is still preserved, and Nonomori seems to have been formed on its peripheral part. The extension of this homate is distinctly shown by the panoramic view looking down from Ōmori-yama of the Aoso Volcano (Fig. 3).

Another one is a strato-homate associated with central cones and rises up to 1817.1 meters above the sea-level as the main part of the Byōbu Volcano, but it is now deformed and dissected to some extent. The large pre-existing crater here is obscured by the formation of central cones and the destruction of crater wall due to explosions. It is, however, not impossible to suppose the position of the crater from the direction of inclination of lavas and ejecta exposed on such peaks as Byōbu-dake, Fubō-zan, Ushiro-eboshi-dake, Mae-eboshi-dake, Nyūdō-san and Manokami-dake. This center of activity is located on the southern extension of the weak line which passes through those of the Zaō Proper and Ryū-zan Volcano.

The structure of the Byōbu Volcano is more complicated by the lavas and ejecta erupted from other sources. They are the lava and agglomerate of Sugiga-mine and the mud flow of Nanokahara and the Kara-sawa.

As has already been stated elsewhere, the volcano under consideration rises up on the foundation composed of the Tertiary formation, granite, aplite, plagioliparite, propylite, felsite, felsophyre, andesite and basalt. It is constructed by two-pyroxene andesite, olivine-bearing two-pyroxene andesite, olivine two-pyroxene andesite and various kinds of ejecta. Some of these volcanic products are alternately piled up, starting mostly with the eruption of agglomerate or tuff. Such a structure is commonly seen on Ushiro-eboshi-dake, Sugiga-mine, Fubō-zan and Nyūdō-san as well as along the lower course of the Sumi-kawa. In the last case, the thick lava flow extends northwards or northwestwards beyond the Sumi-kawa and even the Nigori-gawa at some places. Its exposure is highly cliffed and rests upon base rocks along these valleys (Fig. 5).

So far as is known at present, a part of this volcanic area seems to have been subjected to faulting. For example, the eastern cliff of Byōbu-dake, which is about 300 meters high and extends straightly from north to south, looks like a fault scarp (Fig. 8). Moreover, it is necessary to describe the trend of the Sumi-kawa and Nanba-zawa. They rise from a divide between Sugiga-mine and Katta-dake and run down to the opposite side, taking a course from southwest to northeast and from northeast to southwest respectively. The northeastern extension of this line almost agrees with the trend of the Mae-kawa, passing the vicinity of Monomi-iwa and Aone, whereas its opposite trend is traceable southwestwards to Kayadaira. It is also noticeable that various kinds of base rocks are frequently exposed on these two valleys which are parallel to the Hanoki-zawa dislocation line.

Crater

There are two craters in this volcanic area (Fig. 1). They are respectively found at its central part and eastern periphery. At present, the former disappears beneath two central cones surrounded partly by Byōbu-dake, Fubō-zan and Ushiro-eboshi-dake. The location of pre-existing crater is, however, inferable from the structure of this volcano, although the original topographical feature was largely destroyed later by explosions and dislocations.

The latter is, on the other hand, well preserved on the hilly lands between the Akiyama-zawa and Tashiro-zawa (Fig. 3). This crater had been overlooked until it was recently confirmed by the writer. Its diameter is 1200 meters from east to west, but 1000 meters from north to south. It has a crater wall, about 100 meters high from its bottom, and is opened in agglomerate. This is supposed to have been the earliest center of activity.

Explosion Craters

The Byōbu Volcano is characterized by the frequency of explosion craters, large or small, by which the present topographical feature of this volcano is considerably affected (Fig. 1). They are found in the area around the pre-existing crater. One of remarkable explosion craters is preserved at Numa, where the mud flow poured out at the last stage of activity and rushed down eastwards along the Akiyama-zawa (Fig. 3). The explosion crater here is semicircularly surrounded by a steep wall of about 100 meters high on the southern flank of Mae-eboshi-dake. It opens southwards, and its bottom is filled up with an accumulation

of mud flow. The undulatory surface of this mud flow is thickly covered by a beautiful forest of beech and is adorned with many small swamps from which the name "Numa" was taken.

Besides this, another explosion crater seems to have been opened farther up the Akiyama-zawa. It was, however, subjected intensely to the subsequent erosion of the Akiyama-zawa and its tributaries, resulting in a remarkable modification of the original form.

There is also a similar explosion crater at the source of the Ō-sawa. It is situated behind Nyūdō-san and is semicircularly walled by Byōbu-dake and Fubō-zan, although its inner part is intricately dissected by the Ō-sawa with an undulation of Chōchogamori. The highest point of this wall is estimated to the about 400 meters above the bottom of the main valley.

In connection with it, several explosion craters are located on the southern flank of Fubō-zan. They are scattered here and there, some of these being found near the crest line between its summit and S. Byōbu-dake. Such explosion craters are represented by horse-shoe-shaped or semicircular hollows opened mostly southwards or southwestwards. The largest one is sccoped out downwards from near the summit of Fubō-zan and is surrounded by a wall composed of thickly accumulated lavas and agglomerates which incline about 30° southwards. It is the source of the Owaka-zawa, a tributary of the Yoko-gawa.

Moreover, the presence of a large explosion crater is noticed at the uppermost course of the Nanba-zawa, being situated between Katta-dake and Sugiga-mine. It has a diameter of about 1500 meters from northwest to southeast. This crater seems to have exploded southwestwards, and a part of its wall shows an alteration due to solfataric action. It is about 300 meters high above its bottom, where granite and Tertiary sediments are exposed. A small explosion crater is also known on the southern flank of Nyūdō-san.

Central Cones

Two central cones rise up in the pre-existing crater obscured by the eruption of their lavas and ejecta. These central cones are Nyūdō-san and Manokami-dake (Fig. 10). They stand side by side with a trend from east to west, showing that the eruptions took place in succesion. The lava flow and agglomerate of Nyūdō-san partly disappear beneath the Manokami-dake lava. This fact evidently suggests that Nyūdō-san is older than Manokami-dake. Their structures can be ex-

amined by going up along the Akiyama-zawa, Kara-sawa and Tashiro-zawa as well as along their tributaries. One remarkable feature is the existence of a horse-shoe-shaped hollow on the southern flank of Nyūdō-san. It looks like an explosion crater, being partly surrounded by a wall on which lava and agglomerate are well exposed with an inclination of about 30° southwards. Both central cones are strikingly dissected along the Akiyama-zawa, where they are highly cliffed here and there, but thickly forested. In this case, the agglomerate of Nyūdō-san exposed near the bottom of the Akiyama-zawa passes into a lava flow upwards. The similar order of eruption is indicated by volcanic products of Manokami-dake.

Possible Source of the Sugiga-mine Lava and Agglomerate

There is no evidence that the Sugiga-mine lava and agglomerate were erupted from the pre-existing crater beneath Nyūdō-san and Manokami-dake. These volcanic products begin to be exposed on the western flank of Byōbu-dake and spread extensively down to the Yoko-gawa, Sumi-kawa and their tributaries. The highest point rises up as a large dome called Sugiga-mine which is now eroded deeply by such several tributaries of the Yoko-gawa as the Nanba-zawa, Ōyanagi-zawa, Koyanagi-zawa and others on its western flank. The present summit is partly fringed by swampy terraces and is free of any crater-like hollow. It is, however, not unreasonable to say from the distribution and inclination of lava and agglomerate exposed here that they were supplied from a source somewhere near the summit.

Mineral Composition of Lavas and Ejecta

(1) *Andesite fragments of the Nonomori agglomerate*:—Angular or subangular fragments of two-pyroxene andesite or olivine-bearing two-pyroxene andesite are abundantly contained in the Nonomori agglomerate, being cemented by a tuffaceous matrix in which they are found without any regular arrangement. The writer collected many specimens of these fragments from various parts of this agglomerate, particularly along the Akiyama-zawa and also on the hilly land between the Tashiro-zawa and Akiyama-zawa where it is extensively exposed. Although these andesite fragments indicate somewhat different features from place to place, most of them are compact and remarkably porphyritic. They have a dark grey or black color and assume a grey or reddish

brown color by alteration.

The specimens examined under the microscope are mainly composed of plagioclase, augite, hypersthene and magnetite with a minor or almost negligible amount of hornblende, olivine, biotite, quartz, apatite, tridymite, chlorite, pyrite, goethite and limonite. The last four minerals are secondary products.

The most predominant mineral is plagioclase. Its phenocryst takes a rectangular or tabular form and belongs to labradonite or bytownite with a composition of An_{60-76}. In this case, the crystal is generally euhedral or subhedral, and the largest one is 3 mm.-4 mm. long or across. It has a fresh appearance and is well zoned. The phenocryst is sometimes turbid along the periphery or at the inner part of crystals. Such a feature is seen in the specimens obtained along the trail traversing the hilly land mentioned above from northwest to southeast. Some of it encloses augite or magnetite crystals and is characterized by a worm-eaten structure. It is also noteworthy that phenocrystic plagioclase is occasionally altered to chlorite along its crack or cleavage.

Minute lath-shaped or rectangular plagioclase is an important ingredient of the groundmass, showing a fluidal arrangement in some cases. It is commonly 0.03 mm.-0.25 mm. in length and is represented by labradorite.

Augite occurs as phenocrysts, granular aggregates and ingredients in the groundmass. In these cases, phenocrystic augite is often twinned on (100) or (101) and has a subhedral or anhedral form, being 2.55 mm. long and 1.02 mm. across in its largest crystal. The extinction angle, $Z \wedge c$, is 39°-40°. When it is found in association with hypersthene, the latter is fringed by the former. There are also zoned crystals in which the inner part has a large extinction angle as compared with the periphery. The phenocrystic augite generally encloses magnetite. The augite crystal of the groundmass is abundantly present with magnetite, hypersthene and minute lath-shaped plagioclase. It takes a prismatic or granular form which is 0.01 mm.-0.13 mm. in length or diameter.

The phenocrystic hypersthene usually shows a frequency slightly higher than augite. It has a long or stout prismatic habit, being 4.15 mm. long and 1.53 mm. across in the largest crystal. Of these, the long prismatic crystal is occasionally euhedral. It contains magnetite and is partly chloritized along cracks. Hypersthene is also a remarkable ingredient in the groundmass of a certain specimen. In such a

case, it is mostly represented by a long prismatic crystal 0.05 mm.–0.15 mm. long.

Table I. Compositions and optical characters of plagiocalse, augite and hypersthene phenocrysts of the andesite fragments in Nonomori agglomerate (Measured by F. Hori).

	No. 1 (T.I. 47102502)	No. 2 (T.I. 47102801)	No. 3 (T.I. 47102805)
Plagioclase	$\alpha=1.559\pm0.003$ $\gamma=1.575\pm0.003$ An_{60-71}*	$\alpha=1.562\pm0.003$ $\gamma=1.577\pm0.003$ An_{63-76}*	$\alpha=1.564\pm003$ $\gamma=1.577\pm0.003$ An_{67-76}*
Augite	$\beta=1.683\pm0.003$ $(+)2V=53°$ $Wo_{44}En_{46}Fs_{10}$**	$\beta=1.692\pm0.003$ $(+)2V=47°$ $Wo_{39}En_{43}Fs_{18}$**	$\beta=1.685\pm0.003$ $(+)2V=54°$ $Wo_{45}En_{44}Fs_{11}$**
Hypersthene	$\gamma=1.713\pm0.003$ $(-)2V=58°$ Mg=63%***	$\gamma=1.710\pm0.003$ $(-)2V=60°$ Mg=65%***	$\gamma=1.711\pm0.003$ $(-)2V=58°$ Mg=63%***

* After F. Chayes's chart [Am. Min. Bowen Volume, (1952) 95].
** After H.H. Hess's chart [Am. Min., 34 (1949) 634].
*** After H. Kuno's chart [Am. Min., 39 (1954) 40].

No. 1. = Andesite fragment in the Nonomori agglomerate exposed along the Akiyama-zawa.
No. 2. = 〃 〃 exposed on Yariga-mine
No. 3. = 〃 〃 exposed near Hakuundai.

A noticeable feature of andesitic fragments is the abundance of magnetite as an enclosure in other minerals and in the groundmass of some specimens. The octahedral or granular crystals of this mineral is sometimes more than 1.20 mm. in its diameter, but is usually 0.01–0.04 mm. across.

The occurrence of olivine phenocrysts is restricted to the specimens obtained at the bottom of the Tashiro-zawa and on the hill between the Tashiro-zawa and Akiyama-zawa as well as from Haku'undai. It is a rare ingredient in these specimens and takes an unhedral form, 1.1 mm. in its maximum diameter.

Subhedral or anhedral hornblende is seen in the xenoliths of several specimens. It is long prismatic and has a fresh appearance, being characterized by such a pleochroic scheme as light yellow (X), light brown (Y) and yellowish brown (Z). The absorption is $Z>Y>X$, and the largest crystal is 1.22 mm. long and 0.4 mm. across. The mineral shows a small extinction angle, $Z\wedge c$, of 18° or thereabouts. Some of it twins

on (100) and contains minute magnetite grains.

Biotite and apatite seldom occur in the groundmass. The former is strongly pleochroic from dark brown (Y and Z) to yellow (X), whereas the latter has a dark brown color due to decomposition in the inner part of prismatic crystals. The maximum length is 0.48 mm.

Tridymite fills up the interstices of the ingredient minerals in the groundmass. Quartz is, on the other hand, a xenocryst supplied from base rocks and is subjected to the magmatic corrosion. This mineral is scarcely found in the fragment of olivine-bearing two-pyroxene andesite. Pyrite is richly present in a specimen from the Akiyama-zawa. It traverses the rock as veinlets or irregular networks. Chlorite, goethite and limonite are the decomposition products due to weathering.

The groundmass reveals a pilotaxitic texture, consisting of plagioclase, augite, hypersthene, biotite, tridymite, magnetite and apatite. Besides these, some specimens contain gabbroic, noritic or basaltic inclusions composed of plagioclase, augite, hypersthene, hornblende and magnetite.

(2) *Sumi-kawa lava and agglomerate*:—The Sumi-kawa lava and andesite fragments of its agglomerate have similar feature and mineral composition, being almost composed of olivine-bearing two-pyroxene andesite or olivine two-pyroxene andesite with or without a glassy groundmass.

They are usually hard and compact rocks with a black or dark grey color and remarkable porphyritic texture. These andesites are, however, scoriaceous at the bottom of lava flows which are found in contact with base rocks, as is indicated along the Nigori-gawa, particularly on the cliff opposite to the Gaga Hot Spring. Moreover, one of characteristic features to these andesite lavas is the occurrence of a pitchstone with a porphyritic texture and black color. It is exposed along the trail between Ōdaira and Hakuryūno-taki.

The specimens collected by the writer consists of plagioclase, augite, hypersthene, olivine, hornblende, magnetite, quartz, tridymite, apatite, biotite, chlorite, bowlingite and brown glass.

The most important ingredient is plagioclase which occurs mostly as euhedral or subhedral crystals, 3.91 mm. long and 1.39 mm. across in the largest crystal. These crystals are commonly well zoned and frequently turbid. Such a turbid part is formed by a cloudy aggregate of unknown substance, and it is present at the periphery or inner

portion of crystals, being surrounded by clear zones free of enclosures. The phenocrystic plagioclase is also characterized by the predominance of worm-eaten structure and includes such ingredients as augite, hypersthene, magnetite and irregular patches of brown glass. The indices of refraction measured on (010) suggest that this plagioclase ranges from labradorite to bytownorthite with a composition of An_{58-81}. The plagioclase of the groundmass is represented by minute lath-shaped or rectangular crystals, 0.01 mm.–0.25 mm. long. It is labradorite.

Augite and hypersthene are very common minerals in all specimens, although the proportion between them varies in different localities. Of these minerals, the phenocrystic augite generally takes a subhedral form with a stout prismatic habit, whereas the phenocrystic hypersthene is mostly euhedral or subhedral and occurs as a long prismatic crystal. They are sometimes associated together, which shows that hypersthene is always fringed by a minute aggregate of augite. Both kinds of minerals commonly include magnetite, but rarely glass and plagioclase. Some of the crystals are also marked by the presence of a worm-eaten structure as in the case of plagioclase.

The augite crystal is 3.48 mm. long and 1.78 mm. across in the largest one and twins on (100) or (101), forming frequently a poly-synthetic twin in cross section. It is also noteworthy that there are minute aggregates of granular augite around the skeletal crystal of magnetite. The extinction angle, $Z \wedge c$, is 38°–41°, and it gradually decreases inwards in zoned crystals.

The phenocrystic hypersthene is found as well-defined crystals as compared with augite, the largest one being 2.72 mm. long and 0.71 mm. across. It is partly chloritized.

In the groundmass, augite is a predominant ingredient, but hypersthene occurs in less amount. They are prismatic or granular, and most of these are 0.02 mm.–0.08 mm. in length or diameter.

The compositions and optical characters of phenocrystic plagioclase, augite and hypersthene are summarized in the following table (Table II).

The occurrence of olivine is restricted only to the phenocryst. The high frequency of this mineral is known in the specimens collected from the area including the Niizeki Hot Spring, Kanagarabutsu, Shin-dōgoya, Sangai-taki and Aone. It is, however, mostly found in a small amount. The crystal is generally anhedral or subhedral, being occasionally surrounded by minute aggregates of augite, hypersthene,

magnetite and plagioclase. It is 4.91 mm. across in the largest crystal and includes magnetite. In alteration, such a phenocrystic olivine passes into bowlingite along its periphery and crack. Chlorite is, furthermore, its decomposition product.

All thin sections contain magnetite in varying amounts. It occurs as an enclosure of phenocrystic minerals or a main ingredient of the groundmass. The crystal with an octahedral, granular or skeletal form is 1.75 mm. across in the largest one, but commonly ranges between 0.01 mm. and 0.08 mm. in dismeter.

Quartz is a xenocryst supplied from granites or other quartz-bearing rocks. The crystal is subjected to magmatic corrosion and has a subangular or rounded form, 1.5 mm. in its maximum diameter. Exclusive of some examples shown by several specimens, quarts is a rare ingredient.

Apatite is contained only in three specimens obtained from the lower course of the Sumi-kawa and the uppermost course of the Nigori-gawa. It takes a long prismatic form, 0.17 mm.–0.34 mm. in length. Its inner part has a grey or dark brown color due to decomposition and is closely striated. Biotite, hornblende and tridymite are also minor ingredients. Of these, biotite takes an irregular flaky form, but this mineral is absent in most specimens. Hornblende is represented by a brown variety with a subhedral form, showing such a pleochroic scheme as X=light yellow, Y=yellowish brown, Z=dark brown and an extinction angle, $Z \wedge c$, of 15°–17°. Tridymite is seen in several specimens and fills up the interspaces of various ingredients of the groundmass. The brown glass is, on the other hand, noticed frequently in the phenocrystic plagioclase and hypersthene as well as in the groundmass.

The groundmass consists of plagioclase, augite, hypersthene, magnetite, apatite, biotite, tridymite, quartz and brown glass. In this case, there are many specimens with a pilotaxitic groundmass which is quite similar to the Tōmori-yama lava of the Aoso Volcano.[4] The specimens collected from the lower part of the Sumi-kawa lava are mottled by the frequent occurrence of leucocratic parts due to decomposition. When the groundmass has a hyalopilitic texture, the brown glass is contained in varying amounts. The extreme case rich in the brown glass is pitchstone with swarms of microlites.

Besides various ingredients mentioned above, the occurrence of xenoliths, large or small, is known in almost all specimens. They are gabbroic, noritic or basaltic rocks formed by the confused aggregates

4) T. ICHIMURA, *op. cit.*, (1953), 140–142.

Table II. Compositions and optical characters of plagioclase, augite, and hypersthene phenocrysts in Sumi-kawa lava (Measured by F. Hori)*

	No. 1 (T.I. 47101401)	No. 2 (T.I. 47101406)	No. 3 (T.I. 47101902)
Plagioclase	$\alpha=1.560\pm0.003$ $\gamma=1.574\pm0.003$ An_{61-70}	$\alpha=1.559\pm0.003$ $\gamma=1.574\pm0.003$ An_{60-70}	$\alpha=1.561\pm0.003$ $\gamma=1.579\pm0.003$ An_{62-81}
Augite	$\beta=1.688\pm0.003$ (+)2V=48° $Wo_{40}En_{44}Fs_{16}$	$\beta=1.685\pm0.003$ (+)2V=47° $Wo_{39}En_{48}Fs_{13}$	$\beta=1.690\pm0.003$ (+)2V=49° $Wo_{41}En_{43}Fs_{16}$
Hypersthene	$\gamma=1.705\pm0.003$ (−)2V=63° Mg=68%	$\gamma=1.715\pm0.003$ (−)2V=56° Mg=61%	$\gamma=1.707\pm0.003$ (−)2V=63° Mg=68%

	No. 4 (T.I. 47101909)	No. 5 (T.I. 47102104)	No. 6 (T.I. 47110402)
Plagioclase	$\alpha=1.560\pm0.003$ $\gamma=1.573\pm0.003$ An_{61-69}	$\alpha=1.560\pm0.003$ $\gamma=1.574\pm0.003$ An_{61-72}	$\alpha=1.557\pm0.003$ $\gamma=1.574\pm0.003$ An_{58-70}
Augite	$\beta=1.688\pm0.003$ (+)2V=49° $Wo_{41}En_{44}Fs_{15}$	$\beta=1.683\pm0.003$ (+)2V=50° $Wo_{41}En_{47}Fs_{12}$	$\beta=1.694\pm0.003$ (+)2V=45° $Wo_{37}En_{42}Fs_{21}$
Hypersthene	$\gamma=1.702\pm003$ (−)2V=65° Mg=70%	$\gamma=1.710\pm0.003$ (−)2V=58° Mg=63%	$\gamma=1.710\pm0.003$ (−)2V=59° Mg=64%

*To confirm An, WoEnFs ratio and Mg% the charts devised by F. Chayes, H.H. Hess and H. Kuno were respectively used.

No. 1.= The Sumi-kawa lava from near Jizō-taki.
No. 2.= 〃 from the cliff opposite to the Gaga Hot Spring.
No. 3.= 〃 from the road cutting, about 700 m. from Gaga.
No. 4.= 〃 from near Aone.
No. 5.= 〃 from the upper course of the Nigori-gawa where it rests directly upon the eroded surface of granite.
No. 6.= 〃 from the cutting of bus road near Aone.

of plagioclase, augite, hypersthene, olivine, magnetite and brown glass.

(3) *Byōbu-dake lava*:—The lava flow of Byōbu-dake is exposed on its eastern cliff and western flank as well as at the area dissected deeply by the Owaka-zawa, Katsura-zawa and the uppermost course of the Sumi-kawa. The specimens collected by the writer has a remarkable porphyritic texture and dark grey color. Some of these are finely porous, whereas the others are very compact, both passing into one

Table II. (continued.)

	No. 7 (T.I. 48092009)	No. 8 (T.I. 48092010)	No. 9 (T.I. 48092101)
Plagioclase	$\alpha=1.560\pm0.003$ $\gamma=1.574\pm0.003$ An_{61-70}	$\alpha=1.558\pm0.003$ $\gamma=1.574\pm0.003$ An_{59-70}	$\alpha=1.562\pm0.003$ $\gamma=1.577\pm0.003$ An_{63-76}
Augite	$\beta=1.690\pm0.003$ $(+)2V=47°$ $Wo_{39}En_{44}Fs_{17}$	$\beta=1.688\pm0.003$ $(+)2V=52°$ $Wo_{42}En_{43}Fs_{15}$	$\beta=1.693\pm0.003$ $(+)2V=46°$ $Wo_{38}En_{42}Fs_{20}$
Hypersthene	$\gamma=1.713\pm0.003$ $(-)2V=56°$ $Mg=61\%$	$\gamma=1.709\pm0.003$ $(-)2V=58°$ $Mg=63\%$	$\gamma=1.711\pm0.003$ $(-)2V=61°$ $Mg=66\%$

	No. 10 (T.I. 48100705)
Plagioclase	$\alpha=1.561\pm0.003$ $\gamma=1.576\pm0.003$ An_{62-75}
Augite	$\beta=1.685\pm0.003$ $(+)2V=48°$ $Wo_{40}En_{47}Fs_{13}$
Hypersthene	$\gamma=1.711\pm0.003$ $(-)2V=58°$ $Mg=63\%$

No. 7. = The Sumi-kawa lava from the cliff, situated about 1500 meters northwest from Kanagarabutsu.
No. 8. = 〃 from the northwestern part of Sainokawara.
No. 9. = 〃 from the bottom of the Sanzuno-kawa near Kanagarabutsu.
No. 10. = 〃 from the lower course of the Sumi-kawa.

another. They are sometimes similar to the Sumi-kawa lava.

The microscope reveals that the Byōbu-dake lava is composed of plagioclase, augite, hypersthene, olivine, magnetite, hematite, apatite and brown glass. Of these, the amount of the phenocrystic olivine varies from place to place, and there are some specimens quite devoid of this mineral. The occurrence of brown glass is an exceptional case, whereas apatite is a negligible ingredient and is mostly absent.

Plagioclase is the most important mineral which occurs as a phenocryst or an ingredient of the groundmass. The phenocrystic plagioclase belongs to labratownite with a composition ranging from An_{61} to An_{69}. The crystal is commonly euhedral or subhedral, taking a tabular or rectangular form. It is generally well zoned and frequently turbid. The worm-eaten structure is also one of noticeable features in this

phenocrystic plagioclase, the largest crystal being 2.88 mm. long and 1.28 mm. across. In such a case, augite, hypersthene and brown glass are sometimes found as enclosures.

The plagioclase of the groundmass has a lath-shaped or rectangular form, 0.02 mm.–0.2 mm. long and indicates a fluidal arrangement around phenocrystic minerals.

Similarly, augite and hypersthene are predominant ingredients as phenocrysts and components in the groundmass. They are found in varying proportion, the former being frequently present abundantly as compared with the latter in some sections.

In all specimens, the phenocrystic augite takes a subhedral or anhedral form, 2.12 mm. long and 0.68 mm. across in the largest crystal. It twins on (100) or (101), and its extinction angle, $Z \wedge c$, is 39°–41°. When this mineral occurs together with hypersthene, the latter is always surrounded by the former. A glomeroporphyritic texture is also formed by the granular aggregate of minute augite crystals associated with magnetite and brown glass. Most of the phenocrystic hypersthene have a long prismatic habit, and the largest crystal is 1.6 mm. long and 1.02 mm. across. The crystal is usually euhedral or subhedral. It contains magnetite as in the case of the phenocrystic augite. In the groundmass, augite is more abundant than hypersthene, and its short or long prismatic crystal is 0.02 mm.–0.1 mm. in length.

Table III. Compositions and optical characters of plagioclase, augite and hypersthene phenocrysts in Byōbu-dake lava from the summit of Byōbu-dake (Measured by F. Hori).

	(T.I. 49082309)
Plagioclase	$\alpha=1.560\pm0.003$, $\gamma=1.573\pm0.003$ An_{61-69}*
Augite	$\beta=1.692\pm0.003$ $(+)2V=49°$ $Wo_{40}En_{42}Fs_{18}$**
Hypersthene	$\gamma=1.703\pm0.003$ $(-)2V=60°$ Mg = 65%***

* After F. Chayes's chart.
** After H.H. Hess's chart.
*** After H. Kuno's chart.

Olivine is richly present as a phenocryst in the specimen collected

from near the summit of Byōbu-dake, but it is almost or entirely absent in some thin sections obtained from the lava which is exposed on its western flank. This mineral is always anhedral and has a longer diameter of 0.4 mm.-1.2 mm. It encloses magnetite, being frequently surrounded by the aggregate of hypersthene crystals.

Magnetite takes an octahedral or irregular form. It is mostly 0.01 mm.-0.08 mm. across, although some crystals are 0.4 mm. or more in diameter. In this case, the former is scattered in the groundmass, whereas the latter is generally contained in phenocrystic ingredients, xenoliths and aggregates of augite crystals.

Of such negligible ingredients as apatite and hematite, the former has a subhedral prismatic form, 0.24 mm. long in the largest crystal. The inner part is characterized by a dark brown color due to decomposition. The occurrence of brown glass is known in the specimens from the summit or western flank of Byōbu-dake, filling up the interstices of other ingredients of the groundmass.

The groundmass has a pilotaxitic or hyalopilitic texture and consists of plagioclase, augite, hypersthene, magnetite, hematite, apatite and brown glass. The xenolith is a gabbroic or basaltic rock composed of plagioclase, augite, hypersthene, magnetite and olivine.

(4) *Fubō-zan lava and ejecta*:—The Fubō-zan lava is intercalated with various kinds of ejecta, being traversed by some basaltic dykes. It is mostly characterized by the abundance of plagioclase phenocrysts which are partly composed of big bytownorthite crystals. The writer has also collected intensely magnetic specimens from near the summit. They are, however, found only to a small extent.

The andesite here, including lava flows and fragments in ejecta, is compact or porous and has a dark color. They take on a reddish color in oxidized specimens. Under the microscope, the lava flows and fragments of ejecta consist of plagioclase, augite, hypersthene, olivine, magnetite, tridymite, bowlingite and brown glass; but the amount of such ingredients as olivine, tridymite and brown glass is quite variable even in the same lava flow. Commonly, there is a tendency of the andesite with big bytownorthite phenocrysts to be rich in olivine crystals as compared with other kinds of andesite largely exposed here on Fubō-zan.

The predominance of phenocrystic plagioclase gives a remarkable poprhyritic texture to the Fubō-zan lava. Such a phenocrystic plagioclase is occasionally represented by bytownorthite with a composition of An_{80-82},

and it is frequently 1 cm. across, assuming mostly an euhedral or subhedral form. In the groundmass, plagioclase is more acidic and belongs to bytownite or labradorite. It occurs as a lath-shaped or rectangular crystal, mostly 0.02 mm.–0.2 mm. in its longer diameter. Some of it shows a fluidal arrangement around the phenocrystic plagioclase, giving a pilotaxitic or hyalopilitic texture to the groundmass.

Augite is a very common ingredient in the groundmass, whereas the occurrence of its phenocrystic crystal is rather scarce in most specimens. Specimens devoid of phenocrystic augite are also known. Moreover, it is worthnoting that there are many examples of this mineral associated closely with hypersthene. In such a case, the former is always fringed by the latter. The subhedral or anhedral phenocryst occasionally twins on (100) or (101), and the largest one is 2.38 mm. long and 1.03 mm. across. The crystal reveals an extinction angle, $Z \wedge c$, of 39°–40°. and contains magnetite. In the groundmass, augite is usually found as a minute prismatic crystal, 0.02 mm.–0.08 mm. in length.

Hypersthene indicates, on the other hand, a high frequency as compared with augite. Its long prismatic crystal has a euhedral or subhedral form and is 1.29 mm. long in the largest one. Besides phenocryst, it occurs as an ingredient of the groundmass. Its phenocryst encloses magnetite.

Table IV. Compositions and optical characters of plagioclase, augite and hypersthene phenocrysts in Fubō-zan lava (Measured by F. Hori).

	No. 1 (49082610)	No. 2 (51071804)
Plagioclase	$\alpha=1.564\pm0.003$, $\gamma=1.580\pm0.003$ An_{67-82}*	$\alpha=1.560\pm0.003$, $\gamma=1.579\pm0.003$ An_{61-81}*
Augite		$\beta=1.692\pm0.003$ $(+)2V=490$ $Wo_{40}En_{42}Fs_{18}$**
Hypersthene	$\gamma=1.704\pm0.003$ $(-)2V=65°$ Mg=70%***	$\gamma=1.704\pm0.003$ $(-)2V=64°$ Mg=69%***

* After F. Chayes's chart.
** After H.H. Hess's chart.
*** After H. Kuno's chart.
No. 1. = The Fubō-zan lava from the southern flank of Fubō-zan.
No. 2. = 〃 from the southern foot of Fubō-zan.

Olivine is found as a phenocrystic ingredient. It is commonly present in a small amount, but there are some specimens rich in this mineral. It is represented by a subhedral or anhedral crystal, and the largest one is 1.34 mm. across. Such olivine phenocryst are frequenty surrounded by minute augite crystals and contain magnetite, passing into bowlingite along its crack and periphery.

Tridymite and biotite are rarely seen in the groundmass. The presence of brown glass is restricted to a small extent. It is exceedingly abundant in scoriaceous ejecta.

The groundmass is composed of plagioclase, augite, hypersthene, magnetite, tridymite, biotite and brown glass. In most thin sections, it has a pilotaxitic or hyalopilitic texture, but the groundmass with an orthophyric texture is also seen. The xenolith is mostly absent. It consists of plagioclase, augite, hypersthene and magnetite.

(5) *Sugiga-mine lava and agglomerate*:—Most of the Sugiga-mine lava and andesite fragments of its agglomerate are not so remarkably porphyritic as compared with the Byobu-dake lava exposed largely at the adjacent area. They have a dark grey or black color in fresh specimens, but take on a grey color after subjected to weathering. Such specimens were collected from various parts of lava flow and agglomerate, and the thin sections examined by the writer are composed of plagioclase, augite, hypersthene, olivine, magnetite, brown glass, tridymite and chlorite.

In these thin sections, plagioclase phenocrysts are found as euhedral or subhedral crystal which are frequently well zoned. Some of the phenocrysts indicate a very clear appearance without any inclusion or turbid part, but there are many crystals characterized by a worm-eaten structure, which consists of irregularly outlined pores filled up with such substances as brown glass or other ingredients of the groundmass. These pores are arranged with their longer axes parallel to the elongated direction of the crystals. The phenocryst ranges from labratownite to bytownite with a composition of An_{63-71}, and the largest one is 3.62 mm. long and 1.87 mm. across in thin sections. The plagioclase is also a very important ingredient in the groundmass. It occurs as a lath-shaped or rectangular crystal, 0.02 mm.–0.2 mm. long, showing occasionally a fluidal structure.

Subhedral or anhedral augite phenocrysts are usually more abundant than those of hypersthene, although there are some specimens in which the latter exceeds the former in its amount. The crystal takes a

stout or long prismatic form, twinning frequently on (100) or (101) or (201). In the last case, the penetration twin is formed. It is sometimes found in close association with hypersthene. In such a case, the long prismatic hypersthene has a narrow fringe of augite. The largest crystal is 3.31 mm. long and 1.19 mm. across. The extinction angle, $Z \wedge c$, is 38°–41°. When the crystal is zoned, the extinction angle gradually decreases outwards. Moreover, the phenocrystic augite encloses magnetite and plagioclase, being partly invaded by the groundmass. The minute augite crystals of the groundmass have a prismatic or granular form and are abundantly found together with lath-shaped plagioclase. Most of these are 0.01 mm.–0.05 mm. in length or diameter.

The occurrence of hypersthene is mostly known as phenocryst. This mineral shows an euhedral or subhedral and long or stout prismatic form, 1.7 mm. long and 1.19 mm. across in the largest crystal. Most of hypersthene phenocrysts contain magnetite as enclosure.

Table V. Composition and optical characters of plagioclase, augite and hypersthene phenocrysts in Sugiga-mine lava from the summit of Sugiga-mine (Measured by F. Hori).

	(T.I. 48092503)
Plagioclase	$\alpha=1.562\pm0.003$, $\gamma=1.575\pm0.003$ An_{63-71}*
Augite	$\beta=1.688\pm0.003$ (+)2V=50° $Wo_{41}En_{44}Fs_{15}$**
Hypersthene	$\gamma=1.703\pm0.003$ (−)2V=64° Mg=69%***

* After F. Chayes's chart.
** After H.H. Hess's chart.
*** After H. Kuno's chart.

Olivive is seen in almost all thin sections, but it is commonly present as a subordinate ingredient as compared with other colored minerals. It is found only as a phenocryst and takes generally an anhedral form except in several cases in which euhedral or subhedral crystals are observed. In the well-defined and largest crystal, it is

1.31 mm. long and 0.51 mm. across. The mineral encloses minute magnetite crystals and passes into bowlingite or some chloritic substance along its periphery or crack, being sometimes corroded by the groundmass and being also surrounded by a granular aggregate of augite.

One of characteristic features indicated by this lava and andesite fragments of agglomerate is the abundance of magnetite in the groundmass. The magnetite under consideration is octahedral or granular or skeletal in its form. It is mostly 0.01 mm.-0.03 mm. in diameter except the skeletal crystals which are 0.85 mm. across in the largest one. Some of these skeletal crystals aggregate together with granular augite to form small rounded dots.

Brown glass on the other hand, is seen only in two specimens collected by the writer on the northern branch and southern flank of Sugiga-mine. It fills up the interstices of other ingredients. Besides it, a minor amount of tridymite is present in the groundmass of the lava exposed on the western cliff near the summit of Sugiga-mine.

The groundmass exhibits a pilotaxitic or hyalopilitic texture and consists of such minerals as plagioclase, augite, hypersthene, magnetite, tridymite and brown glass. Gabbroic or noritic xenolith is noticed in several specimens. It is commonly represented by a coarse or fine aggregate of plagioclase, augite, hypersthene and magnetite. In xenolith, olivine is not an important ingredient, and its occurrence is restricted to the specimen from the southern flank of Sugiga-mine.

(6) *Ushiro-eboshi-dake lava and ejecta*:—The Ushiro-eboshi-dake lava is repeatedly intercalated by agglomerate, pumiceous bed and other ejecta. Although lava has somewhat different features from place to place, it is mostly represented by a compact and porphyritic rock with a dark grey or black color in fresh specimens, but a grey or reddish color in those subjected to weathering.

The agglomerate is composed of such andesite fragments as mentioned above and sandy or tuffaceous matrix. In these cases, most specimens collected by the writer are represented by olivine-free andesite different from the underlying Sumi-kawa lava in various points.

The lava flows and andesite fragments under consideration consist of plagioclase, augite, hypersthene, olivine, magnetite, apatite, quartz, biotite, tridymite, bowlingite, chlorite and brown glass. Of these ingredients, the phenocrystic plagioclase belongs to labradorite or bytownorthite with a composition of An_{59-80}. Generally, it takes an eu-

hedral or subhedral form, being 3.5 mm. long and 2.72 mm. across in the largest crystal. Some of plagioclase phenocrysts are well zoned and turbid. There are also many crystals with a worm-eaten structure formed by the invasion of brown glass or other ingredients of the groundmass, Moreover, such phenocrysts frequently enclose minute crystals of augite, hypersthene and magnetite. More acidic plagioclase occurs as an ingredient of the groundmass where lath-shaped or rectangular crystals, 0.03 mm.–0.17 mm. long, are abundant, showing the fluidal arrangement in some specimens.

The augite phenocryst mostly reveals a high frequency as compared with hypersthene. Subhedral or anhedral phenocrysts of this mineral frequently twin on (101) or (100) and have an extinction angle, $Z \wedge c$, of 38°–41°. The largest crystal examined in the thin section is 1.78 mm. long and 0.68 mm. across. In the groundmass, augite crystals are prismatic or irregular, being commonly 0.02 mm.–0.2 mm. in length or diameter. Sometimes they aggregate together with skeletal crystals of magnetite. Hypersthene is also an important colored mineral, but it is scarcely seen in the groundmass. Most of this mineral have an euhedral or subhedral form and a long prismatic habit.

Table VI. Compositions and optical characters of plagioclase, augite and hypersthene phenocrysts in Ushiro-eboshi-dake lava from the summit of Ushiro-eboshi-dake (Measured by F. Hori).

	(T.I. 49082205)
Plagioclase	$\alpha = 1.558 \pm 0.003$, $\gamma = 1.578 \pm 0.003$ $An_{59-8)}$*
Augite	$\beta = 1.694 \pm 0.003$ (+)2V=50° $Wo_{41}En_{39}Fs_{20}$**
Hypersthene	$\gamma = 1.709 \pm 0.003$ (−)2V=60° Mg%=65***

* After F. Chayes's chart.
** After H.H. Hess's chart.
*** After H. Kuno's chart.

The occurrence of olivine is an exceptional case for the Ushiro-eboshi-dake lava and andesite fragments in agglomerate. It is contained in the specimens obtained on the summit of Ushiro-eboshi-dake and

its northwestern foot as well as from near Tengu-iwa of Mae-eboshi-dake. Even the largest phenocryst is 1.04 mm. long and 0.68 mm. across in thin sections and euhedral crystals are absent. Bowlingite is formed from this mineral along its crack and peripheral part.

Magnetite is the commonest ingredient in the groundmass. Minute octahedral or irregular crystals, commonly 0.01 mm.–0.08 mm. across, are most abundant, although there are some crystals attaining to a diameter of 1 mm. or thereabouts. Magnetite is occasionally enclosed by such minerals as plagioclase, augite, hypersthene and olivine.

Quartz is only found as a xenocryst which was probably supplied from granitic rocks. It has a rounded form due to the magmatic corrosion, and the largest grain is 1.54 mm. across. Apatite is rarely present in the specimen collected from the southeastern flank of Ushiro-eboshi-dake. It is a long prismatic crystal, 0.39 mm. in length, and its inner part has a brownish grey color resulting from decomposition. Tridymite fills up the irregular interstices of minute ingredients in the groundmass, and biotite is an unimportant mineral in xenoliths. Chlorite is, on the other hand, a secondary mineral and partly replaces the phenocrystic plagioclase.

Besides various ingredients mentioned above, the occurrence of brown glass is known in the phenocrystic plagioclase and also in the groundmass of the specimen from Tengu-iwa. In the latter case, it occupies the main part of the groundmass, and a hyalopilitic texture is formed.

The groundmass is composed of plagioclase, augite, hypersthene, magnetite, apatite, tridymite and brown glass. It has mostly a pilotaxitic texture. The groundmass of some specimens are intensely decomposed, and it is not clear whether the groundmass has a pilotaxitic or hyalopilitic texture. Moreover, leucoratic spots, rounded or irregular, are abundantly seen, as is indicated by the decomposed groundmass of the Sumi-kawa lava and Byōbu-dake lava. Xenolith is an aggregate of plagioclase, augite, hypersthene and magnetite with a minor amount of biotite flake. It has a gabbroic, noritic or basaltic character and is commonly found in all specimens.

(7) *Andesite fragments of the Kara-sawa mud flow*:—So far as is known at present, there are two kinds of andesite fragments in the Kara-sawa mud flow. They are two-pyroxene andesite and olivine-bearing two-pyroxene andesite, being composed of plagioclase, augite, hypersthene; magnetite and tridymite with or without olivine pheno-

crysts. Of these, the olivine-free andesite is more extensively distributed, and its groundmass has a fine pilotaxitic texture. A similar type of andesite is frequently seen in the Ushiro-eboshi-dake lava. Olivine-bearing andesite is, however, found to a small extent and seems mostly to have been supplied from the Fubō-zan lava.

In such two kinds of andesite fragments, the phenocrystic plagioclase, euhedral or subhedral, is 2.89 mm. long and 1.86 mm. across in the largest crystal. It is always characterized by the frequent presence of a worm-eaten structure, being occasionally turbid and well zoned. The crystal includes augite and magnetite. When the phenocrystic augite reveals a worm-eaten structure, the cavities are filled up by brown glass or other ingredients. Minute lath-shaped plagioclase, mostly 0.02 mm.–0.08 mm. in length, is abundant in the groundmass of olivne-free andesite, whereas the rectangular form, 0.02 mm.–0.2 mm. long, is very common in olivine-bearing variety, giving an orthophyric texture to its groundmass.

In thin sections, the phenocrystic augite is generally 2.38 mm. long and 1.13 mm. across in the largest crystal. Its frequency is commonly higher than the phenocrystic hypersthene. It twins on (100) or (101), and the extinction angle, $Z \wedge c$, is 40°. Hypersthene has a long prismatic habit, and the largest crystal is 1.07 mm. long and 0.59 mm. across. These two minerals contain magnetite, and are sometimes associated together. In this case, hypersthene is fringed by a narrow zone of augite. Minute augite crystals, stout prismatic or irregular in form, are abundant in the groundmass. They are 0.03 mm.–0.08 mm. in longer diameter.

Octahedral or ill-defined magnetite crystals are one of important ingredients in the groundmass, where they are mostly 0.01 mm.–0.08 mm. across, although there are large skeletal crystals, the largest one being 1.36 mm. across in the andesite fragments obtained near Misumi. The occurrence of anhedral olivine crystals is known in several specimens. It is 1.1 mm. long in the largest phenocryst and partly or wholly passes into bowlingite. The groundmass consists of plagioclase, augite, magnetite and tridymite, but noritic xenoliths are almost absent.

(8) *Nyūdō-san lava and agglomerate*:—All the specimens collected by the writer on Nyūdō-san are two-pyroxene andesite. They are compact and porous rocks with a dark grey or black color and porphyritic texture. Some of these specimens are characterized by the frequent occurrence of large plagioclase phenocrysts and xenoliths of plagioliparite.

The former is seen in those obtained on the summit or western flank, whereas the latter is commonly observed in the andesite fragments of agglomerate exposed on the ridge extending south-southeastwards from the summit. The andesite fragments of agglomerate, which constructs the bottom of volcanic products here, are, however, free of such xenoliths and are frequently alunitized to some extent.

The microscopical examination of thin sections shows that they contain plagioclase, augite, hypersthene, magnetite, tridymite, bowlingite and chlorite.

Of these ingredients, phenocrystic plagioclase takes an euhedral or subhedral form, 4.65 mm. long and 1.6 mm. across in the largest one. It is labratownite or bytownite with a composition of An_{63-76}. Sometimes, the crystal looks clear without any inclusions and turbid portion, but it has occasionally a worm-eaten structure due to the invasion of the groundmass. In the latter case, some of phenocrysts enclose minute crystals of augite, hypersthene and magnetite, being frequently subjected sporadically to chloritization. Zoned phenocrysts are also seen commonly in these specimens. Lath-shaped plagioclase crystals, mostly 0.03 mm.–0.08 mm. long, are found abundantly in the groundmass, where they partly reveal a fluidal arrangement.

The augite phenocryst is generally found in high or nearly same frequency as compared with that of hypersthene and occurs as a subhedral or anhedral crystal. It twins on (100) or (101) and contains magnetite and hypersthene crystals. Some of augite crystals indicate a zonal structure with hypersthene. Its largest phenocryst is 3.8 mm. long and 1.76 mm. across. The extinction angle, $Z \wedge c$, is 40°–41°, and the crystal encloses magnetite grains. It is, however, worthnoting that the phenocrystic augite is almost absent in the specimens obtained on the ridge branching south-southeastwards from the summit.

Hypersthene is generally found as phenocryst, but is a scarce ingredient in the groundmass. It has a long or stout prismatic habit, and the largest crystal measured by the writer is 2.35 mm. long and 0.51 mm. across. The crystal includes magnetite and is occasionally altered to bowlingite along its periphery and crack.

Magnetite is always an important mineral in the groundmass, where it occurs as an octahedral or ill-defined crystal, commonly 0.005 mm.–0.08 mm. in diameter, although there are some large skeletal crystals, 0.3 mm.–0.5 mm. across. Tridymite is, on the other hand, a rare ingredient in the groundmass, and it is found filling up the interspaces

Table VII. Compositions and optical characters of plagioclase, augite, hypersthene phenocrysts in Nyūdō-san lava from the western flank of Nyūdō-san (Measured by F. Hori).

	(T.I. 49082310)
Plagioclase	$\alpha=1.562\pm0.003$, $\gamma=1.577\pm0.003$ An_{63-76}*
Augite	$\beta=1.694\pm0.003$ $(+)2V=50°$ $Wo_{41}En_{39}Fs_{20}$
Hypersthene	$\gamma=1.709\pm0.003$ $(-)2V=61°$ Mg=66%***

* After F. Chayes's chart.
** After H.H. Hess's chart.
*** After H. Kuno's chart.

of other minerals. The groundmass has a pilotaxitic texture and consists of plagioclase, augite, hypersthene, magnetite and tridymite. Usually, it contains gabbroic or noritic xenoliths and also some fragments of plagioliparite.

(9) *Manokami-dake lava*:—The lava and andesite fragments collected from agglomerate have a dark grey color, when they are fresh, but takes on a grey color in the process of weathering and a reddish color when reheated. These rocks are finely porphyritic and frequently contain xenoliths. Some of the lava and agglomerate are intensely subjected to the solfataric action, by which they are kaolinized and opalized, being widely pyritized. Such an alteration can be seen along the Akiyama-zawa.

Microscopically, the mineral components of the writer's specimens are represented by plagioclase, augite, hypersthene, olivine, hornblende, magnetite, apatite, brown glass, bowlingite, calcite and chlorite. In such a case, it is worthnoting that the occurrence of olivine is restricted only to the specimens obtained on the southern flank of Manokami-dake.

Of these, the phenocrystic plagioclase is labratownite or bytownite with a composition of An_{63-74}. The euhedral or subhedral crystal of this mineral is occasionally invaded by the groundmass and shows a characteristic worm-eaten structure. The largest crystal is 4.33 mm.

long and 2.8 mm. across. It contains augite and magnetite in frequent association with brown glass and chlorite, being sometimes turbid and well zoned. Besides these, minute lath-shaped or rectangular plagioclase, mostly 0.02 mm.-0.2 mm. long, is abundantly present in the groundmass where it reveals a fluidal arrangement.

Augite and hypersthene are found in varying amount, the former being more abundant than the latter or *vice versa*. In almost all specimens, the phenocrystic hypersthene occurs as a well defined crystal as compared with the phenocrystic augite. When these minerals are associated together, the latter is always fringed by the former. In the writer's specimens, the phenocrystic augite is 1.84 mm. long and 0.8 mm. across in the largest one, and its extinction angle, $Z \wedge c$, is 38°-41°. The crystal has a tendency to be twinned on (100) or (101), and a polysynthetic twinning is seen in some thin sections. It encloses plagioclase and magnetite. In the former case, an ophitic texture is formed occasionally between them. The groundmass contains many small crystals of the stout prismatic or granular augite, 0.02 mm.-0.2 mm. in length or diameter. The alteration product of augite are bowlingite and calcite, but the latter is very rare in its occurrence. The phenocrystic hypersthene is generally characterized by a long prismatic habit. The largest crystal of this mineral is 1.39 mm. long and 0.33 mm. across. Frequently, it contains plagioclase, augite and magnetite. The alteration to bowlingite and hematite is known in the specimens subjected to oxidation.

Table VIII. Compositions and optical characters of phenocrystic plagioclase, augite and hypersthene in Manokami-dake lava from the eastern foot of Manokami-dake (Measured by F. Hori).

	(T.I. 47102603)
Plagioclase	$\alpha=1.562\pm0.003$, $\gamma=1.575\pm0.003$ An_{63-74}
Augite	$\beta=1.685\pm0.003$ $(+)2V=57°$ $Wo_{42}En_{46}Fs_{12}$**
Hypersthene	$\gamma=1.711\pm0.003$ $(-)2V=57°$ Mg=62%***

* After F. Chayes's chart.
** After H.H. Hess's chart.
*** After H. Kuno's chart.

The occurrence of the phenocrystic olivine is noticed in the specimen collected at the uppermost course of the Tashiro-zawa which starts on the southern flank of Manokami-dake. The anhedral crystal of this mineral passes into bowlingite at its periphery as well as along its crack. Magnetite is, on the other hand, the most predominant ingredient in the groundmass of all specimens. It takes an octahedral or granular or skeletal form, usually 0.01 mm.–0.08 mm. in diameter, but 0.5 mm. across in the largest skeletal crystal. Apatite and hornblende are very scanty minerals in the writer's specimens. They are found only in the specimen from the uppermost course of the Tashiro-zawa. Of these two minerals, apatite has a long prismatic form, 0.12 mm. or more in length, being more or less decomposed, whereas hornblende, 0,24 mm. long in the largest crystal, is closely associated with augite and hypersthene in parallel intergrowth and reveals the following pleochroic scheme. X=light yellow, Y=brownish yellow and Z=yellowish brown.

The groundmass is composed of plagioclase, augite, hypersthene, magnetite and apatite. It has a pilotaxitic or hyalopilitic texture which is often obscured by the formation of leucocratic dots due to decomposition. Noritic, gabbroic and basaltic xenoliths are sporadically found in the groundmass, being composed of plagioclase, augite, hypersthene and magnetite.

(10) *Andesite fragments of the Nanokahara mud flow*:—Andesite fragments of this mud flow were supplied from the Ushiro-eboshi-dake lava, because the mud flow here erupted from the explosion crater of Numa surrounded by a semi-circular wall of the Ushiro-eboshi-dake lava. All of these andesite fragments are, therefore, two-pyroxene andesite with a dark grey or black color and remarkably porphyritic texture. They are composed of plagioclase, augite, hypersthene, magnetite and apatite imbedded in the groundmass with a pilotaxitic texture. Various characters of such ingredients are almost same as those of the Ushiro-eboshi-dake lava. In the specimens collected by the writer, the largest phenocrystic plagioclase is 4.67 mm. long and 2.35 mm. across. As in the case of the Ushiro-eboshi-dake lava, most of these are characterized by a worm-eaten structure.

As to augite and hypersthene phenocrysts, there is no remarkable feature different from those of the Ushiro-eboshi-dake lava, the former being more abundant than the latter. Apatite is a very rare ingredient, 0.2 mm. long in the largest crystal. It has a dark brown

color in its inner part and is somewhat rounded. Subjected to weathering, the groundmass yields a leucocratic dots by which its pilotaxitic texture is obscured.

History of Igneous Activities

The extensive distribution of lavas and ejecta suggests that there was once an important active center in the Byōbu volcanic area. The activity here seems to have taken place at different sources in concert with other area of the Zaō Volcanoes. It is supposed to have been repeated several times, resulting in the formation of such remarkable peaks as Byōbu-dake, Fubō-zan, Ushiro-eboshi-dake, Sugiga-mine, Nyūdō-san and Manokami-dake.

The forerunner of these repeated activities is represented by the eruption of the Nonomori agglomerate which had its source at the southeastern corner of this volcanic area. It spreaded over the eroded surface of base rocks composed of the Tertiary formation and various kinds of extrusives. The eruption of the Nonomori agglomerate was followed by those of the Sumi-kawa lava and agglomerate which were abundantly supplied from the center opened newly at the west of the former source. This crater was deformed and obscured later by erosion, explosion and faulting as well as by the formation of central cones, although it is believed to have been a big crater in the beginning.

The Sumi-kawa lava poured out successively after the eruption of its agglomerate, running down northwards beyond the area now dissected by the Sumi-kawa and Nigori-gawa where the Tertiary formation, granite (granodiorite) and other intrusives or extrusives are well exposed.

In the next activity, the Byōbu-dake lava also poured forth through this crater and covered older volcanic products or base rocks. This was followed by other eruptions from the same crater, as is indicated by lavas and ejecta accumulated thickly on Fubō-zan and Ushiro-eboshi-dake. There is, however, no evidence to confirm the relationship between them. The same may be said of the Sugiga-mine lava and agglomerate ejected from the source situated on the western flank of Byōbu-dake.

After these repeated activities, explosion craters which opened between Fubō-zan and Ushiro-eboshi-dake poured out the Kara-sawa mud flow down to Misumi and its surrounding area. As a result of the eruption subsequent to this activity, two central cones such as

Nyūdō-san and Manokami-dake were successively formed within the pre-existing crater.

The activity of the Byōbu Volcano moved from here to Numa at its final stage. It is indicated by the explosion which happened on the southern flank of Mae-eboshi-dake and also by the ejection of the Nanokahara mud flow which extended northeastwards presenting a very characteristic topographical feature.

At the Byōbu volcanic area, even the last activity mentioned above is of the pre-histric time, and it is one of the noteworthy points which differ from the Zaō Proper where the activity is still expected.

Summary

(i) The South Zaō is constructed by such two volcanoes as Byōbu and Aoso. Of these, the Byobu Volcano occupies the western half of this area and includes Nonomori, Byōbu-dake, Fubō-zan, Ushiro-eboshi-dake, Mae-eboshi-dake, Sugiga-mine, Nyūdō-zan, and Manokami-dake, rising to 1817.3 meters above the sea-level at the highest point. They are now deeply dissected and thickly forested as compared with the Zaō Proper.

(ii) The Byōbu Volcano rests upon the eroded surface of such base rocks as Upper Miocene sediments, granite and other intrusives or extrusives. It is built up of various volcanic products represented by the Nonomori agglomerate, Sumi-kawa lava and agglomerate, Byōbu-dake lava, Fubō-zan lava and ejecta, Sugiga-mine lava and agglomerate, Ushiro-eboshi-dake lava and ejecta, Kara-sawa mud flow, Nyūdō-san lava and agglomerate, Manokami-dake lava and Nanokahara mud flow.

(iii) The largest source of these lavas and ejecta is the pre-existing crater or explosion crater which opened at the central part of this volcanic area. It is now surrounded by Byōbu-dake, Fubō-zan and Ushiro-eboshi-dake, but is partly deformed and obscured by the explosion and erosion as well as by the formation of the central cones. Other craters and explosion craters ejected the Nonomori agglomerate, Sugiga-mine lava and agglomerate and Nanokahara mud flow. The most characteristic explosion crater is preserved on the southern flank of Mae-eboshi-dake.

(iv) The beginning of activities repeated here is shown by the eruption of the Nonomori agglomerate, which was followed by the eruption of the Sumi-kawa lava and agglomerate. The latter is the biggest eruption of the Byōbu Volcano, and a large amount of lava

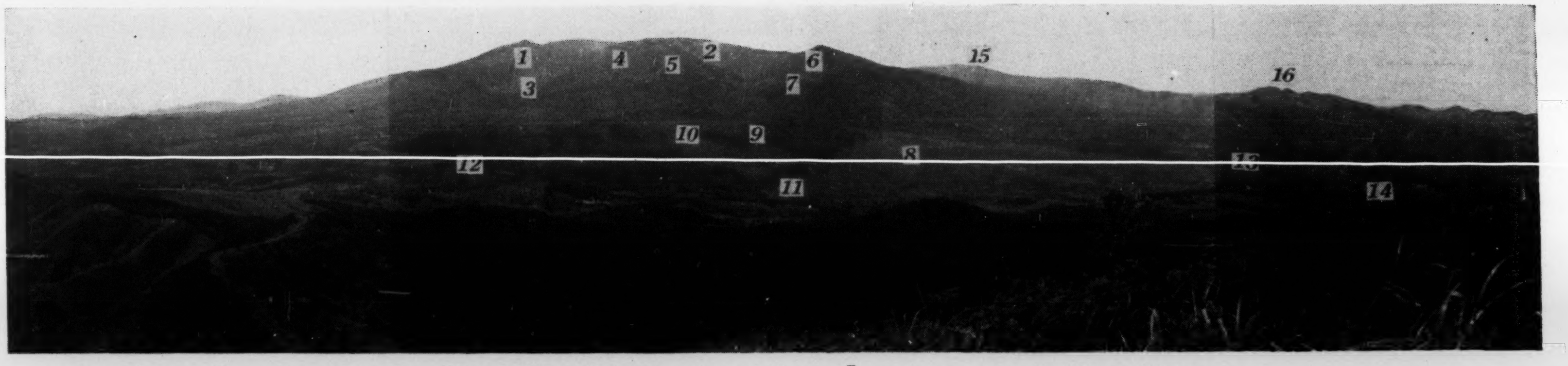

Fig. 3. The Byōbu Volcano viewed from Ōmori-yama of the Aoso Volcano.

1=Fubō-zan, 2=Byōbu-dake, 3=Kara-sawa mud flow, 4=Nyūdō-san, 5=Manokami-dake, 6=Ushiro-eboshi-dake, 7=Numa, 8=Nanokahara mud flow, 9=Nonomori, 10=Crater, 11=The Akiyama-zawa, 12=The Tashiro-zawa, 13=The Sumi-kawa, 14=The Nigori-gawa, 15=Kumano-dake, 16=Gando-yama.

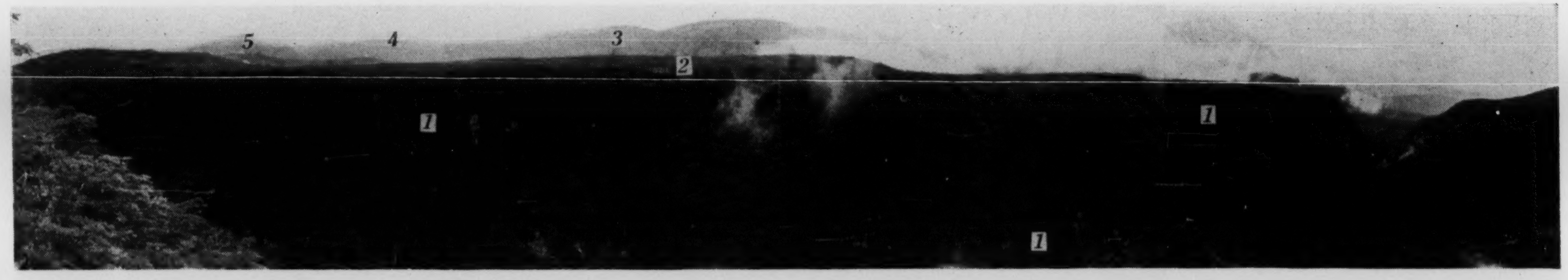

Fig. 4. The Sumi-kawa lava exposed along the Sumi-kawa.

1=Sumi-kawa lava, 2=Nanba-zawa lava underlain by Sumi-kawa lava, 3=Kumano-dake, 4=Goshiki-dake, 5=Katta-dake.

(震研彙報 第三十三号 図版 市村)

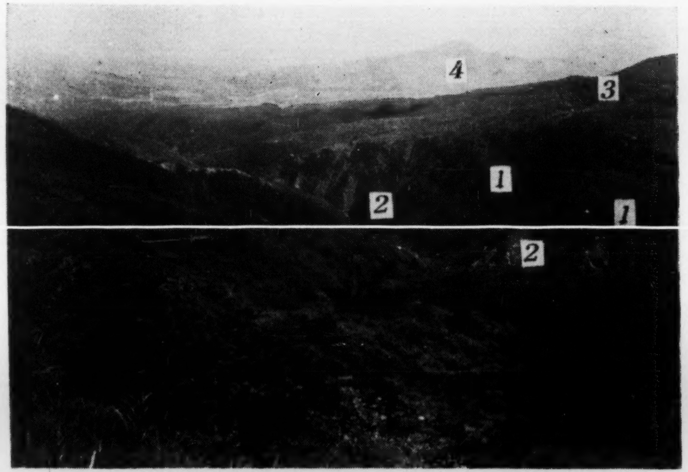

Fig. 5. The Sumi-kawa lava resting upon the eroded surface of granite. 1=Sumi-kawa lava, 2=Granite, 3=Sainokawara, 4=Aoso Volcano.

Fig. 6 Columnar joints of the Sumi-kawa lava at the bottom of the Sumi-kawa.

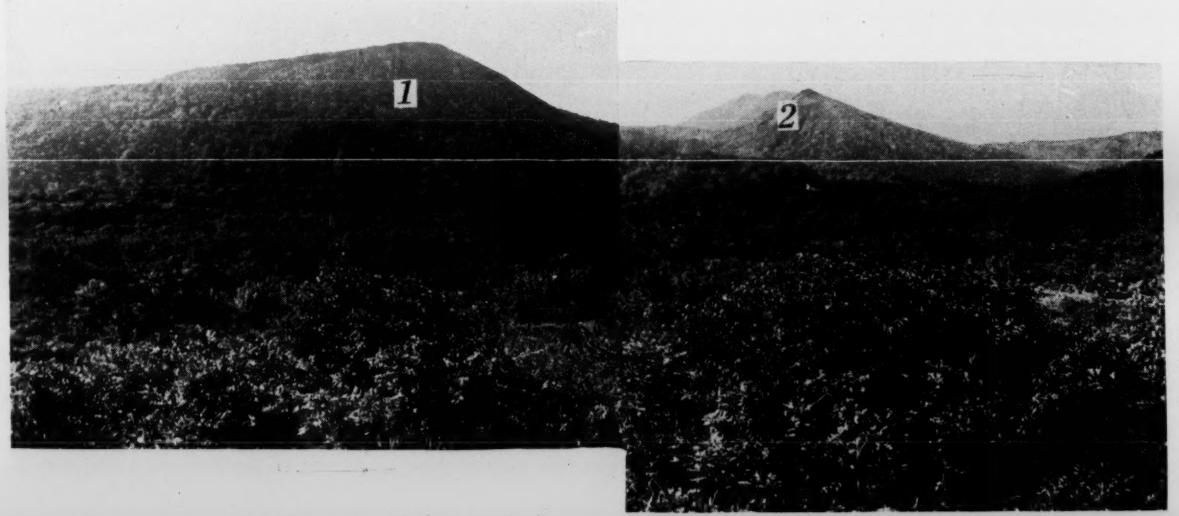

Fig. 7. Byōbu-dake and Ushiro-eboshi-dake viewed from Sainokawara.
1=Ushiro-eboshi-dake,
2=Byōbu-dake.
The eastern side of Byōbu-dake slopes steeply downward and forms here a sharp cliff in contrast with its western gentle slope.

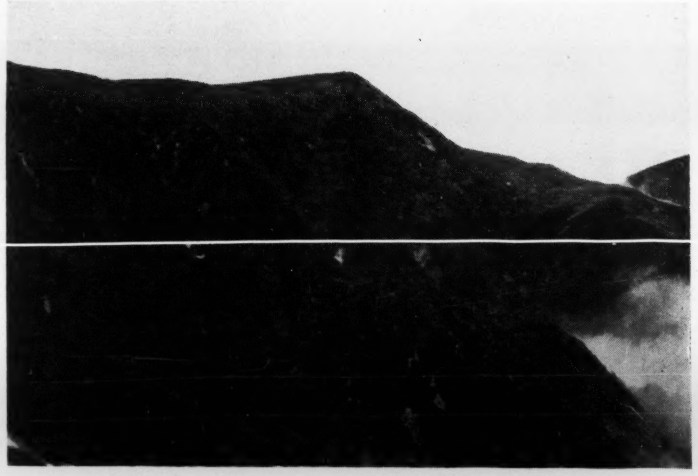

Fig. 8. The eastern cliff of Byōbu-dake looking like a faultscarp.

Fig. 9. Fubō-zan viewed from near the summit of N. Byōbu-dake.

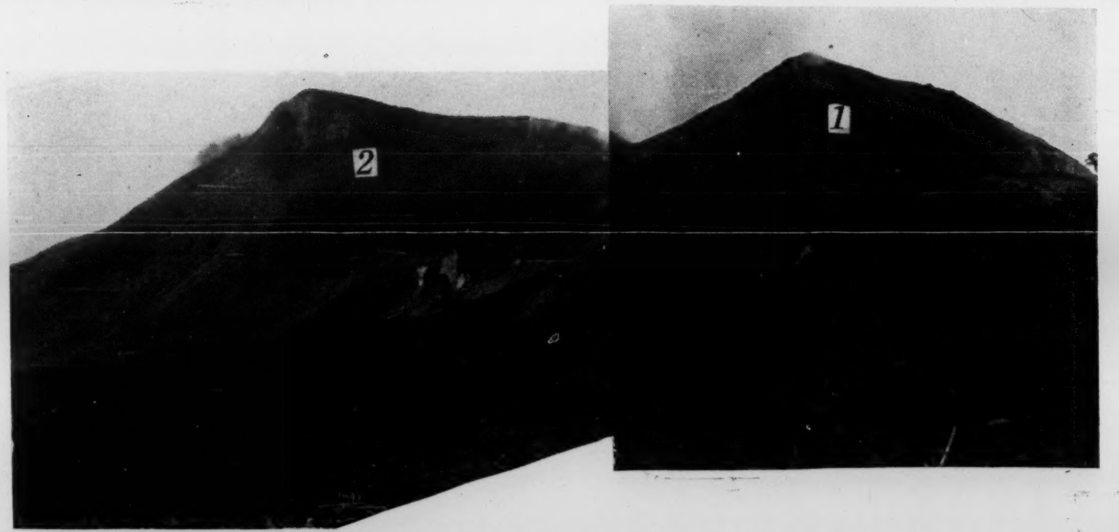

Fig. 10. Nyūdō-san and Manokami-dake, two central cones of the Byōbu Volcano. 1=Nyūdō-san, 2=Manokami-dake.

(震研彙報 第三十三号 図版 市村)

flowed down northwards beyond the Nigori-gawa and Sumi-kawa at that time. Such activities had happened several times until the Nanokahara mud flow poured out finally from the explosion crater near Numa, but there has been no activity in the historic time.

(v) Two central cones were succesively formed within the preexisting crater or explosion crater mentioned above. These cones were formed at the last stage of several activities, being composed of two-pyroxene andesite and its agglomerate. They are characterized by the absence of such dacite as is exposed on the central cones of the neighbouring volcano.

(vi) The geological age of the first eruption here may be the Pleistocene. It is inferred from the fact that the lavas and ejecta of the Byōbu and Aoso Volcanoes erupted together, and the oldest mud flow of the latter is unconformably underlain by alternate beds of clay, sand and gravel assigned to Pleistocene.

In conclusion, the writer wishes to offer his hearty thanks to Dr. N. Nasu and Dr. H. Tsuya who helped him to continue his work even after he had been transferred from the Earthquake Research Institute of Tokyo University to Yamagata University. The writer's sincere thanks are also due to Mr. F. Hori for his co-operation in the petrographical investigations of lavas and ejecta obtained from this volcano. A part of this investigation was carried out with the aid of the Education Ministry Grant for Natural Science.

---

39. 蔵王火山の地質学的研究 (第 3 報)

山形大学 市 村 毅

遠刈田温泉に近い青麻火山の西方に，大きく根を張る屏風火山は，屏風岳，不忘岳，杉ケ峰，後烏帽子岳，前烏帽子岳，入道山，馬神岳，ノノ森などよりなり，蔵王火山群の重要なる部分を占めるものである．この火山は，花崗岩（花崗閃緑岩），新第三系，これ等を貫き，或は被覆する各種火成岩を基盤として，その侵蝕面上に盛上り，火山体を構成する多量の橄欖石複輝石安山岩，含橄欖石複輝石安山岩，複輝石安山岩，砕屑岩は，極めて複雑なる分布を見せている．現在不忘山，屏風岳，後烏帽子岳により包囲され，入道山，馬神岳の両中央火口丘が存在する地域は，屏風火山活動の主要な中心と考えられ，又これに接近してノノ森噴火口，沼爆裂火口，その他からも，熔岩，集塊岩，泥流などが噴出しているのを見ることが出来る．この火山地域の活動は，ノノ森噴火口の生成に始まり，七日原泥流の噴出を以て，終りを告げたものと見做し得可く，青麻火山や蔵王火山群の他の火山と相呼応し，恐らく第四紀に入つてから活動が開始されたものと想像される．ただしこの火山では，青麻火山と同じ様に，有史以後の活動が知られていない．

40. *A Short Discussion on Ripples in Earthquake Shocks.* (*Aftershocks of the Boso-Oki Earthquake.*)

By Keichi KASAHARA,

Earthquake Research Institute.

(Read July 19, Sept. 27, 1955.—Received Sept. 30, 1955.)

1. Introduction

A great earthquake took place on the Pacific coast of Japan on November 26, 1953, and the shocks were felt severely in the central and eastern parts of the Japan Islands. According to the report of the Central Meteorological Observatory of Japan[1], the earthquake, named the Boso-Oki Earthquake showed a magnitude as large as that of the Great Kwanto Earthquake of 1923 and was located as follows:

longitude......141°51.8′ E,
latitude....... 34° 3.3′ N,
depth......... 84.2 km.

In the vicinity of the origin many aftershocks took place which were observed by the network stations of C.M.O. as well as by our stations located around Tokyo. In the Seismological Bulletins and the other report[2] we can find detailed descriptions of the occurrence of aftershocks, namely, the numbers of monthly occurrence, the locations and other necessary data of aftershocks of considerable magnitude. As shown in Table I, aftershocks occurred most frequently in November and December of 1953 and became less active in the following several months. Although the seismic active area was not so close to the land, through the seismological network of high density we could

Table I. Numbers of monthly occurrence of aftershocks.

1953	November	420
	December	215
1954	January	39
	February	42
	March	7
	April	7
	May	11

(after C.M.O.)

1) *Seismological Bulletin, C.M.O.*, No. 35, 36, 37, 38.
2) W. INOUYE, *Quart. Journ. Seis., C.M.O.*, **19** (1954), 8.

determine the locations of each shock of considerable magnitude. Table II shows these aftershocks whose origins were reported with an accuracy of 0.1° both in longitude and in latitude. As to the depths, most aftershocks occurred at places 20 to 50 km under the earth's surface, while a few occurred in places very shallow or deeper than 60 km. From these results, we may infer that the shadowed space of conical shape (Fig. 2) was severely affected by the main shock resulting in numerous aftershocks which took place there. If this supposition is reasonable, the present case of aftershocks offers useful materials in studying the physical properties of the so-called seismic-active regions. Suppose the said regions have some properties differing from the surrounding area (which is not severely affected by the main shock and is thus non-active), seismic waves passing through this area may be affected and may have peculiar features differing from those which do not pass through it.

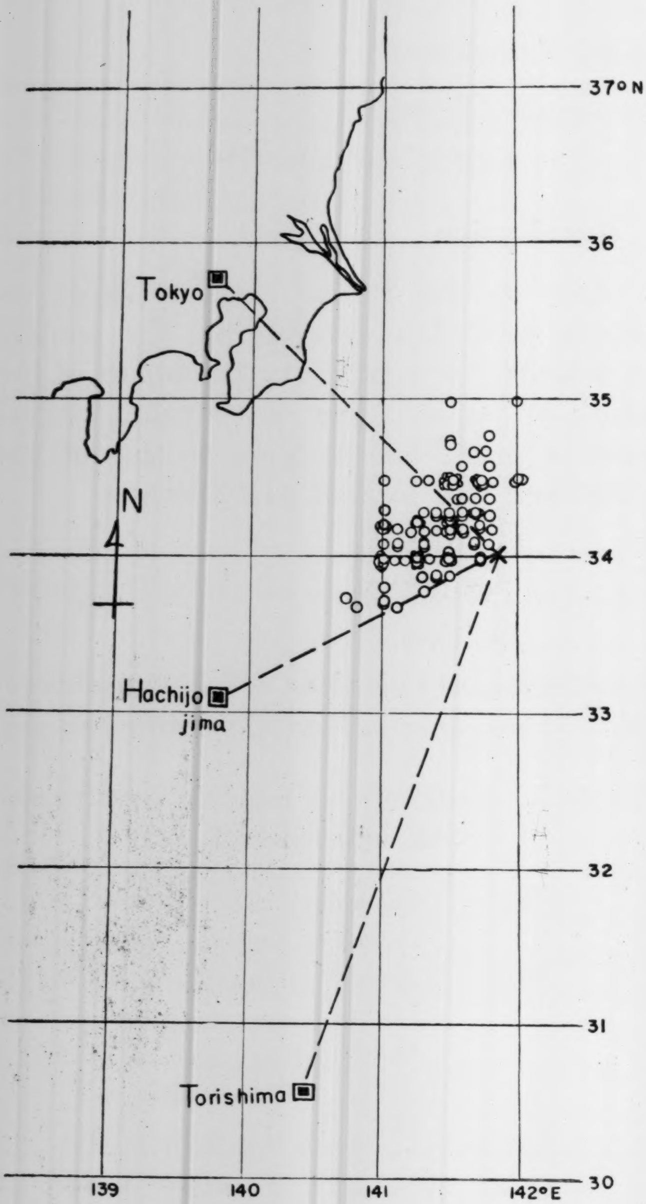

Fig. 1. Locations of the seismic active region and stations.

×: main shock, ○: aftershocks.

(after C.M.O.)

We shall, therefore, compare the two groups of seismograms, one corresponding to waves traveling through the active region and the other corresponding to waves passing through normal areas only. Prof. Matuzawa deter-

Table II. Aftershocks.

No.	Time (G.M.T.)	Location		Magnitude	Type of ripples		
		φ	λ		Tokyo	Hachijo-jima	Torishima
1114	Nov. 26th 23^{h} 36^{m}	24°.2 N	141°.6 E	r	C	—	C
1115	00 03	34.4	141.8	r	C	A	B
1117	10 47	34.2	141.8	r	C	C	C
1119	02 24	34.5	141.5	s	A	A	—
1120	03 24	34.3	141.5	r	A	—	—
1124	05 04	34.5	141.6	s	A	A	—
1126	08 14	34.3	141.6	r	C	B	C
1127	08 20	—	—	r	—	—	—
1131	11 36	34.5	141.5	u	B	A	—
1139	27 00 01	34.0	141.5	m	B	B	—
1143	11 30	34.3	141.6	r	A	B	—
1144	18 31	33.8	141.0	s	A	A	—
1145	28 02 10	34.0	141.3	u	C	B	—
1147	04 25	34.2	141.5	u	B	B	—
1154	29 04 07	34.8	141.8	u	C	C	C
1156	30 03 40	34.6	141.6	u	C	C	—
1157	13 43	34.5	141.5	m	B	B	B
1208	Dec. 2 06 10	34.1	141.1	u	A	B	—
1209	09 47	33.7	141.1	r	B	B	B
1215	3 21 40	34.1	141.0	m	A	—	—
1217	5 09 41	34.3	141.4	r	A	A	B
1218	14 54	34.0	141.2	u	A	A	—
1219	17 20	34.2	141.3	u	A	B	—
1220	18 39	34.2	141.6	m	A	A	—
1235	20 21 20	34.3	141.0	m	A	A	—
1236	21 02 42	34.1	141.0	m	A	A	—
1313	Jan. 18 14 45	33.9	141.4	r	A	—	—
1416	Feb. 22 06 11	34.3	141.7	r	A	—	—
1417	10 26	34.1	141.7	r	A	—	—
1425	23 51	34.2	141.1	r	A	—	—

mined formerly the underground structure[3] which is considered most suitable in interpreting the travel times of earthquakes in the Kwanto district. A schematic view of the result is shown in Fig. 2, in which are drawn ray-paths for transversal waves generated from origins whithin (A) and without (B) the active region, at the same time.

3) T. MATUZAWA, K. YAMADA and T. SUZUKI, *Bull. Earthq. Res. Inst.*, **7** (1929), 241.

Waves from origins A and B will travel along the common path DEF making the first (S) arrival at a station 200 or 300 km distant from the origin. However, the wave from A must travel along the path ACDE while the wave from B travels along BDE, and the different paths ACD and BD is the reasonable condition which interprets some differences found commonly between seismograms of group A and B.

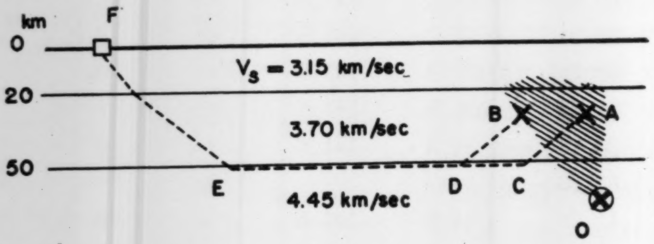

Fig. 2. Seismic wave paths from the active region.
⊗: main shock, ×: aftershocks, □: station.

For the present purpose, aftershocks with focal depths of 20 to 50 km look most suitable, since in the case of the other aftershocks which are located in shallower or deeper places it is difficult for us to decide if the wave paths from them travels through the shadowed region or not. Aftershocks listed in Table II are those which satisfy the above-stated condition.

2. Ripples in seismograms

It is a well known phenomenon in seismology that some seismograms show remarkable vibrations of very short period superposing on fundamental motions of longer period. This kind of phenomenon of "ripples" has been left unstudied for a long time. According to K. Kanai, who has developed his study on this phenomenon recently[4], "the wave form of ripple is due to the multiple reflection of seismic waves in the surface layer, when waves with period equal to or shorter than the natural period of the surface layer are found among the incident seismic waves." In the present case of aftershocks, we also found clearly ripples in seismograms, of which some were remarkable and some faint. For example, Figs. 4 and 9 illustrate typical seismograms obtained at Tokyo University. Although seismograms No. 1115 and No. 1235 have large amplitudes which are comparable to each other, the former shows far less amplitudes of ripples than the latter.

4) K. KANAI, *Bull. Earthq. Res. Inst.*, **32** (1954), 361.

To develop our discussion on the character of ripples, we have to prepare a certain scale which indicates the magnitude of ripples relatively to that of fundamental vibrations. For this purpose, we shall define the ripple factor as follows:

$$r=(a_r/a_f)\times 100\,(\%)\ ,$$

where a_r and a_f means respectively the maximum amplitude of ripples and fundamental vibrations, both being measured in the same part of the seismogram. In this way we can find a time series of ripple factors for the succeeding parts of the seismogram under our test. The problem of separating ripples from the original trace is, however, not a simple one, as we have no convenient filters (mechanical or electronical) which can filtrate wave of necessary range of frequencies accurately. Fortunately,

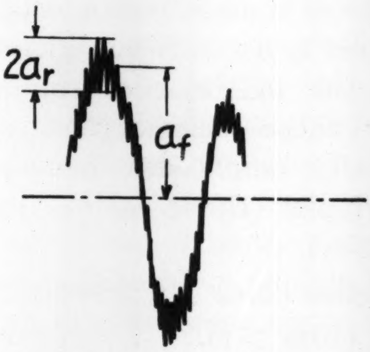

Fig. 3. Determination of ripple factors.

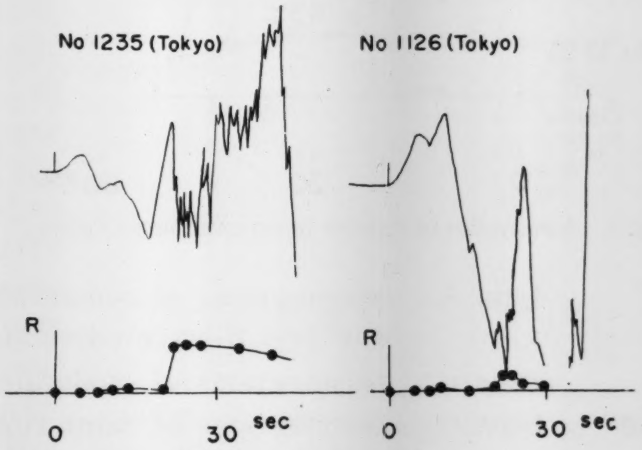

Fig. 4. Typical seismograms and ripples.

clear seismograms obtained with long period pendulums at Tokyo University suggest the possibility of estimating ripple factors even without special instruments. That is, as ripples show far shorter periods than the period of fundamentals, we can easily see the double amplitudes of ripples at each extremity of fundamental events in seismograms. This method of separation will not give a high accuracy to the result but still it will be of use for rough estimation of ripples (see Figs. 3 and 4). Figs. 4 and 5 illustrate amplitudes of ripples separated from the original in this way, and in them we notice remarkable increase of ripples at the beginning of S-phase. This fact may be understood well from the standpoint of Kanai's theory and instead of treating the whole part of seismograms, it may be allowed to limit our discussions to the said

part. The numbers in Fig. 5 indicate the ripple factor determined in this way for each seismogram.

Throughout the active period of aftershock occurrence, we could determine factors r for only several shocks from seismograms obtained at Tokyo, and it was considered to be difficult for us to carry out our studies on such few examples. Thus we had to use more seismograms of smaller aftershocks (*f.i.* Fig. 10). In this case ripple factors could not be determined accurately, and classification of them had to be done on a more rough scale. Three types were considered as the indicator of ripples for these seismograms of smaller amplitudes, namely,

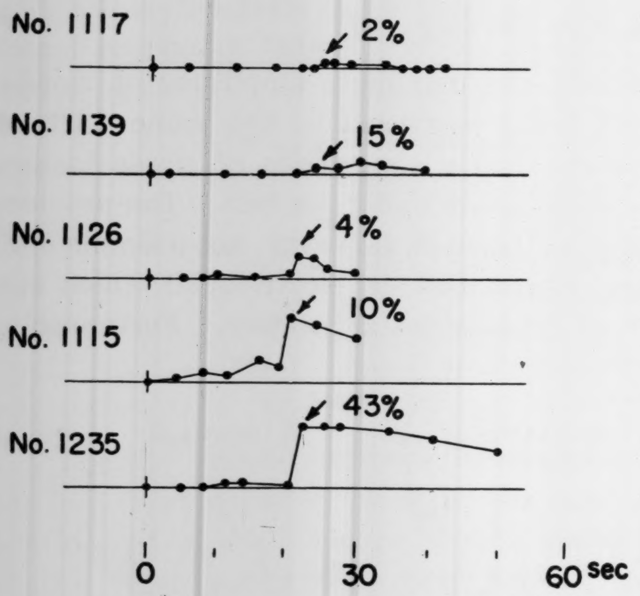

Fig. 5. Amplitudes of ripples in seismograms (Tokyo).

type A: seismograms of remarkable ripples (ripple factors for the first S-wave exceeding 25%),

type B: seismograms of moderate ripples ($25\% > r \geqslant 10\%$),

and type C: seismograms of faint ripples ($10\% \geqslant r$).

By comparing it with typical seismograms of larger amplitudes, we could determine to which type a seismogram belongs even when the ripple factor was unmeasurable. Types were determined for 29 aftershocks in total, as are listed in Table II. Figs. 10, 11 and 12 show representative seismograms belonging respectively to the said three types.

3. Discussion

To show the results more clearly, epicenters of aftershocks classified into three types of ripples are plotted in Fig. 6. It should be noticed that most of the aftershocks of type A are located only in the northwestern (or inner side) part of the active region, while shocks of type C are found most frequently in the southeastern (or outer side) part of the region. Shocks of the intermediate type B can be seen in the

central part. Before entering into further discussion, we should go over the mechanism of generation of ripples[5]. As was discussed in the last chapter, seismic waves making the first S-arrival at Tokyo traveled along the path DEF, which is believed to be also the path for all aftershocks under our test. Referring to Kanai's conclusion, we may suppose, in the present case, that the remarkable increase of ripples in the beginning part of S-phase was induced by incidence of the initial S-wave from the lower layer to the surface. With this supposition as well as the condition of the wave path DEF being common to all shocks, we shall come to the following conclusion: a) ripple factors (or ripple types A, B, C) determined on the surface should be understood as characteristic indicaters of waves propagated along the lower layer from their origins, and b) it is more natural to explain the causation of different ripple types by conditions in the seismic active region than by conditions of propagation, which are considered to be almost common to both types.

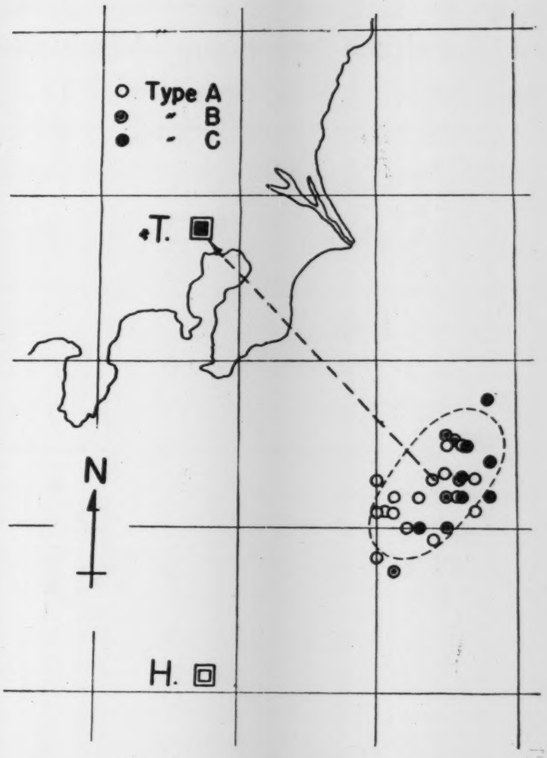

Fig. 6. Distribution of ripple types based on seismograms at Tokyo.

In this meaning of ripple factors, the following two possibilities will be considered to interpret the result illustrated in Fig. 6. They are,

a) aftershocks in the southeastern part of the active region occur initially with low ripple factors to be observed as type A at Tokyo while those in the northwestern part occur with higher ripple factors, and

b) all the aftershocks occur initially with equivalent ripple factors, and it is the absorption or the other effect of the active region that modifies the factor larger or smaller in the course of wave propagation.

To find out which of the two is more probable, further discussion must be done on various points of the phenomena. It would be useful

5) K. KANAI, *loc. cit.*, 4).

to ascertain if ripple types determined from seismograms at Tokyo show the distribution identical with those determined at other stations. That is, if explanation b) holds good, aftershocks must show another ripple type at stations located in a different direction from the centre. And if a) holds good the ripple types should be determined equivalently at stations of different directions. Seismograms of Hachijo-jima and Torishima were considered most suitable for this purpose (Fig. 1). Torishima is located on the opposite side of Tokyo 350 km distant from the active region while Hachijo-jima is 150 km to the west of the centre. Both stations, however, were not equipped with seismometers with natural period as long as that of Tokyo, so we had to determine the ripple types with instruments of shorter period (4 sec). As can be seen in Figs. 11 and 12, vibrations of longer periods were not recorded at these stations so clearly as at Tokyo and the determination of the ripple types was somewhat a difficult task. In Table II are listed the ripple types of aftershocks recorded at the two stations for reference, but these results should be understood as only a rough approximation. We see in the table or in Figs. 7 and 8 that the aftershocks which were found to be of types A, B, or C at Tokyo seem to correspond generally to those of other stations. This fact suggests that the explanation a) is more probable than the other. In other words, the systematic distribution of ripple types in the active region seems to be interpreted more plausibly from the viewpoint of initial conditions of occurrence of each aftershocks than from a certain effect (as supposed in the last chapter) of the active region on the characters of seismic waves passing through it. Special absorption of higher frequencies in the said region, however,

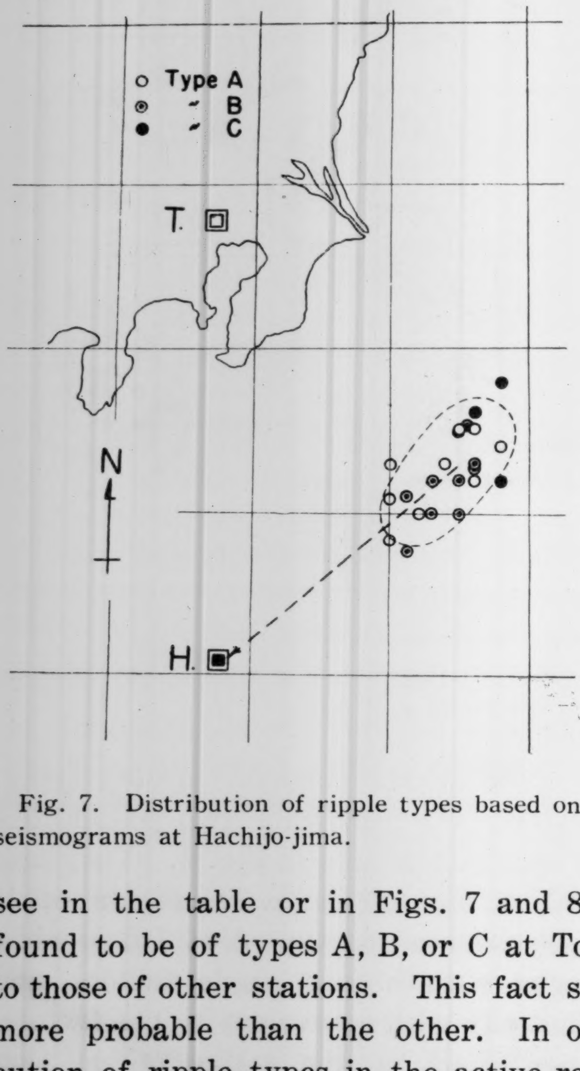

Fig. 7. Distribution of ripple types based on seismograms at Hachijo-jima.

is not the only abnormality which can be imagined in the region affected greatly by the main shock, and other possible case should be investigated in parallel with the present one. We must, however, remember that the locations of aftershocks were not determined so accurately in the case of the Boso-Oki Earthquake, and that we could not use the seismograms of Hachijo-jima and Torishima obtained through long-period seismometers. Both conditions provided unavoidable uncertainties in the determination of ripple types. Aftershocks occurring in the land area are considered to be most suitable for obtaining accurate conclusions on the present project.

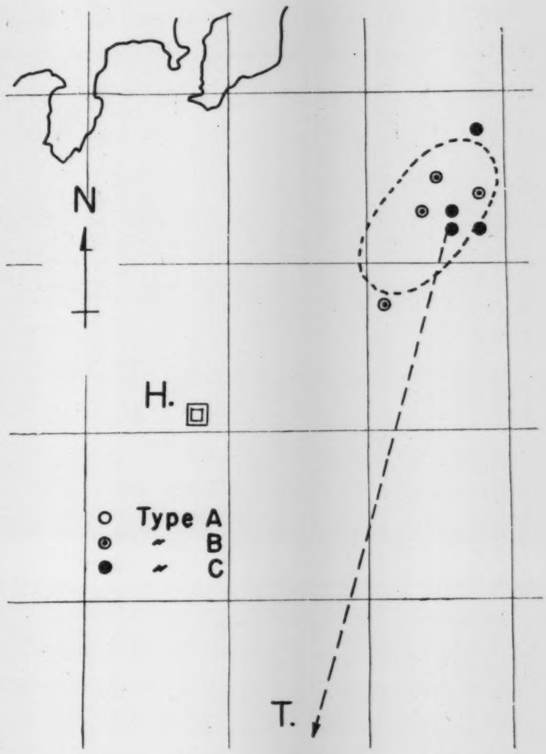

Fig. 8. Distribution of ripple types based on seismograms at Torishima.

4. Concluding remarks

Ripples in aftershocks of the Boso-Oki Earthquake of November 26, 1953 were studied to find out special effects of the "seismic active region" on the propagation of seismic waves passing through it. As to ripple types, aftershocks which brought seismic waves of remarkable ripples to Tokyo were located most frequently in the inner side of the active region and most of the shocks with faint ripples were found in the outer side of the same region. Although it is possible to explain the result by an abnormally remarkable absorption of rapid vibrations in the said region, it was considered more natural to explain it by the initial condition of generation of ripples given at each origin of aftershocks. Because seismograms obtained at Hachijo-jima and Torishima showed the distribution of ripple types which is similar with that obtained at Tokyo.

The author considers that the problem on the property of the seismic active region should be investigated furthermore. A group of after-

shocks occurring in the land area would be more suitable for the present purpose, since locations of each origin could be determined more accurately and observations made under the best condition in that case.

The present author owes very much to the Seismological Division of C.M.O. as well as to the Observation Branch of this institute, which both kindly offered necessary seismograms at his request. He wishes to express hearty thanks to them and to Prof. T. Hagiwara of this institute, who showed an interest in this study and kindly put various facilities at the author's disposal.

---

40. 地震動に含まれる短週期震動（リップル）について
—— 房総沖地震の余震の場合 ——

地震研究所　笠　原　慶　一

比較的近い地震の記象を見ると，リップルともいうべき顕著な短週期震動が長週期震動に重畳している場合がある．余震のように限られた区域に発生する地震群を離れた地点で観測すると，伝播経路がほとんど同一と見なされるので，上記のリップル成分を調べることによつて，余震活動域の性質を知る可能性が考えられる．

各余震のリップルの大小を相対的に表示する量としてリップル率（及びリップル型）をとり，房総沖地震に伴う余震の東京（本郷）における変位記象を分類して見ると，余震域の外側（北東側）に位置する余震は低いリップル率を示し，内側のものは高いリップル率を示するいう系統的な分布が見出された．地震波の伝播経路がこの場合殆んど共通であることを考え合わせると，次の説明が想定される．即ち，

a）余震の発震機構（リップル成分に関しての）そのものが，上記のような傾向をもつているとするか，

b）リップル成分に関する発震機構においてはどの余震も大差なく，上記の傾向が生ずるのは，余震活動域一帯の特性（例えばその中を通過する地震動の短週期成分を特に減衰させるというような）によるものである，と考える

かである．この点を判断する目的で八丈島及び鳥島での記象（簡単微動計による）を調べたところ，a）の説明の方が有力らしく思われる．

[Bull. Earthq. Res. Inst., Vol. XXXIII, Pl. LXXXIV.]

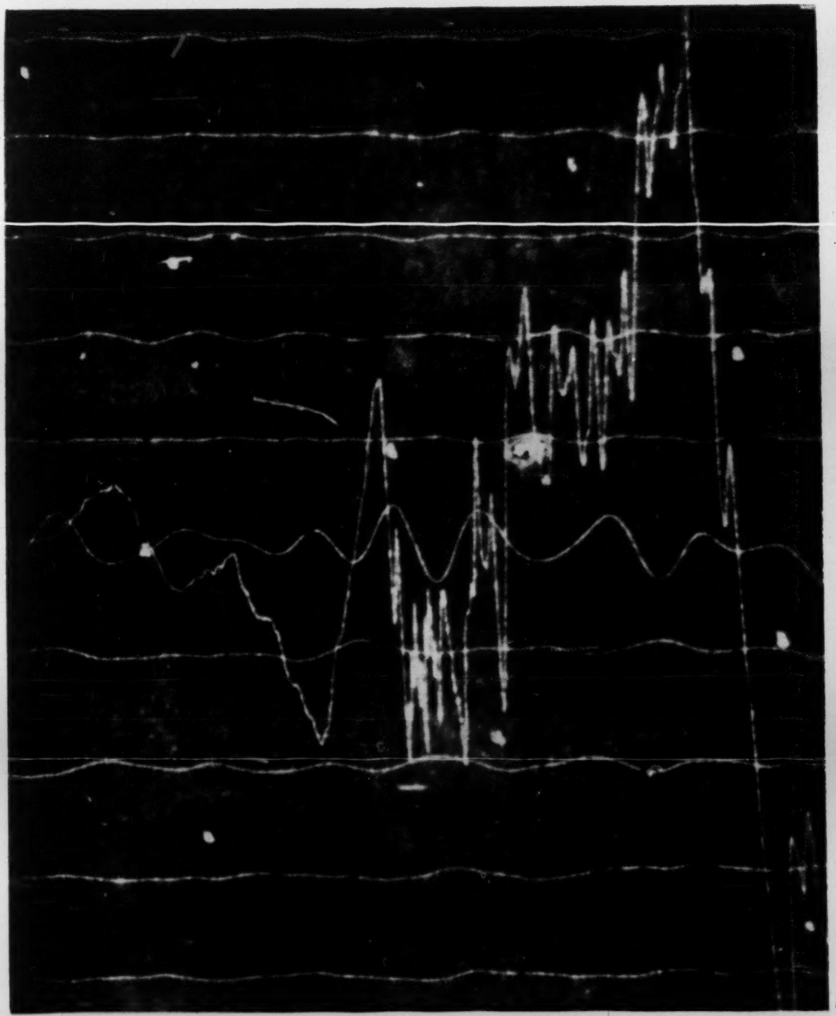

Type "A". No. 1235

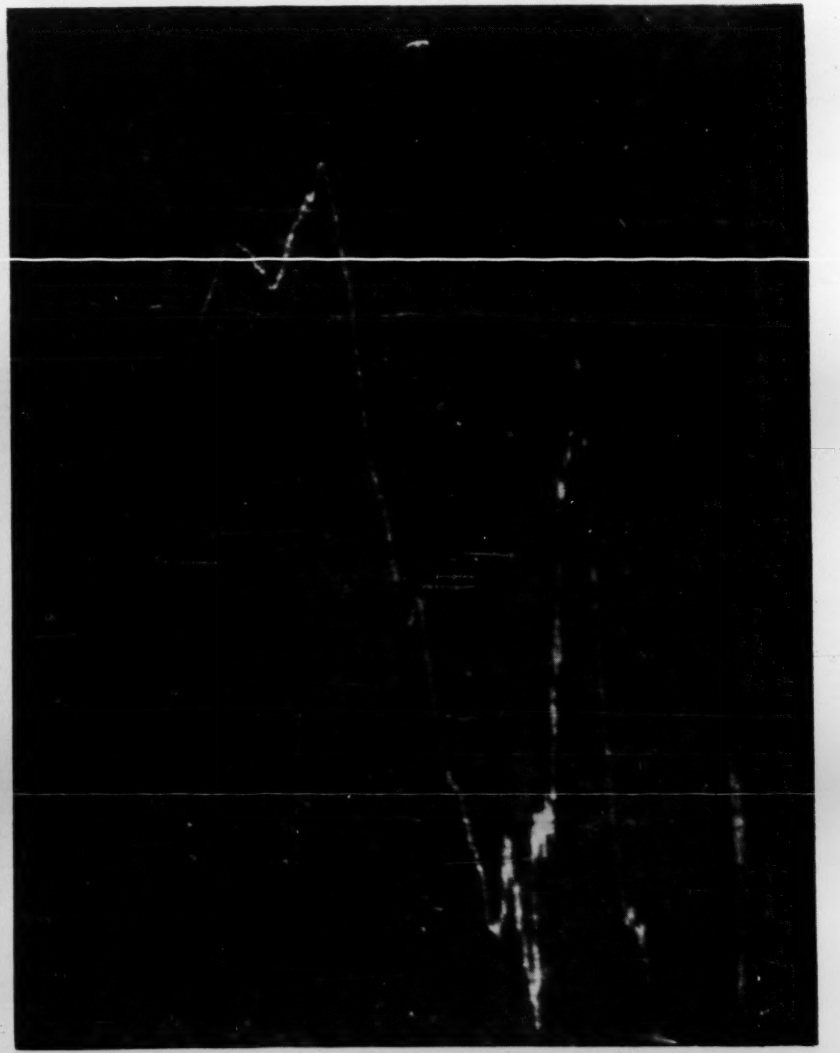

Type "C". No. 1126.

Fig. 9. Typical seismograms of high and low ripple factors (Tokyo). (original ×4)

(震研彙報 第三十三号 図版 笠原)

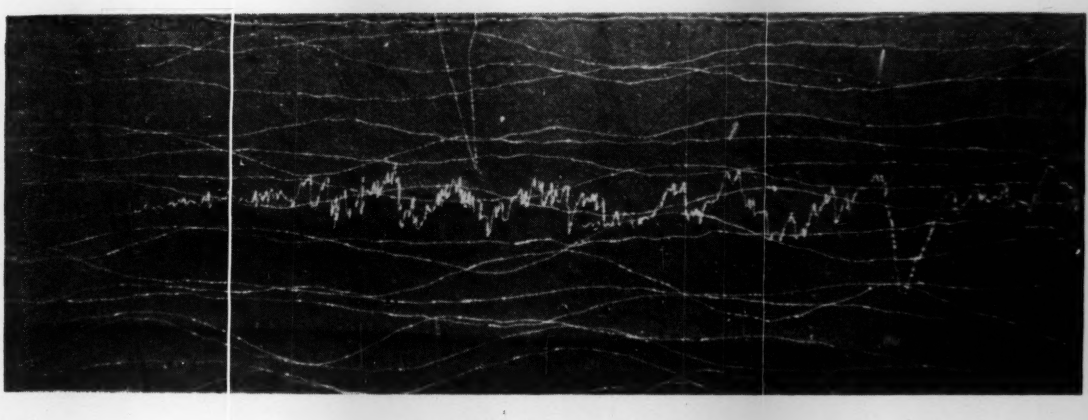

Type "A". No. 1220

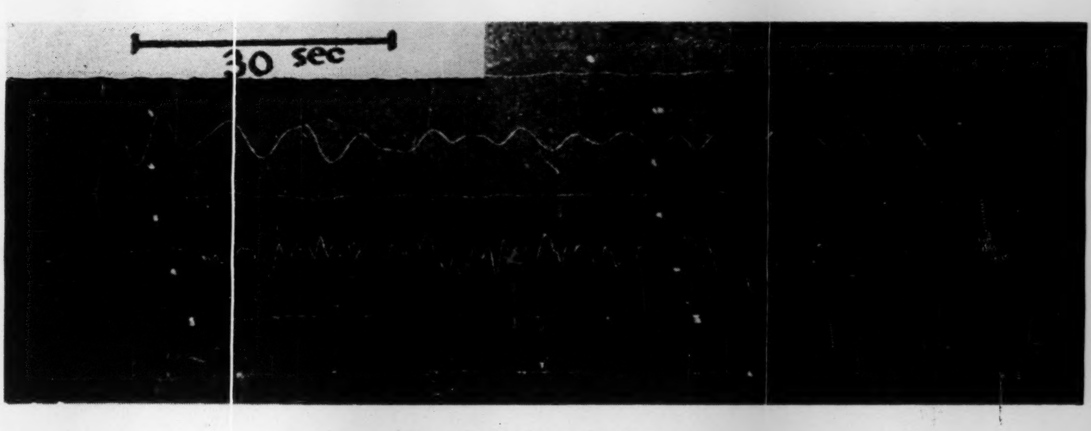

Type "B". No. 1158

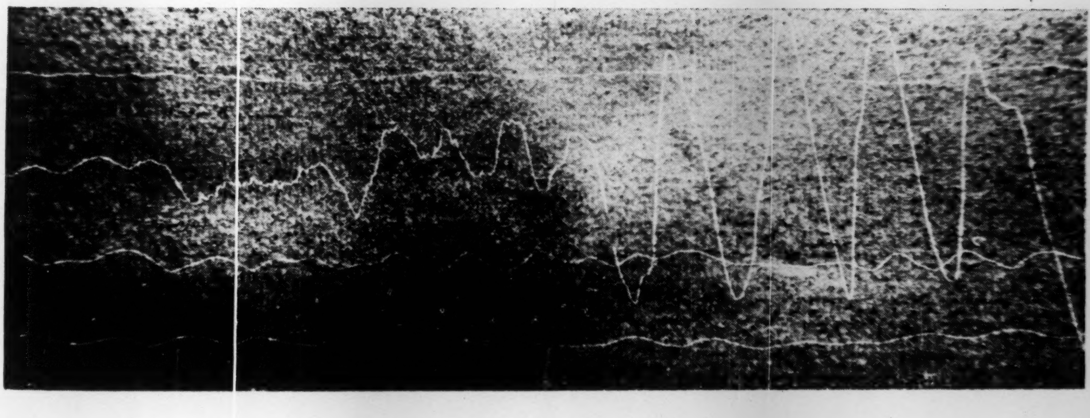

Type "C". No. 1154

Fig. 10. Seismograms classified into three types of ripples (Tokyo). (original ×2)

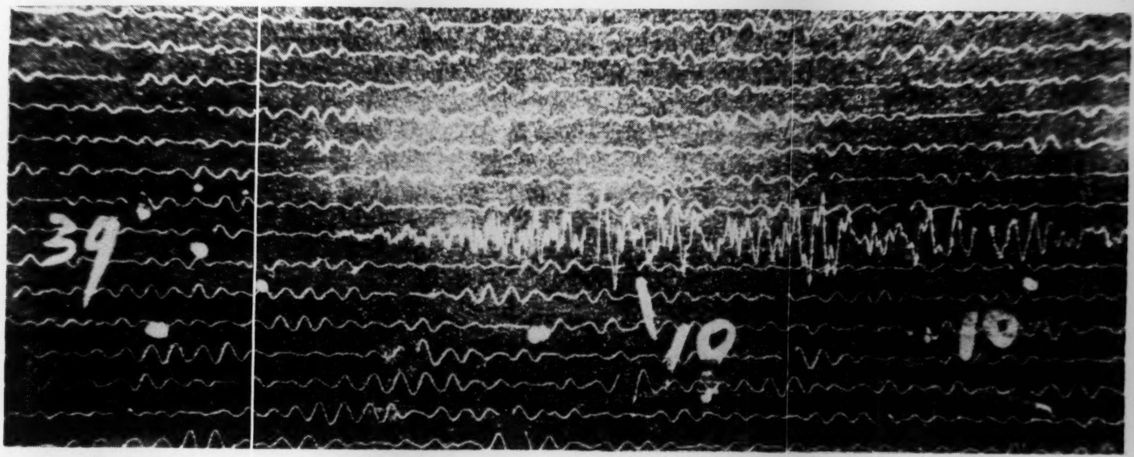

Type "A". No. 1220

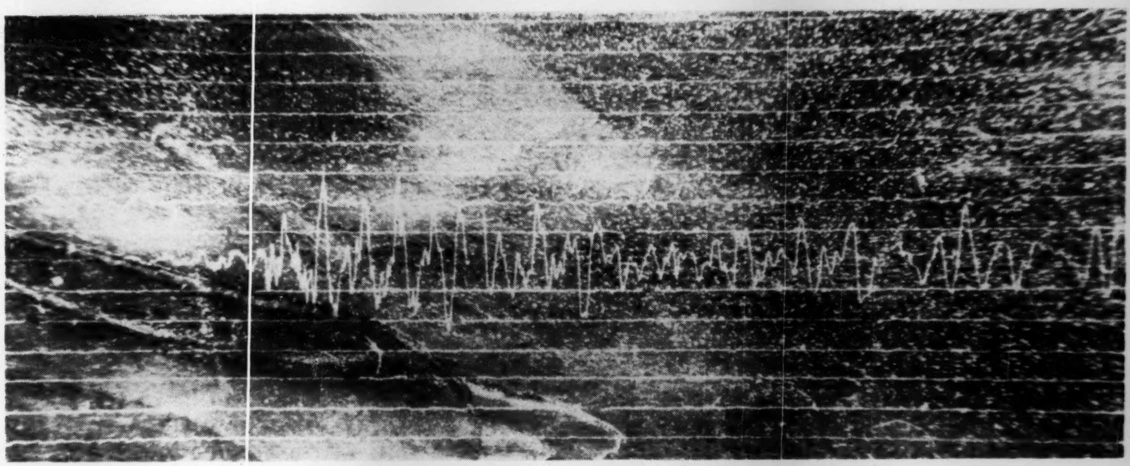

Type "B". No. 1157

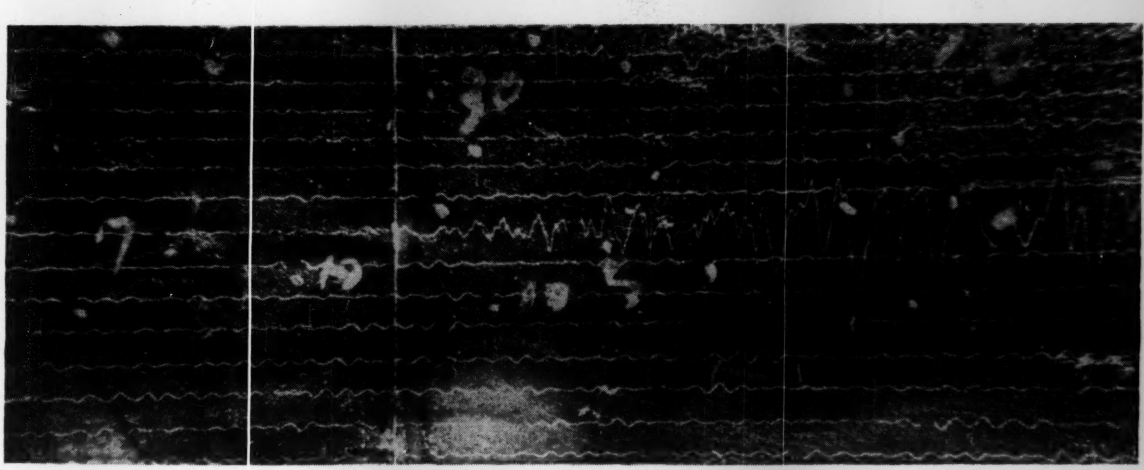

Type "C". No. 1154

Fig. 11. Seismograms classified into three types of ripples (Hachijo-jima). (original ×2)

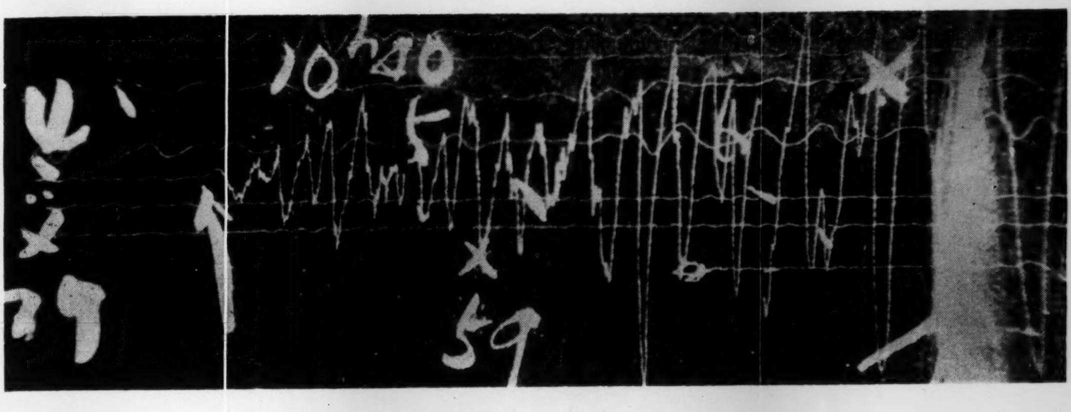

Type "B". No. 1115

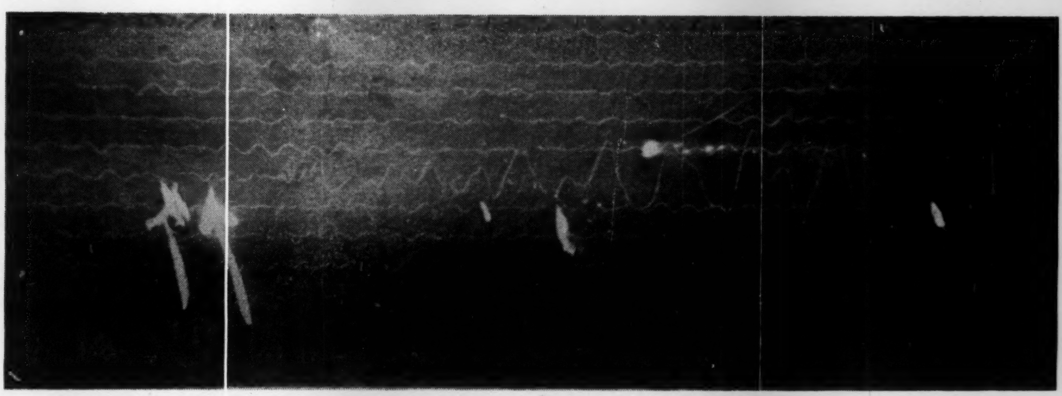

Type "C". No. 1154

Fig. 12. Seismograms classified into three types of ripples (Torishima). (original ×2)
No seismograms of type "A" were recorded.

(震研彙報 第三十三号 図版 笠原)

41. *Aftershocks that accompanied the Tottori Earthquake of Sept. 10, 1943.* (*The 2nd Paper*)

By Syun'itiro OMOTE,

Earthquake Research Institute.

(Read Sept. 16, 1953.—Received Sept. 30, 1955.)

1. Introduction

On the evening of Sept. 10, 1943, the Tottori area was shaken by a severe earthquake. This area is near the coast of the Japan Sea in the western part of the Island of Honshu. The magnitude of this earthquake was estimated as 7.4 by the Gutenberg Richter scale. It resulted in the destruction of more than 7000 dwelling houses and the loss of more than 1000 human lives. Tottori is the largest city in the damaged area and the earthquake is named after it. Prior to this Tottori earthquake, this same area was shaken by two somewhat slighter shocks on March 4 and 5 of the same year which resulted only in the destruction of five houses[1]. After these shocks a somewhat large number of afterschocks, about 537 times in all, were felt in the same area before the destructive earthquake broken out on Sept. 10. The Tottori earthquake was highly destructive in the epicentral area and was the biggest one to occur in these parts along the coast of the Japan Sea after the great Tango earthquake of March 3, 1944, that was originated 80 km to the east of this earthquake.

In less than 24 hours after the outbreak of the Tottori earthquake a field party of our Institute was organized and dispatched to the shaken area, the writer being held responsible for the observation of aftershocks. After a seismometer was installed at Igumi (Fig. 1) on the Sept. 12, seismic stations were established one after another and by the evening of Sept. 14 eight stations, each having one component of horizontal pendulum, were in operation.

The observation of aftershocks was continued for about a month and the description of the distribution of seismic foci of some selected aftershocks was given in a preliminary report published in 1944[2]. As

1) S. OMOTE, *Bull. Earthq. Res. Inst.*, **21** (1943), 453.
2) S. OMOTE, *Bull. Earthq. Res. Inst.*, **22** (1944), 33.

this map of foci was prepared in a great hurry on the basis of rough calculations made immediately after the main shock took place, it was necessary to prepare a more complete report. However, as the war became gradually severe the analysis of the seismograms had to be put aside for many years till recently when all the seismograms were thoroughly readjusted in order to locate the more reliable foci of aftershocks. The results of the readjustment are reported here.

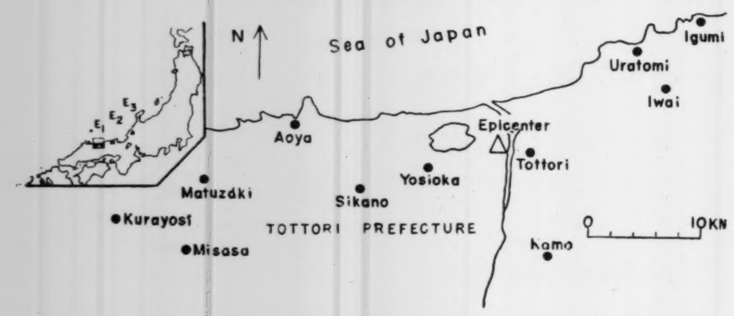

Fig. 1. Map of Tottori district, showing locations of the epicenter of the main shock and the observation network of the aftershocks.

● observation point
△ epicenter of the main shock
▲ E_1, Tottori Earthq.: E_2, Tango Earthq.: E_3, Fukui Earthq.

2. General sketch of the activity of the Tottori aftershocks

From the data of the station observatories, the epicenter was located by the Central Meteolorogical Observatory[3] at 134.°2 E longitude, 35.5° N latitude. The observation network for the aftershocks was placed at the beginning over the eastern part of the Prefecture, but later a seismic fault was found on Sept. 16 near Sikano Town, 15 km to the south-west of Tottori, and on Sept. 28, a fairly large shock of intensity IV according to the Japanese Intensity Scale broke out near Kurayosi Town, and the network had to be shifted gradually to the west.

In this observation of the Tottori aftershocks, as was the case with the other earthquakes, the driving power of the recording drum of the seismograph was fed by an AC motor. The electric power supply, however, was shut off owing to the disconnection of power cables at many places caused by the severe earthquake vibrations. Owing to the wartime situation, the repair works of the damaged power cables went on very slowly, especially in the hilly regions of the southern part of the Prefecture. From this reason we encountered some restrictions in distributing the observation points.

Locations of the observation points, the types of the seismographs

3) *Seismological Bulletin of the CMO*, Japan, for the year 1943.

installed and their instrumental constants and the length of the period of observations are tabulated in Table I. In order to set up as many observation stations as possible, we were compelled to do with only one seismometer at each station, as there were only eight seismometers in all that were available for us.

Table I. Instrumental constants of the seismometers installed at the temporary observation points and the length of the period of observation.

Observation point	Component	Observed Period from month	date	to month	date	Weight of the mass of pendulum	Free oscillation period	Magnification
Uradomi	H-1	IX	16	IX	18	7.5kg	0.12sec	ca. 100
Iwai	〃	IX	27	X	8	6	6.0	21
Igumi	〃	IX	12	IX	23	7.5	0.12	100
Tottori	〃	IX	13	IX	23	7.5	0.12	100
	〃	IX	23	X	12	13	0.15	213
Kamo	〃	IX	13	IX	20	7.5	0.12	100
Yosioka	〃	IX	15	X	11	6	6.0	21
Makihara	〃	IX	21	X	5	7.5	0.12	100
Sikano	〃	IX	14	X	9	7.5	0.12	100
Aoya	〃	IX	18	X	9	7.5	0.12	100
Kurayosi	〃	IX	16	IX	24	6	6.0	21
	〃	IX	24	X	10	7.5	0.12	100
Matuzaki	〃	X	7	X	11	7.5	0.12	100
Misasa	〃	X	8	X	10	7.5	0.12	100

3. Number of aftershocks

On the third day after the great earthquake the first seismograph of our field party was installed in the shaken area but it took two more days before the network of our observation of aftershocks could be completely established and began its operations in full. The Tottori Branch Station of the CMO counted the number of aftershocks (of course only the sensible ones) and the hourly number of the aftershocks felt is reproduced in Fig. 2 by the courtesy of CMO[4]. This figure attracts our attentions especially in the point the hourly number of aftershocks is seen increasing for the first few hours after the occurrence of the

4) W. INOUYE, *Report of the Tottori Earthquake of Sept. 10 1943, CMO,* (1943), (in Japanese).

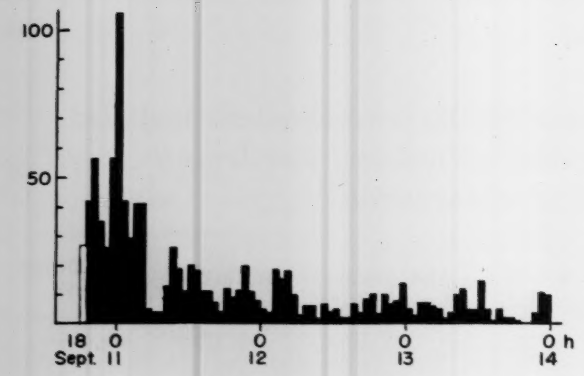

Fig. 2. Hourly number of aftershocks felt at Tottori Branch Station of CMO.

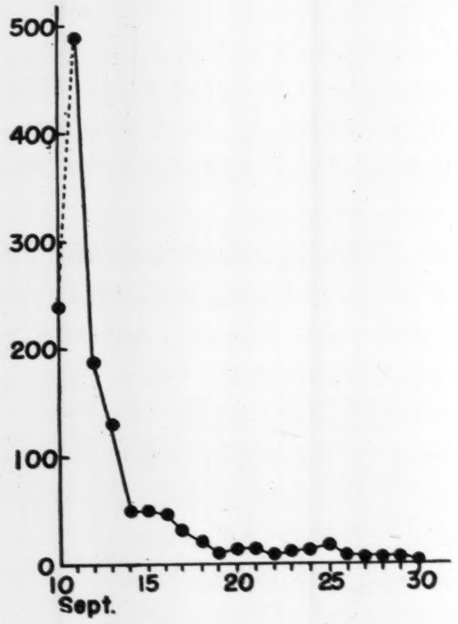

Fig. 3. Daily number of felt aftershocks at the Tottori Branch Station of CMO.

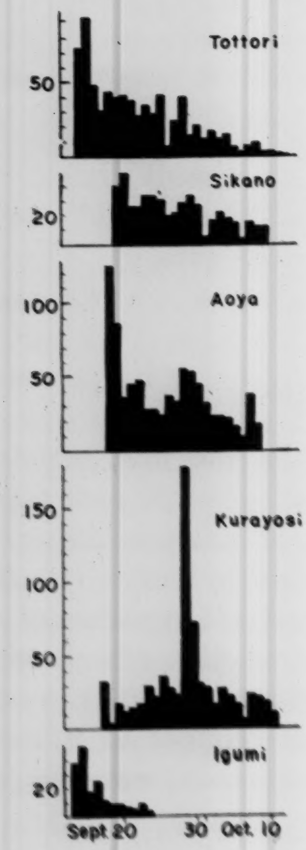

Fig. 4. Daily number of aftershocks.

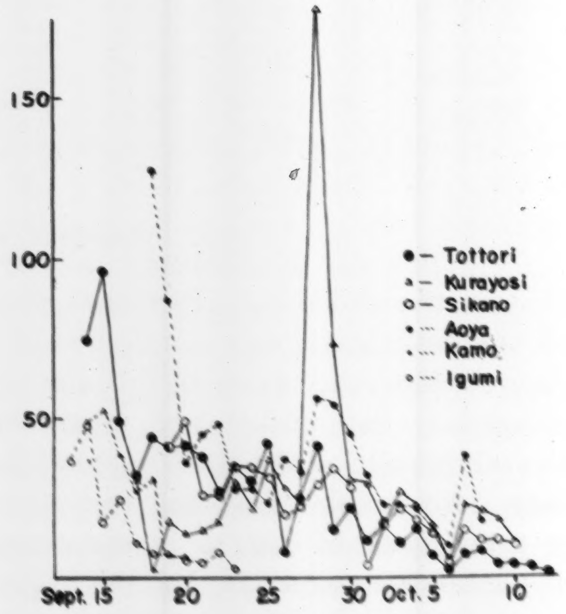

Fig. 5. Daily number of aftershocks at Tottori, Sikano, Kurayosi, Igumi, Kamo and Aoya.

main shock. Six hours after the main shock the hourly number of aftershocks reached its maximum and then it began to decrease rapidly with the lapse of time. The daily number of aftershocks is seen in Fig. 3. The figure shows that the generation of aftershocks was very active for two or three days after the main shock but after Sept. 14 the activity became less vivid. From this it will be seen that, though our observation net was installed in a great hurry, the most active and important period for the study of the aftershocks escaped our observations. The daily number of aftershocks recorded at each station of our seismograph network is given in Fig. 4.

For the purpose of showing the general tendency of the seismic activity throughout the entire shaken area, the daily number of the aftershocks at different stations is shown together in one sheet (Fig. 5). From this figure it is seen that such stations as Igumi, Kamo and Tottori, that are situated in the eastern area were active in the early period of our investigation, while they became inactive as time went on compared with the activity of the western stations. The most noticeable activity is seen in the curves of Kurayosi Station. In this station the number of shocks was rather few compared with that of the Tottori Station until Sept. 28, but after that date, on which date a strong shock took place near the Kurayosi Station, the number of shocks observed at the Kurayosi Station is seen to exceed the number of any other station.

4. Frequency distribution of P-S time

Fig. 6 shows the frequency diagrams of P-S time at respective stations. We notice in the first place that the maximum frequency of P-S time appears to be at about 1 second at the respective stations. On further examination, however, it is found that at Tottori Station the most frequently occurring P-S time is 0.6–1.0 sec., and at Sikano and Kurayosi Stations 0.9–1.0 sec., while at Aoya and Kamo it becomes somewhat longer, being 1.5 sec. or so. In the second place we notice that a very short P-S time is observed at almost every station, especially in Tottori Station, where such a short P-S time as only 0.2–0.4 sec. is observed for about 20 times. If we assume, for instance, that the P–S time is 0.2 sec., it turns out that the distance between the station and the hypocenter is only 1.6 km or so. This means that we have to expect that the earthquake occurs in such a shallow point even if it took place right under the observation station. In general these earthquakes with very short P-S time are also small in their amplitudes and from this

fact we are inclined to think that quite a number of very small shocks were taking place over a wide area covering the whole disturbed area. With respect to the Aoya Station no such shock with very short P-S time was to be seen taking place. In the third place, we notice that in this case of the Tottori aftershocks, fairly long P-S times were also observed at some stations, though they were small in number. At the Sikano Station, which is situated in the central part of our observation network, shocks with P-S time longer than 5 seconds were not recorded at all. At the Tottori and Igumi Stations situated in the eastern part of our observation network, or at the Kurayosi and Aoya Stations situated at the western end of our network, the P-S time exceeding 7 or 8 seconds could be observed though small in number. These facts may give some indication as to the geographical distribution of the foci of the aftershocks.

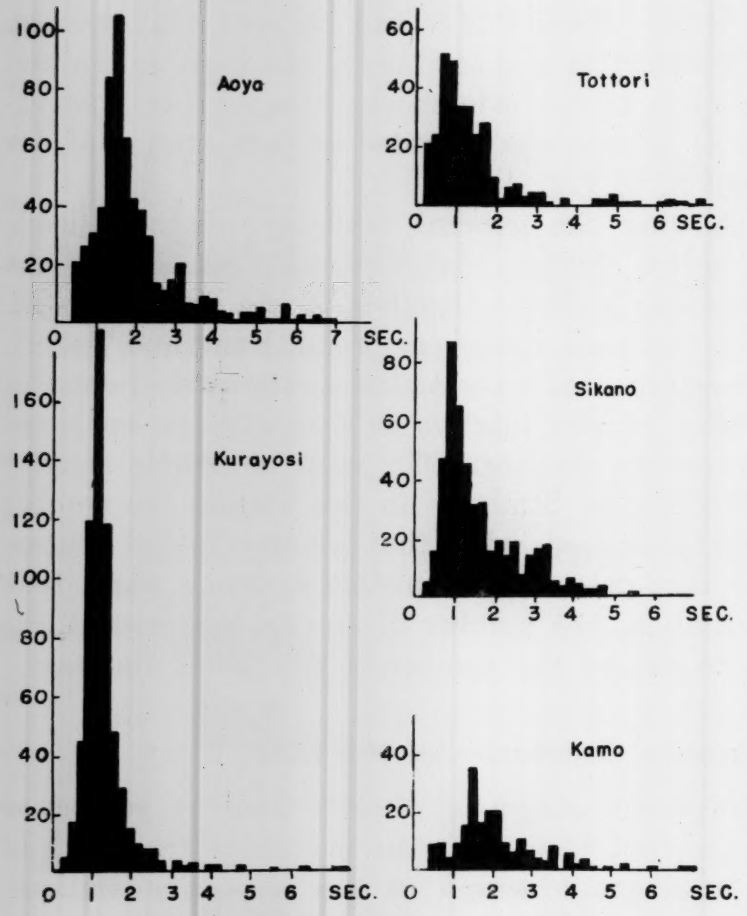

Fig. 6. Frequency diagram of P-S time.

A word should be added as to the P-S time of the Kurayosi Station. In Fig. 7 the frequency diagram of P-S time observed at the Kurayosi Station is shown, in which (b) is in the period from Sept. 16 to Sept. 27 and (a) from Sep. 28 to Oct. 10. As we have already seen, on Sept. 28 a fairly large shock took place near the Kurayosi station and subsequently the seismicity of this station became suddenly active from that date, so that it was considered that there may be seen some differences in the form of frequency diagrams between the two periods. As will

be shown in Figs. 7-a and b, in which (b) is a P-S diagram in the former period and (a) in the latter period, shocks of the shorter P-S time appear to be somewhat active in the latter period.

5. Determination of epicenters

The P-S interval method was introduced in determining the foci of shocks. In this method the value of k, the constant factor in the formula $D=kt$[5], has been determined graphically through those earthquakes that have given good records at least four stations. Those shocks which were used for the determination of k are tabulated in Table II with the value of k

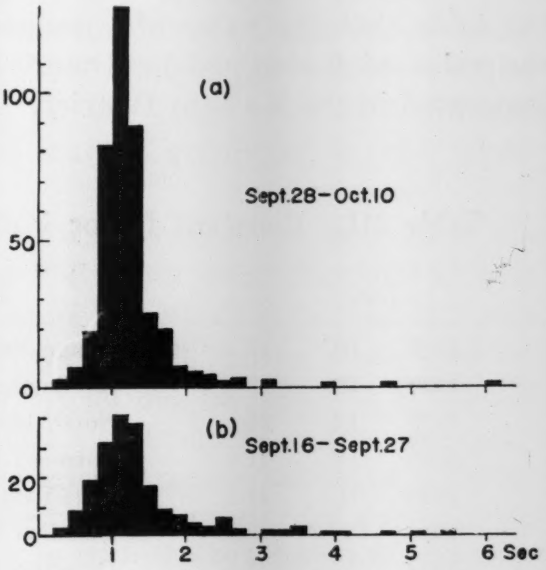

Fig. 7. Frequency diagram of P-S time at Kurayosi Station.

Table II. List of aftershocks for the determination of k. P-S time, value of k and H, the depth of focus.

Earthq. No.	Time of occurrence			Tottori	Yosi-oka	Maki-hara	Sika-no	Aoya	Matu-zaki	Kura-yosi	Misasa	k	H
	Sept.	h	m	sec.	sec.	sec.							km
1*	15	0	25	1.0	1.0							7.4	4.8
7	21	14	32	1.6	1.4	1.4	1.7					8.3	10.8
11	24	3	25	1.8	1.3	1.8	1.1	2.4				7.0	9.3
13	24	13	20	4.2		2.9	2.7			1.9		9.0	11.4
14	27	01	33	2.7		1.7	1.3			2.3		8.6	10.3
17	28	06	41	4.3		2.8	2.4	2.4		1.2		8.1	5.0
	Oct.												
28	3	02	10			3.2	2.7	2.1		1.8		8.8	13.1
29	3	02	11			3.7	3.0	2.6		2.2		9.0	18.8
32	7	5	30					1.9	1.0	1.2	0.8	8.0	6.4
36	7	22	11				2.6	2.1	0.9	0.9	0.9	7.1	4.6
38	9	5	28					1.6	1.1	1.5	1.2	8.1	8.2
											mean	8.1±0.45	

* Igumi, 3.1 sec; Kamo, 1.9 sec.

5) F. OMORI, *Rep. Imp. Earthq. Inv. Comm.*, (*in Japanese*), **88 A** (1918), 1.

as well as their P–S times. The mean value of k is obtained as 8.1 ± 0.4.

The numerical value of k is found to be much smaller in the usual case of other aftershocks, as is shown in Table III. It is seen from the table that the value of k ranges from 4 to 6 which is smaller than the value of k obtained by Omori through the earthquakes that were generated in the Kwanto District. In the usual case of the observation

Table III. Constant factor k obtained at different earthquakes.

Date			Earthquake	k
1927	III	17	Tango Earthquake[6]	8.41
1930	III	—	Ito Earthquake Swarm[7]	4.70
1930	IX	26	North Idu Earthquake[8]	5.13 ± 0.29
1935	IV	21	Formosa Earthquake[9]	4.79
1936	II	21	Koti-Yamato Earthquake[10]	6.15
1938	VI	—	Ooshima Swarm[11]	$2.2 + 0.4d$
1939	V	1	Ogasima Earthquake[12]	5.1 ± 0.3
1940	XII	12	Miyake-sima Eruption[13]	(2)
1943	IX	10	Tottori Earthquake	8.1 ± 0.41
1944	XII	7	Tōkaido Earthquake[14]	$7.1 + 0.02d$
1945	I	13	Mikawa Earthquake[15]	5.7
1948	VI	28	Fukui Earthquake[16]	7.2
1949	XII	26	Imaichi Earthquake[17]	7.1 ± 0.4

of aftershocks, even the largest epicentral distance does not exceed 40 or 50 km, so that it is considered that the P–S times may be derived from the waves $\bar{P}(\bar{S})$ or $P^*(S^*)$. These facts, together with the shallow depth of their foci, may be responsible for the small value of k. Com-

6) N. NASU, *Jour. Facul. Sci. Imp. Univ. Tokyo*, II, **3** (1929), 29.
7) N. NASU, F. KISHINOUYE and T. KODAIRA, *Bull. Earthq. Res. Inst.*, **9** (1931), 32.
8) N. NASU, *Bull. Earthq. Res. Inst.*, **13** (1935), 400.
9) N. NASU, *Bull. Earthq. Res. Inst.*, *Suppl. Vol.*, **3** (1936), 75.
10) N. NASU and T. HAGIWARA, *Bull. Earthq. Res. Inst.*, **14** (1936), 285.
11) R. TAKAHASI, *do.* **16** (1938), 87.
12) T. HAGIWARA *do.* **18** (1940) 252.
13) T. HAGIWARA, *do.* **19** (1941) 260.
14) T. MINAKAMI and S. UTIBORI, *do.* **24** (1946), 19.
15) S. OMOTE, *do.* **24** (1946), 77.
16) S. OMOTE, *et. al. Report of the Fukui Earthq.*, (1949), 37.
17) EARTHQ. RES. INST., *Bull. Earthq. Res. Inst.*, **28** (1951), 387.

pared with these small values of k, the Tottori earthquake is noticeable for its large value of k. A large value of k is also seen in the case of the Tango earthquake in 1927 and the Fukui earthquake in 1948. The Tottori area is very near the Tango district (Fig. 1) and these areas, existing in the northern part of Western Honsyu, are widely covered by granitic rocks.[18] The main reason for the large value of k obtained at the Tottori and Tango earthquakes may be attributed to the geological structures of the districts.

Making use of this value of k, it was possible to determine the epicenters of such shocks of which the P–S times were observed at only three stations. In the case of the Tottori aftershocks, as was the case with the other ones, large number of very small shocks were seen occurring very near a station, while they could not be recorded at distant stations. Moreover, in the case of Tottori aftershocks it was especially difficult to find correspondence between seismograms obtained at different stations, because the supply of the electric AC commercial current was interrupted from time to time, stopping in turn the revolution of a recording drum several times a day. Shocks of which the correspondence was not so reliable were rejected from our calculation and only those shocks of which correspondence was good were used in the determination of epicenters. There are 100 shocks of which the epicenters were determined. Geographical distribution of the epicenters is shown in Fig. 8. Epicenters were found to be distributed in the area 40 km long and 20 km wide with Tottori City situated in the eastern border and Kurayosi Town in the western border of the seismically active area. Such distribution of seismic foci of aftershocks as seen in Fig. 8, may of course have something to do with the distribution of the observation net itself, but nevertheless it will be safe to say that this map shows the seismic active area of the Tottori aftershocks.

In the case of the Tottori earthquake, two seismic faults, Sikano and Yosioka faults, were formed. With respect to these faults, a detailed description is given by Tsuya[19] and their locations are reproduced after him in the map of foci of aftershocks (Fig. 8). We note that almost all the foci of aftershocks are generated in the northern area of the fault, although nothing can be said for a small number of foci that are located on the other side of the fault. We find from this figure that the seismic activity is to be seen mainly in the area bounded by

18) H. TSUYA, *Bull. Earthq. Res. Inst.*, **4** (1928), 139.
19) H. TSUYA, *Bull. Earthq. Res. Inst.*, **22** (1944), 1.

two lines, the line of the coast of the Japan Sea to the north, and the fault line that ties Tottori and Sikano to the south. In the period from the beginning of our observation (Sept. 14), to Sept. 28 seismic

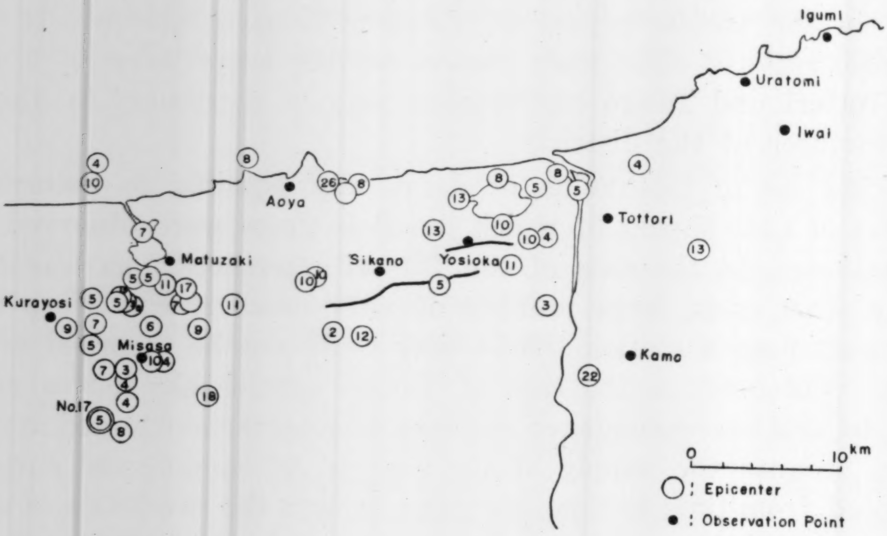

Fig. 8. Distribution of seismic foci.

foci are seen densely distributed in the eastern part of the area described above, while from Sept. 28 to Oct. 5 they are much more densely distributed in the western part of the area.

6. Cubic distribution of the foci

In Fig. 8 the numerals in the circles indicating the epicenters represent the depth of the focus in kilometers. The frequency distribution of the depth of focus is shown in Fig. 9. As shown by the numerals the focal depths of some shocks are very small, while those of some others are as deep as 25 km, but, in most cases, the depth is about 10 km. For the purpose of making clear the cubic distribution of the aftershocks the seismic foci that are distributed in the area bounded by the fault line in the south and the coastal line of the Japan Sea in the north are projected to the vertical plane intersecting the surface along the line of the Sikano fault (line B–B' in Fig. 10–a). As in Fig. 10–b, somewhat deep shocks are generated in the central area while shallow shocks are generated in the east and west parts. In Figs. 10–c and 10–d are shown the cubic distribution of foci that are projected

to the verical plane intersecting the surface along the lines AA' and CC' with respect to the aftershocks that are generated in the areas A and C (Fig. 10-a), respectively. As to the Tottori area (Fig. 10-c)

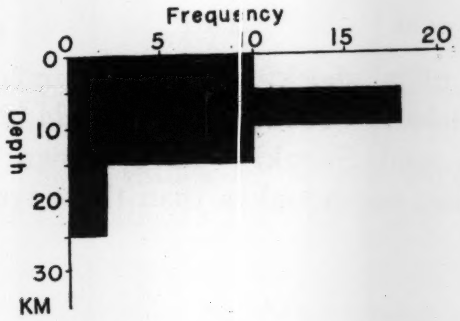

Fig. 9. Frequency diagram of focal depth.

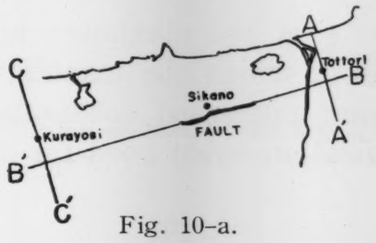

Fig. 10-a.

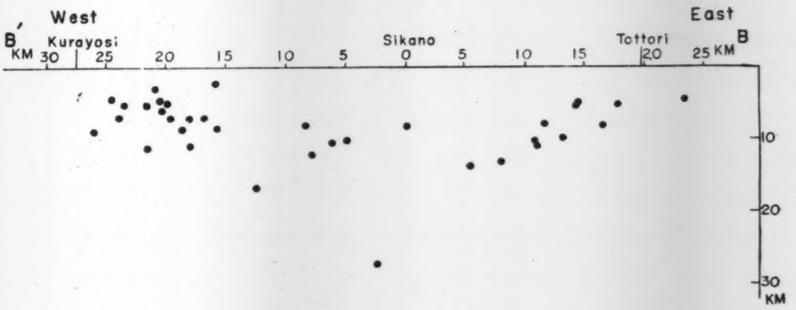

Fig. 10-b. Cubic distribution of seismic foci projected to the vertical plane BB' that runs parallel to the fault line.

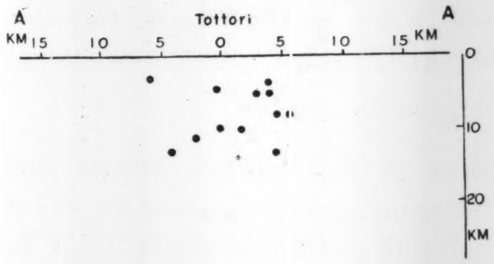

Fig. 10-c. Cubic distribution of seismic foci projected to the vertical plane AA' that is perpendicular to the fault line.

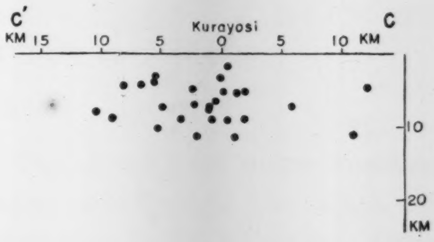

Fig. 10-d. Cubic distribution of seismic foci projected to the vertical plane CC' that is perpendicular to the fault line.

deeper foci is seen in the southern part and in the Kurayosi area (Fig. 10-d) shocks of the very shallow origin are seen to have taken place.

7. Frequency distribution of maximum amplitude

Ishimoto and Iida[20] have proposed an empirical formula on the frequency distribution of maximum amplitudes of earthquakes observed at Tokyo of the form:

$$N(a)=ka^{m} \tag{1}$$

where a is the maximum amplitude of a shock, $N(a)$ the number of shocks of which the maximum amplitude is between a and $a+da$, k and m being numerical constants. Asada and Suzuki[21] have shown that this relation holds good for much smaller earthquakes than those treated

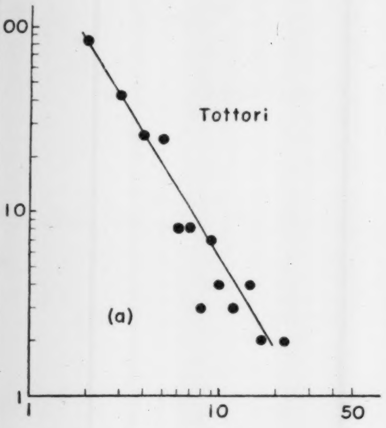

Fig. 11 (a)

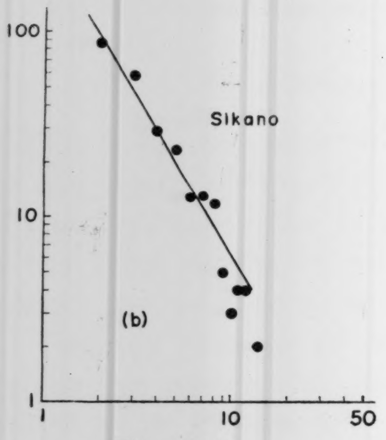

Fig. 11 (c)

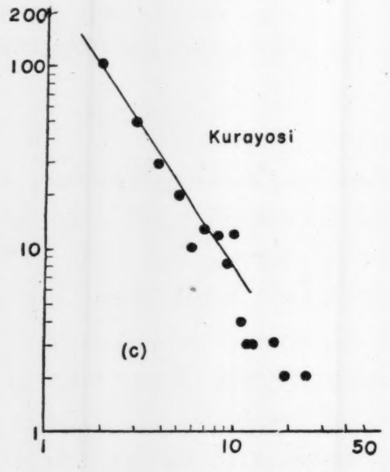

Fig. 11 (b)

Fig. 11. Frequency distribution of maximum amplitudes at different stations.
a; Tottori Station, b; Sikano Station, c; Kurayosi Station.

20) M. ISHIMOTO and K. IIDA, *Bull. Earthq. Res. Inst.*, **17** (1939), 443.
21) T. ASADA and Z. SUZUKI, *Geophys. Notes*, **2** (1949), No. 2.

by Ishimoto and Iida. The frequency of maximum trace amplitudes of earthquake as a function of amplitude observed at three stations, Tottori, Sikano and Kurayosi are shown in Fig. 11.

The values of m in equation (1) calculated from these figures are

Tottori	$m=-1.82\pm0.16$
Sikano	$m=-1.88\pm0.12$
Kurayosi	$m=-1.79\pm0.07$

These values of m are very near to those obtained in the case of other aftershocks such as Fukui[22] and Imaichi[23].

8. Magnitudes of observed aftershocks

Many authorities have proposed methods of determining the magnitude of an earthquake from the trace amplitudes observed at seismic stations. We made some study of finding out the magnitude of aftershocks recorded at our temporary stations. In our observations the distribution of seismic net was limited to the area in Fig. 1, so that there was no means of knowing the amplitude or intensities of shocks at its epicentral distance at 100 km. Tsuboi[24] has proposed a formula which can conveniently be used for determining the Richter-Gutenberg's instrumental magnitude M of an earthquake from the observation at any epicentral distance. The proposed formula is

$$M=0.20\Delta+0.67\log A+3.80\,,\qquad \Delta<5 \tag{2}$$

where Δ is the epicentral distance measured in 100 km and A the maximum vibration amplitude of the ground measured in micron. After the present paper was read, Tsuboi[25] revised his formula as follows:

$$M=1.73\log\Delta+\log A-0.83$$

the reason being that the coefficient of log A will be more reasonably taken as unity. But as asserted in the paper referred to the main object of calculating the magnitude of an earthquake is to estimate approximately the intensity of the earthquake, so for convenience' sake the values of the magnitude M of each aftershock, which has been calculated by using the former formula were adopted in this paper without modi-

22) T. ASADA, *Report of the Fukui Earthq.*, (1949), 58.
23) T. ASADA and Z. SUZUKI, *Bull. Earthq. Res. Inst.*, **28** (1950), 415.
24) C. TSUBOI, *Geophysical Notes*, **4** (1951), No. 5.
25) C. TSUBOI, *Zisin* (*Jour. Seis. Soc. Japan*) [ii], **7** (1954), 185.

fying them by using the latter formula.

In the course of the calculation of the magnitude from equation (2), it becomes necessary to know the epicentral distance and the maximum displacement amplitude of the ground. An epicentral distance will easily be known from the P–S time multiplied by $k(=8.1)$, while the amplitude of the ground displacement is not so easy to know. As we have already seen in Table I, the free oscillation period of our seismometers are about 0.1 sec. while the period of a large amplitude of a ground wave ranged from 0.2 to 0.6 sec. Accordingly it may be said that the seismometer records the acceleration of the earth movement.

Theoretically speaking, it is possible to have a computed displacement seismogram from a accelerogram observed[26], provided one does not shrink from the labour of calculation, and from such a computed displacement seismogram the true maximum amplitude will easily be obtained. But considering the accuracy and the nature of the problem of determining the magnitude of an earthquake, such a troublesome calculation is not worth while at all. As may be seen in the plates the maximum acceleration is given by the waves in the beginning part of *S* phase, while according to our experience the maximum amplitude of the displacement seismogram of a near shock is also seen in the waves in the beginning part of *S* phase[27]. Such being the case, it is probably not so misleading if we assume the result calculated from the maximum trace acceleration amplitude to be the maximum displacement amplitude. From this standpoint we assumed that the maximum displacement amplitude Ae is given by

$$Ae=\frac{1}{V}\cdot\frac{T^2}{4\pi^2}\alpha_e$$

where α_e is the maximum trace acceleration amplitude, T the period of that acceleration, and V the magnification constant of that instrument. Moreover, there lies another difficulty in calculating the true maximum displacement amplitude of the ground, because in the case of our observation, only one seismometer was installed at each station. In the calculation of the magnitude, the maximum amplitude A is defined as the one which is the square root of the sum of the squares of the component maximum amplitudes Ae, the east-west component, and An, the north-south component, and the fact that Ae and An are not necessarily

26) T. HAGIWARA, *Bull. Earthq. Res. Inst.*, **13** (1935), 138.
27) T. ASADA, *Zisin* (*Jour. Seis. Soc. Japan*) [ii], **6** (1953), 69.

the two components of one and the same vibration is ignored. Only one component is available from our stations, so that assuming that $Ae=An$ (this assumption seems not to be a too unreasonable one judging from the reports of seismometrical observations)[28], the maximum displacement amplitude A was taken as $A=\sqrt{2}Ae$. Through such procedures as described above, since Δ and A are known for each shock observed at the respective stations, the magnitude M of each shock is easily determined from the formula (2).

Table IV. Magnitude M determined at different stations.

Earthq. No.	Time of occurrence	Tottori	Maki-hara	Sikano	Aoya	Matu-zaki	Kura-yosi	Misasa	Mean of M
	Sept. h m								
7	21 14 32	3.6	3.7	3.5					3.58±0.08
10	23 21 58	3.4	3.5	3.9					3.58±0.20
11	24 3 25	3.5	3.5	3.6	3.6				3.53±0.06
13	24 13 20	3.3	3.3	3.4			3.4		3.36±0.04
14	27 01 33	3.5	3.3	3.4			3.5		3.38±0.09
15	27 12 17	3.1	3.9	3.3			3.1		3.33±0.24
17	28 6 41	4.2	4.3	4.5			4.3		4.13±0.12
	Oct.								
25	2 01 50	2.5		2.7	2.1		2.7		2.49±0.20
26	2 18 46	3.5		3.2	3.1		3.4		3.28±0.12
27	2 02 07	3.6		3.5	3.4		3.0		3.38±0.16
28	3 02 10	3.6	3.4	3.6	3.6		4.0		3.64±0.16
29	3 02 11	2.5	2.6	2.9	2.5		2.4		2.57±0.12
30	4 01 11			2.7	2.5		2.4		2.53±0.01
32	7 05 30			3.0	3.2		2.6	3.2	3.00±0.14
33	7 09 05				3.3		3.8	3.5	3.50±0.17
34	7 11 01	4.2		4.0	4.1		4.1		4.11±0.04
36	7 22 11			3.2	3.1	3.2	3.0	3.8	3.27±0.20
38	8 03 37				2.7	2.6	2.4	3.0	2.66±0.16
39	8			3.0	3.2	2.9	3.0	2.9	2.99±0.01
41	9 05 28					2.3	2.1	2.3	2.20±0.08
42	10					2.4	2.3	2.2	2.30±0.06

With respect to these aftershocks of which the foci have been determined from the observations at four stations (Table II), the magnitudes were also calculated on the basis of each record obtained at the four respective stations and the result is shown in Table IV. As will be

28) For instance, *CMO, The Seismological Bulletin of CMO, Japan.*

seen in the table the diversity in the value of M is not so large and the probable deviation δM is given in the last column of the table. The shocks listed in this table are rather large ones which accompanied the Tottori earthquake. With these rather large shocks it is seen from the table that the magnitude M ranges from 4 to 5.

From these values of M the energy will be calculated through the formula[29]

$$\log E = 12 + 1.8\,M\,.$$

M and E were calculated with respect to all the aftershocks recorded at four stations, Tottori, Sikano, Aoya and Kurayosi.

For the purpose of studying the seismic activity in the area covered by the observation net as a whole, we divided the whole area into three semispheres that have their centers at Tottori, Sikano and Kurayosi respectively, and the radii of which are 9.7 km, 10.5 km and 15.4 km respectively (Fig. 12). This means that in the first semisphere all the shocks observed at the Tottori station with the P–S time less than 1.2 sec. are included in it, and in the second and the third semisphere, likewise, all the shocks recorded at Sikano and Kurayosi with P–S time under 1.3 sec. and 1.9 sec. respectively, are included in the respective semisphere.

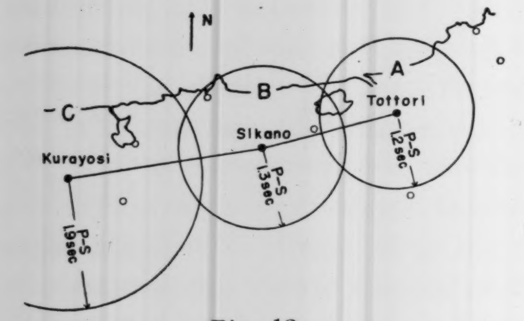

Fig. 12.

As we know from Table I, there are very few shocks that have a focal depth less than 6 km, so that it will be safe to say that the shocks that are recorded at three stations, Tottori Sikano and Kurayosi, and having the P–S time less than 1.2, 1.3, and 1.9 sec. respectively are included in any one of these three semispheres without repetition. Now we will call these semispheres A, B and C in order from east to west.

In order to know some measure on the amount of the energy released from the aftershocks that have taken place in the respective areas A, B and C, the square root of the energy E calculated from the shocks observed at stations Tottori, Sikano and Kurayosi were summed up with time respectively and is shown in Fig. 13–a, b, c where each circular dot represents an increment of energy from a single shock. We see from this figure that the sum of energies released increases step-wise by

29) B. GUTENBERG and C.F. RICHTER, *Bull. Seis. Soc. Amer.*, **32** (1942), 163.

every relatively large shock.

Seismic energies sent out from the areas *A*, *B* and *C* respectively every two days are shown by three curves in Fig. 14, from which

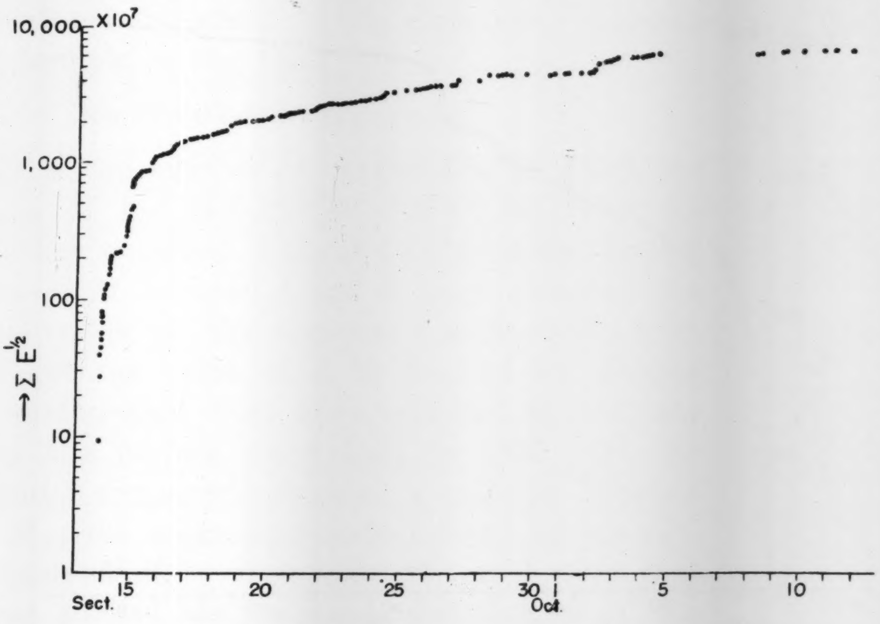

Fig. 13–a. Strain increment in the A area.

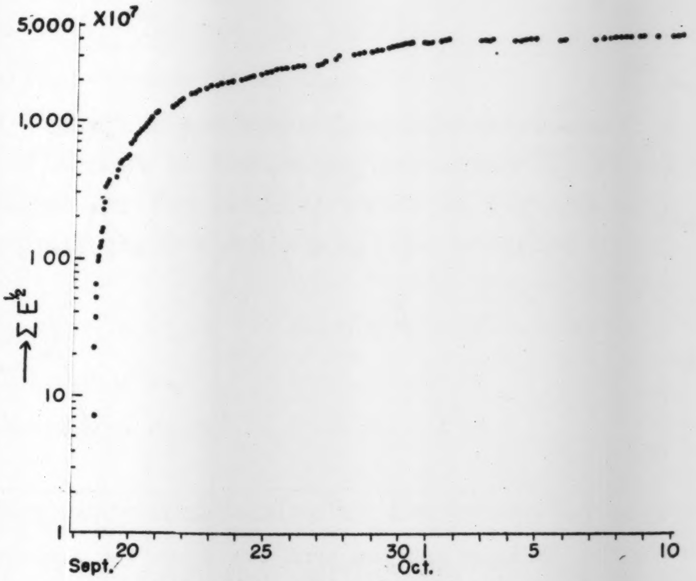

Fig. 13–b. Strain increment in the B area.

seismic activities in the respective areas will clearly be seen. In the *A* area, namely the Tottori area, seismic activity is found to be moderately

high through the entire period observed, while in the C area seismic activity is found to be somewhat low in the first half of the period, while after Sept. 28 the seismicity becomes more active than the two

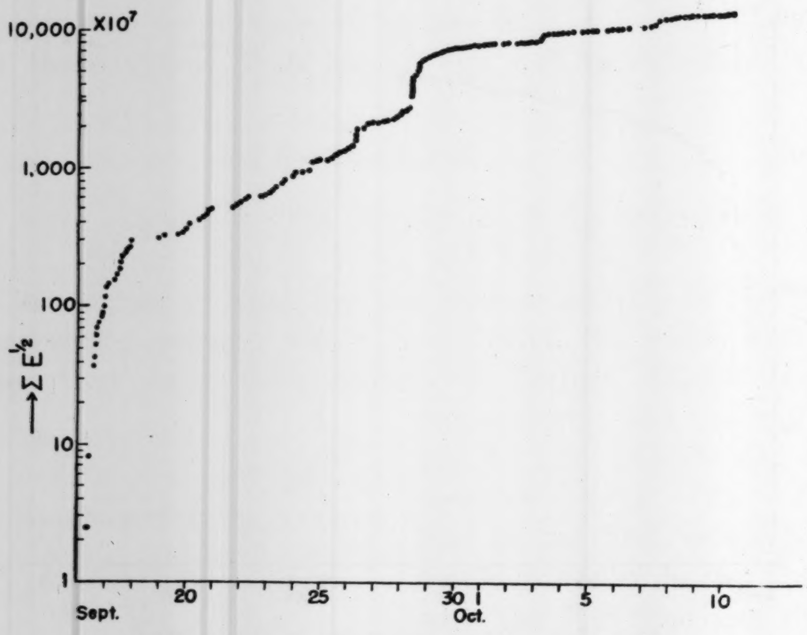

Fig. 13-c. Strain increment in the C area.

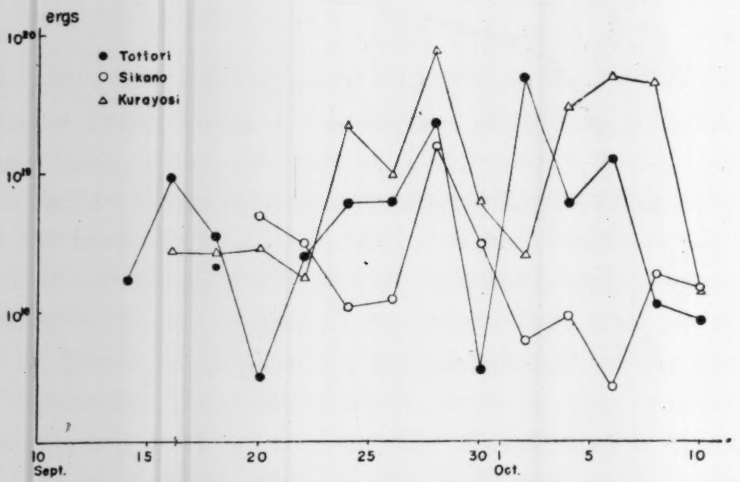

Fig. 14. Seismic energies send out from the respective areas A, B and C, every two days.

other areas. With respect to the B area (Sikano area) it is found that the activity is the lowest compared with the former two areas.

9. Frequency distribution of the magnitude of aftershocks

Since the statistical studies of energy and frequency of earthquake were first made by Gutenberg and Richter[30] in 1944, many authorities have developed the study in this direction. Gutenberg and Richter proposed a formula in the form

$$\log N = a + b(8 - M)$$

where N is the number of earthquake of which the magnitude M is M-$0.25 < M < M + 0.25$. For the shocks which occurred in South California and having the value of M between 4 and 6 they obtained the numerical value of the constant b as $b = 0.88 \pm 0.03$. Tsuboi[31] got the value of b as $b = 1.04$ by making use of earthquakes that have occurred in and near Japan in the periods from 1931 to 1950. On the other hand Kawasumi[32] obtained a relation between N and M_K, the magnitude scale defined by himself, of the form $N(M_K) = \text{const} \times 10^{-0.56 M_K}$, and after that Asada has studied the frequency distribution of the magnitude M_K through the minor earthquakes that occurred in the Kwanto District. In his case M_K was between 4 to 1. He got the relation

$$\log N(M_K) = \text{const} - 0.58\, M_K .$$

In the case of Tottori aftershocks frequencies of the magnitude M of shocks in the respective areas A, B and C, are shown in the semilog paper in Fig. 15. By the least square method values of the constant b are given as

A	area (Tottori area)	$b = 0.95 \pm 0.05$
B	area (Sikano area)	$b = 1.09 \pm 0.06$
C	area (Kurayosi area)	$b = 0.88 \pm 0.04$

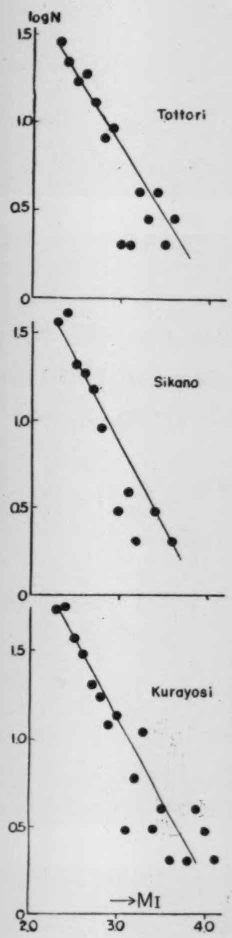

Fig. 15. Frequency diagram of equal interval of magnitude *M*.

10. Frequency distribution of the energy of aftershocks

Instead of classifying the earthquake by the equal intervals of magnitude M, let us now consider the number of earthquakes classified

30) B. GUTENBERG and C. F. RICHTER, *Bull. Seis. Soc. Amer.*, **34** (1944), 185.
31) C. TSUBOI, *Jour. Physics of the Earth*, **1** (1952), 47.
32) H. KAWASUMI, *Bull. Earthq. Res. Inst.*, **30** (1952), 185.

by the equal interval of energy E.

Asada[33] and others have derived an equation

$$N(E)E\,dE=\text{const}\times E^{-0.5}dE \tag{3}$$

where $N(E)$ is the number of earthquakes of which the energy is between E and $E+dE$. We transfer the equation (3) in the form

$$\log N=\text{const}-(1+\alpha)\log E,$$

and from the data here obtained, the value of constant α will be determined as

in the area B $\quad \alpha=0.54\pm0.12$

in the area C $\quad \alpha=0.54\pm0.14$

with respect to all the shocks originated in the whole areas, A, B and C, we get the relation between $\log N$ and $\log E$ as will be seen in Fig. 14 and from it we obtain the value of constant α as $\alpha=0.55\pm0.15$. This value is a little larger compared with the theoretical value, but anyhow this result shows that, as Asada and others already pointed out, according to the classification of equal interval of energy, the total energy released in the class E and $E+dE$ becomes smaller with the increase in E.

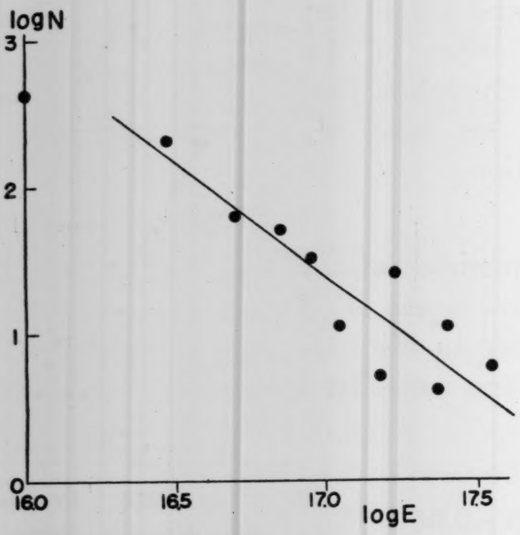

Fig. 16. Frequency diagram of equal interval of E.

As we have already seen in paragraph 7, the Ishimoto Iida's formula was applied satisfactorily in this case of Tottori earthquake, so that it is quite natural that we should have come to this conclusion concerning the frequency of energies of aftershocks. And this in turn may indicate that the magnitude scale here adopted is usefull in the determination of the magnitude of such small earthquake as aftershocks.

In conclusion the author wishes to express his hearty thanks to

---

33) T. ASADA, Z. SUZUKI and Y. TOMODA, *Bull. Earthq. Res. Inst.*, **29**, (1951), 289.

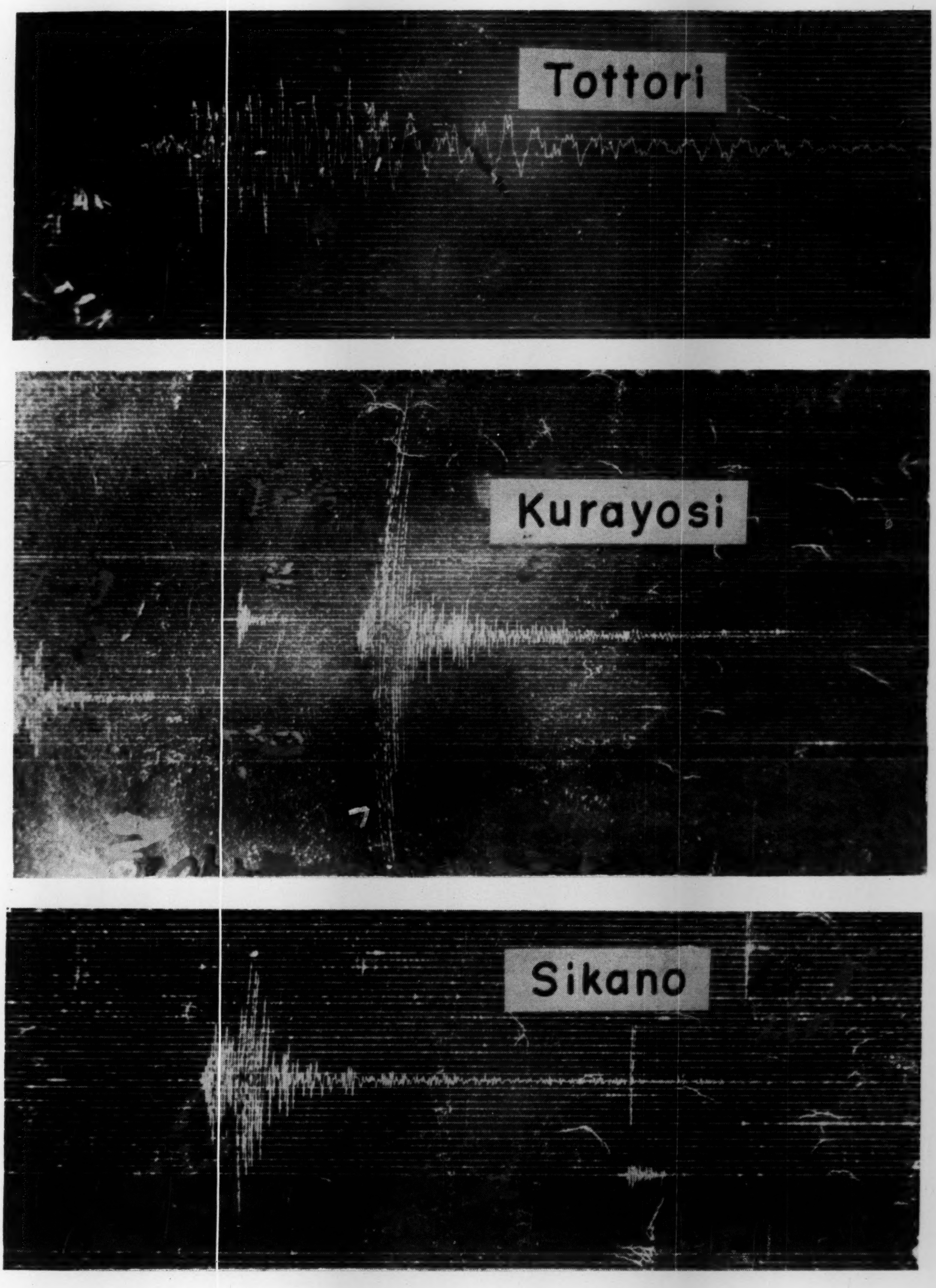

Seismograms of the Tottori aftershocks.

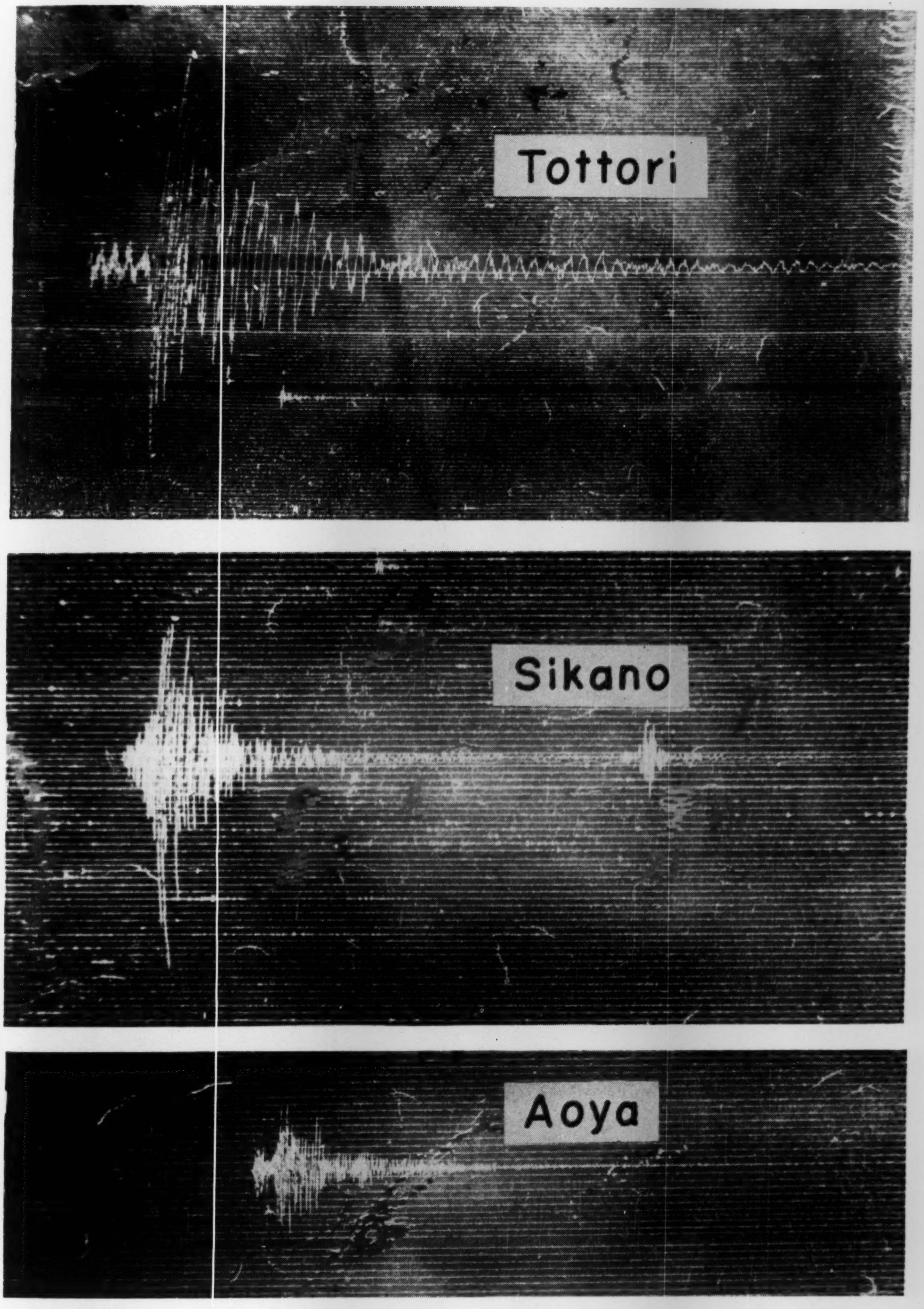

Seismograms of the Tottori aftershocks.

（震研彙報 第三十三号 図版 表）

Mr. Akira Jitsukawa who has cooperated with him for the observation of aftershocks, and the author's sincere gratitude is also due to Professor Takahiro Hagiwara for his valuable advices and encouragements.

---

41. 鳥取地震余震観測 (第 2 報)

地震研究所 表 俊 一 郎

昭和 18 年 9 月 10 日夕刻鳥取市及びその附近に大きな災害をもたらした大地震に際しては顕著な地震断層が発現したのでこの断層の追跡，断層面の動きについての精密測定，地電流変化の測定，精密水準測量等興味ある観測が多くの研究者により行はれた．筆者はこの地震の余震の観測を担当し 8 箇所の臨時観測点をもうけて余震観測を行つた．結果の概報は地震直後の彙報に報告せられたけれども，精しい記録の整理は其の後の戦局の激化にあつて延期させられた侭になつていたが今回機会を得て記録の整理を行うことができたのでここにその結果を報告する次第である．震源をきめるにはこの場合も亦専ら *P-S* 時による方法を用いなくてはならなかつた．距離係数 k の値は $k=8.1$ となつた．この値は丹後地震の k の値とほぼ等しく，他の多くの余震観測より得られている値よりは可なり大きい．丹後，鳥取等の余震の k の値が大きいのは山陰地方の地質構造と密接な関係があると考へられる．

鳥取余震の場合には，本震後 18 日目に倉吉附近に震度 IV の可なりの地震が発生し (No. 17 Fig. 8) その後は，いはばこの地震の余震ともいうべき小地震がこの地震の北東の地域に非常に沢山発生するのが見られた．

余震活動域全域にわたつて余震活動の消長がどのような経過をたどつたかを見るために鳥取，鹿野，倉吉の 3 つの観測点をえらび，夫々の観測点で観測された地震の中適当な大きさの地域の中で起つたと考へられる地震について坪井の 式 に従つてそれら 1 つ 1 つの地震の magnitude M をきめそれよりエネルギー E を求めてそれらの M, E 等について若干の考察を行つた．

---

42. *Ice Tremors Generated in the Floating Lake Ice (Part 1).*

By Syun'itiro OMOTE, Yoshio YAMAZAKI, Naoyoshi KOBAYASHI,
Earthquake Research Institute,
and Sadanori MURAUCHI,
National Science Museum.

(Read Mar. 18, 1952; Dec. 21, 1954.—Received Sept. 30, 1955.)

1. Introduction

We seismologists have long been paying keen attention to the phenomena seen in some floating lake ice. In some lakes, when a few days after the lake has frozen over it happens that the air temperature falls considerably, large fractures are formed at midnight in the ice sheet without any artificial cause, running from one shore to the other across the lake, and split the ice sheet into two or three parts. According to the inhabitants of the district, the formation of the fractures is often accompanied by such a severe shock that it awakens the sleeping people in areas around the lake. This phenomenon is of special interest to seismologists because of the elastic waves generated at the moment of formation of the fractures in the ice.

The opening thus made in the ice-sheet is soon filled up with new ice, but the new ice does not grow as thick as the older ice immediately, and the crack remains as a week line in the ice-sheet. Usually the weather is very fine on the day following such a cold night, so that the whole surface of the lake-ice is heated by the radiation from the sun, causing the expansion of the ice-sheet. As a result, the margins of the two ice-sheets bounded by the weak line are pushed up, and a peculiar ridge of ice is formed along the weak line. The ridge thus produced has been called "Omiwatari" (the sacred crossing) by the inabitants of the Suwa district from ancient times. Local tradition has it that the ridge of ice marks the path along which the God of the Suwa Shrine walked from the Upper Shrine where he lives to the Lower Shrine across the lake in which the Goddess lives. Lake Suwa is famous for this phenomenon of "Omiwatari." This phenomenon has attracted the lakeside people's attention since long ago, and the dates

of the freezing over of the lake and the formation of "Omiwatari" have been recorded almost every year for about 500 years beginning in 1397. The record has been investigated by Fujiwara[1~3] and Arakawa in recent years as a very valuable material in the field of climatology.

The formation of a crack in the ice-sheet causes vibration of the ice-sheet. The significance of this vibration to us consists in that it is not generated by any artificial force but by a natural force. No doubt, vibrations are also to be generated by causing artificial explosions in the ice, but it is difficult to determine what similarity there is between the vibration caused by artificial method and that of earthquakes in their mode of occurrence. On the other hand, it may be safely assumed that vibrations caused by the formation of cracks in the ice-sheet closely resemble those of natural earthquakes in many respects.

By the contraction or expansion of the ice-sheet due to the variation of the air temperature, stress is accumulated in the ice-sheet until the strain overcomes the breaking strength of the material. When at last rupture is caused, the accumulated strain energy is converted into elastic waves.

Many theoretical and seismometrical studies on the mechanism of the occurrence of earthquakes have been carried out by good authorities[4~7], mainly on the basis of data obtained at seismological stations. However, the rapid progress of theoretical seismology makes it necessary to employ a much closer observation net in order to improve the seismometrical study on the mechanism of earthquake occurrence. However, chief difficulty in this direction consists in financial restrictions. Such being the case, it has been found necessary to introduce experimental methods to the study of seismology, and recent years seismic model experiments have been carried out by many investigators[8~14] to study the

1) S. FUJIWHARA and H. ARAKAWA, *Jour. Meteorological Res.* (C.M.O.) (in Japanese) **6** (1955), 123.
2) H. ARAKAWA, *Jour. Meteorological Res.* (C.M.O.) **6** (1955), 584.
3) S. FUJIWHARA, *Geophys. Magazine*, **26** (1954), 1.
4) H. KAWASUMI, *Bull. Earthq. Res. Inst.*, **11** (1933), 403; **12** (1934), 660.
5) H. HONDA, *Geophys. Mag.*, **4** (1931), 185; **5** (1932), 69.
6) W. INOUE, *Bull. Earthq. Res. Inst.*, **14** (1936), 582; **15** (1937), 90, 674.
7) H. KAWASUMI and R. YOSHIYAMA, *Proc. Imp. Acad.* **10** (1934), 345.
8) K. KASAHARA, *Bull. Earthq. Res. Inst.*, **30** (1952), 259; **31** (1953), 71, 235, **32** (1954), 67.
9) Y. KATO and A. TAKAGI, *Sci. Rep. Tohoku Univ. Geophys.*, **7** (1955), 35.
10) T. D. NORTHWOOD and D. V. ANDERSON, *Bull. Seis. Soc. Amer.*, **43** (1953), 239.
11) J. OLIVER, F. PRESS and M. EWING, *Geophys.*, **19** (1954), 202. *ibid.* 388.
12) J. F. EVANS, C. H. HODLEY, J. D. EISLER and D. SILVERMAN, *Geophys.*, **19** (1954), 220.
13) F. K. LEVIN and H. C. HIBBARD, *Geophys.*, **20** (1955), 19.
14) PETER N. S. O'BRIEN, *Geophys.*, **20** (1955), 227.

generation and propagation of elastic waves. It is also along this line that our studies on the lake ice were planned and carried out, in the hope that the mode of occurrence of such tremors generated in the floating ice-sheet may serve as a model for that of the natural earthquake.

Our studies on the floating ice of Lake Suwa were begun in the winter of 1949/50. To record the vibration generated by such a great shock caused by the formation of Omiwatari, the great crack, would be easy enough in itself, for the vibration has a very large amplitude. But, from the standpoint of carring out observations, there arises the very difficult problem of how to catch without fail the rare phenomenon which occurs usually only one time in one winter. In order to preclude the possibility of missing the great chance that will not come around until next winter, it is necessary to record smaller tremors that occur much more frequently all through the winter in the ice-sheet. These tremors, however, are so small in their amplitudes, that they require much more sensitive seismometers than those used for the major tremors.

In the first year of our study we had great difficulties in the observation of ice tremors, as we had no knowledge beforhand of their amplitude range, of the frequency of the generation, or of the location of their occurrence. First of all, we had to know what sort of tremors were being generated in the floating ice. The first and second winters were spent on the preliminary experiment for the study of these subjects. In the third year detectors were installed in such disposition as shown in Fig. 1 and with these eleven detectors the observation of the tremors was carried out. By analysing the records obtained from the observations we learned that, although we were able to catch a large number of tremors, it was extremely difficult to locate the foci of the tremors that occurred in the area covered by our observation net. It was found that a great many of the tremors traced in our record were generated at points very near the lake shore, presumably by minor fractures in the ice-sheet near the shore line of the lake. Therefore in the next winter of 1953, our observation net was set up far into the lake, at a distance of some 500 meters from the shore, and

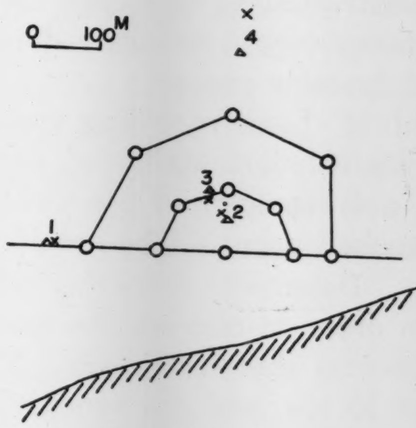

Fig. 1. Location of detectors on the ice-sheet in the winter of 1951/2.

in this same winter we used, in addition to the seismograph equipment, such other instruments as extensometers, thermocouples, etc.

2. Instruments used

Prior to the description of the phenomenon taking place in the ice-sheet, a brief sketch of the instruments used in the observation of ice tremors will be given.

a). Equipments for the recording of the ice tremors.

In recording the ice tremors two systems of recording assemblies were used. Both systems were alike in that the detectors were placed on the ice-sheet, and that the recording equipments were installed in the Suwa Branch Station of CMO standing on the lake shore. They differed, however, in that one system had a very long recording time, longer than twelve hours, while the other had a very short recording time with a high paper speed, about 40 mm/sec. Also the latter was so constructed as to record the oscillation curves of the vibration of a single tremor caught by many detectors simultaneously side by side on a sheet of bromide paper.

i) Long recording system. This long recording time system consists, fundamentally, of detector—preamplifier—direct current amplifier —galvanometer of pen-writting type—and recording drum wrapped with smoked paper. The specifications of each unit are as follows—

Detector: A moving coil type electro-magnetic detector was employed in order to convert the mechanical energy due to the vibration of the ice into the electric one. The natural period of the detector was adjusted at 10 cps, and the sensitivity at this cycle was about 0.1 volt/kine.

Preamplifier and direct current amplifier: The overall frequency response of the tube amplifying units was about 90 db in the range from 1 to 50 cps. The details of the frequency characteristics of the preamplifier and the D.C. amplifier will be described elsewhere.

Pen-writing galvanometer: In order to have a visual recording, a pen-writing galvanometer recording tremors not on photographic paper but on smoked paper was used. This enabled us to record continuonsly for more than 12 hours with a paper speed of 4 mm/sec. In carrying out the observation, overall gains of the amplifying units were adjusted at such a sensitivity as the input of 100μV at the preamplifier produces a deflection of 1 mm at the end of the index of the galvanometer. Time markings were put on the record at every six seconds.

ii) Multi-channel recording system. This system consists, fundamentally, of—12 detectors—12 amplifiers—12 channel oscillograph—and a recording camera. In the operation of this system each of the 12 detectors was connected by a cable to the recording equipment which contained 12 low frequency amplifiers, one for each detector, and an oscillograph to record the ice tremors on a sheet of photographic paper. This multi-channel recording of the output from the twelve detectors was aided by the time-makings of light line across the paper placed at intervals of 10 milliseconds, making possible the picking up of the time of onset of energy to the nearest millisecond. The photographic recording paper was made to run through the oscillograph camera with the speed of 40 mm/sec and a role of bromide paper 25 meters long was consumed in 11 minutes.

b). Extensometer

Extensometers were used for the purpose of measuring the contraction and expansion of the ice-sheet. The construction of this instrument is as follows: One end of a bar about one meter long made of fused silica is fixed to a wooden plate frozen to the ice-sheet, and the other end is placed on a roller supported on a frame also fixed on the ice. The rotation of the roller is magnified by a bow—and—string mechanism and recorded automatically on a paper wrapped around a drum. In this manner the relative movement of the silica bar and the ice was recorded, magnified to 10^4 times the actual amount. In the winter of 1952/3, extensometers were set in two different directions, making an angle $\pi/2$ to each other.

c). Temperature measurement

In the study of the phenomena in the ice-sheet, needless to say, temperature measurement is indispensable. Strictly speaking, it is desirable that the air temperature should be measured on the lake ice, but as the Suwa Branch Station[*] of CMO, standing so near the lake shore, was kind enough to place its record of temperature measurement at our disposal, we used the temperatures measured at the station, to whose courtesy our heartfelt thanks are due. In order to know the temperature within the ice-sheet we used in the first year an underground thermometer and in the second year a thermometer of a thermojunction type.

3. Generation of the ice tremors

In order to show the general manner of the occurrence of the ice

tremors, an example of the record obtained with the smoked paper seismograph is given in Fig. 2 (Plate). As is seen in the figure, sometimes many tremors take place one after another in a day, while on other days they occur only very rarely. We see from the figure that the

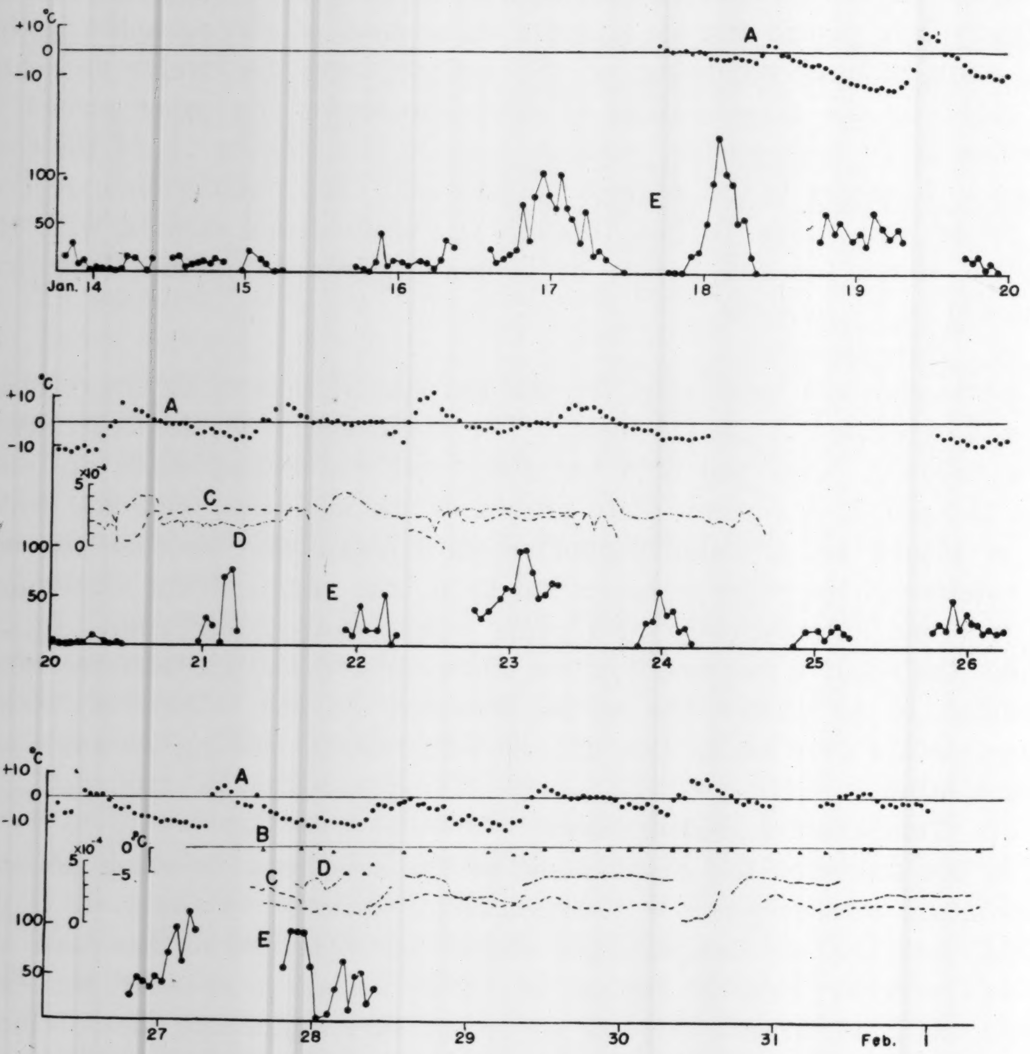

Fig. 3. Diagrams of frequency of ice tremors, contruction and expansion of ice-sheet, and the temperature in the ice and of the air.

tremors resemble more an earthquake in type than a microseism in that they can be counted one by one. From our observation it became clear that these tremors were taking place all day long, but since in the daytime there were too many man-made disturbances caused by skaters, anglers, etc., we gave up taking record of ice tremors until night, when, according to the custom of the district, and in view of the obvious

danger, no one went out on the ice to affect our records. Our observation was therefore restricted to the time between nightfall and the dawn. Vicissitude of tremors observed in the winter of 1953 is shown in Fig. 3. The observation was kept from Jan. 13 to Feb. 1, and the number of tremors was counted every hour, which rose to more than one hundred in the most active period, but sank very low in some cases and there were whole nights when no tremor took place at all. In the

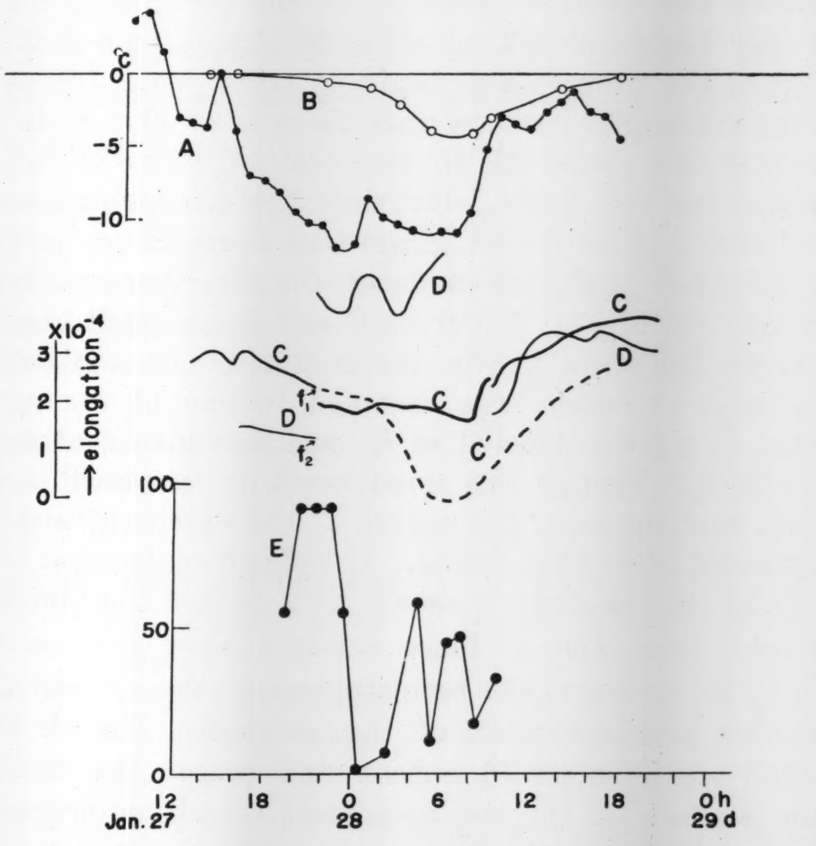

Fig. 4. An enlargement of part of the curves in Fig. 3, on Jan. 27 and 28. A is the air temperature, B is the temperature in the ice-sheet, C and D are records of extensometers and E is the frequency of ice tremors.

figure, curve A represents the air temperature, curve B the temperature in the ice-sheet, curves C and D the records of the extensometers, and curve E the frequency of the tremors in the ice-sheet. In Fig. 3, these results have been put together. A glance at this figure makes it clear that on days when diurnal variation of the air temperature was small tremors were inactive in there occurrence, while on days when the temperature variation was conspicuous, a large number of ice tremors

were generated. However, on looking over more carefully, we find that the relation of the two is not always so close. In order to study the relation between the two, we have to examine every part of Fig. 3 in greater detail. For this purpose we have reproduced in Fig. 4 a part of the former figure covering the period from Jan. 27 to 28, as in this period all cases are represented. In this figure we notice that although the air temperature begins to fall at about 15 o'clock, the temperature of the ice-sheet remains at the freezing point for some time, and only begins to fall, at about 20 o'clock, and that as soon as this fall begins the tremors also begin to occur more frequently. The curves of the extensometers show that there is no change in the length of the ice-sheet soon after the air temperature begins to fall below the freezing point, but two hours later since the air temperature becomes below the freezing point the extensometers begin to contract, and soon after the ice-sheet begins to contract the ice tremors also begin to occur. In the case of Fig. 4 (curves C and D), a small crack seems to have run under the silica bar in the course of its contraction and a sudden stepwise extension was recorded in one of the curves of the extensometer at a point denoted as f_2, and a sudden contraction in the other curve at f_1. Though this small crack is supposed to have been filled up with new ice soon, the curves of the extensometers look somewhat complicated after that points. Calculated contraction based on the temperature in the ice-sheet is shown by a broken line denoted as C′.

As is seen from Fig. 4, there exists a close relation among the generation of ice tremors, the temperatures of the air and the ice, and the contraction and expansion of the ice-sheet. The air temperature begins to fall rapidly after 16 o'clock and passes the freezing point, but on the surface of the ice-sheet there is still water remaining unfrozen in consequence of the warm temperature in the daytime, while the ice-sheet itself stays at 0°C. As the air temperature goes down lower and lower, this surface water on the ice finally begins to freeze. As soon as the surface water is converted into ice the surface temperature of the ice-sheet begins to fall below zero degree. It is just at this moment that ice tremors begin to take place. To sum up, as soon as the surface water is frozen, the surface of the ice-sheet comes into direct contact with the cold air, so that the ice-sheet is cooled and begins to contract, but because of the poor conductivity of heat of the ice, the lower part of the ice-sheet remains at 0°C for a little while, and the stress is accumulated in the ice and finally causes the formation

of small crack. It should also be noticed in this figure that at about half past 23 o'clock, the approach of warm air mass caused the temperature to rise by about five degrees, and as if to correspond to this rise, the occurrence of tremors became inactive, until at last at one o'clock there were no tremors at all.

4. The frequency of the amplitude of the tremors

There is a well-known relation existing between the maximum amplitude of natural earthquakes and its frequency. The relation is:—

$$N(a)a^m = k^{15)},$$

where a is the observed maximum amplitude of an earthquake and $N(a)$ the number of earthquakes whose maximum amplitudes range from a to $a+da$, and m and k are mumerical constants.

The values of the constant m with respect to some earthquakes are given

$m=1.92\pm0.04$	Micro earthquakes of Fukui aftershocks[16]
$m=1.8\pm0.16$	Micro earthquakes of Imaichi aftershocks[17]
$m=1.8\pm0.16$	Aftershocks of the Tottori Earthquake[18].

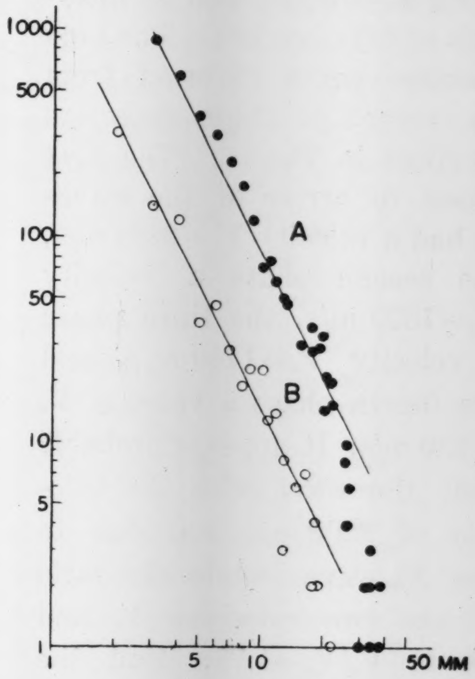

Fig. 5. Frequency distribution of maximum amplitude of the ice tremors. The data of the curve A are obtained from the detector installed at D_1 in Fig. 9, and of curve B from D_2.

The frequency diagram of the amplitude of ice tremors is shown in Fig. 5. From this figure the value of m can be calculated as

$$m=1.8\pm0.2$$

15) M. ISHIMOTO and K. IIDA, *Bull. Earthq. Res. Inst.*, **17** (1939), 443.
16) T. ASADA, *Rep. Fukui Earthq.*, (1949), 58.
17) T. ASADA and Z. SUZUKI, *Bull. Earthq. Res. Inst.*, **28** (1950), 415.
18) S. OMOTE, *Bull. Earthq. Res. Inst.*, **33** (1956), 641.

This agrees well with the value of m obtained with respect to natural earthquakes.

5. Velocity of the elastic waves in the ice-sheet

As to the velocity of elastic waves that propagate in the ice-sheet many authorities[19~26] have made many reports. We also made some study on the point, which will be roughly sketched below. A shock due to a small quantity of explosive caused to burst in ice was picked up by eleven detectors arranged along a straight line at intervals of fifty meters. The time distance curve deduced from the record of these detectors is given in Fig. 6. The first phase to arrive of the waves at had a velocity $V_1=3200$ m/s, the second phase a velocity $V_2=1820$ m/s, the third phase a velocity $V_3=1460$ m/s, and the fourth phase a velocity $V_4=330$ m/s. It appears probable that the wave with the velocity of 3200 m/s was due to the P wave, while the ratio of the two velocities V_1 and V_2 is $V_1/V_2=1.78$. Had the second wave been an S wave (phases due to the shear waves), this ratio would have been about 2 in the ice-sheet, so that this velocity due to the second phase can hardly be accepted as that of S waves. The third phase apparently is due to the waves that passed through the water

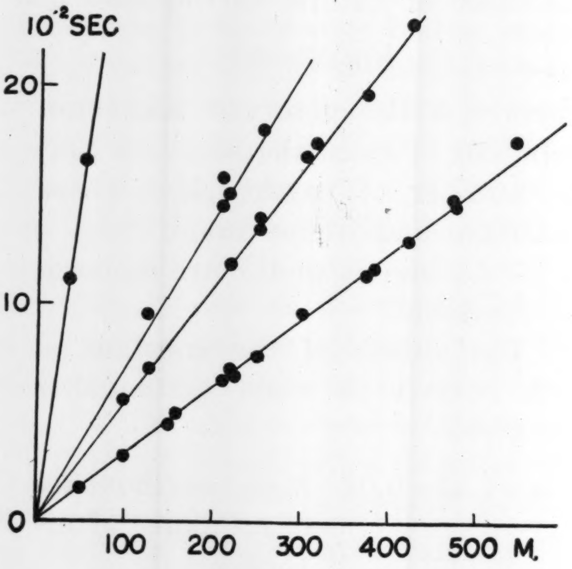

Fig. 6. Travel time curves for various event due to the detonation from the small charges measured on the ice.

19) M. Ewing, A. P. CRARY and A. M. THORNE, *Physics*, **5** (1934), 165.
20) M. Ewing and A. P. CRARY, *do*, **5** (1934), 181.
21) F. PRESS, A. P. CRARY, J. OLIVER and S. KATZ, *Trans. Amer. Geophys. Uni.*, **32** (1951), 166.
22) F. PRESS and M. EWING, *Jour. Appl. Physics*, **22** (1951), 892.
23) A. JOSET et J. J. HOLTZSCHERER, *Ann. d. Géophys.*, **9** (1953), 330.
24) A. JOSET, *do.*, **9** (1953), 345.
25) F. KISHINOUYE, *Bull. Earthq. Res. Inst.*, **21** (1943), 298.
26) Y. SATÔ, *Bull. Earthq. Res. Inst.*, **29** (1951), 223.

beneath the ice-sheet. These three phases were followed up by still another wave with a definitly long period, of which the velocity was calculated as 330 m/s. These velocities here obtained, however, were by no means constant in all cases. For example, in Fig. 7 the values of P waves observed at the same place every two hours are contrasted to the air temperature at which the observation of velocity was made. As is seen from the result, the velocity differs in the range from 2900 m/s to 3230 m/s. The velocity obtained from a single shot may be accepted as fairly accurate as the probable errors were small as shown in Fig. 7. This may indicate that the elastic constant of the ice-sheet itself has changed. In it will be noticed that the velocity increases as time goes on, in the same way as it increases as the temperature goes down. In the daytime, when the air temperature is 5°C and the ice is soft, waves with a velocity of 2900 m/s propagate in the ice, while as it becomes cold at night and the temperature is -10°C or so, the velocity is 3230 m/s.

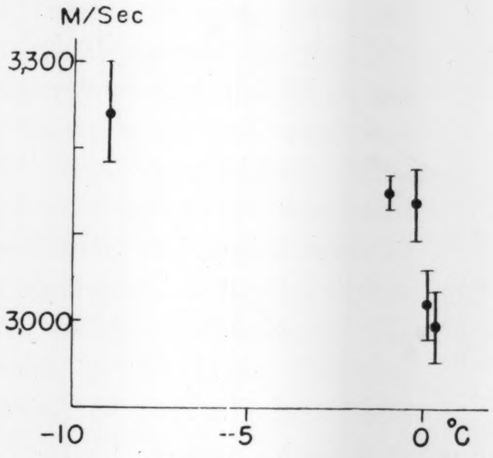

Fig. 7. Velocity of p waves in the ice versus air temperature.

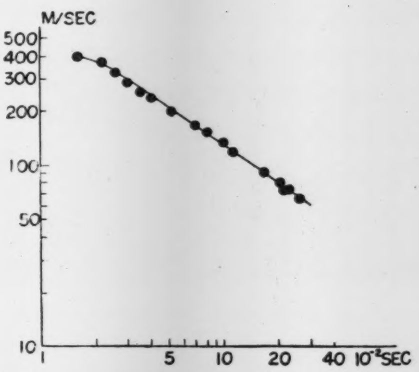

Fig. 8. Dispersion curve of flexural waves in the ice-sheet.

The fourth phase may be considered due to the flexural waves of the ice-sheet. Glancing at a record of this type we at once notice the dispersive nature of the waves. A dispersion curve will be shown in Fig. 8. As is well-known the thickness of the ice-sheet has a great bearing upon the velocity of the flexural wave, and so the measurement of the thickness of the ice-sheet was made once every day, we found from the measurement that the ice-sheet became thicker as days go on by 0.25 cm/day on the average.

6. Determination of epicenters of the ice tremors

As the ice tremors were known to be of the shock type in nature, we wished to know the point from which tremors originate[27]. For this purpose 12 detectors were distributed on the ice-sheet as is shown in Fig. 9 and the position of each detector was measured with great care by using the Wild theodolite and a steel tape 100 meters long. With

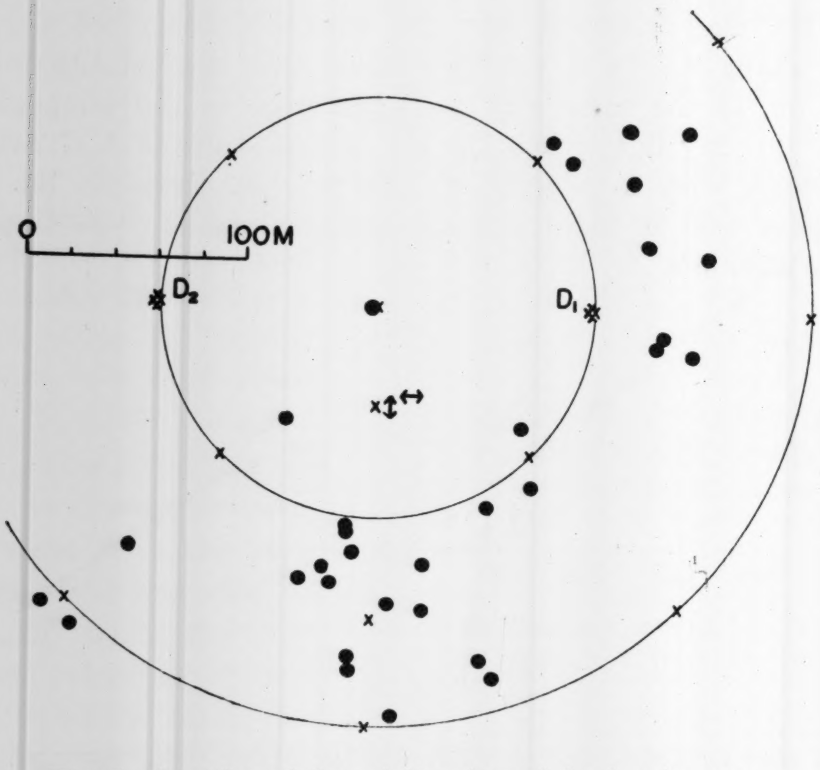

Fig. 9. Location of the origin points of the ice tremors.
× Location of detectors connected to the recording oscillograph.
⋇ Location of detectors connected to pen-galvanometer.
↔ Location of extensometers.
● Origin points of the ice tremors.

these twelve detectors the observations of the ice tremors were carried out. As is seen in Fig. 3, the occurrence of tremors is irregular, that is, under some conditions there take place so many tremors, while under others they are very few. While recording the tremors close attention was paid every night not to miss the time of the most active occurrence of tremors which lasted for one hour or so on the average.

27) A. P. CRARY, *Bull. Seis. Soc. Amer.*, **45** (1955), 1.

Vibrations due to an ice tremor picked up by the respective detectors were recorded side by side on a sheet of bromide paper. An example of the record of ice tremors is reproduced in Fig. 10 and Fig. 12 (Plate). By reading off the commencement time from these records the foci of tremors can be easily calculated. In order to obtain some measure on the accuraey of a focus of an ice tremor, a small amount of explosive was caused to burst at a known instant and at a known place. From the commencement times of vibrations caused by this explosion recorded at 12 points the location of this explosion point was determined. This calculated epicenter was compared with the actual spot of the explosion, and the result is tabulated in Table I. As is seen in the table, the two values, for the calculated and

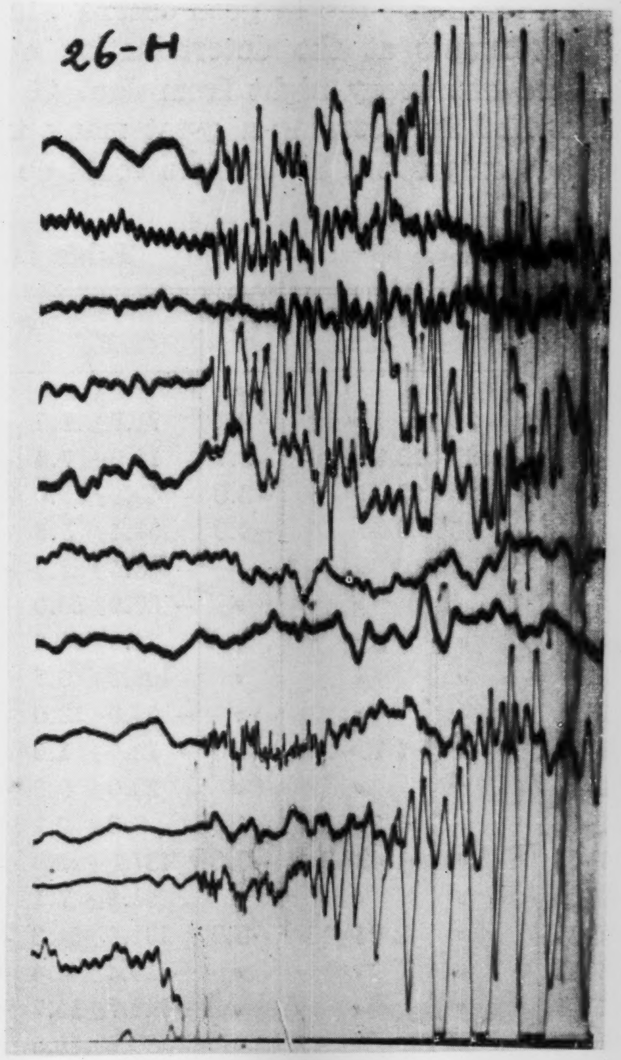

Fig. 10. An example of record of ice tremor on bromide paper.

Table I. Comparison of the calculated and the true origin points due to explosion of small charges.

No.	Co-ordinate of the true origin point		Co-ordinate of the calculated origin point		Calculated origin time	Calculated velocity
	X_0	Y_0	X	Y	T_0	V
	m	m	m	m	$\times 10^{-2}$ sec	m/S
1	0	0	4.9 ± 1.1	-2.8 ± 1.2	-1.4 ± 0.1	3290 ± 70
2	0	0	-4.5 ± 5.1	-0.5 ± 4.7	$+1.5\pm0.5$	3360 ± 170
3	0	0	-3.9 ± 2.8	$+4.4\pm2.9$	$+1.1\pm0.1$	3306 ± 106

given locations, are in good accord with each other.

Attempts at the determination of sourse points of tremors was carried out every night from Jan. 25 to Feb. 1, 1953. Thus we have succeeded in recording a great many tremors, of which, however, the foci of only about 30 tremors could de located. In the calculation of a

Table II.

No.	Date	Observed time	T^*	Epicenter X_0	Epicenter Y_0	Velocity	Number of obs. point
		h m	T°C	m	m	Km/sec	
F-1	Jan. 21	20 10~20	−2.1	71.9± 1.5	− 82.1± 8.8	2.62 ±0.03	10
F-2	23	18 12~20	−2.7	11.9± 7.4	−192.1±31.0	3.45 ±0.13	10
F-3	27	23 57~09	−3.8	− 40.0±59.0	− 53.1±29.0	3.24 ±02.0	10
F-4	28	0 15~25	−4.0	57.4± 5.8	−172.2± 8.0	2.90 ±0.07	9
F-5	〃	〃	〃	− 8.4±22.9	−114.5±32.3	2.95 ±0.15	9
F-6	〃	〃	〃	− 68.9±30.0	− 57.9±36.0	3.01 ±0.27	9
F-7	〃	〃	〃	24.0±12.0	−141.9±18.0	3.05 ±0.03	10
F-8	〃	〃	〃	121.3± 6.7	30.1± 2.8	3.05 ±0.37	9
F-9	〃	〃	〃	− 66.0±13.0	−129.0±23.0	2.84 ±0.11	10
F-10	〃	1 10~20	−4.6	− 12.0± 1.0	−105.0±18.0	2.99 ±0.23	8
F-11	〃	〃	〃	23.0± 0.9	−119.3± 3.8	2.85 ±0.04	11
F-12	〃	1 21~31	−4.8	8.3± 2.1	−209.3± 6.5	2.90 ±0.09	10
F-13	〃	1 49~2 00	−5.3	137.0±22.8	8.4±12.1	2.50 ±0.09	12
F-14	〃	〃	〃	66.2± 7.1	− 55.7± 5.3	3.38 ±0.20	11
F-15	〃	2 04~15	−5.5	191.0±14.2	− 77.6± 7.3	2.52 ±0.04	9
F-16	〃	〃	〃	− 19.4± 4.4	−126.8± 7.5	2.85 ±0.24	10
F-17	〃	〃	〃	−149.7±14.7	−141.0±11.1	3.14 ±0.07	12
F-18	〃	〃	〃	75.5±19.0	98.3±11.0	2.83 ±0.18	10
F-19	〃	〃	〃	147.0±13.0	26.0± 5.0	2.85 ±0.11	10
F-20	〃	〃	〃	−135.3±20.0	−151.6±19.0	3.19 ±0.30	11
F-21	〃	6 17~23	−2.2	7.6± 4.0	−139.3± 9.1	2.87 ±0.03	11
F-22	〃	6 30~33	〃	113.0±28.0	59.0±18.0	2.69 ±0.16	10
F-23	〃	〃	〃	149.8±14.8	− 21.4± 6.9	2.80 ±0.09	7
F-24	〃	7 07~10	−2.1	9.5± 4.9	−165.5±14.0	3.05 ±0.08	10
F-25	〃	0 15~25	−4.0	17.2± 3.7	−169.1± 8.1	3.08 ±0.25	9
F-26	Feb. 1	20 14~17	〃	48.0± 1.5	100.0±30.0	2.65 ±0.01	7

* T: Air temperature.

focus its depth was assumed to be zero as the thickness of the ice-sheet was not more than only 19 or 20 cm. Accordingly in calculating the focus of a tremor we had only four unknowns, namely, the coordinates

of the focus, x and y; the velocity V of the elastic wave that propagates in the ice; and the origin time T_0. In this case of the observation, 12 detectors were used, and we were able to determine those four unknown quantities by means of the least square method. In Table II the results of calculation are shown. The diversity of the calculated values of velocity is about 10 percent. Some noticeable foci are reproduced in Fig. 9.

It has a great significance that we could determine the epicenters of these ice tremors.

Among these 30, three shocks, F–4, 5 and F–6, in Table II are especially interesting. These three shocks, as is seen in the table, took place successively in the interval of about 100 milliseconds. As is seen in Fig. 11, the distance between F–4 and F–5 is 80 m and the time interval between the two is 63 milliseconds, while the distance and the time interval between F–5 and F–6 are 120 m and 215 milliseconds respectively. These facts may indicate that a crack that started from the focus of F–4 proceeded to F–5 and then to F–6. It will be seen from this example that a crack generated at one point in the ice-sheet sends out elastic waves from its origin point and at the same time the crack itself goes forward with some finite velocity smaller than the commpressional elastic P waves in the ice, and in the course of its progress releases a strain energy in the ice-sheet in the form of elastic waves. The progressive velocity of a crack will be given as 1270 m/s and 560 m/s from the curve F_4–F_5–F_6 in Fig. 11. These numerical values may not be highly accurate as the speed of progress of a crack, but the tendency of the speed of the earlier stage to be greater than that of the latter stage seems to have some meaning, because in the formation of a crack, a large amount of strain energy will be released and converted into elastic waves by the first shock, and lesser part of the energy is due to the second shock, and

Fig. 11. Progress of a fracture in the ice-sheet.

when a less strained field of stress energy is released, the speed of the progress of a crack will be retarded.

A word will be added on the determination of the epicenter. We have a few foci which were determined by means of the commencement times of the flexural waves. The beginning of the flexural waves is not so distinct as that of the initial P waves, but not so indistinct as the beginning of the surface waves of natural earthquakes.

The probable errors of the foci thus determined from the flexural waves are of course somewhat large as compared with those due to the errors in the P waves. Seeing from the facts that the two foci are quite near in their positions, and the probable errors of the respective locations of these two foci are so small it will not be too much to say that the two waves, the compressional wave and the flexural wave, started from the same point at the same instance.

In our coming paper more detailed description on the nature of the ice tremors will be attempted.

Acknowledgement

In conclusion, we express our hearty thanks to Dr. K. Wadati, Director of the Central Meteorological Observatory, to Dr. Y. Kodaira, Director of the Tokyo District Meteorological Observatory, and to Mr. T. Tsubota, Chief of the Suwa Branch Station of CMO., who were so kind as to allow us to carry out our observations in a room in the Suwa Branch Station of CMO.

We also cordially express our indebtedness to the Nippon Telegraph & Telephone Public Corporation, especialy to Dr. T. Nakao, Chief Engineer, to Dr. S. Yonezawa, Director of the Maintenance Bureau, to Mr. Nagata, Director of the Material Supply Bureau, who lent us as many cables as desired for our experiment and by whose cooperation our observations could be carried out. Our hearty thanks are also due to Mr. M. Kanai, then Mayor of the Suwa City, to K. Kinoshita, then Director of the Suwa Branch Station of the Department of Civil Engineer of Nagano Prefecture. Last but not least our thanks are due to Drs. N. Nasu and H. Tsuya, Director and Ex-Director of our Institute for their kind encouragement in the entire course of our study. A part of the cost of our study was expended from the Grant in Aid of Scientific Rerearch from the Ministry of Education.

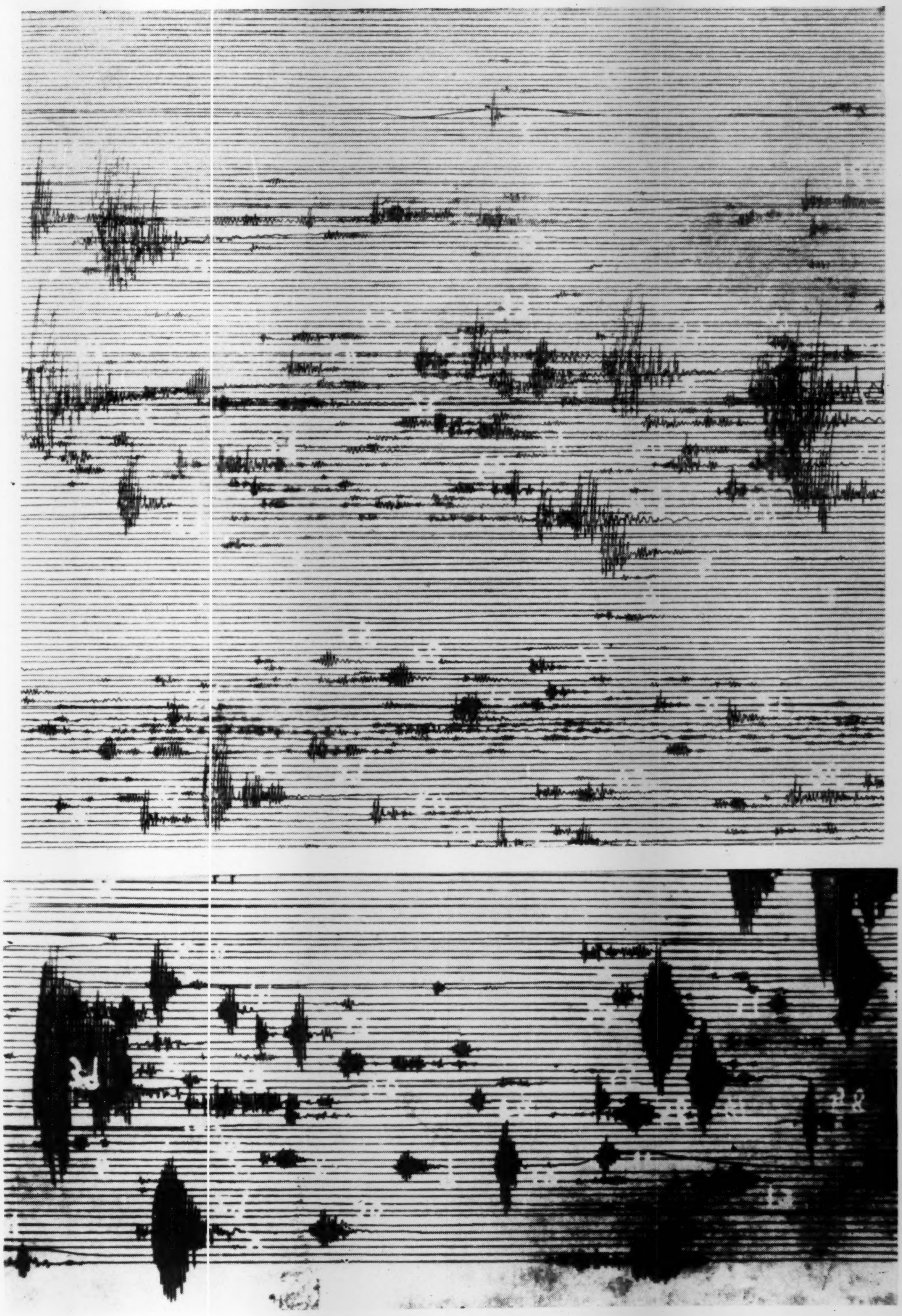

Fig. 2. Record of ice tremors by pen-galvanometers (full size).

(震研彙報 第三十三号 図版 表・山崎・小林・村内)

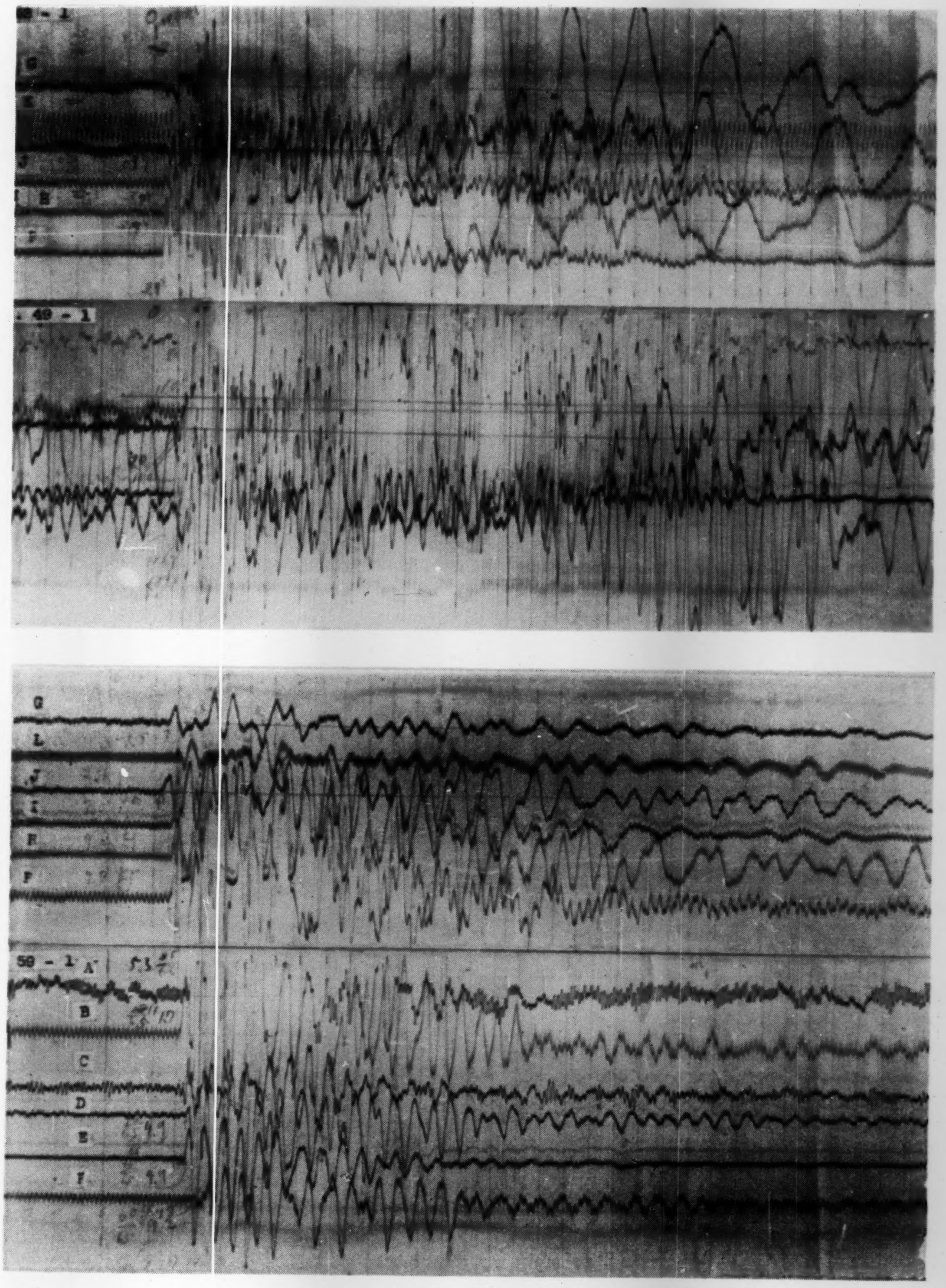

Fig. 12. Record of ice tremors. (full size)

（震研彙報 第三十三号 図版 表・山崎・小林・村内）

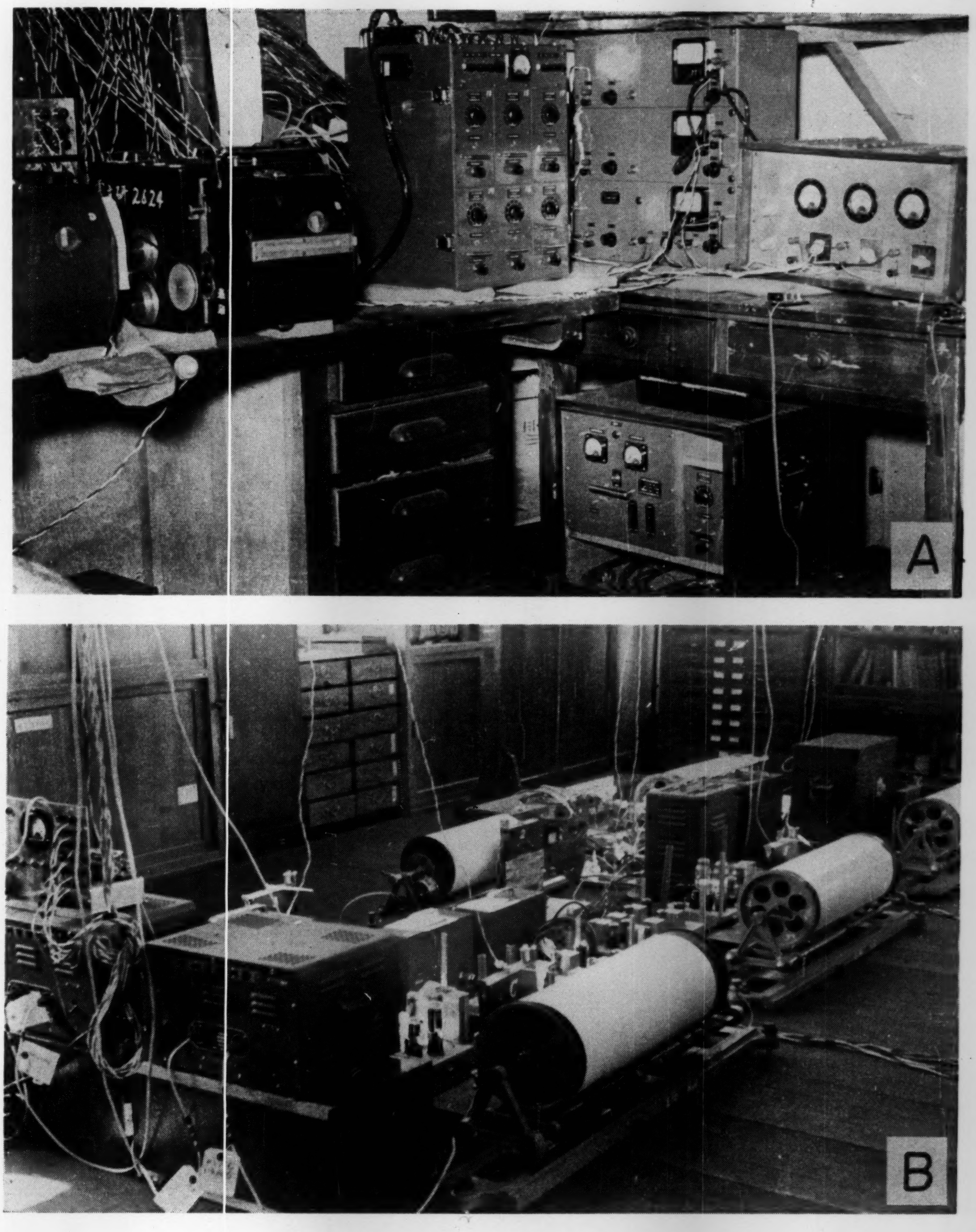

Assemblage of recording instruments.

A: Amplifiers and oscillographs.

B: Long recording time system.

Cables that connect detectors to the recording equipments.

A: Cables mounted on bamboo poles.

B: Getting cables ready.

（震研彙報 第三十三号 図版 表・山崎・小林・村内）

[S. OMOTE, Y. YAMAZAKI, N. KOBAYASHI and S. MURAUCHI.] [Bull. Earthq. Res. Inst., Vol. XXXIII, Pl. XCIV.]

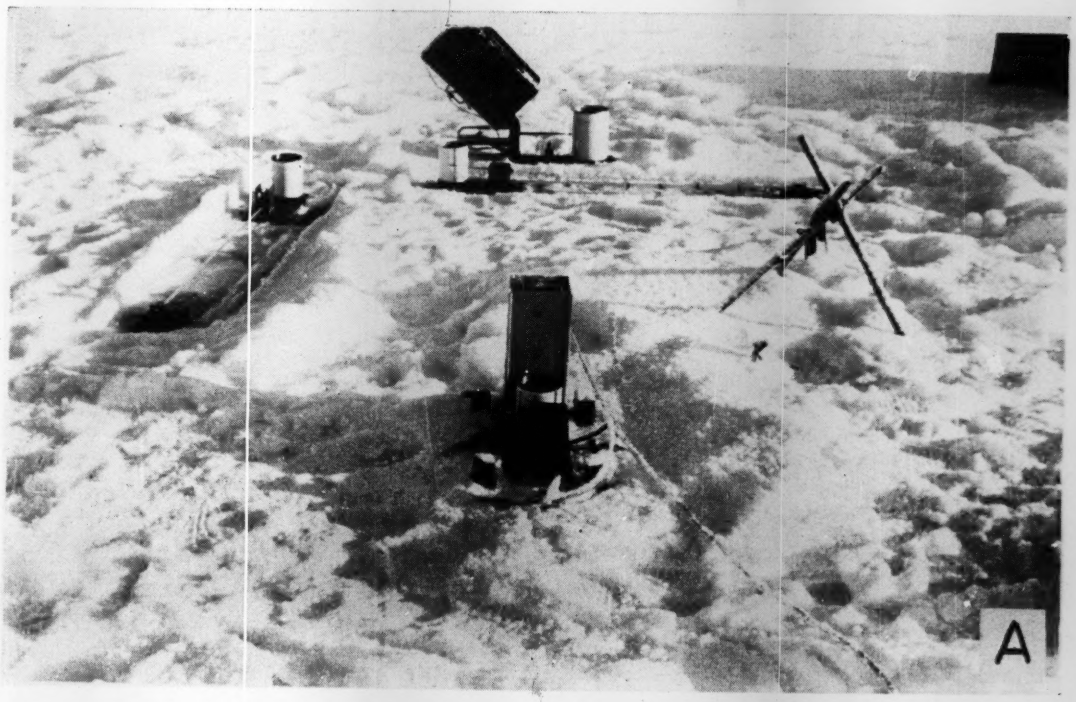

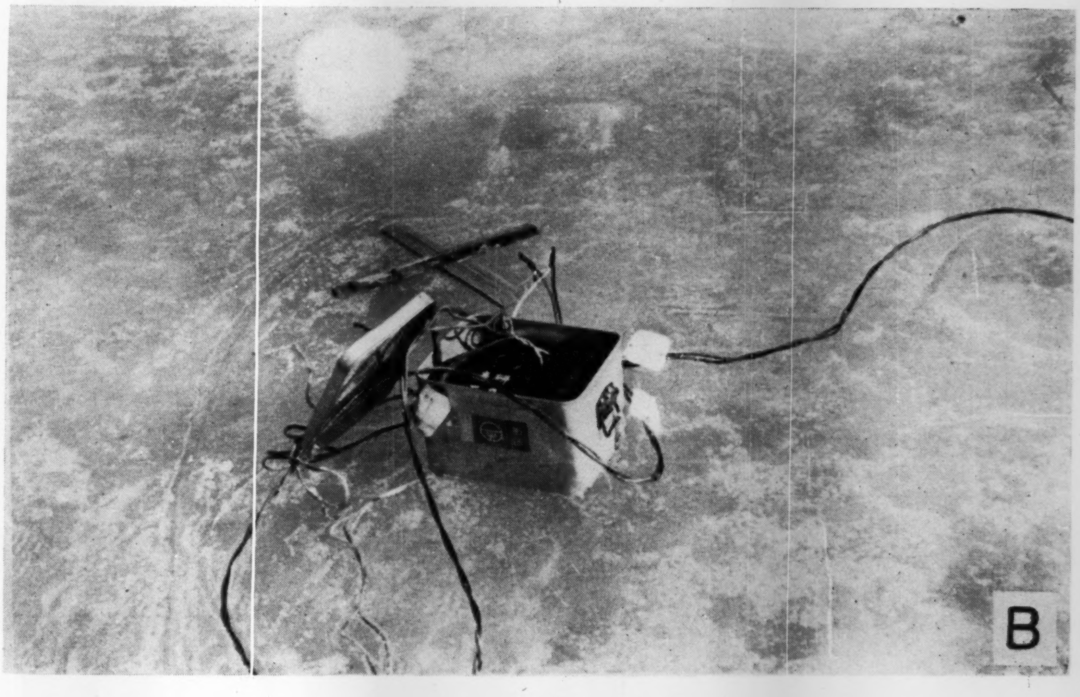

Instruments set up on ice.

A: Extensometers and thermo-couples.

B: Detectors.

(震研彙報 第三十三号 図版 表・山崎・小林・村内)

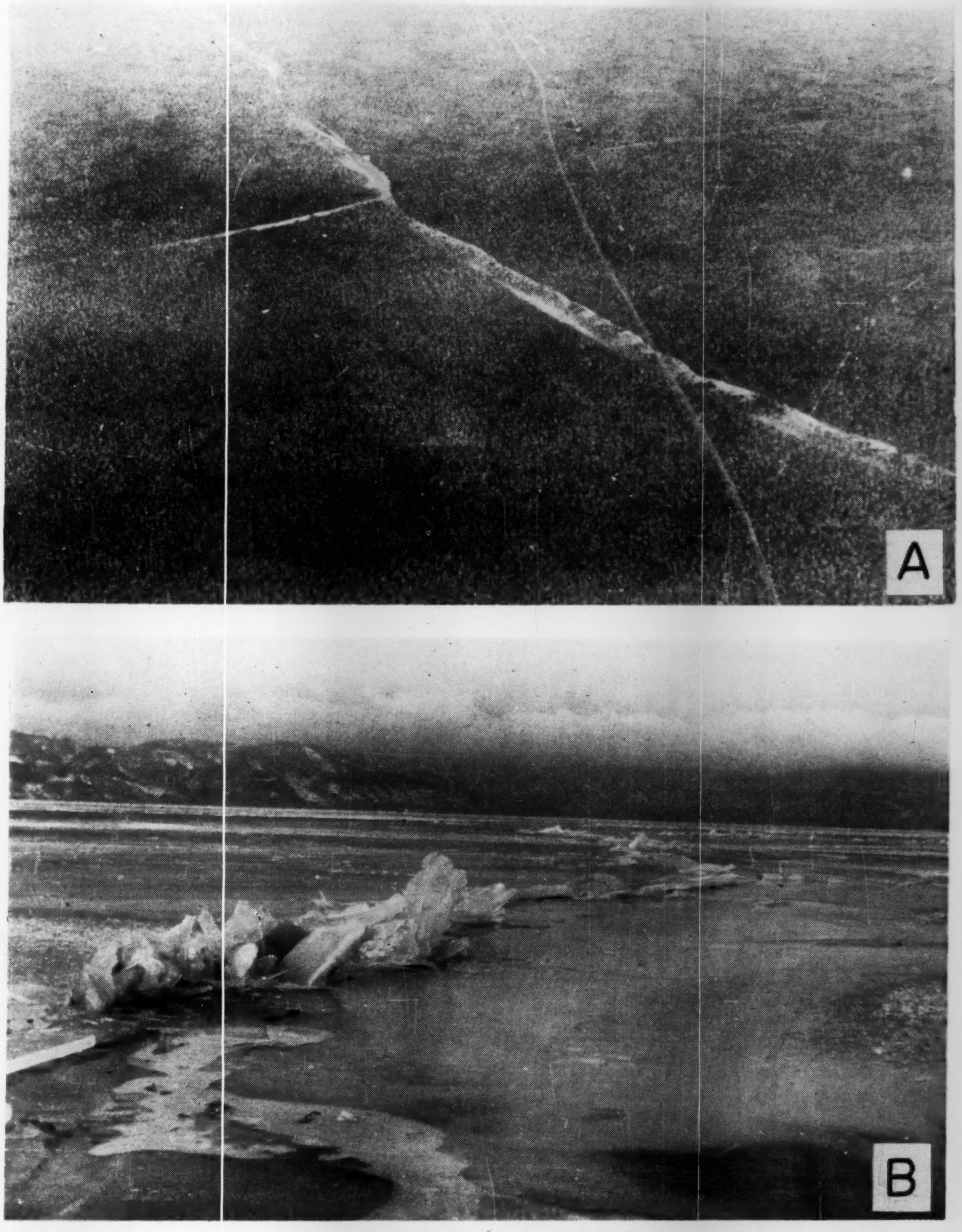

Fractures in the ice-sheet.

A: Small cracks.

B: *Omiwatari* of a small scale.

(震研彙報 第三十三号 図版 表・山崎・小林・村内)

42. 湖氷中に発生する自然震動の研究 (第 1 報)

地震研究所 表 俊 一 郎
山 崎 良 雄
小 林 直 吉

国立科学博物館 村 内 必 典

冬に湖水が全面結氷した後，夜間の冷えこみ，昼間の日光直射等により湖氷が収縮，膨脹を行うに際し氷の中に自然に割目が生じそれに伴つて可なり大きな音がきかれることが気付かれていた．長野県諏訪湖の有名な「御神渡」はこのような現象の顕著なものと考へられる．氷自身の収縮膨脹により氷の中に歪が蓄積せられ遂いに自然に破壊が起つて弾性波を送り出すという機構は地震の研究を行つている者に特別な注意を呼びおこすものである．最近地震の波の発生について model seismology の分野にめざましい発展がなされつつあるが，我々も諏訪湖の湖氷上に換震器を設置して氷の中に起る自然震動—氷震—の観測を行い，これを 1 つの地震の model と考えて氷震発生の機構を研究してみようと試みた．

氷震の発生と，気温，氷中温度，氷の伸縮等との間には第 3, 4 図に示されているように密接な関係が見られる．気温が 0°C 以下に降下して後 2 時間位遅くれて氷中温度も 0°C 以下に下り始め同時に氷の収縮が始まり，ほとんどこれと同時に氷震も起り始めるのが見られる．これらの氷震は，例えば第 2 図又は第 10 図の記録に見られるようにいわば shock type であるので氷震の震央をもとめることが出来る．氷の厚さが僅か十数糎であるので深さは O として普通の地震の場合のように震央の座標 X, Y, 発震時 T_0, 波の速度 V を未知数として 10 ケ位の観測点の発震時を用いて最少自乗法によつて計算を行つた結果は第 II 表及び第 9 図に示されている．これらの図及び表から見るように氷の上に見られる割目は長く延びているけれども割目の始めの所は点としてその origin をきめることが出来ることが知られた．このようにして発生する氷震の振幅の頻度分布について石本飯田の係数 m をもとめた結果は普通の地震の場合に得られている値とほとんど一致していることが知られた．

氷の中をつたはる波の速さについては多くの人々の研究がある．我々もこれについて 2, 3 の測定を行つたので，氷震による初動の押し引きの問題と共に第 2 報において詳述することとしたい．

43. Relation between the Periods of Microseisms and the Situation of Typhoon.*

By Ryôhei IKEGAMI,

Tokyo Gakugei University.

(Read Nov. 3, 1954**.—Received Sept. 30, 1955.)

Introduction

It has been studied by many authors, and by means of various methods, that the patterns of microseismic waves vary according to the situations of severe atmospheric depressions like typhoons or hurricanes. In general, the nearer the depression approaches a station, the larger the amplitudes of microseisms and the longer their periods become, but, on some occasions, the amplitudes or the periods of microseisms are not always related with the distances of the depression.

We have already pointed out that the periods of microseisms are intimately related with the directions of approach of microseisms.

In this paper, in order to study more precisely the relation between the periods of microseisms and the situations of low depression, we constructed the periodograms of the microseismic periods and considered the relations between their patterns and the situations of the typhoon. In addition, we applied Tomoda's simplified correlation method to the same data, and also considered the results obtained.

Materials and Methods Used

The microseismograms used in this paper are those which were observed at the yard of the Tokyo Astronomical Observatory by means of Kishinouye Microseismometers (magnification: 2000, natural period: 10 sec., magnetic damper: critical damping). Periodograms were constructed by ordinary periodogram analysis for five days (from September 11 to 15, 1950), when the Typhoon "Kezia" came up north from the southwest Pacific, passed through Kyushu and Chugoku Districts, and passed over the Japan Sea for Hokkaido. The path of this Typhoon is

* Communicated by F. KISHINOUYE.

** Read at the Meeting of the Seismological Society of Japan.

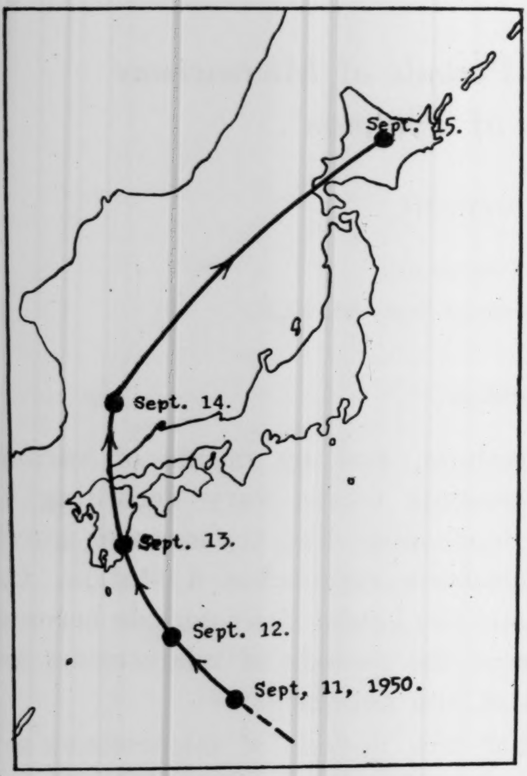

Fig, 1, The path of the Typhoon "Kezia."

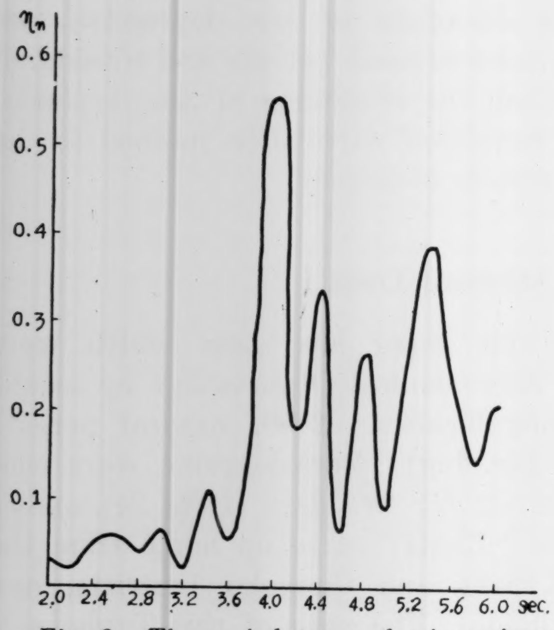

Fig. 2. The periodogram of microseisms observed on Sept. 11, 1950.

shown in Fig. 1.

We restricted the examined periods to the range of 2.0–6.0 sec., for these periods were apparently predominating on the seismograms of those days. The seismograms recording continuously for one minute were used, and the amplitudes of microseismic waves were measured every 0.2 sec. Then we got 300 measured values from the record of each day. Let σ be the standard deviation of the measured values, and let σ_n be the standard deviation to n sec. period in the ordinary periodogram analysis. Then the correlation ratio η_n to n sec. period is given by $\eta_n = \sigma_n / \sigma$, where n stands for 2.0, 2.2, 2.4, 2.6, ... 6.0 sec. The periodograms were constructed by plotting the values of η_n and period n in the ordinate and the abscissa, respectively, and these periodograms are illustrated in Figs. 2–6 for those days of observation.

We applied Tomoda's simplified correlation method[1)] which was published recently to the same microseismic data, and got the correlation coefficients for every n sec. period. The results are shown in Figs. 7 and 8.

Discussion of the Results

In Figs. 2 and 3 the periodograms show one pronounced maxi-

1) Y. TOMODA, *Zisin* (*Journ. Seism. Soc. Japan*, [ii]), **7** (1954), 55, (in Japanese).

mum of correlation ratio at the periods 4.0 sec. and 4.4 sec., respectively, (η_n=0.553 in Fig. 2, η_n=0.759 in Fig. 3), and the ratios for the other periods all have values less than 0.5. We see from these results that the microseismic waves of these 2 days (Sept. 11 and Sept. 12) were predominated by periods of 4.0 sec. and 4.4 sec., respectively, and that the waves of the other periods were insignificant.

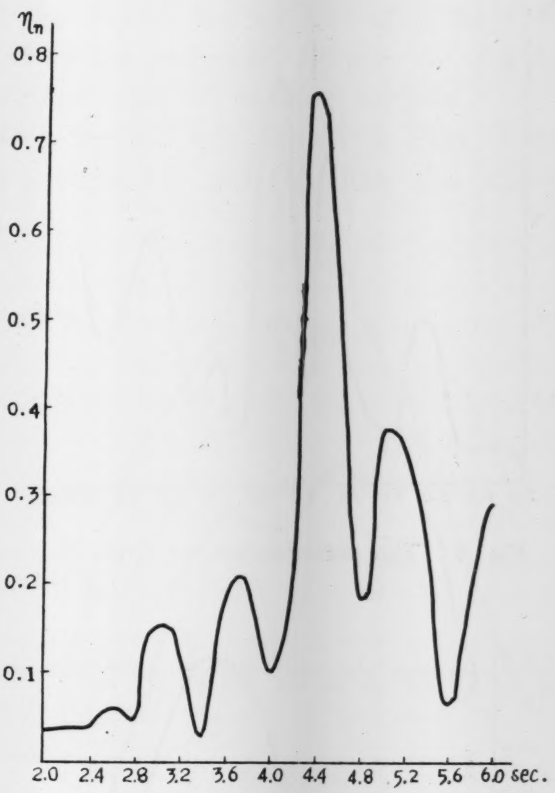

Fig. 3. The periodogram for Sept. 12.

On the other hand, the periodograms of Sept. 13, Sept. 14, and Sept. 15 are markedly different from the above-mentioned ones. In Figs. 4–6, the values of correlation ratio are all less than 0.5, and there is no pronounced maximum. We find on the seismograms that the microseismic waves have various periods in the wide range of about 2.2–5.0 sec. on Sept. 13, 14, and 15. (See Fig. 10.)

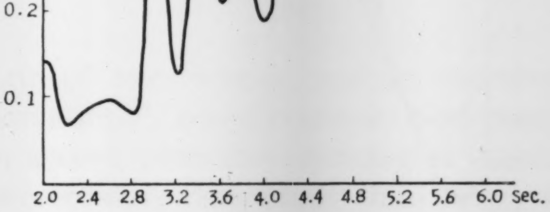

Fig. 4. The periodogram for Sept. 13.

Then we may classify the following two groups of the periodograms in accordance with their characteristics, namely, (a) the periodograms which have a sharp peak, the correlation ratio of which is more than 0.5, (Sept. 11 and 12), (b) the ones which have no striking peak, (Sept. 13, 14 and 15). It is clear that the microseismic waves belonging to the group (a) are markedly predominated by the period of 4.0 sec. (Sept. 11), or 4.4 sec. (Sept. 12), and that the ones belonging to the group (b)

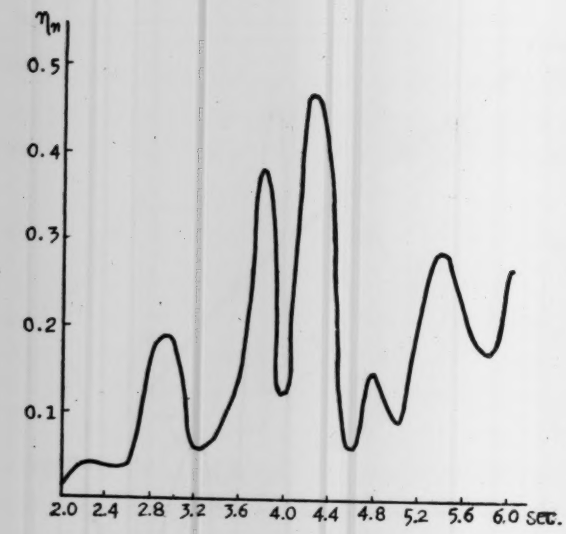

Fig. 5. The periodogram for Sept. 14.

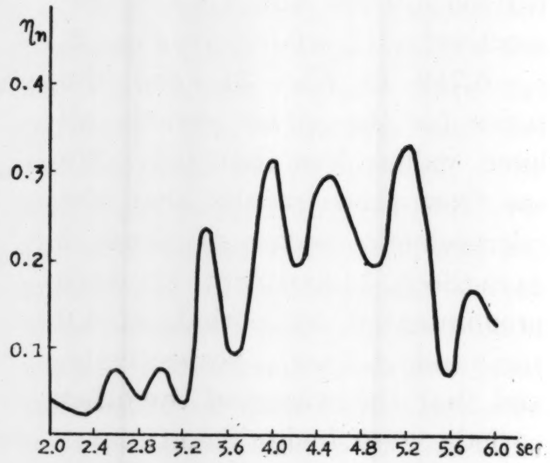

Fig. 6. The periodogram for Sept. 15.

Fig. 7. Microseismic period spectra for Sept. 11 and Sept. 12.

– – – – Sept. 11,
——— Sept. 12.

are mixed with waves of various periods.

According to the weather charts of those days, the Typhoon "Kezia" was situated in the Pacific Ocean to the south of Japan on Sept. 11 and 12, 1950, and struck the shore of Kyushu on the morning of Sept. 13, passed over the land and the Japan Sea rapidly, and reached Hokkaido on Sept. 15.

It has been frequently pointed out that there may be a conspicuous relation between the microseisms at Tokyo and the severe atmospheric depressions over the Pacific Ocean. We may consider that the predominant microseisms with 4.0–4.4 sec. period, which appeared on Sept. 11 and 12, were directly related with the Typhoon "Kezia" over the Pacific Ocean. When

she was moving over the land and the Japan Sea on and after Sept. 13, the regular microseisms predominated by the period of 4.0 sec. or 4.4 sec. disappeared, and gave place to irregular ones of various periods.

The results obtained by Tomoda's method are shown in Figs. 7 and 8. They can be classified into two groups, (a) and (b), like the above-mentioned periodograms, but they have a maximum value at the period of 4.6 sec. on Sept. 11 and 12, respectively. This is different from the above-mentioned results of periodograms, and the difference may be due to the simplified method.

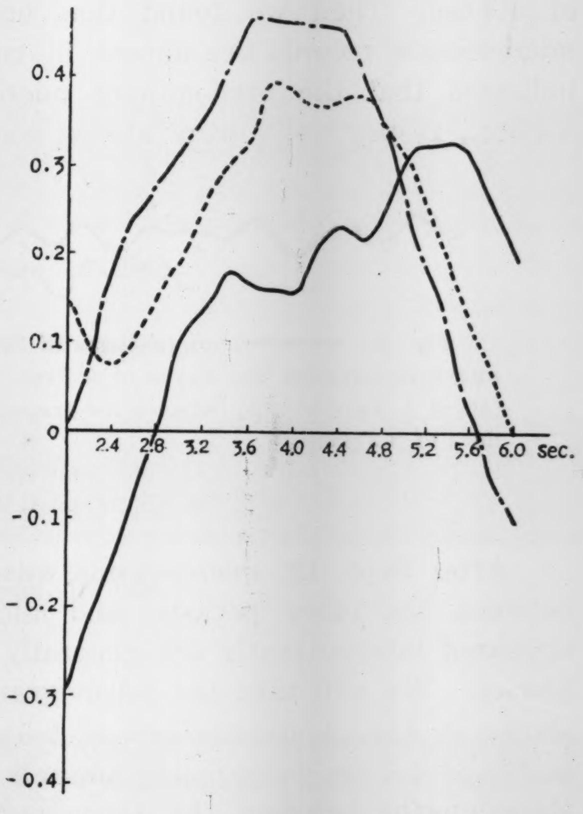

Fig. 8. The period spectra for Sept. 13, 14, and 15.

——— Sept. 13,
— — — Sept. 14,
- - - - Sept. 15.

F. Kishinouye[2] has constructed the frequency distribution diagram of the periods, using the same record of Sept. 11, 1950, and it shows a predominant maximum at the period of 4.0 sec. in both the NS- and EW-components.

Therefore we suppose that the results obtained in this paper is certainly a corroborative evidence of the close relation between the predominant microseisms observed at Tokyo and the severe depression over the Pacific Ocean. Those microseisms may be caused actually by the depression, but there are still many doubtful points about the origin of microseisms, and on the occasion of our preceding tripartite observations[3], the directions of approach of microseisms were not always in accord with the situation of atmosphere depression over the ocean. Accordingly, we admit that the predominant microseisms of Sept. 11 and 12 had some relations with the Typhoon "Kezia" over the Pacific Ocean, but we can not hastily con-

2) F. KISHINOUYE, *Bull. Earthq. Res. Inst.*, **29** (1951), 577.
3) R. IKEGAMI, *Bull. Earthq. Res. Inst.*, **29** (1951), 313.

clude that the center of the Typhoon was the real origin of the microseisms.

For the purpose of studying the nature of microseismic waves, we made an attempt to lay on the microseismic record of Sept. 11, sinusoidal waves with the amplitudes adequately adjusted and the period of 4.0 sec., and on the microseismic record of Sept. 12 those with the period of 4.4 sec. Then we found that both the sinusoidal waves and the microseismic records are almost in concord with each other. This fact indicates that the predominant microseisms with the period of 4.0 and 4.4 sec., respectively, were almost continuous.

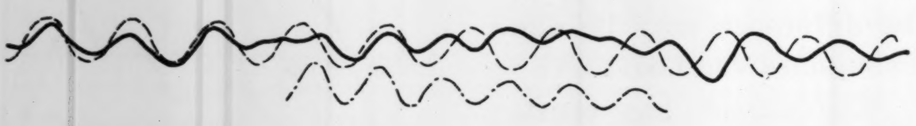

Fig. 9. ———: microseisms of Sept. 14. The waves of 3.5 sec. period intervene between the waves of 4.2 sec. period, and there is a phase difference (about $\frac{1}{4}$ wave-length) between the preceding waves of 4.2 sec. and the following ones of 4.2 sec.

- - - - -: the sinusoidal waves with the period of 4.2 sec.

— — — -: the sinusoidal waves with the period of 3.5 sec.

After Sept. 13, microseismic waves of a certain period intervened between the other periods, and microseisms of the same period which appeared intermittently are generally different from each other in their phases. We will take the seismograms of Sept. 14 as an example. As shown in Fig. 9, microseisms of 3.5 sec. period intervene between microseisms of 4.2 sec. period, and there is the phase difference (about quarter wave-length) between the preceding microseisms of 4.2 sec. period and the following ones of 4.2 sec. period. From this instance, we may say that the irregular microseisms consist of many isolated waves with various periods (possibly, with different origins).

Summary

Periodograms of periods of microseismic waves have been constructed for the five days from September 11 to 15, 1950, when the Typhoon "Kezia" passed over Japan. The following results have been obtained:

1. The periodograms may be classified into two groups; (a) the periodograms of one group show a sharp peak, the correlation ratio of which is more than 0.5 (Sept. 11 and 12) (Figs. 2 and 3): (b) those of

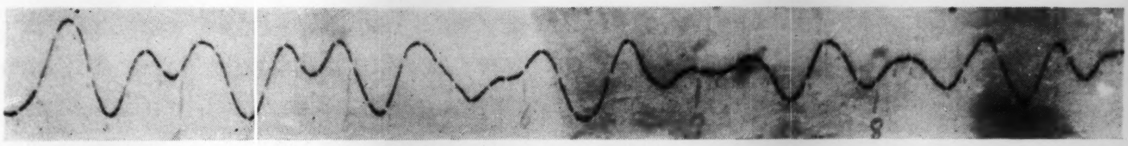

Sept. 11, 1950.

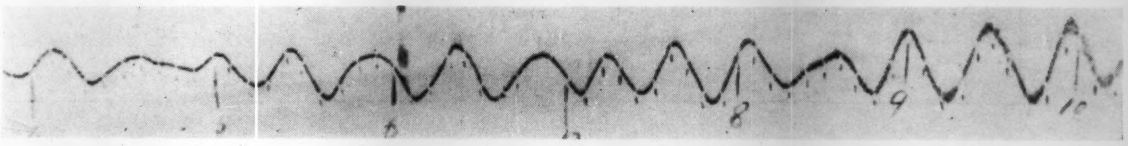

Sept. 12, 1950.

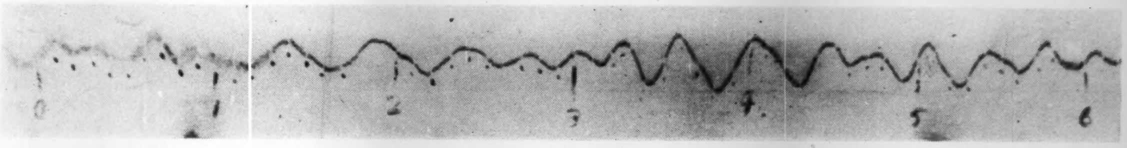

Sept. 13, 1950.

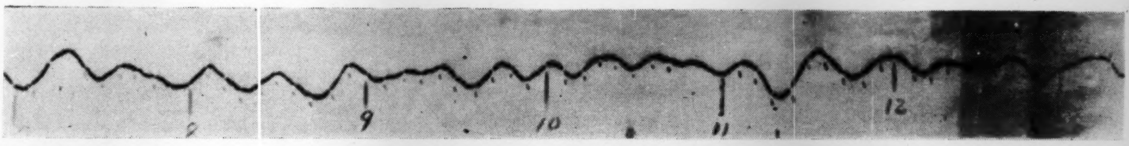

Sept. 14, 1950.

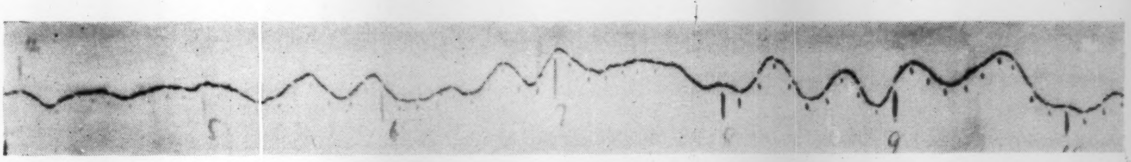

Sept. 15, 1950.

Fig. 10. Microseisms at Tokyo (×0.418).

(震研彙報 第三十三号 図版 池上)

the other group show no striking peak, (Sept. 13 to 15), (Figs. 4–6).

2. It may be considered that the predominant microseisms of Sept. 11 and 12 were directly related with the Typhoon "Kezia" over the Pacific Ocean. But microseismic waves did not always approach the station from the center of the Typhoon.

3. The individual waves of very irregular microseisms from Sept. 13 to 15 had different phases, and may possibly have been of different origin.

4. Microseismic period spectra have also been constructed by means of Tomoda's simplified correlation method (Figs. 7 and 8). The results obtained were also similar to the above-mentioned results.

---

43. 土地の脈動の周期と台風位置との関係

東京学芸大学　池　上　良　平

1950 年 9 月 11 日～15 日の 5 日間に東京に於て観測された脈動記録 (第 10 図) を用いて，周期のペリオドグラムを作つた．このペリオドグラムと台風位置 (第 1 図) とを比較して次の結果を得た．

1. ペリオドグラムは 2 群に分類できる．

(a) 相関比の値が 0.5 以上の著しい極大を有するもの．(11 日及び 12 日の脈動で，第 2 図及び第 3 図に示す)．

(b) 相関比の値に著しい極大のないもの．(13 日以後の脈動で，第 4 図～第 6 図に示す)．

2. 11 日及び 12 日の優勢な脈動は，太平洋上の台風 "Kezia" と密接な関係を持つている．然しこれらの脈動波が台風の中心地域から，東京まで伝播して来たものであると速断することはできない．

3. 13 日以後の非常に不規則な脈動の個々の波は，夫々異つた位相を持つていた．(一例を第 9 図に示す)．この事実は，これらの脈動波は，種々な周期と振幅を持つたいくつかの弧立波の集合である事を示すものであると考えられる．脈動波が一連の同一方向から連続して伝播して来る波であると考えることに，なお疑いを残している．

4. 友田氏の簡単化された相関係数計算法を用いて，同一脈動記録から周期解析を行つた．その結果は第 7, 8 図に示してある．上述の結果と大体同じ結果を示している．

---

44. *Steady State Non-linear Vibration of Two Story Buildings.*

By Toshihiko HISADA and Kyoji NAKAGAWA,

Building Research Institute.

(Read Sept. 27, 1955.—Received Sept. 30, 1955.)

Introduction

For the past several years, vibration tests have been performed on full size structures of new fire-resisting constructions to investigate their aseismic properties. In each test a small or a gigantic shaking machine was installed on the floor or a building so that it might produce forced vibration through the centrifugal shaking force. When the amplitude of the test structure is small, its dynamical behaviour can be regarded as linear but, if the amplitude becomes so large as to do some damage to the building, the response features are no longer linear but present non-linearity. Of these problems the authors already presented two papers[1)2)] in which they dealt with some theoretical and experimental problems on the masonry and two-story frame structures.

In this paper the analysis is shown for the steady state non-linear vibration of the two-storied frame structure which is subjected to shaking force by a machine and its application was investigated on the test results obtained from a pre-stressed concrete frame structure.

In steady state vibration of a building, the relation between the restoring force and the relative displacement of each story would usually make a figure of loop in their co-ordinate but, in the analysis shown in this paper, the relation is assumed as a curve passing through the origin of the co-ordinate, and the damping proportional to the velocity of relative deformation is considered. The vibrational properties of the test building including dampings in large vibrations are computed from this analysis and compared with the ones in small amplitudes.

---

1) T. HISADA and K. NAKAGAWA, "An Analysis of Vibration of Masonry Buildings," *Report of the Building Research Institute*, **12** (1953).

2) T. HISADA, "Non-Linear Vibration of Two Story Buildings" *Trans. Architectural Institute of Japan*, **50** (1955).

1. Forced Vibration by Shaking Machine

Assumptions

In this analysis, the following assumptions are employed:

The building is considered as a system of two degrees of freedom and the restoring force of each story has terms of displacement having odd power (up to 7 in this paper).

The damping force of each story is considered as viscous and proportional to the relative velocity of deformation.

Notations

The following notation is used in this paper:

m_i=mass, $i=1, 2$

$\overline{m}=m_2/m_1$

x_i=instantaneous displacement of mass m_i, $i=1, 2$

c_i=coefficient of the linear term in the algebraic expression for a non-linear restoring force.

$\mu_i^2, \nu_i^4, \xi_i^6$=ratios of the coefficients of the non-linear terms to that of the linear term in the algebraic expression for a non-linear restoring force, $i=1, 2$

$\kappa_i^2=c_i/m_i$, $i=1, 2$

$\overline{\kappa}^2=\kappa_2^2/\kappa_1^2$

$\overline{\mu}^2=\mu_2^2/\mu_1^2$

$n_i=10\nu_i^4/9\mu_1^4$, $i=1, 2$

$l_i=35\xi_i^6/27\mu_1^6$, $i=1, 2$

b_i=coefficient of damping force, $i=1, 2$

$D_i=b_i/2m_i\kappa_i$=dimensionless relative damping, $i=1, 2$

Q_i=amplitude of harmonically varying displacement of mass m_i, $i=1, 2$

$\overline{Q}_i=\sqrt{3/4}\mu_1 Q_i$=dimensionless amplitude of displacement of mass m_i, $i=1, 2$

M=eccentric mass of shaking machine

r=arm of eccentric mass

$s=Mr/m_1$

$\overline{s}=Mr/m_1\cdot\sqrt{3/4}\mu_1$

α_i=difference of phase of the sinusoidal motion of mass m_i $i=1, 2$

Ω=circular frequency of shaking machine

$\eta=\Omega/\kappa_1$

t=time

$\tau=\Omega t$

General Relations

The differential equations of motion of the system shown in Fig. 1 are

$$m_1\ddot{x}_1 + c_1[x_1 - \mu_1^2 x_1^3 + \nu_1^4 x_1^5 - \xi_1^6 x_1^7]$$
$$- c_2[(x_2 - x_1) - \mu_2^2(x_2 - x_1)^3 + \nu_2(x_2 - x_1)^5$$
$$- \xi_2^6(x_2 - x_1)^7] + b_1\dot{x}_1 - b_2(\dot{x}_2 - \dot{x}_1) = 0 \qquad (1.1)$$
$$m_2\ddot{x}_2 + c_2[(x_2 - x_1) - \mu_2^2(x_2 - x_1)^3 + \nu_2^4(x_2 - x_1)^5$$
$$- \xi_2^6(x_2 - x_1)^7] + b_2(\dot{x}_2 - \dot{x}_1) - Mr\Omega^2 \cos \Omega t = 0 \qquad (1.2)$$

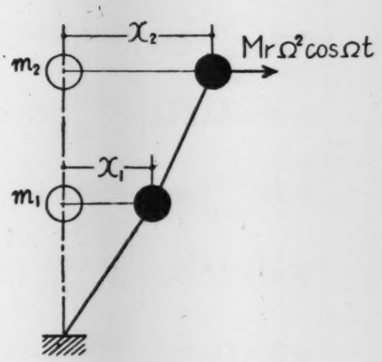

Fig. 1.

or

$$E_1 \equiv \ddot{x} + \kappa_1^2[x_1 - \mu_1^2 x_1^3 + \nu_1^4 x_1^5 - \xi_1^6 x_1^7] - \overline{m}\kappa_2^2[(x_2 - x_1)$$
$$- \mu_2^2(x_2 - x_1)^3 + \nu_2^4(x_2 - x_1)^5 - \xi_2^6(x_2 - x_1)^7]$$
$$+ 2D_1\kappa_1\dot{x}_1 - 2\overline{m}D_2\kappa_2(\dot{x}_2 - \dot{x}_1) = 0 \qquad (1.3)$$
$$E_2 \equiv \ddot{x}_2 + \kappa_2^2[(x_2 - x_1) - \mu_2^2(x_2 - x_1)^3 + \nu_2^4(x_2 - x_1)^5 - \xi_2^6(x_2 - x_1)^7]$$
$$+ 2D_2\kappa_2(\dot{x}_2 - \dot{x}_1) - s\Omega^2/\overline{m} \cdot \cos \Omega t = 0 \qquad (1.4)$$

We assume the following periodic solution:

$$\tilde{x}_1 = Q_1 \cos(\tau - \alpha_1), \qquad \tilde{x}_2 = Q_2 \cos(\tau - \alpha_2) \qquad (1.5)$$

The Ritz averaging method[3] gives the following four conditions:

$$\left.\begin{aligned} &\int_0^{2\pi} E_1(\tilde{x}_1, \tilde{x}_2) \cos \tau d\tau = 0, \qquad \int_0^{2\pi} E_1(\tilde{x}_1, \tilde{x}_2) \sin \tau d\tau = 0 \\ &\int_0^{2\pi} E_2(\tilde{x}_1, \tilde{x}_2) \cos \tau d\tau = 0, \qquad \int_0^{2\pi} E_2(\tilde{x}_1, \tilde{x}_2) \sin \tau d\tau = 0 \end{aligned}\right\} \qquad (1.6)$$

Introducing (1.5) into (1.3) and (1.4), and furthermore putting those two equations in (1.6), we obtain the following four equations:

$$[(1 + \overline{m}\overline{\kappa}^2 - \eta^2)\overline{Q}_1 - (1 + \overline{m}\overline{\kappa}^2\overline{\mu}^2)\overline{Q}_1^{\,3} + (n_1 + \overline{m}\overline{\kappa}^2 n_2)\overline{Q}_1^{\,5} - (l_1 + \overline{m}\overline{\kappa}^2 l_2)\overline{Q}_1^{\,7}] \genfrac{}{}{0pt}{}{\cos}{\sin} \alpha_1$$
$$+ [-\overline{m}\overline{\kappa}^2\overline{Q}_2 + \overline{m}\overline{\kappa}^2\overline{\mu}^2\overline{Q}_2^{\,2} - \overline{m}\overline{\kappa}^2 n_2\overline{Q}_2^{\,5} + \overline{m}\overline{\kappa}^2 l_2\overline{Q}_2^{\,7}] \genfrac{}{}{0pt}{}{\cos}{\sin} \alpha_2$$
$$+ \overline{m}\overline{\kappa}^2\overline{\mu}^2\overline{Q}_1^{\,2}\overline{Q}_2\left[2\genfrac{}{}{0pt}{}{\cos}{\sin}\alpha_2 + \genfrac{}{}{0pt}{}{\cos}{\sin}(2\alpha_1 - \alpha_2)\right] - \overline{m}\overline{\kappa}^2\overline{\mu}^2\overline{Q}_1\overline{Q}_2^{\,2}\left[2\genfrac{}{}{0pt}{}{\cos\alpha_1}{\sin\alpha_1} + \genfrac{}{}{0pt}{}{\cos}{\sin}(2\alpha_2 - \alpha_1)\right]$$
$$+ \overline{m}\overline{\kappa}^2 n_2\overline{Q}_1\overline{Q}_2^{\,4}\left[2 \genfrac{}{}{0pt}{}{\cos}{-\sin}(\alpha_1 - 2\alpha_2) + 3\genfrac{}{}{0pt}{}{\cos}{\sin}\alpha_1\right] - \overline{m}\overline{\kappa}^2 n_2\overline{Q}_1^4\overline{Q}_2\left[2 \genfrac{}{}{0pt}{}{\cos}{-\sin}(\alpha_2 - 2\alpha_1)\right.$$
$$\left. + 3\genfrac{}{}{0pt}{}{\cos}{\sin}\alpha_2\right] + \overline{m}\overline{\kappa}^2 n_2\overline{Q}_1^3\overline{Q}_2^2\left[6\genfrac{}{}{0pt}{}{\cos}{\sin}\alpha_1 + \genfrac{}{}{0pt}{}{\cos}{-\sin}(2\alpha_2 - 3\alpha_1) + 3\genfrac{}{}{0pt}{}{\cos}{\sin}(2\alpha_2 - \alpha_1)\right]$$

3) K. KLOTTER, "Non-linear Vibration Problems Treated by the Averaging Method of W. Ritz," *Proc. First U. S. National Congress of Applied Mechanics*, 1951, ASME.

$$
\begin{aligned}
&-\bar{m}\bar{\kappa}^2 l_2\bar{Q}_1\bar{Q}_2^6\left[3\begin{matrix}\cos\\-\sin\end{matrix}(\alpha_1-2\alpha_2)+4\begin{matrix}\cos\\\sin\end{matrix}\alpha_1\right]+\bar{m}\bar{\kappa}^2 l_2\bar{Q}_1^2\bar{Q}_2^5\left[3\begin{matrix}\cos\\-\sin\end{matrix}(2\alpha_1-3\alpha_2)\right.\\
&\left.+6\begin{matrix}\cos\\\sin\end{matrix}(2\alpha_1-\alpha_2)+12\begin{matrix}\cos\\\sin\end{matrix}\alpha_2\right]-\bar{m}\bar{\kappa}^2 l_2\bar{Q}_1^3\bar{Q}_2^4\left[\begin{matrix}\cos\\-\sin\end{matrix}(3\alpha_1-4\alpha_2)\right.\\
&\left.+4\begin{matrix}\cos\\\sin\end{matrix}(3\alpha_1-2\alpha_2)+12\begin{matrix}\cos\\-\sin\end{matrix}(\alpha_1-2\alpha_2)+18\begin{matrix}\cos\\\sin\end{matrix}\alpha_1\right]\\
&+\bar{m}\bar{\kappa}^2 l_2\bar{Q}_1^4\bar{Q}_2^3\left[\begin{matrix}\cos\\-\sin\end{matrix}(3\alpha_2-4\alpha_1)+4\begin{matrix}\cos\\\sin\end{matrix}(3\alpha_2-2\alpha_1)+12\begin{matrix}\cos\\-\sin\end{matrix}(\alpha_2-2\alpha_1)\right.\\
&\left.+18\begin{matrix}\cos\\\sin\end{matrix}\alpha_2\right]-\bar{m}\bar{\kappa}^2 l_2\bar{Q}_1^5\bar{Q}_2^2\left[3\begin{matrix}\cos\\-\sin\end{matrix}(2\alpha_2-3\alpha_1)+6\begin{matrix}\cos\\\sin\end{matrix}(2\alpha_2-\alpha_1)+12\begin{matrix}\cos\\\sin\end{matrix}\alpha_1\right]\\
&+\bar{m}\bar{\kappa}^2 l_2\bar{Q}_1^6\bar{Q}_2\left[3\begin{matrix}\cos\\-\sin\end{matrix}(\alpha_2-2\alpha_1)+4\begin{matrix}\cos\\\sin\end{matrix}\alpha_2\right]+2D_1\eta\bar{Q}_1\begin{matrix}\sin\\-\cos\end{matrix}\alpha_1\\
&+2\bar{m}D_2\bar{\kappa}\eta\bar{Q}_1\begin{matrix}\sin\\-\cos\end{matrix}\alpha_1-2\bar{m}D_2\bar{\kappa}\eta\bar{Q}_2\begin{matrix}\sin\\-\cos\end{matrix}\alpha_2=0 \qquad \cdots\cdots\begin{cases}(1.7.1)\\(1.7.2)\end{cases}
\end{aligned}
$$

$$
\begin{aligned}
&[-\bar{m}\bar{\kappa}^2\bar{Q}_1+\bar{m}\bar{\kappa}^2\bar{\mu}^2\bar{Q}^3-\bar{m}\bar{\kappa}^2 n_2\bar{Q}_1^5+\bar{m}\bar{\kappa}^2 l_2\bar{Q}_1^7]\begin{Bmatrix}\cos\\\sin\end{Bmatrix}\alpha_1\\
&+[\bar{m}(\bar{\kappa}^2-\eta^2)\bar{Q}_2-\bar{m}\bar{\kappa}^2\bar{\mu}^2\bar{Q}_2^3+\bar{m}\bar{\kappa}^2 n_2\bar{Q}_2^5-\bar{m}\bar{\kappa}^2 l_2\bar{Q}_2^7]\begin{Bmatrix}\cos\\\sin\end{Bmatrix}\alpha_2\\
&-\bar{m}\bar{\kappa}^2\bar{\mu}^2\bar{Q}_1^2\bar{Q}_2\left[2\begin{Bmatrix}\cos\\\sin\end{Bmatrix}\alpha_2+\begin{Bmatrix}\cos\\\sin\end{Bmatrix}(2\alpha_1-\alpha_2)\right]\\
&+\bar{m}\bar{\kappa}^2\bar{\mu}^2\bar{Q}\bar{Q}_2^2\left[2\begin{Bmatrix}\cos\\\sin\end{Bmatrix}\alpha_1+\begin{Bmatrix}\cos\\\sin\end{Bmatrix}(2\alpha_2-\alpha_1)\right]\\
&-\bar{m}\bar{\kappa}^2 n_2\bar{Q}_1\bar{Q}_2^4\left[2\begin{Bmatrix}\cos\\\sin\end{Bmatrix}(\alpha_1-2\alpha_2)+3\begin{Bmatrix}\cos\\\sin\end{Bmatrix}\alpha_1\right]\\
&+\bar{m}\bar{\kappa}^2 n_2\bar{Q}_1^4\bar{Q}_2\left[2\begin{Bmatrix}\cos\\-\sin\end{Bmatrix}(\alpha_2-2\alpha_1)+3\begin{Bmatrix}\cos\\\sin\end{Bmatrix}\alpha_2\right]\\
&+\bar{m}\bar{\kappa}^2 n_2\bar{Q}_1^2\bar{Q}_2^3\left[6\begin{Bmatrix}\cos\\\sin\end{Bmatrix}Q_2+\begin{Bmatrix}\cos\\-\sin\end{Bmatrix}(2\alpha_1-3\alpha_2)+3\begin{Bmatrix}\cos\\\sin\end{Bmatrix}(2\alpha_1-\alpha_2)\right]\\
&-\bar{m}\bar{\kappa}^2 n_2\bar{Q}_1^3\bar{Q}_2^2\left[6\begin{Bmatrix}\cos\\\sin\end{Bmatrix}\alpha_1+\begin{Bmatrix}\cos\\-\sin\end{Bmatrix}(2\alpha_2-3\alpha_1)+3\begin{Bmatrix}\cos\\\sin\end{Bmatrix}(2\alpha_2-\alpha_1)\right]\\
&+\bar{m}\bar{\kappa}^2 l_2\bar{Q}_1\bar{Q}_2^6\left[3\begin{Bmatrix}\cos\\-\sin\end{Bmatrix}(\alpha_1-2\alpha_2)+4\begin{Bmatrix}\cos\\\sin\end{Bmatrix}\alpha_1\right]\\
&-\bar{m}\bar{\kappa}^2 l_2\bar{Q}_1^2\bar{Q}_2^5\left[3\begin{Bmatrix}\cos\\-\sin\end{Bmatrix}(2\alpha_1-3\alpha_2)+6\begin{Bmatrix}\cos\\\sin\end{Bmatrix}(2\alpha_1-\alpha_2)+12\begin{Bmatrix}\cos\\\sin\end{Bmatrix}\alpha_2\right]\\
&+\bar{m}\bar{\kappa}^2 l_2\bar{Q}_1^3\bar{Q}_2^4\left[\begin{Bmatrix}\cos\\-\sin\end{Bmatrix}(3\alpha_1-4\alpha_2)+4\begin{Bmatrix}\cos\\\sin\end{Bmatrix}(3\alpha_1-2\alpha_2)\right.\\
&\qquad\qquad\left.+12\begin{Bmatrix}\cos\\-\sin\end{Bmatrix}(\alpha_1-2\alpha_2)+18\begin{Bmatrix}\cos\\\sin\end{Bmatrix}\alpha_1\right]
\end{aligned}
$$

$$-\overline{m}\,\bar{\kappa}^2 l_2 \overline{Q}_1^4 \overline{Q}_2^3 \Big[\begin{Bmatrix} \cos \\ -\sin \end{Bmatrix} (3\alpha_2 - 4\alpha_1) + 4 \begin{Bmatrix} \cos \\ \sin \end{Bmatrix} (3\alpha_2 - 2\alpha_1)$$
$$+ 12 \begin{Bmatrix} \cos \\ -\sin \end{Bmatrix} (\alpha_2 - 2\alpha_1) + 18 \begin{Bmatrix} \cos \\ \sin \end{Bmatrix} \alpha_2 \Big]$$
$$+ \overline{m}\,\bar{\kappa}^2 l_2 \overline{Q}_1^5 \overline{Q}_2^2 \Big[3 \begin{Bmatrix} \cos \\ -\sin \end{Bmatrix} (2\alpha_2 - 3\alpha_1) + 6 \begin{Bmatrix} \cos \\ \sin \end{Bmatrix} (2\alpha_2 - \alpha_1) + 12 \begin{Bmatrix} \cos \\ \sin \end{Bmatrix} \alpha_1 \Big]$$
$$- \overline{m}\,\bar{\kappa}^2 l_2 \overline{Q}_1^6 \overline{Q}_2 \Big[3 \begin{Bmatrix} \cos \\ -\sin \end{Bmatrix} (\alpha_2 - 2\alpha_1) + 4 \begin{Bmatrix} \cos \\ \sin \end{Bmatrix} \alpha_2 \Big]$$
$$+ 2\overline{m} D_2 \bar{\kappa} \eta \overline{Q}_2 \begin{Bmatrix} \sin \\ -\cos \end{Bmatrix} \alpha_2 - 2\overline{m} D_2 \bar{\kappa} \eta \overline{Q}_1 \begin{Bmatrix} \sin \\ -\cos \end{Bmatrix} \alpha_1 - \begin{Bmatrix} \bar{s}\eta^2 \\ 0 \end{Bmatrix} = 0 \quad \cdots\cdot \begin{Bmatrix} (1.7.3) \\ (1.7.4) \end{Bmatrix}$$

For undamped systems, by putting $\alpha_1 = \alpha_2 = 0$ and $D_1 = D_2 = 0$ in (1.7.1) and (1.7.3), we have

$$(1-\eta^2)\overline{Q}_1 - \overline{Q}_1^3 + n_1 \overline{Q}_1^5 - l_1 \overline{Q}_1^7 - \overline{m}\,\bar{\kappa}^2 (\overline{Q}_2 - \overline{Q}_1) + \overline{m}\,\bar{\kappa}^2 \bar{\mu}^2 (\overline{Q}_2 - \overline{Q}_1)^3$$
$$- n_2 \overline{m}\,\bar{\kappa}^2 (\overline{Q}_2 - \overline{Q}_1)^5 + l_2 \overline{m}\,\bar{\kappa}^2 (\overline{Q}_2 - \overline{Q}_1)^7 = 0 \qquad (1.8.1)$$

$$\overline{m}\,\bar{\kappa}^2 (\overline{Q}_2 - \overline{Q}_1) - \overline{m}\,\bar{\kappa}^2 \bar{\mu}^2 (\overline{Q}_2 - \overline{Q}_1)^3 + n_2 \overline{m}\,\bar{\kappa}^2 (\overline{Q}_2 - \overline{Q}_1)^5$$
$$- l_2 \overline{m}\,\bar{\kappa}^2 (\overline{Q}_2 - \overline{Q}_1)^7 - \overline{m}\eta^2 \overline{Q}_2 - \bar{s}\eta^2 = 0 \qquad (1.8.2)$$

From those two equations, we can compute the response curves which represent the relations between $\overline{Q}_i$ and η^2 by using graphical method.

To see the behavior of free vibration of undamped systems, we put $\bar{s}=0$ in (1.8.1) and (1.8.2), then we have

$$\overline{Q}_2 = \frac{(1-\eta^2)\overline{Q}_1 - \overline{Q}_1^3 + n_1 \overline{Q}_1^5 - l_1 \overline{Q}_1^7}{\overline{m}\eta^2} \qquad (1.9)$$

Introducing (1.9) into (1.8.1), we obtain

$$\overline{m}^6 \eta^{14} [(1-\eta^2) - \overline{Q}_1^2 + n_1 \overline{Q}_1^4 - l_1 \overline{Q}_1^6] - \overline{m}^6 \bar{\kappa}^2 \eta^{12} [(1-\eta^2 - \overline{m}\eta^2) - \overline{Q}_1^2 + n_1 \overline{Q}_1^4 - l_1 \overline{Q}^6]$$
$$+ \overline{m}\,\bar{\kappa}^2 \bar{\mu}^2 \eta^8 [(1-\eta^2 - \overline{m}\eta^2) - \overline{Q}_1^2 + n_1 \overline{Q}_1^4 - l_1 \overline{Q}_1^6]^3 \overline{Q}^2 - \overline{m}\,\bar{\kappa}^2 n_2 \eta^4 [(1-\eta^2 - \overline{m}\eta^2)$$
$$- \overline{Q}_1^2 + n_1 \overline{Q}_1^4 - l_1 \overline{Q}_1^6]^5 \overline{Q}_1^4 + \bar{\kappa}^2 l_2 [(1-\eta^2 - \overline{m}\eta^2) - \overline{Q}_1^2 + n_1 \overline{Q}_1^4 - l_1 \overline{Q}_1^6]^7 \overline{Q}_1^6 = 0 \qquad (1.10)$$

(1.10) is the formula for "backbone" curves of $\overline{Q}_1$ and represents the relation between amplitude Q_1 and frequency η^2 in free vibration, while (1.9) represents the relationship between $\overline{Q}_1$ and $\overline{Q}_2$ on their "backbone" curves.

For damped systems, we can get the response curves by solving (1.7.1), (1.7.2), (1.7.3) and (1.7.4) simultaneously. The computations take very long and are tedious, so, if the dampings of the system are small, we allow ourselves to infer the general tendency of the damped systems

from the response curves of the undamped ones. In this case, it is necessary and most important to determine the behavior of the system at resonance for the first mode. For this, we put $\alpha_1=\alpha_2=\pi/2$ in (1.7) and, by adding (1.7.1) and (1.7.2) and also (1.7.3) and (1.7.4), we obtain

$$(1-\eta^2)\overline{Q}_1-\overline{Q}_1^3+n_1\overline{Q}_1^5-l_1\overline{Q}_1^7-\overline{m}\overline{\kappa}^2(\overline{Q}_2-\overline{Q}_1)+\overline{m}\overline{\kappa}^2\overline{\mu}^2(\overline{Q}_2-\overline{Q}_1)^3$$
$$-\overline{m}\overline{\kappa}^2n_2(\overline{Q}_2-\overline{Q}_1)^5+\overline{m}\overline{\kappa}^2l_2(\overline{Q}_2-\overline{Q}_1)^7+2D_1\eta\overline{Q}_1+2\overline{m}D_2\overline{\kappa}\eta\overline{Q}_1-2\overline{m}D_2\overline{\kappa}\eta\overline{Q}_2=0 \tag{1.11}$$

$$\overline{m}\overline{\kappa}^2(\overline{Q}_2-\overline{Q}_1)-\overline{m}\overline{\kappa}^2\overline{\mu}^2(\overline{Q}_2-\overline{Q}_1)^3+\overline{m}\overline{\kappa}^2n_2(\overline{Q}_2-\overline{Q}_1)^5-\overline{m}\overline{\kappa}^2l_2(\overline{Q}_2-\overline{Q}_1)^7$$
$$-\overline{m}\eta^2\overline{Q}_2+2\overline{m}D_2\overline{\kappa}\eta(\overline{Q}_2-\overline{Q}_1)-\overline{s}\eta^2=0 \tag{1.12}$$

Adding (1.11) and (1.12) and using the relation in (1.9), we obtain

$$2D_1\overline{Q}_1-\overline{s}\eta=0 \tag{1.13}$$

The crossing point of (1.13) and the backbone curve of $\overline{Q}_1$ represents the amplitude of Q_1 at resonance and we can find the corresponding point of Q_2 on its backbone curve.

As to the dampings, we obtain from (1.11), (1.12) and (1.9) the the following formulas:

$$D_1=\{-\overline{m}\eta^2Q_2+\overline{m}\overline{\kappa}^2(\overline{Q}_2-\overline{Q}_1)-\overline{m}\overline{\kappa}^2\overline{\mu}^2(\overline{Q}_2-\overline{Q}_1)^3+\overline{m}\overline{\kappa}^2n_2(\overline{Q}_2-\overline{Q}_1)^5-\overline{m}\overline{\kappa}^2l_2(\overline{Q}_2-\overline{Q}_1)^7$$
$$+2\overline{m}\overline{\kappa}\eta(\overline{Q}_2-\overline{Q}_1)D_2\}/2\eta Q_1 \tag{1.14}$$

$$D_2=\{-\overline{m}\overline{\kappa}^2(\overline{Q}_2-\overline{Q}_1)+\overline{m}\overline{\kappa}^2\overline{\mu}^2(\overline{Q}_2-\overline{Q}_1)^3-\overline{m}\overline{\kappa}^2n_2(\overline{Q}_2-\overline{Q}_1)^5+\overline{m}\overline{\kappa}^2l_2(\overline{Q}_2-\overline{Q}_1)^7+\overline{m}\eta^2\overline{Q}_2$$
$$+\overline{s}\eta^2\}/2\overline{m}\overline{\kappa}\eta(\overline{Q}_2-\overline{Q}_1) \tag{1.15}$$

2. Analysis of Large Vibration Tests of A Pre-Stressed Concrete Structure

Vibration Tests[4] were performed on a two-storied frame structure of prestressed concrete construction by installing a small or a large shaking machine on the roof floor. In those tests eccentric moments *Mr* were 137 kg.cm and 3960 kg.cm respectively. In the case of small vibration no damage was done to the structure but, in the first large vibration test, many cracks appeared in the cement mortar filled in the connections of the frame. Keeping the eccentric moment of machine at a constant value, the test was continued and, in the third test, the steady state response features shown in Fig. 2 were obtained.

4) K. NAKAGAWA and others, "Vibration of A Prestressd Concrete Structure," *Report, Architectural Institute of Japan*, **31** (1955).

For this analysis we computed the relation between the restoring force and displacement of each story by using the period and amplitude at resonance, considering the structure as a system of two degrees of freedom, and obtained Fig. 3 where the results calculated frow small and large vibration tests are plotted.

In this figure we assume curves R_1 and R_2 for the first and second stories respectively. The numerical values used here are as follows:

$m_1 = 10300\ \text{kg}/980\ \text{cm.sec}^{-2}$
$\quad = 10.5\ \text{kg.sec}^2.\text{cm}^{-1}$

$m_2 = 15500\ \text{kg}/980\ \text{cm.sec}^{-2}$
$\quad = 15.85\ \text{kg.sec}^2.\text{cm}^{-1}$

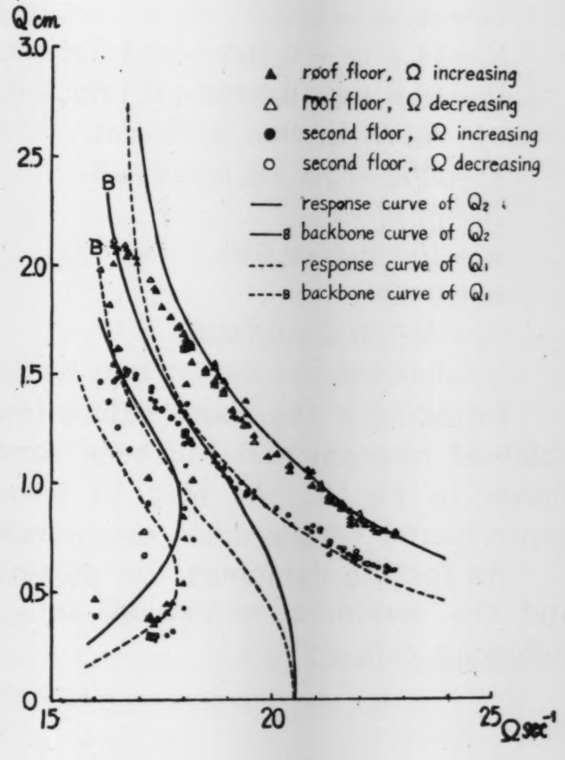

Fig. 2.

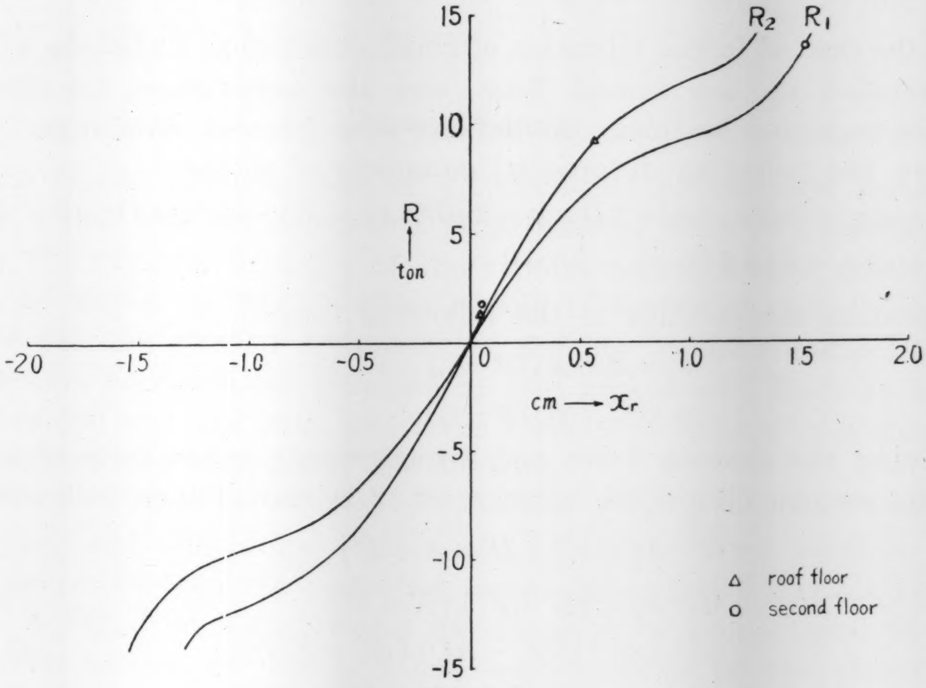

Fig. 3.

$\bar{m}=m_2/m_1=1.51$

$R_1=14.7\ (x_r-0.506x_r^3+0.147x_r^5-0.000267x_r^7)$

$R_2=18.8\ (x_r-0.506x_r^3+0.147x_r^5-0.000267x_r^7)$

R_1, R_2 in ton, x_r in cm.

$\bar{\kappa}^2=\kappa_2^2/\kappa_1^2=c_2/m_2\cdot m_1/c_1=0.846$

$\bar{\mu}^2=\mu_2^2/\mu_1^2=1$

$n_1=10\nu_1^4/9\mu_1^4=0.638$

$n_2=0.638$

$l_1=35\xi_1^6/27\mu_1^6=0.00266$

$l_2=0.00266$

Introducing the above values into (18.1), (18.2) (1.9) and (1.10), we obtained response and backbone curves for the undamped systems as shown in Fig. 2. As may be seen in this figure, the analytical and experimental results show considerable good agreement.

As for the dampings, by putting the resonant circular frequency and the maximum amplitudes into (1.14) and (1.15), we obtained the following values:

$$D_1=0.057 \qquad (1.14')$$

$$D_2=0.094 \qquad (1.15')$$

3. Analysis of Small Vibration Tests of the Same Structure

In the case of forced vibration of small amplitudes, a shaking machine was installed on the second floor, and the behavior of the structure could be regarded as linear oscillations with viscous dampings. Then, we have the following differential equations of motion:

$$\ddot{x}_1+\kappa_1^2x_1-\bar{m}\kappa_2^2(x_2-x_1)+2D_1\kappa_1\dot{x}_1-2\bar{m}D_2\kappa_2(\dot{x}_2-\dot{x}_1)-s\Omega^2\cos\Omega t=0 \qquad (3.1)$$

$$\ddot{x}_2+\kappa_2^2(x_2-x_1)+2D_2\kappa_2(\dot{x}_2-\dot{x}_1)=0 \qquad (3.2)$$

Representing the solution in the following forms

$$\left.\begin{aligned}x_1&=Q_1\cos(\Omega t-\gamma_1)\\x_2&=Q_2\cos(\Omega t-\gamma_2)\end{aligned}\right\} \qquad (3.3)$$

and giving the shaking force and displacements as the form of complex number, we can obtain the solution of (3.1) and (3.2) as follows:

$$Q_1=s\eta^2\sqrt{(C^2+D^2)/(A^2+B^2)} \qquad (3.4.1)$$

$$Q_2=s\eta^2\sqrt{(E^2+F^2)/(A^2+B^2)} \qquad (3.4.2)$$

$$\gamma_1=\tan^{-1}\{(BC-AD)/(AC+BD)\} \qquad (3.4.3)$$

$$\gamma_2=\tan^{-1}\{(BF-AF)/(AE+BF)\} \qquad (3.4.4)$$

where

$$\left.\begin{aligned} A&=\eta^4-(1+\bar{\kappa}^2+\bar{m}\bar{\kappa}^2+4D_1D_2\bar{\kappa})\eta^2+\bar{\kappa}^2\\ B&=2\bar{\kappa}(\bar{\kappa}D_1+D_2)\eta-2(D_1+\bar{\kappa}D_2+2\bar{m}\bar{\kappa}D_2)\eta^3\\ C&=\bar{\kappa}^2-\eta^2\\ D&=2\bar{\kappa}D_2\eta\\ E&=\bar{\kappa}^2\\ F&=2\bar{\kappa}D_2\eta \end{aligned}\right\} \qquad (3.5)$$

Numerical values for the small vibration test are as follows;

$Q_2=0.1\,\text{cm}, \qquad Q_2=0.057\,\text{cm}$

$Mr/m_1=0.0133\,\text{cm}$

$\bar{m}=1.51$

$\bar{\kappa}^2=c_2/(c_1\bar{m})=(29500\,\text{kg/cm})/(30600\,\text{kg/cm})\times\bar{m}=0.638$

$\eta^2=\Omega_r^2m_1/c_1=28.3\times10.5/30600=0.275$

where Ω_r=resonant circular frequency

Introducing the above values into (3.4.1) and (3.4.2), and calculating the values of D_1 and D_2 which satisfy both equations, we have

$$\left.\begin{aligned} D_1&=0.041\\ D_2&=0.029 \end{aligned}\right\} \qquad (3.6)$$

Comparing these values with those in large vibration, we find that the former is smaller than the latter.

4. General Results

In the forced vibration test of a two-storied pre-stressed concrete structure which was subjected to a large shaking force by a mechanical oscillator, the response behavior of the structure represented non-linear features as shown in Fig. 2 where Q and Ω denote the amplitude of each floor and the circular frequency of shaking machine respectively. The maximum accelerations obtained at roof and second floors at resonance were 580 and 420 gals, and some structural damage was done to the connections and columns of the skeleton.

In analysis of the test results, considerable good agreement between experimental and theoretical values are obtained, if we consider the relation curves between the restoring forces and relative displacements as shown in Fig. 3 and the viscous dampings to be proportional to the relative deformations for the first and second stories of the structure regarded as a system of two degrees of freedom. The fractions of

critical damping for the stories computed from the test results are 0.057 and 0.094, and those in the vibration of small amplitudes 0.041 and 0.029 respectively. It is noteworthy that the dampings assumed as viscous in large vibration are larger than those in small amplitudes.

The method presented in this paper may be considered as one of the analytical treatments for the steady state non-linear vibration of two-storied buildings.

The authors are greatly indebted to Professor K. Klotter of Stanford University for his guidance and advice. Thanks are also due to Mr. T. Uchida and Mr. T. Sato who were in charge of the computation.

---

44. 二層建物の非線形定常振動

建設省建築研究所 久田俊彦
中川恭次

プレストレスト・コンクリート造 2 階建建物の屋上に大型起振機を据えて之に大振動（屋上最大振幅約 2 cm，最大加速度 580 ガル）を与えるとその共振曲線は Fig. 2 に示したように非線形的性状を示し，構造体に相当の損傷を生じた．

この場合各階の復元力と相対変形の関係を Fig. 3 に示すような 7 次の曲線で表わし，且相対変形速度に比例する粘性減衰を各階がもつものとし，Ritz の方法で解を求めると実験結果をかなりよく説明出来るようである．この場合の減衰常数を実験値から求めると 1 階 0.057，2 階 0.094 となるが同じ建物の大振動前の微振動時（屋上最大振幅 0,1 cm）に於ける値は夫々 0.041，0.029 であつて大振動時の場合より小さい．

本報文に示した方法及び数値は二層建物の塑性定常振動の解析に関する一資料となるであろう．

45. The Fifth Explosion Seismic Observations carried out in North-eastern Japan.

By the Research Group for Explosion Seismology.*

(Read Nov. 24, 1953.—Received Sept. 30, 1955.)

1. Introduction

At 3 h 4 m 57.074 sec., Sept. 13, 1953, the second big blast was operated at the Kamaisi Mine of the Nippon Iron Works. The Research Group for Explosion Seismology made the observation which was the fifth opportunity in North-eastern Japan.

The blast operation was made in a similar way at a spot adjacent to the previous one[1]. The general features of the blast may be summarized as follows: (1) the aim was to remove dangerous gangue rocks as a safety measure, (2) the amount of explosives was 42 tons, (3) the blast was operated in seven steps, at nominal intervals of 20 milliseconds. However, according to our observation, it took 84 milliseconds instead of 120 milliseconds from the first to the last step.

A blast which is operated successively in several steps is less effective in generating elastic waves in the ground than a simultaneous blast

---

* Members of the group, who participated in the project are as follows (in alphabetic order):

T. AKIMA, S. ASANO, T. DAIKUBARA, M. HORI, I. KARAKAMA, K. KASAHARA, H. KAWASUMI, Naoyoshi KOBAYASHI, S. KOMAKI, H. MATUMOTO, T. MATUMOTO, S. MIYAMURA, K. MOGI, T. MORISITA, A. OKADA, K. OSADA, S. SAITO, M. SIBANO, E. SIMA, T. SUZUKI, H. TAJIMA, T. TANAKA, M. TSUJIURA, Y. YAMAZAKI, M. YANAGISAWA, M. WATANABE, (E. R. I.) K. AKAMATU, T. ASADA, N. DEN, M. MATUZAWA, Y. OGUTI, R. SATO, (*Geophys. Inst. Tokyo Univ.*) K. AIHARA, T. HASEBA, S. HISAMOTO, W. INOUYE, M. ICHIKAWA, E. KOBAYASHI, T. OGAWA, O. SAKAI, J. SUYEHIRO, T. USAMI, T. UTSU, (C. M. O.) A. ISHIGAKI, E. MINE, K. NAKAMURA, K. NORITOMI, G. OSSAKA, H. SIMA, Z. SUZUKI, A. TAKAGI, (*Geophys. Inst., Tohoku Univ.*) K. TAZIME, Y. UYEDA, S. YAMASITA, (*Akita Univ.*) S. SAKUMA (*Hokkaido Univ.*) H. HASEGAWA, M. HAYAKAWA, S. HURUYA, K. ICHIKAWA, T. KANEKO, K. MORI, S. NAGUMO, S. SANO, T. TATEISHI, J. CHUJYO, (*Geol. Surv.*) T. ASANUMA, S. HONDA, S. MURAUCHI (*Nat. Sci. Mus.*) A. KOZUKI, K. MIKUMO, E. NISHIMURA, K. OKANO, K. SASSA, I. TAMAKI, M. YOSHIKAWA, (*Kyoto Univ.*) S. ABE, T. HATTORI, G. MURAKAMI, T. SASAKI, T. SUGAWA, (*Mizusawa Lat. Obs.*) Naota KOBAYASHI, (*Chuo Univ.*) K. I-IDA, T. WADA, (*Nagoya Univ.*) I. MURAMATSU, (*Gifu Univ.*) T. HAGIWARA (*Miyamoto Explor. Co.*).

1) The Research Group for Explosion Seismology, *Bull. Earthq. Res. Inst.*, **32** (1954) 79.

with the same amount of explosives used. Taking this fact into account, we laid out the most sensitive instruments at every 20 km. from $\Delta=170$ km. The main purpose of the present observation was focussed upon ascertaining the existence of a layer of 8.2 km./sec. which had been expected in the past experiment[2]. No stations were set up farther than $\Delta=332$ km. and to the west of the blast point.

In addition to these stations, a special station was established at Umanokiuti, $\Delta=4.63$ km., to make observations of reflected waves.

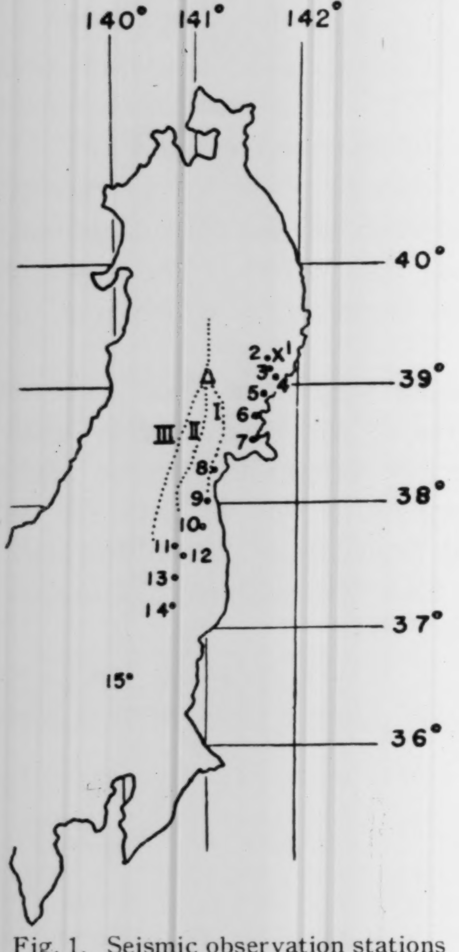

Fig. 1. Seismic observation stations for the 2nd Kamaisi explosion.

△: Isibuti
I: The 1st seismic explosion observation.
II: The 2nd seismic explosion observation.
III: The 3rd seismic explosion observation.

2. Observations

Stations, epicentre, seismographs and observers are listed in Table I, and the distribution of stations is shown in Fig. 1. The electromagnetic seismographs principally used were of proper frequency of 3 c/s and those of 10 c/s and 1 c/s were also supplementarily used. In Mukaiyama, Kawamata, Siraiwa, Nogisawa and Motegi, two or three seismographs were connected in series in order to increase the sensitivity for the seismic waves relative to the noise. As for the amplifier, some new types were employed. In Kanayama a smoked-paper recorder converted from a pen-recording galvanometer was used, with quite satisfactory results.

For time keeping, in addition to receiving directly the radio time signals, we also had the J. J. Y. especially broadcast in medium frequency band by the Nippon Hōsō Kyōkai (N.H.K.) in cooperation.

2) The Research Group for Explosion Seismology, *loc. cit.*, 1).

Table I.

	Station	λ (E)	φ (N)	Δ km	Electro-magnetic Seismograph	Observers
1	Shot point	141°41′32″.9	39°17′39″.9	0~2	10 c/s Vert. E.T.L.	Mori, Kojima
2	Umanokiuti	38 15.4	17 24.4	4.63	SIE-P-11.	Yamazaki, Kobayashi (Naota), Koike
3	Nakasone	39 10.4	11 56.4	11.2	3 c/s Vert.	Mikumo, Nakagawa, Tsushima
4	Sakari	42 46.	04 48.	23.92	3 c/s Vert.	Shima, Shibano, Yanagisawa
5	Kesenuma	34 31.0	38 53 57.4	45.04	3 c/s Vert., Hor.	Matsumoto (T), Karakama
6	Sizugawa	26 35.2	40 24.4	72.25	3 c/s Vert. 1 c/s Hor.	Tanaka, Suzuki (T)
7	Onagawa	27 26.9	26 14.7	97.32	3 c/s Vert., Hor.	Noritomi, Takagi, Osaka
8	Mukaiyama	140 51 32.4	14 33.7	137.38	3 c/s Vert., Hor. 1 c/s Hor.	Usami, Uzu, Ogawa
9	Funaoka	46 43.5	02 50.7	159.6	3 c/s Vert.	Kobayashi (Naoyoshi), Saito
10	Kanayama	47 53.1	37 53 46.0	173.67	3 c/s Vert., Hor.	Akima, Matsumoto (H)
11	Ōsasao	25 17.9	48 16.3	199.04	3 c/s Vert.	Kasahara, Sato (R)
12	Kawamata	37 07.4	40 39.0	202.46	3 c/s Vert.	Tazime, Asano, Akamatsu
13	Siroiwa	29 31.7	29 37.3	225.71	3 c/s Vert.	Den, Hasegawa, Kato
14	Nogisawa	25 05.2	10 05.8	261.04	3 c/s Vert. 1 c/s Hor.	Murauchi, Asanuma, Uchida
15	Motegi	11 42.1	36 33 08.9	331.59	3 c/s, 0.7 c/s Vert.	Suzuki (Z), Mine, Ishigaki

3. Results of Observation

Fortunately, the first motion could be clearly identified in most stations, and a phase corresponding to S was also identified in almost every station.

The data are tabulated in Table II, and the travel-time curves in Fig. 2. Reading was made independently by several persons, and no appreciable discrepancy was found.

Table II.

Shot time: $03^{h}04^{m}57^{s}.074$

Station	Δ km	P		S	
		I	II or II′	I	II or II′
1	0~2				
2	4.63	$3^{h}\,04^{m}\,57^{s}.976$			
3	11.2	59.10			
4	23.92	05 01.15		$05^{m}\,04^{s}.48$	
5	45.04	04.65		10 .78	
6	72.25	09.03			
7	97.32	13.10		25.24	
8	137.38	20.00		37.48	
9	159.6	23.07			
10	173.67		$05^{m}\,25^{s}.20$		$05^{m}\,47^{s}.45$
11	199.04				
12	202.46		28.89		54.13
13	225.71		32.38		59.53
14	261.04				06 06.54
15	331.59		46.1		

The equations of travel-times derived by the method of least squares are:

$$\text{I}: \quad t=\frac{\Delta}{6.05\pm0.03}+(-2.83\pm0.05)\,,$$

$$\text{II}: \quad t=\frac{\Delta}{7.27\pm0.22}+(1.22\pm0.85)\,, \qquad \text{(sec. and km.)}$$

and

$$\text{II}': \quad t=\frac{\Delta}{7.55\pm0.10}+(2.23\pm0.42)\,.$$

I corresponds to the direct wave, and both II and II′ to the refracted

wave. The Funaoka Station happened to be situated nearly on the intersection of Line I and Line II, and therefore this point was omitted in deriving the equation. Since the time accuracy in the farthest station Motegi is relatively low owing to the disturbance caused by the preceding

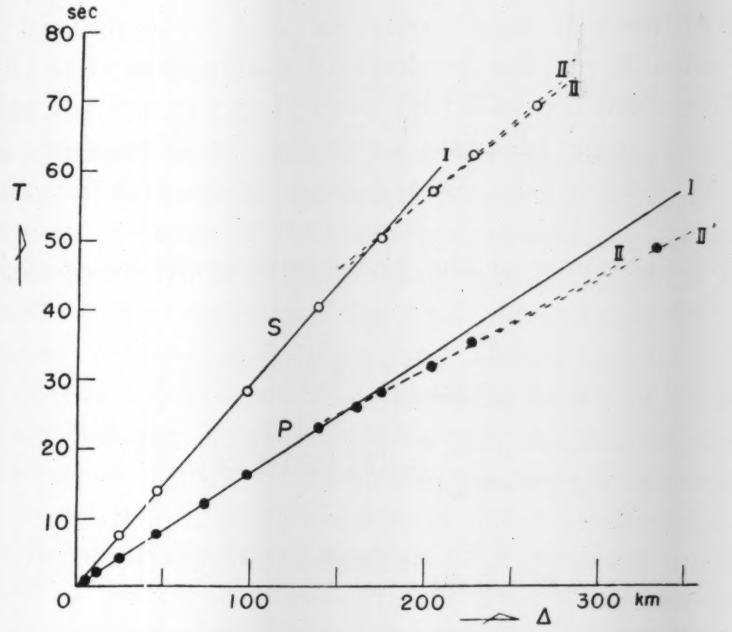

Fig. 2. Travel-time curves obtained from the 2nd Kamaisi explosion.

natural earthquake, this station was excluded in deriving equation II, and included in equation II'. Assuming that the layers are horizontal, the depths are:

from I and II $\qquad Z_{12} = (22.2 \pm 4.9)$ km.

from I and II' $\qquad Z_{12'} = (25.6 \pm 2.2)$ km.

As for the velocity in the upper layer, the value in the previous experiment was 6.19 km./sec., and that in the present blast is 6.05 km./sec. In the southern profile of the second Isibuti blast it was 5.91 km./sec. and in the eastern profile, 6.08 km./sec.[3] In the third Isibuti blast, in the southern profile the velocity was 5.98 km./sec. Some differences are found as stated above[4]. As for the lower layer, the velo-

3) The Research Group for Explosion Seismology, *Bull. Earthq. Res. Inst.*, **30** (1952), 279.

4) The Research Group for Explosion Seismology, *Bull. Earthq. Res. Inst.*, **31** (1953), 281.

city of 8.2 km./sec. which was considered most probable in the previous experiment could not be found, but a velocity which may correspond to the 7.37 km./sec. which was considered the next most probable in the previous experiment was found. Therefore the difference in computed depths in the present and previous experiments is of an order of 10 km. Though these differences may partly be due to errors in observation, they mostly arise from the inadequate assumption that the layers are horizontal. Therefore the velocities derived so far are all apparent ones, and by assuming some adequate structure the differences are supposed to be explained reasonably. Our future study will be aimed at this problem.

The travel-time curve of the phase corresponding to S is also shown by a broken like,

$$\text{I}: \quad t=\frac{\Delta}{3.46\pm0.03}+(-2.42\pm0.25)\,,$$

$$\text{II}: \quad t=\frac{\Delta}{4.75\pm0.14}+(11.65\pm1.46)\,,$$

and

$$\text{II}': \quad t=\frac{\Delta}{4.57\pm0.09}+(9.68\pm0.97)\,.$$

In this case, the Kanayama Station coincides with the break point of the curve, therefore II excludes the station and II′ includes the station on the assumption that the first motion is the refracted wave.

Thus the depths are

from I and II $Z_{12}=(35.8\pm4.0)$ km.

and from I and II′ $Z_{12'}=(32.4\pm2.9)$ km.

which are about 10 km. greater than those computed from P waves.

Fig. 3 is the record of reflected waves. By reducing the weathered layer correction, it is found that 12 components indicate nearly the phase, and the phase, therefore, is undoubtedly the reflected wave from below. Its travel-time is 7.33 sec., and the depth derived from the formula

$$(6.05\text{ km./sec.}\times7.33)/2=\{(5\text{ km./2})^2+Z^2\}^{1/2}$$

is 22.13 km. This value agrees fairly well with the depth $Z_{12}=22.2$ km. which is derived from I and II of P wave. A phase clearly recorded shortly after the first motion is still to be definitely interpreted. Other phases due to multiple reflections or reflection at a supposed discontinuity of 32–35 km. in depth are not yet identified.

Though reflection method is very popular in seismic prospecting, reflected waves from a depth of scores of kilometres have very rarely been recorded. Therefore, the present result is of great importance, and this method seems to be a promising one in the future explosion seismology.

4. Summary

In the present experiment, effort of observation was concentrated in a region to the south of the blast point and with Δ within 300 km. From P waves, a layer of 6.05 km./sec. should overlie a lower layer of 7.2 or 7.6 km./sec. with a corresponding thickness of 22 or 25 km. This result is sufficiently supported by the observation of reflected waves. From S waves, a layer of 3.46 km./sec. should overlie a layer of 4.5 or 4.8 km./sec. with a corresponding thickness of 32 or 36 km.

As stated before, discrepancies in the results of the past several experiments arise probably from the inadequate assumption that the crustal structure is uniformly horizontal. The accumulation of data made so far may be sufficient for deduction of a more complicated structure which must be nearer the real state. This deduction should be made with all the available data by taking the geological and gravitational evidences into consideration.

5. Acknowledgement

Our sincere gratitude goes to the following organizations for their kind cooperations. Without them, successful results would not have been obtained. They are Tokyo Central Station, Sendai Central Station and Morioka Station of N.H.K., Kamaisi Iron Works, Tohoku District Construction Office of the Ministry of Construction, Sendai Central Headquarters and Morioka Central Headquarters of National Police, Morioka Administrative Office of National Railroad, Morioka, Kamaisi and Kassi Telephone Offices, and the village and town offices where our stations were established. The Radio Time Signal Committee, the Broadcast Station of Standard Frequency and the Institute of Astronomy of Tokyo University gave us important helps for this experiment.

Financial aid for this experiment was partly granted by the Ministry of Education.

Note: The interpretation in this paper is based on the present

observations alone, and other series of observations in the same region are entirely disregarded. A general analysis on all the available data has partly been presented orally before the general convention of I. U. G. G. in Rome, 1954. A printed publication shall follow in the near future.

---

45. 東北日本に於ける第 5 回爆破地震動観測

爆破地震動研究グループ

1953 年 9 月 13 日に日鉄鉱業釜石鉱業所に於いて前回の 1952 年 12 月 7 日の大爆破に引続き第 2 回の爆破作業が実施せられた．爆破は前回同様落盤による災害発生防止のため脈石除去を目的とし，場所は前回の隣接地点で薬量は総計約 42 ton である．但し爆発は計画によれば 20 ms づつおいて 7 段に分けてなされ，観測によると初段より終段まで 84 ms を要した．爆破時刻は前回迄と同様な方法により，オッシログラムより $3^h\,04^m\,57.074^s$ と求められた．

地震動観測は，前回予想せられた 8.2 km/sec の速度の検討を主眼とし南方測線のみ 15 点で行い，使用計器は略前回同様である（第 I 表，第 1 図）．今回は，各点で良好な記録が得られ主な位相の読みは第 II 表の如くで，走時曲線は第 2 図に示されている．直線として最小自乗法で求めた初動に対する式は次の如くである．（単位は Δ: km; t: sec.）

$$\text{I}: \quad t=\frac{\Delta}{6.05\pm0.03}+(-2.83\pm0.05)$$

$$\text{II}: \quad t=\frac{\Delta}{7.27\pm0.22}+(1.22\pm0.85)$$

$$\text{II}': \quad t=\frac{\Delta}{7.55\pm0.10}+(2.23\pm0.42)$$

不連続面の深さ:

I, II より $Z_{12}=(22.2\pm4.9)$ km.

I, II′ より $Z_{12'}=(25.6\pm2.2)$ km.

最も遠い茂木は誤差 0.1 s 以内であるが時間の精度が稍々悪いため，II はそれを含めて計算した式であり，II′ はそれを除いて求めた式である．この結果，上層の速度は，各観測毎に多少の差異があり，又，前回の 8.2 km/s の速度は認められない事が判つた．この様な点に関し，我々は，東北地方に於いてかなりの資料を集めたので今後統一的に考えてみる事が必要である．

又，今回は S 波に相当する位相もかなり明瞭に認められ，最小自乗法で求めた式は次の如くである．

$$\text{I}: \quad t=\frac{\Delta}{3.46\pm0.03}+(-2.42\pm0.25)$$

$$\text{II}: \quad t=\frac{\Delta}{4.75\pm0.14}+(11.65\pm1.46)$$

$$\text{II}': \quad t=\frac{\Delta}{4.57\pm0.09}+(9.68\pm0.97)$$

不連続面の深さ:

I, II より $Z_{12}=(35.8\pm4.0)$ km.

I, II′ より $Z_{12'}=(32.4\pm2.9)$ km.

II, II′ を求めた意味は，金山が丁度 I, II の交点付近に当り，II はそれを除いて計算した式であり，II′ は P 波の結果よりそれを含めて求めた式である．P 波に比して精度が劣る事は否定出来ないが，上の如く定め得た意義は大きいものと考えられる．

更に今回は反射波の記録をとるために $\Delta=4.67$ km の馬木内に観測点を設けたが，反射波をとら

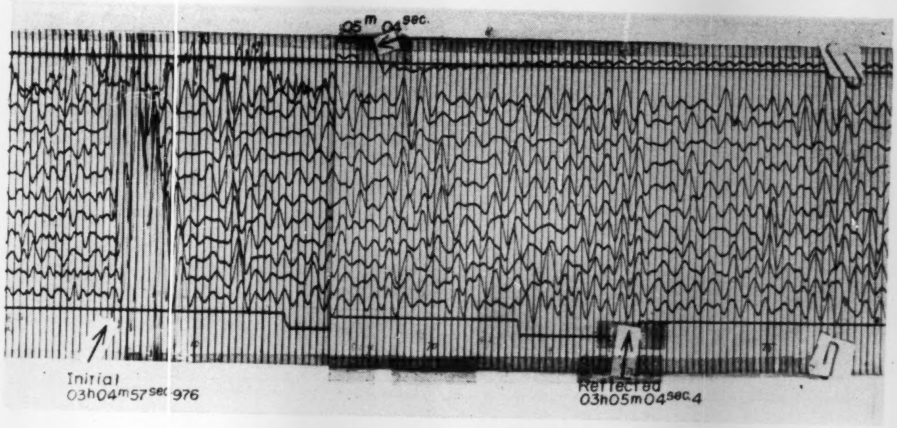

Fig. 3. Record of Reflection Wave at Umanokiuti.

(*A*)

(*B*)

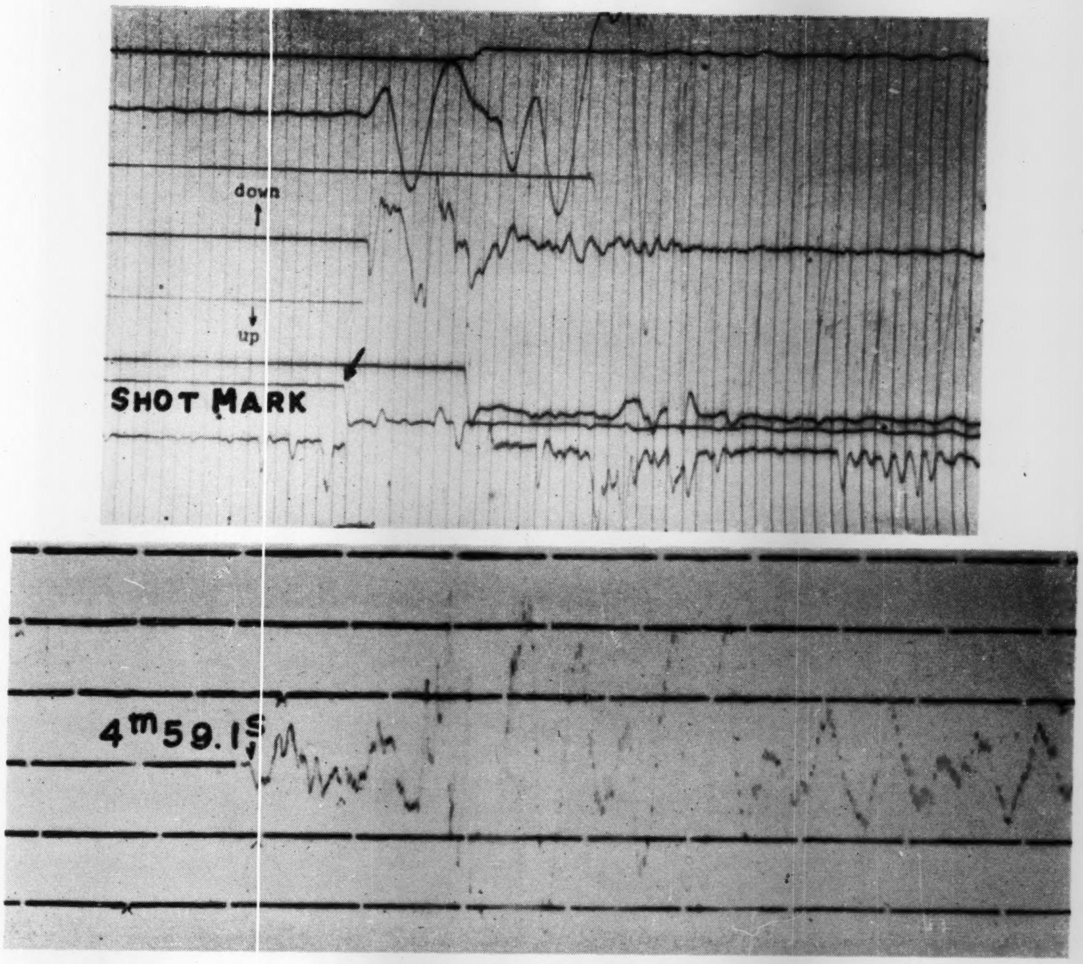

Fig. 4. Seismograms obtained at Shot point (*A*) and Nakasone (B).

(A)

(B)

(C)

(D)

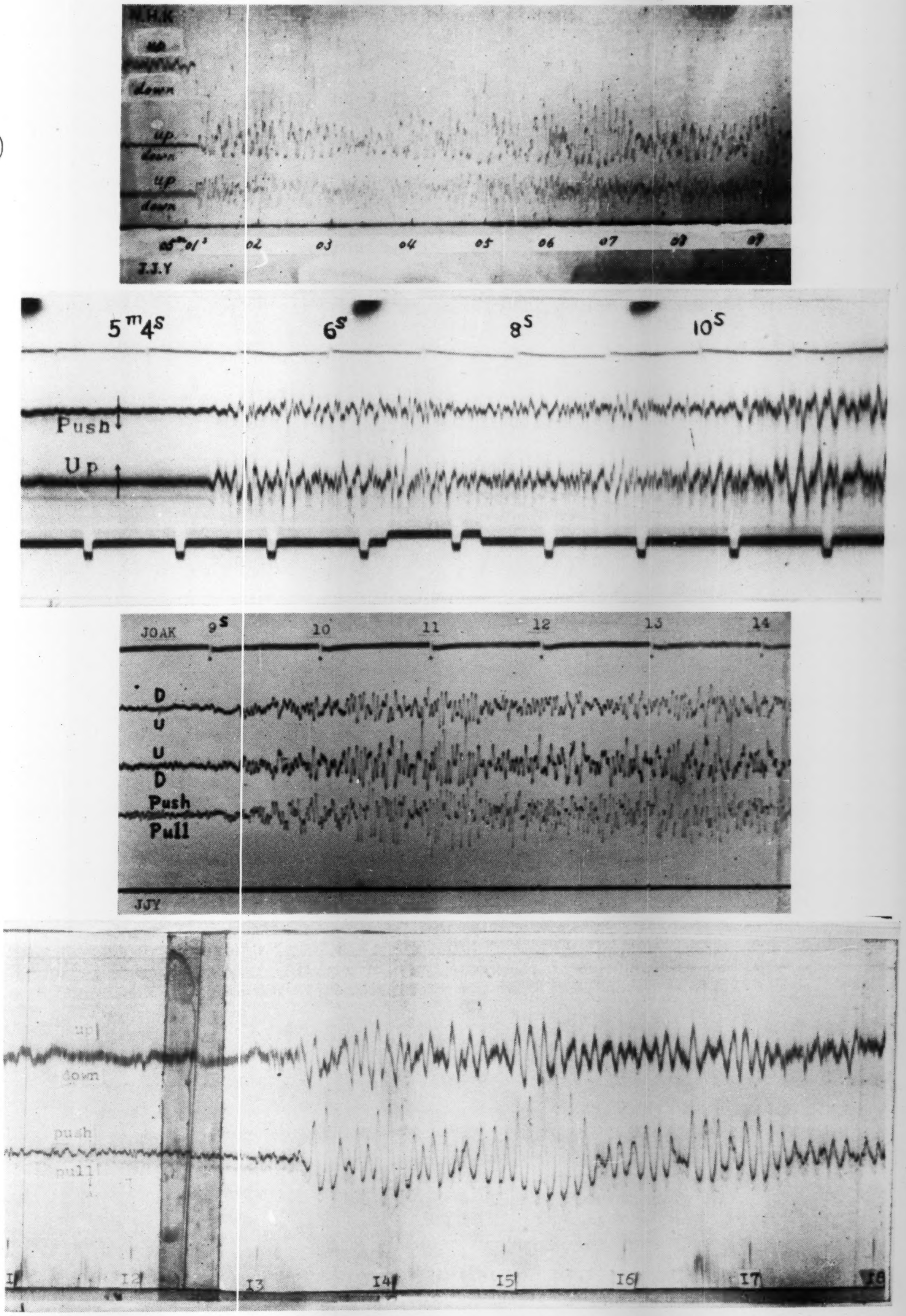

Fig. 5. Seismograms obtained at Sakari (*A*), Kesennuma (*B*), Sizugawa (*C*) and Onagawa (*D*).

(A)

(B)

(C)

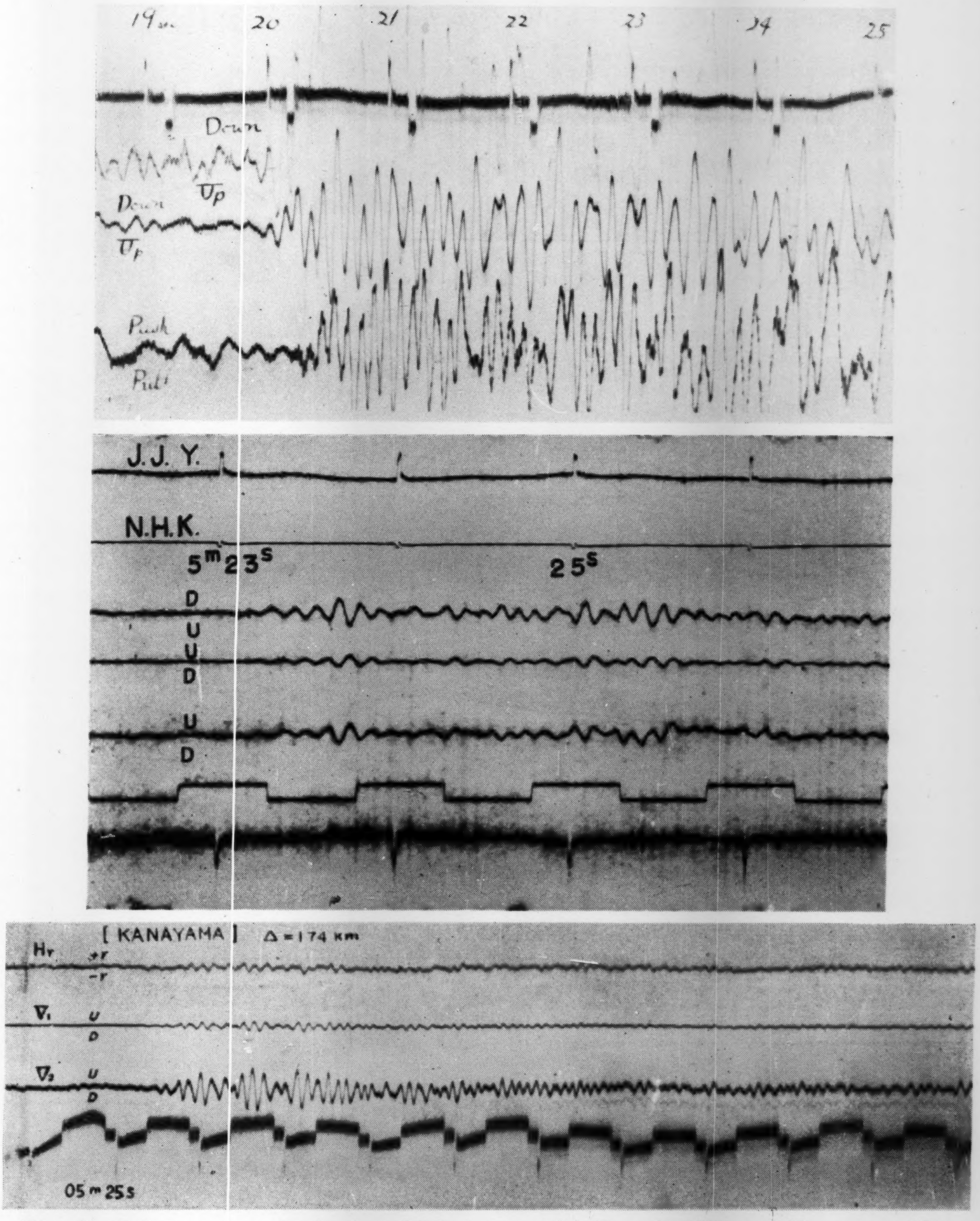

Fig. 6. Seismograms obtained at Mukaiyama (*A*), Funaoka (*B*) and Kanayama (*C*).

（震研彙報 第三十三号 図版 爆破地震動研究グループ）

(*A*)

(*B*)

(*C*)

(*D*)

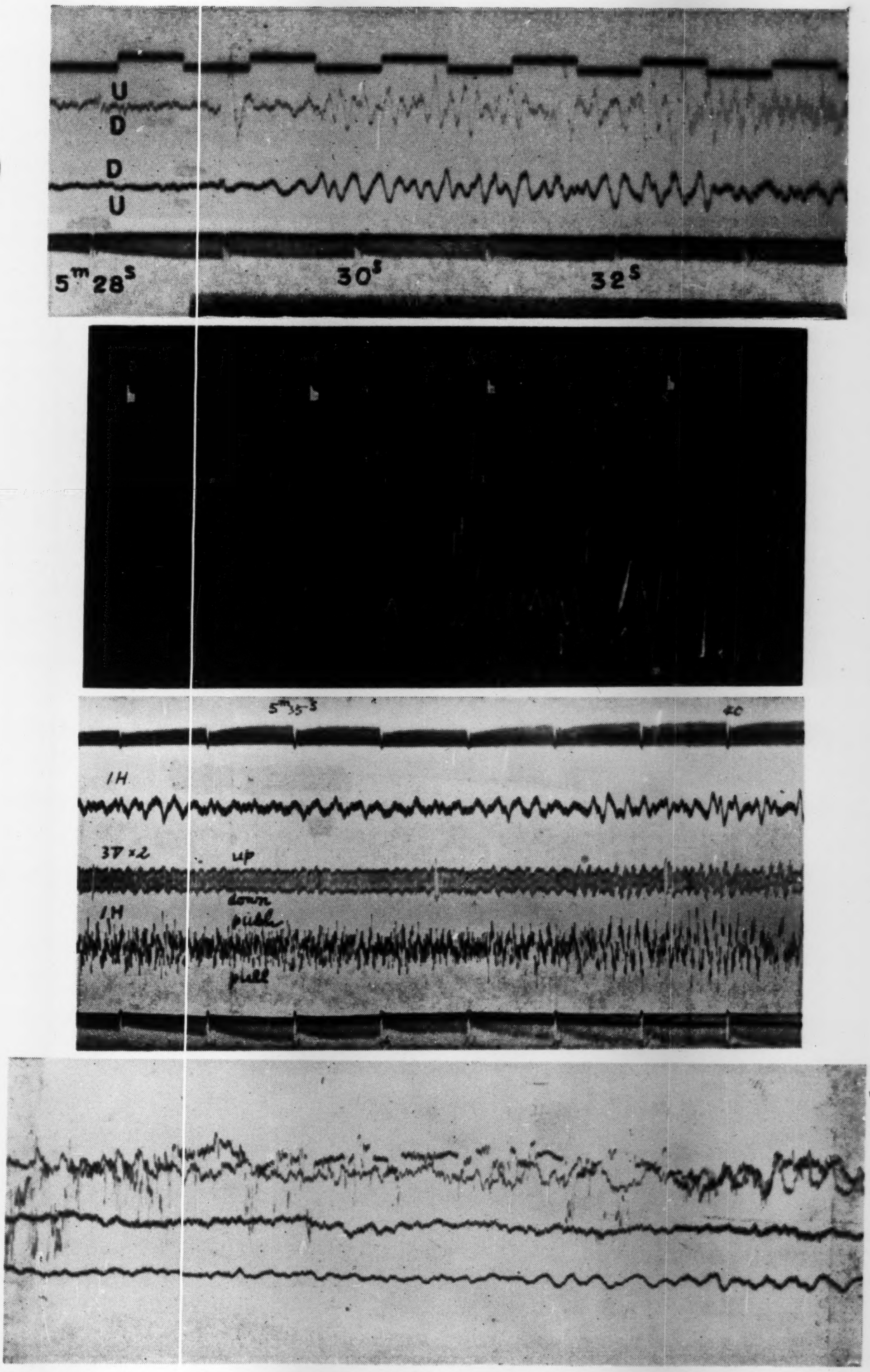

Fig. 7. Seismograms obtained at Kawamata (*A*), Siroiwa (*B*), Nogisawa (*C*) and Motegi (D).

（震研彙報 第三十三号 図版 爆破地震動研究グループ）

える事に成功し，その走時は 7.33 秒でこれより反射面の深さは 22.13 km と求められ，P 波より求めた深さ $Z_{12}=22.2$ km と非常によく一致した結果が得られ，今後新しい有力な手段として大いに期待している．

尚，今回の実験についても前回同様多大の御協力を賜つた日鉄鉱業釜石鉱業所；N.H.K. 東京中央放送局，仙台中央放送局，盛岡放送局；建設省東北地方建設局；国警仙台管区本部，同岩手県本部；盛岡鉄道管理局；電々公社盛岡電話局，釜石電話局，甲子郵便局；各観測点所在官民各機関及び各観測班附属機関関係者各位に篤く御礼申し上げる次第である．

尚，本研究経費の一部は文部省科学研究費によるものである．記して謝意を表する．

註　尚，本報告に於ける結果は，今回の観測のみを用いて独立に整理されたものである．今迄東北地方で合計 5 回の爆破地震動の観測が行われているが，その全部の資料を統一的に説明する地殻構造は既に求められ，1955 年 9 月 ローマに於ける I.U.G.G. の総会で発表せられており，近き将来印刷される．

46. 局地的地震観測網のための有線搬送式遠隔刻時装置

地震研究所 { 宮村摂三
辻浦賢

(昭和 26 年 2 月 20 日発表—昭和 30 年 8 月 31 日受理)

§1. はしがき

地震観測における刻時の重要性についてはすでに充分認識されているが，特に近地地震，局地的地震群，余震群などの観測では，非常にたかい精度の刻時が要求される．近地地震で 1/10 秒の時間精度が必要とすれば，局地的地震の観測では，それは 1/100 秒の精度に達することがのぞましい．もちろん，この時刻精度は絶対時刻の必要はなく，所要の観測網内の各点が共通の時計で支配されてさえいればよい．地震観測に標準電波による天文台の時計からの分秒報時 (たとえば JJY, 4 Mc) を利用することは，すでに実用されているが，それを各観測点で直接地震記録記象に記入する方式は，非常にのぞましいにもかかわらず，実際上なかなか困難があつて，うまくゆかない．実際には大抵，地震記象には時計により刻時を記入し，別に時計と JJY の信号をクロノグラフにとるか，あるいわ1日のうち何回か記象に JJY をも直接記入するという形式が採用される．フェーディング，雑音，混信等で地震記象がよごされることをさけるためでもある．高い時刻精度をえるためには，一方，記録紙速度をはやくし，刻時間隔をせばめることが，記録紙速度の一様性の向上をはかるよりずつと楽でかつ有効であることも強調したい．分秒接点をもつ精巧な標準時計 (Chronometer) を局地地震観測のための臨時的観測網の各点にそなえることは，経費も高いし，運搬に手がかかり，また，精度もそろわず，規制にともなう換算などでまちがえも生じやすい．また，よほど精巧な時計でないかぎり，1 日に数回以上の標準時報による規制を必要とする．

これらの点を考慮すると，局地的地震観測網に対しては，独自の刻時を，一つの基地点においた標準時計から送信して，この同一の信号を，その観測網の各点で受信し，これを地震記象に直接記入する方式をとるのが一番よいとおもわれる．このような方式によれば，それぞれの観測目的に応じた刻時をおくりだすことができ，また種々の必要とする合図をも，各点の記象紙上に直接同時にあたえることができる．またその送信に音声回線をもうけるなら基地からの連絡通話も可能となり，その指令にもとづき一整に各点の記象紙とりかえ，記録のスタートを規制するなどの便もえられる．

このような臨時的地震観測網のための遠隔刻時装置として，われわれは 1946 年ごろから無線周波帯域 (100～300 kc) で，簡単な有線搬送方式による遠隔伝送装置の開発をここ

ろがけ，1950 年すでに報告したような装置を試作した[1]．これをいま LTC–I 型 (Line Telerecording Chronograph, Type I) となづける．1953 年和歌山附近頻発地震群の臨時観測にはこれを利用して，精密観測の効果をあげることができた．[2] 翌 1954 年には観

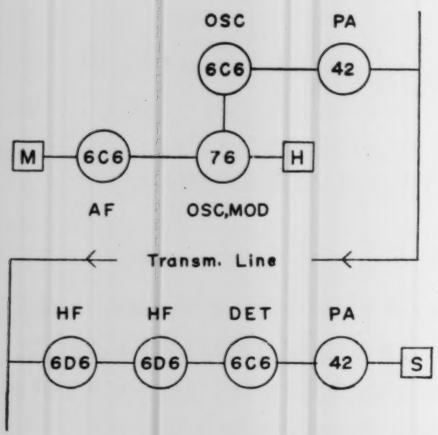

第 1 図 有線搬送式遠隔刻時装置 LTC–I 型構成図． Schematic diagram of Line Carrier Telerecording Chronograph, Type LTC–I.

送信機 Transmitter.

M: マイクロホン Microphone; 6C6. AF: 音声増幅管 Audio Freq. Amplifier; H: 標準時計 Chronometer; 76. OSC, MOD: 発振変調管 AF Oscillation (600 c/s) and Modulation Tube; 6C6 OSC: High Freq. (Carrier Freq.) oscillator; (100～200 kc variable) 42 PA: 送信出力管 Transmitting Power Amplifier.

受信機 Receiver.

6D6 HF: 高周波増幅管 High Frequency Amplifier; 6C6 DET: 検波管 Detector; 42 PA: 出力管 Power Amplifier; S: 地震計刻時装置 Seismograph Time-marker.

伝送線 Transmission Line.

電力会社，営林署などの専用電話線を利用． Telephone Network of Electric Company Bureau, Forestry Bureau, etc.

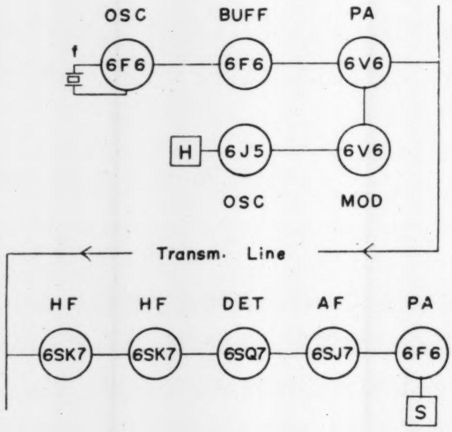

第 2 図 有線搬送式遠隔刻時装置 LTC–II 型構成図． Schematic diagram of Line Carrier Telerecording Chronograph, Type LTC–II.

送信機 Transmitter.

H: 標準時計 Chronometer; 6J5 OSC: 音声周波発振管; AF. Oscillator; 6V6 MOD: 変調管 Modulator Tube; 6F6 OSC: 水晶制禦搬送周波発振管; Crystal controlled H.F. Carrier oscillator (f=100 or 150 kc); 6F6 BUFF: 緩衝管 Buffer Tube; 6V6 PA: 送信出力管 Transmitting Power Amplifier.

受信機 Receiver.

6SK7 HF: 高周波増巾管 H.F. Amplifiers; 6SQ7 DET: 検波管 Detector; 6SJ7 AF 音声周波増巾 A.F. Amplifier; 6F6 PA: 出力管 Power Amplifier; S: 地震計刻時装置 Seismograph Time-marker.

伝送線 Transmission Line

電力会社．営林署などの専用電話線を利用． Telephone Network of Electric Company, Forestry Bureau, etc.

---

1) 宮村摂三・辻浦賢 既設電話線利用搬送方式による地震観測刻時伝送および保守通話 (S. MIYAMURA, M. TSUJIURA, Pri la transdono de temposignaloj kaj parola komuniko por sisma observado pere de la alt-frekvenca telefonado tra la funkianta telefon-fadeno.) *Zisin* (*Journ. Seism. Soc. Japan*), [ii] **4** (1951). No. 2.

2) 宮村摂三・外 和歌山附近頻発地震群の観測 (第 2 報). 1954 年 3 月 23 日第 309 回地震研究所談話会.

測網の拡充にともない，さらに送信出力をまし，安定度をたかめた LTC–II 型をつくった[3]．これらについて，ここに，その概要を報告する次第である．

§2. 装置の概要

LTC–I 型の送信機および受信機の構成はすでに発表したとおり[1]，ほぼ第 1 図のごときものであり，外観は第 3 図の写真にみられるとおりである．若干の要項は第 I 表にしめす．

LTC–II 型の構成は第 2 図のとおりであり，外観は第 3 図にしめす．LTC–I 型とことなるおもな点は，送信機においては水晶によつて発振周波数を固定し，きりかえにより 100 kc または 150 kc で送信できるようにしたこと，電源を別とし，送信部は現用，予備の 2 組をもち，故障に対しただちにきりかえて，刻時送信の中断をきたさぬようにしたこと，などである．現場で継続的に使用するという目的に適するよう，種々細部の工夫を加えたことはいうまでもない．器械の要点は第 I 表にまとめてある．使用周波数は，送受信端のあいだの距離，分岐線の状況などにより適当なものをえらぶよう I 型では 100 ～300 kc の可変としたが，和歌山での経験では II 型のように 2 波程度のきりかえで充分

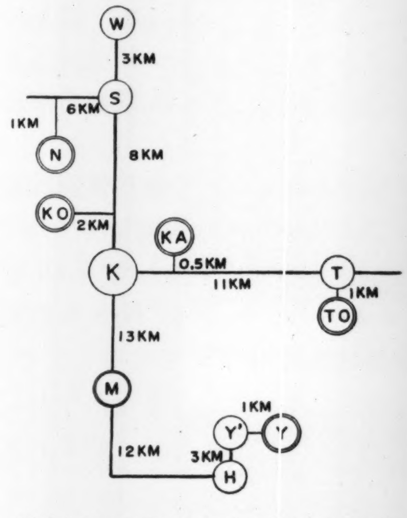

第 4 図　和歌山地震群臨時観測網における関西電力専用電話線による有線搬送式遠隔刻時系統図．(細線は地震観測用臨時架設線) Time Signal System for Local Temporary Network of Wakayama Earthquake Swarms by LTC through Telephone Lines of Kansai Electric Company (Thin lines are especially installed lines for the observation)

刻時送信基地 Time Signal Transm. Base	K:	海南変電所 [海南市筑地]; (Kainan Transformer Station, Tukizi, Kainan
地震観測点 Seism. Stations	N:	星林高校 [和歌山市西浜] (Seirin High School, Nisihama, Wakayama)
	KO:	琴浦発電所 [和歌山市毛見] (Kotonoura Electric Power Plant, Kemi, Wakayama)
	KA:	海南高校 [海南市大野中] (Kainan High School, Ōnonaka, Kainan)
	TO:	大成高校 [東野上町動木] (Taisei High School, Todoroki, Higasinogami)
	M:	箕島変電所 [有田町箕島] (Minosima, T.S., Minosima, Arita)
	Y:	耐久高校 [湯浅町湯浅] (Taikyu High School, Yuasa)
分岐点 Branch Points	W:	和歌山変電所 [和歌山] Wakayama T.S., Wakayama)
	S:	カマ山散宿所 [三田] (Kamayama Branch Point, Santa)
	T:	動木変電所 [東野上町] (Todoroki T.S., Higasinogami)
	H:	広変電所 [広町] (Hiro T.S., Hiro)
	Y':	湯浅営業所 [湯浅町] (Yuasa Branch Office, Yuasa)

3) 宮村摂三・外　和歌山附近頻発地震群の観測，中間報告．1954 年 11 月 3 日地震学会第 14 回学術講演会 (京都)．

第 I 表 有線搬送式遠隔記録刻時装置 LTC-I 型, LTC-II 型要項
Essentials of line telerecording chronograph, LTC-I and LTC-II.

	LTC-II			LTC-I	
	送信機 Transmitter		受信機 Receiver	送信機 Transmitter	受信機 Receiver
	Transmitter	Power Supply			
外形	550× 230× 430 mm	270× 230× 450 mm	220× 170× 350 mm	190× 160× 330 mm	240 ×190 ×400 mm
重量	13 kg	16 kg	5 kg	5 kg	7 kg
真空管	GT 5	GT 1, ST 1	GT 6	ST 5	ST 5
電源	DC 350 V DC 250 V AC 6 V	AC 100 V 50～60 c/s 100 W	AC 100 V 50～60 c/s 40 W	AC 100 V 50～60 c/s 60 W	AC 100 V 50～60 c/s 40 W
備考	現用・予備 組込				

であつた．線路状況の天候其他による変化も受信感度の低い場合は影響があるが，線路の減衰よりも，分岐点における結合容量 (0.01 μF) による低下がいちぢるしく，2 個所以上の分岐をへるとほとんど実用不能であつた．濾波器なしの簡易搬送としての限界と思われる．

1954 年度和歌山におけるこの有線搬送式刻時系統は関西電力株式会社の専用電話線系統による第 4 図のごときものであり，基地海南変電所より湯浅町耐久高校観測室までは 3 中継を要するので，箕島変電所にて LTC-I 送信機により，波長をかえて中継している．石本式加速度計 3 成分をそなえた N, KO, KA, TO, M, Y の 6 点のうち，N は N-S の線路が非常にわるかつたことと，S-KO 間に有線搬送式遠隔記録地震計 (LTS) をのせたため，それが刻時 (LTC) の搬送波よりたかい水準ではいり，周波数分離が充分できなかつたので失敗したが，その他の 5 点は，ほぼ良好な刻時を受信記録することができ，約 2 ケ月の精密観測に成切した．

§3. 謝　　辞

本装置の開発については，初期において，もと本所職員島津孝，竹野清両氏の協力をえた．実験段階においては東京電力（当時関東配電）株式会社工務部の御後援をえたが，特に西山給電係長（現東電通信課長）はじめ給電課の方々，田畑・花畑・市川・越谷・小松川各変電所の方々にお世話になつた．和歌山における観測に実用するにあたつては，関西電力株式会社工務部，同火力事務所，同和歌山支店，特に電路課の後援助をうけ海南・野上・広・箕島各変電所，琴浦発電所其他のお世話になつた．これらの御後援に対してここに心から感謝の意を表したい．

なお本装置の開発施設に要した実験費，設備費は文部省科学研究費，本所特殊研究費（大地震危険地帯の地球物理的研究），および和歌山県よりの援助によるものである．

LTC. I 送信機 (Transmitter) 標準時計 (Chronometer) 無線時報受信機 (Time Signal Radio Receiver)

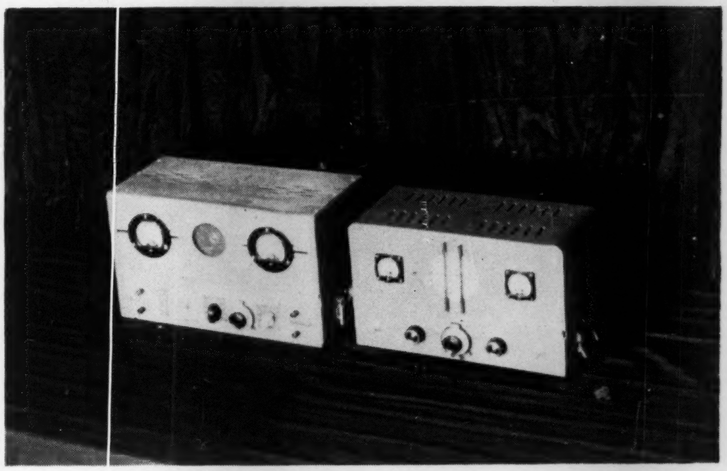

LTC. I 受信機 (LTC. I Receiver) LTC. II 受信機 (LTC. II Receiver)

交流電源部 (AC Power Supply) 送信部 (現用・予備) (Transmitter) 標準時計 (上) (Chronometer)

LTC. II 送信機 (LTC. II Transmitter) 無線時報受信機 (下) (Time Signal Radio Receiver)

第3図 有線搬送式遠隔刻時装置 LTC. I 型および LTC. II 型
(Line Carrier Telerecording Chronographs, Type LTC. I and LTC. II.)

46. *Line Carrier Telerecording Chronograph (abbr. LTC) for Local Seismological Network.*

By Setumi MIYAMURA and Masaru TSUJIURA,

Earthquake Research Institute.

Since 1946 the authors have developed a telerecording chronograph making use of the high-frequency carrier waves of 100–300 kc through civil telephone lines, for the purpose of giving accurate time marks and other necessary signals, including vocal communications, from a central base station of local seismological network to its branch stations. As early as in 1950 they constructed a simple practical transmitter and receiver for this time-marking system (cf. Ref. 1). They introduced it into their seismological network on the occasion of swarm earthquake of Wakayama in 1953. The result was satisfactory. It carried on quite efficient observation work of high accuracy, giving to every 5 branch stations of the network the minute and second time signals to be placed on the seismograms from the standard chronometer at the central base station (Kainan) which was calibrated by the standard time signals of JJY from the Tokyo Astronomical Observatory. Nevertheless, some practical inconveniences or defects were, of course, revealed during the expedition, and the authors developed new types of transmitter and receiver in 1954. In the autumn of the same year the authors used the new line telerecording chronograph (LTC–II) together with the former instrument (LTC–I) in Wakayama with satisfactory results.

Some essential points of these apparatus are reported here. Schematic diagrams of the LTC–I and LTC–II are shown in Fig. 1 and Fig. 2 respectively, while the transmitters and receivers of LTC can be seen in the photographs of Fig. 3. Some details of the instruments are shown in Table I. Fig. 4 shows the transmission line system of Kansai Electric Company in the neighbourhood of Wakayama, which we could use freely in applying these telerecording chronographs to our seismometric network in 1954. (Read Feb. 20th 1951.)

47. 有線搬送式遠隔記録地震計

地震研究所 { 宮 村 摂 三
松 本 英 照

(昭和 30 年 6 月 28 日発表—昭和 30 年 9 月 30 日受理)

§1. はしがき

既設の電話線を利用し，簡単な高周波裸線搬送装置により，地震観測用の刻時その他の信号を伝送し，観測精度の向上と観測業務の機能増進をはかるこころみについては，すでに報告した.[1] その後，和歌山附近の頻発地震群の観測にこれを利用し,[2] さらに改良を加えたあたらしい刻時用有線搬送機器を製作した．これらについてもまた本号において別に報告した.[3] このようにして，和歌山附近の頻発地震群研究のための観測を 1952 年来つづけてくるにつれ，観測点の増設は種々の点から，切実に要望されてきた.[4] 一方，初動の確度の向上のためと，地震活動の低下にそなえるために，地震計の感度をたかめることも必要になつてきた．かぎられた人数で，これらの要求にこたえるためには，電気式高感度地震計の遠隔記録をおこない，多数の無人観測点を設置することがのぞましい．それにより，遠隔観測点の震動を基地にあつめて記録できるならば，刻時精度においてもまた一段と向上が期待できる．特にこの場合，ひきがね式のはやおくり記録法をもちい，電磁オッシログラによる並列記録をとることも容易であり，これにより，もつとも早い発震時の 1，2 点の記録をのぞいては，初動から完全に記録することもできる．

さて，このような無人地震計のための遠隔記録法は，電気式地震計の場合には，地震計換震器の位置から記録点までのあいだに実際の回線を架設すればよいので，地震探鉱其他の場合実施されていることである．しかしながら，その距離は大体数粁が限度であつて，永久施設としてはともかく，臨時的施設としては経費と労力とがかかつて，ある程度以上遠距離の伝送にこのような専用回線の架設をおこなうことは実際にははなはだ困難である.*

---

1) 宮村摂三・辻浦賢 既設電話線利用搬送方式による地震観測刻時伝送および保守通話. (S. MIYAMURA, M. TSUJIURA, Pri la transdono de temposignaloj kaj parola komuniko por sisma observado pere de la alt-frekvenca telefonado tra la funkcianta telefon-fadeno.) *Zisin* (*Journ. Seism. Soc. Japan*), **[ii] 4** (1951), No. 2.

2) 宮村摂三・外 和歌山附近頻発地震群の観測 (第 2 報) 1954 年 3 月 23 日 地震研究所談話会

3) 宮村摂三・辻浦賢 局地的地震観測網のための有線搬送式遠隔刻時装置 (S. MIYAMURA, M. TSUJIURA, Line Carrier Telerecording Chronographs for Local Seismological Network.) 震研彙報 (*Bull. Earthq. Res. Inst.*) **33** (1955), 709.

4) 宮村摂三・其他 和歌山附近頻発地震群の観測，中間報告. 1954 年 11 月 3 日地震学会第 14 回学術講演会 (京都).

* 表俊一郎博士は浅間山西部において 1953, 54 年約 2 km の低周波伝送による観測に成功し，水上武博士は 1955 年最長 6 km を含む 4 点の低周波直接伝送による集中記録をおこない，浅間山頂一帯の微小地震観測をすすめている.

そこで，このように，超低周波の地震動による振動電流を直接伝送するかわりに，適当な高周波搬送電流を地震動で変調し，いわゆる搬送方式伝送によることにすれば，適当な既設の線路を利用できる場合は有線搬送方式，適当な線路のえられない場合は無線搬送方式によつて，それぞれ目的とする遠隔記録をおこなうことができるはずである．しかも，このような方式によれば，直接伝送とちがつて，伝送距離の延長も，きわめて容易になり，さらに1点から多成分の伝送をおこなうことも，多重通信方式の採用により多数の実回線をもうけることなく実現することができる．

このような，搬送式遠隔記録法を地震学の分野に導入したものには，すでに公表されたものとしては P.G. Gane ら[4] が超短波無線により，Witwatersand の局地地震の研究に利用しているものがあるだけである．有線搬送式のものについては，筆者ら[5]がすでに簡単に報告したものがある．これをいま LTS–I 型 (Line Telerecording Seismograph, Type I) となずけ，その後改良した LTS–II 型とともに，ここに装置の概要をまとめて報告する．

§2. LTS-I 型遠隔記録地震計

すでにのべたように，本機の概要と簡単な実験結果は他に報告しておいたが，[5] その後多少変更した点*もあるので，あらためてここに簡単にのべておきたい．構成の大要は，第1

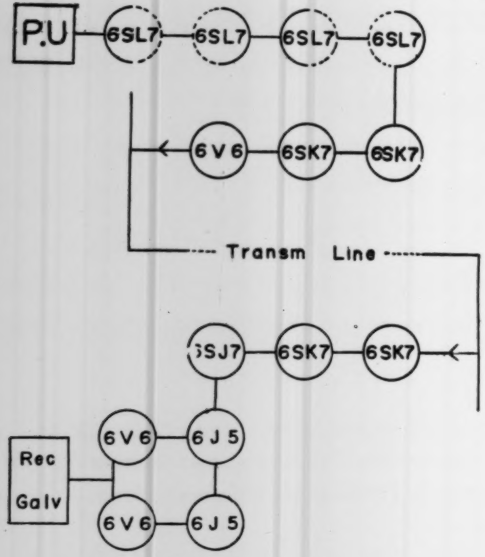

第1図 有線搬送式遠隔記録地震計 LTS–I 型構成図 (Schematic diagram of line carrier telerecording seismograph, Type LTS–I)
送信部 Transmitter
P.U.: 地震計 Seismometer (Pick Up); 6SL7–6SL7: 超低周波増巾器 VLF Amplifier; 6SK7–6SK7–6V6: 搬送周波送信機 Carrier Frequency Transmitter.
受信部 Receiver.
6SK7-6SK7–6SJ7 搬送周波受信機 Carrier Freq. Receiver. 6J5–6V6 P.P.: プッシュプル超低周波増巾，電力増巾，Push Pull VLF Amp. and Power Amp.; Rec. Galv.: 記録電流計 Recording Galvanometer.

4) P. G. GANE, H. J. LOGIE, and J. H. STEPHENS, "Triggered telerecording equipment for seismic observations," *Bull. Seism. Soc. Am.*, **39** (1949), 117–143.

5) 宮村摂三・辻浦賢・松本英照 高周波裸線搬送による地震動波形の遠隔記録 (S. MIYAMURA, M. TSUJIURA and H. MATUMOTO, Telerecording of Seismic Wave Forms by High Frequency Bare Line Carrier Waves.), *Zisin*, [ii], **6** (1954), No. 4, 57–58.

* LTS–I も前の報告[5]では 1000 Hz の補助搬送波をもちい，二段の振巾変調方式をとつたが，その後安定度の点から補助搬送波をもちいず，ここにのべるような直接振巾変調式に改造した．

図の模式図にしめすとおりであつて，送信端では，超低周波増巾器で増巾された地震計からの震動が，送信機で発振された 100～300 kHz の搬送波を直接振巾変調し，線路におくりだされる．受信端ではこれを検波増巾して，記録用電流計をふらせる．地震計としては動線輪型電磁地震計（爆破グループ型 MC3V），送信端の超低周波増巾器としては田[6]の設計による MGIV 型の増巾器を用い，記録用電流計は，三栄測器製ペンライター用電流計（1R102 型 30 c/s, 感度 1 mA/mm, 抵抗 3000 Ω）をもちいた．

装置の外観は第 2 図の写真でみるとおりのものである．おもな要項は第 I 表に表示する．

この装置をもちいて，1953 年夏浅間山麓軽井沢町千ケ滝西区内の営林署専用電話線約 2 km を利用，送信波形と受信波形をくらべてみたところ，ほとんど伝送によるひずみのないことがわかつた．（文献 5 附図参照）また，この実験において約 20 日間の連続記録が安定におこないうることもわかつた．[5]

その後これを和歌山地方の観測において使用したが，実際にはつぎの 3 つの欠点があり，線路状態によつては，充分の伝送距離がえられないことがわかり，応用範囲が限定された．

1) 変調方式が直接変調であるため，波形を忠実にすることにつとめると，送信能率があまり上らなくなり，受信有効距離がみじかい．

2) 受信端における到来搬送波が，線路の雑音の数倍の電圧をもつていないと，検波した地震波形がひずみをうけ雑音と同程度の受信水準ですでに観測不能となり，和歌山において利用した関西電力専用電話線においては，意外に雑音がおおく，はじめ目的とした大崎町海南変電所間約 15 km では伝送に失敗した．

3) 線路の伝送特性は時間的変化をするが，これが，直接の振巾変調であるため，この遠隔記録地震計の綜合感度を直接左右するので，一定感度の観測ができないし．また記録に雑音としてでることも抑制できない．

以上のような欠点を改良するため，われわれはつぎの LTS-II 型を設計した．しかし，この LTS-I 型も，上述の諸点を考慮するなら，雑音量のすくない，特性変化のあまりない線路で，最低数粁程度の伝送は可能であり，また発震時刻だけなら波形の忠実性をギセイにしてある程度の伝送ができるので，なお実際の観測において使用することが可能である．

§3. LTS-II 型遠隔記録地震計

前節で指摘したような LTS-I の欠点を改良し，さらに，磁気録音テープを用いた記録装置を受信端の記録装置として使用することを考慮して，この LTS-II 型遠隔記録地震計を設計，試作した．（磁気録音テープを用いた記録装置については，すでに一成分用のものが完成報告され[7]，現在多成分用のものが研究試作されている）．

6) 田望　爆破観測用超低周波増巾器 (N. DEN, VLF Amplifiers for Explosion Seismology) *Zisin*, [ii], **6** (1953), No. 2. 101–108.

7) S. OMOTE, S. MIYAMURA and Y. YAMAZAKI, "Triggered Magnetic Tape Recorder for Routine Seismic Observations," *Bull. Earthq. Res. Inst.*, **33** (1955), 397.

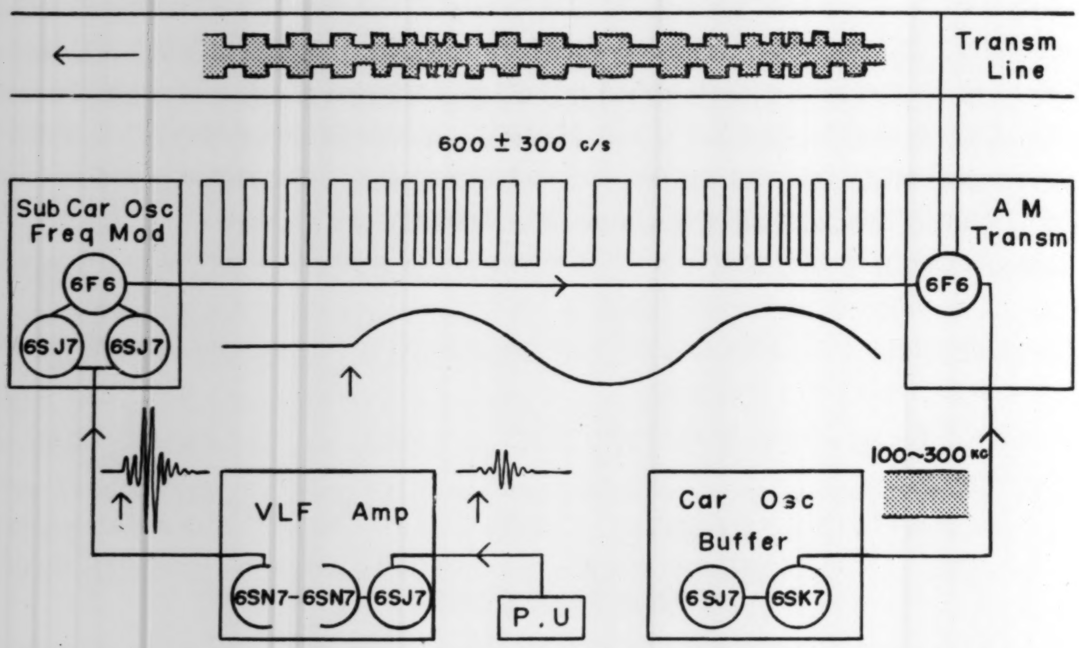

第 3 図 有線搬送式遠隔記録地震計 LTS-II 型送信端構成図 Schematic diagram of transmitting station of Line Carrier Telerecording Seismograph, Type LTS-II.

P.U.: 地震計 Seismic pick up.; VLF Amp: 地震周波増巾器 Amplifier of seismic frequency.; Sub. Car. Osc., Freq. Mod.: 副搬送周波発振ならびに周波数変調部 Subcarrier oscillator and freqency modulation; Car. Osc., Buffer: 搬送周波発振ならびに緩衝部 Carrier frequency oscillator and buffer.; AM Transm.: 振巾変調送信部 AM Transmitter; Transm. Line: 伝送線 Transmission line.

本機の構成および動作の大要は第 2 図（送信端），第 3 図（受信端）にしめすとおりであり，装置の外観は第 5 図のようなものである．おもな要項は第 I 表にしめす．

まず第 2 図にみるように，地震動により換振器に生じた地震周波の電圧変化は超低周波増巾器 6SJ7, 6SN7 により増巾され，6SJ7 2 本より構成され約 600 Hz の矩形波を発振するマルチバイブレーターの格子に電圧変化をあたえる．マルチバイブレターの発振周波数は第 6 図のように格子電圧の変化によつてその中心周波数のまわりに直線的に変化する．こうして，地震動の波形にしたがつて周波数変調されたマルチバイブレターの出力矩形波が補助搬送波となり，送信機の搬送波 100～300 kHz を振巾変調し，送信管で電力増巾され，約 2.5 watt の出力で線路におくりだされる．すなわち F.M.−A.M. 型 2 段変調方式になつている．地震動のない場合は中心周波数 600 Hz の矩形波で A.M. された搬送波がたえずでており，地震がくるとこの周波数がかわる．

送信搬送波の周波数は設置された送受信端局間の線路特性，その附近における妨害電波などに応じ，100～300 kHz の間で適当にえらばれることは，別に報告した LTC についてと同様である．[1,3)]

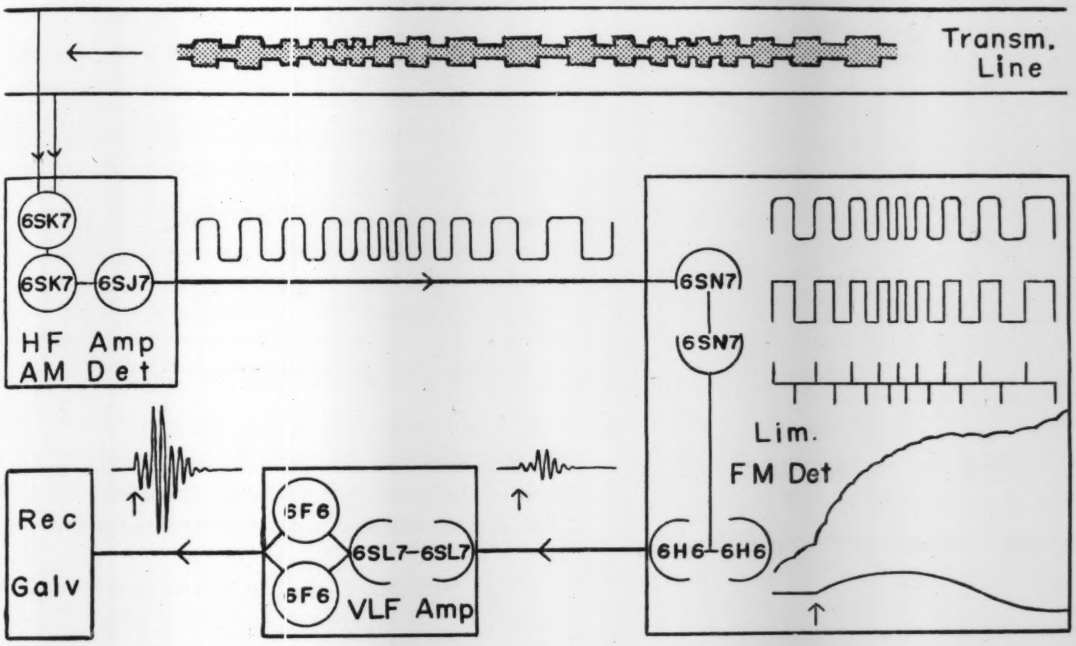

第 4 図　有線搬送式遠隔記録地震計 LTS-II 型受信端構成図. Schematic diagram of receiving station of Line carrier Telerecording Seismograph, Type LTS-II.

Transm. Line: 伝送線; HF Amp. AM Det.: 搬送周波 (100～300 kHz) 増巾, 振巾変調検波. Carrier frequency amplifier, AM detector; Lim. FM Det.: 制限器, 周波数変調検波 Limitter and FM detector; VLF Amp.: 超低周波増巾器. Amplifier of seismic frequency, Rec. Galv.: 記録電流計 Recording galvanometer.

線路におくりだされた搬送波は，LTC の場合と同様，フィルター等を一切もちいてないので，送信点から受信点の方向と同時にその反対方向にもすすむ．これはあきらかに損失となつているが，簡易な装置であるのでやむをえない．

さて，第 3 図にしめされたように，線路によつて減衰をうけた搬送波が受信端に達すると，まず受信機で高周波 2 段の増巾をうけたのち，振巾検波されるが，これは図のように線路ひずみと変調ひずみにより相当ひずんだ矩形波になつているから，これを 2 段のリミターにくわえて，定電圧の，ひずみのない矩形波に再現する．ついで，これを小容量のコンデンサー C_1 で衝撃波化し (微分回路)，つぎに大容量コンデンサー C_2 にその正電圧衝撃波のみをくわえてゆく (積分回路乃至計数回路)．こうすると時間とともに直線的に増加する電圧に地震波の振巾に応じた頻度で単位衝撃波電圧が重畳して段階的に昇圧する．これから一定の直線増加分をのぞいて，地震動による電圧分だけをとりだすと，周波数検波された形でもとの地震動が再現される．これを超低周波 3 段増巾により出力を記録電流計にあたえると，換振器にあたえられた地震動を増巾拡大した記録がえられる．以上がこの LTS II 型遠隔記録地震計の動作原理であり，各部の変換，増巾等のおもな特性は第 6～9 図にある．第 9 図は換振器から電流計までふくめたこの地震計の綜合周波数特性で，黒丸は変位計，白丸は速度計としての特性である．

LTS-II は上述のような FM-AM 2 段変調方式をとつたために，LTS-I にくらべ非

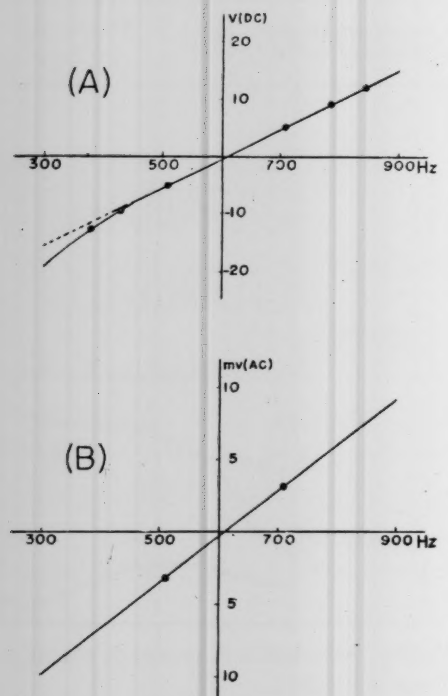

第 6 図 LTS–II 周波数変調特性
(A) 送信機 (B) 受信機
Frequency modulation characteristics of LTS–II. (A) Sender (B) Receiver.

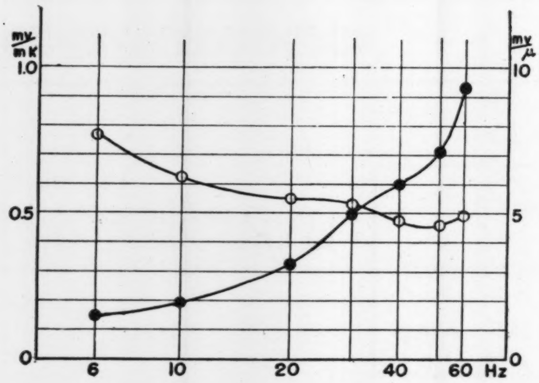

第 7 図 使用地震計換震器 (爆破グループ型 3 c/s 動線輪型電磁式) の周波数特性. Frequency characteristics of used seismometer transducer (RGES type 3 cps moving coil electro-magnetic pick up).

よこ軸 Ordinate: 周波数 Frequency in Hz or c/s. たて軸 Abscissa (for ○): left, 速度感度 Velocity Sensitivity (mk = milikine = kine × 1/1000 = 10^{-3} cm/sec); (for ●) right, 変位倍率 Displacement Magnification. 検定に使用した振動台は地震研究所技術部所属 (明石製作所製) のもので, 強制変位全振巾 20μ constant にて実験し, Pick Up の出力電圧をはかり, 逆算したものである.

常に性能がよくなつた. すなわち受信端の入力レベルが線路雑音と同一か, または多少それよりひくくても, 周波数変調であるため, 矩形波として再現されさえすれば, 忠実に地震波を再現でき, 線路の減衰に対し, 非常につよくなり, LTS-I の約 4 倍くらい受信可能距離がのびた. 1954 年の和歌山における観測では基地琴浦より約 8 km のカマ山 (三田(サンタ)) に無人観測点として, 本機の送信所をおき, 約 40 日間観測を実施した. なお, 実験によれば, 和歌山地方の関西電力の電話線で約 25 km の伝送は可能であつた. カマ山における観測は, 線路の故障其他の事情で途中 17 日間は地震はとれなかつたが, 装置としては連続動作していた. えられた記録の一例は, 同時におこなつた無線式遠隔記録地震計[8]によるものとともに第 10 図 (Pl. CIV) にしめす[9]. なお連続使用の場合, 毎日受信基地で矩形波の監視をブラウン管オシログラフでおこない, 必要に応じ調整し, 一定感度を保守することは容易であつた.

なお, 受信機のリミターの出力矩形波は, すでにのべた本所の磁気録音テープ式遅延記録装置[7]の録音テープにそのままくわえることができるし, 第 2 周波数検波出力をそのト

8) S. MIYAMURA and M. TSUJIURA, "A VHF Radio Telerecording Seismograph," *Bull. Earthq. Res. Inst.*, **33** (1955), 725

9) 文献 8) 第 9 図 (Pl. CVIII) にも LTS-II による記象がある.

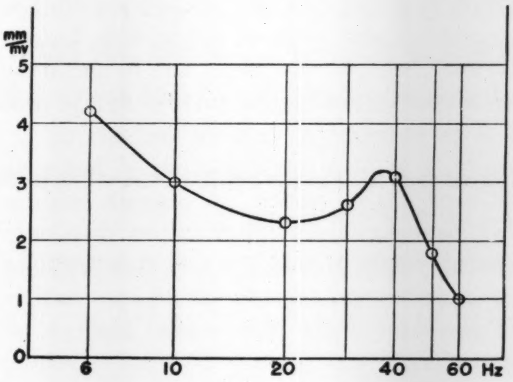

第 8 図 LTS-II の送受信装置 (換震器をのぞき, 記録電流計をふくむ) の周波数特性. Frequency characteristics of LTS-II (including recording galvanometer, but excepting pick up)

よこ軸 Ordinate: 周波数 Frequency in Hz or c/s. たて軸 Abscissa: 単位入力電圧 (P.U. 出力) に対する記録電流計の全振巾 (Double amplitude of recording galvanometer per unit input voltage (output from pick up) impressed by test-oscillator).

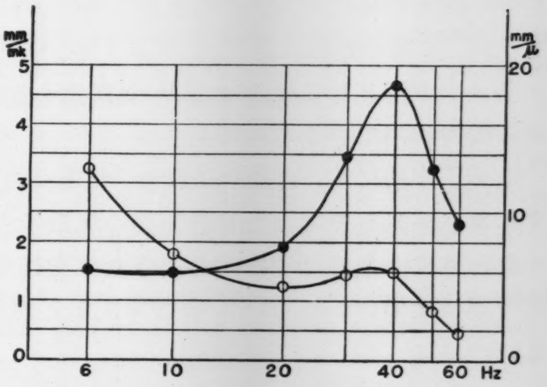

第 9 図 LTS-II 綜合周波数特性 (換震器および記録電流計をふくむ). Overall frequency characteristics of LTS-II, including pick up and recording galvanometer.

よこ軸 Ordinate: 周波数 Frequency in Hz or c/s. たて軸 Abscissa (for ○): 速度感度 Velocity Sensitivity in mm/milikine, (for ●): 変位倍率 Displacement Magnification in mm/micron.

第 I 表 有線搬送式遠隔記録地震計 LTS 要項. Essentials of the line carrier telerecording seismographs LTS-I and LTS-II.

	LTS-II				LTS-I		
	Transmitter		Receiver		Transmitter		Receiver
	送信部 HF.LF.VLF	電源部 Power Supp.	受信部 HF.LF.VLF	電源部 Power Supp.	送信部 HF	電源部 Power Supp.	HF. VLF
外形	230 × 200 × 400 mm	270 × 230 × 450 mm	250 × 230 × 500 mm	270 × 236 × 450 mm	170 × 130 × 250 mm	270 × 230 × 450 mm	550 × 230 × 430 mm
重量	5 kg	15 kg	5 kg	15 kg	2 kg	15 kg	20 kg
真空管	GT. 8	ST. 1 Special 2	GT. 8	ST. 1 Special 2	GT. 3	ST. 1 Special 2	GT. 7 ST. 1 Special 2
電源	DC 250 V DC 6 V AC 6 V	AC 100 V 50～60 c/s 80 w	DC 250 V DC 6 V AC 6 V	AC 100 V 50～60 c/s 80 w	DC 250 V DC 6 V	AC 100 V 50～60 c/s 50 w	AC 100 V 50～60 c/s 80 w
備考	6 V Battery and rectifier		6 V Battery and rectifier		6 V Battery and rectifier		6V Battery and rectifier

リガー回路にあたえて，その装置により，精密記録をとることができることは，いうまでもない．本機の電源は送受共 5Z3 1本，定電圧放電管 2 本を使用し，使用電力約 100 W，ヒラメント用として現在は 6 V 蓄電池を充電しながら用いているが，これはセレンと塞流線輪で代用できるものである．

なお，本機にも，自動利得調整，電源部其他不足の点もあり，特性感度についても改良すべき点があるので，なお各方面の御教示をえたいと存ずる次第である．

おわりに，本機は和歌山のような群発地震以外にも，大地震の余震，大爆破の観測など随時適当な場合にもちいて有効であると思われるので，今後はそれらにも利用してゆきたい．

§4. 謝　辞

この研究は有線搬送刻時装置[1,2]の研究の延長であつたが，約 10 年前にその第 1 歩をふみだしたころから，その実験につねに御協力をあたえて下さつた東京電力株式会社(当時関東配電)工務部通信課および関係した変電所の方々，最近 3 年間和歌山地方における観測にあらゆる便宜をあたえ，協力して下さつている関西電力株式会社工務部，同大阪火力事務所，同和歌山支店電路課，管内変電所関係者の方々に心からの感謝をささげたい．

また本研究の大部分は同僚辻浦賢，堀実両氏の協力をえたものであるが，特に LTS–I の設計はむしろ大部分辻浦氏のものであつたので，しるして感謝の意を表したい．本機の振動台による検定については萩原研究室斎藤貞夫氏の御世話になつた．あつく謝意を表する．また本機に使用した換震器は爆破地震動観測用のものを転用したので，好意ある配慮をえた爆破地震動研究グループの同僚諸氏に感謝したい．

LTS–I の浅間山麓の実験では水上研究室内堀貞雄氏，軽井沢町，岩村田営林署，国土開発興業株式会社等の御協力をえたことをしるし，あらためてお礼したい．

本装置の試作実験に要した経費は筆者の一人に与えられた文部省科学研究費，地震研究所に対する大地震危険地帯特別研究費，および国際地震観測事業費のうちより支弁された．本研究の推進を支援された津屋前所長，那須所長，萩原観測部長，実川技術部長に感謝する．

---

47. Line Carrier Telerecording Seismograph (abbr. LTS)

By Setumi MIYAMURA and Hideteru MATUMOTO,

Earthquake Research Institute.

Needless to say, a central registration of multichannel seismic outputs, made by means of exclusively laid wires from several separate transducers with an oscillograph, is of outstanding use in the interpretation of seismograms. But now the procedure has, as is

widely known, lost its novelty in exploration seismology. However, the increasing necessity of raising the level of observation accuracy in explosion seismology, or seismic deep sounding of the earth's crust, and natural earthquake seismology has led to the introduction of the central registration method into these fields of pure science.

In the last several expeditions of R.G.E.S. in N-E Japan some parties, especially those detached in the neighbourhood of explosion sites, adopted the method and recorded the seismic signals by means of the several pickups separated some hundreds of meters respectively on an oscillograph papers. G.A. Gamburtseff of USSR has introduced a correlation method of seismic observation into his natural earthquake research program, making use of the central registration. T. Asada and others have introduced the method on a small scale into their micro-earthquake studies as the so-called tripartite station method. Into the seismic investigations of the ice-break mechanism on Lake Suwa by S. Omote and volcanic activities of Mt. Asama by T. Minakami the method has been introduced on a wider scale. Especially in the summer of 1955, T. Minakami installed wires as long as 6 kms around the summit of the mountain, which is perhaps one of the longest installation of wires for geophysical purposes. Nevertheless, such direct transmission of seismic output from ordinary electro-dynamic transducer to a central station is limited in distance, because the output is weak in general and also because the installation of exclusive wires is a painstaking and expensive work.

In order to remove these defects and to extend the transmission distance, the authors introduced the carrier telephony techniques and instead of using exclusively laid wires made use of the already existing communication lines in civil or private operation.

Of late the authors have developed a system of time signal telerecording by high frequency carriers through local telephone network for the purpose of sending standard time signals to their seismological stations in the Wakayama swarm earthquake region (cf. Ref. 1.). In designing the present telerecording seismographs, we made good use of the experience gained by developing the line carrier telerecording chronograph (LTC), and constructed the first type of line carrier telerecording seismograph (LTS-I) in 1953. Distortionless transmission of seismic wave-forms was experimented and verified by this set as shown in the preliminary report. (See reproduction in Ref. 2 which demonstrates similarity of transmitted and received wave forms of various ground oscillations). In the autumn of that year (1953) the authors introduced it into their seismological network in Wakayama, in order to add a station which might be operated unattendedly. But the result was not satisfactory, owing to the bad condition of the lines and some defects in the instrument. In the following year we improved the design and constructed a new set (LTS-II) which was utilized in the observation of Wakayama swarm earthquakes with success in 1954.

Schematic diagrams of the construction of LTS-I and LTS-II are shown in Fig. 1 and Figs. 3-4 respectively, while their appearances with some accessaries are shown in the photographs in Fig. 2 and Fig. 5 respectively. The working principle of FM-AM double modulation and demodulation of LTS-II transmitter and receiver are demonstrated in the inserted figures of wave forms of respective steps in Fig. 3 and Fig. 4. Curves in Figs. 6-9 are results of experiments showing the characteristics of LTS-II. Verification of distortionless transmission by LTS-II was not experimented, but we have no reason to suspect the accuracy to be lower than LTS-I.

Seismograms of an earthquake shown in Fig. 10 (Pl. CIV) are examples of a central registration executed by the authors in the autumn of 1954 for the seismometric investigation into Wakayama earthquake swarms. The reproduction labelled as S is a seismogram received or picked up at Santa, an unattended station, and transmitted through private

telephone lines of Kansai Electric Co. to the central recording station Kotono-ura, Wakayama, about 8 kms from Santa. The other reproductions are those also recorded at Kotono-ura. D is a radio-linked record of the same earthquake at Dezima, Waka-ura, ca. 5 km from Kotono-ura. (About this radio-linked telerecording seismograph see Ref. 4). Ko is a record of the shock by an ordinary electronic seismograph near the central recording station. (The amplifier used was R.G.E.S. H-type designed by N. Den. Cf. Ref. 6) Some essentials of these apparatus are given in Tables I. (Read June 28th, 1955.)

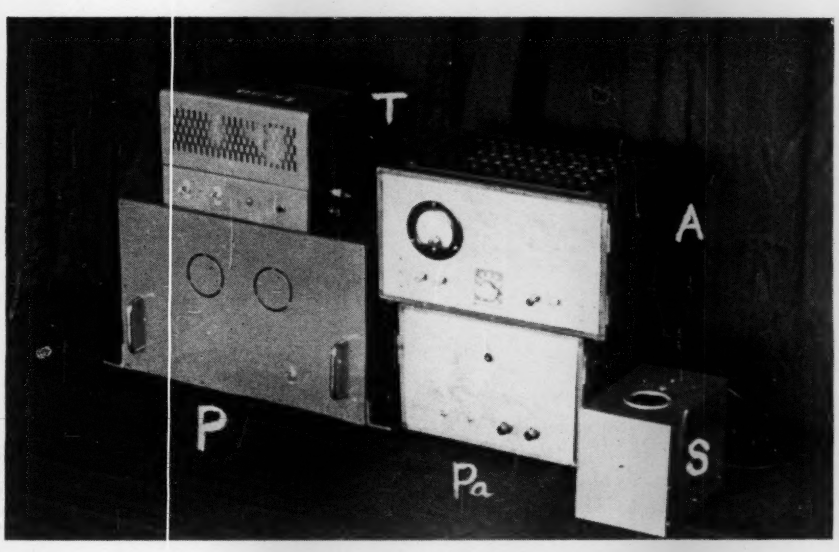

(A)

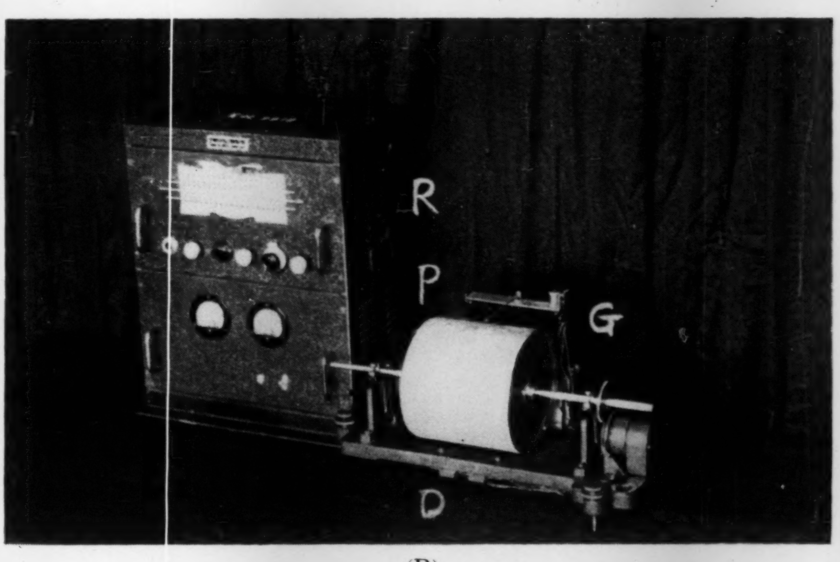

(B)

第 2 図　有線搬送式遠隔記録地震計 LTS-I 型 (Line Carrier Telerecording Seismograph, Type LTS-I.)

(A) 送信部 Transmitting Set.　(B) 受信部 Receiving Set.

S: 地震計 [爆破グループ型動線輪型電磁換振器] Seismometer (R.G.E.S. Type Moving Coil E.M. Transducer], A: 超低周波増巾器 [爆破グループ IV 型] VLF Amplifier [R.G.E.S. Type IV], Pa: 超低周波増巾器用交流電源装置 AC Power Supply for VLF Amp., T: LTS-I 送信機 Transmitter, P: LTS 交流電源 AC Power Supply, R: LTS-I 受信機 Receiver, G 記録電流計 Recording Galvanometer (Ink Writer of SAN-EI Co.), D: 交流用記録円筒 Recording Drum (A.C.)

（震研彙報 第三十三号 図版 宮村・松本）

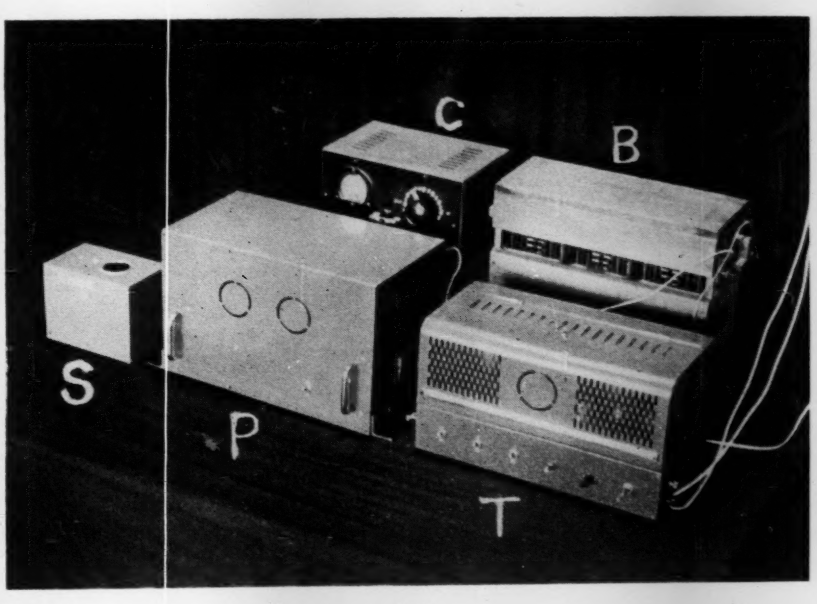

(A)

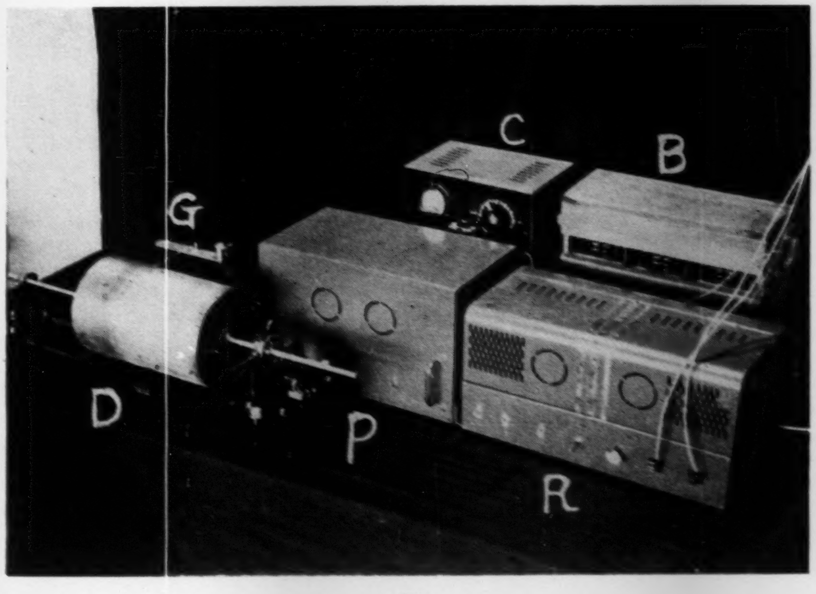

(B)

第 5 図 有線搬送式遠隔記録地震計 LTS II 型 (Line Carrier Telerecording Seismograph, Type LTS-II).

(A) 送信部 Transmitting Set. (B) 受信部 Receiving Set.

S: 地震計 (換震器) [爆破グループ型] Seismometer (E.M. Transducer) [R.G.E.S. Type], P: 交流電源装置 A.C. Power Supply, B: 蓄電池 Battery, C: 充電器 Charger, T: LTS-II 送信機 Transmitter, R: LTS-II 受信機 Receiver, G: 記録電流計 [三栄] Recording Galvanometer [SAN-EI Co.], D: 記録円筒 Recording Drum (A.C.)

(第 10 図　和歌山附近頻発地震群の遠隔記録地震計による記録の一例の説明)

和歌山市琴浦基地観測点にて記録せる 1954 年 11 月 28 日の小地震の記象．S および D は和歌山市カマ山（三田），および和歌浦（出島）の無人観測点にて，有線搬送式遠隔記録地震計 LTS および無線搬送式遠隔地震計 RTS* により受震，これを琴浦基地に送信し記録したもの．KOは基地琴浦にて普通の電子管地震計で記録したもの．三田，出島，琴浦のこれら地震計の綜合感度はそれぞれ 150, 30 および 10 μV eff/mm.　三田では雑微動が大きく，感度があげられなかつたので，D および KOの写真で右下にでている小さい地震は S ではみえない．

Seismograms of a small shock of Nov. 28. 1954 recorded at the base station Kotono-ura Wakayama City. S and D are those which were picked up at the unattended branch stations, Santa and Dezima by LTS and RTS* respectively, and were transmitted to the base station Kotono-ura for central registration. KO is that which was obtained by an ordinary electronic seismograph at Kotono-ura. Sensitivities of these instruments at Santa, Dezima and Kotonoura were 150, 30, aud 10 μV eft/mm respectively. As the ground noise at Santa was great, sensitivity of LTS could'nt be raised and a very small shock, appeared in the right down part of the reproductions of D and KO, are missing in that of S.

* Radio Telerecording Seismograph. cf. Ref. 8).

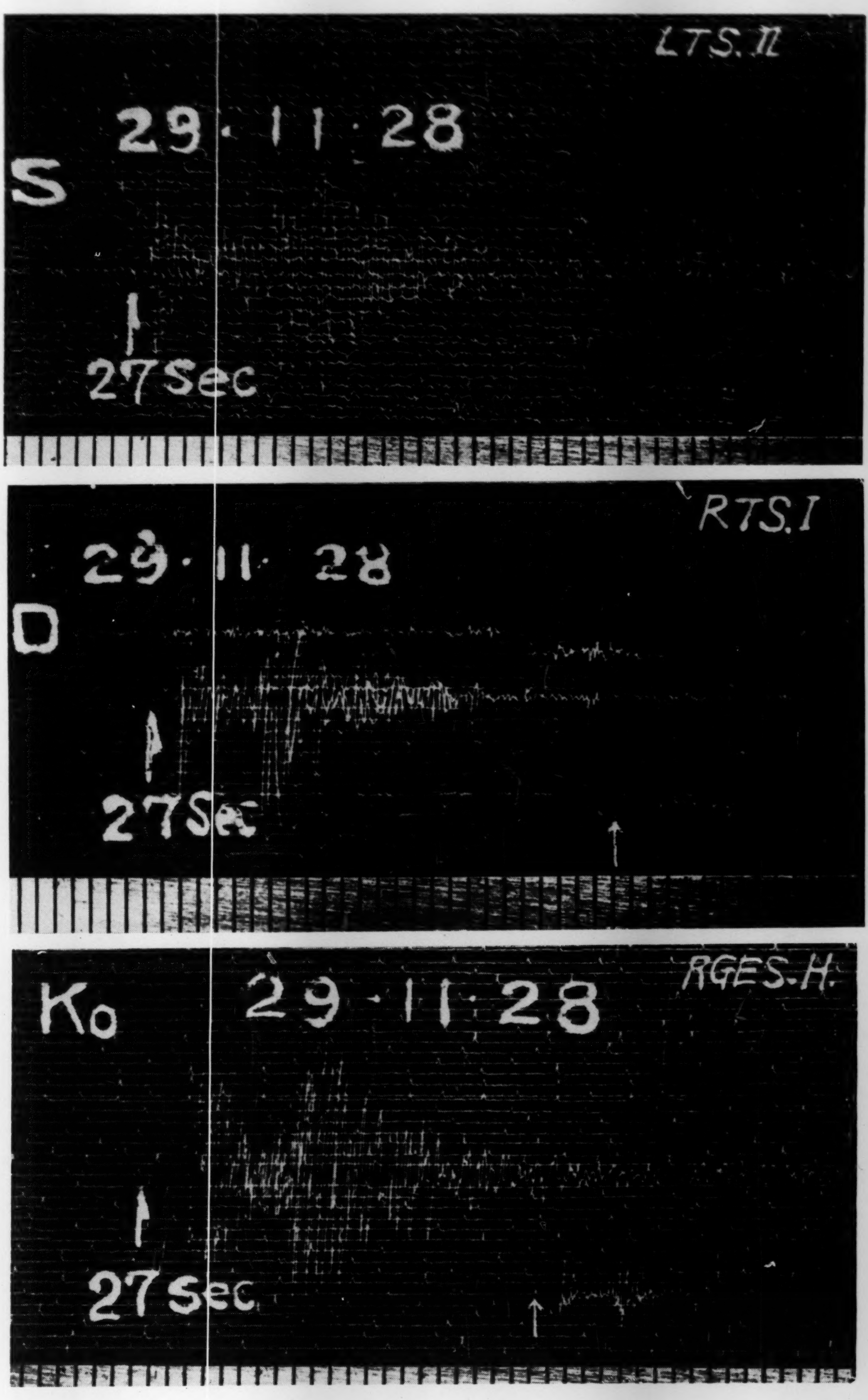

第 10 図　和歌山附近頻発地震群の遠隔記録地震計による記録の一例（説明左頁）

48. 超短波無線搬送式遠隔記録地震計

地震研究所 { 宮村攝三 / 辻浦賢

(昭和 30 年 6 月 28 日発表—昭和 30 年 9 月 30 日受理)

§1. はしがき

有線搬送式遠隔記録地震計 LTS-I および LTS-II については別に報告した.[1-2] 一般に無人観測点用搬送式遠隔記録地震計の必要性とそれらによる集中記録の地震観測上の利点については，そこでくわしくのべたので，ここではそれらのことがらは省略し，簡単に本機を製作した目的をのべ，装置の概要，動作原理，特性等を説明し，なお改良すべき点や，今後の応用などについてしるし，読者の批判をえたいと思う次第である.

1952 年からはじめた和歌山附近頻発地震群研究のための臨時精密観測網では，関西電力の専用電話線を利用し有線搬送式遠隔刻時方式を採用し，また有線搬送式遠隔記録地震計による無人観測点を設置してきたが，海岸方面など必要な方面において，利用しうる適当な既設電話線のないところから観測点の不足があり，これをおぎなうために無線搬送式の遠隔記録地震計による無人地震観測点を設置する必要が生じた.[3] このような無線式遠隔地震計は有線搬送式のものと同様，大地震にともなう余震の観測，大爆破による地震動の観測，噴火にともなう地震群の観測，あるいわ常時微動による地盤調査などにも利用でき，観測の能率化と精度の向上に役立つとおもわれ，さらに将来は，ある程度常時観測業務にもとりいれられ，特につなみ警報など，すみやかに資料の整理計算を必要とする業務に採用されれば，非常に有効であろうと考えられる.

われわれは 1954 年 10 月 60.17 メガサイクル A9 電波全国陸上移動局として，周波数認可をうけ，1954 年 11 月に開局した. 1954 年 11～12 月和歌山地震群の観測に利用し，1955 年 2 月大阪市地盤調査に試験的に使用，1955 年 6 月以降筑波山支所の微小地震観測を東京の本所で受信記録して長時間使用試験をおこない，充分実用の域に達したと思われるに到つた.

§2. RTS-I 型遠隔記録地震計

無線搬送式遠隔記録地震計としては GANE ら[4]が Johannesburg, South Africa で Wit-

1) 宮村攝三・辻浦賢・松本英照 高周波裸線搬送による地震動波形の遠隔記録 (S. MIYAMURA, M. TSUJIURA, H. MATUMOTO, Telerecording of Seismic Wave Forms by High Frequency Bare Line Carrier Weves), *Zisin*, [ii], **6** (1954), No. 4.

2) 宮村攝三・松本英照 有線搬送式遠隔記録地震計 (S. MIYAMURA and H. MATUMOTO, Line Carrier Telerecording Seismograph.), *Bull. Earthq. Res. Inst.*, **33** (1955), 715.

3) 宮村攝三・外 和歌山附近頻発地震群の観測，中間報告. 1955 年 11 月 3 日地震学会第 14 回学術講演会 (京都).

4) P. G. GANE, H. J. LOGIE and J. H. STEPHENS, "Triggered Telerecording Equipment for Seismic Observations," *Bull. Seism. Soc. Am.*, **39** (1949), 119-143.

watersrand 附近の局地地震を観測するのにつくつたものがあるが，われわれのものも，それとほとんど同様で，使用波長も同じく超短波帯のものである．有線搬送式を LTS というのに対し，この無線搬送式のものを RTS (Radio Telerecording Seismograph) となづける．

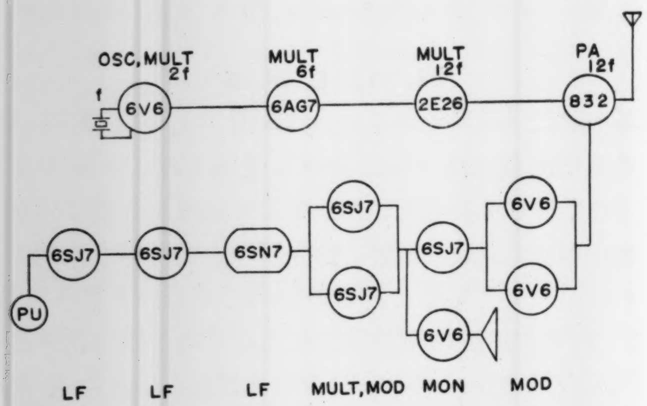

第 1 図　超短波無線搬送式遠隔記録地震計 RTS–I 型構成図　送信部．Schematic diagram of VHF radio telerecording seismograph, Type RTS–I. Transmitting Part.

f=60.17/12 Mc=5014.167 kc. Crystal Oscillator. OSC. 発振管 Oscillator, MULT: 逓倍管 Multiplier, PA: 送信出力管 Transmitting Power Amplifier, PU: 地震計換振器 Seismometer (Moving-Coil Transducer RGES Type), LF: 低周波増巾管 Low Freq. Amplifier, MULT: マルチ発振管 Multivibrator, MOD: プッシュプル変調管 Push-Pull Modulator. MON: モニター Monitor.

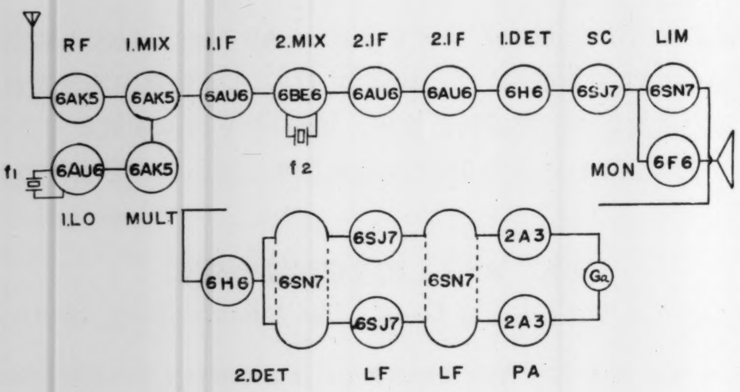

第 2 図　超短波無線搬送式遠隔記録地震計 RTS–I 型構成図　受信部．Schematic diagram of VHF radio telerecording seismograph, Type RTS–I. Receiving Part.

RF: 無線周波増巾管 Radio Freq. Amplifier, MIX: 混合(変換)管 Mixer, IF: 中間周波増巾管 Intermediate Freq. Amplifier, LO: 局部発振管 Local Oscillator, $f_1=(60.17-5)/12$ Mc= 4.5975 Mc, DET: 検波管 Detector, SC: 副搬送周波増巾管 Subcarrier Freq. Amplifier, LIM: 制限管 Limitter, MON: モニター Monitor, LF: 低周波増巾管 Low Freq. Amplifier, PA: 電力増巾管 Power Amplifier, Ga: 記録電流計 Recording Galvanometer.

本機 RTS-I 型の構成の大要は，送信部第1図，受信部第2図にしめすとおりである．装置の外観は送信部第 3 図，受信部第 4 図にみるごときものである．つぎに本機の動作原理を簡単に説明する．まづ無人観測点となるべき送信部を説明する．

電磁地震計換振器に誘起した地震動による電圧は 6SJ7, 6SJ7, 6SN7 3 段の超低周波増巾器によつて増巾され，6SJ7 2 本よりなるマルチ発振回路の格子にくわえられる．そうすると，LTS の報告[2)]で説明したように，マルチ発振回路の中心周波数 (800 Hz) を中心として最高 ±300 Hz の周波数変調がおこなわれる．入力がくわわらない場合，すなわち換振器の出力電圧がない場合，このマルチ回路の発振は 800 Hz の短形波であるが，入力がくわわるとき，つまり地震動がくるときは，これが 800±300 Hz 以内で周波数変調される．

このマルチ発振回路の 800 Hz を補助搬送波 (Subcarrier) とし，これを 6SJ7 で増巾し，変調管 6V6 Push Pull を励振する．

無線搬送波は，割当周波数 60.17 MHz の 1/12 (5014.17 kHz) の基本周波数の水晶で発振し，これを 6V6, 6AG7, 2E26 で 2×3×2=12 逓倍して，出力管 832 に 60.17 MHz の励振をあたえる．補助搬送波がここでこれを振巾変調し，出力 10 watt にて三素子八木空中線により水平偏波として空中に輻射される．饋電線は同軸型インピーダンス 75 Ω, 15 m, 減衰は 0.07 db/m になつている．

つぎに受信部を説明する．受信空中線は送信空中線に対応した三素子八木空中線水平偏波受信空中線をもちいている．饋電線は高周波平衡型 15 m，インピーダンス 300 Ω である．受信機は 0 db 入力に対し S/N 20 db の電気的特性を有し，第 1 中間周波数 5 MHz, 第 2 中間周波数 455 kHz のダブルスーパーヘテロダイン方式で，各周波数変換部はともに水晶により制禦されている．空中線で受信した電波は 6AK5 で 1 段増巾し，これをつぎの 6AK5 で第 1 中間周波数に周波数変換をおこない，これをつぎの 6AU6 で 1 段増巾し，さらにつぎの第 2 中間周波変換管 6BE6 によつて 455 kHz の中間周波数をつくり，これを 6AU6 の 2 段で増巾，つぎの 6H6 で検波して 800±300 Hz の補助搬送波を再現する．ここでまた，同時に AVC, ANL を附加し，回路の安定化をはかつている．あとは大体 LTS-II の回路方式と同様であるが，ただ低周波部は第 2 検波以後全部プッシュ・プルでとりだし，出力管は 2A3 の Push Pull である．

電源は商用交流 50〜60 c/s 切かえ，90〜110 V, 消費電力は送信 約250 W 受信約 200 W である．

第 5 図は送受信機の周波数特性で，低周波発振器の出力を 30 μV (実効値) 一定として，地震周波数入力のかわりにあたえたときの，記録振巾の周波数による特性をあらわしたものである．第 6 図は電磁式地震計もふくめた装置全体の周波数特性であり，地震計を振動台[5)]にのせて記録した結果で，振動台の振巾は 20 μ 一定として検定した．第 7 図の直線 a はこの装置の最高感度特性ともいうべきもので，地震周波数雑音 (地震計換振器をおいた土地の地面の雑振動) と無線周波数雑音 (送受信局間の空中雑音，特に受信

5) 明石製作所製.

点近傍の雑音）とがすくない場合は，この感度で観測ができる．しかし実際にはこれらの雑音があつてこの感度では観測できないことが多く，和歌山附近あるいは筑波一東京での観測ではたとえば第 6 図の直線 *b* の感度 (30 μV eff./mm double amplitude) で観測をおこなつた．観測された記録の例は第 9, 10 図にしめす．[6)]

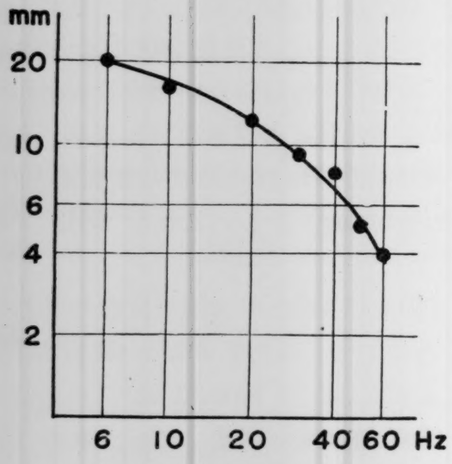

第 5 図　RTS–I 送受信機綜合特性（換振器をのぞく）Frequency characteristics of RTS–I (excepting pickup).

よこ軸 Abscissa: テストオッシレーター周波数 Frequency of test-oscillator in Hz or c/s. たて軸 Ordinate: 記録振巾 Recorded amplitude of the galvanometer. （テストオッシレーターによる入力電圧 30 μV 一定にて実験． Input voltage 30 μV constant by test-oscillator.）

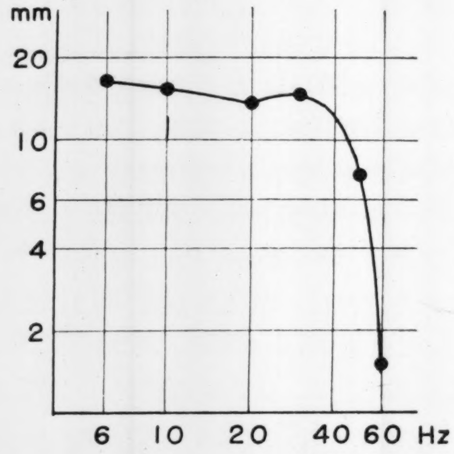

第 6 図　RTS–I 送受信機綜合特性（換振器をふくむ） Over-all frequency characteristics of RTS–I (including pickup).

よこ軸 Abscissa: 振動台周波数 Frequency of vibration table in Hz or c/s. たて軸 Ordinate: 記録振巾 Recorded amplitude of the galvanometer（振動台は 20μ 一定の変位振動をあたえる． Vibration table displacements are 20 μ constant）

第 8 図 T, H は送受信側で同一地震動を同時に記録した例であり，筑波山 (T) に送信機を，本郷 (H) に受信機をおき，送信側の低周波増巾部 6SN7 に別個の電力増巾器をつないでとつた記録 (T) と，本郷で記録した本装置として記録 (H) とを対比してある．本機の送受信機の低周波部の特性は同一でなく，受信部で高周波を切つてあるので，その影響がややみえているが，それ以外はまつたく相似の波形をしめしているので，一応正しい遠隔記録がおこなわれているとみなされる．

なお，本機の電波到達距離，すなわち観測可能限界は，地形により左右されるが，市街地で約 20 km，筑波山一本郷のような見とおしのところでは大体 100 km あまりとおもわれる．

以上で RTS–I 型遠隔記録地震計についての概要をのべたが，最後に現在の装置の欠点として，電源変動に対する安定装置其他の不備があるし，観測の安定に対する妨害とし

6)　文献 2) Fig. 10 にもあり．

て，受信点近傍の自動車雑音，おそらくは飛行機々体による反対電波の干渉とおもわれるゆつくりした時間的に対称な振動（第 10 図の左上に 2ケ所その後半分があらわれてる）などが時々本郷ではあらわれた．電源安定装置は将来施設するとしても，あとの受信電波の妨害は現在対策がない．自動車雑音については将来 FM 方式のものを採用すれば，ずつと改良されるであろうと思われる．

今後このような遠隔記録地震計を多重化して，すくなくとも 1 点から 2 成分以上を送れるようにし，一方そのような無人観測点を数点つくり，それらの集中記録により自然地震および爆破地震の観測の精度向上（特に後者の場合深部反射の検出も容易になろう）とそれら野外作業の業務能率の増進に資したい．その場合この方式では特に各点ごとに別の周波数割当をえなくてはならないので，今日わがくにの電波事情から超短波帯（VHF）では非常に問題となる．現在 UHF において，指向性空中線により偏波面を利用一つの周波数で何点もの無人点からの記録を分離して受信し，遠隔記録をおこなうような方向に研究をすすめている．

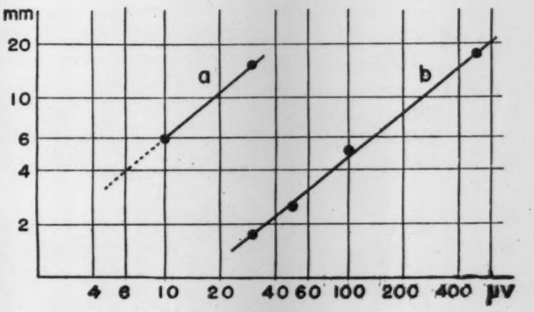

第 7 図 RTS–I 感度特性の直線性 Linearity of sensitivity characteristics of RTS–I.
よこ軸 Abscissa: テストオッシレーター 10 c/s 入力電圧 Input voltage from test-oscillator at 10 c/s. たて軸 Ordinate: 記録振巾 Recorded amplitude of the galvanometer.
a. High Sensitivity Curve
b. Medium Sensitivity Curve

§3. 謝　　辞

本装置の開発をはじめるにあたり，御後援，御教示をたまわつた，郵政省電波局元陸上課長谷村功氏（現電気通信大学教授），同鈴木清次氏はじめ同局陸上課，周波数課および関東電波監理局の関係官各位にあつく御礼申しあげたい．また本装置の製作に従事された岩井電気株式会社の八木純一氏の御協力に感謝したい．松下電器株式会社よりは和歌山における観測網に 60 MHz 帯を利用できるか否かをしらべるための電波伝播試験に協力をえた．御援助を感謝する．なお和歌山では県および関西電力株式会社よりつねにあらゆる面で御援助をえているので特に記して深甚の謝意をのべておく．

本機の製作費は主として地震研究所の「国際地震観測」の特別事業費より支出され，実験費の一部は和歌山県より支出された．後者については和歌山県副知事荒木和成氏，前土木部長鈴木直彦氏および前企画広報課長藤田定基氏に，前者については本所那須所長および萩原教授に御後援を感謝する．なお本研究によせられた本所技術部長実川技官はじめ技術部の方々の御援助に感謝の辞をのべたい．筑波山支所での実験観測には同支所渡辺正雄氏，技術部鈴木喜吉氏および観測部の方々の御支援をえた．振動台による検定には萩原研究室斎藤貞夫氏のお世話をうけた．同僚松本英照氏，堀実氏には本研究中たえず御協力をえた．附記して感謝する次第である．

第 I 表　超短波無線搬送式遠隔記録地震計 RTS–I 型要項

	VHF Radio Telerecording Seismograph, RTS–I					
	送信機 Transmitter			受信機 Receiver		
	送　信　部 RF	増幅·変換部 VLF·LF	電　源　部 Power Supply	受　信　部 RF	変換·増幅部 LF·VLF	電　源　部 Power Supply
外形	220 × 350 × 400 mm	220 × 350 × 400 mm	220 × 350 × 400 mm	220 × 350 × 400 mm	220 × 350 × 400 mm	220 × 350 × 400 mm
重量	13 kg	13 kg	32 kg	14 kg	13 kg	31 kg
真空管	GT 6 Special 1	GT 6 Special 2	ST 3	MT 8 GT 3	GT 6 ST 2	GT 1 ST 2
電源	DC 350 V DC 250 V AC 6 V	DC 250 V DC 6 V AC 6 V	AC 100 V 50∼60 c/s 250 W	DC 250 V AC 6 V	DC 250 V DC 6 V AC 6 V	AC 100 V 50∼60 c/s 180 W
備考	60.17 MHz A9 wave. 10 W	VLF 3∼20 Hz (Seismic freq.) LF (Subcarrier) 800±300Hz		Double Super-heterodyne 1. IF 5 MHz 2. IF 455 kHz	Output 50 W	
空中線	半固定用軽金属組立式水平偏波三素子八木空中線 長さ 2.5 m, 重さ約 2 kg, 支柱の高さ 3 m. 利得 5.5 db.					

48. *A VHF Radio Telerecording Seismograph* (*abbr. RTS*).

By Setumi MIYAMURA and Masaru TSUJIURA,

Earthquake Research Institute.

A VHF radio-linked telerecording seismograph was designed and constructed, in order to add an unattended substation for the local seismological network of Wakayama earthquake swarms in those regions, where no telephone lines were available for either transmitting the time signals by line telerecording chronograph system (LTC) or sending the seismograms by carrier line telerecording seismograph (LTS). Being constructed as portable, these telerecording systems will be also usefull for other seismometric observations in earthquake and explosion seismology. It may also be useful in the future routine seismological network, especially in speeding up the tunami warnings.

Schematic diagrams in Figs. 1 and 2 show the essentials of the transmitting and receiving sets of the radio telerecording seismograph named RTS–I. Appearances of the antennae and sets of RTS–I are shown in Figs. 3 and 4. The transmitting waves used are VHF waves of 60.17 Mc, that is, the amplitude modulated by 800 c/s subcarriers, the

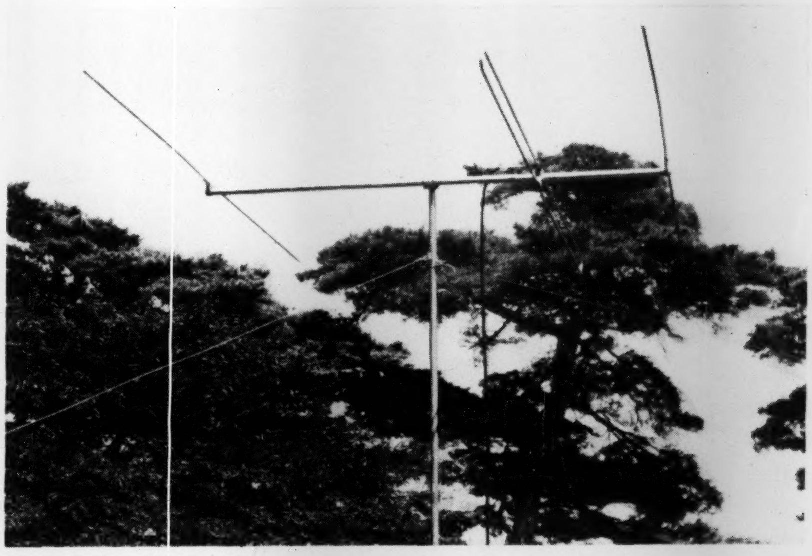

A

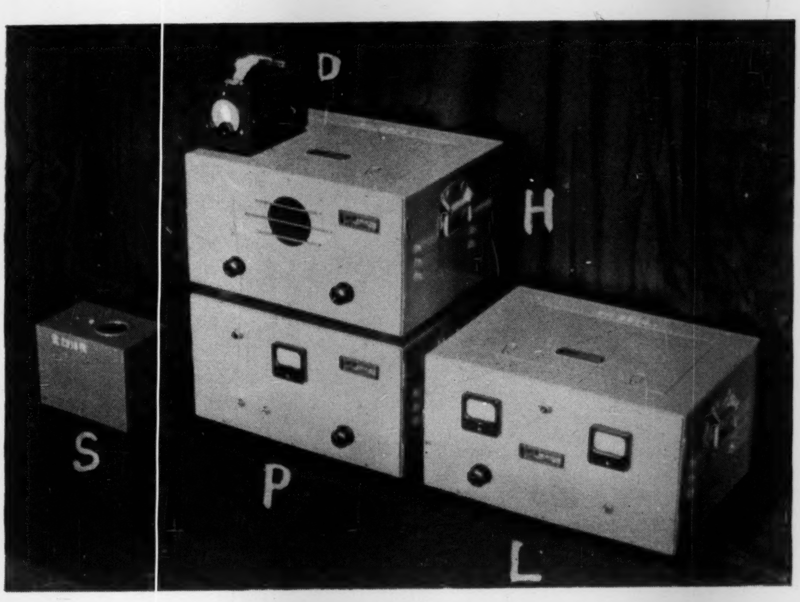

B

第 3 図 超短波無線搬送式遠隔記録地震計 RTS–I 型送信部. VHF Radio Telerecording Seismograph, Type RTS-I. Transmitting Part.

A: 送信空中線. 三素子水平偏波指向性八木空中線 (筑波支所屋上設置) Transmitting antenna. 3-elements horizontal polarized directive YAGI antenna. (On the roof of Tukuba-san Seism. Obs., E.R.I.)

B: 送信装置. Transmitting Set.—S: 地震計 Seismic transducer, D: 擬似空中線 Dummy load, P: 交流電源部, AC Power supply, L: 低周波増巾部 Low freq. amplifier, R: 無線周波送信部 Radio freq. transmitter.

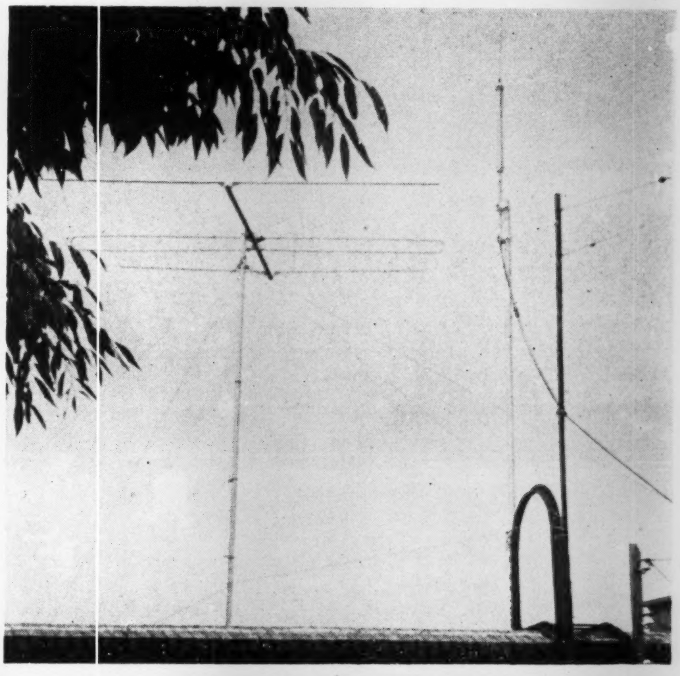

A

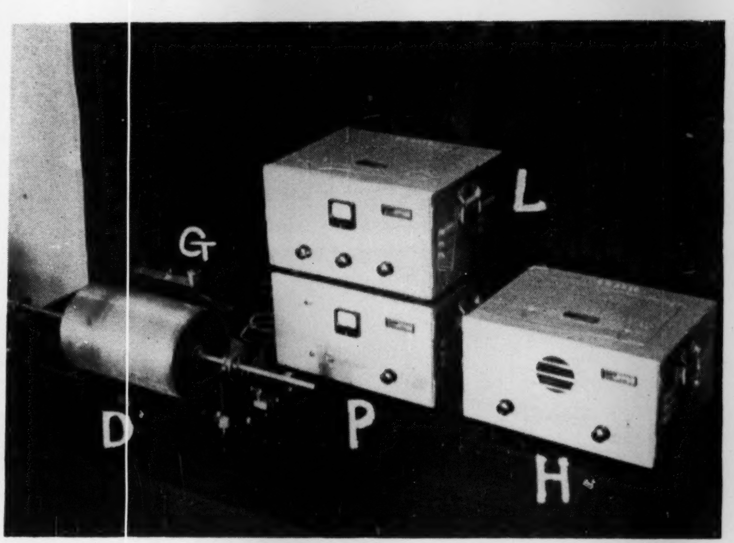

B

第 4 図 超短波無線搬送式遠隔記録地震計 RTS–I 型受信部 VHF Radio Telerecording Seismograph, Type RTS–I. Receiving Part.

A: 受信空中線 (本郷震研屋上) Receiving antenna. (On the roof of the Institute, Hongo) 右は VHF (150 Mc) 通話用無線局空中線および時報受信用短波空中線の一部. Righthand canbe seen VHF slive antenna for communication and HF receiving anntenna for standard time signal.

B: 受信装置 Receiving Set.—H: 無線周波受信部 Radio freq. receiver, L: 低周波増巾部 Low freq. amplifier, P: 交流電源部 AC Power supply, G: 記録電流計 Recording galvanometer, D: 記録円筒 Recording drum.

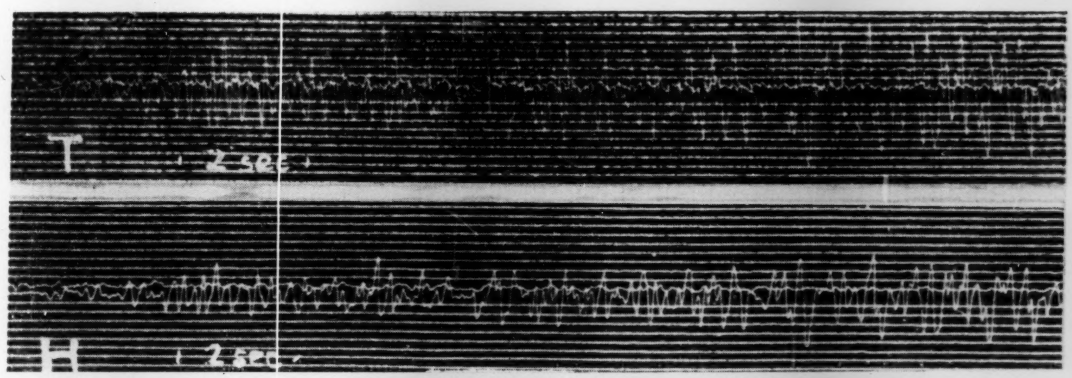

A ×1.8

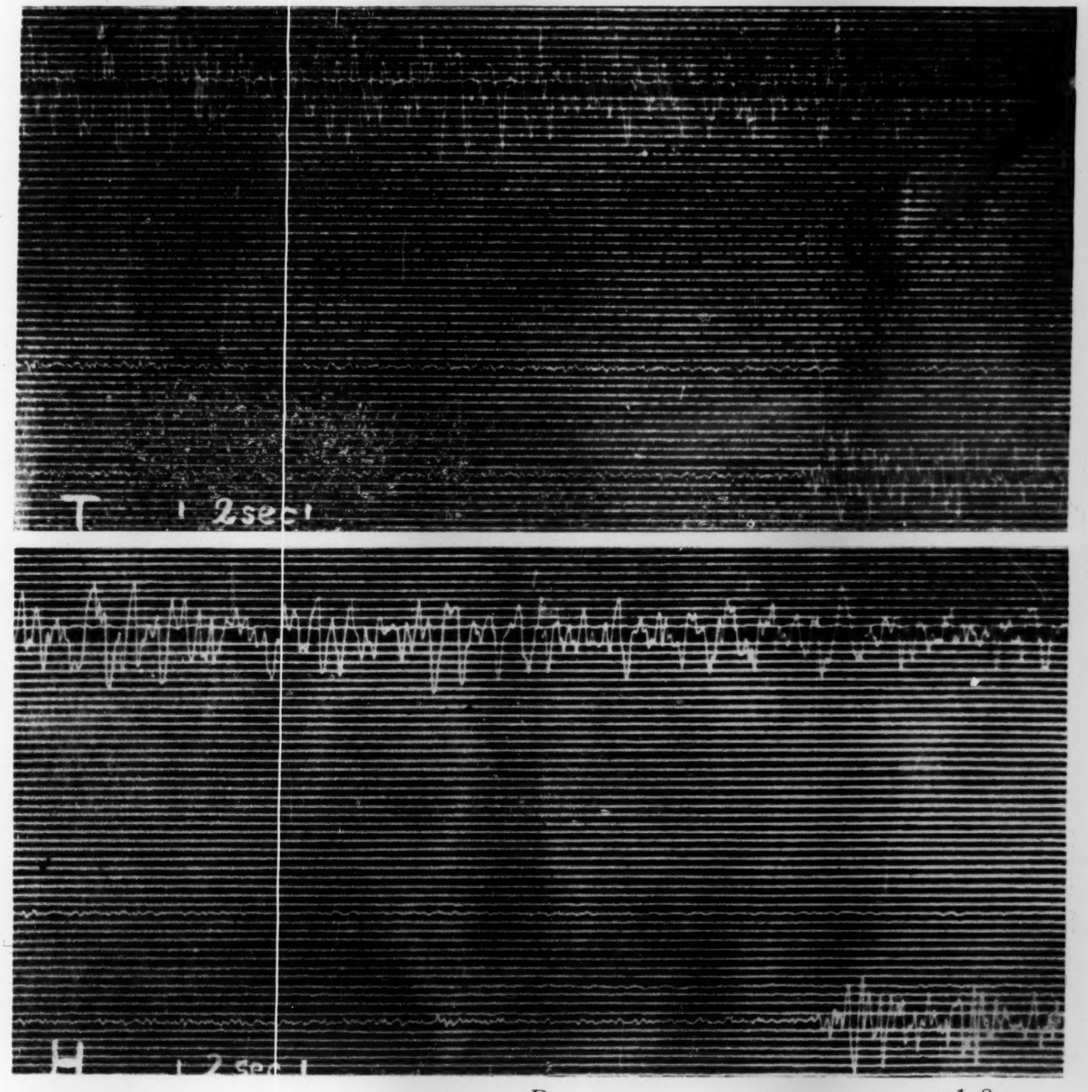

B ×1.8

第 8 図　RTS–I の送信波形 (T) と受信波形 (H) との比較.　Comparison of transmitted (T) and received (H) wave forms by RTS–I.

1955 年 6 月 7 日の小地震を筑波で RTS–I の低周波増巾部から別の電力増巾器を通じ記録したもの (T) と，本郷で受信記録したもの (H) であり，B の上部の振動は A の地震のつづきである.

（震研彙報　第三十三号　図版　宮村・辻浦）

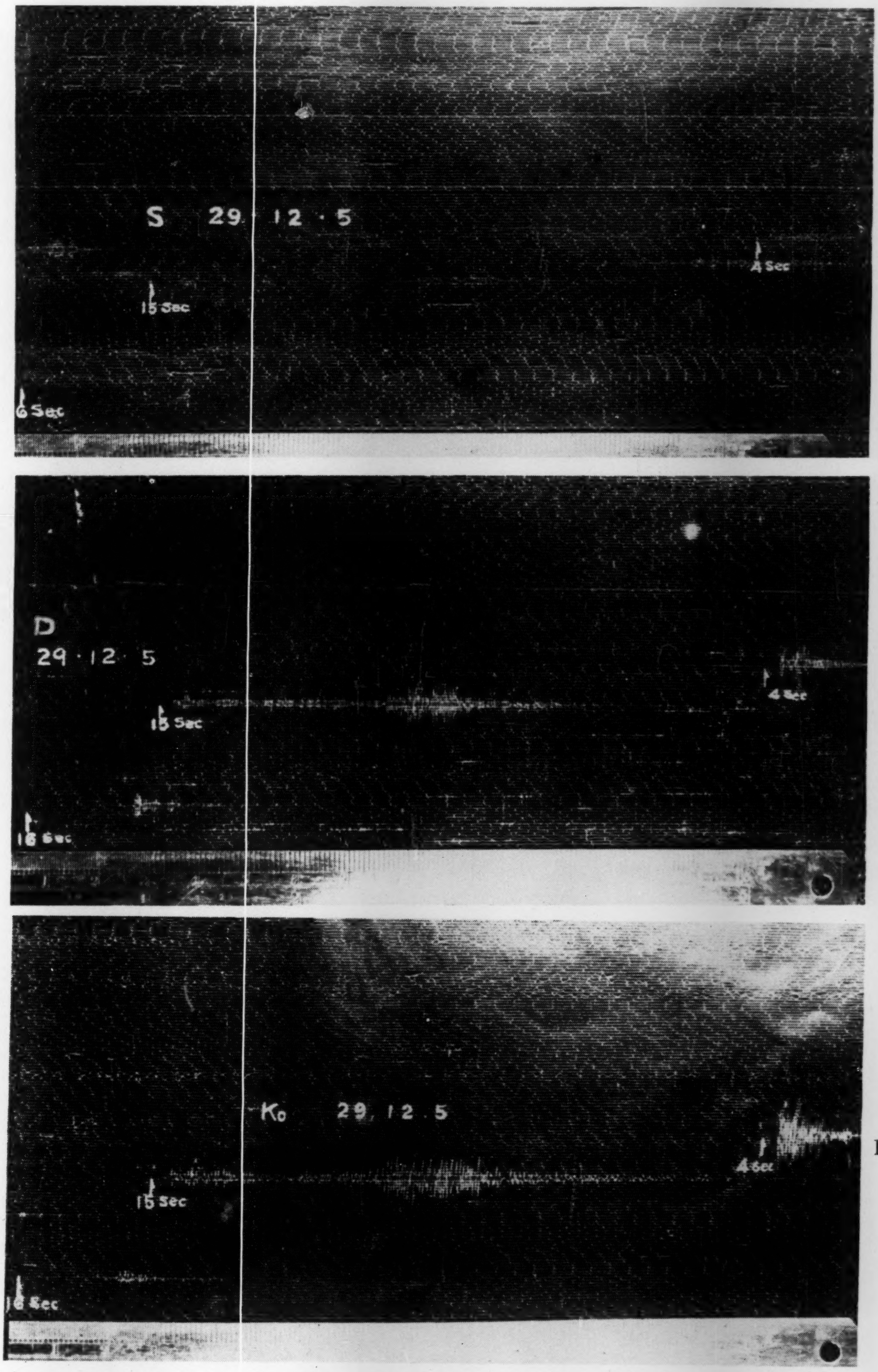

S

D

Ko

第 9 図　和歌山地震群の琴浦 (Ko) 基地における集中記録の一例. An example of central registration of Wakayama earthquake swarms at Kotono-ura.

S: 三田無人観測点の震動 (V) の LTS による記録 Seismogram of shocks at unattended station, Santa, recorded at Kotono-ura by LTS.

D: 出島無人観測点の震動 (H) の RTS による記録 Seismogram of shocks at unattended station, Dezima recorded at Kotonoura, by RTS.

Ko: 琴浦基地における震動 (V) Seismogram of shocks at the central station, Kotono-ura recorded at the same place. Sensitivity: S 150 μV/mm, D 30 μV/mm, Ko 10 μV/mm (effective voltage/double amplitude)

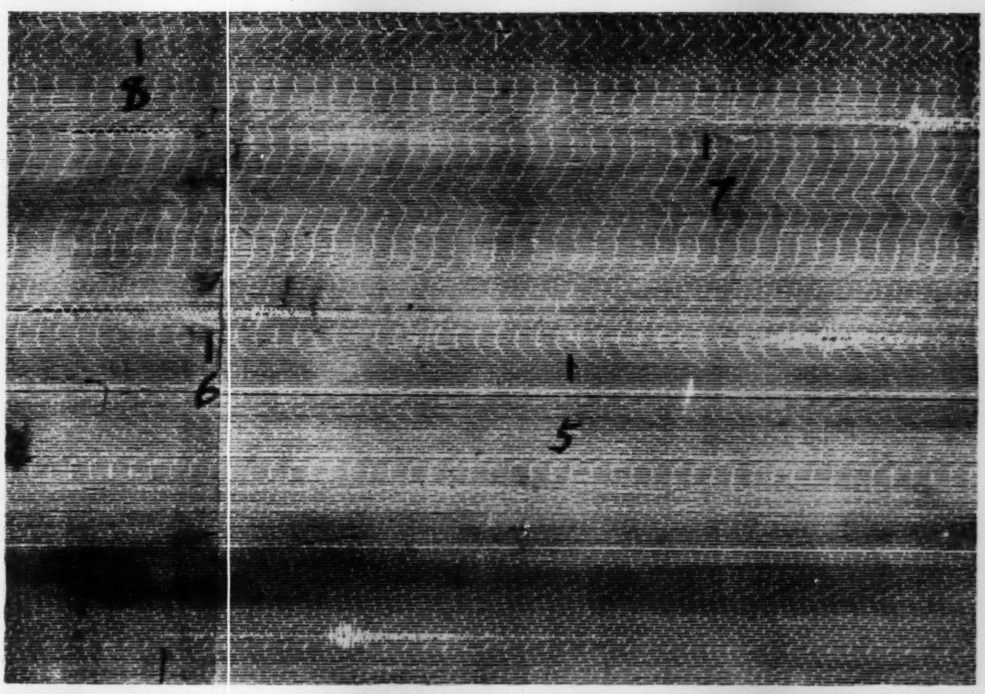

第 10 図　RTS-I により筑波山支所における小地震を約 75 km はなれた本郷地震研究所内にて記録観測せる一例. 1955 年 6 月 12～13 日.　感度: 30 μV eff/mm 全振巾.

An example of seismograms of small earthquakes at Tukuba recorded in the institute at Hongo, about 75 kms from Tukuba. Seismograms on June 12～13, 1955. Sensitivity 30 μV effective value/mm double amplitude.

latter being the frequency modulated within the range of ± 300 c/s by seismic frequencies. Antennae used are the three-elements directive YAGI-antennae with horizontal polarizations, which are constructed of several light metal sections so as to be portable.

Some details of the transmitter and receiver are given in Table I. Frequency and sensitivity characteristics of the set are given in the Figs. 5–7. Distortionless transmission by the instrument was verified by the results of experiment executed between Tukuba and Hongo, ca. 75 kms in distance. Transmitted and received seismograms are compared wave to wave in the reproduction of Fig. 8.

As an unattended substation in the swarm earthquakes observations in Wakayama region in 1954, RTS–I worked for a considerable time (from October to December) in excellent condition with over-all sensitivity of 30 μV/mm (Effective voltages to double amplitude). From June to August in 1954 it was used to record small earthquakes of Tukuba in the laboratory of the Institute at Hongo, during which observations the above-mentioned experiment on distortionless transmission was done. Seismograms obtained in Wakayama and Hongo are reproduced in Figs. 9 and 10 respectively. (Read June 28th, 1955.)

49. 携帯用石本式加速度地震計の野外実地使用に対する二三の基礎実験

地震研究所 { 宮村摂三
堀　　実

(昭和 30 年 9 月 27 日発表—昭和 30 年 9 月 30 日受理)

§1. はしがき

地震動の加速度を直接記録する地震計として，加速度地震計が石本巳四雄により考案製作されてから，すでに 1/4 世紀になる[1]．その間，いわゆる石本式加速度計は当初の光学記録・油減衰器のものから，すすがき・空気減衰器のものにかわり[2]，水平動にくわえて上下動もでき，[3] 固定観測点用のもののほか，小型の携帯用 (感度 1/2) のものもでき[4]，計測地震学のひろい分野で，おおくの人々に利用され，近代日本の地震学発展にめざましい貢献をしてきたことは，ひろく知られているとおりである．また，こうして石本式加速度計の利用がさかんになるにつれて，主として萩原尊礼によつて，この地震計の理論的実際的研究の進展がおこなわれてきたことも，周知のことである[5]．

最近においても，石本式加速度計の改良された大型の携帯用(微動計にきりかえられる)が開発されて，大地震の余震観測や各地の地盤の比較観測にひろく利用されてきた．また 1949 年来地震研究所で萩原教授のもとに編成整備された大地震にそなえての余震観測班[6]でも，これは基準地震計として採用されるにいたつた．

このようにして，石本式加速度地震計の野外における実用が頻繁となるにつれ，そのための観測法基準をさだめることが，実際に要望され，それに関連して，若干の点についでは，なお基礎的な研究の不足が感じられた．

1955 年 6 月，本所余震観測班においては，その編成を強化し，観測法についても，細部にわたり基準をきめることになつた．この基準については別に報告される機会があるとおもうが，そのなかで特に問題となつた点は，制振比のとり方であつた．よつてわれわれは，この要望にこたえて，若干の実験および観測をこころみ，結論をえたいとおもつた．ここに，附随的におこなつた二三の実験の結果をもあわせて，簡単にその結果を報告する．制振比の問題についてかならずしも，最後的結論をえたわけではないが，実際に現在野外で石本式加速度計を使用している実情について，その調整法あるいは，検定法の限界をし

1) M. Ishimoto, *Bull. Earthq. Res. Inst.*, **9** (1931), 159-167.
2) M. Ishimoto, *Bull. Earthq. Res. Inst.*, **9** (1931), 316-332.
3) M. Ishimoto, *Bull. Earthq. Res. Inst.*, **11** (1933), 717-723.
4) N. Nasu and T. Hagiwara, *Bull. Earthq. Res. Inst.*, **14** (1936), 290-296.
5) T. Hagiwara, *Bull. Earthq. Res. Inst.*, **12** (1934), 776, **13** (1935), 138, 783.
6) 萩原尊礼　1953 年 4 月 21 日 第 299 回地震研究所談話会発表.

り，さらに今後改良すべき点についても考える参考資料をえたとおもわれるので，発表する．

§2. 実験使用器械および実験要項

実験に使用した地震計は大型携帯用石本式加速度地震計水平動用(保坂製作所製) 8 台で，その要項は第 I 表にしめす．常数検定等の実験には，はやおくりのときは，小型軸型

第 I 表　携帯用石本式加速度地震計常数表

No.	周期 T_0 sec.	基本感度 S mm/gal. 基本倍率 V	幾何倍率 V_G	摩擦値 ρ mm	目標制振度 v_A (h_A)	備考
1	0.103 ±0.003	0.407±0.0003 150	204	0.005	2.8 (0.3)	1951 年保坂製 (震校 2617)
2	0.102 ±0.005	0.406±0.0002 160	231	0.05	臨界制振 (1.0)	同上 (震校 2618)
3	0.100 ±0.006	0.410±0.0004 160	195	0.005	10.5 (0.6)	同上 (震校 2624)
4	0.100 ±0.002	0.405±0.0003 160	212	0.01	制振器解放 (<0.01)	同上 (震校 2625)
5	0.104 ±0.005	0.408±0.0003 160	210	0.015	過減衰 (>1.0)	1952 年保坂製 (震校 2777)
6	0.104 ±0.003	0.407±0.0003 160	185	0.01	7.9 (0.55)	1951 年保坂製 (震校 2619)
7	0.107 ±0.003	0.437±0.0002 150	193	0.025	6.15 (0.5)	1949 年保坂製 (震文研 24 〃)
8	0.106 ±0.002	0.430±0.0000 150	194	0.015	4.0 (0.4)	同上 (震文研 24 〃)

旧式記録円筒 1 台，観測およびおそおくりの実験には余震観測班用の大型軌条型記録円筒 3 台をもちいた．時間基準の刻時には標準電波分秒報時 (JJY) および余震観測班用刻時時計 15 秒接点を利用した．実験および観測は，本郷弥生町地震研究所第 2 号館地上階室内でおこなわれた．自然地震の観測は 1955 年 4 月より 5 月まで，記録紙速度 2 mm/sec で実施した．

なお使用地震計中 No. 1～4 は余震観測班宮村研究室担当班のもの，No. 6 は同 萩原研究室担当班使用予定のもの，No. 5, No. 7, No. 8 は宮村研究室所属のものである．

これらの地震計の自己周期は現在の観測用記録装置では現場で正確にもとめることはできないが，大体 0.100～0.104秒 (No. 7, 8 は 0.106) である (第 I 表) 基本倍率を 3 ケタ感度試験からもとめるためには，さらに精確な周期の測定が必要である．

§3. 固体摩擦

地震計のふりこの運動をかんがえるとき，固体摩擦ははなはだ厄介なもので，これはで

きるだけちいさいことが，地震計としてのぞましい．拡大部分のてこの廻転軸，すす紙とはり先の部分などで生ずる固体摩擦が，どの程度あるかは，地震計の利用にあたりまずしらべる必要がある．使用した8台の地震計について，それぞれ空気制振器についている2個のコックの1つだけを全部はずして自由振動をかかせ，その記象から教科書[7]にある方法で，流体抵抗(制振比)とともに，固体摩擦値をもとめた．これが第I表にしめした摩擦値 ρ であつて，これらはすべて記録線の太さを考えると充分無視できるほど小さい．よつて一応固体摩擦の影響はないとみて今後の実験をおこなう．なお，こころみにコックをはめて，大体 $h=0.3$, 0.5 程度の制振をあたえて自由振動をさせた記録からも ρ をもとめてみたが，この値にあまり変りはみられなかつた．

§4. 静感度(基本感度)試験

実際に余震観測で使用する場合，各点の使用地震計の感度乃至倍率は正確に現地で検定してから，もちいる必要がある．上下・水平の3成分観測をする場合，同一点の3成分の特性は特にそろつている必要がある．振巾の比較を重視する地盤の比較観測でも，各点そろつた感度で観測するのが便利である．現地で簡単に感度をはかり，またそろえるには，てこによる幾何学的倍率を，その腕の長さをはかつてもとめるのでは，なかなか精度がでない．余震観測班では第1図に P でしめすように，空気減衰器中央上部に質量 m をのせ，それにより生ずる記録紙上のふれ a を測定するという方法を採用した．この場合感度 S は $S=a/\alpha$ (cm/gal), $\alpha=mg/M$, M は振子の質量，g は重力加速度である[8]．ある一定の感度が要求されている場合は，ある質量のおもりをのせ，その際のふれをコンパスではかり，所要のふれに近づくよう，てこの比(麦わらの長さ一定とし，その劣腕の長さ)をすこしづつかえてゆく．

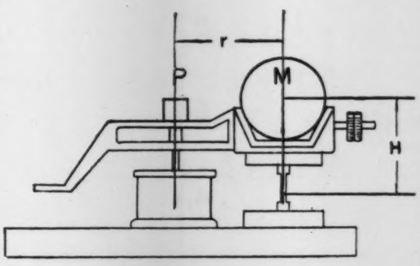

第1図 質量添加法による静感度試験法. Methode d'étalonnage statique par addition des masses.

今回の実験においても，感度を一定とする必要があるので，このようにして，感度をそろえ，第I表 S のような値にして実験をはじめた．No. 7, No. 8 は都合により他とすこしちがう感度になつたが，この方法で大体 2～3% の誤差で一定感度とすることができることがわかつた．

この試験において，加重 m を 25 gr より 600 gr までかえて，加重すなわち負荷加速度と記録紙上のふれとの関係をしらべると，たとえば第2図のごとく直線性をもつているが，No. 1, No. 5 などではある程度以上の力に対し，感度特性が直線からはずれる．この限界は各地震計の特性であり，わるいものでは大体 1.2 cm 約 30 gal まで，が直線性の範囲のようである．したがつて，振巾の比較にはこのことを充分考慮しなくてはならな

7) 萩原尊礼 振動測定 宝文館 (1945) p. 44–47.
8) 萩原尊礼 同 上 p. 339.

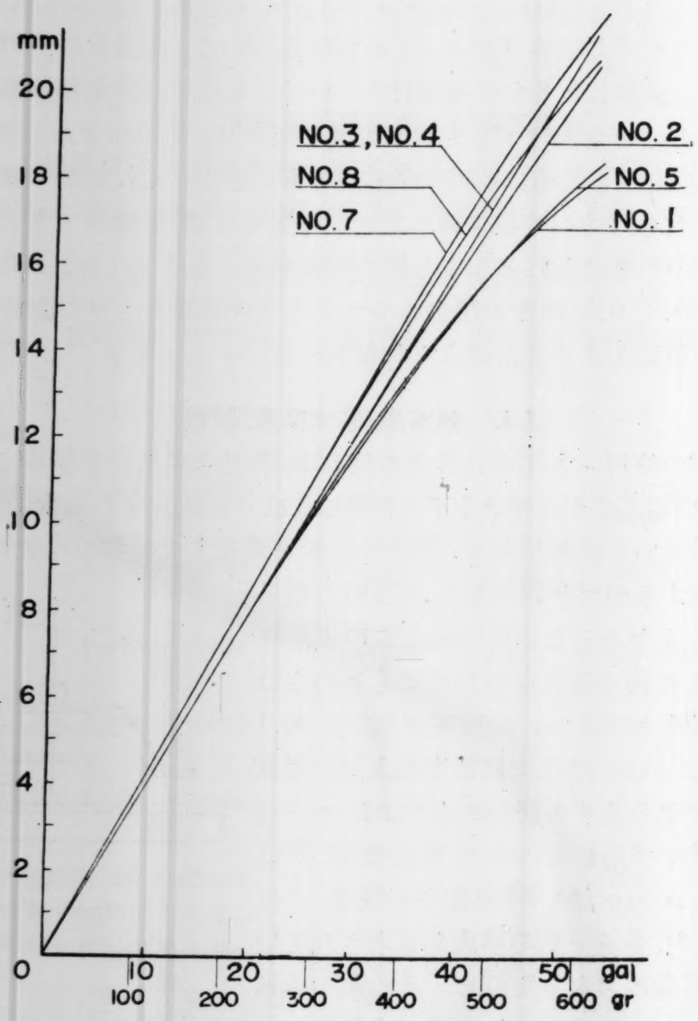

第 2 図　質量添加法による静感度試験特性. Courbes d'étalonnage statique par addition des masses.

い. 勿論これは描針の弧による影響は考えてあるがこれは大したことはない.

第 I 表の基本倍率はこの重量添加法からだした感度 S と前節ではかつた自己周期 T とから $V=4\pi^2 S/T^2$ の関係により算出したものである[8].

このとき別に, てこ倍率をノギスではかつて計算した拡大率が第 I 表の幾何倍率, 乃至てこ倍率 V_G である. V と V_G の差は, 大体はてこの慣性能率の影響による*.

なお, この質量添加試験法では当然ふりこの一方むきのふれだけしか与えられないので, 左右対称性についての保証はないが, 一応これは問題ないとしておく.

* 萩原尊礼　振動測定 p. 174 によればこれは約 17% であるという. ここでは約 20% になつている.

§5. 制振比と動感度試験

5.1 たたき試験法による減衰自己振動からえられる制振比 v_T 乃至制振常数 h_T

現在実際にこの石本式加速度地震計を調整して，適当な制振をあたえ，観測をはじめる場合，普通におこなわれている手つづきは，まず空気制振器のコックをはずし，重錘をかるくたたいて，この充分小さい制振において，きれいな自由振動をえがくように，制振器と，てこの各部などを調整し，ついで制振器のコックをしめつつ，重錘をたたいて左右に自己振動をかかせ，その制振比を円筒のすす紙上で，目的の制振比にあわせた比例コンパスをあててしらべ，所要の制振比に近づけてゆく．こうして，目的の制振比がえられたと思つたら，そこでコックを固定し，なおたたき法で減衰自己振動をたくさんかかせ，にすづけして，これらをよみとり制振比乃至制振常数を決定するのである．こうしてもとめた制振比乃至制振常数をわれわれはここでたたき試験法 (Tapping Test) によるものという意味で v_T 乃至 h_T とかくことにする．

ところで，実際の経験によると，こうしてもとめた v_T または h_T は，はじめ目標とした制振の値 v_A 乃至 h_A とはくいちがつてしまうことがおおい．そこで今回たたき試験による制振比決定の精度をしらべるため，これについて，つぎのような実験をこころみた．

まず，第 I 表にしめすように，各地震計の目標制振値をさだめ，これを目標として，それぞれ上述の方法で，調整時間を約 5 分間とかぎり実施し，v_T の値をもとめ，これを N 回くりかえした．その結果をしめすのが，第 3 図であり，よこ軸は各実験回数，たて軸は 1 回 5 分間の調整でえられた制振状態での減衰振動記録左右 10 ケづつから算出した制振比 v_T の平均値と誤差（標準偏差）である．この 1 回の実験がすむと，つぎにはこの状態をくずしてまた 5 分間に目標値に制振化が近づくように調整し，たたきの記録をとる．なを実線は目標値，破線は各回 v_T 全部の平均とその誤差（標準偏差）をしめすものである．

これによれば，あきらかに目標制振度が大きいほど，これに対する，たたき試験でえられた値のはずれは大きく，かつ各回ならびに全体としての偏差も大きい．大きい制振比ほど，この方法では，目標にそろえるのが困難ということをしめしている．勿論，これには個人誤差もかなりふくまれるであろうが，一応の基準となるものとおもわれる．

なお，臨界制振および過制振をねらつて調整した No. 2 および No. 5 の地震計では，たたき試験による減衰自己振動の記録が，円筒回転がのろいため信頼できず，等時間間隔分割により振巾減衰をよんで制振比をもとめる方法による結果は信用できなかつた．したがつて，このような大きい制振比の場合の問題は，なお今後の研究課題としておきたい．

5.2 たたき試験法によりもとめた制振比と記録紙速度との関係

記録紙速度と固体摩擦の関係はかつて岸上冬彦[9]がしらべたことがあるが，これは今回は実験にさしつかえないことがわかつたが，おかしなことに，記録紙速度をかえてたたき法で制振比をもとめてみると第 II 表のように，$v_A=6$ 以上では，速度がはやくなると，も

9) F. KISHINOUYE, *Zisin* (*Journ. Seism. Soc. Japan*), [i], **15** (1943), 44–68.

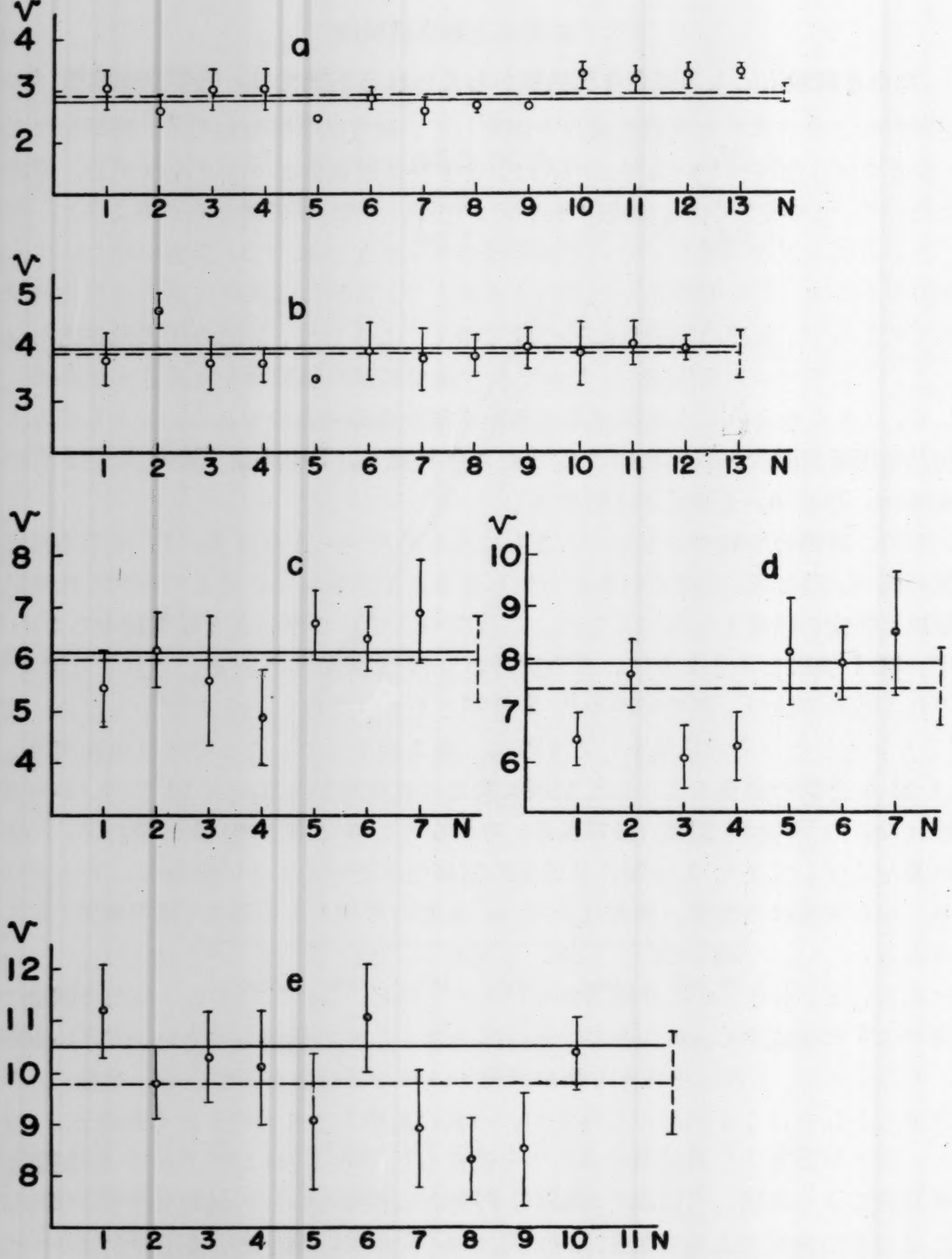

第 3 図 たたき試験法による制振比の目標値 v_A (実線) に対する決定値 v_T およびその平均値 $\bar{v}_T$ (破線). Rapport de l'amortissement visé v_A (——) et celui déterminé v_T et son moyen $\bar{v}_T$ (- - -) par éxamen de tapement.

	a	b	c	d	e
v_A	2.8	4.0	6.15	7.9	10.5
$\bar{v}_T$	2.94±0.23	3.91±0.45	6.02±0.85	7.36±0.78	9.77±0.97

第 II 表　制振度 v_T と記録紙速度の関係

記録速度 ＼ ねらい 制振度 v_A	2 mm/sec.	4 mm/sec.	8 mm/sec.	20 mm/sec.
1	1.03±0.00	1.03±0.00	1.03±0.00	1.03±0.00
2.8	3.35±0.15	3.47±0.19	3.5 ±0.24	4.0 ±0.44
4	5.7 ±1.10	5.5 ±1.12	5.9 ±0.64	5.6 ±1.09
6.15	6.9 ±1.05	7.48±1.43	7.45±1.43	9.1 ±1.75
7.9	8.5 ±1.22	9.4 ±1.18	10.8 ±1.29	12.9 ±3.31
10.5	10.5 ±0.6	11.6 ±0.73	12.61±1.51	15.0 ±1.55

とめられる制振比 v_T がふえてゆく傾向がみられる．これは余震観測班では 4 mm/sec という一定速度で記録するので問題はないが，場合により注意を要する．ただし，このような事実を示す原因は不明なので，なお今後検討を要すると思われる．

5.3　動感度試験とそれから推定される制振比 v_D 乃至制振常数 h_D

現場で加速度計の動感度(振動特性)をはかる簡単な方法としては第 4 図のようにゴム糸の一端 A を重錘の中央にとりつけ，他端 B にながい糸をつけその先を回転円板の中心から r の距離にある C 点にとりつけ，円板をいろいろの回転数 ω でまわし，そのときのこの力による強制振動の記録をとり，振巾 a と周期 T' をはかる方法が用いられる[10]．

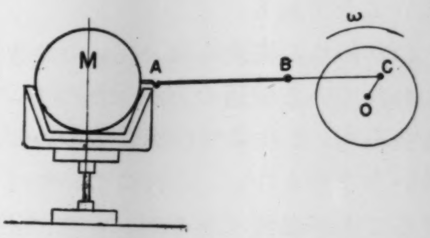

第 4 図　ゴム糸による動感度試験法．
Methode d'étalonnage dynamique par un fil de cautchouc.

この方法で No. 1〜No. 8 の地震計の振動特性をしらべたものが，第 5 図 a—h の丸印である．破線はこの丸印にもつともよくあうようにひいた正弦定常力による強制振動の理論的振動特性，すなわち，地震計の加速度感度係数 $F_a(u, h)=u/\sqrt{(u^2-1)^2+4h^2u^2}$ $(u=T/T')$ をかいたもので，その場合の h を動感度試験による制振常数という意味で h_D となずける．実線をもつて，おなじ地震計の制振比を（勿論制振器は同一の状態で）たたき試験法によりもとめた h_T に対応する理論的特性曲線をかいてあるが，この両者はあきらかに h_T の決定誤差をはるかにこえた不一致をしめす．

h_D と h_T をくらべてみると第 III 表のようになり，ほぼ h_D は h_T より 3 割あまり小さく，動感度試験によると，たたき試験によるよりも，制振があまいようにみえることになる．

このような事実はすでに著者の 1 人[11] が今市地震の余震観測を栃木県船生 (Hunyū, Totigi Pref.) でおこなつたとき，$h=0.6$ くらいをねらつて調整した加速度計（ここに

10)　萩原尊礼　振動測定　p. 340.
11)　S. MIYAMURA and T. AKIMA, *Bull. Earthq. Res. Inst.*, **28** (1951), 421–432.

第 III 表　各種の制振常数の比較

h_A	0.01>	0.3	0.4	0.5	0.55	0.6	1.0	>1
h_D	0.009>	0.25	0.27	0.35	0.38	0.49	0.68	1.1
h_T	0.009	0.35	0.49	0.53	0.56	0.62	—	
h_D/h_T	1>	0.71	0.55	0.66	0.68	0.79	—	

もちいた No. 7 と No. 8) について，同様の方法で動感度試験をおこない，$h=0.35$ 程度の動感度係数曲線をえて，報告したことがある．この場合たたき試験による決定のばらつきに関する今回の実験を考慮しても，やはりこの差は否定できない．

一方，すでに萩原尊礼[12]が論じたように，空気制振器の制振力は正確には速度に比例しない．このような場合について，鈴木次郎[13]は空気制振器をもつ地震計の振動特性が普通の理論による場合とちがつてくることを指摘し，石本式型の地震計についての特性曲線を実際に計算した．それによると，自己振動からもとめた h の値に対する従来の理論による曲線よりも制振があまい傾向になり，その程度は制振が大きいほどはなはだしい．

この傾向は，われわれの実験結果と定性的には一致するものである．しかし，定量的には，種々の常数が鈴木のしめした計算とちがうことを考慮しても，なお必ずしも一致はしないようである．

われわれの実験において，たたき試験法と動感度試験法とは，ともに現在，現場でおこなわれている普通の方法であつて，ともに実験法としては同等の資格をもつものである．もちろん，この2つの実験法のいづれか，または両方ともが多少の欠点をもつていることはいうまでもない．これについては，現場で実用になる，より正しい制振比決定法を考案することが必要であるが，一方，理論の方にも，また問題があるかもしれない．萩原・鈴木の研究はこの線にそう貢献であつたわけである．もちろん理論を考慮するということは，逆にいえば地震計の設計製作面あるいは調整法使用法の面で，従来の理論にあうような器械をつくるという努力，乃至より正しい使用法をとるようにする努力を考慮することをふくむわけである．しかし，いづれにしても，現在どおりの石本式加速度計の野外実用の状況では，上述の結果を充分考慮する必要があろう．

§6. 自然地震の観測結果

上述の実験をおこないつつ，あわせて，これら8種類のことなつた制振比をあたえた同一自己振動週期をもつ地震計をもつて，同一方向成分の地震動観測を実施してみた．

観測実施中にえられた4ヶの地震のそれぞれについて，各地震計の記象をくらべてみると，無制振にちかい No. 4 をのぞき，ほとんど完全に波の対応がつく．No. 4 も高周波がかさなつているが，大体の見当はつく．記象の一例は Fig. 6 (Pl. CX) にしめしてある．

12) T. HAGIWARA, *Bull. Earthq. Res. Inst.*, **13** (1935), 783.
13) Z. SUZUKI, *Zisin*, [**ii**], **5**, (1952), No. 4.

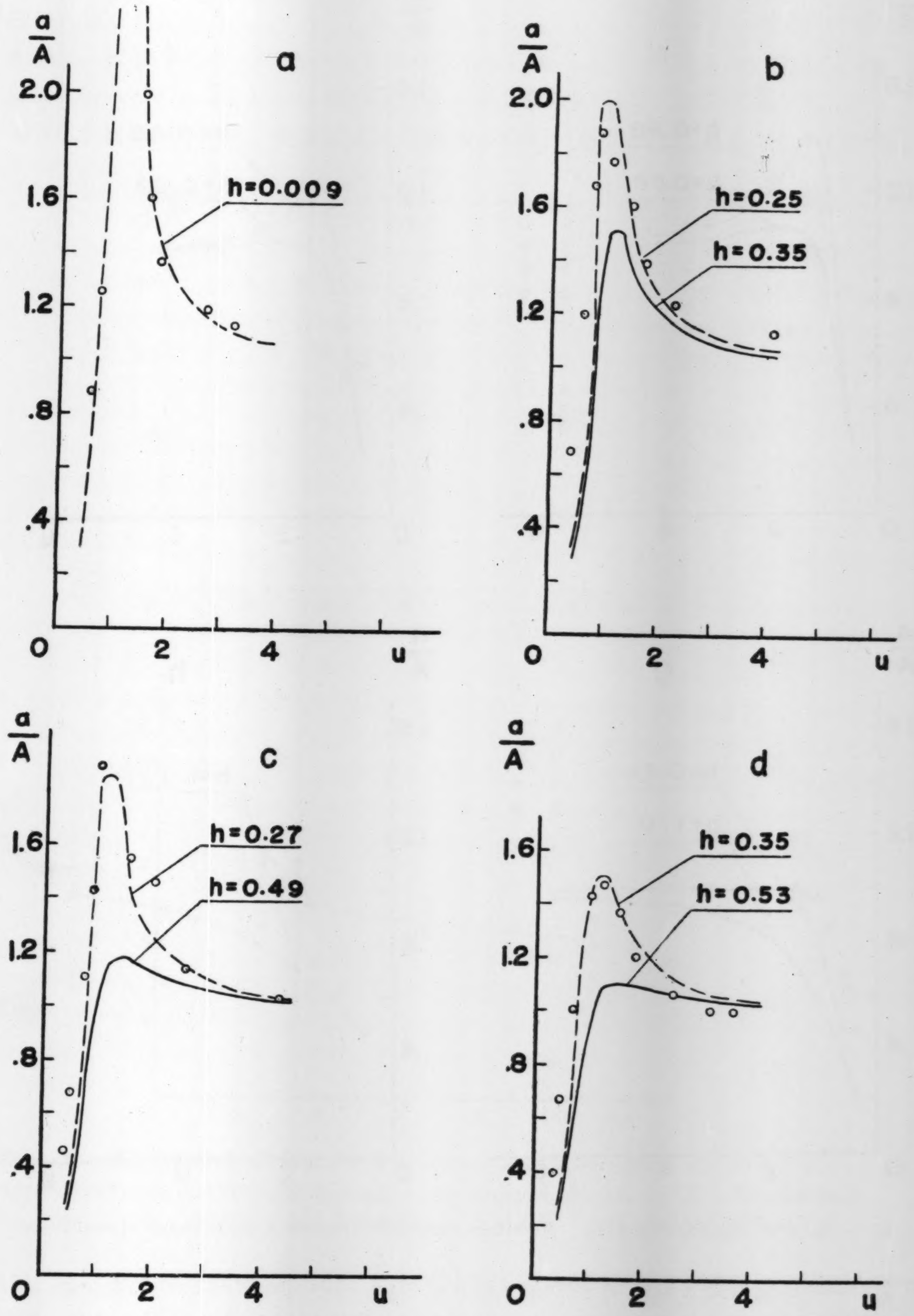

第 5 図，a–d 動感度試験特性 Courbes caractéristiques d'étalonnage dynamique.

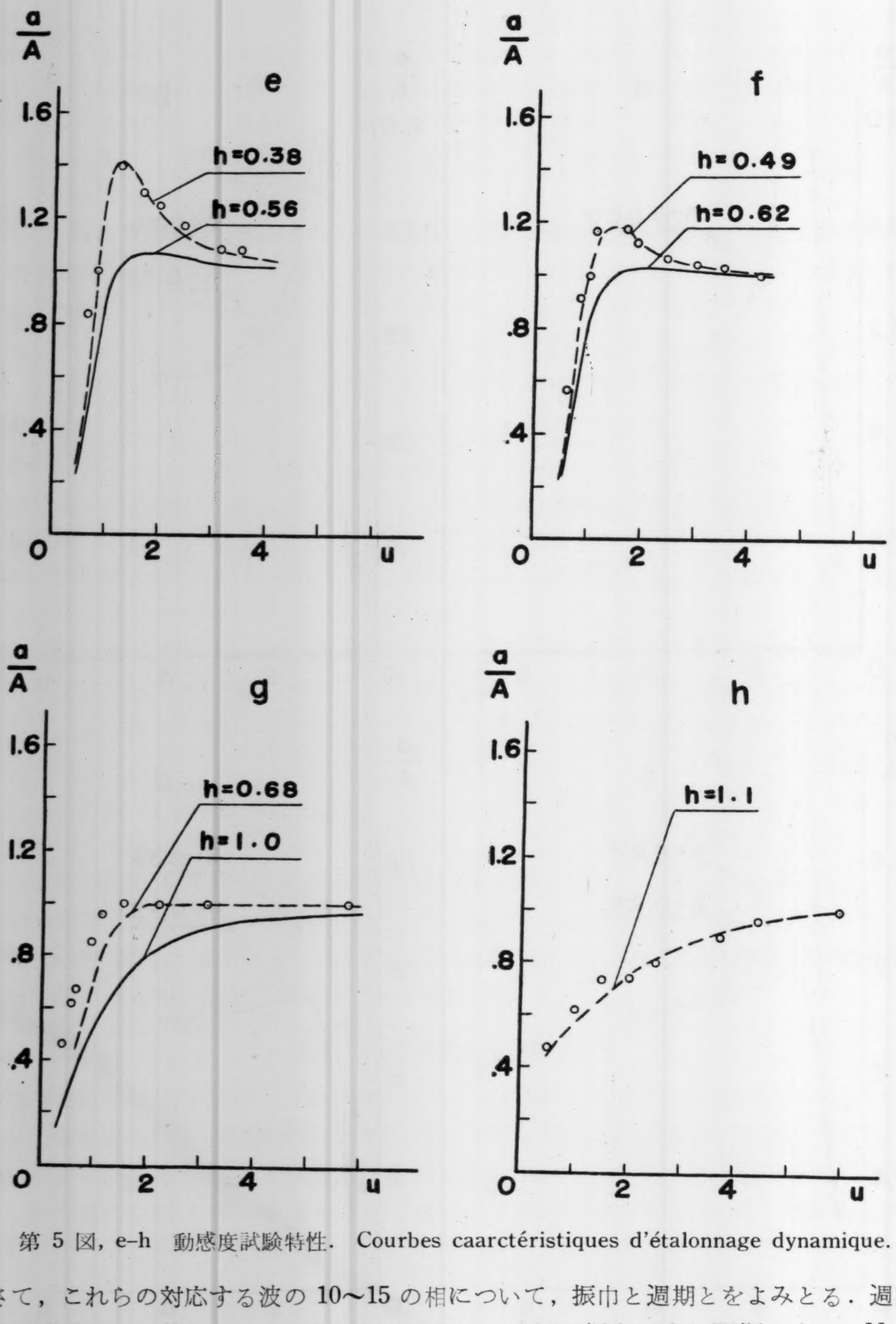

第 5 図，e–h　動感度試験特性．Courbes caarctéristiques d'étalonnage dynamique.

さて，これらの対応する波の 10〜15 の相について，振巾と週期とをよみとる．週期の方は地震計による差はほとんどみられないので，今回は振巾だけを問題にする．No. 7, No. 8 については静感度補正をおこなつたうえ，各相につき $h_T=0.56$ の地震計のかい

た振巾 A_0 を標準とし，これに対する振巾比 A/A_0 をもとめる．この振巾比を各地震につき平均した値をしめしたものが第 7 図 a, b であつて，よこ軸には各地震計の制振常数 h をとつた．破線はめのこでひいた平均線である．h として a では h_T, b では h_D をとつてある．h_T の方は $h \geq 1$ では値がはつきりきまらないので，多少問題があるが，ともかく $h=0.6$ 程度以下では，制振比による振巾のちがいが，かなりあることがわかる．し

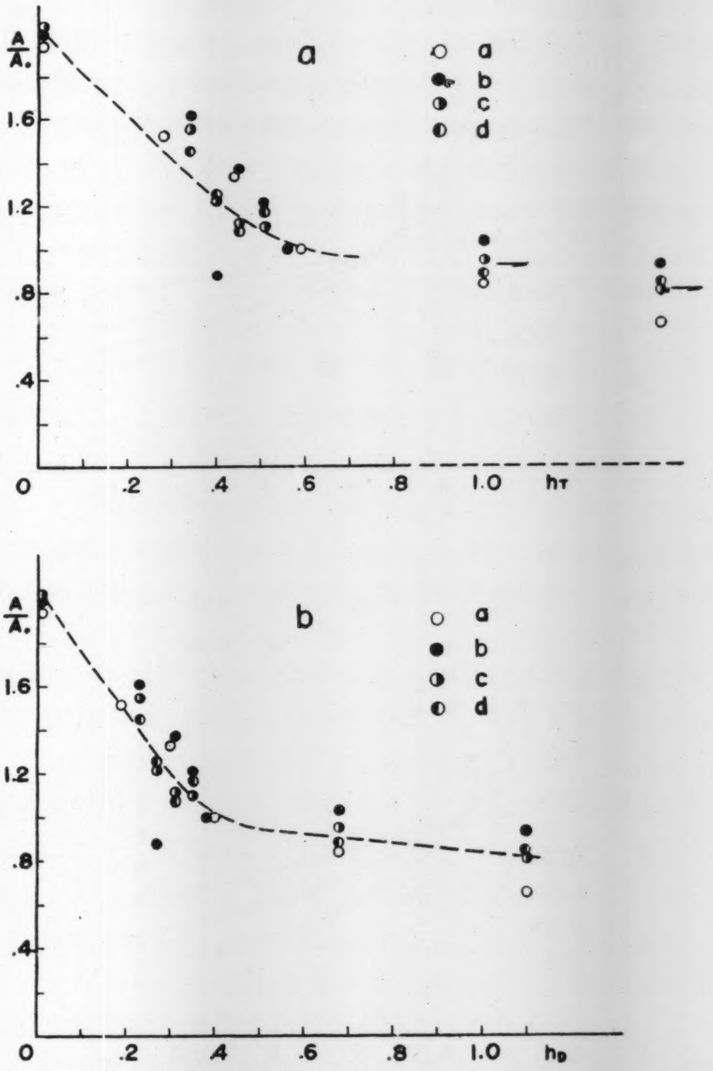

第 7 図　自然地震動振巾の制振度によるちがい（$h_T=0.56$ の振巾 A_0 を 1 とする.）
a: 1955. IV. 15. $13^h 53^m$ 茨城県沖地震,　　b: 1955. V. 12. $17^h 36^m$ 茨城県沖地震
c: 1955. V. 13. $10^h 59^m$ 千葉県北部地震,　　d: 1955. V. 15. $19^h 40^m$ 頃震央不明.

たがつて，制振比がそろつていないと，振巾をくらべるときに注意を要することになる．h がちいさければ，§5 にみたように，制振常数決定の精度は高いけれど，振巾を補正なしでつかうには，かならずしも都合がよくないわけである．§5.3 でのべた点に関連

し，鈴木次郎は結論として，制振比の小さい状態での使用を1つの解決としてすすめているが，これは定量的に記録を処理するにはもつともよい方法であり，§4の点からもよいわけであるが，簡単によみとり値の振巾をそのままつかうような使用方法乃至目的の場合はこれはさけなければならない，制振比決定を精確におこなわないなら，むしろ h を 0.6 以上にすることにしておいた方が安全であるということになる．

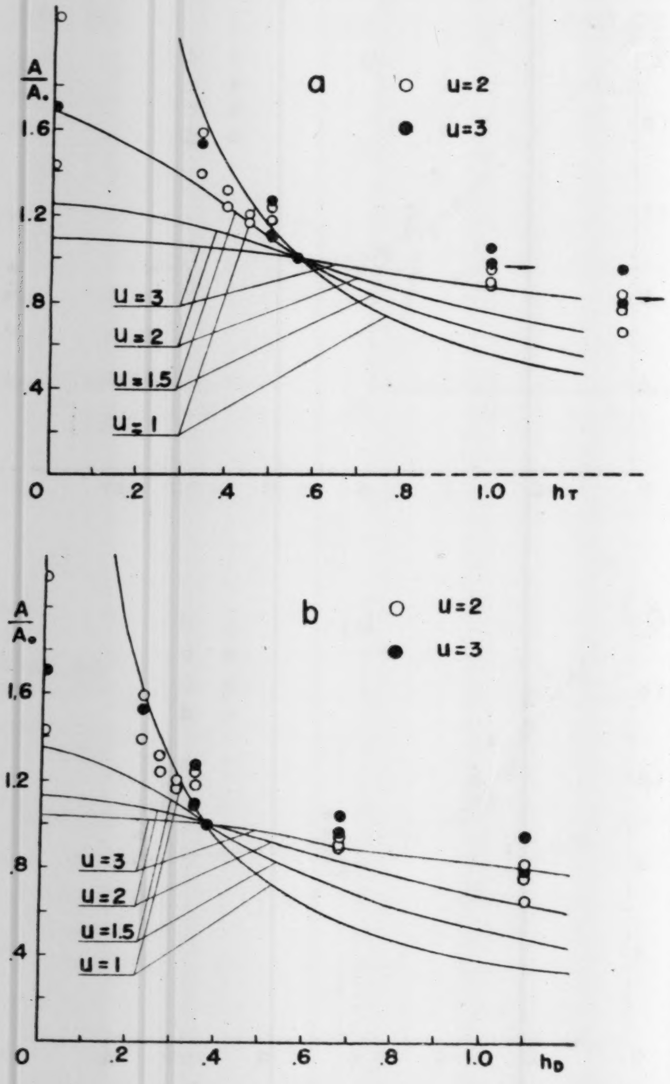

第 8 図　自然地震振巾の制振比によるちがいを波の週期の振子の週期に対する比によりわけて，普通の理論とくらべる．

なお，第 8 図では各相の振巾比をすべて 1 つの地震の 1 つの地震計の記象につき，みなあつめて平均したが，これらをその週期でふるいわけ，$u \fallingdotseq 2$ のもの，$u \fallingdotseq 3$ のもの（地震計週期 0.10秒一定）をとりだし平均してみると，第 8 図の白丸印乃至黒丸印になる．一方，この図には普通の理論による動感度係数 $F_a(u,h)=u/\sqrt{(u^2-1)^2+4h^2u^2}$ で $u=\mathrm{const}$

として，h を変数としたときの値を $h=0.56$ を基準とし，それに対する比とした曲線，すなわち $y(u,h)=F_a(u,h)/F_a(u,0.56)$, $u=1,1.5,2,3$, の曲線をかいてある．もしこの理論がこの地震計の地震時の運動をあらわしているなら(地震動は正弦振動の連続でないから当然ちがいはあるが，普通動感度補正をこの理論で考えることもよくあるから)，その場合にはこの白丸印，黒丸印は夫々 $y=(u,h)$, $u=2$ またわ 3 の曲線のうえにのるべきである．

h として h_T をとつた図 (第 9 図 a) では，これはまつたくあわないが，h として h_D をとつた図 (第 9 図 b) をみると，$u=2$ については $h_D \geqq 0.3$ で，$u=3$ では $h_D \geq 0.35$ で，ほぼこの理論曲線のまわりに点があるようにみえる．これからかんがえると，自然の地震動を記録している状態では，記録振巾は地震計の制振常数として h_D をとれば制振常数の小さい範囲をのぞいて，定常的正弦強制の普通の理論が大体はあてはまつているようにみえる．鈴木次郎の研究によれば，制振比の大きいほど普通の理論とのくいちが大きいのであるが，この結果はそれとは反対の傾向になる．鈴木のとりあげた以外の問題もこの地震計の運動にふくまれていることをしめすものである．

§8. 結　　論

現在一般に実用されている状態での大型携帯用石本式加速度地震計（水平動成分）について若干の実験をおこなつた結果つぎのことがわかつた．

1) 質量添加法による静感度試験では，3% 程度までその感度をそろえることは容易であつたが，感度の直線性は地震計によりことなり，片振巾 10 mm (加速度約 30 gal) くらいから感度がおちるものもある．したがつて，振巾の比較についてはこの点に注意を要する．

ただし地盤の比較などでは，これは大きい振巾のところがますます大きい振巾になるむきであるから，振巾比が 1 より大ならより大きく，1 より少ならより小さくなるわけであり，従来もしこの注意をしてなかつたとき地盤差につき出した結論より，地盤差はよりいちじるしくなるだけだから，従来の結論がちがつてくることはない．

2) たたき試験法により制振比 v_T を目標値にちかづけるのは，制振比が大きいほど困難になり，制振比をたたき試験による減衰自由振動記録のよみとりからもとめる決定精度もわるくなる．臨界制振にちかいもの以上は，この方法でうまくきめられなかつた．装置の考案を要する．これらの点からは定量的な記録処理には制振比が精確にきまるよう制振のすくない常態で地震計を使用する方がよいことになる．

3) $v_T>6$ くらいになると，たたき法による制振比の決定には，記録紙速度の影響があり，はやいおくりで記録をとつて v_T をもとめると，のろいおくりでもとめるより大きい値がえられる．原因は不明である．今後の研究を要する．

4) 正弦強制力をあたえてえた動感度曲線に，普通の理論曲線をあてはめて，制振常数をきめると，その値 h_D はつねに h_T より小さく．そのちがいは制振の大きいほどいちぢるしい傾向がみられる．これは鈴木次郎の計算と定性的にあうが，定量的にはかならずしもあわない．

5) 現在実際にもちいられる2つの制振度決定法によつてえた制振常数 h_T, h_D に測定誤差をこえたくいちがいのあることは，1° 2つの実験法のいづれか1つ，または両方ともが欠点をもつか，2° この実験で h というものを考える基礎の理論に不完全な点があるかであり，いずれの場合も，その解決には 1° 実験法の改良と 2° 理論の改良（地震計にあう理論をつくる）および地震計の改良（理論にあう地震計をつくる）のいづれか，または両方を考慮してゆく必要がある．

6) 自然地震 4 ヶを制振常数のちがう 8 ヶの石本式加速度計で観測した記象は波の位相ははつきり対応がつくが，その振巾は制振のちいさいほど大きい．$h_T=0.56$ の地震計 ($h_D=0.38$) の振巾に対する比をとると，それより小さい制度比では振巾は急にふえるが，過制振にとつたつもり（実際は $h_D=0.7$）の地震計の振巾は $h_D=0.38$ のものとあまりちがわない（1割以内）．したがつて，この点からは，制振は $h_T \geqq 0.6$($v_T \geq 10$) でねらつておけば，3) によりその決定精度はわるくても，そのまま振巾を補正せずにつかうためには比較的安全といえる．

8) 自然地震動の周期によつて，制振比による振巾の差がどうなるかをしらべ，これを普通の定常正弦強制の理論からだした曲線とくらべると，あまりよくあわない．$h_D > 0.5$ くらいではある程度あつているともいえるが，制振の小さい部分では，まつたくくいちがう．

§9. 謝　　辞

本実験につき御協力御後援をえた本所余震観測班の各位，技術部工作係の方々，および自然地震の観測を分担された辻浦賢，松本英照両氏に感謝する．

---

49. Quelques essais au laboratoire pour utilisation pratique du sismographe accélerometrique du type d'Ishimoto.

Par Setumi MIYAMURA et Minoru HORI,

Institut de recherches sur tremblement de terre.

Nous avons éxécuté quelques expériences fondamentales pour utilisation pratique du sismographe accélérométrique du type d'Ishimoto. Cet appareil est aujourd'hui employé chez nous par beaucoup des gens en plusieurs branches de sismologie scientifique et appliquée. Donc nous avons été demandé d'établir une methode typique de la manipulation de l'accélérometre d'Ishimoto du côté des gens, qui s'occupents dans observation pratique par cet appareil en campagne, et essayé des expériences rapportées ici.

En premier lieu sont préparés 8 sismographes du type d'Ishimoto pour les composantes horizontales, qu'ils ont été construits portatives pour observations en campagnes des régions épicentrals des grands tremblements de terre futures à notre institut par la fabrique Hosaka. Les sensibilités statiques des 8 appareils sont calibrés et égalisés dans les limites de 2–3%. Les courbes d'étalonnage étaient obtenues, en posant des poids m les uns les

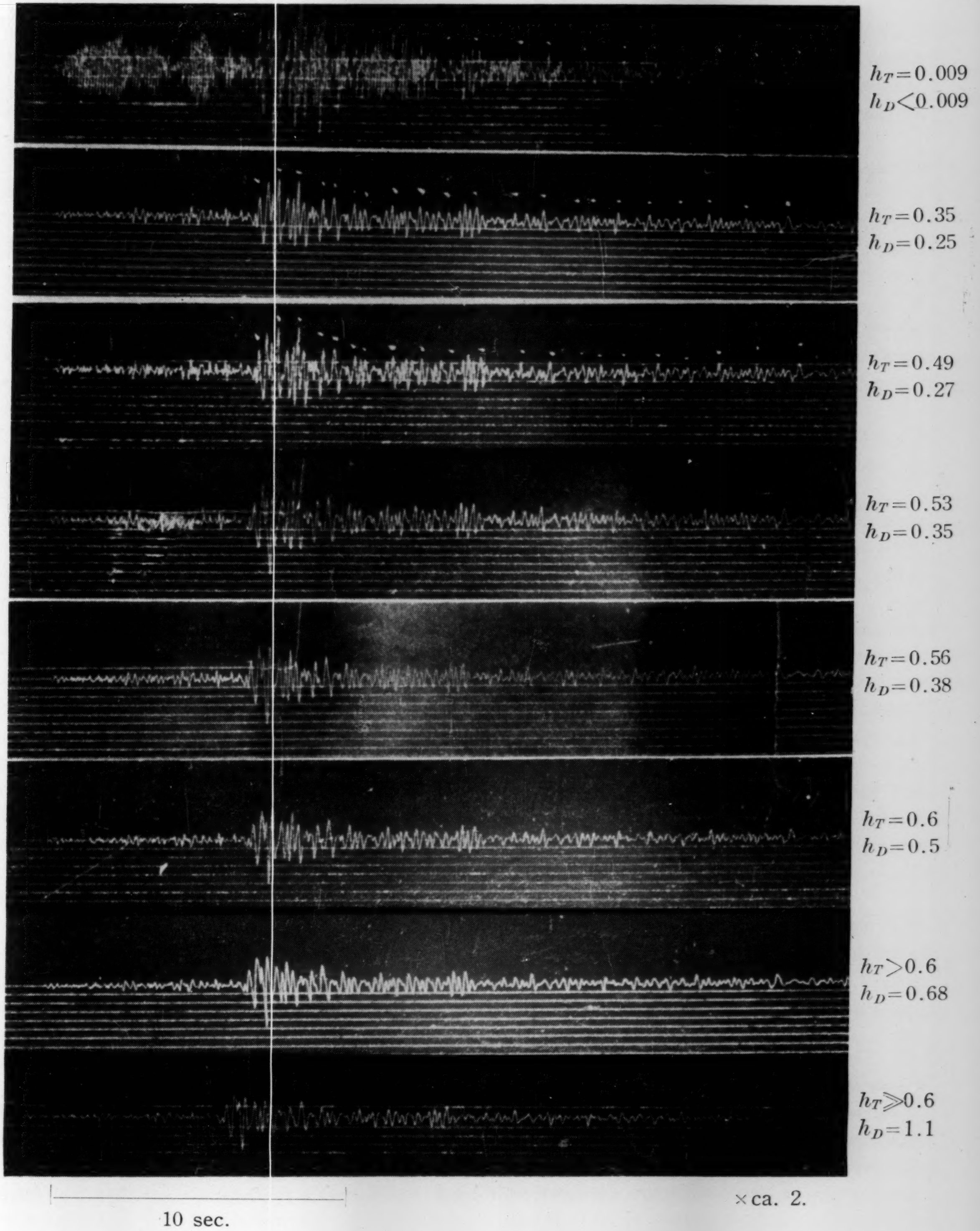

Fig. 6. 種々の制振比をあたえた石本式加速度地震計による地震記象の例.
(1955 年 5 月 13 日 10 時 59 分千葉県北部地震)

Sismogrames des accéléromètres du type d'Ishimoto avec differentes amortissements. (Tremblement de terre du 13. mai, 1955, Kwanto sud, enregistré à Hongo.)

autres sur la jointure P du piston de l'amortisseur de chaque appareil (v. Fig. 1), et mesurant des déviations inscrites par la plume successivement. Comme ils sont montré dans la Fig. 2, les courbes sont linéaires jusqu'a la déviation 20 mm, correspondante a l'accélération des 50 gals excepté quelque-uns avec caractères inferieurs. (par example, No. 1, No. 5 etc.)

Les frottements solides ρ sont très petits, et nous pouvons négliger ces influences sur sismogrammes. (v. Table I)

Pour adjuster l'amortisseur et décider la valeur de la constante d'amortisseur, nous avons adopté la methode d'examen par tapement. Après nos expériences, qui nous avons éxécuté, en donant 8 differents amortissements pour 8 sismographes respectivement, nous pouvons tirer les conclusions suivantes. Comme nous pouvons voir dans les figures de a–h de Fig. 5, il est plus difficile atteindre à la valeur d'amortissment forte deteriminé d'avance, que à la valeur faible. En outre, la précision de la constante, déteriminée par enregistrements des oscillations libres, est aussi plus base pour le sismographe fort amortissé, que pour celui amortissé faible. (v. Fig. 3)

Après nos éxperience il semble que la vitesse de papier de registration influe sur la valeur de la constante d'amortissement déterminée par tapement: mais maintenent nous n'avons pas trouver des explications raisonables. (v. Table II)

Pour verifier les lensibilités dynamiques des appareils avec differants amortissements, nous avons éxécuté l'étalonnage à l'aide d'un fil élastique de cautchouc, dont une éxtrémité est atachée à la masse du pendule, l'autre éxtrémité étant animée d'un mouvement sinusoïdal d'amplitude constante et differentes périodes. (v. Fig. 4) En conséquence nous avons obtenu séries des points montré dans Fig. 5 a–h, suivant le degré d'amortissement du sismographe. Deux courbes dans chaque diagramme de Fig. 5 sont les courbes charactéristiques de la théorie ordinaire pour les valeurs d'amortissments, s'accordantes avec les éxperiences dynamiques et avec l'examens par tapements. Les figures dans Fig. 5 montrent clairement, que la constante d'amortissement h_D, correspondante à l'étalonnage dynamique, est toujours petite que cela du même sismographe h_T par tapements. Il est en harmonie qualitativement avec computations théoriques de Z. SUZUKI, basés sur l'investigation de T. HAGIWARA. Mais, quantitativement il n'y a pas l'accordance entière entre nos résultats et calculs de SUZUKI. Laquelle des deux valeurs des constantes d'amortissements h_T h_D est-elle correcte, nous ne pouvons pas dire immédiatement, mais le fait, qu'il y a deux h differents, semble en tout cas indéniable.

Les observations pour comparaison de l'effect de l'amortissement sur sismogramme ont été effectuées par ces 8 sismographes, et nous avons réussi à enregistré 4 séismes prochaines, une desquelles est montrée par example dans Fig. 6. Dans la Fig. 7 nous mettons les valeurs moyennes des raisons d'amplitudes des phases correspondantes aux sismogrammes de differentes amortissements avec ceux de l'amortissement normale, c'est-à-dire $h_T \doteqdot 0.56$.

Evidement nous pouvons dire que la variation des amplidudes suivant le degré d'amortissment, est considérable dans le région de petite amortissement ($h_T < 0.6$ ou $h_D < 0.4$). Donc il est sûr, que nous adoptons $h_T > 0.6$, si nous voulons utiliser le sismographe des amplitudes sans correction. Au contraire, il est nécessaire prendre $h_T < 0.6$, comme il est mentionné plus haut, si l'on utiliser les sismogrammes quantitativement, en déterminant la valeur de h_T exactement. Fig. 8 montre, que la théorie ordinaire du pendule forcé sinusoïdalement n'est pas correcte, en classifiant les points dans Fig. 7 par ses périodes.
(Lu le 27. sept., 1955.)

50. 黒沢尻附近の水準測量結果

地震研究所　岡　田　　惇

(昭和 30 年 9 月 27 日発表-昭和 30 年 9 月 30 日受理)

§1. まえがき

東北地方の地殻構造についての地球物理学的研究は，既に数多く行われているが，特に最近，坪井忠二教授及び実川顕，田島広一両氏による精密な重力測定より得られた，Bouger Anomaly の分布，[1] また爆破地震動研究グループの速度層分布の研究[2] によつて，地球物理学的な地殻構造の全貌も次第に明らかになつた．いつぽう過去数十年間に亘り全国的に実施されている，地理調査所（旧陸地測量部）の一等水準測量の検測結果は，東北地方に関しても地殻の永年変動を明瞭に示している．[3] このような広区域の地殻運動については，地理調査所の大測量に俟つこととし，ここでは，上記の重力測定結果に示された Bouger Anomaly 分布に見られる大きな構造線いわゆる盛岡〜白河 line[4] に注目して，これらの構造線を含む地域の永年的な地殻運動について触れることにしたい．筆者は活動褶曲構造に関して大塚弥之助教授，宮村摂三助教授等[5-6]によつて試みられたように，小区域ながら適当なルートを選んで，一等水準測量の再測を試み，このような永年運動の有無を調べて見た．すでに大地震や，火山の活動に伴う顕著な地殻変動は，しばしば研究され，数多くの報告が出されており，また，一方西日本における，地殻の垂直変動と重力異常に関しては，宮部直巳博士[7] の御研究があり，東北地方についても同様な研究を進めて行きたいと考えているが，ここには，地理調査所の測量によつて見出される変動の中間過程に進行していると考えられる緩慢な変動を調べ，活動構造運動論 (Lebende Tektonik) の発展に資することを期した．なおこれが併せて 20〜30 年毎に繰返して再測量される，地理調査所の大測量の間隙を補うことに役立てば幸せである．

§2. 測量とその結果について

まえがきに述べたように，第 1 図に示されている東北地方の Bouger Anomaly の分

1) C. TSUBOI, A. JITSUKAWA, H. TAJIMA, *Proc. Japan Acad.*, **29** (1953), No. 9.
C. TSUBOI, *Bull. Earthq. Res. Inst., Suppl. Vol.*, **4** (1954), 125.

2) 爆破地震動研究グループ会報　第 10 号 (1954)，第 11 号 (1955).

3) N. MIYABE, *Bull. Earthq. Res. Inst.*, **30** (1952), 127.

4) 前掲 1) 506 頁.

5) 大塚彌之助 「日本の地質構造」(1942).
大塚彌之助 「地質構造とその研究」(1952).

6) 宮村摂三　地震研究所彙報 **21** (1943), 197.
宮村摂三・岡田惇　地震研究所彙報 **27** (1949), 141.
杉村新　地震研究所彙報 **30** (1952), 163.

7) N. MIYABE, *Bull. Earthq. Res. Inst.*, **12** (1934), 163.

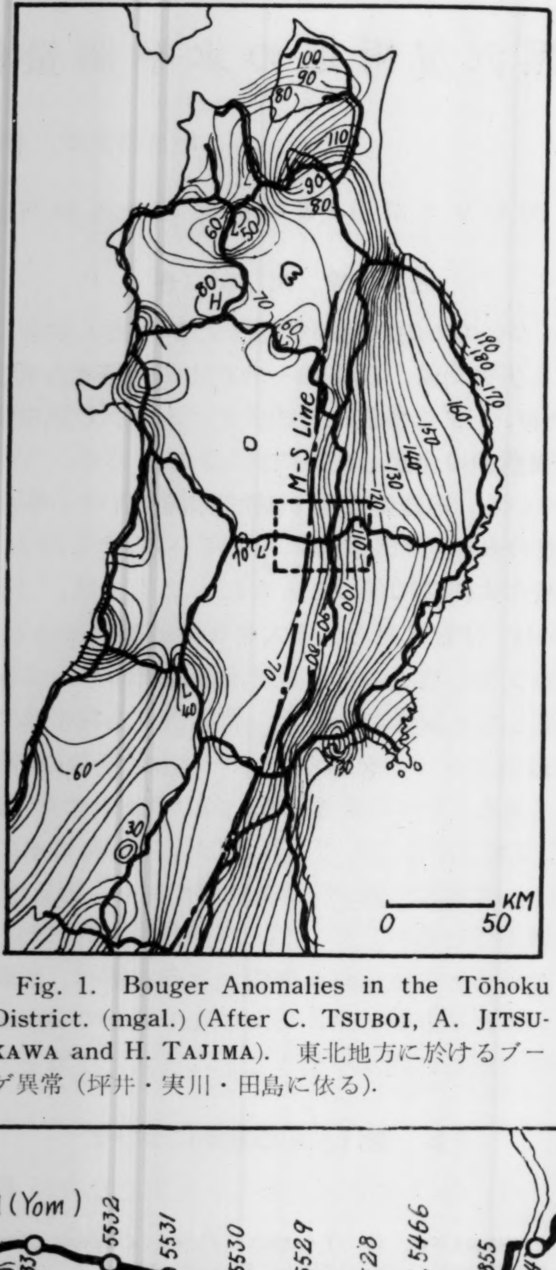

Fig. 1. Bouger Anomalies in the Tōhoku District. (mgal.) (After C. TSUBOI, A. JITSUKAWA and H. TAJIMA). 東北地方に於けるブーゲ異常（坪井・実川・田島に依る）.

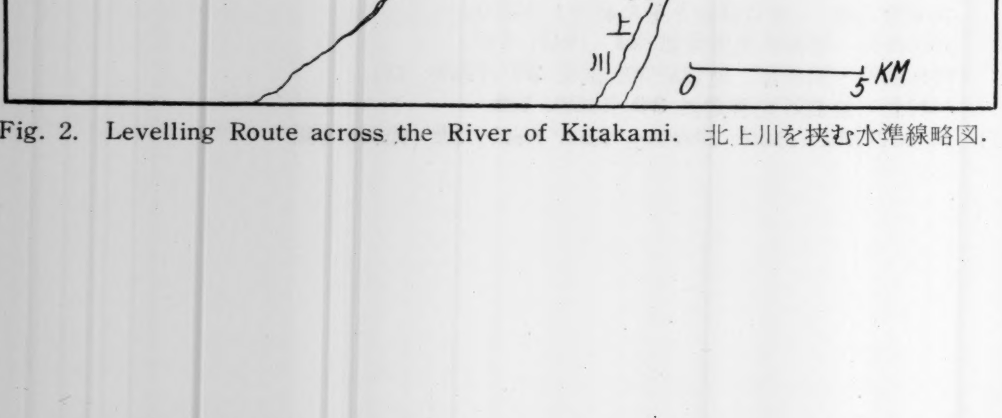

Fig. 2. Levelling Route across the River of Kitakami. 北上川を挟む水準線略図.

布図から，まづ黒沢尻附近を選び，東西約 28 粁に亘る小区域の再測量を，1954 年 9 月下旬より，10 月上旬にわたつて実施した．検測した区間は，第 2 図に示してある．第 3 図はこの水準路線の全域，すなわち横手～黒沢尻～釜石間についてのこれまでの再測結果の変動量[8-9]である．

今回再測した区間 BM. No. 5536 (横川目)～J. 5466 (黒沢尻)～6852 (中内) について，No. 5536 を不動と仮定した新旧の比較は，第 4 図のようになつた．以上の結果から見ると，とりわけてこの期間，すなわち 1933, 1934–1954 の 20 年間には，議論されるほどの変化は，見出されなかつたが，一般的に見て，東側北上山脈の方が中央山系より上昇の傾向にあるように思われる．重力異常から見られる構造線には，特にいちぢるしい変化はなかつたようである．水準点個々に就ては 2, 3 事故点と認られるものもあつたが，事故点の変動量は，誤差の範囲外で全体の傾向よりかなり離れているので，直接地殻あるいは地盤の動きと考えられない．第 I 表には，今回の測量成果を，BM. No. 5536 を不動と仮定して算出した値を示した．

この測量に使用した器械は，つぎの通りである．

Wild, 1st Order Precise Level (No. 1514),

Zeiss, Invar Precise Staff (Nos. 841, 842)

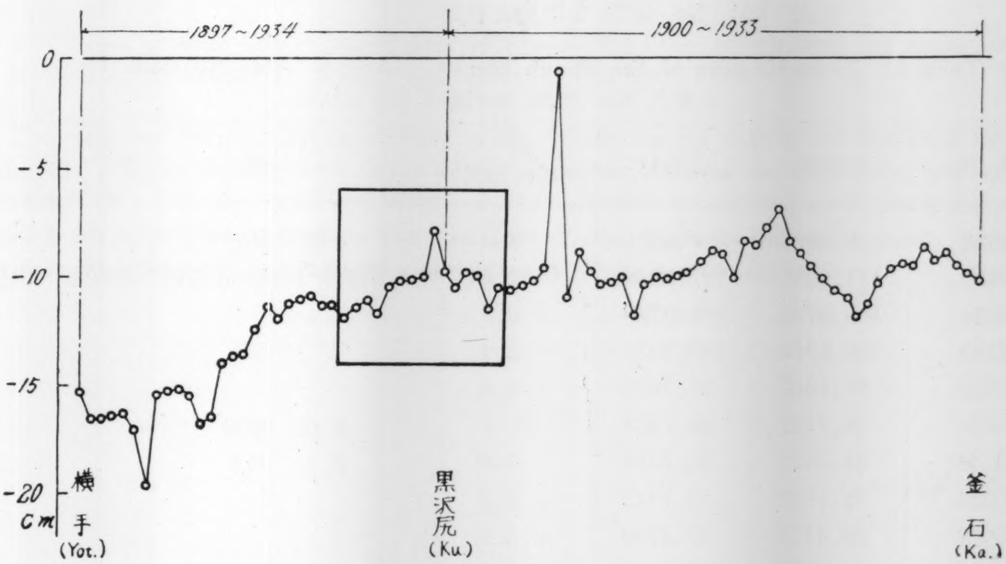

Fig. 3. Change of Heights of the Bench Marks on the Route from Yokote to Kamaishi. 横手～黒沢尻～釜石間に於ける水準点変動図.

8) 「黒沢尻～秋田間水準測量成果」 地震研究所彙報 **12** (1934), 860.
9) N. MIYABE, *Bull. Earthq. Res. Inst.*, **30** (1952), 127.

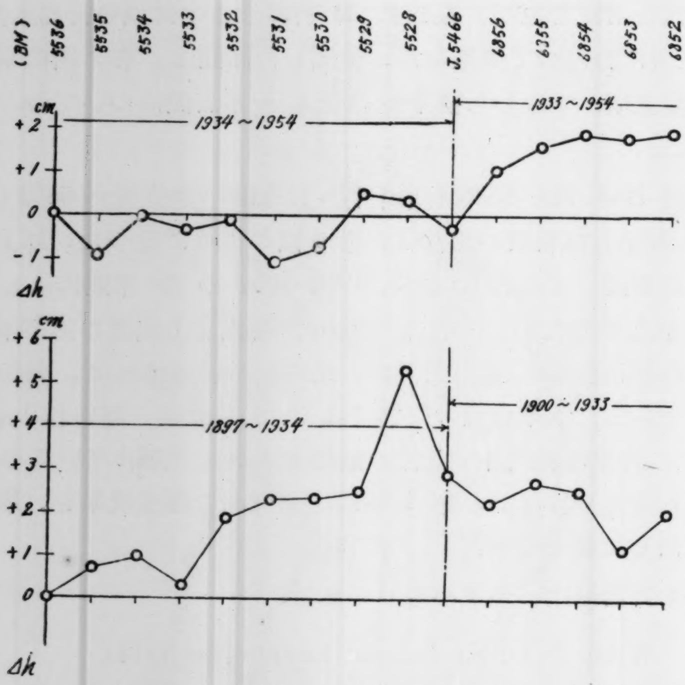

Fig. 4. Change of Heights of the Bench Marks in the Neighbourhood of the Town of Kurosawajiri (Assum. BM. No. 5536=Zero). 黒沢尻附近の水準点変動図 (BM. No. 5536 を不動と仮定).

Table I. True Heights of the Bench Marks. (Assum. BM. No. 5536 Fixed)
水準点 No. 5536 を不動とした真高値

(BM. No.)	(1934)	(1954)	Δh (1954-1934)	(備 考)
5536	m 150,4474	m 150,4474	mm 0.0	不動と仮定
5535	121,5691	121,5596	− 9.5	石羽根ダムのため水面と略同じ（旧道上）
5534	108,9780	108,9773	− 0.7	
5533	108,5063	108,5029	− 3.4	
5532	97,1637	97,1623	− 1.4	
5531	88,7127	88,7020	−10.7	路傍，傾斜
5530	81,2592	81,2514	− 7.8	同上，同上
5529	73,7522	73,7572	+ 5.0	
5528	67,4755	67,4789	+ 3.4	
J.5466	63,1337	63,1307	− 3.0	
6856	57,6973	57,7076	+10.3	
6855	59,8283	59,8444	+16.1	
6854	73,3440	73,3634	+19.4	
6853	99,8827	99,9015	+18.8	
6852	223,6913	223,7110	+19.7	

§3. あ と が き

測量に際して，水準標石箇々の異常の有無に就ては，第 I 表中備考欄に記して参考とした．この調査の結果が緩慢な地殻運動の研究という大きな課題の一端として役立つことを期待している．また，この調査で見出された地殻変動と，東北地方に於ける重力異常との相関関係等も調べる必要があろう．

最後にこの測量は“東北日本の地殻構造の綜合研究”の一部として行われたもので，終始御指導を賜つた坪井忠二教授，並びに宮村摂三助教授に厚く感謝する次第である．現地では，岩手県土木部の多大な御便宜と御助力を受けた．深く謝意を表するものである．

---

50. *Results of Precise Levellings in the Neighbourhood of Kurosawaziri, Iwate Prefecture, Northeastern Japan.*

By Atsushi OKADA,

Earthquake Research Institute.

Precise levellings were carried out along a route, about 28 kilometers in length, running from the east to the west in the neighbourhood of Kurosawaziri, Iwate Prefecture (Fig. 2).

The route crosses the so-called Morioka-Sirakawa Line which was characterized by the steep gradient band of Bouger anomalies as has been made clear by Prof. C. Tsuboi (Fig. 1).

The relative vertical displacements of the bench marks, which are obtained by comparing the present results with those of the earier surveyings in 1933–1934, are not remarkable. We can see, however, that a slight upheaval movement took place during the period from 1933–1934 to 1954 on the east side of the Morioka-Sirakawa Line, while no conspicuous movement is found on the west side (Fig. 4, and Table I).

所　報

◎ 談話会記事

第324回談話会（昭和30年7月19日）

1.	電磁直結型地震計の簡単な検定法	笠原慶一 斎藤貞夫
2.	房総沖地震余震群について（余震域を通過する地震波の問題）	笠原慶一
3.	ストンレー波の速度及び軌道について	佐藤泰夫 山口林造
4.	連続的に変化する地層による地震波の反射及び屈折	松沢武雄
5.	三原山の噴火に伴うその噴火口の地形変化について	津屋弘逵 岡田惇 渡辺佐
6.	振動解析器の理論（補遺）	河角広
7.	南海地震後に於ける四国地方の地盤変動	河角広

第325回談話会（昭和30年9月27日）

1.	房総沖地震の余震群について（前回に対する補遺）	笠原慶一
2.	地下深所における地震動の観測結果 （第6報　地盤係数に関係した問題）	金井清 長田甲斐男 吉沢静代
3.	融解点附近の弾性（第2報）ナトリウムの場合	下鶴大輔
4.	地磁気ダイナモに於ける磁場の成長	力武常次
5.	地球核内の有限振幅電磁流体振動　—地球磁場逆転の可能性—	力武常次
6.	2層建物の起振機による非線型定常振動について	久田俊彦 中川恭次
7.	携帯用石本式加速度地震計の制振度に関する二，三の実験	宮村摂三 堀実
8.	和歌山附近の地殻変動について（続報） （和歌山—御坊間水準測量結果）	岡田惇 宮村摂三
9.	黒沢尻附近の水準測量結果について	岡田惇
10.	富士山山麓の地表傾斜変化の研究（続報）（昭和30年の水準測量）	表俊一郎 笠原慶一 小林直吉

第326回談話会（昭和30年10月25日）

1.	砂層の中を伝わる波の波形について	表俊一郎 小牧昭三 兵頭盛也
2.	土地の脈動について	岸上冬彦
3.	庄内平野における常時微動の測定　第1報	田中貞二 金井清 那須信治
4.	東京都内における常時微動の測定　第3報（九段—駿河台）	田中貞二 長田甲斐男 金井清
5.	常時微動の振幅について　第1報	田中貞二 金井清

6. 地下深所における地震動の観測結果 第7報（継続時間の問題）	金井清 長田甲斐男 吉沢静代
追加 Note on a Paper by Satô.	Hansjürger Dürbaum （代読 佐藤泰夫）

第327回談話会（昭和30年11月22日）

1. スペクトラム分析を用いた地震計特性の検定法	松本利松 斎藤貞夫 唐鎌郁夫 岩田孝行
2. 分散した地震波の解析（4）	佐藤泰夫
3. 三原山の地球磁気学的研究 第7報（噴火に伴う熱過程）	横山泉
4. 桜島噴火の調査報告	茂木清夫
5. 桜島火山の最近の噴火	津屋弘逵
6. 阿蘇火山の最近の活動と噴出物	津屋弘逵
7. 二ツ井地震について I	嶋悦三 柴野睦郎
8. 米代川にそう1部水準路線の測量（第3報） ——二ツ井地震に関連しての速報——	宮村摂三 岡田惇
9. 二ツ井地震に関連した重力の測定	実川顕 田島広一

第328回談話会（昭和30年12月20日）

1. 二ツ井地震について II	嶋悦三 柴野睦郎
2. 弾性波の伝播に関する実験（其の1）	嶋悦三
3. 弾性波の発生機構に関する実験（第8報）	笠原慶一
4. 古記録による弘化4年の善光寺地震調査	佐山守 河角広
5. 湖氷中に発生する自然震動の研究（続報）	表俊一郎 山崎良雄 小牧昭三 小林直吉 森下利三
6. 地震観測用スターターの製作	田中貞二 金井清
7. 地盤と建物振動との関係 第5報	金井清 鈴木富三郎 吉沢静代
8. 地震による建物の振動と建物の特性	河角広
9. 弾性地盤上に立つ建築物の振動	佐藤泰夫 山口林造

Index to Vol. XXXIII.

Page

ASANO, S., (13) On the Accuracy of Hypocentre Determination II. (in English) 199

HISADA, T. and NAKAGAWA, K., (44) Steady State Non-linear Vibration of Two Story Buildings. (in English) 689

HORI, M. et MIYAMURA, S., (49) Quelques essais au laboratoire pour utilisation pratique du sismographe accélérometrique du type d'Ishimoto. (en japonais) 733

ICHIMURA, T., (26) Some Heavy Accessory Minerals in Granitic Rocks from the Tsukuba District, Ibaraki Prefecture. (in English) ... 385

ICHIMURA, T., (29) Activities of the Gassan Volcano. (in English) .. 419

ICHIMURA, T., (39) Geological Investigations on the Zaō Volcanoes. III Byōbu Volcano. (in English) 593

IKEGAMI, R., (43) Relation between the Periods of Microseisms and the Situation of Typhoon. (in English) 681

KANAI, K., (20) On Sezawa-waves (M_2-waves). Part II. (in English) 275

KANAI, K., (21) An Explanation for the Ground Vibration caused by Periodically Exerted Force. (in English) 283

KANAI, K. and SUZUKI, T., (8) Relation between the Property of Building Vibration and the Nature of Ground. (Observation of Earthquake Motion at Actual Buildings.) II. (in English) 109

KASAHARA, K., (28) Experimental Studies on the Mechanism of Generation of Elastic Waves V. (in English) 411

KASAHARA, K., (40) A Short Discussion on Ripples in Earthquake Shocks. (Aftershocks of the Boso-Oki Earthquake.) (in English) 631

KISHINOUYE, F., (14) Human Susceptibility to Shock Vibrations of the Ground. (in English) 207

KISHINOUYE, F. and OSSAKA, J., (10) Earth-flow on July 26, 1953, at Sōunzan, Hakone. (in Japanese) 153

KITAGAWA, Y. and MINATO, M., (24) Die Veränderung des Salzgehaltes in den küstennahen Seen Hokkaidos. (im Deutschen) .. 333

KOBAYASHI, N.; OMOTE, S.; YAMAZAKI, N. and MURAUCHI, S., (42) Ice Tremors Generated in the Floating Lake Ice. (Part 1). (in English) 663

MAEKAWA, H.; NAGATA, T. and OGUTI, T., (36) Model Experiments of Electromagnetic Induction within the Earth. (in English) ... 561

MATUMOTO, H. and MIYAMURA, S., (47) Line Carrier Telerecording Seismograph (abbr. LTS). (in Japanese) 715

MATUZAWA, T., (34) Reflexion und Refraktion der seismischen Wellen durch eine kontinuierlich verändernde Schicht. I. SH Welle. (im Deutschen) 543
MINATO, M., (30) Die zeitliche Verteilung der Vulkane im Quartär Hokkaidos. (im Deutschen) 433
MINATO, M. und KITAGAWA, Y., (24) Die Veränderung des Salzgehaltes in den küstennahen Seen Hokkaidos. (im Deutschen) . . 333
MIYAMURA, S.; YAMAZAKI, Y. and OMOTE, S., (27) Triggered Magnetic Tape Recorder for Routine Seismic Observations. (in English) 397
MIYAMURA, S. and TSUJIURA, M., (46) Line Carrier Telerecording Chronograph (abbr. LTC) for Local Seismological Network. (in Japanese) 709
MIYAMURA, S. and MATUMOTO, H., (47) Line Carrier Telerecording Seismograph (abbr. LTS). (in Japanese) 715
MIYAMURA, S. and TSUJIURA, M., (48) A VHF Radio Telerecording Seismograph (abbr. RTS). (in Japanese) 725
MIYAMURA, S. et HORI, M., (49) Quelques essais au laboratoire pour utilisation pratique du sismographe accélerometrique du type d'Ishimoto. (en japonais) 733
MORIMOTO, R.; OSSAKA, J. and TSUYA, H., (7) The 1950–1951 Eruptions of Mt. Mihara, Oshima Volcano, Seven Izu Islands, Japan. Part II. The 1951 eruption. B. Activity of the third period. (in English) 79
MORIMOTO R. and OSSAKA, J., (16) The 1952–1953 Submarine Eruption of the Myôjin Reef near the Bayonnaise Rocks, Japan (I). (in English) 221
MURAI, I., (9) Tectonic Analysis of the District Surrounding Fukui Plain. (in Japanese) 121
MURAI, I. and SHIMOZURU, D., (5) Elasticity of Marble with Special Reference to its Elastic Aeolotropy. (in English) 65
MURAUCHI, S.; OMOTE, S.; YAMAZAKI, Y. and KOBAYASHI, N., (42) Ice Tremors Generated in the Floating Lake Ice. (Part 1). (in English) 663
NAGATA, T.; OGUTI, T. and MAEKAWA, H., (36) Model Experiments of Electromagnetic Induction within the Earth. (in English) . . . 561
NAKAGAWA, K. and HISADA, T., (44) Steady State Non-linear Vibration of Two Story Buildings. (in English) 689
OGUTI, T.; NAGATA, T. and MAEKAWA, H., (36) Model Experiments

of Electromagnetic Induction within the Earth. (in English)... 561
OKADA, A., (50) Results of Precise Levellings in the Neighbourhood of Kurosawaziri, Iwate Prefecture, Northeastern Japan. (in Japanese)........ 749
OMOTE, S., (41) Aftershocks that accompanied the Tottori Earthquake of Sept. 10, 1943. (The 2nd Paper) (in English)...... 641
OMOTE, S.; MIYAMURA, S. and YAMAZAKI, Y., (27) Triggered Magnetic Tape Recorder for Routine Seismic Observations. (in English).. 397
OMOTE, S.; YAMAZAKI, Y.; KOBAYASHI, N. and MURAUCHI, S., (42) Ice Tremors Generated in the Floating Lake Ice. (Part 1). (in English)........ 663
OSSAKA, J. and KISHINOUYE, F., (10) Earth-flow on July 26, 1953, at Sōunzan, Hakone. (in Japanese)........ 153
OSSAKA, J. and MORIMOTO, R., (16) The 1952–1953 Submarine Eruption of the Myôjin Reef near the Bayonnaise Rocks, Japan (1). (in English)........ 221
OSSAKA, J.; TSUYA, H. and MORIMOTO, R., (7) The 1950–1951 Eruptions of Mt. Mihara, Oshima Volcano, Seven Izu Islands, Japan. Part II. The 1951 eruption. B. Activity of the third period. (in English)........ 79
OTUKA, Y., (32) Shizukawa Group and Tertiary Crustal Movements in Japan. (in Japanese)........ 449
RIKITAKE, T., (1) Magneto-hydrodynamic Oscillations in the Earth's Core. (in English)........ 1
RIKITAKE, T., (12) Magneto-hydrodynamic Oscillations of a Conducting Fluid Sphere in a Uniform Magnetic Field. (in English)... 175
RIKITAKE, T., (37) Growth of the Magnetic Field of the Self-exciting Dynamo in the Earth's Core. (in English)........ 571
RIKITAKE, T., (38) Magneto-hydrodynamic Oscillations of Finite Amplitude of a Conducting Fluid Sphere. (in English)........ 583
RIKITAKE, T. and YOKOYAMA, I., (23) The Anomalous Behaviour of Geomagnetic Variations of Short Period in Japan and Its Relation to the Subterranean Structure. The 6th report. (The results of further observations and some considerations concerning the influences of the sea on geomagnetic variations.) (in English)........ 297
SANTÔ (AKIMA), T., (4) Comparative Studies of Surface Waves Travelling Across Tibet Plateau and Sea of Japan, with Some Notes on the Method of Finding the Velocities of Surface Waves for

a Limited Portion of their Path. (in English) 49
SATÔ, Y., (3) Analysis of Dispersed Surface Waves by means of Fourier Transform I. (in English) 33
SATÔ, Y., (15) Relation between Seismic Intensity and Epicentral Distance. (2) (in English) 211
SATÔ, Y. and YAMAGUCHI, R., (19) Range of Possible Existence of Rayleigh- and Sezawa-Waves in a Stratified Medium. (in English) 265
SATÔ, Y. and YAMAGUCHI, R., (35) Stoneley Wave—Its Velocity, Orbit and the Distribution of Amplitude. (in English) 549
SHIMOZURU, D., (6) A Note on the Elasticity of Marble. (in English) 73
SHIMOZURU, D., (31) Elasticity of Rocks under the Initial Stresses, with Special Reference to the Fracture Problem. (in English).. 437
SHIMOZURU, D. and MURAI, I., (5) Elasticity of Marble with Special Reference to its Elastic Aeolotropy. (in English) 65
SUZUKI, T. and KANAI, K., (8) Relation between the Property of Building Vibration and the Nature of Ground. (Observation of Earthquake Motion at Actual Buildings.) II. (in English) 109
TAKAHASI, R., (18) A Short Note on a Graphical Solution of the Spectral Response of the Ground. (in English) 259
TAKAHASHI, T., (22) Analysis of the Dispersion Curves of Love-Waves. (in English).. 287
TSUJIURA, M. and MIYAMURA, S., (46) Line Carrier Telerecording Chronograph (abbr. LTC) for Local Seismological Network. (in Japanese) 709
TSUJIURA, M. and MIYAMURA, S., (48) A VHF Radio Telerecording Seismograph (abbr. RTS). (in Japanese) 725
TSUYA, H., (25) Geological and Petrological Studies of Volcano Fuji, V. 5. On the 1707 eruption of Volcano Fuji. (in English) 341
TSUYA, H.; MORIMOTO, R. and OSSAKA, J., (7) The 1950–1951 Eruptions of Mt. Mihara, Oshima Volcano, Seven Izu Islands, Japan. Part II. The 1951 eruption. B. Activity of the third period. (in English) 79
YAMAGUCHI, R. and SATÔ, Y., (19) Range of Possible Existence of Rayleigh- and Sezawa-Waves in a Stratified Medium. (in English) 265
YAMAGUCHI, R. and SATÔ, Y., (35) Stoneley Wave—Its Velocity, Orbit and the Distribution of Amplitude. (in English)......... 549
YAMAGUTI, S., (2) On the Changes in the Heights of Mean Sea-levels, before and after the Great Earthquakes. (in English) .. 27
YAMAZAKI, Y.; OMOTE, S. and MIYAMURA, S., (27) Triggered

Magnetic Tape Recorder for Routine Seismic Observations. (in English) 397
YAMAZAKI, Y.; OMOTE, S.; KOBAYASHI, N. and MURAUCHI, S., (42) Ice Tremors Generated in the Floating Lake Ice. (Part 1). (in English) 663
YOKOYAMA, I., (11) Magnetic Survey in Temmabayashi District, Aomori Prefecture. (in Japanese) 163
YOKOYAMA, I., (17) Geomagnetic Studies of Volcano Mihara. The 6th Paper. (Continuous Observation of Changes in Geomagnetic Declination during the Period from 1951 to 1954) (in English) . 251
YOKOYAMA, I. and RIKITAKE, T., (23) The Anomalous Behaviour of Geomagnetic Variations of Short Period in Japan and Its Relation to the Subterranean Structure. The 6th report. (The results of further observations and some considerations concerning the influences of the sea on geomagnetic variations.) (in English) .. 297
SUBSOIL RESEARCH TEAM, THE EARTHQUAKE RESEARCH INSTITUTE, (33) Investigation into Seismic Characteristics of Subsoils in Tokyo. (in Japanese) 471
The Research Group for Explosion Seismology, (45) The Fifth Explosion Seismic Observations carried out in the North-eastern Japan. (in English) 699

索 引 第33号

頁

浅野周三 (13) 震源決定の精度について (第2報) (英文) 199

久田俊彦・中川恭次 (44) 二層建物の非線形定常振動 (英文) 689

堀 実・宮村摂三 (49) 携帯用石本式加速度地震計の野外実地使用に対する
二三の基礎実験 (邦文) 733

市村 毅 (26) 筑波地方産花崗岩の副成分重鉱物 (英文) 385

市村 毅 (29) 月山火山の活動 (英文) 419

市村 毅 (39) 蔵王火山の地質学的研究 (第3報) (英文) 591

池上良平 (43) 土地の脈動の周期と台風位置との関係 (英文) 683

金井 清 (20) 妹沢波 (M_2 波) について (第2報) (英文) 275

金井 清 (21) 周期的加力による地盤振動に対する1つの解釈 (英文) 283

金井 清・鈴木富三郎 (8) 建物の振動的性質と地盤の性質との関係 (実在建物
における地震動観測) 第2報 (英文) 109

笠原慶一 (28) 弾性波の発生機構に関する実験 (第5報) (英文) 411

笠原慶一 (40) 地震動に含まれる短週期震動 (リップル) について——房総沖
地震の余震の場合—— (英文) 631

岸上冬彦 (14) 衝撃による地動に対する人体感覚 (英文) 207

岸上冬彦・小坂丈予 (10) 1953年7月26日の早雲山山津波の調査 (邦文) 153

北川芳男・湊 正雄 (24) 北海道・海岸湖の鹹度変化 (独文) 333

小林直吉・表 俊一郎・山崎良雄・村内必典 (42) 湖氷中に発生する自然震動の研
究 (第1報) (英文) 663

前川英夫・永田 武・小口 高 (36) 地球内電磁誘導現象の模型実験 (英文) 561

松本英照・宮村摂三 (47) 有線搬送式遠隔記録地震計 (邦文) 715

松沢武雄 (34) 連続的に変る地層による地震波の反射及び屈折 (独文) 543

湊 正雄 (30) 北海道・第四紀火山の時代的分類 (独文) 433

湊 正雄・北川芳男 (24) 北海道・海岸湖の鹹度変化 (独文) 333

宮村摂三・山崎良雄・表 俊一郎 (27) 地震観測用磁気テープ利用ひきがね式遅
延記録装置 (英文) 397

宮村摂三・辻浦 賢 (46) 局地的地震観測網のための有線搬送式遠隔刻時装置
(邦文) 709

宮村摂三・松本英照 (47) 有線搬送式遠隔記録地震計 (邦文) 715

宮村摂三・辻浦 賢 (48) 超短波無線搬送式遠隔記録地震計 (邦文) 725

宮村摂三・堀 実 (49) 携帯用石本式加速度地震計の野外実地使用に対する
二三の基礎実験 (邦文) 733

森本良平・小坂丈予・津屋弘逵 (7) 伊豆大島三原山昭和25年及26年の噴火 その2

昭和26年の噴火 (B) 第3期の活動 (英文) 79

森本良平・小坂丈予 (16) 明神礁の昭和27—28年の噴火 (1) (英文) 221

村井 勇 (9) 福井平野周辺地域の地質構造解析 (邦文) 121

村井 勇・下鶴大輔 (5) 大理石の弾性，特にその異方性に就いて (英文) 65

村内必典・表 俊一郎・山崎良雄・小林直吉 (42) 湖氷中に発生する自然震動の研究 (第1報) (英文) 663

永田 武・小口 高・前川英夫 (36) 地球内電磁誘導現象の模型実験 (英文) 561

中川恭次・久田俊彦 (44) 二層建物の非線形定常振動 (英文) 689

小口 高・永田 武・前川英夫 (36) 地球内電磁誘導現象の模型実験 (英文) 561

岡田 惇 (50) 黒沢尻附近の水準測量結果 (邦文) 749

表 俊一郎 (41) 鳥取地震余震観測 (第2報) (英文) 641

表 俊一郎・宮村摂三・山崎良雄 (27) 地震観測用磁気テープ利用ひきがね式遅延記録装置 (英文) 397

表 俊一郎・山崎良雄・小林直吉・村内必典 (42) 湖氷中に発生する自然震動の研究 (第1報) (英文) 663

小坂丈予・岸上冬彦 (10) 1953年7月26日の早雲山山津波の調査 (邦文) 153

小坂丈予・森本良平 (16) 明神礁の昭和27——28年の噴火 (1) (英文) 221

小坂丈予・津屋弘逵・森本良平 (7) 伊豆大島三原山昭和25年及26年の噴火 その2 昭和26年の噴火 (B) 第3期の活動 (英文) 79

大塚弥之助 (32) 静川層群について (附 第三紀地殼運動の一考察) (邦文) 449

力武常次 (1) 地球核内の電磁流体振動 (英文) 1

力武常次 (12) 一様磁場内の導電流体球の電磁流体振動 (英文) 175

力武常次 (37) 地磁気ダイナモに於ける磁場の生長 (英文) 571

力武常次 (38) 地球核内の有限振幅電磁流体振動 (英文) 583

力武常次・横山 泉 (23) 日本に於ける地磁気短周期変化の異常と地下構造 (第6報) (その後の観測結果及び地磁気変化におよぼす海の影響) (英文) 297

三東哲夫 (旧姓秋間) (4) チベット高原と日本海を通過する表面波について，及びある限られた地域を通過する表面波の速度を計算で見出す場合の二，三の注意 (英文) 49

佐藤泰夫 (3) 分散した地震波の解析 I (英文) 33

佐藤泰夫 (15) 震度と震央距離との関係 (2) (英文) 211

佐藤泰夫・山口林造 (19) 表面層をもつ媒質内の Rayleigh 波と妹沢波の存在限界 (英文) 265

佐藤泰夫・山口林造 (35) Stoneley 波——その速度，軌道及び振巾の分布 (英文) 549

下鶴大輔 (6) 大理石の弾性に関するノート (英文) 73

下鶴大輔 (31) 応力と岩石の弾性，特に破壊領域に就いて (英文) 437

下鶴大輔・村井　勇 (5) 大理石の弾性，特にその異方性に就いて (英文) 65
鈴木富三郎・金井　清 (8) 建物の振動的性質と地盤の性質との関係 (実在建物における地震動観測) 第2報 (英文) 109
高橋龍太郎 (18) 地盤のスペクトル応答を求める図式解法 (英文) 259
高橋健人 (22) Love 波の分散曲線の解析 (英文) 287
辻浦　賢・宮村摂三 (46) 局地的地震観測網のための有線搬送式遠隔刻時装置 (邦文) 709
辻浦　賢・宮村摂三 (48) 超短波無線搬送式遠隔記録地震計 (邦文) 725
津屋弘逵 (25) 富士火山の地質学的並びに岩石学的研究 (V) 5. 富士山の宝永4年噴火について (英文) 341
津屋弘逵・森本良平・小坂丈予 (7) 伊豆大島三原山昭和25年及26年の噴火 その2 昭和26年の噴火 (B) 第3期の活動 (英文) 79
山口林造・佐藤泰夫 (19) 表面層をもつ媒質内の Rayleigh 波と妹沢波の存在限界 (英文) 265
山口林造・佐藤泰夫 (35) Stoneley 波——その速度，軌道及び振巾の分布 (英文) 549
山口生知 (2) 大地震前後に於ける平均海水面の変化について (英文) 27
山崎良雄・表　俊一郎・宮村摂三 (27) 地震観測用磁気テープ利用ひきがね式遅延記録装置 (英文) 397
山崎良雄・表　俊一郎・小林直吉・村内必典 (42) 湖氷中に発生する自然震動の研究 (第1報) (英文) 663
横山　泉 (11) 青森県天間林地域における磁気探鉱 (邦文) 163
横山　泉 (17) 三原山の地球磁気学的研究　第6報 (1951～1954年間の偏角変化の連続観測) (英文) 251
横山　泉・力武常次 (23) 日本に於ける地磁気短周期変化の異常と地下構造 (第6報) (その後の観測結果及び地磁気変化におよぼす海の影響) (英文) 297
地震研究所地盤研究会 (33) 東京都地盤調査報告 (邦文) 471
爆破地震動研究グループ (45) 東北日本に於ける第5回爆破地震動観測 (英文) 699

BULLETIN

OF THE

EARTHQUAKE RESEARCH INSTITUTE

TOKYO UNIVERSITY

VOL. XXXIII

1955

30TH ANNIVERSARY VOLUME

東京大学

地震研究所彙報

第 33 号

昭和 30 年

創立30周年記念号

CONTENTS.

VOL. XXXIII.

30TH ANNIVERSARY VOLUME

Part 1. March, 1955.

Papers and Reports.

Page

1. T. RIKITAKE, Magneto-hydrodynamic Oscillations in the Earth's Core. (in English) 1
2. S. YAMAGUTI, On the Changes in the Heights of Mean Sea-levels, before and after the Great Earthquakes. (in English).. 27
3. Y. SATÔ, Analysis of Dispersed Surface Waves by means of Fourier Transform I. (in English) 33
4. T. SANTÔ AKIMA, Comparative Studies of Surface Waves Travelling Across Tibet Plateau and Sea of Japan, with Some Notes on the Method of Finding the Velocities of Surface Waves for a Limited Portion of their Path. (in English) ... 49
5. D. SHIMOZURU and I. MURAI, Elasticity of Marble with Special Reference to its Elastic Aeolotropy. (in English) 65
6. D. SHIMOZURU, A Note on the Elasticity of Marble. (in English) 73
7. H. TSUYA, R. MORIMOTO and J. OSSAKA, The 1950–1951 Eruptions of Mt. Mihara, Oshima Volcano, Seven Izu Islands, Japan. Part II. The 1951 eruption. B. Activity of the third period. (in English) 79
8. K. KANAI and T. SUZUKI, Relation between the Property of Building Vibration and the Nature of Ground. (Observation of Earthquake Motion at Actual Buildings.) II. (in English) 109
9. I. MURAI, Tectonic Analysis of the District Surrounding Fukui Plain. (in Japanese) 121
10. F. KISHINOUYE and J. OSSAKA, Earth-flow on July 26, 1953, at Sōunzan, Hakone. (in Japanese) 153
11. I. YOKOYAMA, Magnetic Survey in Temmabayashi District, Aomori Prefecture. (in Japanese).......................... 163

Part 2. June, 1955.

12. T. RIKITAKE, Magneto-hydrodynamic Oscillations of a Conducting Fluid Sphere in a Uniform Magnetic Field. (in English).... 175

13. S. ASANO, On the Accuracy of Hypocentre Determination II. (in English) 199
14. F. KISHINOUYE, Human Susceptibility to Shock Vibrations of the Ground. (in English) 207
15. Y. SATÔ, Relation between Seismic Intensity and Epicentral Distance. (2) (in English) 211
16. R. MORIMOTO and J. OSSAKA, The 1952–1953 Submarine Eruption of the Myôjin Reef near the Bayonnaise Rocks, Japan (I). (in English) 221
17. I. YOKOYAMA, Geomagnetic Studies of Volcano Mihara. The 6th Paper. (Continuous Observation of Changes in Geomagnetic Declination during the Period from 1951 to 1954) (in English) 251

Part 3. September, 1955.

18. R. TAKAHASI, A Short Note on a Graphical Solution of the Spectral Response of the Ground. (in English) 259
19. R. YAMAGUCHI and Y. SATÔ, Range of Possible Existence of Rayleigh- and Sezawa-Waves in a Stratified Medium. (in English) 265
20. K. KANAI, On Sezawa-waves (M_2-waves). Part II. (in English) 275
21. K. KANAI, An Explanation for the Ground Vibration caused by Periodically Exerted Force. (in English) 283
22. T. TAKAHASHI, Analysis of the Dispersion Curves of Love-Waves. (in English) 287
23. T. RIKITAKE and I. YOKOYAMA, The Anomalous Behaviour of Geomagnetic Variations of Short Period in Japan and Its Relation to the Subterranean Structure. The 6th report. (The results of further observations and some considerations concerning the influences of the sea on geomagnetic variations.) (in English) 297
24. M. MINATO und Y. KITAGAWA, Die Veränderung des Salzgehaltes in den küstennahen Seen Hokkaidos. (im Deutschen). 333
25. H. TSUYA, Geological and Petrological Studies of Volcano Fuji, V. 5. On the 1707 eruption of Volcano Fuji. (in English).. 341
26. T. ICHIMURA, Some Heavy Accessory Minerals in Granitic Rocks from the Tsukuba District, Ibaraki Prefecture. (in English) 385
27. S. OMOTE, S. MIYAMURA and Y. YAMAZAKI, Triggered Magnetic Tape Recorder for Routine Seismic Observations. (in English) 397

28. K. KASAHARA, Experimental Studies on the Mechanism of Generation of Elastic Waves V. (in English).............. 411
29. T. ICHIMURA, Activities of the Gassan Volcano. (in English) .. 419
30. M. MINATO, Die zeitliche Verteilung der Vulkane im Quartär Hokkaidos. (im Deutschen)................................ 433
31. D. SHIMOZURU, Elasticity of Rocks under the Initial Stresses, with Special Reference to the Fracture Problem. (in English) 437
32. Y. OTUKA, Shizukawa Group and Tertiary Crustal Movements in Japan. (in Japanese).................................. 449
33. SUBSOIL RESEARCH TEAM, THE EARTHQUAKE RESEARCH INSTITUTE, Investigation into Seismic Characteristics of Subsoils in Tokyo. (in Japanese).................................. 471

Part 4. December, 1955.

Director, Earthquake Research Institute: Past Thirty Years Since Its Establishment
34. T. MATUZAWA, Reflexion und Refraktion der seismischen Wellen durch eine kontinuierlich verändernde Schicht. I. SH Welle. (im Deutschen)... 543
35. R. YAMAGUCHI and Y. SATÔ, Stoneley Wave—Its Velocity, Orbit and the Distribution of Amplitude. (in English)...... 549
36. T. NAGATA, T. OGUTI and H. MAEKAWA, Model Experiments of Electromagnetic Induction within the Earth. (in English) 561
37. T. RIKITAKE, Growth of the Magnetic Field of the Self-exciting Dynamo in the Earth's Core. (in English) 571
38. T. RIKITAKE, Magneto-hydrodynamic Oscillations of Finite Amplitude of a Conducting Fluid Sphere. (in English)......... 583
39. T. ICHIMURA, Geological Investigations on the Zaō Volcanoes. III Byōbu Volcano. (in English) 593
40. K. KASAHARA, A Short Discussion on Ripples in Earthquake Shocks. (Aftershocks of the Boso-Oki Earthquake.) (in English) 631
41. S. OMOTE, Aftershocks that accompanied the Tottori Earthquake of Sept. 10, 1943. (The 2nd Paper). (in English) 641
42. S. OMOTE, Y. YAMAZAKI, N. KOBAYASHI and S. MURAUCHI, Ice Tremors Generated in the Floating Lake Ice. (Part 1). (in English)... 663
43. R. IKEGAMI, Relation between the Periods of Microseisms and the Situation of Typhoon. (in English).................... 681
44. T. HISADA and K. NAKAGAWA, Steady State Non-linear Vibration

of Two Story Buildings. (in English) 689
45. The Research Group for Explosion Seismology, The Fifth Explosion Seismic Observations carried out in the North-eastern Japan. (in English) 699
46. S. MIYAMURA and M. TSUJIURA, Line Carrier Telerecording Chronograph (abbr. LTC) for Local Seismological Network. (in Japanese) 709
47. S. MIYAMURA and H. MATUMOTO, Line Carrier Telerecording Seismograph (abbr. LTS). (in Japanese) 715
48. S. MIYAMURA and M. TSUJIURA, A VHF Radio Telerecording Seismograph (abbr. RTS). (in Japanese) 725
49. S. MIYAMURA et M. HORI, Quelques essais au laboratoire pour utilisation pratique du sismographe accélérometrique du type d'Ishimoto. (en japonais) 733
50. A. OKADA, Results of Precise Levellings in the Neighbourhood of Kurosawa-ziri, Iwate Prefecture, Northeastern Japan. (in Japanese) 749

目　次

第 33 号
創 立 30 周 年 記 念 号

第 1 冊　昭和 30 年 3 月

論文及報告

			頁
1.	地球核内の電磁流体振動 (英文)	力 武 常 次	1
2.	大地震前後に於ける平均海水面の変化について (英文)	山 口 生 知	27
3.	分散した地震波の解析 I (英文)	佐 藤 泰 夫	33
4.	チベット高原と日本海を通過する表面波について，及びある限られた地域を通過する表面波の速度を計算で見出す場合の二，三の注意 (英文)	三 東 哲 夫 (旧姓秋間)	49
5.	大理石の弾性，特にその異方性に就いて (英文)	下 鶴 大 輔 村 井 勇	65
6.	大理石の弾性に関するノート (英文)	下 鶴 大 輔	73
7.	伊豆大島三原山昭和 25 年及 26 年の噴火 その 2 昭和 26 年の噴火 (B) 第 3 期の活動 (英文)	津 屋 弘 逵 森 本 良 平 小 坂 丈 予	79
8.	建物の振動的性質と地盤の性質との関係 (実在建物における地震動観測) 第 2 報 (英文)	金 井 清 鈴木富三郎	109
9.	福井平野周辺地域の地質構造解析 (邦文)	村 井 勇	121
10.	1953 年 7 月 26 日早雲山山津波の調査 (邦文)	岸 上 冬 彦 小 坂 丈 予	153
11.	青森県天間林地域における磁気探鉱 (邦文)	横 山 泉	163

第 2 冊　昭和 30 年 6 月

12.	一様磁場内の導電流体球の電磁流体振動 (英文)	力 武 常 次	175
13.	震源決定の精度について (第 2 報) (英文)	浅 野 周 三	199
14.	衝撃による地動に対する人体感覚 (英文)	岸 上 冬 彦	207
15.	震度と震央距離との関係 (2) (英文)	佐 藤 泰 夫	211
16.	明神礁の昭和 27--28 年の噴火 (1) (英文)	森 本 良 平 小 坂 丈 予	221
17.	三原山の地球磁気学的研究　第 6 報 (1951～1954 年間の偏角変化の連続観測) (英文)	横 山 泉	251

第 3 冊　昭和 30 年 9 月

頁

18. 地盤のスペクトル応答を求める図式解法（英文）……………… 髙橋龍太郎 259

19. 表面層をもつ媒質内の Rayleigh 波と妹沢波の存在限界（英文）… {山口林造 / 佐藤泰夫} 265

20. 妹沢波（M_2 波）について（第 2 報）（英文）……………… 金井　清 275

21. 周期的加力による地盤振動に対する 1 つの解釈（英文）……… 金井　清 283

22. Love 波の分散曲線の解析（英文）……………… 髙橋健人 287

23. 日本に於ける地磁気短周期変化の異常と地下構造（第 6 報）（その後の観測結果及び地磁気変化におよぼす海の影響）（英文）… {力武常次 / 横山　泉} 297

24. 北海道・海岸湖の鹹度変化（独文）……………… {湊　正雄 / 北川芳男} 333

25. 富士火山の地質学的並びに岩石学的研究（V）
    5. 富士山の宝永 4 年噴火について（英文）……………… 津屋弘逵 341

26. 筑波地方産花崗岩の副成分重鉱物（英文）……………… 市村　毅 385

27. 地震観測用磁気テープ利用ひきがね式遅延記録装置（英文）…… {表俊一郎 / 宮村摂三 / 山崎良雄} 397

28. 弾性波の発生機構に関する実験（第 5 報）（英文）……………… 笠原慶一 411

29. 月山火山の活動（英文）……………… 市村　毅 419

30. 北海道・第四紀火山の時代的分類（独文）……………… 湊　正雄 433

31. 応力と岩石の弾性，特に破壊領域に就いて（英文）……………… 下鶴大輔 473

32. 静川層群について（附　第三紀地殻運動の一考察）（邦文）……… 大塚彌之助 449

33. 東京都地盤調査報告（邦文）……………… 地震研究所地盤研究会 471

第 4 冊　昭和 30 年 12 月

創立以来 30 年間の地震研究所……………… 所　長

34. 連続的に変る地層による地震波の反射及び屈折（独文）……… 松沢武雄 543

35. Stoneley 波—その速度，軌道及び振幅の分布（英文）……… {山口林造 / 佐藤泰夫} 549

36. 地球内電磁誘導現象の模型実験（英文）……………… {永田　武 / 小口　高 / 前川英夫} 561

37. 地磁気ダイナモに於ける磁場の生長（英文）……………… 力武常次 571

38. 地球核内の有限振幅電磁流体振動（英文）……………… 力武常次 583

39. 蔵王火山の地質学的研究（第 3 報）（英文）……………… 市村　毅 593

40. 地震動に含まれる短週期震動（リップル）について
    —房総沖地震の余震の場合—（英文）……………… 笠原慶一 631

			頁
41.	鳥取地震余震観測（第2報）（英文）	表　俊一郎	641
42.	湖氷中に発生する自然震動の研究（第1報）（英文）	表　俊一郎 山崎良雄 小林直吉 村内必典	663
43.	土地の脈動の周期と台風位置との関係（英文）	池上良平	681
44.	二層建物の非線形定常振動（英文）	久田俊彦 中川恭次	689
45.	東北日本に於ける第5回爆破地震動観測（英文）	爆破地震動研究グループ	699
46.	局地的地震観測網のための有線搬送式遠隔刻時装置（邦文）	宮村摂三 辻浦　賢	709
47.	有線搬送式遠隔記録地震計（邦文）	宮村摂三 松本英照	715
48.	超短波無線搬送式遠隔記録地震計（邦文）	宮村摂三 辻浦　賢	725
49.	携帯用石本式加速度地震計の野外実地使用に対する二三の基礎実験（邦文）	宮村摂三 堀　　実	733
50.	黒沢尻附近の水準測量結果（邦文）	岡田　惇	749

昭和31年3月25日印刷
昭和31年3月30日發行

東京都文京區本富士町一番地
東京大學構內
編纂兼發行者　東京大學地震研究所

東京都千代田區富士見町一丁目十番地
印刷者　笠井康頼

東京都千代田區富士見町一丁目十番地
印刷所　株式會社國際文献印刷社

賣捌所　東京都千代田區神田一ツ橋通
岩波書店

東京都中央區日本橋通二丁目六番地
丸善株式會社

Sold by
Iwanami Shoten,
Hitotsubashi dôri, Chiyoda-ku, Tôkyô,
and
Maruzen Co., Ltd.,
Nihonbashi dôri, Chûô-ku, Tôkyô.
Price of this copy: 804 Yen. (Postage exclusive.)

BULLETIN OF

THE EARTHQUAKE RESEARCH INSTITUTE

TOKYO UNIVERSITY

Vol. XXXIII, Part 4. December, 1955.

30TH ANNIVERSARY VOLUME

Contents.

Earthquake Research Institute: Past Thirty Years Since Its Establishment.. Director

Papers and Reports.

Page

34. T. MATUZAWA, Reflexion und Refraktion der seismischen Wellen durch eine kontinuierlich verändernde Schicht. I. SH Welle. (im Deutschen) 543
35. R. YAMAGUCHI and Y. SATÔ, Stoneley Wave—Its Velocity, Orbit and the Distribution of Amplitude. (in English) 549
36. T. NAGATA, T. OGUTI and H. MAEKAWA, Model Experiments of Electromagnetic Induction within the Earth. (in English) 561
37. T. RIKITAKE, Growth of the Magnetic Field of the Self-exciting Dynamo in the Earth's Core. (in English) 571
38. T. RIKITAKE, Magneto-hydrodynamic Oscillations of Finite Amplitude of a Conducting Fluid Sphere. (in English) 583
39. T. ICHIMURA, Geological Investigations on the Zaō Volcanoes. III Byōbu Volcano. (in English) 593
40. K. KASAHARA, A Short Discussion on Ripples in Earthquake Shocks. (Aftershocks of the Boso-Oki Earthquake.) (in English) 631
41. S. OMOTE, Aftershocks that accompanied the Tottori Earthquake of Sept. 10, 1943. (The 2nd Paper). (in English) 641
42. S. OMOTE, Y. YAMAZAKI, N. KOBAYASHI and S. MURAUCHI, Ice Tremors Generated in the Floating Lake Ice (Part 1). (in English) 663
43. R. IKEGAMI, Relation between the Periods of Microseisms and the Situation of Typhoon. (in English) 681
44. T. HISADA and K. NAKAGAWA, Steady State Non-linear Vibration of Two Story Buildings. (in English) 689
45. The Research Group for Explosion Seismology, The Fifth Explosion Seismic Observations carried out in the North-eastern Japan. (in English) 699
46. S. MIYAMURA and M. TSUJIURA, Line Carrier Telerecording Chronograph (abbr. LTC) for Local Seismological Network. (in Japanese) 709
47. S. MIYAMURA and H. MATUMOTO, Line Carrier Telerecording Seismograph (abbr. LTS). (in Japanese) 715
48. S. MIYAMURA and M. TSUJIURA, A VHF Radio Telerecording Seismograph (abbr. RTS). (in Japanese) 725
49. S. MIYAMURA et M. HORI, Quelques essais au laboratoire pour utilisation pratique du sismographe accélérometrique du type d'Ishimoto. (en japonais). 733
50. A. OKADA, Results of Precise Levellings in the Neighbourhood of Kurosawaziri, Iwate Prefecture, Northeastern Japan. (in Japanese) 749

Institute Notes.
Index.

(For the papers written in Japanese or in occidental languages, the abstracts are given in occidental languages or in Japanese respectively.)